Comprehensive Treatise of Electrochemistry

7

Kinetics and Mechanisms of Electrode Processes

Edited by

Brian E. Conway

J. O'M. Bockris

Ernest Yeager

S. U. M. Khan

Ralph E. White

Comprehensive Treatise of Electrochemistry

Volume 7

Kinetics and Mechanisms of Electrode Processes

COMPREHENSIVE TREATISE OF ELECTROCHEMISTRY

Volume 1	THE DOUBLE LAYER Edited by J. O'M. Bockris, Brian E. Conway, and Ernest Yeager
Volume 2	ELECTROCHEMICAL PROCESSING Edited by J. O'M. Bockris, Brian E. Conway, Ernest Yeager, and Ralph E. White
Volume 3	ELECTROCHEMICAL ENERGY CONVERSION AND STORAGE Edited by J. O'M. Bockris, Brian E. Conway, Ernest Yeager, and Ralph E. White
Volume 4	ELECTROCHEMICAL MATERIALS SCIENCE Edited by J. O'M. Bockris, Brian E. Conway, Ernest Yeager, and Ralph E. White
Volume 5	THERMODYNAMIC AND TRANSPORT PROPERTIES OF AQUEOUS AND MOLTEN ELECTROLYTES Edited by Brian E. Conway, J. O'M. Bockris, and Ernest Yeager
Volume 6	ELECTRODICS: TRANSPORT Edited by Ernest Yeager, J. O'M. Bockris, Brian E. Conway, and S. Sarangapani
Volume 7	KINETICS AND MECHANISMS OF ELECTRODE PROCESSES Edited by Brian E. Conway, J. O'M. Bockris, Ernest Yeager, S. U. M. Khan, and Ralph E. White

Comprehensive Treatise of Electrochemistry

Volume 7

Kinetics and Mechanisms of Electrode Processes

Edited by

Brian E. Conway
University of Ottawa
Ottawa, Ontario, Canada

J. O'M. Bockris
Texas A&M University
College Station, Texas

Ernest Yeager
Case Western Reserve University
Cleveland, Ohio

S. U. M. Khan
Texas A&M University
College Station, Texas

Ralph E. White
Texas A&M University
College Station, Texas

PLENUM PRESS • NEW YORK AND LONDON

Library of Congress Cataloging in Publication Data

Main entry under title:

Kinetics and mechanisms of electrode processes.

(Comprehensive treatise of electrochemistry; v. 7)
Includes bibliographical references and index.
1. Electrodes. 2. Electrochemistry. 3. Chemical reaction, Rate of. I. Conway, B. E. II. Series.
QD552.C64 vol. 7 541.3′7s [541.3′724] 83-17831
[QD571]

ISBN-13: 978-1-4613-3586-3 e-ISBN-13: 978-1-4613-3584-9

DOI: 10.1007/978-1-4613-3584-9

©1983 Plenum Press, New York

Softcover reprint of the hardcover 1st edition 1983

A Division of Plenum Publishing Corporation
233 Spring Street, New York, N.Y. 10013

All rights reserved

No part of this book may be reproduced, stored in a retrieval system, or transmitted in any form or by any means, electronic, mechanical, photocopying, microfilming, recording, or otherwise, without written permission from the Publisher

Contributors

A. J. Appleby • Electric Power Research Institute, 3412 Hillview Avenue, Palo Alto, California

John O'M. Bockris • Department of Chemistry, Texas A&M University, College Station, Texas

Evengi B. Budevski • Central Laboratory of Electrochemical Power Sources, Bulgarian Academy of Sciences, Sofia 1040, Bulgaria

B. E. Conway • Department of Chemistry, University of Ottawa, Ottawa, Ontario, Canada

Aleksandar R. Despić • Faculty of Technology and Metallurgy, University of Belgrade, Belgrade, Yugoslavia

R. R. Dogonadze • Institute of Electrochemistry of the Academy of Sciences of the USSR, Moscow, USSR

M. Enyo • The Research Institute for Catalysis, Hokkaido University, Sapporo, Japan

D. Inman • Department of Metallurgy & Materials Science, Imperial College, London SW7 2BP, United Kingdom

Shahed U. M. Khan • Department of Chemistry, Texas A&M University, College Station, Texas

L. I. Krishtalik • Institute of Electrochemistry of the Academy of Sciences of the USSR, Moscow, USSR

A. M. Kuznetsov • Institute of Electrochemistry of the Academy of Sciences of the USSR, Moscow, USSR

D. G. Lovering • Chemistry Branch, R.M.C.S., Shrivenham, Swindon SN6 8LA, United Kingdom

R. Memming • Philips GmbH Forschungslaboratorium Hamburg, D-2000 Hamburg 54, Federal Republic of Germany

E. J. Judd • Eltech Systems Corporation, Technical Center, Fairport, Ohio

Andrzej Sadkowski • Institute of Physical Chemistry, Warsaw, Poland

M. R. Tarasevich • Institute of Electrochemistry of the Academy of Sciences of the USSR, Moscow, USSR

Ernest Yeager • Case Laboratories for Electrochemical Studies, Case Western Reserve University, Cleveland, Ohio

Preface to Comprehensive Treatise of Electrochemistry

Electrochemistry is one of the oldest defined areas in physical science, and there was a time, less than 50 years ago, when one saw "Institute of Electrochemistry and Physical Chemistry" in the chemistry buildings of European universities. But after early brilliant developments in electrode processes at the beginning of the twentieth century and in solution chemistry during the 1930s, electrochemistry fell into a period of decline which lasted for several decades. Electrochemical systems were too complex for the theoretical concepts of the quantum theory. They were too little understood at a phenomenological level to allow the ubiquity in application in so many fields to be comprehended.

However, a new growth began faintly in the late 1940s, and clearly in the 1950s. This growth was exemplified by the formation in 1949 of what is now called The International Society for Electrochemistry. The usefulness of electrochemistry as a basis for understanding conservation was the focal point in the founding of this Society. Another very important event was the choice by NASA in 1958 of fuel cells to provide the auxiliary power for space vehicles.

With the new era of diminishing usefulness of the fossil fuels upon us, the role of electrochemical technology is widened (energy storage, conversion, enhanced attention to conservation, direct use of electricity from nuclear–solar plants, finding materials which interface well with hydrogen). This strong new interest is not only in the technological applications of electrochemistry. Quantum chemists have taken an interest in redox processes. Organic chemists are interested in situations where the energy of electrons is as easily controlled as it is at electrodes. Some biological processes are now seen in electrodic terms, with electron transfer to and from materials which would earlier have been considered to be insulators.

It is now time for a comprehensive treatise to look at the whole field of electrochemistry.

The present treatise was conceived in 1974, and the earliest invitations to authors for contributions were made in 1975. The completion of the early volumes has been delayed by various factors.

There has been no attempt to make each article emphasize the most recent situation at the expense of an overall statement of the modern view. This treatise is not a collection of articles from *Recent Advances in Electrochemistry* or *Modern Aspects of Electrochemistry*. It is an attempt at making a mature statement about the present position in the vast area of what is best looked at as a new interdisciplinary field.

Texas A & M University	John O'M. Bockris
University of Ottawa	Brian E. Conway
Case Western Reserve University	Ernest B. Yeager
Texas A & M University	Ralph E. White

Preface to Volume 7

The present volume deals with electrode kinetics, the heart of electrochemistry. After much progress in the 19th century, at the beginning of the present century the field went into a period of decline from which it did not emerge for about fifty years. Now, it is by far the most populated area in electrochemical research.

It must be admitted, however, that the selection of authors for the present Volume has not been an easy one because there are controversies at the basis of the subject. There is no agreement upon the nature of the activation processes in the fundamental act. A number of fundamental electrochemists limit their activities to the study of redox systems (because of the complexities of bonding in other systems), whereas others consider that by so doing many of the essential features of electrode kinetics remain uninvestigated and that, therefore, a less representative picture of the field may be obtained.

Partly because of the heterogeneous character of the interests of fundamental electrochemists, it seemed desirable to have similar fields described by authors with alternative viewpoints.

University of Ottawa	B. E. Conway
Texas A&M University	J. O'M. Bockris
Case Western Reserve University	E. Yeager
Texas A&M University	S. U. M. Khan
Texas A&M University	R. White

Contents

1. Quantum Electrochemical Kinetics: Continuum Theory

R. R. Dogonadze and A. M. Kuznetsov

1. Introduction 1
2. The Model 8
3. General Expressions for the Transition Probability 11
4. Transition Probability for Fixed Coordinates of the Ions and Reactants . 15
5. Proton Transfer Reactions 20
   5.1. Proton Transfer in the Case of Strong Coupling with the Medium . 20
   5.2. Proton Transfer in the Case of Weak Coupling with the Medium . 25
6. Effect of the Discrete Structure of the Electrical Double Layer on the Kinetics 27
7. The Step of Electrochemical Desorption of Hydrogen Atoms . . . 31
8. The Role Played by the Electronic Structure of the Electrode . . . 33
9. Experimental Verification of the Theory 36

References 37

2. Molecular Aspects of Quantum Electrode Kinetics

S. U. M. Khan and J. O. M. Bockris

1. Introduction 41
2. Correlation between Electrochemical Electron and Spectroscopic Photon Transfer Process 46
3. Applicability of Time-Dependent Perturbation Theory for Electron Transfer Processes at Electrodes 49
4. Proton Transfer at Interfaces 51
   4.1. Gurney's Quantum Mechanical Model of Proton Transfer . . . 51
   4.2. Butler's Modification of Gurney's Model 51
   4.3. The Quantum Character of Proton Transfer 52
   4.4. Degree of Validity of the WKB Tunneling Probability Expression for Proton Transfer 54
   4.5. A Model of Electrochemical Hydrogen Evolution Reaction . . . 57
5. Quantal Aspects of Photoelectrochemical Kinetics 61
   5.1. Photoeffect at Metal–Solution Interface 61
   5.2. Non-Tafel Behavior of Photocurrent at Metal–Solution Interface . 63
   5.3. Photoeffect at Semiconductor–Solution Interface 64

6. Tunneling at the Oxide-Covered Electrode 68
7. Fermi Energy in Solution 71
8. Distribution of Electron States in Ions in Solution 74
9. The Adiabaticity and Nonadiabaticity in Electron Transfer Reactions . 76
  9.1. Landau–Zener Formulation 77
  9.2. Transmission Coefficient, κ, for Homogeneous Redox Reactions . 78
10. Transition Probability of the Electron at the Electrode–Solution Interface 80
11. Concluding Remarks 83
References 84

3. Kinetics of Electrochemical Reactions at Metal–Solution Interfaces

L. I. Krishtalik

1. Introduction: Steps of Electrode Processes 87
2. Phenomenological Theory of the Elementary Act of an Electrode Reaction 93
  2.1. Brønsted-Polanyi Relation and Electrode Reaction Activation Energy 93
  2.2. Electronic Work Function and Related Values in Electrochemical Kinetics 102
  2.3. Activity Coefficient of an Activated Complex 108
  2.4. Temperature Dependence of Electrode Reaction Rates 110
  2.5. Activationless and Barrierless Electrode Processes 116
3. Formal Kinetics of Electrode Reactions 127
  3.1. Kinetic Equations 127
  3.2. Stoichiometric Numbers 133
4. Electrode Double-Layer Structure and Electrode Reaction Rate . . 140
  4.1. Basic Relations 140
  4.2. Hydrogen Evolution 142
  4.3. Reduction of Anions 155
  4.4. Electrode Reactions of Organic Compounds 165
References 168

4. Electrocatalysis

A. J. Appleby

1. Introduction 173
2. Electrocatalysis and Catalysis 177
  2.1. General 177
  2.2. Effect of Potential on Rate 181
3. The Rates of Complex Processes 191

4. Potential Energy Diagrams and Electrocatalysis 197
   4.1. General 197
   4.2. Some Correlations 204
5. Some Quantum Mechanical Aspects 205
   5.1. General 205
   5.2. Radiationless Transfer Theories 206
6. Some Electrocatalytic Reactions 217
   6.1. General 217
   6.2. Hydrogen Electrode Reaction 218
   6.3. Oxygen Electrode Reactions 228
   6.4. Organic Oxidations 233
   6.5. Chlorine Evolution 234
   6.6. General Remarks on Practical Electrocatalysts 234

References 235

5. Hydrogen Electrode Reaction on Electrocatalytically Active Metals

M. Enyo

1. Introduction 241
2. Adsorption of Hydrogen on Metal Electrodes 242
   2.1. Hydrogen Wave by a Potential Sweep Technique 242
   2.2. Adsorption Isotherm for Atomic Hydrogen 244
   2.3. Structure of the Hydrogen Wave and Experiments on Single-Crystal Planes 247
3. Basic Kinetic Equations 248
4. Experimental Behavior and Possible Mechanisms—Existence of a Unique Rate-Determining Step 251
   4.1. Possible Reaction Routes and Mechanisms 251
   4.2. The Stoichiometric Number 252
   4.3. The Tafel Slope 254
   4.4. Magnitude of the Tafel Slope 255
   4.5. The Reaction Orders 259
5. Mechanism with No Unique Rate-Determining Step 261
   5.1. Tracer Experiments 261
   5.2. Tafel Lines and Reaction Orders 262
   5.3. Absence of rds and Affinity Distribution among the Constituent Steps 264
   5.4. Synthesis of the Overall Kinetics 267
   5.5. Transient Experiments on the Pd Hydrogen Electrode 270
6. Related Topics 280
   6.1. Effect of Catalytic Poisons upon the Individual Step Rates . . . 280
   6.2. Hydrogen Pressure Equivalent to Hydrogen Overpotential . . . 282
   6.3. Electrolytic Hydrogenation of Organic Substances 285
7. Electrode Materials 289
   7.1. Pure Metals 289
   7.2. Composite Materials 292

References 293

6. Oxygen Electrochemistry

M. R. Tarasevich, A. Sadkowski, and E. Yeager

1. Introduction 301
2. Thermodynamics of the Oxygen Electrode 302
3. Open-Circuit Potentials 306
4. Oxygen Adsorbed Species and Anodic Films on Platinum and Other Noble Metals 312
   4.1. Electrochemical Studies 314
   4.2. *In Situ* Optical Studies 336
   4.3. *In Situ* Surface Conductivity Measurements 339
   4.4. *Ex Situ* Characterizations 340
5. The Anodic Oxygen Evolution Reaction (OER) 341
   5.1. General Features 341
   5.2. Kinetics and Mechanisms of the Oxygen Evolution Reaction on Metal and Oxide Electrodes 344
6. Cathodic Reactions of Oxygen (Oxygen Cathodes) 353
   6.1. The General Scheme of Parallel and Series Reactions of Oxygen and Hydrogen Peroxide 353
   6.2. The Kinetics of Molecular Oxygen Reduction on Different Metallic Electrodes 362
   6.3. Oxygen Reduction on Nonmetallic Materials 374
7. Concluding Remarks 388

References 390

7. Deposition and Dissolution of Metals and Alloys. Part A: Electrocrystallization

E. B. Budevski

1. Introduction 399
2. Kinetics of Atom Incorporation 400
   2.1. The Structure of a Crystalline Surface 400
   2.2. The Propagation Rate of Steps 404
   2.3. The Current Density on a Stepped Crystal Face 408
3. Metal Deposition on a Perfect Crystal Face 409
   3.1. Energy and Rate of Formation of Two-Dimensional Nuclei . . . 410
   3.2. Kinetics of Step Propagation and Mechanism of Metal Deposition . 413
   3.3. Deposition Kinetics on Perfect Crystal Faces 418
4. Metal Deposition on Faces Intersected by Screw Dislocations . . . 424
   4.1. The Theory of Spiral Growth 424
   4.2. Current Density and Morphology of Growth 428
5. Electrolytic Phase Formation 433
   5.1. Equilibrium Forms and Forms of Growth of Crystals 433
   5.2. The Nucleation Rate 435
   5.3. The Nucleation-Rate–Overpotential Relation 440
   5.4. Comparison with Experimental Data 443

6. Conclusions and Outlook 447
References 448

7. Deposition and Dissolution of Metals and Alloys. Part B: Mechanisms, Kinetics, Texture, and Morphology

A. R. Despić

1. Introduction 451
2. Specific Features of the Thermodynamics of Metal and Alloy Phase Formation and Degradation 453
    2.1. Equilibration of a Metal Surface with Electrolyte Containing Metal Ions—the Problem of the Reversible Potential 453
    2.2. Reversible Potentials of Alloys 456
    2.3. Underpotential Deposition of Metals on Foreign Substrates . . 458
    2.4. Effect of Interactions of the Metal Ion in Solution on the Reversible Potential 460
    2.5. Effect of pH on Electrode Potential 465
3. Likely Mechanisms of Metal Ion Discharge and Their Kinetic Consequences 466
    3.1. Mechanism and Kinetics of the Electrode Process 467
    3.2. Pseudocapacitance Effects and the Concentration of Intermediate Species 480
    3.3. Effect of Anions on the Kinetics of Metal Deposition and Dissolution 483
    3.4. Effect of Substrate on the Kinetics of Activation-Controlled Reactions of Metals 484
    3.5. Kinetics of Codeposition of Metals and Effects on Alloy Phase Formation 485
4. Totally Irreversible Dissolution of Metals 488
    4.1. The "Floating" Electrode Potential 488
    4.2. Dissolution with the Formation of Insoluble Substances 491
    4.3. Acceleration of Anodic Dissolution of Metals under Strain . . . 495
5. Formation and Physical Properties of Metallic Deposits Obtained under Conditions of Slow Discharge and Incorporation 497
    5.1. Effect of Substrate on the Growth of the Deposit 498
    5.2. Factors Affecting Grain Size in a Compact Deposit 499
    5.3. The Appearance of Texture in Metal Deposits 499
    5.4. Development of Stress in Metal Deposits 501
6. Effect of Slow Transport of Species to the Electrode on Surface Morphology of Metal Deposits 507
    6.1. Amplification of Surface Roughness 507
    6.2. The Appearance and Growth of Dendrites 513
    6.3. The Formation of Metal Powders 515
    6.4. Effect of Periodically Changing Conditions of Deposition . . . 517
    6.5. The Phenomenon of Electropolishing 519
7. Effect of Adsorption of Foreign Substances on Surface Morphology of Metal Deposits 521
    7.1. The Growth of Whiskers 522
    7.2. Leveling in Metal Deposition 523

8. Conclusion 525
References 526

8. Processes at Semiconductor Electrodes

R. Memming

1. Introduction 529
2. Potential and Charge Distribution at Solid–Electrolyte Interfaces . . 530
3. Energy Levels in Solids and Electrolytes 535
   3.1. Absolute and Conventional Electrode Potentials 536
   3.2. Energy Levels in Solids 536
   3.3. Energy Levels in Electrolytes 538
   3.4. Energy Levels at Semiconductor–Electrolyte Interfaces 540
4. Electrode Kinetics 544
   4.1. Rate of Electron Transfer (Theory) 544
   4.2. Electrode Reactions in Electrolytes without Redox Systems . . . 548
   4.3. Redox Processes 556
   4.4. Electron Transfer Processes at Organic Insulator Electrodes . . 559
   4.5. Evaluations of Exchange Currents and Determination of Reorientation Energies 560
5. Photoeffects 564
   5.1. Photopotentials and Photocurrents 564
   5.2. Applications in Electrode Kinetics 570
   5.3. Photostimulated Reactions at Organic Electrodes 577
6. Reactions of Excited Molecules at Electrodes 578
   6.1. Energy Levels of Excited Molecules 578
   6.2. Electron Transfer Process 581
   6.3. Relaxation Phenomena, Quenching, Supersensitization 583
   6.4. Competitive Photochemical Reactions in the Electrolyte . . . 585
   6.5. Production of Excited Molecules by Electron Transfer 586
7. Conclusions 588
References 588

9. Electrochemistry in Molten Salts

D. Inman and D. G. Lovering

1. Introduction 593
   1.1. General 593
   1.2. Complex Ions 595
   1.3. Acidity and Basicity 595
   1.4. emf Series and Reference Electrodes 596
2. Electroanalytical Aspects 597
   2.1. General Methodology 597
   2.2. Ion Transport 599
   2.3. Ionic Adsorption 600

2.4. Coupled Chemical Reactions . . . 602
2.5. Solution Stability . . . 603
3. The Metal–Molten Salt Interface . . . 603
3.1. General Aspects . . . 603
3.2. The Electrical Multilayer Close to $E_q = 0$ . . . 604
3.3. The Electrical Multilayer Remote from $E_q = 0$ . . . 606
4. Kinetics and Mechanisms of Electrode Reactions . . . 608
4.1. Problems and Methods of Approach . . . 608
4.2. Electrode Reactions Involving Homogeneous Redox Reactions . 609
4.3. Electrode Reactions at Liquid Metal Electrodes . . . 609
4.4. Electrode Reactions at Solid Metal Electrodes . . . 611
4.5. The Electroactivity of Nonmetallic Anions . . . 613
5. Applications . . . 616
5.1. General . . . 616
5.2. Metals Recovery and Processing . . . 616
5.3. Batteries . . . 620
5.4. Fuel Cells . . . 621
5.5. Corrosion . . . 622
5.6. Anodizing . . . 625
6. Experimental Procedures . . . 627
6.1. Materials, Electrodes, and Operating Conditions . . . 627
6.2. Nitrates . . . 629
6.3. Halides . . . 630
6.4. Other Salts . . . 632
References . . . 634

10. Organic Electrode Processes: Kinetics, Mechanisms, and Prospects for Commercial Development

E. J. Rudd and B. E. Conway

1. Historical Aspects . . . 641
2. Introduction and Nature of Organic Electrode Processes . . . 645
3. Classification of Organic Electrode Reactions . . . 647
4. Kinetic Equations for Electrochemical Reactions . . . 650
4.1. Factors in the Kinetics of Organic Electrode Reactions . . . 650
4.2. Electrode Potential, E, and the Rate Equations for Electron Transfer Reactions . . . 651
4.3. Treatments for More Complex Electrochemical Reactions . . . 656
4.4. Dependence of Rates of Organic Electrode Reactions on the Electrode Material . . . 661
5. Reaction Yields in Relation to Coulombic Efficiency and Conditions of Electrolysis . . . 663
5.1. Current Efficiencies and Coulombic Yields . . . 663
5.2. Significance of Controlled Potential Electrolysis . . . 666
5.3. Coulometry . . . 667
5.4. Preparative Methods . . . 669

6. Role of Adsorption in Electro-Organic Reactions 670
  6.1. Factors in Adsorption and the Formulation of Isotherms . . . 670
  6.2. Methods for Investigation of Adsorption of Organic Substances . 675
  6.3. Reaction Order and Adsorption in Kinetics of Electro-Organic Processes 677
  6.4. Adsorption and Solvation: Solvent Effects in Organic Adsorption . 678
  6.5. Adsorption and the Electrode Metal 681
7. Organic Reactions under Diffusion Control at Electrodes 681
  7.1. Introduction 681
  7.2. Diffusion-Limited Electrode Processes at Solid Metals 682
  7.3. Polarographic Conditions: Diffusion at Mercury Drops 684
  7.4. The Mass Transport Problems in Preparative Electro-Organic Chemistry and Cell Design 685
8. Polarographic Methods and Related Techniques for the Study of Electro-Organic Reactions 687
  8.1. Introduction 687
  8.2. Fundamental Aspects of Polarography 688
  8.3. Criteria of Polarographic Reversibility 697
  8.4. What Information May Be Obtained from Classical Polarography? . 700
  8.5. Other Electrochemical Techniques Related to Polarography . . 700
  8.6. Polarographic Studies of pH Effects and Reaction Mechanisms . . 709
9. Steric Aspects of Electro-Organic Reaction Mechanisms 714
  9.1. Adsorption of Intermediates and Stereochemical Effects . . . 714
  9.2. Alkyl Halide Reduction and Stereochemical Effects 717
10. Isotope Effects in Mechanistic Studies 725
11. Electrocatalytic Types of Reaction with Small Organic Molecules . . 726
12. Anodic Reactions with Thick-Film Oxides on Electrodes 728
  12.1. Reactions at Bulk-Type Base Metal Oxide Films 728
  12.2. Reactions of Organic Substances at High Anodic Potentials on Thick Noble Metal Oxide Films 732
13. Discussion of Some Reactions and Their Mechanisms That Have Possibilities for Commercial Development 733
  13.1. Oxidation of Aliphatic Hydrocarbons 734
  13.2. Anodic Substitution Reactions with Aromatic Hydrocarbons . . 738
  13.3. Electroreduction Processes 741
  13.4. Coupling Reactions 749
  13.5. Electroinitiated Polymerizations 756
14. Economic and Commercial Aspects of Organic Electrode Processes . . 758
15. Conclusions Regarding Industrial Applications 761
References 762

Index 773

1

Quantum Electrochemical Kinetics: Continuum Theory

R. R. DOGONADZE and A. M. KUZNETSOV

1. Introduction

Development of the quantum theory of electrochemical kinetics originates from the work of Gurney(1) (1931), who suggested that an electrochemical electron transfer reaction be considered as a process of electron tunneling from the metal to the ion in the solution. Since that time, the theory has been developed further in the works of many investigators. At present, two main approaches in the theory of the elementary act of the electrochemical process can be distinguished.

One of them originates from the work of Horiuti and Polanyi(2) (1935). Subsequently, it was developed mainly by Bockris and his co-workers.(3) In these works, attention was paid essentially to the behavior of one chemical bond in the course of the reaction. It was assumed that the energy distribution is determined by the thermal equilibrium of the reactant with the medium. However, the calculations did not take into account the dynamic behavior of the solvent. The activation energy and the tunnel corrections to the classical expressions for the reaction rate were calculated using various models for the potential energy profile. In a number of works, this theory is referred to as a "thermal" one. The earlier works of Christov(4) also fall into this category. Subsequently, Christov also considered general problems of the theory of the chemical kinetics and, in recent works, he has brought into consideration

---

R. R. DOGONADZE and A. M. KUZNETSOV • Institute of Electrochemistry of the Academy of Sciences of the USSR, Leninsky Prospekt 31, Moscow V-71, USSR.

explicitly the degrees of freedom describing the behavior of the solvent in the course of the reaction.(5,6)

The other direction is connected with the work of Libby(7) (1952), who suggested that a considerable part of the Frank–Condon barrier in the reaction is due to the *solvent* polarization. Since, in the first works of this kind, attention was paid mainly to the role played by the solvent in the reaction and since the solvent was described using the concept of the polarization of the medium per unit volume, theories of this kind are referred to in the literature sometimes as "continuum" ones (see, e.g., Ref. 8).

We shall show below that a description of the solvent using the concept of the medium polarization itself does not signify the continuum approximation. Moreover, in a number of works, both the change of state of the solvent and that of the intramolecular degrees of freedom in the course of the reaction were taken into account. However, to distinguish these works from those of the first kind, we retain here for the former the name "continuum theory." Below, a brief survey of the development of this (second) type of approach will be given. In order to present the modern development of this kind of theory, we shall consider the proton transfer reaction as an example.

In 1954, Platzmann and Frank(9) indicated the possibility of using the so-called radiationless theory of transitions developed by Lax(10) for polyatomic molecules, and by Pekar(11) for polar crystals, to the process involving charge transfer in liquids. The most general method in the theory of the radiationless transitions was suggested by Kubo and Toyozawa(12) in 1955. Subsequently it was used in many other works. The first calculations for processes in polar liquids in the framework of the polaron theory were performed by Davydov(13) and Deygen,(14) who investigated the properties of metal–ammonia solutions.

The most consistent development of the idea on the role played by nonequilibrium solvent polarization in charge transfer reactions was given by Marcus(15) in 1956 in the framework of a classical description of the solvent for homogeneous outer sphere adiabatic electron transfer reactions. These contributions have played an important role in the development of electron transfer theory. They are successfully used at present for some reactions. A shortcoming of Marcus's approach consisted in the fact that, although in Ref. 15 adiabatic reactions were considered, the expression for the activation free energy given corresponds in fact to a nonadiabatic reaction, since the calculation in Ref. 15 does not take into account the resonance splitting of the potential energy surfaces. As for the preexponential factor, it was calculated in Ref. 15 as the number of reactant encounters, by analogy with the theory of reactions in the gas phase. It was shown in the subsequent quantum mechanical calculations that the preexponential factor is determined by both the transmission coefficient and effective frequency associated with the solvent, the latter parameter being dependent on the characteristics of the medium and the reactants (see Section 5).

Subsequently, Marcus extended his theory to electrochemical electron transfer reactions.(16–19) However, the role played by the electron energy spectrum in the electrode in these works was not elaborated. All the calculations were performed for a simplified model, where the potential energy surfaces for different electronic states were replaced by two potential energy surfaces (one for the initial state and one for the final state). Further calculations have shown that such considerations do not enable us to explain the fact that the transfer coefficient, α, for electrochemical reactions takes values in the interval from 0 to 1. In particular, it does not enable us to explain the existence of barrierless and activationless process (see Chapter 3 by Krishtalik in this volume).

Another method was suggested by Hush.(20) He assumed that the electronic state follows adiabatically the change of configuration of the molecules for the solvent and for the inner coordination sphere (adiabatic reaction) and that the distribution of the electron density between two reacting ions in the transition state is an intermediate one: the charge of one ion decreases by the quantity, λ^+, and that of the second ion increases by the same quantity, where λ^+ is a charge parameter. According to this charge distribution, the classical work was calculated, i.e., the free energy required to attain the transition state, $\Delta F^{\ddagger}$. The change of $\Delta F^{\ddagger}$ due to the resonance splitting of the electronic energy levels was not taken into account.

In 1960, Gerischer(21) developed the theory of nonadiabatic electrochemical electron transfer reactions at semiconductors. This approach was a statistical one. It took into account that, owing to the thermal fluctuations in the solvent, there is a statistical distribution of the electronic states, corresponding to the oxidized and reduced forms of the reactants. Gamow's formula was used to calculate the probability of electron tunneling. For an entirely classical system, this approach enables the correct value of the activation energy to be calculated but not the preexponential factor, since the Gamow formula is applicable only for the description of the tunneling through the time-independent potential barriers.

The first entirely quantum mechanical calculation was performed in 1959 by Levich and Dogonadze(22) for nonadiabatic, homogeneous outer-sphere electron transfer reactions. To describe the solvent in Ref. 22, the simplest model of harmonic oscillators of one unchanged frequency was used. In later works,(23,24) the calculations were extended to the model involving the dispersion of the vibration frequencies. However, for this model, the relation between the parameters of the model and the characteristics of the medium and the reactants was not explored. In 1961, Dogonadze(25) calculated the transition probability for both the nonadiabatic and adiabatic electron transfer reactions in the framework of semiclassical considerations (see also Ref. 26). This method also does not take into account the lowering of the activation barrier due to the resonance splitting of the electron energy levels.

The first quantum mechanical calculations for nonadiabatic electrochemical electron transfer reactions at metals and semiconductors were performed by Dogonadze, Chizmadzhev, and Kuznetsov(27,28) (1962–1964). In Ref. 27 the totally degenerated Fermi gas model was used to describe the state of the electrons in the electrode, and in Ref. 28 an integration over the energy spectrum was performed, taking account of the Fermi distribution of the electrons over a range of energy. Later that theory was extended to other processes at semiconductors and thin semiconductor films.(29)

In 1967, Dogonadze and Kuznetsov(30) performed a quantum mechanical calculation of the electron transfer probability, taking into account the change of the intramolecular state of the reactants in the simple harmonic oscillator model. Somewhat later (1968), this problem was considered independently by Hush(31) for the limiting case of classical intramolecular vibrations.

Dogonadze and Kuznetsov(30) showed for the first time the way to take into account the processes of transfer of heavy particles for reactions in liquids. This work was the basis for the first simplest quantum mechanical model of the electrochemical proton transfer process which was proposed by Dogonadze, Kuznetsov, and Levich(32) in 1967 (see also Ref. 33). The expressions and conclusions of Dogonadze and Kuznetsov's work(30) were used in a number of subsequent papers (also in some recent works, see, e.g., Ref. 34). Therefore, it is necessary to consider this approach in more detail.

A general expression for the probability of a nonadiabatic transition was derived in Ref. 30 for a rather arbitrary form of the frequency dispersion of the type $\omega_k = p_k \Omega$ where p_k are integer numbers and Ω is some small frequency:

$$W_{if} = \frac{2\pi}{\hbar^2}|V_{if}|^2 \exp\left(\frac{J_i - J_f}{2kT} - \sum_k z_k \cosh\frac{\hbar\omega_k}{kT}\right) \sum_{l_k} \prod_k I_{l_k}(z_k) \qquad (1)$$

where $2V_{if}$ is the resonance splitting of the electronic energy levels, J_i and J_f are the minimal energies of the initial and final states, $z_k = \frac{1}{2}(q^f_{k0} - q^i_{k0})^2 \operatorname{csch} \hbar\omega_k/2kT$, q^i_{k0} and q^f_{k0} are the equilibrium values of the dimensionless normal coordinates in the initial and final states, $I_{l_k}(z_k)$ is the Bessel function of the imaginary variable, and the summation in Eq. (1) is performed over all integer values of l_k provided that $\sum_k l_k p_k = (J_f - J_i)/\hbar\Omega$.

Two limiting cases were considered in Ref. 30. The first one corresponds to the inequalities

$$\hbar\omega_{k_0} \ll kT, \qquad z_{k_0} \gg 1; \qquad \hbar\omega_{k_i} \gg kT, \qquad z_{k_i} \ll 1 \qquad (2)$$

where the subscript k_0 denotes the quantities for the degrees of freedom of the solvent outside the coordination layer of the reactants and k_i denotes those for the intramolecular degrees of freedom of the reactants. For this case, the transition probability proves to be

$$W_{if} = \exp\left[-\sum_{k_i} (q^i_{k_i0} - q^f_{k_i0})^2\right] \cdot W^{\text{out}} \qquad (3)$$

where W^{out} is the transition probability for the corresponding outer-sphere reaction (i.e., for $q^{i}_{k_i0} = q^{f}_{k_i0}$), viz.

$$W^{\text{out}} = (\pi/\hbar^2 kTE_{r0})^{1/2}|V_{if}|^2 \exp[-(J_f - J_i + E_{r0})^2/4E_{r0}kT] \tag{4}$$

and $E_{r0} = \frac{1}{2}\sum_{k_0} \hbar\omega_{k_0} (q^{i}_{k_0} - q^{f}_{k_00})^2$ is the reorganization energy of the solvent. Equations (3) and (4) show that the intramolecular vibrations are quantal ones, and the change of the intramolecular structure leads to an additional factor in the expression for the transition probability which is independent of the temperature and is equal to the square overlapping integral of the wave functions of the initial and final ground vibrational states, provided the inequalities (2) hold.

The second limiting case corresponds to the inequalities

$$\hbar\omega_{k_0} \ll kT, \qquad z_{k_0} \gg 1; \qquad \hbar\omega_{k_i} \ll kT, \qquad z_{k_i} \gg 1 \tag{5}$$

Then the expression for the transition probability is similar to Eq. (4) except that E_{r0} should be replaced by the total reorganization energy $E_r = E_{r0} + \frac{1}{2}\sum_{k_i} \hbar\omega_{k_i} \ (q^{i}_{k_i0} - q^{f}_{k_i0})^2$. Thus, in this case, the change of the intramolecular state occurs by a classical way.

The other limiting cases of Eq. (1) were also given in Ref. 33 where proton transfer reactions were considered (see also Ref. 35). As was noted above from the theoretical point of view, the transfer of a heavy particle (e.g., a proton) from one molecule to another does not differ in principle from an intramolecular transfer. Therefore a number of equations prove to be formally the same both for proton transfer reactions and for electron transfer involving an intramolecular change of structure.

In particular, the limiting case of Eq. (1) corresponding to one intramolecular degree of freedom and an "infinite" number of degrees of freedom of the solvent was given(33) as

$$W_{if} = \left(\frac{\pi}{\hbar^2 kTE_s}\right)^{1/2} |V_{if}|^2 \sum_{m=-\infty}^{\infty} I_m(z_p) \exp\left(-z_p \cosh\frac{\hbar\omega_p}{2kT} - \frac{m\hbar\omega_p}{2kT}\right) \times \exp\left[\frac{-(J_f - J_i - m\hbar\omega_p + E_s)^2}{4E_s kT}\right] \tag{6}$$

where E_s is the reorganization energy of the solvent, subscript p denotes the quantities for the intramolecular degree of freedom (proton). This formula may be further simplified depending on the values of the parameters involved.†

Later this model was used by Levich *et al.*(38) to calculate the rate constant of the homogeneous proton transfer reaction and by German *et al.*(39) for the calculation of the kinetic H/D isotopic effect in the electrochemical reaction of hydrogen evolution.

This stage of development of the theory was reviewed in a number of papers.(26,40–42) In this period, the idea on the dynamical role of the solvent became commonly accepted but the quantum mechanical calculations used very simplified models. Further development of the theory is characterized by the application of modern quantum mechanical collision theory and by the complication of the models used. The range of applicability of the theory has also been extended. The models used for the calculations on particular reactions have become much more realistic.

---

† In 1968 Marcus(37) took into account the change of the intramolecular state of the reactants in the framework of the classical description of the movement of nuclei and suggested an expression for the activation energy of the proton transfer reaction. However, the derivation of this expression was not given in Ref. 37 and the parameters involved were not clearly defined.

First of all, the model of the solvent was materially improved. In 1969 Dogonadze and Kuznetsov(26) took into account the spatial correlation of the polarization fluctuations in the medium. In Refs. 43–46 the frequency dispersion of the dielectric constant was also taken into account.† Using this model, Vorotyntsev *et al.*(47) performed quantum mechanical calculations of the transition probability for both nonadiabatic and adiabatic homogeneous electron transfer reactions. The lowering of the activation barrier due to the resonance splitting of the electronic energy levels was correctly derived.(47) Adiabatic electrochemical reactions were also considered in the framework of the semiclassical approach.(48) In 1972, Dogonadze, Kuznetsov, and Vorotyntsev(49) gave the general analysis of the transition probability with account of the change of vibrational frequencies and entangling of the normal coordinates. It embraced practically all the limiting cases of the harmonic vibration model. A considerable part of the results of these works was presented in the review papers.(35,36)

The works in recent years embrace three main directions: (i) further development of the general calculational methods and solution of the fundamental problems of the theory, (ii) application of the theory to calculations for particular reactions, and (iii) extension of the theory to other processes and phenomena occurring under unusual conditions.

A number of fundamental problems are related to the calculation of the preexponential factor. In 1973, Schmickler and Vielstich(50) put forward a question about the way in which the Franck–Condon approximation is employed, i.e., at what configuration of the nuclei coordinates does the electronic resonance integral V_{if} have to be taken out of the integral sign over the coordinates of the heavy particles. The solution of this problem was unclear because the integrands of the Franck–Condon factors for the different vibrational states of the nuclei are maximal at different values of the coordinates of the nuclei. It was suggested that V_{if} be taken out at the point corresponding to the initial equilibrium configuration of the nuclei.(50) This conclusion was derived using the assumption that the set of the electronic wave functions is complete.(50) The latter is not, however, the case for chemical reactions.‡

The solution of this problem was given by Dogonadze and Kuznetsov.(51) The general scheme of the calculation of the transition probability was derived,(51) based on the density matrix method (see Section 3). It was shown that V_{if} has to be taken out of the integral sign over the nuclei coordinates at the point at which the product of the density matrices of the initial and final states for the heavy particles is maximal.(51)

---

† The model of medium was also developed by Schmickler(81) and by Schmidt.(84)

‡ For comments on this paper, see Ref. 54.

One more question of principle on the role played by ionic atmosphere and micropotential in the electrochemical kinetics was considered.(51) Later these results were generalized for the case when there is no equilibrium with respect to the reacting ions in the presence of the excess quantity of the supporting electrolyte (Dogonadze and Kuznetsov(52)).

In 1974, Kestner *et al.*(53) calculated the probability of the electron transfer between two complex ions involving the change of intramolecular structure of the complexes. The method of calculation did not differ essentially from that developed earlier.(49,54,79) Efrima and Bixon(55) considered a fast reaction for which the main factor was assumed to be not the change of configuration of the solvent molecules but the change of the intermolecular distance.

The expression for the perturbation operator leading to reaction was discussed in connection with the nonorthogonality of the electronic wave functions of the initial and final states.(53,55) For the first time, this problem was investigated in a two-level approximation in 1964 by Kuznetsov(56) (see also Refs. 31, 35, and 36). The final results for the probability of electron transfer between complex ions obtained in Ref. 53 represent a limiting case of the expressions derived in Refs. 49 and 57. Deviation of some general relations in Ref. 53 from those derived earlier (see, e.g., Ref. 49) is due to a certain mathematical inaccuracy in Ref. 53 (see Ref. 58).

One more fundamental problem concerning the form of the potential barrier for the electron was considered by Dogonadze and Kuznetsov(59) (see also Ref. 36). It was shown(59) that since, in the transition configuration, the solvent polarization is equal to $P^* = (1-\alpha)P_{0i} + \alpha P_{0f}$, where P_{0i} and P_{0f} are its initial and final equilibrium values and α is the symmetry factor or Brönsted coefficient, the potential barrier for the tunneling of the electron between two ions in the simplest case has the form

$$V_e(r) = V_{z_1} + V_{z_2} - e^2\left(\frac{1}{\varepsilon_{\text{opt}}} - \frac{1}{\varepsilon_{\text{st}}}\right)\left(\frac{1-\alpha}{r} + \frac{\alpha}{|r-R|}\right) \tag{7}$$

where V_{z_1} and V_{z_2} are the interaction energies of the electron with the first and the second ions in the medium considered as a static dielectric, ε_{opt} and ε_{st} are the optical and static dielectric constants, and R is the distance between the ions.

The corresponding expression for the electrochemical reaction has the form

$$V_e(r) = V_{eM} + V_{ez} - e^2\left(\frac{1}{\varepsilon_{\text{opt}}} - \frac{1}{\varepsilon_{\text{st}}}\right)\frac{\alpha}{|r-R|} \tag{8}$$

where V_{eM} is the energy of interaction of the electron with the electrode. The expressions for a more general case were given in Ref. 36.

In a number of works, the calculations for some particular homogeneous and heterogeneous reactions were performed using the general methods developed in Refs. 60–64. In particular, Kharkatz and Ulstrup(61) calculated the polarization characteristics for the hydrogen evolution reaction over a large range of overpotentials.

In 1969 Schmidt(65) made the first attempt to calculate quantum mechanically the probability of the elementary act of the bridge-assisted electron transfer reaction. However, the transitions were only taken into account for which the energy is conserved in all the states including the intermediate one.(65) In a number of subsequent papers, a more detailed quantum mechanical calculation for the reactions of this kind was performed.(66–72) Recently the theory was extended to adiabatic bridge-assisted reactions.(73)

Finally, investigation of reactions occurring under unusual conditions (e.g., at low temperatures or for large heats of reaction or processes of light absorption) becomes of great interest. These fields are beyond the scope of the present paper. An exception is the highly exothermic (or highly endothermic) type of reaction. For these reactions, one should mention effects of two kinds: (i) barrierless and activationless transitions and (ii) decrease of the transition probability with increase of the absolute value of the free energy of the reaction.

The first barrierless electrochemical processes were predicted and investigated experimentally by Krishtalik(74,75) for the hydrogen evolution reaction at metals with high overpotential. The theory of barrierless transitions (and therefore also of the activationless transitions for the reverse process) for the hydrogen evolution reaction at metals was given by Dogonadze *et al.*(32,33) in 1967. Hale(64) in 1968 calculated the limiting electric current for an electron transfer reaction associated with the activationless process. The degenerate Fermi gas model was used to describe the electrons in the metal.

Recently calculations were performed for highly exothermic homogeneous reactions(44,58,76,77) for which the unusual dependence of the transition probability on the reaction free energy, mentioned above, was discovered.

Concluding this brief survey, we may note that most of the papers on this aspect of chemical kinetics derive from the further development of the theory of radiational and radiationless transitions. The most general approach is the density matrix method developed in recent years(51) which is a generalization of the method of Kubo and Toyozawa.(12)

This method will be described below in particular in relation to the proton transfer reaction. However, all the formal results will also be valid for electron transfer reactions involving changes of the intramolecular structure of the reactants since, as was noted above, there is no difference of principle between the intramolecular and intermolecular transfer of a heavy particle.

2. The Model

The reaction of proton transfer from an ion AH^+ to the adsorbed state of H at the electrode surface is one of the steps (often the rate determining one) of the electrochemical hydrogen evolution reaction. This reaction is rather important, both with respect to its practical application and from the general theoretical point of view. It is a chemical reaction in the full sense involving the destruction and formation of chemical bonds. At the same time, it is rather simple since the mass of the particle transferred (the proton) is small compared with the mass of the reactants.

This reaction leads to a change of the electronic state of the molecule A, of its intramolecular structure, of the configuration of the solvent molecules near it, and of the electronic state of the electrode. The characteristic valence bond frequencies for the proton in the chemical compounds are rather large (of the order $4 \times 10^{14}\,\text{sec}^{-1}$). The frequencies of the other intramolecular vibrations, the state of which also can be changed in the course of the reaction, depend on the type of chemical compound involved. For simplicity, we shall consider these frequencies to be rather low ($\ll kT/\hbar$). The parameters for the adsorbed state of the proton are not known exactly. According to rough estimates, however, the valence bond frequency of the adsorbed H is also rather large ($\sim 2 \times 10^{14}\,\text{sec}^{-1}$).(75)

The peculiarity of electrochemical reactions consists in the fact that the potential energy surfaces corresponding to various electronic states in the electrode are usually located very closely one to another, owing to the continuous character of the electronic energy spectrum. This situation very much complicates the calculation for the case of adiabatic reactions.(48) At first we shall consider the transition between two local electronic states in order to consider both the entirely nonadiabatic, and the partly and entirely adiabatic reactions. Such a situation arises, e.g., in homogeneous reactions and also for hydrogen adsorption at a negatively charged surface center at a semiconductor where the energy lies in the band gap. The reaction takes place because of the interaction of the proton with this surface center.

The potential energy surface of the system has two asymptotic regions, one corresponding to the initial state (reactants) and one corresponding to the final state (products). These two are separated by a potential barrier. The transition from the initial state to the final one occurs over the rather narrow intermediate region.

It is assumed that there is thermal equilibrium in the asymptotic region corresponding to the initial state. In particular, we assume that there is an equilibrium coordinate distribution of the ions and molecules in the solution and equilibrium Gibbs's energy distribution, both for the solvent and for the reactant AH^+, i.e., the ion AH^+ and the solvent are considered, as in reality, to be in thermal equilibrium. The method of calculation does not require the existence of an equilibrium coordinate distribution of the ions in the total volume of the solution. The local equilibrium in the asymptotic region corresponding to the initial state (which usually is rather small compared with the solvent volume) is sufficient.†

---

† We specially emphasize here the existence of thermal equilibrium between the reactants and the solvent because it has been stated in some papers that, in this theory, there is *no* equilibrium between them; see, e.g., Refs. 3 and 8.

The thermal equilibrium between the reactants and the solvent is maintained owing to the interaction between them. This interaction is of a double character. Firstly there is the electrostatic interaction of the charge with the dipolar molecules of the medium leading to the change of their orientation with respect to the reactants. This interaction is usually strong and determines a considerable part of the solvation energy of the ion causing the essential change of the average solvent polarization near it.

In addition, there is the interaction of any intramolecular vibrations with the vibrations of the solvent molecules. This interaction is responsible for the shift of the intramolecular vibrational frequencies and for the widening of the intramolecular vibrational states. If this interaction is strong, the total dynamic system "proton + solvent" has to be considered, taking into account this interaction explicitly. However, the interaction is usually rather small (this is maintained by small shifts of the frequencies(78)) and may be neglected in the first approximation. It will be taken into account only to the extent that the intramolecular vibrational energy distribution is assumed to be the equilibrium one.

As for the long-range electrostatic interaction of the first type, we shall consider both limiting cases: (i) strong coupling and (ii) weak coupling with the medium.

The energy of interaction of the reactants with the solvent we shall write in the form

$$V_{i,f} = -\int P(r)\mathscr{E}_{0i,f}(r)\,dr \tag{9}$$

where $P(r)$ is the dipole moment per unit volume of the solvent, and $\mathscr{E}_{0i}(r)$ and $\mathscr{E}_{0f}(r)$ are the electric fields created by the reactant and the product in the medium. The form of the interaction in Eq. (9) does not itself signify the macroscopic description of the solvent since one may imply that $P(r)$ is equal to the sum of the dipole moments of the medium molecules located in a given volume, δV: $P(r) = \sum_{\delta V} d_i \delta(r - r_i)$.

The dynamical behavior of the inertia polarization, $P_{\text{in}}(r)$, in such a complex system like an electrolyte solution may be described by considering $P_{\text{in}}(r)$ as a superposition of a large number of harmonic oscillations, viz.,

$$P_k = \sum_{\nu} A_{k\nu}\pi_{k\nu} \tag{10}$$

where P_k is the Fourier transformation of the inertial polarization, $\pi_{k\nu}$ are the normal coordinates of the νth vibrational mode, and $A_{k\nu}$ are some coefficients. The frequencies of the effective oscillators of the medium, ω, and the oscillator strength are determined by the imaginary part of Green's function, $G_{\alpha\beta}(k, \omega)$, for the polarization operators, i.e., by the quantity, $\text{Im}\, \varepsilon(k, \omega)/|\varepsilon(k, \omega)|^2$, where $\varepsilon(k, \omega)$ is the dielectric function of the medium.†

---

† In general, $G_{\alpha\beta}$ and ε are functions of two variables, k and k', since the system is nonhomogeneous near the electrode and the reactants.

The Hamiltonian of the effective oscillators of the medium for the spatially homogeneous system is of the standard form:

$$H_s = \frac{1}{2}\sum_\nu \hbar\omega_{k\nu}\left(q_{k\nu}^2 - \frac{\partial^2}{\partial q_{k\nu}^2}\right) \tag{11}$$

where $q_{k\nu}$ are the real normal coordinates related to the complex quantities, $\pi_{k\nu}$, by the linear equations of the type

$$\pi_{k\nu} = \left(\frac{\hbar\omega_{k\nu}}{2\phi_{k\nu}}\right)^{1/2}\begin{cases} q_{-k\nu} + iq_{k\nu}, & k_x > 0 \\ -q_{k\nu} + iq_{-k\nu}, & k_x \le 0 \end{cases} \tag{12}$$

where the quantities $\phi_{k\nu}$ characterize the properties of the medium itself. The summation rule is derived for the quantities, $\phi_{k\nu}$ and $A_{k\nu}$, which permits them to be related to the complex dielectric function of the medium, $\varepsilon(k, \omega)^{(35,36,45)}$:

$$4\pi^2 \sum_\nu \frac{|A_{k\nu}|^2}{2\phi_{k\nu}} f(\omega_{k\nu}) = \int_0^\infty \frac{\operatorname{Im}\varepsilon(k,\omega)}{|\varepsilon(k,\omega)|^2}\cdot\frac{f(\omega)d\omega}{\omega} \tag{13}$$

The use of the effective Hamiltonian is convenient for the calculations. However, it should be noted that this is entirely equivalent to decoupling of the higher correlation function for the polarization operators to the pair correlation functions (see Section 4).

As for the ion AH^+ itself, the calculation for the entirely nonadiabatic reaction does not require any serious limitations in the choice of the model. The calculation may be performed, taking account of all the intramolecular vibrations. However, for simplicity, we shall consider at first a simple model in which the reaction leads to a change of the characteristics of only the proton vibrational states and thus to be able to treat also partly adiabatic reactions (Figure 1).

3. General Expressions for the Transition Probability

If the interaction between the reactants leading to the reaction is weak enough (nonadiabatic processes), the transition probability per unit time may be calculated using the formula of the first order in quantum mechanical

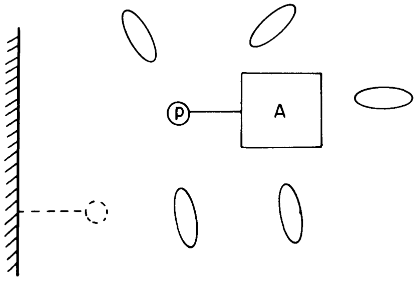

Figure 1. Model for proton transfer at electrode with elements of surrounding solvent dipoles; orientation (1) of proton source.

perturbation theory:

$$W_{if} = \frac{2\pi}{\hbar} \exp\left(\frac{F_i}{kT}\right)$$

$$\times \sum_{\alpha,\{n\}} \exp\left(\frac{-E^i_{\alpha\{n\}}}{kT}\right) \sum_{\beta,\{m\}} |\langle\psi^f_{\beta,\{m\}}|V^{\mathrm{nd}}_i|\psi^i_{\alpha,\{n\}}\rangle|^2 \delta(E^i_{\alpha,\{n\}} - E^f_{\beta,\{m\}}) \tag{14}$$

where F_i is free energy of the initial state, $\psi^i_{\alpha,\{n\}}$, $E^i_{\alpha,\{n\}}$ and $\psi^f_{\beta,\{m\}}$, $E^f_{\beta,\{m\}}$ are the wave functions and the energies, respectively, of the initial and final channels of the reaction described by the Hamiltonian H_i and H_f; V^{nd}_i is the nondiagonal with respect to the states of the initial and final channels part of the interaction operator between the reactants, subscripts α and β denote the quantum numbers of the electronic states of the molecules, and n and m are the quantum numbers of the heavy particle states.

It should be noted that Eq. (14) contains only the nondiagonal part of the interaction operator between the reactants, V^{nd}_i. Its diagonal part, causing the "distortion" of the reactant states in each channel, is included in the Hamiltonian H_i and H_f.

At first, we shall calculate the transition probability for fixed quantum numbers of the electrons, α and β. The subscripts α and β will, however, be temporarily omitted. To separate the electronic and nuclear movements in the channels of the reaction, we shall use the Born–Oppenheimer approximation. Introducing the integral representation of the δ function, Eq. (14) may be transformed to

$$W_{if} = \frac{1}{i\hbar kT} \int_{c-i\infty}^{c+i\infty} d\theta \exp\left(\frac{F_i}{kT}\right) \mathrm{Tr}\,\{L_i\rho_i(1-\theta)L_i^+\rho_f(\theta)\}, \qquad 0 < c < 1 \tag{15}$$

where $\rho_i(1-\theta) = \exp[-(1-\theta)H^a_i/kT]$ and $\rho_f(\theta) = \exp(-\theta H^a_f/kT)$ are the statistical operators of the initial and final channels of the reaction at the effective temperatures, $T/(1-\theta)$ and T/θ; H^a_i and H^a_f are the adiabatic Hamiltonians of the reaction channels and L_i is an operator containing the electron resonance integral:

$$L_i = \mathscr{L}_i\delta(Q - Q') \tag{16a}$$

$$\mathscr{L}_i = \int \phi_{f\beta}(x, \{Q\})V^{\mathrm{nd}}_i\phi_{i\alpha}(x, \{Q\})\,dx \tag{16b}$$

where $\phi_{i\alpha}(x, \{Q\})$ and $\phi_{f\beta}(x, \{Q\})$ are the electronic wave functions of the reactants and products.

Since, in the transitional configuration (at $\{Q = Q^*\}$), the quantity $2\mathscr{L}_i$ is equal to the resonance splitting of the potential energy surfaces, $\Delta E_e(\{Q^*\})$, in the following, we shall use for $\mathscr{L}_i$ the notation, $\mathscr{L}_i = \Delta E_e(\{Q\})/2$ also at arbitrary values of the heavy particle coordinates, $\{Q\}$. In the two-level approximation, the change $2\mathscr{L}_i$ by ΔE_e is essentially a change of notation. However, in the more general case, $2\mathscr{L}_i$ is not equal to ΔE_e. A more detailed analysis shows that the formulas for the transition probability involve the resonance splitting of the potential energy surfaces, but not the electronic resonance integral for two given energy levels.

Neglecting the terms of the order $S_{if} = (\int \phi_{i\alpha}\phi^*_{f\beta}\,dx)^2$ in the two-level approximation with respect to the electrons for $\mathscr{L}_i$, we obtain(35,36)

$$\mathscr{L}_i = \Delta E_e(\{Q\})/2 = \int \phi^*_{f\beta}V_i\phi_{i\alpha}\,dx - \int |\phi_{i\alpha}|^2 V_i\,dx \int \phi_{i\alpha}\phi^*_{f\beta}\,dx \tag{17}$$

where V_i is the energy of interaction between the reactants. The expressions for more general cases can also be derived.(53)

Equation (17) shows that, in the approximation used, the nondiagonal part of the interaction operator, V_i^{nd}, has the form†

$$V_i^{\mathrm{nd}} = V_i - V^{\mathrm{d}} = V_i - \int |\phi_{i\alpha}|^2 V_i\,dx \tag{18}$$

Trace in Eq. (17) operates only with respect to the quantum states of the heavy particles at fixed states of the electrons. Calculating trace in the coordinate representation, one has, in general, to take into account that $\mathscr{L}_i$ and $\mathscr{L}_i^+$ depend on the coordinates of the heavy particles. If this dependence is weak, they may be taken out of the integral at the point corresponding to the maximum of the product of the density matrices $\rho_i\rho_f$. Just this procedure may be called the Franck–Condon approximation for chemical reactions.

Equation (15) takes into account the change of the reactant electronic state and of its intramolecular nuclear configuration, involving the transfer of the heavy particles, the change of the solvent polarization near the reactants and the effect of the reactants on the structure of the solvent contacting them, the approach of the reactants one to another and the separation of the products, the change of the ionic atmosphere around the reacting particles, and finally the effect of the electrode properties and the electric field on the probability of the elementary act and the rate of the electrochemical processes as a whole.

The final analytical expressions for the transition probability, W_{if}, may be found using certain approximations for the density matrices, ρ_i and ρ_f.

Since the movement of the reactants as a whole in liquids is the slowest, we use the adiabatic approximation to separate this movement from the other types of movements, assuming that all the degrees of freedom follow adiabatically the movement of the reactants. In addition, we shall assume that the interaction of the ions with the solvent and with each other does not change essentially the excitation spectrum of the solvent and the intramolecular vibrational spectrum and, for the sake of simplicity, the small change of the mass of the reactants due to the transfer of the proton or some other particle will be neglected.

---

† Strictly speaking, the interaction operator is an operator matrix. The expression (18) gives only one element of this matrix. The expressions for the other matrix elements may be derived in a similar way.

Then, taking into account that the density matrices of the ions, ρ^i_{ion} and ρ^f_{ion}, as functions of the difference, $s = R - R'$ (where R and R' are the coordinates of their centers of mass) have a sharp maximum at $R = R'$, Eq. (15) may be transformed to the relation$^{(51)}$ (see also Ref. 79)

$$W_{if} \simeq \int d\Delta j \int d\{r\}\phi(\{r\}; \Delta j)\, W_{if}(\{r\}, \Delta j) \tag{19}$$

where

$$\Phi(\{r\}; \Delta j) = \frac{1}{2\pi i kT} \exp\left(\frac{F^i_{\text{ion}}}{kT}\right) \int_{c-i\infty}^{c+i\infty} d\theta \exp\left[-\beta\theta(\Delta J - \Delta j)\right]\Delta\{s\}$$
$$\times\, \rho^i_{\text{ion}}(\{r\}, \{r\}; \beta(1-\theta))\rho^f_{\text{ion}}(\{r\}, \{r\}; \beta\theta) \tag{20}$$

and

$$W_{if}(\{r\}; \Delta j) = \frac{1}{i\hbar kT} \exp(\beta F^i_v) \int_{c-i\infty}^{c+i\infty} d\sigma \exp(-\beta\sigma\Delta j)$$
$$\times\, \tfrac{1}{4} \int d\{q\}d\{q'\}\Delta E_e(\{q\}, \{r\})\Delta E_e(\{q'\}, \{r\})$$
$$\times\, \rho^i_v(\{q\}, \{q'\}; \{r\}; \beta(1-\sigma))\rho^f_v(\{q\}, \{q'\}; \{r\}; \beta\sigma) \tag{21}$$

where $\beta = 1/kT$, $\Delta\{s\}$ is the interval of the values of the variables $s = R - R'$, making the major contribution to the integral over $R - R'$, F^i_{ion} and F^i_v are the free energies of the ionic system and the vibrational subsystem in the initial state, $W_{if}(\{r\}, \Delta j)$ is the probability of the elementary act of the reaction at an arbitrary fixed configuration of the ions and for the reaction free energy Δj, ρ^i_{ion}, and ρ^f_{ion} are the ionic density matrices, $r = (R + R')/2$. The function $\Phi(\{r\}; \Delta j)$ is related to the reorganization probability of the ionic subsystem. If the motion of the ions is classical, $\Phi(\{r\}; \Delta j)$ takes the form

$$\phi(\{r\}; \Delta j) = \Phi(\{r\})\delta(\Delta\tilde{J} - \Delta j) \tag{22}$$

where $\Delta\tilde{J} = \Delta J + U^f_{\text{ion}}(\{r\}) - U^i_{\text{ion}}(\{r\})$ is the reaction-free energy for fixed coordinates of all the ions, $\Phi(\{r\})$ is the coordinate distribution function of the ions given by

$$\Phi(\{r\}) = \exp\{\beta[F^i_{\text{ion}} - U^i_{\text{ion}}(\{r\})]\} \tag{23}$$

Here $U^i_{\text{ion}}(\{r\})$ and $U^f_{\text{ion}}(\{r\})$ are the free energies of the system at given values of the ionic coordinates in the solvent considered as a static dielectric which play a part of the potential energy for the ions.

In this case, the expression for W_{if} takes the form

$$W_{if} = \int d\{r\}\phi(\{r\})\, W_{if}(\{r\}, \Delta\tilde{J}) \tag{24}$$

If the concentration of reactants is small, so that their effect on each other and on the potential distribution in the electrical double layer may be neglected, Eq. (24) may be generalized to the case of the local equilibrium. Since the reaction occurs in a small reaction zone, to derive the formula (24) in this case it is sufficient for the distribution function, $\Phi(\{r\})$, with respect to the reactant coordinates to be the equilibrium one only in the vicinity of the reaction region, but not necessarily in the whole volume of the solution. Therefore, Eq. (24) is valid also in those cases when the macroscopic distribution of the reactant concentration is not the equilibrium one.

4. Transition Probability for Fixed Coordinates of the Ions and Reactants

Let us consider the transition probability for a fixed distance between the reactants (or, for an electrochemical reaction, with a fixed distance between the ion and the electrode) and at fixed values of the ionic coordinates, $W_{if}(\{r\}, \Delta\tilde{J})$.

The reaction leads to a change of the reactant electronic state. Therefore, the effective size of the cavity in the solution where the reactants are located is also changed. The surface of the cavity fluctuates owing to the thermal (acoustic) fluctuations of the medium. The interaction of the acoustic modes with the reactants leads to a change of the electronic energies of the reactants. This factor should be taken into account in general when one calculates the transitional configuration corresponding to the equalization of the electronic energies of the initial and final states.

Assuming that the acoustic modes are separated from the optical ones, we can transform the formula for the transition probability, $W_{if}(\{r\}, \Delta\tilde{J})$, to the form similar to Eqs. (19)–(21), viz.,

$$W_{if}(\{r\}, \Delta\tilde{J}) = \int d\Delta j \int d\{\xi\}\phi(\{\xi\}; \Delta j) W_{if}(\{r\}, \{\xi\}; \Delta j) \tag{25}$$

where $\phi(\{\xi\}; \Delta j)$ is related to the change of size of the cavity and is determined by an expression similar to Eq. (20), and $W_{if}(\{r\}, \{\xi\}, \Delta j)$ is the transition probability at fixed values of the coordinates, $\{\xi\}$, of the degrees of freedom describing the acoustic modes leading to the fluctuations of the size of the cavity.

The probability, $W_{if}(\{r\}, \{\xi\}, \Delta j)$, depends on $\{\xi\}$. In general, this dependence should be taken into account along with that of $\phi(\{\xi\}, \Delta j\}$ on $\{\xi\}$ for the determination of the transitional configuration with respect to the coordinate, $\{\xi\}$, in Eq. (25). However, $\phi(\{\xi\}, \Delta j)$ depends on $\{\xi\}$ much more strongly than does $W_{if}(\{r\}, \{\xi\}, \Delta j)$, so that the latter may approximately be taken out of the integral sign over $\{\xi\}$ in Eq. (25) at the point $\{\xi^*\}$ corresponding to the transitional configuration.

Since the repulsion of the electronic envelopes of the reactant from the nearest molecules of the medium is very sharp, it may be expected that the potential, $U_i(\{\xi\})$ (or $U_f(\{\xi\})$) describing the change of the cavity size is strongly asymmetric. Its more smooth branch corresponds to the increase of the cavity size and its more sharp one corresponds to the decrease of the latter. Therefore, it is expected that the transitional configuration with respect to $\{\xi\}$ will be close to the equilibrium configuration corresponding to the larger cavity of the two. Thus, if the reaction leads to a decrease of the cavity size, $\{\xi^*\}$ will be close to the final equilibrium configuration. If the cavity size fluctuations are classical, Eq. (25) takes the form

$$W_{if}(\{r\}, \Delta\tilde{J}) \simeq \exp\left[\frac{F_i^{\{\xi\}} - U_i(\{\xi^*\})}{kT}\right] W_{if}(\{r\}, \{\xi^*\}, \Delta\bar{J})\delta\{\xi\} \tag{26}$$

where $\Delta\bar{J} = \Delta\tilde{J} + U_f(\{\xi^*\}) - U_i(\{\xi^*\})$ is the local reaction free energy at the transitional configuration over $\{\xi\}$, $\delta\{\xi\}$ is the interval of the $\{\xi\}$ values giving an essential contribution to the transition probability.

The quantities $U_i(\{\xi^*\})$ and $U_f(\{\xi^*\})$ may apparently be estimated as the work required to create a cavity of a given size.

Now we consider the probability $W_{if}(\{r\}, \{\xi\}, \Delta\bar{J})$. It is determined by an expression similar to Eq. (21) and involves the density matrices $\rho^i_{cs}(\{z\}, \{z'\}; \{r\}, \{\xi\}; \beta(1-\theta))$ and $\rho^f_{cs}(\{z\}, \{z'\}; \{r\}, \{\xi\}; \beta\theta)$ describing the initial and final states of the solvent and the reactants. Taking into account that the product $\rho^i_{cs}\rho^f_{cs}$ as a function of $\{z - z'\}$ has a sharp maximum at $\{z = z'\}$, the expression for $W_{if}(\{r\}, \{\xi\}, \Delta\bar{J})$ may be approximately written in the form

$$\begin{aligned} W_{if}(\{r\}, \{\xi\}, \Delta\bar{J}) \simeq \frac{1}{i\hbar kT} e^{\beta F^i_{cs}} \int_{c-i\infty}^{c+i\infty} & d\sigma \exp(-\beta\sigma\Delta\bar{J}) \\ \times\tfrac{1}{4} \int & d\{\xi\}[\Delta E_e(\{\zeta\}, \{r\}, \{\xi\})]^2 \Delta(\{\zeta\}) \\ & \times \rho^i_{cs}(\{\zeta\}, \{\zeta\}; \{r\}, \{\xi\}; \beta(1-\sigma)) \cdot \rho^f_{cs}(\{\zeta\}, \{\zeta\}; \{r\}, \{\xi\}; \beta\theta) \end{aligned} \tag{27}$$

where $\Delta(\{\zeta\})$ is the corresponding interval of $\{z - z'\}$ variables and $\{\zeta\}$ is the set of the coordinates of the optical modes of the medium and intramolecular coordinates of the reactants.

The diagonal elements of the density matrices in Eq. (27) represent the distribution functions, $\phi^i_{cs}(\{\zeta\}, 1-\sigma)$ and $\phi^f_{cs}(\{\zeta\}, \sigma)$ over the $\{\zeta\}$ coordinates. They are maximal at the points corresponding to the initial and final equilibrium configurations, respectively. They may be rewritten in the form

$$\begin{gathered} \phi^i_{cs}(\{\zeta\}, 1-\sigma) = \phi^{i0}_{cs}(1-\sigma) \exp[-\beta(1-\sigma)w_i(\{\zeta\}, \sigma)] \\ \phi^{i0}_{cs}(1-\sigma) \equiv \phi^i_{cs}(\{\xi_{0i}\}, 1-\sigma) \qquad (28) \\ \phi^f_{cs}(\{\zeta\}, \sigma) = \phi^{f0}_{cs}(\sigma) \exp[-\beta\sigma w_f(\{\zeta\}, \sigma)], \qquad \phi^f_{cs}(\sigma) \equiv \phi^f_{cs}(\{\zeta_{0f}\}, \sigma) \end{gathered}$$

where the new functions, $w_i(\{\zeta\}, \sigma)$ and $w_f(\{\zeta\}, \sigma)$ have been introduced.

If the interaction of the reactants with the medium is strong enough, the integral over σ in Eq. (27) may be calculated by the steepest descent method. The possibility of such a way of making the integral calculation constitutes essentially the general mathematical criterion of strong coupling with the medium. The particular forms of this criterion may be derived using various models.

The transition configuration in this case is determined by the equations

$$\frac{\partial}{\partial \zeta_k}[(1-\sigma)w_i + \sigma w_f + 2kT \ln \Delta E_e(\{\zeta\}, \{r\}, \{\xi\})] = 0 \tag{29}$$

and

$$\frac{\partial}{\partial \sigma}[(1-\sigma)w_i(\{\zeta^*\}, \sigma) + \sigma w_f(\{\zeta^*\}, \sigma)] + \Delta\bar{J} = 0 \tag{30}$$

The expression for the transition probability takes the form

$$\begin{aligned} &W_{if}(\{r\}, \{\xi\}, \Delta\bar{J}) \\ &\quad \simeq \frac{\beta}{\hbar} \exp(\beta F^{i}_{cs})\Delta_\sigma \Delta_\zeta \Delta(\{\zeta^*\})\tfrac{1}{4}[\Delta E_e]^2_* \phi^{i0}_{cs}(1-\sigma^*)\phi^{f0}_{cs}(\sigma^*) \\ &\qquad \times \exp[-\beta\sigma^*\Delta\bar{J} - \beta(1-\sigma^*)w_i(\{\zeta^*\}, \sigma^*) - \beta\sigma^* w_f(\{\zeta^*\}, \sigma^*)] \end{aligned} \tag{31}$$

The expressions above are rather general and enable us to derive explicit analytical formulas using certain models (in particular, the solvent model described in Section 2). However, we shall demonstrate below one more way of deriving the expression for the transition probability which permits the physical significance of the medium model to be visualized in more detail. For the sake of simplicity, we neglect here the dependence of ΔE_e on z.

The transition probability is determined by an equation of the type (21) and involves $\operatorname{tr} \rho^i_{cs}\rho^f_{cs}$. If the interaction between the intramolecular vibrations and the optical modes of the medium may be neglected, the trace is factorized as $\operatorname{tr} \rho^i_{cs}\rho^f_{cs} = \operatorname{tr} \rho^i_c\rho^f_c \cdot \operatorname{tr} \rho^i_s\rho^f_s$, where ρ_c and ρ_s are the density matrices of the reactants and the medium, respectively. If we assume the harmonic approximation for the intramolecular vibrations, $\operatorname{tr} \rho^i_c\rho^f_c$ may be easily calculated. Our aim is to calculate $S \equiv \operatorname{tr} \rho^i_s\rho^f_s$. It is convenient to transform it to$^{(56)}$

$$\begin{aligned} S &= \operatorname{Tr}[\rho^i_s\rho^f_s] = \operatorname{Tr}[\exp[-\beta(1-\theta)H^s_i]\exp(-\beta\theta H^s_f)] \\ &= \operatorname{Tr}\left[\exp(-\beta H^s_i) T \exp\left\{-\frac{i}{h}\int_0^t [H^s_f(y) - H^s_i(y)\, dy]\right\}\right] \end{aligned} \tag{32}$$

where $t = i\theta\beta\hbar$, T denotes the chronological ordering of the operators, H^s_i and H^s_f are the Hamiltonians of the solvent with account of its interaction with the reactants and the reaction products, and

$$H^s_\alpha(y) = \exp\left(\frac{i}{\hbar}H^s_i y\right) H^s_\alpha \exp\left(-\frac{i}{\hbar}H^s_i y\right), \qquad \alpha = i, f \tag{33}$$

Separating from Eq. (9) the interaction with only the inertia medium polarization, P_{in}, the difference $(H_f^s - H_i^s)_{\text{in}}$ may be written in the form

$$(H_f^s - H_i^s)_{\text{in}} = -\int P_{\text{in}}(r)[\mathscr{E}_{0p}(r) - \mathscr{E}_{0i}(r)]\,dr \tag{34}$$

The expansion of the exponential in Eq. (32) taking account of Eq. (34) involves the quantities $\langle\!\langle \delta P(r)\delta P(r') \cdots \delta P(r'')\rangle\!\rangle$, where $\delta P(r) = P_{\text{in}}(r) - P_{\text{in}}^{0i}(r)$ (P_{in}^{0i} is the equilibrium polarization in the initial state). If we make a certain decoupling of these correlation functions to the products of the pair correlation functions, $\langle\!\langle \delta P(r)\delta P(r')\rangle\!\rangle$, then for ln S we obtain(56)

$$\ln S = \tfrac{1}{2}\left(\frac{i}{\hbar}\right)^2 \int_0^t dy_1 \int_0^t dy_2 \sum_{k,k'} (\mathscr{E}_{0f}^k - \mathscr{E}_{0i}^k)^*(\mathscr{E}_{0f}^{k'} - \mathscr{E}_{0i}^{k'}) \times \langle\!\langle T\delta P_k(y_1)\delta P_{k'}(y_2)\rangle\!\rangle \tag{35}$$

Such decoupling in the liquid may be strictly justified only in the long-wave approximation.(80) In this sense, such a procedure is justified for the macroscopic description. However, one should remember that this is the correct method in a number of cases also for short wavelengths. For example, this is the case for phonons in solids. In other cases, such as the "electron gas" in metals (plasmons), acoustic phonons in quantum liquids and so on, this decoupling may be considered as the self-consistent field method or the random phase approximation (the analog of the superposition approximation in the classical theory of liquids).

The above method of calculation leads to the same result which may be obtained using the model of the medium (Section 2). According to the model described, the fluctuations in the medium are represented by the set of effective oscillators whose frequencies and oscillator strengths are determined by the dielectric losses at given characteristic frequencies in the medium. Using the Hamiltonian of the harmonic oscillators whose parameters may be related to the complex dielectric function of the medium $\varepsilon(k, \omega)$ for S, we finally obtain

$$S = \exp[-\phi^{(m)}(\theta)]$$

and

$$\phi^{(m)}(\theta) = \beta \int_0^{\omega_z} d\omega E_r(\omega) \frac{\sinh[\beta h\omega(1-\theta)/2]\sinh(\beta h\omega\theta/2)}{(\beta h\omega/2)\sinh(\beta h\omega/2)} \tag{36}$$

where ω_z is the characteristic frequency of electronic movement in the reactants and $E_r(\omega)$ is the reorganization energy of the effective oscillators of frequency ω

$$E_r(\omega) = \frac{2}{\pi} \cdot \frac{1}{8\pi} \sum_k |\mathscr{E}_{0f}^k - \mathscr{E}_{0i}^k|^2 \frac{\operatorname{Im} \varepsilon(k, \omega)}{\omega |\varepsilon(k, \omega)|^2} \tag{37}$$

In 1976 Schmickler(81) used an interesting method for the calculation of the transition probability starting from the description of the solvent as a set of the point dipole moments. The expressions for the transition probability obtained in Ref. 81 are identical to those derived for the model described in Section 2. The method used in Ref. 81 is stated to have two main advantages: (i) it does not require the special separation of the inertia polarization from the inertialess one and (ii) it permits transition probability also to be calculated in cases where the continuum approximation for the solvent is inapplicable.

However, it should be noted that from the very beginning the dipole moment of the molecule was divided(81) into two parts, $p_i = m_i + \alpha E$, where the first term, m_i, is the permanent part of the dipole moment and the second is the dipole moment induced by the electric field, E, in the medium (α is the electronic polarizability of the molecule). If m_i in this expression is meant to be an operator over all the degrees of freedom, including the electrons, the second term, αE, has to be omitted. However, if some high frequency modes (e.g., electronic or vibrational) are excluded from m_i, the second term, αE, has to be retained, but in this case, m_i is the operator with respect only to the remaining degrees of freedom (i.e., orientational and vibrational, or solely orientational ones). Thus, such separation is essentially equivalent to the use of the concepts of the inertia and inertialess polarizations. In addition, for the calculation of the transition probability, it was necessary to calculate the average quantities of the type $\langle e^{-ap_i}\rangle$.(81) These were expressed in Ref. 81 using quantities of the type $\exp(-b\langle p_i p_k\rangle)$. The derivation presented above shows that such a procedure may be justified only under the same assumptions which were listed above. Therefore, the results obtained by both methods have to be identical.

Thus, both methods are very similar so far as the physical meaning of the models used is concerned, and the results and the range of their validity. However, there are some differences between them. In particular, in our model, liquids with hydrogen bonds may be considered, while Schmickler's model, based on the description of the polarization as the sum of the dipole moments of separate molecules, is not applicable directly to this kind of liquid.

The expression for $\operatorname{tr} \rho_c^i \rho_c^f$ depends on the characteristic intramolecular vibrations and on the model used for their description. In this section, we shall present only one example where the vibrations are harmonic and the entangling of the normal coordinates is absent. (For the general case of the harmonic approximation, see Ref. 49.) Then the expression for the transition probability takes the form(57)

$$
\begin{aligned}
W_{if} = A \exp\Bigg\{ &-\beta\alpha\,\Delta J - \sum_l \frac{m_l}{\hbar}(x_{l0}^i - x_{l0}^f)^2 \omega_l^i \omega_l^f \tanh\frac{\beta\hbar\omega_l^i(1-\alpha)}{2} \\
&\times \tanh\frac{\beta\hbar\omega_l^f\alpha}{2}\left[\omega_l^i \tanh\frac{\beta\hbar\omega_l^i(1-\alpha)}{2} + \omega_l^f \tanh\frac{\beta\hbar\omega_l^f\alpha}{2}\right]^{-1} \\
&\times \exp[-\phi^{(m)}(\alpha)]\Bigg\}
\end{aligned}
\tag{38}
$$

where the summation over l is performed over all the intramolecular degrees of freedom, x^i_{l0}, x^f_{l0} and ω^i_l, ω^f_l are the corresponding equilibrium values of the dimensional normal coordinates and the vibrational frequencies, A involves the electron resonance integral and some other factors unimportant in what follows.

The symmetry factor, α, is determined by the equation

$$\alpha(\Delta J) = -d \ln W_{if}/d\beta\Delta J \tag{39}$$

It should be remembered that in differentiating over ΔJ one has to take into account both the explicit dependence of W_{if} on ΔJ and that contained in $\alpha(\Delta J)$, while values of the other parameters involved in (38) are kept constant. The last condition is essential for the choice of the reaction series, since a change from one reaction to another may lead to a change of the vibration frequencies and of other parameters.†

Writing Eqs. (38) and (39), we used the formulas (30) and (31). According to (30) and (31), the symmetry factor is identical to θ^*.

5. Proton Transfer Reactions

5.1. Proton Transfer in the Case of Strong Coupling with the Medium

Considering proton transfer reactions in polar liquids (e.g., water), it may be expected that the interaction of the reactants with the medium will be strong, i.e., the solvent reorganization energy in the reaction will be large $E_r^{(m)}$, i.e.,

$$\beta E_r^{(m)} \gg (\beta \hbar\omega_m)^2 \tag{40}$$

where ω_m is the characteristic fluctuation frequency of the solvent polarization. The reorganization energy, $E_r^{(m)}$, has the form

$$E_r^{(m)} = \int d\omega\, E_r(\omega) \tag{41}$$

where $E_r(\omega)$ is described by the formula (37).

5.1.1. Entirely Nonadiabatic Reactions

First we shall consider entirely nonadiabatic reactions for which formulas of the quantum mechanical perturbation theory in the first order in the interaction, V_i^{nd}, leading to reaction may be used for the calculation of the transition probability.

---

† It is worth noting that the derivation of the transition probability presented in this section does not require at all the in-phase vibrations of the large number of the oscillators (see Ref. 8). The criticism in Ref. 8 is based on an erroneous calculation of the phase-space volume.

The integrals over σ in Eq. (27) may be calculated by the steepest descent method provided the inequality (40) holds. If the harmonic approximation for the intramolecular proton vibrations is used, analysis of the expression for the transition probability may be carried out in an analytical form for arbitrary orientation of the ion AH^+ with respect to the site of proton adsorption at the electrode surface, taking into account all three vibrational degrees of freedom of the proton. However, for the purposes of the illustration, we shall confine ourselves to two limiting cases of the orientation, (1) and (2), shown in Figures 1 and 2. Then Eq. (38) for W_{if} may be used directly. The frequencies of the proton valence vibrations are rather high ($\sim 3000\,\mathrm{cm}^{-1}$), while the frequencies of the deformation vibrations are rather lower (up to $1500\,\mathrm{cm}^{-1}$). However, they are still large compared with kT ($\sim 200\,\mathrm{cm}^{-1}$ at room temperature). Therefore, if the reaction proceeds in the normal region, i.e., the symmetry factor, α, is not too close to 0 or unity ($\alpha \sim \frac{1}{2}$), the factor in Eq. (38) related to the change of the proton state is temperature independent and is equal to the Franck–Condon factor for the ground initial and final proton vibrational states:

$$S = \langle \psi_{i0} | \psi_{f0} \rangle^2 = e^{-\sigma_T} \tag{42}$$

where the tunneling factor σ_T for the proton is equal to:

$$\sigma_T = \frac{m}{\hbar} \sum_l \frac{(x^i_{l0} - x^f_{l0})^2 \omega^i_l \omega^f_l}{(\omega^i_l + \omega^f_l)} \tag{43}$$

Thus, formally, the change of the proton state is reduced to the change of the electron resonance integral, V^2_{if} by $V^2_{if} \cdot S$. All the temperature dependence of the transition probability for a fixed value of the coordinate of the reactant center of mass is related to the classical overcoming of the Franck–Condon barrier created by the solvent polarization.

The physical mechanism of the transition may be represented in terms of schematic potential energy surfaces as follows. The system moves on the initial potential energy surface along the classical degrees of freedom (the solvent coordinates), the proton being practically in the unexcited vibrational state, up to the point q^* (Figure 3), where the proton energy levels in the initial and final potential wells become equal to each other (Figure 4). In this

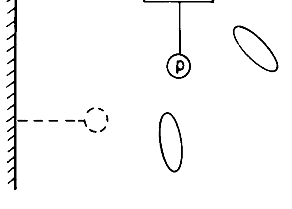

Figure 2. Model as in Figure 1 but for a different orientation (2) of the proton source.

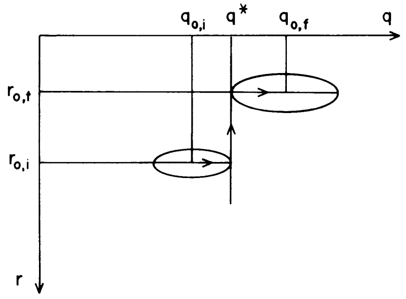

Figure 3. Course of proton transfer reaction showing significance of critical configuration q^*.

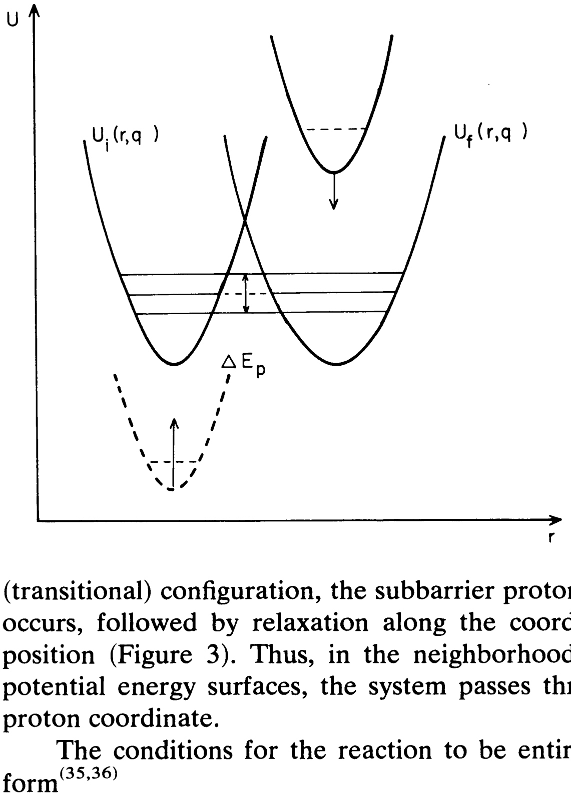

Figure 4. Morse-type potential energy profile diagram for proton transfer showing region where proton energy levels in initial and final energy wells become equal to each other.

(transitional) configuration, the subbarrier proton transition to the final state occurs, followed by relaxation along the coordinate q to the equilibrium position (Figure 3). Thus, in the neighborhood of the intersection of the potential energy surfaces, the system passes through the barrier along the proton coordinate.

The conditions for the reaction to be entirely nonadiabatic are of the form(35,36)

$$\frac{2\pi(\Delta E_e/2)^2}{\hbar|v_p||F_i^p - F_f^p|} \ll 1 \tag{44}$$

$$\kappa_{ep} = \frac{2(\Delta E_p/2)^2}{(\hbar^2\omega_{\text{eff}}^2 kTE_r^{(m)}\pi^{-3})^{1/2}} \ll 1 \tag{45}$$

where v_p is the imaginary velocity of the proton at the intersection of the potential energy surfaces, $F_i^p = \partial U_i(r, q^*)/\partial r$ and $F_f^p = \partial U_f(r, q^*)/\partial r$ are the slopes of the profiles of the potential energy surfaces along the proton coordinate at the transitional configuration q^*, and ΔE_p is the resonance splitting of the proton vibrational energy levels which, in the two-level approximation, is equal to the doubled electron–proton resonance integral (Figure 4), κ_{ep} is the transmission coefficient for partly adiabatic reactions [see Eq. (50) below].

In terms of the adiabatic potential energy surfaces constructed, taking into account all the interactions in the system, the condition (44) is identical with the requirement of a high value for the corresponding nonadiabaticity operator for the total potential energy surfaces (i.e., for the electron terms). The condition (45) means a large value of the nonadiabaticity operator for the adiabatic potential energy surfaces for the degrees of freedom of the solvent at a fixed quantum state of the proton (i.e., for the electron–proton terms).

Equation (38) is convenient if the harmonic approximation is sufficient. However, if the intramolecular vibrations are essentially anharmonic, the formula (46) is more convenient(38,79):

$$W_{if} = \frac{1}{Z} \sum_{m,n} e^{-\beta E^i_m} |\langle \chi^f_n | \chi^i_m \rangle|^2 \cdot W_s(\Delta J + E^f_n - E^i_m) \tag{46}$$

where $S_{mn} = \langle \chi^f_n | \chi^i_m \rangle^2$ is the Franck–Condon factor for two proton vibrational states, m and n, Z is the proton partition function in the initial state, E^i_m and E^f_n are the proton vibrational energies in the initial and final states, and $W_s(\Delta J + E^f_n - E^i_m)$ is the probability of the rearrangement of the electronic subsystem and of the solvent for fixed quantum vibrational proton states, m and n.

The form of W_s depends on the strength of the coupling with the medium. For strong coupling, W_s has the form

$$W_s = \frac{\omega_{\text{eff}}}{2\pi} \kappa_e \exp\left\{-\frac{[E_r^{(m)} + \Delta J + E^f_n - E^i_m]^2}{4E_r^{(m)} kT}\right\} \tag{47}$$

where ω_{eff} is the effective frequency of the solvent polarization fluctuations(35,36), and κ_e is the transmission coefficient taking into account only the change of the electronic state and of the state of the quantum part of the medium polarization.†

Calculations using Eqs. (46) and (47) and, in particular, calculations using electronic computors for the Morse potential model for the proton, with subsequent integration over the electronic energy spectrum in the electrode, gave a *linear* Tafel dependence of rates over a wide potential region, α being close to $\frac{1}{2}$.(61) It should be noted that according to the calculations performed, the major contribution to the transition probability comes from the transitions between the ground states or from transitions with participation of several excited states. Therefore, the activation energy is determined mainly by the solvent reorganization energy and the reaction free energy. The profile of the potential energy surfaces along the proton coordinate determines mainly the transmission coefficient.

---

† Equation (47) is given for the simplest case when the regions of the classical and quantum part of the polarization are separated by a wide transparency band.

5.1.2. Partly Adiabatic and Entirely Adiabatic Reactions

In the normal region, for not too large proton jump distances, the term in Eq. (46) corresponding to the unexcited vibrational proton states is dominant ($m = n = 0$). It may be written in the form

$$W_{if}^{00} = \frac{\omega_{\text{eff}}}{2\pi} \kappa_{ep}^{\text{nonad}} \exp\left(-\frac{E_a^{\text{nonad}}}{kT}\right) \tag{48}$$

$$\kappa_{ep}^{\text{nonad}} = \kappa_e S \tag{49}$$

where E_a^{nonad} may be easily found by comparing Eqs. (48) and (47).

The expressions presented are valid only provided the inequalities (44) and (45) hold. However, for reactions involving heavy particle transfer but without electron transfer from one reactant to another, it may be expected that the electron resonance integral will be large, owing to large overlap of the electronic wave functions, and the inequality (44) will be violated.

The case when an inequality opposite to (44) holds but the inequality (45) is still valid corresponds to a partly adiabatic reaction. This means that the nonadiabaticity operator for the adiabatic electron terms is small and, in the course of the transition, the system remains on the *lower* adiabatic potential energy surface for all the heavy particles including the proton. However, the probability of transition to the final state is still small owing to the small value of the probability of the proton sub-barrier transition.

In this case, the formulas of the first order in the interaction V^{nd} of the quantum mechanical perturbation theory are inapplicable; so are the expressions (45) and (49) which are their consequences. Since the transition occurs with the system remaining on one (lower) potential energy surface, for the calculation of the transition probability, the methods developed for reactions in the gas phase may in principle be used (see, e.g., Ref. 83). However, they are convenient mainly in the cases when the tunneling leads to only small corrections. If the tunneling effects are large (i.e., if the transition takes place between the ground vibrational states), it is more convenient to consider electron–proton potential energy surfaces $\tilde{U}_i^{ep}$ and $\tilde{U}_f^{ep}$ (Figure 5) and to determine the reaction channels. These channels may be introduced unambiguously if the proton is a fast particle compared to movements in the other degrees of freedom. However, if the Born–Oppenheimer approximation is inapplicable, the channels may be introduced in a different way and all the main results will still hold. For example, the channel Hamiltonian may be derived if the electronic term is approximated by the sum of the pair interaction

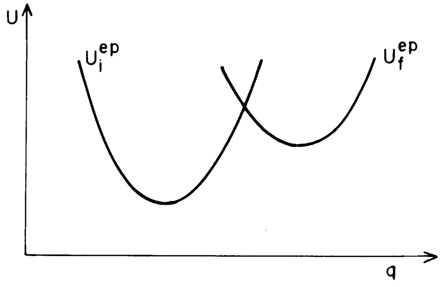

Figure 5. Schematic electron–proton energy surfaces.

potentials between the atoms, omitting the corresponding terms. If the interaction is essentially of a nonpair character, the channels may be introduced separating the reactants to a large distance.(84)

In the Born–Oppenheimer approximation for the proton, the scheme of the calculation is as follows: if a condition similar to (45) holds

$$\kappa_{ep}^{\mathrm{ad}} = \frac{2\pi(\Delta E_{\mathrm{ad}}/2)^2}{\hbar v_T |F_i - F_f|} \ll 1 \tag{50}$$

where ΔE_{ad} is the resonance splitting of the electron–proton potential energy surfaces, v_T is the thermal velocity along the solvent degrees of freedom, $F_i = \nabla_q \tilde{U}^{ep}$ and $F_f = \nabla_q \tilde{U}^{ep}$, and the probability of the transition from this new channel to the new final one may be calculated using the perturbation theory with respect to the quantity ΔE_{ad}. Therefore, one may use the expressions of the foregoing sections, replacing ΔE_e by ΔE_{ad} and making corresponding changes of the other parameters.

In this case, for the transition probability $\bar{W}_{if}^{00}$, we have(35,36)

$$\bar{W}_{if}^{00} = \frac{\omega_{\mathrm{eff}}}{2\pi} \kappa_{ep}^{\mathrm{ad}} \exp\left(-\frac{\tilde{E}_a^{\mathrm{nonad}}}{kT}\right) \tag{51}$$

where E_a^{nonad} is determined by the saddle point on the intersection of the electron–proton potential energy surfaces $\tilde{U}_i^{ep}$ and $\tilde{U}_f^{ep}$.

If conditions opposite to both (44) and (50) hold, the reaction is entirely adiabatic. In this case, the transition probability, W_{if}^{00}, is determined by a formula of the type (51) with the substitution in the last of $\kappa_{ep}^{\mathrm{ad}}$ by unity and $\tilde{E}_a^{\mathrm{nonad}}$ by $E_a^{\mathrm{ad}} = \tilde{E}_a^{\mathrm{nonad}} - \delta E_a$, where δE_a is the lowering of the potential barrier due to the resonance splitting of the potential energy surfaces.

5.2. Proton Transfer in the Case of Weak Coupling with the Medium

We now consider the case of a proton transfer reaction where the interaction of the reactants with the medium is weak. It may be expected that this limiting case arises for some proton transfer reactions in a weakly polar liquid and also for some intramolecular proton transfer processes, in particular, in biological molecules.

The condition of weak coupling with the medium means that the solvent reorganization energy should be small, i.e.,

$$\beta\hbar\omega_m\lambda \equiv \beta E_r^{(m)} \ll (\beta\hbar\omega_m)^2, \qquad \text{i.e., } \lambda \ll 1 \tag{52}$$

In this case, the saddle point method is inapplicable for the calculation of the integral over σ in Eq. (27). The major contribution to the integral comes rather from the large values of $|\sigma|$. This leads to the following expression for the transition probability(85,86):

$$W_{if} = \frac{1}{Z}\sum_{m,n} \exp(-\beta E_m^i)|\langle\chi_n^f|\chi_m^i\rangle|^2 \cdot \frac{1}{\pi}\frac{\lambda kT}{(\Delta J + E_n^f - E_m^i)^2 + (\lambda kT)^2} \tag{53}$$

In the derivation of Eq. (53), Eq. (46) was used.

Equation (53) shows that the dependence of the transition probability on the reaction free energy or on ΔJ is of the form of the sum of Lorentzian maxima weighted by the factors $\exp(-\beta E_m^i)|\langle\chi_n^f|\chi_m^i\rangle|^2$. It should be noted that since coupling with the medium is weak [see Eq. (52)], the width of each maximum is small:

$$\delta = \lambda kT \ll kT \tag{54}$$

The energy difference between the maxima is determined by the quantities $(E_n^f - E_m^i)$ in the denominator of Eq. (53). Since the energies of the proton vibrational quanta are usually large ($\gg kT$), the separation of the maxima is also large. The superposition of the separate maxima is, to a certain degree, incidental. This may arise only at definite "resonance" values of ΔJ. Thus, for example, if the potential energy curves for the proton in the initial and final states are identical, and $\Delta J = E_0^i - E_0^f$, superposition of the maxima with $n = m$ will take place. However, even in this case, most of the maxima with $n \neq m$ will be separated by an energy larger than kT.

In some works (see, e.g., Ref. 34), the resonance dependence of W_{if} on ΔJ is assumed to be smoothed due to the uncertainty in the ΔJ values caused by the interaction between the reactants and the medium. Starting from this assumption, averaging of the transition probability over some interval of ΔJ values around an average value $\Delta\bar{J}$ is performed. The distribution of ΔJ values in this interval is assumed to be uniform.(34)

As for the above, it may be noted that it is the fluctuations of the energetic parameters of the reactants that make possible the fulfillment of the Franck–Condon principle required for the reaction to proceed. For the above fluctuations to smoothen the resonance dependence of the transition probability on ΔJ, the coupling with the medium should be strong (see Section 5.1). In this case, the transition probability has to depend on the characteristics of the medium.

Weak coupling with the medium means that the width of the resonance maxima caused by the interaction between the reactants and the solvent is small. In any case, the correct averaging over ΔJ leads to expressions of the type

$$W_{if} = \frac{1}{Z} \sum_{n,m} \exp(-\beta E^{i}_{m}) |\langle \chi^{f}_{n} | \chi^{i}_{m} \rangle|^{2} \cdot f(E^{i}_{m} - E^{f}_{n}) \tag{55}$$

where $f(\Delta J)$ is the distribution function for the ΔJ values.

Averaging over ΔJ corresponds to the introduction of additional degrees of freedom of the solvent which may be incorporated into the general analysis presented in this section, using various models. Thus, for weak coupling of the reactants with the medium, the dependence of W_{if} on ΔJ is essentially determined by the discrete nature of the proton vibrational energy spectrum and is of the resonance character [see Eqs. (53) and (54)].

It follows from the above that the assumptions regarding weak coupling with the medium and at the same time with regard to the continuous character of the intramolecular vibrational energy spectrum of the reactants, which were made in some papers (see Refs. 3 and 8), to a certain degree contradict each other.

6. *Effect of the Discrete Structure of the Electrical Double Layer on the Kinetics*

In the phenomenological theory, the basis of the electrical double layer effect on the elementary act of an electrochemical reaction is the application of the Brønsted relation which connects the activation energy, E_a, of the process to the heat of the reaction (or reaction free energy)(87):

$$E_a = \text{const} + \alpha \Delta J \tag{56}$$

where α is the symmetry factor. The quantity ΔJ includes the difference of the electrostatic energies of the ion in the solution before and after the electron transition $e\psi$, where ψ is the potential at the point where the reacting ion is located in the double layer.

In most of the earlier works, the average electrostatic potential in the plane where the reacting ions are located was chosen for ψ. This plane was often identified with the outer Helmholtz layer. In this case, the ψ_1 potential calculated according to the Gouy–Chapman theory was used for ψ.

In later works, attempts were made to calculate more exactly the potential at the site of the reactant taking into account the statistical distribution of the ions in the solution.(88–90) These calculations were reduced essentially to the calculation of the average potential at the point where the reacting ion is located at the moment of the electron transition (subtracting the potential of the ion itself). This micropotential was substituted then in formulas of the type of Eq. (55) and was used for the calculation of the polarization characteristics.

All these contributions had a general feature: the average value of the activation energy $\langle E_a \rangle$ was calculated since the average electrostatic potential was inserted directly in the formula for the activation energy. The analysis presented in the foregoing sections shows that, under certain conditions, the total transition probability may be calculated as follows. At first one may calculate the transition probability at arbitrary fixed positions of all the ions in the solution, $W(r_1, r_2, \ldots, r_N)$, and then average $W(r_1, r_2, \ldots, r_N)$ over ionic configurations taking into account their statistical distribution. Thus, according to the correct theory, one should calculate the average transition probability $\langle W(r_1, r_2, \ldots, r_N) \rangle$ but not the average activation energy $\langle E_a \rangle$. As was shown above, under certain conditions the quantum mechanical calculation gives for the transition probability $W(r_1, r_2, \ldots, r_N)$ expressions of the Arrhenius type

$$W(r_1, r_2, \ldots, r_N) = A(r_1, r_2, \ldots, r_N) \exp[-E_a(r_1, r_2, \ldots, r_N)/kT] \tag{57}$$

Thus, unlike the approach mentioned above, one should calculate an average quantity of the type

$$\langle W \rangle = \langle A(r_1, r_2, \ldots, r_N) \exp[-E_a(r_1, r_2, \ldots, r_N)/kT] \rangle \tag{58}$$

but *not* the average activation energy $\langle E_a(r_1, r_2, \ldots, r_N) \rangle$.

The results of the foregoing sections show that the preexponential factor $A(r_1, r_2, \ldots, r_N)$ strongly (exponentially) depends on only the reacting ion coordinates r. Therefore, the dependence of $A(r_1, r_2, \ldots, r_N)$ on the coordinates of the other ions will be neglected in what follows. In addition, for the sake of simplicity, we shall restrict ourselves to the case most frequently encountered experimentally, i.e., when the Brønsted relation is a linear one, i.e., α = const [see Eq. (56)]† and linear Tafel behavior is observed.

If the distribution of all the ions in the double layer is an equilibrium one, the coordinate distribution function of the ions has the form

$$\phi(r, r_1, r_2, \ldots, r_N) = Q_i^{-1} \exp\{-[V_i(r, r_1, r_2, \ldots, r_N) + U_z(r) + U(r_1, \ldots, r_N)]/kT\} \tag{59}$$

where $U(r_1, \ldots, r_N)$ is the interaction energy of all the ions except a given reacting one. It includes the interaction of the ions and their "images" with one another, and with the electrode, and does not depend on the coordinate of the reacting ion, r. $U_z(r)$ is the energy of interaction of the reacting ion, A^z, with its unscreened self-image in the electrode, $V_i(r, r_1, \ldots, r_N)$ is the energy of the interaction of the reacting ion A^z with the other ions and their images and with the electric field of the electrode; Q_i is the statistical sum of the ionic system in the initial state.

---

† For the calculation in the case of an arbitrary E_a versus ΔJ dependence see Ref. 51.

The quantity ΔJ may be written in the form

$$\Delta J = \varepsilon_0 + F_{z-1}^{\text{solv}} - \varepsilon - F_z^{\text{solv}} + e\phi + U_{z-1}(r) - U_z(r) + V_f(r, r_1, r_2, \ldots, r_N) - V_i(r, r_1, \ldots, r_N) \tag{60}$$

where ε_0 is the electron energy in the ion A^{z-1}, ε is the electron energy in the electrode, F_z^{solv} and F_{z-1}^{solv} are the solvation free energies of the ions A^z and A^{z-1}, V_f is the analog of V_i for the final state, ϕ is the potential of the electrode, and $U_z(r)$ and $U_{z-1}(r)$ are the energies of the interactions of the ions A^z and A^{z-1} with their self-images. The quantities $V_i(r, r_1, \ldots, r_N)$ and $V_f(r, r_1, \ldots, r_N)$ may be written in the form

$$V_i(r, r_1, \ldots, r_N) = zv(r, r_1, \ldots, r_N); \; V_f = (z-1)v(r, r_1, \ldots, r_N) \tag{61}$$

where $v(r, r_1, \ldots, r_N)$ is a function independent of the charges of the ions A^z and A^{z-1}.

Introducing a single-particle distribution function for the reacting ions,

$$\phi_z(r) = \int \phi(r, r_1, r_2, \ldots, r_N)\, dr_1\, dr_2 \ldots dr_N \tag{62}$$

we can transform Eq. (59) to the form

$$\phi(r, r_1, r_2, \ldots, r_N) = \phi_z(r) \exp [F_z(r) - V_i(r, r_1, \ldots, r_N) - U(r_1, r_2, \ldots, r_N)]/kT \tag{63}$$

where $F_z(r)$ is the free energy of the ionic system under the condition that a given ion A^z is located at the point r.

Using Eqs. (56) and (58)–(63), we obtain for W_{if}

$$W_{if} = \delta r A(r^*) \exp \{-[E_a^o + \alpha e\phi + \alpha[U_{z-1}(r^*) - U_z(r^*)] + F_{z-\alpha}(r^*) - F_z(r^*)]/kT\} \cdot \phi_z(r^*) \tag{64}$$

where

$$E_a^o = E_a(0) + \alpha(\varepsilon_0 + F_{z-1}^{\text{solv}} - \varepsilon - F_z^{\text{solv}}) \tag{65}$$

The quantity $F_{z-\alpha}(r^*)$ differs from $F_z(r^*)$ only in that it is calculated under the condition that the ion $A^{z-\alpha}$ with the charge $z-\alpha$ is located at the point r^*. r^* denotes in Eq. (64) the distance at which the reaction effectively takes place.†

---

† In general, the location at which the discharging particles find themselves at the moment of the electron transition does not lie in the outer Helmholtz plane. It is determined by the condition that the product of the transition probability and the reactant concentration be maximal. Since the transition probability decreases rather sharply with increasing distance to the electrode, in some cases, the penetration of the particle inside the Helmholtz layer may be required for the reaction to proceed.

It was assumed above that the distribution of all the ions (including the reacting ones) in the solution is an equilibrium or quasiequilibrium one.†

However, if the ions react at an electrode having the same sign of charge as the ions, a deviation from the equilibrium distribution for the reacting ions may arise at sufficiently large values of the current. In this case, the analysis performed above is valid if the supporting electrolyte is present in excess.(52) Indeed the deviation from equilibrium occurs only at small concentrations of the reacting ions in the double layer and the equilibrium distribution is still retained for the ions of the supporting electrolyte. Then $\Phi(r, r_1, \ldots, r_N)$ may be formally written in the same way as Eq. (63) where, in this case, r is the coordinate of a given discharging ion and $r_1, r_2, \ldots, r_N$ are the coordinates of the ions of the supporting electrolyte.‡ The effect of the other reacting ions on a given elementary act of the reaction may be neglected owing to the small values of their concentrations as compared to the concentration of the ions of the supporting electrolyte. In this case, the first cofactor on the right-hand side of Eq. (63) represents the nonequilibrium single-particle distribution function for the reacting ion A^z and the second one is the equilibrium distribution function for the ions of the supporting electrolyte at the fixed position of a given ion A^z.

The calculation using the distribution function described leads to the Eqs. (64) and (65), where the function $\phi_z(r^*)$ may correspond to both the equilibrium and nonequilibrium distributions of the reacting ions.

It should be noted that the result shown in Eqs. (64) and (65) is valid for both steady-state and non-steady-state processes in the frequency region where the capacity of the diffuse part of the double layer is independent of the frequency of the external electric field, i.e., under the condition that the Boltzmann distribution for the ions of the supporting electrolyte, corresponding to a given instantaneous value of the electric field in the solution and to a given configuration of the reacting ions, is retained.

It may be seen from Eq. (64) that the activation factor involves the free energy difference $F_{z-\alpha}(r^*) - F_z(r^*)$ related to the reorganization of the ionic atmosphere around the reactants. According to the Franck–Condon principle, the electron transition takes place at some fixed coordinates of the heavy particles, corresponding to the transitional configuration. In terms of reaction channels, the transitional configuration corresponds to equalization of the electronic energies of the initial and final states. In terms of the adiabatic potential energy surfaces, the transitional configuration corresponds to such an electron density distribution when the charge of the ion A is equal to

---

† If the ion distribution is at equilibrium only in the region of the space charge near the electrode surface (quasiequilibrium), only normalization in Eq. (59) is changed.

‡ The equation (63) is valid if the relaxation time of the Debye ionic atmosphere τ_D is small compared with the characteristic time of the reactant movement or to that of the change of the external electric field in the case of nonstationary processes.

$e(z - \alpha)$.† It follows from Eq. (64) that fluctuations of both the configuration of the medium molecules and of the ionic atmosphere around the reactants are required to attain the transitional configuration. The Eq. (64) solves, in principle, the problem of the effect of the micropotential and the discrete structure of the electrical double layer on the kinetics and reduces it to the calculation of the free energies $F_z(r)$ and $F_{z-\alpha}(r)$, and the distribution function for the reactants $\Phi_z(r)$.

7. The Step of Electrochemical Desorption of Hydrogen Atoms

The proton transition from a donor to an adsorbed state at the electrode surface which is the first step of the hydrogen evolution process at metals was considered above. The total process involves also a second step which is the desorption of the hydrogen atoms to form hydrogen molecules. There are two principal mechanisms of hydrogen atom desorption. In this section, we shall consider the "electrochemical" desorption of hydrogen atoms, which is predominant at metals with high H_2 overvoltages:

$$H_{ads} + e + AH^+ \rightarrow A + H_2 \tag{66}$$

Using the general expressions for the transition probability presented in Sections 3 and 4, one may obtain for the rate of the reaction (66) the expression

$$i = ec_a \frac{\beta L^2}{8\pi^2 i\hbar} \int dR_A \, d\phi_A \, c_A(R_A, \psi_A) \int d\theta \\ \times \exp[-\beta\theta\Delta F(\varepsilon, R_A, \psi_A) - \phi^{(m)}(\theta, R_A, \psi_A) + \beta F_i^{(V)}] \operatorname{Tr} \rho_i(1-\theta)\rho_f(\theta) \tag{67}$$

where $\phi^{(m)}$ is described by a relation of the type of Eq. (36), $F_i^{(v)}$ is the free energy of the intramolecular vibrations of the reactants, $\Delta F(\varepsilon, R_A, \psi_A)$ is the reaction free energy at fixed values of the reactant coordinates and electron energy in the electrode, ε, taking part in the elementary act of the reaction (66), c_a is the concentration of adsorbed hydrogen, c_A is the concentration of the reactants in the solution, L is the electron resonance integral (the reaction is assumed to be a nonadiabatic one), $\rho_i(1 - \theta)$ is the density matrix for the adsorbed hydrogen and for the proton in the molecule AH^+, and $\rho_f(\theta)$ is the density matrix for the hydrogen molecule. The integration is performed over the coordinates of the center of mass of the reactants, R_A, and over their possible orientations ψ_A. The expression (67) should then be averaged over the electronic energies in the electrode (see Section 8).

---

† An assumption of this kind was made in Ref. 20. However, the cited result is obtained here as a consequence of the correct quantum mechanical calculation.

The density matrix for the hydrogen molecule is written in the form

$$\rho_f = \rho_f^{(t)}\rho_f^{(r)}\rho_f^{(v)} \tag{68}$$

where $\rho_f^{(v)}$ is the density matrix for the vibrational motion, $\rho_f^{(t)}$ is the density matrix for the translational motion, which, in the classical limit, has the form

$$\rho_f^{(t)}(R, R') = \left(\frac{M}{2\pi\beta\hbar}\right)^{3/2} \exp\left[-\frac{M}{2\beta\hbar^2}(R - R')^2 - \beta U(R)\right] \tag{69}$$

where R is the coordinate of the center of mass of the hydrogen molecule and $U(R)$ is the effective potential energy of interaction of the hydrogen molecule with the medium.

The density matrix of the rotational motion, $\rho_f^{(r)}$, has the form

$$\rho_f^{(r)}(n, n') = \sum_{l=0}^{\infty} \frac{2l+1}{4\pi} P_l(nn') \exp\left[-\frac{\beta l(l+1)}{\beta_R}\right] \tag{70}$$

where $\beta_R = 2I/\hbar^2$, I is the moment of inertia of the hydrogen molecule, $P_l(nn')$ the Legendre polynomial, and vector n determines the orientation of the hydrogen molecule:

$$n = (r_i - r_a)/|r_i - r_a| \tag{71}$$

where r_i and r_a are the proton coordinates.

The final expression for i may be written approximately in the form

$$i = ec_a \frac{2\pi L^2}{\hbar} \frac{1 - \alpha}{[|\alpha(1 - \alpha)H''(\alpha) - 1|]^{1/2}} \int dXc(X)$$

$$\times \exp\left[-\beta\alpha\Delta F(\varepsilon, X) - \phi^{(m)}(\alpha, X)\right] \int dYdZ \cdot T \tag{72}$$

where $H = \phi^{(m)} - \ln T$,

$$T = \int dr_i \int dr_a \phi_i^{(p)}(r_i, r_a; 1 - \theta)\phi_f^{(p)}(r_i, r_a; \theta) \tag{73}$$

and $\phi_i^{(p)}$ and $\phi_f^{(p)}$ are the diagonal elements of the density matrices ρ_i and ρ_f.

The calculation of the quantity T and the integrals in Eq. (72) using various models have been performed.(91)

On the basis of the analysis presented, the problem of the relation between the quantities of ortho and para modifications of the gaseous hydrogen produced in the course of the reaction was also investigated theoretically.(92) The difference in the rates of production of ortho- and para-hydrogen in the reaction of electrochemical desorption is mainly due to the differences in the density matrices of the hydrogen molecules formed. For para-hydrogen, states with only even values of the orbital angular momentum are possible, since the total nuclear spin is equal to zero. For ortho-hydrogen (the total nuclear spin being equal to unity), the states with only odd values of the orbital angular momentum l arise. Taking into account the three-fold degeneracy with respect to the projection of the total nuclear spin in the ortho-hydrogen molecule, the ratio of the number of hydrogen molecules in ortho modification to that in para modification may be written in the form

$$S_{0-p} = \frac{3\sum_{1}}{\sum_{0}} = \frac{3\sum_{l=1,3,\ldots} (2l+1)\exp[-\beta\theta^{*} l(l+1)/\beta_R]}{\sum_{l=0,2,\ldots} (2l+1)\exp[-\beta\theta^{*} l(l+1)/\beta_R]} \tag{74}$$

It follows from Eq. (74) that for a barrierless process ($\theta^* = 1$), the ratio of ortho- to para-hydrogen should be the equilibrium value but for the activationless process ($\theta^* = 0$) $S_{0-p} = 3$. For small values of $\gamma \equiv \beta\theta^*/\beta_R$, the quantity $1 - S_{0-p}/3$ is small and increases with increasing γ according to the equation$^{(92)}$

$$1 - S_{0-p}/3 \simeq 2\pi(2\pi/\gamma)^{1/2} \exp(-\pi^2/2\gamma) \tag{75}$$

Thus, the difference between S_{0-p} and 3 should increase with the lowering of temperature since $\gamma \sim 1/T$.

8. The Role Played by the Electronic Structure of the Electrode

The transition with participation of electrons occupying local energy levels in the electrode was considered above. Now we shall discuss the question on the role played by the *continuous* electronic energy spectrum in electrochemical kinetics. At first nonadiabatic reactions will be considered. It follows from Eqs. (15) and (16) that the characteristics of the electronic subsystem are involved in the transition probability through the electronic resonance integral and reaction free energy ΔJ which contains the difference of the electronic energies of the initial and final states. In order to obtain the final expression for the transition probability, the quantity (15) should be averaged over initial electronic states and summed over all final electronic states possible.

For electrochemical systems, the calculation of the electron resonance integral and subsequent averaging is very complex since the problem is essentially a many-body one, owing to the strong interaction of the electrons in the metal with each other. Formally, this problem is also important for reactant molecules having a multielectron structure.

Since the interaction is pairwise, the operator of the electron interaction between the electrode and the reactant may be written in the form

$$V = \sum_{k,\alpha} L_{k\alpha} \overset{+}{a}_k a_\alpha + \sum_{k,k',k'',\alpha} U_{kk'k''\alpha} \overset{+}{a}_k \overset{+}{a}_{k'} a_{k''} a_\alpha + \sum_{k,\alpha,\alpha',\alpha''} U_{k\alpha\alpha'\alpha''} \overset{+}{a}_k \overset{+}{a}_\alpha a_{\alpha'} a_{\alpha''} \tag{76}$$

where a_k^+ and a_k are the creation and annihilation operators for the electrons with a quasimomentum k in the metal, a_α^+, a_α are the operators of the creation and annihilation of the electron in the reactant molecule in the state α, and $L_{k\alpha}$, $U_{kk'k''\alpha}$, and $U_{k\alpha\alpha'\alpha''}$ are the one-particle and two-particle matrix elements.

With the use of Eq. (76), the transition probability may be written in the form

$$W_{if} = \frac{\beta}{i\hbar}\int_{c-i\infty}^{c+i\infty} d\theta \exp(\beta F_i)\,\mathrm{Tr}\{\exp[-\beta(1-\theta)H_i]\exp(-\beta\theta H_f)\} \times \langle\!\langle V^+ V(\theta)\rangle\!\rangle \tag{77}$$

where $\tilde{H}_M = H_M - \mu N$ and

$$\langle\!\langle V^+ V(\theta)\rangle\!\rangle = \mathrm{Tr}\{\exp(\beta\Omega + \mu N - H_M)V^+ \exp(-\beta\theta\tilde{H}_M) \times V \exp(\beta\theta\tilde{H}_M)\}$$

The terms of the type $L_{k\alpha}a_k^+ a_\alpha$ in Eq. (76) describe one-particle processes, i.e., the processes leading to the change of state of the one electron transferred from the metal to the reactant (or backward) owing to its interaction with nuclei. In Eq. (76), the terms are omitted which describe the processes of transfer of *two* electrons (one from the reactant to the electrode and another from the electrode to the reactant) which do not contribute to the electric current. Terms are also omitted which describe two-electron transfer to the ion or in the backward direction; these processes are not considered here. The terms $U_{kk'k''\alpha}a_k^+ a_{k'}^+ a_{k'}a_\alpha$ describe the processes of the transition of one electron to the reactant, or backward, followed by a change of the state of the other electrons.

The calculation of average quantities $\langle\!\langle V^+ V(\theta)\rangle\!\rangle$ may be performed in various approximations. One of them is the self-consistent field method which consists in the decoupling of the average values. As a result, we have for $\langle\!\langle V^+ V(\theta)\rangle\!\rangle$

$$\begin{aligned}\langle\!\langle V^+ V(\theta)\rangle\!\rangle = {} & \sum_{k\alpha} g_{kk}(\theta) g^{+}_{\alpha\alpha}(\theta)\Big|L_{k\alpha} + \sum_{k'} N_{k'}(U_{kk'k'\alpha} - U_{k'kk'\alpha}) \\ & + \sum_{\alpha'} N_{\alpha'}(U_{k\alpha'\alpha'\alpha} - U_{k\alpha'\alpha\alpha'})\Big|^2 + \sum_{k\alpha} g_{kk}(\theta) g^{+}_{\alpha\alpha}(\theta) \\ & \times \Big[\sum_{k'k''} N_{k'}N_{k''}(U^*_{kk'k'\alpha} - U^*_{k'kk'\alpha})(U_{kk''k''\alpha} - U_{k''kk''\alpha}) \\ & + \sum_{\alpha'\alpha''} N_{\alpha'}N_{\alpha''}(U_{k\alpha'\alpha'\alpha} - U_{k\alpha'\alpha\alpha'}) \times (U^*_{k\alpha''\alpha''\alpha} - U^*_{k\alpha''\alpha\alpha''})\Big] \\ & + \sum_{kk'k''\alpha} g_{kk}(\theta) g_{k'k'} g^{+}_{\alpha\alpha}(\theta) U^{+}_{k\alpha\alpha'\alpha''}(U_{kk'k''\alpha} - U_{k'kk''\alpha}) \\ & + \sum_{k\alpha\alpha'\alpha''} g_{kk}(\theta) g_{\alpha\alpha}(\theta) g_{\alpha'\alpha'}(\theta) g^{+}_{\alpha''\alpha''}(\theta) U^*_{k\alpha\alpha'\alpha''} \\ & \times (U_{k\alpha\alpha'\alpha''} - U_{k\alpha\alpha''\alpha'})\end{aligned} \tag{78}$$

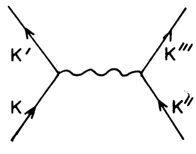

Figure 6. Processes of electron scattering (schematic).

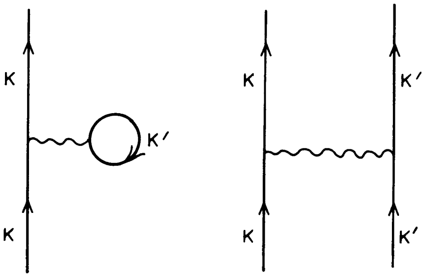

Figure 7. Interaction of electrons with phonons (schematic).

This expression still involves processes of electron scattering with respect to each other in the self-consistent approximation (see Figure 6). If these processes are neglected, retaining only the interaction of the electrons with the phonon particles (Figure 7), i.e., if the random phase approximation is used in the self-consistent field method, we obtain for W_{if}

$$W_{if} \simeq \frac{\beta|\tilde{L}|^2}{i\hbar} \int d\varepsilon \rho(\varepsilon) f(\varepsilon) \int_{c-i\infty}^{c+i\infty} d\theta \exp(\beta F_i) \exp(\beta\theta\varepsilon)$$
$$\times \operatorname{Tr}\{\exp[-\beta(1-\theta)H_i] \exp(-\beta\theta H_f)\} \tag{79}$$

where $f(\varepsilon) = \{1 + \exp[(\varepsilon - \varepsilon_F)/kT]\}^{-1}$ is the Fermi distribution function for the electrons and $\tilde{L}$ is the effective electronic resonance integral. Expressions of this type were used in all the preceding calculations on electrode processes.(93)

The analysis of Eq. (79) shows that the main contribution to the electric current comes from transitions from a small group of electronic energy levels in the electrode near some energy ε^*. The position of the level ε^* is related to the experimentally observed transfer coefficient, α, according to the equation

$$\alpha = 1 - f(\varepsilon^*) \tag{80}$$

and depends on the potential.

Depending on the position of the level ε^* (or on the value of the transfer coefficient, α), one may obviously distinguish three familiar regions: (i) the normal one ($\alpha \sim \frac{1}{2}$), (ii) barrierless ($\alpha \approx 1$), and (iii) activationless ($\alpha \approx 0$). It follows from Eq. (80) that, in the normal region, the electrons occupying the Fermi level mainly take part in the process ($\varepsilon^* \approx \varepsilon_F$). In the barrierless and activationless regions, ε^* lies much higher, or much lower, than the Fermi level, respectively. Since the probability of the occupation of the energy level ε^* by the electron lies in the interval 0 to 1, according to Eq. (80) the transfer coefficient also must lies in this interval ($0 \leq \alpha \leq 1$). Detailed investigation of general properties of the polarization characteristics using the expressions of the type (79) was performed in Refs. 93 and 94.

In concluding this section, we note that nonadiabatic electrochemical reactions were considered above. Calculations on adiabatic electrode processes at metals and semiconductors is more complex. In the model of independent electrons, calculations on such a process were performed in Ref. 48, using the semiclassical method. The physical mechanism of the process consists in the manyfold electron transitions from the electrode to the reactant, and backwards, in the course of variation of the solvent polarization.

9. Experimental Verification of the Theory

The quantum mechanical theory leads to a number of conclusions in respect to the kinetics of electrochemical reactions, in particular to the hydrogen evolution reaction. These conclusions are, to a certain degree, opposite to those of the classical approach. Thus, the consistent incorporation of the electronic energy spectrum in the electrode in the theory leads to the conclusion that barrierless and activationless transitions should be observed under certain conditions. In the theories which consider transitions to only one electronic energy level (the Fermi level), the transition probability should increase, reach a maximum, and then decrease with decrease of the reaction free energy. Experiment shows the existence of the barrierless and activationless processes.(74,75)

Useful information can be obtained from the experimental determination of the activation energy and preexponential factor separately, since they are determined by different factors. According to the quantum mechanical theory, the value of the preexponential factor in proton transfer reactions is determined mainly by the characteristics of the chemical bond to be broken, whereas the activation energy is determined by the Franck–Condon potential barrier associated with solvent polarization. Experimental investigation of the hydrogen evolution reaction from the ions H_3O^+ and CH_3CNH^+ in water and in acetonitrile gave evidence in favor of this conclusion(94) (Table 1). The preexponential factor proves to depend on the nature of the reactant, but it

Table 1
Kinetic Parameters for Proton Transfer Reactions

Solvent	Water		Acetonitrile	
Reactant	H_3O^+	CH_3CNH^+	H_3O^+	CH_3CNH^+
$\log A$	3.4	—	3.2	2.1
E_a	21.9	—	18.2	18.2

is independent of the characteristics of the solvent. The activation energy, on the contrary, is sensitive to changes of the nature of the solvent, but is practically the same for both types of (H^+) ions in the same solvent (see Table 1).

A number of conclusions are concerned with the isotopic effect in the hydrogen evolution reaction and the relation between the ortho and para modifications of H_2 molecules in the gaseous hydrogen evolved. The theory predicts a decrease of the isotopic effect with increasing potential in acid solutions and a weak dependence on the potential in alkaline solutions. This is verified by experiment.(95) Experiments also show that the isotopic effect at various metals is determined by the electric field interacting with the discharging ion, in line with the theory.(95)

The deviation of the relative content of ortho- and para-H_2 species from the equilibrium value predicted by the theory has been observed experimentally.(92) It was found that at 293 K, this relation is identical to the equilibrium one, taking into account the experimental uncertainties. At low temperature (193 K), the content of para-hydrogen in the mixture is equal to 26.1%, whereas the equilibrium composition at this temperature is 25%. Thus, this difference is outside the experimental error. Such a difference (~1%) may be predicted from Eq. (75) if it is assumed that the transfer coefficient for the step of electrochemical desorption is $\alpha = \theta^* < 0.67$. Thus, by investigating the relative content of ortho- and para-hydrogen in the evolved H_2, one may obtain some information about the value of the transfer coefficient for the step of electrochemical desorption.

These, and a number of other experimental facts, give evidence that the physical assumptions on which the theory is based are, in general, correct. In a number of cases, there is also quantitative agreement between theory and experiment. The main difficulty of the theory which is not yet overcome consists in the quantitative description of the transition regions between the normal region of the process, and the activationless and barrierless ones.† It is hoped that this problem will be also solved by further experimental and theoretical investigations.

References

1. R. Gurney, *Proc. R. Soc. London Ser. A* **134**, 137 (1931).
2. J. Horiuti and M. Polyani, *Acta Physicochim. SSSR* **2**, 505 (1935).
3. J. O'M. Bockris and D. B. Matthews, *Proc. R. Soc. London Ser. A* **292**, 479 (1966); *Modern Aspects of Electrochemistry*, Vol. 6, J. O'M. Bockris and B. E. Conway, eds., Butterworths, London (1971), p. 242; J. O'M. Bockris and R. K. Sen, *Molec. Phys.* **29**, 257 (1975); *J. Res. Inst. Catal. Hokkaido Univ.* **21**, 55 (1973).
4. S. G. Christov, *Z. Electrochem.* **62**, 567 (1958); **64**, 840 (1960); *Electrochim. Acta* **4**, 194, 306 (1961), *Z. Phys. Chem. N.F.* **214**, 40 (1960).

---

† See Chapter 3 by Krishtalik in this volume.

5. S. G. Christov, *J. Res. Inst. Catal. Hokkaido Univ.* **16**, 169 (1968).
6. S. G. Christov, *J. Electrochem. Soc.* **124**, 69 (1977); *J. Res. Inst. Catal. Hokkaido Univ.* **24**, 27 (1976).
7. W. Libby, *J. Phys. Chem.* **56**, 863 (1952).
8. J. O'M. Bockris, R. K. Sen, and K. L. Mittal, *J. Res. Inst. Catal. Hokkaido Univ.* **20**, 153 (1972); J. O'M. Bockris, S. U. M. Khan, and D. B. Matthews, *J. Res. Inst. Catal. Hokkaido Univ.* **22**, 1 (1974).
9. R. Platzmann and J. Frank, *Z. Phys.* **138**, 411 (1954).
10. M. Lax, *J. Chem. Phys.* **20**, 1752 (1952).
11. S. I. Pekar, *Investigations of Electronic Theories of Crystals* (Russian edition), Fizmatgiz, Moscow (1951).
12. R. Kubo and Y. Toyozawa, *Prog. Theor. Phys.* **13**, 160 (1955).
13. A. S. Davydov, *Zh. Eksp. Teor. Fiz.* (*Sov. Phys.-JETP*) **18**, 913 (1948).
14. M. F. Deigen, *Tr. Inst. Fiz. Akad. Nauk Ukr. SSR*, Part 5, 119 (1954).
15. R. A. Marcus, *J. Chem. Phys.* **24**, 966, 979 (1956); **26**, 867 (1957).
16. R. A. Marcus, *Can. J. Chem.* **37**, 155 (1959).
17. R. A. Marcus, in *Transactions of the Symposium on Electrode Processes*, E. Yeager, ed. John Wiley and Sons, New York (1961), p. 239.
18. R. A. Marcus, *J. Phys. Chem.* **67**, 853, 2889 (1963).
19. R. A. Marcus, *J. Chem. Phys.* **38**, 1335, 1858 (1963); **39**, 1734 (1963); **41**, 603, 2624 (1964); **43**, 679 (1965).
20. N. S. Hush, *J. Chem. Phys.* **28**, 962 (1958); *Trans. Faraday Soc.* **57**, 557 (1961).
21. H. Gerischer, *Z. Phys. Chem. N.F.* **26**, 223, 325 (1960).
22. V. G. Levich and R. R. Dogonadze, *Dokl. Akad. Nauk SSSR* **124**, 123 (1959).
23. V. G. Levich and R. R. Dogonadze, *Dokl. Akad. Nauk SSSR* **133**, 158 (1960); *Collect. Czech. Chem. Commun.* **26**, 193 (1961).
24. R. R. Dogonadze, *Dokl. Akad. Nauk SSSR* **133**, 1368 (1960).
25. R. R. Dogonadze, *Dokl. Akad. Nauk SSSR* **142**, 1108 (1961).
26. R. R. Dogonadze and A. M. Kuznetsov, in *Itogi Nauki, Elektrochimija 1967*, ed. VINITI of the USSR (Russian edition), Moscow (1969), p. 1.
27. R. R. Dogonadze and Yu. A. Chizmadzhev, *Dokl. Akad. Nauk SSSR* **144**, 1077 (1962); **145**, 848 (1962).
28. R. R. Dogonadze, A. M. Kuznetsov, and Yu. A. Chizmadzhev, *Zh. Fiz. Khim.* **38**, 1195 (1964).
29. R. R. Dogonadze and A. M. Kuznetsov, *Izv. Akad. Nauk SSSR Ser. Chim.* **12**, 2140 (1964).
30. R. R. Dogonadze and A. M. Kuznetsov, *Elektrokhimiya* **3**, 1324 (1967).
31. N. S. Hush, *Electrochim. Acta* **13**, 1005 (1968).
32. R. R. Dogonadze, A. M. Kuznetsov, and V. G. Levich, *Elektrokhimiya* **3**, 739 (1967).
33. R. R. Dogonadze, A. M. Kuznetsov, and V. G. Levich, *Electrochim. Acta* **13**, 1025 (1968).
34. J. Jortner, *J. Chem. Phys.* **64**, 4860 (1976).
35. R. R. Dogonadze and A. M. Kuznetsov, in *Itogo Nauki i Techniki, Ser. Phys. Chim., Kinetics*, Vol. 2, ed VINITI of the USSR (Russian edition), Moscow (1973).
36. R. R. Dogonadze and A. M. Kuznetsov, *Prog. Surf. Sci.* **6**, 1 (1975).
37. R. A. Marcus, *J. Phys. Chem.* **72**, 891 (1968).
38. V. G. Levich, R. R. Dogonadze, E. D. German, A. M. Kuznetsov, and Yu. I. Kharkats, *Electrochim. Acta* **15**, 353 (1970).
39. E. D. German, R. R. Dogonadze, A. M. Kuznetsov, V. G. Levich, and Yu. I. Kharkats, *Elektrokhimiya* **6**, 350 (1970).
40. R. A. Marcus, *Ann. Rev. Phys. Chem.* **15**, 155 (1964).
41. V. G. Levich, in *Advanced Treatise of Physical Chemistry*, Vol. 9B, H. Eyring, D. Henderson, and J. Jost, eds., Academic Press, New York (1970), p. 986.
42. R. R. Dogonadze, in *Reactions of Molecules at Electrodes*, N. S. Hush, ed., Wiley-Interscience, New York (1971), p. 135.

43. R. R. Dogonadze, A. M. Kuznetsov, and V. G. Levich, *Dokl. Akad. Nauk SSSR* **188**, 383 (1969).
44. A. A. Ovchinnikov and M. Ya. Ovchinnikova, *Dokl. Akad. Nauk SSSR* **186**, 76 (1969); *Zh. Eksp. Teor. Fiz.* (*Sov. Phys.-JETP*) **56**, 1278 (1969).
45. R. R. Dogonadze and A. M. Kuznetsov, *Elektrokhimiya* **7**, 763 (1971).
46. R. R. Dogonadze, A. A. Kornyshev, and A. M. Kuznetsov, *Theor. Math. Phys.* **15**, 127 (1973) (Soviet journal).
47. M. A. Vorotyntsev, R. R. Dogonadze, and A. M. Kuznetsov, *Vest. Mosk. Univ. Ser. Fiz.* **2**, 224 (1973); **3**, 352 (1973).
48. R. R. Dogonadze, A. M. Kuznetsov, and M. A. Vorotyntsev, *Croat. Chem. Acta* **44**, 257 (1972); *J. Electroanal. Chem.* **25**, No. 2, App. 17 (1970).
49. R. R. Dogonadze, A. M. Kuznetsov, and M. A. Vorotyntsev, *Phys. Status Solidi B* **54**, 125, 425 (1972).
50. W. Schmickler and W. Vielstich, *Electrochim. Acta* **18**, 883 (1973).
51. R. R. Dogonadze and A. M. Kuznetsov, *J. Electroanal. Chem.* **65**, 545 (1975).
52. R. R. Dogonadze and A. M. Kuznetsov, *Elektrokhimiya* **13**, 1268 (1977).
53. N. R. Kestner, J. Logan, and J. Jortner, *J. Phys. Chem.* **78**, 2148 (1974).
54. R. R. Dogonadze and A. M. Kuznetsov, *Electrochim. Acta* **19**, 961 (1974).
55. Sh. Efrima and M. Bixon, *J. Chem. Phys.* **64**, 3639 (1976).
56. A. M. Kuznetsov, candidate dissertation, University of Moscow, 1964.
57. R. R. Dogonadze and A. M. Kuznetsov, in *Proceedings of the Symposium on Electrocatalysis, San Francisco*, May 1974, M. W. Breiter, ed., Electrochemical Society, Pennington, New Jersey (1974), p. 195.
58. R. R. Dogonadze, A. M. Kuznetsov, and M. A. Vorotyntsev, *Z. Phys. Chem. N.F.* **100**, 1 (1976).
59. R. R. Dogonadze and A. M. Kuznetsov, *Zh. Vses. Khim. Ova.* **19**, 242 (1974).
60. R. R. Dogonadze, J. Ulstrup, and Yu. I. Kharkats, *J. Chem. Soc., Faraday Trans. 2* **68**, 745 (1972).
61. Yu. I. Kharkats and J. Ulstrup, *J. Electroanal. Chem.* **65**, 555 (1975).
62. J. Ulstrup and J. Jortner, *J. Chem. Phys.* **63**, 4358 (1975).
63. W. Schmickler, *Electrochim. Acta* **20**, 137 (1975).
64. J. M. Hale, *J. Electroanal. Chem.* **19**, 315 (1968).
65. P. P. Schmidt, *Austral. J. Chem.* **22**, 673 (1969).
66. M. V. Volkenstein, R. R. Dogonadze, A. K. Madumarov, and Yu. I. Kharkats, *Dokl. Akad. Nauk SSSR* **199**, 124 (1971).
67. V. G. Levich, A. K. Madumarov, and Yu. I. Kharkats, *Dokl. Akad. Nauk SSSR* **203**, 1351 (1972).
68. R. R. Dogonadze, J. Ulstrup, and Yu. I. Kharkats, *Dokl. Akad. Nauk SSSR* **207**, 640 (1972).
69. Yu. I. Kharkats, *Elektrokhimiya* **8**, 1300 (1972).
70. R. R. Dogonadze, J. Ulstrup, and Yu. I. Kharkats, *J. Electroanal. Chem.* **39**, 47 (1972); **43**, 161 (1973).
71. R. R. Dogonadze, J. Ulstrup, and Yu. I. Kharkats, *J. Theoret. Biol.* **40**, 259, 283 (1973).
72. R. R. Dogonadze, Yu. I. Kharkats, and J. Ulstrup, *J. Chem. Soc., Faraday Trans. 2* **70**, 64 (1974).
73. A. M. Kuznetsov and Yu. I. Kharkats, *Elektrokhimiya* **12**, 1277 (1976).
74. L. I. Krishtalik, *Zh. Fiz. Khim.* **33**, 1715 (1959); **34**, 117 (1960); **39**, 642 (1965).
75. L. I. Krishtalik, *Elektrokhimiya* **2**, 1176 (1966).
76. R. P. Van Duyne and S. F. Fischer, *Chem. Phys.* **5**, 183 (1974).
77. W. Schmickler, *J. Chem. Soc. Faraday Trans. 2* **72**, 307 (1976).
78. G. Zundel, *Hydration and Intermolecular Interaction*, Academic Press, New York (1969).
79. M. A. Vorotyntsev, V. M. Kats, and A. M. Kuznetsov, *Vest. Mosk. Gos. Univ. Ser. Fiz.* **4**, 411 (1971).

80. A. A. Abrikosov, L. P. Gor'kov, and I. E. Dsiyaloshinskii, *Methods of Quantum Field Theory in Statistical Physics* (Russian edition), GIFML, Moscow (1962).
81. W. Schmickler, *Ber. Bunsenges. Phys. Chem.* **80**, 834 (1976).
82. W. H. Miller, *J. Chem. Phys.* **61**, 1823 (1974).
83. R. G. Newton, *Scattering Theory of Waves and Particles*, McGraw-Hill Book Company, New York (1969).
84. P. P. Schmidt, *J. Chem. Soc. Faraday Trans. 2* **69**, 1104 (1973); *Z. Naturforsch.* **29a**, 880 (1974).
85. R. R. Dogonadze, E. M. Itskovich, A. M. Kuznetsov, and M. A. Vorotyntsev, *J. Phys. Chem.* **79**, 2827 (1975).
86. R. R. Dogonadze, A. M. Kuznetsov, M. A. Vorotyntsev, and M. G. Zaqaraia, *J. Electroanal. Chem.* **75**, 315 (1977).
87. A. N. Frumkin, *Z. Phys. Chem. A* **164**, 121 (1933).
88. V. S. Krylov, W. R. Fawcett, and V. A. Kiryanov, *Elektrokhimiya* **12**, 424 (1976); **12**, 543 (1976); V. G. Levich, V. A. Kiryanov, and V. S. Krylov, *Dokl. Akad. Nauk SSSR* **155**, 662 (1964); V. N. Gorelkin and V. P. Smilga, *Elektrokhimiya* **2**, 492 (1966); V. A. Kiryanov and V. S. Krylov, *Electrokhimiya* **7**, 1040 (1971).
89. V. A. Kiryanov and V. S. Krylov, *Elektrokhimiya* **7**, 1040 (1971).
90. W. R. Fawcett and S. Levine, *J. Electroanal. Chem.* **43**, 175 (1973).
91. M. A. Vorotyntsev and G. M. Chonishvili, *Dokl. Akad. Nauk SSSR* **225**, 116 (1975).
92. V. M. Tsionsky, G. M. Chonishvili, L. I. Krishtalik, and R. R. Dogonadze, *J. Electroanal. Chem.* **61**, 241 (1975).
93. R. R. Dogonadze and A. M. Kuznetsov, *Elektrokhimiya* **7**, 172 (1971); M. A. Vorotyntsev, R. R. Dogonadze, and A. M. Kuznetsov, *Elektrokhimiya* **7**, 306 (1971).
94. M. A. Vorotyntsev and A. M. Kuznetsov, *Elektrokhimiya* **6**, 208 (1970).
95. L. I. Krishtalik, V. M. Tsionsky, and G. E. Titova, *J. Res. Inst. Catal. Hokkaido Univ.* **22**, 129 (1974).
96. L. I. Krishtalik, *Electrochim. Acta* **13**, 715 (1968); L. I. Krishtalik and V. M. Tsionsky, *Elektrokhimiya* **5**, 1019, 1184, 1502 (1969).

2

Molecular Aspects of Quantum Electrode Kinetics

SHAHED U. M. KHAN and JOHN O'M. BOCKRIS

1. Introduction

The quantum mechanical theory of electrode kinetics has been developed in recent time in two entirely different ways. One is the molecular and mechanistic theory orginated by Gurney(1) as early as 1931. This molecular approach was further developed by Butler,(2) Gerischer,(3,4) Christov,(5–7) Bockris *et al.*,(8–12) Schmickler,(13,14) and Khan *et al.*(15) The other is the continuum and nonmechanistic theory originated by Weiss(16) and Libby(17) and importantly developed by Marcus.(18) Levich *et al.*(19–23) were the first to develop this theory at a quantum mechanical level.

In several recent investigations,(24–30) some striking inconsistencies in the continuum theory of quantum electrode kinetics with respect to experimental results have been pointed out.

For example, Levich and co-workers(19–23) put forward a polaronic energy transfer mechanism (which is applicable firstly in solid crystals) for the activation of ions in solution, the object being to explain the continuity in the current–potential relation. This is because in their view, the vibrational–rotational levels of ions in solution remain separated by the same amounts as in the gas phase. However, this objection is not cogent. Thus, the results of Moore *et al.*(31) show that there are enough translator frequencies in water to justify a model in which liquid water contains a sufficient number of free

---

SHAHED U. M. KHAN and JOHN O'M. BOCKRIS • Department of Chemistry, Texas A&M University, College Station, Texas 77843.

water molecules having an energy distribution corresponding to those of translators, to justify the assumption of a continuum of available levels in solution. Liquid water shows much line broadening, and some of the frequencies making up such broadened peaks correspond to those of translators. In general, the situation of vibrational–rotational levels of ion–solvent bonds in solution is smoothed out, owing primarily to the collisional interaction with the translators in liquid water solvent.

Levich *et al.*$^{(19-23)}$ also suggested that the energy of the individual particle contributing to activation must be less than kT in order to avoid the difficulty of the discreteness of the levels which they thought existed in solution. On this basis, polaronic energy transfer from the solvent librator (which has an energy of less than kT per particle) was thought essential. They also thought that the fraction of particles having energy greater than kT would be too small to be of interest in providing energy for the activation of ions in solution. However, the fraction of particles needing to be in an activated state at any time for a typical electrode reaction (e.g., one having a current density of 10^{-3} A cm^{-2}) is around 10^{-15}, and this amount of activated species in solution can be easily available by the transfer of translational and vibrational energy of solvent molecules.

Hence, a polaronic type of energy transfer mechanism may not be necessary. The polaron is a clear concept in a crystal, but in a liquid the lack of order and periodicity over distances which would be involved in the model suggested by Levich makes efficient energy transfer by this means, over distances above some 10 Å, difficult to accept.

The typical energy of a librator is about 0.001 eV, and so to activate a particle by 1 eV, the cooperation of energy of many solvent librators was suggested,$^{(19-23)}$ without calculation of the frequency with which such fluctuations would occur. Such a calculation is important to establish the validity of this continuum activation approach.†

The current–potential relation given by continuum treatment$^{(19-23)}$ does not give rise to any region of potential which corresponds to Tafel's law, $i = i_0 e^{-\beta\eta F/RT}$, although this is uniformly observed in electrode kinetics. This is because, in the continuum expression of current density, the overpotential appears as a square term. Substantial Tafel linearity (up to eight orders of magnitude in some cases) is noted for *all* electrode reactions, including redox reactions.

The central difficulty of acceptance of the expression for the free energy of activation in the continuum theory (cf. Marcus$^{(18)}$) is that it takes into consideration only the Born part of the many-component solvation energy.

---

† The earlier calculations of Bockris and Sen$^{(32)}$ have a frequency with which a special fluctuation of the *outer* solvent sheath occurred at far less than that needed to support typical current densities. The calculation involved fluctuation theory, but the formalism involved the implicit assumption that $(E_{\text{act}} - \langle E \rangle)$ was $<kT$ (where $\langle E \rangle$ represents average energy), and this is insufficiently general for the calculation to be determinative.

The Born part is less than half the total solvation energy. The ion dipole and other multipole interactions should certainly be taken into account.

Bockris, Khan, and Matthews(27) pointed out that if one plots the value of $\Delta F^{\circ\ddagger}$, calculated on the solvent fluctuation theory for a number of redox reactions in solution, against the corresponding value, calculated from experiment, with the transmission coefficient assumed to be unity, one obtains no correlation, except that the values theoretically predicted are generally below those observed experimentally.

Bockris *et al.*(27) showed that agreement between theoretical and experimental free energy of activation is, however, observed if the stretching contribution (cf. George and Griffith(33)) of the inner coordinated bond is added to the continuum electrostatic contribution.† Fair correlation is observed between theory and experiment for a number of redox reactions, if the outer sphere solvation energy is completely neglected, and the stretching component only taken into account. Hence, concentration on the use of only the continuum expression for the free energy of activation is unrealistic, since no agreement with experiment is observed when it alone is used.

Conway and Currie(34) made a study of the redox reaction, $Fe(CN)_6{}^{3-}/Fe(CH)_6{}^{4-}$, with varying pressure on an electrode, and determined the volume of activation from the pressure, P, dependence of the log $(i)_v$. The observed volume of activation, ΔV^*, corresponds to changes of volumes principally in *short*-range solvent interaction. This conclusion is consistent with an activation process which occurs mainly in the neglected inner shell.

Sahami and Weaver(35) have determined redox reaction rates involving $Co(CN)_3{}^{3-}$, $Co(NH_3)_6{}^{3-}$, and $Co(NH_3)F^{2+}$ complexes in different nonaqueous solvents. They have also obtained up to 10^5 times *decrease* in the reaction rates when transferring from aqueous solutions to those in DMF, DMSO, and NMF. If one puts the value of $(1/\varepsilon_{op} - 1/\varepsilon_s)$ in the Bornian equation for the free energy of activation as 0.5, 0.46, and 0.44 for solvents, H_2O, DMF, and DMSO, respectively, one gets a predicted *increase* in rate constant by five times in DMF and ten times in DMSO compared to those in H_2O.

The optical dielectric constant of water and deuterium oxide is the same, so that, if the Bornian view dominated (as assumed by those whose theoretical concepts follow those originally suggested by Marcus(18)), one would find the reaction rate unchanged by transfer upon aqueous solution to those in deuterium oxide. Weaver, Tyma, and Nettlesky(36) found that the ratio of the rate constants was 2, as an average for several redox reactions.

The Tafel relation predicted by the continuum Bornian view differs even qualitatively from experiment: it should pass through a maximum when $(e_0\eta_c + \Delta F^\circ) > E_s$ and $\eta_c^{\max} = -(\Delta F^\circ + E_s)/e_0$.(30) The condition for Tafel linearity over a significant potential range for the Bornian expression(21) is

---

† This possibility is allowed for in Marcus's paper of 1965,(18) but unfortunately, in the succeeding decades, attention among the users of this work has concentrated upon the dielectric term of 1956 paper.(18) The very large number of publications from the school of Levich and Dogonadze even stressed the absence of a vibrational contribution.

$$(\Delta F^0 + e_0\eta_c)/2E_s \ll 1 \tag{1}$$

where ΔF° is the free energy of reaction, η_c is the cathodic overpotential, and E_s is the solvent reorganization energy. This inequality is seldom observed(37) (Table 1).

Some insight into the nature of E_s can be obtained from the relation from the Bornian view which relates i to η_c.

Thus

$$i = A \exp\left[\frac{-(E_s + \Delta F^\circ + e_0\eta_c)^2}{4E_skT}\right] \tag{2}$$

Hence

$$-\frac{kT\partial^2 \ln i}{e_0\partial\eta_c^2} = \frac{e_0}{2E_s} = \frac{\partial\alpha}{\partial\eta_c} \tag{3}$$

Table 1

Experimental Data to Verify the Applicability of Inequality (31) at Various Overpotentials (0.1 is Considered ≪ 1)

Reaction	ΔF° (eV)	η_c (V)	$\lvert\Delta F^\circ + e_0\eta_c/2E_s\rvert$ for $E_s = 1$ eV	for $E_s = 2$ eV	$\left\lvert\frac{F^\circ + e_0\eta_c}{2E_s}\right\rvert \ll 1$?
$CO^{3+}(aq)/CO^{2+}(aq)$	−1.82	−0.1	0.96	0.48	No
		−0.6	1.21	0.61	
$Fe^{3+}(aq)/Fe^{2+}(aq)$	−0.77	−0.1	0.44	0.22	No
		−0.6	0.69	0.34	
$Fe^{3+}(en)_6/Fe^{2+}(en)_6$	−0.69	−0.1	0.40	0.20	No
		−0.6	0.65	0.32	
$Ru^{2+}(aq)/Ru^{3+}(aq)$	−0.86	−0.1	0.48	0.24	No
		−0.6	0.73	0.37	
$Ag^{2+}(aq)/Ag^{1+}(aq)$	−1.98	−0.1	1.04	0.52	No
		−0.6	1.29	0.65	
$IrCl_6^{-2}/IrCl_6^{-3}$	−1.02	−0.1	0.56	0.28	No
		−0.6	0.81	0.41	
$Ce^{4+}(aq)/Ce^{3+}(aq)$	−1.44	−0.1	0.77	0.39	No
		−0.6	1.02	0.51	
$V^{3+}(aq)/V^{2+}(aq)$	0.25	−0.1	0.07	0.04	Yes
		−0.6	0.18	0.09	
$Cr^{3+}(aq)/Cr^{2+}(aq)$	0.46	−0.1	0.19	0.09	Yes
		−0.6	0.07	0.04	
$Au^{2}(aq)/Au^{1+}(aq)$	−2.70	−0.1	1.85	0.93	No
		−0.6	1.65	0.83	

However, in experimental fact, the transfer coefficient, α, remains constant in a number of electrode kinetic reactions over many decades.(38–42) If, for example, $\partial\alpha/\partial\eta_c = 0.05$, $E_s > 10$ eV. This is an unrealistic value for E_s.

The above relation (2) for current density, i, arises(43) from a more complete equation in which an expression for the current is obtained by integration from the bottom of the conduction band to $E_F + \Phi$, where E_F is the Fermi energy and Φ is the work function of the metal electrode. A similar expression after integration is reported in a recent work.(44,45)

Tafel's law is applicable to redox reactions(38–42) and other reactions(44–47) with remarkable consistency. In some redox reactions, linearity over six orders of magnitude has been observed(41) (Figure 1).

Dogonadze, Kuznetsov, and Levich(19–23)(DKL) treat proton transfer in the same way (i.e., in terms of continuum solvent fluctuation) as that for simple electron transfer reactions, where no breakage or formation of bonds is involved. The reaction takes place only as a result of *continuum solvent polarization fluctuation* without taking into consideration the stretching of the H–OH$_2$ bond and is not connected with the thermal heat sink, which is supposed to give the activated states in other theories.

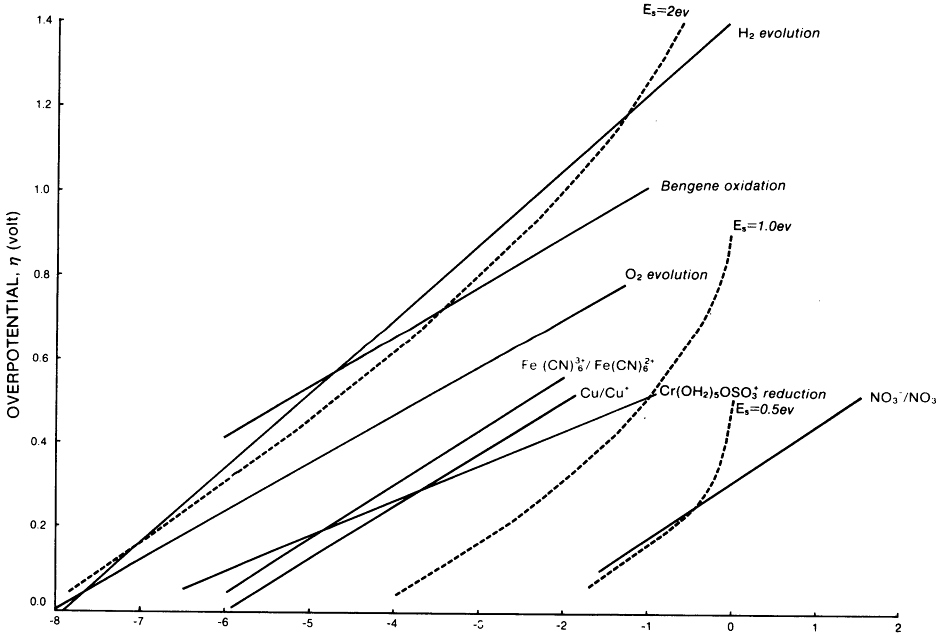

Figure 1. Tafel plots for different reactions: reduction of benzene,(39) oxidation of Cu in solid electrolyte,(40) reduction of $Fe^{3-}(CN)_6$,(32) H_2 evolution reaction,(36,37) O_2 evolution reaction,(38) $Cr(OH_2)_5OSO_3^+$ reduction,(35) and the theoretical plots from the continuum theory expression (----) for various E_s values, i.e., 0.5, 1.0, and 2.0 eV.

Correspondingly, the levels which are supposed to give rise to proton transfer in the DKL view are the lowest levels, i.e., the ground vibrational states of the H–H_2O bond, because the other states are higher, and thus less likely to be activated. Here, DKL involve themselves in the concept that particles which undergo reaction are those which are *most frequently* present and that an activated particle cannot be involved in a reaction mechanism, because it is too infrequent.

In terms of the above model that only the ground state protons take part in the reaction process, DKL thought only the dipoles of the medium are important for the activation process, because during libration the librators perform classical fluctuation ($E_{\text{lib}} < kT$). The number of protons activated above the ground state is small in number and DKL neglected them. A motion effected by the heat sink of the solution occurs only along the solvent coordinate, q, until, owing to a fluctuation of energy *in the outer shell*, the solvent coordinate assumes the value, q^*, corresponding to activated state. Such treatment of the proton transfer reaction cannot explain the absolute straightness of the Tafel line over more than 1 V.†

Christov(48) tried to explain the linearity of the Tafel line for hydrogen evolution, using a harmonic oscillator model having two frequencies, one for the solvent system, ν_x, and the other for the stretching frequency of the H^+–H_2O bond in proton, ν_y (in the case of a redox reaction, ν_y represents the stretching frequency of the inner coordination ion–solvent oscillation), but failed to explain the linearity of Tafel plots.(46,47)

However, Christov(48) clearly pointed out that though a harmonic oscillator model is convenient to use, it greatly overestimates the part played by the solvent in the activation process.

Using two-dimensional models for gas phase reactions of the type $AH + B \rightarrow HB$, it has been shown(47) that there is a considerable stretching of the A–H bond in the transition region. It seems reasonable to assume that this situation takes place in proton transfer in solution, too.

There are, therefore, fundamental and serious inconsistencies in the continuum (solvent fluctuation) approach. Thus, in this chapter, concentration is made on the molecular and mechanistic theory of quantum electrode kinetics and its recent, but limited, development.

2. Correlation between Electrochemical Electron and Spectroscopic Photon Transfer Process

We shall discuss(49,50) here the existence of a fundamental equivalence between the spectroscopic photon emission or absorption and electrochemical electron emission or absorption at the electrode–solution interface.

---

† It is not cogent to say that the oscillations may not be, in fact, harmonic. Thus, in the DKL model, the oscillations considered are around the ground state and, hence, harmonic in nature.

Spectroscopic photon emission and absorption processes have been interpreted in terms of time-dependent perturbation theory.(51–53) The processes of electron emission from an electrode to an acceptor in solution, and the converse processes of electron emissions by particles in solution to the electrode, show phenomenological similarity to the spectroscopic ones.

Figures 2a and 2b show similarities in the dependence of the intensity of absorption upon the energy of photons and electrons, respectively. The spectroscopic intensity increases as a function of the photon energy, and passes through a maximum (Figure 3a). The electrochemical current density increases with electron energy and at sufficiently high energy (corresponding to high applied potential) reaches a point at which its further increase is lessened but does not decline(53,54) (Figure 3b).

These observations may be interpreted in terms of time-dependent perturbation theory.(49,50) The probability of transition can be expressed as(51)

$$P_T = \left| \frac{1}{i\hbar} \int_0^t U_{fi}^0 \exp(i\omega_{fi} t)\, dt \right|^2 \tag{4}$$

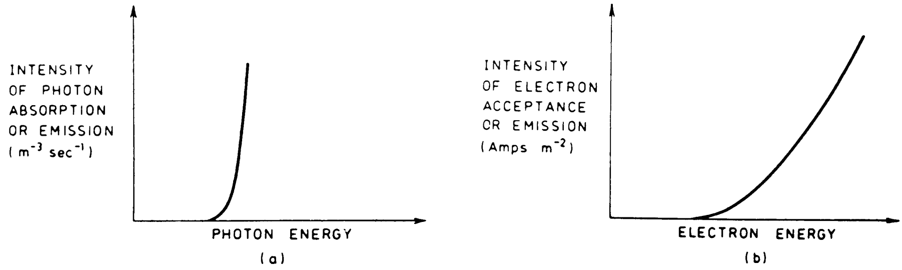

Figure 2. The initial trend of increase in absorption and acceptance of photons and electrons as a function of their respective energies. (a) Increase in intensity of photon absorption or emission with photon energy. (b) Increase in intensity of electron acceptance or emission with electron energy.

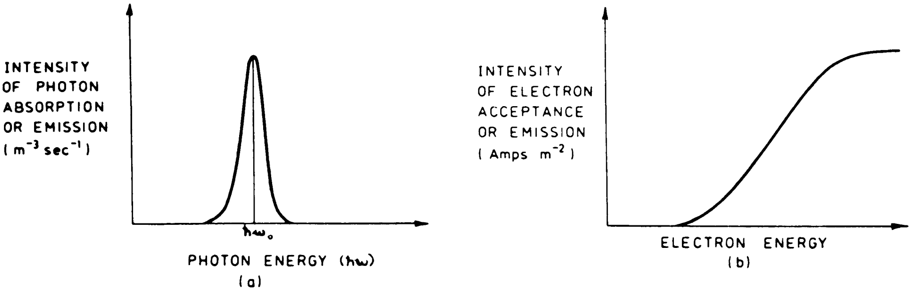

Figure 3. The intensity of absorption and acceptance of photons and electrons as a function of their respective energies. (a) Intensity of photon absorption or emission with photon energy. (b) Intensity of electron acceptance or emission with electron energy.

Using Eq. (4), we can express the intensity–energy relation of spectroscopic absorption as(29,49,50)

$$I = \frac{P_T}{t} N_0 \exp\left(-v\hbar\omega_0/kT\right)$$

$$= \frac{(U^0_{fi}(x))^2 t}{\hbar^2} \frac{\sin^2\{[(E_t - E_i - \hbar\omega)/2\hbar]t\}}{[(E_t - E_i - \hbar\omega)/2\hbar]^2 t^2} N_0 \exp\left(-v\hbar\omega_0/kT\right) \tag{5}$$

where the transition moment matrix $U^0_{fi}(x) = \langle\psi_f|e_0F_0x|\psi_i\rangle$ has the initial state wave function, ψ_i, and the final state wave function, ψ_f, t is the short perturbation time of the process, v is the vibrational quantum number, N_0 is the number of molecular bonds in their ground vibrational quantum state, and ω_0 is the frequency of the photon absorbing bonds. A plot of Eq. (4) against ω indicates the ideal nature of the spectroscopic intensity–energy relation (Figure 3a), which depends upon the fact that the transition moment matrix is independent of ω.

In the corresponding electrochemical case, the electron transition across the metal–solution interface involves a non-time-dependent and nonoscillating perturbing energy.(54)

$$U^0(r) = e_0X_0r \tag{6}$$

where e_0 is the electronic charge, X_0 is the field across the electrode–solution interface, and r is the distance across which the electron travels between the electrode and the acceptor.

Substitution of Eq. (6) into Eq. (4) gives the probability of an electron transition across an interface as

$$P_T = \frac{4(U^0_{fi}(r))^2}{\hbar^2} \frac{\sin^2 \frac{1}{2}\omega_{fi}t}{\omega^2_{fi}} \tag{7}$$

from which the probability of transition passes through a maximum at $\omega_{fi} = 0$.

Thus, Eq. (7) gives the proof of a suggestion made initially by Gurney in 1931(1) concerning the radiationless transition of the electron at interface between the states of equal energy in the electrode metal and in ions in solution.

The intensity of electron transition, i.e., the electrochemical cathodic current density, can be expressed with the use of Eqs. (4), (6), and (7) as(29,49,50)

$$i = \frac{2\pi e_0}{\hbar} |U^0_{fi}(r)|^2 \rho(E_F)F(E_F)N(E_g)$$

$$\times \exp\left[-\beta(E_g + e_0\eta_c - E_F)/kT\right] \tag{8}$$

where $U^0_{fi}(r) = \langle\psi_f|U^0(r)|\psi_i\rangle$ is the matrix element of transition, $\rho(E_F)$ is the density of the final electronic states per unit energy, and $F(E_F)$ is the Fermi function. E_g is the ground state energy of the acceptor, and β is the so-called electrochemical symmetry factor(54) having the range, $0 < \beta < 1$, the significance of which is connected to the force constants of the bonds involved in the reaction. E_F is the energy of the electron and corresponds to the Fermi energy in the metal. The exponential nature of the electrochemical current density–overpotential relation follows from Eq. (8) (Figure 3b).

The origin of the difference in shape of the spectroscopic and electrochemical diagrams (Figures 3a and 3b) lies in differences in expressions (5) and (8); the spectroscopic transitions are from a lower to a higher vibrational state (e.g., for infrared spectra in solution), and hence, the vibrational quantum number, v, and the selection rule of transition, $\Delta v = 1$, are involved. In the electrochemical case, electron transfer is not a transition from a lower to a higher state. Thus, there is no selection rule involved in the electrochemical process [i.e., no zero value of the transition matrix of Eq. (8) can occur], and electrons from the metal electrode can undergo transition to any energy states of the acceptor in solution.

In solution, the collisional interactions cause a blurring of the vibration–rotational states so that there is a semicontinuum of these states.(1) This fact, together with the absence of a selection rule, causes the fulfillment of the Gurney condition at any energy, whereas the Bohr condition applies only for the situation where the transition moment is nonzero. The smooth relation between current density and overpotential, known as Tafel's law,(54) (in contrast to the peaked nature of the intensity–energy situation in spectroscopic phenomena) arises, therefore, from a combination of the absence of selection rules in the electrochemical case, and the presence in solution of a semicontinuum of acceptor and emitter states.

3. Applicability of Time-Dependent Perturbation Theory for Electron Transfer Processes at Electrodes

Several quantum mechanical calculations have been made for electron transfer processes between metals and atoms or ions(55–58) in gaseous medium. In all the cases, the considerations concern the transition of electrons from a metal state to a bound atomic state or to a free continuum state or vice versa. The calculations of transition probabilities in the cited works have been based on "Fermi's golden rule" of time-dependent perturbation theory. However, it was pointed out by Gadzuk(59) that the use of the golden rule usually presents a difficult problem if an estimate of the transition probability is desired, because it requires evaluation of a matrix element: one must specify initial and final state (wave functions) and an interaction. This is not as straightforward as it seems. In a transition, e.g., between an atomic and a conduction band metal state, the initial and final states are eigenfunctions of different Hamiltonians. It seems meaningless to evaluate matrix elements, if the initial and final states are solutions of different Hamiltonians.

The problem stems from the fact that the initial and final states are not orthogonalized, so that a perturbation cannot induce transitions between the metal and atomic states in the solution.

Gadzuk,(59,60) however, has shown a way around this problem. Thus, the transition matrix between states which are, indeed, not the eigenfunctions of the same Hamiltonian and consequently are nonorthogonal can be expressed as

$$M_{if} = \langle X_f | 1 - P_i | U_i^{\text{pert}} | X_i \rangle \tag{9}$$

where P_i is the operator that projects onto the initial state, i, U_i^{pert} is the perturbation when the system is in the initial state, and X_i and X_f are the initial and final state vectors.(43) The operator projecting onto the initial state is given by

$$P_i = |X_i\rangle\langle X_i| \tag{10}$$

Thus, Eq. (9) becomes

$$M_{if} = X_f | U_i^{\text{pert}} | X_i \rangle - \langle X_f | X_i \rangle \langle X_i | U_2^{\text{pert}} | X_i \rangle \tag{11}$$

There is a complete set of states which form a basis for the full Hamiltonian. The completeness is stated by summing over all the products of any state, b, i.e.,

$$\sum_b |b\rangle\langle b| = 1 \tag{12}$$

where the sum becomes an integral if the states are sufficiently close. One might expect that an adequate representation of an atom metal state can be formed by some linear combination of atom and metal state vectors. Thus, summing over all states of the full Hamiltonian can be represented by summing first over all atomic and then over all metal states, and this summation completely spans the Hilbert space. Hence, the sum in Eq. (11) should be taken over all metal and atom states. Using Eq. (12) in Eq. (11), one gets

$$M_{if} = \sum_{a,m} \langle X_f | b \rangle \langle b | U_i^{\text{pert}} | X_i \rangle - \langle X_f | X_i \rangle \langle X_i | U_i^{\text{pert}} | X_i \rangle \tag{13}$$

Gadzuk(59,60) considered the initial state of electron as being in the metal state, ψ_m, in the surface region, and the final state as the electron state, ψ_a, in the ion or the atom. The perturbing potential between these states was taken as the Coulomb potential, $-q^2/r$, of the ion core for a model of adsorption of atoms on a metal surface. With these considerations, Gadzuk obtained the matrix element from Eq. (13) as

$$M_{if} = \left\langle \psi_a \left| \frac{-q^2}{r} \right| \psi_m \right\rangle + \sum_{j \neq m} \left\langle \psi_j \left| \frac{-q^2}{r} \right| \psi_m \right\rangle \langle \psi_a | \psi_j \rangle \tag{14}$$

Thus, the single matrix element, i.e., the first term in Eq. (14), is the contribution due to orthogonalization. To use only the first term in Eq. (14) as the only term for the transition matrix, it is necessary to show that the second term in this equation is zero or gives negligible contribution to the transition matrix, M_{if}. It was, however, shown by Gadzuk that the sum of the matrix element in Eq. (14) (i.e., the second term) *is* zero, i.e.,

$$\sum_{j \neq m} \left\langle \psi_j \left| \frac{-q^2}{r} \right| \psi_m \right\rangle \langle \psi_a | \psi_j \rangle = 0 \tag{15}$$

for the basis, ψ_j, of the following reasonable form, i.e.,

$$|\psi_j\rangle = \frac{1}{\sqrt{n}} \sum_{R_e} e^{ik_j R_j} |a_j, R_j\rangle \tag{16}$$

where $|a_j, R_j\rangle$ is the localized function centered on the lattice site, R_j, of the metal.

Thus, one notices that the use of the first term of Eq. (14) can be used as the transition matrix at the metal–solution interface.

4. Proton Transfer at Interfaces

4.1. Gurney's Quantum Mechanical Model of Proton Transfer

We contrast the molecularly oriented Gurney theory(1) with the continuum dielectric theory, originated by Weiss(16) and Libby(17) and followed by others.(19–23) In proton transfer process, Gurney(1) formulated the rate of electron transfer in terms of a WKB approximation. The model was connected with bonding of the proton to its surrounding solvation sheath. Activation processes considered by Gurney were not associated primarily with the *outer*-shell solvation energy. There is a very distinct difference between Gurney's viewpoint and that of Libby,(17) which treated only Bornian influences. The Gurney model laid stress on the existence of *classically* distributed states in solution, and introduced the symmetry factor, β, which was clearly defined in terms of the potential–energy–distance relations, to control the probability of acceptance of tunneled electrons. The cooperative preliminary fluctuation needed in the Bornian view is not needed. Gurney asserted the smoothed-outness of the vibrational levels for the proton in solution. Spectroscopic contributions made later by Ackerman and Moore *et al.*(31) as by Rudolph and Zimmerman,(62) all confirm quasicontinuum vibrational levels in H_3O^+ from the spectroscopic evidence.

4.2. Butler's Modification of Gurney's Model

An important contribution was made by Butler(2) in 1936. Butler(2) realized that the theory of Gurney did not give reasonable values of the heat of activation, and realized the essential reason, namely, that Gurney did not consider the chemical bonding of hydrogen to the electrode. In the Gurney model, hydrogen atoms were left neutralized as free hydrogen atoms a few angstroms from the electrode. The formation of a bond with the metal substrate is needed to reduce the energy of activation to a reasonable range.

Butler's modification of Gurney's quantum mechanical theory(1) gave rise to the underlay of electrocatalysis, because, with charge transfer as the rate-determining process in proton transfer, the major point about the electrocatalytic aspect is its bonding to hydrogen. Such views (a forerunner of which was the qualitative theory of Horiuti and Polanyi(63)) became the basis of many concepts of electrocatalysis, beginning in the 1960s.(64)

4.3. The Quantum Character of Proton Transfer

Bockris and Matthews(12) measured the separation factor at −71°C by using concentrated HCl solutions. During this work, they accidentally observed an important effect, namely, the considerable variation of the separation factor with potential (Figure 4).

The quantum mechanical correction of separation factor was determined later(59) using the relation

$$\Gamma = \frac{S_q}{S_c} \tag{17}$$

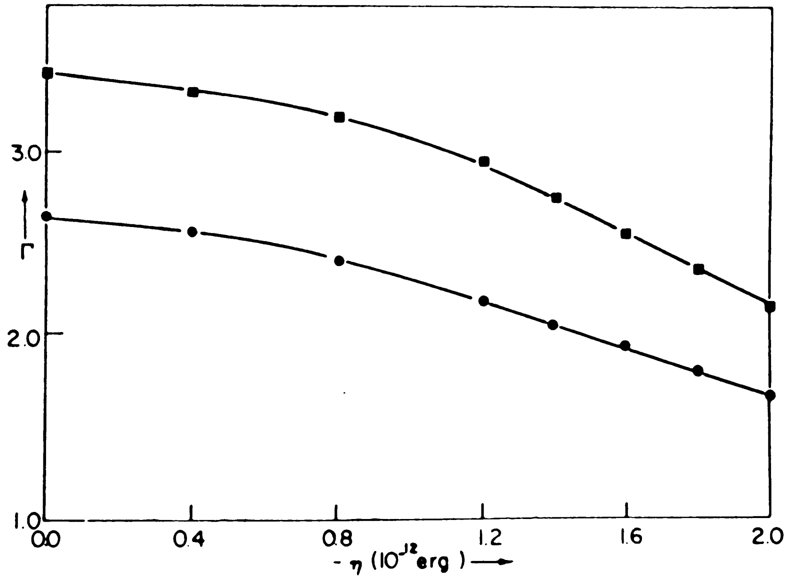

Figure 4. The dependence of Γ on potential. $A_0 = 0$, $T = 298$ K, $2d = 4.0$ Å, $\varepsilon_0^* = 1.0$ eV, ● = $\Gamma_{H,D}$ and ■ = $\Gamma_{H,T}$.

where S_q and S_c are the quantum mechanical and classical separation factors, respectively. S_q for protium–tritium can be expressed as

$$(S_q)_{\mathrm{H,T}} = \frac{\tau_{\mathrm{H}}}{\tau_{\mathrm{T}}}(S_c)_{\mathrm{H,T}} \tag{18}$$

where τ_{H} and τ_{T} are the quantum mechanical transmission coefficients for proton and tritium transfer, respectively.

τ can be defined as

$$\tau = \frac{i_q}{i_c} \tag{19}$$

where i_q and i_c are quantum mechanical and classical rates of electrochemical electron transfer for the discharge step.

One may write i_q as

$$i_q = k_1 C_{\mathrm{H}^+} \int_{E_0}^{\infty} P_T(E) \exp[-(E - E_0)/kT]\, dE \tag{20}$$

where k_1 is a frequency factor, $P_T(E)$ is the probability of proton tunneling at energy level, E, and E_0 is the zero point energy level for the $\mathrm{H^+{-}OH_2}$ bond stretching.

Equation (20) reduces to the classical current, i_c, in the limit of low and wide barriers. Thus

$$i_c = k_1 C_{\mathrm{H}^+} \int_{E^\ddagger}^{\infty} \exp[-(E - E_0)/kT]\, dE \tag{21}$$

where $E^\ddagger$ is the energy of the barrier maximum.

Using Eqs. (20) and (21) in Eq. (19), one gets

$$\tau = (kT)^{-1} \exp[(E^\ddagger - E_0)/kT]J \tag{22}$$

where

$$J = \int_{E_0}^{\infty} \exp[-(E - E_0)/kT] P_T(E) dE \tag{23}$$

Using Eqs. (17) and (18), one gets

$$\Gamma_{\mathrm{H,T}} = \frac{\tau_{\mathrm{H}}}{\tau_{\mathrm{T}}} \tag{24}$$

From Eqs. (22) and (24)

$$\Gamma_{\mathrm{H,T}} = \frac{\exp[(E_{0,\mathrm{T}} - E_{0,\mathrm{H}})/kT] J_{\mathrm{H}}}{J_{\mathrm{T}}} \tag{25}$$

To find Γ, one needs to evaluate J_{H} and J_{T}, and these terms involve tunneling probability factor $P_{\mathrm{T}}(E)$. The tunneling probability, $P_{\mathrm{T}}(E)$, for the unsymmetrical Eckart barrier is given by

$$P_T(E) = \frac{\cosh 2\pi(\lambda + \mu) - \cosh 2\pi(\lambda - \mu)}{\cosh 2\pi(\lambda + \mu) + \cosh 2\pi\sigma} \tag{26}$$

where

$$\lambda = (d/\hbar)(2mE)^{1/2} \tag{27}$$

$$\mu = (d/\hbar)[2m(E - A)]^{1/2} \tag{28}$$

$$\sigma = \tfrac{1}{2}[(2md^2B/\hbar)^2 - 1]^{1/2} \tag{29}$$

$$A = A_0 - e_0\eta, \qquad A_0 = \text{heat of reaction at } \eta = 0 \tag{30}$$

$$B = 4(E_0^{\ddagger} + \beta e_0\eta) \tag{31}$$

and $2d$ is the width of the barrier.

Equation (26) on simplification gives

$$P_T(E) = \frac{\exp[2\pi(\lambda + \mu - \sigma)] - \exp[2\pi(\lambda - \mu - \sigma)] - \exp[-2\pi(\lambda - \mu + \sigma)]}{\exp[2\pi(\lambda + \mu - \sigma)] + 1} \tag{32}$$

From the computed values of J for protium, deuterium, and tritium, the value of Γ was calculated according to Eq. (22) with the use of Eq. (32) for $P_T(E)$. The dependence of Γ on potential is given in Figure 4. This work,(12) therefore, shows the importance of the potential effect of the separation factor upon the quantal character of proton transfer and the helpful effect of such studies upon the calculation of barrier height and shape.

4.4. Degree of Validity of the WKB Tunneling Probability Expression for Proton Transfer

The question of the degree of validity of the WKB method was examined by Sen and Bockris.(66)

Consider a square barrier as is shown in Figure 5. The wave functions may be represented by

$$\begin{aligned} \psi_{\mathrm{I}} &= a_{1i}\exp(ik_1x) + b_{1f}\exp(i_{k1}x) \\ \psi_{\mathrm{II}} &= a_{2i}\exp(-k_2x) + b_{2f}\exp(k_2x) \\ \psi_{\mathrm{III}} &= a_{3i}\exp(ik_3x) + b_{3f}\exp(-ik_3x) \end{aligned} \tag{33}$$

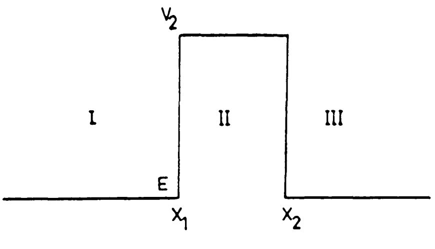

Figure 5. Tunneling through a square barrier.

where k_1, k_2, and k_3 are the wave vectors of the particle in regions I, II, and III, respectively (Figure 5).

There is a solution to the tunneling problem provided by these wave functions. It gives for the transition probability, P_T,

$$P_T = \frac{16k_1^2k_2^2}{(k_1^2 + k_2^2)(k_3^2 + k_2^2)} \exp(-2k_2\omega) \tag{34}$$

where $\omega = (x_2 - x_1)$ is the barrier thickness, and $k_2 = [2m(V_2 - E)/h^2]^{1/2}$ and $k_1 = k_3 = [2mE/h^2]^{1/2}$.

The following wave functions for the electron were chosen:

$$\begin{aligned} \psi_i(x) &= a_{2i} \exp(-k_2 x), \qquad x \le x_1 \\ \psi_f(x) &= b_{2f} \exp(k_2 x), \qquad x \ge x_2 \end{aligned} \tag{35}$$

Using the time-dependent part of the wave function and taking the linear combination, one gets

$$\psi_{\mathrm{II}} = C(t)\psi_i(x)\exp(-iE_it) + d(t)\psi_f(x)\exp(-iE_ft) \tag{36}$$

The substitution of Eq. (36) into the time-dependent Schrödinger equation gives us

$$\begin{aligned} C\exp(-iE_it)H\psi_i + d\exp(-iE_it)H\psi_f &= i\dot{C}\psi_i\exp(-iE_it) + C\psi_iE_i\exp(-iE_it) \\ &\quad + i\dot{d}\psi_i\exp(-E_ft) + d\psi_fE_f\exp(-iE_ft) \end{aligned} \tag{37}$$

initially, the electron is in ψ_i. Hence, we can set $C = 1$, $d = 0$, and $\dot{C} = 0$. The latter condition follows from the normalization condition that $d/dt(CC^* + dd^*) = 0$.

One obtains from Eq. (37)

$$\begin{aligned} i\dot{d}\psi_f\exp(-iE_ft) &= (H - E_i)\psi_i\exp(-iE_it) \\ i\dot{d}\psi_f &= \exp[i(E_f - E_i)t]\int \psi_f^*(H - E_i)\psi_i\,dx \end{aligned} \tag{38}$$

The effective transition probability for tunneling is, therefore,

$$T_{if} = \frac{\hbar^2}{2m}\left(\psi_f^*\frac{d\psi_i}{dx} - \psi_i\frac{d\psi_f^*}{dx}\right)_{x_B} = -i\hbar j_{if} \tag{39}$$

where j_{if} is the current operator. Using Eq. (35) and Eq. (39) gives us

$$T_{if} = (\hbar^2/2m)b_{2f}^*a_{2i} \tag{40}$$

One now obtains b_{2f} in terms of a_{3f}, and a_{2i} in terms of a_{1i}, by solving the standard matching problem at x_1 and x_2 of Figure 5, and introduces them into Eq. (40), obtaining

$$T_{if}^2 = \frac{\hbar^4k_2^2}{m^2}\frac{16k_1^2k_3^2|a_{1i}|^2|b_{3f}|^2}{(k_1^2 + k_2^2)(k_3^2 + k_2^2)}\exp(-2k_2\omega) \tag{41}$$

Using Fermi's golden rule, the current is therefore

$$j_f = \hbar^{-1}|T_{if}|^2\, dn/dE_f \tag{42}$$

where dn/dE_f is the density of states without spin in the transmitted wave at the Fermi level of the metal, and can be written as

$$dn/dE_f = |b_{3f}|^{-2} m/2\pi\hbar^2 k_3 \tag{43}$$

The incident current is therefore

$$j_i = (\hbar k_1/m)|a_{1i}|^2 \tag{44}$$

so that the transition probability becomes

$$P_T = \frac{j_f}{j_i} = \frac{16k_1^2k_2^2k_3^2}{i_1k_3(k_1^2 + k_2^2)(k_3^2 + k_2^2)} \exp(-2k_2\omega) \tag{45}$$

using for j_f the expression resulting from Eqs. (41), (42), and (43). The difference in the preexponential expressions for P_T given by the WKB method [Eq. (34)], and that given by the time-dependent perturbation theory [Eq. (45)], is k_3/k_1. As k_1 and k_3 have the same order of magnitude, the factor k_3/k_1 does not introduce any significant difference.

If the tunneling time is *less* than the fluctuation time of the barrier, the usual tunneling expression will be valid. Sen and Bockris(66) indicated this effect by consideration of the situation in Figure 6. Owing to the permeability of this barrier, there is a splitting in the energy levels in two wells. Let this be represented, energywise, by a δE.

Using the time-dependent Schrödinger equation, one gets

$$\psi = \exp(-iE_0t/\hbar)(\psi_{\text{II}} + \psi_{\text{IV}}) \exp(+i\delta Et/\hbar) + (\psi_{\text{II}} - \psi_{\text{IV}}) \exp(-iEt/\hbar) \tag{46}$$

If the particle is in well II at $t = 0$, it is in well IV at $t = \frac{1}{2}\hbar\pi/\delta E$. The tunneling time can be defined as $\frac{1}{2}\hbar\pi/\delta E$.

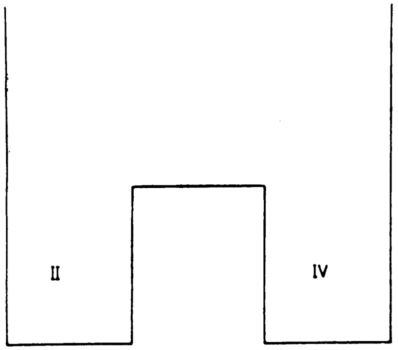

Figure 6. Double-well potential.

The evaluation of the tunneling time depends upon a calculation of δE. To do this, Sen and Bockris$^{(66)}$ utilized an expression, due to Uhlenbeck and Dennison,$^{(67)}$ which is

$$\delta E = \frac{\hbar[2m(E - V)]^{1/2}}{2\pi ml\{\exp[(2\pi l/\hbar)(2m(E - V))^{1/2}]\}^2} \tag{47}$$

where $(E - V)$ is the barrier height, l is the barrier thickness,$^{(68)}$ and m is the mass of the tunneling particle. The magnitude of the tunneling time can be seen in Table 2.

4.5. A Model of Electrochemical Hydrogen Evolution Reaction

Recently, Ovchinnikov and Benderskii$^{(69)}$ gave a quantum mechanical model of the hydrogen evolution reaction at a metal electrode. In this model, they have emphasized the importance of Gurney-based model rather than that of Marcus, Levich, and Dogonadze. However, they tried to combine the principal features of the two models. They have pointed out that transition along the reaction coordinate, rather than the solvent coordinate, was important to explain the Tafel behavior and the constancy of the transfer coefficient.

They considered the hydrogen ion discharge with the formation of adsorbed hydrogen atoms, followed by electrochemical desorption of H_{ads} with the participation of the H_3O^+ ions. But the electron transfer process at the interface, i.e., the tunneling to the reaction complex was considered as the rate-determining step. The tunneling path was considered greater than the Helmholtz layer thickness. The schematic configuration and scheme of reaction complex is shown in Figure 7 for the discharge step.

The probability of electron transfer from metal to the reaction complex is given by

$$W = \int_0^\infty \frac{\chi(E)\theta(E)}{1 + \exp[(E - E_F)/kT]}\,dE \tag{48}$$

Table 2
Data Relevant to Calculation of the Splitting Energy in Proton Transfer$^{(67)}$

Reaction	$(E - V)$ (kcal/mol)	I (Å)	δE (eV)	Tunneling time (sec)	Comments about WKB approximation
1. $CH_2BrC \cdot MePh \cdot H + QEt^-$	22.1	1.59	0.006	1.6×10^{-14}	Valid
2. $RH + D_2O$	13.1	1.26	0.008	1.3×10^{-14}	Valid
3. $RH + F^-$	18.0	1.17	0.090	1.2×10^{-14}	Valid
4. $RH + F\{H_2O + NaBr(5\,M)\}$	24.2	1.46	0.010	1.1×10^{-13}	Doubtful
5. $C_6H_2(NO_2)_3CH_2^- + HOAc$	10.1	1.66	10.060	1.6×10^{-14}	Valid
6. $H_3O^+ + H_2O$			0.12	8.47×10^{-15}	Valid

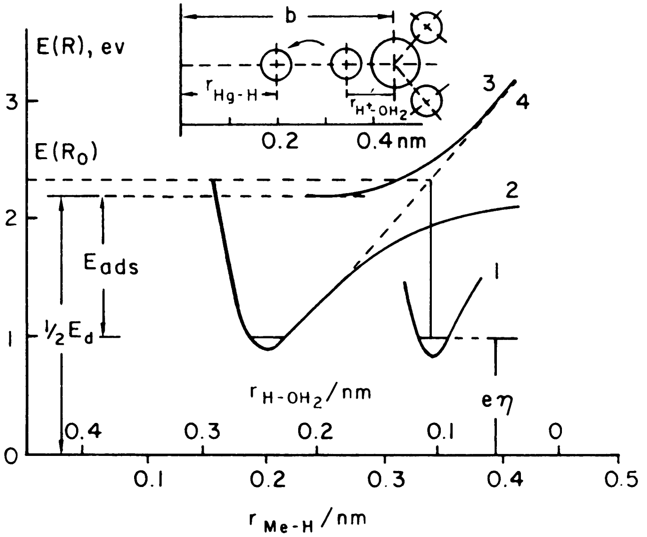

Figure 7. Approximate configuration and scheme of reaction complex terms of discharge step of hydrogen evolution reaction. The equilibrium Hg–H bond length is taken as measured in gas phase (0.18 nm); $r_{H\pm H} = 0.105$ nm. The final state term (dashed line 4) has been plotted as the basis of Morse curve for H_{ads} (curve 2) and H_3O decay curve (curve 3). Electron tunneling length is taken to be 0.45 nm. Curve 1 is the H_3O^+ term.

where $\chi(E)$ is the electron tunneling probability for electrons with energy, E, to a distance of d along the x axis directed normally to the metal surface, $\theta(E)$ is the Frank–Condon factor of this transition, and E_F is the Fermi energy of electrons in the metal.

$\chi(E)$ was calculated on the basis of the general theory of electron tunneling(71) from metal and expressed as

$$\chi(E) = \frac{2\pi}{\hbar} g \int |T_{0,\mathbf{K}}|^2 \delta[E - E(\mathbf{K})] \frac{d^3\mathbf{K}}{(2\pi\hbar)^3} \tag{49}$$

where $T_{0,\mathbf{K}}$ is a matrix element defined by the formula(70)

$$T_{0,\mathbf{K}} = \frac{\hbar^2}{2m} \int (\psi_0 \nabla \psi_{\mathbf{K}}^* - \psi_{\mathbf{K}} \nabla \psi_0^*)\, dy\, dz \tag{50}$$

which accounts for the current through the metal surface plane, $x = 0$, and $g = 2$ is a spin degeneracy factor. The $\psi_0(r)$ and $\psi_k(r)$ are solutions of a three-dimensional Schrödinger equation with an axial-symmetrical potential $V(r)$ (Figure 8), and these wave functions were expressed (for $y = z = 0$) as(70)

$$\psi_{\mathbf{K}}(r) = \sqrt{2} \sin \frac{k_\perp x}{\hbar} e^{ik_\parallel \rho/\hbar} \tag{51}$$

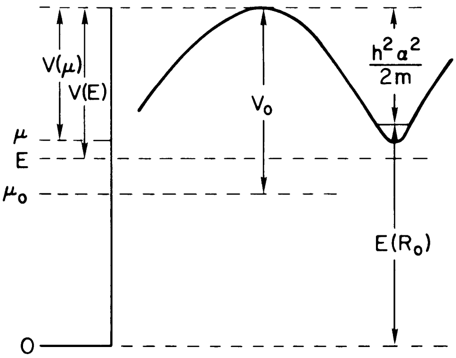

Figure 8. Electron metal-reaction complex tunneling transition barrier, $V(x) = V(r)/y = z = 0$.

In the region, $x = 0$, $\psi_0(r)$ was represented by a quasiclassical formula:

$$\psi_0(r) = C \exp\left(-1/\hbar \int_0^x |P| dx\right) \exp\left(-\rho^2 K/2b^2\hbar\right) \tag{52}$$

where

$$\begin{aligned} \rho &= [2mV(x)]^{1/2} \\ V(x) &= V(r)|_{y=z=0} \\ k &= [2mV(E)]^{1/2} \end{aligned} \tag{53}$$

and the normalization factor, C, was selected from the condition of potential box linking of this function with the electron wave function in the region $x \simeq b$. Expressing $\psi_0(r)$ in the vicinity of $x = b$, $y = z = 0$ as

$$\psi_0(r) = \frac{(\alpha/2\pi)^{1/2} e^{-\alpha r}}{r} \tag{54}$$

the normalization factor, C, can be determined from Eqs. (52) and (54) to be

$$C = \frac{1}{b}\left(\frac{\alpha}{2\pi}\right)^{1/2} \tag{55}$$

where the parameter, α, can be determined by the state of the potential energy curve at $x = b$, such that

$$\frac{\alpha^2\hbar^2}{2m} = V_0 - E(V_0) - E(R_0) \tag{56}$$

where $E(V_0)$ and $E(R_0)$ are shown in Figure 8. Using Eqs. (50)–(56) and carrying out the necessary transformation, one gets

$$|T_{0,\mathbf{K}}|^2 = \frac{4\pi\hbar^4\alpha k_\perp^2}{k^2m^2} \exp\left(\frac{-k_\parallel^2 b}{\hbar\kappa} - \frac{2}{h\int_0^b |P|\, dx}\right) \tag{57}$$

For a model of isotropic electron gas in metal, the momentum integral of Eq. (49) was carried out, and the tunneling probability was expressed as(70)

$$\chi(E) = \frac{2\alpha(2mE)^{1/2}}{m\kappa} \exp\left(-2\hbar \int_0^b |P| dx\right) \tag{58}$$

The Franck–Condon factor, $\theta_0(E)$, along the reaction coordinate, R, is determined using

$$\theta_0(E) = \left|\int \phi_0(R)\phi_E(R)\, d^3R\right|^2 \tag{59}$$

where $\phi_0(R)$ is the initial state vibrational wave function, and $\phi_E(R)$ is the repulsive final state H-atom vibrational wave function.

In a momentum representation, these vibrational, harmonic, oscillator-type wave functions take the form

$$\phi_0(P) = \frac{1}{\pi^{1/4}P_0^{1/2}} \exp\left(\frac{-P^2}{2P_0^2}\right) \tag{60}$$

and

$$\phi_E(P) = \frac{1}{(2\pi\hbar F)^{1/2}} \exp\left[\frac{i}{\hbar F(P^3/6M - EP)}\right] \tag{61}$$

where

$$P_0 = \frac{\hbar}{\delta}$$

$$\delta^2 = \frac{\hbar}{WM_{\mathrm{H}}} \tag{62}$$

F = slope of the potential energy curves

Use of these wave functions from Eqs. (60) and (61) in Eq. (59) gives

$$\theta_0(E) \simeq \frac{1}{[F\delta\pi(1+\nu)]^{1/2}} e^{-a^2} \tag{63}$$

with $a = E(R_0) - E/F\delta$, $\nu = 12ab$, and $b = \hbar\omega/6F\delta$.

Ovchinnikov and Benderskii(69,70) also considered that the continuum solvent coordinates are changed during electron transition and used the Franck–Condon factor, $\theta_P(E)$, due to charge along solvent coordinate, and the total Franck–Condon factor was obtained using the relation

$$\theta(E) = \int_{\infty}^{\infty} \theta_0(E)\theta_P(E)\, dE \tag{64}$$

Thus, using Eqs. (58), (60), (61), and (64) in (48), the transition probability W was determined. Since the authors(69,70) introduced the continuum solvent effect, they end up with an expression of transition probability similar to that of DKL. If they had not included the Franck–Condon factor for continuum solvent coordinate change and also would not have used vibrational harmonic wave function for the bonds, they would get a realistic expression for transition probability, $W(E)$, which would have agreed with Tafel linearity. However, inclusion of the Franck–Condon factor for the transition along the reaction coordinate improved the agreement of transition rate with experimentally observed Tafel linearity.

5. Quantal Aspects of Photoelectrochemical Kinetics

5.1. Photoeffect at Metal–Solution Interface

Brodskii and Gurevich(72–74) developed a quantum mechanical theory of photoemission at the metal–electrolyte interfaces. They have given an expression for the photocurrent which involved the following assumptions:

(a) Photoemission of electrons from the electrode to the electrolyte is the rate-determining step.

(b) The surface of the metal electrode is illuminated by monochromatic light of frequency, ω.

(c) The general expression used for the photocurrent is

$$I_p = \int J_x(E_i, p_{11}, A) f(E_i, E_f) \rho(E_i, p_{11})\, dE_i p_{11} \tag{65}$$

where $j_x(E_i, p_{11}, A)$ is the partial current due to electrons having an initial energy, E_i, and momentum p_{11} and influenced by the electromagnetic field, A. The Fermi distribution function of the initial electrons inside the metal, $f(E_i, E_f)$ and $\rho(E_i, p_{11})$, is the density-of-state function of electrons in the metal electrode.

(d) The partial current (i.e., the photocurrent at a given energy level), j_x, is that due to the electron flow along the x axis normal to the electrode surface and is obtained by using the quantum mechanical expression for flux or current, i.e.,

$$j_x = \frac{e_0 i\hbar}{2m_e}\left(\psi_e \frac{\partial\psi^* e}{x} - \Psi_e^* \frac{\partial\Psi e}{\partial x}\right) \tag{66}$$

(e) The wave function of the electron, ψ_e, is obtained by solving the Schrödinger equation, using the image interaction term only as the potential energy of the electron.

(f) Using the wave function of the electron thus obtained in (66), the expression for the partial current was found by Brodskii and Gurevich(72–75) to be

$$j_x = \frac{P_\alpha}{m_e} |\Lambda|^2 (1 - e^{-P_\alpha/P})^{-1} \tag{67}$$

where

$$P_\alpha = \frac{2\pi e_0^2 m_e}{4h\varepsilon_s} \tag{68}$$

where ε_s is the dielectric constant of the electrolyte medium into which the photoemission of the electron takes place, p is the momentum of the electron, and Λ is a dimensionless constant which depends on the properties of the metal and the interface.

(g) Using the value of j_x from Eq. (67) in Eq. (68), Brodskii and Gurevich(72–74) obtained an expression for the photocurrent as

$$i_p = \tfrac{4}{15}A_0\chi|\Lambda|^2 \frac{\hbar^2}{k_B^2\omega_0^{1/2}}(n\omega_p - \omega_0)^{5/2} \tag{69}$$

where n is the number of photons observed by one electron, k_B is the Boltzmann constant, ω_p is the actual photon frequency, and ω_0 is the threshold frequency (i.e., the minimum frequency required to eject an electron from the electrode).

Equation (69) is obtained under the condition

$$\frac{(\hbar\omega_p - \hbar\omega_0)}{P_\alpha^2/2\omega_e} \gg 1 \tag{70}$$

The condition (70) is satisfied when the dielectric constant of the medium is >10.

In Eq. (69), $A_0 = 4\pi e_0 k_B^2 m_e/(2\pi\hbar)^2$ is a dimensionless function which distinguishes between the behavior of electrons in the metal, described by the ideal Fermi gas model, for which $\chi = 1$.

Equation (69) represents a 5/2 law of photocurrent and is called Brodskii's law.

Brodskii *et al.*(72–74) determined the partial current using the quantum mechanical expression for flux [Eq. (66)], but the wave function used was obtained by solving a Schrödinger equation, using only the image potential of the electron at the metal–solution interface. Thus, Brodskii's model neglects the Coulombic interaction of the electron with ions in the outer Helmholtz plane (OHP) of the double layer, the field effect at the interface, and the solvating effect of the solvent. It is, in effect, a treatment of cold emission in vacuum.

Correspondingly, Brodskii's model, Eq. (69), does not take into account the distribution law for the solvent acceptor states.

Lastly, Brodskii's treatment neglects any account of the interaction of photons with the metal, i.e., it avoids the possibility of understanding the spectral property of metal as a function of frequency. Electron–electron and electron–phonon interactions are neglected. Scatterings in the metal are neglected.(72–75)

A theory of the photoelectrochemical kinetics of the hydrogen evolution reaction at the metal–solution interface was developed by Bockris, Khan, and Uosaki.(76) This theory(76) takes into account photoemission into the solution, the reflective properties of the electrode material, absorption of light by the electron, and the excitation probability from photon–electron interactions, electron–phonon, and electron–electron scattering, the probability of barrier penetration, and the presence of acceptor states and their distribution in solution. The double layer is taken into account in constructing the barrier at the electrode–solution interface.

From this treatment, an expression of photocurrent was obtained as

$$I_p = \frac{e_0 A' C_A}{Q\ C_T}\int_{h\nu}^{\infty}\left[\exp\left(\frac{E_f - e_0 V - E_x}{kT}\right) + 1\right]^{-1} \tag{71}$$

$$\ln\left[1 + \exp\left(\frac{E_f + h\nu - e_0 V - E_x}{kT}\right)\right] P_T(E_x) G(E_x)\, dE_x$$

where the normalization factor Q can be expressed as[76]

$$Q = \int_{h\nu}^{\infty} \rho(E)[1 - f(E)]\rho(E - h\nu) f(E - h\nu)\, dE \tag{72}$$

and tunneling probability expression is

$$P_T(E_x) = \exp\left\{-\frac{\pi^2 l}{h}[2m(U_m - E_x)]^{1/2}\right\} \tag{73}$$

where U_m is the height of the barrier at the interface, and l is the width of the barrier

$$G(E_x) = \exp\left[-\beta(E_g - E_x)/kT\right] \tag{74}$$

where E_g is the ground state energy of the acceptor, E_x is the energy of the photoelectron corresponding to the x component of velocity of an electron, and β is the electrochemical symmetry factor.

This model does not take into account certain secondary effects such as the dependence of I_p on the angle of incidence, the plane of polarization of the radiation, and the effect of different crystal faces of the electrode. It cannot be used to interpret anodic photocurrent at metals in its present form.

Some refinements should be made; for example, the effect of the potential-dependent field at the double layer on the barrier height has not been accounted for.

5.2. Non-Tafel Behavior of the Photocurrent at Metal–Solution Interface

It is well known that electrochemical dark currents follow Tafel's law, but one observes that the photocurrent at the metal–solution interface does not follow it (Figure 9).

For the hydrogen evolution reaction, dark current electrons come from the Fermi level, because, even if the potential is as high as 2 V (vs. the p.z.c.), the Fermi level is still below the ground state of the acceptor H_3O^+ ions, such that the electrons go to it and not to the solvent state. As the acceptor states

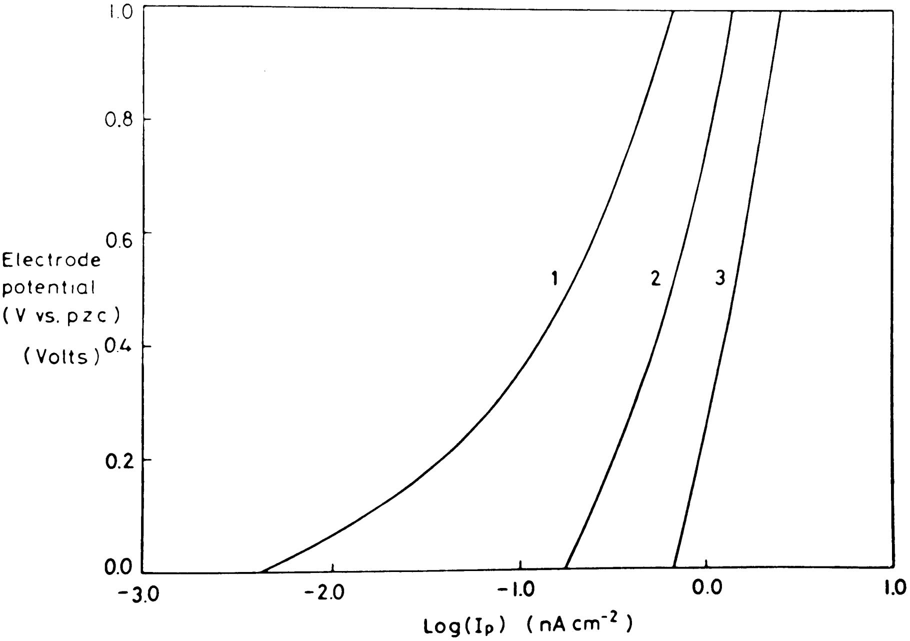

Figure 9. The dependence of the logarithm of the photocurrent I_p on the electrode potential (shows non-Tafelian behavior): (1) $h\nu = 3.0$ eV, (2) $h\nu = 3.5$ eV, (3) $h\nu = 4.0$ eV.

are classically distributed [see Eq. (71)] in solution, one gets an exponential behavior of the dark current with potential [since in Eq. (74), $E_x = E_f - e_0 V$], and therefore the logarithmic Tafel law is followed.

For photocurrents, the photon energy is such that the Fermi electron can be excited to an energy state above the ground state energy of the acceptor (Figure 10). The major contribution to the photocurrent is then due to the photoelectrons which tunnel through the potential barrier, and go to solvent states above the energy of the H_3O^+ states. The number of these states per unit area is not distributed Boltzmannianly, and, hence, the photocurrents do not depend on the availability of exponentially distributed vibration–rotational states in H_3O^+, and accordingly do not follow Tafel law for the exponential dependence of current on potential.

5.3. Photoeffect at Semiconductor–Solution Interface

There appeared several treatments(77–84) of photoeffect at the semiconductor–solution interface which, except few, concentrated mainly on the happenings inside the semiconductor and neglected the properties of the interface and the acceptor or donor ions in solution. These treatments are all classical and hence no discussions are given here.

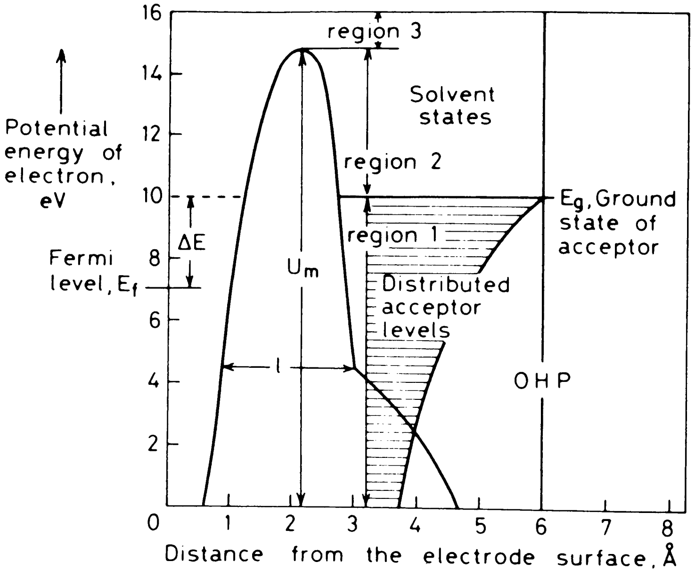
16
14
12
10
8
6
4
2
0
Potential energy of electron, eV
Fermi level, E_f
ΔE
region 3
Solvent states
region 2
region 1
U_m
l
Distributed acceptor levels
E_g, Ground state of acceptor
OHP
1
2
3
4
5
6
7
8
Distance from the electrode surface, Å

Figure 10. The schematic diagram of the barrier for the photoelectron at the metal electrode–solution interface.

A quantal treatment of photoeffect at the semiconductor–solution interface can be obtained using the general expression of the photocurrent of the following form:

$$i_p = e_0 P_{ex}(\omega) \int_{E_c}^{\infty} \delta N_P(x = 0) f(E, h\nu) T(E, h\nu) D_a(E_0, h\nu)\, dE \qquad (75)$$

where e_0 is the electronic charge, $P_{ex}(\omega)$ is the excitation probability of electrons from valence band to conduction band by photon of frequency, ν, δ is the distance between the semiconductor surface and the reaction plane at OHP, and $N_P(x = 0)$ is the number of photoexcited minority carriers per unit volume in the surface region of the semiconductor which arrive from the interior of the semiconductor to this region. $f(E, h\nu)$ is the Fermi distribution of photoexcited minority carrier. This quantity, $N_P(x = 0)$, depends on the intensity, energy, and absorption coefficient of incident light, diffusion length of electron in the semiconductor, and its band gap, etc. Furthermore, it depends on the charge transfer phenomena and the surface recombination rate at the interface. The surface recombination rate constant depends on the induced density of surface states due to adsorbed anions at the electrode–solution interface. The recombination rate constant can be expressed as(77)

$$K_r = \sigma_c \int_{E_c}^{E_v} S_P(E) D_{ss}(E) f_s(E)\, dE \qquad (76)$$

Surface recombination rate constant, K_r, at the interface is one of the most important factors that influence the overall rate, and this quantity depends mainly on the density of surface states, $D_{ss}(E)$ and can be determined quantum mechanically, using the Anderson Hamiltonian formalism.(85,86) In this expression (76), σ_c is the recombination cross section. The value of σ_c can be obtained using the scattering theory. $S_P(E)$ is the velocity of photoexcited electron, and $f(E)$ represents the distribution of surface states which one may consider to be of Gaussian type of distribution, centered at the midgap energy.

In Eq. (75), $T(E, h\nu)$ is the transition rate which determines the fraction of the photocarriers that can transfer across the interface and join an electronic state in an ion in solution per unit time.

In Eq. (75), $D_a(E_0, E, h\nu)$ is the density of the electronic acceptor state in solution, which depends on the ground electronic energy, E_0, of the ion corresponding to the ground vibrational–rotational state of the ion–solvent bond. They can be expressed in terms of a Maxwellian distribution, i.e.,

$$D_a(E_0, E, h\nu) = \frac{\partial N_a(E_0, E, h\nu)}{N_a^0 \partial E} = \frac{\beta}{kT} \exp\left[-\frac{\beta(E_0 - h\nu - E)}{kT}\right] \tag{77}$$

where N_a^0 is the concentration of the acceptor ions at $E = E_0$.

Thus, to have a proper estimate of photocurrent from expression (75), it is desirable to calculate the transition probability, $T(E, h\nu)$, using the time-dependent perturbation theory. The general expression of $T(E, h\nu)$ in terms of Fermi's golden rule of time-dependent perturbation theory is:(29,87)

$$T(E, h\nu) = \frac{2\pi}{\hbar} |\langle \psi_f(r) V'(r) | \psi(r) \rangle|^2 \rho(E_f) \tag{78}$$

where $\hbar$ is the Planck's constant divided by 2π, $\psi_i(r)$ and $\psi(r)$ are, respectively, the wave functions of photoexcited electrons in the initial state in the semiconductor conduction band, and final state in the acceptor ion in solution (after electron transfer). $V'(r)$ is the perturbing potential at the interface, and $\rho(E_f)$ is the density of final state. The excitation probability of the electron from the valence band to the conduction band due to the interaction of electromagnetic field of light can be expressed as(88)

$$P_{ex}(\omega) = \frac{2\pi\tau}{\hbar} |\psi_{CB}(r), n_\lambda - 1 \cdots |H'| \psi_{VB}(r), n_\lambda \cdots|^2 \rho(\omega) \tag{79}$$

where $\psi_{CB}(r)$ and $\psi_{VB}(r)$ are, respectively, the wave functions of electrons in the conduction band and valence band. n_λ and $n_\lambda - 1$ are, respectively, the intensity of incident and transmitted photons, $\rho(\omega) = \omega^2 V/(2\pi C)^3 h$ is the number of states of the radiation field in the volume, V, per unit energy interval and per unit solid angle, and τ is the short time of perturbation.

The Hamiltonian, H', which represents the interaction between the electron and the radiation, can be expressed as

$$H' = \frac{e_0}{mc}(\mathbf{A} \cdot \mathbf{P}) + \frac{e_0^2}{2mc^2}\mathbf{A}^2 \tag{80}$$

where **A** is the vector potential of electromagnetic radiation field, and can be expanded in plane waves and expressed as

$$A = \sum_{\lambda} (b_\lambda A_\lambda + b_\lambda^+ A_\lambda) \tag{81}$$

with

$$A_\lambda = \mathbf{e}_\lambda \left(\frac{4\pi c^2}{V}\right)^{1/2} e^{ik_\lambda \cdot r} \tag{82}$$

where $k_\lambda = \omega_\lambda / c$ and $\mathbf{e}_\lambda$ includes the two possible directions of polarization, V is the volume of the normalization cube, and c is the velocity of light. b_λ and b_λ^+ are, respectively, the photon creation and annihilation operator. **P** represents the momentum operator for electron.

Using the properties of creation and annihilation operators, one can express $P_{\mathrm{ex}}(\omega)$ as

$$P_{\mathrm{ex}}(\omega) = \frac{4\pi^2 e_0^2 n_\lambda}{V\omega m_e^2} |\langle \psi_{\mathrm{CB}}(r)\, e^{ik\cdot r}(\mathbf{P}\cdot\mathbf{e})|\psi_{\mathrm{VB}}(r)\rangle|^2 \rho(\omega)\, d\Omega \tag{83}$$

This can be simplified to the following expression, i.e.,

$$\rho_{\mathrm{ex}}(\omega) = \frac{\omega^3 n_\lambda}{2\pi hc^3} |\langle \psi_{\mathrm{CB}}(r)|e^{-ik\cdot r}\mathbf{d}\cdot\mathbf{e}|\psi_{\mathrm{VB}}(r)\rangle|^2 \sin^2\theta\, d\Omega \tag{84}$$

when $\mathbf{d} = e_0\mathbf{r}$ is the electric dipole moment operator of the electron.

In expression (75), $N_P(x = 0)$ can be obtained as a solution of transport equations for the photoelectrons inside the semiconductor. This can be expressed as

$$N_P(x = 0) = \frac{[1 - (t_\nu + R_\nu)]I_0(\nu)}{K_t + K_r + D_e\, e^{-e_0 V_s/kT}/[L_{\mathrm{D}} + P_1(W)]} \times \left[1 - \frac{e^{-\alpha_\nu W}}{(1 + \alpha_\nu L_D)(1 + P_1(W)L_D^{-1})} - \frac{P_2(W)}{L_D + P_1(W)}\right] \tag{85}$$

where t_ν and R_ν are, respectively, the frequency-dependent transmission and reflection coefficients of photon in the semiconductor. $I_0(\nu)$ is the intensity photon per unit area and time incident on electrode, L_D is the diffusion length of electron in semiconductor, W is the width of the space charge region in the semiconductor (Figure 11), D_e is the diffusion coefficient of electron, and $P_1(W)$ and $P_2(W)$ are two Gaussian integrals involving the parabolic type of

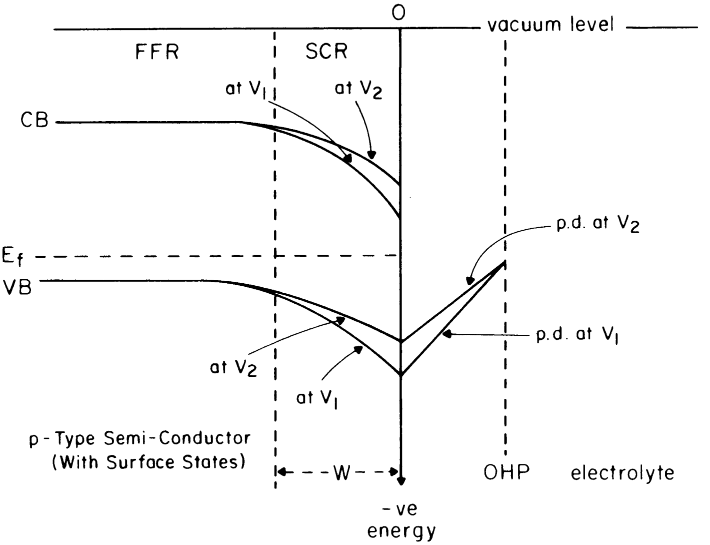

Figure 11. A schematic diagram to show the potential drop in the space charge region of width, *W*, in the *p*-type semiconductor and that in Helmholtz layer.

potential at the space charge region and can be expressed as

$$P_1(W) = \frac{1}{2}\left(\frac{\pi kT}{e_0 V_s}\right)^{1/2} W \tag{86}$$

where V_s is the potential drop inside the semiconductor and

$$P_2(W) \simeq \left(\frac{\pi kT}{4e_0 V_s}\right)^{1/2} We^{-\alpha_\nu W} \tag{87}$$

where α_ν is the frequency-dependent absorption coefficient of the photon in the semiconductor electrode. In Eq. (85) K_t is the electron transfer rate constant at the semiconductor–solution interface and can be expressed as

$$K_t \simeq 2kTS_P(E, h\nu)T(E, h\nu)D_a(E_0, h\nu) \tag{88}$$

6. Tunneling at the Oxide-Covered Electrode

Schmickler(89) put forward a theory of resonance tunneling through the electrochemically generated oxide film covered on metal electrodes to explain some important experimental findings,(90–92) such as a downward bending of anodic current density at low overpotential, small transfer coefficients in the anodic and cathodic Tafel regions, and an upward bending of both branches at high overpotentials. In the theory of resonance tunneling, Schmickler(89) derived an expression for the resonance current based on the second-order perturbation theory with respect to the electronic tunneling factor. In the model, it is considered that a metal electrode is covered by an oxide film of uniform thickness, a, in contact with a redox electrolyte. The film is uniformly doped with impurities, the energy levels of which lie at a fixed distance below the bottom, V_B, of the conduction band and vary linearly with distance, x, from the metal–oxide interphase, and measure all energies with respect to the Fermi level, E_F, of the metal. In this way, the value of $V_R = V_B(a)$ at the electrolyte–oxide interphase depends on the applied overpotential, η, while $V_L = V_B(0)$ at the metal–oxide interphase does not. The potential drop over the outer Helmholtz plane is considered constant so that $V_L = V_L^0 + e_0\eta$. For simplicity, a one-dimensional model is considered for the system, and thus, only electrons with zero transverse momentum, which give the dominant contribution to the tunneling current, are taken into account.

The rate of electron transfer from the electrolyte to an electronic level in the metal with an energy E (with respect to the Fermi level) can be expressed in the form

$$j(\Delta E, \eta) = C|T(\Delta E, \eta)|^2[1 - n(\Delta E)]D(\Delta E, \eta)\rho(\Delta E) \tag{89}$$

where C is a constant containing the concentrations of the reactants, T is the electronic matrix element for the tunneling process, $n(\Delta E)$ denotes the Fermi function, $D(\Delta E, \eta)$ is the probability of finding the solvent subsystem on the saddle point of the reaction hypersurface, and $\rho(\Delta E)$ is the density of electronic states in the metal. The reaction is considered to take place via the saddle point of the reaction hypersurface.

The matrix element for an electronic transition from a state $|e\rangle$ in the redox electrolyte via a localized impurity state $|r\rangle$ in the film to a state $|m\rangle$ in the metal is according to second-order perturbation theory$^{(93)}$

$$T = \frac{\langle e|V_1|r\rangle\langle r|V_2|m\rangle}{E - E_r - \frac{1}{2}\Gamma(E)} \tag{90}$$

where the states $|e\rangle$ and $|m\rangle$ have the same electronic energy E and E_r is the energy of the impurity state and its lifetime broadening. V_1 is a perturbation operator coupling $|e\rangle$ and $|r\rangle$ and V_2 couples $|r\rangle$ and $|m\rangle$. Eq. (90) describes an electronic transition with $|r\rangle$ as a virtual intermediate state. The direct transitions not involving $|r\rangle$ and interference between these two processes are neglected.

Inserting Eq. (90) into Eq. (89) gives for the anodic resonance current due to the impurity state $|r\rangle$

$$\vec{j}_r(\eta) = C\int d(\Delta E)\,\frac{|\langle e|V_1|r\rangle|^2|\langle r|V_2|m\rangle|^2}{(E - E_r)^2 + \frac{1}{4}\Gamma^2}[1 - n(\Delta E)]D(\Delta E, \eta) \tag{91}$$

For reasonably thick barriers ($a > 10$ Å), the width of the Lorentzian distribution of resonance state is smaller than the range over which the other factors in Eq. (91) vary appreciably and, therefore, the other factor can be evaluated at $E = E_r$ and taken then in front of the integration sign.

Thus, the following expression for the anodic current density can be obtained after integration:

$$\vec{\mathrm{j}}_r(\eta) = 2\pi C[1 - n(E_r)]D(E_r, \eta)\rho(E_r)|\langle e|V_1|r\rangle|^2|\langle r|V_2|m\rangle|^2\Gamma^{-2}(E_r) \tag{92}$$

The lifetime broadening is, to a first-order perturbation,

$$\Gamma = (2\rho/h)[\rho(E_r)|\langle m|V_2|r\rangle|^2 + |\langle r|V_1|e\rangle|^2] \tag{93}$$

We next require approximate expressions for the two matrix elements in order to derive a workable expression for the resonance current. Let the impurity be positioned at $x = l$ and have an effective width of $2w$. Then we have, in the WKB approximation,(102)

$$|\langle r|V_1|e\rangle|^2 \simeq c_2 \exp\left(-2\int_{1+w}^{a} k_x\, dx\right) \tag{94}$$

$$|\langle m|V_2|r\rangle|^2 \simeq [1/\rho(E_r)]c_1 \exp\left(-2\int_{0}^{l-w} k_x\, dx\right) \tag{95}$$

where $k_x = \{2m_{\text{eff}}/h[V_R(x) - E_r(l)]\}^{1/2}$ is the WKB propagation constant in the barrier, and m_{eff} is the effective mass of the electron in the oxide. c_1 and c_2 are slowly varying functions of the energy, which depend also on the angular parts of the wave functions $|e\rangle$ and $|r\rangle$. A procedure for the evaluation of c_1 and c_2 has been given by Gadzuk.(94)

For the electronic terms in the electrolyte, Schmickler(89) did not use the usual harmonic approximation, since this always produces a curvature of Tafel plots at high overpotentials even for redox reactions at bare metal electrodes. There is little experimental evidence for such an effect. In this study, there is a particular interest in possible curvature of the theoretically deduced Tafel lines caused by the resonance nature of the electron transfer. The electronic term in the electrolyte, using the linear approximation, is expressed as

$$D(E_r, \eta) = \exp\{-[E^\circ_{\text{act}} + (E_r - e\eta)/2]/kT\} \tag{96}$$

corresponding to a constant transfer coefficient of 0.5, which would give straight Tafel lines for reactions at a bare metal electrode and also for direct elastic tunneling through the film. Thus, if curvature appears from the theory, it will not be due to the effects of squared terms arising from continuum theory but due to resonance tunneling.

The final expression for the contribution to the anodic current of an impurity situated at $x = l$ is

$$\begin{aligned} \Delta\vec{\mathrm{j}}(l) = c_1 2\pi C[1 - n(E_r)] \exp\{-[2E^\circ_{\text{act}} + (E_r - e\eta)]/2kT \\ \times R_1(l)R_2(l)/[R_1(l) + R_2(l)] \end{aligned} \tag{97}$$

where

$$R_1(l) = \exp\left(-4/3\sqrt{}(2m_{\mathrm{eff}})^{1/2}/hg\{[V_L - E_r(l) + g(l - w)]^{3/2} - (V_L - E_r)3/2\}\right) \tag{98}$$

$$R_2(l) = \exp\left(-4/3\sqrt{}(2m_{\mathrm{eff}})^{1/2}/hg\{(V_R - E_r)^{3/2} - [V_L + g(1 + w) - E_r]^{3/2}\}\right) \tag{99}$$

and $g = (V_R - V_L)/a$ is the slope of the barrier. Note that E_r also depends on l:

$$E_r = E_r^\circ + gl \tag{100}$$

The average contribution of a single impurity to the anodic resonance current is

$$\vec{\mathrm{j}}_r = (1/a)\int_0^a \Delta j(l)\, dl \tag{101}$$

The corresponding expression for the cathodic direction [cf. Eq. (97)] is

$$\overleftarrow{\mathrm{j}}_r = \frac{1}{a} 2\pi C c_1 \int_0^a n(E_r) \exp\left\{-\frac{[E_{\mathrm{act}}^\circ - (E_r - e\eta)/2]}{kT}\right\} \times \frac{R_1(l) R_2(l)}{R_1(l) + R_2(l)}\, dl \tag{102}$$

Figure 12 shows the distribution of the resonant current onto impurities situated at different distances from the metal–oxide interphase.

Figure 13 shows Tafel plots for the anodic and cathodic current densities, $\vec{\mathrm{j}}_r$ and $\overleftarrow{\mathrm{j}}_r$. Here, the barrier is flat at equilibrium and relatively low ($V_B = 0.2$ eV at $x = 0$); E_r^0 varies in the range -0.05 to -0.2 eV.

7. Fermi Energy in Solution

The redox potential on the vacuum scale can be expressed$^{(95,96)}$ as

$$V_{\mathrm{redox}}(\text{vacuum scale}) = {}^m\Delta^s\phi - \mu_e^m/e_0 \tag{103}$$

where ${}^m\Delta^s\phi$ is the Galvani potential difference at the metal–solution interface, μ_e^m is the chemical potential of electrons in the metal, and e_0 is the electronic charge.

If one writes for the electrical equilibrium at the metal–solution interface (considering equilibrium between the metal electron and the electron in redox ions in solution) that

$$\bar{\mu}_e^m = \bar{\mu}_e^s \tag{104}$$

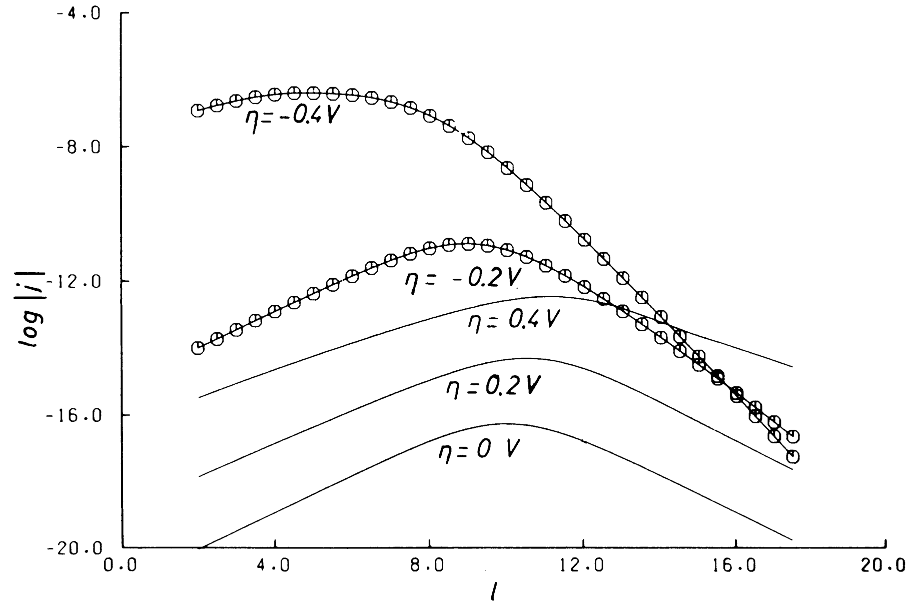

Figure 12. Distribution of the anodic (——) and cathodic (–O–) resonance current over impurities situated at different positions in the barrier. Barrier dimensions (at equilibrium): $V_L = V_R = 0.4$ eV, $E_r^\circ = 0.1$ eV, $a = 20$ Å (from Ref. 13).

then

$$^{m}\Delta^{s}\phi = {}^{m}\Delta^{s}\mu_e/e_0 = {}^{m}\mu_e/e_0 - \mu_e^{s}/e_0 \tag{105}$$

where $\bar{\mu}$ is the electrochemical potential.

Using Eq. (105) in Eq. (103), one gets

$$V_{\text{redox}}(\text{vacuum scale}) = -\mu_e^{s}/e_0$$

or

$$\mu_e^{s} = -e_0 V_{\text{redox}}(\text{vacuum scale}) \tag{106}$$

Thus, from Eq. (106), the *chemical* potential of an electron in solution is equal to the negative of the vacuum scale redox potential.

It can be shown in the following way that the Fermi energy of redox ion in solution, $E_{\text{F,redox}}$, as defined earlier, is, in fact, equal to $-e_0 V_{\text{redox}}$(vacuum scale). According to Gerischer,[98] the Fermi energy for the redox electrolyte is expressed as

$$\begin{aligned} E_{\text{F,redox}} &= \Delta\mu_{\text{redox}} \\ &= \mu_{\text{M}_1^{2+}} - \mu_{\text{M}_1^{3+}} \end{aligned} \tag{107}$$

where $\mu_{\text{M}^{2+}}$ and $\mu_{\text{M}^{3+}}$ are, respectively, the chemical potential M^{2+} and M^{3+}

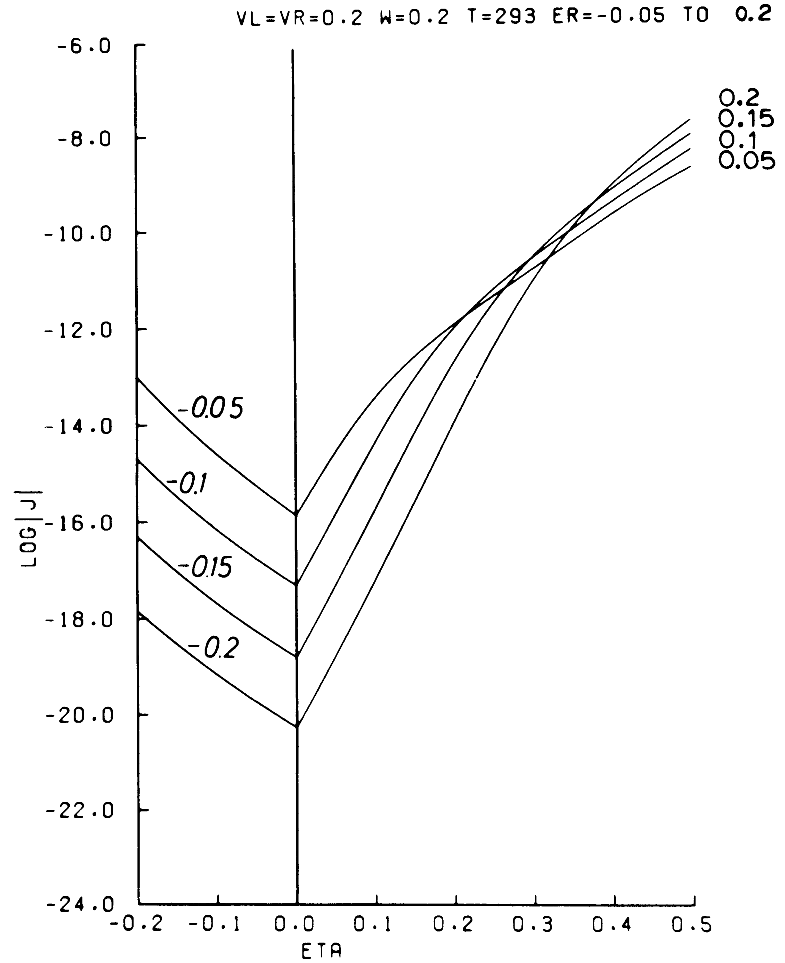

Figure 13. Tafel plots for the anodic and cathodic resonance current densities for various values of the impurity state energy E_r°. Barrier dimensions (at equilibrium) (from Ref. 13): $V_L = V_R = 0.2$ eV, $a = 20$ Å.

ion in a redox reaction of the type, $M_1^{3+}(aq) + e_{vac} \rightarrow M_1^{2+}(aq)$. For the reaction of the type

$$M_1^{3+} + e_m \rightleftarrows M_1^{2+} \tag{108}$$

one can write

$$\bar{\mu}_{M_1^{3+}} + \bar{\mu}_e^m = \bar{\mu}_{M_1^{2+}}$$

which, on rearrangement, gives

$$(\mu_{M_1^{2+}} - \mu_{M_1^{3+}}) = \mu_e^m - \phi^m + \phi^s \tag{109}$$

or

$$E_{\mathrm{F,redox}} = -e_0{}^m\Delta^s\phi + \mu_e^m$$
$$= -e_0 V_{\mathrm{redox}}(\text{vacuum scale}) \tag{110}$$

when Eq. (103) and Eq. (107) are used.

There seem to be two difficulties associated with this result.

(a) It is conventional$^{(98-102)}$ to equate μ_e^s, i.e., $-e_0 V_{\mathrm{redox}}$(vacuum scale), with the Fermi level of energy in the metal at equilibrium. Thereby lies a misunderstanding. One can only equate the electrochemical potential (which is defined as Fermi energy) but not the chemical potential with the Fermi energy in the metal or semiconductor.

Thus, μ_e^m is not equal to the Fermi energy in a semiconductor, which reduces the validity of equating $-e_0 V_{\mathrm{redox}}$(vacuum scale) with the Fermi energy at the solution (for it is a chemical, not an electrochemical, potential).

What is the appropriate expression for thermodynamic equilibrium? From Eq. (103),

$$\mu_e^m - e_0\phi_s^m = -e_0 V_{\mathrm{redox}}(\text{vacuum scale}) - e_0\phi^s$$

or

$$\bar{\mu}_e^m = -e_0 V_{\mathrm{redox}}(\text{vacuum scale}) - e_0\phi^s \tag{111}$$

The right-hand side is [cf. Eq. (106)] the electrochemical potential of the electron in the solution. Equation (111) is the condition for equilibrium. Hence, $-e_0 V_{\mathrm{redox}}$(vacuum scale) is *not* the potential at which an interface is in equilibrium. One needs to include $e_0\phi^s$, which is not obtainable at this time. Moreover, it will depend upon the solution of the system concerned.

Hence, at equilibrium, $-e_0 V_{\mathrm{redox}}$(vacuum scale) (which is known as $E_{\mathrm{F,redox}}$) cannot be equal to Fermi level energy in metal or semiconductor, since $-e_0 V_{\mathrm{redox}}$(vacuum scale) is the chemical (and not the electrochemical) potential of electrons in the solution.

8. Distribution of Electron States in Ions in Solution

It has become common in the photoelectrochemical literature to portray the number of states available for electrons in solution in terms of a bell-shaped curve (Figure 14), which is referred to as Gaussian.$^{(45,98)}$

There are a number of unusual models of presentation in the paper in which the original derivation$^{(19)}$ pertaining to such curves is written down. For example, the density of states is plotted not as a function of energy, E, with respect to vacuum (cf. Gurney$^{(1)}$), but as a function of the difference of energy, ΔE, of the electron in the oxidized and reduced ion.$^{(98)}$

Utilizing $\rho_{\mathrm{ox}}(E)$ for the density of electronic states in the oxidized ion of a redox couple at ΔE apart (with neglect of weighting factor for simplicity) as$^{(98)}$

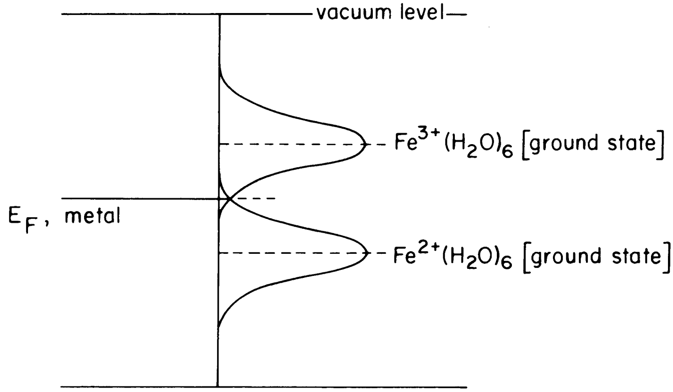
vacuum level—
$Fe^{3+}(H_2O)_6$ [ground state]
E_F, metal
$Fe^{2+}(H_2O)_6$ [ground state]

Figure 14. The schematic bell-shaped diagram of the distribution of electronic energy states of redox ions at an electrode–solution interface (from ref. 3).

$$\rho_{ox}(E) = \frac{\exp[-(E - E^\circ_{ox})/kT]}{\int_{E^\circ_{ox}}^{\infty} \exp[-(E - E_{ox})/kT]\,dE} = \frac{\exp[-(E - E^\circ_{ox})/kT]}{kT} \tag{112}$$

a similar expression for ρ_{red}(E) can be written.

The value of $E - E^\circ_{ox}$ is that of the various vibration–libration states in the ion–solvent complex, and E°_{ox} is the ground state energy of the oxidized ion. If one plots $\rho_{ox}(E)$ and $\rho_{red}(E)$ as a function of E, but not as a function of ΔE, one gets the distribution of density of states as in Figure 15 (cf. Gurney[1]).

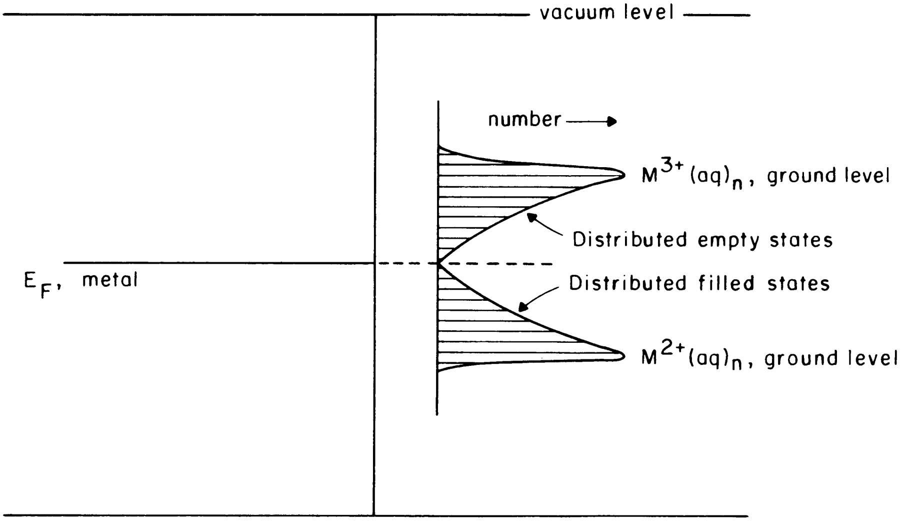
vacuum level
number →
$M^{3+}(aq)_n$, ground level
Distributed empty states
E_F, metal
Distributed filled states
$M^{2+}(aq)_n$, ground level

Figure 15. The plot of the density of electronic energy states, $\rho(E)$, as a function of E, measured with respect to vacuum.

The energy states of electrons in the ion–solvent entities represent states analogous to vibration–rotation states in molecular entities. They do not represent fluctuations of the ground state of the ion symmetrical in both directions around the ground state.

Such considerations (Gaussian or Maxwellian) have implications for the form of the current–potential relation. According to the Gaussian model, the cathodic current is related to overpotential by(45)

$$i_c = i_0 \exp\left(\frac{E_s}{4kT}\right) \exp\left[-\frac{(E_s + e\eta_c)^2}{4kTE_s}\right] \tag{113}$$

However, for the Maxwellian model(103)

$$\begin{aligned} i_c = \text{const} \int_0^{E_0} E^{1/2} \frac{1}{\{\exp[(E - E_\text{F})/kT] + 1\}} P_\text{T}(E) \\ \times \exp[-(E_0 + \beta e_0 \eta_c - E)/kT]\, dE \end{aligned} \tag{114}$$

where E_0 is the ground electronic state energy of the acceptor ion in solution, where $P_\text{T}(E)$ is the tunneling probability at E, and β is the symmetry factor.

After integration,

$$i = i_0 \exp(-\beta e_0 \eta_c / kT) \tag{115}$$

Equation (113) is inconsistent with experiment,(38–42) while Eq. (115) is consistent with it.

9. The Adiabaticity and Nonadiabaticity in Electron Transfer Reactions

A reaction is called adiabatic when the reacting system moves during the whole course of the reaction along the same potential energy curve corresponding to the given electronic state (as shown in Figure 16 by arrow *a*). A nonadiabatic reaction is one in which the reacting system undergoes transition during the course of the reaction from one potential energy curve to another corresponding to a higher energy electronic state of the activated complex (as shown in Figure 16 by arrow *b*).

These two possibilities of reaction processes make much difference in calculating the rate of any chemical reaction. According to the transition state theory formalism, these two types of reactions (i.e., adiabatic and nonadiabatic) influence the value of the transmission coefficient, κ, which is a preexponential term in the absolute rate expression. The value of κ is considered unity for the adiabatic reaction and less than unity for a nonadiabatic reaction.

Physically, in the adiabatic case, the reactants attract strongly at their closest approach when the probability of reaction is a maximum and the

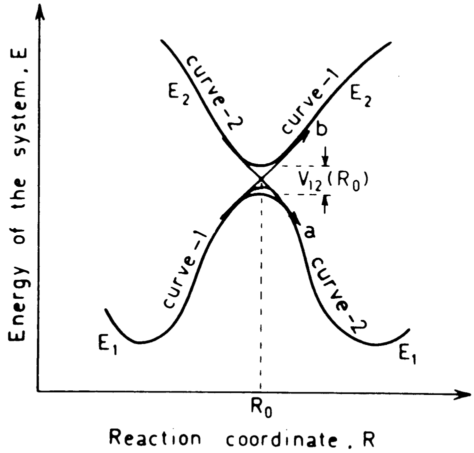

Figure 16. The plot of energy of the reacting system as a function of reaction coordinate. Arrow *a* represents adiabatic and *b* represents nonadiabatic motion in the region of closest approach of two potential curves.

system remains in a lower energy curve, since the gap between the lower and higher potential energy curves (Figure 16) increases and the probability of transition to the upper curve becomes unfavorable. The reverse is the case for the nonadiabatic situation.

Landau(104) and Zener(105) made the first attempts to formulate the probability of transition of the reacting system from a lower electronic state to an upper one, and thus, to find the adiabaticity and nonadiabaticity of a reaction.

9.1. Landau–Zener Formulation

Landau(104) and Zener(105) independently gave the first mathematical formulation of the condition of adiabatic and nonadiabatic reactions in terms of probability factors.

The probability that a reaction will occur adiabatically is expressed as(104,105)

$$P_{\mathrm{ad}} = 1 - \exp\left[-\frac{2\pi|V_{12}|^2}{hV_r(S_1 - S_2)}\right] \tag{116}$$

The probability that the reaction will occur nonadiabatically can be expressed as

$$P_{\mathrm{nonad}} = 1 - P_{\mathrm{ad}} \tag{117}$$

where V_{12} in Eq. (116) is the splitting energy of the two potential energy surfaces in the transition state, and its value depends on the degree of interaction between two reacting systems and is expressed as(104,105)

$$V_{12} = \langle \phi_1 | V' | \phi_2 \rangle \tag{118}$$

where ϕ_1 and ϕ_2 are two electronic states of interacting reacting systems and V' is the perturbing interaction potential between them.

In Eq. (116), V_r is the relative velocity of approach of the one reactant to another during reaction, and $(S_1 - S_2)$ is the net force exerted on the system tending to restore to its original state or take it to a final state. Hence, the probability of the adiabatic transition is dominant. If V_{12} is small, the probability of a nonadiabatic transition is dominant. If the relative kinetic energy corresponding to relative velocity of approach of the reaction systems, V_r, is large compared to V_{12}, the reaction becomes nonadiabatic.

If P_{ad} in Eq. (116) is unity, the reaction is adiabatic, which corresponds to a transmission coefficient, $\kappa = 1$, in the absolute reaction rate expression. If P_{ad} is less than unity, the probability of a nonadiabatic process, P_{nonad} [cf. Eq. (117)], is not zero, and then the transmission coefficient, κ, becomes less than unity.

Bates(106) criticized the Landau–Zener(104,105) treatment for finding the probability of transition. He mentioned that the assumption by Landau–Zener that the transition occurs only in the zone of crossing of two potential energy surfaces is not necessarily correct; the transition may occur away from the crossing, and he calculated the width of the transition zone as

$$\Delta R = \left(\frac{4\pi V_r h}{\alpha}\right)^{1/2} \tag{119}$$

whence it is observed that the width of the transition zone is proportional to the square root of the velocity of the relative motion of the reactants, V_r. α is a constant and equal to e_0^2/R_0^2, where e_0 is the electronic charge and R_0 is the equilibrium position of the reactant state.

Serious error is likely to arise in the treatment of Landau(104) and Zener(105) unless the wave functions ϕ_1 and ϕ_2 are spherically symmetrical and unless the velocity of the relative motion is low. For example, in a charge transfer process which involved electron transfer between p and d states, the Landau–Zener result will be less applicable.

9.2. Transmission Coefficient, κ, for Homogeneous Redox Reactions

Newton(107) determined the transmission coefficient, κ, for the homogeneous electron transfer reaction between $Fe^{2+}(H_2O)_6$ and $Fe^{3+}(H_2O)_6$ redox couples in solution. The transmission coefficient was expressed in terms of the Landau–Zener(104,105) probability factor, P_{12}^0, i.e.,

$$\begin{aligned}\kappa &= P_{12}^0 \\ &= 1 - \exp\{-4\pi^2 H_{AB}/[h\bar{v}(|S_A - S_B|)]\}\end{aligned} \tag{120}$$

where H_{AB} is the matrix element of the electronic Schrödinger Hamiltonian,

H, and is expressed as

$$H_{AB} = \int \psi_A H \psi_B \, d\tau \qquad (121)$$

where ψ_A and ψ_B are, respectively, the reactant and the product state electronic wave functions and $d\tau$ is the volume element. The factor $\bar{v}|S_A - S_B|$ has been expressed as $8\nu_{\text{eff}}(\pi RTE^*)^{1/2}$, where $\bar{v}$ is used as the thermally averaged velocity and S_A and S_B are the slopes of the energy surfaces. The effective frequency is defined as

$$\nu_{\text{eff}}^2 = \frac{\sum^N \nu_i^2 E_i^*}{\sum E_i^*} \qquad (122)$$

where $\nu_i = \frac{1}{2}\pi(F_i/\mu_i)^{1/2}$, μ_i being the effective mass of the ith mode of ion-solvent bond, F_i is the force constant of such ith bond, E^* is the activation energy that consists of both inner and continuum contribution, and E_i^* is the inner-shell contribution to activation energy.

The model Hamiltonian, H, for the $Fe^{2+}(H_2O)_6$ and $Fe^{3+}(H_2O)_6$ interactions includes explicitly all 11 valence electrons of Fe^{2+} and Fe^{3+}, simulating the core electrons using an *ab initio* effective core potential$^{(108)}$ and representing the field of the 12 first shell H_2O molecules through the use of point charges 0.49 for H and −0.98 for O, located at the H and O atomic positions (the intramolecular H_2O geometry was taken from the gas phase data: $r_{OH} = 0.957$ Å < HOH = 104.5$^{(109)}$). These point charges establish the proper local geometry of the reactive super molecule and were chosen so as to reproduce roughly the binding energy of the hydration shell when Fe^{2+}(aq) and Fe^{3+}(aq) are close together.

The wave functions ψ_A and ψ_B were obtained from open-shell SCF calculations based on the 11-valence-electron Hamiltonian, using the face-to-face geometry and imposing T_h symmetry on the atomic configuration of each inner-sphere complex and a common point characteristic of both reactants in the activated complex.

The off-diagonal matrix element H_{AB} was obtained from ψ_A and ψ_B. Since ψ_A and ψ_B are not constructed from a common set of orthonormal MOS, H_{AB} was evaluated using the method of corresponding orbitals.$^{(110)}$ In view of the orthogonality of ψ_A and ψ_B, the proper coupling element designated below as H'_{AB} for the use in the golden rule and Landau–Zener expression is as follows$^{(10-12)}$:

$$H'_{AB} = H_{AB} - S_{AB}H_{AA} \qquad (123)$$

where $H_{AA} = H_{BB}$ for symmetric exchange reactions, S_{AB} is the overlap integral.

The matrix element H_{AB} was evaluated over the range $R_{\text{Fe-Fe}} = 5.6$–8.1 Å and the value of transmission coefficient, κ, was found to vary for 6.9×10^{-2} to 5×10^{-6} (Table 3). At the traditional contact distance of 6.9 Å, the value

Table 3
Comparison of H'_{AB} and S_{AB} Values[107]

$R_{\text{Fe-Fe}}$ (Å)	H'_{AB} (cm^{-1})	S_{AB}	H'_{AB}/S_{AB} (cm^{-1})	P^0_{12}
5.61	$-91.2(-91.0)$	0.399×10^{-2}	-1.19×10^4	6.9×10^{-2}
5.86	$-65.7(-66.0)$	0.286×10^{-2}	-2.30×10^4	3.7×10^{-2}
6.11	$-46.4(-46.2)$	0.199×10^{-2}	-2.33×10^4	1.8×10^{-2}
6.36	$-30.8(-30.9)$	0.131×10^{-2}	-2.35×10^4	8.0×10^{-3}
6.61	$-19.5(-19.4)$	0.814×10^{-3}	-2.40×10^4	3.2×10^{-3}
6.86	$-11.3(-11.2)$	0.455×10^{-3}	-2.48×10^4	1.1×10^{-3}
7.11	$-5.6(-5.6)$	0.209×10^{-3}	-2.68×10^4	2.6×10^{-4}
7.36	$-2.0(-2.0)$	0.584×10^{-4}	-3.42×10^4	3.4×10^{-5}
7.61	$0.0(0.0)$	-0.193×10^{-4}	0.0	0.0
7.86	$+0.9(+0.8)$	-0.543×10^{-4}	-1.66×10^4	5.0×10^{-6}
8.11	$+1.0(+0.8)$	-0.524×20^{-4}	-1.91×10^4	4.8×10^{-6}

of P^0_{12} is 1.1×10^{-3}. These results show considerable nonadiabatic character of such homogeneous redox reactions.

10. Transition Probability of the Electron at the Electrode–Solution Interface

In most theory concerning the electron transfer at the electrode–solution interface, the electronic transition probability is generally kept unevaluated or determined in terms of the WKB treatment. The WKB treatment is applicable for situations where the potential at the interface does vary fairly slowly. This situation is rare. Use of time dependent perturbation theory is needed to have a proper evaluation of the transition probability, P_T, of electrons at the interface. One attempt(15) of calculation of electronic transition probability $T(E)$ from electrode Fermi level to an available redox ion, e.g., $Fe^{3+}(H_2O)_6$, state is given.

According to time-dependent perturbation theory, P_T can be expressed as

$$P_T = \frac{2\pi\tau}{\hbar} \langle\psi_F|V(r)|\psi_I\rangle|^2 \rho(E_f) \tag{124}$$

where ψ_I and ψ_F are, respectively, the initial and final state wave functions of the electron. The initial state of the electron is that in the metal surface, corresponding to energy equal to that of the Fermi level, and can be expressed as a plane wave, using effective mass approximation, and the final state is that of the electron in the reduced ion. τ is the time during which the electron in the electrode surface experiences a perturbation(113) before it joins the acceptor ion after crossing the interface. $V(r)$ is the perturbing potential energy which causes the transition. $\rho(E_f)$ is the density of electronic states in the final state in the acceptor metal ion for the cathodic process and in metal for the anodic process.

To calculate the transition probability, $T(E)$, it was considered that an electron transfers from the electrode to an available $Fe^{3+}(H_2O)_6$ ion in solution having equal energy.

The *initial state* wave function, ψ_I, of a conducting electron in the electrode (metal) can be expressed in terms of spherical harmonies $Y(r)$ and Bessel function, $j(kr)$, as

$$\psi_I(r) = L_0^{-3/2} 4\pi \sum_{l=0}^{\infty} \sum_{m=-l}^{l} i^l j_l(kr) Y_{lm}^*(\hat{\mathbf{k}}) Y_{lm}(\hat{\mathbf{r}}) \tag{125}$$

The perturbed final state wave function in Fe^{2+}(aq) ion was expressed using the time-independent perturbation theory as(15)

$$\begin{aligned}\psi_d^{(1)} &= \psi_d(r) Y_{20}(\hat{\mathbf{r}}) + \frac{3\xi}{\sqrt{35}(E_d^\circ - E_f^\circ)} \left\langle \psi_f(r) Y_{30}(\hat{\mathbf{r}}) \left(\frac{1}{|R-r|^2}\right) \psi_d(r) Y_{30}(\hat{\mathbf{r}}) \right\rangle \psi_f(r) \\ &\quad \times Y_{30}(\hat{\mathbf{r}}) + \frac{2\xi}{\sqrt{15}(E_d^\circ - E_p^\circ)} \\ &\quad \times \left\langle \psi_p(r) Y_{10}(\hat{\mathbf{r}}) \left(\frac{1}{|R-r|^2}\right) \psi_d(r) Y_{10}(\hat{\mathbf{r}}) \right\rangle \psi_p(r) Y_{10}(\hat{\mathbf{r}})\end{aligned} \tag{126}$$

where the ion dipole perturbing potential was used and expressed as $V'_{\text{ion dipole}} = 6e_0\mu/|R - r|^2$. Using Hein's expansion of the term, $1/|\mathbf{R} - \mathbf{r}|^2$, in terms of Legendre function, Q_l, and spherical harmonics, one can express the first integral in Eq. (126) as

$$\begin{aligned}M_1 &= \sum_{l,m} \frac{4}{2R} Y_{lm}^*(\hat{\mathbf{R}}) \left[\int_0^\infty r^2\, dr\, \psi_f(r) \frac{1}{r} \psi_d(r) Q_l\left(\frac{R^2 + r^2}{2Rr}\right)\right] \\ &\quad \times \langle Y_{30}(\hat{\mathbf{r}}) | Y_{lm}(\hat{\mathbf{r}}) | Y_{30}(\hat{\mathbf{r}}) \rangle\end{aligned} \tag{127}$$

Expressing the angular integral, $\langle Y_{30}(\hat{\mathbf{r}}) | Y_{lm}(\hat{\mathbf{r}}) | Y_{30}(\hat{\mathbf{r}}) \rangle$, in terms of the $3j$ symbol, one gets

$$M_1 = \frac{2l+1}{2R} \sum_l (2l+1) \begin{pmatrix} 3 & l & 3 \\ 0 & 0 & 0 \end{pmatrix}^2 P_l(\cos\Omega) \int_0^\infty r^2\, dr\, \psi_f(r) \frac{1}{r} \psi_d(r) Q_l\left(\frac{R^2 + r^2}{2Rr}\right) \tag{128}$$

Similarly, the second integral of Eq. (126) becomes

$$M_2 = \frac{2l+1}{2R} \sum_l (2l+1) \begin{pmatrix} 1 & l & 1 \\ 0 & 0 & 0 \end{pmatrix} P_l^2(\cos\Omega) \int_0^\infty r^2\, dr\, \psi_P(r) \frac{1}{r} \psi_d(r) Q_l\left(\frac{R^2 + r^2}{2Rr}\right) \tag{129}$$

Now, using Eqs. (128) and (129) in Eq. (126), the perturbed state wave function of $Fe^{2+}(H_2O_6)_6$ ion can be expressed as

$$\psi_d^{(1)} = \psi_d(r)Y_{20}(\mathbf{r}) + A\psi_f(r)Y_{30}(\mathbf{r}) + B\psi_p(r)Y_{10}(\mathbf{r}) \tag{130}$$

where

$$A = \frac{3\xi|M_1|}{\sqrt{35}(E_d^\circ - E_f^\circ)} \tag{131}$$

and

$$B = \frac{2\xi|M_2|}{\sqrt{15}(E_d^\circ - E_p^\circ)} \tag{132}$$

Putting the perturbed third state wave function, $\psi_d^{(1)}$, from Eq. (130) in Eq. (124) in place of ψ_F, one gets the matrix element as

$$\begin{aligned} M &= \langle\psi_F|V(r)|\psi_I\rangle \\ &= \langle\psi_d(r)Y_{20}(\hat{\mathbf{r}})|V(r)|\psi_I\rangle + A\langle\psi_f(r)Y_{30}(\hat{\mathbf{r}})|V(r)|\psi_I\rangle \\ &\quad + B\langle\psi_p(r)Y_{10}(\hat{\mathbf{r}})|V(r)|\psi_I\rangle \end{aligned} \tag{133}$$

Hence, the transition probability can be expressed as

$$P_T = \frac{2\pi\tau}{\hbar}|M|^2\rho(E_f) \tag{134}$$

where the matrix element, M, simplifies to

$$\begin{aligned} M &= \frac{4\pi}{L_0^{3/2}} \sum_{m=-2}^{2} Y_{2m}(\hat{\mathbf{k}})(-1) \int_0^\infty r^2\,dr\,j_2(kr)V(r)\psi_d(r) \\ &\quad + \frac{4\pi A}{L_0^{3/2}} \sum_{m=-3}^{3} Y_{3m}(\hat{\mathbf{k}})(-i) \int_0^\infty r^2\,dr\,j_3(kr)V(r)\psi_f(r) \\ &\quad + \frac{4\pi B}{L_0^{3/2}} \sum_{m=-1}^{1} Y_{1m}(\hat{\mathbf{k}})(i) \int_0^\infty r^2\,dr\,j_1(kr)V(r)\psi_p(r) \end{aligned} \tag{135}$$

The quantitative calculation of the probability of transition of an electron from the platinum electrode to $Fe^{3+}(H_2O)_6$ has been carried out from Eq. (134) using $|M|^2$ from Eq. (135).

The density of states of the electron is taken as that in the metal electrode at the Fermi level at the reversible potential (where electron transition rates from or to metal are equal) and is expressed as

$$\rho(E_f) = \frac{m^*k_fL_0^3}{2\pi^2h^2} \tag{136}$$

where k_f is the wave number of electrons corresponding to the energy, $E_{f,\text{rev}}$.

For the typical value of $\tau = 1.66 \times 10^{-16}$ sec, the transition at the reversible potential of $Fe^{3+}(aq)/Fe^{2+}(aq)$ becomes

$$P_T = 7.2 \times 10^{-3} \tag{137}$$

One can determine the potential dependence of P_T. From the value of P_T for hydrogen and oxygen evolution reaction, one can study the electrocatalytic property of metal electrodes.

11. Concluding Remarks

It is valuable to make some concluding remarks (written in 1982), which attempt to bring together some general perception of the developing subject of the quantum theory applied to the rate phenomena of interfacial systems.

(1) It is unfortunate that so much attention has been given by so many workers to the nonmolecular theoretical point of view, in which, apart from the avoidance of models, no account is taken of the structure of the interface, and there is such a marked qualitative (and of course) quantitative disagreement with experiment.

(2) Correspondingly, most theorists are involved in continuing to push forward a model involving only *solvent fluctuation* when there is much evidence that in redox reactions, the assumptions that the solvent fluctuation aspect is important gives discrepancy with experimental result (in reactions which involve bond formation with the electrode surface, solvent fluctuation would be expected to have less strength as a contributor to a model than with non-bond-forming models).

(3) The molecular model approach to the quantum mechanical formulation of a kinetic theory of velocity of reaction rates at surfaces is a little-developed subject, and the first difficulties are as follows:

(a) There is, as yet, no clear understanding of what happens in a charge transfer reaction. Can a transition state viewpoint be maintained in a situation where the electron transfer itself occurs in a time small compared with the time of existence of activated complexes?

(b) Although there has been some attempt to calculate the transmission coefficient, there is, as yet, no quantum mechanical approach to the calculation of the probability of activation.

(c) The scope of work on the molecular approach is small. There has been no application to reaction outside those of redox and proton transfer.

(d) The greatest weakness of the approach is the avoidance of calculations involving bonding and absorption (and, thus, electrocatalysis): there has been no consideration of the *chemical* aspects of electrochemical reactions, although surface *chemical* reactions are often rate determining in electrochemical reactions, particularly electroorganic reactions.

(4) *The path forward*:

(a) It is desirable to put forward a theory of the kinetics of electrochemical reactions which is related to models accepted in the theory of reactions in solution. It seems anomalous that one should have a completely separate treatment (via continuum theory) for electrochemical reactions.

(b) It is necessary to make quantitative calculations which avoid the use of continuum dielectrics when treating interfacial processes.

(c) It is desirable to tackle electrochemical reactions other than simple proton transfer or redox reactions in quantum mechanical terms, e.g., metal dissolution or photoelectrochemical reactions.

References

1. R. W. Gurney, *Proc. R. Soc. London Ser. A* **134**, 137 (1931).
2. J. A. V. Butler, *Proc. R. Soc. London Ser. A* **157**, 423 (1936).
3. H. Gerischer, *Z. Phys. Chem.* **26**, 223 (1960); **29**, 325 (1960).
4. H. Gerischer, *Z. Phys. Chem.* **27**, 48 (1961).
5. S. G. Christov, *Electrochim. Acta* **4**, 306 (1961).
6. S. G. Christov, *Electrochim. Acta* **9**, 575 (1964).
7. S. G. Christov, *J. Res. Inst. Catal., Hokkaido Univ.* **16**, 169 (1968).
8. J. O'M. Bockris and D. B. Matthews, *Proc. R. Soc. London Ser. A* **292**, 479 (1966).
9. J. O'M. Bockris and D. B. Matthews, *J. Chem. Phys.* **44**, 298 (1966).
10. J. O'M. Bockris and S. Srinivasan, *J. Electrochem. Soc.* **111**, 853 (1964).
11. J. O'M. Bockris, S. Srinivasan, and D. B. Matthews, *Discuss. Faraday Soc.* **39**, 239 (1965).
12. J. O'M Bockris and D. B. Matthews, *Electrochim. Acta* **11**, 143 (1966).
13. W. Schmickler, *J. Electroanal. Chem.* **82**, 65 (1977).
14. W. Schmickler, *J. Electroanal. Chem.* **84**, 203 (1977).
15. S. U. M. Khan, P. Wright, and J. O'M. Bockris, *Electrokhim.* **13**, 914 (1977).
16. J. Weiss, *J. Chem. Phys.* **19**, 1066 (1951).
17. W. Libby, *J. Phys. Chem.* **56**, 863 (1952).
18. R. A. Marcus, *J. Chem. Phys.* **24**, 966 (1956); **43**, 679 (1965).
19. V. G. Levich, *Adv. Electrochem. Electrochem. Eng.* **4**, 249 (1966).
20. R. R. Dogonadze, A. M. Kuznetsov, and V. G. Levich, *Electrochim. Acta* **13**, 1025 (1968).
21. V. G. Levich, in *Physical Chemistry: An Advanced Treatise*, Vol. 9B, H. Eyring, D. Henderson, and W. Jost, eds., Academic Press, New York (1970), Chap. 12.
22. E. D. German, V. G. Davali, R. R. Dogonadze, and A. M. Kuznetsov, *Electrokhimiya* **12**, 639 (1976).
23. R. R. Dogonadze, in *Reactions of Molecules at Electrodes*, N. S. Hush, ed., Wiley-Interscience, New York (1971), Chap. 3.
24. J. O'M. Bockris, B. E. Conway, and R. K. Sen, *Nature* **240**, 143, 197 (1972).
25. J. O'M. Bockris, R. K. Sen, and K. Mittal, *J. Res. Inst. Catal., Hokkaido Univ.* **20**, 153 (1972).
26. A. J. Appleby, J. O'M. Bockris, and R. K. Sen, *MTP International Review of Science*, Vol. 6, J. O'M. Bockris, ed., Butterworths, Washington, D.C. (1973).
27. J. O'M. Bockris, S. U. M. Khan, and D. B. Matthews, *J. Res. Inst. Catal., Hokkaido Univ.* **22**, 1 (1974).
28. J. O'M. Bockris and S. U. M. Khan, in *Proceedings of the Third Symposium on Electrode Processes*, Vol. 80-3, Electrochemical Society, Princeton, New Jersey (1980), p. 34.

29. J. O'M. Bockris and S. U. M. Khan, *Quantum Electrochemistry*, Plenum Press, New York (1979).
30. S. U. M. Khan and J. O'M. Bockris, *J. Res. Inst. Catal., Hokkaido Univ.* **28**, 249 (1980).
31. R. E. Moore, R. O'Ferral, G. Koepple, and A. Kroege, *J. Am. Chem. Soc.* **93**, 1 (1971).
32. J. O'M. Bockris and R. K. Sen, *Mol. Phys.* **29**, 357 (1975).
33. P. George and J. S. Griffith, in *The Enzymes*, Vol. 17, P. D. Boyer, H. Lardy, and K. Myrback, eds., Academic Press, New York (1959), Chap. 8, p. 347.
34. B. E. Conway and J. C. Currie, *J. Electrochem. Soc.* **125**, 257 (1978).
35. S. Sahami and M. J. Weaver, *J. Electroanal. Chem.* **124**, 35 (1981).
36. M. J. Weaver, P. Tyma, and S. M. Nettles, *J. Electroanal. Chem.* **114**, 53 (1980).
37. S. U. M. Khan and J. O'M. Bockris, in *Proceedings of Photoelectrochemical Processes and Measurement Techniques*, W. L. Wallace, A. J. Nozik, K. Deb, and R. H. Wilson, eds., Electrochemical Society, Pennington, New Jersey (1982).
38. A. M. T. Olmedo, R. Pereiro, and D. J. Schiffrin, *J. Electroanal. Chem.* **74**, 9 (1976).
39. M. J. Weaver and F. C. Anson, *J. Phys. Chem.* **80**, 1861 (1976).
40. P. Tyma and M. J. Weaver, *J. Electroanal. Chem.* **111**, 195 (1980).
41. S. W. Burr, K. Guyer, and M. J. Weaver, *J. Electroanal. Chem.* **111**, 41 (1980).
42. R. D. Armstrong, T. Dickinson, and R. Taylor, *J. Electroanal. Chem.* **57**, 157 (1974).
43. J. O'M. Bockris and S. U. M. Khan, *Quantum Electrochemistry*, Plenum Press, New York (1979), Chap. 13.
44. K. Kolbayashi, Y. Aikawa, and M. Sukizara, *Chem. Lett., Chem. Soc. Japan*, 1211 (1981).
45. S. Kapusta and N. Hackerman, *J. Electrochem. Soc.* **128**, 2607 (1981).
46. A. Damjanovic and J. O'M. Bockris, *Electrochim. Acta* **11**, 376 (1966).
47. J. O'M. Bockris, H. Wroblowa, E. Gileadi, and J. Piersma, *Trans. Faraday Soc.* **61**, 2531 (1965).
48. S. G. Christov, *J. Electrochem. Soc.* **124**, 69 (1977).
49. J. O'M. Bockris and S. U. M. Khan, *J. Res. Inst. Catal., Hokkaido Univ.* **25**, 63 (1977).
50. J. O'M. Bockris and S. U. M. Khan, *Trans. SAEST* **12**, 165 (1977).
51. P. W. Atkins, *Molecular Quantum Mechanics*, Clarendon Press, Oxford (1970).
52. S. Grasiorweiz, *Quantum Physics*, John Wiley and Sons, New York (1974).
53. C. R. Gatz, *Introduction to Quantum Chemistry*, Charles E. Merrill, Columbus, Ohio (1971).
54. J. O'M. Bockris and A. K. N. Reddy, *Modern Electrochemistry*, Plenum Press, New York (1970).
55. L. J. Vornerin, *Phys. Rev.* **91**, 859 (1953).
56. W. I. Harrison, *Phys. Rev.* **123**, 85 (1961).
57. R. Gomer and L. W. Swanson, *J. Chem. Phys.* **38**, 613 (1963).
58. M. Remy, *J. Chem. Phys.* **53**, 2487 (1970).
59. J. W. Gadzuk, *Surf. Sci.* **6**, 159 (1966).
60. J. W. Gadzuk, *Phys. Rev.* **1**, 2110 (1970); *Surf. Sci.* **6**, 133 (1967).
61. T. Ackerman, *Discuss. Faraday Soc.* **24**, 180 (1957).
62. J. Rudolph and H. Zimmerman, *Z. Phys. Chem.* **43**, 311 (1964).
63. J. Hoiuti and M. Polanyi, *Acta Physicochim. USSR* **16**, 169 (1942).
64. J. O'M. Bockris, R. J. Mannan, and A. Damjanovic, *J. Chem. Phys.* **48**, 1989 (1968).
65. R. Parsons and J. O'M. Bockris, *Trans. Faraday Soc.* **47**, 914 (1951).
66. R. K. Sen and J. O'M. Bockris, *Chem. Phys. Lett.* **18**, 166 (1973).
67. D. M. Dennison and G. E. Uhlenbeck, *Phys. Rev.* **41**, 313 (1932).
68. E. F. Caldin and M. Kaspvian, *Discuss. Faraday Soc.* **39**, 25 (1965).
69. A. A. Ovchinnikov and V. A. Benderskii, *J. Electroanal. Chem.* **100**, 563 (1979).
70. A. A. Ovchinnikov, V. A. Benderskii, S. D. Bubenko, and A. G. Krivenko, *J. Electroanal. Chem.* **91**, 321 (1978).
71. J. Bardeen, *Phys. Rev. Lett.* **6**, 57 (1961).
72. A. M. Brodskii and Yu. Ya. Gurevich, *Zh. Eksp. Teor. Fiz.* **54**, 213 (1968).

73. A. M. Brodskii and Yu. Ya. Gurevich, and V. G. Levich, *Phys. Status Solidi* **40**, 139 (1970).
74. A. M. Brodskii and Yu. V. Pleskov, *Prog. Surf. Sci.* **2**, 1 (1972).
75. D. B. Matthews and S. U. M. Khan, *Aust. J. Chem.* **28**, 253 (1975).
76. J. O'M. Bockris, S. U. M. Khan, and K. Uosaki, *J. Res. Inst. Catal., Hokkaido Univ.* **24**, 1 (1976).
77. R. H. Wilson, *J. Appl. Phys.* **48**, 4292 (1977).
78. J. Reichmann, *Appl. Phys. Lett.* **36**, 574 (1980).
79. H. Reiss, *J. Electrochem. Soc.* **125**, 937 (1978).
80. W. J. Albery and P. N. Bartlett, *J. Electrochem. Soc.* **128**, 1492 (1981).
81. A. K. Ghosh and H. P. Maruska, *J. Electrochem. Soc.* **125**, 223 (1978).
82. J. O'M. Bockris and K. Uosaki, *J. Electrochem. Soc.* **125**, 223 (1978).
83. D. Hanemann and J. F. McCann, *Phys. Rev.* **B24** (1981).
84. S. U. M. Khan and J. O'M. Bockris, *J. Appl. Phys.* **52**, 7270 (1981).
85. P. W. Anderson, *Phys. Rev.* **124**, 41 (1961).
86. J. W. Gadzuk, J. K. Hartman, and T. N. Rhodin, *Phys. Rev.* **B115**, 2110 (1970); **B4**(2), 241 (1971).
87. E. E. Anderson, *Modern Physics and Quantum Mechanics*, W. B. Saunders, London (1971), p. 359.
88. F. Constantinescu and E. Magynri, *Problems in Quantum Mechanics*, Pergamon Press, Oxford (1971).
89. W. Schmickler, *J. Electroanal. Chem.* **82**, 65 (1977).
90. J. Schultze and K. J. Vetter, *Electrochim. Acta* **18**, 889 (1973).
91. K. J. Vetter and J. W. Schultze, *Ber. Bunsenges. Phys. Chem.* **77**, 995 (1973); P. Kohl and J. W. Schultze, *Ber. Bunsenges. Phys. Chem.* **77**, 953 (1973).
92. J. W. Schultze and U. Stimming, *Z. Phys. Chem. N.F.* **98**, 285 (1975).
93. K. H. Gundlach, *Festkorperprobleme* **11**, 273 (1971).
94. J. W. Gadzuk, *Phys. Rev.* **B1**, 2110 (1970).
95. J. O'M. Bockris and S. D. Argade, *J. Chem. Phys.* **49**, 5133 (1968).
96. S. Trasatti, *J. Electroanal. Chem.* **66**, 155 (1975).
97. S. Trasatti, in *Comprehensive Treatise of Electrochemistry*, Vol. 1, J. O'M. Bockris, B. E. Conway, and E. Yeager, eds., Plenum Press, New York (1980), Chap. 2.
98. H. Gerischer, *Z. Phys. Chem. N.F.* **26**, 223 (1960).
99. H. Gerischer, in *Special Topics in Electrochemistry*, P. A. Rock, ed., Elsevier, Amsterdam (1977), p. 35.
99. R. Memming, in *Electroanalytical Chemistry*, Vol. 11, A. J. Bard, ed., Marcel Dekker, New York (1979).
100. S. R. Morrison, *Electrochemistry at Semiconductor and Oxide Metal Electrodes*, Plenum Press, New York (1980).
101. A. J. Nozik, *Ann. Rev. Phys. Chem.* **29**, 189 (1978).
102. R. E. Malpas, K. Itaya, and A. J. Bard, *J. Am. Chem. Soc.* **103**, 1622 (1981).
103. J. O'M. Bockris and S. U. M. Khan, *J. Electrochem. Soc.* **128**, 2606 (1981).
104. L. Landau, *Phys. Z. Sowjetunion* **2**, 46 (1932).
105. C. Zener, *Proc. R. Soc. London Ser. A* **137**, 696 (1932); **140**, 660 (1933).
106. D. R. Bates, *Proc. R. Soc. London Ser. A* **257**, 22 (1960).
107. M. D. Newton, *Int. J. Quantum Chem. Quantum Chem. Symp.* **14**, 363 (1980).
108. B. D. Olafson and W. A. Goddard III, *Chem. Phys. Lett.* **28**, 457 (1974).
109. K. Kuchitsu and Y. Morino, *Bull. Chem. Soc. Japan* **38**, 814 (1965).
110. S. P. Dolin, E. D. German, and R. R. Dogonadze, *J. Chem. Soc., Faraday Trans.* **273**, 648 (1977).
111. N. R. Kestner, J. Logan, and J. Jortner, *J. Chem. Phys.* **78**, 2148 (1974).
112. J. Halpern and L. E. Orgel, *Discuss. Faraday Soc.* **29**, 32 (1960).
113. H. L. Strauss, *Quantum Mechanics, An Introduction*, Prentice-Hall, Englewood Cliffs, New Jersey (1968), p. 140.

3

Kinetics of Electrochemical Reactions at Metal–Solution Interfaces

L. I. KRISHTALIK

1. Introduction: Steps of Electrode Processes

Electrode reactions occurring at the metal–solution interface are very often multistep processes. Like any heterogeneous reactions, they involve steps of transport of reagents and products, as well as chemical and electrochemical transformation steps at the interface.

Effects of transport processes, which are, in some cases, complicated by chemical transformations within the solution, may, in principle, either be taken into account or eliminated. These problems have been dealt with in another volume of the present Treatise and therefore will not be considered here.

With the exception of some simple single-electron reactions, most electrode processes involve several electrochemical or chemical steps. For example, the hydrogen evolution reaction, described by the overall equation

$$2H^+ + 2e \rightarrow H_2 \qquad \text{(A)}$$

may include the following steps:

$$H^+ + e \rightleftarrows H_{ads} \qquad \text{(B)}$$

L. I. KRISHTALIK • Institute of Electrochemistry of the Academy of Sciences of the USSR, Leninsky Prospekt 31, Moscow V-71, USSR.

$$2H_{ads} \rightleftarrows H_2 \tag{C}$$

$$H_{ads} + H^+ + e \rightleftarrows H_2 \tag{D}$$

These processes (B), (C), and (D) are often referred to, respectively, as Volmer,(1) Tafel,(2) and Heyrovsky(3) reactions after the names of the investigators who were the first to distinguish and point out their significance.

The overall reaction (A) may involve the following three combinations of elementary steps: (a) double occurrence of the discharge step (B) in the cathodic direction followed by the recombination step (C); (b) a single occurrence of the discharge step (B) followed by the electrochemical desorption step (D); and (c) a single occurrence of the dissociative adsorption of the H_2 molecule (C), directed from right to left, with the electrochemical desorption (D) subsequently occurring twice. These three possibilities determine three different paths of the reaction as a whole.

The possibility, in principle, of several reaction paths is a principal feature of multistep processes. In certain cases, a reaction follows several routes at the same time.

Defining the path of a reaction does not solve the problem of its mechanism. In a given sequence of stages, the kinetic behavior of a process as a whole may vary, depending on the characteristics of each step.

Consider, for instance, evolution of hydrogen involving the path: discharge-electrochemical desorption. If the process is stationary, the rate of formation of the adsorbed hydrogen (B) [i.e., the number of acts of reaction (B) per second per cm^2 of the electrode] V_B is equal to the rate of its removal through D, V_D; otherwise, the surface concentration of hydrogen, hence, the reaction rate would vary in time, i.e., the process would not be stationary. Each of the steps may proceed in a forward as well as a backward direction, so that the total rate, V_i, is the difference of the two rates $\overrightarrow{V}_i$ and $\overleftarrow{V}_i$. With this in view, the steady state condition is written as follows:

$$\overrightarrow{V}_B - \overleftarrow{V}_B = \overrightarrow{V}_D - \overleftarrow{V}_D = V \tag{1}$$

Here, V is the rate of the reaction as a whole. A *steady state condition* of this type may be written for a sequence of any number of steps, except that, in general case, one should take into account the *stoichiometric number* ν_i, i.e., the number of its recurrences along the path of the overall reaction:

$$(\overrightarrow{V}_1 - \overleftarrow{V}_1)/\nu_1 = \cdots = (\overrightarrow{V}_i - \overleftarrow{V}_i)/\nu_i = \cdots = (\overrightarrow{V}_n - \overleftarrow{V}_n)/\nu_n = V \tag{2}$$

For example, in the case of a discharge-recombination sequence (B, C), $\nu_B = 2$ and $\nu_C = 1$; therefore,

$$(\overrightarrow{V}_B - \overleftarrow{V}_B)/2 = \overrightarrow{V}_c - \overleftarrow{V}_c = V \tag{3}$$

The greater the deviation of a potential from its equilibrium value, the higher is the current or, which is equivalent, the reaction rate V; also the greater is the degree by which the rate of each step in the forward direction exceeds that in the backward direction. There are two typical extreme cases: an irreversible and a quasireversible (quasiequilibrium) reaction. If the rate of any reaction in the backward direction can be neglected, compared to its rate in the forward direction ($\overrightarrow{V}_i \gg \overleftarrow{V}_i$), then this step is practically irreversible. If, on the other hand, the rates of the forward and backward reactions are comparable enough for their difference to be small compared with their absolute values ($\overrightarrow{V}_i \simeq \overleftarrow{V}_i$; $\overrightarrow{V}_i - \overleftarrow{V}_i \ll \overrightarrow{V}_i, \overleftarrow{V}_i$), then equilibrium in this step is almost unaffected, and it may be considered as quasireversible.

The degree of irreversibility of individual steps depends, because of the steady state condition, on the conditions of the process and the characteristics of a given step, as well as of any other steps associated with the latter. For example, if the total rate V of a reaction (or the total current i, equal to nFV) is much lower than the rate of a given step in the forward and backward directions at the equilibrium potential $\overrightarrow{V}_{i0} = \overleftarrow{V}_{i0} = V_{i0}$ (corresponding to this rate is the *exchange current* $i_{i0} = n_iFV_{i0}$), then this step is a quasiequilibrium one. In the case of a reversed relation between i and i_{i0}, the ith stage is expected to be irreversible. In complex multistep processes, there is a possibility that this condition is not met if the concentration of an intermediate product participating in the back reaction increases rapidly with the potential. Let it be assumed that, under the experimental conditions and for a given sequence of steps, one of them, namely the ith step, is irreversible, while the others are quasireversible:

$$(\overrightarrow{V}_1 - \overleftarrow{V}_1)/\nu_1 = \cdots = \overrightarrow{V}_i/\nu_i = \cdots = (\overrightarrow{V}_n - \overleftarrow{V}_n)/\nu_n \tag{2a}$$

Then, the rate of the reaction as a whole is simply the rate of the ith step in the forward direction (taking into account, of course, the stoichiometric number of the step). For example, the hydrogen ion discharge being irreversible in the discharge-electrochemical desorption route

$$V = \overrightarrow{V}_B \tag{1a}$$

i.e., the number of H_2 molecules formed per unit of time is equal to that of the discharged H^+ ions [the second hydrogen atom is introduced into each H_2 molecule in reaction (D)]. The same holds true for a discharge-recombination sequence, i.e.,

$$V = \overrightarrow{V}_b/2 \tag{3a}$$

Thus, the kinetic law of a reaction as a whole, with a single irreversible step, is determined in a simple way; it is identical to the stoichiometric factor with the kinetic equation for this irreversible step. This step is known as the *rate-determining* or *limiting* step. Use is often made of the term "slow" step. This term should be taken only colloquially bearing in mind that, as has been mentioned above, the resulting rate of each one of the sequential steps is the *same* in accordance with the steady state condition. However, in the case of the irreversible step, its resulting rate is a rate in the forward direction, while in the case of quasireversible steps, this rate is the *difference* between those in the forward and backward directions. In this case, the rate-determining step is "slow" in the sense that, in the forward direction, its rate is minimal.

The latter statement also holds near the equilibrium potential, when none of the steps can be considered fully irreversible. If, however, $\vec{V}_i$ is much lower than the $\vec{V}$ of each of the remaining steps, then, although $\overleftarrow{V}_i$ relative to $\vec{V}_i$ could not be ignored, the kinetic pattern of the process is still determined by the *i*th step. For all the other steps, the relative deviation from equilibrium is much less than for the *i*th step. The above situation arises when the current i is lower than the exchange current i_{i0}, and, at the same time, much lower than the exchange currents of the remaining steps.

Finally, one more remark with regard to the Eqs. (1a)–(3a). The overall reaction rate equals that of the limiting step and is fully determined by its kinetic parameters. This does not mean, however, that other steps do not affect the reaction rate. In cases where the rate of the limiting step depends substantially on the intermediate product concentration, the latter being determined by equilibrium in the quasireversible steps, the effect of the quasireversible steps on the process is considerable. This effect, however, is indirect and manifests itself only through concentration changes in the kinetic equation of the limiting step.

Consider now a case involving a number of irreversible stages, e.g., two:

$$(\vec{V}_1 - \overleftarrow{V}_1)/\nu_1 = \cdots = \vec{V}_i/\nu_i = \vec{V}_k/\nu_k = \cdots = (\vec{V}_n - \overleftarrow{V}_n)/\nu_n = V \quad (2b)$$

Here, the concept of the limiting step becomes more complicated. In such a system, a later irreversible step utilizes the intermediate product formed in an earlier irreversible step (this applies both to a direct product of that step and to products of its subsequent quasireversible transformations). In the steady state, the concentration of the intermediate product is such as to ensure equality of the respective rates. It is therefore convenient, as proposed by Frumkin,$^{(4)}$ to compare the rates of these two steps under such condition that the effect of the intermediate product concentration is excluded and, thereby, to discriminate the slow step. For example, the rate of a discharge reaction varies with the fraction of the free electrode surface

$$\vec{V}_B = k_B(\phi)(1 - \theta)C_{\mathrm{H}^+}, \quad (4)$$

where $k_B(\phi)$ is the rate constant depending on potential ϕ, θ is the degree of coverage of the surface with adsorbed hydrogen, and C_{H^+} is the hydrogen ion concentration.† On the other hand, the desorption rate varies with the surface coverage in the following manner:

$$\vec{V}_D = k_D(\phi)\theta C_{\mathrm{H}^+} \quad (5)$$

---

† Equations (4) and (5) are written in a form corresponding to Langmuir's adsorption isotherm. Formally, they apply to any other isotherm; however, in such a case, the rate constants depend not only on ϕ, but also on θ.

If the rate $\vec{V}_B$ at $\theta = 0$, i.e., at $(1 - \theta) = 1$, is compared with $\vec{V}_D$ at $\theta = 1$ (i.e., if in fact the rate constants are compared), the reaction whose rate is lower can be regarded as rate determining. Indeed it is precisely its kinetic pattern that determines the kinetic equation for the reaction as a whole, whereas the characteristics of another process will only affect the absolute value of the stationary coverage, θ_{st}. Thus, in the sequence under consideration, when $\vec{V}_B = \vec{V}_D$,

$$\theta_{st} = \frac{k_B(\phi)}{k_B(\phi) + k_D(\phi)} \tag{6}$$

It can easily be seen that if $k_B(\phi) \ll k_D(\phi)$, i.e., $\theta_{st} \ll 1$,

$$V = k_B(\phi)C_{H^+} \tag{6a}$$

i.e., the rate is completely dependent on the discharge characteristics. If it is the desorption step that is slow $[k_D(\phi) \ll k_B(\phi)$ and $\theta \simeq 1]$, the rate of the overall process will be determined by the desorption reaction parameters

$$V = k_D(\phi)C_{H^+} \tag{6b}$$

A similar expression for a discharge–recombination sequence is

$$V_C = k_C\theta^2 \tag{7}$$

Here, k_C is independent of ϕ. Then

$$\theta_{st} = \frac{-k_B(\phi)C_{H^+} + [k_B(\phi)^2C_{H^+}^2 + 4k_Ck_B(\phi)C_{H^+}]^{1/2}}{2k_C} \tag{8}$$

and

$$V = \frac{2k_C + k_B(\phi)C_{H^+} - [k_B(\phi)^2C_{H^+}^2 + 4k_Ck_B(\phi)C_{H^+}]^{1/2}}{2k_C}k_B(\phi)C_{H^+} \tag{9}$$

For the slow discharge step $k_B(\phi)C_{H^+} \ll k_C$, $\theta \ll 1$, and

$$V = k_B(\phi)C_{H^+} \tag{9a}$$

For a slow recombination step $k_B(\phi)C_{H^+} \gg k_C$, $\theta \simeq 1$, and

$$V = k_C \tag{9b}$$

Thus in the limiting cases where the rate constants of two (or more) irreversible steps differ greatly, it is desirable to distinguish one of these steps as the rate-determining step. If, on the other hand, both reaction steps have comparable rate constants, the concept of a single rate-determining step, of course, makes no more sense, so that kinetics of the process would be substantially dependent on the parameters of both steps [see Eqs. (6) and (9)].

Note that a higher rate constant does not necessarily mean a higher exchange current, because the latter depends not only on the rate constant at the equilibrium potential ϕ_e, but also, for many reactions, on the equilibrium *concentrations* of the intermediate product. For example, if the condition $k_B(\phi_e) \ll k_D(\phi_e)$ is met, the inequality $k_B(\phi_e) \times (1 - \theta_e) \gg k_D(\phi)\theta_e$ may be valid at the same time, i.e., the discharge exchange current can be much greater than the electrochemical desorption exchange current. In this case, far from equilibrium, where both discharge and desorption reactions are irreversible, the rate-determining step is the discharge process while in the vicinity of the equilibrium potential, we deal with a situation in which $i_{D0} \leq i \ll i_{B0}$, i.e., the discharge is quasireversible, whereas the desorption is essentially irreversible and rate determining. Such an interchange of the limiting steps in different potential regions is a quite common phenomenon. In addition to the above reason, it may occur for a number of others. For example, if the type of dependence of the rate constants of two steps on the potential is different, the relationship between them may be opposite in different potential regions. Another reason why the limiting step may change is if a limiting intermediate product concentration is attained so that the rate of the step in which the intermediate product is involved can no longer adapt itself to the rate of the preceding step, which is precisely why the last irreversible step becomes rate determining.

As was mentioned earlier, when current flows, the electrode potential, of course, deviates from its equilibrium value. The greater this deviation, i.e., the greater the *polarization*, the greater is the current, all other things being equal. Since the current flow is an irreversible process, thermodynamically speaking, it becomes obvious that at least one of the reaction steps is substantially irreversible. If this irreversibility is only due to transport of reagents and hence can be expressed in terms of the concentration near the electrode, then the difference between the equilibrium potential ϕ_e and its value ϕ when current flows through the electrode is referred to as *concentration polarization*. If the transport is quasireversible, i.e., if the reagent concentrations near the electrode (i.e., at the boundary of the diffuse layer) are almost the same as their bulk values, one of the steps of the electrode process proper is then irreversible. In this case, the difference between ϕ and ϕ_e is known as *overpotential*. It is usually denoted by η.† Depending on which step is rate determining, one speaks of a discharge overpotential (or, in a broader sense, transfer overpotential, for each step associated with charge transfer across the metal–solution interface), a chemical reaction overpotential, a crystallization overpotential, etc. If the reaction kinetics is materially affected by a number of irreversible steps (e.g., diffusion and discharge), in the general case, polarization cannot be expressed simply as a sum of terms characteristic of each irreversible step. The relationship between polarization and the kinetic parameters of individual steps is determined by the kinetic equations of these steps and the steady state conditions of the process as a whole. The only example when polarization arising in no matter how complicated a mechanism can be expressed as a sum of overpotentials for the individual steps is the case of very small polarizations ($|\phi - \phi_e| \ll RT/F$), i.e., when the rate of each step is a linear function of the respective overpotential.

---

† In most cases, η is assumed to represent the *absolute* value of $|\phi - \phi_e|$, although some authors prefer the definition: $\eta = \phi - \phi_e$. In the latter case, $\eta > 0$ for an anodic process and $\eta < 0$ for a cathodic process.

In what follows in this chapter, we shall consider only the steps of charge transfer across the electrode–solution interface. It is precisely these steps that are specific for electrode processes and set them apart from other heterogeneous reactions.

Over many years, the predominant opinion in electrochemistry was that, in all cases, overpotential is due to the slow rate of chemical and diffusion steps; it was assumed that, in a way similar to the reactions of neutralization or precipitation of insoluble salts, the process of discharge of ions was practically instantaneous. For the first time, the finite discharge rate and the effect of the electrode potential drop seems to have been discussed in a semiquantitative form already back in 1924 by Audubert(5) and Butler,(6) who tried to rationalize the Nernst equation kinetically. In contemporary form, the notion of a slow discharge as the limiting step of the hydrogen evolution process was brought forth by Erdey-Gruz and Volmer in their fundamental work.(1) They clearly outlined the concept of a direct effect of the potential on the discharge activation energy and introduced the notion of the *transfer coefficient*, α, which characterized the magnitude of this effect.

At first, however, it seemed that the slow discharge theory was irreconcilably at variance with experimental data since in solutions of pure acids the hydrogen overpotential was found to be independent of the acid concentration. This inconsistency was solved in Frumkin's classical work(7) in which he took into consideration the effects of the double-layer structure on the discharge rate. The numerous studies by Frumkin and his coworkers, as well as the work of other electrochemists, that followed, have provided experimental proof of the limited rate of electrode reactions involving transfer of a charge across the metal–solution interface.

2. Phenomenological Theory of the Elementary Act of an Electrode Reaction

2.1. Brønsted–Polanyi Relation and Electrode Reaction Activation Energy

While following the general pattern of heterogeneous chemical reactions, electrode reactions are additionally characterized by being associated with the transfer of electric charge across the interface between two conductive phases. This is why the energetics, hence, the rate of charge transfer from one phase to the other, depends on the electric potential difference between these phases. Thus, in addition to the variables commonly involved in chemical kinetics, a new independent variable, viz., electrode potential, appears in electrochemical kinetics.

The basic relationship between the potential and electrode reaction rate (expressed in terms of the electrical units, i.e., current density i) was empirically found by Tafel in 1905(2):

$$\eta = a + b \log i \tag{10}$$

where a and b are constants depending on the properties of a given system. In a different form, Eq. (10) can be written as follows:

$$i = i_0 e^{\eta/b'} \tag{10a}$$

where $b' = b/2.3$ and $a = -b \log i_0 = -b' \ln i_0$.

This specifically electrochemical law is, as was shown by Frumkin,(8) a direct consequence of an important general kinetic rule formulated by Brønsted in the 1920s(9) and later elaborated by Polanyi, Semenov, and other investigators.(10–13) In the beginning, this rule was formulated for certain homogeneous processes of proton transfer, then applied to other types of reactions. The essence of this rule originates from the fact that for a series of homologous reactions, there is a relation between the reaction rate constants k and the equilibrium constants K of the form

$$k = k_0\left(\frac{K}{K_0}\right)^{\alpha} \tag{11}$$

Here, α is the so-called transfer or Brønsted coefficient, and subscript 0 is used to denote constants for the reaction selected as a conventional standard. In terms of the theory of absolute reaction rates, whereby the rate constant is expressed through standard free activation energy $\Delta G^{\ddagger}$,

$$k = \kappa \frac{kT}{h} e^{-\Delta G^{\ddagger}/RT} \tag{12}$$

relation (11) is equivalent to

$$\Delta G^{\ddagger} = \Delta G_0^{\ddagger} + \alpha(\Delta G^{\circ} - \Delta G_0^{\circ}), \tag{13}$$

where ΔG° is the standard free reaction energy (or, to be more precise, the standard free energy of the slow step to which $\Delta G^{\ddagger}$ applies).

Frumkin noted that, at different potentials, an electrode reaction may be regarded as a series of similar reactions differing only in the value of ΔG°, this difference being equal to $nF\Delta\phi$ (in the case of electrode reactions, one should consider the overall free energy change, including electrical work; in what follows, this value will be denoted $\Delta\bar{G}^{\circ}$; n is the number of electrons transferred within an elementary act of a slow process step). Therefore, for electrochemical reactions, Eq. (13) takes the form $\Delta G^{\ddagger} = \Delta G_0^{\ddagger} + \alpha nF\Delta\phi$.

Substituting this expression into Eq. (11), we have

$$i = k' \exp\left(-\frac{\alpha nF\Delta\phi}{RT}\right) \tag{14}$$

i.e., a Tafel equation with $b' = RT/nF$ results. Incidentally, it can be seen that the transfer coefficient α introduced by Erdey-Gruz and Volmer is identical with the Brønsted coefficient.

The physical meaning of the Brønsted relation is normally explained by means of a diagram of potential (similarly, free-) energy curves representing the system's internal energy U (or its energy $G°$) as a function of a reaction coordinate x (Figure 1). The nature of this coordinate and the reasons why U depends on x are considered with the aid of concrete molecular models of an elementary act and, in principle, may be different. However, from a purely phenomenological point of view, the mere existence of this relation is quite sufficient for some important conclusions to be drawn.

Equilibrium coordinates x_i° and x_f° of a system in its initial and final states are, generally speaking, different, i.e., the minima of respective potential curves U_i and U_f are shifted relative to each other. This immediately suggests that, in the general case, there exists a potential barrier $U^* - U_i$ which is determined by the point of intersection of the potential curves. The vertical shift of U_i and U_f relative to each other, i.e., corresponding to a variation in the heat of the elementary act, $\Delta U° = U_f^\circ - U_i^\circ$ (in the case of an electrode reaction, a variation in $U°$ practically equals $nF\Delta\phi$) causes an energy variation at the intersection point x^*. This variation is usually smaller than the variation in $\Delta U°$; therefore, the activation energy varies, too.† For example, as the energy of the initial state U_i° increases by $nF\Delta\phi$, U^* increases by $\beta nF\Delta\phi$ while the activation energy $U^* - U_f^\circ$ decreases, respectively, by $\alpha nF\Delta\phi$. It follows, correspondingly, that the activation energy $U^* - U_f^\circ$ of the backward reaction increases by $\beta nF\Delta\phi$. Since, in view of the microscopic reversibility principle, the forward and backward reactions pass through the same activated state, the difference between their activation energies is equal to the heat of the reaction, hence, $\alpha + \beta = 1$. As can be easily seen, the value of α (and β)

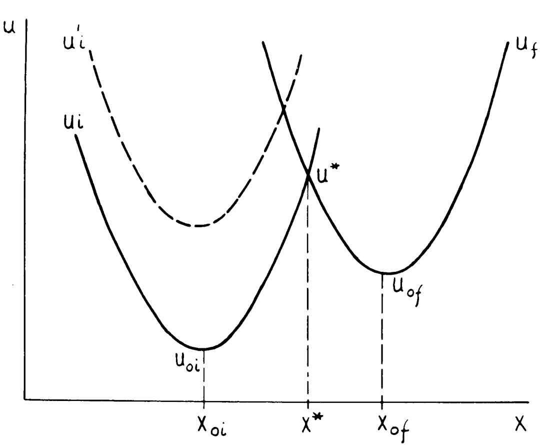

Figure 1. Potential curves of the initial (U_i) and final (U_f) states. X, generalized coordinate; X_{0i} and X_{0f}, its equilibrium initial and final values. For other designations see text.

---

† The case where $\Delta U^* > \Delta(\Delta U°)$ will be considered in Section 2.5.

is determined formally by the relation between the slopes of the potential curves at the point of their intersection.

Harmonic potential energy curves may be linearized only within a narrow energy interval; therefore, it is to be expected that the relation between their slopes, and hence α, must vary smoothly over a sufficiently great variation in $\Delta U°$. However, the linearization interval is broader if the curves $U(X)$ have an inflection typical of, for example, an anharmonic oscillator, but near the minimum of the curves, where they can always be approximated by a parabola, the linearity is inevitably disturbed. In fact, when a certain series of homogeneous reactions of proton transfer were studied over a sufficiently broad range of $\Delta U°$ (about 80 kJ mol^{-1}), a smooth variation in α was observed(14); however, nobody has so far reliably established a smooth variation in the true value of α with the potential† for any electrode reaction; moreover, in the case of the hydrogen evolution reaction, a good constancy in α is observed over an interval of overpotentials of about 1.5 V.(15–17) This difference in the behavior of chemical and electrode reactions has not yet found a plausible explanation in any of the existing molecular theories of the elementary act. In fact most theories of electron transfer predict that α is potential dependent owing to a use of the harmonic oscillator model. We shall return to the dependence of α on the potential in Section 2.5.

The Brønsted relation operates with free energies, while potential diagrams involve internal energies. Transition from one to the other implies that in a homologous reaction series the entropy variations are constant or vary systematically with the internal energy. Such relations are known to have been observed in a great number of most diverse processes [see, for example, (18)].

Regardless of the constancy of α, the Brønsted relation permits a number of quantitative conclusions to be drawn. To this end, there is no need to resort to the linear relation (13); it is sufficient to use a statement which may be considered as a generalized Brønsted relation(19)—between the free energies of activation and of overall reaction, there exists a single-valued functional relation

$$\Delta G^{\ddagger} = f(\Delta G°) \tag{15}$$

A similar relationship can be written for internal energies as well:

$$U^{*} - U_i^{\circ} = f(\Delta U°) \tag{15a}$$

Consider now the effect of variation in heats of adsorption of reagents, using Eq. (15a). In Figure 2, curve 1 corresponds to the initial state of the discharge step, while curves 2 and 3 correspond to the final state, i.e., adsorbed product (e.g., an hydrogen atom), the heat λ of adsorption in the case of

---

† Variations in the apparent value of α are often related to a gradual change in the ψ_1 potential, a secondary effect.

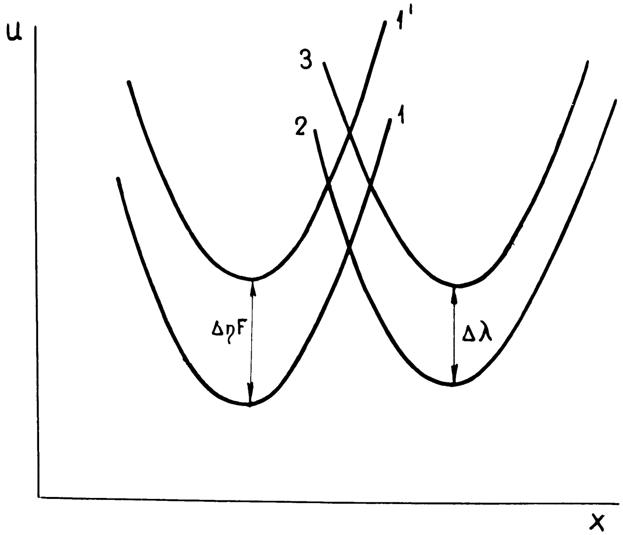

Figure 2. Potential curves. Curve 1, initial state; 2 and 3, final state. Curves 2 and 3 correspond to different heats of adsorption of the product (λ_f). Curve 1' is in fact curve 1 shifted vertically by $\Delta\eta F = -\Delta\lambda_f$.

curve 2 being greater than in the case of curve 3 (we compare two different electrode materials).

We shall now apply a procedure first proposed by Temkin,$^{(20)}$ namely, the initial state curve will be shifted up by a value equal to the difference of heats of adsorption $|\Delta\lambda_f|$, i.e., we apply, in fact, additional overpotential $\Delta\eta = -\Delta\lambda_f/F$. Now, the relative positions of curves 1 and 3 are the same as those of curves 1 and 2; hence, in accordance with the generalized Brønsted relation, corresponding to these curves the same activation energies arrive and, all other things being equal, therefore the same rates. In other words, at the same current density, the difference in overpotentials at two metals is determined by the difference in heats of adsorption of the immediate product of the discharge step.† (This statement holds true if it is assumed that the entropies of activation are equal; in the case of hydrogen evolution, it has to be modified somewhat, first of all because of the different probability of proton tunneling at different cathode materials.)

The energy of adsorption of the intermediate product affects not only the activation energy, i.e., the reaction rate constant, but also its surface concentration. At an equilibrium potential, the surface coverage is at equilibrium and represents a single-valued function of the adsorption energy, e.g., with Langmuir isotherm

---

† This conclusion is implicit in Butler's treatment in 1936, using potential energy curves for chemisorption at electrodes. (See also Ref. 10.)

$$\frac{\theta_0}{1-\theta_0} = KCe^{-\lambda/RT} \tag{16}$$

where C is the volume concentration of the adsorbed substance, and K is a constant independent of the nature of the adsorbent.

An increase in the heat of adsorption decreases the discharge activation energy ($E^* = E_0^* - \alpha\lambda$), i.e., increases the rate constant

$$k = k_0 e^{\alpha\lambda/RT} \tag{17}$$

However, at the same time, the equilibrium coverage increases, too, i.e., the free surface area $(1 - \theta_0)$ is reduced, which diminishes the exchange current. As a result, depending on λ, the exchange current passes through a maximum; at a low adsorption energy, $1 - \theta_0 \simeq 1$ and the most significant effect is the increase in k, while at high λ, $\theta_0 \simeq 1$ and the predominant role is played by a sharp decrease in $(1 - \theta_0)$. Quantitatively, this is suggested by a combination of Eqs. (14), (16), and (17):

$$i_0 = k(1 - \theta_0) = k_0 \frac{e^{\alpha\lambda/RT}}{1 + Ke^{\lambda/RT}} \tag{18}$$

Such a "volcano" relation† between the exchange current and the heat of adsorption is typical not only of the discharge stage, but also other processes such as electrochemical desorption, recombination, etc. As can be inferred from its physical significance, it is common for any heterogeneous reactions, as was shown by Balandin.(21)

Interestingly, if the adsorption isotherm is of a different form, independence of the exchange current on λ may be observed within a certain range of values of λ.

Consider a case where λ depends on surface coverage θ. The simplest form of this dependence is the linear Temkin relation

$$\lambda = \lambda^0 - fRT\theta \tag{19}$$

This effect may be associated either or both with the repulsive interaction of the adsorbed particles and with the inhomogeneity (or, to be more precise, regular inhomogeneity) of the surface.(20) Therefore, the coefficient f is often referred to as the inhomogeneity coefficient.

Substitution Eq. (19) into (16) (the latter equation expresses nothing more or less than the equality of the chemical potentials of a given substance throughout the volume and on the surface), we obtain an isotherm which, at intermediate surface coverages, i.e., as $\theta/(1 - \theta) \sim 1$, gives Temkin's logarithmic isotherm

---

† This kind of treatment was given by Parsons in 1958 in some detail for various mechanisms of the H_2 evolution reaction at a series of metals having increasing strength of chemisorption of H.(25) See also (24).

$$\theta_0 = \frac{1}{f}\ln K + \frac{\lambda^0}{fRT} + \frac{1}{f}\ln C \tag{20}$$

Strictly speaking, such substitution of Eq. (19) into (16) is justified only if the relationship between λ and θ is due to repulsive interactions. However, if it involves adsorption sites with a spectrum of adsorption energies, one should average all Langmuir isotherms for each type of adsorption center.(20) The result of such averaging coincides with Eq. (20), accurate to the constant.

Taking into consideration the Nernst relationship between the equilibrium potential and the concentration C of electrochemically active substance, we have

$$\theta_0 = \text{const} \pm \frac{1}{f}\frac{nF}{RT}\phi \tag{21}$$

Here, the sign (+ or −) depends on whether the substance is an oxidant or a reductant, and n stands for the number of electrons necessary to yield the adsorbed product.

The relationship between λ and the surface coverage leads to a corresponding activation energy relation. For example, in the case of a discharge, a decrease in λ corresponds to an increase in $E^\ddagger$ by $\alpha\Delta\lambda$, i.e., by $\alpha fRT\theta$. A potential shift in a direction facilitating discharge increases the equilibrium value of θ by $1/f \cdot nF/RT \cdot \Delta\phi$, i.e., it increases the activation energy by $\alpha nF\Delta\phi$. This increase exactly compensates for the normal decrease in the activation energy $-\alpha nF\Delta\phi$, so that the reaction rate under conditions corresponding to equilibrium, at a given potential, is independent of the potential.(20) This theoretical deduction was corroborated in an experiment with the reaction of hydrogen ion discharge on platinum.(22)

In the case of two different metals with various λ^0 the θ_0 values differ by $\Delta\lambda^0/fRT$ so that at different equilibrium values of θ_0, λ_0, which is the heat of adsorption under equilibrium conditions, is constant. Hence, the activation energy is constant too and accordingly, the reaction rate does not depend on the nature of the metal. This conclusion is true to the extent to which variations in $(1-\theta)$ and the transmission coefficient κ can be ignored. The same applies to the independence of the exchange current on the potential.

Strictly speaking, this conclusion is not restricted to a specific form of the logarithmic isotherm. Indeed, in the case of an equilibrium, chemical (and electrochemical, in the case of an electrode reaction) potentials μ (or, respectively, $\bar{\mu}$) throughout the volume and on the surface are equal. In the region of intermediate coverages, a variation in the adsorbed substance's chemical potential, due to the variable term $RT\ln\theta/(1-\theta)$, is small; therefore, the essential role in the equalization of μ is played by a variation in λ with θ. This means that at a given value of μ, λ for various metals will be practically the same although θ will be different. This result is obtained with any form of the relationship between λ and θ, i.e., for any isotherm, provided the dependence of λ on θ is sufficiently strong that this contribution to the concentration dependence of the chemical potential is predominant as compared to $RT \ln \theta/(1-\theta)$.(23)

The form of the adsorption isotherm determines the shape of the polarization curve, influencing the magnitude of Tafel slope b, since θ, varying with the potential, leads to a variation in λ and hence in the activation energy. This effect has been discussed at length, starting with the first work by Temkin(20) (see, for example, Ref. 23). A most vivid illustration of the foregoing is the independence of the current on the potential.

A low ($\theta \ll 1, \lambda = \lambda_0$) or high ($1 - \theta \ll 1, \lambda \simeq \lambda_{\min}$) coverages, however, the variation in $RT \ln \theta/(1-\theta)$ becomes predominant; then the adsorption isotherm becomes practically Langmuirian (at very low θ or $1 - \theta$—Henry's law isotherm), and the kinetic relations become similar to those described at the very beginning of this chapter.

In the case of a multistep process, the energy of adsorption of the intermediate product produces different effects on the kinetic parameters of various steps. This results in different relations between constants and different reaction mechanisms (route, slow step) for metals with different adsorption properties. For example, for hydrogen evolution on metals with a low bonding energy for H, the most probable limiting step is slow discharge, while in the case of metals strongly adsorbing H, the limiting step is electrochemical desorption and, in some cases, slow recombination, at low overpotentials. For medium bonding energies of H, also at low overpotentials, an adsorption–electrochemical mechanism is probable.(24–28)

It might be useful to point out a factor which is essential when we consider the mechanism of a reaction involving a particular series of metals. In some cases, comparison of electrochemical data with data on adsorption of, for example, hydrogen from the gaseous phase gives good results. In many cases, however, the energy of adsorption from the gas phase differs greatly from the value which produces an immediate effect on overvoltage. The reasons for this may be different including, for example, strong chemisorption of the solvent.

However, it is desirable to draw attention to another considerable effect. A situation may arise when, owing to high adsorption energy, at the equilibrium, or at even lower potential, virtually complete saturation of the monolayer is achieved, yet adsorption sites of a different type with a substantially lower adsorption energy, which had existed on the metal initially or have appeared as a result of filling of the first monolayer, remain vacant. At a sufficiently strong polarization, the H_2 evolution process will take place precisely at these sites with lower adsorption energy, while the strongly bonded first monolayer is practically inert. This is precisely what happens when hydrogen is evolved on tungsten(29,30) and, probably, on other metals, e.g., Mo, with the highest bonding energy for H. Studies on evolution of oxygen on platinum have furnished convincing proof of only weakly bonded oxygen from the second and even third monolayer participating in the process.(31–33)

In a similar way, one can establish the effect of the energy of adsorption of the initial particles on the activation energy. The more strongly a particle is bonded, the more difficult is its discharge; hence, the discharge activation energy is

$$E^{\ddagger} = E_0^{\ddagger} + \alpha\lambda_i \tag{22}$$

The adsorption of a particle which is being discharged may be both specific and electrostatic, in which case it is associated with the potential difference between the site of the discharging particle and the solution volume, ψ_1, somewhere in the double-layer. The electrostatic component of the energy of adsorption of a particle with charge z_i is equal to $z_i F\psi_1$, and the corresponding contribution to the activation energy is $\alpha z_i F\psi_1$.

It should be noted, however, that all this reasoning based on the Brønsted relation is related to the energy of activation of the elementary act proper of the step under consideration without any account being taken of the possible equilibria preceding this step. Such an activation energy is known as the "true" value† and can be determined experimentally from the temperature dependence of the rate of the overall reaction at a constant concentration of the reagents in a state immediately preceding the elementary act, i.e., in the case of electrode processes, at a constant *surface* concentration of the reagents.

It is more convenient, however, to compare reaction rates at a constant concentration in the solution. The activation energy determined under such conditions is known as the "apparent" value and represents the energy of activation of the elementary act itself as well as heat change of the preceding equilibrium. At low surface concentration C_s of a reagent (in the Henry's isotherm region), C_s varies with volume concentration C and exponentially depends on the heat of adsorption

$$C_s = KCe^{\lambda_i/RT} \tag{23}$$

Substituting Eq. (23) into the expression for the reaction rate

$$V = k_0 C_s e^{-E^{\ddagger}/RT} \tag{24}$$

we obtain a relationship for the apparent activation energy

$$E^{\ddagger}_{\text{app}} = E^{\ddagger}_{\text{true}} - \lambda_i \tag{25}$$

Taking into consideration the dependence of E_{true} on the heat of adsorption (22), we obtain

$$E^{\ddagger}_{\text{app}} = E_0^{\ddagger} - (1 - \alpha)\lambda_i \tag{26}$$

---

† "True" and "apparent" activation energies are different to "ideal" and "real" ones given in Temkin's treatment of the temperature dependence of an electrochemical rate measured at a constant potential with respect to a reference electrode in the same solution, i.e., when the real (unknown) reference electrode potential is changing with temperature. (See Section 2.4.)

or, in the case of purely electrostatic adsorption,

$$E^{\ddagger}_{\text{app}} = E^{\ddagger}_{0} - (1 - \alpha)z_iF\psi_1 \tag{27}$$

To obtain a full expression for $E^{\ddagger}_{\text{app}}$, one should take into account the effect of ψ_1 potential on the adsorption energy of the product, i.e., add to Eq. (27) a term $\alpha(Z_i - n)\psi_1F$, where n is the number of electrons being transferred during an elementary act.

It can be seen that the energy of adsorption of the reagent produces two opposite effects on the reaction rate: one through the activation energy of the elementary act and the other through the surface concentration of the reagent. When $\alpha < 1$, the latter effect is predominant. These effects are well known in ordinary surface reactions, e.g., in heterogeneous catalysis.

Simple addition of the true activation energy and the heat of adsorption takes place only in the case of the Henry's law isotherm; with other isotherms, the picture becomes more complicated and must be analyzed separately in each specific instance.

2.2. Electronic Work Function and Related Values in Electrochemical Kinetics

The role of the electronic work function in the kinetics of electrode reactions was elucidated in 1935 by Frumkin$^{(34)}$ and has been discussed many times.

Consider the same electrode reaction on electrodes of different metals, for example,

$$\overset{+}{\mathrm{A}}_{\mathrm{sol}} + \overset{-}{\mathrm{e}}_{\mathrm{M}} \rightleftarrows \mathrm{A} \tag{E}$$

Here, ion A^+ is in the solution, the electron is in the metal, and substance A is in a macroscopic phase, e.g., in the solution or in the gaseous phase.

Electron chemical potentials $\mu_e(1)$ and $\mu_e(2)$ in different metals are different, which might suggest that the energetics of reaction (E) on different metals must differ greatly, resulting in appreciable differences in the activation energy of the reaction. However, when we determine the energetic effect of a reaction, we must consider not only the chemical but also the electrical component of the free enegy, i.e., electrochemical potentials, $\bar{\mu}_e$. The electrode potential is taken the same for the two different metals: i.e., $\bar{\mu}_e(1) = \bar{\mu}_e(2)$ (the emf of any galvanic circuit is nothing but the electrochemical potential difference of the electrons at the terminals of this circuit, expressed in electrical units; the electrode potentials being equal, the emf of the circuit between them is zero). Hence, the electrons in both metals are energetically equivalent and therefore do not affect the energetics of the process. But if the heat (or free energy) of an elementary act on both metals is the same, then, in accordance with the generalized Brønsted relation (Eq. (15)), the activation (free) energy is the same, too, at a given electrode potential.

The difference in the nature of the metal manifests itself in that, at the same electrode potential, the Galvani potential drop at the metal–solution interface is different, the Galvani potential difference being equal to the difference of μ_e's. Since, however, the absolute value of an individual potential drop cannot be measured, but only the overall energetic effect, these differences are impossible to observe.

Using the terminology which will be considered in detail in 2.4, we can say that, with different metals, the ideal activation energy (at a constant potential drop) is different, but the real activation energy (at constant *electrode potential*) is the same. It is the *latter* that lends itself to observation.

Thus, the energy of activation of reaction (E) turns out to be independent of the nature of the metal. This holds true for that form, precisely, in which reaction (E) is written, i.e., when all components are within respective phases. If the reaction proceeds through substances in an adsorbed state or, to be more precise, if the energy of the adsorbed substances differs greatly from their energy in the bulk, the nature of the metal affects the adsorption energy and, as was described in the previous section, the apparent activation energy for the overall reaction. However, the energy level of the electron in the metal produces no direct effect on the activation energy.

This can be easily seen from an example of a reaction involving reduction of some anions which do not exhibit any tangible specific adsorbability, while significant electrostatic adsorption effect (ψ_1 effects) can, in fact, be quantitatively taken into account.

This has been done in the works by Frumkin and Nikolaeva-Fedorovich *et al.*, which will be discussed in Section 4.3. In particular, Figure 25 in that section suggests that the marked differences in the kinetics of persulfate reduction on various metals are associated with the differences in the structure of the double layer on these metals. After the data are corrected for the ψ_1 effect, the rate of the process on most diverse metals becomes the same.

Note the peculiarities of the work functions in a nonconducting medium (vacuum, pure solvent) and a conducting medium (electrolyte solution): when two metals contact each other, an electron equilibrium is always established between them, i.e., the condition $\bar{\mu}_e(1) = \bar{\mu}_e(2)$ is met. The work function W is defined as the work of electron transfer from a metal to a point in the nonmetallic phase which is in the proximity to the interface at such a distance that the potential variation with distance can be ignored, i.e., beyond the superficial electric double layer, including the region in which the image forces are active:

$$W = \bar{\mu}_e(\text{met}) - \bar{\mu}_e(\text{nonmet}) \tag{28}$$

When the nonmetallic phase is nonconductive, the potentials on the surface of both metals are not equal. This potential difference, the Volta potential $\Delta\psi$, makes an appropriate contribution to the electrochemical potentials of the electrons in this phase, $\bar{\mu}_e(\text{Nm})$:

$$\bar{\mu}_e(\text{Nm } 1) = \bar{\mu}_e(\text{Nm } 2) - e\Delta\psi \tag{29}$$

As can be seen, the Volta potential is equal to the work function difference of the two metals (expressed in electrical units). The Volta potential is due to the surface of the metals being charged as a result of the electron migration from one metal to the other. Since the excess surface electron density in a metal charged to common Volta potential values is low as compared to the electron concentration on the surface of the uncharged metal, it cannot produce any tangible effect on the distribution of the electron density near the metal surface, i.e., on the surface potential drop. Therefore, the work functions for an uncharged metal or a metal in contact with another is practically the same.

If the nonmetallic phase is highly conductive, the potential in this phase, at any point beyond the double layer, is the same; hence, the electrochemical potential, $\bar{\mu}_e(\text{Nm})$, is the same, too. Therefore, the electronic work function in metal–solution systems for two metals which are in direct or indirect contact (i.e., at the same electrode potential) is the same. It stands to reason that this applies equally well to different faces of the same metal.

This deduction has found direct proof in experiments conducted by Pleskov *et al.*,$^{(35,36)}$ aimed at studying the photoemission of electrons from metals into an electrolyte solution. Figure 3 illustrates the relationship between photocurrent to the power 2/5 and the potential for a number of electrode materials (this relationship must, in accordance with Brodsky's and Gurevich's theory$^{(37)}$, be rectilinear). Although the difference of the point of zero change (p.z.c.), i.e., the difference in the work functions at the metal–pure-water interface for the metals under investigation, reaches 0.5 V, all straight lines can, within the accuracy of the experiment, be extrapolated to a single point

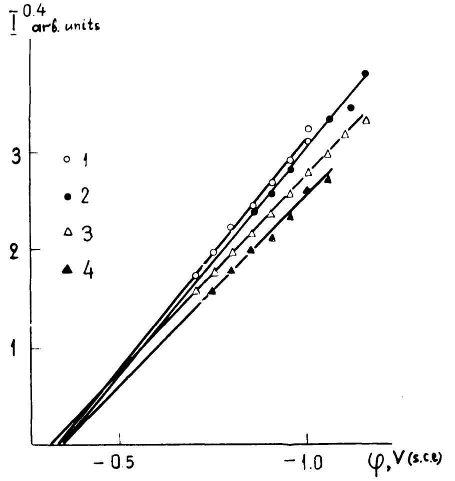

Figure 3. Emission current to the power 2/5 versus potential for the following electrode materials: 1, mercury; 2, amalgam of Tl; 3, amalgam of In (18%); 4, amalgam of In (50%) (according to Ref. 35).

corresponding to the potential at which the work function coincides with the energy of the light quantum used in the experiments (electrochemical photoelectric effect).

The electrochemical potential difference of the electron in the metal and in the solution naturally depends on the electrode potential:

$$W = W_0 + e(\phi - \phi_0)$$

The linear relationship between the work function and the potential was corroborated both for electron photoemission and for dark cathodic generation of electrons in solutions in aprotic solvents in which sufficiently high negative potentials can be achieved, i.e., sufficiently low values of the work function can be obtained even without illumination. These low values allow a substantial rate of electron emission(38,39) to arise. These experiments have also demonstrated that the effective work function is independent of the nature of the metal (Figure 4).

When dealing with the problem of the electronic work function at the metal–solution interface, one should also consider the possible role of formation of solvated electrons as intermediate products of cathodic reduction reactions. The hypothesis according to which this step is practically universal for a cathodic process was advanced in recent years by a number of investigators.(40–44) Their reasoning, however, is not convincing, as was first shown by Conway(45): neither the kinetic pattern nor the relations between thermodynamic parameters correspond, for the usual interval of potentials, to such a mechanism (this discussion is summarized in Refs. 38, 39 and 45). Walker's attempt(41) to demonstrate, with the aid of optical measurements, the appearance of solvated electrons in the cathode layer was also refuted.(46,47)

A typical picture representing the possible sphere of action of the mechanism of reduction by solvated electrons is shown in Figure 4. The upper straight line corresponds to the dark generation of solvated electrons on various cathodes in hexamethyl phosphorus triamide (HMPA) solutions of salts. In

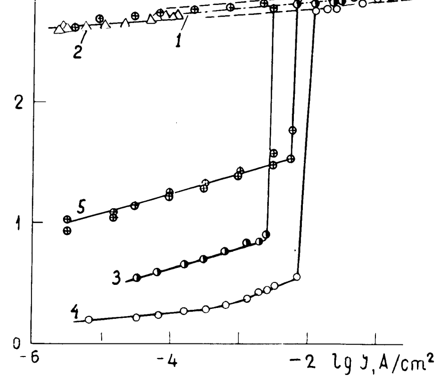

Figure 4. Cathodic polarization curves in HMPA solutions, 1, 0.2 *M* LiCl on electrodes from Pt, Cu, and Cd; (broken lines indicate the limits of the scatter in the data obtained under these conditions); 2, 0.2 *M* NaBr, Pt; 3, 0.2 *M* LiCl + 0.15 *M* HCl, Cu; 4, 0.2 *M* LiCl + 0.18 *M* HCl, Pt; 5, 0.2 *M* LiCl + 0.17 *M* HCl, Cd (according to Ref. 38).

this solvent, solvated electrons form rather stable intensely blue solutions. The bottom group of straight lines corresponds to evolution of hydrogen in slightly acidified solutions of the same salts. This process, which exhibits practically the same pattern as in an aqueous solution, occurs at potentials 1.5–2.5 V more positive than those at which solvated electrons are formed. Thus, in this range of potentials, participation of solvated electrons in the cathodic reduction of hydrogen ions (as well as any other substance) is absolutely out of the question. If, on the other hand, limiting current densities are reached and the potential sharply increases, at a potential of about −3 V a new increase in current takes place; the polarization curve then virtually coincides with the electron generation curve, and slight coloration is observed near the cathode. Under these conditions, solvated electrons are formed, which diffuse through the hydrogen-ion-depleted diffusion layer, then react with the ions in the solution. Such a mechanism of indirect cathodic reduction may apply to a great variety of reactions, provided only that *sufficiently high* negative potentials are attained.

Coming back to the effect of the work function, as a characteristic of a metal on the kinetics of an electrode reaction, it should be pointed out that in a number of works a clear correlation between the work function and hydrogen overpotentials is actually observed.(48–55) As has already been mentioned above, the work function (as well as the electron chemical potential and absolute Galvani potential drop) can exert no *direct* influence on the heat of an electrode reaction and hence on the activation energy. In other words, the work function (and related quantities) is not directly involved in the kinetic equations.

Its indirect influence may manifest itself through a shift of the point of zero charge and a related change in the double-layer structure, as was mentioned above in connection with data on electroreduction of anions. However, in the above-mentioned hydrogen overpotential correlations, the ψ_1 effect did not play any significant role.

The decisive factor here is the relation between changes in W and the heat λ_H of hydrogen adsorption on a given metal, i.e., a parameter directly affecting the overpotential.

The approximate correlation between W and λ_H is, in principle, not surprising, for both parameters are, in the final analysis, determined by the electronic structure of the metal. The process of hydrogen adsorption can be conceived as a sequence of reactions of hydrogen ionization, then electron transfer into the metal (energy gain W) and proton transfer to the metal surface with energy gain Q. If the values of Q for different metals differ to a lesser degree than those of W (or if they change in parallel), we may assume parallelism between the heat of adsorption and work function. Needless to say, these correlations will be approximate as indicated experimentally.

Detailed studies were made by Delahay and Ruetschi and by Conway and Bockris on these correlations between W and λ, and the latter authors

Table 1
Hydrogen Overpotential in Nonaqueous Solutions(70)

	Variation relative to water	
Solvent	Hydrogen overpotentials, V	Proton solvation energy, eV
Methyl alcohol	−0.10 to −0.16	−0.1 to −0.02
Ethyl alcohol	−0.07 to −0.16	−0.02
Propyl alcohol	−0.27	~−0.02
Ethylene glycol	−0.1	−0.07
Ethyl ether	~−0.05	~0.0
Formic acid	~−0.1	−0.47
Acetic acid	~−0.1	~−0.5
Acetonitrile	−0.15	−0.14
Ammonia	+0.1 to +0.2	+0.9
Dimethylsulfoxide	−0.15	+0.34

pointed out the importance of taking into account electronegativities of substrate metal M and of H in the MH bond strength.

It is not only the electron chemical potential that does not directly affect the energy of activation of an electrode reaction, but also the standard† chemical potentials of all the other reagents. Take, for example, a different energy of solvation of ion A^+, by using a different solvent. In principle, this would change the activation energy of the reaction but we should take into account that a change in the solvation energy automatically, due to the equilibrium (E), leads to an equal and opposite change in the Galvani potential so that the total energy of the initial state *remains the same.*

In fact, if we consider reaction (E) at its standard equilibrium potential, ϕ^0_e,

$$\mu^0_{A^+} + \bar{\mu}_e = \mu^0_A$$

i.e., the standard free energy of the process is equal to zero. At any other potential with respect to ϕ^0_e, the standard free energy of the process is no longer equal to zero but to $(\phi - \phi^0_e)$, i.e., this energy is the same for any electrode material and solvent. Hence, on the basis of the generalized Brønsted relation, we may conclude that the free energy of activation is the same as well. Thus, the values of the solvation energies are *not* involved in the kinetic equations either and produce no direct effect on the activation energy.(56)

The absence of a direct relationship between the hydrogen ion solvation energies and the overpotential of the ion's discharge in various solvents can be seen from Table 1; no quantitative relation exists between these values and, in the case of dimethylsulfoxide, a reversal of signs is even observed.

---

† We are here speaking of standard chemical potentials since the concentration-dependent part of μ is distinguished in an explicit form, being used in the kinetic equations as a product of concentrations, while the exponent includes only the standard free energy of activation.

2.3. Activity Coefficient of an Activated Complex

The kinetic equations obtained within the framework of the absolute reaction rate theory include an activity coefficient $\gamma^{\ddagger}$ of an activated complex, which is a value representative of the change in the energy of the activated state in a real solution as compared to an ideal one.

If a reaction is to some degree governed by the Brønsted rule, which is the case with most electrochemical reactions (in compliance with the Tafel equation), it becomes possible to express the activated complex activity coefficient $\gamma^{\ddagger}$ in terms of the activity coefficients of initial (γ_i) and final (γ_f) states of the reaction.(57,58)

The Brønsted relation stipulates that for similar reactions, the change $\delta\Delta G^{\ddagger}$ in the standard free energy of activation represents a fraction $\alpha(\leq 1)$ of the corresponding change $\delta\Delta G^{\circ}$ in the standard free energy of an elementary act of this reaction:

$$\delta\Delta G^{\ddagger} = \alpha\delta\Delta G^{\circ}$$

Consider a reaction which proceeds in an ideal solution (all γ's = 1), then in a real solution. Both cases can be regarded as two similar reactions with slightly different ΔG° values, to which the Brønsted relation is applied. The change in the standard free energy of an elementary act of the process, if transferred from the ideal to the real solution, is determined by the activity coefficient of the initial and final substance:

$$\delta\Delta G^{\circ} = RT\ln \Pi\gamma_f/\Pi\gamma_i. \tag{30}$$

Similarly, for a change in the free activation energy,

$$\delta\Delta G^{\ddagger} = RT\ln \gamma^{\ddagger}/\Pi\gamma_i \tag{30a}$$

Substituting $\delta\Delta G^{\circ}$ and $\delta\Delta G^{\ddagger}$ from Eqs. (30) and (30a) into the Brønsted relation (13), we obtain

$$\gamma^{\ddagger} = \Pi\gamma_f^{\alpha}\Pi\gamma_i^{\beta} \tag{30b}$$

where $\beta = 1 - \alpha$.

In the equation for the electrode reaction rate expressed through overpotential [see Section 3.1, Eq. (61a)], a kinetic activity factor is present:

$$\Gamma = \frac{\Pi\gamma_f^{\alpha}\Pi\gamma_i^{\beta}}{\gamma^{\ddagger}} \tag{31}$$

If Eq. (30b) is taken into consideration, this factor becomes equal to unity, i.e., the reaction rate at a given overpotential is independent of the activity coefficients of the components.

Here, the following reservation should be made. The Brønsted relation includes values characterizing the reagents in the states immediately preceding and following an elementary act of the slow stage, i.e., for the electrode reaction in the double layer, whereas the reaction rate equation includes the values of γ related to the initial and final states in the entire chain of transformations. Therefore, the kinetic activity coefficient will become equal to unity only in the case where the participants of the elementary act are the same as in the reaction as a whole, and provided their activity coefficients in the adsorbed state are essentially the same as the bulk ones. The latter assumption with not too high coverages of the surface by the reagents seems to be highly probable since, in the above deductions, γ described only the effects of interaction with the closest environment, while the important contribution to the free energy of the adsorbed substances, associated with the ψ_1 potential, has been made a separate term.

We now write the kinetic activity coefficient for the hydrogen evolution reaction

$$\Gamma = \frac{\gamma_{H_2}^{\alpha/2}\gamma_{H_3O^+}^{\alpha}\gamma_{H_2O}^{\alpha}}{\gamma^{\ddagger}} = \frac{\gamma_{H_2}^{\alpha/2}\gamma_{H_3O^+}^{\beta}\gamma_{H_2O}^{\alpha}}{\gamma_{H_s}^{\alpha}\gamma_{H_2O_s}^{\alpha}\gamma_{H_3O_s^+}^{\beta}} \tag{32}$$

This expression takes into account that the products of an elementary act and the reaction as a whole are different, namely, an adsorbed hydrogen atom and an H_2 molecule in the gaseous phase, as well as that adsorbed particles participate in the elementary act. For gaseous H_2, $\gamma_{H_2} = 1$; for mercury-type cathodes, for which the surface coverage with adsorbed hydrogen is quite small, $\gamma_{H_s} = 1$. If γ for adsorbed H_3O^+ and H_2O, as well as the same particles in the bulk are made equal, the kinetic activity coefficient will be equal to unity. Even if this relation is not strictly accurate, the value will be close to unity and only a minor variation with a change in the solution composition is likely:

$$\Gamma = \frac{\gamma_{H_2O}^{\alpha}\gamma_{H_3O^+}^{\beta}}{\gamma_{H_2O_s}^{\alpha}\gamma_{H_3O_s^+}^{\beta}} \tag{32a}$$

Iofa and Frumkin(59) found that the hydrogen overpotential in concentrated chloride solutions as a supporting electrolyte does not change from LiCl to KCl, although the activity coefficient of the H_3O^+ ion should undergo a substantial change (the mean ionic activity coefficient of HCl changes 1.87 times). This is indicative of the fact that the term in Eq. (32a), associated with H_3O^+, is, in fact, practically constant. For highly concentrated solutions of LiBr for which the activity coefficient of water falls to 0.1, in the region of barrierless discharge of hydrogen ions, an increase in overpotential only by 12 mV has been found, compared to behavior in more dilute solutions, this result practically coincides with the shift caused by a change in the mole fraction (8 mV), but much smaller than in a case where the activity of water would have a certain effect (0.060 V).(58,60)† Hence, $\gamma_{H_2O}/\gamma_{H_2O_s} \simeq 1$. All of the above data confirm the validity of Eq. (32) and, consequently, the general relation (31) for the activated complex activity coefficient.

---

† Such a comparison is possible only for barrierless hydrogen ion discharge, since, in this case, the ψ_1 effects, normally predominant in concentrated solutions, disappear (see below, in Section 2.5).

2.4. Temperature Dependence of Electrode Reaction Rates

The rate of an electrode process directly depends on magnitude, ϕ, of the potential drop at the electrode–solution interface. Therefore, while determining the activation energy from the temperature dependence of the reaction rate, we would have to maintain constant not only such common independent variables as pressure P and concentration m, but also ϕ:

$$\left(\frac{\partial \ln i}{\partial T}\right)_{P,m,\phi} = \frac{W^{\ddagger}}{RT^2} \tag{33}$$

It is assumed here that the composition of the bulk phase is such that its constancy ensures also that of the surface concentration, i.e., there is no difference in the true and apparent activation energies. A corresponding correction factor has been described in Sections 2.1 and 4, and is not considered here.

However, the magnitude of a single potential drop cannot be measured directly, therefore, it is not possible to control its constancy, i.e., we cannot conduct an experiment to determine the value $W^{\ddagger}$, similar to the energy of activation of a common chemical reaction. This value, $W^{\ddagger}$, which is impossible to measure is called, according to Temkin,(61) the "ideal" activation energy.

A practical activation energy can be experimentally found at a constant measured electrode potential, but usually this value has no definite physical meaning since the selection of the reference electrode is arbitrary. It acquires a definite physical meaning only when a reversible electrode is chosen as the reference one, on which equilibrium of the reaction of interest is achieved. In this case, the electrode potential being measured is the overpotential

$$\eta = |\phi_e - \phi| \tag{34}$$

The activation energy found experimentally at a constant overpotential has been termed by Temkin the "real" activation energy

$$\left(\frac{\partial \ln i}{\partial T}\right)_{P,m,\eta} = \frac{A^{\ddagger}}{RT^2} \tag{35}$$

Consider now the relationship between the ideal ($W^{\ddagger}$) and the real ($A^{\ddagger}$) activation energies. Since current density is a function of the independent variables P, T, m, and ϕ, we may write an expression for the exact differential $\ln i$

$$d \ln i = \left(\frac{\partial \ln i}{\partial T}\right)_{P,m,\phi} dT + \left(\frac{\partial \ln i}{\partial m}\right)_{P,T,\phi} dm + \left(\frac{\partial \ln i}{\partial P}\right)_{T,\phi,m} dP + \left(\frac{\partial \ln i}{\partial \phi}\right)_{P,T,m} d\phi \tag{36}$$

With P, m, and η being constant,

$$\left(\frac{\partial \ln i}{\partial T}\right)_{P,m,\eta} = \left(\frac{\partial \ln i}{\partial T}\right)_{P,m,\phi} + \left(\frac{\partial \ln i}{\partial \phi}\right)_{P,T,m} \left(\frac{\partial \phi}{\partial T}\right)_{P,m,\eta} \tag{37}$$

The dependence of ln i on ϕ at constant P, T, and m is expressed in Tafel equation (14) which, when differentiated, easily gives

$$\left(\frac{\partial \ln i}{\partial \phi}\right)_{P,T,m} = -\frac{\alpha F}{RT} \tag{38}$$

The minus sign in Eq. (38) corresponds to a cathodic process; in the case of an anodic process, the derivative is equal to $+\beta F/RT$.

At a constant overpotential, as can be seen from Eq. (34), the temperature derivative of the potential drop, when current is passing, is equal to the equilibrium potential drop derivative (which, naturally, is independent of η)

$$\left(\frac{\partial \phi}{\partial T}\right)_{P,m,\eta} = \left(\frac{\partial \phi_e}{\partial T}\right)_{P,m} \tag{39}$$

Substituting Eqs. (38) and (39) into Eq. (37), we have

$$\left(\frac{\partial \ln i}{\partial T}\right)_{P,m,\eta} = \left(\frac{\partial \ln i}{\partial T}\right)_{P,m,\phi} - \frac{\alpha F}{RT}\left(\frac{\partial \phi_e}{\partial T}\right)_{P,m} \tag{40}$$

This relation was for the first time derived by Agar$^{(62)}$ and Temkin.$^{(61)}$ Comparison of Eq. (40) with (33) and (35) gives

$$A^{\ddagger} = W^{\ddagger} - \alpha FT\left(\frac{\partial \phi_e}{\partial T}\right)_{P,m} \tag{41}$$

For an anodic process, the expression is similar, viz.,

$$A^{\ddagger} = W^{\ddagger} + \beta FT\left(\frac{\partial \phi_e}{\partial T}\right)_{P,m} \tag{41a}$$

As can be seen from Eq. (41), the ideal activation energy cannot be found from the value of the real energy for it would require knowledge of the temperature coefficient of an individual potential drop, which is impossible to measure or to calculate *a priori* thermodynamically.

For a clearer definition of the physical meaning of the relationship between $A^{\ddagger}$ and $W^{\ddagger}$, we should take into account certain thermodynamic relations describing a reaction on an individual electrode. From the equality of the sum of the electrochemical potentials of the initial compounds and products ($\sum \bar{\mu}_i = \sum \bar{\mu}_f$), we find the equilibrium potential drop

$$F\phi_e = \sum \mu_i - \sum \mu_f = \Delta G_a = -\Delta G_k \tag{42}$$

Here ΔG is the Gibbs free energy of the reaction at given reagent concentrations, ΔG_a being written for the reaction in the anodic direction and ΔG_k, for the cathodic direction.

Taking into consideration the relation between entropy and the temperature derivative of the free energy

$$\Delta S = -\left(\frac{\partial \Delta G}{\partial T}\right)_{P,m}$$

we obtain

$$A^\ddagger = W^\ddagger - \alpha T \Delta S_k \tag{43}$$

for the cathodic process, and

$$A^\ddagger = W^\ddagger - \beta T \Delta S_a \tag{43a}$$

for the anodic process.

The value $T\Delta S$ is nothing but q, which is the latent equilibrium heat of an electrode process or, in other words, the heat absorbed at an equilibrium potential during transformation of stoichiometric amounts of reagents to products. Accordingly, Eqs. (43) and (43a) take the forms

$$A^\ddagger = W^\ddagger - \alpha q_k \tag{44}$$

$$A^\ddagger = W^\ddagger - \beta q_a \tag{44a}$$

Relations (43)–(44) derived for the first time by Temkin[61] have made it possible for him to define the physical meaning of activation energies deduced theoretically by the potential diagram method. Let us now analyze this problem using Temkin's approach.

Consider a specific example—the hydrogen evolution reaction following the slow discharge mechanism. The rate-determining stage is

$$H_3O^+_{sol} + e = H_{ads} + H_2O_{sol} \tag{b}$$

The overall process is

$$H_3O^+_{sol} + e = 1/2H_{2\,gas} + H_2O_{sol} \tag{a}$$

We now construct a potential energy diagram for the discharge process (Figure 5). Regardless of the mechanism of the elementary act, i.e., what precisely is the reaction coordinate X, to construct the diagram we must know the vertical distance between the minima of the potential curves or, in other words, know the respective energy differences. The reference level is assumed

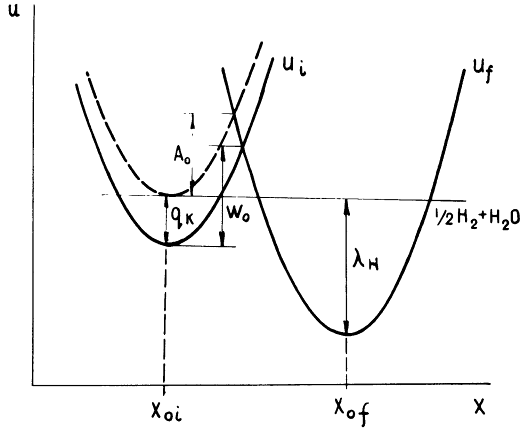

Figure 5. Potential curves for H_3O^+ ion discharge. The horizontal line defines the energy level corresponding to the state $H_{2\,gas} + H_2O_{sol}$. Curve U_i, state $H_3O^+_{sol} + e_M$; curve U_f, $H_{ads} + H_2O_{sol}$. The dashed line represents curve 1 shifted upward by q_k.

to be the $H_2 + H_2O$ energy level shown conventionally by the horizontal line in Figure 5. Then, the equilibrium level of the final state of the slow stage (b), i.e., $H_s + H_2O$, will be lower by λ, which is the heat of adsorption of 1 g-atom of hydrogen and is a positive value if heat is liberated during adsorption. Correspondingly, we construct final state potential curve $U_f(X)$ with reference to this level.

Consider now the energy of the initial state $H_3O^+ + e$. At an equilibrium potential, transformation of the initial substances to the final ones, $1/2H_2 + H_2O$, is accompanied by absorption of the latent equilibrium heat, q_k, of the cathodic process, i.e., the minimum of the initial state potential curve $U_i(X)$ is lower than the $H_2 + H_2O$ level by the value q_k. Thus, we have established the true mutual arrangement of the potential curves at an equilibrium potential.

Their intersection gives us the "ideal" activation energy $W_0^\ddagger$ at $\eta = 0$. At any other value of η, the initial state curve is shifted upward by ηF, and the new point of intersection determines the ideal activation energy at a given overpotential

$$W_\eta^\ddagger = W_0^\ddagger - \alpha\eta F$$

The foregoing suggests that in order to calculate theoretically the activation energy, one should know the latent heat q_k of the electrode process which can neither be experimentally found nor strictly theoretically calculated.

Now consider the result of shifting the initial state potential curve further up by q_k, as shown in Figure 5 by the dashed line. Such an upward shift of the potential curve q_k must lower the activation energy by αq_k, since we could have caused this shift by applying an overpotential $\eta = q_k/F$, while our process obeys the Tafel equation. Hence the activation energy corresponding to the dashed curve will be equal to $W_0^\ddagger - \alpha q_k$. This value, however, is, as can be seen from comparison with Eq. (44), nothing but the real activation energy at the equilibrium potential $A_0^\ddagger$. At any overpotential, η, the curve will be shifted by another ηF, and the real activation energy will be equal to $A_0^\ddagger - \alpha\eta F$.

Thus, the foregoing shows how the real activation energies must be calculated—they can be derived from potential energy diagrams constructed on the assumption that the latent equilibrium heat of the electrode process is zero.

As is known, the Arrhenius equation for the reaction rate constant k takes the form

$$k = k_0 \exp(-W^\ddagger/RT) \tag{45}$$

where k_0 is the preexponential factor.

For electrode reactions, as has been described above, the "ideal" activation energy $W^\ddagger$ cannot be found experimentally. However, we can measure the real activation energy $A^\ddagger$, associated with $W^\ddagger$ through the above relations. If we substitute Eq. (43) into (45),

$$k = k_0 \exp(-\alpha \Delta S/R) \exp(-A^\ddagger/RT) \tag{46}$$

Here, the value $k_0 \exp(-\alpha \Delta S/R)$, which does not contain the exponential temperature dependent term,was termed the "real pre-exponential factor" by Temkin.(63) Unlike the "ideal" preexponential term k_0, the value can be determined experimentally and, as was for the first time shown by Temkin,(63) calculated within the limits of certain assumptions.

The "ideal" preexponential factor can be expressed in terms of absolute reaction rate theory as

$$k_0 = \kappa \frac{kT}{h} \exp\left(\frac{S^{\ddagger} - S_i^{\circ}}{R}\right) \tag{47}$$

The main difficulty in calculating this value normally lies in the determination of the activated complex entropy.

Temkin has proposed that a system at two close temperatures, T and $T + \Delta T$, be considered as two solutions having a slight difference in the activity coefficient of the activated complex. Then, the difference in its free energies can be expressed, on the basis of relations (30)–(31), through the respective differences in the free energies of the reagents:

$$\Delta G^{\ddagger} = \alpha \Delta G_f^{\circ} + \beta \Delta G_i^{\circ} \tag{31a}$$

Division of Eq. (31a) by ΔT, proceeding to the limit, and substitution of the temperature derivatives of G by respective S's, gives(64)

$$S^{\ddagger} = \alpha S_f^{\circ} + \beta S_i^{\circ} \tag{48}$$

The similarity with the activity coefficients or, in other words, values associated with interactions with the medium, which follows from the foregoing, suggests that Eq. (48) relates not to the usual full entropy values, but only to the contribution determined by the interaction with the medium. The full values differ by the contributions associated with intramolecular vibrations. In the case of particles with rigid internal chemical bonds, this contribution to entropy is small and can be represented in the form of Eq. (48), with the error introduced thereby being ignored. Therefore, for such particles such as, for example, H_3O^+ and, of course, monatomic ions, Eq. (48) can be considered accurate enough.

In the limiting cases of an activationless ($\alpha = 0$) or barrierless ($\alpha = 1$) discharge, Eq. (48) takes the form of simple formulas having a clearly defined physical meaning since, for these processes, the activated complex becomes identical with the initial or final states, respectively (see Section 2.5).

From Eq. (48) we obtain for the activation entropy

$$S^{\ddagger} - S_i^{\circ} = \alpha S_f^{\circ} - \alpha S_i^{\circ} \tag{49}$$

This value cannot be calculated accurately because S_f° and S_i° (or at least one of them) include absolute entropies of individual ions, which cannot be determined purely thermodynamically. Therefore, the ideal preexponential factor, as well as the ideal activation energy, is impossible to calculate.

These difficulties disappear, however, in the case of a real preexponential factor for which the entropy term $-\alpha \Delta S^\circ$ is added [see Eq. (46)].† Here, ΔS° is a variation in entropy in the case of the overall reaction. It differs from $S_f^\circ - S_i^\circ$ by the difference in the entropies of the intermediate states—participants of an elementary act, and entropies of the first and last reagent in the chain of transformations. For example, for a discharge of H_3O^+, S_i° is $S_{H_3O_s^+}^\circ$ and S_f° corresponds to $S_{H_s}^\circ + S_{H_2O_s}$, while the overall reaction includes H_3O^+ and H_2O in the solution, and H_2 in the gaseous phase, i.e., ΔS° differs from $S_f^\circ - S_i^\circ$ by adsorption entropies

$$\Delta S_{a_{H_3O^+}} + \Delta S_{a_{H_2O}} + (1/2 S_{H_2}^\circ - S_{H_s}^\circ)$$

Therefore, ΔS° can be represented as $S_f^\circ - S_f^\circ + \sum \Delta S_a^\circ$. Thus, the entropy term for calculating the real preexponential factor is

$$S^\ddagger - S_i^\circ - \alpha \Delta S^\circ = \alpha S_f^\circ - \alpha S_i^\circ - \alpha (S_f^\circ - S_i^\circ + \sum \Delta S_a^\circ) = -\alpha \sum \Delta S_a^\circ \qquad (50)$$

This expression no more includes absolute entropies of individual ions; therefore, it can be calculated, in principle.

The transmission coefficient κ which is also included in the expression for the preexponential factor, cannot be calculated using a purely phenomenological approach, but involves the quantum mechanical theory of an elementary act. For most simple electron transfer reactions, $\kappa = 1$.

2.4.1. Electrode Reaction Rate as a Function of Pressure

Differences in ideal and real values may manifest themselves not only through the temperature dependence of the electrode reaction rate, but also in the dependence of the latter on other intensive parameters, external pressure being one of them.(65)

The pressure derivative of the reaction free energy is known to be equal to the change in volume during the reaction. Similarly, from the pressure derivative of the activation free energy (i.e., logarithm of the rate constant), the volume of activation is found.

However, the same difficulty is encountered here: a variation in the external pressure causes a change in the equilibrium potential drop. Therefore, it is impossible to determine the ideal activation volume, and only a corresponding real value can be found.

Using the approach described above, one can demonstrate that the experimentally determined real activation volume $\Delta V_r^\ddagger$ differs from the ideal value, $\Delta V_{\text{id}}^\ddagger$, thus

$$\Delta V_r^\ddagger = \Delta V_{\text{id}}^\ddagger - \alpha \Delta V \qquad (51)$$

where ΔV is the change in volume in an overall electrode process.(66,67)

---

† The expression is given for standard reagent concentrations. At different concentrations, one should take into account the difference of ΔS in Eq. (46) from ΔS°.

2.5. Activationless and Barrierless Electrode Processes

We have already mentioned a most important feature of electrode processes—the dependence of the activation energy on the potential, for example, in a cathodic process:

$$W_k^{\ddagger} = W_k^{\ddagger\circ} + \alpha\phi F$$

and, in an anodic process:

$$W_a^{\ddagger} = W_a^{\ddagger\circ} - \beta\phi F$$

For a sufficiently strong shift of the potential in the negative direction to such a value of ϕ that $|\alpha\phi F| \simeq W_k^{\ddagger\circ}$, the activation energy of a cathodic reaction becomes zero. A similar result—zero activation energy of an anodic process—is obtained at a high positive potential.

A negative value of the true ideal activation energy has no physical meaning. Therefore, it is natural to assume (this assumption will be corroborated in what follows) that a further shift of the potential, after $W_k^{\ddagger}$ (or accordingly, $W_a^{\ddagger}$) has become zero, will not result in any further increase in $W^{\ddagger}$, i.e., $W^{\ddagger}$ varies monotonically with the potential. A constant value of $W^{\ddagger}$, equal to zero, formally corresponds to $\alpha = 0$.

Processes with $W^{\ddagger} = 0$ and $\alpha = 0$ may be referred to as *activationless*. The possibility of such processes has been discussed in the literature over many years. The first mention of such a situation can be found in a paper by Iofa and Mikulin,(68) who attributed to the activation energy becoming zero the fact that the extrapolated Tafel lines for different temperatures intersect at a single point. Audubert,(69) who proceeded from the potential curve diagram, also arrived at the conclusion that the activation energy tends to zero at sufficiently high overpotentials. Later, various aspects of this problem were studied by a number of investigators (for a review see Ref. (70)).

Consider another limiting case. Assume that the potential is shifted in the positive direction. This leads to a decrease in the anodic reaction activation energy. At a sufficiently low cathodic, or a sufficiently high anodic, potential, $W_a^{\ddagger}$ will become zero. Then, $\beta = 0$ and, consequently, $\alpha = 1$. Unlike activationless processes, those corresponding to $\alpha = 1$ require a considerable amount of the activation energy. At the same time, in contrast to the relations in an ordinary discharge, this activation energy is equal to the heat of a reaction's elementary act, for the activation energy of the backward process is zero. On the potential diagram of the process, the hump usually present, viz., the activation barrier, is not seen any more, which is why such processes have been termed *barrierless.*(27)

In view of the possible existence of three types of electrode processes, namely, barrierless, ordinary and activationless, the polarization curve can be as shown schematically in Figure 6. The possibility of experimentally examining a selected portion of the curve depends on the kinetic characteristics of the process, in particular, its energetics.

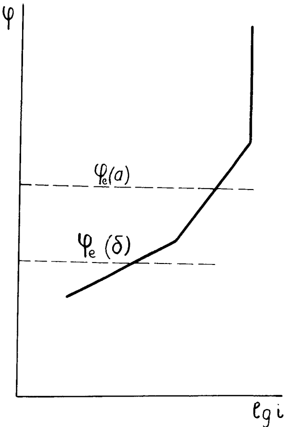

Figure 6. Polarization curve shown schematically in a broad potential range. Horizontal lines *a* and *b* represent two possible positions of the equilibrium potential.

For a barrierless process to occur, an elementary act of the reaction should involve absorption of heat, for activation energy is essentially a positive quantity. In other words, at the equilibrium potential and within a certain overpotential interval, the energy level of the final state must be higher than that of the initial state. Consequently, in the case of slow discharge of hydrogen ions, for example, a barrierless process may involve only metals which poorly adsorb hydrogen. On the other hand, in the case of slow electrochemical hydrogen desorption, a barrierless process may occur, in principle, only if the hydrogen–metal bond energy is high.

Initially, in the theory of barrierless and activationless processes, it was postulated that the activation energy varies monotonically with the potential; after $W^{\ddagger}$ has decreased all the way to zero, its increase was considered impossible. Corroboration of this monotony principle can be found when the energy spectrum of electrons in a metal is taken into account.(71–74)

When the energy spectrum is taken into account, one should define precisely at which of the possible energy levels the electron is. Assume that curve 1 (Figure 7) corresponds to the initial state of the ion + electron system on the Fermi level; and curve 1′ corresponds to that of the same system below the Fermi level.

Evidently, the activation energy in the former case is perceptibly smaller than in the latter, so that transition from the Fermi level is more probable than from the lower level. Consider now a state corresponding to an electron at the excited level which is above the Fermi level by a value equal to ΔE (curve 1″). In this case, the activation energy $E^{\ddagger\prime\prime}$ is less than the respective value corresponding to curve 1 ($E^{\ddagger}$). However, an additional factor should be taken into account, namely, the low concentration of electrons on the excited levels.

At a sufficient distance from the Fermi level ($\Delta E \gg kT$), the population of the electron levels exponentially decreases. The probability of transition from an excited level is proportional to the product of the probability of an

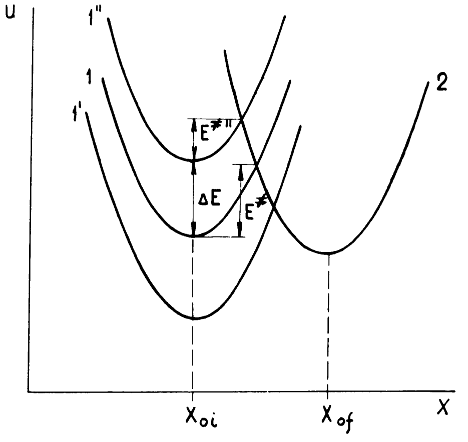

Figure 7. Potential curves taking into account the distribution of electrons by energies in the metal. For designations see text.

electron occupying this level [exp $(-\Delta E/kT)$] and the exponent of respective activation energy $E^{\ddagger''}$, i.e., $\exp[-(\Delta E + E^{\ddagger''})/kT]$. The total effective activation energy $\Delta E + E^{\ddagger''}$ is substantially greater than $E^{\ddagger}$, i.e., a process with the participation of an electron at the Fermi level is most probable.

The deduction as to the preferential participation of electrons from the Fermi level (or, to be more precise, from a band several kT wide near this level, as was first shown by Gerischer$^{(75)}$) holds true only in the case of an ordinary discharge, but is quite different with respect to barrierless and activationless processes.

Consider, for instance, Figure 8 in which curve 1 corresponds to the state of electrons on the Fermi level at a certain electrode potential ϕ_1 marking the onset of a barrierless process. If we reduce the potential by $\Delta\phi$, the corresponding curve assumes a position 1′. In this case, a barrier reappears between the initial and final states, but on the other side of the minimum of curve 2. If the process involved only the Fermi level as before, during transition of curve 1 to position 1′, the activation energy would increase by a value greater than $F\Delta\phi$, i.e., the transfer coefficient α would exceed unity.

With such an arrangement of the potential curves, however, discharge from the Fermi level is no more optimal. This can be seen from consideration of the potential curve corresponding to the excited level which is above the Fermi level at the value $F\Delta\phi$. At a potential ϕ_1, corresponding to this level is curve 1″ (Figure 8); hence, a high effective activation energy arises. However, at a potential ϕ_2, when the curve corresponding to the Fermi level shifts to position 1′, it will assume position 1 for an excited level. The effective activation energy $F\Delta\phi + E_1^{\ddagger}$, corresponding to the excited level, is now lower than for the Fermi level. Therefore, at all potentials below ϕ_1, the process will follow a barrierless path, the activation energy variation will be equal to $F\Delta\phi$, and $\alpha = 1$. A similar approach will show that in the case of an activationless process, $\alpha = 0$, and the electron transfer proceeds from levels below the Fermi level.

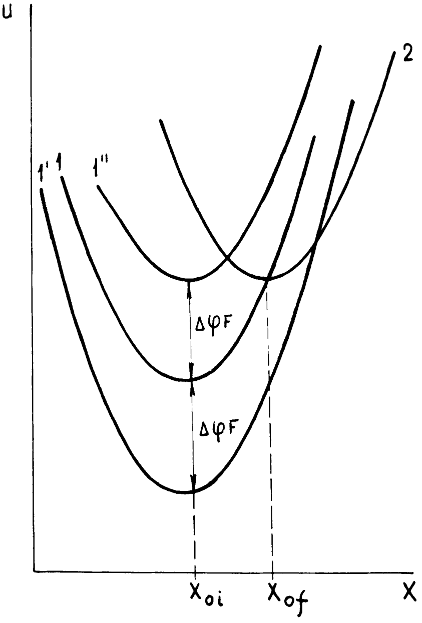

Figure 8. Potential curves for highly endothermal reactions. For designations see text.

Quantitative analysis has shown that $n^* = 1 - \alpha$, where n^* is the population of the level making the greatest contribution to the process. For example, for $\alpha = 0.5$, $n^* = 0.5$, which corresponds to the Fermi level. When $\alpha \to 1$, $n^* \to 0$, i.e., the principal role is played by the excited levels whose population is negligible. Similarly, in the case of activationless processes, $\alpha \to 0$, and $n^* \to 1$, i.e., the contribution of the deep-lying, practically filled levels is predominant. The value of α is always anywhere between 0 and 1.

All the foregoing applies to a cathodic process, or equally well to an anodic reaction, except that, in this case, a hole at a certain level in the metal is involved, rather than an electron.

A barrierless cathodic process involves an excited electronic state. In an activationless process, electrons from deep levels take part, i.e., as a result of the reaction's elementary act, a hole is formed at a level below the Fermi level. This state is known to be a nonequilibrium one or, in other words, is characterized by an excess of energy. Thus, a barrierless process involves an excited initial state, while an activationless process, an excited final state. This holds true even in the case where not only electronic, but also other, for example, vibrational degrees of freedom may be excited.

Consider now some specific features of the kinetics of barrierless and activationless processes. At a constant potential and for invariant double-layer structure, the discharge rate varies directly with the discharging particle concentration. This, of course, applies to any discharge process, be it an ordinary, barrierless or activationless one. If, however, we make a comparison at a constant overpotential, rather than at a constant potential, the relations are quite different. A higher concentration of the discharging particles, e.g., H_3O^+ ions, reduces the equilibrium potential with the result that, at a constant overpotential, the rate increases directly with $C_{H_3O^+}^{1-\alpha}$, and not with $C_{H_3O^+}$ [see Section 3.1, Eq. (61)].

In the case of ordinary discharge, $\alpha = 1/2$ and the current density is proportional to $C_{H_3O^+}^{1/2}$. In the case of barrierless discharge, $\alpha = 1$, and the reaction rate at a constant overpotential is independent of the concentration; the acceleration of the discharge owing to an increase in the number of the discharging particles is balanced out by its deceleration due to a decrease in the equilibrium potential. This is true for slow barrierless discharge of any particles, provided that the number of electrons transferred per particle in the overall reaction and during the slow stage is the same.

A similar situation occurs when we consider the effect of the ψ_1 potential. A shift of the ψ_1 potential affects the reaction rate both because of the variation of the surface ion concentration and because of the changing potential drop in the dense part of the double layer (see Section 4.1). In the case of ordinary discharge, the former factor is predominant since the latter one involves a ψ_1 potential with $\alpha = 1/2$. In the case of barrierless discharge, $\alpha = 1$, and both effects may balance out each other. This compensation of ψ_1 effects is possible only with n-electron reduction of an n-charged cation (or a corresponding anion oxidation). In other cases, there is no compensation of the effect of the ψ_1 potential on surface concentration and potential drop.

As can be inferred from the above, in the case of barrierless discharge of hydrogen ions, for example, the overpotential is practically independent of the solution composition, which, along with $\alpha = 1$, i.e., $b = 59$ mV, is a most typical feature of slow barrierless discharge.

As far as activationless discharge is concerned, since in this case, the discharge rate does not depend on the potential, this process is unaffected by whatever factors may be associated with the magnitude of the equilibrium potential or the potential drop in the compact double layer.

The rate of activationless discharge varies directly with the surface concentration of the discharging particles, i.e. with their bulk concentration and $\exp(-z\psi_1 F/RT)$ [this can be easily seen from Eq. (92) if $\alpha = 0$ is substituted therein]. A characteristic feature of an activationless process is the appearance of a limiting current not associated with the slow rate of any preceding step.

In order to experimentally detect barrierless discharge, the reaction of hydrogen evolution on mercury was chosen in the first place, since the hydrogen adsorption energy on this metal is low; hence, one could expect a sufficient endothermicity of the discharge act.

Experiments were conducted with large concentrations of salts with surface-active anions, I^- and Br^-, as supporting electrolytes since they greatly reduce the overpotential of ordinary discharge (ψ_1 effect) without affecting the barrierless process. Therefore, one would expect a substantial shift, toward higher current densities, of the point of transition from one type of discharge to the other.

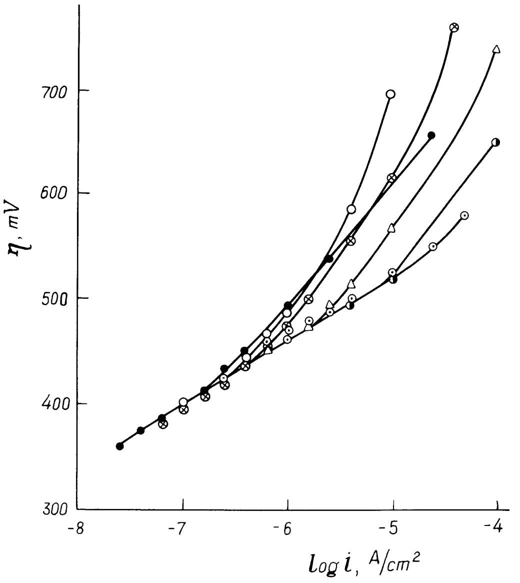

Figure 9. Hydrogen overpotential on mercury cathode at 25°C in acidified salt solutions of the following composition: ○, 0.8 *M* KI + 0.8 *M* HCl; ⊗, 3.2 *M* KI + 0.15 *M* HCl; △, 3.2 *M* KI + 0.45 *M* HCl; ◑, 6.0 *M* KI + 0.55 *M* HCl; ⊙, 3.0 *M* KI + 0.9 *M* HCl + 1.3 10^{-3} *M* $N(C_4H_9)_4Br$; ●, 6.6 *M* NaBr + 0.85 *M* HCl (according to Refs. 76 and 77).

Some typical experimental results obtained on a stationary mercury cathode are shown in Figure 9. The polarization curves include two portions with slopes corresponding to ≥100 mV and about 60 mV (the mean value of the slope of the bottom portion, according to Refs. 76 and 77, for 31 solutions of different composition is 58 mV, which agrees well with the theoretical value of 59 mV).

The variation in slope has nothing to do with the effect of impurities or self-dissolution of the cathode. This is corroborated both by the good reproducibility of the overpotential values and by their invariability when the cathode is changed and, which is most important, by their insensitivity to the vigorous stirring of the solution, i.e., transport of possible impurities to the cathode or self-dissolution products from it.

The low slope of the polarization curve does not seem to be related to the peculiarities of kinetics following a logarithmic adsorption isotherm, since the concentration of adsorbed hydrogen on mercury is very low. Nor has it anything to do with the restructuring of the double layer near the potential of zero charge; in some cases, inflections of the curves were observed sufficiently far from the zero charge potentials after the characteristic changes in the kinetics of hydrogen evolution, owing to the restructuring of the double layer that had taken place.

The slope corresponding to 0.059 V could have been related to the equilibrium discharge-ionization mechanism with subsequent activationless desorption. However, in this case, the rate of the overall process would be a second-order one with respect to the hydrogen ion, at a constant potential (or, a first-order one, at a constant overpotential), which is inconsistent with the experiment (zeroth order at η = const, i.e., first order at ϕ = const). A more detailed analysis of these, as well as other possible explanations of the slope corresponding to 0.059 V, is given in Ref. 70.

At the same time, the experimental data can be easily explained if one assumes that the curve portion with $b \simeq 0.06$ V corresponds to the barrierless hydrogen ion discharge, whereas the top portion corresponds to ordinary slow discharge. The top portion is characterized, just as expected for an ordinary discharge, by a strong dependence of the overpotential on the hydrogen ion concentration, as well as on the nature and concentration of surface-active ions.

The overpotential difference in solutions of different compositions used in the experiment attained in this region equals 0.20 V and higher. At the same time, in the region where $b \simeq 0.060$ V, all curves lie in a 0.020 V-wide interval, most of them being in an interval 0.010 V wide. The whole interval was extended to 0.020 V for some data in the most concentrated solutions where the overpotential is somewhat higher because of the low mole fraction of water. The divergence of the curves corresponding to different solutions has the same order of magnitude as that of the curves obtained in independent experiments with solutions of the same composition. Therefore, it can be stated with confidence that, in the region where $b \simeq 0.060$ V, the overpotential is practically independent of the solution composition, which is typical of barrierless discharge of hydrogen ions.

Barrierless discharge of H_3O^+ ions was established with a sufficiently high degree of certainty in the case of hydrogen evolution on another cathode material—silver.(78) Figure 10 illustrates the relations derived for this case. It is quite possible that on cathodes from some other materials (e.g., Bi, Sb) which have not yet been studied as closely, the process of hydrogen evolution may be barrierless as well.(70)

The independence of the barrierless H_3O^+ discharge rate from the ψ_1 potential permits this process to be used for studying a number of electrode kinetics problems.(70) It was shown, for example, that even if deceleration of

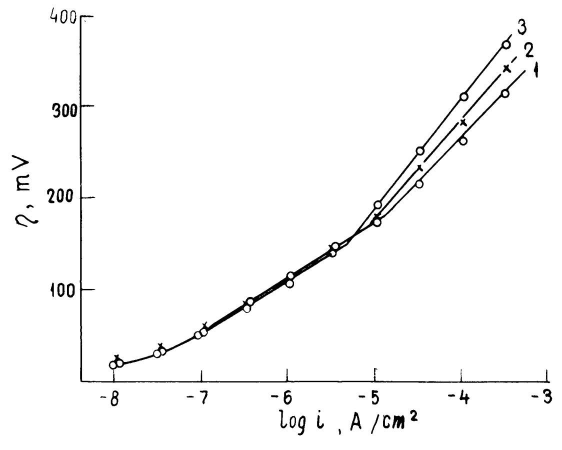

Figure 10. Hydrogen overpotential on silver cathode at 25°C in: 1, 0.1 *M* HCl; 2, 0.033 *M* HCl; 3, 0.01 *M* HCl (according to Ref. 78).

a barrierless H_3O^+ discharge with tetrabutylammonium ions is a reality, it lies at the boundary of experimental error. Hence, such an ion does not produce any sizable screening effect on the discharge of H_3O^+, and its strong influence on an ordinary discharge of H_3O^+ is primarily due to the ψ_1 effect. Then, as has been mentioned above, the ψ_1 effect is absent in a barrierless cation discharge, but is significant in the discharge of a neutral molecule. For this reason, it has become possible to demonstrate discharge of undissociated hydrohalic acids (molecules or ion pairs) in their concentrated solutions. Finally, the absence of ψ_1 effects has made it possible to study highly concentrated solutions of salts in connection with the problem of the effect of the water activity coefficient, which was considered above in Section 2.3.

In the case of barrierless discharge, the activation energy equals the heat of the elementary act. Therefore, experimental determination of the energy of activation of H_3O^+ discharge enables the energy of hydrogen adsorption to be estimated. By this approach, a value for this quantity at mercury was found to be $\Delta H = 23$ kcal, which corresponds to a Hg–H bond energy of 29 kcal. Note that this value virtually coincides with the estimate given by Frumkin *et al.*(79) as a result of comparing hydrogen overpotential on mercury and platinum (27 kcal).

A barrierless process, i.e., when $\alpha = 1$, is indicative of the fact that, in the same interval of potentials, $\beta = 0$, or, in other words, the process of ionization is activationless. Therefore, the data cited above can be regarded as an indirect proof of the existence of activationless electrode processes. Direct observations of limiting activationless currents of hydrogen discharge have not yet become possible. However, as was shown by Pleskov, Rotenberg, and co-workers(80,81) it is possible to determine from photoemission measurements, a summed α value for the processes of electrochemical desorption and ionization of adsorbed H together. For a mercury cathode, this sum was found equal to 0.5, which is a strong argument in favor of an activationless electrochemical desorption mechanism. For a bismuth cathode, within a certain potential interval, this sum is zero, which is indicative of both reactions being activationless.

Together with cathodic hydrogen evolution, a kinetic pattern characteristic of barrierless processes has also been revealed for a number of other reactions. Of greatest interest among these is the anodic evolution of chlorine.(70,82–86)

Figure 11 represents polarization curves for chlorine evolution on graphite, from highly acidified concentrated chloride solutions in which the secondary process of oxygen evolution and formation of CO_2 is practically suppressed. The curve includes two Tafel regions with slopes corresponding to 120 and 200–240 V. Since graphite is highly porous, the true values of the slopes, as follows from the theory of porous electrodes, are half these values, viz., 0.06 and 0.1 $\sim$ 0.12 V. These are precisely the slopes that can be observed if the pores of graphite are filled with melts of $PbCl_2$ or AgCl.(82)

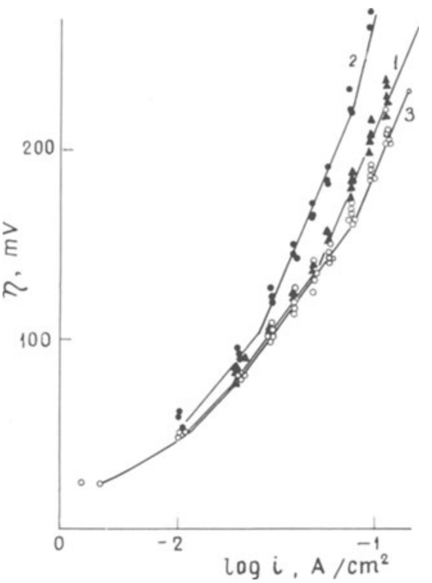

Figure 11. Overpotential of chlorine evolution on porous graphite electrode at 25°C. Solutions: 1, 4.4 M Cl^- + 1.5 M H^+: 2, solution 1 + 0.2 M SO_4^{2-}; 3, solution 1 + 0.1 M Fe^{3+} (according to Ref. 82).

It is not possible to change the chloride concentration significantly for the process under investigation because a lower concentration will intensify the side reaction of graphite oxidation. This is why the effect of this factor could not be examined as properly as was desired. However, the effects of specifically adsorbed ions are clearly manifested. As can be seen from Figure 11, addition of an Fe^{+3} cation causes an appreciable decrease, while SO_4^{2-} causes an increase, in the chlorine overpotential at the top part of the curve, whereas the bottom part remains practically unaffected. This fact, in combination with the electrode capacity, stoichiometric number and cathodic chlorine reduction data, have made it possible to establish the following mechanism of the process: slow discharge (barrierless or, at higher η, ordinary) with subsequent electrochemical desorption.

The kinetics of the chlorine reaction has been studied in more detail over a broad range of chloride concentrations (in particular, with an excess amount of sulfate), on an electrode made from titanium coated with a solid solution of RuO_2–TiO_2 (30 mol % RuO_2), "DSA" electrode. Typical curves are represented in Figure 12. Characteristic features of the kinetics of this process include flatness of the anodic curve with slopes corresponding to 0.030 V and higher overpotentials, to 0.040 V, a limiting non-diffusion-controlled cathodic current equal to the extrapolated anodic exchange current (extrapolation with respect to the bottom Tafel region), and the following reaction orders, at a constant potential: anodic process—first order with respect to chloride, zeroth order with respect to Cl_2; cathodic process—first order with respect to Cl_2 and negative first order with respect to Cl^-. These orders of the reaction completely rule out such mechanisms as slow recombination and

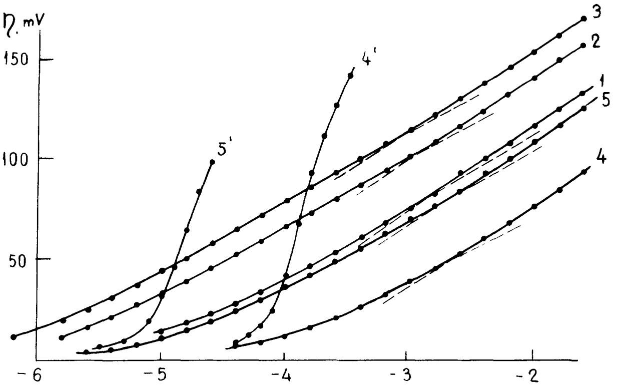

Figure 12. Anodic (1–5) and cathodic (4′, 5′) polarization curves on 35% RuO_2 + 65% TiO_2 at 30°C, ~0.03 g/m^2 Ru_{met}; compositions of the solutions: 1,2,3—1.5 *M* HCl + 2.5 *M* NaCl; 4,4′,5″—1.54 *M* HCl; P_{Cl_2}: 1,4,4′—1 atm; 2—0.1 atm; 3—0.039 atm; 5′,5—0.043 atm (according to Ref. 86).

electrochemical desorption (requiring second-order kinetics with respect to Cl^- for the anodic process, and zeroth order for the cathodic process). A complete analysis of all possibilities led to the following mechanism:

$$Cl^- - e \rightleftharpoons Cl_{ads} \qquad \text{(F)}$$

$$Cl_{ads} - e \rightarrow Cl^+ \qquad \text{(G)}$$

$$Cl(+1) + Cl^- \rightleftharpoons Cl_2 \qquad \text{(H)}$$

In this case, the kinetic data do not permit it to be established in which form the univalent positive chlorine species is present—in the form of an adsorbed Cl^+ cation, ClO^- ion, etc. (incidentally, it is hardly possible to draw a distinction between the Cl^+ ion chemisorbed on the lattice oxygen and chemisorbed ClO^- ion). The slow step is (G), and its rate is determined as

$$i_a = k_a[Cl_{ads}]\exp\left(\frac{\beta\phi F}{RT}\right) = k_a'[Cl^-]\exp\left[\frac{(1+\beta)\phi F}{RT}\right] \qquad (52)$$

For the backward reaction,

$$i_k = k_k[Cl^+]\exp\left(\frac{\alpha\phi F}{RT}\right) = k_k'\frac{[Cl_2]}{[Cl^-]}\exp\left(\frac{\alpha\phi F}{RT}\right) \qquad (53)$$

In Eqs. (52) and (53), due account has been taken of the equilibrium steps (F) and (H), preceding the slow step.

For $\beta = 1$, i.e., in the case of a barrierless discharge, the slope of the anodic curve corresponds to 0.030 V, while with $\beta = 1/2$ (ordinary discharge), it corresponds to 0.040 V. Near the equilibrium potential, $\beta = 1$, hence, $\alpha = 0$. In fact, in the cathodic region, a limiting current is observed, just as would be expected in an activationless process.

In other barrierless reactions, particularly chlorine evolution on graphite, no limiting current in the backward process was observed, the reason being that, in these cases, the slow step of the forward reaction was the transfer of the first electron, followed by that of the second, e.g., in an electrochemical desorption step. In the backward process, the slow activationless step is, in this case, preceded by the transfer of a single electron. The relationship between the rate of this process and the potential masks the limiting current phenomenon.

A barrierless condition also arises when azide is anodically oxidized to nitrogen on a platinum electrode.(87) The probability of this condition is also high when this reaction proceeds on a number of other metals of group VIII, as well as in the case of certain other anodic processes.(70)

It is not always, of course, that a barrierless ($\beta = 1$) or activationless ($\beta = 0$) process produces slopes corresponding, respectively, to 60 mV and ∞. As can be seen, for example, from Eq. (52), under conditions where a preceding equilibrium step is involved, these values of β may result in slopes corresponding to 0.030 and 0.060 V, respectively. Conversely, it is equally possible that in certain cases, such slopes which are sometimes interpreted as indicative of a slow chemical step, correspond, in fact, to the limiting cases of the electrochemical reaction *per se*, considered above.

We have seen that α becoming equal to unity or zero is determined by rather general phenomenological factors. However, one thing remains unclear, namely, the sharp change in the value of α from 1/2 to 1. Figures 9–12 suggest that α should change within a very narrow interval of potentials, on the order of RT/F. A similar picture would be expected if the potential curves were rectilinear all the way to the minimum. However, all the estimates so far indicate that the potential curves are close to parabolic at rather long distances from the minimum.

Consistent with the parabolic shape of the curves is a smooth change in α from unity to zero within a wide range of energies for homogeneous reactions of proton transfer.(14) At the same time, in the case of similar electrochemical reactions, the change in α, as has been mentioned above, is over a very narrow range of energies. The reason for such a discrepancy between the elecrochemical and chemical experiments remains unknown.

Strictly speaking, the values of $\alpha = 1$ or 0 are not necessarily associated with complete disappearance of the energy barrier between the two states. This barrier suffices to be potential independent. Such processes may be called quasibarrierless and quasiactivationless. An explanation of the reason why, even with a significant potential shift, there remains a permanent barrier, is beyond the scope of the phenomenological theory. This phenomenon was predicted on the basis of the quantum mechanical theory of an elementary act, and it was shown that certain reactions, particularly those of chlorine evolution, are, in fact, quasibarrierless. A detailed discussion of this problem can be found in Ref. 70. Here we shall only point out that the reason for this effect resides in the presence of two basically different reaction coordinates, one behaving in a classical manner all the time, while the other changes, in the course of the process, from quantum to classical behavior. The barrier disappears for the path along the purely classical coordinate, but remains for the other coordinate. In particular, in the case of chloride ion discharge, the coordinate representing the behavior of the solvent is purely classical, while that which represents the distance from the chlorine atom to the electrode may behave quantum mechanically.

3. Formal Kinetics of Electrode Reactions

3.1. Kinetic Equations

Consider the kinetic equation for the simplest single-step, single-electron reaction:

$$\mathrm{A}^z + \mathrm{e}_\mathrm{M}^- \rightleftarrows \mathrm{A}^{z-1}$$

The reaction rate in the cathodic direction, in accordance with the mass action law, is

$$\vec{V} = \vec{k}[\mathrm{A}^z]_S \tag{54}$$

where $[\mathrm{A}^z]_S$ is the concentration of substance A^z at the electrode surface in the state immediately prior to the reaction. The fact that we distinguish between the surface and bulk concentrations is already, strictly speaking, a digression from the assumption that the reaction is a single-step one, for an adsorption step is then, in effect, introduced before the electrode reaction proper. It is normally assumed that this step is quasireversible, i.e., $[\mathrm{A}^z]_S$ is practically an equilibrium value relative to that in the bulk, $[\mathrm{A}^z]$. Therefore, $[\mathrm{A}^z]_S$ in Eq. (54) can be substituted by a suitable function for $[\mathrm{A}^z]$. In the simplest case, this relation is described by the Henry's law isotherm but, for most systems, more complex relations are expected.

For the simplest case,

$$\vec{V} = \vec{k}'[\mathrm{A}^z] \tag{54a}$$

Similarly, for the backreaction,

$$\overleftarrow{V} = \overleftarrow{k}'[\mathrm{A}^{z-1}] \tag{55}$$

so that the net rate is

$$V = \vec{V} - \overleftarrow{V} = \vec{k}'[\mathrm{A}^z] - \overleftarrow{k}'[\mathrm{A}^{z-1}] \tag{56}$$

The electrode reaction rate constant depends on the difference of potentials ϕ between the electrode and the site of the discharging particle. This dependence stems from the fact that the reaction involves a charge (electron) transfer from the electrode to the particle (or in the opposite direction).

The following exponential relation, empirically found by Tafel$^{(2)}$ has gained wide acceptance, though it is not yet substantiated in a fully quantitative way from the theoretical point of view (for semiquantitative interpretation of this problem see Section 2.1):

$$\overrightarrow{k} = \overrightarrow{k}_0 \exp\left(-\frac{\alpha\phi F}{RT}\right)$$

$$\overleftarrow{k} = \overleftarrow{k}_0 \exp\left(+\frac{\beta\phi F}{RT}\right) \tag{14a}$$

Here, α and β are constants having values from 0 to 1 (normally, about 1/2), as treated earlier.

Then,

$$V = \overrightarrow{k}_0' \exp\left(-\frac{\alpha\phi F}{RT}\right)[\mathrm{A}^z] - \overleftarrow{k}_0' \exp\left(+\frac{\beta\phi F}{RT}\right)[\mathrm{A}^{z-1}] \tag{56}$$

At equilibrium, $\overrightarrow{V} = \overleftarrow{V} = V_0$, which is the exchange rate at the equilibrium potential ϕ_0

$$V_0 = \overrightarrow{k}_0' \exp\left(-\frac{\alpha\phi_0 F}{RT}\right)[\mathrm{A}^z] = \overleftarrow{k}_0' \exp\left(\frac{\beta\phi_0 F}{RT}\right)[\mathrm{A}^{z-1}] \tag{57}$$

From this equation it is easy to find the relationship between the equilibrium potential and concentration of the components:

$$\phi_0 = \text{const} + \frac{RT}{(\alpha+\beta)F} \ln \frac{[\mathrm{A}^z]}{[\mathrm{A}^{z-1}]} \tag{58}$$

Comparison of Eq. (58) with the Nernst thermodynamic equation indicates that $\alpha + \beta = 1$ is the result which had been obtained earlier (see Section 2.1) when analysis of activation energies was made.

Substituting V_0 into Eq. (56) and introducing electrical units, i.e., current densities $i = FV$, we have

$$i = i_0\left[\exp\left(\frac{\alpha\eta F}{RT}\right) - \exp\left(-\frac{\beta\eta F}{RT}\right)\right] \tag{59}$$

where $\eta = \phi_0 - \phi$ is the cathodic overpotential.

At sufficiently high cathodic ($\eta \gg RT/\alpha F$) or anodic ($-\eta \gg RT/\beta F$) overpotentials, Eq. (59) takes the form of the Tafel equation

$$\eta = a + b \log i$$

$$-\eta = a' + b' \log i \tag{10}$$

where $a = b \log i_0$, $a' = b' \log i_0$ and $b = 2.3(RT/\alpha F)$, $b' = 2.3(RT/\beta F)$.

At low overpotentials ($|\eta| \ll RT/\alpha F$), Eq. (59) gives a linear relationship

$$i = i_0 \frac{\eta F}{RT} \tag{60}$$

similar to Ohm's law, so from Eq. (60), it is seen that RT/i_0F has the nature of an effective resistance, the so-called reaction resistance or Faradaic resistance familiar in a.c. impedance studies of electrode reactions.

The exchange current density depends on the component concentrations, as stipulated both by the mass action law and by the equilibrium (Nernst) potential [Eq. (58)] being a function of these concentrations. Substituting the latter relationship into Eq. (57), we obtain

$$i_0 = i_0^0[\mathrm{A}^z]^\beta[\mathrm{A}^{z-1}]^\alpha \tag{61}$$

where i_0^0 is the standard exchange current (with all concentrations being equal to unity).

At a constant potential, the reaction rate is proportional to the concentration of each respective reagent. On the other hand, at a constant overpotential, as can be inferred from, for example, Eqs. (59) and (61), it is proportional to $[\mathrm{A}^z]^\beta$ as well as to the product concentration to the power α. This is due to the equilibrium potential being dependent on the concentration of all participating species in the reaction.

As will be seen from what follows, similar (sometimes, even more complex) relationships between the reaction rate and concentration apply to multistep processes as well. Determining the order of the reaction for each component is an essential method of studying the mechanism of electrode processes.(88) The selection of appropriate conditions (ϕ = const or η = const) under which the determination is made is based on the specific features of the system of interest. Needless to say, both methods are equivalent although, in some cases, the first method is preferable (e.g., when a reversible electrode for the electrode under kinetic study cannot be realized, i.e., when the overpotential cannot be measured directly), while, in other cases, preference is given to the second method (e.g., near the equilibrium potential, i and $[\mathrm{A}^z]$ when ϕ = const are no longer proportional, while when η = const they remain proportional at any overpotential; moreover, in concentrated solutions, it is practically impossible to meet the condition ϕ = const in an experiment over a wide range of concentrations, while the condition η = const can be met with a high degree of accuracy).

The foregoing calls for two comments: Firstly, while discussing equilibrium, one should bear in mind that the Nernst thermodynamic equation includes the full potential difference between the electrode and solution, rather than the potential difference between the electrode and the discharging particle's site (or charge transfer point ϕ_s).

This holds true if both values coincide or differ by a constant value independent of the electrode potential and the discharging particle's concentration. If this condition is not met, the equations must be modified (see below, Section 4). In this case, however, the kinetic approach will certainly lead to the Nernst equation. Indeed, the equilibrium potential automatically implies that there is equilibrium between particles on the electrode surface and those in the solution, i.e., the condition of equality of their electrochemical potentials obtains.

Taking this into account eventually leads to the result that the final expression for the equilibrium potential includes only the full metal–solution potential difference as well as the bulk concentrations, i.e., the same values that form part of the Nernst thermodynamic equation.

The second comment is similar to the first one, and has to do with the discharging particle's concentration. The kinetic equation (54) includes the surface concentration, but the expression for the equilibrium potential includes only the bulk concentration (or activity).

The correctness of the above can be easily seen if one uses more general kinetic equations which can be derived by the transition state method:

$$\vec{V} = \kappa \frac{kT}{h} \frac{\{\mathrm{A}^z\}_s}{\gamma^\ddagger} \exp\left(- \frac{\Delta \vec{G}_0^\ddagger + \alpha \phi_s F}{RT} \right) \tag{62}$$

$$\overleftarrow{V} = \kappa \frac{kT}{h} \frac{\{\mathrm{A}^{z-1}\}_s}{\gamma^\ddagger} \exp\left(\frac{\Delta \overleftarrow{G}_0^\ddagger - \beta \phi_s F}{RT} \right) \tag{62a}$$

Here, κ is the transmission coefficient, $\{\mathrm{A}^i\}$ is activity, $\gamma^\ddagger$ is the activity factor of the activated complex, $\Delta \vec{G}_0^\ddagger$ and $\Delta \overleftarrow{G}_0^\ddagger$ are the standard free energies of activation at $\phi_s = 0$, the remainder of the terms having their usual significance.

If the adsorption equilibrium is taken into account, the adsorption isotherm having an arbitrary form, i.e., any form of the relationship between $\{\mathrm{A}\}$ and $[\mathrm{A}]$, we obtain (from the equality of respective electrochemical potentials)

$$RT \ln \frac{\{\mathrm{A}\}_s}{\{\mathrm{A}\}} = Z_{\mathrm{A}}(\phi - \phi_s)F \tag{63}$$

where Z_{A} is the charge of the particle concerned. Substituting Eq. (63) into Eqs. (62) and (62a) and writing the rates equal at the equilibrium potential ϕ_0, we have

$$\phi_0 = \text{const} + \frac{RT}{(\alpha + \beta)F} \ln \frac{\{\mathrm{A}^z\}}{\{\mathrm{A}^{z-1}\}} \tag{58a}$$

i.e., when $\alpha + \beta = 1$, the Nernst equation is again recovered in a form applicable to all solutions, including nonideal ones if activities are employed. Here, just as before, the principle of microscopic reversibility has been used, i.e., the fact that the transition complex of the forward and backward reactions is the same, hence, values $\gamma^\ddagger$ in Eqs. (62) and (62a) are equal.

From Eqs. (62) and (58a), the following relationship between the exchange current and solution composition is derived:

$$i_0 = i_0^0 \frac{\{\mathrm{A}^z\}^\beta \{\mathrm{A}^{z-1}\}^\alpha}{\gamma^\ddagger} = i_0^0 \frac{\gamma_{\mathrm{A}^z}^\beta \gamma_{\mathrm{A}^{z-1}}^\alpha}{\gamma^\ddagger} [\mathrm{A}^z]^\beta [\mathrm{A}^{z-1}]^\alpha \tag{61a}$$

The so-called kinetic activity factor, determined by the activity coefficients of the components and activated complex, was discussed in Section 2.3.

We have considered the kinetics of a single-step electrode reaction. In the case of multistep processes, the same approach is used in deriving the kinetic equations for each step. These equations, however, include the concentrations not only of the final and initial substances, but also the intermediate products participating in the various steps.

These concentrations are defined from steady state conditions. Thus, the procedure for analysis of such processes is as follows: for each step, equations of the type (56) or (62) are derived and substituted into the steady state condition (2). As an example, we shall write the kinetic equations for a two-step process:

$$\mathrm{A}^+ + \mathrm{e} \rightleftarrows \mathrm{A}, \qquad \mathrm{A} + \mathrm{e} \rightleftarrows \mathrm{A}^-$$

$$\vec{k}_1 \exp\left(-\frac{\alpha_1 \phi F}{RT}\right)[\mathrm{A}^+] - \overleftarrow{k}_1 \exp\left(\frac{\beta_1 \phi F}{RT}\right)[\mathrm{A}] =$$

$$= \vec{k}_2 \exp\left(-\frac{\alpha_2 \phi F}{RT}\right)[\mathrm{A}] - \overleftarrow{k}_2 \exp\left(\frac{\beta_2 \phi F}{RT}\right)[\mathrm{A}^-] \tag{64}$$

In the above, it is assumed that intermediate product A does not undergo any chemical transformations and its transport is sufficiently fast for that process to be ignored.

It is easy to derive from this expression equations for, e.g., a cathodic reaction far from the equilibrium potential if it is the first step that is limiting, viz.,

$$i = 2\vec{k}_1[\mathrm{A}^+] \exp\left(-\frac{\alpha_1 \phi F}{RT}\right) \tag{64a}$$

or, if the first step is quasireversible and the second step is slow,

$$i = 2\frac{\vec{k}_1}{\overleftarrow{k}_1}\vec{k}_2 \exp\left[-\frac{(1+\alpha_2)\phi F}{RT}\right][\mathrm{A}^+] \tag{64b}$$

Factor 2 takes into account that each occurrence of the first step is associated with that of the second step in which another electron is transferred. Similarly, equations may be derived for a process near the equilibrium potential, for an anodic reaction, etc. In the general case, when none of the four reaction rates can be ignored relative to others, the following equation is derived:

$$i = 2\vec{k}_1 \exp\left(-\frac{\alpha_1 \phi F}{RT}\right)[\mathrm{A}^+] - 2\overleftarrow{k}_1 \exp\left(\frac{\beta_1 \phi F}{RT}\right) \times$$

$$\times \frac{\vec{k}_1 \exp(-\alpha_1 \phi F/RT)[\mathrm{A}^+] + \overleftarrow{k}_2 \exp(\beta_2 \phi F/RT)[\mathrm{A}^-]}{\vec{k}_2 \exp(-\alpha_2 \phi F/RT) + \overleftarrow{k}_1 \exp(\beta_1 \phi F/RT)} \tag{65}$$

which does not reduce to the form of a Tafel equation even if the deviation from the equilibrium potential is considerable, viz., substantially greater than RT/F. However, at a sufficiently high overpotential when it is possible to disregard certain terms, we again obtain a Tafel equation.

For example, at a definite potential, let $\overleftarrow{k}_2 \exp(\beta_2\phi F/RT)[\mathrm{A}^-] \ll \vec{k}_1 \exp(-\alpha_1\phi F/RT)[\mathrm{A}^+]$. A further shift of the potential in the negative direction will not affect this inequality since its left-hand side decreases and the right-hand side increases. Then, Eq. (65) can be simplified to

$$i = \frac{2\vec{k}_1 \exp(-\alpha_1\phi F/RT) \cdot \vec{k}_2 \exp(-\alpha_2\phi F/RT)}{\vec{k}_2 \exp(-\alpha_2\phi F/RT) + \overleftarrow{k}_1 \exp(\beta_1\phi F/RT)}[\mathrm{A}^+] \tag{65a}$$

This is not yet a Tafel equation. If condition $\vec{k}_2 \exp(-\alpha_2\phi F/RT) \ll k_1 \exp(\beta_1\phi F/RT)$ is also met, i.e., if the back reaction rate of the first step is much greater than the forward rate of the second step, the first step is quasireversible and Eq. (65a) takes the form, as would be expected, of Eq. (64b). This Tafel expression features a low slope having the value $RT/(1 + \alpha_2)F$, which is a typical result for the case where the rate-limiting stage is preceded by a quasireversible electrode process [the transfer of n electrons results in a relationship between the intermediate product concentration and potential $\sim\exp(n\phi F/RT)$]. With potentials shifted further in the negative direction, the step rate ratio must change and, ultimately, inequation $\vec{k}_2 \exp(-\alpha_2\phi F/RT) \gg k_1 \exp(\beta_1\phi F/RT)$ will be true. Then, Eq. (65a) becomes (64a), i.e., an expression for the first step as the limiting stage. This result compounds, as the overpotential increases, to a situation where a transition takes place from a later to an earlier rate-limiting step in the chain of successive electron transfers; this change of the identity of the limiting step is such that the Tafel slope b becomes larger; this effect is rather general and applies to mechanisms involving any number of successive steps. An exception is the case where the intermediate product concentration has a certain limit, for example, the product is an adsorbed substance. In this case, as the overpotential increases, the number of the limiting step may be higher, but even in this case the slope b tends to become larger at higher η values.

It should be noted that the orders of the reaction (for the condition ϕ = const and η = const) follow the above-mentioned simple relations only at sufficiently high overpotentials (but not necessarily only in the Tafel regions).

A similar analysis should be made for each of the possible mechanisms of a reaction of interest, and comparison of the results of such an analysis (as well as analysis of the ψ_1 effects; see below, Section 4) with the experimental results permits selection of the most probable mechanism.

Another peculiarity of multistep reactions is to be noted, namely, a more complicated definition of the exchange current. For each step, this concept is unambiguous, but for the reaction as a whole it may be introduced only with certain reservations. For example, for the two-step reaction described above, we may determine the exchange currents of each stage; i_{01} and i_{02}, but if we try to find out what is precisely the exchange current of the reaction as a whole, its definition turns out to depend on the method by which it is determined. For example, we can find i_0 for the Tafel regions experimentally, using the Tafel equation (the so-called extrapolated exchange current).

Thereby, depending on which step is rate determining corresponding to the extrapolated Tafel region, we find different exchange currents $i_0 = 2i_{01}$ or $i_0 = 2i_{02}$.

Since, in principle, different steps must be rate limiting over different ranges of overpotential, if the process has been studied over a sufficiently broad range of η, we shall obtain *two* values of the extrapolated exchange current. A different value is obtained if we want to determine the exchange current through the effective conductance of the reaction near the equilibrium potential, i.e., through the value $(\partial i/\partial\eta)_{\eta=0}$ [cf. Eq. (60)]. Equation (65) suggests (we omit rather cumbersome intermediate transformations) so that

$$\left(\frac{\partial i}{\partial \eta}\right)_{\eta=0} = \frac{F}{RT}\,\frac{4i_{01}i_{02}}{i_{01}+i_{02}} \tag{66}$$

In this formula, the function of the exchange current is performed by the expression $2i_{01}i_{02}/(i_{01}+i_{02})$ [see below, Section 3.2, Eq. (81b)]. As can be seen, it coincides with the extrapolated exchange current only under the condition that the exchange current of one of the stages is much greater than that of the other.

The picture becomes more complicated if the reaction follows *parallel* paths. For example, in the case of cathodic hydrogen evolution with simultaneous occurrence on the electrode of three steps: discharge, desorption, and recombination, we can always describe the process as a combination of two of the possible paths, and, in some cases, three different combinations describe the situation adequately. Obviously, in this case, such a notion as the exchange current of a reaction following a particular path is purely conventional.

3.2. Stoichiometric Numbers

Valuable information on the mechanism of a process can be obtained when the kinetics of the reaction are examined near the equilibrium potential and compared with the characteristics of the Tafel region(s). We have already given some formulas for particular mechanisms [Eqs. (60) and (66)] indicative of the linear relationship between the current and overpotential near the equilibrium, the proportionality factor (effective conductance $(\partial i/\partial\eta)_{\eta=0}$) being determined by the value of the exchange current.

These formulas represent a particular case of the general linear relationship between the rate (V) and affinity (A) of a reaction, originating from the thermodynamics of irreversible processes(89):

$$V = \left(\frac{\partial V}{\partial A}\right)_{A=0} \cdot A \tag{67}$$

The quantity $(\partial V/\partial A)_{A=0}$ is known as the phenomenological coefficient of a reaction. It can be written as V_0/RT, where V_0 is the exchange rate and the coefficient RT renders value A dimensionless. The affinity of a reaction is determined according to de Donder as the chemical (or electrochemical, for charged particles) potential difference of products (f) and initial substances (i), multiplied by the respective stoichiometric factors:

$$A = \sum_f x_f \bar{\mu}_f - \sum_i x_i \bar{\mu}_i \tag{68}$$

At equilibrium, this difference is known to be equal to zero; hence, the affinity of a reaction determines the degree of its deviation from equilibrium. At low deviations ($A \ll RT$), the linear relationship (67) is true. For electrode reactions involving transfer of n electrons,

$$A = nF\eta \tag{69}$$

and the current density is

$$i = nFV \tag{70}$$

Consider now a more general case, namely, a multistep reaction following a number of parallel routes, as is shown schematically, for example, in Figure 13a. The analysis will be conducted along the lines proposed by Erenburg.(90–92)

As is shown in Figure 13b, cases of branching are possible when one of the steps involves two or more routes. In this case, it is convenient to break down its rate into two or more components and to associate each of them with one of the paths, i.e., the diagram of Figure 13b can be reduced to that of Figure 13a.

We denote the values relating to one of the routes (p) by subscript p, while subscript i is given to the numbers of steps within a given route. For example, the affinity of a given step on a given route is designated A_{pi}, its stoichiometric number (the number of its recurrences on a given path) is

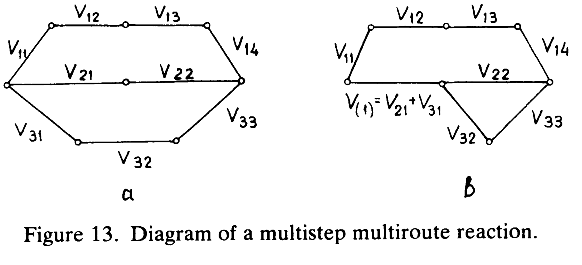

Figure 13. Diagram of a multistep multiroute reaction.

designated ν_{pi} and its rate, V_{pi}. The latter is the difference of the rates in the forward and backward directions: $V_{pi} = \vec{V}_{pi} - \overleftarrow{V}_{pi}$. For each route, we may write a steady state condition (2′):

$$\frac{V_{p1}}{\nu_{p1}} = \cdots = \frac{V_{pi}}{\nu_{pi}} = \cdots = \frac{V_{pn}}{\nu_{pn}} = V_p \tag{2′}$$

The rate of the reaction as whole is the sum of its rates on all parallel paths:

$$V = \sum_p V_p \tag{71}$$

At true equilibrium, not only $A = 0$, but also, since all steps are in equilibrium, all $A_{pi} = 0$. Should a deviation from equilibrium occur, the affinity of each step becomes, generally speaking, not equal to zero. The total deviation from equilibrium with respect to all successive stages (with their recurrences being taken into account) is equal to the overall affinity of the reaction, i.e.,

$$\sum_i \nu_{pi} A_{pi} = A \tag{72}$$

This relation holds, naturally, for each one of the parallel routes. It is similar to the sum of voltage drops across each of the serially connected resistors in each parallel branch of an electric circuit. This similarity to an electric circuit will be seen in what follows, which is not accidental; in fact, Ohm's law is just another case of a linear relationship between flow and generalized force, similar to Eq. (67); Kirchhoff's law is similar to Eq. (71), etc.

Also written for each rate of an individual step can be a linear relationship similar to Eq. (67), but, in this case, one should take into account that the rate of this step may, generally speaking, be dependent not only on the affinity of this step, but also on the affinity of other steps, i.e.,

$$V_{pi} = \sum_k \left(\frac{\partial V_{pi}}{\partial A_{pk}}\right)_{A_{pk}=0} \cdot A_{pk} \tag{73}$$

However, in the case where $(\partial V_{pi}/\partial A_{pk})_{k \neq i} \neq 0$ it can be shown, using the steady state condition, that the rate of a given step can always be expressed as a linear function of affinity of only this step, viz.,

$$V_{pi} = \left(\frac{V^0_{pi}}{RT}\right) A_{pi} \tag{74}$$

where the coefficient V^0_{pi}/RT is not necessarily identical with $(\partial V_{pi}/\partial A_{pi})_{A_{pi}=0}$.

Some transformations are now performed which permit finding the phenomenological coefficient of the reaction as a whole, i.e., $(\partial V/\partial A)$. First, the rate derivative with respect to A for an individual step is found:

$$\left(\frac{\partial V_{pi}}{\partial A}\right)_{A=0} = \frac{V^0_{pi}}{RT}\left(\frac{\partial A_{pi}}{\partial A}\right)_{A=0} \tag{75}$$

The derivative $\partial A_{pi}/\partial A$ forming part of the above expression also occurs when Eq. (72) is differentiated:

$$\sum_i \nu_{pi}\left(\frac{\partial A_{pi}}{\partial A}\right)_{A=0} = 1 \tag{76}$$

The value of the derivative from Eq. (75) is substituted into Eq. (76):

$$\sum_i \nu_{pi}\frac{RT}{V^0_{pi}}\left(\frac{\partial V_{pi}}{\partial A}\right)_{A=0} = 1 \tag{77}$$

From the steady state condition (2):

$$\frac{1}{\nu_{pi}}\left(\frac{\partial V_{pi}}{\partial A}\right)_{A=0} = \left(\frac{\partial V_p}{\partial A}\right)_{A=0} \tag{78}$$

Substituting Eq. (78) into Eq. (77), we find

$$\frac{\partial V_p}{\partial A} = \frac{1}{RT}\left(\sum_i \frac{\nu^2_{pi}}{V^0_{pi}}\right)^{-1} \tag{79}$$

For the reaction as a whole, $\partial V/\partial A = \sum_p (\partial V_p/\partial A)$ [see Eq. (71)], i.e.,

$$\left(\frac{\partial V}{\partial A}\right)_{A=0} = \frac{1}{RT}\sum_p\left(\sum_i \frac{\nu^2_{pi}}{V^0_{pi}}\right)^{-1} \tag{80}$$

Since the value of interest is normally the rate of the reaction as a whole, it is precisely expression (80), determining the "conductance" of reactions, that represents the relationship on which further analysis of the experiment is to be based.

For electrode reactions, this expression can be written, using Eqs. (69) and (70), as

$$\left(\frac{\partial i}{\partial \eta}\right)_{\eta=0} = \frac{n^2F^2}{RT}\sum_p\left(\sum_i \frac{\nu^2_{pi}n_{pi}F}{i^0_{pi}}\right)^{-1} \tag{81}$$

Here, $i^0_{pi} = n_{pi}FV^0_{pi}$ and n_{pi} is the number of electrons transferred during this step ($\sum_i n_{pi} = n$). Writing the result in this form is not convenient in cases where purely chemical steps are involved, not accompanied by any charge transfer, i.e., $n_{pi} = 0$ and $i^0_{pi} = 0$. It is more useful to introduce the effective exchange current determined as

$$I^0_{pi} = nF\frac{V^0_{pi}}{\nu_{pi}} \tag{82}$$

This value is numerically equal to the current flowing through the entire sequence of steps if a given step proceeds at a rate equal to a respective exchange rate. Then,

$$\left(\frac{\partial i}{\partial \eta}\right)_{\eta=0} = \frac{nF}{RT}\sum_p\left(\sum_i \frac{\nu_{pi}}{I^0_{pi}}\right)^{-1} \tag{81a}$$

Formula (81a) is nothing but an expression for the conductance of a composite circuit with series and parallel connections of its elements whose conductance is $(I^0_{pi}/\nu_{pi})/(RT/nF)$.

Assume that we are dealing with a single-route reaction. Then,

$$\left(\frac{\partial i}{\partial \eta}\right)_{\eta=0} = \frac{nF}{RT}\left(\sum_i \frac{\nu_i}{I^0_i}\right)^{-1} \tag{81b}$$

If only one rate-limiting step is involved, i.e., its exchange current $I^0_k \ll I^0_{i(i\neq k)}$, in the sum of Eq. (81b) all the terms except for that belonging to the kth step can be omitted. The result will be written in the following form for ν_k:

$$\nu_k = (nF/RT)I^0_k/(\partial i/\partial \eta)_{\eta=0} \tag{83}$$

This formula for determining the stoichiometric number of the rate-limiting step was for the first time derived by Horiuti, who introduced the concept of the stoichiometric number into kinetics and showed its significance.(93,94)

In order to determine the stoichiometric number from Eq. (83) one should, on the one hand, measure relation $i(\eta)$ in the region of sufficiently low η (determination of $\partial i/\partial \eta$ in the region of proportionality of i to η)† and, on the other, find I^0_k. If condition $I^0_k \ll I^0_i\,(i \neq k)$ is met, i.e., if a single slow step is involved, I^0_k can be easily found by way of extrapolation to the equilibrium potential of the Tafel region of the polarization curve.

If the exchange currents of different steps are comparable, then, as has been suggested by analysis of a number of particular mechanisms made by different authors, the relationships become more complicated; the value of ν determined formally from Eq. (83), using the effective exchange current instead of I^0_k, may then be of any magnitude and loses its physical meaning as the number of recurrences of a step. Attempts to use values of I^0 determined, for example, by the isotopic exchange method instead of from extrapolated exchange currents do not yield the desired results either.

In the literature, one may often come across the term "stoichiometric number of reactions." It implies the number of recurrences of the slow step only if a single-route reaction has a single slow step. In the case of more complex mechanisms, one can speak of the number of recurrences, i.e., the stoichiometric number, with reference to a single step and not to the reaction as a whole.

We now examine what information can be provided by experimental determinations of stoichiometric numbers from an equation similar to Eq. (83), without assuming *a priori* that the reaction involves a single route and a single slow step.

---

† The potential interval within which i is proportional to η to a good degree of accuracy, is always significantly smaller than $\pm RT/nF = \pm 25/n$ mV, and, for certain mechanisms, e.g., discharge–recombination, it may be as small as fractions of a millivolt.

Generally speaking, with arbitrary exchange current ratios between different steps and routes, the shape of the polarization curve may be so complex that it will not lend itself to straightforward analysis. However, if we take a great number of various mechanisms, it turns out that within a definite range of overpotentials the principal role is played by one of the paths, while over a different potential range, by another, each of these ranges being subdivided into several possible Tafel regions corresponding to particular rate-determining steps. Extrapolation of these Tafel regions allows the so-called extrapolated exchange currents, I^e_{pi}, to be evaluated. The latter coincide with true I^0_{pi} if both the corresponding Tafel region and the region near $\eta = 0$ are characterized by a similar coverage of the electrode with the intermediate product—in both cases, either $\theta \ll 1$ or $\theta \simeq 1$. This condition is sufficient but not necessary. For some mechanisms, I^e_{pi} coincides with I^0_{pi} at mean coverages. Another prerequisite of I^e_{pi} coinciding with I^0_{pi} is the constancy of the true value of α over the entire potential range under investigation.

Substituting the extrapolated values of the currents into Eq. (83), we obtain an effective value of ν^e_{pi} of the stoichiometric number. It is not equal to the number of recurrences of step *pi* and may, in principle, be nonintegral (the equality to the theoretical value ν_{pi} is possible, as has been mentioned above, only in the case of a single-route reaction with a single slow step; it corresponds to a polarization curve with a single cathodic Tafel region and a single anodic region, which are extrapolated to the *same* exchange current). If the extrapolated exchange current coincides with the true I^0_{pi}, substituting it into the Horiuti formula gives

$$\nu^e_{pi} = \frac{(nF/RT)I^0_{pi}}{(\partial i/\partial \eta)_{\eta=0}} \tag{84}$$

Combining this formula with Eq. (81a) gives

$$\sum_p \left(\sum_i \frac{\nu_{pi}}{\nu^e_{pi}}\right)^{-1} = 1 \tag{85}$$

This formula may serve as a criterion for agreement of the experimental data with the proposed reaction mechanism. If this criterion is not met, then either the mechanism is inappropriate or the extrapolation conditions ($I^e_{pi} \neq I^0_{pi}$) are not complied with, for example, as a result of a change in the true value of α. Examples of using this criterion both for defining parallel paths and for proving the fact of a change in the true value of α are given in Refs. 86 and 92.

In the case of a single-route reaction, Eq. (85) becomes

$$\sum \frac{\nu_i}{\nu^e_i} = 1 \tag{85a}$$

It can be easily seen from this equation that

$$\nu^e_i \geq \nu_i \tag{86a}$$

In the case of a branched process, each path of which involves only one slow step,

$$\sum_p \frac{\nu_p^e}{\nu_p} = 1 \tag{85b}$$

Then,

$$\nu_p^e \leq \nu_p \tag{86b}$$

These relations suggest that the deviation of a particular experimental value ν^e from theoretical values ν (especially, nonintegral values ν^e) is a serious proof of the existence of several (parallel or successive) limiting steps.

Consider now relations elucidating the physical meaning of effective stoichiometric numbers. Comparing formulas (75), (69), and (82), we can easily obtain

$$\left(\frac{\partial I_{pi}}{\partial \eta}\right)_{\eta=0} = \frac{nF}{RT} I_{pi}^0 \left(\frac{\partial A_i}{\partial A}\right)_{A=0} \tag{87}$$

if the reaction is a single-route one, the total reaction current $i = I_i$ (route subscript p may be omitted here). Then,

$$\frac{(nF/RT)I_i^0}{(\partial I_i/\partial \eta)_{\eta=0}} = \frac{(nF/RT)I_i^0}{(\partial i/\partial \eta)_{\eta=0}} = \nu_i^e$$

i.e.,

$$\frac{1}{\nu_i^e} = \left(\frac{\partial A_i}{\partial A}\right)_{A=0} \tag{88}$$

Hence the physical meaning of $1/\nu_i^e$: for a single-route reaction, it is the measure of nonequilibrium (fraction of affinity) introduced by a single act of step i (ν_i acts are responsible for the quantity ν_i/ν_i^e). The significance of Eq. (85a) becomes clear as well: the total extent of nonequilibrium of all steps recurring the required number of times is equal, as would be expected, to unity.

Consider another limiting case, a reaction following a number of parallel routes each involving only one slow step. If we could measure the current corresponding to one of the routes, we would be able to determine, with the aid of the Horiuti formula, the true stoichiometric number of the slow step of this route (since there is only one slow step, the *true* ν_p is determined)

$$\nu_p = \frac{(nF/RT)I_p^0}{(\partial I_p/\partial \eta)_{\eta=0}} \tag{83a}$$

Experimentally, the total current $i = \sum I_p$ is determined, as well as, respectively, the effective stoichiometric number

$$\nu_p^e = \frac{(nF/RT)I_p^0}{(\partial i/\partial \eta)_{\eta=0}} \tag{83b}$$

Division of this formula by the preceding one gives

$$\frac{\nu_p^e}{\nu_p} = \left(\frac{\partial I_p}{\partial i}\right)_{\eta=0} \tag{89}$$

i.e., the ratio of the effective stoichiometric number to the true one gives the fraction of current near the equilibrium potential for a given route. Naturally, the sum of these values is equal to unity [Eq. (85b)]. In the general case of a multiroute reaction with a plurality of nonequilibrium steps, the contributions of parallel routes are summed up taking into consideration the irreversibility of each one of the successive steps [Eq. (85)].

4. Electric Double-Layer Structure and Electrode Reaction Rate

4.1. Basic Relations

An electrode process occurs at the electrode–solution interface. This is why the structure of this interface, i.e., the structure of the electric double layer, naturally produces a tangible effect on the electrode reaction rate. This simple though exceptionally important concept was first put forth by Frumkin(7) in 1933 and has played a decisive role in the development of modern electrochemical kinetics. Needless to say, the structure of the reaction zone is substantial for any chemical processes, but in electrochemistry it has a particular significance; we can, first of all, change the double-layer structure over an extremely wide range without affecting the mechanism of the electrode reaction itself (by changing, e.g., ionic strength of the solution) and secondly, using various techniques, certain information on the structure of the double layer can be obtained, i.e., on the reaction zone.

The ψ_1 effect in the kinetics of electrode reactions has been dealt with in a number of important reviews(15,95–100) which can be recommended to readers who wish to have further knowledge on this topic (particularly detailed information can be had from the relevant chapters in the monographs by Delahay(99) and Frumkin(100)).

An ion in the double layer, in particular an ion at a point which is optimum for discharge, is, generally speaking, at a potential different from that in the solution. This potential difference is generally known as the ψ_1 potential. Its existence gives rise to two effects.

Firstly, the concentrations C_s of ions in a respective plane differ from their mean concentrations in the solution (C_0). If the surface coverage with discharging particles is small and if the passage of a particle from the bulk to the surface is not accompanied by a substantial change in its standard chemical potential, the relation between C_s and C_0 takes a simple form:

$$C_s = C_0 \exp\left(-\frac{Z\psi_1 F}{RT}\right) \tag{90}$$

where Z is the ion valency.

Secondly, the ion is acted upon not by the full metal–solution potential difference ϕ, but only by a part of it, viz., $\phi - \psi_1$. This means that the value of the true activation energy varies with the potential by $\alpha(\phi - \psi_1)F$:

$$E^{\ddagger} = E_0^{\ddagger} + \alpha(\phi - \psi_1)F \tag{91}$$

[Eq. (91) is written for a single-electron cathodic reaction.]

Both the above ψ_1 effects are, in principle, independent, the first being capable (depending on the sign of the charge of the discharging particle) of producing a directly opposite effect and disappears completely in the case of a neutral reagent ($Z = 0$). Together, the two effects lead to the following expression for the rate of an electrode reaction:

$$i = kc_0 \exp\left[-\frac{(z-\alpha)\psi_1 F}{RT}\right] \exp\left(-\frac{\alpha\phi F}{RT}\right) \tag{92}$$

or, taking overpotential into consideration,

$$\eta = \text{const} + \frac{Z-\alpha}{\alpha}\psi_1 - \frac{1-\alpha}{\alpha}\frac{RT}{F}\ln C_0 + \frac{RT}{\alpha F}\ln i \tag{93}$$

A similar expression can be easily written for multielectron processes as well as for a reaction in the anodic direction.

In the absence of specifically adsorbable ions, the double-layer structure is adequately described in terms of the Gouy–Chapman–Stern theory. The outer Helmholtz plane potential ψ^0 (distinguished by Grahame) is associated with a surface charge density σ through the relation

$$\psi^0 = \frac{2RT}{ZF}\sinh^{-1}\left(\frac{\sigma}{2A\sqrt{C}}\right) \tag{94}$$

where C is the total concentration of a Z, Z-charged electrolyte (for a nonsymmetrical electrolyte, the expression is more cumbersome; see, for example, Ref. 99; at high surface charges, the determining effect is produced by Z and C of an ion charged oppositely to the electrode), and

$$A = \left(\frac{\varepsilon RT}{2\pi}\right)^{1/2}$$

where ε is dielectric permittivity.

At low surface charges ($\sigma/2A\sqrt{C} \ll 1$), taking into account that if $x \ll 1$, $\sinh^{-1} x \simeq x$,

$$\psi^0 \simeq \frac{RT\sigma}{ZFA\sqrt{C}} = \frac{\sigma}{ZF}\left(\frac{2\pi RT}{\varepsilon C}\right)^{1/2} \tag{95}$$

At high charges ($\sigma/2A\sqrt{C} \gg 1$), taking into account $\sinh^{-1} x \div \ln(x + x^2 + 1)$, we have

$$|\psi^0| \simeq \text{const} + \frac{2RT}{ZF} \ln |\sigma| - \frac{RT}{ZF} \ln C \tag{96}$$

At positive surface charges, ψ^0 is positive, while at negative charges, it is negative. The absolute value of ψ^0 gradually increases with the absolute magnitude of the charge and decreases as the electrolyte concentration increases.

At high surface charges, the integral electrode capacity K can be assumed to be more or less constant and, taking into consideration $\sigma = K\phi_a$, where ϕ_a is a potential shift relative to the zero charge potential, we have

$$\psi^0 \simeq \text{const}' + \frac{2RT}{ZF} \ln |\phi_a| - \frac{RT}{ZF} \ln C \tag{96a}$$

In some cases, a very simple relation is expected between ψ^0 and ψ_1 which forms an integral part of the electrochemical kinetic equations.

4.2. Hydrogen Evolution

The application of the "ψ_1 effect" of Frumkin was first done for the hydrogen ion discharge reaction.$^{(7)}$ Therefore, we shall start the discussion with the classical topic.

In the presence of an excess of a supporting electrolyte, when total $C \gg C_0$, the value of the ψ_1 potential is practically independent of the hydrogen ion concentration. Therefore, it can be assumed constant to a first approximation. Then, from Eq. (93) it follows that

$$\eta = a - \frac{1-\alpha}{\alpha}\frac{RT}{F} \ln C_0 + \frac{RT}{\alpha F} \ln i + \frac{1-\alpha}{\alpha}\frac{RT}{F} \ln C \tag{97}$$

With $\alpha = 1/2$, we obtain (at 298 K)

$$\left(\frac{\partial \eta}{\partial \log i}\right)_{C_0,C} = -0.118\text{ V}, \qquad \left(\frac{\partial \eta}{\partial \text{pH}}\right)_{i,C} = 0.059\text{ V}, \qquad \text{and}$$

$$\left(\frac{\eta}{\partial \log c}\right)_{i,C_0} = 0.059\text{ V} \tag{98}$$

Values close to these limits have been frequently found experimentally. The independence of ψ_1 on C_0 does not mean, however, that it is strictly constant. If it is assumed, as a first approximation, that in the absence of specific adsorption of ions, the ψ_1 potential varies under the action of external factors just as the ψ^0 potential does, corresponding effects can be evaluated using Eqs. (96) or (96a).

When overpotential on mercury is measured in a 1 N acid, for example, in the current density range of 10^{-6} to 10^{-2} A cm^{-2} the potential range of -0.70 to -1.17 V is involved or, in other words, the ϕ_a range of -0.51 to -0.98 V. According to Eq. (96a), in this range, the ψ^0 potential will shift in the negative direction by 0.033 V, which results in the mean value of $\partial\eta/\partial \log I$ decreasing by 0.008 V, i.e., down to 0.110 V. This effect is slightly mitigated by a shift farther away from the potential of zero charge, i.e., as the current density or pH of the solution increases (e.g., in a 1 N acid at $i = 10^{-2}$–10^{0} A cm^{-2}, $b = 0.112$ V; in a 1 N solution of a uni-uni-valent electrolyte with pH = 3 and $i = 10^{-6}$–10^{-2} A cm^{-2}, $b = 0.113$ V). Close values are also obtained when the more rigorous Eq. (96) is used instead of Eq. (96a), together with experimental data on surface charges. The results of such calculations, expressed in terms of the apparent value of α, are shown in Figure 14.

A variation in the ψ_1 potential should also be manifest with varying pH of the solution since, in this case, a substantial change in the electrode potential with respect to the potential of zero charge occurs owing to the varying equilibrium potential and overpotential. For example, at $i = 10^{-4}$ A cm^{-2}, a variation in pH from 0 to 5 corresponds to a variation in ϕ_a from -0.74 to -1.33 V, which leads to a shift of ψ^0 by -0.030 V, i.e., a decrease in $\partial\eta/\partial$ pH by 0.006 V. A similar effect is to be expected when we consider the influence of the concentration of an indifferent salt, namely, a decrease in $\partial\eta/\partial \log C$ by several millivolts. Practically, if the Tafel slope is expressed as $2.3(RT/\alpha' F)$, where α' is an effective factor differing from the true α because of the dependence of ψ_1 on ϕ, then the derivatives of η with respect to pH and log C will differ from the value of 0.059 V by a factor very close to $(1-\alpha')/\alpha'$.

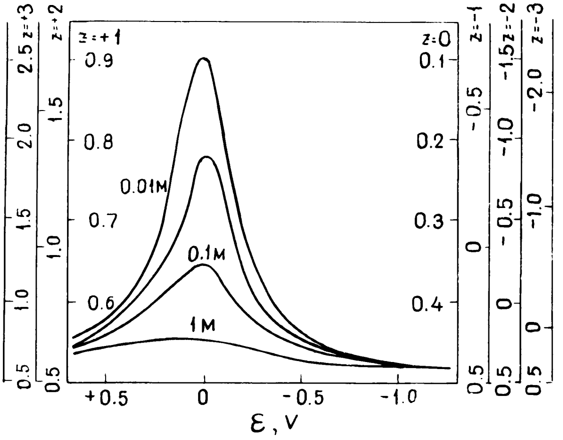

Figure 14. Effective transfer coefficient α' (true value $\alpha = 0.5$) in the case of reduction of an ion with valency Z versus potential, with respect to the zero charge potential in surface-inactive supporting electrolytes of different concentrations (according to Ref. 95).

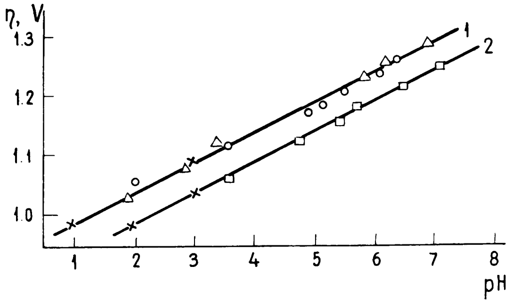

Figure 15. Hydrogen overpotential on mercury versus pH at a current density of 10^{-4} A/cm^2. □, 0.01 M $K_3PO_4 + xM$ HCl; ○, 0.1 M $K_3PO_4 + xM$ HCl; △, 0.01 M $K_3PO_4 + 0.3M$ KCl $+ xM$ HCl; ×, HCl + KCl. The total electrolyte concentration for the top curve is 0.3 N and for the bottom curve, 0.03 N (according to Ref. 101).

We are speaking of minor deviations from the values of the derivatives given by Eq. (98), but careful measurements reveal these deviations. For instance, in HCl solutions and in the presence of potassium salts, values of b, $\partial\eta/\partial$ pH, and $\partial\eta/\partial \log C$ have been found, corresponding to $\alpha' = 0.53$, i.e., practically coinciding with the calculated values (see Figure 15).(101)

When there is no surplus amount of an indifferent electrolyte, the total concentration C of the electrolyte coincides with the acid concentration C_0, and two respective terms in Eq. (93) [after the dependence of ψ_1 on C has been substituted in accordance with Eqs. (96) or (96a)] are automatically balanced out. It should be pointed out that this compensation is practically independent of the assumption that σ or ϕ_a is constant. In fact, as has been shown above, a corresponding relationship results in a variation in the effective value of α', which is the same for the dependence on pH as on total electrolyte concentration. Since the terms in $\ln C$ and $\ln C_0$ have the same coefficient $(1 - \alpha')/\alpha'$, the compensation is almost exact.

Experiments have revealed the constance of η in the acid concentration range 0.001–0.1 M. At higher concentrations, the ψ_1 potential, now relatively low, varies slower with the electrolyte concentration than in accordance with Eq. (96), and the influence of the variation in the hydrogen ion concentration [the term with C_0 in Eq. (93)] becomes predominant, i.e., increase in the acid concentration causes a certain decrease in overpotential.

So far we have considered only data quantitatively described by theory with the assumption that $\Delta\psi_1 = \Delta\psi^0$. Certain facts, however, are inconsistent with this assumption. For example, the effects of addition of a neutral salt is close to the theoretical predictions only in the case of potassium salts. In the presence of lithium salts, it is less strong, while with a cesium salt, the effect is more pronounced.(102)

This may be partially due to the known minor extent of specific adsorption of Cs^+, but, at least in the case of Li^+, the discrepancy is to be accounted for by the difference between ψ_1 and ψ^0.

Interestingly, best agreement with theory is observed in the case of the K^+ cation which is very close in size to the H_3O^+. Here, we may expect a closer similarity of structures of the dense part of the double layer. A similar

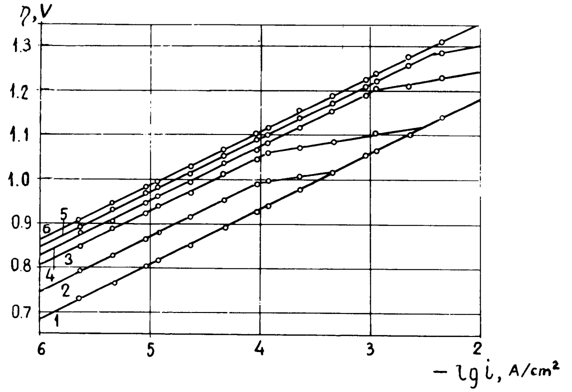

Figure 16. Effect of tetrabutylammonium addition on hydrogen overpotential on mercury in 1 *N* HCl. $N(C_4H_9)_4\ _2SO_4$ concentration: 1, 0; 2, 10^{-5} *N*; 3, 10^{-4} *N*; 4, 5×10^{-4} *N*; 5, 10^{-3} *N*; 6, 5×10^{-3} *N* or 5×10^{-2} *N* (according to Ref. 105).

situation arises in other systems as well. For example, good agreement with theory can be seen in the case of Ga^{3+} ion discharge on mercury in the presence of the Al^{3+} ion which is comparable in size and is also trivalent, while with Na^+ and Mg^{2+} salts as supporting electrolytes, the agreement with theory is much worse.(103)

Particularly pronounced ψ_1 effects are observed in the presence of specifically adsorbed ions. For example, addition of tetrabutylammonium ion causes a dramatic increase in overpotential, even in a 1 *M* acid (Figure 16). A specific feature of the behavior of large organic cations is their ability, just as with many other organic molecules, to desorb from the electrode within a narrow interval of potentials, depending on the surface-active ion concentration. This results in an abrupt break of the polarization curve and its convergence to the pure acid curve.

The effect of adsorption of substituted ammonium ions is due, primarily, to the variation in the ψ_1 potential; the overpotential shift is close in magnitude to that of the zero charge potential in the positive direction, in the presence of the same concentrations of NR_4^+ ions. In addition, the influence of tetraalkylammonium salts on the rate of cation and anion discharge is directly opposite, just as would be expected for a ψ_1 effect.

At the same time, the adsorption of tetraalkylammonium ions must produce another inhibiting effect, that of surface blocking. In principle, this effect should take place for any adsorbing particle, but, in this case, it becomes particularly pronounced owing to the large size of these ions. For example, in chromate anion reduction, when the cation adsorption brings about an accelerating ψ_1 effect, inhibition also occurs as a result of surface screening. Consequently, the dependence of the reaction rate on the surface-active ion concentration passes through a maximum the occurrence of which depends on the size of the ion—the larger the ion, the sooner it appears.(104)

The screening action depends not only on the size of the substituted ammonium ion, but also on the characteristics of the discharging particle. For example, if, in the case of CrO_4^- discharge, the blocking of the surface with the $(nBu)_4N^+$ ion is pronounced, hydrogen evolution in the barrierless dis-

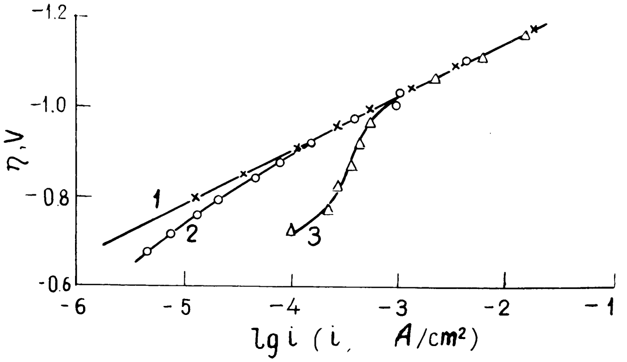

Figure 17. Polarization curves of hydrogen evolution from 1 *M* HCl + 2 *M* KCl (1), +2 *M* KBr (2), +2 *M* KI (3) (according to Ref. 108).

charge region, where no ψ_1 effect is present, reveals only an insignificant increase in overpotential, commensurate with the experimental error.(70,76,77) The screening effect is predominant when uncharged molecules are adsorbed, although, in this case, a certain ψ_1 effect is observed, which is due to the orientation of the dipole of the adsorbed substance.(106)

Specific adsorption of anions must be accompanied by a sharp drop in the hydrogen overvoltage. This deduction from theory was for the first time tested by Iofa, Kabanov, and co-workers(107) and repeatedly confirmed later (see Figure 17). The value of η turns out to be extremely sensitive to anion adsorption; a decrease in η is perceptible at such potentials at which the anion adsorption is not yet seen on the electrocapillary curves.

The point is that the ψ_1 potential is directly associated, not with surface tension, but with the surface charge, to variations of which the electrocapillary curve [which is integrated with respect to σ, ϕ curve] is less sensitive. A variation in η, on the other hand, strictly correlates with a variation in σ.

Since adsorption of small ions gradually changes over a wide potential range, a respective gradual change in overpotential is observed. In the presence of two specifically adsorbed ions of different signs (e.g., I^- and NBu_4^+), mutual intensification of their adsorption and ψ_1 effects is observed(109) over a certain potential range. The phenomena of coadsorption of two ions are due not only to the adsorbability of each separate ion, but also, as was analyzed in detail by Gierst *et al.*,(98,104) to their tendency to associate forming adsorbed ion pairs in the double layer, the charge centers of two associated ions lying, as a rule, in different planes.

The behavior in the presence of adsorbed anions vividly demonstrates the difference between effects of ψ_1 and ψ^0 potentials. Figure 18 represents polarization curves which would have been expected if ψ_1 were equal to ψ^0. These curves have been derived by Parsons and collaborators(110) from data on double-layer structure in various solutions. Evidently, neither the shape

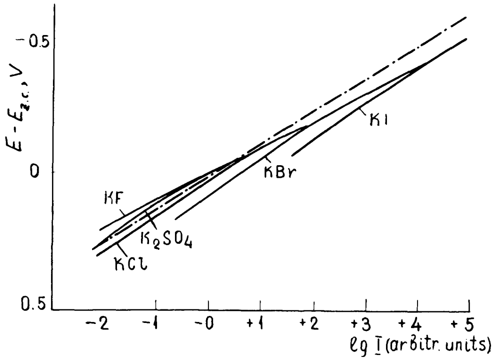

Figure 18. Calculated polarization curves of reduction of single-charged cation in 0.1 M solutions of various supporting electrolytes. In the calculation, it was assumed that $\psi_1 = \psi^0$; ψ^0 being determined from the double-layer structure data. The dot-and-dash line corresponds to $\psi_1 = 0$ (according to Ref. 110).

of the curves nor the value of the overpotential decrease are consistent with the experimental results (cf. Figure 17).

The overpotential shift should be compared with the outer and inner Helmholtz plane potentials, ψ^0 and ψ^i. According to Grahame,(111,112) at $\sigma = -10\ \mathrm{C\ cm^{-2}}$ ($E_{\mathrm{n.c.e.}} = -1.051$ V) in 1 N KI, the ψ^0 potential is -0.050 V, while $\psi^i = -0.188$ V. In the absence of specific adsorption (0.92 M MaF) at the same electrode potential, $\sigma = -11.4\ \mu\mathrm{C\ cm^{-2}}$ and $\psi^0 = -0.046$ V.

Interpolation of the data from Refs. 76, 77, and 108 indicates that, in the presence of 1 M KI, the maximum overpotential decrease (in the lower Tafel region) is 0.16–0.20 V. If it is assumed that in the absence of specific ion adsorption $\psi_1 \simeq \psi^0$, the overpotential shift, which can be identified with the shift of the ψ_1 potential, is much closer to the variation in ψ^i (0.14 V) than to the variation in ψ^0 (0.01 V).

Despite the approximate nature of this calculation, it provides a strong argument in favor of the discharging ion being closer to the electrode than the outer side of the double layer, i.e., of its being in the layer of water molecules immediately adjacent to the electrode. The same inner layer also accommodates the anions specifically adsorbed on the electrode, although, of course, the planes in which lie the charge centers of anions and H_3O^+ may not coincide.†

Parsons(114) has pointed out that, if we equate $\Delta\eta$ to the ψ_1-potential shift, we must assume that the concentration of H^+ ions in the double layer increases in the presence of iodide by several orders of magnitude. However, electrocapillary measurements give no indication of the H^+ ion adsorption increasing under these conditions. Therefore, Parsons assumed that the overpotential decrease is due to the influence of the iodide on the activity coefficient of the activated complex, rather than on the ψ_1-potential shift.

However, as was shown in Section 2.3, the activated complex activity coefficient is related to that of the ion as follows:

$$\gamma^{\ddagger} = \gamma_{H_3O_s}{}^{\beta}\gamma_{H_2O_s}{}^{\alpha} \qquad (31a)$$

---

† It was first assumed that ψ_1 is close to ψ^i in Ref. 113 for the nitromethane reduction reaction.

This means, that the hypothesis of the sharp decrease in $\gamma^{\ddagger}$ is equivalent to the assumption of a sharp decrease in $\gamma_{\mathrm{H_3O_s}}$, i.e., strong adsorption of H_3O^+ Thus, the above-mentioned discrepancy remains.

If Eq. (31a) is substituted into the kinetic equation for discharge, the term including γ and ψ_1 takes the form

$$\left(\frac{\gamma_{\mathrm{H_3O^+}}}{\gamma_{\mathrm{H_3O_s^+}}}\right)^{\beta} \exp\left(-\frac{\beta\psi_1 F}{RT}\right) \tag{99}$$

On the other hand, taking into account the activity coefficients, Eq. (90) can be written as

$$\frac{C_s}{C_0} = \frac{\gamma_{\mathrm{H_3O^+}}}{\gamma_{\mathrm{H_3O_s^+}}} \exp\left(-\frac{\psi_1 F}{RT}\right) \tag{90a}$$

The absence of measurable specific adsorption means that $C_s/C_0 \leq 1$. Hence, factor (99), forming part of the kinetic equation, is a value roughly equal to, or less than, unity and, consequently, the varying activity coefficients and the ψ_1 potential cannot explain, in terms of this model, the increase in the discharge rate by several orders of magnitude.(115,116)

The above problem of the overpotential decrease, however, can be avoided(115,116) if it is assumed that only those hydroxonium ions discharge which have penetrated† the first monolayer of water molecules adjacent to the electrode. The major part of cations, including H_3O^+ ions, are in the second water monolayer. The concentration of the H_3O^+ ions which are in direct contact with the electrode is low and constitutes merely a fraction of their total amount in the double layer (because of the requirement that expenditure of energy is necessary to incorporate an ion in the monolayer of electrode-oriented water molecules). Then, Eq. (90a) takes the form

$$C_s = KC_0 \frac{\gamma_{\mathrm{H_3O^+}}}{\gamma_{\mathrm{H_3O_s^+}}} \exp\left(-\frac{\psi_1 F}{RT}\right) \tag{90b}$$

where $K \ll 1$. With such an expression, we, in fact, give up the assumption made earlier while deriving Eq. (90) that the standard chemical potentials of ions in the bulk and in the state immediately prior to discharge are equal $[K = \exp(-\Delta\mu^0/RT)]$. Although the concentration of the ions immediately adjacent to the electrode is low, it is precisely these ions that discharge since their discharge is accompanied by hydrogen being more easily adsorbed; hence, their discharge is more facile than that of H_3O^+ ions in the outer Helmholtz plane.

One might think that a similar situation is common for all cases where the primary discharge product must, from energy considerations, be associated with the electrode, e.g., when amalgams of metals are formed. And when the discharge product remains in the solution, e.g., in ordinary redox reactions, localization of the discharging particle near the outer Helmholtz plane may be preferable. Such a model explains the possibility of major ψ_1-potential shifts which may result in the discharging ion concentrations increasing by several orders of magnitude without any perceptible increase in the total adsorption of H^+.

---

† Note that H^+ can easily move from an outer water layer to the inner layer by the prototropic transfer mechanism, as in its conductance.

If it is not assumed that the activity coefficient of discharging hydrogen ions differs greatly from the corresponding value in the bulk [the related overpotential correction factor is $-[(1-\alpha)RT/\alpha F]/\ln(\gamma_{H_3O^+}/\gamma_{H_3O_s^+})$], then the ψ_1-potential shift can be evaluated from the overpotential change.

The equality $\Delta\eta = -[(1-\alpha)/\alpha]\Delta\psi_1$ can be checked as follows. As is known, the kinetic isotopic effect in the case of hydrogen ion discharge is, to an appreciable extent, dependent on the potential. Irrespective of how this phenomenon is explained, it is obviously determined by the electric field directly acting upon the ion, i.e., $\phi - \psi_1$.

As can be inferred from Figure 19a, in the presence of adsorbed ions, the relationship between the protium–tritium separation factor $S_{H/T}$ and the potential varies greatly. If, however, it is assumed that a variation in the local ψ_1 potential equals that in overpotential and if corresponding $S - \phi$ curves are shifted by $\Delta\eta = \Delta\psi_1$, we can compare solutions of different composition at the same $\phi - \psi_1$. Such a comparison is shown in Figure 19b. It can be seen that, after having been reduced to the same local potential drop, all data merge into a single curve, which corroborates the assumption as to the overpotential variations being due, primarily, to variations in the ψ_1 potential.(116,117)

It is most essential that good agreement is observed in the presence of surface-active anions and cations despite the different double-layer structure. The coincidence of corrected curves in the presence of adsorbed anions and such a large cation as tetrabutylammonium is indicative of the fact that, in all cases, the plane of localization of the centers of the discharging H_3O^+ ions is the same, just as it should be if they occupy the *inner* Helmholtz layer.

The fact that in the absence of specific ion adsorption, variations in ψ_1 practically coincide with those in ψ^0 may be explained assuming that, under such conditions, the effective permittivity, hence, the capacity for the layer between the electrode and discharging ion localization plane, are much lower than the corresponding values for the layer between the inner and outer Helmholtz planes. Then, the potential drop is concentrated, mainly, in the layer between the electrode and discharging ions, i.e., $\psi_1 - \psi_0$, is a relatively small value. Model-based evaluations of respective permittivity values corroborate this picture.(116)

We have so far dealt with experimental data obtained on a mercury cathode. In the case of other electrodes poorly adsorbing hydrogen, where the discharge step is undoubtedly the rate-limiting stage, data are less comprehensive and, as a rule, less accurate. By far the most comprehensive and reliable data have been obtained for liquid gallium, some liquid alloys, and

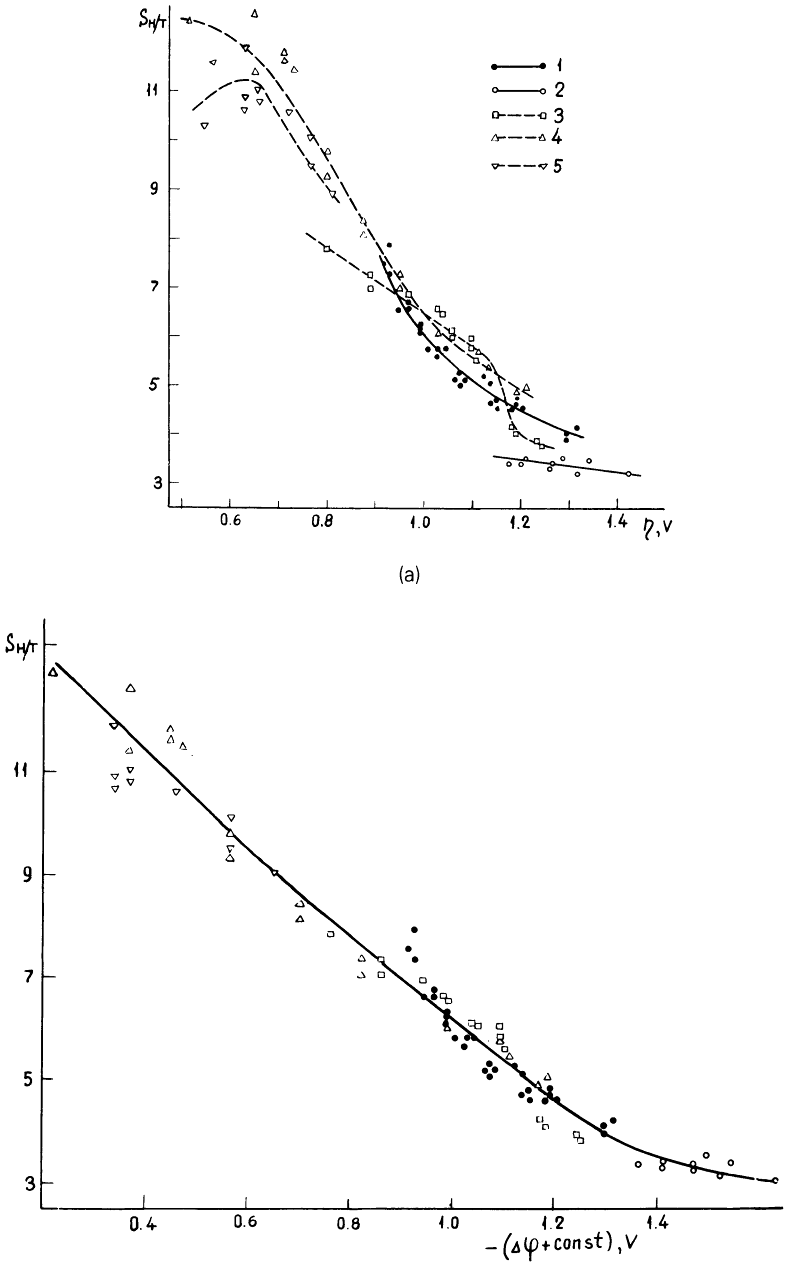

(a)

(b)

Figure 19. Separation factor of hydrogen isotopes (H and T) on mercury cathode versus overpotential (a) and potential drop $\phi - \psi_1$ (b) in solutions: 1, 0.1 M HCl; 2, 0.1 M HCl + 5 × 10^{-3} M $N(C_4H_9)_4Br$; 3, 2 M HCl; 4, 1 M HCl + 2.9 M NaI; 5, 1 M HCl + 2.9 M NaI + 5 × 10^{-3} M $N(C_4H_9)_4Br$ (according to Ref. 117).

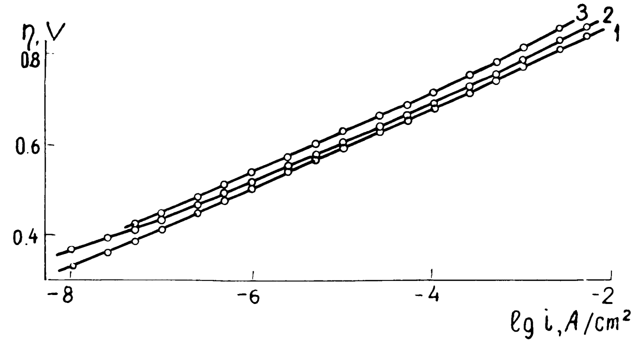

Figure 20. Polarization curves of hydrogen evolution on bismuth in solutions of the following composition: 1, 1 *M* $HClO_4$; 2, 0.1 *M* $HClO_4$; 3, 0.1 *M* $HClO_4$ + 0.9 *M* $LiClO_4$ (according to Ref. 118).

a solid bismuth electrode. The latter case is of particular interest because the potential of zero charge of this metal falls into the hydrogen evolution region, which permits the overpotential to be measured in the absence of specifically adsorbed ions on both a negatively and a positively charged surface. The results obtained by Palm and Tenno(118–120) are presented in Figure 20. In full agreement with theory, a certain decrease in η is observed at negative charges, and an increase, at positive charges, which results in a marked distortion of the Tafel curve. However, good linearity is observed after correction by the value of the ψ_1 potential calculated as ψ^0 from the surface charge data. According to Ref. 121 a substantial overpotential drop takes place near the point of zero charge. However, as was shown in Refs. 118–120 this effect is observed only if the solution has not been properly freed from traces of oxygen. The same applies, e.g., to gallium, tin, and antimony electrodes (cf. Refs. 121 and 122–124). Evidently, near the point of zero charge, where the electrode can most easily adsorb various impurities, oxidation of the surface is facilitated, as a result of which the surface is considerably modified. This is another indication of the need to keep experimental cells and solutions extremely clean, especially in the zero charge potential region.

A lower overpotential, in the region of potential close to the zero charge potential, was found for some solid metals by Kolotyrkin *et al.*(125–131) as a result of specific anion adsorption. The specific adsorbability of corresponding anions, including sulfate, on lead was confirmed by independent experiments.

Trasatti(54) suggested that this overpotential drop is caused by the different orientation of water molecules on the positively and negatively charged electrode surface. Hence, this drop should occur on all metals. In fact, however, some metals do not exhibit it at all, including some electrodes on which Trasatti based his assumption.

In the case of specific anion adsorption, many metals exhibit another effect which has not been observed in studies involving a mercury cathode, namely, the adsorption of anions produces not only accelerating, but also

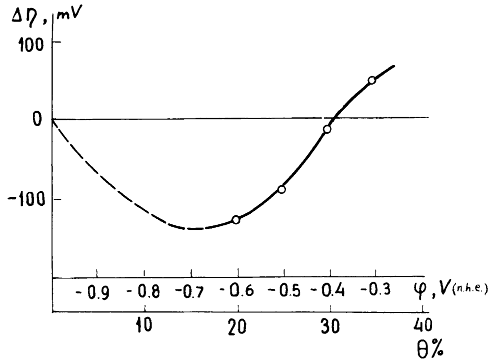

Figure 21. Relationship between hydrogen overpotential shift on lead electrode and surface coverage with adsorbed iodide ions in 1 N $H_2SO_4 + 10^{-3}$ N KI (according to Ref. 130).

inhibiting action. An example of such behavior can be seen in Figure 21, which shows transition from acceleration to inhibition as the adsorbed iodide concentration on lead increases.

Specific adsorption of ions of the iodide type is most probably accompanied by a partial transfer of a charge to the metal, i.e., by forming a bond of the covalent or metallic type. The collectivization of electrons during adsorption causes, according to Temkin,(132) occupation of the surface electron levels of the metal, and, as a consequence, an increase in the system's energy. This results in effective repulsion between adsorbed particles. If charge transfer in adsorption of an ion is appreciable (electrosorption valency effect), this may bring about a substantial interaction with the adsorbed hydrogen, hence, weakening its bond with the metal. This effect seems to be the most probable cause of the increase in overpotential in the case of specific anion adsorption.(28)

The adsorbability of a particle is determined not only by the energy of its bond to the metal of the electrode, but also by the energy of adsorption of the water which is expelled from the surface during adsorption of the substance of interest. Therefore, on gallium, for example, the adsorbability of an iodide is lower than on mercury, but this is due to the stronger adsorption of water, rather than the weaker bond between the ion and metal. The bond of iodide with gallium, as such, is stronger than with mercury, which causes a rise in overpotential, partially compensating for the normal ψ_1 effect.(133)

The appreciable adsorption of water molecules linked with gallium through their oxygen atoms must, in principle, result in a higher overpotential. This increase may be caused both by the surface being partially blocked by molecules oriented in such a way that they cannot transform to hydroxonium ions with the O–H bond directed toward the metal, and by the fact that the chemisorption of water will weaken, just as adsorption of other donor particles, the adsorption bond of hydrogen.

Such an effect was in fact observed recently(134); it is vividly illustrated in Figure 22. In the region of high pH, the electrode is exposed to sufficiently negative potentials at which, as is known from double-layer structure data,

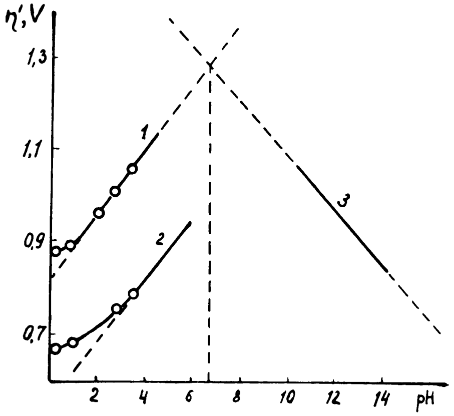

Figure 22. Curves representing the dependence of $\eta' = \eta - (1 - \alpha)/\alpha\psi_1$ on pH in the case of hydrogen evolution on Ga at a current density of 10^{-2} A/cm^2 (curves 1, 3) and 10^{-4} A/cm^2 (curve 2) (curves 1, 2 according to Ref. 134 and curve 3 according to Ref. 140).

the water molecules are oriented with their hydrogen atoms toward the metal, and the bond there is rather weak. Thus, in this case, the structure of the dielectric layer is similar to that at a mercury electrode. Under such conditions, there is a normal relationship between overpotential and pH ($\partial\eta/\partial\,\mathrm{pH} \simeq 0.06$ V) which also applies to mercury and other hydrophobic electrodes. However, at low pH, the hydrogen evolution potential lies in the region of substantial chemisorption of water, and the overpotential increases markedly as compared to the value which would correspond to a linear relationship between η and pH.

4.2.1. Hydrogen Evolution from Alkaline Solutions

When hydrogen evolves from water molecules at alkaline pH, the ψ_1 potential does not affect the surface concentration of the discharging particle, but the influence on the potential drop $(\phi - \psi_1)$ remains. Therefore, the ψ_1 effect during water molecule discharge is opposite in sign to that during hydroxonium ion discharge. As a result, for example, in solutions of pure alkalis, the effects related to variations in pH and in the ψ_1 potential do not cancel each other as in pure acids, but add, so that the dependence of η on the alkali concentration is strong ($\partial\eta/\partial \log C = -0.12$ V).

Although in highly concentrated solutions, the ψ_1 effects are minor, because of the different sign in acid and alkaline solutions, they become significant when the kinetics of H_3O^+ and H_2O discharge are compared. The data presented in Figure 22 have been corrected by the value of the ψ_1 potential. For gallium and some other electrodes, e.g., Hg and such alloys as Hg–Ga and In–Ga, the pH value at which the rates of H_3O^+ and H_2O discharge are equal is about 7–8. In earlier works, mention was made of pH = 9–10, but then the ψ_1 correction was not taken into account.

For the rate of H_2O discharge on mercury, evaluations were made, based on the kinetics of decomposition of amalgams of alkali metals at high pH.

As was shown by Korshunov *et al.*$^{(135,136)}$ in pure alkaline solutions, decomposition of amalgams follows a chemical mechanism, which makes it impossible to determine directly the H_2O discharge rate. However, the rates of two competing paths of the process differ but slightly. Therefore, under special conditions, one can determine the rate of H_2O discharge on mercury.$^{(135,137)}$

As was demonstrated by Kabanov *et al.*,$^{(138)}$ incorporation of an alkali metal in the material of the cathode is also exhibited by a number of *solid* metals, which renders it difficult to interpret the data on hydrogen evolution on these metals in alkaline solutions. In the case of liquid gallium and certain alloys, no incorporation of alkali metal cations takes place; this observation has made it possible to use the above-mentioned systems in quantitative studies of the process of discharge of water molecules.

The pH value for transition from H_3O^+ and H_2O discharge, equal to 7, results from the Brønsted relation being applied to the rate constants of both reactions ($7 = -\log(K_w)^{1/2}$, where K_w is the ionic product of water). This value, however, cannot be regarded as a rigorous result of the theory, for K_w represents the ratio of acid–base characteristics of H_3O^+ and H_2O in the solution, while we are interested in the reaction *rate* at the surface. Therefore, this ratio must be corrected by $\exp(\Delta G/RT)$, where ΔG stands for differences of free energies of adsorption of H_3O^+ and OH^- ions, adsorption of H_2O molecules in two orientations in which they act as proton donors (alkaline solutions), and as a base remaining after proton detachment (acid solutions), as well as adsorption of the H atoms which are in direct contact with the H_2O molecule (after H_3O^+ discharge) or the OH^- ion (after H_2O discharge). Although all these differences seem to be small, there is no reason why they should be ignored or exactly compensated. Therefore, a certain spread about pH = 7, depending on the nature of the metal, seems quite natural.

When hydrogen evolves from alkaline solutions, a marked influence of the nature of the cation on the overpotential is observed.$^{(135,139-145)}$ The general trend exhibited by various cathodes is that in the series of alkali metals, the overpotential drops as the cations increase in size; with alkaline-earth cations, the overpotential decreases with the size of ions, whereas in the presence of tetraalkylammonium salts, the overpotential increases considerably. A higher specific adsorbability of cations is conducive to a ψ_1-potential shift in the positive direction, i.e., an increase in the absolute value of $\phi - \psi_1$, hence, acceleration of the discharge of water molecules. It is impossible, however, to account for the above behavior only by cation adsorption. Another factor which plays a decisive role originates from the fact that the double-layer field is not evenly distributed, but, because of the discrete nature of the ion charges, is concentrated on them. And this is precisely where, i.e., at the point of high field intensity, the discharge of water molecules is facilitated. This effect is inversely proportional to the cation size and directly proportional to its charge.$^{(145)}$

4.3. Reduction of Anions

Another group of processes for which ψ_1 effects have been studied with particular care involve anion reduction reactions. These reactions are interesting because, as can be seen from Eq. (92), a strong inhibiting effect must occur at high negative ion charges and negative ψ_1 potentials (owing to the sharp decrease in the surface concentration of the anion being reduced). Particularly interesting relations are expected near the potential of zero charge.

At low surface charges, the absolute value of ψ^0 increases with the charge [see Eq. (95)]. In dilute solutions, the coefficient of proportionality between ψ^0 and σ is great; therefore, at small deviations of the potential from the zero charge value, the major portion of the potential shift is accounted for by a variation in ψ^0. If it is assumed that $\psi_1 \simeq \psi^0$, then, since ψ_1 forms part of a kinetic equation with coefficient $|(z - \alpha)| > 1$, while ϕ forms part of an equation with a coefficient $\alpha < 1$, the inhibiting effect of the negative value of ψ_1 is predominant and, as the potential shifts in the negative direction, the reduction current drops instead of rising. At potentials shifted further in the negative direction, the variation in ψ_1 becomes insignificant and the predominant role is now played by an increase in $\exp(-\alpha\phi F/RT)$. Thus, the reduction current passes through a minimum. This minimum was for the first time observed by Kryukova(146) in the case of $S_2O_8{}^{2-}$ anion reduction, while the above interpretation of this phenomenon was made by Frumkin and Florianovich.(147)

When various anions are reduced, two limiting cases are possible. One of them involves disappearance of the minimum as the supporting electrolyte concentration increases. Typical curves for this case are shown in Figure 23 (reduction of $S_2O_8{}^{2-}$). The disappearance of the minimum is due to the double layer being less diffuse. These data are adequately described by theory with the assumption that $\psi_1 \simeq \psi^0$, i.e., with the assumption that the anion being reduced is not specifically adsorbed and is localized near the outer Helmholtz plane.

The other case, of which $PtCl_4{}^{2-}$ reduction (Figure 24) is a typical example, is characterized by a very weak influence of the electrolyte concentra-

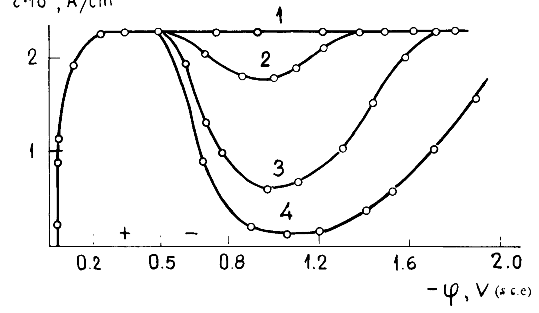

Figure 23. Polarization curves of reduction of 10^{-3} N $K_2S_2O_8$ on rotating amalgamated copper electrode at a supporting electrolyte (Na_2SO_4) concentration of : 1, 1 N; 2, 0.1 N; 3, 0.008 N; 4, 0 (according to Ref. 148).

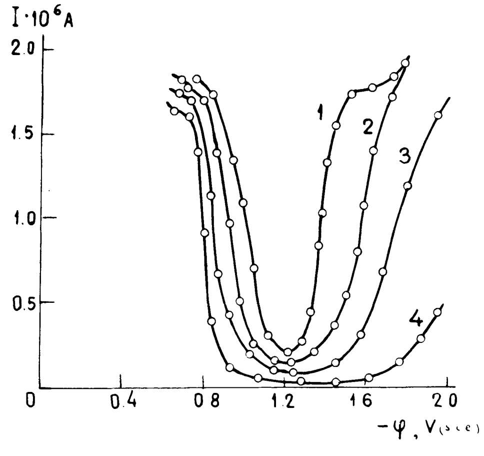

Figure 24. Polarization curves of reduction of $10^{-3}\,N$ K_2PtCl_4 on mercury-dropping electrode at a supporting electrolyte (KCl) concentration of: 1, $1\,N$; 2, $0.1\,N$; 3, $0.009\,N$; 4, 0 (according to Ref. 148).

tion on the depth of the minimum; when an indifferent salt is added, the minimum does not disappear but becomes narrower. Such behavior can be explained only by assuming a pronounced specific adsorption of the discharging anion, which is almost insensitive to variations in the diffuseness of the double layer. For such a process, $\psi_1 \simeq \psi^i$, the value of ψ^i being largely determined by the adsorption of the discharging anion.(148)

The observed phenomena being related to a rapid variation in the ψ_1 potential near the point of zero charge is vividly illustrated by the fact that when various cathode materials are used, a drop in current occurs near the respective zero charge potentials.(149,150)

At a potential more positive than the point of zero charge, the ψ_1 effect changes sign, which is why one should expect intersection, at this point, of the polarization curves obtained with various salt concentrations. In aqueous solutions, the rate of reduction of persulfate on the positively charged surface is so high that it cannot be measured—diffusion limitations come into play. However, in such a nonaqueous solvent as dimethylsulfoxide, the process turned out to be much slower and it becomes possible to observe directly the intersection of the polarization curves.(151,152)

The same behavior was observed in an aqueous solution, on a disk electrode rotating at high speed, which enabled mixed kinetic conditions to be attained.(150)

Quantitative comparison of the experimental results with theory should be made preferably by the method of corrected Tafel plots (C.T.P.), proposed by Delahay *et al.*,(103) or by the graphical method of constructing polarization curves at constant ψ^0, proposed by Gierst.(153) The first method is based on reducing Eq. (92) to the form

$$\ln i + \frac{Z\psi_1 F}{RT} = \text{const} - \frac{\alpha(\phi - \psi_1)F}{RT} \qquad (100)$$

from which a straight line should be derived in the coordinates $(\log i + 2.3Z\psi_1F/RT) - (\phi - \psi_1)$, the slope of which would be indicative of the value of α. Used as ψ_1 are the values of ψ^0, calculated from experimental data on the double layer in the supporting electrolyte. The same data are used in Gierst's method where the $\psi^0 - \phi$ curves obtained at different supporting electrolyte concentrations are intersected by the $\psi^0 = \text{const}$ lines. The resulting values of ϕ are transferred onto experimental polarization curves (corrected, if necessary, for concentration polarization) corresponding to the same electrolyte concentrations and the constant concentration of the discharging ion. Joining the intersection points gives a curve of $\log i$ *vs.* ϕ for $\psi^0 = \text{const}$.

In Figure 25 are shown corrected Tafel curves for reduction of $S_2O_8^{2-}$ on a number of metals. As can be seen, after the ψ_1 correction has been introduced, the curve with the minimum becomes the straight line. This is another proof that the theory adequately describes the experimental situation. In the case of a mercury cathode, though, slight curvature remains in the bottom portion, which may be attributed to the effect of weak specific adsorption of the anion.

An important factor is the coincidence of corrected Tafel curves for different cathode materials, but the divergence between uncorrected curves is rather great (up to 0.5 V and even higher). As was described in Section 2.2, in the absence of specific adsorption of reagents, the rate of a reaction† is independent of the nature of the metal. This deduction is in full agreement with the experimental data given in Figure 25. On the other hand, it confirms the absence of specific adsorption of the reagents and products under the conditions of the experiments discussed above.

The independence from the nature of the metal was deduced in Section 2.2 for the case where processes on different metals belong to the same series of reactions, i.e., when the only possible distinction between them is the difference in the heat of an elementary act. This means that other characteristics of the elementary act, including all components of the reorganization energy, remain invariable.

In the case of redox reactions, the most essential component of the reorganization process is reorganization of the solvent. The coincidence of data for different metals is indicative of the fact that the microenvironment around discharging ions is the same. This corroborates the assumption that persulfate ions discharge in the region which is beyond the dense part of the double layer, since the difference in capacity in this part, hence, in its dielectric properties, is substantial for the metals of interest.(150)

---

† Strictly speaking, it is the activation energy that is independent of the nature of the metal, but in the case of simple electron transfer reactions, one can hardly expect significant changes in the preexponential factor. Therefore, it is more appropriate to speak of the independence of the reaction rate.

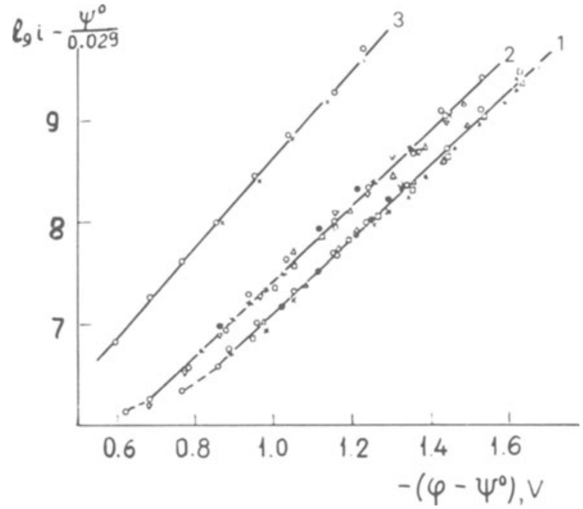

Figure 25. Corrected Tafel plots for $S_2O_8^{2-}$ anion reduction. 1, $5 \times 10^{-4}\,M$ $Na_2S_2O_8 + 9 \times 10^{-3}\,M$ NaF; 2, $5 \times 10^{-4}\,M$ $K_2S_2O_8 + 9 \times 10^{-3}\,M$ KF; 3, $5 \times 10^{-4}\,M$ $Cs_2S_2O_8 + 9 \times 10^{-3}\,M$ CsF. Electrode symbols: Sb (▽), amalgamated Cu (○), Bi (×), Sn (●), Pb (△), Cd (□), In (✻) (according to Ref. 150).

The introduction of the ψ_1 correction raises the problem of the charge Z of the reacting particle, in view of the well-known situation that multicharged ions tend significantly to form ion pairs, which accordingly, reduces their effective charges. The question as to what the charge of the reacting particle may be can be answered, according to Frumkin, on the basis of quite general relations.(100,154,155)

We first take Gibbs's adsorption equation

$$d\gamma = -\sigma d\phi - RT\Gamma_c d\ln C - RT\Gamma_a d\ln C \tag{101}$$

In the absence of specific adsorption and at a sufficiently high negative charge, the adsorption of anions can be ignored as compared to the adsorption of cations $|\Gamma_a| \ll |\Gamma_c|$. [In Eq. (101), account is taken only of the supporting electrolyte at concentration C, while the effect of a low concentration, C_i^0, of the reagent is disregarded.] Then, the last term in Eq. (101) can be omitted. From the properties of perfect differentials, there follows the equality of cross derivatives

$$\left(\frac{\partial\sigma}{\partial \ln c}\right)_\phi = RT\left(\frac{\partial\Gamma_c}{\partial\phi}\right)_C$$

Under the defined conditions, the charge of the electrode is almost completely neutralized by that of cations in the double layer, $\Gamma_c = -\sigma/Z_cF$. Hence,

$$\left(\frac{\partial\sigma}{\partial \ln c}\right)_\phi = -\frac{RT}{Z_CF}\left(\frac{\partial\sigma}{\partial\phi}\right)_C \tag{102}$$

From Eq. (102) it follows that

$$\sigma = f\left(\phi - \frac{RT}{Z_C F} \ln C\right) \tag{103}$$

It can be easily seen that differentiation of this function with respect to ϕ and $\ln C$ gives the same (accurate to the factor $RT/Z_C F$) result, i.e., relation (102) will be true for any form of the functional dependence. We may vary both ϕ and C, but if the constancy of $\phi - (RT/Z_C F) \ln C$ is met, corresponding to it is a single particular value of σ. At a given value of σ, however, in the absence of specific adsorption, it is the potential drop in the dense part of the double layer that is constant (as was shown by Grahame,(156) the capacity of the dense part at a given value of σ does not depend on the electrolyte concentration).

At high negative charges on the metal, the concentration of cations in the dense part of the double layer and in a certain part of the adjacent diffuse layer, whose thickness is less than the characteristic length of the latter, is much higher than that of anions. The potential distribution in this cation layer is fully determined by the distribution of cations, i.e., it is, in the final analysis, merely a function of σ or, in other words, a function of $\phi - (RT/Z_C F) \ln C$.

If the locality of a discharging particle does not go beyond the cation layer, we may assume that, at a given value of σ, $\phi - \psi_1$ is constant. The combination of conditions

$$\phi - \frac{RT}{Z_C F} \ln C = \text{const} \tag{104}$$

and

$$\phi - \psi_1 = \text{const} \tag{105}$$

leads to

$$\psi_1 - \frac{RT}{Z_C F} \ln C = \text{const} \tag{106}$$

Consider now reaction rates, in a supporting electrolyte concentration, varying with the potential, so that condition (104) is met in this case. In compliance with (105), all of the current variation will be related only to the change in *surface* concentration C_i^s. At constant bulk concentration C_i^0, C_s depends on the ψ_1 potential in accordance with Eq. (90), i.e., $d \ln C_i^s = -Z_i(F/RT)\, d\psi_1$.

Substituting Eq. (106) into this expression, we find

$$d \ln C_i^s = -\frac{Z_i}{Z_c} d \ln C$$

The final expression is

$$\left(\frac{\partial \ln i}{\partial \ln C}\right)_{\phi - RT/Z_C F \ln C,\, C_i^0} = -\frac{Z_i}{Z_c} \tag{107}$$

The value of the derivative in Eq. (107) can be found experimentally from polarization curves at different salt concentrations, and the charge Z_i may be found as a result. It should be emphasized that, according to this deduction, this charge belongs to that particle in the solution with which the discharging particle is at equilibrium.

In aqueous solutions, if the derivative in Eq. (107) is determined at sufficiently negative potentials when the above simplifications hold true with a high degree of accuracy, values of Z_i are obtained, in all examined cases, close to the charge of a respective free anion. This agrees well with the fact that the degrees of association of the anions of interest with singly charged cations, are not high. If we take solutions in solvents with lower permittivities, in which association of ions is much stronger, the experimental value of Z_i considerably decreases. For example, when persulfate is reduced in ethylene glycol solutions of Na^+ and K^+ salts, $Z_1 \simeq -1$, which corresponds to $(MS_2O_8)^-$ pairs being predominant in the bulk.$^{(157)}$

Strictly speaking, in the case of salt association in the bulk, both free ions and any pairs or triplets are at equilibrium with the discharging particles. Obtaining one of the two limiting values of Z_i is due to the fact that the experiment is conducted at a constant total concentration of the anion, in the form of both free ions and ion pairs. The relationship between these two forms depends, in general, on the supporting electrolyte concentration, but the simplest results are obtained when either the ion pair or the free ion concentration is negligibly small over the entire range of C. For more information on the effective value of Z_i in the case of association see Ref. 158.

Now, consider a case for which ion pair discharge is predominant and association in the solution is practically nil. In this case, for the surface concentration of a discharging particle, particularly, at some potential well displaced from the zero charge potential, Eq. (90) can be written as follows:

$$C_i^s = K\theta C_i^0 \exp\left(-\frac{z_i\psi_1 F}{RT}\right) \tag{108}$$

Here, Z_i is the free anion charge, and the ψ_1 potential stands not for the mean potential in the plane of centers of charges of the discharging anions, but a local potential near the cation or, to be more precise, at the point which is the center of the discharging anion forming the ion pair. The constant K is representative of the energy of specific nonelectrostatic interaction between the cation and anion and, in particular, the contribution of the variation in the ion-pair solvation energy as opposed to the solvation energy of individual ions.

The value of K is independent of the electrolyte concentration, but may depend strongly on the cation's nature. The value of θ determines the fraction of the surface which may be occupied by the anions immediately in contact with the double-layer cations, i.e., anions forming ion pairs with the latter.

This value is defined by the effective radii of both ions and by the surface cation concentration which, in turn, is determined by the electrode charge and, if it is sufficiently far from the point of zero charge, changes gradually with the potential, so that the variation in this factor can be ignored as compared to the terms which are exponentially dependent on the potential.

The local ψ_1 potential differs significantly from the ψ^0 potential even if the anion centers lie in the outer Helmholtz plane. However, at a constant and sufficiently negative surface charge, the structure of the cation layer is practically the same and independent of the nature of the electrode metal and the electrolyte concentration. Therefore, the difference between ψ_1 and ψ^0 is also a function only of charge and is independent of the electrode material and electrolyte concentration. Hence, the corrected Tafel plots for which ψ^0 is used, while differing from the true ones, should be independent of the electrode material and supporting electrolyte concentration. Thus, taking the discharge of ion pairs into account, leads to the same conclusion which is in good agreement with experiment, just as in the case of the simpler model involving the potential averaged in the Helmholtz plane.

At the same time, owing to the contribution of specific interactions to the formation of ion pairs [the constant K in Eq. (108)], their surface concentration for various cations is different even if the surface charge is the same. Hence the shift of the corrected Tafel plots, in parallel with each other, is understood for salts of different cations, as can be seen from experiment (see Figure 25).

The role of formation of ion pairs on the surface has been clearly demonstrated by Gierst *et al.*,(98) who showed that the effect of the nature of the supporting electrolyte on the kinetics of some reactions correlates not only with the adsorbability of foreign ions, but also with their ability to form ion pairs with a discharging ion.

The temperature dependence of the rate of persulfate anion reduction at the minimum of the polarization curve suggests that the activation energy depends† strongly on the nature of the cation and can even become negative in Cs^+ solutions. Such behavior can be accounted for only by a preequilibrium with a negative enthalpy increment, the absolute value of which exceeds that of the true energy. Such a preequilibrium is provided by the formation of an ion pair on the surface.(150,159)

The model of ion pair being discharged is a limiting case of a more general, but difficult to analyze, situation where the anion can discharge at any point in the double layer, the probability of discharge and the probability of its being at a given point being determined by the local value of both the electrostatic and nonelectrostatic potentials (the energy of specific interaction with the cations and, in the case of specifically adsorbed anions, with the metal). If these local potentials are spatially distributed in such a manner that a position near the cation (i.e., formation of an ion pair) is more favorable than others, then it is only this position that is practically essential. Otherwise, one should sum up the contributions from all variations of locality of the discharging anions.

---

† Since the current near the minimum is practically independent of the potential, the difference between the ideal and real activation energies becomes insignificant.

The concept of the three-dimensional potential distribution as opposed to an averaged one-dimensional model or, as it is often referred to, the concept of the discreteness of charge in the double layer as a possible cause of significant kinetic effects, was for the first time proposed way back in 1935.(160,161) It is still most important in another respect which will be considered later.

So far, we have considered all reactions assuming that there is equilibrium between ions in the bulk and on the surface of the electrode. In 1949, however, Levich(162,163) suggested that this assumption may be wrong. In the case of multicharged anions, the rate of their diffusion toward the electrode through the diffuse part of the double layer is slowed down by their being repelled from the negatively charged surface of the electrode to such an extent that the process of ion transfer in the double layer may become rate determining.

Since repulsion increases with the charge density, this mechanism leads to a monotonic decrease in current as the potential increases. To explain the further increase in the current, i.e., to account for the experimentally observed minimum in the curve, an additional assumption has to be made when this model is used. Namely, one has to assume that at high negative potentials it becomes possible to reduce the anions at a certain distance from the electrode, beyond the region of a considerable potential drop within the diffuse double layer, by way of tunneling of electrons over corresponding distances.(164,165)

Thus, it becomes possible to suggest two reasons for the minima on the anion reduction polarization curves, one being a static (change in the equilibrium surface concentration) and the other, a dynamic (change in the rate of transport toward the electrode) ψ_1 effect (using the terminology proposed by Gierst(153)). We have already shown in the foregoing how well the experimental data are described by the concept of the static ψ_1 effect. On the other hand, the dynamic effect does not give a good fit with experiment. This can be seen if we compare, all others things being equal, the behavior of different electrode materials.(166) At the same surface charge, we may expect the same effect of anion repulsion, hence, coincidence of the downsloping polarization curve regions reduced to the same charge. However, the electron tunneling, being dependent on the energy difference between the initial and final states, is determined by the electrode's potential rather than by its charge; to be more precise, by the potential difference between the metal and the point of tunneling. That is, a correction factor of the ψ_1 type in the static effect should be introduced. However, since tunneling is here assumed to be beyond the region of the main potential drop in the diffuse layer, this correction is actually insignificant. It is much less than ψ^0; hence, taking it into consideration would not have led to any coincidence of the corrected Tafel plots for different metals.

Since the difference in the potential of various electrodes at a constant charge may be quite significant, it becomes evident that the upsloping portions of the polarization curves for various metals must coincide in substantially different coordinates than the downsloping portions. In other words, we cannot, in terms of the dynamic effect, give an adequate description of the entire length of the polarization curve for different metals, which, as is well known, can be easily done using the static ψ_1 effect model. Therefore, preference should be given to that interpretation of experimental data which describes them in terms of the static ψ_1 effect.

The relationship between the static and dynamic effects has another very important aspect. Quantitative analysis, based on Levich's theory, indicates that the rate of transport of multicharged anions toward the electrode, under corresponding experimental conditions, must by several orders of magnitude be lower than the actual experimentally observed reaction rates. It would thus seem that the whole behavior must be determined by the dynamic ψ_1 effect, while the experimentally observed rates would not have been realized.

To solve this inconsistency, one should definitely take into account the discrete ionic structure of the double layer. In Levich's theory, use is made of a one-dimensional potential distribution model so that the anion diffusing toward the electrode everywhere meets the same repulsion field. If the discrete nature of charges in the double layer is taken into consideration, certain parts of the repulsion field turn out to be stronger than the average, while other parts of this field, near the cations, are weaker. As a result, directions appear in which anion diffusion is facilitated. No strict quantitative theory of diffusion in a discrete double layer has been elaborated so far, but semiquantitative evaluations of these effects, made by Krylov,(167) indicate that diffusion of anions in the model of a discrete double layer should, in fact, be much faster than in a one-dimensional model, and the above discrepancy is removed at least for doubly charged anions.

Thus, examples of anion reduction reactions clearly indicate that it is precisely the local value of the ψ_1 potential and, in some cases, specific nonelectrostatic, i.e., narrowly localized ionic interactions, that should be taken into account. Needless to say, this is not a specific feature only of such reactions, although the corresponding effects are particularly manifest here because of the significant ψ_1 effects. We observed similar phenomena also in the case, for example, of hydrogen ion discharge in the presence of adsorbing anions or when hydrogen evolves from water in solutions of various alkalis.

The extent to which the effects having a discrete nature are exhibited may differ widely, particularly depending on the magnitude and sign of the charge of the supporting electrolyte ions prevailing in the double layer and of the discharging ions. However, taking this factor into account may be essential for treatment of any processes. Elaboration of a theory enabling evaluation of the effect of the discrete nature of charges in the double layer on the kinetics of electrode reactions is one of the currently topical problems in electrochemical kinetics (see, for example, Refs. 168–175).

We have discussed ψ_1 effects on the basis, primarily, of experimental results for two reactions: hydrogen evolution and persulfate reduction. It is

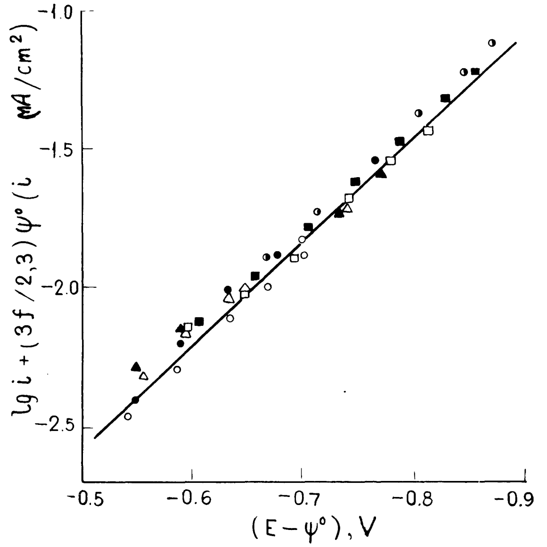

Figure 26. Corrected Tafel plots for reduction of 1×10^{-3} *M* Ga^{+3} on mercury in 0.02 *M* $HClO_4$ at $Al(ClO_4)_3$ concentrations: ○, 0.0 mM $Al(ClO_4)_3$; ●, 0.5 mM; △, 1 mM; ▲, 2 mM; □, 4 mM; ■, 8 mM; ◑, 16 mM (according to Ref. 103).

to be understood, however, that the above conclusions apply equally well to the most diverse ion discharge processes.

Referring the reader again to some of the above-cited reviews,(95–100) we shall confine ourselves to a brief mention of another two clear examples. Shown in Figure 26 are the corrected Tafel plots for Ga^{3+} ion reduction, according to Delahay *et al.*,(103) indicative of an adequate description by theory of the effect of the supporting electrolyte concentration. Figure 27 illustrates anodic oxidation of Eu^{2+} according to Gierst and Cornelissen.(153)

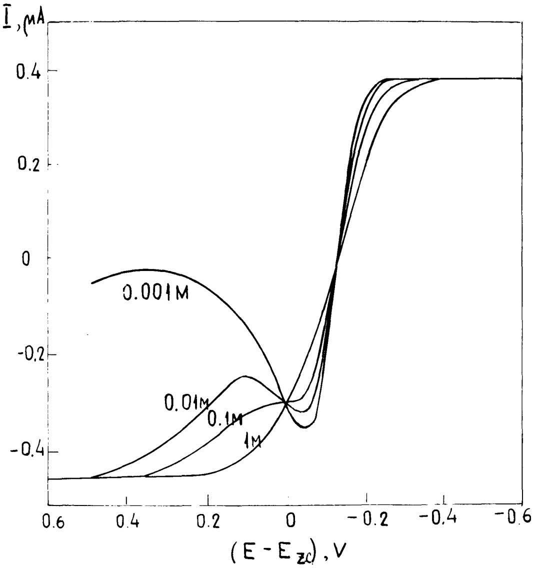

Figure 27. Polarograms of 10^{-4} $Eu^{+3} + 10^{-4}$ Eu^{+2} in supporting $HClO_4$ solution having a concentration as given in the figure (according to Ref. 153).

The process of cation oxidation is absolutely identical with that of anion reduction; the same anodic current minimum is observed owing to the cation being repelled from the positively charged surface. The repulsion becomes weaker and finally disappears as the supporting electrolyte concentration increases. Of particular interest in this case is the fact that the curves for all supporting electrolyte concentrations intersect at a point corresponding to the zero charge potential.

4.4. Electrode Reactions of Organic Compounds

At the end of this section, it would be worthwhile pointing out another example of the electric double layer affecting the kinetics of electrode reactions, namely, its effect on the rate of reactions of physically adsorbed organic substances. Of course, common ψ_1 effects are possibly involved here too, which were long ago experimentally demonstrated.(176) In addition, since such organic molecules are polar, their adsorption changes the potential distribution, thereby influencing the ψ_1 effect. For simplicity, in what follows, we shall not take the ψ_1 effects into consideration.

If we consider an organic surfactant, its adsorption is strongly dependent on the potential even if it is not charged. As has already been discussed at length in the chapter dealing with adsorption of organic substances on electrodes, this dependence is caused by the expulsion of the substance less polar than water out from the double-layer capacitor when the electric field becomes sufficiently large (treatments of Frumkin and Butler). Therefore, the free energy of adsorption of the organic substance depends on the potential. In the simplest case, this dependence is described by the square law

$$\Delta G_{\mathrm{ads}} = \Delta G_{\mathrm{ads}}^{\max} + a(\phi - \phi_N)^2 \tag{109}$$

where a is a constant characteristic of the adsorbate substance, and ϕ_N is the potential at which its adsorption is a maximum. The potential ϕ_N is generally rather close to the zero charge potential.

Just as in the case of ψ_1 effects, the potential dependence of the adsorption energy has two consequences. Firstly, the surface concentration is dependent on the potential. In the region of low coverages, this dependence can be expressed approximately as follows:

$$C_s = KC_0 \exp\left[-\frac{a(\phi - \phi_N)^2}{RT}\right] \tag{110}$$

The second effect originates from the influence of variations of the adsorption energy on the energy of the elementary discharge act, hence, in accordance with the Brønsted relation, influencing the activation energy of the process. Therewith, it should be taken into account that potential affects the adsorption energy of both the initial substance (given the subscript i) and the final one (subscript f), with both effects influencing the energy of the elementary act. Note that earlier, when trying to explain the ψ_1 effect, the term $\alpha\psi_1 F$ was introduced to take account of this effect precisely. In the case of a single-electron reaction, $\psi_1 F$ represents the difference in the electrostatic energies of the oxidized and reduced forms of the reagent. Taking both of the above factors into consideration, and combining them with the ordinary Tafel relation, we obtain the following expression for the rate of reduction of an adsorbed organic substance:

$$i = kc_0 \exp\left[\alpha \frac{a_i(\phi - \phi_{Ni})^2 - a_f(\phi - \phi_{Nf})^2}{RT}\right] \exp\left(-\frac{\alpha\phi F}{RT}\right) \exp\left[\frac{a_i(\phi - \phi_{Ni})^2}{RT}\right] \tag{111}$$

At potentials remote from the value ϕ_N, the organic substance is almost completely desorbed from the electrode, and the reaction slows down (the last exponent tending to zero, prevails over the growth of the second term). Antropov was the first to see the possibility of such a slowdown of the reaction.$^{(177)}$ A typical example of such a slowdown as a result of desorption is shown in Figure 28.

When studying reactions of organic compounds, it is often possible to directly determine, using an appropriate method, the concentration of the adsorbed substance. In this case, one can obtain polarization curves at a constant concentration on the surface rather than in the bulk.

These curves are described by the equation

$$i = kC_s \exp\left[\frac{a_i(\phi - \phi_{Ni})^2 - a_f(\phi - \phi_{Nf})^2}{RT}\right] \exp\left(-\frac{\alpha\phi F}{RT}\right) \tag{112}$$

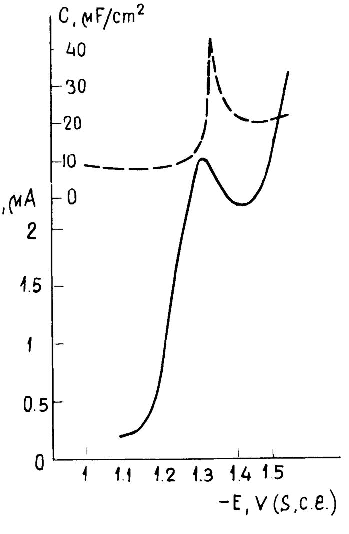

Figure 28. Polarogram and curve of differential capacity (dashed line) of 10^{-3} *M* *N*-(2-methoxybenzoyl) caprolactam. Note the current drop near the desorption peak (according to Ref. 178).

The properties of large organic molecules are usually quite similar both in the oxidized and reduced forms; therefore, their adsorption energy is affected almost similarly by the electric field, i.e., $a_i \simeq a_f = a$, whereas the maximum adsorption potentials for particles of dissimilar charges (e.g., in the case of a neutral molecule and an anion, the product of its reduction) may differ markedly. That is why Eq. (112) can be approximately written as

$$i = k'C_s \exp\left\{-\frac{\alpha[1 - 2a(\phi_{Nf} - \phi_{Ni})]\phi F}{RT}\right\} \tag{113}$$

Thus, the effect of expulsion of adsorbed substances by the electric field may manifest itself through a variation in the effective value of α. Estimates suggest that, for appropriate values of the parameters, this variation may amount to 10%, i.e., it lies at the limits of accuracy of experiments commonly conducted with organic compounds.(179)

It has already been mentioned earlier that the problem had been discussed for the case of sufficiently concentrated electrolyte solutions, permitting the diffuse nature of part of the double layer to be ignored. If, however, the diffuseness is significant, it should be taken into account in Eqs. (109)–(113) by noting that the expulsive action on the organic molecule is exerted not by the entire potential (field), but only by the potential drop (field) in the *compact part* of the double layer.

It is appropriate here to mention another effect of the supporting electrolyte concentration, which has nothing to do with the double layer. It is known that the presence of an electrolyte, particularly at high concentrations, changes the activity coefficient of the dissolved molecules, this phenomenon being referred to (in the bulk situation) as *salting out*. As a result, adsorption tends to become stronger so that the electrode reaction rate increases.(180)

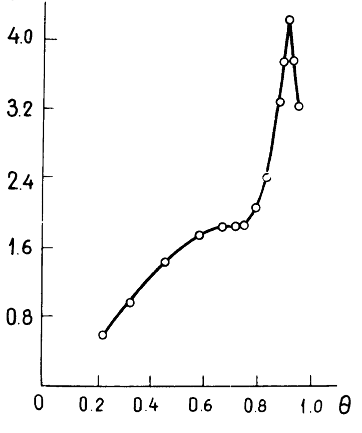

Figure 29. Rate of reduction of diphenyl ammonium ions versus electrode coverage with organic substance (according to Ref. 181).

The rate of an electrode reaction is proportional to the surface concentration of the adsorbed substance. This proportionality is usually met only if the coverage θ is not too high, but at medium and high θ this linearity is disturbed for various reasons, such as non-Langmuirian adsorption behavior, variations in the double-layer structure, etc. Moreover, in some cases, even a *decrease* in the reaction rate is observed as the coverage increases, the so-called "effect of high coverages" revealed by Tedoradze and collaborators(181,182) (see Figure 29).

At present, it is difficult to provide an unambiguous interpretation of this phenomenon. One of the most plausible explanations may be that, in the course of the reaction, at least in the transition state, the area occupied by the molecule increases or its reorientation is considerable. All this requires a certain free area near the reacting particle; therefore, the high degree of coverage produces an autoinhibiting effect on the reaction.

References

1. T. Erdey-Gruz and M. Volmer, *Z. Phys. Chem. A* **150**, 203 (1930).
2. J. Tafel, *Z. Phys. Chem.* **50**, 641 (1905).
3. J. Heyrovsky, *Rec. Trav. Chim. P.B.* **44**, 499 (1925).
4. A. N. Frumkin, *Zh. Fiz. Khim.* **10**, 568 (1937).
5. R. Audubert, *J. Chim. Phys.* **21**, 351 (1924).
6. J. A. V. Butler, *Trans. Faraday Soc.* **19**, 729 (1924).
7. A. N. Frumkin, *Z. Phys. Chem. A.* **164**, 121 (1933).
8. A. N. Frumkin, *Z. Phys. Chem. A.* **160**, 116 (1932).
9. J. N. Brønsted and K. Pedersen, *Z. Phys. Chem.* **108**, 185 (1924); see also J. N. Brønsted, *Chem. Rev.* **5**, 231 (1928).
10. J. Horiuti and M. Polanyi, *Acta Physicochim. URSS* **2**, 505 (1935).
11. R. A. Ogg and M. Polanyi, *Trans. Faraday Soc.* **31**, 604 (1935).
12. M. G. Evans and M. Polanyi, *Trans. Faraday Soc.* **34**, 11 (1938).
13. N. N. Semenov, *O nekotorykh problemakh khimicheskoy kinetiki i reaktsionnoy sposobnosti*, Academy of Sciences of USSR, Moscow (1958).
14. M. Eigen, *Pure Appl. Chem.* **6**, 97 (1963); *Angew. Chem.* **75**, 489 (1963).
15. A. N. Frumkin, V. S. Bagotsky, Z. A. Jofa, and B. N. Kabanov, *Kinetika elektrodnykh protsessov*, Moscow State University (1952).
16. H. W. Nürnberg, *Fort. Chem. Forsch.* **8**, 241 (1967).
17. G. C. Barker, H. W. Nürnberg, J. A. Bolzan, in *Osnovnye voprosy sovremennoi teoreticheskoi elektrokhimii* (Proceedings of the 14th CITCE Meeting), A. N. Frumkin, ed., Mir, Moscow (1965), pp. 91–117.
18. E. Cremer, in *Advances in Catalysis*, Vol. 7, W. G. Frankenburg, V. I. Komarewsky, and E. K. Rideal, eds., Academic Press, New York (1955), pp. 75–91.
19. L. I. Krishtalik, *Elektrokhimiya* **2**, 229 (1966).
20. M. I. Temkin, *Zh. Fiz. Khim.* **15**, 296 (1941).
21. A. A. Balandin, in *Voprosy khimicheskoy kinetiki, kataliza i reaktsionnoy sposobnosti*, V. N. Kondratiev and N. M. Emanuel, eds., Academy of Sciences of USSR, Moscow (1955), pp. 461–483.
22. P. I. Dolin and B. V. Ershler, *Zh. Fiz. Khim.* **14**, 886 (1940).

23. E. Gileadi and B. E. Conway, in *Modern Aspects of Electrochemistry*, Vol. 3, J. O'M. Bockris and B. E. Conway, eds., Butterworths, London (1964), p. 347.
24. H. Gerischer, *Z. Phys. Chem. N.F.* **8**, 137 (1956); see also H. Gerischer, *Bull. Soc. Chim. Belge* **67**, 506 (1958).
25. R. Parsons, *Trans. Faraday Soc.* **54**, 1053 (1958).
26. L. I. Krishtalik, *Zh. Fiz. Khim.* **33**, 1715 (1959).
27. L. I. Krishtalik, *Zh. Fiz. Khim.* **34**, 117 (1960).
28. L. I. Krishtalik, in *Advances in Electrochemistry and Electrochemical Engineering*, Vol. 7, P. Delahay, ed., Interscience, New York (1970), p. 283.
29. B. B. Kuz'menko and L. I. Krishtalik, *Elektrokhimiya* **9**, 130 (1973).
30. L. I. Krishtalik and B. B. Kuz'menko, *Elektrokhimiya* **9**, 664 (1973).
31. L. A. Khanova, E. V. Kasatkin, and V. I. Veselovsky, *Elektrokhimiya* **9**, 562 (1973).
32. L. A. Khanova, E. V. Kasatkin, and V. I. Veselovsky, *Elektrokhimiya* **10**, 800 (1974).
33. L. A. Khanova, E. V. Kasatkin, and V. I. Veselovsky, *Elektrokhimiya* **10**, 1098 (1974).
34. A. N. Frumkin, see footnote on p. 524 of Ref. 10.
35. Z. A. Rotenberg and Yu. V. Pleskov, *Elektrokhimiya* **4**, 826 (1968).
36. Yu. V. Pleskov and Z. A. Rotenberg, *J. Electroanal. Chem.* **20**, 1 (1969).
37. A. M. Brodsky and Yu. Ya. Gurevich, *Electrochim. Acta* **13**, 1245 (1968).
38. L. I. Krishtalik and N. M. Alpatova, *Elektrokhimiya* **12**, 163 (1976).
39. L. I. Krishtalik, *Electrochim. Acta* **21**, 693 (1976).
40. D. C. Walker, *Can. J. Chem.* **44**, 2226 (1966).
41. D. C. Walker, *Can. J. Chem.* **45**, 807 (1967).
42. D. C. Walker, *Anal. Chem.* **39**, 896 (1967).
43. I. A. Kenney and D. C. Walker, in *Electroanalytical Chemistry*, Vol. 5, A. J. Bard, ed., Marcel Dekker, New York (1971), p. 1.
44. L. I. Antropov, in *Itogi Nauki, Elektrokhimiya*, Vol. 6, V. V. Bondar', ed., Vsesoyuznyi Institut Nauchnoy i Teknicheskoy Informatsii, Moscow (1971), p. 5.
45. B. E. Conway, in *Modern Aspects of Electrochemistry*, Vol. 7, B. E. Conway and J. O'M. Bockris, eds., Butterworths, London (1972), p. 83.
46. D. Postl and U. Schindeworlf, *Ber. Bunsenges. Phys. Chem.* **75**, 662 (1971).
47. A. Bewick, B. E. Conway, and A. M. Tuxford, *J. Electroanal. Chem.* **42**, App. 11 (1973).
48. J. O'M. Bockris, *Trans. Faraday Soc.* **43**, 417 (1947).
49. J. O'M. Bockris, in *Modern Aspects of Electrochemistry*, Vol. 2, J. O'M. Bockris and B. E. Conway, eds., Butterworths, London (1954), p. 201.
50. B. E. Conway and J. O'M. Bockris, *J. Chem. Phys.* **26**, 532 (1957).
51. A. T. Petrenko, *Zh. Fiz. Khim.* **39**, 2097 (1965).
52. H. Kita, *J. Electrochem. Soc.* **113**, 1095 (1966).
53. V. L. Kheifets, B. S. Krasikov, and A. L. Rotinian, *Elektrokhimiya* **6**, 916 (1970).
54. S. Trasatti, *J. Electroanal. Chem.* **39**, 163 (1972).
55. S. Trasatti, *J. Chem. Soc. Faraday Trans. 1* **68**, 229 (1972).
56. L. I. Krishtalik, *Zh. Fiz. Khim.* **31**, 2403 (1957).
57. L. I. Krishtalik, *Zh. Fiz. Khim.* **41**, 2883 (1967).
58. L. I. Krishtalik, *Electrochim. Acta* **13**, 715 (1968).
59. Z. A. Jofa and A. N. Frumkin, *Zh. Fiz. Khim.* **18**, 268 (1944).
60. L. I. Krishtalik, *Elektrokhimiya* **2**, 1123 (1966).
61. M. I. Temkin, *Zh. Fiz. Khim.* **22**, 1081 (1948).
62. J. N. Agar, *Discuss. Faraday Soc.* **1**, 81 (1947).
63. M. I. Temkin, in *Trudy Soveshchaniya po Elektrokhimii* 1950, A. N. Frumkin, ed., Academy of Sciences of USSR, Moscow (1953), p. 181.
64. L. I. Krishtalik, *Elektrokhimiya* **2**, 1176 (1966).
65. G. J. Hills and D. R. Kinnibrugh, *J. Electrochem. Soc.* **113**, 1114 (1966).
66. L. I. Krishtalik, *J. Electrochem. Soc.* **113**, 1117 (1966).

67. R. Parsons, *J. Electrochem. Soc.* **113**, 1118 (1966).
68. Z. A. Jofa and K. P. Mikulin, *Zh. Fiz. Khim.* **18**, 137 (1944).
69. R. Audubert, *Discuss. Faraday Soc.* **1**, 72 (1947).
70. L. I. Krishtalik, *Elektrodnye reaktsii, Mekhanism Elementarnogo acta,* Nauka, Moscow (1979).
71. R. R. Dogonadze, A. M. Kuznetsov, and V. G. Levich, *Elektrokhimiya* **3**, 739 (1967).
72. R. R. Dogonadze, A. M. Kuznetsov, and V. G. Levich, *Electrochim. Acta* **13**, 1025 (1968).
73. M. A. Vorotyntsev and A. M. Kuznetsov, *Elektrokhimiya* **6**, 261 (1970).
74. M. A. Vorotyntsev, R. R. Dogonadze, and A. M. Kuznetsov, *Elektrokhimiya* **7**, 306 (1971).
75. H. Gerischer, *Z. Phys. Chem. N.F.* **26**, 325 (1960).
76. L. I. Krishtalik, *Zh. Fiz. Khim.* **39**, 642 (1965).
77. L I. Krishtalik, *Electrochim. Acta* **13**, 1045 (1968).
78. V. I. Bystrov and L. I. Krishtalik, *Elektrokhimiya* **3**, 1345 (1967).
79. A. N. Frumkin, Z. A. Jofa, and V. S. Bagotsky, *Zh. Fiz. Khim.* **25**, 1117 (1951).
80. Z. A. Rotenberg, V. I. Lakomov, and Yu. V. Pleskov, *Elektrokhimiya* **6**, 515 (1970).
81. Z. A. Rotenberg, Yu. A. Prishchepa and Yu. V. Pleskov, *J. Electroanal. Chem.* **56**, 345 (1974).
82. L. I. Krishtalik and Z. A. Rotenberg, *Zh. Fiz. Khim.* **39**, 907 (1965).
83. R. G. Erenburg and L. I. Krishtalik, *Elektrokhimiya* **4**, 923 (1968).
84. R. G. Erenburg, L. I. Krishtalik, and I. P. Yaroshevskaya, *Elektrokhimiya* **11**, 1068 (1975).
85. R. G. Erenburg, L. I. Krishtalik, and I. P. Yaroshevskaya, *Elektrokhimiya* **11**, 1072 (1975).
86. R. G. Erenburg, L. I. Krishtalik, and I. P. Yaroshevskaya, *Elektrokhimiya* **11**, 1236 (1975).
87. L. I. Krishtalik and G. E. Titova, *Elektrokhimiya* **4**, 285 (1968).
88. K. J. Vetter, *Elektrochemische Kinetik*, Springer-Verlag, Berlin (1961).
89. R. Haase, *Thermodynamik der Irreversiblen Prozesse*, Dr. D. Steinkopff Verlag, Darmstadt (1963).
90. R. G. Erenburg, *Dokl. Akad. Nauk SSSR* **211**, 1149 (1973).
91. R. G. Erenburg, *Elektrokhimiya* **10**, 457 (1974).
92. R. G. Erenburg, thesis, Inst. of Electrochem. Acad. Sci. USSR, Moscow (1975).
93. J. Horiuti and M. Ikusima, *Proc. Imp. Acad. (Tokyo)* **15**, 39 (1939).
94. J. Horiuti, *J. Res. Inst. Catal. Hokkaido Univ.* **1**, 8 (1948).
95. R. Parsons, in *Advances in Electrochemistry and Electrochemical Engineering*, Vol. 1, P. Delahay, ed., Interscience, New York (1961), p. 2.
96. A. N. Frumkin, in *Advances in Electrochemistry and Electrochemical Engineering*, Vol. 1, P. Delahay, ed., Interscience, New York (1961), p. 65.
97. A. N. Frumkin, in *Advances in Electrochemistry and Electrochemical Engineering*, Vol. 3, P. Delahay, ed., Interscience, New York (1963), p. 287.
98. L. Gierst, E. Nicolas, and L. Tytgat-Vandenberghen, in *The Chemistry of Solid/Liquid Interfaces, Proc. of Int. Summer School*, B. Težak and V. Pravdić, eds., *Croatica Chem. Acta*, Special Publication No. 1, pp. 37–67, Zagreb (1971).
99. P. Delahay, *Double Layer and Electrode Kinetics*, Interscience, New York (1965).
100. A. N. Frumkin, *Potentsialy Nulevogo Zaryada*, Nauka, Moscow (1979).
101. V. S. Bagotsky and I. E. Yablokova, *Zh. Fiz. Khim.* **23**, 413 (1949).
102. E. A. Maznichenko, B. B. Damaskin, and Z. A. Jofa, *Dokl. Akad. Nauk SSSR* **138**, 1377 (1961).
103. K. Asada, P. Delahay, and A. Sundaram, *J. Am. Chem. Soc.* **83**, 3396 (1961).
104. L. Gierst, J. Tondeur, R. Cornelissen, and F. Lami, in *Osnovnye Voprosy Sovremennoy Teoreticheskoy Elektrokhimii*, Proc. of 14th CITCE Meeting, A. N. Frumkin, ed., Mir, Moscow (1965), pp. 425–452.
105. E . P. Andreeva, *Zh. Fiz. Khim.* **29**, 699 (1955).
106. B. B. Damaskin and B. N. Afanasiev, *Elektrokhimiya* **13**, 1099 (1977).
107. Z. A. Iofa, B. N. Kabanov, E. M. Kuchinsky, and F. Chistyakov, *Zh. Fiz. Khim.* **13**, 1105 (1939).

108. Tza Chuan-sing and Z. A. Iofa, *Dokl. Akad. Nauk SSSR* **126**, 1308 (1959).
109. Tza Chuan-sing and Z. A. Iofa, *Dokl. Akad. Nauk SSSR* **125**, 1065 (1959).
110. K. M. Joshi, W. Mehl, and R. Parsons, in *Transactions of the Symposium on Electrode Processes*, E. Yeager, ed., J. Wiley, New York (1961), pp. 249–265.
111. D. C. Grahame, *J. Am. Chem. Soc.* **76**, 4819 (1954).
112. D. C. Grahame, *J. Am. Chem. Soc.* **80**, 4201 (1958).
113. M. Breiter, M. Kleinerman, and P. Delahay, *J. Am. Chem. Soc.* **80**, 5111 (1958).
114. R. Parsons, *J. Electroanal. Chem.* **21**, 35 (1969).
115. L. I. Krishtalik, *Elektrokhimiya* **6**, 1165 (1970).
116. L. I. Krishtalik, *J. Electroanal. Chem.* **35**, 157 (1972).
117. V. M. Tsionsky and L. I. Krishtalik, *Elektrokhimiya* **5**, 1184 (1969).
118. T. T. Tenno and U. V. Pal'm, *Elektrokhimiya* **8**, 1381 (1972).
119. T. T. Tenno and U. V. Pal'm, *Elektrokhimiya* **9**, 1545 (1973).
120. T. T. Tenno and U. V. Pal'm, *J. Electroanal. Chem.* **42**, 457 (1973).
121. A. B. Kilimnik and A. L. Rotinian, *Elektrokhimiya* **5**, 1234 (1969).
122. E. Preis, K. Szabo, S. Raicheva and I. A. Bagotskaya, *Elektrokhimiya* **2**, 1209 (1966).
123. Yu. A. Kukk, S. I. Suurman, and V. E. Past, *Dvoynoy Sloy i Adsorbtsia na Tverdych Elektrodakh, III*, Proc. of Symp., Tartu State University, Tartu, 1972, pp. 143–150.
124. K. Punning and V. Past, *Uch. Zap. Tartuskogo Gos. Univ.* **235**, 35 (1969).
125. Ya. M. Kolotyrkin and N. Ya. Bune, *Zh. Fiz. Khim.* **21**, 581 (1947).
126. N. Ya. Bune and Ya. M. Kolotyrkin, *Dokl. Akad. Nauk SSSR* **100**, 295 (1955).
127. Ya. M. Kolotyrkin and N. Ya. Bune, *Zh. Fiz. Khim.* **29**, 435 (1955).
128. Ya. M. Kolotyrkin and L. A. Medvedeva, in *Trudy Soveshchaniya po Elektrokhimii, 1950*, A. N. Frumkin, ed., Academy of Sciences of USSR, Moscow (1953), pp. 369–379.
129. Ya. M. Kolotyrkin and L. A. Medvedeva, *Zh. Fiz. Khim.* **25**, 1355 (1951).
130. L. A. Medvedeva and Ya. M. Kolotyrkin, *Zh. Fiz. Khim.* **31**, 2668 (1957).
131. Ya. M. Kolotyrkin, *Trans. Faraday Soc.* **55**, 455 (1958).
132. M. I. Temkin, in *Voprosy Khimicheskoy Kinetiki, Kataliza i Reaktsionnoy Sposobnosti*, V. N. Kondratiev and N. M. Emanuel, eds., Academy of Sciences of USSR, Moscow (1955), pp. 484–495.
133. A. M. Morozov, I. A. Bagotskaya, and E. A. Preis, *Elektrokhimiya* **5**, 40 (1969).
134. L. N. Sviridova, V. N. Korshunov, and B. B. Damaskin, *Elektrokhimiya* **12**, 1608 (1976).
135. V. N. Korshunov and Z. A. Jofa, *Dokl. Akad. Nauk SSSR* **141**, 143 (1961).
136. V. N. Korshunov, A. N. Frumkin, and I. V. Ivanova, *Elektrokhimiya* **4**, 1120 (1968).
137. V. M. Tsionsky and V. A. Krasikov, *Elektrokhimiya* **12**, 961 (1976).
138. B. N. Kabanov, I. I. Astakhov, and I. G. Kiseleva, *Usp. Khim.* **34**, 1813 (1965).
139. Z. A. Jofa, A. N. Frumkin, and E. A. Maznichenko, *Zh. Fiz. Khim.* **31**, 2042 (1957).
140. I. A. Bagotskaya, N. M. Genkina, and V. G. Boytsov, *Elektrokhimiya* **5**, 132 (1969).
141. I. A. Bagotskaya and E. N. Potapova, *Elektrokhimiya* **5**, 1465 (1969).
142. I. A. Bagotskaya and E. N. Potapova, *Elektrokhimiya* **6**, 855 (1970).
143. V. E. Past and M. E. Haga, *Elektrokhimiya* **5**, 319 (1969).
144. Yu. A. Kukk and V. E. Past, *Elektrokhimiya* **7**, 1860 (1971).
145. I. P. Gladkikh and V. N. Korshunov, *Elektrokhimiya* **9**, 250 (1973).
146. T. A. Kryukova, *Dokl. Akad. Nauk SSSR* **65**, 517 (1949).
147. A. N. Frumkin and G. M. Florianovich, *Dokl. Akad. Nauk SSSR* **80**, 907 (1951).
148. G. M. Florianovich and A. N. Frumkin, *Zh. Fiz. Khim.* **29**, 1827 (1955).
149. N. V. Nikolaeva, N. S. Shapiro, and A. N. Frumkin, *Dokl. Akad. Nauk SSSR* **86**, 581 (1952).
150. A. N. Frumkin, N. V. Nikolaeva-Fedorovich, N. P. Berezina, and Kh. E. Keis, *J. Electroanal. Chem.* **58**, 189 (1975).
151. N. V. Fedorovich, M. D. Levi, B. B. Damaskin, and A. V. Shlepakov, *Dokl. Akad. Nauk SSSR* **225**, 148 (1975).
152. N. V. Fedorovich, M. D. Levi, and A. V. Shlepakov, *Elektrokhimiya* **13**, 89 (1977).

153. L. Gierst, in *Transactions of the Symposium on Electrode Processes*, E. Yeager, ed., John Wiley, New York (1961), pp. 109–144.
154. A. N. Frumkin and O. A. Petry, *Dokl. Akad. Nauk SSSR* **147**, 418 (1962).
155. A. N. Frumkin, O. A. Petry, and N. V. Nikolaeva-Fedorovich, *Electrochim. Acta* **8**, 177 (1963).
156. D. C. Grahame, *Chem. Rev.* **41**, 441 (1947).
157. D. I. Dzhaparidze and V. V. Shavgulidze, *Elektrokhimiya* **9**, 1390 (1973).
158. O. A. Petry and B. B. Damaskin, *Elektrokhimiya* **10**, 756 (1974).
159. A. N. Frumkin and N. V. Nikolaeva, *J. Chem. Phys.* **26**, 1552 (1957).
160. A. N. Frumkin, *Usp. Khim.* **4**, 987 (1935).
161. A. N. Frumkin, *Couche Double. Electrocapilarité. Surtension.* (*Actualités Scientifiques et Industrielles N373*), Hermann, Paris (1936).
162. V. G. Levich, *Dokl. Akad. Nauk SSSR* **67**, 309 (1949).
163. V. G. Levich, *Dokl. Akad. Nauk SSSR*, **124**, 869 (1959).
164. A. N. Frumkin, *Usp. Khim.* **24**, 933 (1955).
165. A. N. Frumkin, *Z. Elektrochem.* **59**, 807 (1955).
166. D. Bieman and W. R. Fawcett, *J. Electroanal. Chem.* **34**, 27 (1972).
167. V. S. Krylov, *Elektrokhimiya* **12**, 331 (1976).
168. R. Guidelli and M. Foresti, *Electrochim. Acta* **18**, 301 (1973).
169. W. R. Fawcett and S. Levine, *J. Electroanal. Chem.* **43**, 175 (1973).
170. W. R. Fawcett and S. Levine, *J. Electroanal. Chem.* **65**, 505 (1975).
171. V. S. Krylov and V. A. Kiryanov, *Elektrokhimiya* **12**, 536 (1976).
172. V. S. Krylov and V. A. Kiryanov, *Elektrokhimiya* **12**, 1071 (1976).
173. V. S. Krylov, W. R. Fawcett, and V. A. Kiryanov, *Elektrokhimiya* **12**, 424 (1976).
174. V. S. Krylov, W. R. Fawcett, and V. A. Kiryanov, *Elektrokhimiya* **12**, 543 (1976).
175. V. A. Myamlin and V. S. Krylov, *Elektrokhimiya* **13**, 1581 (1977).
176. E. S. Levin and Z. I. Fodiman, *Zh. Fiz. Khim.* **28**, 601 (1954).
177. L. I. Antropov, *Zh. Fiz. Khim.* **24**, 1428 (1950).
178. G. A. Tsagareli, A. M. Shkrob, and A. B. Ershler, *Izvestiya ANSSSR, Seriya Khimicheskaya*, 1952 (1967).
179. A. B. Ershler, *Elektrokhimiya* **13**, 408 (1977).
180. A. B. Ershler, E. D. Belokolos, and G. A. Tedoradze, *Elektrokhimiya* **1**, 1429 (1965).
181. A. N. Frumkin, D. I. Dzhaparidze, and G. A. Tedoradze, *Dokl. Akad. Nauk SSSR* **152**, 164 (1963).
182. G. A. Tedoradze and D. I. Dzhaparidze, *Elektrokhimiya* **1**, 910 (1965).

4

Electrocatalysis

A. J. APPLEBY

1. Introduction

"Electrocatalysis" is inevitably an extension of, and a qualification of, "catalysis." Catalysis has been typically defined as that part of chemistry in general which concerns the increase in the rate of chemical reactions giving preferred products by substances which do not themselves show a permanent chemical change. The word itself, first used in the chemical sense (after literary analogies) by Berzelius in 1835, is derived from Greek *kata* (down) and *lyein* (to loosen or let, its Indo-European analogs), giving "letting down" or "easing," "aiding."

Catalysis may occur as a result of homogeneous or heterogeneous additives, and it was early recognized that the latter could be extended to the heterogeneous surface representing the electrode in electrochemical reactions. Bowden and Rideal(1) in their well-known 1928 paper speak of catalytic effects at electrodes, and the measurement of catalysis for certain reactions by the magnitude of the currents generated at different electrodes under the same conditions of potential. It does not require a very long step to coin a new word, "electrocatalysis," from these early observations. This word may then be defined as the study of heterogeneous catalytic reactions that involve reactant and product species transferring electrons through an electrolyte–catalyst interface. However, this implies a considerable qualification of the overlying concept of catalysis in general, since efficient electrocatalysis will inevitably require relatively long ionic and electronic pathways, hence efficient ionically conducting solutions and electronically conducting catalyst materials. In normal heterogeneous chemical catalysis, chemical changes involving bond breaking (and the inevitable redistributions of electrons associated with it)

A. J. APPLEBY • Electric Power Research Institute, 3412 Hillview Avenue, Palo Alto, California 94303.

occur only over atomic distances, hence substrates and supporting media are not subject to the above special requirements. In addition, in electrode reactions a further degree of freedom affecting rate is involved: that of the electrode potential. This adds to those normally considered in chemical processes: reactant concentration (including pressure), and temperature, in addition to the specific "catalytic" properties of the homogeneous environment and heterogeneous surface. These variables will be discussed in further detail in the next section.

There has been some dispute as to who first introduced the neologism "electrocatalysis" into the literature. According to Frumkin,(2) it first occurs in the German language Soviet literature in prototype form during the period 1934–1936, in papers by Kobosev and Monblanowa.(3) However, these references appear to have been largely ignored by English language readers until the advent of fuel cells made maximization of reaction rates at electrodes imperative. Thus, the first use of the word "electrocatalysis" in the reviewed English scientific literature appears in a well-known paper by Grubb(4) in 1963. After this time, its utilization became widespread.

A semantic point should be mentioned: the term *electrocatalysis* cannot strictly be applied to electron transfer steps or simple electron transfer reactions since there cannot be any *non*catalyzed equivalent pathway in the absence of an electrode surface. However, adsorption effects specific to the electrode surface can influence the kinetics of an electron transfer step involving adsorbed products and/or reactants and in this limited sense "electrocatalysis" could arise in an electron transfer reaction. The term *electrocatalysis*, however, applies more correctly to the influence of electrode material and the state of electrode surfaces on the behavior of those types of chemical-catalyzed steps, e.g., dissociative chemisorption in some fuel cell oxidations, that are *coupled* with electron transfer processes.

Discussions of the phenomenon of electrocatalysis, in particular, referring to the improvement of the kinetic characteristics of contemporary (direct hydrocarbon) fuel cells, had started to appear somewhat earlier—ca. 1960.(5) This evidence of a rapidly rising interest in this newly defined branch of chemistry and electrochemistry is shown by the appearance of the first full-fledged review attempting to consider all the factors and documented reactions involved, by Wroblowa and Bockris(6) in 1964. However, while this review was entitled "Electrocatalysis," the subject had been implicitly referred to in earlier discussions, which considered the "role of the substrate in determining reaction rates at electrodes." One may particularly cite Bockris,(7) Bockris and Potter,(8) Ruetschi and Delahay,(9,10) Conway and Bockris,(11,12) Parsons(13,14) and Gerischer,(15) since their contributions represent the most general analyses of "electrocatalytic" reactions at the time of their publication. Many other, rather more specialized discussions of the effect of substrate properties on reaction rates were published during the same time interval. These are discussed in following sections.

An extended review of the general field, as newly defined, authored by Wroblowa, Srinivasan, and Bockris appeared in 1967.(16) This was essentially an updating of Ref. 6. Other reviews have followed subsequently. These have been either rather limited in scope, e.g., confined to acid fuel cells,(17) and oxygen electrode reactions,(18) or alternatively, have attempted a more comprehensive viewpoint.(19)

The importance of electrocatalysis is considerable. While it must inevitably deal with situations which are less general than those in catalysis as a whole, due to the constraints imposed by the required properties of the supporting medium (the electrolyte) and of the heterogeneous substrate (the electrode material), it nevertheless allows the use of the electrode potential parameter as a further rate-influencing factor. Changes in electrode potential, over relatively small ranges, may allow very large changes in rate of reaction on a given substrate, for example, changes of three to ten orders of magnitude for a potential variation of, say, 400 mV. Such a change in reaction rate is outside the normal possibilities of chemical processes occurring in solution, since under isothermal conditions the only available variable would be concentration change, or in gaseous systems, pressure change. The only comparable parameter capable of affecting the rates of *chemical* processes to this sort of degree is temperature. In some ways, this may be regarded as analogous to electrode potential, since a temperature perturbation will change the rates of different reactions to varying degrees, according to their activation energies. However, a variation of ten orders of magnitude in reaction rate for processes at the higher end of activation energy spectrum under normal conditions ($\sim 80\ \text{kJ mol}^{-1}$) will require a temperature excursion of several hundred degrees. The rate variation will of course be correspondingly less for reactions possessing lower activation energies. Under such drastically imposed energetic conditions, thermal excitation will be such that side reactions (bond breaking, polymerization, etc.) will inevitably occur.

This underlines the potentially important significance of electrocatalysis, compared with conventional chemical catalysis. For selectivity, i.e., for differentiating between a number of chemical steps of varying activation energy, wide variations of the temperature conditions may be required in the latter case, whereas in the former only the effect of varying potential may be used. The effect of selectivity of rates between different processes will then correspond to their different potential sensitivities, i.e., to the differences between their Tafel slopes. This point, however, illustrates the potential value of electrocatalysis as a preparative technique: with it, selectivity of reactions can be achieved at high rates under nondrastic conditions, so that high yields are possible for sensitive processes—e.g., many organic chemical procedures.

Certain electrocatalytic, or at very least electrochemical, processes correspond to classical preparative techniques in organic chemistry: such preparations as those involving sodium–alcohol and zinc-dust–acid reductions, or indeed the many processes using different heterogeneous reductive agents that are involved in the reduction of nitrobenzenes to give a wide range of products, are examples of electrocatalytic procedures. In them, the electrocatalytic preparation involves the use of dissolving electrodes to provide both the effectively controlled potential environment and the heterogeneous surface. In other words, dissolution of the reducing metal provides the equivalent of a mixed potential (resulting from a corrosion–reduction reaction) and a catalytic surface. This, of course, reduces the number of possible degrees of freedom in the preparative process.

Since the surface must simultaneously corrode, reduce, and catalyze, it is clear that very specific substrates will normally be necessary for "ordinary" chemical catalytic processes. They must possess just the right combination of catalytic and reductive properties so that, when exposed to their reactive environment, they produce an electrochemical potential that gives the correct rate (bearing in mind their own "electrocatalytic" character) for the preparative process desired. The correct products will thereby result. Clearly, it would be much easier if the "electrocatalytic" and "potential" characteristics could be separated by the use of specialized conductive electrode surfaces, combined with a suitable electronic potentiostat, respectively. In this way, electrocatalysis could become of great future importance in certain types of preparative organic chemistry.

However, electrocatalysis shows a much more important potential usefulness in energy conversion devices. In these, the object is to retain the greatest possible rate (thus using a minimum device area or minimum investment) at potentials as close as possible to the reversible value, or the maximum allowed by thermodynamics, so that maximum second-law efficiency may be expected. The latter energy value will then correspond to the reaction free energy, a value which cannot be exceeded by the total free energy (in the form of electricity) produced. This will require the greatest possible reaction rates for the primary oxidation and reduction processes involved in the device which has, since the late 1950s, carried the name "fuel cell," since it is a battery using a "fuel" as the oxidizable medium and oxygen (or air) as the oxidizing or depolarizing medium. Hence, the reaction rates at both electrodes must be not only maximized by the use of large surface areas, but must also be "catalyzed" so that the effective potentials under load are as close as possible to the theoretical values for both oxidation and reduction processes.

Overall, therefore, "electrocatalysis" is a specialized branch of catalysis. However, its importance in three areas may be stressed:

1. Using the potential variable, it may give a route to high rates of formation of certain organic materials which have a high specificity in regard to preparative procedure (surface and temperature effects).
2. By allowing great specificity at high rates, it may give a higher energy efficiency than that for thermal preparation routes.
3. Finally, and most important, electrocatalysis allows a route to direct energy conversion of the free energy of combustion into dc electricity via

anodic and cathodic processes in a fuel cell. This requires the maximum possible reaction rates close to the equilibrium potential for the anodic and cathodic reactions, and provides a great challenge for the electrochemist and electrochemical engineer. If this challenge can be taken up and exploited using low-capital cost, long-lived conversion devices, there seems little doubt that the fuel cell will have an increasingly important impact for energy conversion on a utility and nonutility basis. Its high efficiency, especially under part-load conditions, together with its ability to be dispersed close to the point of load use in small, efficient units, is expected to result in fuel and capital savings compared with state-of-the-art Carnot-limited machines. In addition, its low emission, its lack of high levels of noise, and low cooling requirements are further points in its favor, compared, for example, with combined-cycle gas and steam turbines. Finally, the possibility of its close proximity to the point of ultimate energy use, as determined by the efficiency and environmental characteristics listed above, should allow further energy conservation by the economic utilization of its waste heat. A recent account of the fuel cell (20) stresses all the above points.

2. Electrocatalysis and Catalysis

2.1. General

Conventional catalytic reactions, of the type represented by the overall gas phase or liquid phase process

$$\mathrm{A + B \rightarrow AB} \tag{1}$$

may be accelerated in rate by certain homogeneous or heterogeneous additives, C. It was early proposed that this rate increase was a result of the formation of rapidly decomposed intermediates between the reactants A and B and the catalyst C. For example, we may write

$$\mathrm{A + C \rightarrow AC} \quad \text{rapid} \tag{2}$$

$$\mathrm{AC + B \rightarrow AB + C} \quad \text{rapid} \tag{3}$$

in which it is implied that both steps are more rapid than the rate of reaction (1) above. This explanation essentially still remains as the basis of current knowledge of catalysis, though the intermediates that form may be indeed of very short lifetime in practice.

More concrete notions of catalysis occurred after Arrhenius had formulated his integrated rate law(21)

$$r = \text{const} \prod \{\text{reactants}\} \exp\left[-E/RT\right] \tag{4}$$

where r is forward rate, $\prod$ {reactants} is the product of the reactant concentrations for all the reactant molecules appearing in the slowest step (i.e., taking into account reaction orders), and E is a certain "energy of activation" corresponding to the energy required to place the molecular bonds involved in a favorable position to react. R and T are the gas constant and absolute temperature, respectively. Ostwald was apparently the first to point out that changes in r, hence changes in E, were associated with catalysis.

As the above example shows, catalysis implies consecutive reactions. One of the historically most useful ideas in the treatment of such processes has been the steady state assumption—i.e., that the intermediates in such a reaction sequence might rapidly reach a given stationary concentration, which then, in the steady state, remains invariant. This concept was first used by Bodenstein(22) and by Michaelis and Menten,(23) and was generalized by Christiansen and Kramers(24) to reactions involving possible chain mechanisms in the gas phase. It is of some importance, since it illustrates early concepts in the collision theory of reactions.

For a concentration of reacting gas n, undergoing decomposition to yield a product, we can suppose that at a given time we have concentrations of activated reactants a and activated products a'. We assume that the activated reactants and activated products have energies sufficient to surmount the Arrhenius energy barrier, and that all activation occurs by direct collisions with normal molecules of reacting gas. Then the rate of formation of active reactants will be

$$\frac{da}{dt} = k_1n^2 + \alpha k_1'na' - k_2a - k_3na \tag{5}$$

when we assume that all activations occur through collisions with other normal reactant species, and hence contain an n term. α is a factor which is included to show that not all activated product–normal reactant molecule collisions are effective in producing activated reactant molecules. The k's are the various rate constants for the individual steps (formation, respectively, of a from n, of a from a' from a via spontaneous decomposition at the top of the energy barrier, and of n from a). It is also clear that

$$\frac{da'}{dt} = k_2a - k_1'na' \tag{6}$$

hence from (5) and (6), using the steady state hypothesis ($da'/dt = da/dt = 0$)

$$-\frac{dn}{dt} = k_2a = \frac{k_1n^2}{(k_3/k_2)n + (1-\alpha)} \tag{7}$$

This relationship is interesting historically, since it shows how a normal decomposition reaction involving collision-type activation can transform from a unimolecular to a bimolecular type of mechanism. For example, if collisional *deactivation* of activated reactants is much more rapid than spontaneous deactivation ($k_3n \gg k_2$), then $-dn/dt = (k_1k_2/k_3)n$, i.e., the reactor is unimolecular. However, if the opposite is true, and if $(1-\alpha)$ is not excessively small, then $-dn/dt \propto n^2$, i.e., the process is bimolecular. In other cases, the reaction order may be these two extremes, depending on the various rate constants and α values. If, on the other hand, we consider that a homogeneous *catalyzed decomposition* reaction occurs, then the implication is that the process will involve the formation of activated a' molecules consisting of a combination of reactant molecules and catalyst molecules, whose (unactivated) concentration is n. Equation (7) then becomes

$$-\frac{dn}{dt} = \frac{k_1 nn'}{(k_3/k_2)n + (1-\alpha)} \tag{8}$$

assuming that the catalyst concentration n' is relatively small compared with n. Hence, if the activated molecule can be rapidly deactivated and decomposed by collisions ($k_3 n \gg k_2$), the reaction will be essentially zero order in reactant molecules, but first order in catalyst molecules. However, if the decomposition process to give the reaction product is essentially *spontaneous*, i.e., the activated molecule dissociates in less than the time for a normal high-energy molecular collision, then for a "typical" nonchain process with $\alpha \simeq 0$, the overall rate will be given by $-dn/dt \simeq k_1 nn'$. In other words, the reaction will be first order in both reactant molecules and catalyst molecules. This characteristic of "typical" gas phase catalytic processes was first demonstrated by Clusius and Hinshelwood(25) in 1930 for the decomposition of various aldehydes and ethers in the vapor phase, catalyzed by molecular iodine. This appears to be the first experimental proof that "catalysis" as observed does indeed imply the formation of chemical intermediates that have a transient existence, which is less than that for collisional deactivation.

In this review, it is unnecessary to continue the historical development of homogeneous catalysis in the gas phase, since electrocatalysis, as generally understood, is a heterogeneous, solution phase phenomenon. However, it may be permissible to consider briefly the homogeneous catalytic problem in a liquid phase situation, since this has considerable relevance to the mechanism of "activation" of molecules (i.e., of energy transfer), in electrolytic environments. In general, if we reconsider the question implied by Eq. (5) in a liquid phase, rather than in an overall dilute, perfect gas environment, then $k_1 n^2$ in the first term will be replaced by a term $k_1'' n$, where k_1'' contains a true rate constant, related to some collision number, and some effective concentration or collision probability term that will depend on the number of indifferent liquid molecules per reacting molecule. It is easy to show that the n term in the denominator of (7) will similarly disappear, into a new k_3 term, which may be called k_3'. In such cases, the overall reaction will always be first order in n. If heterogeneous catalysis occurs, then the situation may change.

If the surface catalyst concentration is relatively small compared with the concentration of reagent molecules, n, available in its vicinity, then the amount of active catalytic sites available for reaction, $(n' - a)$, may no longer be negligible. In such cases, the reaction may be zero order in n (though first order in n').[23] Normally, chain processes will be unimportant, i.e., α will tend to zero. In the general case, neglecting for simplicity reactions involving product molecules a' crossing the Arrhenius barrier (i.e., neglecting the backreaction), A again being the transient complex concentration:

$$\frac{da}{dt} = (n' - a)nk_1'' - ak_3' - k_2a \tag{9}$$

with $-dn/dt = k_2a$, and using the steady state assumption, we obtain

$$-\frac{dn}{dt} = \frac{k_1''k_2nn'}{nk_1'' + k_2 + k_3'} \tag{10}$$

This differs from the corresponding reaction made for the homogeneous case by including nk'' in the denominator. $-dn/dt$ is now a surface rate within a thin "zone of reaction" containing n reacting molecules/unit area, in which a transient complex can form. If the $nk_1'' \gg k_2 + k_3'$, i.e., if $n' \simeq a$, the reaction may be zero order in n, and be limited by the available number of n' sites. This is important for certain electrocatalytic reactions, which are always of the electrode (surface) type.

By definition, "electrocatalytic" reactions† involve electron transfer to or from charged particles. The electron transfer step may be rate determining, for example in the sequence

$$\mathrm{A} + \{\mathrm{S}\} \rightarrow \mathrm{A}\{\mathrm{S}\} \tag{11}$$

which is postulated to be rapid, and where {S} is a catalytic site on an electrode surface, followed by

$$\mathrm{A}\{\mathrm{S}\} + \mathrm{e}^- \rightarrow \mathrm{A}\{\mathrm{S}\}^- \tag{12}$$

and

$$\mathrm{A}\{\mathrm{S}\}^- \rightarrow \{\mathrm{S}\} + \mathrm{A}^- \tag{13}$$

in which (12) (electron transfer) may be rate determining. Similarly, if both (11) and (12) are rapid, the ion transfer reaction (13) may be rate determining. Alternatively, (11) and (12), or (12) and (13) may be combined into single steps, i.e.,

$$\mathrm{A} + \{\mathrm{S}\} + \mathrm{e}^- \rightarrow \mathrm{A}\{\mathrm{S}\}^- \tag{14}$$

$$\mathrm{A}\{\mathrm{S}\} + \mathrm{e}^- \rightarrow \{\mathrm{S}\} + \mathrm{A}^- \tag{15}$$

The actual path followed will clearly depend on the heights of the activation energy barriers for the individual steps, so that the overall rate is maximized. In general, only one pathway, and rate-determining step, will *predominate* on a given surface. There may be occasional exceptions to this rule, particularly in the case of the reduction of molecular oxygen. These are discussed in a later section.

---

† See semantic discussion on p.174.

As can be seen from the above discussion, the chemical reaction orders for electrochemical reactions will generally be "normal", i.e., reactions which are written first order will normally show true first order kinetics, with reactions of higher order behaving similarly. Exceptions to the above may occur when the catalytic sites have a low concentration, or when the overall rate is sufficient to saturate available sites. This will be discussed in a later section; for the moment, we will assume that $k_2 + k_3' \gg nk_1''$ in Eq. (10). When the rate-determining step involves an electron transfer, as in reactions (12), (14), or (15) above, the lifetime of the activated state will be expected to be long (10^{-11} sec) compared with time for transfer of an electron (10^{-16} sec). Hence, if the electron can be readily accepted by the activated reactants, the transition probability will be close to unity and the rate of deactivation back to initial reactants low. Hence, $k_2 \gg k_3'$, and the overall rate will be $k''nn'$. In some processes, the electron may *not* be readily accepted. In such cases $k_2 \ll k_3'$, and the overall rate will be $(k_2k_1''/k_3')nn'$. Such processes are termed "non-adiabatic" in the quantum mechanical sense and are discussed in a later section. For the case of purely chemical rate-determining steps, for example a surface recombination of two radicals, the chemical step may be very slow—it may, for example, involve surface diffusion to other sites. In such cases, the possibility of deactivation before reaction may again be high; reactions of this type will also be discussed in more detail in a later section.

2.2. Effect of Potential on Rate

Electrochemical reactions are characterized by potential-dependent rate constants. If we consider the sequence of reactions represented by (11)–(15), assuming for the moment (15) to be rate determining with a high transition probability, then, under some given conditions of Galvani potential (ϕ) the rate of (12) will be given by

$$r = (\mathrm{A}\{\mathrm{S}\})\rho k \exp\left[-E(\phi)/RT\right] \qquad (16)$$

where r is a rate constant, $[\mathrm{A}\{\mathrm{S}\}]$ is the concentration of reagents in the rate-determining step [i.e., the surface concentration of the complex formed in (11)], k is a number with the dimensions of a frequency, which expresses the rate of activation, and $E(\phi)$ is an Arrhenius activation energy at Galvani potential ϕ. ρ is a term representing some electron "concentration" within the electrode.

It will be noted above that, apart from ρ, the frequency factor is assumed not to depend on the Galvani potential, since it depends simply on some collisional or vibrational energy transfer from the liquid. We will attempt to test this hypothesis below, and at the same time, determine the standard potential at which electrode reaction rates should be compared.

Early work by Bockris and co-workers(7,8,26) first indicated a relationship between the log rate of the electrocatalytic hydrogen evolution reaction, which involves adsorbed atomic hydrogen intermediates, and the electronic work function over a series of metal electrodes. Since log rate is proportional to $(\log k) \times E(\phi)/RT$, we may express these terms in the form $\Delta G(\phi)^{\ddagger}/RT$, where $\Delta G(\Phi)^{\ddagger}$ is the free energy of activation at the Galvani potential ϕ. Let us define a standard free energy of activation, $\Delta G'^{\ddagger}$, to go from reactants to products in the rate-determining step, given by

$$\Delta G'\ddagger = \bar{\mu}^{\circ}(\text{trans}) - \bar{\mu}^{\circ}(\text{init}) \tag{17}$$

where $\bar{\mu}^{\circ}(\text{trans})$, $\bar{\mu}^{\circ}(\text{init})$ are the standard electrochemical potentials of the transition and initial states, respectively, as shown in Figure 1 for reaction (15). We can write

$$\bar{\mu}^{\circ}(\text{init}) = \bar{\mu}^{\circ}_{\text{A\{S\}}} + \mu_e - \phi_m F \tag{18}$$

$$\bar{\mu}^{\circ}(\text{trans}) = \mu^{\circ}(\text{trans}) + (1-q)\mu_e - qF\phi_d - (1-q)F\phi_m \tag{19}$$

where q is the fractional charge on the transition state and F is the Faraday, ϕ_m is the Galvani potential of the metal, and ϕ_d that of the zone in which the transition state occurs. We will use the conventional postulate that this is at the interface between the Helmholtz and diffuse double layers.

The potential V of a metal with respect to an independent reference electrode in the same solution may be expressed in the form[(27)]

$$V = m\Delta s\phi - m'\Delta s\phi + m'\Delta m\phi \tag{20}$$

where the $m\Delta s\phi$ terms are the Galvani potential differences across the various interfaces, and where m' represents the reference electrode metal. Since m, m' are in electronic contact, they are in electronic equilibrium, and

$$\bar{\mu}_e(m) = \bar{\mu}_e(m') \tag{21}$$

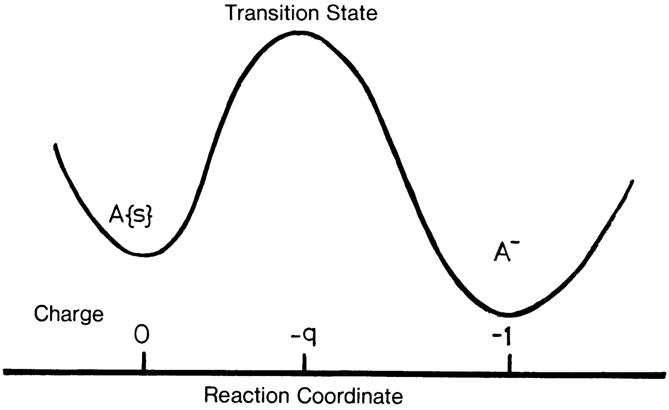

Figure 1. Charge change along reaction coordinate in a one-electron cathodic charge transfer process.

and

$$m'\Delta m\phi = [\mu_e(m') - \mu_e(m)]/F \tag{22}$$

i.e.,

$$\phi_s - \phi_m = s\Delta m\phi = -V - m'\Delta s\phi + [\mu_e(m') - \mu_e(m)]/F \tag{23}$$

Putting $\phi_s = \phi_d$ (i.e., ignoring the diffuse double layer(28) in concentrated solutions), then from Eqs. (18), (19), and (23),

$$\Delta G'^{\ddagger} = \mu^\circ(\text{trans}) - \mu^\circ_{A\{S\}} + qF[V + m'\Delta S\phi] - q\mu_e(m') \tag{24}$$

This contains no electron term for the electrode metal.

Based on the above argument, the electron free energy (or the work function) is therefore not the phenomenon lying behind the characteristic electrocatalytic properties of the electrode material. A number of arguments have been previously used in the literature to establish that the work function of the electrode at least *approximately* cancels out of the rate equation when the rates of a given electrocatalytic reaction are compared on different electrode materials under the same conditions at a potential measured with respect to some independent reference electrode.(14,29) In general, these have revolved around the use of the zero charge potential of the electrode ($V_{\text{p.z.c.}}$) as a reference point. At this potential, $s\Delta m\phi$ is equal to zero. The arguments have considered that $V_{\text{p.z.c.}}$ is approximately proportional to ϕ, where ϕ is the electrode metal work function under vacuum conditions. This is discussed in Ref. 30. It may be shown(27) that

$$V_{\text{p.z.c.}} = \Phi/F - \chi^s + \delta\chi + m'\Delta s\phi + \mu_e(m')/F \tag{25}$$

where χ^s, $\delta\chi$ are terms resulting from the location of electrode metal m in the electrolytic solution, χ^s being an energy term depending on the orientation of solvent dipoles, and $\delta\chi$ an energy term depending on electron overlap effects. $V_{\text{p.z.c.}}$ is therefore proportional to Φ provided that the χ terms are metal independent. The assumption that $\mu_e(m) = -\Phi$, as in Ref. 29, leads to a difficulty which is apparent when Eqs. (23) and (25) are compared. From Eq. (23), which is based on a valid thermodynamic and electrostatic argument

$$V_{\text{p.z.c.}} = \mu_e(m) - m'\Delta s\phi + \mu_e(m')/F \tag{26}$$

Hence, comparing Eqs. (25) and (26), it is clear that on the m' reference scale, $\chi^s + \delta x$ (representing the differences between χ^s, δx for m and m') is, in practice equal to zero, since the terms for m and m' cancel each other (cf. also the arguments in Ref. 29b and references quoted therein). Thus, there is no question(29c) that the mean free energy of the electrons in an electrode metal is not a factor in determining reaction rates at different metal electrodes, provided that these rates are measured in the same medium at a fixed potential against an independent reference electrode. This may, of course, conveniently be the reversible potential of the reaction being studied, i.e., that potential at which the free energy of the overall process is zero, so that the process has no net rate in either forward or reverse directions.

In general, therefore, the rates of the same electrocatalytic reaction on a series of electrode substrates should predominantly be given by the differences in the *chemical* potentials of the transition state $\mu^{\circ}_{\text{trans}}$ when rates are compared at the same reference potential. This is apparent from Eqs. (16), (17), and (24), and it is illustrated graphically for reaction (15), preceded by reaction (11), in Figure 2. This figure makes it clear that the standard free energy of activation in the rate-determining step will generally be different from the standard free energy of an *overall* process. This results from the standard free energy difference between the reactants in their primary state in the bulk solution and in their "catalyzed" state in the form of the complex prior to reaction in the rate-determining step.

The rate of the overall process is to be determined by looking at the system from the outside (reactants in bulk solution). The overall standard free energy of activation, $\Delta G^{\ddagger}$, is given by $\Delta G'^{\ddagger} + \Delta\Delta G^{\circ}$, where $\Delta\Delta G^{\circ}$ is the standard free energy change between the reactants in the bulk solution and in their state before the rate-determining barrier is crossed. This is discussed in detail in Section 3.

In the past, there has been some dispute as to the "zero potential" at which rates on different metals should be compared. Most early discussions centered around the use of the p.z.c. of the metal (Antropov, Ref. 31; Grahame, Ref. 32: the latter calling the scale "the rational potential scale"). Bockris and Potter(8) decided that the rates of the electrocatalytic hydrogen evolution reaction should be compared at the zero-charge potentials of different metals, because of the log rate—Φ correlations reported in Ref. 7. This comparison is not only difficult to make, on account of the general problem of accurately determining the p.z.c. values in most cases,(30) but, as shown above, is also not necessary. Indeed, it is clear that wide variations in

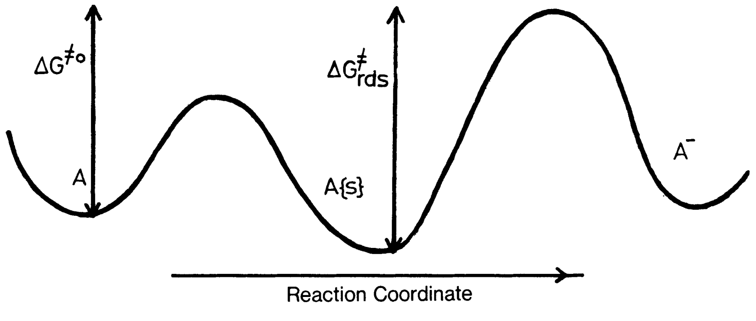

Figure 2. Standard free energy of activation ($\Delta G^{\ddagger\circ}$) for the overall process (left) and for the rate-determining step (rds) in a two-step cathodic one-electron transfer reaction involving adsorption.

rates observed on different metals for certain electrocatalytic processes at constant reference potential are not a direct result of the variation of the electronic work function, but are rather a result of a variation of the chemical potential of the "transition state," which itself is influenced by the same electronic factors which control the thermionic work function. In other words, the factors influencing the rates of catalytic reactions involving electron transfer are the same as those influencing purely chemical catalytic processes, the extra energy required to extract an electron from the electrode being cancelled out in the external electronic circuit.

A lack of appreciation of this fact caused occasional confusion in the electrochemical literature up to the early 1960s (cf. Refs. 6, 33: compare Refs. 9, 14, 28). If it should prove possible, it would be useful from a theoretical viewpoint to put the value of V in Eqs. (20), (23), and (24) on an *absolute* scale, so that the absolute values of $\mu^{\circ}_{\text{trans}}$ can be determined and compared with the values for purely chemical reactions under similar environmental conditions. It can be seen that this will be related to the effective Φ value of the reference electrode metal under working electrolyte conditions at its own p.z.c. [Eq. (24)]. Attempts have been made to determine this "absolute" potential scale.(27,29b)

Before discussing the purely chemical potential factors influencing the free energy of the transition state on different metals at a given potential V [Eq. (24)], we shall consider the fact that the rate-constant values [k in Eq. (16)] depend on potential (V on a reference scale) in processes where electron transfer is involved. It is clear from Eq. (24) that $\Delta G'^{\ddagger}$ depends on V, the standard reference potential. Using Eqs. (23) and (24), we obtain

$$\Delta G'^{\ddagger} = \mu^{\circ}_{\text{trans}} - \mu^{\circ}_{\text{A}\{\text{S}\}} - qF\phi_s - q[\mu_e(m) - F\phi_m] \tag{27}$$

where

$$\mu_e(m) - F\phi_m = \bar{\mu}_e(m) \tag{28}$$

$\Delta G'^{\ddagger}$ therefore depends on the Galvani potential of the metal, since we may assume for the moment that ϕ_s, the Galvani potential of the electrolytic solution close to the electrode surface, will be invariant. Since $\mu_e(m)$, the potential of electrons in the electrode at $\phi = 0$, is the Fermi level of the electrode, it is clear that $\Delta G'^{\ddagger}$ is a function of the change of Fermi level due to externally imposed changes in ϕ.

$\Delta G'^{\ddagger}$ is therefore strictly a standard electrochemical free energy of activation, $\overline{\Delta G}'^{\ddagger}$, defined so that $\overline{\Delta G}'^{\ddagger} = \Delta G^{\ddagger}$ at $\phi = 0$ for a given value of ϕ_s (i.e., in a given electrolyte). The most important characteristic of the variation of $\overline{\Delta G}'^{\ddagger}$ with ϕ is that the slope of the energy of activation vs. ϕ plot is equal to q. q represents the charge on the transition state complex, and in the case of reaction (15) it will vary along the reaction coordinate (the abscissa of Figure 1) from limiting values of 0 to 1. Figure 1 can be redrawn (Figure 3) to show this effect, where the reaction coordinate is now effectively the change

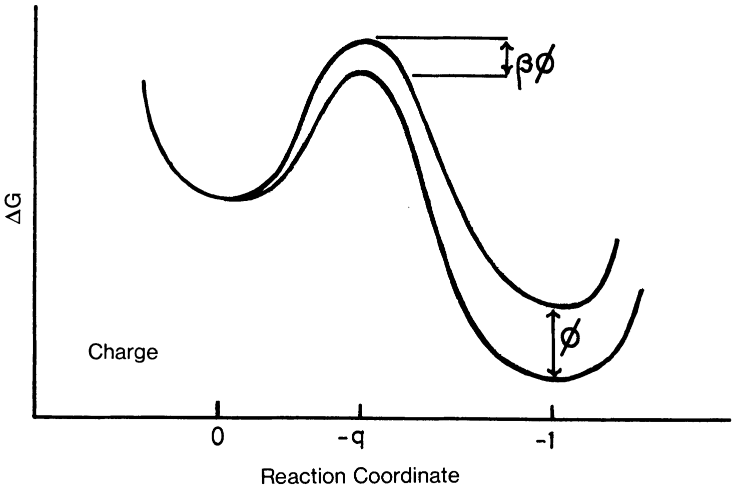

Figure 3. The effect of applied potential (ϕ) on the free energy of the transition state in an electrochemical process. The fraction β (the symmetry factor) is the same as q in Figure 1.

in charge as the system moves from reactants to products. The transition state, i.e., the free energy maximum of the system $A - \{S\} \rightarrow \{S\} + A^-$, as the A–{S} bond is geometrically reconfigured and the electron donated from the metal could, in principal, lie anywhere along the abscissa; however, for a symmetrical free energy barrier (which may be typical), $q \simeq 0.5$. Writing $q = \beta$, we therefore obtain in a given electrolyte

$$\Delta G'^{\ddagger} = \Delta G'^{\ddagger} + \beta F \phi_m \tag{29}$$

or alternatively

$$\Delta G'^{\ddagger} = \Delta G'^{\ddagger}(V = 0) + \beta F V \tag{30}$$

In the case of Eq. (30), the standard value of electrochemical free energy is defined at $V = 0$, where V is on a standard reference scale rather than on an absolute (Galvani) potential scale. β is normally called the "symmetry factor" of the electrode reaction.

The rate of reaction (15) may therefore be written in the form

$$r = [A\{S\}]\rho \exp(-\Delta G''/RT) \exp(-\beta F V/RT) \tag{31}$$

where $\Delta G'' = \overline{\Delta G'}^{\ddagger}(V = 0)$. ΔG_{act}, the overall free energy of activation at $V = 0$, is given by $\Delta G'' + \Delta\Delta G^{\circ}$, where

$$[A\{S\}] = [A][\{S\}] \exp(-\Delta\Delta G^{\circ}/RT) \tag{32}$$

where [A] is the solution value of A. r may be expressed in current density units by multiplying by the electronic charge if (31) is in molecule $\text{cm}^{-2}\,\text{sec}^{-1}$ units.

Equation (31) is of course a Langmuir isotherm, and Eqs. (31) and (32) give the overall rate of the process represented by reactions (14) and (15), i.e.,

$$r = [\text{A}][\{\text{S}\}]\rho \exp(-\Delta G_{\text{act}}/RT) \exp(-\beta FV/RT) \qquad (33)$$

Alternatively, we can write a further rate expression:

$$r = [\text{A}][\{\text{S}\}]\rho k \exp(-\Delta\Delta G^\circ/RT) \exp(-\beta FV/RT) \qquad (34)$$

where k is an equilibrium constant equal to $\exp(-\Delta\Delta G^\circ/RT)$ in (32). It is therefore clear that reactions proceeding before the rate-determining step can, in general, be represented as a series of equilibrium constants multiplying the rate equation for the rate-determining step, provided that their rates are rapid, in both directions, compared with that of the rate-determining step itself. In general, a tenfold difference in rate will allow a sufficiently good approximation. This effect will be examined in more detail in the next section.

If we now observe the situation, supposing that the rate-determining step (rds) is of the reaction (12) type, i.e., that the electron is transferred from the metal electrode to a particle adsorbed on its surface, which then does not desorb and go off into the bulk solution, the following conclusions are reached. Such a particle will only see a proportion of the total $\phi_s - \phi_m$ potential change. A change in ϕ_s will in this case only cause a fraction of the driving force change (i.e., change in $\overline{\Delta G'^{\ddagger}}$) as compared with the previous assumption. One possible reaction in which this may occur is in oxygen reduction under certain conditions, for example (34):

$$\text{O}_2 + \{\text{S}\} \rightarrow \text{O}_2\{\text{S}\} \qquad (35)$$

$$\text{O}_2\{\text{S}\} + \text{e}^- \rightarrow \text{O}_2^-\{\text{S}\} \quad \text{(rds)} \qquad (36)$$

In this case, we can suppose that, to a first approximation, the ion produced in the rds (O_2^-) is adsorbed at a distance from the electrode surface which is a constant (potential-dependent) fraction of the width of the Helmholtz double layer. Thus, in Eq. (19), we should multiply the fractional charge on the transition state by a further fraction, γ, which represents the fraction of $\phi_s - \phi_m$, seen by the adsorbed species on the electrode. Equation (31) will then effectively contain a term equal to $\beta\gamma$, rather than β. The value of the $V \sim \log i$ slope will then be $RT/\beta\gamma F$, rather than $RT/\beta F$, i.e., it will be considerably larger than $2RT/F$, assuming β to have a "typical" value of about 0.5.

Cases of this type have been discussed by Gnanamuthu and Petrocelli(35) and by Parsons.(14) Whether they actually occur in practice is another matter, since linear $V \sim \log i$ slopes for primary electron transfer reactions that are greater than $2RT/F$ (120 mV/decade at 298 K) are rarely observed in practice, except with processes at barrier layer oxide films. This observation would seem to indicate that steps involving a charge transfer to an adsorbed species at the electrode surface are rarely rate determining—when they occur, they are probably rapid reactions since the amount of bond ordering and electrostatic reordering around the adsorbed ion is likely to be relatively small. Since the concept of "reordering" of the local molecules near the reacting particle is the basis of the reaction activation energy in electron transfer processes, the corresponding activation energy is likely to be small, hence the rate relatively high. This is discussed again in detail in Section 4.(40)

Thus, such reactions will be unlikely to be rate determining. In fact, it would appear that their occurrence may be rather rare (whether rate determining or not) and that charge transfer steps will normally involve the complete transfer of electrons between the electrode and bulk solution species or vice versa. Hence, cathodic electrocatalytic reactions will normally involve electron transfer to an adsorbed species which desorbs in a reduced condition [cf. reaction (15)], or a bulk solution species which adsorbs on the electrode in a reduced form [reaction (14)]. For anodic processes, involving electron donation, the exact opposite will occur. Hence, the most probable types of electrocatalytic reactions involving rate-determining electron transfer are as follows:

$$\mathrm{A} + \{\mathrm{S}\} + \mathrm{e}^- \rightarrow \mathrm{A}^-\{\mathrm{S}\} \qquad \text{(cathodic)} \tag{37}$$

$$\mathrm{A}\{\mathrm{S}\} + \mathrm{e}^- \rightarrow \mathrm{A}^- \qquad \text{(cathodic)} \tag{38}$$

$$\mathrm{A}^- + \{\mathrm{S}\} \rightarrow \mathrm{A}\{\mathrm{S}\} + \mathrm{e}^- \qquad \text{(anodic)} \tag{39}$$

$$\mathrm{A}^-\{\mathrm{S}\} \rightarrow \mathrm{A} + \{\mathrm{S}\} + \mathrm{e}^- \qquad \text{(anodic)} \tag{40}$$

In all the above cases, the charge is transferred between the electrode and a species which is ultimately found or ultimately starts from outside the Helmholtz double layer. Of course, reactions involving electron transfer to or from adsorbed species may well occur in relatively complex reaction sequences. While they will be unlikely to be rate determining, they may be expected to influence reaction rates as a function of potential. Since the rate of the overall process may be described by the rate of the rds multiplied by the equilibrium constants for preceding rapid reactions, then, for cathodic processes involving a previous electron transfer, we can write

$$K(V) = K(V = 0) \exp(-nFV/RT) \tag{41}$$

where K is the equilibrium constant for the preceding steps at potential V on a standard reference scale, and K is the corresponding quantity at $V = 0$. n is the number of electrons transferred up to the rate-determining reaction steps. Overall, the rate equation will contain a term $\exp[-(n + \beta)FV/RT]$, where $(n + \beta)$ is α, the effective transfer coefficient (see below). It should be noted that n can be "partial," i.e., it may involve a single step in which charge is transferred over only a fractional part of the total double-layer distance, as was demonstrated above.

For example, if we consider a sequence of reactions involving an overall two-electron transfer,

$$\mathrm{A} + \{\mathrm{S}\} + (\mathrm{e}^-)\mathrm{A}\{\mathrm{S}\}^{\delta e^-} \tag{42}$$

$$\mathrm{A}\{\mathrm{S}\}^{\delta e^-} + (\mathrm{e}^-) \rightarrow \{\mathrm{S}\} + \mathrm{A} = \mathrm{rds} \tag{43}$$

in which the (δe^-) terms represent nonunit amounts of electronic charge transferred across the totality of the Helmholtz double layer, then using the same arguments as in Eqs. (18)–(24),

$$i = [\mathrm{A}\{\mathrm{S}\}^{\delta e^-}]K \exp - q\frac{FV}{RT} \tag{44}$$

However, since

$$[\mathrm{A}\{\mathrm{S}\}^{\delta e^-}] = [\mathrm{A}][\{\mathrm{S}\}]K(V = 0) \exp - \frac{\delta FV}{RT}$$

overall, we obtain

$$i = [\mathrm{A}][\{\mathrm{S}\}]K(V = 0) \exp\left[-\frac{(q + \delta)FV}{RT}\right] \tag{45}$$

where q, as before, is the effective change in charge on the transition state. Clearly, if $q \simeq \frac{1}{2}$, as in the previous discussion, the overall value of the transfer coefficient will deviate from that determined following Eq. (41), for a one-electron rapid process preceding a one-electron rate-determining step, for which $n = 1$ and $\beta \simeq \frac{1}{2}$, giving a transfer coefficient $\alpha \simeq 1.5$. In this case, for a rate-determining one-electron transfer step following a partial charge transfer, α would be expected to be substantially less than 1.5.

However, a further examination shows that higher values are more probable. The overall stoichiometry of the reaction indicates that the initial state of the rate-determining step should start off with the charge $-\delta$ $(\delta < 1)$, the final state in the bulk solution having a charge of -2. The overall change of charge on the transition state as it goes from charge $-\delta$ to -2, assuming it to have a structure roughly midway between that of the initial and final states, will be on the order of $-[(2 - \delta)/2]$.

This is shown in diagrammatic form in Figure 3, and is equal to the q value of Eq. (45). The overall transfer coefficient will therefore be equal to $q + \delta$ or $1 + \delta/2$. If we consider δ equal to, say, 0.6, this would be 1.3 overall, rather than 1.1 if q is considered to have the "normal" value of 0.5. Such a process would lead to Tafel slopes in the range 45–50 mV/decade at ordinary temperatures ($\alpha \simeq 1.25$ or 1.3), rather than the expected value of 40 mV/decade for a rate-limiting one-electron transfer, following a complete reversible preceding charge transfer step. If q is assumed to be 0.5, with $\delta \simeq 0.6$, the corresponding value would be about 50 mV/decade.

It is indeed possible that, even following a partial charge transfer, the reaction proceeds in stages, i.e., that a rapid relaxation of the double layer occurs before the rate-determining second electron transfer step can occur. If this possibility exists, the net result should be a lower activation energy for rate-determining charge transfer process, since the net charge to be transferred is lower.

The theoretical basis for this is discussed in Section 4 where, in particular, the improbability of simultaneous two-electron transfers will be stressed. In fact, increasing complexity of individual steps (i.e., steps involving multi-ion and/or multielectron transfer) will render them increasingly improbable, so that all reactions will be expected to proceed via steps involving only one bond breaking and/or forming event at a time. This stepwise progression, on the "Occam's razor" principle, will result in the highest possible overall rate since the successive activation energy barriers will be lowest if the process proceeds in this manner, despite the increasing number of overall steps involved. This has important implications in complex electrocatalytic processes, particularly in oxygen reduction and in the electro-oxidation of organic molecules. These will be considered in more detail in a later section. In this respect, there is a strong resemblance between electrocatalytic and heterogeneous catalytic processes.(36)

As a final point in this section, we may consider the effect of the diffuse double layer on rates of reactions. This results from the fact that the value of the Galvani potential difference ($d\Delta\phi s$) between the outer Helmholtz plane and the bulk solution depends on the total metal–solution Galvani potential difference.(37) In turn, the concentration of ionic reactants (and products) will change at the outer Helmholtz plane due to this potential difference. As shown in Ref. 38, this will make a small difference to the rates of reactions at constant potential over a range of metals, since [Eq. (25)] the $m\Delta\phi s$ value depends on metal work function. According to Grahame and Soderberg's results on mercury in $1\,M$ SO_4^{2-} the $\partial(m\Delta\phi s)/\partial\Phi$ slope is linear and equal to about -0.12.(39) Hence, since from Ref. 40,

$$C_d = C_b \exp(-z(d\Delta\phi s)F/RT) \tag{46}$$

where C_d, C_b are the outer Helmholtz plane and bulk concentrations of a reacting ion of charge z, then the rate of a reaction at constant potential would be expected to vary with Φ of the electrode metal (using the data in Ref. 38) by an amount equal to about +1 decade/V for $z = +1$ (i.e., $\partial \log_{10} i/\partial\Phi \simeq +z$). For univalent positive ions (e.g., protons) a rate change of about a factor of 2–3 would be expected over the noble metals due to this effect, the change being less in concentrated solutions. It is, therefore, certainly an effect of second order, but it should be borne in mind that, in any rate correlations with other properties affecting bonding of intermediates, it may result in some small perturbations.

3. The Rates of Complex Processes

In the previous section, we have referred to the way in which the overall rate of the reaction depends on the chemical potential of the transition state when rates for identical processes are compared under identical conditions on different substrates. It was also implied that an equilibrium could be assumed between processes taking place before the rate-determining step in simple cases. This concept will be examined in more detail in this section for the case of more complex processes in which parallel reaction pathways can and do occur. One of the most characteristic (and one of the simplest and most studied) of such processes is that of hydrogen evolution, where three possible steps involving adsorbed species are generally considered to occur.(41) These are known respectively as the discharge or Volmer process, the electrochemical desorption or Heyrovsky process, and the hydrogen atom combination (Tafel) reaction, as follows (written in the cathodic direction):

$$H^+ + e^- \rightarrow H_{ads} \tag{47}$$

$$H^+ + H_{ads} + e^- \rightarrow H_2 \tag{48}$$

$$2H_{ads} \rightarrow H_2 \tag{49}$$

The first two are electron transfer steps, the third chemical. All of the above can, in principle, contribute to the rate of the overall process. In general, however, a combination of any two will predominate. Since the rate constant of (49) is independent of potential, whereas the rate constants of the other two are potential dependent, the pair of reactions predominating may change as the potential is varied on any given surface. The rates of the individual processes will be given by the expressions

$$r_1 = [H^+](1-\theta)\vec{k}_1 - \theta\overleftarrow{k}_1 \tag{50}$$

$$r_2 = [H^+]\vec{k}_2 - p_{H_2}(1-\theta)\overleftarrow{k}_2 \tag{51}$$

$$r_3 = \theta^2\vec{k}_3 - p_{H_2}(1-\theta)^2\overleftarrow{k}_3 \tag{52}$$

where θ is the coverage with H_{ads} and the k's are the respective forward and backward rate constants for the formation or removal of one H_{ads}. Without making any initial assumptions as to which pair of processes predominates, it is possible to derive the equilibrium coverage (θ) under dynamic conditions and hence the overall rate of the reaction. This calculation was first performed by Bockris and Mauser.(42) The overall reaction rate

$$(-d[H^+]/dt) \qquad \text{or} \qquad (+\tfrac{1}{2}dp_{H_2}/dt)$$

will be given by

$$-d[\mathrm{H}^+]/dt = [H^+](1-\theta)\vec{k}_1 - \theta(\overleftarrow{k}_1 - [\mathrm{H}^+]\vec{k}_2) - (1-\theta)p_{H_2}\overleftarrow{k}_2 \tag{53}$$

In the steady state, we may assume, as usual, that $d\theta/dt = 0$. This gives us, in the general case,

$$(\overrightarrow{k}_3 - [\mathrm{H}_2]\overleftarrow{k}_3)\theta^2 + (p_{\mathrm{H}_2}\overrightarrow{k}_1 + \overleftarrow{k}_1 + p_{\mathrm{H}_2}\overrightarrow{k}_2 + p_{\mathrm{H}_2}\overleftarrow{k}_2 + 2p_{\mathrm{H}_2}\overleftarrow{k}_3)\theta$$
$$-([\mathrm{H}^+]\overrightarrow{k}_1 + p_{\mathrm{H}_2}\overleftarrow{k}_2 + p_{\mathrm{H}_2}\overleftarrow{k}_3) = 0 \tag{54}$$

The real solution to this quadratic gives a general expression for θ, but it is not very useful unless certain simplifying assumptions are made. The simplest of these assumptions is to regard the process as taking place in a potential region where the combination reaction is unimportant, i.e., to ignore $\overrightarrow{k}_3$ and $P_{\mathrm{H}_2}\overleftarrow{k}_3$ compared with the other rate terms. We then obtain:

$$\theta = \left(1 + \frac{\overleftarrow{k}_1 + [\mathrm{H}^+]\overrightarrow{k}_2}{[\mathrm{H}^+]\overrightarrow{k}_1 + p_{\mathrm{H}_2}\overleftarrow{k}_2}\right)^{-1} \tag{55}$$

Using Eq. (54), and counting the cathodic direction positive, the overall rate is then equal to

$$r = 2\left(\frac{[\mathrm{H}^+]^2\overrightarrow{k}_1\overrightarrow{k}_2 - p_{\mathrm{H}_2}\overleftarrow{k}_1\overleftarrow{k}_2}{[\mathrm{H}^+]\overrightarrow{k}_1 + \overleftarrow{k}_1 + [\mathrm{H}^+]\overrightarrow{k}_2 + p_{\mathrm{H}_2}\overleftarrow{k}_2}\right) \tag{56}$$

This refers to all possible combinations of reactions (47) and (48), in both forward and backward directions, and where the factor 2 arises from the stoichiometry of the overall process. We can now make some specific assumptions regarding the rates of the individual steps. If reaction (48) is rate determining in the cathodic direction, we may ignore the backreaction in (51) and write $\overrightarrow{k}_1 \gg \overrightarrow{k}_2$, so that

$$r = \frac{2[\mathrm{H}^+]\overrightarrow{k}_2}{1 + \overleftarrow{k}_1/[\mathrm{H}^+]\overrightarrow{k}_1} \tag{57}$$

Thus, if $[\mathrm{H}^+]\overrightarrow{k}_1$ is large compared with $\overleftarrow{k}_1$,

$$r \simeq 2[\mathrm{H}^+]\overrightarrow{k}_2 \tag{58}$$

and, from Eq. (55), $\theta \simeq 1$, i.e., the reaction is proceeding at high coverage. This will apparently, therefore, be the normal situation if reaction (48) is rate determining, in the absence of reaction (49), under sufficiently cathodic conditions. A more general expression, where we do not make the above simplifying rate assumption, will be

$$r = \frac{2[\mathrm{H}^+]\overrightarrow{k}_2}{1 + \overleftarrow{k}_1/[\mathrm{H}^+]\overrightarrow{k}_1 + \overrightarrow{k}_2/\overrightarrow{k}_1} \tag{59}$$

However, this will be always essentially the same as Eq. (57) since, by definition, the ratio $\overrightarrow{k}_2/\overrightarrow{k}_1$ will be small when reaction (48) is rate determining. We can consider the weak adsorption case where $\overleftarrow{k}_1$ is large compared with $[\mathrm{H}^+]\overrightarrow{k}_1$

[though this is unlikely at cathodic overpotentials, due to the exp $(1 - \beta)F\eta/RT$, exp $(-\beta F\eta/RT)$ multipliers contained in $\overleftarrow{k}_1$, $\vec{k}_1$, respectively]. The overall rate would be given by

$$r = \frac{2[\mathrm{H}^+]\vec{k}_2}{1 + \overleftarrow{k}/[\mathrm{H}^+]\vec{k}_1} \simeq \frac{2[\mathrm{H}^+]^2\vec{k}_1\vec{k}_2}{\overleftarrow{k}_1} \tag{60}$$

$$= 2\mathrm{K}_1[\mathrm{H}^+]\vec{k}_2 \tag{61}$$

where K_1 is the equilibrium constant of step (47). This is, of course, the equivalent of assuming that the rate simplifies to $\theta[\mathrm{H}^+]k_2$ overall, since if $\overleftarrow{k}_1 > [\mathrm{H}^+]\vec{k}_1$, from Eq. (55), θ is small. Using the same argument, we can suppose that $\theta \to 1$, and then Eq. (58) will result. However, this argument throws less light on which process is likely to be the most probable as the individual rate constants (and θ values) change.

Using similar reasoning to that given above, the rate of the overall process, with reaction (47) rate determining and reaction (48) rapid, will be given by

$$r = \frac{[\mathrm{H}^+]\vec{k}_1}{1 + \vec{k}_1/\vec{k}_2 + p_{\mathrm{H}_2}\overleftarrow{k}_2/[\mathrm{H}^+]\vec{k}_2} \tag{62}$$

The final term in the denominator is normally small at high overpotentials (low coverage conditions), and $\vec{k}_1/\vec{k}_2$ will also be small. Hence, the most probable rate-determining step will be reaction (47) under low-coverage conditions, and the rate will be

$$r = 2[\mathrm{H}^+]\vec{k}_1 \tag{63}$$

where 2 is inserted for the stoichiometry of the complete process.

It should be noted that the rate expressions under high-coverage conditions are zero order in reactants, as in the chemical catalysis case [Eq. (10)], whereas at low coverage the reaction has the correct (expected) chemical reaction orders (under conditions where diffuse layer effect are invariant). The most probable cases [reaction (47) rate determining, low coverage, and reaction (48) rate determining, high coverage] have rates that depend on $\vec{k}_1$, $\vec{k}_2$, respectively, and will therefore have the same potential dependence, log rate/V being $-2RT/F$ with $\beta \sim 0.5$. The high-coverage [reaction (47)] case, and the low-coverage [reaction (48)] case, if they occur, will show a dependence of $-RT/(1 + \beta)F$. This results from the K and $\vec{k}$ terms, since K will vary as exp $(-FV/RT)$ and $\vec{k}$ as exp $(-FV/\beta RT)$.

In the anodic direction, a similar analysis shows that the situation will be reversed compared with the above. The most probable rate-determining steps will be reaction (47), this time under high-coverage conditions, or reaction (48) under low-coverage conditions. The respective rates will be given by

$$r = \frac{\overleftarrow{k}_1}{1 + [\mathrm{H}^+]\vec{k}_2/p_{\mathrm{H}_2}\overleftarrow{k}_2} \simeq \overleftarrow{k}_1(\theta \to 1) \tag{64}$$

$$r = \frac{p_{\mathrm{H}_2}\overleftarrow{k}_2}{1 + [\mathrm{H}^+]\overrightarrow{k}_1/\overleftarrow{k}_1} \simeq p_{\mathrm{H}_2}\overleftarrow{k}_2(\theta \to 0) \tag{65}$$

where the θ values are obtained by simplification of Eq. (55). Again, reaction orders are zero under high-coverage conditions.

If we now consider the situation for sequences in which reaction (49) participates, then a similar analysis to the above shows if reaction (49) is rate determining in the cathodic direction:

$$r \simeq \theta^2\overrightarrow{k}_3 = \frac{\overrightarrow{k}_3}{[1 + (\overleftarrow{k}_1 + [\mathrm{H}^+]\overrightarrow{k}_2)/([\mathrm{H}^+]\overrightarrow{k}_1 + p_{\mathrm{H}_2}\overleftarrow{k}_2)]^2} \tag{66}$$

The value of the θ^2 term may be high or low, depending on the relative k_1, k_2 values. If the predominant rapid process is (47), then $[\mathrm{H}^+]\overrightarrow{k}_1 \gg p_{\mathrm{H}_2}\overleftarrow{k}_2$, and $\overrightarrow{k}_1 > \overrightarrow{k}_2$, hence

$$\theta \simeq [1 + \overleftarrow{k}_1/[\mathrm{H}^+]\overrightarrow{k}_1]^{-1} \tag{67}$$

Since, under sufficiently cathodic conditions, $\overleftarrow{k}_1 < [\mathrm{H}^+]\overrightarrow{k}_1$, i.e., $\theta \to 1$, the rate will be $\overrightarrow{k}_3$, again zero order in reactants and with zero potential dependence. If process (48) predominates, a similar argument shows that

$$r = \overrightarrow{k}_3/(1 + [\mathrm{H}^+]\overrightarrow{k}_2/p_{\mathrm{H}_2}\overleftarrow{k}_2)^2 \tag{68}$$

$$\simeq (p_{\mathrm{H}_2})^2/[\mathrm{H}^+]^2(\overleftarrow{k}_2/\overrightarrow{k}_2)^2\overrightarrow{k}_3 \tag{69}$$

This time the reaction orders are as expected and the potential dependence, given by the $(\overleftarrow{k}_2/\overrightarrow{k}_2)^2$ term, will be $\exp[+2FV/RT]$, i.e., the process will become *less* rapid with increasing overpotential. The combination of processes (49) rate determining, (48) rapid will therefore be improbable. In any case, since $\overleftarrow{k}_2 < \overrightarrow{k}_2$ under sufficiently cathodic conditions, (69) will always be slow and will be rapidly overtaken by a combination of reactions (47) and (48) as overpotential increases.

In the anodic direction, the opposite will again occur. If the predominant process is (47),

$$\theta \simeq [1 + \overleftarrow{k}_1/[\mathrm{H}^+]\overrightarrow{k}_1]^{-1} \qquad \text{with } \overleftarrow{k}_1 > [\mathrm{H}^+]\overrightarrow{k}_1,$$

hence, $\theta \to 0$. The rate will then be

$$r = p_{\mathrm{H}_2}\overleftarrow{k}_3 \tag{70}$$

with normal reaction orders and no potential dependence. If (48) predominates,

$$\theta \simeq [1 + [\mathrm{H}^+]\overrightarrow{k}_2/p_{\mathrm{H}_2}\overleftarrow{k}_2]^{-1} \simeq 1$$

The $(1 - \theta)^2$ term in (52) will thus be equal to

$$(1 - \theta)^2 = \left(\frac{[\mathrm{H}^+]\overrightarrow{k}_2/p_{\mathrm{H}_2}\overleftarrow{k}_2}{1 + [\mathrm{H}^+]\overrightarrow{k}_2/p_{\mathrm{H}_2}\overleftarrow{k}_2}\right)^2 \tag{71}$$

$$\simeq ([\mathrm{H}^+]\overrightarrow{k}_2/p_{\mathrm{H}_2}\overleftarrow{k}_2)^2 \tag{72}$$

and the rate will be

$$r = ([\mathrm{H}^+]/p_{\mathrm{H}_2})(\vec{k}_2/\overleftarrow{k}_2)^2\overleftarrow{k}_3 \tag{73}$$

where the chemical reaction orders arise from the $(1 - \theta)$ term. The potential dependence, arising from the $(\vec{k}_2/\overleftarrow{k})^2$ term, will be $\exp[-2FV/RT]$. It is again clear that the condition reaction (49) rate determining, with reaction (48) rapid, will be unlikely, since r in Eq. (70) will always have a value greater than in Eq. (73) under sufficiently anodic conditions. In any case, the rate in Eq. (70) will be rapidly overtaken by the combination of reactions (47) and (49), owing to their log rate $\vartheta_s V$ dependence. Hence, the most probable combinations will be (cathodic) $r = \vec{k}_3$, $\theta \rightarrow 1$, with reaction (47) in quasiequilibrium; (anodic) $r = p_{\mathrm{H}_2}\overleftarrow{k}_3$, again with reaction (47) in pseudoequilibrium, and only at relatively small overpotentials.

Finally, we can consider the case where reaction (49) is rapid with either reaction (47) or (48) rate determining. Solution of the quadratic Eq. (54) shows that

$$\theta \simeq [(\vec{k}_3/p_{\mathrm{H}_2}\overleftarrow{k}_3)^{-1/2} + 1]^{-1} \tag{74}$$

The corresponding cathodic rates will be (a) with reaction (47) rate determining,

$$\vec{k}_3 > p_{\mathrm{H}_2}\overleftarrow{k}_3 \qquad \text{(weak adsorption)}$$

$$r = 2[\mathrm{H}^+]\vec{k}_1 \tag{75}$$

$$\vec{k} < p_{\mathrm{H}_2}\overleftarrow{k}_3 \qquad \text{(strong adsorption)}$$

$$(1 - \theta) \simeq (\vec{k}_3/p_{\mathrm{H}_2}\overleftarrow{k}_3)^{1/2} \tag{76}$$

$$r = 2(\vec{k}_3/p_{\mathrm{H}_2}\overleftarrow{k}_3)^{1/2}[\mathrm{H}^+]\vec{k}_1 \tag{77}$$

with reaction (48) rate determining, the corresponding values will be

$$r = 2(\vec{k}_3/p_{\mathrm{H}_2}\overleftarrow{k}_3)^{-1/2}[\mathrm{H}^+]\vec{k}_2 \tag{78}$$

and

$$r = 2[\mathrm{H}^+]\vec{k}_2 \tag{79}$$

We should note that Eq. (75) is identical with Eq. (63), i.e., for the rate of reaction (47) occurring under low-coverage conditions with reaction (48) in equilibrium. Since at sufficiently cathodic overpotentials $\vec{k}_2 > \vec{k}_3$, owing to the $\exp[-\beta FV/RT]$ term in $\vec{k}_2$, the rate of reaction (48) will always overtake that of reaction (49), and the overall process will exhibit a transition from (47) rds, (49) in quasiequilibrium to (47) rds, or (48) in quasiequilibrium (low-coverage conditions). Similarly, under high-coverage conditions, Eq. (79) is identical in form to Eq. (58), and the process will exhibit a transition from reaction (48) rds, (49) in quasiequilibrium to reaction (48) rds, (47) in quasiequilibrium. The corresponding anodic cases can easily be evaluated: they will transition to reaction (47) rds (high coverage); reaction (48) in quasiequilibrium, reaction (48) rds (low coverage); reaction (47) in quasiequilibrium at sufficiently high anodic overpotentials. Reaction (49) in quasiequilibrium (when it can occur) would only therefore be expected over a rather limited overpotential range.

Despite the apparent complexity of the hydrogen reaction scheme given above, it is still comparatively simple compared with many important electrocatalytic processes, particularly oxygen reduction and hydrocarbon oxidation. Only one intermediate (H_{ads}) is postulated to be involved, though it occurs in a rather complex manner as either the product or reactant in two electrochemical steps, or as a reactant (in the cathodic direction) in a chemical step. This is clearly an oversimplification, since it has often been supposed that other intermediates, e.g., H_2^+, may be involved as short-lifetime species.(43) In addition, other problems can arise, for example, the fact that several states of adsorbed hydrogen may occur on a number of metals. This is particularly apparent in the case of platinum.(44)

Such effects will clearly complicate the course of the reaction from that given above, since the mobility and adsorption of the species differ. The most active species may well be that which is the weakest adsorbed, at least in the case of platinum, as the arguments in the next section will show. The consequence of this will be that the θ value in the previous equations will be some effective value, rather than the total surface fraction used above. In addition, this will render the combination reaction events somewhat less probable, since the probability of finding two suitably adsorbed H atoms on neighboring sites will be reduced.

In principle, any complex process can be analyzed in the manner indicated above, though the generalized expressions for the rates will become increasingly complex as the number of intermediates and steps increases. This will be particularly true for multielectron processes, of which one of the simplest is oxygen reduction involving overall four electrons and (in acid solutions) four protons per oxygen molecule. The latter can be imagined to be a specialized site when it is adsorbed on the electrode surface, onto which successive proton transfers occur. In fact, the majority of electrocatalytic processes involving oxidation or reduction in aqueous systems involve simultaneous electron and proton transfer steps, though some reactions of importance are exceptions, e.g., Cl^- discharge to form Cl_2.(44a)

The complexity of some of these processes can be illustrated by the free energy "map" (Figure 4) for the oxygen reduction process (for acidic solutions). One axis represents changes involving only the O–O bond, the other changes involving O–H bonds; the actual path followed will depend on the heights of the energy barriers between possible intermediates. As already remarked, the simplest steps (usually involving single electron–proton transfers) are likely to show the lowest activation energies, and these will be involved in the preferred pathways. In general, a number of different adsorbed oxygen species will be present, which must be taken into account in the rate equations. True oxides may also be present; thus the competition for suitable

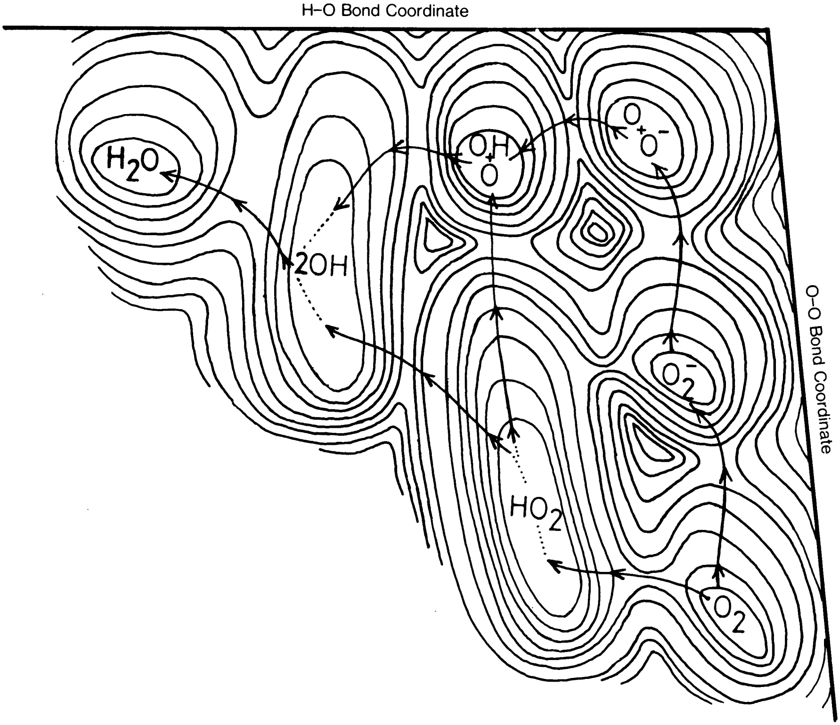

Figure 4. Energy "map" for various possible pathways for a complex process (dioxygen reduction in acid solution), as a function of O–O and H–O bond coordinates, admitting only single sequential electron transfer, electron–atom transfer, or atom transfer steps.

sites will be considerably greater than in the simple case of the hydrogen reaction. A further factor must also be considered: the fact that the effective bond strengths of noble metal oxygen bonds are "time dependent"(46) (owing to oxide film reconstruction processes). As shown in the next section, this will affect the rate constants of slow processes. These factors (complexity, number of intermediates, time dependence of adsorption reactions to give irreversibly adsorbed intermediates) all contribute to rates that are much lower for the oxygen reduction process than for the hydrogen reactions on the same substrate. Typically, the ratio of rates may be 10^8. Rates are similarly low for organic oxidation processes. This will be discussed in more detail in the following section.

4. Potential Energy Diagrams and Electrocatalysis

4.1. General

As shown above, we can generally assume that processes involving adsorbed reactants can be written with the rate of the rate-determining step multiplied by a series of equilibrium constants calculated of Langmuir absorption of intermediates under high- or low-coverage conditions. Taking one low-coverage case,

$$r = \theta\kappa = \prod [\mathrm{R}]K\kappa \tag{80}$$

where [R] is the concentration of reactants in the bulk solution, K is the equilibrium constant for the formation of intermediates, and κ is the rate constant of the rate-determining step. Under high-coverage conditions, the corresponding expression will be (for the sample case of a unimolecular adsorbate in one rate-determining step):

$$r \approx \frac{\prod [\mathrm{R}]K\kappa}{1 + \prod [\mathrm{R}]K} \approx \kappa \tag{81}$$

We must now examine the change in κ as K (i.e., $\exp[-\Delta G_{\mathrm{ads}}(RT)]$ changes. Figure 5 shows the situation involved in the form of ΔH_{ads} (approximate potential energy) and ΔG_{ads} diagrams, both for adsorbed reactants and products. If the ground states change because of adsorption, then provided the curves do not change in shape or relative position owing to the effects of this change in ground state, displacements in the ground state of reactants in the rate-determining step will result in displacements in the intersection point of the energy curves of reactants and products, as shown in Figure 5. Simple geometric considerations show that for small displacements, this change will be $\beta \Delta H_{\mathrm{ads}}$ for reactants, where the height of the barrier as seen by the adsorbed species *increases* with increasing degree of adsorption (see Figure 5). Similarly, the barrier height for the adsorption of products will *decrease* as seen by the reactants, by an amount equal to $-\beta \Delta H_{\mathrm{ads}}$. If we can assume that the lines of the energy curves are, to a good approximation, straight near the point of intersection, then β will be approximately constant over a wide range of ΔH_{ads}. The heights of the barriers—i.e., the activation energies—will

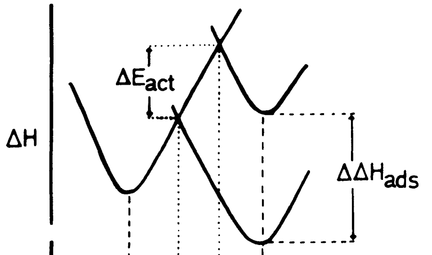

Figure 5. Effect of heat adsorption ($\Delta\Delta H_{\mathrm{ads}}$) in reducing activation energy by ΔE_{act} of electrocatalytic reaction. Entropy change along reaction coordinate also shown.

therefore depend fractionally on the heats of adsorption of reactants and products in the rate-determining step, giving a roughly linear relationship. This is one of the oldest concepts in catalysis (cf. Brønsted, Ref. 45), and was first considered in electrochemistry (the hydrogen evolution reaction) by Horiuti and Polanyi.(47)

In order to determine the effect of this activation energy term on the overall rate of reaction, we must also consider the effect of the change in the $T\Delta S$ term as the system moves from reactants to products. Normally, this is a factor which has been largely ignored in most analyses of reaction rates. However, in many reactions involving adsorbed species, the change in entropy as the system moves from reactants to products in any given step may be quite considerable, since as bonds form or break, and solvational changes occur with ions, changes in activated vibrational or translational energies would be expected. Whether the $T\Delta S$ term will go through a maximum is unclear, but it seems improbable, since in the normal transition state formulation of reaction rates,(48) all partition function changes taking place along the axis of the reaction coordinate are conventionally represented by a classical frequency factor, kT/h, which is identical for all processes, whereas the off-axis changes can be expected to involve gradual vibrational–translational loosening or tightening as the system passes from reactants to products. The $T\Delta S$ surface, as a function of distance along the reaction coordinate, may well, therefore, change in a somewhat linear manner, without exhibiting a maximum (Figure 5). ΔG_{ads} changes will, therefore, be expected to follow the same rule as ΔH_{ads} changes, and affect the overall reaction rate in a similar manner. This implies that, since the intersection point of the potential energy curves (or, to a first approximation, the ΔH curves) for reactants and products of the rate-determining step has a position on the reaction coordinate axis which varies with ΔH_{ads}, then the entropy of the configuration at the point of intersection may also vary with ΔH_{ads}. This has some important potential consequences,(19,49) which will be considered later in the discussion of the oxygen electrode reaction.

In general, using the above highly simplified approach, we can write k in the form

$$\kappa = \kappa' \exp(+\beta \Delta G^{R}_{\text{ads}}/RT) \exp(-\beta \Delta G^{P}_{\text{ads}}/RT) \tag{82}$$

where the R, P values refer to adsorbed reactants and products, respectively, and where κ' is a rate constant value under conditions of zero adsorption ($\Delta G^{R,P}_{\text{ads}} = 0$). κ' will thus be a substrate-independent quantity. We will show below that the ΔG_{ads} values in (82) are expressed at constant ϕ or V, i.e., they represent the change in the chemical potential of the transition state discussed in Section 2. If the $T\Delta S$ change can be ignored, then the ΔG_{ads} values can be replaced by ΔH_{ads} values, or by the (negative) bond strength values of reactants and products, if these are known.

If we now put K in Eq. (80) equal to $\exp(-\Delta G_{\mathrm{ads}}/RT)$, then from Eqs. (80) and (82):

$$r = \prod[\mathrm{R}]k' \exp[-1-\beta)\Delta G^{\mathrm{R}}_{\mathrm{ads}}/RT]\exp(-\beta\Delta G^{\mathrm{P}}_{\mathrm{ads}}/RT) \tag{83}$$

for the low-coverage case (for both reactants and products). It can be seen from this expression that, under low-coverage conditions, adsorption of both reactants and products increases the rate of the overall process, the $\log r \simeq \Delta G_{\mathrm{ads}}$ slopes being $-(1-\beta)$ for reactants, and $-\beta$ for products, respectively. These slopes are normally called the Brønsted coefficients, and, as we shall see below, β will generally be equal to the corresponding electrochemical symmetry factor for adsorption of one reactant molecule and/or one product molecule. Under high-coverage conditions, we must write for the general case of this type:

$$\theta^R = \prod[\mathrm{R}](1-\theta^R-\theta^P)\exp(-\overline{\Delta G}^R_{\mathrm{ads}}/RT) \tag{84}$$

where θ^{P}, the coverage with reaction product under dynamic conditions, must be calculated by using the steady state assumption. However, ignoring the back reaction in the rate-determining step (a reasonable supposition), we can simply assume that θ^P is in equilibrium with reaction products, i.e.,

$$\theta^R = \prod[\mathrm{P}](1-\theta^R-\theta^P)\exp(-\overline{\Delta G}^P_{\mathrm{ads}}/RT) \tag{85}$$

Solving the simultaneous Eqs. (84) and (85), we find that $(1-\theta^R-\theta^P)$, the site availability term in the overall rate equation, is

$$[1+\prod[\mathrm{R}]\exp(-\Delta G^R_{\mathrm{ads}}/RT)+\prod[\mathrm{P}]\exp(-\Delta G^P_{\mathrm{ads}}/RT)]^{-1}$$

Hence, the rate under high-coverage conditions must be multiplied by this factor. If the reactant is under high-coverage conditions, Eq. (83) becomes

$$r = K'\exp(\beta\Delta G^R_{\mathrm{ads}}/RT)\exp(-\beta\Delta G^P_{\mathrm{ads}}/RT) \tag{86}$$

which, as expected, is zero order in reactants and has a $\log r/\Delta G^R_{\mathrm{ads}}$ slope of $+\beta$. If the *product* is under high-coverage conditions,

$$r = \prod[\mathrm{R}]K'\exp[-(1-\beta)\Delta G^R_{\mathrm{ads}}/RT]\times\prod[\mathrm{P}]^{-1}\exp(1-\beta)\Delta G^P_{\mathrm{ads}}/RT] \tag{87}$$

Hence, under conditions of high coverage by reaction products, the rate of overall reaction will not only contain the $\prod[\mathrm{P}]$ term as a *negative* reaction order, but the $\log r/\Delta G^P_{\mathrm{ads}}$ slope will be $(1-\beta)$. Similar arguments show that the transfer coefficients will be (low-coverage) $(n+\beta)$; (high-coverage reactants) β; (high-coverage products) $(n'+\beta)$, where n, n' are the number of electrons transferred before and after each *unit* rate-determining step to complete the whole process.† The corresponding free energy profiles for these hypothetical mechanisms are given in Figure 6.

† $n+n'+1=N/\nu$, where N is the number of electrons transferred in the overall process and ν, the stoichiometric number, is the number of times the rate-determining step occurs in the overall process. α, the "transfer coefficient," is $n+\beta$ in the cathodic direction at low coverage.

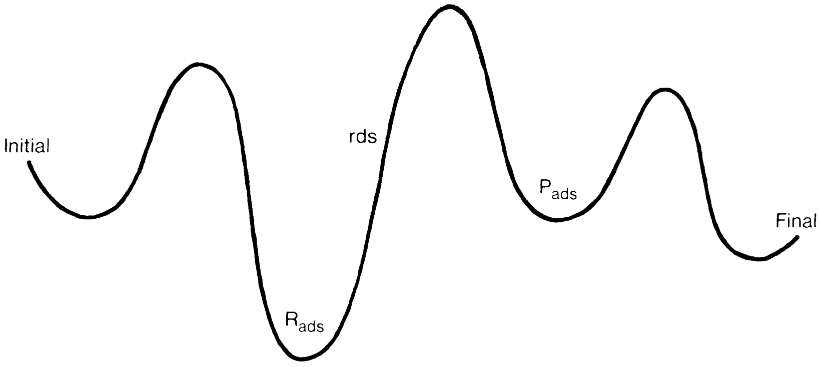

Figure 6. Energy profile in a complex process involving adsorption reactants (R_{ads}) and products (P_{ads}) in rate-determining step (rds).

From the above discussion, it is clear that various kinetic criteria (reaction orders, Tafel slopes, and log i–ΔG_{ads} plots on different electrode materials, where appropriate) can be used to determine the reaction mechanism and the coverage conditions. For reactions involving protons, the separation factors (H–T or H–D) can also be used as another criterion, since the barrier heights vary characteristically with mechanism because of the relatively large zero point energy difference between the isotopes and their different quantum mechanical tunneling properties. This is evaluated in Refs. 50 and 51, and may be used to confirm other evidence.

Equations (83), (86), and (87) under generalized coverage conditions will usually be applicable for both adsorbed reactants and adsorbed products, though they refer to a simple case of only one adsorbed reactant intermediate and/or one adsorbed product. As we have seen above, if both reactant and product are adsorbed, the step is unlikely to be rate determining unless charge is transferred completely across the double layer, e.g., as protons. However, chemical steps that are rate determining may involve both adsorbed reactant and product species, in which case the corresponding α values will be (low-coverage) n, (high-coverage reactants) 0, (high-coverage products) n'.

It is instructive to consider what will happen as we go through a potential region where coverage has intermediate values, i.e., $0.1 < \theta_{total} < 0.9$. In this case, it is possible that we will go through a condition where $\Delta \bar{G}^\circ_{ads}$ is coverage-dependent, i.e., some generalized isotherm of Frumkin type$^{(52)}$:

$$(\theta/1 - \theta_{total}) = \prod [R] \exp[-(\Delta G^\circ_{ads} + q\theta_{total})/RT] \tag{88}$$

applies, in which ΔG_{ads} varies linearly (or otherwise) with θ. If similarly bonded species are adsorbed on the electrode, then one should expect the ΔG_{ads} values of *all* species to be affected similarly as the predominant species goes through the medium-coverage region.

Since in the medium-coverage range, $d\ \ln(\theta/1-\theta)/d\theta = 1/\theta(1-\theta) \simeq 4$, we can write Eq. (88) in a form generalizing the $q\theta$ term as $f(\theta)$, i.e., putting $\Delta\bar{G}_{\text{ads}}$ as $\Delta G^{\circ}_{\text{ads}} + nFV + f(\theta)$ (for a cathodic process); then

$$4RT = \frac{df(\theta)}{d\theta} + nF\frac{dV}{d\theta} \tag{89}$$

If the right-hand terms are both large compared with $4RT$ (i.e., if ΔG_{ads} changes by substantially more than ~3 kcal as θ changes), then we have

$$\frac{df(\theta)}{dV} = \frac{d\Delta G_{\text{ads}}}{dV} = -nF \tag{90}$$

Since we are considering a cathodic process, this is the appropriate expression for reactants at medium coverage. For products, the corresponding

$$d\Delta G_{\text{ads}}/dV = +n'F$$

In the medium-coverage region for *reactants*, we can neglect (to a first approximation) the preexponential θ term in Eq. (80). Differentiating the rate with respect to V using Eqs. (41) and (90) gives

$$d\ \log r/dV = -(\beta F/RT) - (\beta nF/RT) - (\beta n'F/RT) \tag{91}$$

in which the three successive terms represent the differential of κ, the effect of the change of $\Delta G^{R}_{\text{ads}}$ as the reactant coverage changes in the medium coverage range, and the *consequent* effect of the change of reactant coverage on the ΔG_{ads} of the product, by dipole or other interaction effects (for review, see Ref. 19). Thus, in the intermediate region of coverage, quite complex Tafel behavior may be expected. However, it is important to note that no *a priori* knowledge of the $\Delta G_{\text{ads}} - \theta$ function is required to predict the Tafel slope: it will always be roughly linear, with a slope given by the above expression, if the inequality in Eq. (89) remains valid. If we take the alternative case (medium-coverage products, low-coverage reactants), then the preexponential θ term cannot be neglected. The corresponding Tafel slope will therefore have a term equal to $-nF/RT$ added to expression (81).

Closer inspection of Eq. (88) shows that reaction orders will change in the event that ΔG_{ads} is strongly dependent on θ.[†] Neglecting the preexponential part of Eq. (88) in the medium coverage region, the isotherm becomes

$$\Delta G_{\text{ads(eff)}} = \Delta G^{\circ}_{\text{ads}} + f\theta = RT\ln\prod[\text{R}] \tag{92}$$

where the $\Delta G_{\text{ads(eff)}}$ are the effective values of free energy of adsorption of reactants and products in the potential and θ regions, where ΔG_{ads} is strongly coverage dependent. Hence, if reactants are at medium coverage, from Eqs.

[†] The usual assumption is that ΔG_{ads} varies *linearly* with θ, following the "Temkin isotherm".(54) However, this does not have to be assumed to obtain the special "intermediate coverage" Tafel slopes, as shown above ($df(\theta)/d\theta \gg 4RT$, Eq. 89).

(80) and (92), neglecting the preexponential θ, the reaction order will be $\prod [R]^{\beta}$. If products (or, indeed, any other "blocking" material) are at medium coverage, then the preexponential in Eq. (80) cannot be neglected, and the overall reaction order will be $\prod [R](\prod [P])^{-\beta}$. These and the Tafel slopes are compromise values between the low- and high-coverage conditions.

It is also clear that various other possible medium-coverage cases can occur, for example, "blocking material" affecting an adsorbed reaction product at low coverage, with no adsorbed reactant. In this case, it is clear from Eqs. (88) and (92) that the Tafel slope will be $-\beta(1 + n'')$ and the reaction order $\prod [R](\prod [M])^{-\beta}$, where the [M]'s are the activities of the free-solution species contributing to the blocking coverage, which requires n'' electrons transferred (anodically) overall. Other combinations can easily be worked out: the above has been particularly useful in explaining certain aspects of oxygen reduction on noble metals,(53) on which the reaction under certain conditions was shown to have order 1 for p_{O_2}, 3/2 (i.e., $1 + \beta$) for H^+, and with a Tafel slope of $-RT/F$. The latter might be characteristic of a *chemical* rate-determining step under low-coverage conditions, following a rapid one-electron transfer step involving a proton. However, for this type of process, a nonfractional reaction order would have been expected. Temkin or other medium-coverage conditions are characterized by Tafel slopes having values which are multiples of RT/F and fractional reaction orders. The explanation(53) involved a rate-determining step

$$O_2 + H^+ + e^- \rightarrow O_2H_{ads} \tag{93}$$

where the product ΔG_{ads} is changed by that of OH_{ads} produced under medium coverage conditions by water oxidation:

$$H_2O \rightarrow OH_{ads} + H^+ + e^- \tag{94}$$

In Eq. (93), the reaction order for H^+ is -1, hence, the overall order is $[p_{O_2}][H^+]^{(1+\beta)}$, and the transfer coefficient $\alpha \simeq 1$.

We should finally note two general points: under Temkin or other medium-coverage conditions, one of the ΔG_{ads} terms (either for reactants, products, or "blocking material," whichever applies) is inevitably close to zero (at least if the standard state for θ is taken to be 0.5). When the potential is such that this situation occurs (at least for simple cases), the rates on all material surfaces showing the same reaction mechanism should be approximately equal. The potential ranges in which these similar rates occur may be different, since they will represent the absolute ΔG_{ads} differences on the different materials. This was first pointed out by Parsons.(13) The second point concerns the low Tafel slopes implied by transfer coefficients of $(n + \beta)$ (low-coverage reactants) or $\beta(n + 1)$ (medium-coverage reactants). Reactions with large n values will, in general, not be rate determining, since their rates will rapidly overtake those with smaller n values as overpotential increases. Indeed, in complex processes with very low exchange currents, which only give significant rates at high overpotentials, primary electron transfers or chemical steps will most probably be rate determining.

4.2. Some Correlations

Equations (82)–(87) imply that, for any rate-determining step, on different substrates, log rate at constant potential should depend linearly on the increasing negative free energies of adsorption of rate-determining-step intermediates in the low-coverage region, going through a maximum in the $0.1 > \theta$ total > 0.9 region, when Eq. (88) may apply. This region will be followed by a fall of log rate with increasingly negative free energy of adsorption in the high-coverage region. Overall, the process should show a log rate–ΔG_{ads} dependence like that in Figure 6. However, the question may arise as to the change of rate-determining step as the reaction takes place on different substrates. Inspection of Eqs. (83)–(86) shows that, if complex reactions occur in which more than one reactant particle is involved in the rds, then the $\log r/\Delta G^{R}_{\text{ads}}$ slope for reactants under low-coverage conditions will not be $-(1-\beta)$, but $-x(1-\beta)$, where x is the number of reactant particles involved (x is unlikely to be greater than 2). The similar slope for high coverage would be $+x\beta$. Adsorbed products would behave similarly. Thus, a situation similar to that shown in Figure 7 may occur where two competing rds are shown in a two-step process, for example,

$$A^{+} + e^{-} \rightarrow A_{\text{ads}} \tag{95}$$

$$2A_{\text{ads}} \rightarrow A_2 \tag{96}$$

Clearly, the $\log r$ vs. $\Delta G^{\circ}_{\text{ads}}$ slopes will be twice as great for the second step as for the first, as shown by the corresponding plots A and B for each step, respectively. Such plots are called "Volcano plots," and their existence was first discussed in the case of purely catalytic processes by Balandin;(55) they were theoretically discussed by Parsons(13) and Gerischer(15) for the

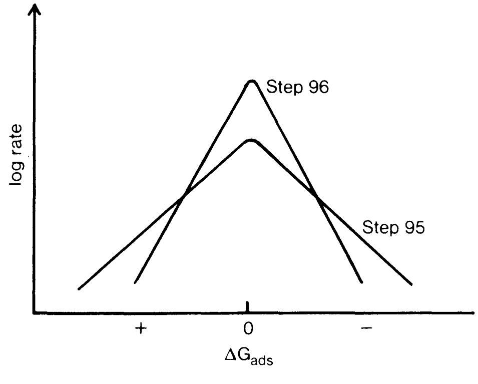

Figure 7. Volcano plots for steps (95), (96).

electrocatalytic hydrogen evolution reaction. The corresponding fit to experimental data was first proposed by Conway and Bockris.(11) This will be discussed in more detail in a later section.

In Figure 7, we can see that, at very positive and very negative ΔG_{ads} values, the rate of step (96) is less than that of step (95); therefore, it will be rate determining. The reverse is true in the slightly positive to slightly negative range of values. Thus, in complex processes, the rates may vary with the substrate ΔG_{ads}, especially for reactions with similar k values. However, the "volcano" effect should always be there, though not necessarily in the form of a smooth curve. In addition, the volcanoes may be skewed if β departs significantly from 0.5. Finally, at high rates, the shapes may be perturbed by tunneling effects for light nuclei, particularly protons.

5. Some Quantum Mechanical Aspects

5.1. General

Reactions involving proton transfer are characteristic of a wide range of electrochemical processes, for example, oxygen reduction in aqueous solutions, and hydrocarbon oxidation. In the above, a proton transfer involving adsorption is involved. Adsorption takes place to or from a foreign atomic or molecular species on an electrode surface in the above cases, whereas in hydrogen evolution it occurs either directly onto the surface [as in the discharge process, reaction (47)] or onto a hydrogen atom adsorbed on the surface [as in the electrochemical process, reaction (48)]. Proton transfer with accompanying electron transfer therefore differs only in degree, rather than in kind, between the simplest proton discharge and (say) a complex biochemical step involving proton transfer onto, or from, an electron donor or acceptor molecule of high molecular weight. For this reason, the microscopic mechanism of the proton plus electron transfer process is of great importance.

In the previous section, it has been dealt with in a purely phenomenological way, whereas in this section we shall attempt a more basic treatment. We shall consider only the cathodic discharge reaction (Ref. 41), since it may be used as a model for more complex processes. Two models of the reaction have been considered in the literature: first, one consisting of a partly bonded proton transition state(47,48) between the donor molecule and the acceptor atom (or surface) in the cathodic case, and second, a process in which it is supposed that the electron transfer process occurs instantaneously, so that the proton finds itself bonded to the new site after one single-electron transition. The two represent extreme limiting cases of the same phenomenon ("slow" and "rapid" electron transfer). It is convenient to discuss the "instantaneous transfer" process first, since it was the first case to be seriously suggested as a proton transfer mechanism, by Gurney in 1931.(56) This paper is of historic importance in representing the first application of the quantum theory to chemical mechanisms. Both of the above models involve, either implicitly or explicitly, radiationless electron transfer. However, since the role of the electron or a model for its transfer was not originally specified in the transition state approach,(47,48) it suffices to label the various "instantaneous transfer" models in the literature as "instantaneous transfer theories."

5.2. Radiationless Transfer Theories†

The basic concepts of these models were originally introduced by Gurney in 1931(56) for transfer between protons and unadsorbed hydrogen atoms in solution. They were then modified to include adsorption by Butler in 1936.(57) The concept used in Gurney's well-known paper was relatively simple and universally applicable: an activated proton in the solution will find itself on some sort of energy-configuration curve whose abscissa represents the configurational position of all the atoms considered in the discharging system, in n-dimensional space. If the electron energy of this proton then corresponds to that of an occupied metal electronic level, radiationless electron transfer from the metal to the proton (i.e., discharge) may result, via an "electron tunneling" effect.

We emphasize two points: (a) the "electron tunneling," while obviously distance dependent, may not be classical tunneling through a fixed Gamow-type barrier(58) as Gurney assumed for the unadsorbed hydrogen atom case, since the barrier between a proton and the nearby metal surface changes according to the electron position during the act of transfer, and (b) the electron energy associated with the proton *after discharge* must be the same as that of the metal level from which the electron arrives, so that the radiationless transfer condition is obeyed. In all cases, the Born–Oppenheimer (Frank–Condon) principle is assumed for the nuclei, i.e., their movement may be neglected during the electron transfer. The theory is then straightforward, and envisages a first-order reaction for electrons and protons for each metal level. The energy diagram is shown schematically in Figure 8. The overall reaction rate v will be given by

$$V = \int_{E=-\infty}^{E=\infty} \nu(E)\tau(E)\kappa(E)N(E)n(E)\rho(E)\,dE \tag{97}$$

where $\nu(E)$ is the frequency of energy transfer to the proton, $\tau(E)$ is the proton transmission coefficient, and $\kappa(E)$ is the electron transmission coefficient, the two latter terms together representing the probability of completing the elementary act when protons and electrons of energy E are in an appropriate position for reaction. $N(E)$ is the number of protons of electron energy E (i.e., after discharge) in the reaction zone, $n(E)$ is the Fermi–Dirac distribution for electrons in the metal, and $\rho(E)$ is the density of

---

† See also Chapter 1 in this volume by Dogonadze and Kuznetzov.

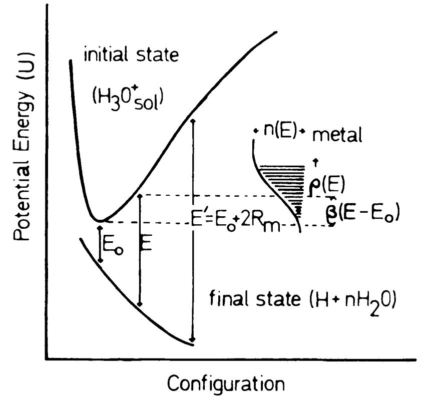
Potential Energy (U)
initial state
($H_3O^+_{sol}$)
• n(E)• metal
ρ(E)
E′=E₀+2Rₘ
β(E-E₀)
E₀
E
final state (H+nH₂O)
Configuration

Figure 8a. Modified Gurney model for charge transfer.

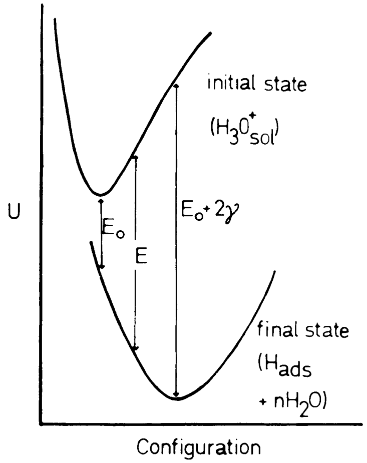
initial state
($H_3O^+_{sol}$)
U
E₀+2γ
E₀
E
final state
(H_{ads}
+ nH₂O)
Configuration

Figure 8b. Modified Butler model for charge transfer with adsorption.

states at level E. Strictly, a double integral (E terms as a function of distance) should be used, but the above simplification suffices.

In order to evaluate the integral, it is necessary to know E as a function of configuration (see Figure 8). In a particularly prophetic insight, Gurney assumed that the electron terms for reactants and products could be roughly linearized, so that approximately

$$\beta(E - E_0) = E_{act} \tag{98}$$

where the energy terms are identified in Figure 8, and where β is constant, assuming linear terms. Then, if the $\nu(E)$, $\tau(E)$, $\kappa(E)$, and $\rho(E)$ terms are regarded as having a relatively small variation with E, the integral can be evaluated.

The $N(E)$ term is given by the Boltzmann distribution $N_0 \exp[-\beta(E - E_0)/kT]$, where N_0 is the number of protons in the ground state, $n(E)$ is the

Fermi distribution, $[1 + \exp(E_f - E)/kT]^{-1}$. The resulting integral does not have analytical solutions, so approximations are necessary to give a useful result. Several approximations have been used,(56,59,60) the simplest being that used by Gurney, i.e., the replacement of the Fermi distribution by a Boltzmann distribution, with interception of the integration limits at the Fermi level(56) and by the assumption that the maximum rate value as a function of E is very sharp.(60) In the latter case, the Laplace least-descent method may be used in which the integrand is expanded as a Maclaurin series near the maximum value (i.e., E_f). Both methods lead to the same essential result,(61) namely, that

$$i_{\text{cath}} \sim eN_0\kappa^*\rho^*\nu\frac{kT}{1-\beta}\exp[\beta(E_0 - E_f)/kT] \tag{99}$$

$$i_{\text{anodic}} \sim eN_0'\kappa^*\rho^*\nu\frac{kT}{\beta}\exp[-(1-\beta)(E_0 - E_f + 2\gamma)/kT] \tag{100}$$

where κ^*, ρ^*, γ are mean values, N_0' is the atomic concentration of adsorbed H and E_0 is the energy difference between the ground state of the proton and the products in the same nuclear configuration, $E_0 + 2\gamma$ being the same quantity for the ground state of the product (adsorbed H) (Figure 8).

In both cases, the overpotential is contained in the E_f term, since the effect of the potential is to slide the metal acceptor surface level up and down on the energy scale. Hence, the rates contain $\exp[-\beta eV/kT]$ (cathodic) and $\exp[(1-\beta)eV/kT]$ (anodic), thus giving the Tafel relationships. Provided that the relative positions of the minima of the curves do not move along the configuration coordinate with increasing adsorption, then E_0 and γ both contain the adsorption potential energy of hydrogen. Putting this equal to ΔH_{ads} as a first approximation, the rates therefore contain $\exp[-\beta\Delta H_{\text{ads}}/kT]$ (cathodic) and $\exp[-(1-\beta)\Delta H_{\text{ads}}/kT]$ (anodic), i.e., the Brønsted relations,(45) as in Eq. (83).

The complete calculation shows that practically all the electrons come from within $\pm kT$ of the Fermi level. This is to be expected on thermodynamic grounds, since the Fermi level is the effective electrochemical free energy of the electrons, which are transferred to the metal surface without having to overcome a barrier. As remarked above, Gurney supposed that a simple tunnel mechanism for the electron transfer occurs; however, as we have seen above, this is unlikely to be the case for adsorbed H as a product. In addition, Gurney did not identify the ν term, representing the rate at which activated protons arrive at reaction sites, i.e., the rate of *energy* transfer in the system. In order to obtain an expression for an exchange current from Eqs. (99) and (100), we must write an isotherm for the adsorbed H atoms. If, for example, we suppose that the combination mechanism is in equilibrium, then

$$c'/N(1-\theta) = (p_{H_2})^{1/2}\exp(-\Delta G_{\text{ads}}/RT) \tag{101}$$

where c' is the total concentration of H_{ads}, of fractional coverage θ and N is the total number of adsorption sites per unit area. Remembering that metal sites are reactants in the process, we should insert $(1 - \theta)$ in Eq. (99). By equalizing Eqs. (99) and (100), and by the use of the isotherm [Eq. (101)], we obtain (61):

$$I_{\text{exchange}} = 2ec^{(1-\beta)} p_{H_2}^{\beta/2} N^{\beta} (1 - \theta) f_i^{-(1-\beta)} f_f^{-\beta/2} \times \kappa^* \rho^* \nu kT \exp[-\beta(1-\beta)2\gamma/kT] \exp(-\beta U_{\text{ads}}/kT) \tag{102}$$

where c is the proton concentration in the reaction zone and where the partition functions for the initial and final states (f_i, f_f) have been introduced by the use of the Gibbs distribution function, i.e., $N_0 = cf_i^{-1}$, $N_0' = c'f_{\text{ads}}^{-1}$, $\exp[-\Delta G_{\text{ads}}/RT] = f_f^{-1} f_{\text{ads}} \exp[-U_{\text{ads}}/kT]$, where f_{ads} is the partition function for H_{ads}. Hence, apart from N and ρ^*, the only metal property that enters into the rate is the energy of adsorption of the intermediate, thus confirming the "thermodynamic" results discussed in Section 2. Equation (102) is essentially the same as Eq. (83).

When later authors made use of this model, they regarded the electron as emerging through a transparent barrier from the Fermi level with a 100% probability of capture by activated protons (see Refs. 12 and 62). This concept became inevitably confused with transition state theory (see below), and the energy curves of H^+ and H_{ads} were regarded as those for "bond stretching," i.e., of the H^+–H_2O and $H_{(\text{ads})}$–M bonds in the initial and final states. As Levich has pointed out(63) this is unreasonable, since the "tightness" of these bonds implies that they must all be essentially in the ground state, with a ~15 kcal energy difference between this and the first excited vibrational state. For such bonds to be activated, a "classical subsystem" superimposed on the ground state is therefore necessary. Such a classical subsystem might consist of translational levels (as in the gas phase), or coupled vibrational levels of low frequency.

In recent years, the pre-transition-state idea of Gurney has been taken up again by Dogonadze, Levich, and co-workers,(60)† who have used a model for the classical subsystem that is based on Landau's work,(64) and which was applied by Mott and Gurney(65) and Pekar(66) to crystals, and in modified form by Libby(67) and Weiss(68) to electrolytes. This idea makes use of continuum physics to obtain a description of the potential energy of an ion in solution, in a highly simplified model which is purely electrostatic.

Dogonadze *et al.*(60) based their conceptual interpretation of the activation phenomenon on certain ideas of Marcus(69) for redox processes. In the latter, the continuum reorganization energy on transfer of charge may be put equal to the difference between the Born electrostatic free energy terms for charge stabilization using the static and optical frequency dielectric constants. This results because of the Frank–Condon approximation, which implies that heavy nuclei will be unable to keep up with changes in the surrounding electrostatic

---

† See Chapter 1 in this volume by Dogonadze and Kuznetzov.

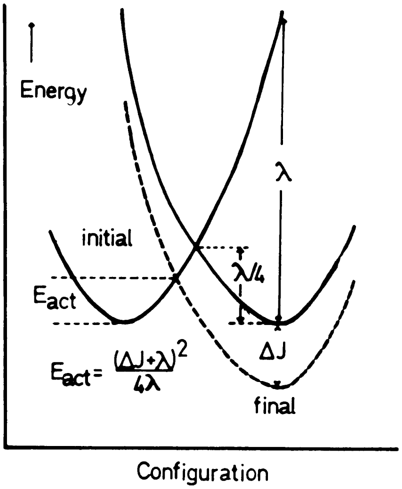

Figure 9. "Electrostatic" model for charge transfer.

field on the optical frequency transfer of an electron. Since the entropy terms in the two expressions are equal,$^{(70)}$ the difference in energy λ is therefore the potential energy for system rearrangement between reactants and products. It is the equivalent of γ in Figure 8, i.e., it is the energy required to change the ground state of the reactants to the state of the neutralized products in the same nuclear configuration (i.e., implying normalization of the curves by addition of the electron energy terms, so that at equilibrium $\Delta G_{\text{reactants}} = \Delta G_{\text{products}}$ as in Figure 9. λ† in this simple electrostatic model is given$^{(71)}$ by

$$\lambda = e^2/2(1/a - 1/R)(1/n^2 - 1/\varepsilon) + \Delta w \qquad (103)$$

for a one-electron transfer; it is derived from the simple Born equation

$$E = z^2e^2/2r(1 - 1/\varepsilon) \qquad (104)$$

for the stabilization energy of a charge of radius r and charge z, in a medium of dielectric constant ε. In Eq. (103), a is the effective radius of the ion in the activated condition, and R is twice the ion–electrode distance. Δw is a (small) electrostatic work term for assembling the reactants and n is the refractive index of the solvent.$^{(71)}$ It is clear from Eq. (104) that for a z-electron transfer, λ would be multiplied by z^2, thus enormously increasing the activation energy for charge transfer. As disucssed in Section 2, transfers other than those involving a single electron are therefore most unlikely on electrostatic and activation energy grounds.

Having established a hypothetical λ value using this simple model, Dogonadze and Levich$^{(60)}$ then considered the problem of ν. They considered that the rate of energy transfer should be given by the frequency of stationary waves of "polaron" type within the dielectric continuum ($\sim 10^{11}\ \text{sec}^{-1}$) (cf. discussion by Levich for redox processes, Ref. 72). Finally, in an original contribution to the theory of charge transfer, they considered the possibility of non-adiabatic transitions, i.e., those in which the possibility of the energized reactants finding themselves on the curve for the products is small, owing to the lack of coupling between the two respective energy surfaces). Thus they used the classical Landau–Zenner method$^{(73)}$ to calculate the probability of a transition between states for a transfer process involving an energy barrier that depends on the position of the particles themselves.

---

† In Marcus's notation, Ref. 72. Note that Marcus regards this term as a free energy difference, not a potential energy difference.

An up-to-date account of their model is given Chapter 1 of this volume. Their model, then, involves a formalism for eventually calculating the transfer rate: the transmission coefficients in Eqs. (99), (100), and (102) are, in principle, given by appropriate Landau–Zener-type expressions (see below) and the ν value by the frequency of polaron waves. The shapes of the curves, hence the β values as a function of E, are considered to represent coupled harmonic vibrations of the electrostatic environment in phase space. Since these are considered to depend only on this environment, it follows that they are therefore geometrically similar for reactants and products, and are, owing to the harmonic assumption, parabolic in form. In this case, a simple geometrical argument shows that the free energy of activation in the normalized form for the initial and final electron energy terms is given by (cf. Figure 9):

$$\Delta G_{\text{act}} = (J + \lambda)^2/4\lambda \tag{105}$$

$\beta(= \partial\Delta G_{\text{act}}/\partial J)$ is therefore equal to $0.5 + J/2\lambda$.

After integration, Dogonadze and Levich arrive at an expression that is relatively similar to Eq. (99), but which contains an effective β value equal to the expression given above.

The main problems involved with the Levich–Dogonadze model are those of agreement with experiment and of the fundamental hypotheses used. They are probably correct in assuming that the transition between the different electronic terms should, in principle, be calculated (if this is possible) using the perturbation theory approximation for a quantum transition probability (w) from a process of Landau–Zener type, i.e.,

$$w = (2\pi/\hbar)\text{Av}\sum_{n'} |\langle\psi_{\beta n'}|L_{\beta\alpha}|\psi_{\alpha n}\rangle|^2 \delta(E_{\beta n'} - E_{\alpha n}) \tag{106}$$

where $\psi_{\beta n}$, $\psi_{\alpha n}$ are the wave functions of the final and initial states of the solvent in the n'th and nth states of energies $E_{\beta n'}$, $E_{\alpha n}$; δ is the Dirac δ function indicating conservation of total energy, and $L_{\beta\alpha}$ is the exchange integral between the two states. The expression is integrated over all classical initial system states, which are averaged statistically to give an expression of the form$^{(63)}$

$$w = (\pi/\hbar^2 kT\lambda)^{1/2}|L|^2 \exp[-(J + \lambda)^2/4\lambda kT] \tag{107}$$

where L is the overall exchange integral. Comparison of Eqs. (105) and (107) shows that for the transfer of electrons alone,

$$\nu\kappa^* \sim (\pi/H^2kT\lambda)^{1/2}|L|^2 \tag{108}$$

where κ^* is ~ 1 for a sufficiently large splitting between the electron energy terms of the initial and final states (i.e., for an adiabatic process).

Since, for the case of proton transfer, they assume two separate coupled Franck–Condon transitions, first for electrons, then for electrons coupled with protons, their κ^* term will contain two separate transition probabilities. According to their model, the proton is considered to make a quantum transition over a very short distance (0.5 nm), to a level of equal proton energy in the product state. During the classical activation process, energetics represented by the curve for the reactants in Figure 9, the proton coordinate (i.e., the proton bond length to a water molecule) is considered not to change, i.e., the proton remains in the ground state. The proton, therefore, makes its transition from its ground state in the reactants to that in the products.

Concerning the agreement between the results offered by the above theory and experiment, the first evidence concerns the nature of the Tafel line. Tafel lines on mercury show linear behavior over almost 1.5 V (a total of 12 decades of current density if the early results of Bowden and Grew(74) are considered). This is quite inconsistent with the parabolic classical energy curves assumed in Ref. 60 and with the β values indicated by Eq. (105). The only possible conclusion is that the sides of the energy wells in reality must be almost straight.

In addition, the experimental values of H–T separation factors are difficult to account for using the Dogonadze–Levich model. Normally, they have been explained by supposing that the different hydrogen isotopes possess different zero point energies, so that when activation occurs the barrier heights differ for the three species. A correction for quantum mechnical tunneling is, of course, required for low, thin barriers, which will favor penetration by the lightest particles (i.e., protons).(50,51) In the Dogonadze–Levich theory, no activation, as such, of the proton bond can be considered to occur. Experimental separation factor values are, therefore, imagined to result from the non-adiabatic nature of the proton transition, for which the κ^* value varies strongly with overpotential.(75) The electron transmission coefficient may be imagined to be unity (i.e., an adiabatic process is involved, with complete splitting of the energy terms for reactants and products (see Refs. 69 and 71). The κ^* variation is considered to result from a discharge distance-overpotential relationship due to adsorption.

While not entirely impossible, this concept is highly improbable. It implies an even greater disagreement between the experimental Tafel slope and that predicted from the β value following from Eq. (105). Besides, the overall preexponential factor in the rate expression, if nonadiabatic proton transfer is assumed, it would give rates that are too small. A second problem of the basic model is the fact that it can *only* apply to protons and perhaps marginally to a few other light nuclei. It could never, for example, give an adequate description of potassium ion transfer, which is an extremely rapid process.(76) This ion, which resembles the proton–H_2O combination in size and which must be surrounded by a fairly similar solvation sheath of tightly bound water molecules, would have to tunnel out of the latter if the Dogonadze–Levich approach were valid.(61)

While a partly classical "inner-sphere" contribution to the activation energy in cases where the "electrostatic continuum" approximation applies has been assumed by Marcus(77) for a redox-type (i.e., non-atom-transfer) process, no successful efforts have been made to describe the "instantaneous" radiationless electron transfer mechanisms for heavy nuclei (see, however, Ref. 78). Overall, it seems reasonable to conclude that the "instantaneous transfer" theory is an unlikely hypothesis for combined atom and electron transfer. A more reasonable approach is dependent on the fact that the lifetime of an activated molecule (i.e. the proton tightly bound to its neighboring water molecules, e.g., in $H_3O_4^+$) is very long compared with the transition time for one single-electron passage.(61)

During each single-electron "passage," we can consider the Born–Oppenheimer approximation to be obeyed. However, between passages, and at constant electron energy, we can imagine small changes in bond length in the tightly bound molecular bonds between the proton and its neighboring water molecules, which result from the slowly changing charge distribution (in a resonance effect), provided that the electron transfer is adiabatic. This is, therefore, a definition of a transition state, i.e., a cumulative bonding phenomenon, or a cumulative multiplicity of electron transfers on the same energy level. This seems to be the only mechanism that will allow an orderly transition between the "tight" quantized proton–H_2O bond and the low-frequency classical bond concept required to explain atom transfer involving a progressive movement of several atoms over rather longer distances. Such a mechanism seems necessary for the combined electron and atom transfer case, especially for heavy nuclei.

Such a view is in accord with recent developments (e.g., Bockris and Sen(79) and Marcus(80)). The latter author feels that the potential energy surface will then be similar to that given by the BEBO model.(81,82) This has been applied to the case of the electrocatalytic hydrogen reaction. In simple cases, this will predict a rather curved Tafel line,(82,83) similar to that derived on the Dogonadze–Levich theory. However, with some corrections for electrostatic effects,(84) a fairly constant value of β may be obtained. Essentially, the shape of the Tafel plot is that of the energy surface. A straight plot therefore indicates a straight-sided energy well.(61,70) While a Morse curve has normally been considered as the well shape for a dissociating molecule, the well may be better represented as that of the tight $H_9O_4^+$ or H_3O^+ ion in a "cage" in the case of the hydrogen evolution reaction.(61) This "cage" may well be, for example, sinusoidal, i.e., practically straight-sided.

A final point that requires discussion is that of reaction adiabaticity concerning the electron transfer elementary step. Any theory in which the reactants are "suddenly" transformed into products without an intermediate transition state being formed invokes this problem (Bockris$^{(85)}$ and Wright, Khan, and Bockris$^{(86)}$).

However, if a true transition state is formed in which the electron essentially makes a multitude of transitions during the total lifetime of the state (which would be the assumption in the case of the BEBO or similar models), then it is hard to see how the reactions can be other than adiabatic. Basically, the rate equations predicted will be similar to the classical approach in Eqs. (82)–(87). The only modification introduced is the effect of the electronic density of states [cf. Eq. (99)], which is generally small. In the case of semiconductors, however, this may be different.

A final word should be said about the situation when a semiconducting electrode is involved. While the properties of semiconductors involved as electrodes for reactions not involving adsorption (i.e., redox processes) is relatively well known, and was first discussed by Gerischer$^{(87)}$ using essentially Gurney's theory of charge transfer,$^{(56)}$ the semiconductor–solution interface when adsorption is involved has been much less discussed. Figure 10 shows a diagram of *n*- and *p*-type semiconductors in the dark in contact with an electrolytic solution. The actual degree of band-bending depends on the difference between the E_f value at the flat-band potential of the individual semiconductor and the "effective E_f" in the electrolyte. By using arguments similar to those used in Eqs. (99) and (100), it can be shown that the equilibrium rate of the reaction is equal to that on a metal multiplied by the factor

$$(\rho \text{ semiconductor}/\rho \text{ metal}) \exp\left(-\frac{\beta|E - E_p|}{kT}\right) \tag{109}$$

where E is the band edge energy at the electrode–solution interface for the predominant band involved in the process (the conduction band in Figure 10b) and E_f is the Fermi level. The ρ's are the corresponding densities of states at the band edge and Fermi level, respectively. The Tafel slope will be different from that in metals;$^{(88)}$ essentially, the apparent symmetry factor value when diffusion of minority carriers is not limiting (as it might be for the *p*-type material in Figure 10, but not for the *n* type), is given by

$$\beta_{\text{app}} = 1 - \frac{(1-\beta)\Delta\Delta\phi_{dl}}{\Delta\Delta\phi_i + \Delta\Delta\phi_s} \tag{110}$$

where $\Delta\Delta\phi_i$ is the potential change in the semiconductor and $\Delta\Delta\phi_{dl}$ is that in the Helmholtz double layer, the total drop being the sum of both. In nondegenerate semiconductors (i.e., those with $|E - E_F| > 3kT$, $\Delta\Delta\phi_{dl}$ is negligible, and $\beta_{\text{app}} \simeq 1$).

Equation (109) appears to indicate that the rate of a reaction on a semiconductor can never be as high as that on a metal (at least under

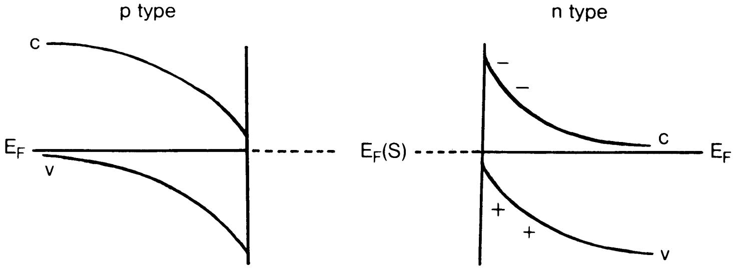

Figure 10. p- and n-type semiconductors in contact with an electrolytic solution. E_F = Fermi level; $E_F(S)$ = so-called Fermi level of redox system in solution (activation barrier energy).

equilibrium conditions). However, the effect of the lower Tafel slope will be soon to lower the $|E - E_F|$ value on the semiconductor, and so introduce degeneracy leading to the same effective rate as on a corresponding metal with the same adsorption properties. The final difference between semiconductors and metals is in the density-of-states term. It is possible that this may be very high for the conduction band of a wide-gap semiconductor, compared with that at the E_F value of a metal,$^{(87)}$ thus leading to a partial compensation.

Finally, in reactions involving adsorption (electrocatalytic processes) the problem of degeneracy will arise, since the presence of the adsorbate implies the existence of surface states (Figure 11). In such cases, the electrons or holes involved in the process will essentially arise from the energy level of the surface state, and the ρ term will be that for the surface concentration of the surface state. If one considers an oxidizing process on an n-type semiconductor (Figure 11), E_1 will represent a "low-coverage" adsorbate, and E_2 a "high-coverage" adsorbate. The surface concentration as a fraction of total coverage (θ) will presumably be given by

$$\frac{\theta}{1-\theta} = A^-_{\text{soln}} \exp\left(-\frac{|E - E_F|}{kT}\right) \tag{111}$$

for the process

$$A^- \rightarrow A_{\text{ads}} + e^- \text{ (rds)}, \qquad A_{\text{ads}} \leftrightarrows A^-_{\text{soln}} \tag{112}$$

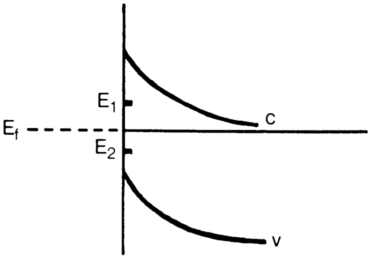

Figure 11. As Figure 10, showing n-type semiconductor with surface states E_1, E_2.

or

$$\theta = \{[A]\exp(-|E - E_F|/kT)\}\{1 + [A]\exp(-|E - E_F|/kT)\}^{-1} \quad (113)$$

in the general case. This becomes an effective density-of-states term, and the overall rates will be [using Eqs. (109) and (113)]

$$\text{(low coverage)} \quad A\exp[-(1+\beta)|E - E_F|]/kT \quad (114)$$

$$\text{(high coverage)} \quad \exp[-\beta|E - E_F|]/kT \simeq 1 \quad (115)$$

times that on a metal [Eqs. (82)–(87)] for reactions involving adsorbed products.

We can now write $|E - E_F| = \Delta G^p_{\text{ads}}/N$ (low-coverage case) or $|E - E_F| = -\Delta G^p_{\text{ads}}/N$ (high-coverage case), where N is Avogadro's number. This relationship arises because of the identity of the E value with the adsorbate itself (Figure 11). So, using Eq. (82) (and considering the case of adsorbed products only), then we find that the overall rate on a semiconductor will be

$$\begin{array}{ll} \text{low coverage, } \Delta G^p_{\text{ads}} \text{ positive:} & k \sim k' \exp[-2\Delta G^p_{\text{ads}}/RT] \\ \text{high coverage, } \Delta G^p_{\text{ads}} \text{ negative:} & k = k' \exp[(1-\beta)\Delta G^p_{\text{ads}}/RT] \end{array} \quad (116)$$

Similar cases can be calculated for reactions involving adsorbed reactants. Thus, in general, a different type of volcano expression would be expected on semiconductors with active surface states, with a more rapid rise on the low-coverage side, with the same behavior as a metal on the high-coverage side for reactions involving adsorbed products (Figure 12). Unlike the case of

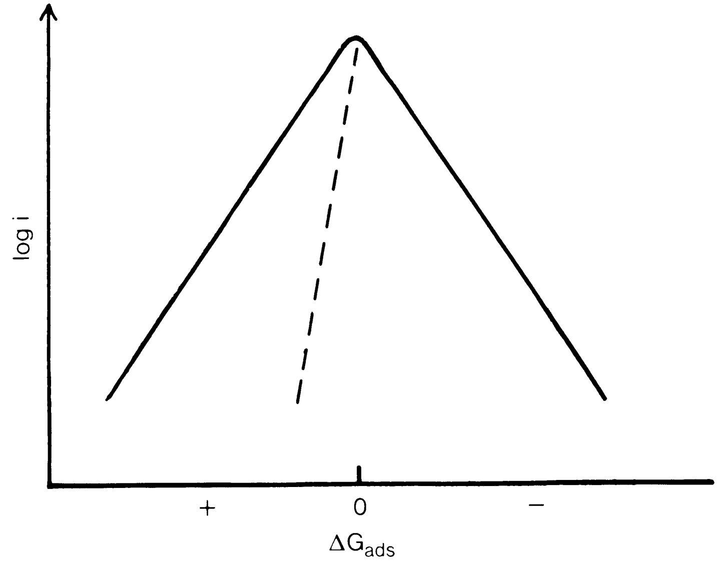

Figure 12. Volcano plots for an electrocatalytic process on a metal electrode and on a semiconductor where the adsorbate forms surface states. Dashed line: rising side on semiconductor. Falling side on semiconductor same as on metal.

metal electrodes, insufficient data exist to confirm this. In the case of thin semiconducting layers on metals, "some of the above discussion may break down," since the layer may be insufficiently thick to support a space-charge region. The film will then be effectively "metallized." While it has been suggested that Auger spectroscopy may be of value in looking at such films,(85) few useful data have so far been obtained. We may imagine that, in general, Eqs. (82)–(87) will apply to surfaces involving reversible adsorbates on thin films, where electrons may tunnel through from or to the metal Fermi level.

6. Some Electrocatalytic Reactions

6.1. General

In an earlier section it was remarked that, in a number of processes, complications may arise which render Eqs. (82)–(87) difficult to use and interpret. These would include the existence of several species of different bonding energies on the surface of the electrode (all of which have the same chemical nature, but may or may not be reaction intermediates), or cases where the bond strengths of intermediates are time dependent. The first is characteristic of hydrogen on platinum,(44,90) the second oxygen on noble metals.(45) In the first case, the question at issue will be which type of sites are indeed active in the reaction, and which coverage term is involved, for example, when reaction (48) or (49) is rate determining in the cathodic direction.

Since a volcano expression will always be expected, it seems probable that the most active form of hydrogen, when several different forms are present, will be the species whose free energy of adsorption is closest to zero. This transient species will have only a limited coverage (θ perhaps equal to 0.2) at any given time. In addition, adsorbates always exhibit at least some Temkin behavior [Eq. (92)] in the medium-coverage region. In the second case, that of reactions involving oxygen, the problem of strongly adsorbed reaction intermediates [–OH or –O monolayers, or "proto-oxides" involving place exchange (Ref. 46)] may influence reaction rates by physical "blockage" of sites, as well as by induced heterogeneity (Temkin-type) effects [Eq. (92), Refs. 46 and 53]. As we shall see below, this is also involved in processes involving oxidation of organic compounds. Finally, "foreign" adsorbates (surfactants, certain specifically adsorbed ions, poisons, long-chain molecules) may block surface sites and introduce Temkin effects.

It is impossible in a review of this length to deal in detail with all the above, together with other electrocatalytic processes [e.g., chlorine evolution (see Ref. 44a), reduction of organics, etc.]. These are dealt with in mechanistic terms in other chapters in these volumes, to which the reader is referred. In many cases, insufficient data are available to allow correlation of rates between different materials, and to determine the predicted changes in the rate-determining step with substrate. Some of these are reviewed elsewhere in some detail.(19,44a,91) Recent symposia on electrocatalysis should also be consulted, since they summarize recent and ongoing work in an assimilable manner.(92–96) In addition, for the hydrogen and oxygen electrodes, an exhaustive list of nonmetallic compounds that have been screened as electrocatalysts has been given by Kuhn.(97)

In this final section, electrocatalysis of hydrogen, oxygen, and organic oxidation processes is briefly summarized, and practical implications discussed.

6.2. Hydrogen Electrode Reaction

The six possible combinations of three simple reactions [discharge, electrochemical desorption, and combination steps, reactions (47)–(49)] will all show volcano relations. An analysis(19) shows that their rates are as given below. For simplicity, all reactions are considered to occur for $\Delta G_{\text{ads}} \neq 0$ at the V value considered, i.e., Langmuir conditions.

6.2.1. Discharge rds

Equilibrium electrochemical desorption:

$$i = k_1[\text{H}^+] \exp[-\beta \Delta G_{\text{ads}}/RT] \exp[-\beta FV/RT], \qquad \theta < 1/2 \qquad (117)$$

$$i = k_1[\text{H}^+]^2 (p_{\text{H}_2})^{-1} \exp(1-\beta)\Delta G_{\text{ads}}/RT] \exp[-(1+\beta)FV/RT], \qquad \theta > 1/2 \qquad (118)$$

6.2.2. Electrochemical Desorption rds

Equilibrium combination:

As Eq. (117), $\theta < 1/2$ (119)

$$i = k_1[\text{H}^+](p_{\text{H}_2})^{1/2} \exp[(1-\beta)\Delta G_{\text{ads}}/RT] \exp[-\beta FV/RT], \quad \theta > 1/2 \qquad (120)$$

$$i = k_2[\text{H}^+]^2 \exp[-(1-\beta)\Delta G_{\text{ads}}/RT] \exp[-(1+\beta)FV/RT], \qquad \theta < 1/2 \qquad (121)$$

$$i = k_2[\text{H}^+] \exp \beta \Delta G_{\text{ads}}/RT \exp[-\beta FV/RT], \qquad \theta > 1/2 \qquad (122)$$

Equilibrium combination:

$$i = k_2(p_{\text{H}_2})^{1/2}[\text{H}^+] \exp[-(1-\beta)\Delta G_{\text{ads}}/RT] \exp[-\beta FV/RT], \qquad \theta < 1/2 \qquad (123)$$

As Eq. (122), $\theta > 1/2$. (124)

6.2.3. Combination rds

Equilibrium discharge:

$$i = k_3[\mathrm{H}^+]^{-2} \exp[-2(1-\beta)\Delta G_{\mathrm{ads}}/RT] \exp[-2FV/RT], \qquad \theta < 1/2 \quad (125)$$

$$i = k_3 \exp[2\beta \Delta G_{\mathrm{ads}}/RT], \qquad \theta > 1/2 \quad (126)$$

Equilibrium electrochemical desorption:

$$i = k_3[\mathrm{H}^+]^2 p_{\mathrm{H}_2} \exp[-2(1-\beta)\Delta G_{\mathrm{ads}}/RT] \exp[+2FV/RT], \qquad \theta > 1/2 \quad (127)$$

As Eq. (126), $\theta > 1/2$ (128)

In the above analysis, again for simplicity, we assume that the symmetry factor (β) value is the same for each rds. The k_1, k_2, k_3 values are the intrinsic rate constants for each process at $V = 0$, $\Delta G_{\mathrm{ads}} = 0$. On platinum, at the reversible hydrogen potential, ΔG_{ads} is approximately 0 (i.e., $\theta \sim 1/2$), as is shown by the roughly unit coverage shown by cyclic scans.(44,90) Using experimental data obtained under these conditions, it is possible to estimate the appropriate k values.(13) In acid solution at 298 K, they are about 10^{-1}, 10^{-4}, and 10^{-2} A cm^{-1}, respectively (see Ref. 98 for review of values for k_1). The k_3 value is somewhat unreliable, owing to the possible occurrence of a diffusion-controlled hydrogen evolution process on the platinum metals; however, the value above is consistent with other considerations.(49)

Any combination of two of the three possible elementary steps may, in principle, represent the overall process. In the general case (except over very limited regions of $\Delta\bar{G}_{\mathrm{ads}}$ or V), one step will be rate determining, and the other will be to a first approximation in quasiequilibrium. The rates indicated by Eqs. (117)–(128) are purely theoretical (or rather "virtual"), but a consideration of them will enable the appropriate path to be determined for given ΔG_{ads} and/or V values. The path (i.e., the combination of two reactions) will always be that giving the highest rate, i.e., that in which the slowest step is more rapid than the slowest step in any other possible pair. The slowest step of the pair is defined by the condition that the *inverse* path (i.e., the "rapid" step presumed to be rate determining with the "slow" step at equilibrium) must possess a higher "virtual" rate than that of the real path itself, otherwise the physical rate-determining assumption is impossible. The other step of the path will necessarily be the fastest that can occur under the given conditions. Using these simple selection rules, the various possible mechanisms and overall log rates can be constructed graphically as a function of ΔG_{ads} at constant V (i.e., either at the equilbrium potential or at some positive overpotential). The experimental Brønsted slopes can, therefore, be established. Alternatively, log i–V plots can be established at constant ΔG_{ads}, i.e., for a given metal, and the changes in mechanisms determined under anodic and cathode conditions. The Brønsted and Tafel slopes thus obtained can be compared with experiment, at least under the conditions where the above rate expressions apply (i.e., $\theta \to 0$ or $\theta \to 1$, as appropriate).

In the intermediate regions ($0.2 < \theta < 0.9$), intermediate Tafel or Brønsted slopes between those at the extreme coverages will apply; but, as Eqs. (88)–(92) show, these will be only over rather short free energy ranges.

In general, most attempted analyses of electrocatalytic properties have involved correlations based on the measured or estimated exchange currents. These often suffer from the disadvantage of doubtful extrapolations over long ranges of overpotential. However, for simplicity, we can first discuss the reaction based on correlations at $\eta = 0$, and then attempt to extend this to higher overpotential regions in establishing the appropriate experimental conditions.

Superimposed volcano plots for the six possible pairs of reactions, at $\eta = 0$, are shown in Figure 13, assuming the k_1, k_2, k_3 values given above. The rate-determining combinations are immediately clear from the selection rules, and the solid line represents the presumed true volcano plot from the process. It is possible that the true plots are skewed ($\beta \neq 0.5$), especially for the combination reaction.$^{(99)}$ Near $\Delta G_{\text{ads}} = 0$ (at least if the k_3 value is correct) the combination should be rate determining in a range ~ ± 12 kJ mol^{-1}, with the discharge step in quasiequilibrium. Since adsorption data show that the platinum metals must possess $\overline{\Delta G}_{\text{ads}}$ values close to zero at $\eta = 0$ (cf. Refs. 44 and 90), this is in agreement with the (disputed) experimental evidence and with the Tafel slopes measured. For ΔG_{ads} values that are negative, a

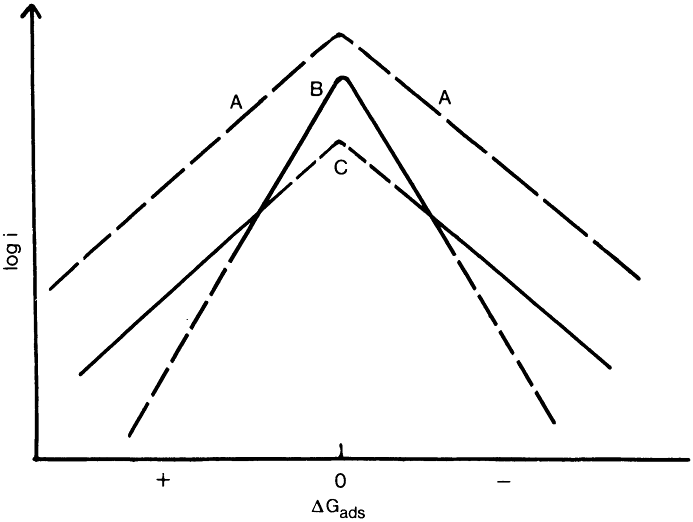

Figure 13. Apparent volcano plots (on metallic electrodes) for different hydrogen evolution reactions at zero overpotential. A, discharge reaction; B, combination reaction; C, electrochemical desorption reaction.

descending arm of the volcano should be observed, in which the rate-determining step is the electrochemical desorption process with the discharge step in equilibrium. For ΔG_{ads} values that are positive, an ascending branch of the volcano plot should be observed, with the same numerical $\log i \simeq \Delta G_{\text{ads}}/RT$ slope (~0.5), where the rate-determining step is again the electrochemical desorption process with the discharge step in equilibrium.(13,15) For metals on which data can be obtained near equilibrium, this is in general accord with experiment. For metals on which only out-of-equilibrium data are available, which are then extrapolated to obtain an i_0 value, the above analysis would not apply, since the relative positions of the volcano curves on both vertical and horizontal axes change with V, as a result of the Tafel slope difference for the two halves of each (i.e., from the effect of the $\exp(FV/RT)$ term in the isotherm for each process.

This is illustrated for cathodic polarization in Figure 14. "Virtual" combinations (i.e., those that are physically impossible) are represented by dashed lines, whereas "real" but unimportant combinations are given in solid lines. Thick lines represent the rates of the major paths followed.

We can see that, for a relatively small value (~1.0 decades of c.d. or 120 mV in potential) the combination reaction becomes much reduced as a rds on the $-\Delta G_{\text{ads}}$ side at $\eta \sim 180$ mV, and on the $+\Delta G_{\text{ads}}$ side at $\eta \sim$ 360 mV. At higher potentials, the volcano becomes of simple structure, with ascending and descending branches having a slope equal to $\pm 1/2$. The slow *discharge* step [reaction (47)] is rate determining in the ascending branch, which continues up to $\Delta G_{\text{ads}} = +F\eta/2$, when it intersects with the descending branch for which the *electrochemical* reaction [reaction (48)] is rate determining, with the discharge step in quasiequilibrium. This is in accord with the conclusions of Eqs. (50–79), and those of Conway and Bockris.(12) It should be noted that a change of the equilibrium step should be observed in the ascending branch at ΔG_{ads} values between $+3F\eta/2$ and $+F\eta/2$, i.e., from the electrochemical desorption step to the combination step. This cannot be confirmed by experiment, since this region of ΔG_{ads} properties is not easily physically accessible under normal conditions.

A further analysis, carried out on the equivalents of Eqs. (117)–(128) in the anodic region, leads to the opposite conclusions: at η values close to equilibrium, the combination reaction should be rate determining for ΔG_{ads} small and negative,(100) while farther away from equilibrium, the "reverse" electrochemical discharge process should become the rds with the "reverse" electrochemical discharge step in quasiequilibrium for $\Delta G_{\text{ads}} < 0$, the inverse being the case for $\Delta G_{\text{ads}} > 0$. There are presently insufficient electrochemical data to support all these conclusions.

Figure 14 allows us to determine the validity of the electrocatalytic model in terms of available experimental cathodic data. The major conclusions are essentially in accord with mechanistic determinations on the individual metals, as established by Tafel parameters (slopes are generally reported as $2RT/F$

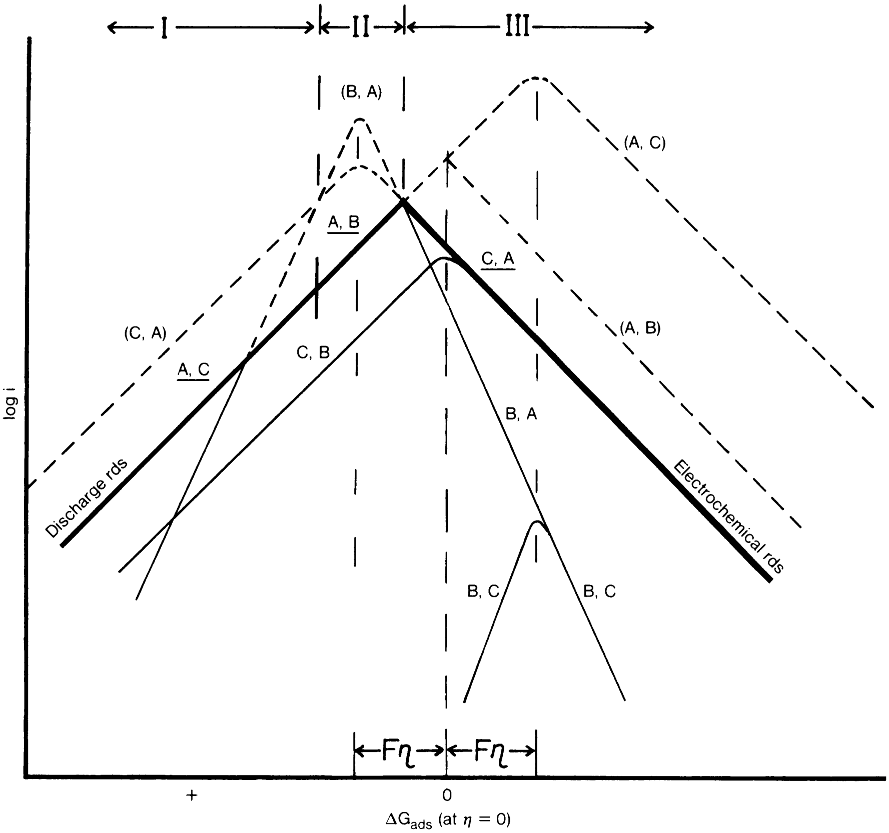

Figure 14. As Figure 13, but at overpotential η, showing shift of volcanos. Volcanos for each possible reaction pair are shown, with first member of pair rate determining, e.g., C, B = electrochemical rds, combination in equilibrium. Thick lines are the major contributing pairs (reaction pairs underlined: left to right A, C, followed by A, B up to $\Delta G_{ads} = 0$, then C, A). Thin lines: volcanos for pairs with minor contributions to overall rate. Dotted lines (pairs in parentheses): "virtual" combinations, in which the first member of each cannot be rate determining, since it is faster than the second member.

for the two branches at higher overpotentials), separation factors, and stoichiometric number determinations (see Ref. 91 for a fuller discussion). In general, all these methods agree in regard to the mechanism followed, but some ambiguities have occasionally occurred. For example, for iron electrodes, mechanistic data imply a rate-determining electrochemical desorption process, whereas separation factors indicate the combination mechanism.$^{(100)}$ It is possible that this results from small changes in experimental conditions, especially in the lower overpotential range. However, another possible explanation is discussed below.

Close to equilibrium (particularly in the anodic direction) on the platinum metals, the combination reaction should be rate determining. This is confirmed by experiments on H_2–D_2 exchange(101) and pressure dependence of rate.(102)

After establishing that the mechanistic predictions are as expected, we turn to the electrocatalytic implications of Figure 14. If, instead of attempting a correlation at constant η, we try a correlation at constant i (i.e., overpotential at constant current density as a function of ΔG_{ads}), a rather convenient and direct comparison with experimental data is possible, avoiding extrapolations over wide potential ranges in the case of many metals. A convenient i value, which occurs in practically all experimental Tafel plots, is 10^{-3} A cm^{-2}.

Two major problems occur—firstly, which data to select, and secondly, the ΔG_{ads} values that should be used in the correlation. For the former, we shall use data on plane electrodes in the cleanest solutions (most stringent experimantal conditions). For the transition metals, the ΔG_{ads} value gives no difficulty, as the Eley–Pauling equation can be used directly in a first round calculation. Assuming for the moment that entropy changes are relatively small as a function of ΔG_{ads}, ΔH_{ads} values in the gas phase may be equated with ΔG_{ads} values with a correction for solvent effects and adsorbate entropy, the latter being estimated asuming that $\Delta G_{\text{ads}} = 0$ at $\eta = 0$ is close to the ΔH_{ads} value for platinum. The major difficulty lies in establishing a correct scale of ΔG_{ads} for the *sp* metals. In general, Eley–Pauling calculations for these metals give ΔH_{ads} values that are too large, as Conway and Bockris first pointed out.(12) This results from the electronic structures of these metals. As previously pointed out, *a priori* calculations have not generally proved helpful.(85) Gas phase measurements indicate values that are about 180 kJ mol^{-1} more positive than those derived from Eley–Pauling calculations, and it has been suggested that in the electrolytic environment, about the mean of the two values should apply.(19) This is supported by some experimental evidence for ΔH_{ads} for mercury, for which a value of 120 kJ mol^{-1} has been estimated.(83,104) Consequently, it seems reasonable to put ΔH_{ads} values on the *sp* metals equal to the Eley–Pauling values plus 90 kJ mol^{-1}, to normalize their values with that estimated for mercury.

A plot of $-\Delta H_{\text{ads}}$ vs. η at 10^{-3} A cm^{-2} is given in Figure 15, using a combination of the Conway–Bockris data(12) supplemented by those originally selected by Kita.(105) An inverted volcano is indeed observed as expected, with a right branch in which the electrochemical desorption process is rate determining (except possibly for the Pt metals for which η is close to the equilibrium zero value when the combination reaction is rate determining) and a left branch (the *sp* metals) for which the corresponding process is slow discharge. The large gap in ΔH_{ads} values between -160 and -240 kJ mol^{-1} is apparent. This cannot be bridged by *d–sp* alloys because of their electronic structures. The slopes for each branch, according to Eqs. (117) and (122), should be $\pm 1/F$ (23.06 kcal/V) since the Brønsted and transfer coefficients for ΔG_{ads} and η, respectively, are identical. Slopes of these values have been

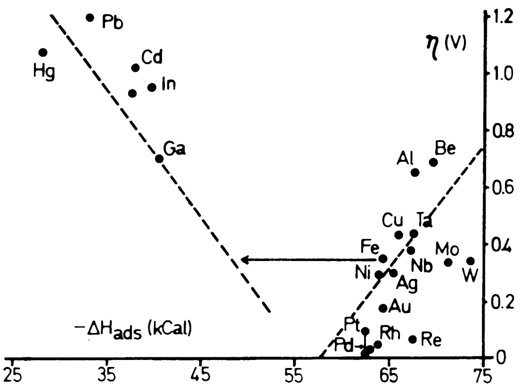

Figure 15. Volcano plots for hydrogen evolution in acid solution at 1 mA/cm^2. Overpotential data and heat of adsorption from references quoted in Ref. 19, p. 411. Arrow for Fe shows position assuming discharge rds, and ΔH_{ads} data quoted in Ref. 109.

inserted on the plot and are in satisfactory agreement with the experimental data.

Again, using Parsons' figures(13) for the k_1 and k_2 values, $i = 10^{-3}$ A cm^{-2} corresponds to an overpotential for the electrochemical discharge rds of 0.12 V for a metal with $\Delta G_{\text{ads}} = 0$ at $\eta = 0$. This corresponds on the plot to a $-\Delta H_{\text{ads}}$ value of about 244 kJ mol^{-1}, which must, therefore, be equated with $\Delta G_{\text{ads}} = 0$, close to the position occupied by platinum and palladium. In contrast, the discharge process for a metal with $\Delta G_{\text{ads}} = 0$ at $\eta = 0$ should have a rate of 10^{-1} A cm^{-2} at $\eta = 0$ or 10^{-3} A cm^{-2} at $\eta = +0.24$ V. The line inserted does indeed pass through this η value at $\Delta H_{\text{ads}} = 244$ kJ mol^{-1}, in excellent agreement with the theoretical predictions. We may, therefore, conclude that the general theory and ΔH_{ads} values are essentially correct, and that Figure 15, which previously has been given elsewhere,(19,91) is the most satisfactory electrochemical correlation to date between theoretical and experimental catalytic data for the hydrogen electrode process (at least for the cathodic reaction).

Though the overall picture is reasonably satisfactory, certain more detailed problems remain. One is the effect of coverage on the ideal heat of adsorption values discussed above. A second problem is the effect of proton tunnelling, and of other possible changes of preexponential factor in the rate expression. The latter will invalidate the assumption of constant entropy of adsorption or activation.

The effect of change in heat of adsorption with coverage should only be apparent on the right side of the volcano (electrochemical desorption rds). Conway and Bockris(12) show a log i_0–heat of adsorption plot for the transition metals, using an experimental gas phase heat of adsorption rather than calculated values. This plot is given in Figure 9 of Ref. 19. The value for Pt is that in the high-current density region (electrochemical step rate determining). According to Eq. (122), the slope of the $\log_{10} i_0$–ΔG_{ads} plot should be $-\beta/2.3RT$, or about 0.36 with $\beta = 0.5$ at 298 K. The value between Pt and Ni in Ref. 12 is considerably greater than this, whereas that between Fe and

Ta is much less. The difference in the first case may be explained by the length of the Temkin region (where and if it occurs) on each metal. The effect of this region is to give an effective ΔG_{ads} value different from that estimated, which corresponds to the effective value for low coverage, at a standard state of $\theta = 1/2$. The "high coverage" value may be several kJ mol^{-1} more positive. Whether this effect can explain the rate difference between Pt and Ni is open to question, since it implies that the ΔH_{ads} values for Pt are under high-coverage conditions, whereas those for Ni refer to low coverage. There are insufficient available experimental data to establish this point, but some evidence exists in alkaline solution that suggests a low coverage of H on Ni.(105) The problem becomes even more complicated by the fact referred to earlier that, for platinum, iridium, and probably for other metals, several states of adsorbed hydrogen are identifiable. Results between Ni and Ta are complicated by the effect of formation of stable oxide films, and it is not certain that the reaction is, indeed, taking place on the bare metal surface.

For the most part, Eq. (122) appears to give a reasonably good account of the kinetics of hydrogen evolution on transition metals at moderate to high overpotentials. It would be interesting to see if some of the second order discrepancies discussed above might be due to "preexponential" term changes in rate by the ΔH_{ads} part of ΔG_{ads}. This hypothesis could be confirmed if data on activation energies for the process on different substrates were available under comparable experimental conditions. Unfortunately, with some rare exceptions, this is not the case. Glasstone *et al.*(48) quote some early references that indicate a similarity of preexponential terms. Certain later values (reviewed in Ref. 91) showed a similar trend. Similar results were obtained by Breiter.(171)

Parsons(106) made an attempt to derive some theoretical values for the preexponential term for the above processes, based on statistical thermodynamics and classical absolute rate theory. He pointed out the effect of possible surface mobility of the loosely bonded activated complex on the rate of reaction, or rather that of the mobility of the adsorbate, since the latter implies a mobile activated complex. Low bonding strength of H in the electrochemical environment may well allow mobility, provided that the effective free energy of the adsorbed species is less than kT.(107) A further activation entropy effect (the configuration of the solvation sheath of the activated state of the bound proton at the moment of discharge) may also be important in determining overall rate, independent of final adsorbate mobility (cf. Ref. 19, Figure 5, here).

Experimental data on these effects are lacking, and important future work might be oriented in this direction. Some relatively fragmentary data on alloys do, however, show the potential importance of these considerations. Some of these are discussed in Ref. 91. There is some evidence that the Arrhenius preexponential term on copper is higher than that on nickel, whereas the reaction rate on nickel is the higher of the two, i.e., a "compensation effect" occurs.(108)

The details of the overall picture are therefore rather complex. However, the broad outlines of the Balandin–Parsons–Gerischer theory which, after full analysis, gives a good account of the changes in rate-determining steps and at least a macroscopic estimation of rates on individual metals, may be said to be obeyed. However, from a more microscopic viewpoint, complications arise, especially in the case of the transition metals that have medium to high adsorbate coverages.

It has recently been suggested that the correlation may be better carried out using the heat of adsorption estimated assuming that a hydride,(109) rather than a chemisorbate, should be used in the ΔH_{ads} term. (The Eley–Pauling equation corresponds to gas phase measurements of the heat of chemisorption.) The ideas in Ref. 109 may be of considerable importance, since they can explain some of the discrepancies existing in current correlations. For example, Krishtalik,(110) starting from an *a priori* analysis of log rates as a function of heat of adsorption, was led to place Co, Ni, and Fe on the rising ($+\Delta G_{\text{ads}}$) side of the volcano, on the grounds that their measured ΔH_{ads} coverages under various conditions were relatively small. Similarly, cyclic-voltammetric data do not indicate a high coverage on gold. Krishtalik's calculations of a theoretical heat of adsorption relative to other metals not only agree rather well with the estimations of the heat of adsorption of H in the form of a more-or-less covalent hydride, the latter derived from the bond frequency on metal–hydride complexes,(109) but also seem to correlate with kinetic data in certain cases. For example, if we take the case of hydrogen evolution on iron (Bockris and Koch(100)), kinetic data, including stoichiometric number, appear to show a rate-determining electrochemical desorption process at high coverage, with the discharge process in equilibrium.

In fact, as can be seen by comparing Eqs. (117) and (122), no differences in reaction orders and Tafel slopes exist between reaction (49), when rate determining with reaction (47) equilibrium, and reaction (48), rate determining with reaction (49) in equilibrium, under presumed conditions of high and low coverage, respectively. Thus, an important criterion for distinguishing between the two would be coverage. However, even that may not be sufficient, since it is at least possible that a limited number of sites,(111) representing a fraction of the total coverage, may be ultimately responsible for the total rate (though with a lower preexponential factor). In addition, the final diagnostic criterion used by electrochemists, the stoichiometric number, may also not serve to distinguish between different cases, due to the possibility of changes of mechanism in going from anodic potentials in the marginal $\Delta\bar{G}_{\text{ads}}(\sim 0)$ cases. It is, therefore, possible that the only final diagnostic criterion is the separation factor.

Bockris and Koch's results(100) for this quantity seem to place iron among the "more weakly adsorbing" metals, and would thus situate it on the *rising* side of the volcano. Figure 14 shows that it should lie in the transition region, where the combination reaction is rate determining at low overpotential (and low coverage) with a transition to the high-coverage case (electrochemical desorption rate determining). In this region, all three processes are important, and all reactions may, in simlar circumstances, proceed with similar rates. In this case, the equilibrium assumptions normally used are no longer valid, and a more complete calculation using the steady state approximation will show that, in cases where the combination reaction ceases to be important, the process becomes a directly *coupled* discharge—electrochemical desorption reaction, with both single steps increasing equally in rate as overpotential increases. θ is then given (at high overpotentials) by

$$\theta = \frac{\vec{k}_1}{\vec{k}_1 + \vec{k}_2} \tag{129}$$

and the overall reaction rate by

$$\tau = \frac{\vec{k}_1\vec{k}_2}{\vec{k}_1 + \vec{k}_2} \tag{130}$$

where the $\vec{k}$'s are the electrochemical rate constants of each step. It is therefore possible for θ to reach a limiting coverage less than 1, since both $\vec{k}_1$ and $\vec{k}_2$ contain the same overpotential exponent [$\exp(-\beta FV/RT)$]. Equally, the Tafel slope for the overall process will also be $-RT/\beta F$. These observations appear to be in accord with the experimental data. Further research is required in this area.

The question that now may be asked is whether the "hydride" type of bond or the "chemisorption" type of bond applies to all metals, and to all the possible reactions. On platinum, for the gas phase adsorption case, 2M–H_{ads} stretching frequencies are observed at ~2055 and 2105 cm^{-1}.(112) The *stronger* bonded form has the lower frequency. This is attributed to some sort of bridge bond formation, perhaps requiring the occurrence of H_2 in the initial state. Frequencies and bond strengths are given in Ref. 109.

In the electrochemical environment, it seems certain that both the gas phase and hydride values will be too high. A difference of about 20 kJ mol^{-1} was suggested in Ref. 109, which brings the value into line with those used by Krishtalik(110) and those given in Figure 15.

The arrows inserted on this figure represent a correlation assuming "hydride" ΔH_{ads} values for certain metals, which show an excellent electrocatalytic correlation.

We can conclude from the above that the problem of the precise nature of the H_{ads}–metal bond and its influence of reaction rate still is not entirely understood, even though the overall pattern is now apparent. A more complete discussion is given in Ref. 91.

Data in alkaline solution are too few to draw any effective conclusions (see Ref. 91 for a review); however, the same trends appear to apply.

Finally, it should be noted that all the equation pairs describing the rising and falling parts of the superposed "real" volcanos in Figure 14 predict that both log $i_{(\eta)}$ and H_{act} (experimental activation energy) should exist in volcano form as a function of ΔG_{ads}. In particular, ΔH_{act} plotted as a function of $(-)\Delta G_{\text{ads}}$ should be linear, with a slope of $-\beta$ (or $-x\beta$ if x moities are involved in the rds) for ΔG_{ads} positive, go through a minimium at $\Delta G_{\text{ads}} = 0$, and should rise linearly with a slope of $+\beta$ for ΔG_{ads} negative. Such plots should be characteristic of *all* cases of reversible adsorption of reaction intermediates. Unfortunately, again insufficient data exist to test this relationship in the case of hydrogen electrode reactions. It should be noted that while *absolute* ΔH_{act} values cannot be determined experimentally for half-cell processes, relative values on a series of substrates measured at some given potential (or overpotential) against a reference electrode will do just as well.

We should stress that all heat or free energy of adsorption values represent the difference between that of the intermediate and that of the electrolyte displaced.

6.3. Oxygen Electrode Reactions

In acid solution, reaction (93) is normally considered to be rate determining on noble metals.(19,53) In the case of platinum at potentials greater than those at which -O or -OH adsorption from water oxidation occurs, the reaction takes place under Temkin conditions,(53) as discussed in Section IV. This results from the "induced homogeneity" effect due to presence of the adsorbate on the low coverage of (O_2H). In general, little hydrogen peroxide is observed on Pt group metals as a reaction product in purified acid solutions, and it has been suggested that bond breaking actually occurs in the rds,(113) i.e.,

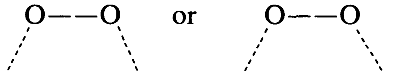

$$\text{O—O} \quad \text{or} \quad \text{O—O} \quad + H^+ = e^- \rightarrow OH + O \qquad (131)$$

Bridge model Griffiths model

In the first case, a "bridge" bonded structure is formed with dioxygen, involving the d_{xz} or d_{yz} orbitals of two surface atoms interacting with sp^2 dioxygen orbitals. In the second case, d_z^2 orbitals are proposed to react with π orbitals with $d_{xz}/d_{yz} - \pi^*$ backbonding on one side.(114) In the case of hydrogen peroxide production from blocked "poisoned" surfaces at low rates, the Pauling(115) model (single-ended adsorption with dioxygen at 120°C, resulting from sp^2–d_z^2 interaction) will then apply.

The electrocatalytic significance of reaction (131) compared with (93) involves the bonding of the reaction products, which should be reflected in the slopes of plots of the volcano type. Volcano relationships are certainly observed in $\eta - \Delta G_{\text{ads}}$ plots at constant i for oxygen reduction in acid solution for platinum group metals, silver and gold, and their alloys. Such a plot, for 85% phosphoric acid, is shown in Figure 16. It is expressed as current density at constant η (extrapolated where necessary), plotted against the potential (*NHE*) at which incipient adsorbed -OH or -O first begins to appear on the

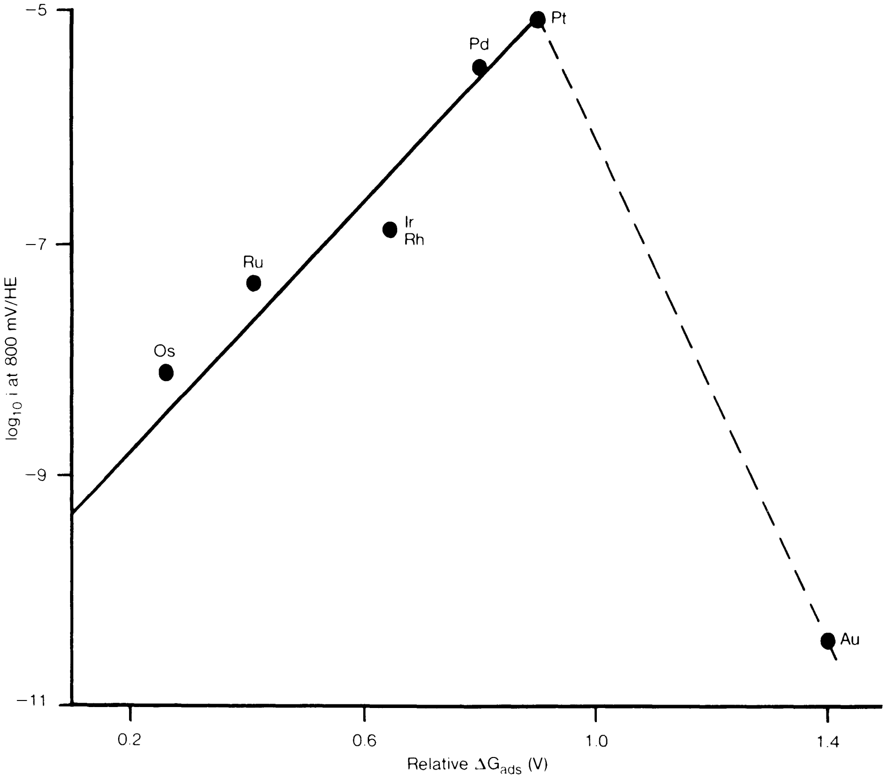

Figure 16. Volcano plots for oxygen reduction in 85% phosphoric acid at 25°C ($\log i$ at 800 mV/HE from Ref. 116). Relative $\Delta G_{ads}(V)$ is incipient -O or -OH adsorption potential from anodic cyclic voltammetry (Ref. 116).

surface of each metal, as determined by cyclic-voltammetric scans. This represents an effective ΔG_{ads} (on a relative scale) for adsorbed oxygen.(116) It should be noted that the $\log_i - \Delta G_{ads}$ slope on the "rising" side of the volcano is 200 mV/decade in voltage terms, equivalent to $\beta = 0.3$. While the descending part (platinum to gold) is somewhat dubious, there is evidence that Pd–Au and Pt–Au solid solutions will fall in this area.(117) Here the slope corresponds to β close to 0.5. (Reference 49 also contains a number of other volcano-type correlations using more traditional parameters such as latent heat of sublimation, or *d*-orbital vacancies, which are related to ΔG_{ads}). It should be pointed out that the most recent data (reviewed in Ref. 118) show somewhat higher values, particularly for Pt, than those reported in Ref. 49, but since orders of magnitude are concerned here, later data under highest-purity conditions will make little difference.

The question is whether the volcano relations of Figure 16 type for oxygen result from the same cause as for the hydrogen electrode. Fortunately, activation energy data (at 460 mV overpotential) are available.(19) These are

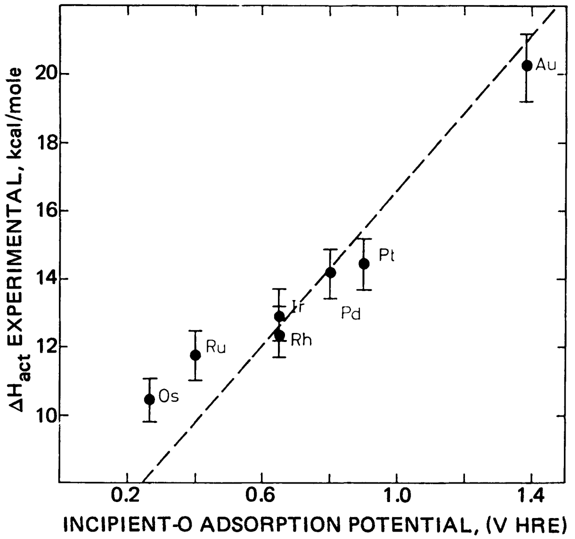

Figure 17. Experimental activation energy (at $\eta = -460$ mV) for oxygen reduction in 85% H_3PO_4 (Refs. 19 and 116) as a function of ΔG_{ads}. Abscissa as in Figure 16.

shown in Figure 17. It is apparent that activation energy is a rising function as free energy of adsorption (or bond strength for weakly bonded, freshly formed oxygenated material) falls. A slope of $\beta = 0.5$ is inserted, but $\beta \simeq 0.3$ at the strongly bonded side of the volcano osmium to platinum) seems to give a somewhat better fit. This essentially means that, at constant potential, a "compensation effect" occurs, with the preexponential term in the rate expression 10^5 times less on osmium than on platinum (Figure 18), more than compensating for the effect of the lower activation energy value. It seems that

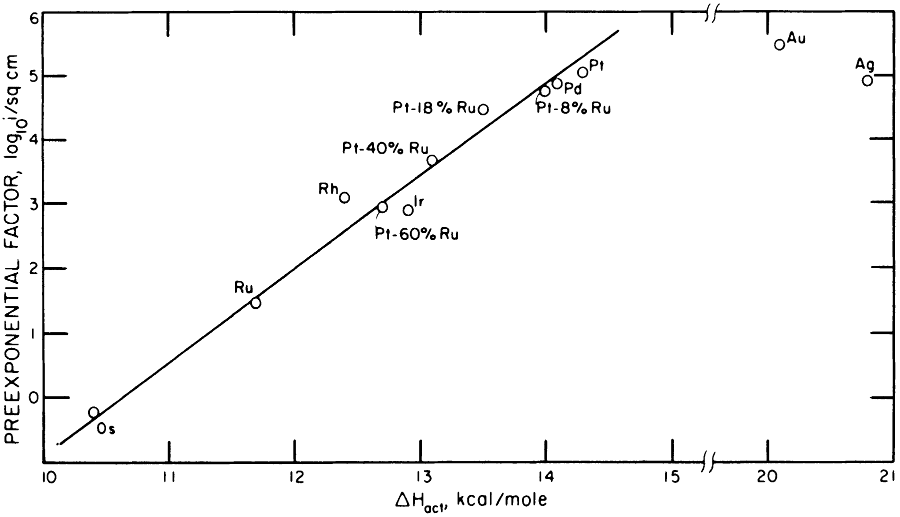

Figure 18. Plot of Arrhenius preexponential factor for data in Figure 17 (Ref. 19) $\eta = -460$ MV as a function of experimental activation energy, showing the existence of a "compensation effect."

this is due to irreversible formation of –O species which are relatively temperature independent and which block surface sites,(118) though other explanations based on entropy of adsorption effects are given in Ref. 19. Further work is required in this area to confirm these findings, which indicate that volcano plots can arise from causes other than those considered in the Balandin–Parsons–Gerischer model. Basically, the observation is that rates on each metal are equal at the potential at which the adsorbed oxygen layer becomes reduced(119) on the Os to Pt side of the volcano.

It is significant that the β value obtained from the activation energy $-\Delta G_{ads}$ plot is fairly close to 0.5, indicating that only *one* reasonably strongly bonded intermediate is involved in the rds. Since the scheme in reaction (131) would seem to result in two intermediates (slope of 2β), then reaction (93), with Pauling-type adsorption followed by rapid O_2H breakdown, appears to be a more likely rds. However, reaction (131) really implies a two-electron transfer, and a bridge-bonded or Griffiths-type oxygen, giving adsorbed –O and a radical, followed by a second electron transfer:

$$O_2 + H^+ + e^- \rightarrow O_{ads} + OH \qquad (132)$$

$$OH + e^- \rightarrow OH^-_{ads} \qquad (133)$$

may be possible steps. The β value also implies that the bonding of dioxygen is slight and not substrate-dependent.

The situation in alkaline solutions is very different. In this case, many materials that exhibit little adsorption of oxygenated material show reasonable rates at high pH. Carbons(120) are good examples. In general, these materials often have low Tafel slopes (typically $3RT/2F$), indicating a chemical step following a preliminary one-electron transfer. The reaction on these materials is pH independent, which implies a process of the type(120):

$$O_2 + e^- \rightarrow O_2^- \qquad (132')$$

$$O_2^- + H_2O + e^- \rightarrow (O_2H)^- + OH^- \quad \text{(rds)} \qquad (133')$$

Other surfaces, typically platinum, show pH-dependent processes which have been variously explained. Damjanović and Brusić(53) believe that the rds is similar to reaction (93) under Temkin conditions, with a Tafel slope or RT/F:

$$O_2 + H_2O + e^- \rightarrow O_2H + OH^- \qquad (134)$$

in which the (OH^-) dependence, resulting from the Temkin term as in reaction (93), is -0.5. Other investigators(121) find an (OH^-) reaction order of -1. i.e. overpotential is independent of pH, with a Tafel slope of about RT/F; the main process is of the following type, under Langmuir conditions:

$$O_2 + H_2O + e^- \rightarrow O_2H + OH^- \qquad (135)$$

$$O_2H \rightarrow OH + O \quad \text{(rds)} \qquad (136)$$

which is probably "electrocatalytic," i.e., it involves strong adsorption.

Overall, it would appear that in alkaline solutions close to ordinary temperatures, a few surfaces show an electrocatalytic pathway, normally characterized by strong adsorption of reaction products, while others operate (at a somewhat lower rate, perhaps an order of magnitude less) more or less via a redox process, reducing oxygen to O_2H^- ($E_0 \sim 0.68$ V/SHE). For the latter materials, the alkaline medium is virtually a homogeneous catalyst, owing to its stabilizing effect on the reaction product, O_2H^-. This is essentially a non-substrate-dependent process, except at a few materials, for example, the basal plane of stress-relieved pyrolytic graphite, which may have no interaction for dioxygen, and shows very low rates (cf. Ref. 122). Thus, the horizontal $\log_i - \Delta G_{ads}$ relationship (for which the η at constant i varies with pH) would appear to be superimposed upon a volcano relationship for a reaction involving adsorption of products whose η at constant i is close to being pH independent (or at least has a smaller dependence). The latter reaction is characteristic of at least some of the platinum group metals, platinum being again close to the volcano maximum. As pH increases, the rates on the two groups of materials become very similar. This implies that meaningful distinctions in the alkaline solution range should be conducted in only moderately basic media, at, for example, pH values around 10.

A special group of compounds, because they introduce another facet of electrocatalysis, are transition metal, square-planar macrocyclics (phthalocyanines, porphyrins, Pfeiffer compounds, tetraazaanulenes, etc.; see, for examples, Ref. 123). The compounds of most importance in electrocatalysis that have emerged are quaternary nitrogen chelates, resembling biochemical materials such as hemoglobin and the cytochromes. Like the latter compounds, they are capable of binding dioxygen via Pauling-type complexes. Suitable compounds (e.g., iron phthalocyanines, polyphthalocyanines, and sulfinated derivatives) show high turnover numbers and have sufficient stabilities to be used as catalysts in alkaline(124) and acid(125) solutions. They appear to function via the "redox catalysis" concept of Beck,(126) which also applies on transition metal oxides(27) and thiospinels.(128) This concept is similar to that previously discussed for surface states on semiconductors: essentially, if the redox couple at the active site has a reversible potential close to that of the couple involved in the electrocatalytic process, optimum rates will result. For example, if the process in alkaline solution

$$M + O_2 \rightleftarrows M^+ - O_2^- \tag{137}$$

has a surface redox potential close to 0.68 V, optimum catalysis to HO_2^- will result. This is exactly the same as saying $\overline{\Delta G}_{ads} = 0$ as in Eq. (82): on platinum in acid solution, $\overline{\Delta G}_{ads} = 0$ occurs at about 0.8 V; the couple being the surface redox process

$$Pr + H_2O + 2e^- \rightarrow PtO + 2H^+ \text{ (or with PtOH)} \tag{138}$$

Hence, volcano relations should also arise as a function of redox potential.

One side of one is shown, with the correct slope, in Ref. 129 for oxygen reduction in alkaline solution. For the macrocyclics, optimum catalysis demands optimum spin crossover(129) and electronic conductivity is of the charge transfer complex type in thin layers via charged reaction intermediates.(124) In acid solutions, rates are lower on the macrocyclics, but some recent work on "face-to-face" cobalt porphyrins is exciting.(130)

6.4. Organic Oxidations†

The most studied reaction has been methanol oxidation(131) (reviewed in Ref. 132), though volcano relations have been noted for ethylene(133) and formic acid oxidation.(134) Useful reviews on methanol oxidation and on specific(132) electrocatalysis have been given by McNichol.(135) Rates of organic oxidations are low. In general, fuels such as methanol are, therefore, reformed to give hydrogen for more efficient oxidation in a fuel cell. Reactions normally involve processes such as,(33,131,136–138)

$$(CH_xO_y)_{ads} + OH_{ads} \rightarrow \text{products} \tag{139}$$

where some of the products are poisons, but are slowly eliminated as CO_2 in the steady state. Initial rates, involving H_{ads} oxidation, may, however, be high. Complex reactions, involving branched chains, have been discussed by Parsons(139) on a volcano basis. OH_{ads} comes from the process

$$M + H_2O \rightarrow MOH + H^+ + e^- \tag{140}$$

and the maximum in the volcano curve occurs at $\Delta G_{ads} \simeq 0$. Platinum is normally close to the maximum, as expected.

An interesting aspect of these processes is that there appears to be a specific "spillover" effect when alloys are used to fine-tune around the maximum of the volcano, for example, with Pt–Sn for methanol oxidation in acid solution.(140,141) "Spillover" was first suggested in electrocatalysis as an explanation for the high activity of surface platinum for oxygen reduction on tungsten bronzes.(142) Reaction intermediates are envisaged to diffuse from sites on one surface phase to another during the reaction, on which adsorption is optimized.

A mention of underpotentially deposited metals may be made after this observation. In general, such layers can mimic the substrate material (e.g., lead on platinum), but no optimization of catalysis has been observed, at least in the case of oxgen reduction in acid solution.(143)

Finally, why are oxgyen reactions, such as dioxygen reduction or hydrocarbon oxidation, slow compared with hydrogen reactions for materials at the top of the volcano relation. This is clear from Figure 4. Oxygen intermediates are multiple, and are all high energy, so that reduction of barrier heights by increasing heat of adsorption is self defeating, since strongly bonded material is irreversibly adsorbed, and finally place exchange occurs with destruction of the (metal) catalyst lattice and complete oxidation of the surface. Activation energies are, therefore, rather high, and preexponential terms are low. In contrast, the hydrogen reaction is a low-barrier, single-adsorbed, intermediate process, with no possible irreversibility on Pt group metals. This permits rates similar to those of reactions with no adsorption (redox processes).

---

† See also Chapter 10 of this volume by Rudd and Conway.

6.5. Chlorine Evolution

The evolution of chlorine from acidic solutions is certainly an electrocatalytic reaction, but experimental difficulties have arisen in fundamental studies, owing to corrosion in the chloride medium. Much work has nevertheless been carried out over the past 12–15 years on the chlorine evolution reaction and its mechanisms. A comprehensive review on this topic, including the relation of electrode performance to chemical composition of oxide films and their band structures, has been given by Novak, Tilak, and Conway in the *Modern Aspects of Electrochemistry* series.(44a)

Traditional electrodes have been graphite based; but since 1970, RuO_2 on TiO_2/Ti has been used(144) very successfully in the chloralkali industry. This material seems to have optimum electrocatalytic properties and exceptional corrosion resistance.

Recent work has been carried out by Conway and Novak(145,146) on the role of the oxide film, plus coadsorbed Cl^- ion at Pt electrodes in the chlorine evolution reaction; optimum electrocatalysis appears to arise at a surface at which appreciable coverage of specifically adsorbed Cl^- ion exists *together* with an incomplete film of OH and O species. Thick oxide films on Ir and Ru electrodes are also very effective electrocatalysts.

6.6. General Remarks on Practical Electrocatalysts

In practical systems or devices, the important characteristic of a catalyst electrode is watts per unit cost, or moles reacted per unit cost. This requires stability, corrosion resistance, high surface area, and sheer performance.

In general, the platinum metals have performances that outweigh their cost, and they can be used at very low loadings. In fuel cells, $0.5\ \mathrm{mg\ cm^{-2}}$ of Pt at $80\ \mathrm{m^2\ g^{-1}}$ will outperform any other catalyst in performance and cost ($\sim$\$45/kW). Poorer catalysts, e.g., silver in alkaline solutions, require heavier loadings to reach comparable levels of performance, and hence function less well (diffusion losses), in a vicious circle.

It is beyond the scope of this chapter to discuss the preparation and properties of high-surface-area catalysts. This is reviewed in detail in Ref. 147.

References

1. F. P. Bowden and E. K. Rideal, *Proc. R. Soc. London Ser. A***120**, 59 (1928).
2. A. N. Frumkin, N. Polianovskaya, I. Bagorskaya, and N. Grigoryev, *J. Electroanal. Chem.* **33**, 319 (1971).
3. N. Kobosev and W. Monblanowa, *Acta Physicochim. URSS* **1**, 611 (1934); see also **4**, 395 (1936); *Zh. Fiz. Khim.* **7**, 645 (1936).
4. W. Grubb, *Nature* **198**, 883 (1963).
5. H. A. Liebhafsky and E. J. Cairns, *Fuel Cells and Fuel Batteries*, Wiley, New York (1968), pp. 474–523.
6. J. O'M. Bockris and H. Wroblowa, *J. Electroanal. Chem.* **7**, 428 (1964).
7. J. O'M. Bockris, *Trans. Faraday Soc.* **43**, 417 (1947).
8. J. O'M. Bockris and E. C. Potter, *J. Electrochem. Soc.* **99**, 169 (1952).
9. P. Ruetschi and P. Delahay, (a) *J. Chem. Phys.* **23**, 195 (1955); (b) **23**, 1167 (1955).
10. P. Ruetschi and P. Delahay, *J. Chem. Phys.* **23**, 566 (1955).
11. (a) B. E. Conway and J. O'M. Bockris, *Naturwiss* **43**, 446 (1956); (b) *Nature* **178**, 488 (1956).
12. B. E. Conway and J. O'M. Bockris, *J. Chem. Phys.* **26**, 532 (1956).
13. R. Parsons, *Trans. Faraday Soc.* **54**, 1053 (1958).
14. R. Parsons, *Surf. Sci.* **2**, 418 (1964); see also A. N. Frumkin, B. B. Damaskin, and O. A. Petrii, *Elektrokhimiya* **12**, 3 (1976), and references quoted therein.
15. H. Gerischer, *Bull. Chim. Soc. Belg.* **67**, 506 (1958).
16. S. Srinivasan, H. Wroblowa, and J. O'M. Bockris, *Adv. Catal.* **17**, 351 (1967).
17. A. J. Appleby, *Catal. Rev.* **4**(2), 221 (1970).
18. J. P. Hoare, *The Electrochemistry of Oxygen*, Wiley, New York (1968).
19. A. J. Appleby, in *Modern Aspects of Electrochemistry*, Vol. 9, B. E. Conway and J. O'M. Bockris, eds., Plenum Press, New York (1974), p. 369.
20. A. P. Fickett, *Sci. Am.* **239**(6), 70 (1978).
21. S. Arrhenius, *Z. Phys. Chem.* **4**, 226 (1889).
22. M. Bodenstein, *Z. Phys. Chem.* **85**, 329 (1913).
23. L. Michaelis and M. L. Menten, *Biochem. Z.* **49**, 333 (1913).
24. J. A. Christiansen and H. A. Kramers, *Z. Phys. Chem.* **104**, 541 (1923).
25. K. Clusius and C. N. Hinshelwood, *Proc. R. Soc. London Ser. A* **128**, 75 (1980).
26. J. O'M. Bockris, *Chem. Rev.* **43**, 525 (1948).
27. J. O'M. Bockris and S. D. Argade, *J. Chem. Phys.* **49**, 5133 (1968).
28. A. N. Frumkin, *Z. Phys. Chem.* **A164**, 121 (1933); *Acta Physicochim. URSS* **6**, 502 (1937).
29. (a) P. Delahay and M. Kleinermann, *J. Am. Chem. Soc.* **82**, 4509 (1960); (b) A. N. Frumkin, *Elektrokhimiya* **1**, 394 (1965); (c) B. E. Conway, *Theory and Principles of Electrode Processes*, Ronald Press, New York (1964).
30. S. Trasatti, *J. Electroanal. Chem.* **33**, 351 (1971).
31. L. Antropov, *Tr. Erevanskogo politekhnich. in-ta* **2**, 7 (1946); *Tr. IV soveshchaniya po elektrokhimii, izd. AN USSR*, Moscow, 1959, p. 34; Kinetics of electrode processes and null points of metals, in *Counc. Scient. Ind. Res.*, New Delhi, 1960; *Zh. Fiz. Khim.* **24**, 1428 (1950); **25**, 1494 (1951); **37**, 965 (1963); *Ukr. Khim. Zh.* **29**, 557 (1963).
32. D. C. Grahame, *Chem. Rev.* **41**, 441 (1947).
33. H. Dahms and J. O'M. Bockris, *J. Electrochem. Soc.* **111**, 728 (1964).
34. M. Brĕzina and A. Hofmanova-Matĕjková, *Electrochim. Acta* **44**, 460 (1973).
35. D. S. Gnanamuthu and J. V. Petrocelli, *J. Electrochem. Soc.* **114**, 1036 (1967).
36. P. Stonehart and P. N. Ross, *Catal. Rev.* **12**, 1 (1975).
37. O. Stern, *Z. Elektrochem.* **30**, 508 (1924).
38. J. O'M. Bockris, R. J. Mannan, and A. Damjonovic, *J. Chem. Phys.* **48**, 1898 (1968).
39. D. C. Grahame and B. A. Soderberg, *J. Chem. Phys.* **22**, 449 (1954).
40. W. J. Plieth and K. J. Vetter, *Z. Phys. Chem. NF* **61**, 282 (1960).

41. J. Tafel, *Z. Phys. Chem.* **50**, 641 (1905); T. Erdey-Gruz and N. Volmer, *Z. Phys. Chem. A* **150**, 203 (1930); J. Horiuti and G. G. Ohamoto, *Sci. Pap. Inst. Phys. Chem. Res. Tokyo* **28**, 231 (1936).
42. J. O'M. Bockris and H. Mauser, *Can. J. Chem.* **37**, 475 (1959).
43. J. Horiuti, T. Keii, and K. Hirota, *J. Res. Inst. Catal. Hokkaido Univ.* **2**, 1 (1951–1953).
44. F. G. Will, *J. Electrochem. Soc.* **112**, 451 (1965); F. G. Will and C. A. Knorr, *Z. Electro. Chem.* **64**, 258 (1960); P. N. Ross, *J. Electroanal. Chem.* **76**, 139 (1977); K. Kinoshita and P. Stonehart, *Electrochim. Acta* **20**, 101 (1975); H. Angerstein-Kozlowska, W. B. A. Sharp, and B. E. Conway, in *Proceedings of the Symposium on Electrocatalysis*, M. W. Breiter, ed., The Electrochemical Society, Princeton, New Jersey (1974), p. 94.

44a. D. M. Novak, B. V. Tilik, and B. E. Conway, *Review in Modern Aspects of Electrochemistry*, Vol. 14, J. O'M. Bockris and B. E. Conway, eds., Plenum Press, New York (1981).

45. J. N. Brønsted, *Chem. Rev.* **5**, 231 (1928).
46. A. J. Arvia, *Israel J. Chem.* **18**, 89 (1979), and references quoted therein; P. Stonehart, W. A. Kozlowska, and B. E. Conway, *Proc. R. Soc. London Ser. A* **310**, 541 (1969); A. J. Appleby, *J. Electrochem. Soc.* **120**, 1205 (1973).
47. J. Horiuti and M. Polanyi, *Acta Physicochim. URSS* **2**, 505 (1935).
48. S. Glasstone, K. J. Laidler, and H. Eyring, *Theory of Rate Processes*, McGraw-Hill, New York (1941).
49. A. J. Appleby, in *Proceedings of the Symposium on Electrocatalysis*, M. W. Breiter, ed., The Electrochemical Society, Princeton, New Jersey (1974), p. 78.
50. B. E. Conway, *Proc. R. Soc. London Ser. A* **247**, 400 (1958).
51. J. O'M. Bockris and S. Srinivasan, *Electrochim. Acta.* **9**, 31 (1964).
52. A. N. Frumkin, P. Dolin, and B. V. Ershler, *Acta Physicochim. URSS* **13**, 779 (1940).
53. A. Damjonovic and V. Brusic, *Electrochim. Acta* **13**, 615 (1967).
54. M. Temkin, *Zh. Fiz. Khim.* **15**, 296 (1941).
55. A. A. Balandin, *The Problems of Chemical Kinetics, Catalysis and Reactivity*, Academy of Sciences, Moscow (1955), p. 462.
56. R. Gurney, *Proc. R. Soc. London Ser. A* **134**, 137 (1931).
57. J. A. V. Butler, *Proc. R. Soc. London Ser. A* **158**, 423 (1936).
58. G. Gamow, *Z. Phys.* **51**, 204 (1928) (for triangular barriers); a more realistic barrier is given by C. Eckart, *Phys. Rev.* **35**, 1303 (1930).
59. J. M. Hale, *J. Electroanal. Chem.*, **19**, 315 (1968).
60. R. R. Dogonadze, A. M. Kuznětsov, and V. G. Levich, *Electrochim. Acta* **13**, 1025 (1968).
61. A. J. Appleby, *J. Electroanal. Chem.* **51**, 1 (1974).
62. R. Parsons and J. O'M. Bockris, *Trans. Faraday. Soc.* **47**, 914 (1951); B. E. Conway and J. O'M. Bockris, *Proc. R. Soc. London Ser. A* **248**, 1394 (1958); *Electrochim. Acta* **3**, 340 (1962); B. E. Conway, *Can. J. Chem.* **37**, 178 (1959); J. O'M. Bockris and D. B. Matthews, *J. Chem. Phys.* **44**, 298 (1966); *Proc. R. Soc. London Ser. A* **292**, 479 (1966); M. Salomon and B. E. Conway, *J. Chem. Phys.* **41**, 3169 (1964); J. O'M. Bockris, S. Srinivasan, and D. B. Matthews, *Discuss. Farday Soc.* **39**, 239 (1965).
63. V. G. Levich, in *Advanced Treatise on Physical Chemistry*, Vol. IXB, *Electrochemistry*, H. Eyring, D. Henderson, and Y. Jost, eds., Academic Press, New York, p. 985.
64. L. Landau, *Phys. Z. Sowjetunion* **3**, 664 (1933).
65. N. F. Mott and R. W. Furney, *Electronic Processes in Ionic Crystals*, Oxford University Press, London (1940).
66. S. I. Pekar, *Investigations of the Electronic Theory of Crystals*, Fizmattiz, Moscow (1951).
67. W. Libby, *J. Phys. Chem.* **56**, 852 (1952).
68. J. Weiss, *Proc. R. Soc. London Ser. A* **222**, 128 (1954).
69. R. A. Marcus, *J. Chem. Phys.* **23**, 966 (1956); **26**, 867 (1957); **38**, 1858 (1963); **39**, 1734 (1963).
70. R. R. Dogonadze, in *Reactions of Molecules at Electrodes*, N. S. Hush, ed., Wiley, New

York (1971).

71. R. A. Marcus, *Can. J. Chem.* **37**, 138 (1959); *Trans. Symp. Electrode Processors*, E. Yeager, ed., Wiley, New York (1961), p. 239.
72. V. G. Levich, in *Advances in Electrochemistry and Electrochemical Engineering*, Vol. 4, P. Delahay and C. W. Tobias, eds., Interscience, New York (1966).
73. L. Landau, *Phys. Z. Sowjetunion* **1**, 88 (1932); **2**, 46 (1932); C. Zener, *Proc. R. Soc. London Ser. A* **137**, 696 (1932); **140**, 660 (1933); see also E. G. C. Stuckelberg, *Helv. Phys. Acta.* **5**, 369 (1932).
74. R. P. Bowden and K. E. W. Grew, *Discuss. Faraday Soc.* **1**, 86 (1947).
75. E. D. German, R. R. Dogonadze, A. M. Kutnetsov, V. G. Levich, and Y. I. Kharkats, *Elektrokhimiya* **6**, 350 (1970).
76. H. Imai and P. Delahay, *J. Phys. Chem.* **66**, 1683 (1962).
77. R. A. Marcus, *Discuss. Faraday Soc.* **29**, 21 (1921); *J. Phys. Chem.* **67**, 853, 2889 (1963); *J. Chem. Phys.* **43**, 679 (1965).
78. L. I. Krishtalik, *Elektrokhimiya* **6**, 507 (1970).
79. J. O'M. Bockris and R. K. Sen, *Mol. Phys.* **29**, 357 (1975).
80. R. A. Marcus, in *Proceedings of the Symposium on Electrode Processes, 1979*, S. Bruckenstein, B. Miller, J. D. E. McIntyne, and E. Yeager, eds., The Electrochemical Society, Princeton, New Jersey (1980), p. 1.
81. H. S. Johnson, *Gas Phase Reaction Rate Theory*, Ronald Press, New York (1966), p. 177.
82. R. A. Marcus, *J. Phys. Chem.* **72**, 891 (1968); R. A. Marcus and A. Cohen, *J. Phys. Chem.* **72**, 4249 (1968).
83. A. J. Appleby, J. O'M. Bockris, B. E. Conway, and R. K. Sen, in *MTP—International Review of Science and Technology—Electrochemistry*, Butterworths, London (1972).
84. C. M. Marschoff and P. J. Aragon, *J. Electrochem. Soc.* **123**, 213 (1966).
85. J. O'M. Bockris, in *Proceedings of the Symposium on Electrocatalysis, San Francisco, 1974*, M. Brieter, ed., The Electrochemical Society, Princeton, New Jersey (1974), p. 64; see also Ref. 49.
86. S. U. M. Khan, P. Wright, and J. O'M. Bockris, *Elektrokhimiya* **13**, 914 (1977).
87. H. Gerischer, *Z. Phys. Chem.* **26**, 223, 325 (1960).
88. M. Green, in *Modern Aspects of Electrochemistry*, Vol. 2, J. O'M. Bockris, ed., Butterworths, London (1959), p. 343.
89. H. Gerischer, *Electrochim. Acta* **13**, 1467 (1968); W. Mehl and F. Lohmann, *Electrochim. Acta* **13**, 1459, 1467 (1968).
90. H. Angerstein-Kozlowska, W. B. A. Sharp, and B. E. Conway, in *Proceedings of the Symposium on Electrocatalysis, San Francisco, 1974*, M. Brieter, ed., The Electrochemical Society, Princeton, New Jersey (1974), p. 94.
91. A. J. Appleby, G. Bronoel, M. Chemla, H. Kita, *et al.*, Hydrogen, in *Electrochemistry of the Elements*, A. J. Bard and H. Lund, eds., Marcel Dekker, New York (1982).
92. *Proceedings of the Symposium on Electrocatalysis*, The Electrochemical Society, Princeton, New Jersey (1974).
93. *Conference Proceedings, Fuel Cell Catalysis Workshop*, EPRI SR-13, Electric Power Research Institute, Palo Alto, California (1975).
94. *Proceedings of the Symposium on Electrode Materials for Energy Conversion and Storage*, The Electrochemical Society, Princeton, New Jersey (1977).
95. *Proceedings of the Symposium on Industrial Water Electrolysis*, The Electrochemical Society, Princeton, New Jersey (1978).
96. *Proceedings of the Workshop on the Electrocatalysis of Fuel Cell Reactions*, The Electrochemical Society, Princeton, New Jersey (1979).
97. A. T. Kuhn, in *Electrochemistry*, H. Bloom and F. Gutmann, eds., Plenum Press, New York (1977), p. 148.
98. D. R. Flinn and S. Schuldiner, *Electrochim. Acta* **19**, 421 (1974).

99. E. Yeager, private communication.
100. J. O'M. Bockris and D. F. A. Koch, *J. Phys. Chem.* **65**, 1941 (1961).
101. W. Vogel, J. Lundquist, P. Ross, and P. Stonehart, *Electrochim. Acta* **20**, 79 (1975).
102. S. Schuldiner, *J. Electrochem. Soc.* **107**, 452 (1960).
103. L. Pauling, *The Nature of the Chemical Bond*, Cornell University Press, Ithaca, New York (1948); D. D. Eley, *J. Phys. Coll. Chem.* **55**, 1017 (1961); see Ref. 19, p. 403.
104. L. I. Krishtalik, *Zh. Fiz. Khim.* **33**, 1715 (1959); **34**, 117 (1960).
105. M. A. V. Devanathan and M. Selvaratriam, *Trans. Faraday Soc.* **56**, 1820 (1960).
106. R. Parsons, *Trans. Faraday Soc.* **59**, 1340 (1960).
107. M. Breiter, *Ann. New York Acad. Sci.* **101**, 709 (1963).
108. B. E. Conway, E. M. Beatty, and P. A. D. DeMaine, *Electrochim. Acta* **7**, 39 (1962); K. Gössner and U. Freyer, *Z. Phys. Chem. N.F.* **63**, 132 (1962); K. Gössner and F. Mansfeld, *Z. Phys. Chem. N.F.* **63**, 143 (1969).
109. D. J. Barclay, *J. Electroanal. Chem.* **44**, 47 (1973).
110. L. I. Krishtalik, in *Advances in Electrochemistry and Electrochemical Engineering*, Vol. 7, P. Delahay and C. Tobias, eds., Interscience, New York (1970), p. 283.
111. S. Schuldiner, *J. Electrochem. Soc.* **107**, 452 (1960).
112. W. A. Pliskin and R. P. Eischens, *Z. Phys. Chem. N.F.* **24** 11 (1960).
113. E. Yeager, in *Electrocatalysis on Non-Metallic Surfaces*, NBS Special Publications 445 (1976), p. 203.
114. J. A. McGinnety, in *MTP International Reviews of Science, Inorganic Chemistry*, Series I, Vol. 5, D. Sharp, ed., Butterworths, London (1972), p. 229; J. S. Valentine, *Chem. Rev.* **73**, 235 (1973).
115. L. Pauling, *Nature* **203**, 183 (1964).
116. A. J. Appleby, *Surf. Sci.* **27**, 225 (1971).
117. A. Damjanovic and V. Brusic, *Electrochim. Acta* **12**, 1171 (1967).
118. A. J. Appleby, p. 23 in Ref. 96.
119. F. G. Will, p. 71 in Ref. 93.
120. A. J. Appleby and J. Marie, *Electrochim. Acta* **24**, 195 (1979).
121. M. Appel and A. J. Appleby, *C.R. Acad. Sci. Paris* **280C**, 551 (1975).
122. I. Morcos and E. Yeager, *Electrochim. Acta* **15**, 953 (1970).
123. H. Alt, H. Binder, W. Linder, and G. Sandstede, *J. Electroanal. Chem.* **31**, App. 19 (1971).
124. A. J. Appleby and M. Savy, in Ref. 94, p. 321, and references therein.
125. E. Yeager, P. Bindra, N. Doddapaneni, J. C. Huang, R. K. Sen, and J. Zagal, EPRI EM-505, Electric Power Research Institute, Palo Alto, California (1977); J. A. van Veen and C. Visser, *electrochim. Acta* **24**, 921 (1979), and references therein.
126. F. Beck, W. Dammert, J. Heiss, H. Hiller, and R. Polster, *Z. Naturforsch.* **28A**, 1009 (1973); F. Beck, *Ber. Bunsenges. Phys. Chem.* **77**, 353 (1973).
127. G. Feuillade, J. Bouet, and B. Chenaux, *Electrochim. Acta* **15**, 1527 (1970).
128. H. Behret, H. Bender, and G. Sandstede, *Electrochim. Acta* **20**, 111 (1975).
129. A. J. Appleby, M. Savy, and P. Caro, *J. Electroanal. Chem.* **111**, 91 (1980).
130. J. P. Collman, P. Denisovich, Y. Konai, M. Marrocco, C. Koval, and F. V. Anson, *J. Am. Chem. Soc.* **102**, 6027 (1980).
131. O. A. Khazova, Yu. B. Vasilev, and V. S. Bagotskii, *Elektrokhimiya* **10**, 606 (1974).
132. B. D. McNichol, p. 93 in Ref. 96.
133. A. T. Kuhn, H. Wroblowa, and J. O'M. Bockris, *Trans. Faraday Soc.* **63**, 1458 (1967).
134. A. Capon and R. Parsons, *J. Electroanal. Chem.* **44**, 239 (1973).
135. B. D. McNichol, *Specialist Periodical Reports on Catalysis*, Vol. 2, The Chemical Society, London (1979).
136. R. Kh. Burshtein, V. S. Tyurin, and A. G. Pshenichnikov, *Dokl. Akad. Nauk USSR* **160**, 629 (1965).
137. V. A. Gromyko, Yu. B. Vasilev, and V. S. Bagotskii, *Elektrokhimiya* **8**, 1238 (1972).
138. V. S. Bagotskiĭ and Yu. B. Vasilev, *Electrochim. Acta* **9**, 69 (1964).

139. R. Parsons, *Discuss. Faraday Soc.* **45**, 40 (1968).
140. B. D. McNichol, R. T. Short, and A. G. Chapman, *J. Chem. Soc. Faraday Trans. 1* **72**, 2735 (1976); *J. Appl. Electrochem.* **6**, 221 (1976).
141. M. R. Andrew, J. S. Drury, B. D. McNichol, C. Pinnington, and R. T. Short, *J. Appl. Electrochem.* **6**, 99 (1976); see also the discussion of R. Parsons, *Surf. Sci.* **18**, 28 (1969).
142. J. O'M. Bockris, and J. McHardy, *J. Electrochem. Soc.* **120**, 53, 61 (1973).
143. E. Yeager, Report EPRI EM 1814 (1981).
144. W. O'Grady, C. Iwakura, J. Huang, and E. Yeager, p. 286 in Ref. 92; S. Pizzini, G. Buzzanca, C. Mari, L. Rossi, and S. Torchio, *Mat. Res. Bull.* **7**, 449 (1972); D. Galizzioli, F. Tantardini, and S. Trassati, *J. Appl. Electrochem.* **4**, 57, 203 (1974).
145. B. E. Conway and D. M. Novak, *J. Electroanal. Chem.* **99**, 133 (1979).
146. B. E. Conway and D. M. Novak, *J. Chem. Soc., Faraday Trans. 1* **75**, 2454 (1979).
147. K. Kinoshita and P. Stonehart, in *Modern Aspects of Electrochemistry*, Vol. 12, B. E. Conway and J. O'M. Bockris, eds., Plenum Press, New York (1977).

5

Hydrogen Electrode Reaction on Electrocatalytically Active Metals

M. ENYO

1. Introduction

Studies on the hydrogen electrode reaction (HER) could probably be traced back to the time of Faraday, who observed loss with time of a mixed gas of H_2 and O_2 once produced and kept in a closed one-compartment electrolysis cell. This was a typical example of what is now called electrocatalysis.(1,2) A parallelism between the hydrogen overpotential and relative rate of catalytic recombination reaction of hydrogen atoms on various metals was already noted by Bonhoeffer in 1924,(3) and the HER was thus accepted as a means by which one may obtain information on the catalytic characteristics of various metallic materials.

Kinetic studies on hydrogen evolution on various electrode materials were conducted early in this century by Tafel.(4) The results of his observations led to the well-known equation

$$\eta = a + b \log i \tag{1}$$

where η is the overpotential, i the current density (c.d.), and a and b are constants. Investigations were then devoted to the mechanistic interpretation of the Tafel relationship on the basis of experimental data, mainly in the cathodic region. In the 1930s, among others we may recall the work by

---

M. ENYO • The Research Institute for Catalysis, Hokkaido University, Sapporo, Japan.

Erdey-Gruz and Volmer(5) and Butler,(6) to whom we owe a rate expression for charge transfer processes. Later, Frumkin(7–10) took into account the potential distribution at the electrode–electrolyte interface and its influence upon the process of discharge of ions. Experimentally observable quantities other than the Tafel constants have also been employed since then in elucidating the mechanism. For example, experimental observations of and attempts of theoretical interpretation of the electrolytic hydrogen–deuterium separation factor were presented by Topley and Eyring,(11) Horiuti,(12–18) and others,(19–26) as briefly reviewed elsewhere.(27)

After a more or less interrupted period in the early 1940s, the field again was studied intensively, beginning in the late 1940s and extending to the 1960s. A large number of reports were published by so many investigators that it would not be possible to list them adequately here. Significant progress was made during this period in experimental techniques as well, in particular the use of transient methods, ac impedance techniques, and isotope tracers. Extensive efforts were also made to ensure stringent purification of systems.

Why is there such a deep interest in this field? We may point out some of the probable reasons, such as (a) a hope to elucidate the HER mechanism as a prototype for heterogeneous reaction kinetics, (b) to obtain a systematic view on the catalytic properties of various metals, (c) the existence of many related important fields such as corrosion of metals, electrolytic hydrogenation of organic substances, etc., and (d) some more up-to-date reasons, such as efficient hydrogen production or use of hydrogen in fuel cells, and seeking a prospect toward the so-called hydrogen economy.

In this short review, it is hoped to examine the present status of mechanistic studies of the HER. Particular stress will be placed on the direction of decomposition of the overall reaction into elementary steps and discussion on the activity of the reaction intermediate. The latter plays an important role in discussing hydrogen pressure equivalent to hydrogen overpotential or electroreduction of substances on the hydrogen electrode. Correspondingly, most of the discussion will be restricted to electrocatalytically active metals, mainly those in groups VIII and Ib of the periodic table.(28,29) It is not intended to review the whole vast area of this field, nor will discussions be given on other important topics, such as charge transfer theory,(30–39) the double-layer effect in electrode kinetics,(8,40,41) effects of anion adsorption,(9,10) the effect of adsorption energy of hydrogen(42) on rates, etc.; many excellent reviews, cited above, are available on those topics.

2. Adsorption of Hydrogen on Metal Electrodes

2.1. Hydrogen Wave by a Potential Sweep Technique

Hydrogen dissociatively adsorbs on many metals from the gas phase, especially on those which are catalytically active.(28) In electrochemical sys-

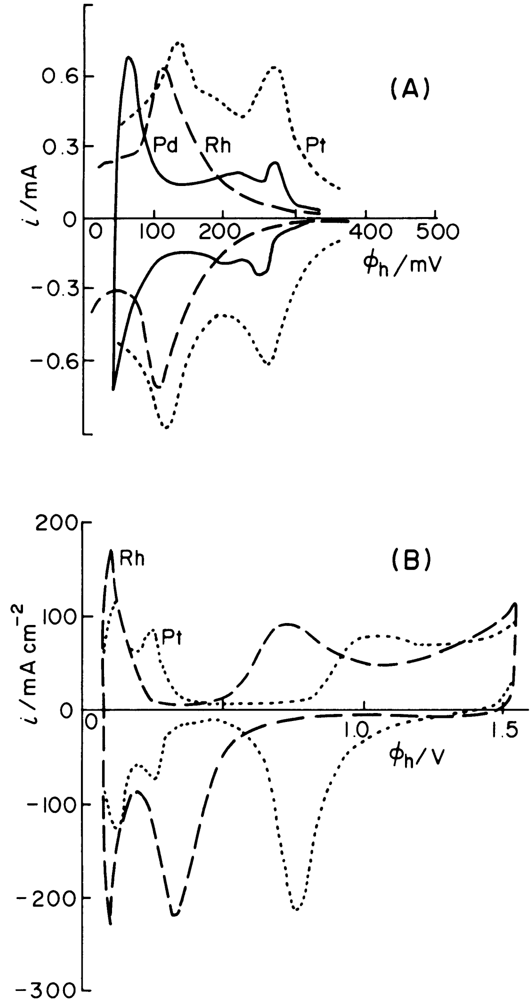

Figure 1. Current–potential profiles at some noble metals obtained by the potential sweep technique. Potential ϕ_h is referred to the reversible hydrogen electrode potential. (a) Pt, Rh, and Pd black electrodes deposited on Au in H_2SO_4 (pH = 1) (Chevillot *et al.*[46]). (b) Smooth Pt and Rh electrodes in 1 *M* H_2SO_4 at 298 K. Potential sweep rate 40 mV sec^{-1} (Baker[47]).

tems, the existence of a hydrogen adatom H(a) on many electrocatalytically active (noble) metals has been demonstrated by observation, by means of the potentiodynamic potential-sweep technique (cyclic-voltammetry) of a current due to its formation or ionization (the hydrogen wave) by the (Volmer) reaction, $H(a) \rightleftharpoons H^+ + e$. Exceptions are those elements in group Ib where no appreciable amount of H(a) is observed in spite of their fair electrocatalytic activity for the HER. The hydrogen wave is obtained at potentials considerably positive to the reversible hydrogen electrode under 1 atm hydrogen pressure.[40,43–45] Typical hydrogen waves are shown in Figure 1.[46,47] It is seen (a) that the hydrogen wave usually appears in the potential region between 0 and 0.4 V (or less) positive to the reversible hydrogen electrode (hence it may be called "underpotential" deposition,[48]) and (b) the anodic (ionization) and cathodic (deposition) waves are almost symmetrical, particularly on platinum metals which are electrocatalytically highly active, indicating a very rapid rate of the Volmer reaction. Not much difference is seen between electrodeposited (Figure 1a) and smooth (Figure 1b) electrodes. That the hydrogen wave indeed originates from adsorbed hydrogen was demonstrated by a technique of thermal desorption at elevated temperatures from the electrode after it was removed from the solution, in the case of tungsten carbide,(49) pyrolytic graphite,(50) and Ni.(51)

The gross amount of electricity involved in the hydrogen wave on Pt is very reproducible and seemingly corresponds to one monoatomic layer (surface coverage unity) of H(a), e.g., $210\,\mu\mathrm{C\,cm^{-2}}$ (true) on Pt, depending somewhat on the crystal surface orientation. Thus, it is likely that the Pt surface is almost fully covered with H(a) at the reversible hydrogen electrode potential under 1 atm hydrogen.(52) An analogous conclusion was also reached on Rh, Ir,(52) and on Pd.(46) On Ni, the data are not consistent among researchers, owing probably to involvement of surface oxidation; thus, the surface coverage by H(a) has been reported to be much smaller than unity(53) or close to unity.(51)

On Pt, this amount has been shown to agree with the true surface area measured by means of the BET method,(54) providing a simple and convenient means for evaluating *in situ* the true surface area of the electrode or knowing the effective area after a fraction of the electrode surface has been covered with some inert substance, e.g., as in electrosorption of organics.

2.2. Adsorption Isotherm for Atomic Hydrogen

By integration along the time axis of the hydrogen wave in Figure 1, one obtains a relation between surface coverage and the electrode potential or, after converting the latter to the corresponding hydrogen pressure $P_{\mathrm{H_2}}$ by a thermodynamic (Nernst) equation, the adsorption isotherm of hydrogen (solid lines in Figure 2).(55) It is observed that the amount of H(a), or the surface coverage, θ, changes approximately linearly with $\log P_{\mathrm{H_2}}$, leading to a semilogarithmic isotherm (the Temkin isotherm)† in a wide region of θ but not very close to zero or unity:

$$\theta = c_1 + c_2 \log P_{\mathrm{H_2}} \tag{2}$$

where c's are constants. When equilibrium in the dissociative adsorption of H_2 obtains, we have, in terms of chemical potentials,

$$\mu_{H_2} = 2\mu_{\mathrm{H(a)}}$$

---

† The fact that in the original cyclic voltammogram for H(a) on, e.g., Pt or Ir, three or four distinct peaks are observed, means that a Temkin adsorption isotherm does *not*, in fact, represent the behavior. Integral isotherms are relatively insensitive for distinguishing Temkin behavior from discrete (3–4 state) multistate adsorption (Eds.).

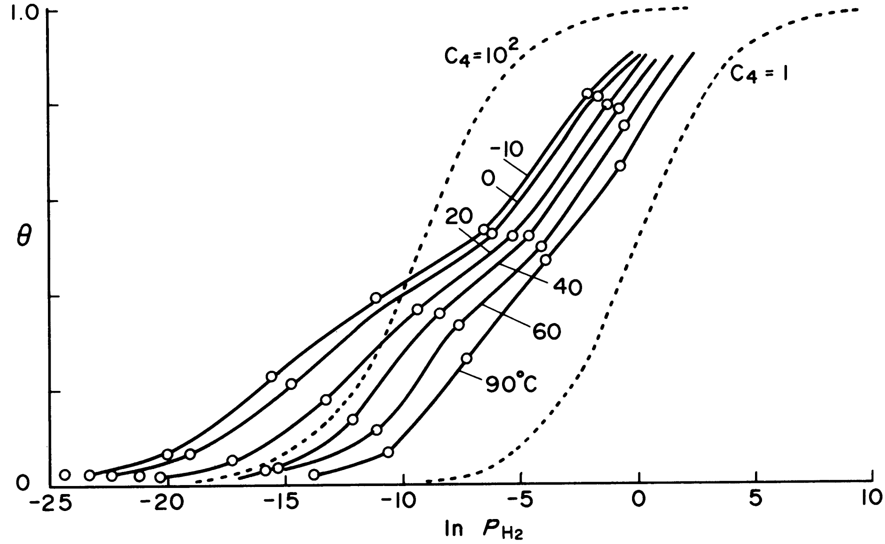

Figure 2. Hydrogen adsorption isotherm on smooth Pt in 2 *M* H_2SO_4 (Böld and Breiter(55)). Dotted lines indicate isotherms expected for the Langmuir isotherm $c_4(P_{H_2})^{1/2} = \theta/(1-\theta)$ with $c_4 = 1$ or 10^2 atm$^{-1/2}$ (see text).

or, in terms of the hydrogen pressure and the H(a) activity a_H,

$$c_3 + (1/2)\ln P_{H_2} = \ln a_H \tag{3}$$

Referring to Eq. (2), this means that θ and a_H are also related to each other by a semilogarithmic relation. It is hence reasonable to write,(56,57)

$$a_H = \frac{\theta}{1-\theta}\exp U\theta \tag{4}$$

where U is a constant which may represent interaction energy (in units of RT) among H(a)'s, or else is called the heterogeneity factor(58) as it may originate from heterogeneous structure of the surface. It is readily seen that Eq. (4) reduces, on the one hand, to the Langmuir isotherm when $U = 0$, and, on the other hand, to the semilogarithmic isotherm when θ is not close to zero or unity (but see footnote on p. 246).

An approximate overall average value of U in Eq. (4) can be deduced from Figure 2. Eliminating a_H in Eq. (4) using Eq. (3), we obtain

$$c_3P_{H_2}^{1/2} = \frac{\theta}{1-\theta}\exp U\theta \tag{5}$$

and hence

$$\frac{d\ln P_{H_2}}{d\theta} = \left[\frac{1}{\theta(1-\theta)} + U\right] \tag{6}$$

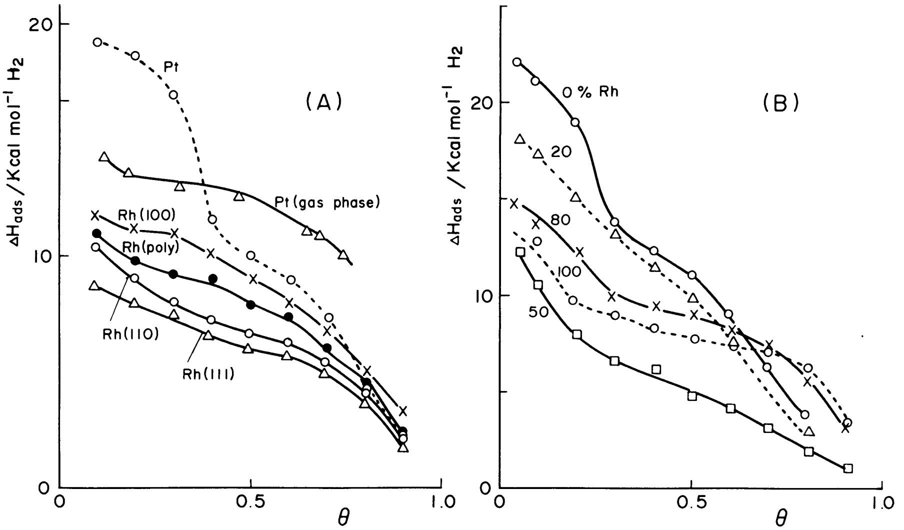

Figure 3. Heat of hydrogen adsorption as a function of surface coverage. (a) Pt[(62)] and Rh[(65)] electrodes in 0.5 M H_2SO_4. (b) Pt–Rh alloy electrodes[(67)] in 0.5 M H_2SO_4.

which predicts a sigmoid shape of the θ vs. $\log P_{H_2}$ relation, in apparent agreement with actual observations. According to Figure 2, or to analogous ones reported by other authors,[(59,60)] the derivative in Eq. (6) at $\theta = 1/2$ takes a value roughly 20 at 303 K. With these data, Eq. (6) readily yields $U = 6$ or corresponds to ~30.2 kJ mol^{-1} H_2 (or 15.1 kJ mol^{-1} H).[†] This is comparable with the value of decrease with surface coverage of the heat of adsorption of hydrogen, ~29.4 kJ mol^{-1} H_2 per unit coverage in gas phase experiments on Pt[(61)], or somewhat smaller than the value 54.6 kJ[(62)] on the Pt electrode obtained from the temperature dependence of curves in Figure 2. Analogous behavior of decrease of the adsorption heat with coverage was also reported on single-crystal planes of Pt[(63,64)] or Rh,[(65)] Pt–Au alloy electrodes,[(66)] Pt–Rh alloy electrodes,[(67)] etc.; cf. Figure 3.[(62,65,67)]

In Figure 2 are also given (dotted lines) typical curves anticipated for the Langmuir isotherm

$$c_4(P_{H_2})^{1/2} = \frac{\theta}{1-\theta}$$

with $c_4 = 1$ or 10^2. As is evident from this equation, the slope at $\theta = 1/2$ should be 8 in the case $U = 0$. This is, however, not usually observed in real experiments, indicating that the interaction–heterogeneity factor is significant in hydrogen adsorption on Pt and several other metals.

[†] The semilogarithmic isotherm $c_3' P_{H_2}^{1/2} = \exp U\theta$ which lacks the term $\theta/(1-\theta)$ in Eq. (5) was used by Klein and Vetter.[(68)] This leads to a higher value of U when it was deduced from adsorption isotherm data. As the slope $d \ln P_{H_2}/d\theta$ would be evaluated around $\theta = 1/2$, the difference would amount to $[\theta(1-\theta)]^{-1}RT = 4RT = 10.1$ kJ mol^{-1} H.

It is possible to evaluate U from direct analysis of the potential sweep curve.(69–71) Assuming reversibility of the hydrogen wave during the potential sweep, we may rewrite Eq. (5) as

$$c_5 \exp(-f\phi) = \frac{\theta}{1-\theta} \exp U\theta \tag{7}$$

where $f \equiv F/RT$ and ϕ is the electrode potential. The hydrogen ionization–deposition current i is given from this equation as

$$i = c_6 \frac{d\theta}{dt} = \frac{-fc_6 v}{[\theta(1-\theta)]^{-1} + U} \tag{8}$$

where $v \equiv d\phi/dt$, the potential sweep rate. At the peak i_{peak}, of the hydrogen wave at which $di/dt = 0$, we obtain $\theta_{\text{peak}} = 1/2$. Further, at the point $i_{1/2} = i_{\text{peak}}/2$, namely, at the half-wave, we find $\theta_{1/2} = \{1 \pm [1 - 4/(8+U)]^{1/2}\}/2$. If $U = 0$, this yields $\theta_{1/2} = (1 \pm 1/\sqrt{2})/2 = 0.8536$ or 0.1464. Substituting these values into Eq. (7), we find the half-wave width to be 92 mV if $U = 0$ or 60 mV if $U = -1.73$. Experimentally, the half-wave width on Rh or on component peaks after deconvolution of the hydrogen wave on Pt was reported to be narrower than 92 mV, thus leading to negative values of U, namely, the "negative" Temkin isotherm.(72,73) However, this seems to be rather unlikely, since the adsorption heat data are always decreasing with θ, namely, the "positive" Temkin isotherm. The cause of this disconcordance is not clear at present.

The complex structure of the hydrogen wave demonstrated in the potential sweep curve or also from impedance data(74) for the Pt electrode indicates the existence of distinguishable kinds of H(a), which are likely to be interchangeable.(75) These adsorbed states of H(a) are different in their chemical stability (strongly or weakly bonded hydrogen, etc.) and correspondingly in their chemical reactivity in, e.g., electrolytic hydrogenation reactions. For instance, it was reported that on Pt only the weakly bonded hydrogen was active for hydrogenation of ethylene in acidic media.(76)

The shape of the hydrogen wave on Pt is not very reproducible in detail, depending on the conditions of preparation of the electrode, on its history, e.g., anodization, on the kind of anion present in the solution,(77) etc. However, on a given electrode in a given solution, the profile is exactly reproducible if impurities are absent. It seems almost established that differences of profiles are caused by coexistence of various crystallographic planes on the electrode surface (see below, Section 2.3).

2.3. Structure of the Hydrogen Wave and Experiments on Single-Crystal Planes

On Pt, the hydrogen wave exhibits a clear structure, consisting of three (or more) separate peaks.(10,78) The structure usually becomes more apparent when a low rate of the potential sweep is employed.

It may be expected that the cause of the structure in the hydrogen wave on polycrystalline Pt is clarified by comparing the curves with those obtained on basic crystallographic planes. Will(79) carried out such observations on Pt single-crystal electrodes in 4 M H_2SO_4 and came to the conclusion that the three major peaks in the order of decreasing positive electrode potential can be attributed to (100), (111), and (110) planes, respectively. Along with recent developments of experimental technique, efforts have been directed to this problem by many investigators.(80–85) Typical results are shown in Figure 4.(80) The assignment of crystallographic planes to each of the peaks on the hydrogen wave does not appear, however, to be perfectly conclusive at present.(86) It is very interesting that the peak position is strongly dependent on the kind of anion present in the solution,(84,85) so that their relative positions can be changed depending on solution composition. Typical waves are shown in Figure 5.(84)

It is not quite clear at present what is the relation between these peaks and, e.g., two of the hydrogen adsorption peaks reported on the Pt (111) face from gas phase experiments(87) or with regard to the theoretical prediction of two adsorbed states of hydrogen on metal surfaces.(88)

3. Basic Kinetic Equations

For a general electrode reaction

$$(-m_1)S_1 + (-m_2)S_2 + \cdots = m_3S_3 + m_4S_4 + \cdots + ne \tag{8}$$

the free energy decrease (the reaction affinity), $-\Delta G$, is given by

$$-\Delta G = -\sum_j m_j\mu_j - n\mu_e \tag{9}$$

where the coefficient m_j for substance S_j is taken negative for the members in the reactants and positive for those in the products. For an easier sign convention, the reaction is written in such a direction that its forward transformation corresponds to the anodic process, e.g., hydrogen ionization in the HER. Both current and overpotential are correspondingly taken positive for a net anodic process.

When the reaction is at equilibrium, denoted by the subscript 0, and if experimental operations are such that all the μ_j's for the irreversible electrode process are kept the same values with those at equilibrium, we have

$$0 = -\sum_j m_j\mu_j - n\mu_{e,0} \tag{10}$$

From the last two equations, we obtain

$$-\Delta G = -n(\mu_e - \mu_{e,0}) = nF\eta \tag{11}$$

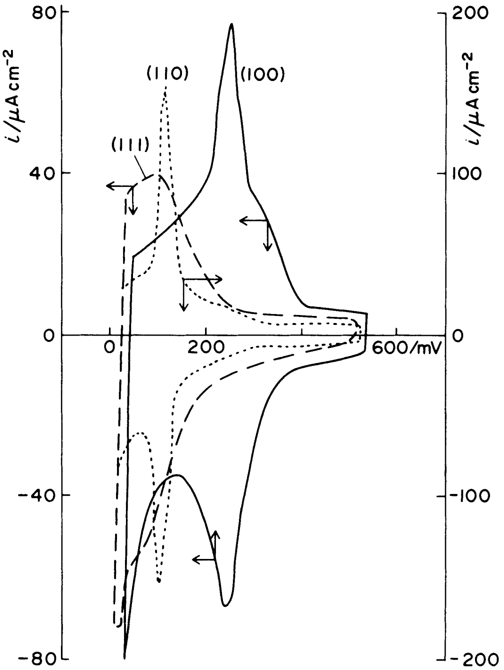

Figure 4. Current–potential profiles obtained by the potential sweep method on Pt single-crystal faces in 0.5 *M* H_2SO_4. Potential sweep rate 50 mV sec^{-1} (Yamamoto *et al.*(80)).

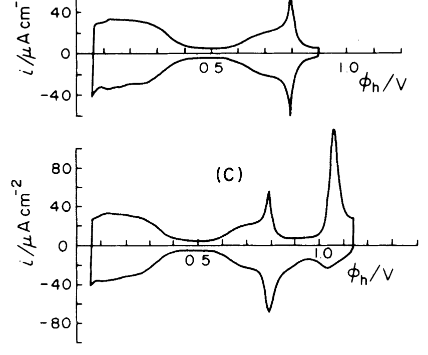

Figure 5. Anion effects on the current–potential profiles obtained by the potential sweep technique on a Pt [111] single-crystal face. Potential sweep rate 50 mV sec^{-1} (Clavilier *et al.*(84)). Arrows in (A) indicate the part of the hydrogen wave split by the anion effect: (A) 0.5 *M* H_2SO_4, (B) 0.1 *M* $HClO_4$ (in the potential range not covering the oxygen region), (C) 0.1 *M* $HClO_4$ (in potential region covering the oxygen region).

If the overall reaction is composed of a set of elementary steps connected in series, $-\Delta G$ is given as the sum of the free energy decreases of these steps multiplied with the stoichiometric number ν_s of step s;(89,90) thus

$$-\Delta G = -\sum_s \nu_s \Delta g_s \tag{12}$$

The step affinity is related to the ratio of the forward to backward unidirectional component rate of the step:(89)

$$\frac{v_{+s}}{v_{-s}} = \exp\left\{-\frac{\Delta g_s}{RT}\right\} \tag{13}$$

In the steady state of the reaction, the overall net reaction rate V, its unidirectional component rates, V_+ and V_-, and those of the constituent steps are interrelated to each other by

$$V = V_+ - V_- = (v_{+s} - v_{-s})/\nu_s \tag{14}$$

Further, these unidirectional rates are related to each other by(91,92)

$$V_+/V_- = \prod_s (v_{+s}/v_{-s}) \tag{15}$$

For electrode processes, it is convenient to convert the rate, v_{+s} etc., to the equivalent c.d., i_{+s} etc. As the rate v_{+s} is counted in terms of the number of times of occurrence per unit time of the step for each unit occurrence of the overall reaction, v_{+s}/ν_s is then equal to the number of times of occurrence of the overall reaction. Multiplying nF by this value, we obtain, therefore, the rate expressed in c.d. units:

$$(nF/\nu_s)v_{+s} = i_{+s} \tag{16}$$

The overall reaction rate is simply converted to c.d. by

$$i = i_+ - i_- = nFV = nF(V_+ - V_-) \tag{17}$$

According to the theory of absolute reaction rates,(93,94) we have

$$i_+ = \kappa(nFkT/AN_0\nu_r h)\exp(\mu_1 - \mu_*)/RT \equiv k_+a_I/f^* \tag{18}$$

$$i_- = \kappa(nFkT/AN_0\nu_r h)\exp(\mu_F - \mu_*)/RT \equiv k_-a_F/f^* \tag{19}$$

where κ is the transmission coefficient (which should be common to both the unidirectional rates under the same condition), A is the surface area of the electrode, N_0 is Avogadro's number, μ_I, μ_F, and μ_* are, respectively, chemical potentials of the initial, final, and activated states, I, F, and $*$, and $f^* \equiv \exp(-\mu_*/RT)$ is the activity coefficient of the activated state. If we consider i_+ and i_- under the same experimental conditions (hence at the same electrode potential), κ and μ_* are common to both i_+ and i_-. Consequently, we immediately obtain from the last two equations

$$\frac{i_+}{i_-} = \exp\left\{\frac{\mu_I - \mu_F}{RT}\right\} \tag{20}$$

4. Experimental Behavior and Possible Mechanisms— Existence of a Unique Rate-Determining Step

4.1. Possible Reaction Routes and Mechanisms

The terms *route* and *mechanism* will be used as defined below:

Route: a reaction pathway or a series combination of elementary steps which correspond to the overall reaction, no specification being given concerning the rate-controlling nature of the steps.

Mechanism: a route with specifications on the rate-controlling nature of the constituent steps, and their coupling.

Among various reaction routes proposed so far, it appears reasonable to consider the following two routes; other "external" causes such as ohmic resistivity of the solution, mass-transfer limitations, film formation, etc., will not be considered.

(A) The Tafel–Volmer route,

$$H_2 \leftrightarrow 2H(a), \qquad H(a) \leftrightarrow H^+ + e$$

(B) The Heyrovsky–Volmer route

$$H_2 \leftrightarrow H(a) + H^+ + e, \qquad H(a) \leftrightarrow H^+ + e$$

where H(a) denotes the hydrogen adatom intermediate, H^+ is proton in the solution, associated with OH^- or H_2O, and e is a free electron at the Fermi level in the electrode. In solutions containing alkali metal ions, a reaction intermediate of the alkali metal adatom or even alloy formation with the electrode metal was often concluded,(95,96) e.g., with Pt. In this case, the Volmer step would be divided into two steps, viz.,

$$H(a) + OH^- + Na^+ \leftrightarrow H_2O + Na(a), \qquad Na(a) \leftrightarrow Na^+ + e$$

We shall, however, not dwell on this matter since this would not affect very much the general analysis to be dealt with below, except that the kinetics might be different from those anticipated on the basis of an ordinary Volmer step. Although the formation of Na(a) on the electrode is probably well established, particularly on soft metals,(97,98) there might still remain a discussion as to Na(a) being actually a reaction intermediate of the HER or simply a by-product. Other reaction routes, involving reaction intermediates such as $H_2^+(a)$, $H^-(a)$, and solvated electrons,(99,100) etc. have not gained sufficient experimental support to demonstrate that these species should be considered seriously. Direct emission of electrons from the electrode into solution,(99–106) followed by their reaction with water yielding hydrogen, would only be significant, if at all, at very high cathodic overpotentials or on metals of high hydrogen overpotentials, and is not likely to be significant on the types of electrodes considered here.(106)

In each of those routes, if either step is sufficiently slow compared with the other, the overall rate should be almost completely controlled by that step; hence the step is called "rate determining," and the other preceding or following step may be approximated as being in quasiequilibrium. Four mechanisms then become possible:

A-1. The slow† Volmer–rapid† Tafel mechanism (the slow-discharge mechanism)

$$H_2 \rightleftarrows 2H(a), \qquad H(a) \leftarrow\!\sqcap\!\rightarrow H^+ + e$$

A-2. The rapid Volmer–slow Tafel mechanism (the slow combination or the catalytic mechanism)

$$H_2 \leftarrow\!\boxed{\ }\!\rightarrow 2H(a), \qquad H(a) \rightleftarrows H^+ + e$$

B-1. The slow Volmer–rapid Heyrovsky mechanism

$$H_2 \rightleftarrows H(a) + H^+ + e, \qquad H(a) \leftarrow\!\boxed{\ }\!\rightarrow H^+ + e$$

B-2. The rapid Volmer–slow Heyrovsky mechanism (the so-called atom + ion desorption mechanism),

$$H_2 \leftarrow\!\sqcup\!\rightarrow H(a) + H^+ + e, \qquad H(a) \rightleftarrows H^+ + e$$

4.2. The Stoichiometric Number

In order to obtain general expressions for various kinetic parameters such as the Tafel slope, it is necessary to take into account the stoichiometric correlation among the steps involved in the overall reaction. The stoichiometric number of the constituent step was thus introduced by Horiuti(107) and employed in steady state reaction rate theory.(89,93,94,108–111)

For the case where a unique rate-determining step (rds) exists in the reaction route, it directly follows from Eq. (12)

$$\Delta G = \nu_r \Delta g_r \tag{21}$$

and from Eqs. (13)–(17)

$$\frac{V_+}{V_-} = \frac{v_{+r}}{v_{-r}} = \exp\left\{\frac{-\Delta G}{\nu_r RT}\right\} \tag{22}$$

---

† The terms *slow* and *rapid* are often used in discussions of multistep reaction where one step is rate controlling. This usage is undesirable (except in transient states) since, in the steady-state, all steps proceed at the *same* rate. It is rather the *rate constant* of one step that is smaller or larger than that of another. Infinitely large magnitudes of the ratio of the rate constants are implied in this usage. The case with the ratio of finite magnitudes will be discussed later (Section 5).

Hence, from Eq. (14)

$$V = V_+\left[1 - \exp\left\{\frac{-\Delta G}{\nu_r RT}\right\}\right] \tag{23}$$

Equation (23) is used in the experimental determination of ν_r by observation of V_+, e.g., by the use of an isotope as a tracer, together with observations of V and $-\Delta G$. For electrode reactions, replacing ΔG with η and counting the rates in units of c.d., Eqs. (22) and (23) are rewritten, respectively, as

$$\frac{i_+}{i_-} = \exp\left\{\frac{nf\eta}{\nu_r}\right\} \tag{24}$$

and hence

$$i = i_+ - i_- = i_+\left[1 - \exp\left\{-\frac{nf\eta}{\nu_r}\right\}\right] \tag{25}$$

Near (at) equilibrium, i_+ takes the particular value i_0, the exchange c.d. We then obtain the well-known relation

$$(di/d\eta)_{\eta\to 0} = i_0 nf/\nu_r \tag{26}$$

Two techniques are employed to obtain i_0, namely, use of an isotope tracer and extrapolation to zero overpotential of a linear portion of the Tafel line at high polarizations. The tracer technique has the advantage that the rate at the reversible potential, i.e., i_0 itself, is directly measured but it may introduce an ambiguity due to the kinetic isotope effect. This is particularly serious in the case where hydrogen is the species concerned, e.g., as exemplified by the electrolytic hydrogen–deuterium separation factor which is reported to exceed 10 under some conditions. However, it was demonstrated(27,112–114) that this difficulty can be removed if one uses concentrated D_2 combined with a solution of light water. In this case, so far as the initial rate is concerned, the unidirectional rate in the anodic direction, hence the exchange c.d., is obtained by a direct observation of transfer rate of deuterium from the gas phase to the solution phase. There exists no contribution of light hydrogen to the total rate of movement of hydrogen in that direction. The exchange c.d. would have a different value from that in the pure light hydrogen system, but both the exchange c.d. and the polarization resistance $(d\eta/di)_{\eta\to 0}$ are obtained just as they are in such an isotopically mixed system. The correct value of ν_r is hence obtained provided that the reaction mechanism is maintained during this change of the system in isotopic composition. Results of the stoichiometric number obtained by this technique will be given later (see Table 1).

The method of extrapolation of a linear section of the Tafel line, which is realized over the high overpotential region, to zero overpotential is much simpler, but it introduces a degree of uncertainty as the method relies upon the assumption of a constant Tafel slope, independent of the overpotential. Experiments, however, often indicate some concave curvature in a "linear"

Tafel line, which would lead to an overestimate of the exchange c.d., and hence, of ν_r. On a Ni hydrogen electrode in alkaline solution, $\nu_r = 2$ was reported,$^{(115)}$ indicating slow discharge followed by a rapid Tafel step on the mechanism.

The stoichiometric numbers of steps other than the rds are not readily accessible by experiment, as these steps are kinetically invisible. The case where there is no unique rds will be discussed later (Section 5).

4.3. The Tafel Slope

The most intensively studied experimental parameter has naturally been the Tafel slope, i.e., the dependence of η upon $\log i$. The Tafel constants, α_+ and α_-, for the anodic and cathodic Tafel lines, respectively, are defined by the relation

$$\alpha_+ = \frac{1}{f}\left(\frac{\partial \ln i}{\partial \eta}\right)_{p_{\mathrm{H}_2}, a_{\mathrm{H}^+}} \quad (\eta \gg RT/F) \tag{27}†$$

$$\alpha_- = -\frac{1}{f}\left(\frac{\partial \ln i}{\partial \eta}\right)_{p_{\mathrm{H}_2}, a_{\mathrm{H}^+}} \quad (-\eta \gg RT/F) \tag{28}$$

These have the significance of a reaction order with respect to the electron.

The kinetic expression which covers the whole overpotential region is

$$\begin{aligned} i &= i_+ - i_- \\ &= i_0[\exp\{\alpha_+ f\eta\} - \exp\{-\alpha_- f\eta\}] \end{aligned} \tag{29}‡$$

---

† Owing to the contribution of the reverse reaction component rate, experimental evaluation of α_- directly from the η–$\log i$ relation is restricted to the region of $-\eta$ of at least several tens of millivolts separated from the equilibrium potential. Neglect of this, such as determining it at overpotentials as low as 20 mV, leads to a loss of certainty of the Tafel slope. If overpotential values smaller than 30 mV are involved, it is helpful to construct a plot of

$$\eta \text{ vs. } \log[i/\exp(nf\eta/\nu_r) - 1]$$

with adequate choice of ν_r of 1 or 2$^{(116)}$ [cf. Eqs. (29) and (30) below]. Although evaluation of α_- in this way, assuming a plausible value of ν_r, is not quite definitive, the values of the parameters are usually obtained with fair accuracy.

‡ Unfortunately, instead of Eq. (29), the following relation frequently has appeared in various publications, and was used in kinetic analyses:

$$i = i_0[\exp\{\beta n_r f\eta\} - \exp\{-(1-\beta)n_r f\eta\}] \tag{29a}$$

where β is the symmetry factor and n_r is the number of electrons involved in the rds. Were this relation valid over the whole range of η values, one should obtain βn_r and $(1-\beta)n_r$ from the Tafel slopes in the anodic and cathodic regions, respectively, and hence n_r by combining them. However, this equation is not generally valid.$^{(117)}$

Since we have a unique rds in the present case, we obtain from Eq. (24)

$$\frac{d \ln i_+}{d\eta} - \frac{d \ln i_-}{d\eta} = nf/\nu_r$$

or

$$\alpha_+ + \alpha_- = n/\nu_r \tag{30}$$

Equation (30) is, in principle, applicable for determining ν_r.(111) However, in practice, it has rather a limited application since, strictly speaking, it is valid only if α_+ and α_- are observed under the same experimental conditions, particularly the same electrode potential. In, e.g., the cathodic region, α_- is directly observable, but α_+ could be obtained only if a special technique is devised, such as the use of an isotope tracer.(118)

Another possibility is, of course, determination of α_- and α_+ in the cathodic and anodic regions, respectively, but it is then a prerequisite that these constants are indeed confirmed to be constant, independent of the electrode potential. Unfortunately, this is not necessarily expected in the case of the HER where a variation with electrode potential of the symmetry factor β is noticeable in some cases (cf. Figure 11 below), and more seriously, the anodic Tafel line does not exhibit any reasonable linearity.

A general expression for α_+ and α_- to cover various mechanisms has been repeatedly presented in the literature.(111,119–128) A simple derivation of these expressions will be given below. An approximation will be made throughout that the reaction conditions are such that the double-layer correction term is always negligible.

4.4. Magnitude of the Tafel Slope

The reaction mechanism of the general electrode reaction may be expressed in the form

$$z_+(1)\mathrm{S}_1 + \cdots + z_+(j)\mathrm{S}_j + \cdots \rightleftarrows \cdots \rightleftarrows I + n_I\mathrm{e} + \rho \tag{31}$$

$$I \leftarrow\!\boxed{}\!\rightarrow F(=F' + n_r\mathrm{e}) \quad \text{(rds)} \tag{32}$$

$$\rho + F' \rightleftarrows \cdots \rightleftarrows z_-(1)\mathrm{S}_1 + \cdots + z_-(j)\mathrm{S}_j + \cdots + n_F\mathrm{e} \tag{33}$$

where $z_+(j)$ and $z_-(j)$ are, respectively, the numbers of moles of S_j that are in equilibrium with I and F of the rds, n_I, n_r, and n_F are, respectively, the number of electrons (which can take the values zero) involved in each step [or possibly a group of steps in the case of Eqs. (31) and (33)], and ρ represents(108,109) an extra intermediate that may be produced together with the formation of I but does not participate in the rds. Here, e.g., a substance in a reduced form, S_R, belongs to the left-hand side of Eq. (31) and hence, $z_+(R)$ is likely to be positive. However, this is not necessarily always the case (e.g., where a disproportionation reaction is involved) and in fact is not implied in Eq. (31).

Since all the steps other than the rds are in quasiequilibrium, we have the following relation; from eq. (31),

$$\mu_I = \sum_j z_+(j)\mu_j - n_I\mu_e - \mu_\rho \tag{34}$$

and from Eqs. (32) and (33),

$$\mu_F = \sum_j z_-(j)\mu_j + (n_r + n_F)\mu_e - \mu_p \tag{35}$$

Substituting these into Eq. (20), we obtain

$$i_+/i_- = \exp\left\{\left(\sum_j z_+(j)\mu_j - \sum_j z_-(j)\mu_j - n\mu_e/\nu_r\right)\Big/RT\right\} \tag{36}$$

where n is related to n_I, etc., by

$$n = \nu_r(n_I + n_r + n_F) \tag{37}$$

Expressions for the individual unidirectional rates are obtained as follows. For brevity, we will assume ρ to be nonexistent. In Eqs. (34) and (35), μ_j is expressed in terms of the corresponding activity, a_j, as

$$\mu_j = \mu_j^0 + RT\ln a_j \tag{38}$$

and μ_e is directly related to the electrode potential ϕ as

$$\mu_e = \mu_e^0 - F\phi \tag{39}$$

where μ^0's are constants. Substituting Eqs. (34) and (35), respectively, into Eqs. (18) and (19), and using the last two equations, we obtain

$$i_+ = k_+\left[\prod_j a_j^{z_+(j)}\right]\exp\{(n_I F\phi - \mu_*)/RT\} \tag{40}$$

$$i_- = k_-\left[\prod_j a_j^{z_-(j)}\right]\exp\{(-[n_r + n_F]F\phi - \mu_*)/RT\} \tag{41}$$

where

$$k_+ = \kappa(nFkT/AN_0\nu_r h)\exp\left\{\left(\sum_j z_+(j)\mu_j^0 - n_I\mu_e^0\right)\Big/RT\right\} \tag{42}$$

and

$$k_- = \kappa(nFkT/AN_0\nu_r h)\exp\left\{\left(\sum_j z_-(j)\mu_j^0 + [n_r + n_F]\mu_e^0\right)/RT\right\} \tag{43}$$

Both electrode potential and activity of the reaction intermediate exert influences upon μ_*. Introducing the symmetry factor β(30,110,111) and the activity coefficient f^* of the activated complex, the above rate expressions may be rewritten as

$$i_+ = k_+\left[\prod_j a_j^{z_+(j)}\right] \exp\{[n_I + \beta n_r]f\phi\}/f^* \tag{44}$$

and

$$i_- = k_-\left[\prod_j a_j^{z_-(j)}\right] \exp\{-[n_F + (1-\beta)n_r]f\phi\}/f^* \tag{45}$$

4.4.1. Low Surface Coverage with H(a)

In this case, we may approximate f^* as unity, because of negligible interaction between $*$ and H(a). Introducing the rate expressions obtained above in Eqs. (27) and (28), we obtain†

$$\alpha_+ = n_I + \beta n_r \tag{46}$$

and similarly,

$$\alpha_- = n_F + (1-\beta)n_r \tag{47}$$

The very frequently observed value of $\alpha_- = 1/2$ strongly suggests, according to Eq. (47), that $n_F = 0$, $\beta = 1/2$, and $n_r = 1$, and hence that the rate-determining step is the Volmer reaction.‡ As it tells nothing about the value of ν_r, it is not possible to decide whether the slow Volmer step is followed by a rapid Tafel or a rapid Heyrovsky step. In other cases, $\alpha_- = 1.5$ (on, e.g., Ag(129)) or 2 (on, e.g., Pt(130–132) and Pd(133,134)) are reported. The former value would indicate $n_F = 1$, $\beta = 1/2$, and $n_r = 1$; hence the rapid Volmer followed by a rate-determining Heyrovsky step, whereas the latter value would indicate $n_F = 2$ and $n_r = 0$, hence the rapid Volmer followed by a rate-determining Tafel step.

---

† These are of a somewhat modified form from analogous expressions derived by Matthews and Bockris:(119)

$$\alpha_+ = (s/\nu_r) + \beta n_r, \qquad \alpha_- = (t/\nu_r) + (1-\beta)n_r$$

where $s(t)$ is the number of electrons transferred prior to the rds for the formation of the required number of $I(F)$ for completion of a unit overall reaction, rather than such a number for the formation of *single* $I(F)$ as used here. It then follows that $n_I = s/\nu_r$ and $n_F = t/\nu_r$.

‡ It is possible to obtain $\alpha_- = 1/2$ in the case of the slow Heyrovsky mechanism. However, the possibility of this value for the rate-determining Heyrovsky step at high cathodic overpotentials, on the basis of the argument that the contribution of exp $(-n_F f\phi)$ in Eq. (45), which represents growth of θ with cathodic overpotential, drops out under that condition, is not generally justifiable (see below, Section 5.4.2).

4.4.2. High Surface Coverage with H(a)

The surface coverage of H(a) will grow to a significant magnitude under certain conditions, so that f^* may not be approximated as unity. If this were the case, e.g., the forward unidirectional rate $i_{+\mathrm{T}}$ of the Tafel step is expressed as, with $n_I = n_r = 0$,

$$i_{+\mathrm{T}} = k_{+\mathrm{T}} P_{\mathrm{H}_2} / f_T^* \tag{48}$$

Further, we may write$^{(108,109)}$ by analogy with Eq. (4),

$$1/f_T^* = \Theta_{*(0)} \exp\{-u^* \theta\} \tag{49}$$

where $\Theta_{*(0)}$ is the probability that the adsorption site for the activated complex is vacant, and u^* (in units of RT) is the interaction energy between the critical complex and the surrounding H(a).

Assuming a two-site activated complex for the Tafel step, we develop Eq. (49) as

$$1/f_{\mathrm{T}}^* = (1-\theta)^2 \psi \exp\{-2\lambda_{\mathrm{T}} U \theta\}$$

where ψ is a function of θ, usually not significantly deviating from unity,$^{(108)}$ and $\lambda_{\mathrm{T}} = u_{\mathrm{T}}^*/2U$ with U defined in Eq. (4). Hence, approximating $\psi = 1$, we have

$$i_{+\mathrm{T}} = k_{+\mathrm{T}} P_{\mathrm{H}_2} (1-\theta)^2 \exp\{-2\lambda_{\mathrm{T}} U \theta\} \tag{50}$$

Similarly, $i_{-\mathrm{T}}$ is expressed, assuming quasiequilibrium Volmer step, hence taking $n_F = 2$ and $n_r = 0$,

$$i_{-\mathrm{T}} = k'_{-\mathrm{T}} a_{\mathrm{H}^+}^2 \exp\{-2f\phi\}/f^* = k_{-\mathrm{T}} a_{\mathrm{H}}^2 / f^*$$

or, employing Eq. (4)

$$i_{-\mathrm{T}} = k_{-\mathrm{T}} \theta^2 \exp\{2(1-\lambda_{\mathrm{T}}) U \theta\} \tag{51}$$

Defining,

$$W \equiv \theta/\theta_0, \qquad Z \equiv (1-\theta)/(1-\theta_0)$$

and

$$Q \equiv \exp\{U(\theta - \theta_0)\} \tag{52}$$

we rewrite Eqs. (50) and (51) as

$$i_{+\mathrm{T}} = i_{0\mathrm{T}} Z^2 Q^{-2\lambda_{\mathrm{T}}} \tag{53}$$

and

$$i_{-\mathrm{T}} = i_{0T} W^2 Q^{2(1-\lambda_{\mathrm{T}})} = i_{0\mathrm{T}} Z^2 Q^{-2\lambda_{\mathrm{T}}} \gamma_{\mathrm{H}}^2 \tag{54}$$

where $i_{0\mathrm{T}}$ is the exchange c.d. of the Tafel step expressed as

$$\begin{aligned} i_{0\mathrm{T}} &= k_{+\mathrm{T}} P_{\mathrm{H}_2} (1-\theta)^2 \exp\{-2\lambda_{\mathrm{T}} U \theta_0\} \\ &= k_{-\mathrm{T}} \theta^2 \exp\{2(1-\lambda_{\mathrm{T}}) U \theta_0\} \end{aligned} \tag{55}$$

and, cf. Eqs. (4) and (52),

$$\gamma_H \equiv (W/Z)Q = a_H/a_{H,0} \tag{56}$$

Equation (53) indicates that i_{+T} is constant only if Z and Q are both approximated as unity, that is, if we have the condition θ, $\theta_0 \ll 1$. Similarly, i_{-T} is proportional to γ_H^2 (i.e., 30 mV slope) only if this condition is satisfied. Otherwise, both the Tafel lines will deviate from the simple behaviors.

Similarly, for the rate-determining Volmer step, we obtain from Eqs. (44) and (45),

$$i_{+V} = k_{+V}P_{H_2}^{1/2}\exp\{\beta f\phi\}/f_V^* \tag{57}$$

$$i_{-V} = k_{-V}a_{H^+}\exp\{-(1-\beta)f\phi\}/f_V^* \tag{58}$$

Assuming a one-site activated complex, we may write,[108,109]

$$1/f_V^* = (1-\theta)\exp\{-\lambda_V U\theta\} \tag{59}$$

where $\lambda_V \equiv u_V^*/U$. Employing this, we have

$$\begin{aligned} i_{+V} &= i_{0V}WQ^{(1-\lambda_V)}\exp\{\beta f\eta\} \\ &= i_{0V}Z\gamma_H Q^{-\lambda_V}\exp\{\beta f\eta\} \end{aligned} \tag{60}$$

$$i_{-V} = i_{0V}ZQ^{-\lambda_V}\exp\{-(1-\beta)f\eta\} \tag{61}$$

where

$$\begin{aligned} i_{0V} &= k_{+V}\theta_0\exp\{(1-\lambda_V)U\theta_0\}\exp\{\beta f\phi_0\} \\ &= k_{-V}a_{H^+}(1-\theta_0)\exp\{-\lambda_V U\theta_0\}\exp\{-(1-\beta)f\phi_0\} \end{aligned} \tag{62}$$

In the present case, however, $\theta = \theta_0 = \text{const}$, because of assumed quasiequilibrium in the Tafel step. Hence, $W = Q = 1$, or Eqs. (60) and (61) both reduce to simple forms, as seen in the literature. The case where W, Q are not equal to unity will be discussed later (Section 5).

4.5. The Reaction Orders

Reaction orders provide useful information in elucidating the reaction mechanism, as widely used in ordinary chemical reactions; their use in electrode processes was discussed in detail by Vetter[135] and others.[136–138]

If we keep μ_e (or the electrode potential ϕ) and all the activities, a_j's, constant except the activity a_k of the kth component S_k, Eqs. (9) and (22) yield[90]

$$\zeta_+(k) - \zeta_-(k) = -m_k/\nu_r \tag{63}$$

where ζ's are the reaction orders of the forward and reverse unidirectional rates with respect to the substance S_k, respectively, defined as

$$\zeta_+(k) \equiv RT\left(\frac{\partial \ln i_+}{\partial \mu_k}\right)_{\phi, a_{j\neq k}} = \left(\frac{\partial \ln i_+}{\partial \ln a_k}\right)_{\phi, a_{j\neq k}} \tag{64}$$

and

$$\zeta_-(k) \equiv RT\left(\frac{\partial \ln i_-}{\partial \mu_k}\right)_{\phi, a_{j\neq k}} = \left(\frac{\partial \ln i_-}{\partial \ln a_k}\right)_{\phi, a_{j\neq k}} \tag{65†}$$

Referring to Eq. (36), we can extend the above relation to

$$\zeta_+(k) - \zeta_-(k) = z_+(k) - z_-(k) = -m_k/\nu_r \tag{66}$$

i.e., the difference in ζ values (at the same value of ϕ) is equal to that in z values. Equation (66) is very useful in determining such ζ values as are not directly observable; e.g., at highly positive potentials, we obtain ζ_+ directly from experiments but not ζ_-. Also, this can be utilized in evaluating ν_r when the ζ's are constant, independent of ϕ and a_k.

The relations between ζ's and z's are readily obtained from Eqs. (40) and (41). These are

$$\zeta_+(k) = z_+(k) - \frac{1}{RT}\left(\frac{\partial \mu_*}{\partial \ln a_k}\right)_{\phi, a_{j\neq k}} \tag{67}$$

and

$$\zeta_-(k) = z_-(k) - \frac{1}{RT}\left(\frac{\partial \mu_*}{\partial \ln a_k}\right)_{\phi, a_{j\neq k}} \tag{68}$$

Equation (67) or (68) indicates that the reaction order ζ_+ (or ζ_-) experimentally observed is not necessarily an integer (or reciprocal integer), or equal to z_+ (or z_-) only if the term $(\partial \mu_*/\partial \ln a_k)_{\phi, a_{j\neq k}}$ is zero. This means that $z_+(z_-)$, which is of great importance in determining the reaction mechanism,(135) is experimentally obtainable if due attention is paid to the possible (change in) interaction of the activated complex with the surroundings. An experimental approach to this problem was discussed elsewhere,(90) and applied to the analysis of the kinetic data, particularly the reaction orders, of the chlorine electrode reaction on Pt, Rh, and Ir electrodes.(139) Fortunately, it appears that the reaction orders usually take values close to integers so that not much difficulty is likely to be involved in the deduction of z values from ζ values.

The reaction orders involved in the HER are pH dependent and affected by the hydrogen pressure. Dependence upon pH of the cathodic hydrogen evolution rate was occasionally studied. For example, no pH dependence was seen on Au, Ag, and Cu in the region of pH 2 ~ 0 in HCl or H_2SO_4

---

† Use of the term(127) "reaction order" for the variation with a_k of i_0 (and not i_+ or i_- at constant ϕ) is not advisable since, in that case, the chemical potential of electron, which is one reactant of the electrode reaction, is not kept constant. In connection with this, it is desirable to plot data obtained under various a_k values in the $\ln i$ vs. ϕ, rather than $\ln i$ vs. η, diagram, because then ζ values are clearly visualized in the figure.

solutions,(140) suggesting the rate-determining Tafel mechanism. On Pt, $i_0 \propto ([H^+])^{1/2}$ was reported in $10^{-3} \sim 0.5M$ H_2SO_4.(141–143) Analogously, the anodic hydrogen ionization rate on micro-Pt electrode(143) was independent of pH in the range 3–14, but dependent in the range <3. No pH dependence was observed on Rh and Ir electrodes.(143) Experimental studies of the pH dependence meet the problem of stringent purification of the system for maintaining reproducible surface state of the electrode during changes of the solution. This would be particularly difficult when supporting neutral salts are added to the system in order to avoid complexities caused by the double-layer correction term.(9,10)

There exist some reports on the hydrogen pressure dependence of the anodic ionization current. These will be presented later (Section 5.2).

5. Mechanism with No Unique Rate-Determining Step

5.1. Tracer Experiments

Use of deuterium in the mechanistic studies of the HER began shortly after its discovery in 1931. It was used in two directions: (a) as a tracer to measure the unidirectional component rate of the reaction, and (b) for examination of the kinetic isotope effect, namely, the electrolytic separation factor.

In tracer experiments, concentrated D_2 was used, combined with a light water solution, in order to avoid the complexity due to the isotope effect.(27,144–154) Further, the observations were made, not only on the isotope exchange rate which yields the exchange c.d., but also on the isotopic composition (D_2, HD, and H_2) of the gaseous hydrogen produced by the exchange reaction. It was then possible (a) to evaluate the stoichiometric number, (b) to determine the route of the HER by observation of time course of the isotopic composition, and (c) to determine individual rates of the elementary steps which constitute the reaction route. If we conduct the exchange experiments on the electrode under polarization, an overpotential dependence will be found of those component rates. The technique was applied to most of the electrocatalytically active metals at which the exchange reaction proceeds with a reasonable rate.

Results of the experiments have been summarized elsewhere,(27) and only brief comments will be given here: (a) results which support the Tafel–Volmer reaction route were obtained on Rh (in acid) and Rh and Ni (in alkaline solution), and partly on Pt, Pd, Ir, Au, and Ag (in acid solutions); (b) elementary step rates are frequently of comparable magnitudes, particularly on Rh and Ni; (c) correspondingly, the stoichiometric numbers often deviate from integer values; and (d) kinetics of the cathodic component rate of the Tafel step was second order in a_H, while that of the Volmer step indicated its symmetry factor $(1 - \beta)$ to be close to unity. Some results are summarized in Table 1.(27)

Table 1
Results of Tracer Experiments. Values of $m_0 \equiv i_{0V}/i_{0T}$ and $\bar{\nu}$. Hydrogen pressure: 20 ± 2 cm Hg, 298 K[27]

Electrode	Solution (pH)	m_0	$\bar{\nu}$ (± 0.1)
Pt	0.5 *M* NaOH (13.5)	$5 \sim 10$	1.1
	0.5 *M* $Na_2SO_4 + H_2SO_4$ ($0.9 \sim 1.9$)	$7 \sim 30$	1.0
Ir	0.5 *M* H_2SO_4	5	1.2
Au	0.5 *M* H_2SO_4	$5 \sim 20$	1.0
Ag	0.5 *M* H_2SO_4	$3 \sim 5$	$1.0 \sim 1.1$
Rh	0.5 *M* H_2SO_4	$1 \sim 3$	$1.0 \sim 1.3$
	0.25 *M* $K_2SO_4 + H_2SO_4$ (2.0)	$1 \sim 2$	$1.4 \sim 1.5$
	0.2 *M* K_2SO_4 + KOH (12.3)	$1 \sim 2$	$1.4 \sim 1.6$
	0.2 *M* K_2SO_4 + KOH (13.5)	$0.9 \sim 1$	$1.1 \sim 1.4$
Ni	0.5 *M* NaOH	$0.4 \sim 3$	$1.0 \sim 1.5$

The experimental fact that the rates (exchange c.d.'s) of the constituent steps, here Volmer and Tafel, are of comparable magnitudes was rather surprising as it was thought so far, through many experimental findings, that one particular step would be controlling the overall rate (a unique rds) and the other steps having sufficiently large rate constants that they do not influence the overall kinetics. In fact, even on Rh and Ni, for which the tracer experiments indicated $m_0 \equiv i_{0V}/i_{0T}$ to be of the order of magnitude of unity, experimentally observed Tafel lines have, nevertheless, ordinary shapes anticipated from the model with a unique rds.

As will be discussed later (Section 5.4), it is quite possible in such cases, with more than one irreversible step, to realize quasilinear Tafel lines which are usually accepted as characteristic of reactions with a unique rds.

5.2. Tafel Lines and Reaction Orders

Typical Tafel lines, cathodic and anodic, on Pt are shown in Figure 6.[155] The cathodic data usually give a linear relation with a slope of ~30 mV, and this is attributed to the rate-determining Tafel step. In good conformity with this, the anodic line exhibits a limiting current behavior, attributed also to this step as the maximum rate of dissociation of H_2 on Pt realized at negligible surface coverage with H(a). These behaviors, together with the first-order dependence upon hydrogen pressure[156-158] (but see other data,[159-162] where orders of 0–1 are found, depending on electrode preparation) are consistent with this mechanism. The cathodic Tafel line often tends to yield 120-mV slope at high cathodic overpotentials, suggesting an approach of the kinetics to the slow Volmer mechanism or indicating a mechanism change with respect to that in the other overpotential region.

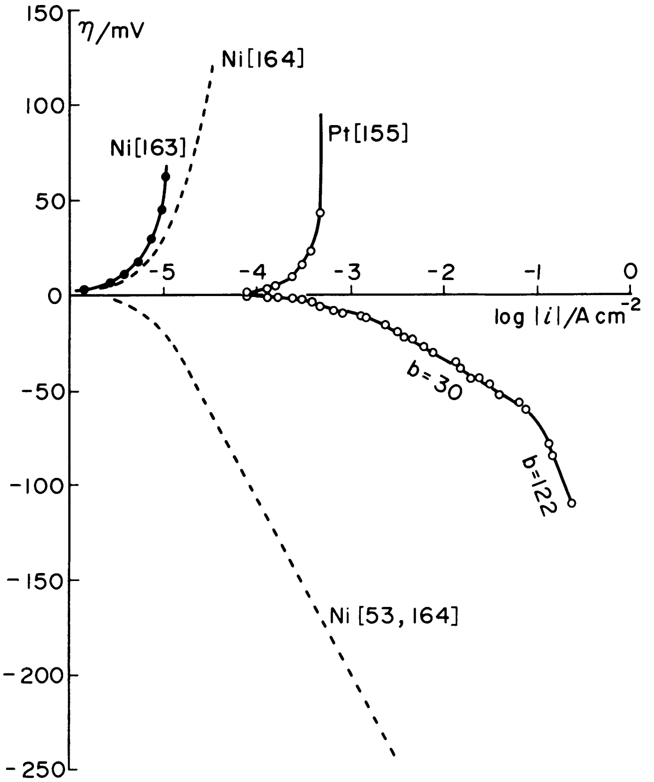

Figure 6. Hydrogen overpotential on Pt and Ni electrodes: Pt in 1 *M* H_2SO_4 (Schuldiner and Hoare(155)); Ni (anodic) in 0.1 *M* NaOH (Makrides(163)) and in 4 *M* KOH (Weininger and Brieter(164)); Ni (cathodic) in 1 *M* NaOH (Devanathan and Selvaratnam(53)) and in 4 *M* KOH (Weininger and Breiter(164)).

Typical Tafel lines on Ni in alkaline solution are seen also in Figure 6.(53,163,164) The anodic limiting current behavior which is observed would be attributable to the rate-determining Tafel step. In support of this, the rate of anodic ionization of H_2 on Ni in 1 *M* KOH or 0.1 *M* KOH was dependent on the first power of P_{H_2}.(165,166) On the other hand, an opposite view was presented,(167) claiming that the limiting current behavior is due to oxidation of the Ni electrode surface after the supply of H_2 by diffusion became insufficient. Because of lower electrocatalytic activity of Ni as compared with that of Pt, it is unlikely to exhibit such a rate control, and hence limiting current behavior, due to diffusion of H_2 in the solution, although the latter effect certainly interferes with the behavior in the case of active Pt electrodes.155)

The cathodic Tafel line on Ni is reasonably linear, with a slope of ~120 mV. However it is not impossible to account for this slope in terms of a rate-determining Tafel step, by considering interaction among H(a) and that between H(a) and the activated complex of the Tafel step,(108) but other experimental evidence seems to support the rate-determining Volmer step, such as tracer experiments cited above(154) and constancy of α_- in rather a wide range of η (cf. Figure 6). Accepting this view, and in conformity with a general trend of the mechanism change with η (see below), we can conclude that the mechanism is different in the anodic region, where the Tafel step is rate determining, and in the cathodic region, where the Volmer step is rate determining.

Reaction kinetics with comparable magnitudes of rate constants of the constituent steps, hence not having any unique rds, was often discussed. Hammett(168) was probably the first to examine such cases. He conducted polarization experiments on Pt in 0.1 *M* HCl or 0.1 *M* KOH and interpreted the data on the model of two steps in the Volmer–Tafel reaction route having similar magnitudes of exchange c.d.'s. The value of m_0 required in interpreting the polarization data on Pt was 7 ~ 18 for the repeated series of experiments.

More detailed analyses were conducted later,(169–176) both for the Volmer–Tafel and the Volmer–Heyrovsky reaction routes, with allowance for comparable magnitudes of exchange c.d.'s of the constituent steps. It became clear that such analyses of the so-called "linked/coupled"† mechanism could well provide an interpretation of some experimental data, as will be discussed later. Meanwhile, some comments will be made concerning the definition of the now widely accepted terms "rds" and other related topics.

5.3. Absence of rds and Affinity Distribution among the Constituent Steps

Two definitions of the rds appear to have been used in the literature which are different in a quantitative sense:

(a) The rds is such a step that it practically controls the overall reaction rate.

(b) In addition to (a), all the other steps are said to be so rapid that they can be treated as in quasiequilibrium during irreversible overall reaction.

The latter definition was, in fact, the basis of the analysis presented above, in Section 4. As already seen, the entire kinetic, as well as the physical, picture could be significantly simplified if one accepts definition (b). How good is such an approximation, in general, in the HER? Various experimental findings presented above in this chapter indicate that this definition of rds may, in some cases, be an oversimplification, and one would have to take a more general approach in the analysis of kinetics which cover a wide range of reaction conditions. This is to use the term rds only in the sense of (a) above.

---

† There has been some difference between the significance of the term "coupled" used by Enyo in earlier publications(170–173) and that used by Parsons(111) or by Bockris.(124,175) In the latter's terminology, "linked" or "dual" was used to mean the cases in which more than two elementary steps have exchange c.d.'s of similar magnitudes. Upon increase of the overpotential beyond a certain limit, the reaction would become "coupled," namely, both the steps become irreversible and have the same rate. These are altogether called "coupled" by Enyo. In the present chapter, the terminology proposed by Parsons and by Bockris will be used. The author is indebted to Professor Bockris for pointing out this difference.

If there is more than one step which is not in quasiequilibrium, one must pay attention to the distribution of the affinity (free energy decrease) of the overall reaction among such steps involved. This can readily be done starting with general equations already presented in Section 3. In short, the analysis would involve evaluation of the overall free energy decrease from free energy decreases of the constituent steps, calculation of the overall rate from rates of the steps, correlation of the forward and backward unidirectional component rates of an elementary step with the free energy decrease associated with it, and connection of the various step rates on the basis of the steady state mass balance requirements.

The affinity distribution in the present example of the Volmer–Tafel route of HER may be expressed by m:

$$m \equiv \Delta g_{\mathrm{T}}/\Delta g_{\mathrm{V}} \tag{69}$$

According to Eq. (14), with $\nu_{\mathrm{T}} = 1$ and $\nu_{\mathrm{V}} = 2$,

$$v_{+\mathrm{T}} - v_{-\mathrm{T}} = (v_{+\mathrm{V}} - v_{-\mathrm{V}})/2$$

or employing Eqs. (13) and (16),

$$i_{+\mathrm{T}}\left[1 - \exp\left\{\frac{\Delta g_{\mathrm{T}}}{RT}\right\}\right] = \frac{v_{+\mathrm{V}}}{2}\left[1 - \exp\left\{\frac{\Delta g_{\mathrm{V}}}{RT}\right\}\right] \tag{70}$$

The step affinities are written as

$$-\Delta g_{\mathrm{T}} = \mu_{\mathrm{H}_2} - 2\mu_{\mathrm{H}} = -2\mathrm{RT}\ln\gamma_{\mathrm{H}} \tag{71}$$

$$-\Delta g_{\mathrm{V}} = \mu_{\mathrm{H}} - (\mu_{\mathrm{H}^+} + \mu_e) = F\eta + RT\ln\gamma_{\mathrm{H}} \tag{72}$$

where γ_{H} is the ratio of a_{H} to that at equilibrium, defined in Eq. (56).

In the vicinity of the overall equilibrium, where $\eta \to 0$, $i_{+\mathrm{T}}$, etc. is replaced by $i_{0\mathrm{T}}$, etc., the exchange c.d. of the step. Hence, from Eq. (70), we find,

$$i_{0\mathrm{T}}\left(-\frac{\Delta g_{\mathrm{T}}}{RT}\right)_{\eta\to 0} = i_{0\mathrm{V}}\left(-\frac{\Delta g_{\mathrm{T}}}{RT}\right)_{\eta\to 0}$$

or

$$\left(\frac{\Delta g_{\mathrm{T}}}{\Delta g_{\mathrm{V}}}\right)_{\eta\to 0} = \frac{i_{0\mathrm{V}}}{i_{0\mathrm{T}}} \equiv m_0 \tag{73}$$

Typical results of calculations of m for the Volmer–Tafel route as a function of η are given in Figure 7.$^{(171-173)}$ It is seen that m has a tendency to approach a value of the order of magnitude of unity for high affinity values,

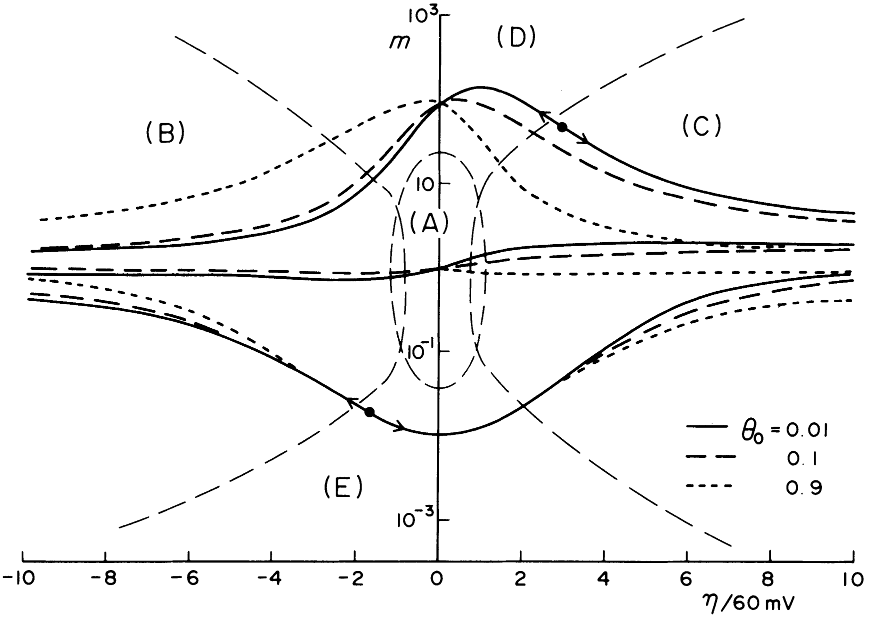

Figure 7. Theoretical curves showing affinity distribution $m \equiv \Delta g_T/\Delta g_V$ for the Tafel–Volmer route as a function of hydrogen overpotential for various values of $m_0 \equiv i_{0V}/i_{0T}$ and of θ_0 as indicated. Temkin isotherm with $u = 5$ and $\beta = 0.5$ are used. Territories indicate schematically the rate-determining characteristics of the constituent steps: (A) linked Tafel–Volmer, (B) rate-determining Volmer with coupled Tafel, (C) rate-determining Tafel with coupled Volmer, (D) Tafel uniquely rate determining, (E) Volmer uniquely rate determining.

both in the anodic and cathodic regions.† Even if m_0 is rather different from unity, say, 10^2, m takes a value less than 10 at $-\eta > 0.1$ V.

This means that the overall affinity is more or less evenly distributed between both steps. Hence, the affinity values of the steps become appreciable, and the "rapid" step should eventually become irreversible as seen from Eq. (13). In Figure 8 is shown the growth of η_V for the case $m_0 = 10^2$ as a function of η. For example, it is seen that the approximation for the Volmer step to be in quasiequilibrium (say, $|\eta_V| < 5$ mV) is permissible only in the overpotential range, $-60 < \eta/\text{mV} < 150$, for the case $\theta_0 = 0.01$. A much larger value of m_0 would be needed in order for η_V to be sufficiently small at cathodic overpotentials, of magnitudes encountered in ordinary experiments.

The rate-determining characteristics of the two steps and their variation with overpotential are schematically illustrated in Figure 7.

First, the situation in the region not too far from the equilibrium potential is described by m_0, namely, rate-determining Tafel behavior if $m_0 \gg 1$, Volmer if $m_0 \ll 1$, or linked if $m_0 \simeq 1$. Upon increase of $|\eta|$ (in the anodic or cathodic

---

† An analogous but symmetric shape of the affinity distribution vs. η relation could be obtained for the Heyrovsky–Volmer route.(171,172)

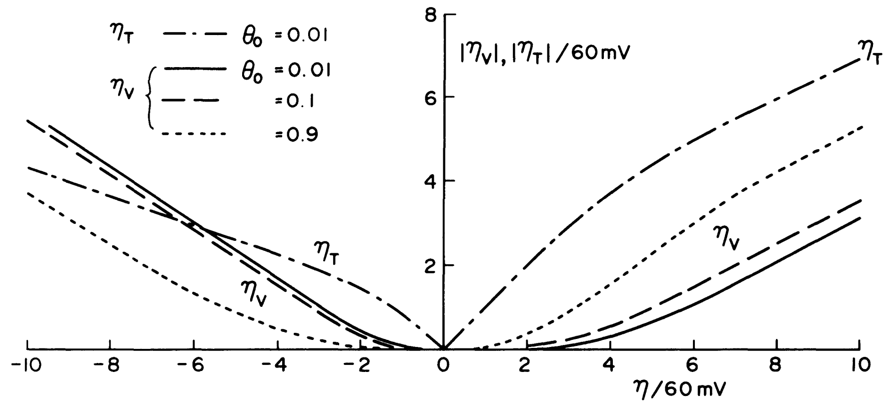

Figure 8. Growth of the component overpotentials $|\eta_V|$ and $|\eta_T|$ as a function of η for the case $m_0 = 10^2$. For further details, see text.

regions), the situation is described by the movement of a point on the curve which is predetermined by m_0 (and other kinetic parameters). Unless m_0 is very large (or small), exceeding, e.g., 10^2 (or 10^{-2}), the point soon moves into the region in which the reaction is coupled, i.e., both steps are completely irreversible.

A modification would be needed of the concept of the stoichiometric number if there exists no unique rds or there are other steps that are not in quasiequilibrium. Nevertheless, quantities included in Eq. (22) are experimentally obtainable without information concerning the rate-determining nature of the steps involved, and hence a "stoichiometric number" can be evaluated. Denoting the value in this sense by $\bar{\nu}$, we may rewrite Eq. (22) as

$$\bar{\nu} = \frac{-\Delta G}{RT \ln V_+/V_-} \tag{74}$$

Employing Eqs. (12), (13), and (15), one finds

$$\bar{\nu} = \sum_s \nu_s \Delta g_s \Big/ \sum \Delta g_s \tag{75}$$

Thus, $\bar{\nu}$ evaluated in this way has the physical meaning of an average of stoichiometric numbers of the constituent steps, each weighted in the affinity values associated with them.

5.4. Synthesis of the Overall Kinetics

5.4.1. The Tafel–Volmer Route

It is easy to derive the expression for the overall net rate i from the component rates of the two steps.(171–173,177) From Eqs. (53), (54), (60), and

(61), we obtain

$$\begin{aligned} i &= i_{+\mathrm{T}} - i_{-\mathrm{T}} = i_{+\mathrm{V}} - i_{-\mathrm{V}} \\ &= i_{0\mathrm{T}} Z^2 Q^{-2\lambda_\mathrm{T}} [1 - \gamma_\mathrm{H}^2] \\ &= i_{0\mathrm{V}} Z Q^{-\lambda_\mathrm{V}} [\gamma_\mathrm{H} - e^{-f\eta}]\, e^{\beta f \eta} \\ &= \frac{1 - \gamma_\mathrm{H}\, e^{-f\eta}}{Q^{2\lambda_\mathrm{T}}/i_{0\mathrm{T}} Z^2 + (\gamma_\mathrm{H} Q^{\lambda_\mathrm{V}}/i_{0\mathrm{V}} Z)\, e^{-\beta f \eta}} \end{aligned} \tag{76}$$

It is seen that the rate-controlling nature of the two steps basically depends on relative magnitudes of the two terms in the denominator of this equation, particularly on the ratio of $i_{0\mathrm{V}}$ to $i_{0\mathrm{T}}$, and further depends on the magnitude of the overpotential included in the second term. This is particularly so as γ_H increases with the negative increase of η. Thus, the ratio of the two terms, r, viz.,

$$r \equiv \frac{i_{0\mathrm{V}}}{i_{0\mathrm{V}}} \frac{Q^{2\lambda_\mathrm{T} - \lambda_\mathrm{V}}}{\gamma_\mathrm{H} Z} e^{\beta f \eta} \tag{77}$$

has a tendency to increase almost exponentially with η, and hence the expression for the overall rate readily changes with η. It is seen that, with large positive increase of η, unless $m_0 \equiv i_{0\mathrm{V}}/i_{0\mathrm{T}}$ has extreme values, Eq. (76) reduces to

$$i = i_{0\mathrm{T}} Z^2 Q^{-2\lambda_\mathrm{T}} \tag{78}$$

which is characteristic of the slow Tafel mechanism. Conversely, with large negative increase of η,

$$i = -i_{0\mathrm{V}} Z Q^{\lambda_\mathrm{V}} e^{-(1-\beta) f \eta} \tag{79}$$

which is characteristic of the slow Volmer mechanism.

Behaviors of the η vs. $\log i$ relation expected under various experimental conditions are reproduced in Figure 9 for the case of the "positive" Temkin isotherm. The shape is naturally dependent upon the adsorption isotherm,(173) but several conclusions below can be drawn without having precise information concerning the isotherm. Generally speaking, the use of the Temkin isotherm yields smoother curves, and possibly better fit with experiment, than the use of the Langmuir isotherm.(173)

(a) If $m_0 = 10^2$, characteristics of the slow Tafel mechanism are seen in the region $\eta > -0.2$ V, whereas those of the slow Volmer mechanism appear at more negative overpotentials.

(b) If $m_0 = 1$, characteristics of the slow Tafel and slow Volmer mechanism appear in the anodic and in the cathodic region, respectively.

(c) If $m_0 = 10^{-2}$, characteristics of the slow Volmer mechanism are seen in the region $\eta < +0.2$ V, but in the region $\eta > +0.2$V, the characteristics of the Tafel step appear.

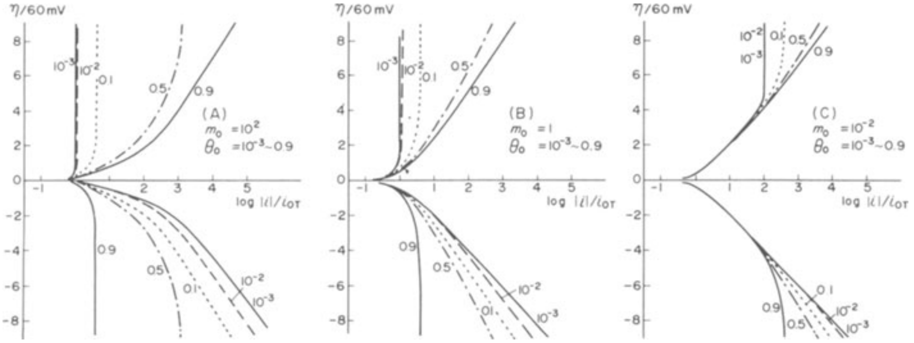

Figure 9. Current–overpotential relations calculated for the Tafel–Volmer route, with (A) $m_0 = 10^2$, (B) 1, or (C) 10^{-2}, with various values of θ_0. Temkin isotherm with $u = 5$ and $\beta = 0.5$ are assumed.

5.4.2. The Heyrovsky–Volmer Route

This route can be analyzed similarly; major results are[(173)]

$$i = Z[1 - e^{-2f\eta}]\left\{\frac{1}{i_{0\mathrm{H}}Q^{-\lambda_\mathrm{H}}\exp(\beta_\mathrm{H}f\eta)} + \frac{1}{i_{0\mathrm{V}}Q^{-\lambda_\mathrm{V}}\exp[(1+\beta_\mathrm{V})f\eta]}\right\}^{-1} \tag{80}$$

$$\frac{1}{Z} = 1 - \theta_0 + \frac{\theta_0}{Q}\exp(-f\eta)\frac{\exp(f\eta) + m'_\mathrm{B}}{\exp(-f\eta) + m'_\mathrm{B}} \tag{81}$$

$$m'_\mathrm{B} = m_{\mathrm{B}0}Q^{(\lambda_\mathrm{V}-\lambda_\mathrm{H})}\exp(\beta_\mathrm{V} - \beta_\mathrm{H})f\eta \tag{82}$$

where $m_{\mathrm{B}0} \equiv i_{0\mathrm{V}}/i_{0\mathrm{H}}$, and λ_H and β_H are defined analogously with those in Section 4.4. With Eq. (80), the steady state η vs. $\log i$ relations quite analogous to those which have appeared in the literature[(111,135,178)] are readily obtained,[(173)] namely, a Tafel constant of 1.5 at low cathodic overpotentials and its change to 0.5 at high overpotentials, resulting in a break on the Tafel line.

However, one finds a significant difference in the meaning of the break from that currently understood. As already mentioned in the footnote to Eq. (47), it is not generally true that such a break is caused by saturation with H(a) of the electrode surface. Suppose that θ_0 is sufficiently small that Z and Q can both be approximated to unity [cf. Eq. (52)]. If $m_{\mathrm{B}0} \gg 1$, then for large cathodic overpotentials, Eq. (80) yields

$$i = -i_{0\mathrm{H}}\exp\{-(2 - \beta_\mathrm{H})f\eta\} \tag{83}$$

which is characteristic of the Heyrovsky step with a Tafel constant around 1.5. If $m_{\mathrm{B}0} \simeq 1$, the second term in the denominator grows rapidly with increase of $-\eta$, hence one finds

$$i = -i_{0V}\exp\{-(1-\beta_V)f\eta\} \tag{84}$$

which is characteristic of the Volmer step. With values of m_{B0}, finite but larger than unity, the Tafel line would exhibit a break. It can be shown that this break is not accompanied with approach of θ to unity.

Suppose now that θ_0 is close to unity. With $\theta_0 \simeq 1$, Eq. (81) reduces to

$$Z = Q[e^{-f\eta} + m'_B]/[1 + m'_B e^{-f\eta}] \tag{85}$$

Substituting this into Eq. (80) and taking the condition $m_{B0} \simeq 1$ and $-f\eta \gg 1$, one finds

$$i = -i_{0H}Q^{(1-\lambda_H)}\exp[-(1-\beta_H)f\eta] \tag{86}$$

which is characteristic of the Heyrovsky step. This appears to agree with views in the literature that the Tafel constant reaches 0.5 as $\theta \rightarrow 1$, when the Heyrovsky step is rate determining. However, the latter view may not be justified, because the difference of Eq. (86) from Eq. (84) originates from Z, or the $(1-\theta)$ term. It seems more appropriate to say that the rate is still determined by the Volmer step but, since the free electrode surface now plays a decisive role, and its magnitude depends on the rate of the Heyrovsky step, the rate expression involves kinetic parameters of that step.(179,180)

In conclusion, the break of the cathodic Tafel line in the Heyrovsky-Volmer route is not due to onset of surface saturation with H(a) with the Heyrovsky step rate determining, but to the Volmer step becoming rate determining.(173)

5.5. Transient Experiments on the Pd Hydrogen Electrode

The Pd hydrogen electrode has been demonstrated to be an excellent system for the experimental demonstration of the concept expressed in Eq. (12). Owing to extensive dissolution of H in Pd, accumulation of H(a) of the magnitude required for steady occurrence of the HER on Pd takes a very long time, so that the process is almost completely separated in the time domain from the Volmer reaction for the formation of H(a) from H^+ (or its consumption to form H^+). Accordingly, when a constant current is applied to a Pd electrode, an overpotential rise transient like that in Figure 10 is observed. An analogous decay transient is obtained when the polarization current is turned off after a steady state overpotential η is reached. In both the overpotential transients, a clear break is seen on the curve, which divides the steady overpotential into two components.(186)

As the corresponding overpotential components in the rise and decay transients are not necessarily equal to each other,(181) they are named separately as η_1 and η_2 or η'_1 and η'_2, respectively.(181-186) The time constant involved in η_1 or η'_1 is $\sim 10^{-4}$ sec. Undoubtedly, this component is determined

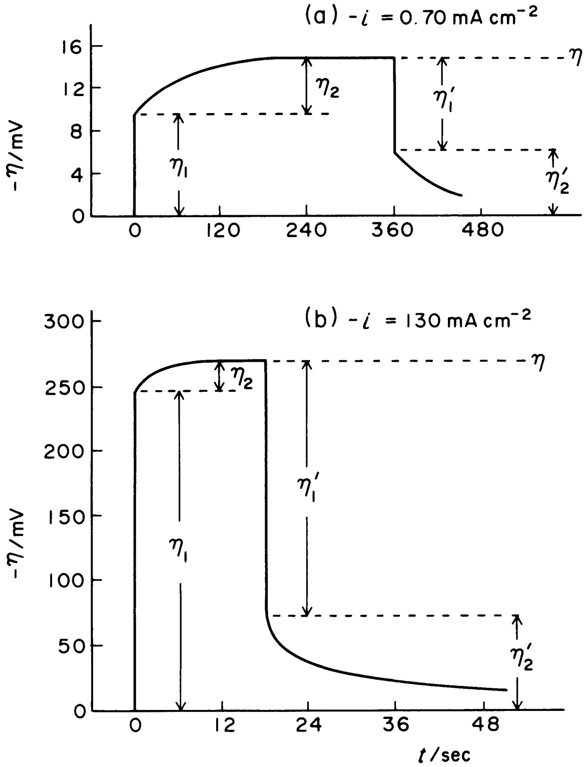

Figure 10. Typical galvanostatic overpotential rise and decay transients on Pd wire, 0.2-mm diameter, in 0.5 M H_2SO_4, at 303 K (Maoka and Enyo(186)).

by a charge transfer process, presumably the Volmer reaction. As the double-layer capacitance is ~50 μF cm^{-2} (apparent), this time constant leads to an equivalent resistance of 2 Ω cm^2 (apparent), or a corresponding exchange c.d. of ~10^{-2} A cm^{-2} (apparent). This is not too far from the exchange c.d. of the overall HER, namely, the charge transfer process is not exceedingly rapid compared with the overall reaction.

The time constant involved in η_2 or η_2' naturally depends on the dimension of the electrode and also on the polarization conditions; it is of the order of 10^2 sec for a Pd foil 10^{-3} cm in thickness. In fact, even on a Pd specimen of this dimension, a time of 1 hr will be needed to establish the reversible hydrogen electrode potential.†

Such a particular shape of the overpotential transient attracted attention of many investigators.(181–186,189–191) Frumkin and Aladjalova(182) employed a Pd membrane electrode and observed the overpotential component η_d "diffused" or "transmitted" through it when the other face of the membrane was polarized cathodically. They observed that $\eta_d = \eta'_2$ and then concluded that η'_2 represents the concentration cell emf of the Pd electrode charged with hydrogen in excess of its amount at the reversible hydrogen electrode potential under 1 atm hydrogen. However, the equality $\eta_2 = \eta'_2$ is not experimentally verified at high overpotential values exceeding several tens of millivolts.(186)

---

† The time constant of the process of hydrogen diffusion in a Pd electrode of this dimension is expected to be roughly 0.2 sec from the diffusion coefficient 1.5 × 10^{-6} cm^2 sec^{-1} (187,188) at 303 K in β-H/Pd. Comparison of this value with the above figure of 10^2 sec indicates that the diffusion process is much quicker than the surface process for such a thin Pd specimen.

Several experiments were carried out later,(183-186) particularly on the value of η'_2 and its relation to log c.d. Not much attention was paid in most of those reports to the difference between the rise and the decay transients, nor on a critical test of the experimental techniques employed to distinguish η'_2 and η'_1. Clamroth and Knorr(183) used an empirical linear relation between the decaying overpotential and volume of hydrogen evolved after the polarization current was terminated. The time range concerned was 10^2 sec or longer, which would possibly mean that the technique is insensitive to a rapidly decaying overpotential component with a time constant of 0.1 sec or shorter which is observable at the beginning of the *slow* portion of the overpotential decay transient.

Much faster observation of η'_2 was carried out by Lewis *et al.*(184) or Maoka and Enyo.(185) In those experiments, Pd(184) or Ag(185) electrodes with a thick layer of electrodeposited Pd were used. After observation of a rapidly decaying overpotential component on smooth Pd electrode,(186) it seemed likely that such a region would escape notice on a porous electrode, because of the time-dependent potential distribution in porous structures during transients.(192-193) Although an interesting view has been proposed by Lewis *et al.*,(194,195) indicating heterogeneity of the electrode surface, we probably need beforehand to investigate carefully the true characteristics of the overpotential transient on Pd.

In some reports cited above, a limiting behavior of η'_2 at high c.d. region was suggested.(183-185,194,196) Further, it was shown by Vetter(197) that such a limiting value could be interpreted in terms of the Heyrovsky–Volmer route of the HER. From the value, he deduced the ratio of the exchange c.d.'s of the two steps. However, careful observations of the overpotential transients on *smooth* Pd electrodes show a continuous increase of η'_2 with the polarization current,(186,198) and suggest that such a saturation behavior might be due either to inaccurate observations of the initial region of the transients or to the use of porous electrodes. The Tafel–Volmer route was instead concluded on the basis of absence of the limiting behavior of η'_2 and also absence of a pH effect upon η'_2.(186,198)

A detailed analysis of the overpotential transient on a smooth Pd electrode was carried out by Enyo and Maoka(186,198-200) in order to extract various kinetic parameters from the observation of the transients. Basic equations which determine the overpotential rise transients at constant polarization c.d.,

i, or the decay transients with $i = 0$, are simultaneous equations which describe the mass balances with respect to electric charge and to hydrogen adatoms on the electrode. Those may be written as

$$C\frac{d\eta}{dt} = i - (i_{V+} - i_{V-})$$

$$= i - i_{0V}\{\gamma_{\uparrow} e^{\beta f \eta} - \gamma_{\downarrow} e^{-(1-\beta)f\eta}\} \tag{87}$$

$$q\frac{d\theta}{dt} = i_{T+} - i_{T-} - (i_{V+} - i_{V-})$$

$$= i_{0T}\{\gamma_{\downarrow}^2 - \gamma_{\uparrow}^2\} - i_{0V}\{\gamma_{\uparrow} e^{\beta f \eta} - \gamma_{\downarrow} e^{-(1-\beta)f\eta}\} \tag{88}$$ †

where C is the double-layer capacitance per unit area of the electrode, $\gamma_{\uparrow}$ and $\gamma_{\downarrow}$ are a function of θ defined below, and q is the amount of electric charge needed to change θ from zero to unity. On a Pd electrode, q is much larger than in ordinary cases (Pt) where only H(a) is involved, since an extra amount of hydrogen is required to charge up the bulk of the electrode with H along with variation of θ for the surface.

In the steady state, we obtain for the Volmer step, from Eqs. (13) and (72),

$$F\eta + RT \ln \gamma_H = RT \ln i_{V+}/i_{V-}$$

or, taking the expressions for i_{V+} and i_{V-} from Eq. (87) and referring to Eq. (56), we find

$$\gamma_H = \gamma_{\uparrow}/\gamma_{\downarrow} \tag{89}$$

Referring to Eq. (4), we may, therefore, write

$$\gamma_{\uparrow} = \frac{\theta}{\theta_0}\exp[\delta U(\theta - \theta_0)], \qquad \gamma_{\downarrow} = \frac{1-\theta}{1-\theta_0}\exp[-(1-\beta)U(\theta - \theta_0)] \tag{90}$$

where δ is a constant $0 \le \delta \le 1$. In the following analysis, we shall assume $\delta = 1/2$, and hence denote $\delta U = (1 - \delta)U \equiv u$. According to Eq. (90), $\gamma_{\uparrow}$ equals γ_H and $\gamma_{\downarrow}$ equals 1 at $\theta_0, \theta \ll 1$, or 1 and $1/\gamma_H$, respectively, at $\theta_0, \theta \simeq 1$.

5.5.1. η (Steady State Polarization)

In the steady state of the polarization, we may take $d\eta/dt = d\theta/dt = 0$ in Eqs. (87) and (88), respectively. Hence, we have

$$\begin{aligned} i &= i_{0V}\{\gamma_{\uparrow} e^{\beta f \eta} - \gamma_{\downarrow} e^{-(1-\beta)f\eta}\} \\ &= i_{0T}\{\gamma_{\downarrow}^2 - \gamma_{\uparrow}^2\} \end{aligned} \tag{91}$$

---

† Hydrogen penetration into Pd and its diffusion in the bulk of Pd are assumed to be fast, compared with the processes taking place at the electrode–electrolyte interface. This was supported by the observation that the β-Pd/H electrode readily sustain a current exceeding 0.1 A cm^{-2} (apparent) during anodic ionization of hydrogen dissolved in it. The exchange c.d. for the surface–bulk penetration reaction was reported to be 0.8 A cm^{-2}.[191]

This indicates that, e.g., the cathodic Tafel plot does not give i_{0V} directly unless $i_{0T}/i_{0V} = \infty$, owing to variation of $\gamma_{\downarrow}$ with θ and hence with η. Tafel lines observed on Pd are shown later in Figure 13.

5.5.2. η_1 (Rise)

The slope of the overpotential rise at the very beginning of the rise transient is given by the first term of Eq. (87), namely, when $d\eta/dt \simeq i/C$. The slope practically vanishes at the moment η reaches η_1, at which the following relation holds:

$$i = i_{0V}\{\gamma_{\uparrow} \exp(\beta f \eta_1) - \gamma_{\downarrow} \exp[-(1-\beta) f \eta_1]\}$$

On Pd, $d\theta/dt$ in Eq. (88) should be very small because of an extremely large value of q, or we may take θ at the time of η_1 to be approximately unchanged from its equilibrium value θ_0, and hence, take $\gamma_{\uparrow} = \gamma_{\downarrow} = 1$. Accordingly, the overpotential component η_1 is given by the relation

$$i = i_{0V}\{\exp(\beta f \eta_1) - \exp[-(1-\beta) f \eta_1]\} \qquad (\eta = \eta_1) \tag{92}$$

After this, $|\eta|$ increases very slowly along with the growth (in the cathodic region) of θ above θ_0. Equation (92) states (i) that a linear plot of η_1 against i at low overpotential directly gives i_{0V}, and (ii) that the slope and the intercept at $\eta_1 = 0$ of the "Tafel line" with respect to η_1 gives β and i_{0V}, respectively. The lines in the cathodic and anodic regions would be symmetrical if $\beta = 1/2$. Typical results of η_1 on Pd HER are given in Figure 11.(199) The cathodic and anodic Tafel lines are, indeed, satisfactorily symmetrical, with the β value reasonably close to 1/2. A more precise analysis led to the value $\beta = 0.43$ at the reversible potential, slightly depending upon η, and $i_{0V} = 0.77$ mA cm^{-2} (apparent).

Cathodic and anodic Tafel lines showing such good symmetry have never been reported for the overall HER on any electrode metals (including Pd itself). This observation is, hence, a strong indication that those asymmetric η vs. $\log i$ lines usually observed on HER are not due to any peculiar characteristics of the proton/water discharge, but to an interference between the Tafel recombination process and the Volmer process. This observation hence indicates that the system lacks a unique rds.

5.5.3. η_1' and η_2' (Decay)

Upon interruption of the current, the overpotential starts to decay, with the slope determined by discharge of the double-layer capacitance through the Volmer process. Analogous to the case of the rise transient, η will jump from η to η_2', at which the discharge is nearly completed, and the value of η_2' is obtained by taking the values of $\gamma_{\uparrow}$ and $\gamma_{\downarrow}$ in Eq. (87) as those for the steady state. After η_2' is reached, η decays, along with the loss (or accumula-

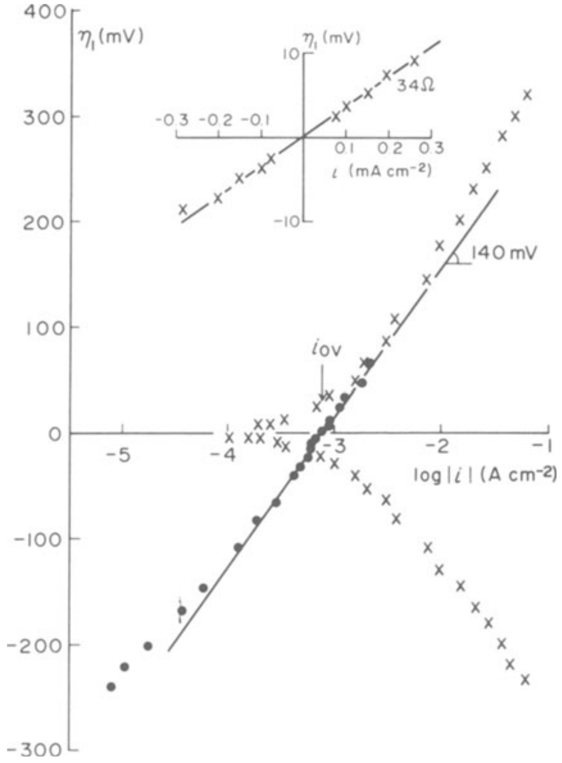

Figure 11. Overpotential component η_1 evaluated from the rise transient on Pd electrode as a function of the polarization current. Pd foil electrode, 10μm thick, 0.5 *M* H_2SO_4 at 303 K. $i_{OV} = 0.77$ mA cm^{-2} and $\beta = 0.43$ are obtained (Enyo and Maoka(199)). (×) η_1 vs. log $|i|$ and (●) η_1 vs. log $[i/(e^{f\eta} - 1)]$.

tion, if it was the anodic polarization) of H(a) through the Tafel step. The decay rate is then determined by the rate constant of the Tafel step and the amount of H to be removed from the electrode.

At the moment η has reached η_2', $d\eta/dt$ may be approximated to zero in Eq. (87). Hence, referring to Eq. (89), we obtain

$$e^{-f\eta_2'} = \gamma_\uparrow/\gamma_\downarrow = \gamma_H \tag{93}$$

Hence, γ_H during the steady polarization prior to the current interruption is readily obtained from η_2'.

One may define the overpotential components, η_s's, for the constituent steps in such a way that

$$\eta = \sum_s \eta_s \tag{94}$$

Referring to Eqs. (11) and (12), one finds

$$-\Delta g_s = (nF/\nu_s)\eta_s \tag{95}$$

Comparison of Eq. (93) with Eq. (71) readily yields

$$\eta_2' = \eta_T \tag{96}$$

and referring to Eq. (94),

$$\eta'_1 = \eta - \eta'_2 = \eta - \eta_T = \eta_V \tag{97}$$

The steady state overpotential components for the elementary steps are therefore obtained by measurements of η and η'_2.

5.5.4. Affinity Distribution as a Function of the Total Overpotential

Distribution of the affinity of the overall reaction amongst elementary steps, already discussed in terms of m in Section 5.3, is directly accessible on Pd(171,172):

$$m \equiv \Delta g_T/\Delta g_V = 2\eta'_2/\eta'_1 \tag{98}$$

Typical results obtained are shown in Figure 12,(199) together with the theoretically expected curves.(171,172) It is seen that theoretical curves calculated on the basis of the Langmuir, or the Temkin (with $\mu = 5$), adsorption isotherm for hydrogen adatoms with $m_0 \equiv (\Delta g_T/\Delta g_V)_{\eta\to 0} = i_{0V}/i_{0T} = 10$, and for low values of θ_0, satisfactorily explain the experimental results. As the m vs. η curve should be symmetrical for the Volmer–Heyrovsky route,(171) the fit of the experimental data to the asymmetric curve, which is obtained from the Volmer–Tafel route, may be taken as a support for the latter pathway.

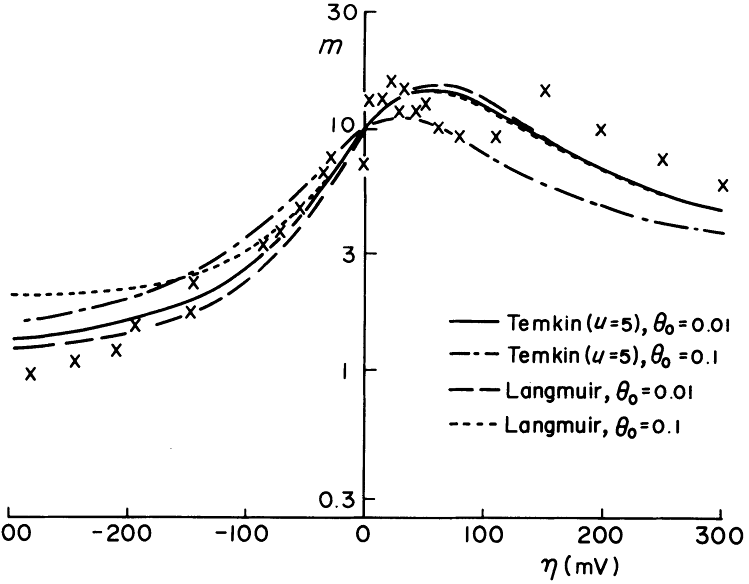

Figure 12. Change of m with η on Pd foil electrode, 10 μm thick, in 0.5 M H_2SO_4 at 303 K and comparison with the theoretical curves calculated for the Temkin or Langmuir isotherms with $m_0 = 10$ and various θ_0 values indicated (Enyo and Maoka(199)).

5.5.5. "Tafel Line" with Respect to η'_2 ($=\eta_T$)

Combining Eq. (91) with (93) and employing Eq. (90), we find

$$\frac{i}{i_{0T}} = \gamma_\downarrow \cdot \gamma_\uparrow\{\exp(f\eta'_2) - \exp(-f\eta'_2)\} = \frac{\theta_0(1-\theta_0)}{\theta(1-\theta)}\{\exp(f\eta'_2) - \exp(-f\eta'_2)\} \tag{99}$$

This indicates that the η'_2 vs. $\log i$ relation would give an approximate linear line. A typical result is given in Figure 13.(199) If $|f\eta'_2| \ll 1$, we have

$$i_{0T} = \frac{\theta_0(1-\theta_0)}{\theta(1-\theta)} \frac{1}{2f}\left(\frac{di}{d\eta'_2}\right)_{\eta'_2 \to 0}$$

but the first quantity on the right-hand side of this equation may be approximated to unity, since θ should be close to θ_0 in the present case. Thus, the data (inserted in Figure 13) lead to the value $i_{0T} \simeq 0.11$ mA cm^{-2} (apparent). Accordingly, we obtain $m_0 \equiv i_{0V}/i_{0T} = 0.77/0.11 = 7.0$. As discussed before (Section 5.3), m_0 of this magnitude should not be large enough that the Tafel step becomes uniquely rate determining.

It can be shown(199) that the slope α'_{-2} of the cathodic Tafel line for η'_2 is obtained from Eq. (99) as

$$\alpha'_{-2} \equiv -\frac{d\ln(-i)}{f\,d\eta'_2} = 1 - \frac{d\ln(\gamma_\uparrow \cdot \gamma_\downarrow)}{f\,d\eta'_2} = \frac{2(1+u\theta)}{1/(1-\theta)+2u\theta} \tag{100}$$

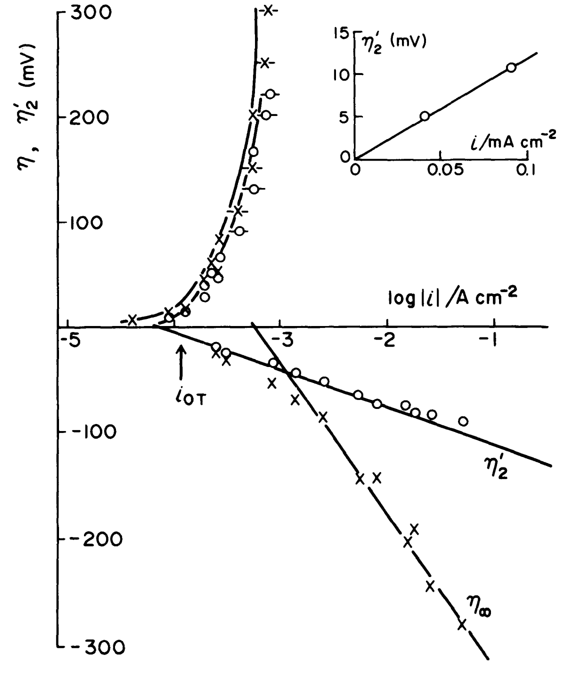

Figure 13. Typical plots of η and η'_2 against c.d. on Pd wire electrode (0.2-mm diameter) in 0.5 M H_2SO_4 (Enyo and Maoka(199)). The arrow indicates i_{0T} evaluated from the polarization resistance at low η'_2 (the figure inserted).

We see that α'_{-2} is generally a function of η, owing to variation of θ with η, and takes a value $\alpha'_{-2} \leq 2$ if $u > 0$ and $\alpha'_{-2} > 1$, if $\theta < 1/2$. It decreases with increase of θ or the Tafel line may have a tendency to bend up under severer cathodic polarizations, finally approaching zero at $\theta \simeq 1$. In special cases (i) if $2u\theta(1-\theta) \gg 1$, then $\alpha'_{-2} \simeq 1$, and (ii) if $u\theta \ll 1$, then $\alpha'_{-2} \simeq 2$.

Accordingly, the slope should be larger than 30 mV/decade. The slope observed (Figure 13) was 36 ~ 40 mV/decade,† depending on electrode pretreatment. Although u is yet unknown, the slope employed in Eq. (100) indicates that θ (under cathodic polarization) must be smaller than (or equal to, if $u = 0$) 0.15 (36 mV) or 0.25 (40 mV). This suggests that the atomic ratio H/Pd is *lower* on the Pd surface than that in the bulk of Pd where it amounts to about 0.7 under 1 atm hydrogen pressure.

At high anodic η'_2, no straight line of η'_2 vs. $\log i$ was experimentally observed. This is presumably due to approach of θ to zero. Thus, from Eq. (99), we obtain$^{(199)}$

$$\alpha'_{+2} \equiv \frac{d \ln i}{f\,d\eta'_2} = 1 + \frac{d \ln(\gamma_\uparrow \cdot \gamma_\downarrow)}{f\,d\eta'_2} = 2\theta \frac{1 + u(1-\theta)}{1 + 2u\theta(1-\theta)} \tag{101}$$

We see that α'_{+2} may approach zero when θ does so under anodic polarization. Namely, there is a general tendency that the anodic Tafel line for η'_2 readily bends up in the anodic region. The prediction is, indeed, substantiated by experiments (Figure 13).

5.5.6. Tafel Lines with Respect to η

5.5.6.1. Cathodic Region

At sufficiently high cathodic overpotentials, we have from Eq. (91),

$$\alpha_- \equiv -\frac{d \ln(-i)}{f\,d\eta} = (1-\beta) - \frac{d \ln \gamma_\downarrow}{d \ln(-i)} \frac{d \ln(-i)}{f\,d\eta}$$

or,

$$\alpha_- = (1-\beta) \Big/ \left[1 - \frac{d \ln \gamma_\downarrow}{d \ln(-i)}\right] \tag{102}$$

From Eq. (89), we have

$$\frac{d \ln \gamma_\downarrow}{d \ln(-i)} = \frac{d \ln \gamma_\uparrow}{d \ln(-i)} - \frac{d \ln \gamma_\mathrm{H}}{f\,d\eta'_2} \frac{f\,d\eta'_2}{d \ln(-i)}$$

but $[d \ln \gamma_\mathrm{H}/f\,d\eta'_2] = -1$ according to Eq. (93). Also, at such high cathodic overpotentials where $-i \simeq i_{-\mathrm{T}} \gg i_{0\mathrm{T}}$, $-i$ is proportional to $\gamma_\downarrow^2$ or

---

† The slope often reported in the literature is 30 mV/decade.$^{(184)}$ Corresponding to this value, slow diffusion of molecular H_2 in the solution was proposed.$^{(182,184)}$

$[d \ln \gamma_\uparrow / d \ln(-i)] = 1/2$. Hence, referring to Eq. (100), we have,

$$\frac{d \ln \gamma_\downarrow}{d \ln(-i)} = \frac{1}{2} - \frac{1}{\alpha'_{-2}} \tag{103}$$

Substituting Eq. (103) into Eq. (102), we obtain

$$\alpha_- = (1-\beta) \Big/ \left[\frac{1}{2} + \frac{1}{\alpha'_{-2}}\right] \tag{104}$$

In the special case of $\theta \ll 1$, and hence $\alpha'_{-2} = 2$ according to Eq. (100), we have, from Eq. (104), $\alpha_- = 1 - \beta$, i.e., the overall Tafel line is not distorted from its ordinary shape. However, α_- becomes smaller than $(1-\beta)$ if θ grows to a significant magnitude, or the Tafel line would become steeper than the one which corresponds to $(1-\beta)$. As the deviation of α'_{-2} from 2 represents interference of the Tafel step in the overall kinetics, Eq. (104) could be an explanation of repeated experimental observations of Tafel slopes steeper than 120 mV/decade for various HER systems at high cathodic overpotentials. A typical cathodic Tafel slope of η on Pd at $-\eta = 100 \sim 250$ mV is 140 mV and the corresponding one for η'_2 is ~37 mV/decade (Figure 13). Hence, we have $\alpha_- = 0.43$ and $\alpha'_{-2} = 1.62$. Using these values in Eq. (104), we find $\beta = 0.52$, as compared with the β value in this region of around 0.47 (Figure 11).

5.5.6.2. Anodic Region

Similar developments in the anodic region yield

$$\alpha_+ = \beta \Big/ \left[\frac{1}{2} + \frac{1}{\alpha'_{+2}}\right] \tag{105}$$

or, referring to Eq. (101),

$$\alpha_+ = \frac{1 + u(1-\theta)}{1 + \theta + 3u\theta(1-\theta)} 2\beta\theta \tag{106}$$

The anodic Tafel line should, therefore, become very steep and show a limiting current behavior when θ approaches zero, or α'_{+2} approaches zero, as indeed is observed on Pd (Figure 13). It seems likely that the same concept also applies to analogous behaviors on some other metals,(201) although similar experiments would no longer be possible for obtaining α'_{+2}.

5.5.7. The Anodic Limiting Current Density, i_{AL}

This is reached when $\theta = 0$. Hence, from Eqs. (90) and (91), we have

$$i_{\mathrm{AL}} = i_{0\mathrm{T}} \gamma_\downarrow^2 = i_{0\mathrm{T}}\, \mathrm{e}^{2u\theta_0}/(1-\theta_0)^2 \tag{107}$$

This may be used to assess the upper limit value of θ_0 from the measurement of i_{AL}/i_{0T}. Then, assuming $u \geq 0$, we obtain

$$\theta_0 \leq 1 - (i_{0T}/i_{AL})^{1/2}$$

Evaluation of i_{AL} on Pd meets some difficulty as the limiting current for H_2 diffusion in the solution readily sets in. An experiment for which results are shown in Figure 13 was therefore carried out, using a deactivated electrode which was once used in an experiment involving organics. The value after a long (15 hr) potentiostatic polarization was $i_{AL} \simeq 0.7\ \text{mA cm}^{-2}$ (apparent). From the value of $i_{0T} \simeq 0.11\ \text{mA cm}^{-2}$ (apparent), evaluated above at low overpotentials, we have

$$(1 - \theta_0)\, e^{u\theta_0} = (i_{0T}/i_{AL})^{1/2} \simeq 0.4$$

or, we obtain $\theta_0 \simeq 0.6$ if $u = 0$, or $\theta_0 \simeq 0.15$ if u is arbitrarily taken to be 5.(171)

5.5.8. Surface Coverage with H(a)

It is to be noted that various pieces of information obtained from kinetic analyses, such as θ_0 being significantly smaller than unity as obtained above, analogous indications obtained from the m vs. η relation (cf. Figure 12), or θ not exceeding ~0.25, as suggested from the cathodic η'_2 vs. $\log i$ relation under cathodic polarization of $-\eta \simeq 200$ mV, altogether indicate that the surface coverage with H(a) on Pd at the reversible HER potential should be much smaller than unity. However, this is not in accord with the corresponding information derived from the potential sweep experiments discussed above (Section 2). The cause of the discrepancy is not well understood yet. It might indicate, e.g., that there is no one-to-one correspondence between H(a) and metal atoms on the surface array, or that the hydrogen wave originates in part from "dermasorbed"(202) hydrogen.

6. Related Topics

6.1. Effect of Catalytic Poisons upon the Individual Step Rates

Intense efforts have been made toward stringent purification of experimental HER systems, in particular during the last three decades.(203) It has been recognized that even a trace of impurity (10^{-10} mol dm^{-3}) poisons the electrode reaction, and there are many inorganic and organic surface active substances (surfactants) which have long been known to retard the rate of the HER.(204–208) On the other hand, when a surfactant is added to the HER system and the activity decreased, it is still not very clear in what way the additive affects the reaction rate, more than just decreasing the overall reaction rate. Not many reports have appeared, to the present author's knowledge, which provide information about the effect of additives upon individual step rates, or possibly changes of mechanism.

Stonehart and Kohlmayr(209) investigated the HER rate on a rotating Pt bead electrode as a function of surface coverage with CO. They concluded(210,211) that the electrocatalytic activity of Pt for the hydrogen ionization is a quadratic, but not a linear, function $(1 - \theta_{\text{poison}})^2$ of the free surface fraction, thus suggesting a rate-determining dual-site step, probably the Tafel reaction. However, this correlation was questioned later by Breiter.(212,213)

In a series of interesting papers by members of the Polish school, the effect of additives upon the improvement of the hydrogen-absorbing property of Ni(214–216) or Fe(217) electrode during cathodic hydrogen evolution was reported. The effectiveness of thiourea(218,219) for this purpose was interpreted by them as catalytic promotion of the hydrogen absorption process. Such a view of the nature of the additive as a promoter, by e.g., affecting the metal–H bond strength,(220) volatile hydride formation,(221) etc. was widely assumed. However, another possibility may exist that the additive acts as a poison of the Tafel step,(222) thus giving rise to an increased activity of H(a) during the steady polarization with a given c.d.(198,223–225)

The effect of additives on the rates of the individual step rates is experimentally traceable in the case of Pd hydrogen electrode.(198) As discussed above in Section 5.5, analysis of the overpotential decay transient on Pd, upon interruption of the current, directly gives information on the affinity values shared by the Volmer and the Tafel steps during steady polarization. Typical results are shown in Figure 14.(198) Tetrabutylammonium ion (Figure 14a) was found to be a typical substance which retards strongly the overall HER rate but not that of the Tafel step. It therefore retards the Volmer step

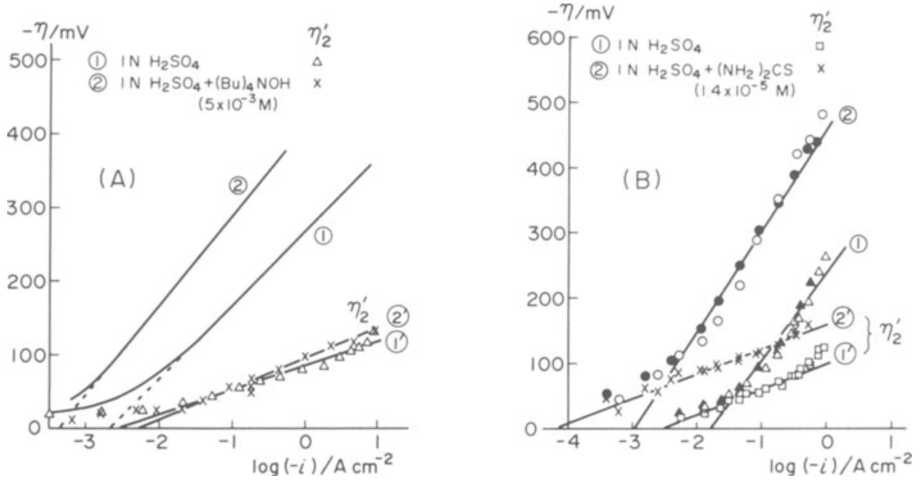

Figure 14. Tafel plots of cathodic η and η'_2 in the presence or absence of surfactants on Pd foil electrode, 10 μm thick (Maoka and Enyo(198)). (A) 0.5 M H_2SO_4 without (curves 1, 1′) or with (curves 2, 2′) the addition of 5×10^{-3} M tetrabutylammonium hydroxide; (B) 0.5 M H_2SO_4 without (curves 1, 1′) or with (curves 2, 2′) the addition of 1.4×10^{-5} M thiourea.

and this conclusion is in conformity with the general recognition that this substance is particularly effective in retarding charge transfer or redox reactions involving simple ions through double-layer effects. On the other hand, thiourea is a typical substance which retards the Tafel step as demonstrated by the significant increase of η_2' (Figure 14b), with some retarding effect also upon the Volmer step. Other substances, As_2O_3, KI, and Na_2S, have intermediate effects.(198)

The overpotential transient experiments on Pd thus provide a convenient means for investigating effects of various surfactants upon elementary processes rather than on the overall reaction. Hopefully, investigations along these lines will offer characterization of surfactant effects on electrocatalytic processes such as those involving corrosion inhibitors and effects of additives on electroreduction processes, etc.

6.2. Hydrogen Pressure Equivalent to Hydrogen Overpotential

Some metals absorb hydrogen when they are placed in a hydrogen atmosphere, or particularly when they are polarized cathodically in a protonic solution, presumably due to the formation of H(a) on the metal surface. It was also known for a long time that cathodes exhibit a strong ability to reduce (hydrogenate) substances, through a species sometimes referred to by the term *nascent hydrogen*.

It was often argued that the particularly strong reducing power of a cathode can be summed up in terms of the "hydrogen pressure equivalent to hydrogen overpotential," here denoted by $P_{\bar{H}_2}$, and further it is stated that this effect should be related to η by a Nernst-like relation

$$P_{\bar{H}_2} = \exp\{-2f\eta\} \tag{108}$$

where the reference pressure at zero overpotential is taken to be 1 atm. This relation predicts indeed a high pressure value, such as 10^4 atm at $\eta = -120$ mV, an ordinary overpotential value encountered in polarization experiments.

The equivalent hydrogen pressure can be visualized with the concept of cavity pressure.(226,227) Thus, when a hydrogen-absorbing metal electrode is cathodically polarized (Figure 15), a steady activity of H(a) may be established, and then a steady hydrogen concentration is generated in the metal below the surface. This hydrogen diffuses into the metal, reaches a cavity forming H(a) on the inside wall, and produces H_2 there by desorption. If activity of H(a) on the outside surface is significantly higher than its value at adsorption equilibrium with 1 atm ambient H_2 pressure, then the cavity pressure would become higher than 1 atm.(223) (This presents one model for hydrogen embrittlement effects.(226)) It is easily seen that the relation below holds for this pressure:

$$\mu_{\bar{H}_2} = 2\mu_{H(a)}$$

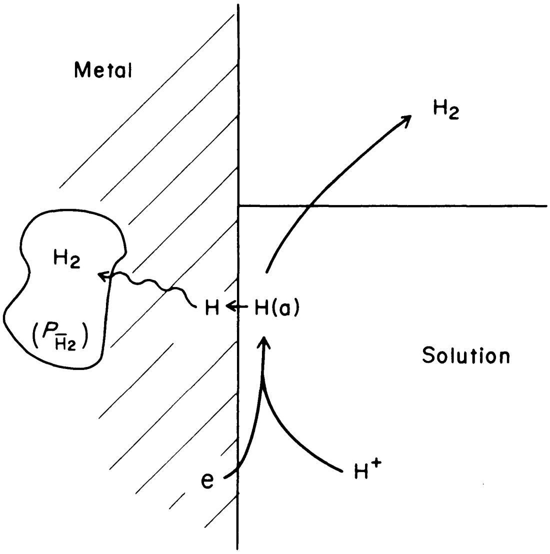

Figure 15. Schematic presentation of the hydrogen pressure equivalent to hydrogen overpotential.

or, cf. Eq. (56),

$$P_{\bar{H}_2} = (a_H/a_{H,0})^2 = \gamma_H^2 \tag{109}$$

It can readily be understood(227) that Eq. (108) would be valid only when mechanism A-1 (or B-1), Section 3 is operative, because in this case we have, from the quasiequilibrium condition of the Volmer step,

$$a_H = a_{H,0} \exp\{-f\eta\} \tag{110}$$

For other mechanisms, Eq. (110) is not valid, and hence, Eq. (108) is no longer obeyed. The degree of metal embrittling effect, along with various HER mechanisms, was discussed by Bockris and Subramanyan.(227)

In the case of the Volmer–Tafel reaction route, the equivalent pressure is readily obtained by substituting Eq. (71) into Eq. (109) and employing the relation between m and η, as calculated (see Figure 7). The resultant log $P_{\bar{H}_2}$ vs. η relation becomes practically linear, and its slope is determined by m_0 and other kinetic parameters.(171)

Experimental observation of the equivalent hydrogen pressure was conducted on a Pd electrode by observing a steady state hydrogen concentration in the Pd electrode during the polarization, cathodic and anodic, and combining the data with hydrogen absorption isotherm which is experimentally accessible(181,228) (Figure 16). It is seen that the data considerably deviate from Eq. (108), although the pressure is still very high. Further, the data are in fair agreement with theoretical lines; a good agreement is obtained if one takes the values of the parameters as follows:

$$m_0 \simeq 10 \qquad \text{and} \qquad u = 5$$

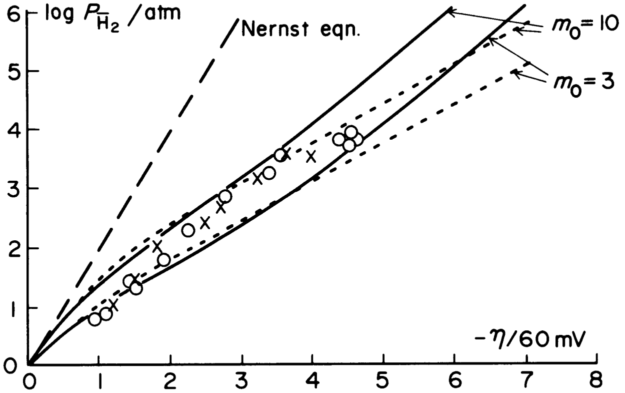

Figure 16. The equivalent hydrogen pressure as a function of cathodic overpotential on Pd foil, 10 μm thick, in (O) 0.5 *M* H_2SO_4 or (×) with the addition of 2×10^{-5} *M* thiourea (Maoka and Enyo(200)). Curves are for the Nernst equation (broken line) and the theoretical lines are for the Langmuir (solid lines) and Temkin (dotted lines, with u = 5) isotherms, with m_0 = 3 or 10 and θ_0 = 0.1.

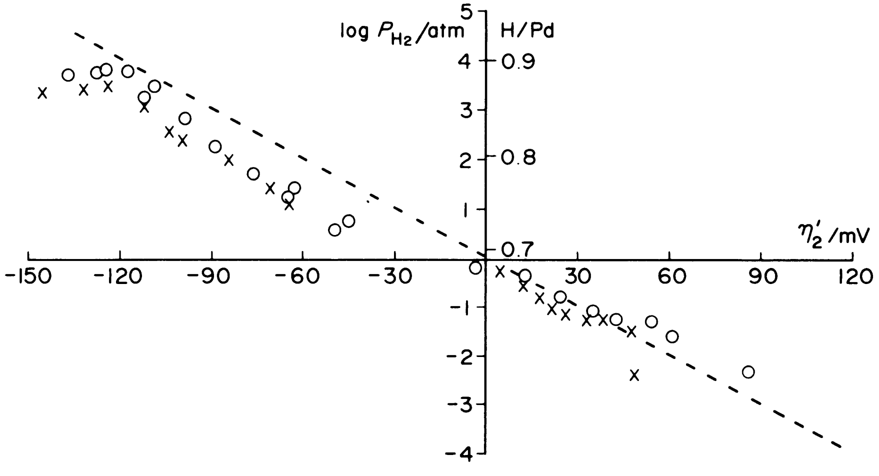

Figure 17. Relation between the equivalent hydrogen pressure (or hydrogen concentration in Pd) and η_2' in the anodic and cathodic regions on Pd foil electrode, 10 μm thick. (O) in 0.5 *M* H_2SO_4 or (×) in 0.5 *M* $H_2SO_4 + 8 \times 10^{-4}$ *M* tetrabutylammonium hydroxide (Maoka and Enyo(200)). The broken line represents the theoretical relation, 30-mV slope, obtained from Eqs. (71) and (109).

Figure 17 shows the relation between $\log P_{\bar{H}_2}$ and η_2'. It is clear from Eqs. (93) and (109) that this should have a slope of 30 mV. Experimental data are in an acceptable agreement with this relation, the dotted line. Also shown in this figure are experimental results obtained after introduction of tetrabutylammonium ion. No systematic difference is seen, supporting the above proposal that η_2' is the main overpotential component which determines H(a) activity and hence $P_{\bar{H}_2}$.

There may be two possibilities for the effect of additives upon increased hydrogen dissolution into the electrode at a given cathodic polarization, namely, retardation of the Tafel step and promotion of the Volmer step. A significant increase of hydrogen dissolution, but with a decrease of the overpotential upon additition of H_2S, were observed on mild steel in $HClO_4 + NaClO_4$ solution.(229) This effect was attributed to an acceleration of the Volmer step. However, there remains the possibility that H_2S retards the Tafel step but, at the same time, an electrode process with H_2S was involved in parallel with the HER, giving rise to a decrease in the overpotential. In support of this, addition of a small amount of H_2S usually results in retardation of the overall HER.(198,229) Also, in gas phase experiments on the recombination reaction of atomic hydrogen on Fe, introduction of H_2S resulted in acceleration of the hydrogen entry into Fe, presumably due to retardation of the recombination reaction.(230)

6.3. Electrolytic Hydrogenation of Organic Substances

Electrolytic hydrogenation of unsaturated compounds might have advantages over the ordinary gas phase catalytic processes as the reaction rate, and possibly the selectivity, could be controlled through the potential of the electrode. Also, the electrochemical system may provide a much stronger reducing condition than with the gas phase reactions.

Survey of the vast field of chemistry of electroreduction of various substances(231–237) is beyond the scope of this short chapter. Therefore, only some sections of the field which have an intimate relation with mechanistic aspects of the HER will be briefly touched on.

6.3.1. Reduction by H(a) and by Electrons

It might appear likely that electroreduction processes take place directly by electrons† on metals which have high hydrogen overpotential and by H(a) on low overpotential metals.(238) Indeed, e.g., electroreduction of acrylonitrile to adiponitrile on Pb or Hg takes place by electronation, followed by proton addition and dimerization,(239) while electrolytic olefin hydrogenation on Pt takes place by transfer of H(a) to the organics.(240–251) Nevertheless, such results are not sufficient evidence to justify the reaction route as determined by the choice of electrode material. On the contrary, it appears likely that the route is dependent on the nature of the reacting substance to be reduced and appropriateness of the electrode material is subsequently determined.

The first step of electroreduction of maleic acid (M) on Hg was reported to be electron transfer forming an ion radical, followed by addition of H^+ (252):

$$M + e \rightarrow M^-(a)$$

$$M^-(a) + H^+ \rightarrow MH \cdots MH_n$$

---

† See also Chapter 10 in this volume by Rudd and Conway.

However, on Pt and other electrocatalytically active metals, the C=C double bond of maleic acid (or ethylene and its derivatives(253)) is considered to be reduced by H(a),

$$H^+ + e \rightarrow H(a)$$

$$M + H(a) \rightarrow MH \cdots MH_n$$

These two possible paths of electroreduction were investigated by von Stackelberg and Weber,(254) using a Pd membrane electrode. To distinguish these alternative paths, a sophisticated experimental technique was later proposed by Wagner(255) and indeed carried out by Takehara.(256) The experiment is based on the use of a Pd (and partly Pt) membrane; what is observed is the effect upon the hydrogenation rate of hydrogen atoms which are supplied by transfer through the membrane from the other side, at which hydrogen was produced by electrolysis. Results led these authors to the conclusion that pickup of electrons or H(a) are both possible on these metals, depending on the nature of the substance to be reduced, e.g., reduction of the $>C=O$ group takes place by direct electron transfer, whereas the C=C bond is reduced by H(a).

It is also possible to distinguish these two alternatives on Pd through observation of η_2'. Thus, if H(a) is primarily involved in the electrolytic hydrogenation, η_2' at a given c.d. will be reduced upon introduction of reducible organics to the system. This is perhaps better expressed by the behavior of m, Eq. (98), because then the absolute electrocatalytic activity of the electrode, which is often difficult to reproduce, especially when organics are added to the system, would not be directly involved. Typical results are shown in Figures 18 and 19.(257) In Figure 18, values of m as obtained on Pd from the overpotential decay transients before and after the addition of (A) I_2 to the solution of 1 N H_2SO_4 containing I^-, and (B) quinone (Q) to the solution of 1 N H_2SO_4 containing hydroquinone (QH_2), are presented as a function of η. No appreciable difference was seen on the m vs. η relation upon addition of these reducible substances. This would simply mean that a fraction of the cathodic polarization current is consumed by the reduction and the HER takes place rather independently corresponding to the rest of the current. This view is in conformity with conclusions reached by other techniques, i.e., reduction proceeds by a direct electronation in the I_2/I^- (258) and Q/QH_2 (259) systems.

In contrast with these cases, the m vs. η relation is significantly different in the absence or presence of reducible substance for the system butenediol–butanediol or allyl alcohol–propanol (Figure 19).(257) Further, it was possible in these systems to observe the case where $\gamma_H < 1$, hence $\eta_2' > 0$ at cathodic hydrogen overpotentials. This indicates that H(a), supplied through the Volmer step, is consumed by the electroreduction process which now exists as a reaction which competes with the Tafel step. The difference between the curves was the smaller the more negative was the electrode potential, namely,

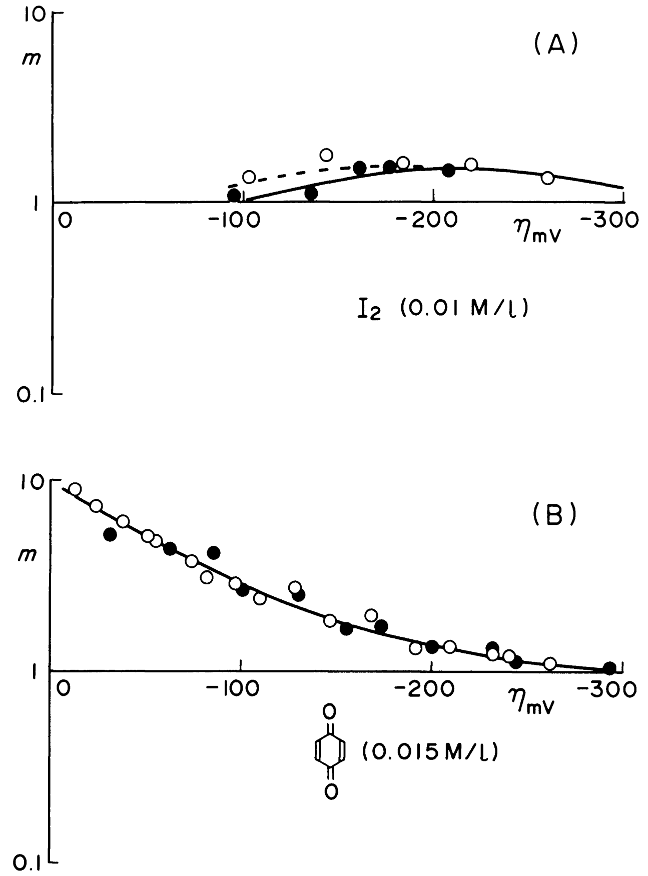

Figure 18. Relation between m and cathodic overpotential during electroreduction of I_2 and quinone on Pd foil electrode, 10 μm thick (Enyo[257]). (A) (○) 0.5 M H_2SO_4 + 0.06 M KI; (●) with the addition of 0.01 M I_2; (B) (○) 0.5 M H_2SO_4 + 0.015 M hydroquinone; (●) with the addition of 0.015 M p-benzoquinone.

greater the cathodic c.d. This appears reasonable as the rate of consumption of H(a) by the organics would have lower dependence upon γ_H than the Tafel step.

6.3.2. Control of Hydrogenation through Electrode Potential

If the electrolytic reduction means the electronation of the substance in question, whether directly itself or after combination with H^+, the reduction is likely to be controlled by the electrode potential which determines the (electro)chemical potential of electrons in the electrode. Not many factors which require further detailed consideration are likely to be associated with such a process.

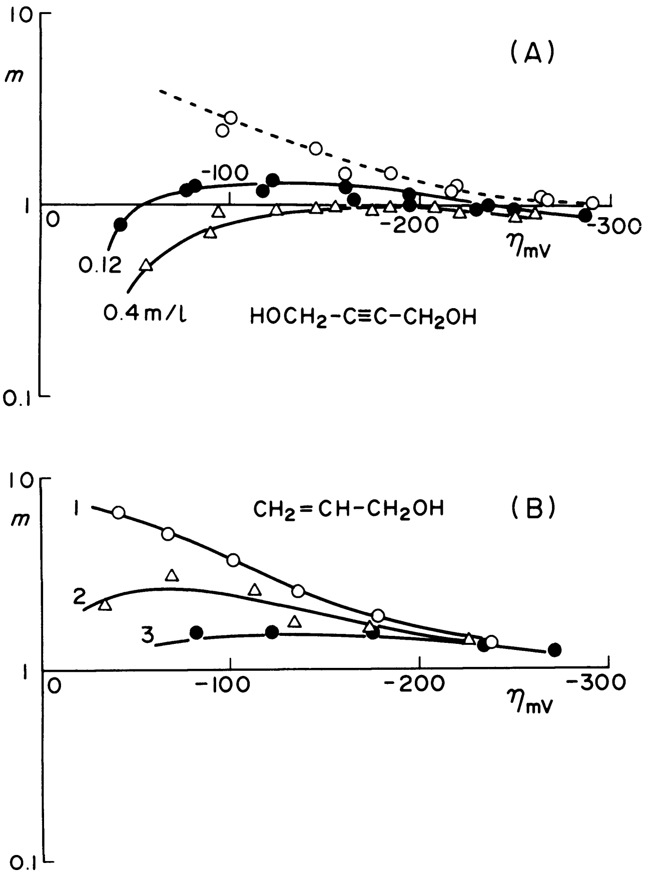

Figure 19. Relation between m and cathodic overpotential during electrolytic hydrogenation of butynediol and allyl alcohol on Pd foil electrode, 10 μm thick (Enyo$^{(257)}$). (A) (○) 0.5 M H_2SO_4 + 0.11 M butanediol; (●) with the addition of 0.11 M or (△) 0.4 M 2-butyne-1,4 diol; (B) (○) 0.5 M H_2SO_4; (△) with the addition of 0.08 M or (●) 0.5 M allyl alcohol.

On the other hand, if the electrolytic reduction involves reaction between H(a) and the substance to be hydrogenated, then γ_H should play the major role, and the electrode potential then controls the reaction in an indirect way, through its influence upon γ_H. This importance of H(a) activity in electrolytic hydrogenation was clearly demonstrated by Beck$^{(260)}$ in investigations on hydrogenation of dimethylethinyl carbinol on Pd–SiO_2 catalyst powder suspended in methanol solution or hydrogenation of butynediol on Pd–Al_2O_3 catalyst in aqueous solution with H_2 bubbling (Figure 20). In both systems, he observed abrupt changes on the time courses of the hydrogenation rate and the potential of the catalyst, and found that the hydrogenations to C≡C triple bonds and to C=C double bonds are well distinguished on such curves. As the catalyst potential would directly represent γ_H, the observations in Figures 20,

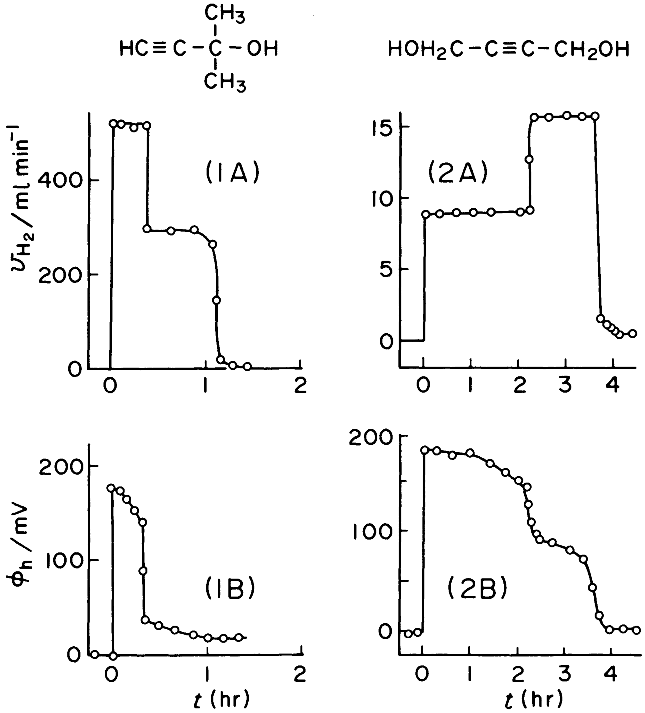

Figure 20. Time courses of hydrogen consumption rate and catalyst potential during hydrogenation on suspended catalyst at 298 K (Beck[260]). (1A, B) Hydrogenation of dimethylethinyl carbinol on Pd (4.5%)/SiO_2 catalyst (5 g). 0.5 *M* in triethanolamine-buffered methanol solution (pH 8), 500 cm^3; (2A, B) Hydrogenation of 2-butyne-1,4 diol on Pd (5%)/Al_2O_3 catalyst (5 g). 0.06 *M* solution in triethanolamine buffered aqueous solution (pH 8), 500 cm^3.

1b, and 2b presumably mean that hydrogenations to triple and double bonds are controlled by γ_H.

As already discussed, γ_H is given as a function of η and involves several kinetic parameters of the HER such as exchange c.d., transfer coefficient, etc. Further, it is possible to control γ_H, not only through η, but also through intentional variation of kinetic parameters of the individual steps of the HER by use of surfactants. Advancement of our understanding on electroreduction processes through systematic observations of γ_H during the reaction may, hence, be anticipated.

7. Electrode Materials

7.1. Pure Metals

From an electrocatalytic point of view, it is almost an ultimate aim of research and development in this field to find electrode materials which have sufficiently high activity, with cheap cost and of sufficient resources. Platinum metals are usually very active but too high in cost for any wide use. Nickel, often impregnated with platinum metals, or of the Raney structure, is used if the hydrogen evolution or ionization reaction is to be conducted in alkaline media.

Observation on kinetics of the HER can be carried out on a large number of metals. In Figure 21, typical results of polarization experiments on some low and medium overpotential metals are given.(53,140,150,163,261–275) On the basis of such data, possibilities of finding a general trend in their electrocatalytic activity have been often discussed in terms of periodicity(276–279) or in terms of physicochemical properties such as melting point,(280–282) cohesive energy,(283) %d character,(284) interatomic distance,(282,285–287) compressibility,(288) heat of sublimation,(289–291) surface energy,(292,293) thermionic work function,(294,302) and heat of hydrogen adsorption.(294,300,303–310)

Understanding of these factors is not yet sufficiently conclusive. Among various difficulties, there is the lack of a solid basis for the operative HER mechanisms on these metals. Certainly, one must be sure beforehand in an analysis of this kind that the electrocatalytic activities of various metals can

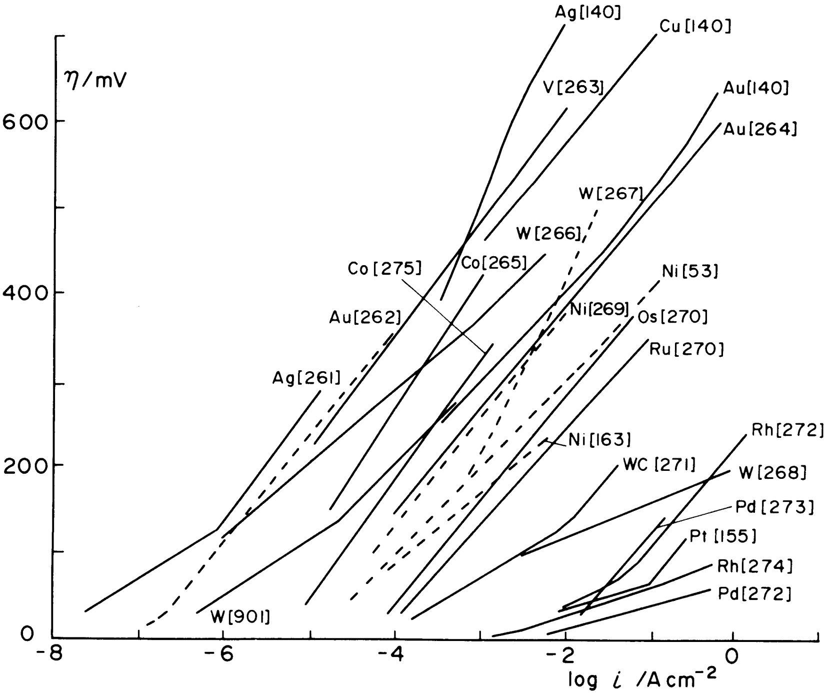

Figure 21. Typical HER Tafel lines for various metals as reported in the literature. Solid lines for acidic solutions and broken lines for alkaline solutions. References are indicated on the figure.

be compared on the basis of a common mechanism, and hence for a common step.

According to the argument concerning the change of the mechanism with overpotential presented in Section 5, one might take almost a common feature, except the case of platinum metals in an active state, of the cathodic Tafel lines on those metals as an indication of mechanism of the rate-determining Volmer followed by rapid or irreversible Tafel or Heyrovsky steps. At present, one possibility is, therefore, to take the attitude that exchange c.d.'s obtained by extrapolation of the Tafel lines to $\eta = 0$ would represent $i_{0\mathrm{V}}$ at least approximately. Another difficulty arises from the fact that, after all, a certain degree of correlation will always exist among various physicochemical properties, and hence there will not be any definite way to disclose the *essential* term among many other terms.(311)

In contrast to the "electronic" properties discussed above, structural factors in electrocatalytic activity have been investigated by several authors. In spite of the extreme difficulty in this kind of work to maintain an unperturbed surface state, free of surface contamination, and to reproduce a defined surface, some interesting results have been reported.

Using single-, as well as poly-, crystalline Pt electrodes in 0.5 *M* H_2SO_4, Bagotzky *et al.*(64,233) have reported that η at a constant cathodic current is in the order

$$\eta_{\mathrm{poly}} > \eta_{(100)} > \eta_{(110)} > \eta_{(111)}$$

i.e., the more densely packed is the surface, the higher is its activity for the HER.

Mechanical deformation was effective in decreasing η on the (100) face of Cu or, to some extent, on Ni,(312) but had no significant effect on Pt.(87) Neutron irradiation was effective in producing electrocatalytically active surface defects.(64) Extensive dispersion of Pt on Au or pyrographite substrates yielded significantly high specific activity of Pt, particularly at low Pt coverage.(313) Effect of grain size, or possibly clusters, upon the activity was recognized in some investigations,(314) suggesting the importance of surface atoms at edges, kinks, etc., namely, the structure-sensitive nature of the HER.(313,315)

A detailed investigation on such structural effects has recently been carried out on Ni by Angely *et al.*(316) They prepared vacuum-deposited films of Ni on, e.g., a vitreous carbon substrate, and investigated their structure (diameter and shape of crystallites, stacking faults, vacancies, etc.) as functions of substrate temperature during the deposition and subsequent annealing, their properties with regard to hydrogen adsorption in an electrochemical system (1 *M* KOH), and the HER kinetics on these electrodes. They concluded that hydrogen adsorption sites which are active for the HER are only those surface Ni atoms with low coordination number, i.e., those on crystallite edges and summits, and correspondingly the electrocatalytic activity of the films is high on those structures which involve high concentrations of unsaturated surface Ni atoms.

7.2. Composite Materials

Efforts toward discovering electrocatalytically active substances have also been directed toward alloys and composite materials. Several alloy systems were investigated. Thus, alloying of Pd with Ni resulted in a decrease of the activity for HER up to 20% Ni and thereafter no significant difference.(317) Analogously, addition of Au (318) or Rh (272) to Pd induced an activity decrease up to 50% Au or 40% Rh, respectively. In contrast with these observations where no improvement of the activity by alloying above the levels of pure metals was seen,(319) an activity peak at 40% Au in Pd was reported.(320) Also, Ross *et al.*(321) reported three times higher activity at 24% Rh in Pt as compared with pure Pt, and Yanagihara(322,323) reported very high electrocatalytic activity for hydrogen evolution at electrodeposited Co electrodes with codeposits of Mo or V (cf. Figure 22). Composite materials, such as tungsten carbide(324) or Na–W bronzes(325–330) were also reported to be active.

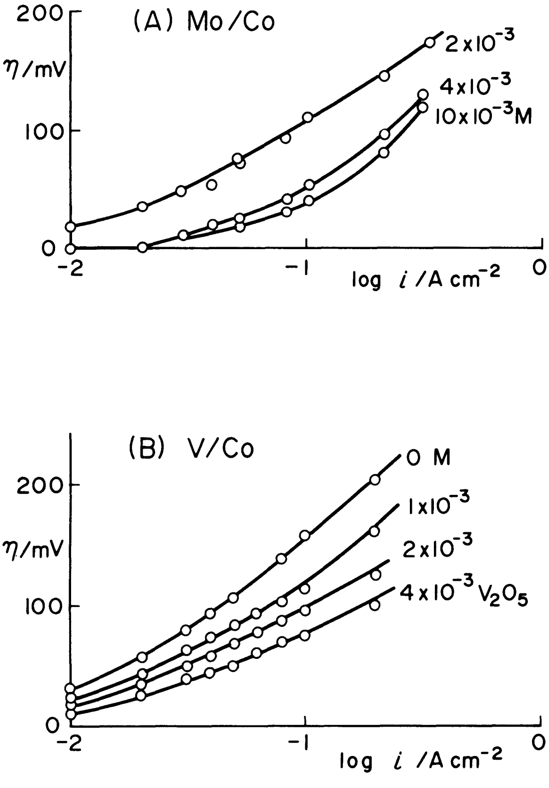

Figure 22. HER Tafel lines obtained for electrodeposited Co electrodes with codeposits of Mo and V in 3 M NaOH at 353 K (Yanagihara(322,323)). (A) Electrodes prepared by electrodeposition on Cu from a cobalt plating bath containing $(NH_4)_2MoO_4$ at the concentrations indicated; (B) electrodes prepared by electrodeposition on Cu from a cobalt plating bath containing V_2O_5 at the concentrations indicated.

In spite of observations of improved activity of Pt metals for anodic oxidation of organic substances by surface modification with other elements such as As, Pb, Se, Ga, Cu, Hg, Bi, etc.,(284,331–339) deposition of Se, Sn, etc. on a Pt substrate,(340,341) Pb, Cd, and Tl on Pt,(342) Pb on Au,(343) or Tl and Pb on Ag,(344) all resulted in a decrease of the activity for the HER. It seems unlikely that good electrode materials for electrocatalysis in the HER will be found from this category of materials.

References

1. N. Kobosev and W. Monblanova, *Acta Physicochim. URSS* **1**, 611 (1934), **4**, 395 (1936); *Zh. Fiz. Khim.* **7**, 645 (1936).
2. W. Grubb, *Nature* **198**, 883 (1963).
3. K. F. Bonhoeffer, *Z. Phys. Chem.* **A113**, 199 (1924).
4. J. Tafel, *Z. Phys. Chem.* **50**, 641 (1905).
5. T. Erdey-Gruz and M. Volmer, *Z. Phys. Chem.* (*Leipzig*) **150**, 203 (1930); **162**, 53 (1932).
6. J. A. V. Butler, *Proc. R. Soc.* (*London*) *Ser. A* **157**, 423 (1936).
7. A. N. Frumkin, *Acta Physicochim. URSS* **18**, 23 (1943).
8. A. Frumkin, *Z. Phys. Chem.* (*Leipzig*) **A164**, 121 (1933).
9. A. N. Frumkin, in *Advances in Electrochemistry and Electrochemical Engineering*, Vol. 1, P. Delahay, ed., Interscience, New York (1961), p. 65.
10. A. N. Frumkin, in *Advances in Electrochemistry and Electrochemical Engineering*, Vol. 3, P. Delahay and C. Tobias, eds., Interscience, New York (1963), p. 287
11. B. Topley and H. Eyring, *J. Chem. Phys.* **2**, 217 (1934).
12. J. Horiuti and G. Okamoto, *Sci. Pap., Inst. Phys. Chem. Res. Tokyo* **28**, 231 (1936).
13. G. Okamoto, J. Horiuti, and K. Hirota, *Sci. Pap., Inst. Phys. Chem. Res. Tokyo* **29**, 223 (1936).
14. J. Horiuti, T. Keii, and K. Hirota, *J. Res. Inst. Catal. Hokkaido Univ.* **2**, 1 (1951).
15. J. Horiuti and T. Nakamura, *J. Res. Inst. Catal. Hokkaido Univ.* **2**, 73 (1951).
16. T. Keii and T. Kodera, *J. Res. Inst. Catal. Hokkaido Univ.* **5**, 105 (1957).
17. T. Kodera and T. Saito, *J. Res. Inst. Catal. Hokkaido Univ.* **7**, 5 (1959).
18. J. Horiuti and K. Müller, *J. Res. Inst. Catal. Hokkaido Univ.* **16**, 605 (1968).
19. H. F. Walton and J. H. Wolfenden, *Trans. Faraday Soc.* **34**, 436 (1938).
20. M. Rome and C. F. Hiskey, *J. Am. Chem. Soc.* **76**, 5207 (1954).
21. B. E. Conway, *Proc. R. Soc.* (*London*) *Ser. A* **247**, 400 (1958); *Can. J. Chem.* **37**, 178 (1959).
22. M. Salomon and B. E. Conway, *J. Phys. Chem.* **68**, 2009 (1964); *Discuss. Faraday Soc.* **39**, 223 (1965).
23. J. O'M. Bockris and S. Srinivasan, *J. Electrochem. Soc.* **111**, 844, 853, 858 (1964).
24. B. E. Conway and M. Salomon, *J. Chem. Phys.* **41**, 3169 (1964).
25. S. G. Christov, *J. Res. Inst. Catal. Hokkaido Univ.* **16**, 169 (1968).
26. P. R. Rowland, *Nature* **218**, 945 (1968); *J. Electroanal. Chem.* **32**, 89, 109 (1971).
27. M. Enyo, in *Modern Aspects of Electrochemistry*, Vol. 11, B. E. Conway and J. O'M. Bockris, eds., Plenum Press, New York (1975), p. 251.
28. G. C. Bond, *Catalysis by Metals*, Academic Press, London (1962).
29. H. Kita, in *Electrochemistry*; *The Past Thirty and the Next Thirty Years*, H. Bloom and F. Gutmann, eds., Plenum Press, New York (1977), p. 117.
30. J. Horiuti and M. Polanyi, *Acta Physicochim. URSS* **2**, 505 (1935).
31. D. B. Matthews and J. O'M. Bockris, in *Modern Aspects of Electrochemistry*, Vol. 6, J. O'M. Bockris and B. E. Conway, eds., Plenum Press, New York (1971), p. 242.

32. R. R. Dogonadze, *Dokl. Akad. Nauk SSSR* **133**, 1368 (1960); **142**, 1108 (1962).
33. R. R. Dogonadze, A. M. Kuznetsov, and T. A. Marsagishvili, *Electrochim. Acta* **25**, 1 (1980).
34. V. G. Levich and R. R. Dogonadze, *Dokl. Akad. Nauk SSSR* **124**, 123 (1959).
35. R. A. Marcus, *J. Chem. Phys.* **24**, 966 (1956); **26**, 867 (1957).
36. H. Gerischer, in *Advances in Electrochemistry and Electrochemical Engineering*, Vol. 1, P. Delahay, ed., Interscience, New York (1961), p. 139.
37. N. S. Hush, *J. Chem. Phys.* **28**, 962 (1962).
38. J. Ulstrup, *J. Chem. Soc. Faraday Trans. 1* **71**, 435 (1975).
39. P. P. Schmidt, in *Electrochemistry* (*The Chemical Society, Specialist Periodical Reports*), H. R. Thirsk (Senior Reporter), Vol. 5 (1975), p. 21; Vol. 6 (1978), p. 128.
40. P. Delahay, *Double Layer and Electrode Kinetics*, Interscience, New York (1965).
41. L. I. Krishtalik, *J. Electroanal. Chem.* **35**, 157 (1972).
42. L. I. Krishtalik, in *Advances in Electrochemistry and Electrochemical Engineering*, Vol. 7, P. Delahay and C. W. Tobias, eds., Interscience, New York (1970), p. 283.
43. A. Slygin and A. Frumkin, *Acta Physicochim. URSS* **3**, 791 (1935).
44. B. Ershler, *Acta Physicochim. URSS* **7**, 327 (1937).
45. M. W. Breiter, C. A. Knorr, and W. Völkl, *Z. Elektrochem.* **59**, 681 (1955).
46. J.-P. Chevillot, J. Farcy, C. Hinnen, and A. Rousseau, *J. Electroanal. Chem.* **64**, 39 (1975).
47. B. G. Baker, D. A. J. Rand, and R. Woods, *J. Electroanal. Chem.* **97**, 189 (1979).
48. S. Hadzi-Jordanov, H. Angerstein-Kozlowska, M. Vukovic, and B. E. Conway, *J. Phys. Chem.* **81**, 2271 (1977).
49. V. Sh. Palanker, E. N. Baybatyrov, and D. V. Sokolsky, *Electrochim. Acta* **20**, 51 (1975).
50. W. Warren and J. T. Kummer, *J. Electrochem. Soc.* **124**, 724 (1977).
51. A. G. Pshenichnikov, R. Kh. Burshtein, and V. D. Kobalevskaya, *Elektrokhimiya* **11**, 1465 (1975).
52. M. Breiter, *Ann. N. Y. Acad. Sci.* **101**, 709 (1963); *J. Electroanal. Chem.* **90**, 425 (1978).
53. M. A. V. Devanathan and M. Selvaratnam, *Trans. Faraday Soc.* **56**, 1820 (1960).
54. M. J. Joncich and N. Hackerman, *J. Electrochem. Soc.* **111**, 1286 (1964).
55. W. Böld and M. Breiter, *Z. Elektrochem.* **64**, 897 (1960).
56. A. N. Frumkin, *Z. Phys. Chem.* **116**, 466 (1925).
57. J. Horiuti, *J. Res. Inst. Catal. Hokkaido Univ.* **4**, 55 (1956).
58. N. P. Keier and S. Z. Roginsky, *Dokl. Akad. Nauk SSSR* **57**, 157 (1947).
59. R. Woods, *J. Electroanal. Chem.* **49**, 217 (1974).
60. K. Kinoshita, D. R. Ferrier, and P. Stonehart, *Electrochim. Acta* **23**, 45 (1978).
61. J. G. Aston, *J. Phys. Chem.* **67**, 2042 (1963).
62. M. W. Breiter, *Trans. Faraday Soc.* **60**, 1445 (1964).
63. V. S. Bagotsky, Yu. B. Vassiliev, and I. I. Pyshnograeva, *Electrochim. Acta* **16**, 2141 (1971).
64. I. I. Pyshnograeva, Yu. B. Vassiliev, I. E. Zimakov, V. S. Bagotsky, and V. L. Spitsyn, *Dokl. Akad. Nauk SSSR* **189**, 1048 (1969); *Elektrokhimiya* **5**, 1503 (1969).
65. A. M. Meretskii, I. V. Kudryashov, and Yu. B. Vasiliev, *Elektrokhimiya* **13**, 447 (1977).
66. M. W. Breiter, *Trans. Faraday Soc.* **61**, 749 (1965).
67. T. M. Grishina, L. I. Logacheva, and G. D. Vovchenko, *Elektrokhimiya* **9**, 1247 (1973).
68. G. P. Klein and K. J. Vetter, *Z. Phys. Chem.* (*N.F.*) **99**, 1 (1976).
69. S. Srinivasan and E. Gileadi, *Electrochim. Acta* **11**, 321 (1966).
70. A. Bewick and B. Thomas, *J. Electroanal. Chem.* **85**, 329 (1977).
71. A. Sadkowski, *J. Electroanal. Chem.* **97**, 283 (1979).
72. K. Kinoshita, J. Lundquist, and P. Stonehart, *J. Catal.* **31**, 325 (1973).
73. K. Kinoshita and P. Stonehart, *Electrochim. Acta* **20**, 101 (1975).
74. T. Yoshida and T. Osaka, *Elektrokhimiya* **14**, 692 (1978).
75. M. Nakamura and H. Kita, *J. Electroanal. Chem.* **68**, 49 (1976).
76. K. Fujikawa, A. Katayama, and H. Kita, *J. Chem. Soc. Faraday Trans. 1* **70**, 1 (1974).
77. J. C. Huang, W. E. O'Grady, and E. Yeager, *J. Electrochem. Soc.* **124**, 1732 (1977).
78. M. Breiter, *Electrochim. Acta* **7**, 25 (1962).

79. F. G. Will, *J. Electrochem. Soc.* **112**, 451 (1965).
80. K. Yamamoto, D. M. Kolb, R. Kotz, and G. Lehmpfuhl, *J. Electroanal. Chem.* **96**, 233 (1979).
81. A. T. Hubbard, R. P. Ishikawa, and J. Katekaru, *J. Electroanal. Chem.* **86**, 271 (1978).
82. E. Yeager, W. E. O'Grady, M. Y. C. Woo, and P. Hagans, *J. Electrochem. Soc.* **125**, 348 (1978).
83. P. N. Ross, *J. Electrochem. Soc.* **126**, 67 (1979).
84. J. Clavilier, R. Faure, G. Guinet, and R. Durand, *J. Electroanal. Chem.* **107**, 205 (1980); J. Clavilier, *J. Electroanal. Chem.* **107**, 211 (1980).
85. P. N. Ross, Jr., *J. Electroanal. Chem.* **76**, 139 (1977).
86. P. N. Ross, Jr., *J. Electrochem. Soc.* **126**, 67 (1979).
87. K. Christmann, G. Ertl, and T. Pignet, *Surf. Sci.* **54**, 365 (1976).
88. T. Toya, *J. Res. Inst. Catal. Hokkaido Univ.* **6**, 308 (1958); **8**, 209 (1960); **10**, 236 (1962); **11**, 84 (1963); J. Horiuti and T. Toya, *Solid State Surf. Sci.* **1**, 1 (1969).
89. J. Horiuti, *J. Res. Inst. Catal. Hokkaido Univ.* **1**, 8 (1948).
90. M. Enyo and T. Yokoyama, *Electrochim. Acta* **16**, 223 (1971).
91. A. Matsuda and J. Horiuti, *J. Res. Inst. Catal. Hokkaido Univ.* **10**, 14 (1962).
92. M. I. Temkin, *Dokl. Akad. Nauk SSSR* **152**, 156 (1963).
93. J. Horiuti, in *Trans. Symp. Electrode Processes, Philadelphia*, Wiley, New York (1959), p. 17.
94. J. Horiuti and T. Nakamura, in *Advances in Catalysis*, Vol. 17, D. D. Eley, ed., Academic Press, New York (1967), p. 2.
95. A. Matsuda and R. Notoya, *J. Res. Inst. Catal. Hokkaido Univ.* **14**, 165, 192, 198 (1966).
96. A. Matsuda, R. Notoya, T. Omori, K. Kunimatsu, and T. Kushimoto, *Elektrokhimiya* **13**, 726, 1659 (1977).
97. B. N. Kabanov, *Electrochim. Acta* **13**, 19 (1968); B. N. Kabanov, I. I. Astakhov, and I. G. Kiseleva, *Electrochim. Acta.* **24**, 167 (1979).
98. Yu. A. Kukk and V. E. Past, *Elektrokhimiya* **7**, 1863 (1971).
99. D. C. Walker, *Can. J. Chem.* **45**, 807 (1967); **44**, 2226 (1966).
100. D. C. Walker, *Q. Rev.* **21**, 79 (1967).
101. D. C. Walker, *J. Electroanal. Chem.* **42**, App. 17 (1973).
102. T. Pyle and C. Roberts, *J. Electrochem. Soc.* **115**, 247 (1968).
103. G. A. Kenney and D. C. Walker, in *Electroanalytical Chemistry*, Vol. 5, A. J. Bard, ed., Marcel Dekker, New York (1971), p. 1.
104. L. I. Krishtalik, N. M. Alpatova, and E. V. Ovsyannikova, *Elektrokhimiya* **12**, 1493 (1976).
105. S. E. Zabusova, M. G. Fomicheva, N. M. Alpatova, and L. I. Krishtalik, *Elektrokhimiya* **14**, 1619 (1978).
106. B. E. Conway and D. J. Mackinnon, *J. Phys. Chem.* **74**, 3663 (1970).
107. J. Horiuti and M. Ikusima, *Proc. Imp. Acad. Tokyo* **15**, 39 (1939).
108. J. Horiuti, *Ann. N. Y. Acad. Sci.* **213**, 5 (1973).
109. J. O'M. Bockris, *J. Electrochem. Soc.* **99**, 366c (1952); *Annual Review of Physical Chemistry*, Vol. 5, Annual Reviews Inc., Palo Alto, California (1954), p. 477.
110. J. O'M. Bockris, in *Modern Aspects of Electrochemistry*, Vol. 1, J. O'M. Bockris and B. E. Conway, eds., Butterworths, London (1954), p. 180.
111. R. Parson, *J. Chim. Phys.* **49**, C82 (1952).
112. T. Matsushima, T. Yokoyama, and M. Enyo, *J. Res. Inst. Catal. Hokkaido Univ.* **17**, 165 (1969).
113. M. Enyo and T. Yokoyama, *J. Res. Inst. Catal. Hokkaido Univ.* **12**, 1631 (1967).
114. T. Matsushima and M. Enyo, *J. Res. Inst. Catal. Hokkaido Univ.* **17**, 14 (1969).
115. J. O'M. Bockris and E. C. Potter, *J. Chem. Phys.* **20**, 614 (1952).
116. A. R. Despic and J. O'M. Bockris, *J. Chem. Phys.* **32**, 389 (1960).
117. J. O'M. Bockris and U. M. Khan, *Quantum Electrochemistry*, Plenum Press, New York (1979), p. 49.
118. A. Matsuda and R. Notoya, *J. Res. Inst. Catal. Hokkaido Univ.* **11**, 193 (1963).

119. D. B. Matthews and J. O'M. Bockris, *Modern Aspects of Electrochemistry*, Vol. 6, J. O'M. Bockris and B. E. Conway, eds., Plenum Press, New York (1971), p. 242.
120. K. B. Oldham, *J. Am. Chem. Soc.* **77**, 4697 (1955).
121. K. J. Bachmann, *J. Electrochem. Soc.* **119**, 1021 (1972).
122. A. C. Makrides, *J. Electrochem. Soc.* **104**, 677 (1957); **109**, 256 (1962).
123. H. Mauser, *Z. Elektrochem.* **62**, 419 (1958).
124. J. O'M. Bockris and H. Mauser, *Can. J. Chem.* **37**, 475 (1959).
125. A. C. Riddiford, *J. Chem. Soc.* 1175 (1960).
126. D. M. Mohilner, *J. Phys. Chem.* **68**, 632 (1964).
127. S. Barnartt, *J. Phys. Chem.* **70**, 412 (1966).
128. A. R. Despic, *Bull. Soc. Chim. (Belgrade)* **30**, 293 (1955).
129. T. Yamazaki and H. Kita, *J. Res. Inst. Catal. Hokkaido Univ.* **13**, 77 (1965).
130. B. E. Conway, *Proc. R. Soc. (London)*, **A256**, 128 (1960).
131. E. J. Kelly, *J. Electrochem. Soc.* **112**, 124 (1965).
132. J. O'M. Bockris and S. Srinivasan, *Electrochim. Acta* **9**, 31 (1964).
133. R. Clamroth and C. A. Knorr, *Z. Elektrochem.* **57**, 399 (1953).
134. J. C. Barton and F. A. Lewis, *Z. Phys. Chem. (N. F.)*, **33**, 99 (1962).
135. K. J. Vetter, *Electrochemical Kinetics*, Academic Press, New York (1967), p. 432.
136. B. E. Conway and M. Salomon, *Electrochim. Acta* **9**, 1599 (1964).
137. B. E. Conway, E. J. Rudd, and L. G. M. Gordon, *Discuss. Faraday Soc.* **45**, 87 (1968).
138. H. Gerischer, *Z. Elektrochem.* **54**, 362 (1950).
139. T. Yokoyama and M. Enyo, *Electrochim. Acta* **15**, 1921 (1970).
140. K. Gossner and F. Mansfield, *Z. Phys. Chem. (N. F.)*, **58**, 19 (1968).
141. D. R. Flinn and S. Schuldiner, *Electrochim. Acta* **19**, 421 (1974).
142. V. S. Bagotsky and N. V. Osetrova, *J. Electroanal. Chem.* **43**, 233 (1973).
143. N. V. Osetrova and V. S. Bagotzky, *Elektrokhimiya* **9**, 48 (1973).
144. M. Enyo and T. Yokoyama, *Electrochim. Acta* **12**, 1631, 1641 (1967).
145. T. Yokoyama and M. Enyo, *J. Res. Inst. Catal. Hokkaido Univ.* **15**, 207 (1967).
146. T. Matsushima and M. Enyo, *J. Res. Inst. Catal. Hokkaido Univ.* **17**, 165 (1969).
147. T. Matsushima and M. Enyo, *J. Res. Inst. Catal. Hokkaido Univ.* **18**, 34 (1970).
148. T. Matsushima and M. Enyo, *Shokubai (Catalyst)*, **13**, 177P (1971) (in Japanese).
149. T. Matsushima and M. Enyo, *Electrochim. Acta* **19**, 117, 125, 131 (1974).
150. M. Enyo, *J. Res. Inst. Catal. Hokkaido Univ.* **22**, 42 (1974).
151. M. Enyo and T. Matsushima, *J. Res. Inst. Catal. Hokkaido Univ.* **22**, 88 (1974).
152. M. Enyo, *J. Res. Inst. Catal. Hokkaido Univ.* **22**, 195 (1974).
153. K. Saito, M. Enyo, and T. Matsushima, *J. Res. Inst. Catal. Hokkaido Univ.* **23**, 26 (1975).
154. T. Matsushima and M. Enyo, *Electrochim. Acta* **21**, 241, 823, 1029 (1976).
155. S. Schuldiner and J. P. Hoare, *Can. J. Chem.* **37**, 228 (1959).
156. E. Heitz and E. Yeager, *J. Electrochem. Soc.* **109**, 850 (1962).
157. M. Makowsky, E. Heitz, and E. Yeager, *J. Electrochem. Soc.* **113**, 204 (1966).
158. K. J. Vetter and D. Otto, *Z. Elektrochem.* **66**, 1072 (1956).
159. V. V. Sobol, A. A. Dmitrieva, and A. N. Frumkin, *Elektrokhimiya* **3**, 1040 (1967).
160. E. Aikazyan and A. Frumkin, *Dokl. Akad. Nauk SSSR* **100**, 315 (1955).
161. E. Aikazyan, *Zh. Fiz. Khim.* **33**, 1016 (1959).
162. A. Frumkin, V. Sobol, and A. Dmitrieva, *J. Electroanal. Chem.* **13**, 179 (1967).
163. A. C. Makrides, *J. Electrochem. Soc.* **109**, 977 (1962).
164. J. L. Weininger and M. W. Breiter, *J. Electrochem. Soc.* **111**, 707 (1964).
165. G. Okamoto, *J. Fac. Sci. Hokkaido Imp. Univ. Ser III*, **2**, 115 (1937).
166. S. M. Salei and A. I. Krasilishichikov, *Elektrokhimiya* **5**, 940 (1969).
167. P. Lukowzew, S. Levina, and A. Frumkin, *Acta Physicochim. URSS* **11**, 21 (1939).
168. L. P. Hammett, *Trans. Faraday Soc.* **29**, 770 (1933).
169. M. Breiter and R. Clamroth, *Z. Elektrochem.* **58**, 493 (1954).
170. M. Enyo, *Int. J. Chem. Kinet.* **7**, 463 (1975).

171. M. Enyo, *Electrochim. Acta* **18**, 155, 163 (1973).
172. M. Enyo, *Electrochim. Acta* **21**, 15 (1976).
173. M. Enyo, *J. Res. Inst. Catal. Hokkaido Univ.* **25**, 17 (1977).
174. I. H. Plonski, *J. Electrochem. Soc.* **116**, 944, 1688 (1969); **117**, 1048 (1970).
175. J. O'M. Bockris and E. C. Potter, *J. Electrochem. Soc.* **99**, 169 (1952).
176. I. Ruzic, *J. Electroanal. Chem.* **52**, 331 (1974).
177. M. Enyo, *Denki Kagaku* (*J. Electrochem. Soc. Japan*) **47**, 2 (1979) (in Japanese).
178. R. M. Hurd, *J. Electrochem. Soc.* **109**, 327 (1962).
179. R. G. Erenburg, *Dokl. Akad. Nauk SSSR* **211**, 1149 (1973).
180. R. G. Erenburg, *Elektrokhimiya* **10**, 457, 703, 641 (1974); **11**, 1068 (1975).
181. M. v. Stackelberg and H. Bischoff, *Z. Elektrochem.* **59**, 467 (1955).
182. A. N. Frumkin and N. Aladjalova, *Acta Physicochim. URSS* **19**, 1 (1944).
183. R. Clamroth and C. A. Knorr, *Z. Elektrochem.* **57**, 399 (1953).
184. J. C. Barton and F. A. Lewis, *Z. Phys. Chem.* (*N. F.*) **33**, 99 (1962).
185. T. Maoka and M. Enyo, *Surf. Tech.* **4**, 277 (1976).
186. T. Maoka and M. Enyo, *Surf. Tech.* **8**, 441 (1979).
187. D. N. Jewett and A. C. Makrides, *Trans. Faraday Soc.* **61**, 932 (1965).
188. E. Wicke and G. Bohmholdt, *Z. Phys. Chem.* (*N.F.*) **42**, 115 (1964).
189. G. W. Castellan, *J. Electrochem. Soc.* **111**, 1273 (1964).
190. R. A. LaPietra and G. W. Castellan, *J. Electrochem. Soc.* **111**, 1276 (1964).
191. P. L. Damour and G. W. Castellan, *J. Electrochem. Soc.* **111**, 1280 (1964).
192. D. I. Leikis, E. S. Sebastianov, and L. L. Knotz, *Zh. Fiz. Khim.* **38**, 1833 (1964).
193. K. Kunimatsu, *J. Res. Inst. Catal. Hokkaido Univ.* **20**, 1, 20 (1972).
194. F. A. Lewis, R. C. Johnston, M. C. Witherspoon, W. F. N. Leitch, S. G. Thompson, A. Obermann, and S. F. Deane, *Surf. Tech.* **4**, 89 (1976).
195. F. A. Lewis, A. Obermann, and G. Hodes, *Surf. Tech.* **4**, 79 (1976).
196. C. A. Knorr, *Z. Elektrochem.* **57**, 599 (1953).
197. K. J. Vetter, *Electrochemical Kinetics*, Academic Press, New York (1967), p. 607.
198. T. Maoka and M. Enyo, *Surf. Tech.* **9**, 147 (1979).
199. M. Enyo and T. Maoka, *J. Electroanal. Chem.* **108**, 227 (1980).
200. T. Moaka and M. Enyo, *Electrochim. Acta* **26**, 607, 615 (1981).
201. S. Schuldiner and C. M. Shepherd, *J. Electrochem. Soc.* **115**, 916 (1968).
202. S. Schuldiner and T. B. Warner, *J. Electrochem. Soc.* **112**, 212 (1965).
203. N. Pentland, J. O'M. Bockris, and E. Sheldon, *J. Electrochem. Soc.* **104**, 181 (1957).
204. N. Kobosev and N. I. Nekrasov, *Z. Elektrochem.* **36**, 519 (1930).
205. J. O'M. Bockris and B. E. Conway, *Trans. Faraday Soc.* **45**, 989 (1949).
206. A. Hickeling and F. W. Salt, *Trans. Faraday Soc.* **37**, 333 (1941).
207. A. I. Oshe, *Zh. Fiz. Khim.* **27**, 1622 (1958).
208. L. V. Tamm, Yu. K. Tamm, and V. E. Past, *Elektrokhimiya* **9**, 1382 (1973).
209. P. Stonehart and G. Kohlmayr, *Electrochim. Acta* **17**, 369 (1972).
210. P. Stonehart and P. N. Ross, *Catal. Rev. Sci. Eng.* **12**, 1 (1975).
211. P. Stonehart, *J. Electroanal. Chem.* **77**, 245 (1977).
212. M. W. Breiter, *J. Electroanal. Chem.* **65**, 623 (1975).
213. M. W. Breiter, *J. Electroanal. Chem.* **77**, 251 (1977).
214. B. Baranowski and M. Smialowski, *Bull. Acad. Polonaise Ser. Sci. Chim.* **7**, 663 (1959).
215. B. Baranowski, *Bull. Acad. Polonaise Ser. Sci. Chim.* **7**, 887, 891, 897, 907 (1959).
216. B. Baranowski, Z. Szklarska-Smialowska, and M. Smialowski, in *Actes de Deuxieme Congres International de Catalyse, Paris, 1960*, Editions Technip, Paris (1961), p. 2269.
217. H. Angerstein-Kozlowska, *Bull. Acad. Polonaise Ser. Sci. Chim.* **7**, 881 (1959); **8**, 49 (1960).
218. B. Baranowski and Z. Szklarska-Smialowska, *Electrochim. Acta* **9**, 1497 (1964).
219. H. Jarmolowicz and M. Smialowski, *J. Catal.* **1**, 165 (1962).
220. K. E. Shuler and K. J. Laidler, *J. Chem. Phys.* **17**, 212 (1949).
221. M. Smialowski, *Hydrogen in Steel*, Pergamon Press, Oxford (1962).

222. W. Beck, A. L. Glass, and E. Taylow, *J. Electrochem. Soc.* **112**, 53 (1965).
223. E. G. Dafft, K. Bohnenkamp, and H.-J. Engell, *Z. Phys. Chem.* (*N.F.*) **108**, 33 (1977).
224. T. D. Radhakrishnan and L. L. Shreir, *Electrochim. Acta* **11**, 1007 (1966).
225. M. A. V. Devanathan, J. O'M. Bockris, and W. Mehl, *J. Electroanal. Chem.* **1**, 143 (1959–1960).
226. J. O'M. Bockris and A. K. N. Reddy, *Modern Electrochemistry*, Plenum Press, New York (1970), p. 1333.
227. J. O'M. Bockris and P. K. Subramanyam, *Electrochim. Acta* **16**, 2169 (1971).
228. P. S. Perminov, A. A. Orlov, and A. N. Frumkin, *Dokl. Akad. Nauk SSSR* **84**, 749 (1952); A. I. Fedorova and A. N. Frumkin, *Zh. Fiz. Khim.* **27**, 247 (1953).
229. A. Kawashima, K. Hashimoto, and S. Shimodaira, *Nippon Kinzoku Gakkaishi* (*J. Japan Soc. Metals*) **38**, 553 (1974) (in Japanese).
230. W. Palczewska and I. Ratajczyk, *Bull. Acad. Polonaise Ser. Sci. Chim.* **9**, 267 (1961).
231. A. M. Sokol'skaya and D. V. Sokol'skii, *Kinetika i Kataliz* **6**, 658 (1965).
232. F. D. Popp and H. P. Schultz, *Chem. Rev.* **62**, 19 (1962).
233. V. S. Bagotzky, Yu. B. Vassiliev, and O. A. Khazova, *J. Electroanal. Chem.* **81**, 229 (1977).
234. P. J. Elving, *Can. J. Chem.* **55**, 3392 (1977).
235. D. V. Sokol'skii, in *Progress in Electrochemistry of Organic Compounds*, Vol. 1, A. N. Frumkin and A. B. Ershler, eds., translated by D. E. Hayler, Plenum Press, New York (1971), p. 377.
236. I. Kiseleva, M. Fioshin, and B. Kabanov, *Elektrokhimiya* **11**, 1544 (1975).
237. I. Kiseleva, M. Fioshin, and B. Kabanov, *Elektrokhimiya* **13**, 773, 1048, 1092, 1516 (1978).
238. S. Glasstone, *Textbook of Physical Chemistry*, D. Van Nostrand, New York (1940), p. 1018.
239. J. O'M. Bockris and D. Drazic, *Electrochemical Science*, Taylor & Francis, London (1972), p. 170.
240. L. D. Burke, C. Kemball, and F. A. Lewis, *Trans. Faraday Soc.* **60**, 913 (1964).
241. L. D. Burke, F. A. Lewis, and C. Kemball, *Trans. Faraday Soc.* **60**, 919 (1964).
242. H. J. Davitt and L. F. Albright, *J. Electrochem. Soc.* **118**, 236 (1971).
243. K. Fujikawa and H. Kita, *J. Chem. Soc. Faraday Trans. 1* **75**, 2638 (1979).
244. K. Fujikawa, H. Kita, K. Miyahara, and S. Sato, *J. Chem. Soc. Faraday Trans. 1* **71**, 1573 (1975).
245. K. Fujikawa, H. Kita, and K. Miyahara, *J. Chem. Soc. Faraday Trans. 1* **69**, 481 (1973).
246. K. Fujikawa, A. Katayama, and H. Kita, *J. Chem. Soc. Faraday Trans. 1* **70**, 1 (1974).
247. M. Byrne and A. T. Kuhn, *J. Chem. Soc. Faraday Trans. 1* **68**, 355 (1972).
248. M. Byrne, A. T. Kuhn, and V. J. Whittle, *J. Chem. Soc. Faraday Trans. 1* **69**, 787 (1973).
249. S. H. Langer, I. Feiz, and C. P. Quinn, *J. Am. Chem. Soc.* **93**, 1092 (1971).
250. S. H. Langer and G. P. Sakellaropoulos, *J. Electrochem. Soc.* **122**, 1619 (1975).
251. X. de Hemptinne and K. Schunk, *Ann. Soc. Sci. Bruxelles* **65**, 591 (1969).
252. P. J. Elving and C. Teitelbaum, *J. Am. Chem. Soc.* **71**, 3916 (1949).
253. H. Kita, T. Nakamura, H. Itoh, and H. Kano, *Electrochim. Acta* **23**, 405 (1978).
254. M. von Stackelberg and P. Weber, *Z. Elektrochem.* **56**, 806 (1952).
255. C. Wagner, *Electrochim. Acta* **15**, 987 (1970).
256. Z. Takehara, *Electrochim. Acta* **15**, 999 (1970).
257. M. Enyo, *Denki Kagaku* (*J. Electrochem. Soc. Japan*) **50**, 743 (1982).
258. K. J. Vetter, *Z. Phys. Chem.* **199**, 285 (1952).
259. K. J. Vetter, *Z. Elektrochem.* **56**, 797 (1952).
260. F. Beck, *Ber. Bunsenges. Phys. Chem.* **69**, 199 (1965).
261. V. I. Bistrov and L. I. Krishtalik, *Elektrokhimiya* **3**, 1345 (1967).
262. N. Pentland, J. O'M. Bockris, and E. Sheldon, *J. Electrochem. Soc.* **104**, 182 (1957).
263. A. Belanger and A. K. Vijh, *J. Electrochem. Soc.* **121**, 225 (1974).
264. E. D. Lebin and A. L. Rotinyan, *Elektrokhimiya* **8**, 240 (1972).
265. I. V. Kudryashov, E. S. Burmistrov, and V. L. Kirgis, *Elektrokhimiya* **6**, 737 (1970).
266. J. O'M. Bockris and D. F. A. Koch, *J. Phys. Chem.* **65**, 1941 (1961).

267. B. B. Kuzimenko and L. I. Krishtalik, *Elektrokhimiya* **9**, 130 (1973).
268. J. O'M. Bockris and R. Parsons, *Trans. Faraday Soc.* **44**, 860 (1948).
269. Yu. K. Tamm and L. V. Tamm, *Elektrokhimiya* **12**, 955 (1976).
270. A. T. Kuhn and P. M. Wright, *J. Electroanal. Chem.* **27**, 319 (1970).
271. R. D. Armstrong and M. F. Bell, *Electrochim. Acta* **23**, 1111 (1978).
272. J. P. Hoare, *J. Electrochem. Soc.* **107**, 820 (1960).
273. J. P. Hoare, S. Schuldiner, and G. W. Castellan, *J. Chem. Phys.* **28**, 22 (1958).
274. S. Schuldiner, *J. Electrochem. Soc.* **107**, 452 (1960).
275. L. P. Bicelli, C. Romagnani, and M. Rosania, *J. Electroanal. Chem.* **63**, 238 (1975).
276. H. J. Ellingham and A. J. Allmand, *Trans. Faraday Soc.* **19**, 748 (1924).
277. H. Kita, *J. Electrochem. Soc.* **113**, 1095 (1966).
278. M. H. Miles and M. A. Thomason, *J. Electrochem. Soc.* **123**, 1459 (1976).
279. M. H. Miles, *J. Electroanal. Chem.* **60**, 89 (1975).
280. E. J. Weeks, *Chem. News* **129**, 17 (1924).
281. J. R. Partington, *Chem. News* **129**, 77 (1924).
282. N. Ontani, *Sci. Rep. Res. Inst. Tohoku Univ.* **A8**, 399 (1956).
283. N. I. Kobozev, *Zh. Fiz. Khim.* **26**, 112 (1952).
284. R. R. Adzic, D. N. Simic, D. M. Drazic, and A. R. Despic, *J. Electroanal. Chem.* **61**, 117 (1975).
285. H. Leidheiser, *J. Am. Chem. Soc.* **71**, 3634 (1949).
286. E. N. Khomatov, *Zh. Fiz. Khim.* **24**, 1201 (1950).
287. S. G. Christov and N. A. Pangarov, *Z. Elektrochem.* **61**, 113 (1957).
288. A. K. Lorentz, *Zh. Fiz. Khim.* **27**, 317 (1953).
289. A. J. Appleby, *Catal. Rev.* **4**, 221 (1970).
290. H. Kita, *J. Res. Inst. Catal. Hokkaido Univ.* **13**, 151 (1965).
291. R. T. Sanderson, *Chemical Periodicity*, Reinhold, New York (1964), p. 86.
292. H. Fischer, *Z. Elektrochem.* **52**, 111 (1948).
293. G. I. Volkov, *Zh. Fiz. Khim.* **29**, 390 (1955).
294. B. E. Conway and J. O'M. Bockris, *J. Chem. Phys.* **26**, 532 (1957).
295. J. O'M. Bockris, *Trans. Faraday Soc.* **43**, 417 (1947).
296. J. O'M. Bockris, *Chem. Rev.* **43**, 525 (1948).
297. J. O'M. Bockris and H. Wroblowa, *J. Electroanal. Chem.* **7**, 428 (1964).
298. J. O'M. Bockris, *Nature* **158**, 584 (1946).
299. B. E. Conway, *J. Electrochem. Soc.* **124**, 410C (1977).
300. A. Belanger and A. K. Vijh, *Elektrokhimiya* **10**, 1854 (1974).
301. S. Trasatti, in *Advances in Electrochemistry and Electrochemical Engineering*, Vol. 10, H. Gerischer and C. W. Tobias, eds., John Wiley, New York (1977), p. 213.
302. A. T. Petrenko, *Zh. Fiz. Khim.* **39**, 2097 (1965).
303. P. Rüetschi and P. Delahay, *J. Chem. Phys.* **23**, 195 (1955).
304. P. Rüetschi and P. Delahay, *J. Chem. Phys.* **23**, 1167 (1955).
305. N. I. Kobozev, *Zh. Fiz. Khim.* **26**, 112, 438 (1952).
306. R. Parsons, *Trans. Faraday Soc.* **54**, 1053 (1958).
307. A. K. Vijh and A. Belanger, *Z. Phys. Chem.* (*N.F.*) **83**, 173 (1973).
308. Y. Takasu and Y. Matsuda, *Electrochim. Acta* **21**, 133 (1976).
309. D. J. Barclay, *J. Electroanal. Chem.* **44**, 47 (1973).
310. H. Gerischer, *Z. Phys. Chem.* **8**, 137 (1956).
311. A. T. Khun, J. Mortimer, G. C. Bond, and J. Lindey, *J. Electroanal. Chem.* **34**, 1 (1972).
312. I. V. Kudryashov and L. A. Falin, *Elektrokhimiya* **8**, 1029 (1972); I. V. Kudryashov, A. V. Izmailov, and Yu. A. Lelikov, *Zh. Fiz. Khim.* **49**, 929 (1975).
313. V. S. Bagotzky, L. S. Kanevsky, and V. Sh. Palanker, *Electrochim. Acta* **18**, 473 (1973).
314. R. N. Ross, K. Kinoshita, and P. Stonehart, *J. Catal.* **32**, 163 (1974); K. Kinoshita and P. Stonehart, *Electrochim. Acta* **20**, 101 (1975).
315. T. Biegler, *Aust. J. Chem.* **26**, 2571, 2587 (1973).

316. L. Angely, G. Bronoel, and G. Peslerbe, *J. Electroanal. Chem.* **96**, 183, 191, 203 (1979).
317. J. P. Hoare and S. Schuldiner, *J. Phys. Chem.* **62**, 229 (1958).
318. S. Schuldiner and J. P. Hoare, *J. Phys. Chem.* **61**, 705 (1957).
319. P. N. Ross, K. Kinoshita, A. J. Scarpellino, and P. Stonehart, *J. Electroanal. Chem.* **63**, 97 (1975).
320. J. H. Fishman and M. Yarish, *Electrochim. Acta* **12**, 579 (1967).
321. P. N. Ross, K. Kinoshita, A. J. Scarpellino, and P. Stonehart, *J. Electroanal. Chem.* **59**, 177 (1975).
322. M. Yanagihara, *Kinzoku Hyomen Gijutsu* (*Metal Surface Finish*) **29**, 590 (1978) (in Japanese).
323. M. Yanagihara, *Kinzoku Hyomen Gijutsu* (*Metal Surface Finish*) **29**, 636 (1978) (in Japanese).
324. D. V. Sokolsky, V. Sh. Palanker, and E. N. Baybatyrov, *Electrochim. Acta* **20**, 71 (1975).
325. D. P. Sepa, A. Damjanovic, and J. O'M. Bockris, *Electrochim. Acta* **12**, 746 (1967).
326. A. Damjanovic, D. P. Sepa, and J. O'M. Bockris, *J. Res. Inst. Catal. Hokkaido Univ.* **16**, 1 (1968).
327. J. O'M. Bockris and J. McHardy, *J. Electrochem. Soc.* **120**, 61 (1973).
328. J. P. Randin, *J. Electrochem. Soc.* **120**, 378 (1973); *Electrochim. Acta* **19**, 87 (1974).
329. J. P. Randin and A. K. Vijh, *Electrochim. Acta* **20**, 37 (1975).
330. D. B. Sepa, D. S. Ovcin, and M. V. Voinovic, *J. Electrochem. Soc.* **119**, 1285 (1972).
331. R. R. Adzic and A. R. Despic, *J. Chem. Phys.* **61**, 3482 (1974).
332. R. R. Adzic, D. N. Simic, D. M. Drazic, and A. R. Despic, *J. Electroanal. Chem.* **61**, 117 (1975); **65**, 587 (1975).
333. R. R. Adzic, M. E. Spasojevic, and A. R. Despic, *J. Electroanal. Chem.* **92**, 31 (1978).
334. R. R. Adzic, D. N. Simic, A. R. Despic, and D. M. Drazic, *J. Electroanal. Chem.* **65**, 587 (1975); **80**, 81 (1977).
335. S. Motoo and M. Watanabe, *J. Electroanal. Chem.* **98**, 203 (1979).
336. R. R. Adzic and A. R. Despic, *Z. Phys. Chem.* (*N.F.*) **98**, 95 (1975).
337. R. R. Adzic and A. V. Tripkovic, *J. Electroanal. Chem.* **94**, 231 (1978); **99**, 43 (1979).
338. M. Uehara, S. Nagaya, H. Aoki, and T. Suzuki, *Denki Kagaku* (*J. Electrochem. Soc. Japan*) **46**, 656 (1978) (in Japanese).
339. Yu. B. Vassiliev, V. S. Bagotzky, N. V. Osetrova, and A. A. Mikhailova, *J. Electroanal. Chem.* **97**, 63 (1979).
340. N. Furuya and S. Motoo, *J. Electroanal. Chem.* **98**, 195 (1979).
341. N. Furuya and S. Motoo, *J. Electroanal. Chem.* **102**, 155 (1979).
342. R. R. Adzic, M. D. Spasojevic, and A. R. Despic, *Electrochim. Acta* **24**, 577 (1979).
343. R. T. Adzic, M. D. Spasojevic, and A. R. Despic, *Electrochim. Acta* **24**, 569 (1979).
344. A. M. A. El-Halim, K. Jüttner, and W. J. Lorenz, *J. Electroanal. Chem.* **106**, 193 (1980).

6

Oxygen Electrochemistry

M. R. TARASEVICH, ANDRZEJ SADKOWSKI, and ERNEST YEAGER

1. Introduction

Oxygen electrochemistry is of major importance to energy conversion storage and conservation. Oxygen-consuming cathodes are used in fuel cell systems and in metal–air batteries. Further, O_2 electrogeneration is involved in water electrolysis and other industrial electrolytic processes as well as in the recharging of metal–air cells. Oxygen-consuming cathodes are also expected to find application in industrial electrolysis cells such as the chloralkali cells in the near future. In aqueous systems, however, O_2 reduction and generation are very irreversible even at temperatures above 100°C and this imposes serious energy losses in electrochemical cells involving O_2 electrodes.

On the other hand, the high overpotential associated with O_2 generation is advantageous in aqueous batteries involving cathodes operating at potentials anodic to the reversible potential of the O_2 electrode. Otherwise the spontaneous generation of O_2 would rapidly discharge such cathodes.

Oxygen reduction also plays a role in the corrosion of metals such as steel in the presence of air. The O_2 reduction drives the potential sufficiently positive to produce the passivation film on ferrous metals, which in turn inhibits corrosion.

M. R. TARASEVICH • Institute of Electrochemistry of the Academy of Sciences of the USSR, Leninsky Prospekt 31, Moscow V-71, USSR. **ANDRZEJ SADKOWSKI** • Institute of Physical Chemistry, Warsaw, Poland. **ERNEST YEAGER** • Case Laboratories for Electrochemical Studies, Case Western Reserve University, Cleveland, Ohio.

The oxygen electrode has been the subject of extensive investigations over the past century. The pronounced irreversibility of the cathodic and anodic reactions in aqueous solutions has imposed severe limitations on the information which can be obtained concerning the pathways from electrochemical kinetic studies. In most instances at current densities practical for kinetic studies, the current–voltage data are not sensitive to the backreaction and hence yield information only up to the rate-controlling step, which usually occurs early in the multiple-step reaction sequence. Further the reduction and oxidation processes are usually studied only at widely separated potentials and thus the surface conditions differ sufficiently such that the reduction and oxidation pathways are probably not complementary. The situation is made all the more complicated by the large number of possible pathways for the O_2 electrode reactions. The relation of the overall anodic and cathodic kinetics to the surface electronic properties is not well understood. With the possible exception of gold cathodes in acid aqueous electrolytes, metal electrodes are covered with anodic films at the potentials of interest for O_2 reduction and for O_2 generation. The surface states of the anodic films are usually strongly potential dependent and also, in most instances, time dependent with the result that quite complex kinetic behavior has been observed as a function of potential.

During O_2 reduction on most electrode surfaces, hydrogen peroxide is generated. In alkaline solutions, the exchange current density for the O_2–peroxide couple on most electrode surfaces is quite high compared to that for the overall four-electron reduction to water. As a consequence, it has been possible to obtain more insight into the pathways for the O_2–peroxide reaction including reaction orders and stoichiometric numbers.

The interest in O_2 electrochemistry includes hydrate melts (e.g., NaOH and KOH monohydrate), molten salts (particularly alkali metal carbonates), and organic solvent systems. This chapter, however, will be limited principally to aqueous systems.

2. Thermodynamics of the Oxygen Electrode

The overall four-electron reductions of O_2 in acid and alkaline aqueous solutions are, respectively,

$$O_2 + 4H^+ + 4e^- \rightleftharpoons 2H_2O, \quad (E^\circ_{\mathrm{NHE}})_{298} = 1.229\ \mathrm{V} \tag{I}$$

$$O_2 + 2H_2O + 4e^- \rightleftharpoons 4OH^-, \quad (E^\circ_{\mathrm{NHE}})_{298} = 0.401\ \mathrm{V} \tag{II}$$

where the standard reduction potentials have been calculated relative to the standard hydrogen electrode (SHE, NHE, or RHE) from the standard free energy of formation of water and OH^- ions.(1) Various component reactions and the corresponding free energies and potentials are listed in Tables 1a and

Table 1a
Selected Thermodynamic Data of Oxygen Species[a] at 25°C

Formula	Standard state	$\Delta G°$, kJ/mol	$\Delta H°$, kJ/mol	$S°$, J/mol/K
O_2	Gas, 1 atm	0	0	205.3
H_2O	Pure liquid	−237.18	−285.83	69.91
OH^-	1 *M*, aq.	−157.29	−230.00	−10.75
H_2O_2	1 *M*, aq. undisc.	−134.1	−191.2	143.9
HO_2^-	1 *M*, aq.	−67.36	−160.3	23.8
O_2^-	1 *M*, aq.	27.4[b,c]	n.a.[d]	n.a.[d]
HO_2	1 *M*, aq.	5.09[b,c]	n.a.[d]	n.a.[d]
OH	Gas, 1 atm	34.23	38.95	183.6

[a] Data from D. D. Wagman, N.B.S. Technical Note 270–3, U.S. Government, Printing Office, Washington, D.C. (1968).

[b] J. Divisek and B. Kastening, *J. Electroanal. Chem.* **65**, 603 (1975).

[c] This value is based on that in footnote *b*, but is open to question (see text).

[d] Not available.

[e] J. Weinstein and B. H. J. Bielski, *J. Am. Chem. Soc.* **101**, 58 (1979).

Table 1b
Standard Electrode Potentials of Selected Oxygen Reactions

Formula	Standard potential vs. SHE, *V*
$O_2 + 4H^+ + 4e^- = 2H_2O$	1.229
$O_2 + 2H_2O + 4e^- = 4OH^-$	0.401
$O_2 + 2H^+ + 2e^- = H_2O_2$	0.695
$O_2 + 2H_2O + 2e^- = H_2O_2 + 2OH^-$	−0.133
$O_2 + H_2O + 2e^- = HO_2^- + OH^-$	−0.065
$H_2O_2 + 2H^+ + 2e^- = 2H_2O$	1.763
$H_2O_2 + 2e^- = 2OH^-$	0.935
$HO_2^- + H_2O + 2e^- = 3OH^-$	0.867
$O_2 + e^- = O_2^-$	−0.284
$O_2 + H^+ + e^- = HO_2$	−0.053
$HO_2 + e^- = HO_2^-$	0.751
$HO_2 + H^+ + e^- = H_2O_2$	1.443
$O_2^- + H_2O + e^- = HO_2^- + OH^-$	0.155
$O_2^- + 2H_2O + 3e^- = 4OH^-$	0.629
$HO_2 + 3H^+ + 3e^- = 2H_2O$	1.656

1b and shown in Figures 1 and 2[(2)] for alkali and acid aqueous solutions at 25°C. The thermodynamic data listed in these tables and used in these figures are the values listed by Hoare.[(1)] Under some exceptional conditions, described in Section 3 of this chapter, the thermodynamically reversible potential for

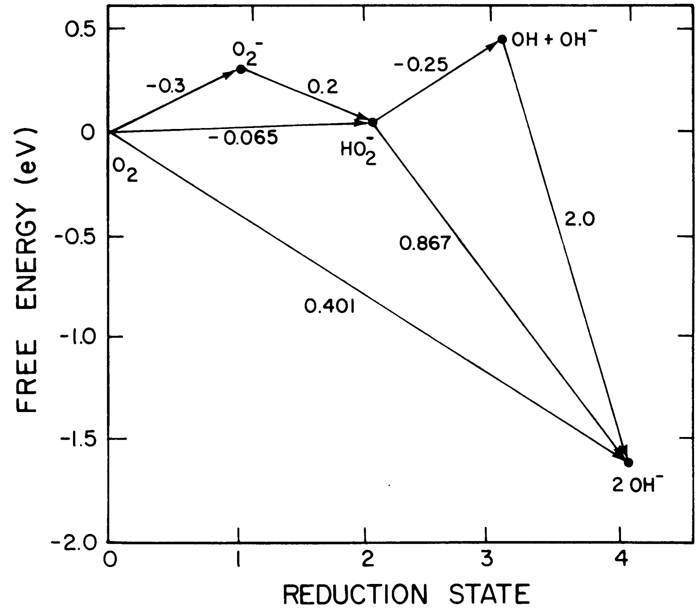

Figure 1. Free energy relationships for the reduction of oxygen in basic solutions at 25°C. Standard reduction potentials in volts are indicated on lines designating steps. Multiply ordinates by $F = 96{,}487$ to obtain free energy in J mol^{-1}.(2)

the four-electron reduction of O_2 has been achieved under open-circuit conditions but this is not generally the situation. The thermodynamic potential, however, is achieved for the O_2–hydrogen peroxide couple in alkaline solutions on electrode surfaces such as graphite, semiconducting NiO, and gold on which the decomposition of the peroxide proceeds only slowly.(3,4,11) The observed pH and peroxide activity dependences are those expected on the basis of the Nernst equation for the reversible reaction

$$O_2 + H_2O + 2e^- \rightleftharpoons HO_2^- + OH^- \tag{III}$$

$$(E_{\text{NHE}})_{\text{III}} = (\overset{\circ}{E}_{\text{NHE}})_{\text{III}} - \frac{RT}{2F} \ln \frac{(a_{HO_2^-})(a_{OH^-})}{(p_{O_2})(a_{H_2O})} \tag{1}$$

The pK values for the first and second ionization of H_2O_2 at 25°C are p$K_1 = 11.69$ and p$K_2 = \sim 20$ at 25°C(7) and therefore in alkaline aqueous electrolytes at pH > 12 the predominant species is HO_2^-.

Hoare in his review of thermodynamic data for O_2 (1) lists a value of $(\overset{\circ}{E}_{\text{NHE}})_{\text{III}} = -0.064$ V at 25°C, calculated from thermodynamic data for the free energy of formation of HO_2^-. Latimer,(10) using earlier free energy of formation data, listed $(\overset{\circ}{E}_{\text{NHE}})_{\text{III}} = -0.076$ V. Experimental values of −0.045 to −0.054 V have been reported by various workers,(4–6) on the basis of electrode potential measurements on mercury, carbon, and graphite. The open-circuit O_2 electrode potentials of Yeager and Kozawa$^{(11)}$ with low-area pure graphite in NaOH + HO_2^- yield a value of $(\overset{\circ}{E}_{NHE})_{III} = -0.067$ V, correcting the data to standard state conditions. This is in reasonable agreement with the value listed by Hoare.$^{(1)}$

The large negative free energy changes associated with the decomposition of H_2O_2 and HO_2^- (see Table 1) suggest that these species should be very unstable in both acid and alkaline aqueous electrolytes. In the absence of impurities, however, the decomposition of hydrogen peroxide is very slow in aqueous solutions, and the homogeneous decomposition reaction most likely proceeds through a redox-dismutation mechanism; i.e.,

$$HO_2^- + HO^- \rightarrow O_2 + H_2O + 2e^- \qquad (IV)$$

$$\underline{HO_2^- + H_2O + 2e^- \rightarrow 3OH^-} \qquad (V)$$

$$2HO_2^- \rightarrow O_2 + 2OH^- \qquad (VI)$$

The stability of the peroxide is principally the result of the need for multielectron transfers with unstable intermediates requiring large increments in free energy and the difficulty of breaking the O–O bond. The latter results in the reduction reaction V being extremely slow.

In principle it should be possible for the potential of the O_2–perioxide couple to approach that for the overall four-electron reduction [reactions (I) or (II)] by depressing the peroxide concentration to the equilibrium value for reaction (VI). In practice this has not proved possible even with extremely effective homogeneous or heterogeneous peroxide decomposing catalyst because the equilibrium peroxide concentration is very low, e.g., $10^{-15}\,M$ HO_2^- in 1 M caustic saturated with O_2.

In the presence of hydrogen peroxide in concentrated alkaline electrolytes, the equilibrium concentration of the superoxide radical ion $O_2^{\cdot-}$ can be surprisingly high. An estimate of the equilibrium concentration of the $O_2^{\cdot-}$ for given HO_2^-, O_2, and OH^- activities can be obtained from the following reactions and potentials:

$$O_2 + e^- \rightleftharpoons O_2^{\cdot-}, \qquad (\overset{\circ}{E}_{NHE})_{VII} \qquad (VII)$$

$$O_2^{\cdot-} + H_2O + e^- \rightleftharpoons HO_2^- + OH^-, \qquad (\overset{\circ}{E}_{NHE})_{VIII} \qquad (VIII)$$

From reaction (VIII) minus reaction (VII),

$$2O_2^{\cdot-} + H_2O \rightleftharpoons O_2 + HO_2^- + OH^-, \qquad (\overset{\circ}{E}_{NHE})_{IX} \qquad (IX)$$

with the standard thermodynamic potential for reaction (IX) given by $(\overset{\circ}{E}_{NHE})_{IX} = (\overset{\circ}{E}_{NHE})_{VIII} - (\overset{\circ}{E}_{NHE})_{VII}$. Divesek and Kastening$^{(8)}$ report a value of $(\overset{\circ}{E}_{NHE})_{VII} = -0.284$ V on the basis of O_2 reduction measurements (first polarographic wave) on Hg in 0.1 M NaOH with 0.05 M triphenyl phosphine while similar data of Chevalet *et al.*$^{(8a)}$ in 1 M NaOH with 0.017 $M\,\alpha$-quinoline as a stabilizing agent yield a standard value of −0.29 V.[(8b)] From radiolysis studies,[(8c)] $(E^{\circ}_{\mathrm{NHE}})_{\mathrm{VII}}$ is estimated to be −0.33 V. Thus, as a compromise value $(E^{\circ}_{\mathrm{NHE}})_{\mathrm{VII}} = -0.30$ V seems to be a reasonable estimate.

The potential for reaction (VIII) can be calculated from E°_{VII} and that for reaction (III), i.e., $(E^{\circ}_{\mathrm{NHE}})_{\mathrm{III}} = -0.064$ V.[(1)] Then $(E^{\circ}_{\mathrm{NHE}})_{\mathrm{VIII}} = 2(E^{\circ}_{\mathrm{NHE}})_{\mathrm{III}} - (E^{\circ}_{\mathrm{NHE}})_{\mathrm{VII}} = 0.17$ V. The value for reaction (IX) is then $(E^{\circ}_{\mathrm{NHE}})_{\mathrm{IX}} = -0.17 - (-0.30\ \mathrm{V}) = -0.47$ V. The equilibrium constant for reaction (IX) at 25°C is

$$K_{\mathrm{IX}} = \frac{(p_{\mathrm{O_2}})(a_{\mathrm{HO_2^-}})(a_{\mathrm{OH^-}})}{(a_{\mathrm{O_2^{\cdot}}})^2(a_{\mathrm{H_2O}})} = \exp\frac{FE^{\circ}_{\mathrm{IX}}}{RT} = 10^{8.0} \tag{2}$$

For a 0.05 *M* HO_2^- + 10 *M* NaOH solution saturated with O_2 at 1 atm, the activities of the various components are estimated to be $a_{\mathrm{OH^-}} \cong 30$, $a_{\mathrm{HO_2^-}} \cong 0.1$, and $a_{\mathrm{H_2O}} \cong 1$. From Eq. (2), then, the value of $a_{\mathrm{O_2^{\cdot}}}$ would be $\sim 2 \times 10^{-4}$ and $C_{\mathrm{O_2^{\cdot}}} \cong 1 \times 10^{-4}$ *M*. This concentration is an order of magnitude higher than the solubility (10^{-5} *M*) of O_2 in this electrolyte and hence the $O_2^{\cdot}$ species may be an important factor in O_2 electrode kinetics in concentrated caustic solutions. In the presence of adsorbed organics, one-electron reduction has been observed on mercury in alkaline solutions. This appears to correspond to reaction (VII).[(8,8a,9)] Dubrovina and Nekrasov,[(9)] however, ascribe this to the formation of an $O_2^{\cdot}$ complex with a surfactant-type adsorbed molecule.

3. Open-Circuit Potentials

The four-electron reduction of oxygen [reaction (I)] is very irreversible and therefore experimental verification of the thermodynamic reversible potential of this reaction is very difficult. The exchange current densities for reactions (I) and (II) are typically 10^{-10}–10^{-11} A/cm² of real surface area for Pt and other noble metals at room temperatures. Any other side reaction, even if slow and otherwise difficult to detect, may compete with reaction (I) or (II) in establishing the rest potential. Indeed, unless special experimental procedures are used, the thermodynamic potential cannot be obtained at ambient temperature in aqueous electrolytes. Even on the most active platinum electrode in pure acid or alkaline aqueous solution under ordinary conditions, the rest potential in the presence of oxygen at 1 atm and ambient temperature usually does not exceed 1.1 V vs. the NHE and most often has a value close to 1.0 V. In early work on O_2 electrochemistry, before reliable thermodynamic data were available, the potential 1.08 V vs. RHE was considered as the reversible value for reactions (I) and (II).[(12)]

Indirect thermodynamic determinations of the free energy of formation of liquid water from the equilibrium potentials of a metal–insoluble metal oxide couple (i.e., Ag–Ag_2O, Hg–HgO) together with the free energy of formation of the metal oxide[(12)] gave values inconsistent with these early direct determinations of the oxygen electrode rest potentials. The same inconsistency with direct potential measurements was revealed also by direct calorimetric determinations of the free energy of liquid water(13) from ΔH and ΔS. The reversible potential 1.23 V was confirmed indirectly by Hoare(14) by extrapolation of the oxygen cathodic and anodic polarization curves on highly oxidized Pt electrode. Similar results were obtained also on various noble electrodes by Bockris and co-workers(15,17) and Hoare,(16) who extrapolated the cathodic and anodic Tafel plots of the polarization curves to yield an intersection at a potential close to 1.23 V. This is surprising, however, considering that these extrapolations were done from high cathodic and high anodic overpotentials where the surface conditions and hence mechanisms for the four-electron reaction might be expected to differ.

Bockris and Huq(18) after long and careful purification with a Pt electrode in oxygen-saturated 0.05 *M* H_2SO_4 obtained for the first time a rest potential of 1.24 ± 0.3 V stable for about 1 hr. After this time, the potential drifted in the cathodic direction but could still be restored to 1.24 V by additional preelectrolysis. Very intensive oxidation of the Pt surface, however, also appears to have been an important factor in the Bockris–Huq procedure, not less important than the purification of solution. The electrode in this work was treated with a hot mixture of concentrated HNO_3 and H_2SO_4 and then treated in pure oxygen for 2 hr at 500°C. A similar procedure was applied later by Watanabe and Devanathan,(19) who succeeded in keeping the electrode at the reversible potential of 1.23 V for many hours. Hoare(20) obtained the reversible potential on a Pt electrode which prior to experiment was kept for 72 hr in concentrated HNO_3. Hoare(21,22) also reported obtaining the reversible O_2–H_2O potential on one side of a Pt membrane electrode, the other side of which was in contact with concentrated HNO_3 saturated with O_2.

Tarasevich *et al.*(13) used a Teflon-bonded, high-surface-area Pt-black electrode semisubmerged in an electrolytic solution with O_2 above the solution to obtain the reversible O_2–H_2O potential in both H_2SO_4 and KOH solutions. These authors attributed the effectiveness of their electrode to easy access of O_2 molecules to active sites on the surface of platinum, whereas access of impurities from the bulk of the solution to these sites was hindered by diffusion through and along the liquid film extending from the meniscus within the porous electrode. Their electrode, however, was also strongly oxidized by heating in oxygen prior to being immersed into solution.

All authors cited above established pH and oxygen pressure dependences for the open-circuit potentials in accord with the Nernst formula. This provided good evidence that the experimentally obtained potentials corresponded to the reversible potentials for the four-electron reaction.

The question remains open as to what is the nature of irreversible rest potential of most "ordinary" platinum and other noble metal electrodes in the presence of O_2 in the solution. The importance of this potential lies in the fact that it is the starting point for the cathodic polarization of practical oxygen (or air) electrodes used in such electrochemical devices as fuel cells and metal–air batteries.

Some experimental features of this rest potential on platinum which are valid also for other noble metal electrode materials are the following:

(1) The dependence on pH is the same as for the reversible potential of reactions (I) or (II), i.e., the rest potential has a 59-mV/pH dependence at 25°C, measured vs. SHE.

(2) The dependence on p_{O_2} is rather irreproducible and somewhat confusing. According to Schuldiner and Roe(24) at very low O_2 concentrations the rest potential decreases to 0.7 V vs. RHE and $dE/d \log p_{O_2} = 60$ mV/decade. These authors suggested that the formation of superoxide radicals according to the reaction

$$O_2 + H^+ + e^- \rightarrow HO_2^{\cdot} \tag{X}$$

is potential determining at low p_{O_2}. The same dependence $dE/d \log p_{O_2} = 60$ mV/decade was found by Wroblowa *et al.*(25) in the range $10^{-3} < p_{O_2} < 1$ atm and by Shepelev *et al.*(26) in the range $1 < p_{O_2} < 100$ atm. Hoare(20) reported a value $dE/d \log p_{O_2} = 15$ mV/decade, Brusic *et al.*(27) a value of 26 mV/decade, and Urbach *et al.*(28) a value of 30 mV/decade. The inconsistency of the data is apparently caused by different oxidation states of the Pt surface.

(3) Quite similar values for the rest potentials in O_2-saturated solutions have been reported for several noble metal electrode materials. The small differences do not have any apparent relation to the metal–metal oxide potentials for these electrodes.

(4) The rest potential is relatively insensitive to stirring.

Various theories have been proposed to explain the nature of the irreversible rest potential. Perhaps the oldest one is the oxide theory,(12,29) which considers the rest potential as corresponding to the equilibrium potential of the metal–metal oxide reaction. This, however, contradicts point (3) above, as well as the fact that this rest potential is established also on electrodes free of bulk oxides such as gold and prereduced Pt. Other theories involve the concept of a mixed potential,(12,17) which is the result of simultaneous occurrence of two or more continuous (steady state) electrode reactions, i.e., the four-electron cathodic reduction of O_2 plus some anodic reaction. The result is a zero overall current and a rest potential in between the equilibrium potentials of these reactions.

The rate of the anodic reaction may be very low, corresponding to the slow rate of the four-electron cathodic reaction at a typical rest potential of ~1.0 V vs. RHE. If the four-electron reaction is assumed to have an exchange current density $i_0 = 10^{-11}$ A/cm^2 and a Tafel slope $(d\eta/d \log i) = -60$ mV/decade,(17) then for a rest potential of 1.00 V vs. RHE the cathodic O_2 reduction current density is 10^{-7} A/cm^2.

Various anodic reactions have been proposed: (1) oxidation of impurities (mostly organic) from the solution(18,25); (2) oxidation of H_2O_2 accumulated in solution as a result of the two-electron oxygen reduction(12); (3) the formation of surface oxides; and (4) platinum anodic dissolution.(30–32)

According to Bockris and his coworkers,(17,25) the anodic current from the oxidation of impurities is under most laboratory conditions sufficient to account for the mixed potential of oxygen electrode. This does not, however, explain the surprising reproducibility of this rest potential independent of the nature and concentrations of impurities in various laboratories. Further, the transport of impurities in the solution phase to the electrode surface should be at least partially rate controlling and hence the rest potential should be sensitive to stirring. The rest potential of platinum, however, usually exhibits little dependence on stirring.

The peroxide theory considers reaction (III) as potential determining. This is based on the well-known experimental fact that on most electrodes reaction (III) is much more reversible than (I) or (II). Therefore, as soon as even a small amount of H_2O_2 accumulates close to the surface of the electrode due to cathodic reaction (III), the potential may be determined mainly by the O_2–H_2O_2 equilibrium.

The achievement of the reversible potential of 1.23 V on highly oxidized platinum in very pure solutions may be explained in terms of peroxide if, as proposed by some investigators,(33) the oxidized platinum is very effective in catalyzing the chemical decomposition of the hydrogen peroxide. The concentration of H_2O_2 close to electrode would be decreased considerably and the O_2–H_2O_2 couple would no longer compete with the four-electron reaction in establishing the rest potential. Such high catalytic activity of platinum oxides, however, is challenged by other authors.(34,35) The peroxide explanation also does not explain the reproducibility of the rest potential of the oxygen electrode even in freshly prepared, pure peroxide-free solutions in contact with an active Pt electrode, which is known to be a good H_2O_2 decomposer. If the rest potential close to 1.0 V were to be determined principally by the O_2–H_2O_2 redox couple in acid electrolytes, then the activity of H_2O_2 close to the electrode surface should be of the order of $10^{-10}\,M$ using a value of $E^{\circ}_{\text{NHE}} = 0.695$ V from Figure 2 and assuming reversible behavior. Such a low concentration would result in transport problems and hence marked sensitivity to convective transport. Such is generally not observed.

A widely accepted explanation for the rest potential of Pt involves the formation of surface oxides of the metal as the anodic reaction which together with reaction (I) or (II) yields the mixed potential control. At the rest potential of ~1.0 V vs. RHE, platinum which has not been exposed to much more oxidizing conditions is not covered with a phase oxide but rather has a chemisorbed layer of an oxygen species, probably OH(ads). Thus the anodic

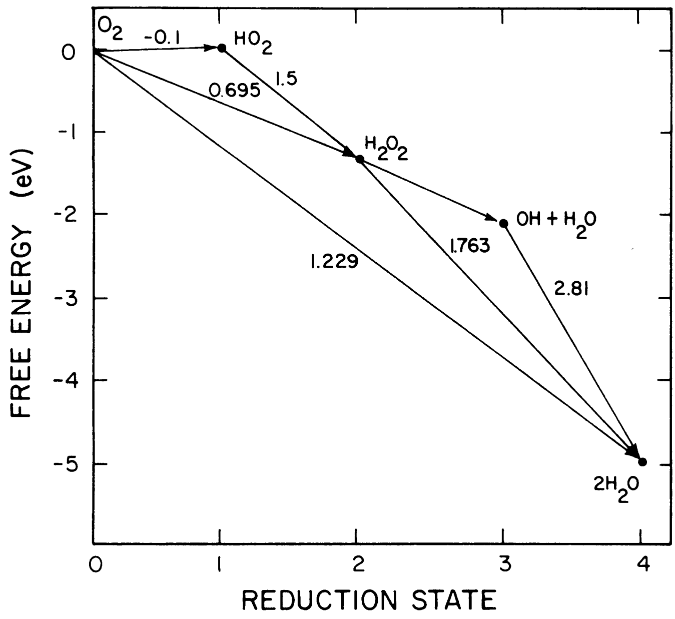

Figure 2. Free energy relationships for the reduction of oxygen in acid solution at 25°C. Standard reduction potentials in volts are indicated on lines designating steps. Multiply ordinates by $F = 96{,}487$ to obtain free energy in J mol^{-2}.⁽²⁾

reaction can be written for acid solutions:

$$\mathrm{Pt} + \mathrm{H_2O} \rightleftharpoons \mathrm{PtOH} + \mathrm{H^+} + e^- \qquad \text{(XI)}$$

and for alkaline solutions:

$$\mathrm{Pt} + \mathrm{OH^-} \rightleftharpoons \mathrm{PtOH} + e^- \qquad \text{(XIa)}$$

If these reactions are essentially reversible, the pH dependence of the potential would be the observed 0.0591 V/pH at 25°C but this is not a sufficient criterion since any process with 1 e^- per H^+ could satisfy this condition.

To act effectively as the complementary anodic reaction in establishing a mixed rest potential, reaction (XI) or (XIa) has to occur continuously, i.e., in a steady state mode. Electrode reactions (XI) and (XIa) at potentials lower than 1.1 V, however, are adsorptive(36) and result in capacitive, non-steady-state behavior, typical for polarizable electrodes. Therefore, a further process must be involved, acting as a "sink" of adsorbed oxygen so as to support steady state platinum oxidation. Oxygen diffusion into the bulk of a metal has been proposed by Hoare(37) and Schuldiner(38) for such a "sink" reaction. These authors present evidence that platinum can dissolve considerable amounts of oxygen forming a metal–oxygen surface alloy ("dermasorbed" oxygen).(39) This view has found additional support in recent experiments reported by Bagotskii *et al.*(40–43) in which ultrahigh vacuum thermal degassing of platinum removed oxygen absorbed by surface layers of the metal. It is questionable, however, whether significant amounts of O enter the Pt at potentials of ~1.0 V vs. RHE.

Evidence exists that platinum dissolves in both acid and alkaline electrolytes(30–32) at potentials of ~1.0 V vs. RHE. Thus the anodic dissolution of Pt may be the steady state complementary reaction. The dissolution may proceed through the direct dissolution of the platinum or through a Pt–OH or Pt–O intermediate.

This mechanism may also explain the attainability of reversible potential of reaction (I) on highly oxidized Pt electrodes in very pure solutions saturated with oxygen. According to Hoare,(12) highly oxidized Pt is covered with a uniform, nonporous, electronically conductive oxide layer which blocks further oxidation of the metal, and therefore only reaction (I) is active in establishing the rest potential. The Pt has been essentially rendered passive. According to Hoare(12,44) such electronically conductive oxide layers which are nonpermeable to metal ions are formed only on Pt and Rh, and only for these metals has the reversible potential of the oxygen electrode been obtained.

The platinum dissolution model can also explain the achievement of the reversible four-electron potential with high-area Teflon-bonded platinum electrodes.(23) At the low concentrations of platinum in the solution phase, the concentration would build up within the pores to the equilibrium value because of slow diffusion and this would suppress the dissolution process.

Some authors have attempted to explain peculiarities of the rest potential of the oxygen electrode by involving the concept of surface potential(45) influenced by adsorbed oxygen dipoles.(46) Such double-layer effects, however, appear to be irrelevant to the establishment of the rest potential because the double layer has purely capacitive character and is featured by ideal polarizability (absence of a "driving force") whereas a stable rest potential may result only from an electrode reaction (or reactions) involving bulk components.

Tseung and Bevan(47) have investigated the perovskites such as $LaCoO_3$ and $La_{1-x}Sr_xCoO_3$ as O_2 electrocatalysts in KOH solutions and found $La_{0.5}Sr_{0.5}CoO_3$ to exhibit reversible behavior for the O_2–H_2O couple. The O_2 partial pressure dependence corresponds to that expected for the four-electron reduction.

The rest potentials of platinum and other electrodes have also been examined in hydrogen peroxide solutions. On surfaces such as carbon, graphite, and lithiated nickel oxide,(3,4,11) the open-current values are the thermodynamically reversible value for the O_2–HO_2^- couple in alkaline electrolytes or close to it. On these surfaces, the further reduction of peroxide [reaction (V)] and the overall four-electron reaction are both very inhibited. These surfaces also do not have much catalytic activity for the heterogeneous decomposition of the peroxide. On the other hand, with platinum the overall four-electron reduction is far less inhibited and the platinum surface is a reasonably effective catalyst for peroxide decomposition. Even so, the open-current potential for platinum in alkaline peroxide solutions has been found to exhibit the expected dependence on peroxide concentration and oxygen partial pressure(48,49) for peroxide concentrations less than 10^{-4} *M*.(50,51)

4. Oxygen Adsorbed Species and Anodic Films on Platinum and Other Noble Metals

Since oxygen evolution and in most instances also O_2 electroreduction occur on electrode surfaces covered with an adsorbed oxygen species or an oxide layer, the properties of such layers control the mechanisms and electrocatalytic activity of the electrode for these processes. The most extensive studies have been carried out on platinum. Some of the conclusions concerning the anodic adsorbed and oxide layers on this surface are probably also valid for other noble metals. Considerable controversy persists, however, concerning the nature of these layers on platinum.

It is well recognized that at high anodic potentials $E_H > 2.0$ V (E_H = potential vs. RHE) an oxide phase is formed on Pt electrode both in acid and alkaline solutions.(52,53) The region of lower potentials from the onset of anodic layer formation ($E_H \cong 0.8$ V) to the evolution of molecular oxygen ($E_H \cong 1.6$ V) is the subject of controversy. Some investigators believe that in this range of potential, hydroxide groups and/or oxygen atoms are strongly and irreversibly adsorbed(52,54,55) according to the reactions

$$OH^- \rightleftharpoons OH_{ad} + e^- \tag{XII}$$

$$H_2O \rightleftharpoons OH_{ad} + H^+ + e^- \tag{XIIa}$$

$$OH_{ad} \rightleftharpoons O_{ad} + H^+ + e^- \tag{XIII}$$

$$OH_{ad} + OH^- \rightleftharpoons O_{ad} + H_2O + e^- \tag{XIIIa}$$

$$2OH_{ad} \rightleftharpoons O_{ad} + H_2O \tag{XIV}$$

Whatever is the mechanism of OH_{ad} and O_{ad} formation, the principal point of this "adsorption theory" is that Pt surface atoms are stable in their positions in the lattice and the integrity of the Pt lattice is retained after an adsorption–desorption cycle in the voltammetry studies. The formation of adsorbed layer is described quantitatively by adsorption isotherms at equilibrium, e.g., Temkin(55) or Frumkin(56) adsorption isotherms and corresponding kinetic equations such as the Elovich equation.(57) Intrinsic to the adsorption theory is the concept of the maximum surface concentration corresponding to monolayer coverage by the ad-particles on all available adsorption sites.(52,58)

Another view considers the anodic layer on Pt as a new phase whose composition and structure more or less correspond to those of bulk Pt oxides. According to this phase oxide model,(59–61) oxygen adsorption—if it

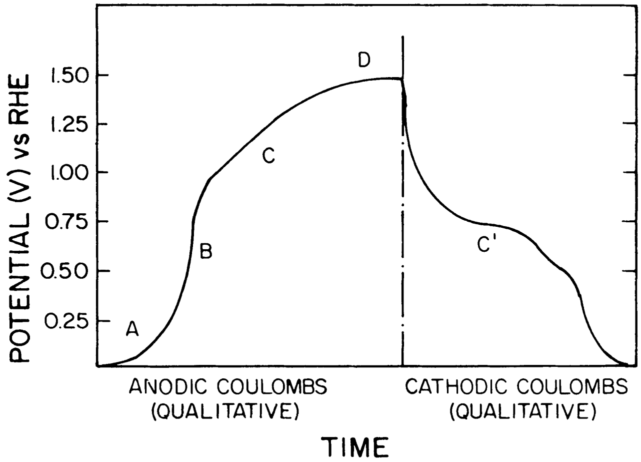

Figure 3. A typical current-step charging curve of Pt in acid solution. Segments of the curve correspond to: A, hydrogen desorption; B, double layer charging; C, oxygen adsorption; D, end of oxygen monolayer buildup; C′, oxygen desorption.

occurs—is only an initial step in the process of oxide buildup (section A of the curve in Figure 3). Deposition of hydroxyl radicals and oxygen atoms destroys the original structure of the Pt surface atoms [e.g., by a place exchange mechanism(62)] and forms a new structure of Pt oxide (sections B–D in Figure 3). Cathodic reduction of this oxide does not restore the original Pt lattice but produces new, partly structureless arrangements of Pt atoms. Repeated cycles of oxide formation–reduction develop surface roughness and cause some dissolution of Pt.

In this phase oxide theory the concept of limiting coverage (monolayer) has not such importance as in the adsorption theory and supporters of the former put forward experimental data against a limiting surface concentration of oxygen.(59,62) This theory does not deal with equilibrium and the concept of adsorption isotherms is considered as irrelevant to oxygen deposition on Pt surface. This is because genuine equilibrium of phase oxide formation should involve not only surface but also the bulk of the electrode material. The kinetics of the phase oxide formation or reduction are described in terms of rate equations specific to the nucleation and growth of the new phase.(61,62)

Discrimination between the oxygen adsorption and oxide phase formation theories has important implications in electrocatalysis. If the adsorption theory is correct, then Pt metal should be considered the electrode material and the adsorbed oxygen-containing species as possible intermediates in the steady state electrode reactions of molecular oxygen or a competition with intermediates for adsorption sites. If the phase oxide theory is correct, then Pt oxide has to be considered as the electrode material with obvious consequences concerning the energies of adsorption of intermediates on Pt oxides and not on the bare metal.

4.1. Electrochemical Studies

4.1.1. Platinum

Most experimental work related to anodic layers on Pt and other noble metals has been done using electrochemical transient methods in which nonstationary relations between the electrode potential and charge or current related to deposition or reduction of oxygen-containing species were analyzed. Comparison of these experimental relations with theoretical predictions resulting from particular models has constituted the basis for choosing the best fitting model.

This procedure involves, however, some uncertainty, mainly because electrochemical methods give only direct, electrical information on the surface charge transfer reactions. Much effort has been directed to *in situ* optical spectroscopic methods to study the electronic properties of these surface layers and to study the interactions of the oxygen species with Pt (see Section 4.2).

The most conspicuous feature of the anodic layers on Pt is the unattainability of adsorption equilibrium. This is seen from the hysteresis of corresponding charge Q vs. E dependences recorded for example in current-step experiments (galvanostatic charging curves; see Figure 3). Equivalent to this hysteresis is the asymmetry of the anodic vs. cathodic branches of linear sweep voltammetry (potentiodynamic curves; see Figure 4). In Figures 4 and 5 the features in the anodic sweep at potentials $E_H > 0.8$ V correspond to the formation of the anodic layers in 0.5 M H_2SO_4. Since the voltammetry

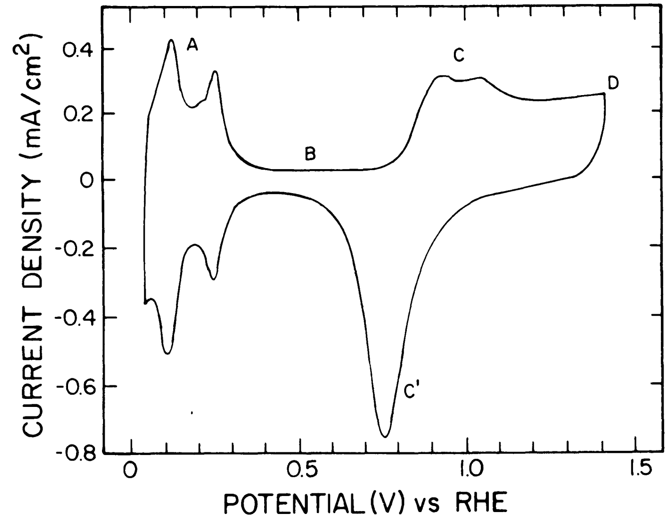

Figure 4. A typical sweep voltammogram (potentiodynamic charging curve) of a Pt electrode in acidic solution (0.5 M H_2SO_4, He-deaerated, $\partial E/\partial t = \pm 0.1$ V/sec). Segments A, B, C, D, C′ correspond to those in Figure 2.

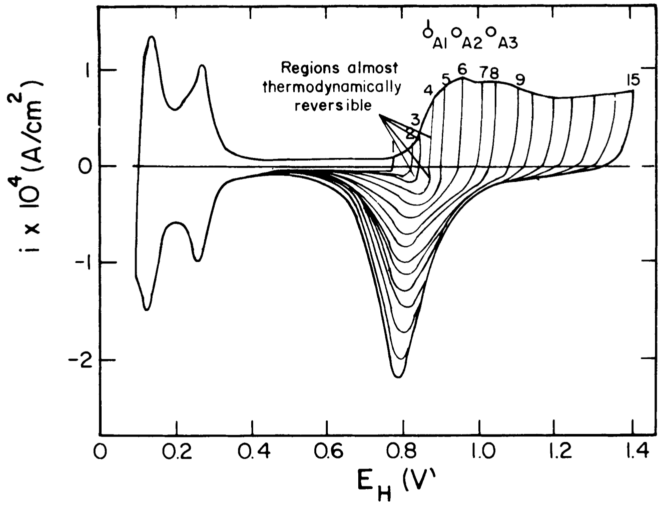

Figure 5. Voltammograms for Pt in 0.5 *M* H_2SO_4. Anodic limit of voltage sweep progressively increased. Peaks O_{A1}, O_{A2}, O_{A3} correspond to sublattice structures of OH adsorbed on Pt with increasing OH : Pt ratios, and O_{A3} corresponds to Pt–OH monolayer (see Figure 6) according to Angerstein-Kozlowska *et al.*(36)

curves are the same in Figure 5 for $E_H < 0.3$ V, hydrogen adsorption–desorption is apparently reversible in that potential range.

The nature of the irreversibility of the anodic layers on Pt as well as on most other metals with the exception of Ir (63) is not clear. This irreversibility is retained even at very low current densities or potential sweep rates. At the same time both anodic and cathodic branches reveal relatively high rates of anodic layer formation and cathodic reduction of the anodic layer. This results in potentiodynamic curves having almost the shame shapes and current proportional to sweep rates over wide ranges of sweep rates.

In the voltammetry curves the anodic sweep is quite different from the cathodic. The latter consists of a single almost symmetrical peak suggesting a single desorption mechanism.(64,65) The kind of irreversibility exhibited by the anodic layer on Pt is referred to by Conway *et al.*(66) as intrinsic or thermodynamic irreversibility(67,68) in opposition to the kinetic irreversibility observed when well-defined complementary peaks are observed in the anodic and cathodic sweeps, but which deviate in position because of kinetic factors (e.g., hydrogen adsorption–desorption at high sweep rates). The intrinsic irreversibility involves different species or states on the surface during the anodic and cathodic sweeps. The kinetic irreversibility is superimposed on the intrinsic irreversibility at faster potential sweep rates and current densities.

In the past when the nonequilibrium characteristics of the anodic layers were not well recognized, premature conclusions were reached concerning the adsorption isotherms based on only the anodic branch of the *Q* vs. *E* curves. This dependence is almost rectilinear and corresponds to the flat part of the anodic curve in the voltammetry curve between 1.0 and 1.5 V in Figure 4 (between C and D). Such dependence has often been interpreted as evidence for the validity of the Temkin adsorption isotherm(55) and therefore as support for the adsorption theory.(69) It is now clear, however, that the irreversibility of the anodic layer formation and reduction renders equilibrium thermodynamic considerations irrelevant.

The intrinsic irreversibility probably results from some kind of phase transformation such as the transformation of the adsorbed layer into a surface phase oxide by a place exchange mechanism.(70) This may lead to different reaction paths for the anodic and cathodic processes.

Another interesting feature of the anodic layers on Pt and also some other metals is their long-time reconstruction or aging effects.(54,71) This is observed, for example, if the electrode is kept for some time at a constant anodic potential at $E > 0.9$ V vs. RHE. The stability of the layer increases with time as may be seen from the shift of the cathodic reduction peaks in the cathodic direction. Potentiostatting at even higher anodic potentials $E > 1.4$ V causes a slow increase of the apparent thickness of the layer as evidenced from the increasing charge associated with its formation as well as its subsequent reduction.

Some researchers have reported reversible adsorption of OH at low coverages, i.e., at $E_H < 0.9$ V.(54) At the same time, however, even at these low coverages, aging effects were observed, which may render the conclusion as to the reversibility of adsorption open to question.

Several representative studies will be discussed suggesting various models pertinent to either the adsorption or phase oxide models.

Using sweep voltammetry Conway *et al.*(54) found at the beginning of oxygen deposition on polycrystalline Pt in very pure 0.5 *M* H_2SO_4 three adsorption peaks followed by a flat minimum (see Figure 5). From charge ratios under the deconvoluted peaks, these workers concluded that these peaks represent OH adsorption in various apparent structural configurations; e.g., for the (100) plane:

$$\text{peak 1:} \quad 4Pt + H_2O \rightarrow Pt_4OH + H^+ + e^- \qquad \text{(XV)}$$

$$\text{peak 2:} \quad Pt_4OH + H_2O \rightarrow 2Pt_2OH + H^+ + e^- \qquad \text{(XVI)}$$

$$\text{peak 3:} \quad Pt_2OH + H_2O \rightarrow 2PtOH + H^+ + e^- \qquad \text{(XVII)}$$

The entities Pt_4OH and Pt_2OH may correspond to adsorbed OH interacting with four and two Pt surface atoms, respectively. Alternatively, the adsorbed OH may interact with only one Pt at a time but the occupied Pt sites may be separated from each other so as to give the indicated surface stoichiometry for the adsorbed layer because of induced heterogeneity, i.e., surface interactions increase the free energy of adsorption at surface sites adjacent to sites occupied by an OH_{ads} (see Figure 6).

The validity of reactions (XV)–(XVII) depends on the accuracy of discriminating between charges of rather weakly distinguishable peaks and has

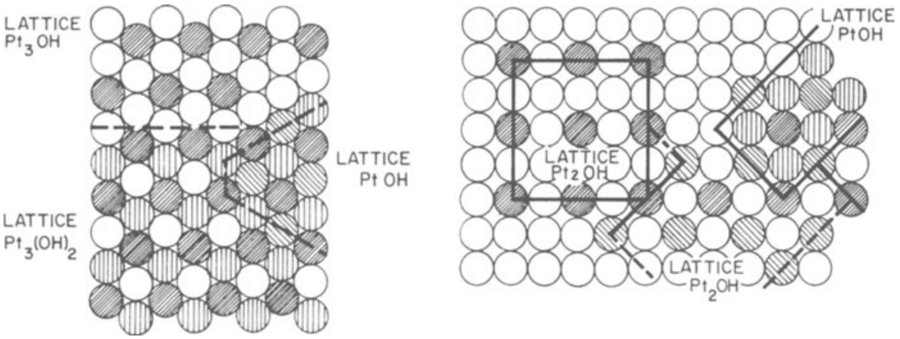

Figure 6. Significant sublattice structures of OH electrosorbed on the (100) and (111) crystal planes of Pt up to monolayer of Pt–OH.(36)

been questioned by various authors(55,73) including Ross.(72) This latter author found that the fine structure of the linear sweep voltammograms at the beginning of oxygen adsorption depends strongly on solution composition and disappears in a solution of HF, i.e., in the absence of specific adsorption of anions. Therefore, according to Ross, the fine structure in the sweep voltammograms is caused by adsorbed anions of the acid electrolyte and not the adsorption of OH.

Using various voltage sweep rates Conway *et al.*(54) showed that the OH adsorption is apparently very fast and in a sense reversible during the anodic sweep, but they observed strong aging effects even in the region of the Pt_4OH structure where the surface concentration of oxygen is low. Close inspection of the voltammograms presented by Conway *et al.*,(54) however, suggests that oxygen adsorption is intrinsically irreversible even at the beginning, since with just very small excursions into the anodic region, asymmetry arises between the anodic and cathodic sweeps. Some support for the reversibility concept, however, has been obtained from ac impedance and electromodulated reflectance experiments.(74) They found no hysteresis in the real component of the admittance $(1/R_p)$ vs. E_H curves or the electromodulation reflectance $[\chi = (1/R)(\Delta R/\Delta E)]$ vs. E_H curves during anodic and cathodic sweeps limited to $E_H \leq 0.85$ V. It is very interesting that the shapes of the $(1/R_p)$ vs. E_H and χ vs. E_H curves are almost identical, suggesting that the same type of charge transfer processes determines both. The same type of similarity has been found between charge vs. E_H and relative reflectance vs. E_H by other workers.(75)

High sweep rate cathodic voltammograms (>1 V/sec), particularly in concentrated acids and at lower temperatures, provide additional evidence of various states of adsorbed oxygen species. Angerstein-Kozlowska *et al.*(54) have postulated that the less reversible adsorbed oxygen species is formed from Pt_2OH and PtOH by a place exchange mechanism:

$$\text{Pt—Pt—OH} \rightarrow \text{Pt—OH—Pt} \qquad \text{(XVIII)}$$

Conway *et al.*,(76) using their concept of various structural configurations of adsorbed OH and O, were able to simulate with a computer the linear sweep voltammograms on Pt in 0.5 *M* H_2SO_4. They used kinetic equations for the electrochemical adsorption compatible with the Frumkin adsorption isotherms for various forms of adsorbed oxygen. This simulation involved 12 adjustable parameters, a fact which reduces the value of this simulation as evidence for the proposed mechanism.

Similar computer simulations of linear sweep voltammograms have been performed by Appleby(77) with the main objective of providing a formal explanation of the intrinsic irreversibility. A two-step reaction of oxygen adsorption was assumed [reactions (XII) and (XIII)] with kinetic equations analogous to these used by Conway *et al.*(65) To account for the intrinsic irreversibility in the voltammograms, the rate constant for reaction (XII) (considered as the rate-controlling step in the anodic sweep) was assumed to depend exponentially on the surface concentration of oxygen in addition to the dependence associated with the Frumkin linear term in the kinetic equation. It was assumed that in the cathodic sweep the rate constant of reaction (XII) retained its final values from the anodic sweep. Reasonable agreement between simulated and experimental voltammograms was obtained. The physical nature of the unconventional changes in the rate constant was not clarified. The problem of intrinsic irreversibility was formally reduced to irreversible changes of the rate constant, which does not contribute much to a better understanding of the nature of irreversibility.

The concept involved in Appleby's work(77) pertains to adsorption theory of an oxide layer on Pt. This is true also for a series of works done by Tarasevich *et al.*,(55,73,78–80,82) who used linear sweep voltammetry to study oxygen adsorption and reduction on Pt, Pd, and Rh in H_2SO_4 and KOH solutions with various pH values. Figure 7 shows linear sweep voltammograms of Pt and Pd in different solutions recorded by these workers. In alkaline solutions they find two pairs of adsorption–desorption peaks which they assign to OH and O. The less anodic peaks (I in Figure 7F) correspond according to Tarasevich *et al.*(55,73) to OH adsorption–desorption [reaction (XII)], while the second peak II represents O adsorption–desorption (a complex reaction). In acid solutions only peak II was found and in contrast to the data of Conway *et al.*(54) no fine structure in the beginning of anodic branch was reported. Tarasevich *et al.* believe that in acid solutions mainly oxygen is adsorbed on Pt ($\theta_{OH} \ll \theta_O$).

Tarasevich *et al.* formulated their kinetic treatment of the O and OH adsorption in terms of the reactions (XII)–(XIV) (also listed in Table 2) and have derived a kinetic equation for these reactions.(55,73) For the overall anodic process,

$$i_a = 2Fk_a(C_{H^+})^{\nu_a}(1 - \theta_O)^{\mu_a} \exp\left(\frac{\gamma_a FE}{RT}\right) \exp(-\gamma'_a f_a \theta_O) \qquad (3)$$

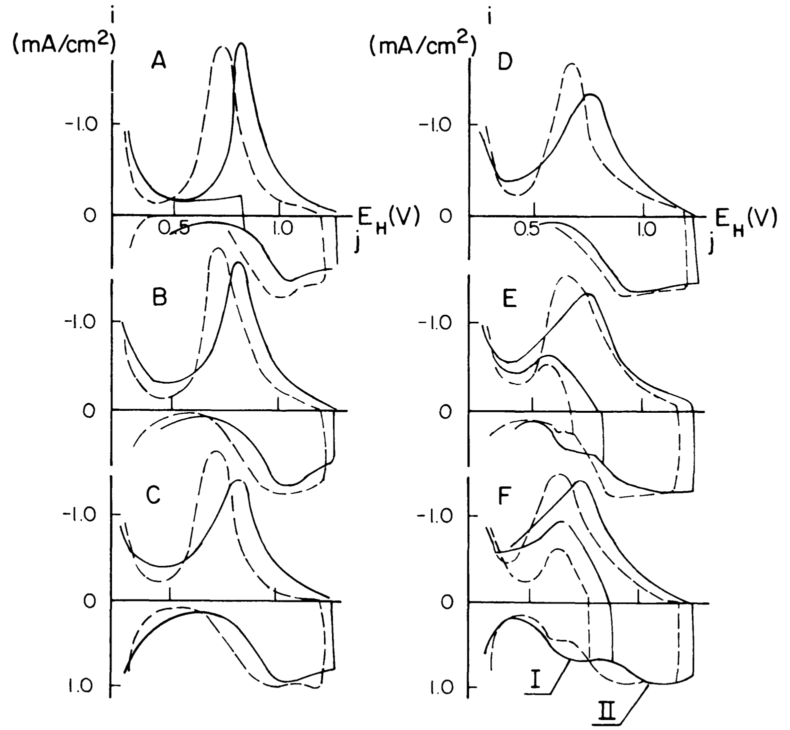

Figure 7. Voltammograms for Pt (solid line) and Pd (dashed line) at a sweep rate of 1 V/sec in solutions of various pH: A, 0.3; B, 3.9; C, 6.0; D, 7.7; E, 11.7; F, 12.6.[73]

for the overall cathodic process:

$$i_c = 2Fk_c(C_{H^+})^{\nu_c}(\theta_O)^{\mu_c}\exp\left(\frac{\gamma_c FE}{RT}\right)\exp(\gamma_c' f_c \theta_O) \qquad (4)$$

where f_a and f_c are the values of the heterogeneity factor for the anodic and cathodic processes. (Because of age of adsorbed oxygen, these quantities may differ for complementary anodic and cathodic processes.) The equations for a two-step process do not contain θ_{OH} because of the assumption $\theta_{OH} \ll \theta_O$. In the event that the adsorption proceeds as a one-step process (S–OH is formed), θ_O is replaced by θ_{OH}. The particular values of ν, μ, γ, and γ' depend on which step is the slow one. The values of these coefficients for all possible slow steps of the anodic and cathodic processes are listed in Table 2. Using these equations Tarasevich *et al.* have analyzed the influence of various factors on the peak potentials E_p in the linear sweep voltammetry curves to find the sequence of the reaction occurring under different experimental conditions and to identify the slow step. The calculated values of the coefficient $\partial E_p/\partial \log s$ ($s = dE/dt$) and $\partial E/\partial\mathrm{pH}$ for different reaction mechanisms are given in Table 2, taking the transfer coefficients = 1/2.

Table 2
Kinetic Parameters of the Oxygen Adsorption and Desorption Reactions (55,73)

Slow reaction	ν	μ	γ	γ'	$\dfrac{\partial E_p}{\partial \ln s}$	$\dfrac{\partial E_p}{\partial(2.3\ \text{pH})}$
			Anodic process			
1	0	1	β	β	$\dfrac{2RT}{F}$	0
2	1	1	β	β	$\dfrac{2RT}{F}$	$-\dfrac{2RT}{F}$
3	−2	2	2	$2+\beta$	$\dfrac{RT}{2F}$	$-\dfrac{RT}{F}$
4	−1	1	$1+\beta$	$1+\beta$	$\dfrac{2RT}{3F}$	$-\dfrac{2RT}{3F}$
5	−2	1	$1+\beta$	$1+\beta$	$-\dfrac{2RT}{3F}$	$-\dfrac{4RT}{3F}$
			Cathodic process			
1′	2	1	$1+\alpha$	$1+\alpha$	$-\dfrac{2RT}{3F}$	$-\dfrac{4RT}{3F}$
2′	1	1	$1+\alpha$	$1+\alpha$	$-\dfrac{2RT}{3F}$	$-\dfrac{2RT}{3F}$
3	2	2	2	$2+\alpha$	$-\dfrac{RT}{2F}$	$-\dfrac{RT}{F}$
4′	1	1	α	α	$-\dfrac{2RT}{F}$	$-\dfrac{2RT}{F}$
5′	0	1	α	α	$-\dfrac{2RT}{F}$	0
		One-step cathodic process involving OH desorption				
1′	1	1	α	α	$-\dfrac{2RT}{F}$	$-\dfrac{2RT}{F}$
2′	0	1	α	α	$-\dfrac{2RT}{F}$	0

$\mathrm{S + H_2O \underset{(1')}{\overset{(1)}{\rightleftharpoons}} SOH + H^+ + e^-}$ (reaction 1)

$\mathrm{S + OH^- \underset{(2')}{\overset{(2)}{\rightleftharpoons}} SOH + e^-}$ (reaction 2)

$\mathrm{2SOH \xrightarrow{(3)} SO + S + H_2O}$ (reaction 3)

$\mathrm{SOH \underset{(4')}{\overset{(4)}{\rightleftharpoons}} SO + H^+ + e^-}$ (reaction 4)

$\mathrm{SOH + OH^- \underset{(5')}{\overset{(5)}{\rightleftharpoons}} SO + H_2O + e^-}$ (reaction 5)

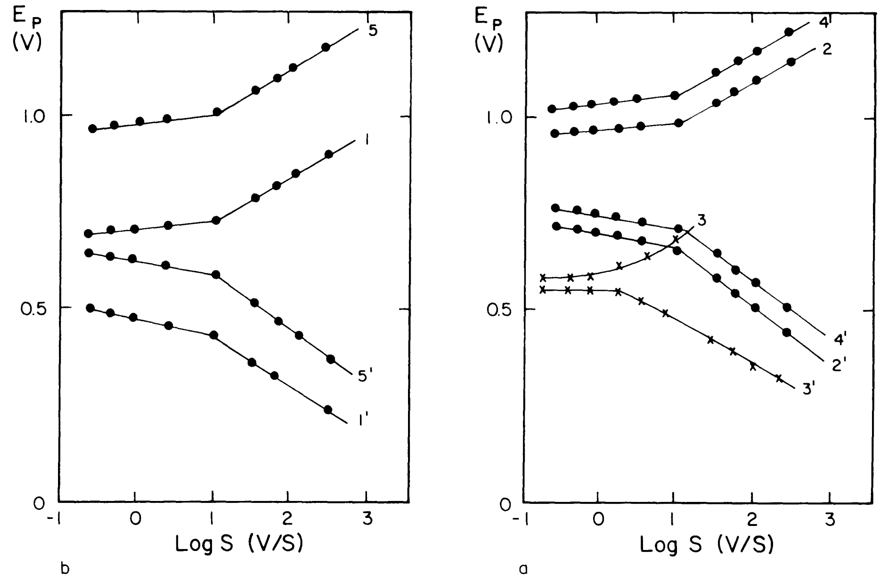

Figure 8. Dependence of oxygen adsorption and desorption peak potentials E_p on logarithm of the sweep rate. (1,1′), Rh; (2,2′,3,3′), Pd; (4,4′,5,5′), Pt. (a) 0.05 M H_2SO_4: (1,5), adsorption in anodic sweep started at 0.5 V vs. RHE, (1′,5′), desorption in cathodic sweep started at 1.1 and 1.4 V, respectively. (b) 0.1 M KOH: (2,4), adsorption in anodic peak started at 0.5 V. Desorption at cathodic sweep started at 0.75 V (3′) and 1.25 V vs. RHE (2′,4′).(73)

The coefficients in the kinetic equations corresponding to different mechanisms have been compared with the experimental data obtained on platinum,(55,82) rhodium,(83) and palladium(84) as a function of sweep rate and pH.

All E_p vs. $\log s$ curves (Figure 8) for Pt, Rh, and Pd have two parts. In the region of slow sweep rates below a critical value ($s < s_{cr}$) the peak potential $(E_p)_I$ depends little on the sweep rate. At $s > s_{cr}$, the dependence is strong. In the region of maximum† I, the value of $\partial(E_p)_I/\partial \log s$ at $s > s_{cr}$ is ~0.12 V/decade. At $s < 1.0$ V/sec the value of $(E_p)_I$ on a palladium electrode is practically independent of the s. Apparently, this is an indication of the reversibility of the adsorption process.

On Pt, Rh, and Pd, both in acid and alkaline solutions, the value of $\partial(E_p)_{II}/\partial \log s$ at $s < s_{cr}$ is 0.03–0.04 V/decade. At $s > s_{cr}$ the slope of the $(E_p)_{II}$ vs. $\log s$ curves rise to 0.12–0.15 V/decade. The increase of slope $(E_p)_{II}$ vs. $\log s$ curves from 0.03 to ~0.12 V/decade indicates that in the region of maximum II, the slow step for a two-step process undergoes a change both in acidic and alkaline solutions.

---

† Maximum I is the maximum in the potential range $E_H < 0.7$ V vs. RHE in alkaline solutions; maximum II is the maximum at $E_H > 0.7$ V.

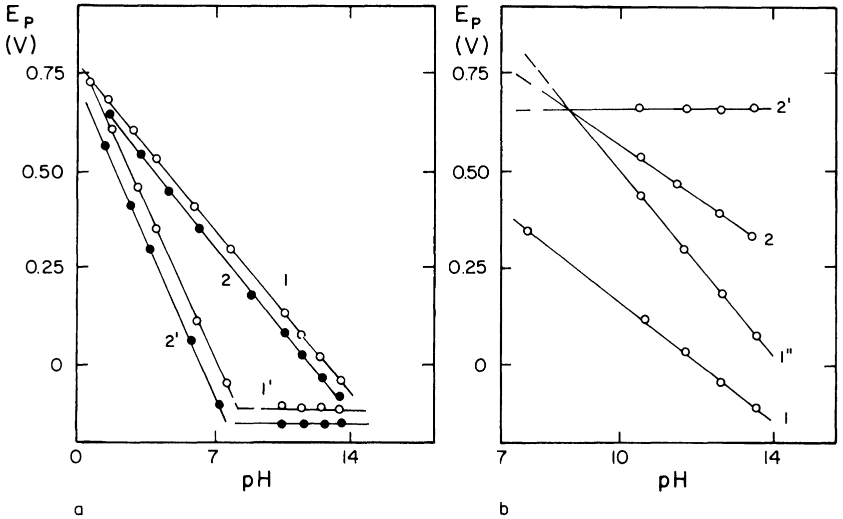

Figure 9. pH dependence of the peak potentials E_p in the voltammograms for Pt and Pd.$^{(73)}$ Potentials on ordinates vs. SHE. (a) Cathodic desorption peaks: 1, Pt sweep rate, 1 V/sec; 1′, Pt sweep rate, 50 V/sec; 2, Pd sweep rate, 1 V/sec; 2′, Pd sweep rate, 50 V/sec. (b) Anodic adsorption peaks: 1, Pt, peak I (see Figure 7F), sweep rate, 1 V/sec; 1′, Pt, peak I (see Figure 7F), sweep rate, 50 V/sec; 2, Pt, peak II (see Figure 7F), sweep rate, 1 V/sec; 2′, Pt, peak II (see Figure 7F), sweep rate, 50 V/sec.

The value of $\partial(E_p)_{\text{I}}/\partial\text{pH}$ at $s < s_{\text{cr}}$ for the anodic and cathodic branches of the i vs. E curves is 0.06 V/decade (Figure 8b, curve 1). At $s > s_{\text{cr}}$, the position of the maximum in the cathodic branch does not depend on pH,$^{(78)}$ but in the anodic branch the value of $\partial(E_p)_{\text{I}}/\partial\text{pH}$ is close to ~0.12 V/decade (Figure 8b, curve 1′). The values of $\partial(E_p)_{\text{II}}/\partial\text{pH}$ for platinum and palladium electrodes in the pH range 0–14 (Figure 9a, curves 1, 2) and at $s < s_{\text{cr}}$ are equal to ~0.06 V/decade. At $s < s_{\text{cr}}$, the value for the cathodic branch of the i vs. E curve is ~0.12 V/decade in acid solutions. In alkaline solutions it does not depend on pH (Figure 9a, curves 1′, 2′). These results were confirmed by the independent analysis of the exchange current of adsorbed oxygen.$^{(82)}$

The comparison of the experimental data with the kinetic parameters given in Table 2 for different slow steps suggests the following mechanism of oxygen adsorption and desorption on platinum, rhodium, and palladium.† In the region of the first maximum in Figure 7, the main form of adsorbed oxygen is the S–OH species, resulting from a one-electron anodic reaction. At low potential sweep rates, the process is practically reversible. With increasing potential sweep rate, the slowness of the electrochemical step begins to be evident. As follows from the dependence of the potential of this maximum on solution pH, the formation of S–OH in the region of maximum I (which

† This mechanism is also applicable to the iridium electrode.$^{(83)}$ In this case the analysis is simpler because the apparent strengthening of chemisorbed oxygen with time is absent.

is practically observed only in alkaline solutions) is the result of the hydroxyl ions discharge according to reaction 2 in Table 2 and not of the water molecules by reaction 1.

In the region of the second maximum, a two-step process occurs. Depending on the rate of potential application, either the first or the second step is limiting. In the range of high rates of potential application, where the maximum depends strongly on s, the first step is the limiting one, both in the anodic and cathodic processes. In the range of small s, the first step becomes an equilibrium step and the process is limited by the second step. As follows from the experimentally derived kinetic parameters, in the region of the second maximum, the anodic formation of S–OH may be the result of the water molecules discharge. Further formation of S–O results from the dismutation of S–OH species according to reaction 3 in Table 2 and is not due to an electrochemical reaction.

The reaction schemes based on the concept of S–O formation via an intermediate formation of S–OH almost over the entire potential range appears to show better agreement with experimental data for various platinum metals than other schemes described in the literature and in particular, for the observed changes of the kinetic parameters with pH.

Another instance of an adsorption theory kinetic approach but with the kinetic analysis based on potential steps is a series of works by Bagotzkii *et al.*(84–86) They investigated the rates of oxygen adsorption and desorption on Pt in 0.1 M NaOH at various potentials and the effect of the aging of oxygen adlayer on these rates. The experimental results (i vs. time) were represented on semilogarithmic or logarithmic coordinates ($\log i$ vs. $\log t$, $\Delta\theta_O$ vs. $\log t$, $\log i$ vs. ΔE) and yielded approximately straight lines. From their analysis of the data these authors(85,86) concluded that kinetic equations of the Elovich type,(57) based on the Temkin adsorption isotherm are valid, i.e.,

$$i_a = k_a \exp(-\alpha f\theta_O) \exp\left(\frac{\alpha FE}{RT}\right) \tag{5}$$

$$i_c = k_c \exp(\beta f\theta_O) \tag{6}$$

with heterogeneity constants f strongly dependent on electrode potential and aging conditions. This was attributed to the partial discharge of adsorbed OH^- anions:

$$OH^- \rightarrow OH^{-\delta} + (1-\sigma)e^- \tag{XIX}$$

where the extent of the charge transferred increases with anodic potential and with electrode aging. According to Bagotzkii *et al.*,(85) the charge remaining on the adsorbed species causes repulsive interactions, as is evident from the higher values of the heterogeneity parameter f. The logarithm-type plots used in these studies, however, did not facilitate distinguishing details of the fine structure of adsorption.

Further use of adsorption theory has been made by Biegler and Woods *et al.*(58,87) (see also the review in Ref. 52). They showed that in Q vs. E data, steps can be seen corresponding to O/Pt ratios equal to 1/1 and 2/1 provided that special precautions are taken in defining the charge equivalent to a monolayer adsorption. This use of the charge corresponding to hydrogen adsorption to obtain the maximum surface site concentration assumes that the same sites are effective for oxygen adsorption.

Phase oxide theory for anodic layers on Pt developed gradually from early experimental investigations by Bockris *et al.*,(70) Ord *et al.*,(88) and Visscher and Devanathan.(89) It is still faced with reluctance by many electrochemists because it applies the concept of bulk phase oxides(90) to the formation of very thin layers and even a submonolayer amount of oxide in the potential region $1.0 < E_H < 1.6$ V (vs. RHE).

The attractiveness of various versions of this theory lies in that it is more flexible in accounting for baffling experimental facts, owing to, among other things, the greater number of adjustable parameters. This makes it easier to construct models which are consistent with experimental findings, particularly relating to intrinsic irreversibility.

Representative of the work using phase oxide concepts are those of Damjanovic *et al.*,(59,62,91,98) Vetter and Schultze,(60,99) and Gilroy.(61,100) Most studies by these workers were done using current and potential pulses with the results often integrated and presented in logarithmic coordinates. This has led some of these workers to conclude that one model and corresponding kinetic equations may be operative for the entire potential region of anodic layer growth from the very onset of oxygen adsorption ($E_H \cong 0.8$ V) to high anodic potentials ($E_H > 1.6$ V) where the existence of a phase oxide is not questioned by adherents of the adsorption theories. Most of these workers, however, believe that the formation of the phase oxide is preceded by the adsorption of OH or O^{2-}(99) at less anodic potentials.

Damjanovic *et al.*(59) from anodic-current step measurements starting from the rest potential of Pt in O_2-saturated 1 *M* H_2SO_4 found that during oxide buildup the potential increased with time as follows:

$$E \sim t \qquad \text{for } 0.98 < E_H < 1.6 \text{ V}$$

$$E \sim \log t \qquad \text{for } E_H > 1.6 \text{ V}$$

From ellipsometric data these authors(59,94) concluded that the thickness of the oxide layer increased linearly with electrode potential under galvanostatic conditions but the slopes of these dependences were different below and above the onset of O_2 evolution. From current steps at various current densities they found the relations

$$\frac{\partial E}{\partial Q} = C \ln \frac{i}{i_0} \tag{7}$$

$$\left(\frac{\partial E}{\partial \ln i}\right)_Q = aQ \tag{8}$$

where a and C are constants and the charge Q is that directly measured assuming the current density for O_2 evolution to be negligible. They assumed also the validity of the functional dependence:

$$E = f(Q, i) = f(Q, \dot{Q}) \tag{9}$$

which implies the absence of long-time electrode surface reconstruction (aging effects). From these they inferred the kinetic equation:

$$i = i_0 \exp \frac{\alpha(E - E_c)}{r(Q + Q_0)} = i_0 \exp \frac{\alpha \Delta E}{d} \tag{10}$$

where i_0 and α are constants, r is a factor relating charge to oxide thickness d $[r = d/(Q + Q_0)]$, Q_0 is the charge equivalent to the adsorbed layer prior to application of the current pulse, and E_c is an empirical constant.

Damjanovic *et al.* interpreted this type of kinetic equation as evidence for a Cabrerra–Mott type of mechanism(101) of the oxide growth, i.e., uniform growth of the oxide phase by field enhanced migration of ions through the existing oxide phase with the rate-controlling process the transfer of ions over an activation barrier to occupy an interstitial position in the oxide matrix. The value of the electrostatic field in question is $(E - E_c)/d = (\phi - \phi_0)/d$, where ϕ_0 is the potential in the oxide at the oxide–electrolyte interface, ϕ is the potential in the oxide at the metal–oxide interface, and $\Delta\phi$ is the drop across the oxide film of the thickness d.

The kinetic growth equation predicted by the Cabrerra–Mott model has the form

$$i = 2N\nu\lambda\omega r^{-1} \exp\left[-\frac{W}{kt}\right] \exp\left[\frac{ze\lambda\,\Delta\phi}{kTd}\right] \tag{11}$$

where N is the cross-sectional density of the migrating ions, ν is their vibration frequency, λ is the jump distance between stable positions in the lattice, ω is the area of the oxide layer per single migrating ion, W is the activation energy for ion transport in the absence of the field, and ze is the charge of the migrating ion.

Damjanovic *et al.* concluded that Pt^{2+} is the migrating ion [from the $2e\lambda$ value calculated from the approximate formula $(\partial^2 E/\partial \ln i \cdot \partial(d) = kT/2e\lambda)$] and that the rate-controlling step is ingress of Pt^{2+} from the metal lattice into the oxide phase with the further migration much faster. This raises some doubts, since the rate equations (10) and (11) are in terms of the field $(\Delta\phi/d)$ in the oxide phase whereas there is no clear relation between this value and the rate of Pt^{2+} ingress into the oxide phase.

Damjanovic *et al.* referred also to the intrinsic irreversibility of oxide formation/reduction, postulating that whereas oxide formation involves uniform (unlocalized) growth, its reduction, on the contrary, is localized (patchwise) with a mechanism analogous to the two-dimensional nucleation and growth of pits on passive layers on Fe. This, however, does not explain the almost ideal symmetry and reproducibility of the cathodic potentiodynamic peaks on Pt in 1 M H_2SO_4 with rather weak dependence of these peaks on the presence of strongly adsorbing halogen anions(59) which are known for their pit-initiating action on Fe passive layers.

The pH dependence of oxide formation, not directly predicted by the Cabrerra–Mott model, was explained(59) with the E_0 term in Eq. (10), using the dependence:

$$E_0 = E_{0,0} - \frac{2.3RT}{F}\text{pH} \tag{12}$$

where $E_{0,0}$ is a constant. No interpretation was put forward for the pH dependence of oxide reduction.

Mutual consistency was found(59) for the results obtained with current-step, potential-step, and potential-sweep measurements and it was reported that all of these methods gave results compatible with the field-enhanced growth mechanism. In particular, it was shown that the reciprocal pseudocapacity $(\partial E/\partial Q)_i$ in the oxide formation region determined in potential-sweep experiments was proportional to $\log s$ over the entire investigated range of sweep rates: $10\ \text{mV/sec} < dE/dt < 10\ \text{V/sec}$. This result is at variance with earlier findings of other workers,(54,103) according to which electrode pseudocapacitance in the oxide region is almost constant over a fairly broad range of sweep rates. This controversy, crucial to oxide layer theories, should be settled by independent, comparative experiments of potentiodynamic and galvanostatic anodic oxide formation on Pt in pure solutions and with careful elimination of instrumental artifacts (e.g., field asymmetry around the electrode and ohmic drop contributions).

Damjanovic *et al.*(62,97) have investigated the temperature dependence of oxide formation. From Eq. (11) they defined "exchange current density" (preexperimental factor for field = 0) as

$$i_0 = 2N\nu\lambda\omega r^{-1} = 2Nze\nu \tag{13}$$

since $ze = \lambda\omega/r$. From the approximate dependence

$$\left(\frac{\partial^2 E}{\partial Q \partial T}\right)_i \cong \frac{kr}{ze\lambda}\ln\frac{i}{i_0} \tag{14}$$

they evaluated i_0 for Pt in H_2SO_4 solution and, assuming $\nu \cong 10^{12}\ \text{sec}^{-1}$ and using Eq. (13), found $N \cong 2 + 10^{15}\ \text{cm}^{-2}$. This value is close to the density of Pt atoms on the surface and hence they conclude that ingress of Pt^{2+} atoms into the oxide phase is rate controlling.

The same procedure was repeated by Damjanovic *et al.*(97) with respect to Pt in 1 M KOH and led to the conclusion that field-enhanced oxide growth is operative also in this case. The "exchange current density," however, was 10^3 times higher than in acid solution. The activation energy W was determined from the equation

$$W = -2.3\,Rd \log i_0/d(1/T) \tag{15}$$

This gave values of 18.5 kcal/mol for 1 M KOH and 25 kcal/mol in 0.5 M H_2SO_4. The difference between these values in W overcompensated the difference in the exchange current densities i_0. To accommodate this difference it was postulated(97) that N in alkaline is ~800 times lower than in acid. This conclusion, as pointed out by these workers, cannot be explained simply in terms of the oxide growth theory postulated for Pt in acid.

A further difficulty associated with the use of this approach [Eqs. (7)–(15)] and the phase oxide theory arises from the aging effects. The analysis of galvanostatic and potentiodynamic experiments with equations of the form of Eq. (9) fails to take into account intrinsic time-dependent effects associated with aging phenomena. The history of the electrode has a major effect as has been revealed particularly in the aging experiments of Folgner and Arvia *et al.*(71)

Vetter and Schultze(60,99) have proposed a model for the formation of the anodic layer on Pt which involves features of both the chemisorbed and phase oxide models. They view the formation of the anodic layer as proceeding through the states represented in Figure 10. They propose that the first step involves the following reaction to yield the chemisorbed layer (Figure 10a):

$$H_2O \rightarrow O^{2-}(\text{ads}) + 2H^+ \tag{XX}$$

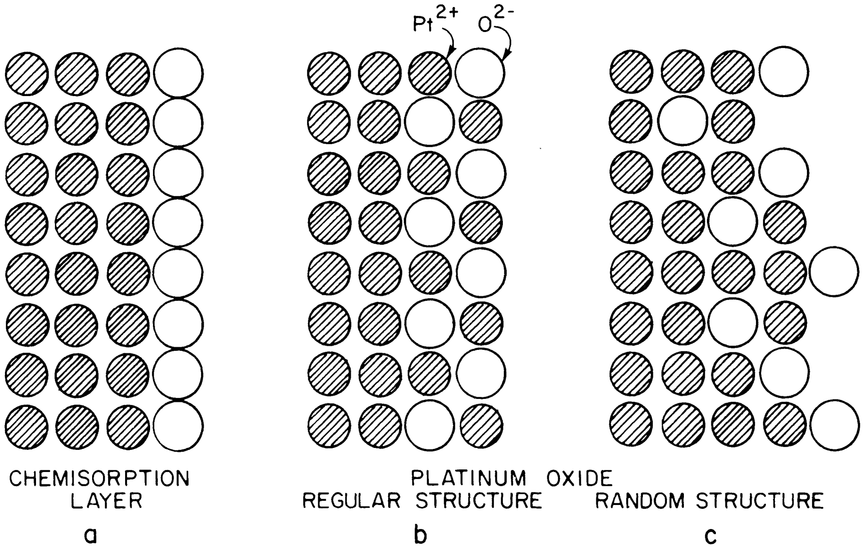

Figure 10. Schematic diagrams of oxygen layers on the (100) face of Pt at a coverage $\theta = 1$.(99)

The adsorbed species O^{2-} is not believed to exceed ~10% on the basis of the available capacity data. While these workers propose reaction (XX), they also point out that on the basis of the pH dependence alone it is not possible to distinguish between O^{2-} and OH^- adsorption. Vetter and Schultze indicate that the species is ionic rather than a covalently bonded species. A clear distinction between ionic vs. covalent bonding is difficult to make on the basis of electrochemical measurements. Even if the adsorption involves an ionic species O^{2-} or OH^-, the compensating charge on the Pt must pass through the external circuit and be equal to that on the adsorbed ionic species except for the small portion compensated by changes in the charge in the outer Helmholtz plane and diffuse layer.

The principal evidence presented by Vetter and Schultze for the model in Figure 10 and reaction (XX) is the observed relation between capacitance data and coverage as determined from galvanostatic cathodic reduction of the layer. The observed capacitance C was found to depend on coverage θ as follows:

$$\frac{1}{C}=\frac{1}{C_i}(1+a_1\theta) \tag{16}$$

where a_1 is a constant. This dependence is interpreted on the basis of the equivalent circuit in Figure 11, where C_{ox} is the capacitance of the oxide layer; C_i and C_o are the capacitances of the inner and outer Helmholtz layers; C_{ad} and R_{ad} are the capacitance and resistance components associated with the adsorption process. In the region of oxide formation, C_{ad} is very large, R_{ad} is very low, and the circuit reduces to a series connection of C_{ox} and C_i; hence

$$\frac{1}{C}=\frac{1}{C_i}+\frac{1}{C_{\text{ox}}} \tag{17}$$

Vetter and Schultze assume that $C_{\text{ox}} \propto 1/\theta$. This follows from the reasoning that capacitance of a parallel plate condenser is $C_{\text{ox}} = D_{\text{ox}}/(4\pi\delta_{\text{ox}})$, where D_{ox} is the dielectric constant of the oxide. The effective thickness of the capacitor δ_{ox} is regarded as proportional to the surface coverage θ. Thus Eq. (17) has a form similar to that of Eq. (16).

At constant potential in H_2SO_4 solution, Vetter and Schultze found the current associated with the adsorption process to follow the relation

$$\log i = \log i_{\theta=0} - k\theta \tag{18}$$

where $i_{\theta=0}$ is the current for layer formation at $\theta = 0$, immediately following the potential step. The relation between the electrode potential and current at constant θ was found to be

$$E = a + b \log i \tag{19}$$

although the experimental E vs. $\log i$ plots deviated somewhat from straight

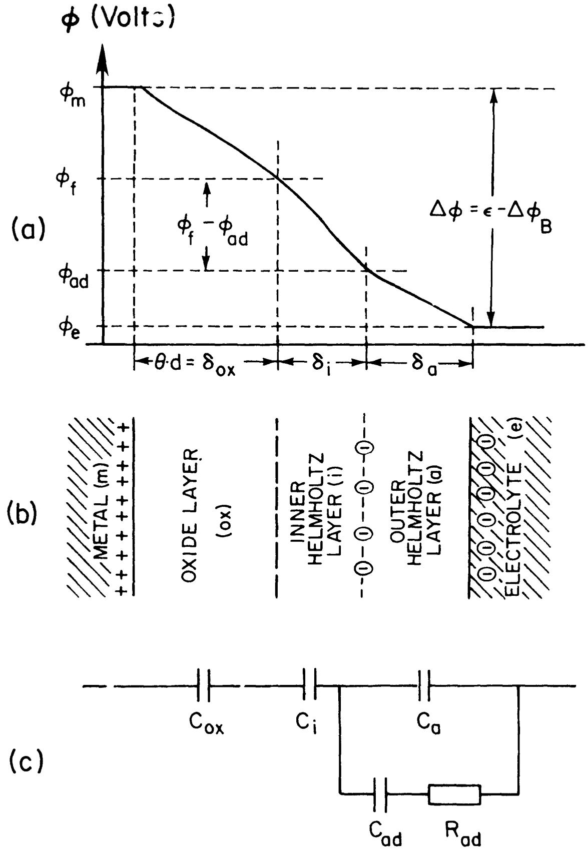
ϕ (Volts)
ϕm
ϕf
ϕad
ϕe
ϕf − ϕad
Δϕ = ε − ΔϕB
θ·d = δox
δi
δa
(a)
(b)
METAL (m)
OXIDE LAYER (ox)
INNER HELMHOLTZ LAYER (i)
OUTER HELMHOLTZ LAYER (a)
ELECTROLYTE (e)
(c)
Cox
Ci
Ca
Cad
Rad

Figure 11. Double-layer model for monomolecular oxide layer with chemisorbed oxygen ions. a, Potential distribution; b, charge distribution; c, equivalent circuit diagram with regard to adsorption equilibrium of oxygen ions. Symbols defined in text.(60)

lines. The Tafel slopes b_a for the anodic currents during formation of the film were found to depend on the coverage as follows:

$$b_a = b_a^0(1 + a_2\theta) \qquad (20)$$

while the value b_c for the reduction was essentially independent of θ. The similarity between the dependence of $1/C$ on θ and b_a on θ lead Vetter and Schultze to conclude that the field across the O^{2-}(ads) layer acts as the driving force for its growth.

Vetter and Schultze proposed that the further stages of growth of the film represented by Figure 10b and c occur through place exchange between adsorbed O^- ions and Pt metal ions under the influence of the potential across the interface. The penetration of O^{2-} into the Pt provides a likely explanation for the aging effects.

Vetter and Schultze also proposed that the reduction of the oxide occurs pathwise (in a localized way) and therefore with kinetics (Tafel slopes) which are almost independent of thickness or average coverage.

Gilroy,(61,104) using the phase oxide concept, proposed that the oxide formation on Pt occurs through a nucleation mechanism from the very beginning. From measurements carried out potentiostatically in 1 M H_2SO_4 over the potential range $1.1 < E_H < 1.8$ V, he found linear Q vs. $\log t$ plots with the lines for various potentials intersecting at a single point. Further, the slopes $\partial Q/\partial \log t$ depended linearly on electrode potential with $\partial Q/\partial \log t = 0$ at $E_H = 0.75$ V. From these measurements, Gilroy found the semiempirical kinetic equation

$$i = \frac{A\eta}{t_0} \exp - \frac{Q}{A\eta} \tag{21}$$

where A and t_0 are constants. This equation is similar in form to that derived theoretically by Fleischmann and Thirsk(105) for electrochemical nucleation. As evidence against adsorption models and in favor of a nucleation theory, Gilroy points out that the adsorption model and the Temkin-type adsorption isotherm lead to a Q vs. $\log t$ equation of the form

$$Q = a \log t + bE + C \tag{22}$$

where a, b, and c are constants. According to this equation, the Q vs. $\log t$ plots for various potentials should be parallel rather than converge to a single point.

Gilroy(61) proposed that the reduction of the oxide layer is uniform and typical of that for a desorption process with charge transfer control. This view is contrary to that of Vetter and Schultze(60) and Damjanovic *et al.*,(98) who propose that the oxide formation is uniform and originates with the formation of an adsorbed layer but that the reduction is patchwise (localized).

The kinetics of the adsorption process and the structure of the oxide layer at potentials more positive than 1.5–1.7 V vs. RHE have been studied by a number of researchers.(106–120) The total oxygen coverage generally increases linearly with the potential to 2.0 V. At this potential the value θ_O reaches approximately two atoms of oxygen per atom of Pt, or a slightly higher figure. In several studies the establishment of a limiting coverage ($\theta_O = {\sim}2.2$) at potentials from 2 to 3 V was observed. Some researchers consider that this limiting coverage provides formal evidence of a monolayer of the chemisorbed oxide $Pt{-}O_2$ (α-oxide(110,111)) and that under more severe oxidation conditions, the formation of phase oxides (β-oxide(110,111)) also occurs. Evidence for the presence of Pt (IV) in the anodic film has been obtained from *ex situ* X-ray photoelectron spectroscopic measurements (see Section 4.4).

The majority of the experiments have dealt with the electrochemical properties of the α phase and its participation in the reaction of O_2 evolution.

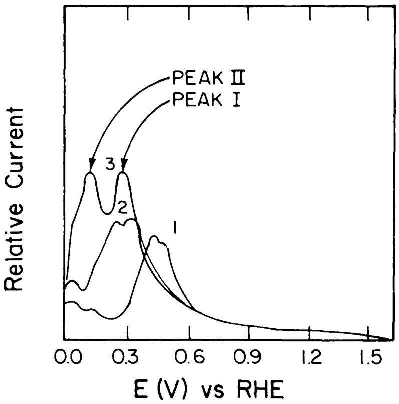

Figure 12. Cathodic sweep voltammograms of Pt electrode preanodized for 15 sec at 2.0 V (vs. RHE) in 5 M $HClO_4$. Various sweep rates: 1, 30 V/sec; 2, 60 V/sec; 3, 300 V/sec.(113) (relative currents only on ordinate).

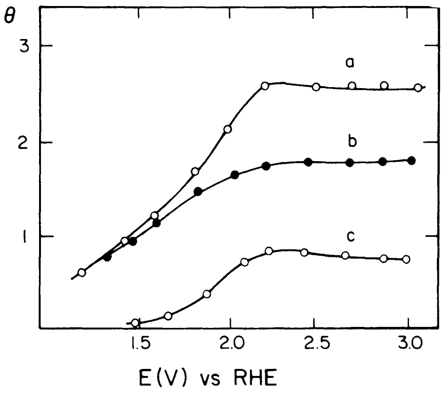

Figure 13. Dependence of surface coverages by oxygen on anodization potential of Pt in 0.5 M H_2SO_4. Anodization time = 120 sec. a, Total oxygen coverage θ_O; b, c, coverages θ_I, θ_{II} associated with oxide forms I and II, respectively.(113)

Typical results are given in Figures 12 and 13. At a low scanning rate, all oxides are reduced at the one peak in the cathodic i vs. E_H curve. With increasing sweep rate, the oxide reduction peak splits into two: a more anodic peak I and a more cathodic peak II (Figure 12). These two maxima are assumed to reflect the existence of two forms of surface oxide. If this is correct, the amount of the first form θ_I and especially the second one θ_{II} increases with increasing formation potential (Figure 13). The properties of these two forms of adsorbed oxygen have been studied in detail by Tyurin and Volodin(109) and Khanova *et al.*(113) The behavior of the second form (II) is quite unusual. On the one hand this oxide behaves as if it were very labile and a considerable proportion of it is lost after only 0.5 sec at 1.5 V vs. RHE. On the other hand, it is reduced at potentials which are more cathodic than those for oxide I. In other words, peak II is more stable in the cathodic process and very labile in the anodic process. These contradictory properties can be explained if it is assumed that the labile form is not the oxide II but its precursor—active oxygen—which takes part in the anodic reaction. With decrease of the potential E_H to 1.5 V this active oxygen may become more stable and be converted into the oxide II, which is more difficult to reduce.

At very anodic potentials, in accordance with the early investigation of Weselovskii(119) the following reaction is proposed to take place:

$$\text{Pt—O[O]} + H_2O \rightarrow \text{Pt—O} + O_2 + 2H^+ + 2e^- \qquad \text{(XXI)}$$

where Pt—O is oxide form I and [O] is the active oxygen. At a potential of 1.5 V reaction (XXI) is accompanied by a parallel and competing reaction involving the conversion of the active oxygen into form II, which can be conditionally written as follows:

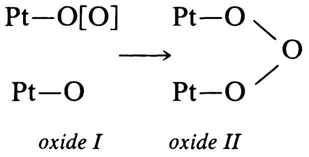

(XXII)

With displacement of the potential in the cathodic direction, reduction of the oxide forms I and II takes place according to reaction (XXIII) and (XXIV) given below and form II is converted into form I in reaction (XXV) with the participation of the free platinum previously formed in reactions (XXIII) and (XXIV):

$$\text{Pt—O} + 2H^+ + 2e^- \rightarrow \text{Pt} + H_2O \qquad \text{(XXIII)}$$

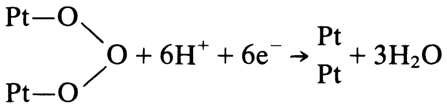

(XXIV)

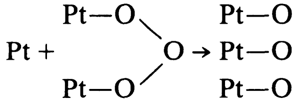

(XXV)

Supporting evidence for this scheme has been obtained using O^{18} isotope labeling.(116,117) It has been shown that part of the oxygen of the second monolayer apparently is strongly involved in the total O_2 evolution process. The main pathway to the evolution of molecular oxygen, however, is proposed to be that via the most labile form of surface oxide Pt—O[O]. This oxide can only be detected when the potentiodynamic reduction curves are recorded very rapidly and the time delay prior to the cathodic sweep is short.(113) As the polarization time is extended, the chemisorbed oxygen becomes more firmly bound and its degree of involvement in O_2 evolution decreases.

In contrast to α-oxide, it has been proposed that the β-oxide grows on the metal at a much slower rate, forming a multilayer. The rate of its formation according to electrochemical and ellipsometric data depends on potential, temperature, length of polarization, and electrode pretreatment. For example, it grows to as many as 60 layers of PtO_2 by galvanostatic anodization for 28 hr in 1 M H_2SO_4. At potentials higher than $E_H = 2.3$ V the growth of the

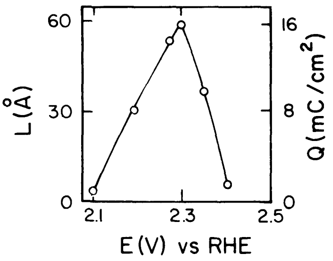

Figure 14. Thickness and charge associated with anodic layer produced on Pt in 0.5 *M* H_2SO_4 after 1 hr of anodic polarization at various potentials.(116)

β-oxide is strongly retarded (Figure 14). Further investigation is required as to the reasons for this retardation.

The growth of the β-oxide is expected to be controlled by the transport rate of the oxidizing species through the oxide phase. When the oxidizing species are ions, their transport rate may depend largely on the strength of the electric field in the oxide phase. According to Khanova *et al.*(116) the surface oxides of platinum have an effect on the anodic generation of O_2. The presence of the α-oxide on a metallic substrate (which has photoelectric properties characteristic of a semiconductor with *n*-type conductivity(115)) leads to a decrease in the anodic O_2 generation current, while the β-oxide phase of platinum (which has photoelectric properties characteristic of a *p*-type semiconductor) leads to an increase in the oxygen evolution current.

Thus, when the potential E_H is increased from 0.7–0.8 to 2.5–3.0 V, the platinum electrode surface passes successively through three stages of oxidation. At 1.4–1.5 V a monolayer of chemisorbed oxygen with a formal Pt:O ratio of 1:1 is formed. At more anodic potentials it is gradually converted into an oxide coating of a different type with a Pt:O ratio of 1:2 to 1:3 (α-oxide), sometimes called the limiting coating. Finally, in the region of 2.1–2.3 V, the formation of an oxide film with phase character (β-oxide) is observed under the α-oxide. The different nature of the three forms of these surface oxides is confirmed by the ellipsometric investigation on a platinum anode.(114,115,120) Evidence for the presence of Pt in the IV valency state in the oxide film has been obtained from *ex situ* photoelectron spectroscopic measurements (see Section 4.4).

4.1.2. Other Noble Metals

The properties of electrochemically formed oxide layers on other noble metals will be discussed briefly. They have been studied much less intensively than Pt and, at least for some of them, the conclusions formulated for Pt have been tentatively adopted. More detailed reviews on this subject are available.(52,53)

Rhodium. Rhodium has the closest resemblance to Pt. Except for the overall cathodic shift by about 0.3 V for the onset of the adsorption and desorption of oxygen, other properties of the oxide layer on Rh seem to be analogous to those for Pt. This is particularly so with respect to the irreversibility of oxygen adsorption and desorption, which on Rh, similarly to on Pt, results in hysteresis in the charge vs. potential curves. Because of the uncertainty in obtaining the surface site concentration from hydrogen monolayer adsorption on Rh, the calculation of the surface concentration (coverage) of adsorbed oxygen on Rh from cathodic reduction is more uncertain.

Whereas a limiting coverage by oxygen corresponding to a monolayer of Rh_2O_3 or RhO_2 has been reported by Wood(121) at $E_H > 2.0$ V, no formation of the phase oxide analogous to β-oxide on Pt was observed on Rh. Instead, coloration of the solution occurs after strong anodic polarization in H_2SO_4 indicating corrosion of the electrode material resulting evidently from greater solubility of Rh oxides. According to Wood,(52) 15% of the anodic charge in slow potentiodynamic cycle is expended for Rh dissolution as compared with 1% for Pt.(52)

Palladium. Because of the solubility of hydrogen in the bulk of this metal, it is almost impossible to determine monolayer coverage by hydrogen and hence the calculation of oxygen coverage is difficult. The properties of Pd–oxide are similar to those for Pt and Rh.(52,53) An important feature of Pd is its higher corrosion, particularly in acids and in the presence of complexing ions. Metal dissolution according to Wood accounts for 17% of charge in slow anodic potentiodynamic sweep experiments. In contrast to Rh, no limiting coverage of Pd by chemisorbed oxygen has been found, but the formation of a phase oxide (analogue of Pt β-oxide) is quite easy and gives diffuse cathodic peaks for reduction in the potentiodynamic curves.(121)

Iridium. The peculiar property of this metal is its ability to form thick (multilayer) surface oxide during, for example, continuous potentiodynamic cycling between hydrogen adsorption and the anodic potential $E_H = 1.5$ V in dilute H_2SO_4 or $HClO_4$. This oxide with a composition supposedly close to IrO_2 is built up irreversibly during cycling and is not stripped off even by deep cathodization. It has very high pseudocapacity, however, as manifested by the reversible anodic and cathodic peaks at $E_H = 0.9$ V.

The hydrogen adsorption on Ir is similar to that on Pt and this makes possible the calculation of the charge corresponding to a hydrogen monolayer with reasonable accuracy. Therefore, the measurement of the equivalent surface concentration of oxygen is also possible. According to Buckley and Burke(63) the charge capacity of surface oxide formed by 5000 slow potentiodynamic cycles ($100 \rightarrow 1500 \rightarrow 100$ mV) accounts to 46 mC cm^{-2}, i.e., the equivalent of about 100 monolayers. Since this oxide is not completely reduced during cathodic cycle, however, it is assumed that only a change of its stoichiometry occurs, for example, according to

$$IrO_2 + 2H^+ + 2e^- \rightarrow IrO(OH)_2 \qquad \text{(XXVI)}$$

Consequently, the surface concentration of oxygen atoms on oxidized Ir has to be at least twice as high as that obtained assuming the overall reversible charge to be attributed to the reaction:

$$MeO_2 + 4H^+ + 4e^- \rightarrow Me + 2H_2O \qquad \text{(XXVII)}$$

The development of this highly capacitive oxide layer is not accompanied by any subsequent considerable change of hydrogen pseudocapacity nor by surface roughening. Reversible electrochromic effects during charging/discharging of the oxide pseudocapacitance have been reported in References 63, 123–126.

In the presence of concentrated acid (e.g., 5 *M* H_2SO_4) or at sufficiently anodic potentials ($E_H > 1.65$ V in 1 *M* H_2SO_4), the highly capacitive oxide layer is dissolved and the original "monolayer" pattern of potentiodynamic curve is restored.

There is still not a clear explanation of what occurs during formation of the oxide layer and its reversible recharging. The original suggestion of Böld and Breiter(127) was that these processes occur because of the expansion of the surface layer of the metal lattice, resulting in easy access of the oxygen atoms to the inner parts of the metal. This has not been confirmed in later investigations.(63,123–126) Rather, it appears to be caused by the buildup of an amorphous oxide(128) of composition close to IrO_2 and with good metallic-like conductivity,(129,130) similar to well-recognized properties of RuO_2 (see below). The charge capacity and reversibility of recharging is due to a reaction of the type (XXVI) involving the transfer of protons and electrons through the thick oxide layer. Indeed, many properties of electrochemically formed Ir oxide exhibit striking similarities to those of thermally generated RuO_2 including high electrocatalytic activity for the anodic oxygen generation(131) which may result from the good electronic and protonic conductivities of these high-surface-area oxide phases.

Ruthenium. Ruthenium corrodes even more than the metals discussed above and has no particular importance by itself. It is its oxide RuO_2 which has attracted the interest of many investigators due to its application in dimensionally stable anodes (DSA) as the catalytic material on Ti substrates for chlorine and oxygen evolution.(132–135) The phase oxide on Ru may be formed similarly as on Ir by continuous potentiodynamic cycling in diluted acid between the potentials for oxygen and hydrogen evolution but this oxide is unstable and easily corrodes. More effective is the thermal decomposition of $RuCl_3$ in air which gives a stable oxide material.(136) Crystals of RuO_2, similarly to IrO_2, have metallic properties and the same is expected for electrochemically formed Ru oxides. According to Trasatti and Buzzanca(136) the properties of RuO_2 obtained by thermal decomposition of $RuCl_3$ on Ti substrate are different from RuO_2 monocrystals, particularly in corrosion resistance.

During the study of O_2 evolution on thermally prepared RuO_x on Ti and other substrates, O'Grady *et al.*(137) examined the voltammetry of this oxide in acid and alkaline electrolytes. The voltammograms indicate complementary peaks in the anodic and cathodic sweeps at $E_H = \sim 1.3$ V in both acid and alkaline electrolytes at sweep rates of $1 < dE/dt < 300$ mV/sec. At slower sweeps $dE/dt \leq 10$ mV/sec, the anodic and cathodic peaks have the same potential, indicating reversible behavior. This peak was attributed by O'Grady *et al.*(137) to a change of the valency state (probably Ru^{4+}–Ru^{5+}) of just the surface Ru species of the oxide on the basis of surface area measurements using the Zn^{2+} adsorption technique of Kozawa(138) and the charge under the 1.3-V voltammetry anodic or cathodic peaks.

4.2. In Situ Optical Studies

While electrochemical methods are very sensitive, they lack the molecular specificity needed to resolve the structure of the anodic layer formed on noble metals. This has prompted various workers to turn to *in situ* optical measurements (for reviews see Refs. 139, 140, and 158). Ellipsometric techniques have received particular attention in studies of the oxide film on Pt. In these studies, elliptically polarized light is specularly externally reflected from the electrode surface and the changes in phase Δ and amplitude ψ of the polarization components (perpendicular and parallel) determined. The ellipsometric data have usually been interpreted in terms of a three-layer model consisting of a layer of thickness small compared to the optical wavelength interposed between two bulk phases—the metal and the electrolyte. Three parameters are needed to describe such a layer—the real and imaginary components of the refractive index and its thickness. The measurement of the changes in Δ and ψ, however, is sufficient only to determine two parameters and hence it has been necessary to make some assumptions, for example, that the thickness can be determined from Coulombic measurements or that the imaginary component of the refractive index of the film is negligible. In more recent ellipsometric studies, the change in the overall optical intensity of the reflected light has also been measured and this has provided the additional data necessary to determine the real and imaginary components of the refractive index and thickness(141–143) without such assumptions. Even so, the use of the three-layer model to calculate the refractive index of a layer of monolayer dimensions is open to question. The optical changes produced by such a layer are not localized to the layer but include the modification of the surface electronic properties of the metal by the interaction with the oxygen species of the anodic layer and modifications in the optical properties of the ionic double layer.

Much of the earlier studies of the anodic layer with ellipsometry were carried out by Bockris and his group.(144–146) Reddy, Genshaw, and Bockris(144,145) followed the formation of the anodic film on Pt using ellipsometry. Whereas oxygen adsorption begins at $E_H = 0.8$ V, these workers found no evidence of such in their ellipsometric measurements below 0.95 V. At more anodic potentials, distinctive changes of Δ were found and attributed to the formation of the oxide film. These workers assumed that real component of the refractive index at the wavelength of their measurements (546 mm) was the same as for bulk PtO · H_2O even though the layer was of the order of a monolayer. On the basis of these results, Reddy *et al.* concluded that there are two types of layers on Pt, one present below 0.95 V with optical constants close to that of water and not readily detected with ellipsometry, and a second above 0.95 V.

In later work using measurements of the change of reflectance (ΔR) as well as Δ and ψ, however, Kim, Paik, and Bockris(146) found that the optical constants of the film on Pt were nearly independent of electrode potential E_H between 0.8 and 1.6 V with only the thickness of the film increasing nearly linearly with potential. Apparently the earlier measurements of Reddy *et al.*(144,145) lacked the sensitivity to follow the film formation when it was a small fraction of a monolayer. On the basis of the later measurements, Kim *et al.* concluded that the anodic film was a phase oxide.

A number of other workers also have examined the anodic layer on Pt with ellipsometry and specular reflectance spectroscopy.(142,143,147–157) In contrast to Kim *et al.*,(146) several of these researchers have found evidence for a change in the optical properties of the film on Pt in acid solution at E_H = 1.0–1.1 V (see, e.g., Greef,(146) Ord and Ho,(148) Angerstein-Kozlowska *et al.*,(155) Horkans *et al.*(143)). Most workers, however, have obtained evidence that the optical properties of the film undergo relatively little or negligible change in the range E_H = 1.1–1.6 V. The agreement as to the values of the optical constants, however, is poor (see Table 3).

Table 3

Complex Refractive Index ($\hat{n} = n - ik$) for the Oxide Layer on Pt Formed at E_H = 1.4–1.6 V in Acid Electrolytes, as Determined by Various Workers(143)

λ_0, nm	n	k	Source
546	2.62	~1.5	Reddy *et al.*(145),[a]
546	3.0	1.5	Visscher(148),[b]
546	2.8	0.7	McIntyre and Kolb(153),[b]
546	3.05	1.35	Parsons and Visscher(150),[b]
546	2.8	1.7	Kim *et al.*(146)
250	2.4 ± 0.3	2 ± 0.3	Barrett and Parsons(151),[b]
290	2.7 ± 0.3	1.6 ± 0.3	
350	3.1 ± 0.3	1.4 ± 0.3	
400	3.1 ± 0.3	1.7 ± 0.4	
440	3.00 ± 0.05	1.49 ± 0.05	Horkans *et al.*(143)
480	3.26 ± 0.05	1.43 ± 0.05	
555	3.45 ± 0.05	1.44 ± 0.05	
600	3.58 ± 0.05	1.39 ± 0.05	
650	3.70 ± 0.05	1.31 ± 0.05	
710	3.82 ± 0.05	1.36 ± 0.05	

[a] Film assumed to have n of PtO·H_2O.

[b] Film thickness determined from charge.

The wavelength dependence has been investigated in the visible range by Horkans *et al.*(143) and in the ultraviolet range by Barrett and Parsons(151,152) (see Table 3). The wavelength dependence is quite small in the visible and perhaps also in the ultraviolet, although the limited accuracy makes this uncertain in the latter case.

Angerstein-Kozlowska *et al.*(155) have pointed out that the breaks in the ellipsometric data vs. potential at $E_H = 1.1$ and 1.6 V occur at coverages corresponding to 0.5 and 1 electron per surface Pt atom in 0.5 *M* H_2SO_4. They considered this evidence that the anodic film consists predominantly of an –OHPt layer formed by place exchange at 1.1 V and that over the range 1.1–1.5 V this is converted to –OPt. It is not clear, however, why the effective optical thickness of the film should increase as –OHPt is converted to –OPt. The reverse might be expected on the basis of interatomic distances. An alternate explanation suggested by Horkans *et al.*(143) is that the surface is covered principally with O bridging to two surface Pt atoms at 1.1 V and this is transformed to Pt–O over the range 1.1–1.5 V, as follows:

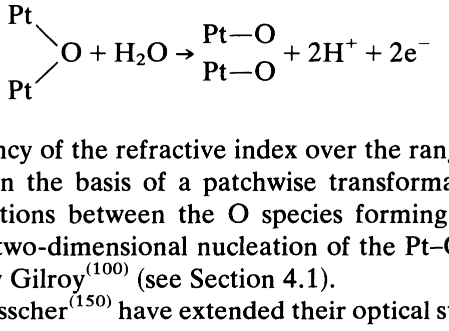

$$\begin{matrix}\mathrm{Pt}\diagdown\\ \quad\mathrm{O}\\ \mathrm{Pt}\diagup\end{matrix} + H_2O \rightarrow \begin{matrix}\mathrm{Pt{-}O}\\ \mathrm{Pt{-}O}\end{matrix} + 2H^+ + 2e^- \qquad \text{(XXVIII)}$$

The relative constancy of the refractive index over the range $E_H = 1.1$–1.6 V can be explained on the basis of a patchwise transformation. This implies short range interactions between the O species forming precursors to the Pt–O patches, i.e., two-dimensional nucleation of the Pt–O phase analogous to that suggested by Gilroy(100) (see Section 4.1).

Parsons and Visscher(150) have extended their optical studies to potentials considerably more anodic than $E_H = 1.6$ V, where O_2 evolution would normally interfere with the optical measurements. Owing to the irreversibility of the oxide film formation, however, the oxide formed at high potentials may be studied by first forming it and then reducing the potential to a value below gas evolution but still above the potential where the film is reduced to any appreciable extent. Using this approach, Parsons and Visscher found limiting values of Δ and ψ for $E_H > 2.0$ V in 0.5 *M* H_2SO_4 and estimated the film thickness to be 8 Å in this region. They attributed this to a Pt–O–Pt–O/solution structure. Vinnikov *et al.*(149) from their ellipsometric data estimated this thickness as 13 Å and attributed it to limiting concentration of oxygen atoms in—as they called it—an α-oxide layer. They propose that beneath this layer phase oxide (β-oxide) is formed continuously during prolonged anodization at $E_H > 2.0$ V (see Section 4.1).

The optical absorption coefficient α, calculated from the complex refractive index or dielectric constant of the film on Pt, exhibits two peaks at ~300 and ~365 mm, as pointed out by McIntyre and Kolb(153) on the basis of their specular reflectance spectroscopic measurements over the wavelength range

200–800 mm. The value cf α is very high ($5 \times 10^5\ \text{cm}^{-1}$). They interpret this as being due to a charge transfer process—probably between the $2p$ level of O^{2-} and a $5d$ level of Pt.

The reflectance of an electrode is modulated when an alternating potential is applied to an electrode. This technique has been applied to the study of the anodic layer on Pt by Conway and Gottesfeld.(156) These ac electromodulation reflectance measurements yield results analogous to ac admittance measurements whereas the change of reflectance and ellipsometric parameters with and without the film present are analogous to the charge vs. potential curves. The ac electroreflectance measurements confirm the reversible adsorption at low coverage ($E_H < 0.9$ V) and the irreversible character of film formation at $E_H > 1.0$ V.

Bewick and Tuxford(154) have used ac electromodulation reflectance spectroscopy with square wave modulation (stair case) from a potential in the double-layer range to various potentials in the anodic film range. They report the detection of film formation already at $E_H = 0.7$ V and that the signal associated with the film formation increases until 1.5 V where it levels off. They conclude that the general features of the wavelength dependence of the reflectance spectrum are determined primarily by the wavelength dependence of the optical properties of the Pt substrate and not by the film.

Despite the extensive studies of the anodic layers on Pt with various ultraviolet–visible optical methods, they have not provided a clear indication of the electronic or structural properties of the layers. Rather these optical methods have been more than just another form of readout to complement the electrochemical measurements of charge and current response of the layer to potential and time. Vibrational spectroscopic data from infrared and Raman measurements would be more helpful in establishing the nature of the layers but it is difficult to use these techniques to study metal–electrolyte and similar interfaces because of solvent interference and sensitivity problems. A noteworthy exception is the quite successful *in situ* use of Raman spectroscopy to study the electrochemically formed oxide layers on silver by Kötz and Yeager.(158) In the instance of silver electrodes, there is a large surface enhanced Raman effect and the signal-to-noise ratio is not a problem. Unfortunately this is not the situation with other metal surfaces such as Pt. Even so, with improved instrumentation there is hope that *in situ* Raman studies of the anodic layers on Pt will become practical.

4.3. *In Situ* Surface Conductivity Measurements

Another *in situ* nonelectrochemical method is the measurement of the electric conductivity of thin Pt films deposited on isolated substrate, usually glass.(159,160) The conductivity of such films changes in a characteristic way with potential as a result of changes in the electronic properties of the metal electrode surface induced by the electric field across the metal–electrolyte interface and by the presence of the adsorbed species or phase oxide. The dependence of the conductivity on electrode potential closely resembles the Q–E_H dependence. In the range of oxide layer formation the conductivity changes of the Pt thin film in contact with the electrolyte follow closely the pattern of changes of electrode reflectivity. This similarity occurs because the same factor, the concentration of surface charge on the metal, is probably the principal factor responsible for changes of both optical reflectance and electrical conductivity.

4.4. Ex Situ Characterizations

Kim, Winograd, and Davis(161) and Allen, Tucker, Capon, and Parsons(162) have used X-ray photoelectron spectroscopy to study *ex situ* the oxide film on Pt. The results from these two groups are quite different. Kim *et al.*(161) have indicated that PtO_{ads}, PtO, and PtO_2 are formed upon electrochemically oxidized Pt electrodes at potentials E_H of 0.7, 1.2, and 2.2 V, and predominantly PtO_2 at 2.2 V. The Parsons group(162) suggest from their experimental results that a single species, probably $Pt(OH)_2$, exists up to potentials of 2.4 V where coulometry(58) indicates a limiting coverage on Pt. No evidence for PtO_{ads} or PtO was found by these workers. Only under extreme oxidizing conditions (at $E_H = 4$ V for 4 hr or more) was PtO_2 detected.

Employing Auger spectroscopy to investigate Pt surfaces, anodized in H_2SO_4 at 500 mA/in.^{2} for 16 hr, Johnson and Heldt(163) have found that the anodized Pt surface contains 50% oxygen and corresponds to a composition of PtO. This stoichiometry also corresponds with the interpretation of Thaker and Hoare's electrochemical data.(164) Johnson and Heldt also claim that it is possible that oxygen is adsorbed or dermadsorbed strongly and that its stoichiometry and stability would be difficult to distinguish from an oxide.

Despite the reasonably extensive use of both *in situ* and *ex situ* spectroscopic tools and electrochemical methods, the understanding of the anodic films on platinum and other metals of interest to O_2 electrochemisry is still very limited. Substantial experimental progress is being made, however, in the study of the interaction of oxygen and water with platinum single-crystal surfaces at the solid–vacuum interface using low-energy electron diffraction (LEED), electron energy loss spectroscopy (EELS), and ultraviolet photoelectron spectroscopy (UPS) (see, e.g., Refs. 165–167 and 210). The insights gained from such studies concerning O and OH layers on Pt and other single-crystal metal surfaces may help in understanding the layers formed at metal–electrolyte interfaces. Such *ex situ* studies, however, are not a substitute for the much needed *in situ* studies with more molecularly sensitive tools. So far, the *in situ* optical spectroscopies have not proved sufficient. Among the promising further *in situ* nonelectrochemical techniques(171) are Mössbauer spectroscopy for certain metals,(168) extended X-ray absorption fine structure (EXAFS),(169) X-ray diffraction from surface layers,(170) perhaps even nuclear magnetic resonance spectroscopy.

5. The Anodic Oxygen Evolution Reaction (OER)

5.1. General Features

The anodic reaction of oxygen evolution on most electrode materials occurs with rather high overvoltage. The kinetic hindrance may differ, however, from that involved in the four-electron reduction of molecular oxygen primarily because no strong oxygen-to-oxygen bond splitting is expected to be involved in OER.

Specific features of OER include the following:

1. The oxygen evolution reaction can occur from either OH^- or H_2O in aqueous solutions [see, e.g., Eq. (1)].

2. In aqueous solutions, OER occurs in a potential range in which relatively few metal electrode materials are corrosion resistant and even this resistance is associated with their strong passivation. In alkaline solutions graphite electrodes are sometimes found to be sufficiently stable at not too high anodic potentials and moderate temperatures.(173) Various bulk metal oxide (particularly mixed) having metallic or semiconductor properties have been found to be efficient catalysts of OER particularly at elevated temperatures. Since either surface oxides layers or highly conductive bulk oxides are inevitably involved in OER, the remark of Gottesfield and Srinivasan(174) that "the science of OER is the science of oxides and their properties" is appropriate.

3. Intermediate products such as H_2O_2 or the corresponding ionized species HO_2^- are normally not detected in the OER. Such species are very unstable in the potential range where OER occurs.

Feature 2 complicates kinetic studies of OER. With thick oxides barriers to charge transfer must be considered both at the oxide–electrolyte and metal–oxide interfaces. The intrinsic resistance (often nonlinear) of thick oxides must also be taken into account particularly at high current density.

The specific features of the electron transfer at the metal–oxide and oxide–electrolyte interfaces are not sufficiently understood, particularly with oxides which are partially hydrated and modified by the electric field. In the case of the very thin oxide layer, such as are formed on Pt in acid electrolyte, charge transfer directly from the metal to adsorbed species may occur by electron tunneling through the oxide.(175)

Of great importance from the mechanistic point of view is the question of the participation of oxygen atoms constituting the oxide layer on metals in OER. Isotopic studies with ^{18}O done by Rosenthal and Veselovskii *et al.*(176,177) have indicated that ^{18}O from the oxide layer on Pt was present in the O_2 gas evolved anodically on this electrode. The excess of ^{18}O in the evolved gas on Pt was strongly dependent on the state of the oxide layer ("history" of its preparation) and on the electrode potential.

The ^{18}O-labeling experiments do not provide a simple "yes" or "no" answer to the important question of whether or not surface adsorbed oxygen atoms on Pt do participate as intermediates in the *steady state* OER. It is important to realize that the answer "yes" would imply a mechanism for the OER involving an elementary step with strong adsorption of O or OH. It is possible that the ^{18}O in the O_2 may arise from a competing reaction to one not involving the oxygen in the anodic layer.

Similar ^{18}O labeling experiments have been carried out by Lee *et al.*(178,179) with anhydrous lithium doped NiO mosaic crystals and have demonstrated that a significant fraction of the O_2 generated at $E_H > 1.6$ V originates from lattice O^{2-} with the fraction from this source potential dependent. Solution equilibration of the surface lattice O^{2-} with the solution phase OH^- and H_2O is much too slow to explain these results. Lee *et al.* have proposed that the *p*-carriers in the lithiated NiO fall into O^{2-} surface traps, generating $O^{\bar{\cdot}}$ or $OH\cdot$ radicals which eventually combine to yield O_2. This mechanism may be represented by the following reactions:

$$O^{2-}(\text{lattice}) + p^+ \rightarrow O^{\bar{\cdot}}(\text{lattice}) \qquad \text{(XXIX)}$$

$$O^{\bar{\cdot}}(\text{lattice}) + H^+ \rightarrow OH\cdot(\text{aq}) \qquad \text{(XXX)}$$

$$4OH\cdot(\text{aq}) \dashrightarrow O_2 + 2H_2O \qquad \text{(XXXI)}$$

$$Ni^{2+}(\text{lattice}) \rightarrow Ni^{2+}(\text{aq}) \qquad \text{(XXXII)}$$

Overall reaction:

$$4NiO + 4H^+ + 4p^+ \rightarrow 4Ni^{2+}(\text{aq}) + O_2 + 2H_2O \qquad \text{(XXXIII)}$$

Reaction (XXXIII) is to be viewed as a competing reaction to O_2 generation from only solution phase species. An interesting feature of reaction (XXXIII) is that it consumes NiO and can proceed even at potentials less anodic than the reversible potential for the O_2–H_2O couple because of the coupling of O_2 generation to the dissolution of NiO. For an acid electrolyte, the calculated standard electrode potential corresponding to this reaction is $\sim +0.5$ V vs. SHE.(178)

Extensive investigations(178–180) at high anodic potentials in concentrated acids indicate that oxyanions (e.g., $SO_4{}^{2-}$, $ClO_4{}^-$) are adsorbed and react anodically on noble metal electrodes. These anions contribute with their oxygen atoms to OER and also give specific oxidation and decomposition products: persulfate ions, ClO_2, ClO_4, $ClO_3{}^-$, etc. The onset of the anodic reactions involving oxyanions is usually accompanied by a drastic change in the polarization curve.

In spite of these well-recognized complications, the kinetics and mechanism of OER have usually been analyzed in terms of classical concepts of formal electrode kinetics with apparently insufficient allowance for the electronic properties of the chemisorbed oxygen and oxide layers and the metal–oxide interface.

The review by Damjanovic(181) offers a comprehensive summary of kinetic data for OER collected mainly by Bockris and his coworkers in the sixties.

In most cases discussed in this review, no firm conclusions could be reached with respect to the actual mechanism even for Pt, the most thoroughly investigated electrode. Instead, two or more mechanisms were cautiously indicated as consistent with experimentally found mechanistic criteria: Tafel slope, reaction orders with respect to H^+, or OH^- and O_2, and stoichiometric number. The use of the stoichiometric number as a mechanistic criterion for oxygen electrode reactions requires caution because its determination from the cathodic and anodic Tafel slopes involves the assumption that the same rate-controlling process is involved for both.(182) This is questionable in view of the large differences in potentials and hence large difference in the state of the electrode surface between the cathodic and anodic branches of the polarization curves.

Most of the early experimental data for the OER(183,184) on various electrode materials consistently indicated a Tafel slope for this reaction in acid solutions as well as often in alkaline solutions of close to 120 mV/decade. The simplest and most natural explanation of this fact is that the first charge transfer step is a rate-determining step (rds). If this is true and the discharge has electrocatalytic character (i.e., involves a strong adsorption bond), then it would be reasonable to expect a linear Brønstedt type of relation between the free energy of activation and the overall free energy change of the elementary step. This should lead to a general correlation between the free energy or enthalpy of oxygen adsorption and the kinetic parameters related to reaction rate (rate constant, exchange currents, overpotentials at a constant current density). Ruetschi and Delahay(185) have derived equations according to which the overpotential for OER at constant current density should be linearly dependent on the enthalpy of adsorption of O or OH. They have correlated data for OER overpotentials published in 1947 by Hickling and Hill(186) with thermodynamically calculated values of the bond energies of M–OH for various metals and found surprisingly good agreement with their theory. The bond energies used by these authors(185) were chosen somewhat arbitrarily. Even so, a simple linear relation between OER overpotential and M–OH bond energy seems to hold quite well for most of the considered metals.

It is interesting that Ruetschi and Delahay(185) were able to correlate sudden variations in overpotential on certain metals (breaks of continuity in the Tafel plots) with variations of the energy of the bond M–OH as a result of sudden changes of the valence of these metals in the surface oxides. According to these authors sudden increases in overpotential occurred in the immediate vicinity of the equilibrium potentials for different oxidation states of the electrode surface. This implies a relation between the mechanism for OER and the state of the surface oxide.

Appleby(187,188) has anticipated more complicated dependences between the kinetic parameters for OER and specific properties of the electrode materials related to the free energy of adsorption of oxygen atoms or OH radicals. According to this author both the exponential (activational) and preexponential (related to surface concentration and charge transfer probability) factors in the rate equation are influenced by the free energy of adsorption. The nature of these dependences should result in a volcano plot for oxygen reaction analogous to the one discussed by many authors for the hydrogen evolution reaction.(189,190) Experimental evidence for a volcano plot has been presented by Appleby(187,191) for oxygen reduction and is discussed in Section 6.

The OER on various electrodes of practical importance will be discussed next. Because of the historically unique role of Pt, this electrode will receive more attention.

5.2. Kinetics and Mechanisms of the Oxygen Evolution Reaction on Metal and Oxide Electrodes

5.2.1. Platinum

As shown in Section 4, in the potential range relevant to OER the Pt electrode at all values of pH is covered with an oxide layer whose nature (thickness, hydration, ionic, and electronic conductivity) may differ according to the conditions of its preparation and the electrode potential. In the dry state, bulk PtO_2 has been found to have semiconducting properties(192) with a negative temperature coefficient of electronic conductivity and relatively high resistance (10^6 Ω cm for compressed PtO_2 powder at room temperature). According to Damjanovic(181) in acid solutions, for the OER

$$\frac{\partial E}{\partial \ln i} = \frac{2RT}{F} \quad \text{and} \quad \frac{\partial E_{\mathrm{NHE}}}{\partial \mathrm{pH}} = \frac{2.303 \cdot R}{2F} \cong 30\ \mathrm{mV/decade}$$

In a more recent publication(193) Damjanovic and Jovanovic invalidated this latter value and found instead

$$\frac{\partial E_{\mathrm{NHE}}}{\partial \mathrm{pH}} = \frac{2.303RT}{F} \cong 60\ \mathrm{mV/decade}$$

In alkaline solutions according to Damjanovic(181)

$$\frac{\partial E_{\mathrm{NHE}}}{\partial \ln i} = \frac{RT}{F} \quad \text{and} \quad \frac{\partial E_{\mathrm{NHE}}}{\partial \mathrm{pH}} = 2.303 \cdot \frac{2RT}{F} \cong 120\ \mathrm{mV/decade}$$

for low current densities and

$$\frac{\partial E_{\mathrm{NHE}}}{\partial \ln i} = \frac{2RT}{F}, \quad \frac{\partial E_{\mathrm{NHE}}}{\partial \mathrm{pH}} = 2.303 \cdot \frac{3RT}{F} \cong 180\ \mathrm{mV/decade}$$

for high current densities.

The Tafel slope $b = 120$ mV/decade at 25°C suggests that the first charge transfer is the rate-determining step (rds) with all of the following elementary steps fast. The same slope may also be obtained for other rds with the specific assumption of a Temkin adsorption isotherm and high surface concentration of the adsorbed oxygen.(181) Because of the specificity of this assumption and some ambiguity of what should be really understood as a high surface concentration of O_{ad} or OH_{ad} the first mechanistic conclusion is "safer." Some difficulty with respect to the adsorption of an oxygen intermediate arises, however, because of the difficulty of distinguishing between oxygen atoms constituting the oxide film and those which directly participate in the oxygen electrode reactions. At high anodic potentials oxygen strongly bonds with Pt to form a stable oxide phase(194) and hence only part of the oxygen surface atoms are expected to have sufficient mobility to be considered as adsorbed intermediates for OER.(177) The concentrations of only the mobile oxygen atoms or OH radicals should be accounted for in the preexponential term of the kinetic equation. In the case of a Temkin type of adsorption isotherm the total surface concentration of oxygen atoms is effective in changing the free energy of adsorption. Consequently, the activation barrier for the electrode reaction may involve a much greater fraction of the surface oxygen atoms (probably all of them) and therefore the exponential term becomes disputable.

This uncertainty makes the kinetic analysis in terms of Frumkin and Temkin adsorption isotherms also uncertain. As long as there is no clear evidence to the contrary, it may be safer to rely on a simple form of a kinetic equation consistent with the Langmuir adsorption isotherm. Therefore, it is usually accepted that in not too concentrated acids the OER occurs on Pt according to

$$S + H_2O \rightarrow SOH + H^+ + e^- \qquad \text{(rds)} \qquad \text{(XXXIV)}$$

$$4S - OH \leftrightarrow 4S + 2H_2O + O_2 \qquad \text{(fast)} \qquad \text{(XXXV)}$$

where S is an adsorption site on the Pt–oxide.

Assuming a low concentration of the adsorbed intermediate (almost constant preexponential term), the kinetic equation for the anodic reaction is

$$i = 4Fk \exp\frac{\beta FE}{RT} \tag{23}$$

and consequently

$$\frac{\partial E}{\partial \ln i} = \frac{RT}{\beta F}, \qquad \frac{\partial E_{\mathrm{NHE}}}{\partial \mathrm{pH}} = 0 \tag{24}$$

The backreaction to the rds [reaction (XXXIV)] is considered to be usually negligible over the entire potential range accessible to kinetic measurements and hence the steps following it cannot be established from anodic kinetic studies.

The pH dependence found experimentally does not agree with Eq. (24) and this somewhat troublesome fact indicates that the kinetic equation needs some refinements, which will be discussed later in this chapter. In alkaline solutions the various Tafel slopes and pH dependences for low and high current densities may be explained either by different reaction paths or by the same path with a different rds at low and high polarization. According to Damjanovic(181) the latter is more probable for Pt in 1 *M* KOH. This author also suggested that, assuming a Temkin adsorption isotherm, the same reaction path and the same rds may be operative at low and high polarizations with the change of Tafel slope being caused by a change in the surface concentration of an adsorbed intermediate.

More difficult to explain is the pH dependence of the OER overpotential in alkaline solution particularly for high current densities:

$$\frac{\partial E_{\mathrm{NHE}}}{\partial \mathrm{pH}} = -2.303 \cdot \frac{3RT}{F} = \sim 90\,\mathrm{mV/decade} \tag{25}$$

which is not consistent with any mechanism cited by Damjanovic. The experimentally found pH dependences, however, are not necessarily very reliable. Double-layer corrections usually are not introduced and an excess of a supporting electrolyte has often not been used. Furthermore, the surface of the Pt with its anodic film is pH dependent and this can change the concentration and intrinsic properties of the surface sites available for the rds.

Two modelistic approaches have been proposed to account for the hinderance of the OER by the oxide layer on Pt. The first, used by Damjanovic and Jovanovic,(93) involves the concept of a double activation barrier, which was proposed earlier by Meyer for electrode reactions on passivated zirconium(195) and adopted by Macdonald and Conway(196) to analyze the OER on Pd–Au alloys. According to this model the charge transfer is hindered at both the oxide–solution (O/S) interface and the metal–oxide (M/O) interface. It is therefore equivalent to a complex electrode reaction with two rate-limiting steps following one another. The mathematical analysis for steady state conditions starts with two separate equations:

$$i_{\mathrm{M/O}} = 4Fk_1c^m \exp\frac{\beta_1 F\Delta\phi_{\mathrm{M/O}}}{RT} \tag{26}$$

$$i_{\mathrm{O/S}} = 4Fk_2c^n \exp\frac{\beta_2 F\Delta\phi_{\mathrm{O/S}}}{RT} \tag{27}$$

At steady state, both currents are equal: $i = i_{\mathrm{M/O}} = i_{\mathrm{O/S}}$ and the overall potential difference (related to the experimentally controlled electrode potential) is equal to the sum of the two individual potential differences: $\Delta\phi_{\mathrm{M/S}} = \Delta\phi_{\mathrm{M/O}} + \Delta\phi_{\mathrm{O/S}}$, assuming no potential drop in the oxide layer itself. Eliminating individual potential differences from the above rate equations we obtain:

$$i = 4Fkc^p \exp\frac{\alpha FE}{RT} \tag{28}$$

where

$$\alpha = \frac{\beta_1\beta_2}{\beta_1+\beta_2}, \qquad p = \frac{n\beta_1 + n\beta_2}{\beta_1+\beta_2} \tag{29a, b}$$

An important result of the double-barrier model is that the transfer coefficient α in the final kinetic equation is lower than that of either individual transfer coefficient β_1 or β_2. This results in a higher value of the Tafel slope than in traditional single-barrier kinetic equations. The apparent reaction order with respect to the active component whose concentration appears in the kinetic equation is also modified.

The equations based on the double-barrier model were utilized by Damjanovic and Jovanovic to account for their experimental results for OER on Pt in H_2SO_4 solutions and particularly to explain the reaction order with respect to H^+ as equal to $-1/2$, i.e.,

$$\left(\frac{\partial E_{\mathrm{NHE}}}{\partial \mathrm{pH}}\right)_i = -60\ \mathrm{mV} \quad \text{or} \quad \left(\frac{\partial E_{\mathrm{H}}}{\partial \mathrm{pH}}\right)_i = 0 \tag{30a, b}$$

which was found in a rather narrow range of pH: $0.3 \leq \mathrm{pH} \leq 2$. It was also concluded that earlier experimental values of pH dependence found by Damjanovic *et al.*⁽¹⁹⁷⁾ and Bockris and Huq⁽¹⁹⁸⁾ were invalid.

Kinetic equations for which agreement was obtained between experiment and the double-barrier model were

$$i_{\mathrm{M/O}} = A \exp \frac{F\Delta\phi_{\mathrm{M/O}}}{RT} \tag{31}$$

$$i_{\mathrm{O/S}} = B(C_{\mathrm{H}^+})^{-1} \exp \frac{F\Delta\phi_{\mathrm{O/S}}}{RT} \tag{32}$$

with the overall rate equation

$$i = 4Fk(C_{\mathrm{H}^+})^{-1/2} \exp \frac{FE}{2RT} \tag{33}$$

The mechanism for OER on Pt in H_2SO_4 proposed by Damjanovic and Jovanovic⁽¹⁹³⁾ is

$$H_2O \rightleftharpoons OH + H^+ + e^- \qquad \text{(fast)} \qquad \text{(XXXVI)}$$

$$S + OH\cdot \rightarrow S{-}OH \qquad \text{(rds)} \qquad \text{(XXXVII)}$$

$$4S{-}OH \rightleftharpoons 4S + 2H_2O + O_2\uparrow \qquad \text{(fast)} \qquad \text{(XXXVIII)}$$

This mechanism is rather unconventional in assuming the existence of OH· radicals in solution and hindrance of their chemical reaction with the electrode surface. This contradicts the generally recognized instability of OH· radicals in aqueous solutions. In spite of some early efforts to calculate their free energy in aqueous solution^(199,200) and to consider them as bulk phase intermediate products of oxygen electrode reactions, OH· radicals do not appear to have been detected in aqueous electrolytes during O_2 generation. These authors also use a transfer coefficient for the oxide–solution charge transfer of $\beta_2 = 1$ corresponding to a barrierless process,(201) which is questionable.

The nature of the barrier to charge transfer at the metal–oxide interface is open to speculation. Assuming semiconducting properties for the Pt–oxide layer, this additional barrier may simply represent the nonlinear resistance of a metal–semiconductor junction, i.e., resistance of a diode biased in the conduction direction. For high bias voltages, the current–voltage relation for such a junction may be expressed by an equation of the form of Eq. (31).

The experimental data of Damjanovic and Jovanovic(193) do not necessarily require such an unconventional explanation as represented by reactions (XXXVI)–(XXXVIII). There is no indication that these authors attempted a double-layer correction,(202) which may be necessary for the rather dilute acids without supporting electrolyte used in their work. Double-layer effects(203) can produce a substantial change in the reaction order with respect to H^+, particularly in systems involving an electrode surface covered with a chemisorbed oxygen or hydroxide layer or oxide layer.

Another modelistic approach to OER on Pt covered with an oxide layer has been proposed by Schultze and Vetter.(175) They did not analyze in detail the mechanism of OER but rather investigated the influence of the oxide layer thickness (expressed as equivalent charge) and temperature on the OER overpotential. As a theoretical basis of their analysis the Gurney–Gerischer theory of charge transfer(204,205) was used. These workers assumed charge transfer (electron tunneling) between the metal phase and the adsorbed OH^- ions to be the rds:

$$H_2O \rightleftharpoons OH^-_{ad} + H^+ \qquad \text{(fast)} \qquad \text{(XXXIX)}$$

$$OH^-_{ad} \rightarrow OH_{ad} + e^- \qquad \text{(rds)} \qquad \text{(XL)}$$

$$2OH_{ad} \rightleftharpoons O_2 + 2H^+ + 2e^- \qquad \text{(fast)} \qquad \text{(XLI)}$$

The role of the oxide layer in this approach was limited to the modification of the frequency factor for electron tunneling. The probability of electron tunneling and hence the current density is then theoretically expected to be inversely exponentially dependent on the layer thickness. Schultze and Vetter showed experimentally that the current at constant overpotential indeed does decrease exponentially with the increase of the oxide layer thickness, calculated from the charge for the cathodic stripping of the oxide, assuming constant composition and density of this oxide.

The influence of the temperature was mainly attributed to the distribution function of electrons in the adsorbed states. They also predicted the possibility of a break in the Arrhenius plot corresponding to a transfer probability = 1 but this was not confirmed by the experimental data of Bowden for Pt in 0.1 *M* H_2SO_4,(206) utilized by Schultze and Vetter for comparison with the theoretically expected temperature dependence.

The final equation proposed by these authors, accounting for the influence of the oxide layer thickness d and temperature, was

$$\log i = A - \frac{U_{\text{Å}}^{\circ} - \alpha F\eta}{2.3RT} - \frac{d}{d_0} \tag{34}$$

where A is the frequency factor corresponding to the current density at $T \to \infty$ with $d = 0$ ($A \cong 9$), $U_{\text{Å}}^{\circ}$ is the activation energy at $\eta = 0$ ($U_{\text{Å}}^{\circ} = 84.9$ kJ/mol); $d_0 = 1.6$ Å, and $\alpha = 0.63$. The transfer coefficient α in this equation, determined from the slope of the plot of the activation energy (from an Arrhenius plot) vs. electrode potential, agrees well with the value of α determined from the Tafel slope.

The Vetter–Schultze approach attributing the exponential decrease of the reaction rate with increasing oxide thickness (oxygen coverage) to the frequency factor in electron tunneling may be looked upon as an alternative to the traditional approach based on the "absolute rate theory" with the oxide coverage then influencing the effective frequency of activation through a Temkin term. The theoretically predicted dependence between $\log i$ and the concentration of adsorbed oxygen (whether expressed as oxide layer thickness or as oxygen coverage) is the same and it is impossible to differentiate between these two different concepts on the basis of electrochemical measurements. The temperature dependence has not provided additional evidence in favor of one or the other of these approaches.

Iwakura *et al.*(207) have investigated OER on platinum oxide deposited on Ti support by repeated painting of Ti foils with a solution of chloroplatinic acid and heat treatment in air. They identified the oxide obtained in this way as PtO_2. The polarization curves for OER in 1 *M* KOH on such electrodes were quite reproducible from the very beginning in contrast to Pt electrodes,(193,198) which gave reproducible polarization curves only after strong anodization.

The comparison of the PtO_2 electrodes and preanodized Pt as anodes in 1 *M* KOH led these authors to the conclusion that they behave similarly and, hence, that Pt preanodized in alkaline solution is covered with a film of $PtO_2 \cdot nH_2O$. They found two Tafel linear regions for OER on Pt–oxide in 1 *M* KOH at 30°C: $\partial E/\partial \ln i = \sim RT/F$ at low current densities and $\partial E/\partial \ln i = \sim 2RT/F$ at high current densities. The pH dependence differed in these two current density regions, i.e., $(\partial \ln i/\partial \ln a_{\text{KOH}})_{E_{\text{NHE}}} = 2$ at low current densities and $(\partial \ln i/\partial \ln a_{\text{KOH}})_{E_{\text{NHE}}} = 1$ at high current densities. On the basis of these findings, Iwakura *et al.* proposed for the OER on PtO_2 in alkaline solutions a mechanism valid according to them also for preanodized Pt:

step (a) $\quad S + OH^- \rightleftharpoons SOH + e^-$ (XLII)

step (b) $\quad SOH + OH^- \rightleftharpoons SO^- + H_2O$ (XLIII)

step (c) $\quad SO^- \rightleftharpoons SO + e^-$ (XLIV)

step (d) $\quad 2SO \rightleftharpoons 2S + O_2$ (XLV)

This mechanism is essentially the same as the Krasilschikov mechanism(208) and was also suggested by Appleby(188) for oxygen reactions on Pt and other noble metals in alkaline solutions. Krasilschikov proposed it originally for OER on Ni in alkaline solutions. Tafel slopes and pH dependences found by Iwakura *et al.*(207) suggest that at low current densities, reaction (XLVII) is the rds whereas at high current densities reaction (XLVI) is the rds.

To accept this conclusion, analogous to that reached also by Appleby (Ref. 188, p. 429) for the OER on Pt in alkaline, one has to admit that the rate of the *chemical* reaction [step (b)] increases faster with increasing anodic polarization than the rate of charge transfer step (a). The reason for such strong acceleration of the chemical reaction by the electrode potential is not clear.

The prospect of a large-scale industrial application of high current density water electrolysis ("hydrogen economy") has stimulated the investigation of the activity of Pt and other noble metals as anodes for OER at elevated temperatures. Miles *et al.*(39) compared the activity of Pt, Ru, Ir, and their equiatomic alloys in 1 M H_2SO_4 and 1 M CF_3SO_3H at $t = 80°C$. They found that Pt was less active than the other electrodes and also adversely influenced the activity of Ru and Ir in alloys. This effect was attributed to the properties of the oxide layers which have high metallic conductivity on Ru and Ir but the much lower electronic conductivity of a semiconductor or insulator on Pt. The Tafel slopes and exchange currents were the same in both sulfuric and trifluoromethane sulfonic acids (no medium effects) and the mechanism of OER probably did not differ from that at ambient temperature.

5.2.2. Iridium

Iridium is very specific in forming thick, highly capacitive (reversibly reduced and oxidized) anodic layers. This property is attributed to the good electronic and protonic conductivity of these oxide layers, the same properties being beneficial for high electrocatalytic activity of Ir in OER. As earlier cited, Miles *et al.*(209) found much higher activity for Ir than Pt for OER in both H_2SO_4 and CF_3SO_3H. Higher activity of Ir both in acid and alkaline solution was also reported earlier by Buckley and Burke.(211) The rate of the corrosion of Ir, however, was found to increase faster with potential than the rate of OER. Two breaks in the polarization curves at $E_H = 1.55$ V and $E_H = 1.85$ V in 1 M H_2SO_4 were attributed to changes of the mechanism of OER following changes of the oxide layer properties. The Tafel slopes were RT/F and $2RT/F$ for $E_H < 1.57$ V and $E_H > 1.57$ V, respectively. At $E_H \geq 1.8$ V in 1 M H_2SO_4 steady state was reached much faster than at $E_H < 1.8$ V, indicating different properties of the anodic oxide layer on Ir at $E_H < 1.8$ V and $E_H > 1.8$ V. Steady state was not reached in 1 M NaOH although the current density on Ir in this electrolyte was also much higher than on Pt for a given potential. Buckley and Burke suggested that the OER at lower current densities (c.d.) involved the adsorption of an OH intermediate, whereas at high c.d. the OER occurred through decomposition and reconstruction of the oxide layer. They associated the time decay of the current with the OH intermediate adsorption mechanism, whereas the stable values of the current were attributed to the oxide decomposition–reconstruction mechanism.

Earlier results for Ir obtained by Bockris' group are summarized in Damjanovic's review.(181) According to Bockris and his coworkers, both in acids and alkali the OER on Ir gives two linear Tafel regions: for acids and alkali: $\partial E/\partial \ln i = (2/3)(RT/F)$ for low c.d. and $\partial E/\partial \ln i = 2RT/F$ for high c.d.; pH dependence: $(\partial E_{\mathrm{NHE}}/\partial \mathrm{pH})_i = -42$ mV/decade for low c.d., $(\partial E_{\mathrm{NHE}}/\partial \mathrm{pH})_i = -105$ mV/decade for high c.d.

According to Damjanovic these data suggest an electrochemical oxide path(212) which for acids is

$$\mathrm{S} + \mathrm{H_2O} \rightleftharpoons \mathrm{SOH} + \mathrm{H^+} + \mathrm{e^-} \qquad \text{(XLVI)}$$

$$\mathrm{SOH} + \mathrm{S} + \mathrm{H_2O} \rightleftharpoons \mathrm{SO} + \mathrm{SH_2O} + \mathrm{H^+} + \mathrm{e^-} \qquad \text{(XLVII)}$$

$$2\mathrm{SO} \rightarrow \mathrm{O_2} + 2\mathrm{S} \qquad \text{(XLVIII)}$$

with the last reaction the rds at low c.d. and the first at high c.d.

5.2.3. Rhodium

Similarly to iridium, two Tafel linear regions for OER have been reported for rhodium by Damjanovic:(181)

$$\text{acid:} \quad \frac{\partial E}{\partial \ln i} = \frac{RT}{F} \text{ at low c.d.,} \qquad \frac{\partial E}{\partial \ln i} = \frac{2RT}{F} \text{ at high c.d.}$$

$$\text{alkali:} \quad \frac{\partial E}{\partial \ln i} = \frac{2RT}{3F} \text{ at low c.d.,} \qquad \frac{\partial E}{\partial \ln i} = \frac{2RT}{F} \text{ at high c.d.}$$

Damjanovic suggested the same mechanism for the OER on Rh in alkaline as for Ir. For OER on Rh in acids, Krasilschikov's mechanism was suggested(208) or its analog resulting from replacement of $\mathrm{OH^-}$ by water molecules.(212)

5.2.4. Nickel

The OER on Ni in alkaline solutions was studied by, among others, Krasilschikov,(208) and the mechanism known by his name is widely accepted for this system. Miles(213) in a comparative study found that Ni is among the most active catalyst for the OER in alkaline. The electrocatalytic activity may be linked with the magnetic properties of nickel oxides.(214,215) The activity increases above the Neel temperature.(214,215)

5.2.5. Metal Oxides

The OER has been examined on a number of defect metal oxides produced by the thermal decomposition of the metal hydroxide on a salt such as chloride (see, e.g., Refs. 178, 179, and 216–218). The overpotential vs. log *i* data are compared in Figure 15 for various oxides on a titanium substrate in 4 *M* KOH.(247) These oxides have porosity and hence some of the difference between the polarization curves for the various oxides in this figure may be due to differences in the ratios of the true to superficial surface areas. Tafel linearity is observed for some of these oxides over two or three decades. The deviation from Tafel linearity is probably caused by ohmic losses within the oxide or between the oxide and the titanium substrate.

The Tafel slopes for some of the oxides (RuO_2, IrO_2, PdO_2) are 40–50 mV/decade in contrast to the considerably higher Tafel slopes observed on platinum and other noble metals in alkaline electrolytes. This suggests that the rate-controlling step is a second-electron rather than a first-electron transfer. The kinetics are first order in OH^- on RuO_2.(217) O'Grady *et al.*(217,218) have proposed the following mechanism to explain these results:

$$\text{step (a):} \qquad S^{+z} + OH^- \underset{k_{-a}}{\overset{k_a}{\rightleftharpoons}} (SOH)^{+z} + e^- \quad \text{(fast)} \qquad \text{(XLIX)}$$

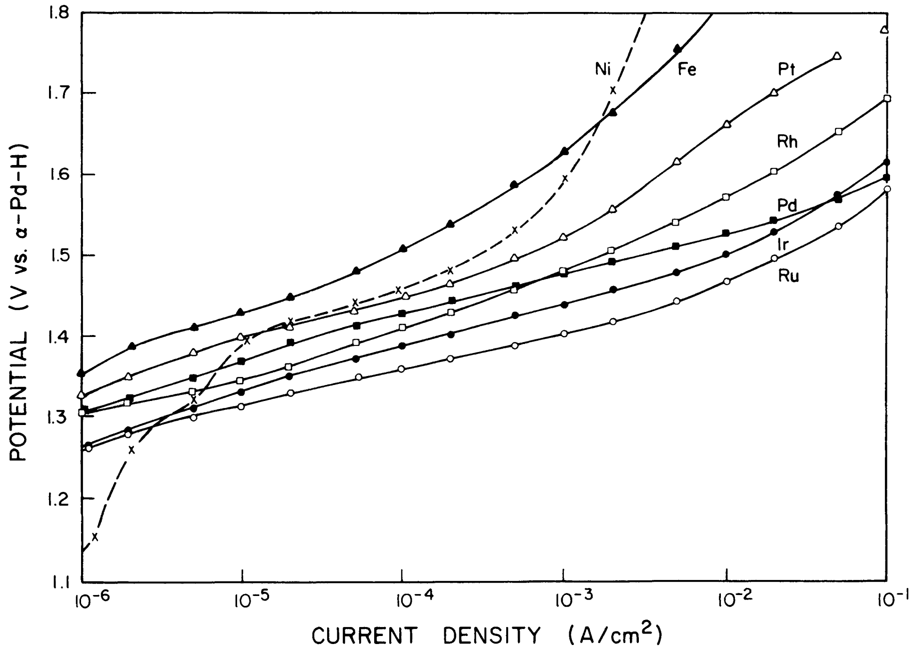

Figure 15. Polarization curves for O_2 generation on various metal oxides produced by thermal decomposition of their salts on a titanium substrate.(218) Measurements recorded with increasing current density in 4 *M* KOH at 22°C.

step (b): $$(\mathrm{SOH})^{+z} \xrightarrow{k_b} (\mathrm{SOH})^{z+1} + \mathrm{e}^- \qquad \text{(rds)} \tag{L}$$

followed by subsequent processes yielding finally O_2 and regenerating the site S^{+z}. As a possibility for such subsequent processes, they suggest

step (c): $$\begin{array}{ccccccccc} (\mathrm{SOH})^{+z+1} & & \mathrm{OH}^- & & \mathrm{S{-}O{-}H\cdots OH^-} & & \mathrm{S}^{+z} & \mathrm{O} & \mathrm{HOH} \\ & + & & \rightarrow & & \rightarrow & + & | & + \\ (\mathrm{SOH})^{+z+1} & & \mathrm{OH}^- & & \mathrm{S{-}O{-}H\cdots OH^-} & & \mathrm{S}^{+z} & \mathrm{O} & \mathrm{HOH} \end{array} \tag{L1}$$

With electrode surfaces involving species with predominantly ionic character, it is appropriate to write the mechanism so as to indicate the changes in the effective valency state of the catalyst sites. With RuO_2, the sites are probably Ru^{+4}. The sites are undoubtedly hydrated and step (a) probably involves the loss of a proton from a water bound to S^{+z} to yield an OH^-(ads). Alternatively step (a) may proceed through an S_N2-type mechanism with an intermediate state involving the expansion of the inner coordination sphere of Ru to 7, as suggested by O'Grady *et al.*(217) Somewhat analogous solution phase reactions involving polymeric Ru complexes appear to proceed through S_N2 mechanisms.(219,220)

With step (b) rate controlling, negligible backreaction and the coverage of $(SOH)^{+z}$ and $(SOH)^{+z+1}$ both low, the current density i is

$$i = 4F \cdot \frac{k_a k_b}{k_{-a}} (C_{\mathrm{OH}^-}) \cdot \exp \frac{(1 + \beta_b)FE}{RT} \tag{35}$$

where k_a, k_{-a}, and k_b are rate constants and β_b is the transfer coefficient for step (b). With $\beta_b = 1/2$, the Tafel slope at 25°C is 0.04 V/decade.

6. Cathodic Reactions of Oxygen (Oxygen Cathodes)

The electrochemical reduction of molecular oxygen on different electrode materials has been studied extensively during the last 20 years principally in connection with electrochemical energetics. Oxygen electroreduction is a multielectron reaction and may include a number of elementary steps forming various parallel–consecutive combinations.

6.1. The General Scheme of Parallel and Series Reactions of Oxygen and Hydrogen Peroxide

Much of the progress in the investigation of possible parallel–consecutive courses of the oxygen reduction reaction is due to the application of the disk–ring method proposed by Frumkin and Nekrasov.(221) The hydrodynamic theory of this method has been reviewed by various authors.(222–225) Mueller and Nekarasov were the first to use the rotating disk–ring method to study O_2 reduction.(226) The O_2 reduction was carried out on the disk while the H_2O_2 was monitored on the ring which was maintained at a potential sufficiently positive to oxidize the peroxide back to O_2 at the diffusion limiting current. Damjanovic *et al.*(227) proposed a diagnostic criterion, based on the rotation dependence of the disk–ring current data, for distinguishing between whether O_2 reduction proceeds through hydrogen peroxide as an intermediate (series mechanism) or whether there is also a parallel four-electron multiple step process leading to H_2O or OH^- without H_2O_2 as an intermediate. Their analysis, however, was restricted to a relatively simple treatment and not sufficiently general.

Later, after substantial rotating disk–ring data were available for O_2 reduction on various electrode materials, Bagotskii *et al.*(228,229) proposed a more general scheme for the series (consecutive)–parallel reactions of O_2 and H_2O_2, i.e.,

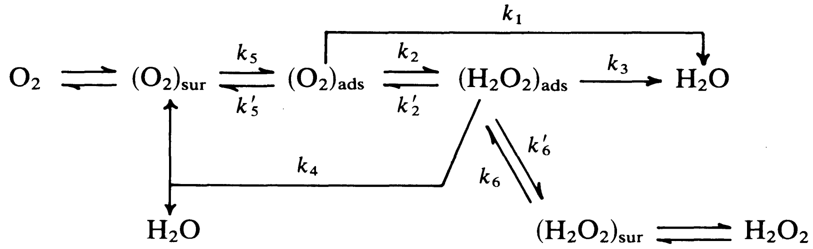

In this reaction scheme, O_2, $(O_2)_{sur}$, and $(O_2)_{ads}$ correspond to molecular O_2 in the bulk solution, in the solution adjacent to the electrode surface, and in the adsorbed state, respectively. The O_2 can be electrochemically reduced either directly to water with the constant k_1 without the intermediate formation of hydrogen peroxide or to hydrogen peroxide (k_2). The adsorbed hydrogen peroxide $(H_2O_2)_{ads}$ can be reduced to water (k_3), oxidized back to O_2 (k'_2), catalytically decomposed on the electrode surface (k_4), or desorbed and diffuse into the bulk of the solution. The constants k_5, k'_5 and k_6, k'_6, are for the adsorption and desorption of O_2 and H_2O_2, respectively. This scheme takes into consideration the heterogeneous decomposition of hydrogen peroxide which can occur electrochemically through coupled oxidation and reduction reactions with electron transfer through the electrode phase and/or nonelectrochemically through a disproportionation reaction involving a direct electron transfer between two $(H_2O_2)_{ads}$ species and not through the electrode phase. In the reaction scheme (LII), the direct $4e^-$ pathway corresponding to k_1 may still proceed through an adsorbed peroxide intermediate but this adsorbed species does not lead to a solution phase peroxide.

Isotopic experiments with ^{18}O in O_2, H_2O_2, and H_2O have played an important role in substantiating this scheme. The investigations on various surfaces(230–233) indicate that all of the peroxide oxygen originates from O_2 and not H_2O or OH^- in the reduction of O_2 to H_2O_2. The experiments with nonequilibrium mixtures of ^{18}O–^{18}O, ^{18}O–^{16}O, and ^{16}O–^{16}O show that both

O atoms in the H_2O_2 come from the same O_2 molecule. Similar isotopic experiments have also been carried out for the heterogeneous decomposition reaction of H_2O_2 on platinized-platinum on open circuit:

$$2H_2O_2 \rightarrow 2H_2O + O_2 \quad \text{or} \quad 2HO_2^- \rightarrow 2OH^- + O_2 \tag{LIII}$$

In pure 1 M KOH and 0.05 M H_2SO_4, the isotopic distribution in the O_2 remains within 10% of the nonequilibrium distribution in the H_2O_2, indicating again that the two oxygens in the O_2 molecule mostly originate from just one of the H_2O_2 molecules. The most likely explanation for this behavior is that reaction (LIII) proceeds principally through coupled electrochemical reactions, i.e., in acid solution

$$H_2O_2 \xrightarrow{k_2'} 2H^+ + O_2 + 2e^- \tag{LIV}$$

$$H_2O_2 + 2H^+ + 2e^- \xrightarrow{k_3} 2H_2O \tag{LV}$$

A possible alternative or competing reaction to (LV) is the overall $4e^-$ reduction of the O_2 produced by reaction (LIV) through a pathway not involving the solution phase peroxide, i.e.,

$$1/2O_2 + 2H^+ + 2e^- \xrightarrow{k_1} H_2O \tag{LVI}$$

The overall peroxide decomposition reaction would still be the same. The electrons in these reactions are assumed to be transferred through the electrode phase.

Tarasevich *et al.*(232,233) have investigated the shift of the isotopic distribution from the nonequilibrium distribution in the O_2 gas produced by peroxide decomposition in both pure 1 M KOH and 0.05 M H_2SO_4 on platinum black. With the addition of alkali earth cations to the 1 M KOH the isotopic distribution shifts further toward equilibration while the addition of $H_2PO_4^-$ or Cl^- to the 0.05 M H_2SO_4 produces small shifts in the reverse direction (see Table 4). These workers have interpreted the partial equilibration as evidence for a second pathway for the heterogeneous decomposition and

Table 4

Fraction (A) of O_2 Gas Produced in the Decomposition of Hydrogen Peroxide on Platinized Platinum Originating from Two Different Peroxide Molecules Rather than Just a Single Peroxide Molecule(232,233)

Electrolyte composition	A, %	Electrolyte composition	A, %
1 M KOH	10	0.05 M H_2SO_4	8
1 M KOH + 10^{-2} M $Ca(OH)_2$	14	0.05 M H_2SO_4 + 0.03 M H_3PO_4	6
1 M KOH + 10^{-2} M $Sr(OH)_2$	20	0.05 M H_2SO_4 + 0.01 M HCl	5.2
1 M KOH + 10^{-2} M $Ba(OH)_2$	50		

propose that this pathway may be nonelectrochemical, e.g., a direct surface reaction between two peroxide molecules.

The so-called direct four-electron reduction of O_2 to H_2O corresponding to k_1 in reaction (LII) probably proceeds through an intermediate step involving the dissociative chemisorption of molecular O_2. Unfortunately proof of the dissociative chemisorption of the molecular oxygen is absent at present, at least under electrochemical conditions. The low-temperature homomolecular oxygen exchange on the gas–solid interface(165–167) provides evidence that the dissociative chemisorption of molecular oxygen of the electrode surface is possible. On the other hand, it is quite possible that on some surfaces the four-electron reduction corresponding to k_1 in reaction (LII) may proceed through an adsorbed superoxide and/or peroxide state. If a peroxide state is involved, this reaction pathway with the rate constant k_1 would then be distinguishable from the series sequence with the rate constants k_5, k_5', k_2, k_2', k_3 only in that the adsorption sites are such that the peroxide does not desorb to any appreciable extent before cleavage of the O–O bond.

The analysis of the parallel–series reactions according to this scheme has been developed for the rotating disk–ring method by Bagotskii *et al.*(228,229) The equations relating the ratio of currents at the disk (I_D) and the ring (I_R) to the electrode rotation rate ω are as follows:

$$\left(\frac{I_D}{I_R}\right)N = \frac{I_D}{I_B} = 1 + 2\frac{k_1}{k_2} + \left[\left(1 + 2\frac{k_1}{k_2}\right)(k_2' + k_3 + k_4) + (k_3 - k_2')\right]\frac{1}{k_6'} + \left[\left(1 + 2\frac{k_1}{k_2}\right)(k_2' + k_3 + k_4) + (k_3 - k_2')\right]\frac{k_6}{k_6'}\frac{1}{\gamma_B\sqrt{\omega}} \tag{36}$$

$$\frac{I_A^\circ - (I_D + I_B)}{I_B} = 2\left(\frac{\gamma_A}{\gamma_B}\right)\left(\frac{k_5'}{k_5}\right)\left(\frac{k_6}{k_6'}\right)\left[\left(1 + \frac{k_1' + k_2}{k_5'}\right)\frac{(k_2' + k_3 + k_4)}{k_2} - \frac{(k_4 + 2k_2')}{2k_2}\frac{k_2}{k_5'}\right] + \left[\left(1 + \frac{k_1 + k_2}{k_5'}\right) + \left(1 + \frac{k_2' + k_3 + k_4}{k_6'}\right)\frac{k_5'}{k_2} - \frac{k_4 + 2k_2'}{2k_6'}\right]\frac{k_5'}{k_5}\frac{2\gamma_A\sqrt{\omega}}{k_5'} \tag{37}$$

where I_B is related to the ring current by the relation $I_B = I_R/N$, where N is the collection efficiency. I_A° is the diffusion-limiting current density if all O_2 reaching the disk undergoes a four-electron reduction. The coefficients γ_A and γ_B relate the diffusion-limiting currents for O_2 and H_2O_2 to the concentrations and rotation rates, i.e.,

$$I_A^\circ = 4F\gamma_A C_A^\circ\sqrt{\omega} \tag{38}$$

and

$$I_B^\circ = 2F\gamma_B C_B^\circ \sqrt{\omega} \tag{39}$$

where the subscripts A and B refer to O_2 and H_2O_2, respectively. The experimental disk–ring data can be represented graphically by plotting I_D/I_B vs. $\omega^{-1/2}$ and $[I_A^\circ - (I_D + I_B)]/I_B$ vs. $\omega^{1/2}$. From these linear plots the slopes and intercepts on the ordinate can be obtained. Typical plots of I_D/I_R are shown in Figures 16 and 17 for Au and Pt electrodes. Similar data to that for Pt in Figure 17 have been reported for Rh in KOH.(238)

Damjanovic *et al.*(227,234) have stated that I_D/I_B vs. $\omega^{-1/2}$ plots having intercepts greater than 1.0 are proof that the parallel mechanism is operative. The analysis of Bagotskii *et al.*,(229) however, shows that the number of rate constants involved in the reaction scheme is greater than the number of

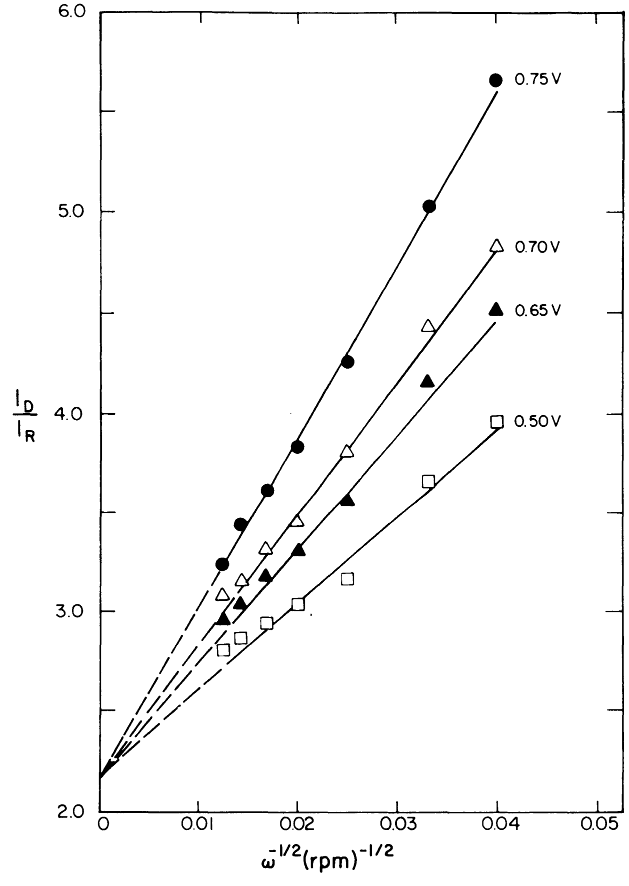

Figure 16. Rotating disk–ring electrode data(237) for O_2 reduction on gold in 0.1 *M* NaOH at 25°C. I_D/I_R vs. $\omega^{-1/2}$ at various disk potentials. Au ring potentiostated at E_H = 1.1 V. N = 0.43.

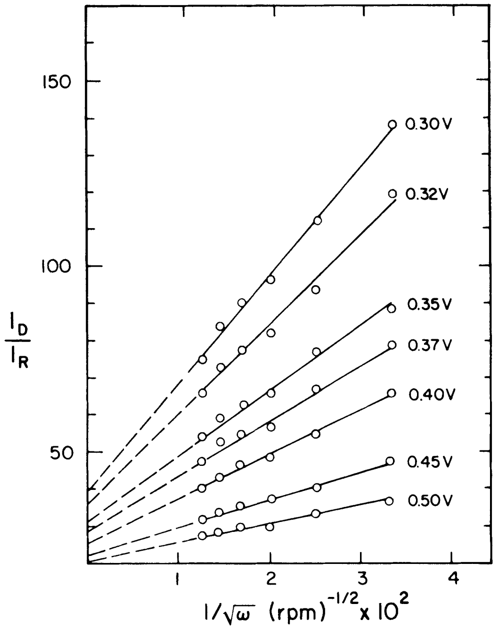

Figure 17. Rotating disk–ring electrode data[237] for O_2 reduction on platinum in 85% H_3PO_4 at 25°C. I_D/I_R vs. $\omega^{-1/2}$ at various disk potentials. Pt ring potentiostated at $E_H = 1.2$ V. $N = 0.40$.

independent equations (see also Ref. 235). Therefore, it is impossible to determine all the above-mentioned constants from rotating disk–ring electrode data for O_2 reduction alone. It is clear from Eq. (36) that intercepts greater than 1.0 can be observed even when the O_2 reduction proceeds only through intermediate formation of hydrogen peroxide ($k_1 = 0$) but the transfer of hydrogen peroxide from the electrode surface to the solution is controlled by the rate of its desorption (k'_6, k_6). This means that within this reaction scheme it is not possible by means of the rotating ring–disk electrode to determine the role of the adsorption stages in the reactions of oxygen and hydrogen peroxide and to prove necessarily that oxygen reduction occurs via k_1 rather than just by k_2 plus k_3 and/or k_4.

Wroblowa *et al.*[235] have used a somewhat simpler reaction scheme which does not consider explicitly an adsorbed $(O_2)_{ads}$ state but does take into account the possibility of slow desorption of H_2O_2. The scheme is as follows:

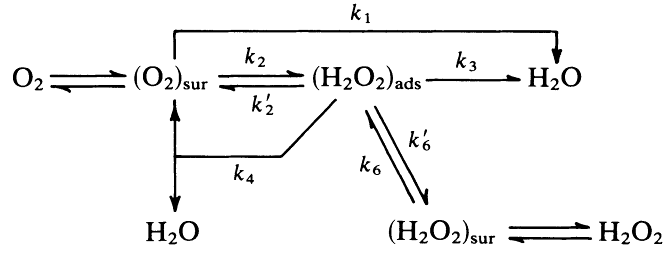

(LVII)

This scheme yields the equation

$$\frac{NI_D}{I_R} = \frac{I_D}{I_B} = 1 + 2\frac{k_1}{k_2} + A + \frac{k_6}{\gamma_A \omega^{1/2}} \cdot A \tag{40}$$

where

$$A = (2k_1/k_2k_6')(k_2' + k_3 + k_4) + (2k_3 + k_4)/k_6' \tag{41}$$

For the series mechanism with peroxide as an intermediate, Eq. (40) reduces to

$$\frac{NI_D}{I_R} = \frac{I_D}{I_B} = 1 + \frac{2k_3 + k_4}{k_6'} + \frac{k_6}{\gamma_A} \cdot \frac{2k_3 + k_4}{k_6'} \cdot \frac{1}{\omega^{1/2}} \tag{42}$$

If an intercept of 1 is obtained, this verifies the series process but a potential-dependent intercept can still be obtained with the series process if the term $(2k_3 + k_4)/k_6'$ is appreciable compared to 1. Equation (40) predicts for the parallel processes that the slopes and intercepts from the I_D/I_B vs. $\omega^{-1/2}$ plots are related by the equation

$$J = 1 + \frac{2k_1}{k_2} + \frac{S\gamma_A}{k_6} \tag{43}$$

where J and S are the ordinate intercepts and slopes at various potentials. For the series process Eq. (42) predicts

$$J = 1 + \frac{S\gamma_A}{k_6} \tag{44}$$

If k_1 and k_2 have the same potential dependence and the potential dependence of k_6 is small, Eq. (43) predicts a linear relation between J and S with the intercept depending on the ratio k_1/k_2. On the other hand, Eq. (44) predicts a linear relation between J and S with an intercept of 1. Figure 18 shows such a plot for Pt in 85% H_3PO_4, prepared from the data in Figure 17. The intercept is much greater than unity, thus providing evidence for the parallel mechanisms with $k_1/k_2 = \sim 2$.

The Wroblowa treatment has two less rate constants than that of Bagotskii *et al.*(229) Even so, the seven rate constants in the Wroblowa treatment still exceed what can be obtained from a treatment of the disk–ring data as a function of rotation rate. Van den Brink, Barendrecht, and Visscher(241) have proposed measurements with just H_2O_2 and no O_2 in solution in order to obtain five rate constants in a reaction scheme similar to that of Damjanovic *et al.*(227,234) which omits the $(H_2O_2)_{ads}$ state and does not consider slow desorption of H_2O_2.

Despite the impossibility of obtaining all of the rate constants in the reaction scheme (LII), the careful examination of the experimental data and the character of the influence of chemisorbed oxygen and ions on the mechanism of molecular oxygen reduction enables one to draw some qualitative conclusions and to gain some insight as to the course of the reaction. Let us discuss some examples which characterize the present state of this problem.

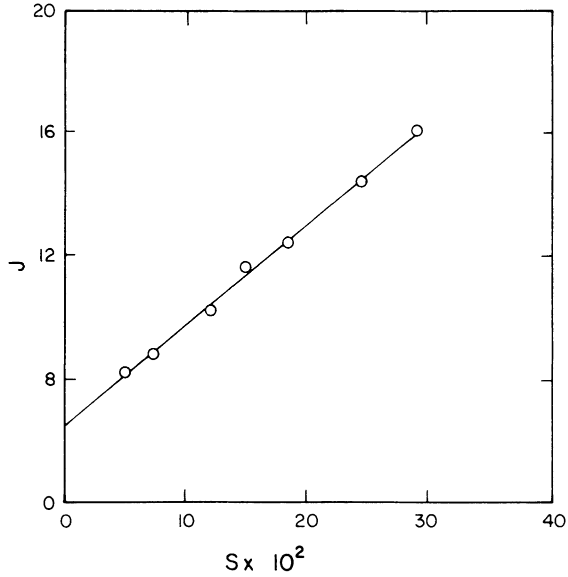

Figure 18. Plot of the intercepts vs. slopes for the disk–ring electrode data(237) in Figure 17 for O_2 reduction on Pt in 85% H_3PO_4 [see eq. (43)].

For molecular oxygen reduction on the gold electrode in alkaline solutions the plots of I_D/I_B vs. $\omega^{-1/2}$ yield intercepts ranging from 1.0 (Ref. 236, see Figure 16) to 7.(239) The higher intercepts may reflect impurity problems. All these authors, however, have concluded the series mechanism to be involved, having taken into consideration the slow desorption of the hydrogen peroxide from the electrode surface. This conclusion is in agreement with the results obtained for the direct reduction of H_2O_2 on gold.(236,237,238)

On platinum and platinum family metals, the O_2 reduction appears to occur by the parallel mechanism with the direct four-electron reduction to water predominant in both acid and alkaline electrolyte in the absence of impurities. Evidence to support this conclusion is to be found in the influence of surface chemisorbed oxygen species (Pt–OH or Pt–O), adsorbed anions, and other adsorbed species on the extent to which the O_2 reduction proceeds to water and to H_2O_2. In rotating disk–ring electrode studies, the intercepts in the I_D/I_B vs. $\omega^{-1/2}$ plots have been found to be greater than unity and potential dependent in both alkaline and acid (Figure 17) electrolytes. This provides evidence for a parallel mechanism scheme provided the adsorption–desorption of H_2O_2 are fast. Further support for the parallel mechanism is the finding that the plots of these intercepts vs. the slopes from the I_D/I_B vs. $\omega^{-1/2}$ plots are linear (Figure 18) in accord with Eq. (43) with the intercept term $1 + (2k_1/k_2)$ large compared to unity.(237)

The increase of the surface coverage θ_O by chemisorbed oxygen formed during the discharge of water molecules inhibits the reduction of molecular oxygen directly to water on platinum(242) and palladium electrodes.(243) The rate of the reaction yielding intermediate formation of hydrogen peroxide

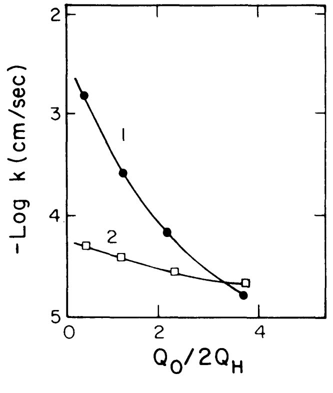

Figure 19. Rate constants k_1 and k_2 for O_2 reduction on a palladium electrode in 0.05 M H_2SO_4 at $E_H = 0.8$ V as a function of the amount of chemisorbed oxygen calculated from the ratio $Q_O/2Q_H$.(243)

decreases more slowly (Figure 19) with increasing total surface coverage (θ_O) with O. Similar results have been obtained on the silver electrode.(244) In a study of the effects of adsorbed anions and cations on oxygen reduction on Pd, an increase of their specific adsorbability has been found to produce a decrease in the rate of O_2 reduction with a preferential decrease for the reaction going directly to water.(245) The same effect is produced on oxygen reduction on platinum by the organic cation of tetrabutylammonium sulfate.(246) The simplest and most logical explanation of these results is that the increase in surface coverage of the electrode by chemisorbed oxygen and by other strongly bonded species leads to a decrease in the number of sites with high bond energy which are available for the dissociative chemisorption of molecular oxygen. Dual adsorption sites may be involved in the dissociation of O_2 while single adsorption sites may be sufficient for the pathway yielding peroxide. Thus the four-electron pathway would be expected to be second order in available sites and hence more adversely affected by the adsorption of O, OH, and other strongly adsorbed species.

The formation of the chemisorbed oxygen layer is dependent on the prior potential treatment and time. This allows one to explain the discrepancies between some literature data, especially in the case of work done without automatic control of the potential of the disk and the ring electrodes and programmed potentiodynamic treatment of the disk.

An analysis of literature results allows one to divide the metallic electrode materials into two groups. The first involves electrodes on which the O_2 reduction proceeds predominantly through intermediate hydrogen peroxide formation while the second involves parallel mechanisms (i.e., both the four-electron and two-electron reductions). Mercury,(247,248) pyrographite,(249-252,255) and other different types of the carbon materials,†(249,251-254) and gold(235,236,239,240) are classified in the first group.

---

† The inclusion of pyrographite with metallic electrode is logical because the band gap in graphite is negligibly narrow and graphite behaves essentially as a metal conductor. On the other hand, the surface chemical structure of carbonic materials is very important for the electrocatalysis. This will be examined in Section 6.3.

The electroreduction of the molecular oxygen occurs only through the intermediate formation of hydrogen peroxide.† The polarization curves are characterized by two waves. The first wave corresponds to the oxygen reduction to H_2O_2. The hydrogen peroxide is reduced in the second wave with a high overpotential. In some instances it is difficult to distinguish the second wave because of the extreme irreversibility of the H_2O_2 reduction.

Platinum,(234,237,242,246) platinum family metals,(238,243,245) and silver(244) are classified in the second group. The oxygen electroreduction on these metals occurs both directly to water and via intermediate formation of hydrogen peroxide. The hydrogen peroxide formed in the parallel reaction is decomposed by chemical or electrochemical mechanisms. The relation between the rates of these processes depends in a complicated way on the nature of the metal, the potential, the coverage of the electrode by the chemisorbed species, and their adsorption character. The polarization curves are characterized by a single wave with a limiting current close to the diffusion current for the four-electron process.

A simple qualitative explanation of this distinction between the first and second groups may be a different affinity of these materials for molecular oxygen and hydrogen peroxide. Apparently, in the case of the first group of the electrodes this affinity is low and it is not sufficient to break the O–O bond.

6.2. The Kinetics of Molecular Oxygen Reduction on Different Metallic Electrodes

The kinetics and mechanism of the oxygen reduction are simpler for the first group of electrodes. We shall use as an example the pyrolytic graphite electrode which has been studied extensively.(250–252,255) The Tafel slopes found by Tarasevich *et al.*(255) are listed in Table 5. In acid solution, the Tafel slope is −0.14 to −0.16 V/decade. In acid solution, the oxidation of H_2O_2 occurs at an appreciable rate only at potentials at least 0.4 V more positive than the reversible value for the O_2–H_2O_2 couple. In alkaline electrolytes, Tarasevich *et al.*(255) have observed two distinct cathodic Tafel slopes. At relatively low polarizations, the Tafel slope is ~ −0.03 V/decade. Further, at low polarization in alkaline solutions

$$(\partial E/\partial \log C_{HO_2^-})_i = (\partial E/\partial \log p_{O_2})_i = 0.029 \text{ V/decade}$$

at 25°C(25) and the polarization curves for O_2 reduction and peroxide oxidation pass into one another continuously near the steady state open-circuit potential (see Figure 20).

Tarasevich *et al.*(255) have found that the pH dependence of the potential at constant reduction current differs at different current densities. With i =

---

†An exception is carbon materials in strong acidic media(253,254) and possibly high-area carbons in alkaline electrolytes(256) where the parallel mechanisms have been reported.

Table 5
Values of Tafel Slopes for O_2 Reduction on Pyrolytic Graphite at ~ 25°C Solutions with Different pH(255)

Composition of solution	pH	$\partial E/\partial \log i$, V/decade Region of low polarization	 Region of high polarization
1 N H_2SO_4	0.3	—	0.170
0.6 N H_2SO_4 + 0.4 N K_2SO_4	1.4	—	0.160
0.2 N H_2SO_4 + 0.8 N K_2SO_4	1.8	—	0.160
0.1 N H_2SO_4 + 0.9 N K_2SO_4	2.2	—	0.160
0.01 N H_2SO_4 + 0.99 N K_2SO_4	3.2	—	0.145
0.005 N H_2SO_4 + 0.995 N K_2SO_4	4.2	—	0.140
0.001 N KOH + 0.999 N K_2SO_4	10.6	0.024	0.130
0.01 N KOH + 0.99 N K_2SO_4	12.1	0.025	0.110
0.1 N KOH + 0.9 N K_2SO_4	13.0	0.035	0.075
0.1 N KOH	14.0	0.030	0.080

$0.5i_D$ (i_D = diffusion-limiting current), the potential remains constant in the pH interval from 1.5 to 14 (Figure 21). Similar behavior has been observed in acid solutions at low current densities. In alkaline solutions at low current densities (where the slope of the polarization curve is close to −0.03 V/decade) increasing the pH displaces the potential toward negative values. Similar results have been reported also for oxygen electroreduction on carbon black(254) and on gold. These effects are also generally similar to those reported for the reduction of oxygen on mercury.(247)

Somewhat different results have been obtained by Morcos and Yeager on pyrolytic graphite(250) and Yeager *et al.* on other carbons.(249) In contrast to the results of Tarasevich *et al.*(255) only one Tafel slope of −0.12 V/decade has been observed in 1 M KOH with a stoichiometric number of 2.0 and a

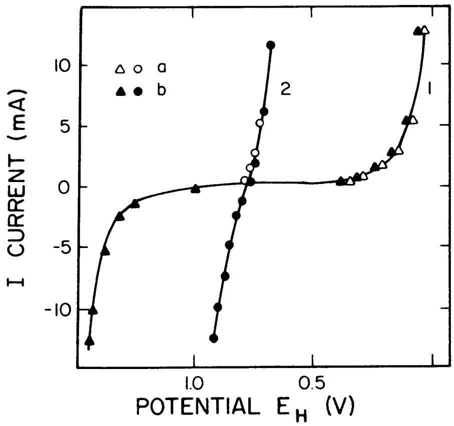

Figure 20. Anodic and cathodic polarization curves on the pyrographite electrode in O_2 saturated solutions, according to Tarasevich *et al.*(255) Curve 1: pH 3.2; curve 2: pH 12.1. △, ○, without H_2O_2 added; ▲, with 10^{-2} M H_2O_2; ●, with 2×10^{-3} M H_2O_2.

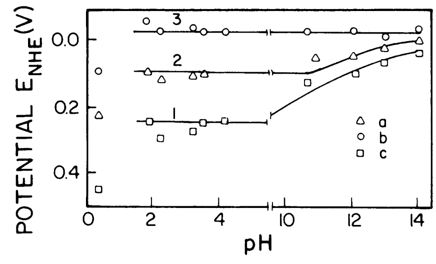

Figure 21. Oxygen reduction on pyrographite according to Tarasevich *et al.*(255) Potential vs. pH at various fractions of the limiting current i_D. Curve 1: $(1/80)i_D$; curve 2: $(1/8)i_D$; curve 3: $(1/2)i_D$.

zero reaction order with respect to C_{OH^-} at pH ≥ 12. This discrepancy in Tafel slopes may be caused by differences in the surface properties of the carbons and graphites. Morcos and Yeager(250) have examined O_2 reduction on stress annealed pyrolytic graphite and found that the O_2 reduction proceeds with a Tafel slope of −0.12 V/decade on the edge plane but is very depressed on the basal plane (see Section 6.3).

Zurilla *et al.*(236) have reported kinetic data for O_2 reduction and peroxide oxidation on gold in akaline solutions which indicate that the Tafel slopes for the O_2 reduction to peroxide as well as the reverse oxidation process are both numerically −0.12 V/decade at 25°C in ultrapure solutions without any platinum contamination.† As with the pyrolytic graphite the stoichiometric number is 2.0 with the reduction reaction first order in O_2 and zero order in OH^- in alkaline solutions over the pH range examined (11.5–12.7). This implies a mechanism similar to that on pyrolytic graphite in alkaline solutions, based on the data of Morcos and Yeager.(250)

Two mechanisms have been proposed in the literature for O_2 reduction on carbon and gold. According to some investigators(253–255) the O_2 reduction proceeds as follows:

step 1: $$S + O_2 \rightarrow S{-}O_2 \tag{LVIII}$$

step 2: $$S{-}O_2 + e^- \rightarrow S{-}O_2^- \tag{LVIX}$$

step 3: $$S{-}O_2^- + H_2O + e^- \rightarrow S + HO_2^- + OH^- \tag{LX}$$

with the retardation of step 1 both in the cathodic and anodic directions. The equation for the polarization curve at low S–O_2 coverage has the form(255)

$$i = \frac{i_D}{1 + (D/\delta)(1/k)\exp(\alpha FE/RT) + [1/C_H + (C_H^+ + K)]\exp[2F(E - E_0)/RT]} \tag{45}$$

---

† Many studies of O_2 reduction have been carried out with Pt counter and/or preelectrolysis electrodes. This leads to contamination of the electrolyte and hence the working electrode with platinum.(236)

where i_D is the diffusion limiting current density for O_2 reduction, D/δ is the diffusion parameter, K the dissociation constant of H_2O_2, and E_0 the standard reversible potential of the couple O_2/H_2O_2. The only quantities which cannot be determined by independent measurements are the transfer coefficients α and the rate constant for the cathodic reaction k. Having determined these values from measurements in one solution, it is possible to calculate the complete polarization curves in other solutions—both acid and alkaline—and the dependence of the potential on the pH. The calculated curves in the pH range from 1.5 to 14 agree satisfactorily with the experimental results in Figure 21. At $\text{pH} < 10$ the reduction of oxygen is controlled by step 1. At more alkaline pH and at relatively low current densities, the system O_2/H_2O_2 approaches equilibrium, and with increasing pH, E is displaced towards negative values.

The pathway represented by reactions (LVIII)–(LX) has a stoichiometric number of 1 and therefore is in conflict with the stoichiometric number of 2.0 found by Morcos and Yeager(250) for pyrolytic graphite and Zurilla *et al.*(236) for gold in carefully purified alkaline solutions. It also is incompatible with the reaction orders found by the latter authors for the oxidation of HO_2^- to O_2 on gold in 0.1 *M* NaOH (i.e., 1/2 order with respect to both OH^- and HO_2^-).

Morcos and Yeager(250) have proposed a pathway for O_2 reduction on graphite with the first two steps the same as reactions (LVIII) and (LVIX) but with the final peroxide producing step a surface dismutation reaction

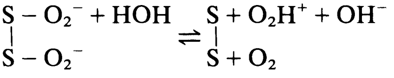

$$\begin{array}{l} S - O_2^- + HOH \\ | \\ S - O_2^- \end{array} \rightleftharpoons \begin{array}{l} S + O_2H^+ + OH^- \\ | \\ S + O_2 \end{array} \qquad \text{(LXI)}$$

Reaction (LVIX) is rate controlling at potentials in the Tafel range and results in the Tafel slope of -0.12 V/decade, while reaction (LVIII) becomes controlling at high cathodic polarization. Zurilla *et al.*(236) have proposed essentially the same mechanism for gold except that they did not find any evidence of a rate-controlling adsorption step preceding the first charge transfer step and hence they write reactions (LVIII) and (LVIX) as a single step in their kinetic analysis, i.e.,

$$S + O_2 + e^- \rightarrow S - O_2^- \qquad \text{(LXII)}$$

With reaction (LXII) slow and reaction (LXI) fast and with the surface coverage of $S\text{–}O_2^-$ small, the potential–current density relationship for both the O_2 reduction to peroxide and peroxide oxidation to O_2 is

$$\eta = \frac{RT}{\alpha_1 F}\ln\frac{(i_0)_1}{i_D} - \frac{RT}{\alpha_1 F}\ln X \qquad (46)$$

where

$$X = \frac{i/(i_D - i)}{1 - [i_D(i_d + i)/i_d(i_D - i)]^{-1/2} \exp(F\eta/RT)} \tag{47}$$

where η is the overpotential for the O_2–HO_2^- couple, i_D and i_d are the diffusion-limiting current densities for O_2 reduction and HO_2^- oxidation, respectively, $(i_0)_1$ and α_1 are the apparent exchange current density and transfer coefficient for reaction (LXII), and i is positive for a net reduction reaction and negative for a net oxidation reaction. Equations (46) and (47) fit the data for Au in NaOH–HO_2^- solutions very well as is evident in Figure 22.

The dismutation reaction (LXI) is rather surprising. Since the rate of the reverse of reaction (LXII) is negligible at substantial cathodic overpotentials ($\eta < 0.1$ V), reaction (LXI) is not just the simple electrochemical oxidation of the superoxide S–$O_2^{\cdot}$ coupled with its further reduction. Further, it is unlikely that reaction (LXI) proceeds by the desorption of $O_2^{\cdot}$ followed by a second-order homogeneous reaction in the solution phase, i.e.,

$$2O_2^{\cdot} + H_2O \rightarrow HO_2^- + OH^- + O_2 \tag{LXIII}$$

The experimental data show that two electrons per O_2 are transported through the Nernst layer in the rotating disk experiments. Consequently, reaction (LXIII) would need to proceed sufficiently fast to be essentially complete within a distance small compared to the Nernst diffusion layer thickness. Thermodynamics imposes an upper limit on the $O_2^{\cdot}$ concentration adjacent to the electrode, using the value of $E^\circ_{\text{NHE}} = -0.30$ V for the O_2–$O_2^{\cdot}$ couple (see Figure 1). At a potential, for example, of $E_{\text{NHE}} = -0.80$ V(287) the upper limit for the $O_2^{\cdot}$ concentration (calculated from the Nernst equation) is $\sim 10^{-3}$ *M*. The upper limit for the second order rate constant for reaction (LXIII), however, has been found(259) to be $100\,M^{-1}\,\text{sec}^{-1}$. Assuming that the reaction must occur in an electrolyte layer of $X = 10^{-3}$-cm thickness, the upper limit on the rate of reaction (LXIII), expressed in units of current density, is 1×10^{-5} A/cm^2. The observed current density i_1 at this potential and a rotation rate of 2500 rpm is 1.8×10^{-3} A/cm^2 or two orders of magnitude greater. It appears, therefore, that reaction (LXI) is a surface process involving the direct interaction of two $O_2^{\cdot}$ adsorbed radicals.

In spite of the difference between these two mechanisms, the assumption of a rate-controlling first electron transfer to yield an adsorbed $O_2^{\cdot}$ explains the basic features of a reduction of molecular oxygen on the first group of electrode materials. Sawyer *et al.*,(260,261) however, have concluded that this one-electron reduction of O_2 to $O_2^{\cdot}$ is essentially reversible and not sensitive to the electrode material. This is not borne out by the experimentally measured rate constants for the first electron transfer, measured on electrode materials in the first group (see Table 6).(262) Nonetheless the question persists as to

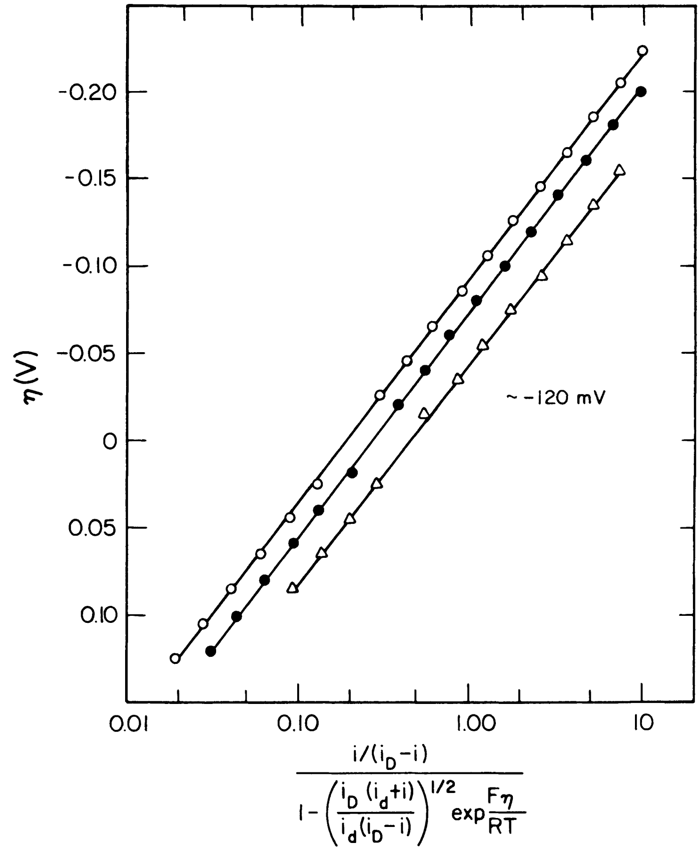

Figure 22. Reduction of O_2 and oxidation of HO_2^- on gold on O_2 saturated 0.1 *M* NaOH containing 8.8×10^{-4} *M* HO_2^- at 26°C according to Zurilla *et al.*(236) Overpotential η for the O_2–HO_2^- couple; see Eqs. (46) and (47). Rotating disk–ring electrode data. Disk area: 0.196 cm^2; ring potential E_H: 0.88 V. ○, 4900 rpm, $i_D = 0.93$, $i_d = 0.47$. ●, 2500 rpm, $i_D = 0.66$, $i_d = 0.34$. △, 900 rpm, $i_D = 0.40$, $i_d = 0.20$ in A (Note: *i* has been taken as positive for cathodic current and negative for anodic.)

what extent the one-electron reduction of O_2 to $O_2^{\cdot-}$ may occur in alkaline solutions by a heterogeneous outer-sphere electron transfer process (outer Helmholtz plane). Only a small change in bond lengths is involved (from 1.20 to 1.28 Å) and hence the inner contribution to the reorganizational free energy of activation ΔF^* for the electron transfer should be small. Since this is usually the major contribution to ΔF^* for outer-sphere electron transfer, the process should be fast. The standard electrode potential for the O_2–$O_2^{\cdot-}$ couple [$E^\circ_{NHE} = -0.30$ V (see Figure 1)], however, is substantially more cathodic than that for the O_2–HO_2^- couple ($E^\circ_{NHE} = -0.065$ V). Therefore, reactions (LVIII) plus (LVIX) or (LXII) involving adsorbed species are expected to be predominant at the potentials where the current is under principally kinetic

Table 6
Current Densities with Pure Kinetic Control (i_k) and Apparent First-Order Heterogeneous Rate Constants (k) Determined from Rotating Disk Electrode Data for $O_2 + e^- \rightarrow O_2^{\cdot -}$ at −0.32 V vs. SCE(262)

Electrode surface	Electrolyte	T, °C	i_k, mA cm^{-2}	$k \times 10^3$, cm sec^{-1}	Ref.
Gold	0.1 M NaOH	26	12	50	236
Graphite edge plane[a]	1 M KOH	22	0.9	4	250
Graphite basal plane (single crystal)	1 M KOH	22	<0.01	<0.04	250
Graphite basal plane[a]	0.1 M NaOH	20	<0.06	<0.24	262
Graphite basal plane[a] with adsorbed layer of Co–TSP	0.1 M NaOH	20	3	13	262

[a] Stress-annealed pyrolytic graphite.

control in the rotating disk–ring electrode measurements. The outer-sphere electron transfer probably becomes significant as a competing process only at potentials in the potential region where transport of O_2 to the disk is controlling.

While the reduction of O_2 to hydrogen peroxide is relatively fast in alkaline solutions on such surfaces as ordinary graphite and gold, it is very slow in acid electrolytes. This difference in kinetics may relate to the ionization constant for the adsorbed superoxide species

$$S{-}O_2H \rightleftharpoons S{-}O_2^- + H^+ \qquad \text{(LXIV)}$$

In alkaline solution $S{-}O_2^-$ would be expected to be the stable form and hence the formation of the adsorbed superoxide to proceed by reactions (LVIX) or (LXII) with just an electron transfer involved. In acid media, reaction (LVIX) is likely to be replaced by

$$\begin{tikzcd} S{-}O_2 \arrow[r, "e^-"] \arrow[dr, "e^-", "H^+"'] & S{-}O_2^- \arrow[d, "H^+"] \\ & S{-}O_2H \end{tikzcd} \qquad \text{(LXV)}$$

The free energy of formation of the $S{-}O_2^-$ species should be quite high, particularly if the ionization constant for reaction (LXIV) is relatively low, and hence the formation of $S{-}O_2H$ is likely to proceed from $S{-}O_2$ through a simultaneous electron and proton transfer. Such a process would be expected to have a higher activation free energy than just the electron transfer and hence the kinetics to be much slower.

The analysis of the mechanism of O_2 electroreduction on platinum and platinum family metals to H_2O or OH^- is more difficult. The possible mechanisms have been examined by various workers (see, e.g., Refs. 238 and 263–266) and have been summarized by Damjanovic.(267) A critical element in the analyzing of the experimental data has been the calculation of the stoichiometric numbers ν in these papers. Experimental values for ν evaluated from the Tafel slopes for the anodic and cathodic polarization data, however, are in question for the reason indicated in Section 1. Nonetheless, these studies have been an important stage in the investigation of O_2 reduction and have strongly influenced present thinking concerning the mechanism of the overall four-electron reduction of O_2.

In principle the analysis of the pH dependence of the O_2 reduction kinetics on the potential at constant current $(\partial E_{\mathrm{NHE}}/\partial \mathrm{pH})_i$ over a wide pH range can be of much help in identifying the rate-controlling step. The kinetic parameters for O_2 reduction on platinum(268–270) and palladium(271) are compared in Table 7 with values for the coverage θ_{O} by chemisorbed oxygen (formed from discharge of water) in the corresponding potential regions. The pH dependences listed in this table are in reasonable agreement with those obtained from the data reported in 1980 by Damjanovic *et al.*(272,273) in acid solutions but not alkaline. The latter authors report the values indicated in parentheses in Table 7. The E vs. $\log i$ curves have a slope of ~ -0.12 V/decade at more negative potentials. Similar data have been obtained on rhodium(238) in alkaline solutions. The value of $(\partial E/\partial \log P_{O_2})_i$ is equal to the value $(\partial E/\partial \log i)$ and consequently the oxygen reduction reaction is first order in O_2. At lower polarizations the value of $(\partial E_{\mathrm{NHE}}/\partial \mathrm{pH})$ remains approximately constant, and amounts to 0.06 V/decade in this potential range for pH from 1 to 13. According to Leites *et al.*(274,275) the value $(\partial E_{\mathrm{NHE}}/\partial \mathrm{pH})$ is equal to about 0.06 V/decade for pH from 2 to 13 at low

Table 7

Kinetic Parameters for the Reduction of Molecular Oxygen on Platinum and Palladium Electrodes as Listed by Tarasevich(257)

Metal	0.1 *M* solution	Range ΔE_{H}, V	$Q_{\mathrm{O}}/2Q_{\mathrm{H}}$	$\frac{\partial E_{\mathrm{NHE}}}{\partial \log i}$, V	$\frac{\partial E_{\mathrm{NHE}}}{\partial \log P_{O_2}}$, V	$\frac{\partial E_{\mathrm{NHE}}}{\partial \mathrm{pH}}$, V
Platinum	H_2SO_4	1.0–0.85	0.36–0.08	0.07	0.06	0.06 (0.09)[a]
		0.85–0.70	—	0.12	0.11	—(0.12)[a]
	KOH	1.0–0.80	0.56–0.27	0.06	0.07	0.06 (0.03)[a]
		0.87–0.75	0.3–0.17	0.12	0.12	—(0)
Palladium	H_2SO_4	0.95–0.82	0.35–0.10	0.06	0.06[b]	0.06
		0.82–0.73	0.10–0.01	0.12	0.12[b]	0.06
	KOH	1.0–0.85	0.70–0.40	0.06	0.06[b]	0.06
		0.85–0.75	0.40–0.10	0.12	0.12[b]	0.06

[a] Values in parentheses are those reported by Sepa, Voinovic, and Damjanovic.(272)

[b] On the basis of the relation I_D/I_B vs. $1/\sqrt{\omega}$ in rotating disk-ring experiments.

current densities and for pH from 3 to 9 at higher current densities. These results agree with the data obtained on "active" electrodes by various researchers.(276–283)

These dependences hold for oxygen reduction directly to water as well as for O_2 reduction via the intermediate formation of hydrogen peroxide(268,271,275) on Pt. Thus for the first group of electrode materials, (e.g., gold, graphite) the value $(\partial E_{NHE}/\partial pH)$ is equal to 0, while for the second group the value $(\partial E_{NHE}/\partial pH)$ is $\sim 2.3RT/F$ at lower polarization. This is an important distinction between the kinetic parameters of these two groups of electrode materials.

A particular feature of platinum-type metals is that in the potential range where molecular oxygen is reduced they have chemisorbed oxygen on their surface that has been formed during the discharge of water molecules (Table 7). The mechanism of the reduction of molecular oxygen on the platinum-group metals can only be understood when the influence of chemisorbed oxygen (and, in the general case, of other chemisorbed species as well) is taken into account.

Polarization curves for oxygen reduction at the rotating palladium electrode and curves showing the surface coverage of this electrode by chemisorbed oxygen are given in Figure 23 (257) for several values of pH. There is a parallel shift of the θ_O–E_{NHE} and log i–E_{NHE} curves toward negative potentials as the pH is increased. One can assume, therefore, that the inhibition of the reduction of molecular oxygen is due to the increase in surface coverage of the electrode by adsorbed oxygen. Increasing coverage by chemisorbed oxygen,(242,243,268) surface oxides,(269) anions, and cations(245) produces a retardation of the reduction reaction going directly to water, as well as a retardation of the reaction going via the intermediate formation of hydrogen peroxide. The $4e^-$ reduction is more retarded than the peroxide-producing reaction by the presence of these adsorbed species. Such behavior has also been observed on Pt in 85% H_3PO_4.(237)

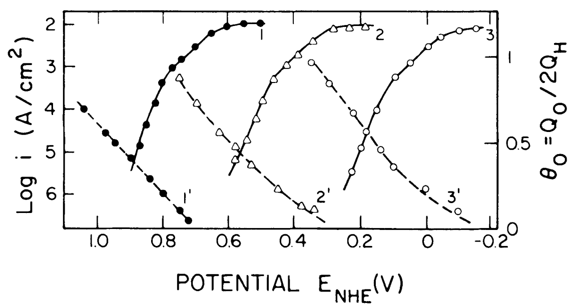

Figure 23. Polarization curves for O_2 reduction and generation on a palladium rotating disk electrode at 6100 rpm.(257) Also shown is the potential dependence of the surface coverage θ_O by chemisorbed oxygen. Current vs. potential plots: 1, pH 1; 2, pH 6; 3, pH 13. Oxygen coverage vs. potential plots: 1', pH 1; 2', pH 6; 3', pH 13.

The number of possible alternatives for the oxygen reduction mechanism is extremely high(284) and it is hardly fruitful to discuss them. One should find it preferable to seek experimental criteria permitting one to reduce the number of possible mechanisms. One such criterion is to compare the rates of cathodic reduction of molecular oxygen and the chemisorbed species S–OH and S–O produced by the discharge of water molecules. Figure 24 shows the exchange current densities of chemisorbed oxygen as well as polarization curves for the reduction of molecular oxygen on platinum and palladium electrodes. The O_2 reduction process is significantly slower than the reduction of chemisorbed oxygen. It follows then that in the electroreduction of O_2 the slow step must precede or include the breaking of O–O bond in the oxygen molecule. For O_2 reduction directly to water, this conclusion also is confirmed by it being first order with respect to O_2.

An important parameter in comparing possible pathways with kinetic data is the stoichiometric number ν. This parameter is usually obtained from either the complementary anodic and cathodic Tafel slopes b_a and b_c using the equation

$$\nu = \frac{nF}{RT}\left(\frac{1}{b_a} - \frac{1}{b_c}\right)^{-1} \tag{48}$$

or from the value of $\partial\eta/\partial i$ at $\eta \to 0$ using the equation

$$\nu = \frac{nFi_0}{RT}\left(\frac{\partial\eta}{\partial i}\right)_{\eta\to 0} \tag{49}$$

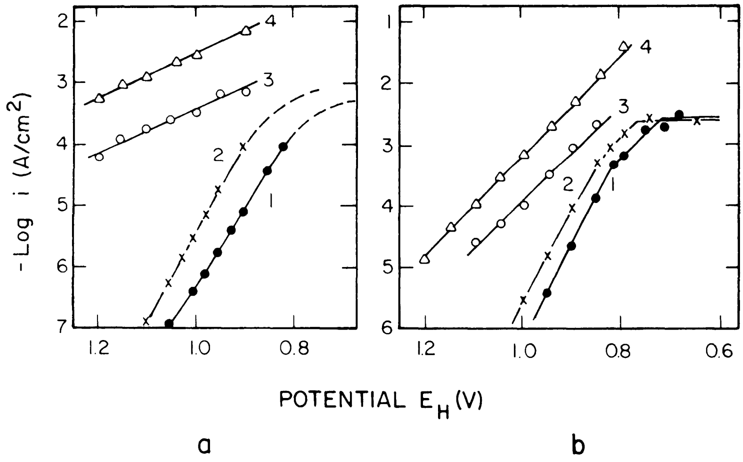

Figure 24. (a) Current density vs. potential curves for O_2 reduction and exchange current density vs. potential curves for the chemisorbed oxygen on platinum in O_2 saturated solutions.(257) Curve 1, O_2 reduction in 0.05 *M* H_2SO_4; curve 2, O_2 reduction in 0.1 *M* KOH; curve 3, exchange current densities for oxygen chemisorption in 0.05 *M* H_2SO_4; curve 4, exchange current densities for oxygen chemisorption in 0.1 *M* KOH. (b) Corresponding curves for palladium.

where n is the number of electrons transferred in the overall process ($n = 4$) and the exchange current density i_0 is evaluated from the intercept of either the anodic or cathodic Tafel plots with the reversible potential.

For the four-electron reduction–oxidation reaction on Pt, it is doubtful that the anodic and cathodic Tafel slopes would be complementary unless evaluated quite close to the reversible potential. Data of this type have been obtained in alkaline solution with a Teflon-bonded high-area Pt electrode by Tarasevich *et al.*(285) (Figure 25a, b). Note that the open-circuit potential corresponds to $E_H = 0$ and that the anodic and cathodic Tafel plots have a common intercept at $E_H = 0$ corresponding to $\log i_0$. The Tafel slopes are $b_a = \sim 0.12$ V/decade and $b_c = \sim -0.12$ V/decade corresponding to a value of $\nu = \sim 4$. This value is close to that deduced by Damjanovic *et al.*(263) but it is questionable as to whether this value is very significant because of the following discrepancy. If ν is evaluated from Eq. (49) and the value of i_0 obtained from the Tafel linear regions in Figure 25b, ν is found to be 0.8 to 1.5 or perhaps $\nu = \sim 1$. This inconsistency with the value of ν evaluated from b_a and b_c implies that it is very questionable to evaluate i_0 from either of the Tafel linear regions and then use it in Eq. (49) to evaluate ν from $(\partial\eta/\partial i)$ at $\eta \to 0$. Further, the cathode Tafel slope of ~ -0.12 V/decade at $E_H = 1.15$ to 1.20 V vs. RHE in Figure 25a differs from the usual low-current-density Tafel slope of -0.06 V/decade on smooth platinum listed in Table 7. It is quite possible that the rate-controlling step and even the mechanism differ at the more positive potentials involved with the Teflon-bonded high-area Pt electrode in Figure 25. Thus the question of the stoichiometric number for the four-electron reduction remains unresolved.

On the basis of the present data, the authors of this chapter have not been able to agree on what is the most likely mechanism for the four-electron

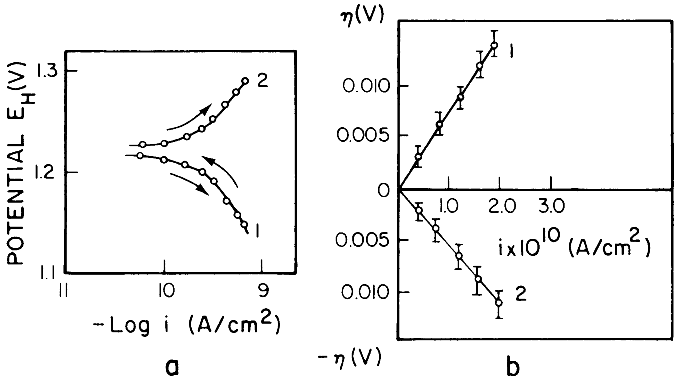

Figure 25. Polarization curves for the O_2 electrode reaction on Teflon-bonded high-area platinum in O_2 saturated 0.1 M KOH.(285) a, $\log i$ vs. E_H; 1, cathodic; 2, anodic. b, i vs. η_H; 1, cathodic; 2, anodic.

reduction on platinum. The first step, however, is probably the adsorption of O_2 on the surface, i.e.,

$$O_2 \rightarrow O_2(\text{ads}) \qquad \text{(LXVI)}$$

but the type of site and configuration are quite uncertain. Some of the possibilities are shown in Figure 26 together with likely overall reaction pathways. These types of interactions of O_2 with transition metal species are well known in inorganic coordination chemistry both in the solid state and in solution with the bonding involving the π and π^* orbitals of the O_2 interacting with the *d* orbitals of the transition metal. These types of interactions are also to be expected on surfaces such as platinum with the relatively localized *d* orbitals of the surface metal atoms. The formation of such O_2-adsorbed species may also be accompanied by electron transfer as has been found with the O_2 adducts formed with some transition metal complexes. For example, the bridged -O-O- model C may involve the formation of a peroxide state

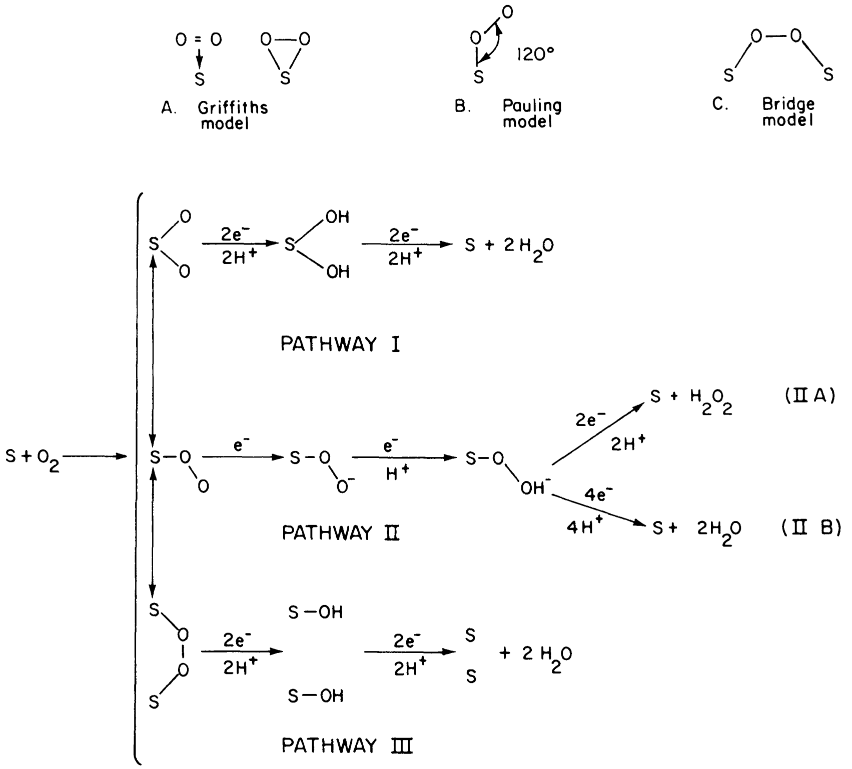
A. Griffiths model
B. Pauling model
120°
C. Bridge model
S + O₂
2e⁻
2H⁺
S + 2H₂O
PATHWAY I
e⁻
H⁺
S + H₂O₂
(II A)
4e⁻
4H⁺
S + 2H₂O
(II B)
PATHWAY II
S–OH
+ 2H₂O
PATHWAY III

Figure 26. Models for O_2 adsorbed on metal sites and likely overall reaction pathways.(2)

either directly or as part of a subsequent electron transfer, e.g.,

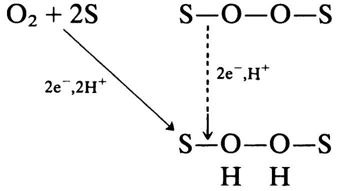

(LXVII)

The reaction sequences in Figure 26 show possible intermediates but not all of the steps. The end-on bonded species M–O–O in Figure 26 would be expected to lead to peroxide formation but in principle can also lead to the four-electron process through rupture of the O–O bond during the desorption step. Models A and C, however, seem more likely to lead to the rupture of the O–O bond and hence the overall four-electron reduction.

6.3. Oxygen Reduction on Nonmetallic Materials

The extensive application of O_2 electrodes, particularly in electrochemical energy conversion, requires inexpensive electrocatalysts of high activity and reasonable stability. This has stimulated a search for semiconductor O_2 electrocatalysts of both inorganic and metallo-organic types.

Two approaches have been involved in studying the dependence of catalytic activity on the electronic properties of semiconductor systems: (1) the macroscopic (collective) approach, based upon the band theory in which the energy of interaction with adsorbates depends on the position of the Fermi level which is determined by the energy levels of electrons in the entire solid catalyst with account taken for the charge of the surface layer; (2) the microscopic (local) approach, based upon the quantum mechanical theory of chemical bonds in solids and in transition metal complexes (the crystal field theory of the ligands); in this case the only interaction taken into account is that with the closest neighbors with the direct participation of the given chemical group (or defect) in adsorption and catalytic acts.

These approaches represent the two extreme viewpoints on the process of adsorption and catalysis. The first one operates with the multielectron collective function of the entire solid body and with the corresponding average macroscopic parameters. The second one considers individual chemical interactions between the reagents and the active center. The macroscopic properties of the solid are regarded only as the background for the catalytic process. These phenomenological models serve as a guide in classifying experimental data and establishing the mechanism and the nature of the slow step of a given electrochemical reaction with the aim of establishing the criteria for the selection of catalytically active sytems.

We shall consider the following three groups of catalysts: heterogeneous inorganic systems, carbon materials, and metallo-organic complexes.

6.3.1. Oxide Catalysts

Most of the work on inorganic semiconductor catalysts for O_2 reduction has been carried out on metal oxides in alkaline electrolytes. A number of these oxides have moderately high electrocatalytic activity with reasonable stability. These include lithiated nickel oxide,(288–290) perovskites,(291) and spinel-structured metal cobaltite $Me_aMe_bO_4$.(292–298)

Anhydrous NiO has been studied in the form of mosaic crystals [(100) orientation] doped with 0.1%–10% Li. This material is a *p*-type semiconductor and hence cathodic processes such as O_2 reduction would be expected to be inhibited. Examination of redox couples such as ferri-ferrocyanide with the rotating disk technique do indicate cathodic inhibition in acid solutions with the anode branch under combined kinetic and diffusion control.(299) Differential capacitance measurements in acid solutions indicate that most of the electrode potential change occurs across the space charge region within the NiO (0.1% Li) at electrode potentials cathodic to 0.8 V vs. SHE.(300) In alkaline solutions, however, the ferri-ferrocyanide couple is no longer cathodically inhibited and both the cathodic and anodic branches are essentially diffusion controlled even at high rotation rates.(299) The flat band potential shifts in alkaline solution to quite negative values relative to the reversible potential of this couple with the result that the potential changes then occur principally across the Helmholtz layer. The reversible potential for the O_2–peroxide couple, however, is more negative and therefore O_2 reduction even in alkaline solution is still quite inhibited.(288) Similar results have been obtained on lithiated polycrystalline NiO produced by high-temperature oxidation of nickel metal in air or in O_2.(289)

^{18}O techniques have been used to demonstrate that the O_2 generated during the oxidation of HO_2^- to O_2 on NiO in alkaline solutions originates only from the HO_2^-.(288) Thus the O–O bond does not appear to be broken during the oxidation process, and presumably also during the reverse reduction of O_2 to HO_2^-.

On NiO(Li) and perovskites, the rate of O_2 reduction at temperatures below 100°C is rather low, but increases rapidly in concentrated solutions (melts) of KOH at temperatures above 150–170°C. Tseung and Beuan(291) have proposed that this effect is connected with the transition through the Neel point with an accelerated chemisorption of O_2 molecules in a "side-on" configuration which facilitates rupture of the O–O bond. The active sites [Co(III)–Co(IV) couples] control the dissociative chemisorption of the O_2 molecule and this is dependent on the thermally induced conversion of low-spin Co^{2+} to high-spin Co^{3+}. It has been reported,(301) however, that the following thermal reaction takes place between the O_2 and alkali at higher temperatures, e.g., 170°C:

$$3/2O_2 + 2OH^- \rightarrow 2O_2^- \cdot + H_2O \qquad \text{(LXVIII)}$$

with $O_2^- \cdot$ formation. Therefore, a possibility is that the reaction in the KOH melt is accelerated primarily because of a transition from the reduction of molecular oxygen to that of the superoxide ion:

$$O_2^- \cdot + 2H_2O + 3e^- \rightarrow 4OH^- \qquad \text{(LXIX)}$$

Metal cobaltites display high electrocatalytic activity even at ambient temperatures. Some authors(292,302) believe that the reduction of oxygen on different cobalt oxides at low temperature proceeds only through the intermediate state of hydrogen peroxide formation, so that the promoting effect of oxide catalysts is due to the acceleration of H_2O_2 decomposition. On the other hand, the data on homomolecular oxygen exchange(303) show that the dissociative low-temperature chemisorption of oxygen on cobaltites is possible. The rotating disk–ring electrode technique has made it possible to resolve this question.

Figure 27 presents the polarization curves for oxygen reduction on carbon black promoted by different cobaltites(294) in alkaline solution. In these rotating disk–ring electrode experiments an extremely thin layer of a catalyst was applied to the pyrographite disk electrode. The analysis of the experimental data has shown that the O_2 in the presence of the cobaltites is reduced mainly to water without the formation of hydrogen peroxide.

Attempts to use nonmetallic catalysts for the catalysis of the oxygen reduction reaction in acid solutions have been unsuccessful. Tungsten–sodium bronzes(304,305) or tungsten oxides, when used for this purpose, have to be promoted by noble metals.(307,308) The intrinsic activity and stability of the chalcogenide compounds are also insufficient.(306)

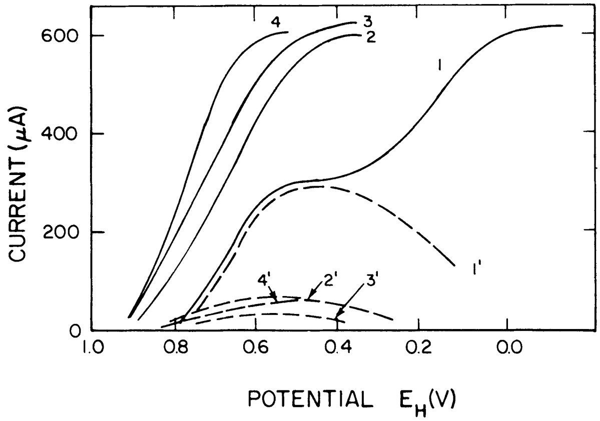

Figure 27. Polarization curves for O_2 reduction in 0.1 *M* KOH on carbon with and without cobaltic oxides using the rotating disk–ring electrode technique.(294) Curve 1, carbon black; 2, carbon black + $CoCo_2O_4$; 3, carbon black + $MnCo_2O_4$; 4, carbon black + $NiCo_2O_4$. Curves 1′ to 4′: corresponding currents for HO_2^- oxidation on a Pt ring. Rotation rate: 655 rpm.

6.3.2. Carbon Materials

The various forms of carbon present in natural and artificial coals, in products of carbonization of organic substances, and in carbon-graphite products used in catalysis and electrocatalysis have a wide range of properties. Graphitelike areas are cross-linked by lateral chains of carbon to form a three-dimensional polymer. Thus, in peripheral regions of the structure the $C-C$, $C=C$, and $C\equiv C$ bonds and orbitals with sp^1, sp^2, and sp^3 hybridization may be present, depending on the nature of the original substances and the conditions of processing.

The development of compact and disperse carboneous materials with a wide range of chemical and electrophysical properties is in progress in an attempt to increase the activity of oxygen and air electrodes. To increase the electrocatalytical activity of carbon materials, however, a better understanding of the nature of the active sites is needed. This problem has been studied extensively by various workers,(258,250,309-311) but the nature of the active sites still remains in doubt.

Typical current–voltage curves obtained with the rotating disk technique are shown in Figure 28 for the edge and basal planes of stress-annealed pyrolytic graphite with X-ray rocking angle $\theta_{1/2} = 0.4°$ in $1\,M$ KOH. The hysteresis evident in these slow sweep curves (10 mV/sec) is caused by changes in the oxidation state of various groups present on the edge orientation. With

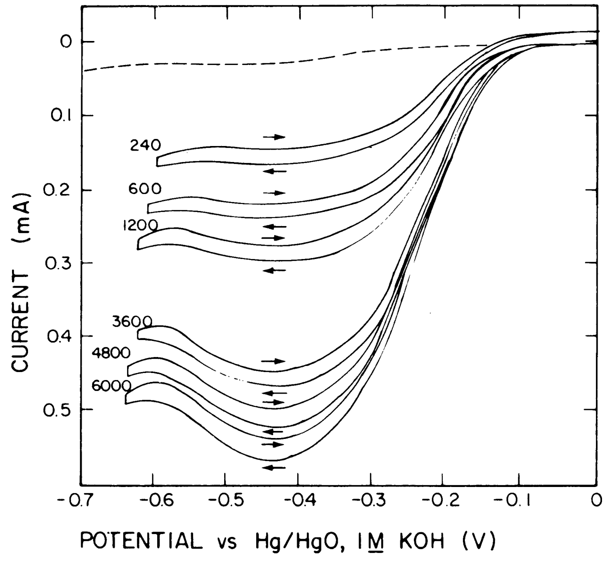

Figure 28. Reduction of O_2 on high-pressure stress-annealed pyrolytic graphite in O_2 saturated $1.0\,M$ KOH using a rotating disk electrode of area $0.20\,\text{cm}^2$. Solid curves: edge orientation; dashed line: basal (cleavage) plane. Rotation rates in rpm's are indicated on curves.(250)

single-crystal graphite and stress–annealed pyrolytic graphite, the O_2 reduction as well as peroxide oxidation reactions are very inhibited on the basal plane with the exchange current at least two orders of magnitude less on the basal plane than on the edge orientation. Imperfections in the basal plane set a lower limit to the checking of how far the exchange current is depressed on this plane.

This depression of the exchange current on the basal plane may be caused by (1) anisotropic surface-semiconductor properties of the graphite, or (2) the lack of suitable functional groups or adsorption sites on the basal plane. The surface area of the edge plane also is probably much greater than unity but it is unlikely that this alone can explain the large difference between the edge and basal planes. The carrier concentration in graphite is rather low near the Fermi level and hence some significant fraction of the applied potential may fall across a space charge region extending perpendicular to this plane.(309,310) The differential capacitance curves and corresponding voltammetry curves are shown in Figure 29 for both 1 M NaOH and 0.5 M H_2SO_4. These curves are in strong contrast to the corresponding curves for

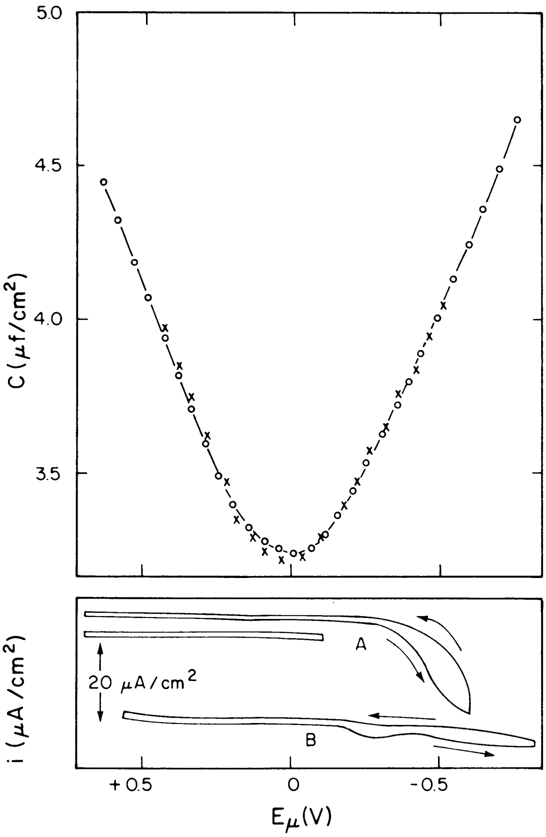

Figure 29. Capacity–potential and current–potential curves for the basal (cleavage) plane of stress-annealed pyrolytic graphite ($\Delta\theta_{1/2} = 0.4°$) in 0.5 M H_2SO_4 (×) and 1 M NaOH (O) at 25°C and at 1000 Hz. Scan rate for current potential curves: 0.01 V/sec. Curve A, in 0.5 M H_2SO_4; curve B, in 1 M NaOH.(311)

the edge orientation(311) which show much structure. The capacitance on the basal plane is much lower than on the edge orientation or on typical metals such as Hg or Au, suggesting that a significant potential drop occurs across a space charge region within the graphite. The potential dependence of the capacitance, however, is close to parabolic rather than the hyperbolic dependence expected for a semiconductor electrode. This may be caused by the high carrier concentration in the graphite, i.e., 6×10^{18} carriers/cm^3.(312) Further, the capacitance curves give no indication of specific adsorption, even in the presence of relatively high concentrations of such anions as iodide.(309,310)

To check further on the extent to which electrode reactions on the basal plane may be impeded by semiconductor effects, the $Fe(CN)_6{}^{3-}$–$Fe(CN)_6{}^{4-}$ redox couple has been examined and found to have an exchange current on the basal plane which is ~1/3 of that on the edge plane. This difference may be caused by a difference in the ratio of true-to-apparent surface area or ionic double-layer effects (different point of zero charge) as well as semiconductor effects but is certainly far less than the two orders of magnitude difference in the exchange current densities for the O_2 reduction on the basal and edge planes.

The most likely explanation for the suppression of O_2 reduction on the basal plane is the lack of suitable adsorption sites for $O_2{}^-$(ads) and O_2H^-(ads) during the reduction. This raises the question as to what particular adsorption sites or functional groups are involved in the O_2 reduction on the edge surface. A large number of functional groups have been proposed to exist on carbon surfaces(313) and some of these should persist on graphite as well as carbon at the potentials for O_2 reduction in alkaline solutions. Even so, it is far from clear which, if any, provide the adsorption sites involved in the O_2 reduction and are effective in alkaline electrolytes but not very effective in acid electrolytes.

Garten and Weiss(314) some years ago proposed that surface quinone groups are involved in the following way:

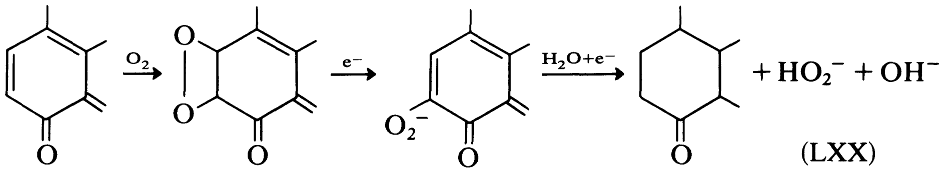

(LXX)

The O_2 first adds to the olefinic bond associated with the quinone group to form the hydroperoxide or molecular oxide. Electron transfer then occurs to form $O_2{}^-$(ads) and subsequently splits off as $HO_2{}^-$ after a further electron transfer. The Garten–Weiss mechanism is compatible with the pathway represented by reactions (LVIII), (LVIX), and (LX), but not with the observed stoichiometric coefficient of $\nu = 2$ and the pathway proposed by Morcos and

Yeager(26) involving a peroxide dismutation–desorption step represented by reaction (LXI) (see Section 6.2). While the Garten–Weiss mechanism is a reasonable one involving the functionality of the carbon or graphite surface groups, it is far from proved. Other functional groups may also be involved. With the graphitic materials, O_2^- and even HO_2^- intercalation may also occur on the edge plane and may play a role in the reaction mechanism.

6.3.3. Transition Metal Macrocyclic Complexes

Many of the transition metal macrocyclic complexes have substantial catalytic activity for O_2 reduction. These catalysts are of interest to the enzyme chemist as well as the electrochemist. Some of the typical macrocyclic ligands are shown in Figure 30. While the coordination to the central transition metal can be through various elements (e.g., N, O, S), the nitrogen-coordinated macrocyclics tend to be more stable with the first transition row elements in alkaline and acid electrolytes. The macrocyclic ligands involve highly conjugated organic structures with delocalized π electrons. As solids, many of the macrocyclics have quite good electronic conductivity. With the phthalocyanines, the conductivity of the polymeric species may be several orders of magnitude higher than that of the corresponding monomer. In general the electrical conductivity and magnetic properties are strongly influenced by the crystalline modification as well as oxygen and water absorption.(315,316)

The studies of O_2 reduction on macrocyclic catalysts have usually been carried out on thin films of the macrocyclic on a carbon, graphite, or metal substrate.(317–330,341–344) These experimental studies can be divided into three groups:

a. Ligand Structure: The first group of experiments is concerned with the influence of the ligand structure, the type of substituent, and the degree of polymerization. The phthalocyanines (Pc),(317–324) tetraphenylporphyrins (TPhP),(324,325) and dibenzotetraazoannulenes (DBTAA)(319,328) display different activity for oxygen electroreduction both in acid and in alkaline solutions. Rotating disk–ring electrode studies show that in alkaline solutions the contribution of the direct $4e^-$ reaction to water is 50% for the polymeric cobalt phthalocyanine $(CoPc)_n$ and 30% for the cobalt tetramethoxy phenyl porphyrin (CoTMPhP).(324) In acid solutions the reaction proceeds only through the intermediate H_2O_2 formation,(324,330) and the activity decreases in the series CoTMPhP > CoTPhP > $(CoPc)_n$ > CoPc. Introduction of electron donors into the phenyl groups of cobalt tetraphenyl porphyrin (R in Figure 30D) decreases its activity in the series OCH_3 > phenyl > SCH_3 > H.(325)

b. Influence of central metal ion: The data (e.g., Refs. 321, 323, 324, 331, and 332) obtained show that, irrespective of pH, the activity of the monomeric phthalocyanines changes in the series Fe(II), Fe(III) > Co(II) ≥ Mn(II) > Ni(II), Cu(II) > $2H^+$. With the polymeric phthalocyanines, the

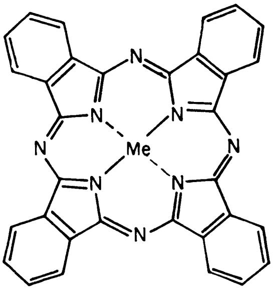

PHTHALOCYANINE (Pc)

a

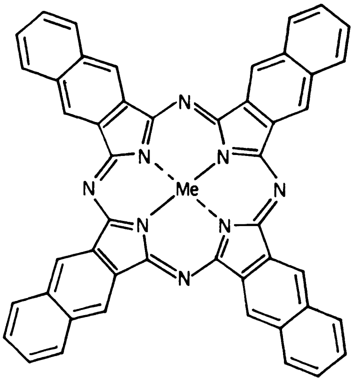

NAPHTHOCYANINE (N Pc)

b

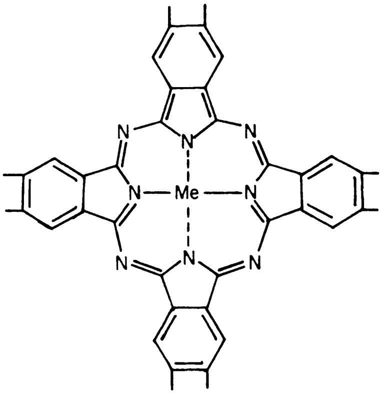

POLYMERIC PHTHALOCYANINE(MPc)n

c

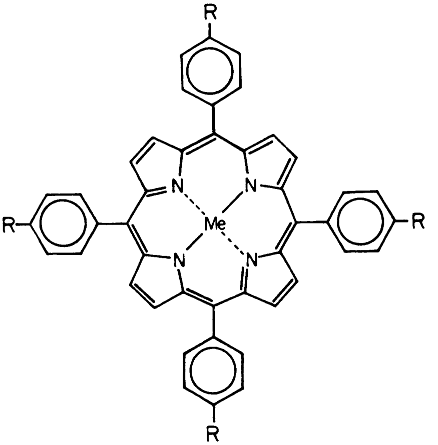

TETRAARYLPORPHYRIN

d

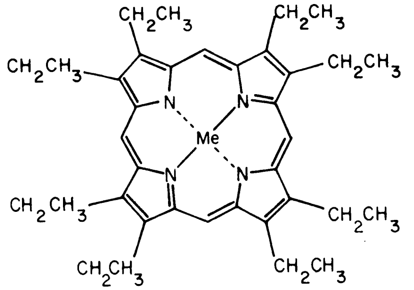

OCTAETHYLPORPHYRIN (OEP)

e

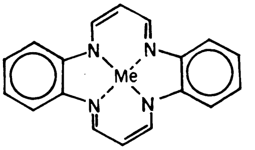

BIBENZOTETRAAZANNULENE (BBTA)

f

Figure 30. Structures of various macrocyclic compounds of interest as catalysts for O_2 reduction.

introduction of Mn, Fe and Co into the polymer chain increases the contribution of the O_2 reduction to water but accelerates the whole reduction process.(324,326) The dependence of the mechanism and kinetics of the reaction on the nature of the central metal ion indicates that the metal is the site where the electrocatalytic process occurs. The observed correlation of electrochemical activity with the first redox potential and the value of the magnetic moment(327) also shows that the local interaction rather than the collective one plays the key role with these metal organic complexes. The activity series of phthalocyanines with the different central ion has been discussed in the literature(325,326) in terms of the electronic structure of the complexes and can be explained in terms of molecular orbital theory. This approach, however, is only qualitative and disregards a number of effects. In order to understand their catalytic activity one must study theoretically and experimentally the overall surface and bulk electronic properties of these metal organic complexes and the adsorptive and also possibly *ab*sorptive interactions of the reaction components, including likely intermediates.

Zagal *et al.*(330–333) have examined the catalytic properties of water-soluble tetrasulfonated phthalocyanines (TSPc) adsorbed as a monolayer on graphite substrates, using the rotating disk–ring electrode technique. These complexes are very strongly adsorbed on graphite and carbon and can be presorbed in a monolayer before introduction into the electrolyte solution in which the O_2 reduction is to be studied. Figures 31 and 32 show the polarization curves for these complexes with various transition metal central ions with the complexes pre-adsorbed on the basal plane of stress-annealed pyrolytic graphite in alkaline and acid electrolytes.(333) The predominant reduction process is to the peroxide on all of these complexes with the exception of FeTSPc for which the four-electron reduction is predominant at potentials positive to the maximum in the polarization curve in Figure 31.

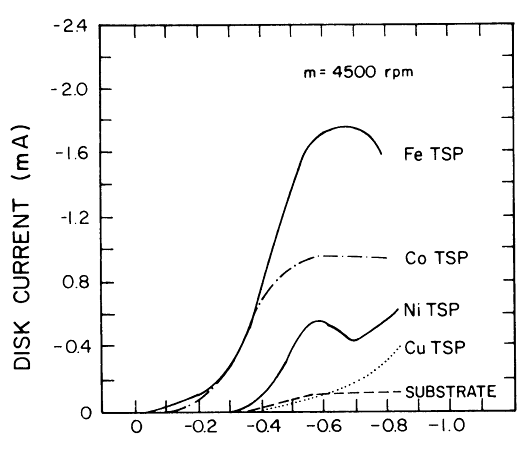

Figure 31. O_2 reduction on adsorbed layers of various transition metal tetrasulfonated phthalocyanines on the basal plane of stress-annealed pyrolytic graphite in 0.1 *M* NaOH. Macrocyclic preadsorbed from aqueous 10^{-3} *M* MeTSPc solution. Rotating disk electrode. Rotation rate: 4500 rpm. Disk area: 0.20 cm^2. Potential scan rate (cathodic): 10 mV/sec. T = 21°C.(333)

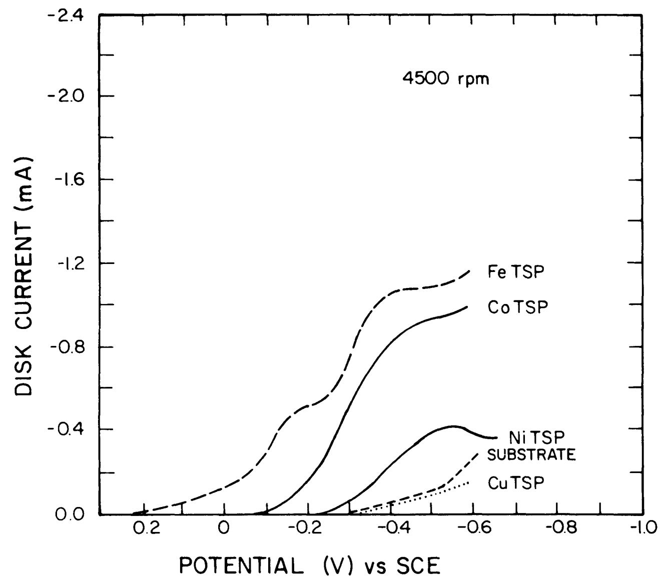

Figure 32. O_2 reduction on adsorbed transition metal tetrasulfonated phthalocyanine in 0.05 M H_2SO_4. Conditions similar to those for Figure 31 except that 10^{-5} M of the MeTSPc present in solution during measurements.(333)

The overall order of decreasing catalytic activity for the adsorbed monolayers of the MeTSPc ($Fe \geq Co > Ni > Cu$) is essentially the same as for the non-water-soluble thicker layers of MePc listed earlier. It is interesting to note that the activity of CuTSPc is even smaller than that for the basal plane of pyrolytic graphite without an adsorbed layer.

c. Electrolyte effects: The third group of experimental data refers to the influence of the electrolyte composition on the kinetics and mechanism of the electrode process. Investigations in this field have been performed for H_2Pc, CoPc, $(CoPc)_n$, and CoTPhP.(323,324) Except for $(CoPc)_n$ in alkaline solution, O_2 reduction on the surface of these compounds proceeds in two stages with the intermediate formation of H_2O_2. The typical kinetic dependences are presented in Figure 33. They resemble those observed for pure carbon materials(255) for which the slow state is the transfer of the first electron to the oxygen molecule:

$$(L—M) + O_2 \rightarrow (L—M)—O_2 \qquad \text{(LXXI)}$$

$$(L—M)—O_2 + e^- \rightarrow (L—M)—O_2^- \qquad \text{(LXXII)}$$

where L is the macrocyclic ligand. The following stages leading to the hydrogen peroxide formation are fast. The behavior of CoTPhP in acid solutions does not correspond to this scheme, because a sharp shift of the half-wave potential towards a positive value is observed. The explanation may be the need for a

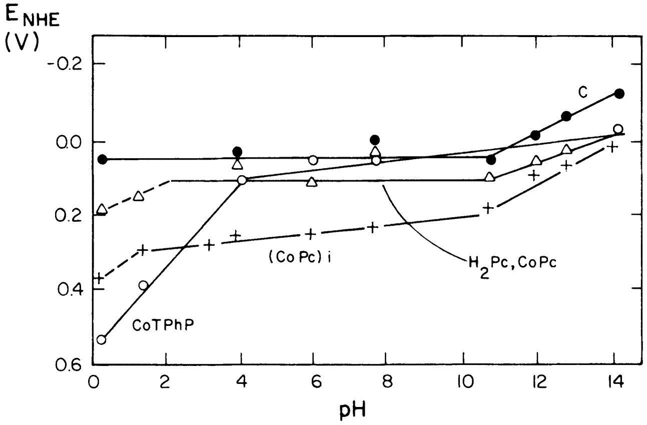

Figure 33. pH dependence of half-wave potentials for O_2 reduction on carbon black with and without macrocyclic catalysts. Rotating disk technique. ●, Carbon black alone; △, H_2Pc or CoPc; +, $(CoPc)_n$; ○, CoTPhP.(324)

simultaneous proton transfer:

$$(L{-}M){-}O_2 + H^+ + e^- \rightarrow (L{-}M){-}O_2H \qquad \text{(LXXIII)}$$

The first electron transfer was proposed as the rds also by Behret *et al.*(328) for the O_2 electroreduction on cobalt tetrabutyltetraazoannulene (CoTBTAA) and by Zagal *et al.*(330,333) for the same reaction on Co(II)TSPc preadsorbed on the graphite surface. The values of the Tafel slope both in acid and alkaline solutions are close to −0.12 V/decade and the half-wave potential at constant rotation rate is practically constant between pH 0.3 and 13. The O_2 electroreduction can be envisaged to proceed according to the following scheme in acid solution with an analogous scheme in alkaline solution:

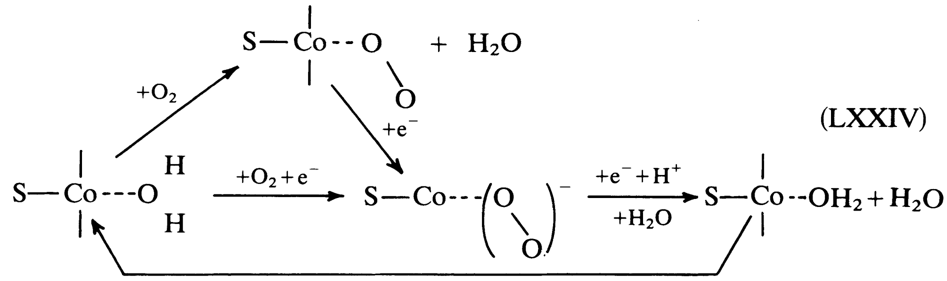

(LXXIV)

where the first step is probably ligand displacement (water or OH^- groups depending on pH) followed by a heterogeneous electron transfer process to give peroxide.

Extensive studies of O_2 reduction with FePc and $(FePc)_n$ on carbon black have been carried out by Appleby, Fleish, and Savy(326) with the rotating disk–ring electrode technique with the macrocyclic/carbon in the form of a paste incorporating purified mineral oil in a cavity. On the polymeric $(FePc)_n/C$ in alkaline solutions, these workers report that the four-electron reduction process occurs with no peroxide as a detectable intermediate in the electrolyte for potentials above $E_H = 0.60$ V. Magner, Savy, and Scarbeck(342) have also reported the four-electron reduction to be predominant with the iron naphthalocyanine on carbon in alkaline electrolytes. This is in contrast to the results discussed earlier for the CoPc and $(CoPc)_n$. Appleby *et al.*(326) have also examined the FePc and $(FePc)_n$ films produced in various ways on gold and carbon substrates with Mössbauer and ultraviolet-visible reflectance spectroscopy and concluded that the presence of five coordinated Fe(III) in the intermediate spin state ($S = 3/2$) probably leads to the highest activity in the films produced by various means. Meier *et al.*(343) have also examined the Mössbauer spectra of FePc on carbon supports after thermal treatment and have concluded that high activity is exhibited only by those FePc complexes in which the iron is directly bonded to the carbon substrate through an Fe–C bond. It is not completely clear, however, what spin state to expect for such Fe species. Melendres(346) has also compared the Mössbauer and Raman spectra of carbon-supported FePc and the pure complex and finds evidence of catalyst-support interactions with the former.

On the basis of rotating disk–ring electrode data in alkaline solutions (pH from 11.8 to 16.4) Appleby *et al.*(326) have proposed the following formal mechanism:

step 1: $O_2 \rightarrow O_2(\mathrm{ads})$ (fast) (LXXV)

step 2: $O_2(\mathrm{ads}) + H_2O + e^- \rightarrow O_2H(\mathrm{ads}) + OH^-$ (fast) (LXXVI)

step 3: $O_2H(\mathrm{ads}) + e^- \rightarrow O_2H^-(\mathrm{ads})$ (fast) (LXXVII)

step 4: $O_2H^-(\mathrm{ads}) + H_2O \rightarrow 2OH + OH^-$ (rds) (LXXVIII)

step 5: $OH + e^- \rightarrow OH^-$ (fast) (LXXIX)

They further propose that the chemisorption of the O_2 occurs *inside* the bulk of the FePc or $(FePc)_n$ to produce a dioxygen radical which then diffuses to the catalyst–electrolyte interface. It is difficult, however, to accept their mechanism, particularly step 4, which leads to the formation of two OH radicals with the simultaneous desorption of the peroxide. Such a complex single step seems very unlikely on the basis of the high free energy needed to form OH free radicals in alkaline electrolytes (see Figure 1).

Zagal and Yeager *et al.*(331–334) have also found O_2 reduction on a monolayer of FeTSPc adsorbed on the basal plane of graphite to yield no detectable peroxide with the rotating disk–ring electrode technique at potentials $E_{NHE} > 0.60$ V for pH from 4.4 to 13.8. At lower values of E_{NHE}, small amounts of peroxide are formed, probably through a parallel mechanism. Since the O_2 reduction is extremely inhibited on the basal plane of graphite, the peroxide generation reaction at $E_{\mathrm{NHE}} < 0.60$ V must involve the FeTSPc and not just some exposed graphite. The polarization curves for various pH are shown in Figure 34. In the lower polarization region where no peroxide is detected, the Tafel slopes are −30 to −35 mV/decade over the pH range 13.8 to 10.8 and then increase to −65 mV/decade at pH 4.4. (Reproducible data were not obtained below pH 4.4.) The apparent limiting current at $\log i/(i_L - 1) = {\sim}0.1$ is not associated with O_2 transport and is independent of pH and first order in O_2 concentration. A chemical limiting process appears to be involved with essentially potential-independent kinetics. Above this limiting current, the Tafel slope is −0.12 V/decade and the kinetics are pH independent over the range 4.4–13.8. On the basis of the rotating disk–ring electrode data and voltammetry studies of the redox properties of the adsorbed FeTSPc layer, Zagal *et al.*$^{(331-333)}$ have proposed the following mechanism for pH > 8 for the region up to the apparent chemical limiting current in Fig. 34.

step 1: $$[(\mathrm{TSPc})\mathrm{Fe^{III}\text{-}OH}]_{\mathrm{ads}} + \mathrm{H_2O} + e^- \rightleftharpoons [(\mathrm{TSPc})\mathrm{Fe^{II}\text{-}OH_2}]_{\mathrm{ads}} + \mathrm{OH^-} \tag{LXXX}$$

step 2: $$[(\mathrm{TSPc})\mathrm{Fe^{II}\text{-}OH_2}]_{\mathrm{ads}} + \mathrm{O_2} \rightleftharpoons [(\mathrm{TSPc})\mathrm{Fe^{III}\text{-}O_2^-}]_{\mathrm{ads}} + \mathrm{H_2O} \tag{LXXXI}$$

step 3: $$[(\mathrm{TSPc})\mathrm{Fe^{II}\text{-}O_2^-}]_{\mathrm{ads}} + e \rightarrow \text{intermediates} \tag{LXXXII}$$

Step 3 is proposed to be rate controlling at low current densities but at the chemical limiting current, step 2 becomes rate controlling. The redox couple

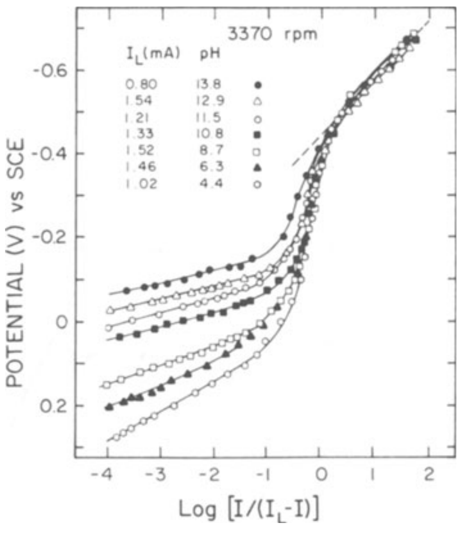

Figure 34. Tafel plots for O_2 reduction on FeTSPc preadsorbed on an ordinary pyrolytic graphite disk in solutions of various pH.$^{(331)}$ Rotation rate: 3370 rpm. T:N 25°C. Note that I_L corresponds to the diffusion-limiting current.

$[(TSPc)Fe^{III}\text{-}OH]_{ads}/(TSPc)Fe^{II}\text{-}OH_2]_{ads}$ plays a critical role and in this aspect the mechanism is similar to the redox-type mechanisms proposed by Beck.(335) Zagal *et al.*, however, do not indicate what happens after step 3. Since the overall $4e^-$ reduction is involved, the O–O bond-breaking step must follow step 3. At high current densities above the chemical limiting current, the behavior is very similar to that on both the preadsorbed CoTSPc layer and the thicker CoPc layers studied by other workers. In this range, Zagal *et al.*(336–338) propose that the mechanism represented by reaction (LXXI) discussed earlier is predominant.

An interesting feature of some of the M–TSPc complexes is the report that some TSPc complexes such as CoTSPc and FeTSPc form dimeric O_2 adducts in aqueous solutions (see, e.g., Refs. 336–338). This has prompted Nikolic, Adzic, and Yeager(339) to propose that perhaps an adsorbed dimeric species (TSPc)Fe–O–O–Fe(TSPc) is involved, similar to such species proposed to exist in aqueous solutions. They have attempted to obtain evidence for such an adsorbed O_2 adduct using visible reflectance spectroscopy.(339) The *in situ* spectra for the adsorbed species on the basal plane of stress annealed pyrolytic graphite and also platinum are very similar to those of the solution phase species for both the CoTSPc and FeTSPc. Further, the changes in the reflectance spectra of the adsorbed complexes at constant potential upon introduction of O_2 into the electrolyte are very similar to the spectral changes for the solution phase species. On the basis of this optical evidence Nikolic *et al.* have proposed the model shown in Figure 35, involving edge-on adsorption. More recent *in situ* Raman studies of the CoTSPc adsorbed on silver, however, have raised some questions concerning this model—at least on silver. Kötz and Yeager(340) have found changes in the Raman spectra which are difficult to explain with the edge-on model in Figure 35. Furthermore the CoTSPc and FeTSPc complexes are very strongly adsorbed on graphite and

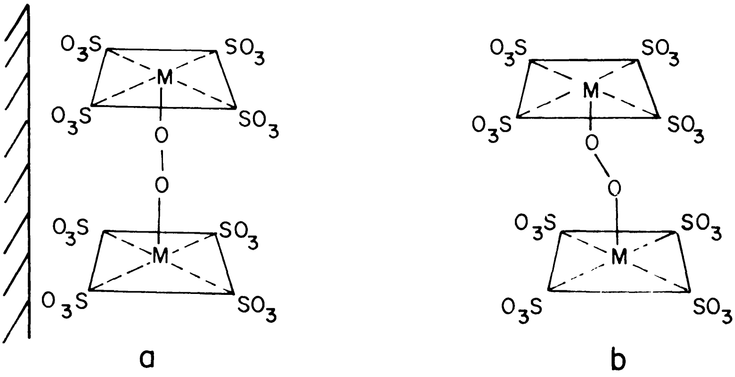

Figure 35. Model proposed by Nikolic, Adzic and Yeager(339) for adsorbed iron and cobalt tetrasulfonated phthalocyanines on the basal plane of stress annealed pyrolytic graphite. a, View parallel to the surface; b, view perpendicular to the surface.

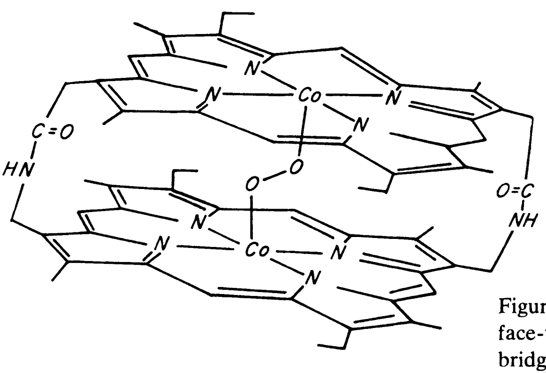

Figure 36. *Syn* diastereomer of the β-linked face-to-face porphyrin with four-atom bridge.(341) The metal-metal distance is ~4 Å.

the edge-on model would not be expected to lead to such strong adsorptions. Consequently, the state of these adsorbed catalysts remains unsettled.

Recently Collman, Anson, and their co-workers(341) have synthesized covalently linked face-to-face dicobalt porphyrin dimers (Figure 36) with the spacing between the parallel cobalt porphyrins controlled by two amino bridges of varying length. They have applied these cofacial metalloporphyrins to graphite and then examined O_2 reduction with the rotating disk–ring electrode technique in acid electrolytes. All of these molecules have exhibited catalytic activity but the product has been normally H_2O_2. With the dicobalt species, however, when the parallel porphyrin groups are linked by a four-atom bridge, the O_2 reduction is almost entirely to water at quite positive potentials. The Co–Co spacing in this diporphyrin is ~4 Å and hence proper to form a Co–O–O–Co bridge, much in the same manner as proposed by Nikolic *et al.*(339) This is an exciting development. Such diporphyrin complexes are expensive to synthesize, however, and stability is likely to be a problem, particularly in concentrated electrolytes such as 85% H_3PO_4 at elevated temperatures.

7. Concluding Remarks

Despite the large research effort and extensive literature on the O_2 electrode reactions, the mechanisms remain mostly a matter of speculation and the relationship of the electrocatalytic activity to surface electronic properties and morphology uncertain. The reasons for this state of uncertainty have been mentioned earlier in this chapter and include the following: (1) the marked irreversibility of the four-electron O_2 electrode reactions in aqueous electrolytes at moderate temperatures, (2) the difficulties of obtaining reproducible results between various laboratories with highly surface demanding reactions, and (3) the difficulty of establishing surface electronic and morphological properties of electrodes.

Among the more promising research areas to advancing our understanding of O_2 electrochemistry are the following:

1. Measurements in aqueous electrolyte solutions at elevated temperatures and pressures. By extending kinetic studies to higher temperatures and pressures, the rate constants can be increased to values at which it should be possible to carry out kinetic measurements at potentials near the reversible values, where the anodic and cathodic processes are complementary. From such measurements it should be possible to obtain stoichiometric numbers and complementary reaction orders for the cathodic and anodic processes. Electrode stability and particularly the solubility may prove to be a problem. It also does not necessarily follow that the mechanism and rds will be the same as at lower temperatures.

2. Isotopic studies. While isotopic tracer and equilibration studies have been carried out for the O_2 electrode reactions, little has been done with kinetic isotopic studies. The anodic generation of O_2 lends itself to isotope fractionation studies with O^{18} using isotope ratio mass spectroscopy. It would be helpful in screening various mechanisms for O_2 generation to know the magnitude of the kinetic isotope effect *under well-defined* kinetic conditions as a function of the electrode surface conditions. Kinetic measurements in deuterated solutions vs. undeuterated solutions may also yield further insight as to the role of protons provided the reproducibility of the measurements is good and impurity effects can be eliminated. While the theory for D/H kinetic isotope effects has been discussed,(345) experimental studies appear to be lacking.

3. Techniques for establishing electrode surface properties. *In situ* techniques for characterizing the surface properties of electrodes are of critical importance and warrant a continuing effort. Of particular importance are efforts to detect and characterize O_2 surface species which may be the precursors to the O–O bond breaking step during the O_2 reduction.

4. Studies of O_2 and H_2O adsorption on metal and semiconductor surfaces *in vacuo*. Powerful techniques are available for studying adsorbed species such as O_2, OH, and H_2O on metal and semiconductor surfaces *in vacuo*. These surface physics techniques can be used to establish the adsorption sites, adsorbate configuration, electronic properties, and vibrational spectra. Insight as to these properties at the solid–vacuum interface will prove helpful in understanding the behavior of O_2, OH, and H_2O at electrochemical interfaces.

Acknowledgments

One of the authors (MT) is pleased to acknowledge support from the International Research and Exchange Board (IREX) for a visit to Case Western Reserve University during which he worked on this chapter. The other two authors (AS and EY) express appreciation to the U.S. Department of Energy for support of their efforts in preparing part of this chapter.

References

1. J. P. Hoare, in *The Encyclopedia of Electrochemistry of the Elements*, Vol. 2, A. J. Bard, ed., Marcel Dekker, New York (1974), p. 220.
2. E. Yeager, in *Electrocatalysis on Non-Metallic Surfaces*, NBS Special Publication 455 (1976), p. 203.
3. W. Berl, *Trans. Electrochem. Soc.* **83**, 253 (1943).
4. E. Yeager, P. Krouse, and K. V. Rao, *Electrochim. Acta* **9**, 1057 (1964).
5. V. S. Bagotskii and D. Motov, *Dokl. Akad. Nauk USSR* **71**, 501 (1950).
6. I. E. Yablokova and V. S. Bagotskii, *Dokl. Akad. Nauk USSR* **85**, 599 (1952).
7. T. Joyner, *Z. Anorg. Allgem. Chem.* **77**, 103 (1912).
8. J. Divisek and B. Kastening, *J. Electroanal. Chem.* **65**, 603 (1975); (a) J. Chevalet, F. Rouille, L. Gierst, and J. P. Lambert, *J. Electroanal. Chem.* **39**, 201 (1972); (b) Y. A. Ilan, G. Czapski, and D. Meisel, *Biochim. Biophys. Acta* **430**, 209 (1976); (c) J. A. Fee and J. S. Valentine, *Superoxide and Superoxide Dismutases*, Academic Press, New York (1977), p. 19.
9. N. I. Dubrovina and L. N. Nekrasov, *Elektrokhim.* **8**, 1503 (1972).
10. W. M. Latimer, *The Oxidation States of the Elements and Their Potentials in Aqueous Solutions*, 2nd ed., Prentice Hall, New York (1952).
11. E. Yeager and A. Kozawa, in *Kinetic Factors in Fuel Cell Systems: The Oxygen Electrode*, Proc. 6th AGARD Meeting, Cannes, France (1964), p. 769–793.
12. J. P. Hoare, *The Electrochemistry of Oxygen*, Interscience, New York (1968).
13. G. N. Lewis, M. Randall, K. Pitzer, and L. Brewer, *Thermodynamics*, 2nd ed., McGraw-Hill, New York (1961).
14. J. P. Hoare, *Proc. R. Soc. London Ser. A* **142**, 628 (1933).
15. A. Damjanovic and J. O'M Bockris, *Electrochim. Acta* **11**, 376 (1966).
16. J. P. Hoare, *J. Electrochem. Soc.* **113**, 846 (1966).
17. A. Damjanovic, in *Modern Aspects of Electrochemistry*, Vol. 5, J. O'M. Bockris and B. E. Conway, eds., Plenum Press, New York (1969).
18. J. O'M. Bockris and A. K. M. S. Huq, *Proc. R. Soc. London Ser. A* **237**, 277 (1956).
19. N. Watanabe and M. A. V. Devanathan, *J. Electrochem. Soc.* **111**, 615 (1964).
20. J. P. Hoare, *J. Electrochem. Soc.* **110**, 1019 (1963).
21. J. P. Hoare, *J. Electrochem. Soc.* **126**, 1502 (1979).
22. J. P. Hoare, *Electrochim. Acta* **20**, 267 (1975).
23. R. Kh. Burshtein, M. R. Tarasevich, and V. A. Bogdsanovskaya, *Elektrokhimiya* **8**, 1542 (1972).
24. S. Schuldiner and R. M. Roe, *J. Electrochem. Soc.* **110**, 1142 (1963).
25. H. Wroblowa, M. L. B. Rao, A. Damjanovic, and J. O'M. Bockris, *J. Electroanal. Chem.* **15**, 139 (1967).
26. V. Ya. Shepelev, M. R. Tarasevich, and R. Kh. Burstein, *Elektrokhimiya* **7**, 999 (1971).
27. Cited in Ref. 17 as their Ref. 56.
28. H. B. Urbach and R. J. Bowden, *Electrochim. Acta* **14**, 927 (1969).
29. R. Lorenz and M. Hauser, *Z. Anorg. Allgem. Chem.* **51**, 81 (1906).
30. D. A. J. Rand and R. Woods, *J. Electroanal. Chem.* **35**, 209 (1972).
31. P. Bindra, S. Clouser, and E. Yeager, *J. Electrochem. Soc.* **126**, 1631 (1979).
32. E. I. Khrusheheva, V. S. Bagotskii, and N. A. Shumilova, *Elektrokhimiya* **16**, 743 (1980).
33. L. Mueller and L. N. Nekrasov, *J. Electroanal. Chem.* **9**, 282 (1965).
34. M. R. Tarasevich and V. S. Vilinskaya, *Elektrokhimiya* **9**, 98 (1973).
35. S. Sh. Leites, V. I. Lukyanycheva, V. S. Bagotskii, A. V. Yuzhanina, and V. S. Konyakina, *Elektrokhimiya* **9**, 620 (1973).
36. H. Angerstein-Kozlowska, B. E. Conway, and W. B. A. Sharp, *J. Electroanal. Chem.* **43**, 9 (1973).

37. J. P. Hoare, *J. Electrochem. Soc.* **121**, 872 (1974).
38. S. Schuldiner, M. Rosen, and D. R. Flinn, *Electrochim. Acta* **18**, 19 (1973).
39. M. Rosen, S. Schuldiner, and D. R. Flinn, *J. Electrochem. Soc.* **119**, 412 (1972).
40. V. I. Lukianycheva, L. A. Fokina, and N. A. Shumilova, All Union Congress of Electrochemistry, Moscow 1974, Proceedings, p. 241 (in Russian).
41. Z. A. Markova, A. A. Mikhailova, N. V. Osetrova, and V. S. Bagotskii, *Elektrokhimiya* **10**, 1794 (1974).
42. A. A. Mikhailova, N. V. Osetrova, and V. S. Bagotskii, *Elektrokhimiya* **13**, 1089 (1977).
43. V. I. Lukyanycheva, L. A. Fokina, N. A. Shumilova, and V. S. Bagotskii, *Elektrokhimiya* **14**, 389 (1978).
44. J. P. Hoare, in *The Encyclopedia of Electrochemistry of the Elements*, Vol. 2, A. J. Bard, ed., Marcel Dekker, New York (1974), p. 191.
45. J. O'M. Bockris and A. K. N. Reddy, *Modern Electrochemistry*, Vol. II, Plenum Press, New York (1970).
46. M. L. B. Rao, A. Damjanovic, and J. O'M. Bockris, *J. Phys. Chem.* **67**, 2508 (1963).
47. A. C. C. Tseung and H. L. Bevan, *J. Electroanal. Chem.* **45**, 429 (1973).
48. D. Winkelman, *Z. Elektrochem.* **60**, 731 (1956).
49. J. Giner, *Z. Elektrochem.* **64**, 691 (1960).
50. R. J. Bowen, H. B. Urbach, and J. H. Harrison, *Nature* **213**, 592 (1967).
51. H. B. Urbach and R. T. Bowen, *Electrochim. Acta* **14**, 927 (1969).
52. R. Woods, in *Electroanalytical Chemistry*, Vol. 9, A. J. Bard, ed., Marcel Dekker, New York (1976), Chap. 1.
53. G. Belanger and A. J. Vijh, in *Oxides and Oxide Films*, Vol. 5, A. J. Vijh, ed., Marcel Dekker, New York (1977), Chap. 1.
54. H. Angerstein-Kozlowska, B. E. Conway, and W. B. A. Sharp, *J. Electroanal. Chem.* **43**, 9 (1973).
55. M. R. Tarasevich and K. A. Radyvshkina, *Elektrokhimiya* **6**, 812 (1970).
56. A. N. Frumkin, *Z. Phys. Chem.* **116**, 466 (1925).
57. D. O. Hayward and B. M. W. Trapnell, *Chemisorption*, 2nd ed., Butterworths, London (1964).
58. T. Biegler and R. Woods, *J. Electroanal. Chem.* **20**, 73 (1963).
59. A. Damjanovic, A. T. Ward, B. Ulrick, and M. O'Jea, *J. Electrochem. Soc.* **122**, 471 (1975).
60. K. J. Vetter and J. W. Schultze, *J. Electroanal. Chem.* **34**, 141 (1972).
61. D. Gilroy, *J. Electroanal. Chem.* **71**, 257 (1976).
62. A. Damjanovic, L. S. R. Yeh, and J. F. Wolf, *J. Electrochem. Soc.* **127**, 874 (1980).
63. D. N. Buckley and L. D. Burke, *J. Chem. Soc., Faraday. Trans. 1* **71**, 1447 (1975).
64. E. Gileadi and S. Srinivasan, *Electrochim. Acta* **11**, 321 (1966).
65. H. Angerstein-Kozlowska, J. Klinger, and B. E. Conway, *J. Electroanal. Chem.* **75**, 45 (1977).
66. B. V. Tilak, B. E. Conway, and H. Angerstein-Kozlowska, *J. Electroanal. Chem.* **48**, 1 (1973).
67. D. H. Everett and W. I. Whitten, *Trans. Faraday Soc.* **48**, 749 (1952).
68. D. H. Everett and F. W. Smith, *Trans. Faraday Soc.* **50**, 187 (1954).
69. V. S. Bagotskii, Yu. B. Vasiliev, and I. I. Pyshnograeva, *Electrochim. Acta* **16**, 2141 (1971).
70. A. K. N. Reddy, M. A. Genshaw, and J. O'M. Bockris, *J. Chem. Phys.* **48**, 671 (1969).
71. M. E. Folger, J. O. Zerbino, N. R. deTacconi, and A. J. Arvia, *J. Electrochem. Soc.* **126**, 592 (1979).
72. P. N. Ross, *J. Electroanal. Chem.* **76**, 139 (1977).
73. V. S. Bagotskii and M. R. Tarasevich, *J. Electroanal. Chem.* **101**, 1 (1979).
74. S. Gottesfield and B. E. Conway, *J. Chem. Soc., Faraday Trans. 1* **69**, 1090 (1973).
75. *Symp. Faraday Soc.* **4** (1970).
76. W. O'Grady, C. Iwakura, J. Huang, and E. Yeager, in *Electrocatalysis*, M. W. Breiter, ed., Electrochemical Society, Princeton, New Jersey (1974), p. 286.

77. A. J. Appleby, *J. Electrochem. Soc.* **120**, 1205 (1973).
78. M. R. Tarasevich and V. A. Bogdanovskaya, *Elektrokhimiya* **7**, 1519 (1971).
79. M. R. Tarasevich, V. S. Vilinskaya, and R. Kh. Burshtein, *Elektrokhimiya* **7**, 1200 (1971).
80. R. Kh. Burshtein, M. R. Tarasevich, and K. A. Radyushkina, *Elektrokhimiya* **6**, 1611 (1970).
81. M. I. Temkin, *Zh. Fiz. Khim.* **15**, 296 (1941).
82. M. R. Tarasevich, V. A. Bogdanovskaya, and V. S. Villinskaya, *Elektrokhimiya* **7**, 1684 (1971).
83. B. D. Kurnikov and Yu. B. Vasiliev, *Elektrokhimiya* **10**, 77 (1974).
84. V. Lukyanycheva *et al.*, *Elektrokhimiya* **7**, 1287 (1971).
85. V. Lukyanycheva *et al.*, *Elektrokhimiya* **10**, 475 (1974).
86. A. V. Yuzhanina *et al.*, *Elektrokhimiya* **10**, 630 (1974).
87. T. Biegler, D. A. J. Rand, and R. Woods, *J. Electroanal. Chem.* **29**, 269 (1971).
88. J. L. Ord and F. C. Ho, *J. Electrochem. Soc.* **118**, 46 (1971).
89. W. Visscher and M. A. V. Devanathan, *J. Electroanal. Chem.* **8**, 127 (1964).
90. D. A. Vermilya, in *Advances in Electrochemistry and Electrochemical Engineering*, Vol. 3, P. Delahay, ed., Interscience, New York (1963).
91. A. Damjanovic, A. T. Ward, and M. O'Jea, *J. Electrochem. Soc.* **121**, 1186 (1974).
92. L. B. Harris and A. Damjanovic, *J. Electrochem. Soc.* **122**, 593 (1975).
93. A. Damjanovic and B. Jovanovic, *J. Electrochem. Soc.* **123**, 374 (1976).
94. A. Ward, A. Damjanovic, E. Gray, and M. O'Jea, *J. Electrochem. Soc.* **123**, 1599 (1976).
95. A. Damjanovic and L. S. R. Yeh, *J. Electrochem. Soc.* **126**, 555 (1979).
96. A. Damjanovic, L. S. R. Yeh, and J. F. Wolf, *J. Electrochem. Soc.* **127**, 1945 (1980).
97. A. Damjanovic, L. S. R. Yeh, and J. F. Wolf, *J. Electrochem. Soc.* **127**, 1951 (1980).
98. A. Damjanovic and A. T. Sard, *MTP Int. Rev. Sci. Phys. Chem. Ser.* **II**, 103 (1976).
99. K. J. Vetter and J. W. Schultze, *J. Electroanal. Chem.* **34**, 131 (1972).
100. D. Gilroy, *J. Electroanal. Chem.* **83**, 329 (1977).
101. N. Cabrera and N. F. Mott, *Rep. Prog. Phys.* **12**, 163 (1949).
102. V. S. Bagotskii, Yu. B. Vasiliev, J. Weber, and J. N. Pirtskhalava, *J. Electroanal. Chem.* **27**, 31 (1970).
103. S. Gilman, in *Electroanalytical Chemistry*, Vol. 2, A. J. Bard, ed., Marcel Dekker, New York (1967), p. 112.
104. D. Gilroy and B. E. Conway, *Can. J. Chem.* **46**, 875 (1968).
105. M. Fleischmann and H. R. Thirsk, in *Advances in Electrochemistry and Electrochemical Engineering*, Vol. 3, P. Delahay, ed., Interscience, New York (1963).
106. S. D. James, *J. Electrochem. Soc.* **116**, 1681 (1969).
107. Yu. M. Tyurin and G. F. Volodin, *Elektrokhimiya* **5**, 1203 (1969).
108. T. Biegler and R. Woods, *J. Electroanal. Chem.* **20**, 73 (1969).
109. Uy. M. Tyurin and G. F. Volodin, *Elektrokhimiya* **6**, 1186 (1970).
110. S. Shibata and M. P. Sumino, *Electrochim. Acta* **16**, 1089 (1971).
111. S. Shibata and M. P. Sumino, *Electrochim. Acta* **17**, 2205 (1972).
112. J. Balej and O. Spalek, *Collect. Czech. Chem. Commun.* **37**, 499 (1972).
113. L. A. Khanova, E. V. Kasatkin, and V. I. Veselovskii, *Elektrokhimiya* **8**, 451 (1972).
114. R. Parsons and W. M. M. Visscher, *J. Electroanal. Chem.* **36**, 329 (1972).
115. Yu. Ya Vinnikov, V. A. Shepelin, and V. I. Veselovskii, *Elektrokhimiya* **9**, 649 (1973).
116. L. A. Khanova, E. V. Kasatkin, and V. I. Veselovskii, *Elektrokhimiya* **9**, 562 (1973).
117. L. A. Khanova, E. V. Kasatkin, and V. I. Veselovskii, *Elektrokhimiya* **10**, 1098 (1974).
118. S. Shibata, *Electrochim. Acta* **22**, 175 (1977).
119. V. I. Veselovskii, in *Proceedings of the Fourth Conference on Electrochemistry, Soviet Electrochemistry*, Vol. 2, New York (1960), p. 163.
120. Yu. Ya. Vinnikov, V. A. Shepelin, and V. I. Veselovskii, *Electrokhim.* **9**, 1557 (1973).
121. D. A. Rand and R. Woods, *J. Electroanal. Chem.* **31**, 29 (1971).
122. M. Pourbaix, *Atlas of Electrochemical Equilibria in Aqueous Solutions*, Pergamon Press, New York (1968).

123. S. Gottesfeld, J. D. E. McIntyre, G. Beni, and J. L. Shay, *Appl. Phys. Lett.* **33**, 208 (1978).
124. S. Gottesfeld and J. D. E. McIntyre, *J. Electrochem. Soc.* **126**, 742 (1979).
125. S. Gottesfeld, *J. Electrochem. Soc.* **127**, 1922 (1980).
126. S. Gottesfeld, *J. Electrochem. Soc.* **127**, 272 (1980).
127. W. Böld and M. Breiter, *Electrochim. Acta* **5**, 109 (1961).
128. J. O. Zerbino, N. R. deTacconi, and A. J. Arvia, *J. Electrochem. Soc.* **125**, 1266 (1978).
129. D. R. Rogers, R. D. Shannon, A. W. Sleight, and J. L. Gilson, *Inorg. Chem.* **8**, 841 (1969).
130. W. D. Ryder, A. W. Lawson, and C. C. Sartain, *Phys. Lett.* **26A**, 209 (1968).
131. V. S. Bagotskii and M. R. Tarasevich, *J. Electroanal. Chem.* **101**, 1 (1979).
132. H. B. Beer, Belg. Patent No. 710551 (1968).
133. V. DeNora, *Chem. Eng. Tech.* **42**, 222 (1970).
134. S. Galizzoli, F. Tantardini, and S. Trasatti, *J. Appl. Electrochem.* **4**, 57 (1974).
135. S. Galizzioli, F. Tartarndini, and S. Trasatti, *J. Appl. Electrochem.* **5**, 203 (1975).
136. S. Trasatti and G. Buzzanca, *J. Electroanal. Chem.* **29**, App. (1971).
137. W. O'Grady, C. Iwakura, J. Huang, and E. Yeager, in *Electrocatalysis*, M. Brutes, ed., The Electrochemical Society, Princeton, New Jersey (1974), pp. 286–302.
138. A. Kozawa, *J. Inorg. Nucl. Chem.* **21**, 315 (1961).
139. J. Kruger, in *Advances in Electrochemistry and Electrochemical Engineering*, Vol. 9, *Optical Techniques in Electrochemistry*, R. H. Muller, ed., J. Wiley and Sons, New York (1973), p. 227.
140. J. D. E. McIntyre, in *Advances in Electrochemistry and Electrochemical Engineering*, Vol. 9, *Optical Techniques in Electrochemistry*, R. H. Muller, ed., J. Wiley and Sons, New York (1973), p. 61.
141. W. K. Paik and J. O'M. Bockris, *Surf. Sci.* **28**, 61 (1971).
142. B. D. Cahan, J. Horkans, and E. Yeager, *Surf. Sci.* **37**, 559 (1973).
143. J. Horkans, B. D. Cahan, and E. Yeager, *Surf. Sci.* **46**, 1 (1974).
144. A. K. N. Reddy, M. A. Genshaw, and J. O'M. Bockris, *J. Electroanal. Chem.* **8**, 406 (1964).
145. A. K. N. Reddy, M. A. Genshaw, and J. O'M. Bockris, *J. Chem. Phys.* **48**, 671 (1968).
146. S. H. Kim, W. Paik, and J. O'M. Bockris, *Surf. Sci.* **33**, 617 (1972).
147. R. Greef, *J. Chem. Phys.* **51**, 3148 (1969).
148. W. Visscher, *Optik* (*Stuttgart*) **26**, 403 (1967).
149. Y. Y. Vinnikov, V. A. Shepelin, and V. I. Veselovskii, *Elektrokhimiya* **9**, 649 (1973).
150. R. Parsons and W. Visscher, *J. Electroanal. Chem.* **36**, 329 (1972).
151. M. Barrett and R. Parsons, *Symp. Faraday Soc.* **4**, 72 (1970).
152. M. A. Barrett and R. Parsons, *J. Electroanal. Chem.* **42**, 1 (1973).
153. J. D. E. McIntyre and D. M. Kolb, *Symp. Faraday Soc.* **4**, 99 (1970).
154. A. Bewick and A. M. Tuxford, *Symp. Faraday Soc.* **4**, 114 (1970).
155. H. Angerstein-Kozlowska, B. Conway, and W. Sharp, *J. Electroanal. Chem.* **34**, 141 (1973); **43**, 9 (1973).
156. B. E. Conway and S. Gottesfeld, *J. Chem. Soc., Faraday Trans. 1* **69**, 1090 (1973).
157. R. M. Lazorenko-Manevich and T. N. Stoyanovskaya, *Elektrokhimiya* **8**, 982 (1972).
158. G. Belanger and A. K. Vijh, in *Oxides and Oxide Films*, Vol. 5, A. K. Vijh, ed., Marcel Dekker, New York (1977), Chap. 1, p. 1.
159. J. O'M. Bockris, B. D. Cahan, and G. E. Stoner, *Chem. Inst.* **1**, 273 (1969).
160. M. Fujihara and T. Kuwana, *Electrochim. Acta* **20**, 565 (1975).
161. K. S. Kim, N. Winograd, and R. E. Davis, *J. Am. Chem. Soc.* **93**, 6296 (1971).
162. G. A. Allen, P. M. Tucker, A. Capen, and R. Parsons, *J. Electroanal. Chem.* **50**, 335 (1974).
163. W. C. Johnson and L. A. Heldt, *J. Electrochem. Soc.* **121**, 34 (1974).
164. R. Thacker and J. P. Hoare, *J. Electroanal. Chem.* **30**, 1 (1971).
165. G. B. Fisher and B. A. Sexton, *Phys. Rev. Lett.* **44**, 683 (1980).
166. B. Z. Sexton, *Surf. Sci.* **94**, 435 (1980).
167. G. B. Fisher and J. L. Gland, *Surf. Sci.* **94**, 446 (1980).
168. W. O'Grady, *J. Electrochem. Soc.* **127**, 555 (1980).

169. P. N. Ross, Observation by XPS and EXAFS of a Crystallite Size Effect with Adsorption of Oxygen on Pt, in International Meeting, The Electrochemical Society, Pittsburgh, October 1978, Electrochemistry Abstracts 78-2, No. 305.
170. M. Fleischmann, private communications (work at the University of Southampton).
171. E. Yeager, in *Non-traditional Approaches to the Study of the Solid–Electrolyte Interface*, T. Furtak, K. Kliewer, and D. Lynch, eds., North-Holland Publishing Co., Amsterdam (1980), p. 1.
172. J. O'M. Bockris, *Discuss. Faraday Soc.* **1**, 229 (1947).
173. G. N. Kokhanov, *Elektrokhimiya* **7**, 1606 (1971).
174. S. Gottesfeld and S. Srinivasan, *J. Electroanal. Chem.* **86**, 89 (1978).
175. J. W. Schultze and K. Vetter, *Electrochim. Acta* **18**, 889 (1973).
176. K. I. Rosental and W. I. Veselovskii, *Dokl. Akad. Nauk SSSR* **III**, 637 (1956).
177. L. A. Khanova, E. V. Kasatkin, and V. I. Veselovskii, *Elektrokhimiya* **10**, 800 (1974).
178. C. H. Lee, A. Riga, and E. Yeager, in *Mass Transport Phenomena in Ceramics*, A. R. Copper and A. H. Heuer, eds., Plenum Press, New York (1974), pp. 489–499.
179. C. H. Lee and E. Yeager, The Dissolution Kinetics of Lithiated Nickel Oxide in Aqueous Solutions, Tech. Report 5, Office of Naval Research Contract Nonr. 14939(05), Case Western Reserve University Cleveland, Ohio (1969).
180. T. R. Beck and R. M. Moulton, *J. Electrochem. Soc.* **103**, 247 (1956).
181. A. Damjanovic, in *Modern Aspects of Electrochemistry*, Vol. 5, J. O'M. Bockris and B. E. Conway, eds., Plenum Press, New York (1969), Chap. 5.
182. R. Parsons, *Trans. Faraday Soc.* **47**, 1332 (1951).
183. J. P. Hoare, *The Electrochemistry of Oxygen*, Interscience, New York (1968).
184. K. Vetter, *Electrochemical Kinetics, Theoretical Aspects*, Academic Press, New York (1967).
185. P. Rüetschi and P. Delahay, *J. Chem. Phys.* **23**, 556 (1955).
186. A. Hickling and S. Hill, *Discuss. Faraday Soc.* **1**, 236 (1947).
187. A. J. Appleby, *Catal. Rev.* **4**, 221 (1970).
188. A. J. Appleby, in *Modern Aspects of Electrochemistry*, Vol. 9, J. O'M. Bockris and B. E. Conway, eds., Plenum Press, New York (1974), Chapt. 5.
189. R. Parsons, *Trans. Faraday Soc.* **54**, 1053 (1958).
190. H. Gerischer, *Bull. Chim. Soc. Belg.* **67**, 506 (1958).
191. A. J. Appleby, *J. Electrochem. Soc.* **117**, 1157 (1970).
192. D. B. Rogers, R. D. Shannon, A. W. Sleight, and J. L. Gilson, *Inorg. Chem.* **8**, 841 (1969).
193. A. Damjanovic and B. Jovanovic, *J. Electrochem. Soc.* **123**, 374 (1976).
194. R. Woods, in *Electroanalytical Chemistry*, Vol. 9, A. J. Bard, ed., Marcel Dekker, New York (1976).
195. R. E. Meyer, *J. Electrochem. Soc.* **107**, 847 (1960).
196. J. J. MacDonald and B. E. Conway, *Proc. R. Soc. London Ser. A* **269**, 419 (1962).
197. A. Damjanovic, A. Dey, and J. O'M. Bockris, *Electrochim. Acta* **11**, 791 (1966).
198. J. O'M. Bockris and K. M. S. Huq, *Proc. R. Soc. London Ser. A* **237**, 277 (1956).
199. W. M. Latimer, *Oxidation Potentials*, 2nd ed., Prentice Hall, New York (1952).
200. A. Hickling and S. Hill, *Trans. Faraday Soc.* **46**, 557 (1950).
201. L. Krishtalik, in *Advances in Electrochemistry and Electrochemical Engineering*, Vol. 7, P. Delahay and C. Tobias, eds., Interscience, New York (1970), pp. 283–340.
202. R. Parsons, in *Advances in Electrochemistry and Electrode Kinetics*, Vol. 1, P. Delahay and C. Tobias, eds., Interscience, New York (1961).
203. A. N. Frumkin, in *Advances in Electrochemistry and Electrochemical Engineering*, Vol. 1, P. Delahay and C. Tobias, eds., Interscience, New York (1961).
204. R. W. Gurney, *Proc. R. Soc. London Ser. A* **134**, 137 (1932).
205. H. Gerischer, *Z. Phys. Chem. NF* **26**, 223, 325 (1960).
206. F. P. Bowden, *Proc. R. Soc. London Ser. A* **126**, 107 (1930).
207. C. Iwakura, K. Fukuda, and H. Tamura, *Electrochim. Acta* **21**, 501 (1976).
208. A. I. Krasilshchikov, *Russ. J. Phys. Chem.* (*Zh. Fiz. Khim.*) **37**, 273 (1963).

209. M. H. Miles, E. A. Klaus, B. P. Gunn, J. R. Locker, W. E. Serafin, and S. Srinivasan, *Electrochim. Acta* **23**, 521 (1978).
210. J. A. Joebstl, *J. Vac. Sci. Technol.* **12**, 347 (1975).
211. D. N. Buckley and L. D. Burke, *J. Chem. Soc., Faraday Trans. 1* **72**, 2431 (1976).
212. J. O'M. Bockris, *J. Chem. Phys.* **24**, 817 (1957).
213. M. H. Miles, *J. Electroanal. Chem.* **60**, 89 (1975).
214. M. H. Miles, G. Kissel, P. W. T. Lu, and S. Srinivasan, *J. Electrochem. Soc.* **123**, 332 (1976).
215. A. C. C. Tseung and S. Jasem, *Electrochim. Acta* **22**, 31 (1977).
216. P. W. Lu and S. Srinivansan, *J. Electrochem. Soc.* **125**, 265 (1978).
217. W. O'Grady, C. Iwakura, J. Huang, and E. Yeager, Ruthenium oxide catalysts for the oxygen electrode, in *Electrocatalysis*, M. Breiter, ed., The Electrochemical Society, Princeton, New Jersey (1976), pp. 286–302.
218. W. O'Grady, C. Iwakura, and E. Yeager, Oxygen electrocatalysts for life support systems, in Proceedings of the Intersociety Conference on Environmental Systems, The American Society of Mechanical Engineers, San Diego, 1976, pp. 37–48.
219. J. Earley and H. Ragavi, *Inorg. Nucl. Chem. Lett.* **9**, 331 (1973).
220. J. Earley and T. Fealey, *Inorg. Chem.* **12**, 323 (1973).
221. A. N. Frumkin and L. N. Nekrasov, *Dokl. Acad. Nauk SSSR* **126**, 115 (1959).
222. Yu. B. Ivanov and V. G. Levich, *Dokl. Acad. Nauk SSSR* **126**, 1029 (1959).
223. S. Bruckenstein, *Elektrokhimiya* **2**, 1085 (1966).
224. Yu. V. Pleskov and V. Yu. Filinovski, *The Rotating Disk Electrode*, Consultants Bureau, New York/London (1976).
225. W. J. Albery and M. L. Hitchman, *Ring Disk Electrodes*, Clarendon Press, Oxford (1971).
226. L. Muller and L. Nekrasov, *Electrochim. Acta* **9**, 1015–1023 (1964).
227. A. Damjanovic, M. A. Genshaw, and J. O'M. Bockris, *J. Chem. Phys.* **45**, 4057 (1966).
228. V. S. Bagotskii, M. R. Tarasevich, and V. Yu. Filinovskii, *Elektrokhimiya* **5**, 1218 (1969).
229. V. S. Bagotskii, M. R. Tarasevich, and V. Yu. Filinovskii, *Elektrokhimiya* **8**, 84 (1972).
230. M. Davies, M. Clark, E. Yeager, and F. Hovorka, *J. Electrochem. Soc.* **106**, 56 (1959).
231. M. R. Tarasevich, G. I. Zakharkin, and R. M. Smirnova, *Elektrokhimiya* **7**, 1298 (1971).
232. M. R. Tarasevich, G. I. Zakharkin, and R. M. Smirnova, *Elektrokhimiya* **9**, 645 (1973).
233. M. R. Tarasevich, G. I. Zakharkin, and R. M. Smirnova, *Elektrokhimiya* **8**, 601 (1972).
234. A. Damjanovic, M. A. Genshaw, and J. O'M. Bockris, *J. Electrochem. Soc.* **114**, 1107 (1967).
235. H. S. Wroblowa, Yen-Chi Pan, and G. Razumney, *J. Electroanal. Chem.* **69**, 195 (1976).
236. R. W. Zurilla, R. K. Sen, and E. Yeager, *J. Electrochem. Soc.* **125**, 1103 (1978).
237. J. C. Huang, R. K. Sen, and E. Yeager, *J. Electrochem. Soc.* **126**, 736 (1979).
238. K. A. Radyushkina, M. R. Tarasevich, and R. Kh. Burstein, *Elektrokhimiya* **6**, 1352 (1970).
239. M. R. Tarasevich, K. A. Radyushkina, V. Yu. Filinovskii, and R. Kh. Burstein, *Elektrokhimiya* **6**, 1522 (1970).
240. B. G. Podlibnor and L. N. Nekrasov, *Elektrokhimiya* **5**, 340 (1969).
241. F. van den Brink, E. Barendrecht, and W. Visscher, *J. Electrochem. Soc.* **127**, 2003 (1980).
242. V. J. Lukyanycheva, A. V. Yuzhenina, B. J. Lentsner, L. L. Knots, N. A. Shumilova, and V. S. Bagotskii, *Elektrokhimiya* **7**, 1287 (1971).
243. M. R. Tarasevich and V. S. Vilinskaya, *Elektrokhimiya* **9**, 96 (1973).
244. G. V. Zhutaeva, N. D. Merkulova, N. A. Shumilova, and V. S. Bagotskii, *Elektrokhimiya* **10**, 1253 (1968).
245. V. S. Vilinskaya and M. R. Tarasevich, *Elektrokhimiya* **9**, 1187 (1973).
246. L. I. Antropov, C. G. Vrzhosek, M. R. Tarasevich, and M. A. Marinich, *Elektrokhimiya* **8**, 149 (1972).
247. V. S. Bagotskii and I. E. Yablokova, *Zh. Fiz. Khim.* **27**, 1663 (1953).
248. M. Homda, T. Kodera, and M. Kita, *J. Res. Inst. Catal. Hokkaido Univ.* **18**, 19 (1970).
249. E. Yeager, P. Krouse, and K. V. Rao, *Electrochim. Acta* **9**, 1059 (1964).
250. I. Morcos and E. Yeager, *Electrochim. Acta* **15**, 953 (1970).

251. M. R. Tarasevich, F. Z. Sabirov, A. P. Mertsalova, and R. Kh. Burstein, *Elektrokhimiya* **4**, 432 (1968).
252. F. Z. Sabinov and M. R. Tarasevich, *Elektrokhimiya* **5**, 608 (1969).
253. R. J. Taylor and A. A. Mumffray, *J. Electroanal. Chem.* **64**, 63 (1975).
254. S. I. Androuseva, M. R. Tarasevich, and K. A. Radyushkina, *Elektrokhimiya* **13**, 253 (1977).
255. M. R. Tarasevich, F. Z. Sabirov, and R. Kh. Burstein, *Elektrokhimiya* **7**, 404 (1971).
256. M. Appel and A. J. Appleby, *Electrochim. Acta* **23**, 1243 (1978).
257. M. R. Tarasevich, *Elektrokhimiya* **9**, 599 (1973).
258. E. Yeager, Electrocatalysis on Non-Metallic Surfaces, NBS Special Publication 455, 1976, p. 203.
259. D. Behar, G. Grapski, J. Rabani, L. M. Dorfman, and H. A. Schwarz, *J. Phy. Chem.* **74**, 3209 (1970).
260. D. T. Sawyer and E. T. Seo, *Inorg. Chem.* **16**, 499 (1977).
261. J. Wilshire and D. T. Sawyer, *Acc. Chem. Res.* **12**, 105 (1979).
262. R. K. Sen, J. Zagal, and E. Yeager, *Inorg. Chem.* **16**, 3379 (1977).
263. A. Damjanovic, A. Dey, and J. O'M. Bockris, *Electrochim. Acta* **11**, 791 (1966).
264. A. Damjanovic, A. Dey, and J. O'M Bockris, *J. Electrochem. Soc.* **113**, 739 (1966).
265. A. Damjanovic and V. Brusic, *Electrochim. Acta* **12**, 615 (1967).
266. A. Damjanovic, M. A. Genshaw, and J. O'M. Bockris, *J. Electrochem. Soc.* **114**, 566 (1967).
267. A. Damjanovic, in *Modern Aspects of Electrochemistry*, Vol. 5, J. Bockris and B. Conway, eds., Plenum Press, New York (1969), p. 369.
268. M. R. Tarasevich, R. Kh. Burstein, and K. A. Radyushkina, *Elektrochimiya* **6**, 372 (1970).
269. M. R. Tarasevich and V. A. Bogdanovskaya, *Elektrokhimiya* **7**, 1072 (1971).
270. M. R. Tarasevich, V. Ya. Shepelev, and R. Kh. Burstein, *Elektrokhimiya* **9**, 1693 (1973).
271. M. R. Tarasevich and V. S. Vilinskaya, *Elektrokhimiya* **8**, 1489 (1972).
272. D. B. Sepa, M. V. Vojanovic, and A. Damjanovic, *Electrochim. Acta* **25**, 1491 (1980).
273. D. B. Sepa, M. V. Vojanovic, and A. Damjanovic, Comparison of the kinetics and mechanisms of O_2 reduction on Pt electrodes over the entire pH range, in National Meeting of The Electrochemical Society, St. Louis, May, 1980, Extended Abstracts 80–1, 1220.
274. S. Sh. Leites, V. I. Lukyanycheva, V. S. Bagotskii, A. V. Vuzhannina, and V. F. Konanykina, *Elektrokhimiya* **9**, 620 (1973).
275. S. Sh. Leites, V. S. Bagotskii, and V. I. Lukyanycheva, *Elektrokhimiya* **9**, 1755 (1973).
276. M. Mochizuki, *J. Electrochem. Soc. Jpn.* **28**, 583 (1960).
277. D. T. Sawyer and L. V. Intervante, *J. Electroanal. Chem.* **2**, 310 (1961).
278. D. T. Sawyer and R. Day, *Electrochim. Acta* **8**, 589 (1963).
279. J. J. Lingane, *J. Electroanal. Chem.* **2**, 306 (1965).
280. D. C. Peters and R. A. Mitchell, *J. Electroanal. Chem.* **10**, 306 (1965).
281. J. D. F. Black and A. S. Buchanen, *Austr. J. Chem.* **19**, 2169 (1966).
282. A. J. Appleby and A. Borucka, *J. Electrochem. Soc.* **116**, 1212 (1969).
283. A. J. Appleby, *J. Electrochem. Soc.* **117**, 328 (1970).
284. P. C. Milner, *J. Electrochem. Soc.* **111**, 228 (1964).
285. V. A. Bogdanovskaya, R. Kh. Burstein, and M. R. Tarasevich, *Elektrokhimiya* **10**, 1011 (1974).
286. J. S. Griffiths, *Proc. R. Soc. London Ser. A* **235**, 73 (1956).
287. L. Pauling, *Nature* **203**, 182 (1964).
288. D. Yoke, A. Riga, R. Greef, and E. Yeager, *Electrochim. Acta* **13**, 1351 (1968).
289. E. Yeager and A. Kozawa, *Proceedings of the 6th AGARD Meeting, Cannes, 1964*, Pergamon Press, Oxford (1965), p. 769.
290. A. Tseung, B. Mobbs, and A. Jantram, *Electrochim. Acta* **15**, 473 (1970).
291. A. Tseung and H. L. Beuan, *J. Electroanal. Chem.* **45**, 429 (1973).
292. K. V. Kadish, in *Handbook on Fuel Cell Technology*, E. Berger ed., Prentice-Hall, Englewood Cliffs, New Jersey (1968), p. 361.
293. M. Savy, *Electrochim. Acta* **13**, 1359 (1968).

294. R. H. Burstein, V. S. Vilinskaya, M. R. Tarasevich, and N. C. Bulavina, *React. Kinet. Catal. Lett.* **4**, 159 (1976).
295. M. R. Tarasevich, V. S. Vilinskaya, A. M. Khutornoi, R. Kh. Burstein, F. V. Makordei, and Vu. A. Tkach, *Elektrokhimiya* **12**, 504 (1976).
296. A. M. Trunov, V. A. Presnov, M. V. Uminskii, Q. F. Rakityanskaya, T. S. Bakutina, and A. I. Kotseruba, *Elektrokhimiya* **11**, 552 (1975).
297. N. A. Shumilova, E. I. Khrushcheva, and O. V. Morabskaya, *Denki Kagaku* **43**, 14 (1975).
298. V. S. Bagotskii, N. A. Shumilova, and E. I. Khrushcheva, *Electrochim. Acta* **21**, 919 (1976).
299. D. M. Tench and E. Yeager, *J. Electrochem. Soc.* **121**, 318 (1974).
300. D. M. Tench and E. Yeager, *J. Electrochem. Soc.* **120**, 164 (1973).
301. S. G. Ogryzko-Zhukovskaya, N. A. Tedotov, and V. P. Belokopytov, *Elektrokhimiya* **10**, 1541 (1971).
302. J. R. Goldstein and A. Tseung, *J. Phys. Chem.* **76**, 3646 (1972).
303. G. K. Boreskov, Vu. A. Borisov, N. N. Bulgakov, V. S. Murykantov, G. I. Panov, and P. G. Tsyrulnilov, *Kinet. Catal.* **16**, 1246 (1975).
304. J. McHardy and J. O'M. Bockris, *J. Electrochem. Soc.* **120**, 53 (1973).
305. J. McHardy and P. Stonehart, in *MTP International Reviews of Science*, Vol. 6, A. Buckingham and J. O'M. Bockris, eds., Series Z, Butterworths, London (1974).
306. M. Behret, M. Binder, and G. Sandstede, *Electrochim. Acta* **20**, 111 (1975).
307. J. P. Randin, *J. Electrochem. Soc.* **120**, 373 (1973).
308. J. P. Randin, *Electrochim. Acta* **19**, 87 (1974).
309. J. P. Randin and E. Yeager, *J. Electrochem. Soc.* **118**, 711 (1971).
310. J. P. Randin and E. Yeager, *J. Electroanal. Chem.* **36**, 257 (1972).
311. J. P. Randin and E. Yeager, *J. Electroanal. Chem.* **58**, 313 (1975).
312. C. A. Klein, *J. Appl. Phys.* **33**, 3357 (1962).
313. R. E. Panzer and P. J. Ebving, *Electrochim. Acta* **20**, 635 (1975).
314. V. A. Garten and D. E. Weiss, *Rev. Pure Appl. Chem.* **7**, 69 (1957).
315. F. Gutmann and L. Lyons, *Organic Semiconductors*, Wiley, New York (1967).
316. H. Tachikawa and L. R. Faulkner, *J. Am. Chem. Soc.* **100**(14), 4379 (1978).
317. R. Jasinski, *J. Electrochem. Soc.* **122**, 526 (1965).
318. A. Kozawa, V. E. Zillion, and R. J. Brodd, *J. Electrochem. Soc.* **117**, 1470 (1970).
319. F. Beck, W. Zammert, J. Heiss, H. Miller, and R. Polster, *Z. Naturforsch.* **28A**, 1009 (1973).
320. M. Savy, P. Andro, C. Bernard, and C. Magner, *Electrochim. Acta* **18**, 191 (1973).
321. M. Savy, P. Andro, and C. Bernard, *Electrochim. Acta* **19**, 403 (1974).
322. K. A. Radyushkina, R. Kh. Burstein, B. D. Berezin, M. R. Tarasevich, and S. D. Levina, *Elektrokhimiya* **9**, 410 (1973).
323. K. A. Radyushkina, M. R. Tarasevich, and S. I. Andrusyova, *Elektrokhimiya* **11**, 1079 (1975).
324. M. R. Tarasevich, K. A. Radyushkina, and S. I. Andrusyova, *Bioelectrochemistry and Bioenergetics* **4**, 18 (1977).
325. H. Alt, H. Binder, and G. Sandstede, *J. Catal.* **28**, 8 (1973).
326. A. J. Appleby, J. Fleish, and M. Savy, *J. Catal.* **44**, 281 (1976).
327. J. P. Randin, *Electrochim. Acta* **19**, 83 (1974).
328. M. Behret, W. Clauberg, and S. Sandstede, *Ber. Bunsenges. Phys. Chem.* **81**, 54 (1977).
329. Chr. Kretzschmar and K. Wiesener, *Z. Phys. Chem. (Leipzig)* **257**, 39 (1976).
330. J. Zagal, R. K. Sen, and E. Yeager, *J. Electroanal. Chem.* **83**, 207 (1977).
331. J. Zagal, P. Bindra, and E. Yeager, *J. Electrochem. Soc.* **127**, 1506 (1980).
332. E. Yeager, J. Zagal, B. Nikolic, and R. R. Adzic, in *Proceedings of the Third Symposium on Electrode Processes*, S. Bruckenstein, J. D. E. McIntyre, B. Miller, and E. Yeager, eds., The Electrochemical Society, Princeton, New Jersey (1979), p. 409.
333. J. Zagal, Oxygen reduction on water soluble phthalocyanines adsorbed on graphite electrodes, Ph.D. thesis, Case Western Reserve University, 1978.
334. E. Yeager, *J. Electrochem. Soc.*, in press.

335. F. Beck, *Ber. Bunsenges. Phys. Chem.*. **77**, 353 (1973); see also *J. Appl. Electrochem.* **7**, 329 (1977).
336. L. C. Gruen and R. J. Blagrove, *Aust. J. Chem.* **25**, 319 (1973).
337. J. Veprek-Siska, E. Schwertnerova, and D. M. Wagnerova, *Chimia* **26**, 75 (1972).
338. D. M. Wagnerova, E. Schwertnerova, and J. Veprek-Siska, *Collect. Czech. Chem. Commum.* **39**, 1980 (1974).
339. B. Z. Nikolic, R. R. Adzic, and E. Yeager, *J. Electroanal. Chem.* **103**, 281 (1979).
340. R. Kötz and E. Yeager, *J. Electroanal. Chem.* **113**, 113 (1980).
341. J. P. Collman, P. Denisevich, Y. Konai, M. Marrocco, C. Koval, and F. C. Anson, *J. Am. Chem. Soc.* **102**, 6027 (1980).
342. G. Magner, M. Savy, and G. Scarbeck, *J. Electrochem. Soc.* **127**, 1076 (1980).
343. H. Meier, U. Tschirwitz, E. Zimmerhackl, W. Albrecht, and G. Zeitler, *J. Phys. Chem.* **81**, 712 (1977).
344. H. G. Jahnke, *Ber. Bunsenges. Phys. Chem.* **72**, 1053 (1968).
345. R. Saloman, *J. Phys. Chem.*
346. C. A. Melendres, *J. Phys. Chem.* **84**, 1936 (1980).

7

Deposition and Dissolution of Metals and Alloys. Part A: Electrocrystallization

EVGENI B. BUDEVSKI

1. Introduction

There are two major factors which have to be considered in the process of the electrolytic metal deposition: (i) the thermodynamic and growth properties of the crystalline phase which can be treated as largely independent of the presence and character of the ambient phase and (ii) the properties of the ionic solution affecting primarily the structure of the interface boundary and the kinetics of the mass and charge transfer across it. In the first part of this chapter the problems connected with the formation and growth of the crystals of the metal deposit will be discussed more closely, while the problems arising from the ionic solution side will be treated as simply as possible (see also Vol. 1 of this series).

In the second part of this chapter, the implications arising from the character and properties of the ionic solution phase will be considered, treating the deposition process as a whole. The texture and the surface morphology of the deposit are strongly affected by both crystalline properties of the depositing metal and mass and charge transfer across the interface boundary. Hence, for these aspects of the deposition process, the reader is advised to consult the second part (Part B) of the chapter.

EVENGI B. BUDEVSKI • Central Laboratory of Electrochemical Power Sources, Bulgarian Academy of Sciences, Sofia 1040, Bulgaria.

2. Kinetics of Atom Incorporation

The incorporation of atoms into the crystal lattice, i.e., the process of growth of a crystal, depends on the crystallographic character of the growing surface and is largely affected by the surface structure itself. The surface of a solid metal electrode has a complex character. Areas occupied by crystallites emerging on the surface with different crystallographic orientations and intergrain boundary regions can be differentiated. In addition, crystal defects, inclusions, adsorbed molecules, oxide layers, etc., complicate the state of the surface. The simplest conditions, to begin with, can be expected when single crystals are considered.

2.1. The Structure of a Crystalline Surface

A crystal is surrounded at equilibrium by flat, atomically smooth, low-index faces or, in Frank's classification,$^{(1)}$ by singular faces. These faces in equilibrium forms are defined by the Gibbs definition of the equilibrium form requiring a minimum of the surface free energy of the crystal at constant volume (see Section 5.1).

2.1.1. The Surface Roughness: Adatoms, Steps, and Kink Positions

At elevated temperatures, due to thermal fluctuations, singular faces acquire a surface roughness manifested by the formation of adatoms and surface vacancies, di- or polyatomic surface clusters, and vacancies and steps with kinks as shown in Figure 1. The surface roughness becomes appreciable only above a critical "roughening" temperature T_r. The theoretical value of T_r for a simple cubic crystal lattice, $T_r = 0.6\psi_1/^{(2)}k$, where ψ_1 denotes the bond energy between two first neighbor atoms, gives temperatures around or above the melting point. In reality T_r is lower but not substantially below the melting point. At room temperatures singular faces of metals have a relatively low degree of roughening, and exhibit only adatoms and monatomic vacancies. At steps, kink positions are also present.

Among the different positions in Figure 1, the kink position, or the "half-crystal" position, as introduced first by Kossel and Stranski, has a special significance for the definition of the equilibrium condition (vapor pressure, concentration, electrode potential, etc.) of an infinitely large crystal with its ambient phase.

The salient feature of the kink position is that if one atom is removed from such a position, for which a dissociation energy ϕ_k will be needed, the initial configuration is not changed and the removal of the next atom would require the same energy. An infinitely large crystal can then be disintegrated (sublimated, dissolved) by removing atoms consecutively from kink positions. The contribution of the boundary atoms being insignificant, the sublimation (dissolution) energy G_s is then $G_s = N_A\phi_k$.

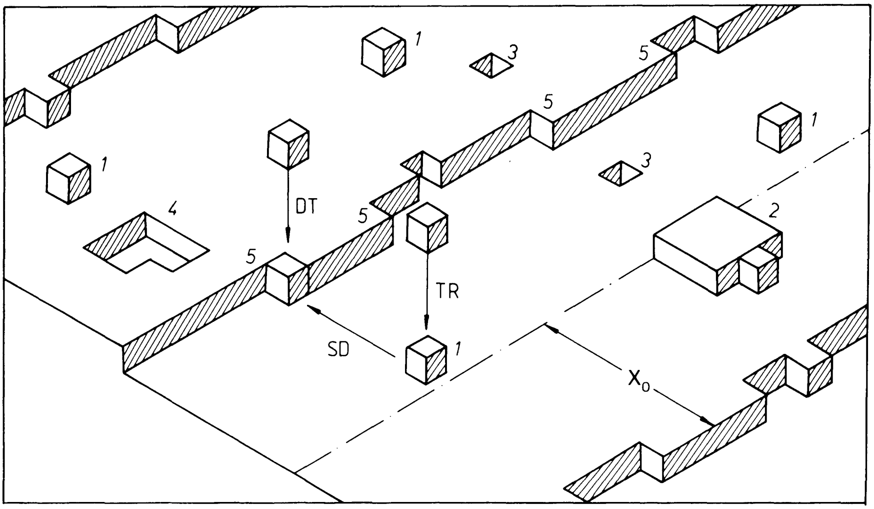

Figure 1. The structure of a crystalline singular face and paths of atom incorporation. 1, Adatom; 2, adatom cluster; 3, vacancy; 4, vacancy cluster; 5, half-crystal (kink) atom; DT, direct transfer to a kink position; TR, transfer to an adatom; SD, surface diffusion and incorporation; x_0 step half-distance.

2.1.2. The Equilibrium Potential and the Kink Atom Position

Now it is also understandable that the exchange of kink atoms with the ambient phase can be used for the definition of the equilibrium, because it requires the same Gibbs free energy per atom as the average disintegration free energy of the crystal per atom, i.e., just equal to the chemical potential of the crystalline phase.

One cannot, however, mechanically transfer the problem of crystal-vapor equilibrium to the case of electrocrystallization. In the first case ϕ_k is obtained from the sublimation energy: $\phi_k = G_s/N_A$, or from the energy of interaction ψ_1 between first neighbor atoms and the number of first neighbors of a kink atom (e.g., six, as in the case of a fcc or hcp crystal: $\phi_k = 6\psi_1$). In the second case, however, charge transfer across the electric field of the double layer as well as the ion-solvent interaction have to be also considered.

According to Kaischew$^{(3)}$ the frequencies of deposition and dissolution of atoms on/from a site i of the crystal surface are given for the case of electrocrystallization by

$$\omega_{\text{dep},i} = p_i c \exp(-\Delta G^{\ddagger}_{\text{dep},i}/kT) \exp(-\beta z e_0 E/kT) \tag{1}$$

$$\omega_{\text{diss},i} = q_i \exp(-\Delta G^{\ddagger}_{\text{diss},i}/kT) \exp[(1-\beta) z e_0 E/kT] \tag{2}$$

where E is the electrode potential. The $G^{\ddagger}$'s are the activation energies of deposition and dissolution of an atom on/from the site i at a standard concentration. The values of the activation energies for any particular site are interrelated with the energy ϕ_i of the transfer of an atom from that particular site i to the solution: $-(\Delta G^{\ddagger}_{\text{dep},k} - \Delta G^{\ddagger}_{\text{dis},i}) = \phi^{\ddagger}_{i,s}$.†

At equilibrium, i.e., at the equilibrium potential, of an infinitely large crystal with its ambient phase present, the deposition and dissolution frequencies of kink atoms must be equal, and then from (1) and (2), bearing in mind $-(\Delta G^{\ddagger}_{\text{dep},k} - \Delta G^{\ddagger}_{\text{diss},k}) = \phi_{k,s}$, it follows that

$$ze_0E_r = \phi_{k,s} + kT\ln(p_k/q_k) + kT\ln c \tag{3}$$

It is seen that the reversible potential, E_r, is related to the dissociation energy of a kink atom $\phi_{k,s}$. In the case of the electrocrystallization process, however, $\phi_{k,s}$ cannot be obtained directly from the sublimation energy or the bond energy ψ_1; additional effects such as energy of ionization, energy of hydration, etc., have of course also to be taken into account.

2.1.3. The Step Roughness

From the viewpoint of the deposition or growth process, it would be of interest to have a quantitative description of the surface structure. At room temperatures, thermal roughening is not expected to produce monatomic steps(2) but, if present, they may show a rather high concentration of kinks. The mean distance δ_0/a between kinks in atomic diameters is given for the most dense step on a (100) face of a fcc crystal(2,4) by

$$\delta_0/a = [2 + \exp(\psi_1/2kT)]/2 \tag{4}$$

With a typical value of $\Delta G_s = 150\ \text{kJ mol}^{-1}$ or $\psi_1 = 4.1 \times 10^{-20}$ J per bond, thermal roughening causes every 75th atom of the step to be in a kink position.

---

† As seen in contrast to a homogeneous (liquid) surface in the case of deposition on a crystal face for any particular site, a different value of the deposition and dissolution frequencies can be ascribed, determined by the energy barriers G_{dep} and G_{diss} and the constants p_i and q_i. If there are n_i sites per unit area of the type i, an exchange current density per unit area of atoms deposited on these sites with the ions in the solution may be defined by analogy to a homogeneous surface:

$$i_{0,i}/ze_0 = \omega^{\text{rev}}_{\text{dep},i}n^0_i = \omega^{\text{rev}}_{\text{diss},i}n^0_{i+1} \tag{a}$$

where n_i are the number of sites of the type i per unit area which by addition of one atom are transformed to sites of the type $(i + 1)$. For example, a free surface site "0" is transformed by addition of one atom to an adatom site "ad," or a vacancy "v" to a free surface site "0." The equality $\omega^{\text{rev}}_{\text{dep},i}n^0_i = \omega^{\text{rev}}_{\text{diss},i}n^0_{i+1}$ is fulfilled only at the equilibrium potential when the equilibrium concentrations n^0_i and n^0_{i+1} are established. Only in the case of the kink atom sites "k" is the number of kink sites n_k undefined but this has no effect on the equilibrium because the addition of one atom to a kink site does not change the number of kink sites, i.e., $n_i = n_{i+1}$ in Eq. (a). Hence, the equilibrium potential is defined by the dissolution–deposition frequencies only, $\omega^{\text{rev}}_{\text{diss},k} = \omega^{\text{rev}}_{\text{dep},k}$, irrespective of the number of kink sites n_k. The intensity of the exchange of kink atoms per unit area with ions in the solution, however, gives the exchange current density of kink atoms and, as seen from Eq. (a), is proportional to the number of kink sites n_k and, hence, to the step density, the step roughness being defined by the temperature (see Section 2.1.3).

Owing to the solid-solvent phase boundary interaction, however, this density may be increased significantly. A more reasonable value in such a case may be obtained when ψ_1 is calculated from the specific surface energy σ or the specific edge energy ε, e.g.,$^{(2)}$

$$\varepsilon a = \frac{\psi_1}{2} - 2kT \exp\left(-\frac{\psi_1}{kT}\right) \tag{5}$$

It is obvious that ψ_1 calculated in this way, i.e., from ε, includes a part of the hydration energy of the surface atoms, as was considered by Conway and Bockris. For the case of silver in $6\,M$ $AgNO_3$ at 318 K, a value of $\varepsilon = 2.1 \times 10^{-13}$ J cm^{-1} has been found giving for $\psi_1(\varepsilon) = 1.52 \times 10^{-20}$ J per bond. With $a = 2.88 \times 10^{-8}$ cm, Eq. (4) shows that every fourth atom is in a kink position.

2.1.4. The Concentration and Mean Displacement of Adatoms

The equilibrium adatom concentration C^0_{ad}, mol cm^{-2}, of a sufficiently large crystal is given by

$$n_{\text{ad}} = C^0_{\text{ad}} N_A = n_0 \exp(-W/kT) \tag{6}$$

where the preexponential term contains the entropy factor and is roughly equal to the surface atomic density n_0.$^{(2)}$ $W = \phi_k - \phi_{\text{ad}}$ is the energy of transfer of an atom from a kink position to the adsorption site. $\phi_k = \Delta G_s/N_A$ is a constant characteristic for the crystal. ϕ_{ad} depends on the crystallographic character of the face and contains a part of the hydration energy of adatoms.$^{(5,6)}$ This makes the assessment of C^0_{ad} rather difficult.

Adatoms exchange with ions in solution. Equations (1) and (2), applied to the adsorption sites of a face, give for the deposition and dissolution rates in terms of current densities, A cm^{-2},

$$i_{c,\text{ad}} = \omega_{\text{dep,ad}} z e_0 n_0 \quad \text{and} \quad i_{a,\text{ad}} = \omega_{\text{diss,ad}} z e_0 n_{\text{ad}} \tag{7}$$

The density of adatoms n_{ad} is assumed to be much smaller than n_0 and is neglected with respect to n_0 in the first equation. At any potential E the dissolution and deposition rates can equalize producing a stationary value of n_{ad} or C_{ad}. From (7), (1), and (2) with $i_a = i_c$ follows

$$C_{\text{ad}}(E) = \frac{n_0}{N_A} \frac{p_{\text{ad}}}{q_{\text{ad}}} c \exp\left(\frac{\phi_{\text{ad}}}{kT}\right) \exp\left(-\frac{z e_0 E}{kT}\right) \tag{8}$$

where $\phi_{\text{ad}} = -(\Delta G^{\ddagger}_{\text{dep,ad}} - \Delta G^{\ddagger}_{\text{diss,ad}})$ is the desorption energy of an adatom. At the equilibrium potential, $E = E_{\text{rev}}$ (where $i_c = i_a = i_0$), $C_{\text{ad}}(E_{\text{rev}}) = C^0_{\text{ad}}$, i.e., the adatom concentration is a constant independent of c or E_{rev} because of their relation through the Nernst equation. The potential independence of C^0_{ad} follows also from Eq. (6) directly.

The mean residence time of adatoms on the face is given by $1/\tau_r = \omega_{\text{diss,ad}}$ or with Eq. (7) for any arbitrary potential when the dissolution and deposition rates have equalized:

$$\tau_r = C_{\text{ad}}zF/i_{a,\text{ad}} = C_{\text{ad}}zF/i_{c,\text{ad}} \tag{9}$$

The mean residence time depends on potential. At the equilibrium potential, $\tau_r^0 = C_{\text{ad}}^0 zF/i_{0,\text{ad}}$.†

During their stay on the surface, adatoms migrate at random across the surface making an average displacement λ_s given by

$$\lambda_s^2 = D_s\tau_r = \frac{zFC_{\text{ad}}^0}{i_{0,\text{ad}}}D_s \exp\left[-\frac{(1-\beta)ze_0\eta}{kT}\right] \tag{10}$$

where D_s is the surface diffusion coefficient, $i_{0,\text{ad}}$ the exchange current density, and $\eta = E - E_{\text{rev}}$, the overpotential. The mean displacement distance λ_s is a function of the overpotential. At the equilibrium potential, $\lambda_s^0 = (zFC_{\text{ad}}^0 D_s/i_{0,\text{ad}})^{1/2}$.

2.2. The Propagation Rate of Steps

If the potential of an atomically smooth (stepless) singular face is changed, e.g., to a value below the reversible potential, the enhanced deposition rate would increase the adatom concentration above its equilibrium value, C_{ad}^0, until the opposite reaction $i_{a,\text{ad}}$, increasing with C_{ad}, takes the balance with $i_{c,\text{ad}}$. Then, with $i_{c,\text{ad}} = i_{a,\text{ad}}$, from Eq. (8) it follows that

$$C_{\text{ad}}(\eta) = C_{\text{ad}}^0 \exp(-ze_0\eta/kT) \tag{11}$$

2.2.1. Surface Diffusion

If steps are present, in close vicinity of the step edge the kink-atom–adatom exchange reaction will keep the adatom concentration at its equilibrium value, C_{ad}^0. At a distance greater than λ_s, however, adatoms deposited on the face cannot reach the step edge during their residence time, so that the adatom concentration will remain unaffected by the presence of the step equal to $C_{\text{ad}}(\eta)$. This causes a diffusion flux $D_s(C_{\text{ad}} - C_{\text{ad}}^0)/\lambda_s$ of adatoms toward the step edge where these are incorporated into the crystal lattice. At room temperature, where the average kink distance is of the order of several atoms (see Section 2.1.), diffusion along the step edge can be neglected. The incorporation of atoms in the step causes a propagation of its edge with a rate $v = (zF/q_{\text{mon}})D_s\Delta C_{\text{ad}}/\lambda_s$, or with Eqs. (11) and (10);

$$v_{\text{SD}} = \frac{2i_{0,\text{ad}}\lambda_s}{q_{\text{mon}}}V(\eta) \tag{12}$$

---

† Note that τ_r^0 is a function of the bulk concentration c or E_{rev} through $i_{0,\text{ad}}$.

where

$$V(\eta) = \exp[(1-\beta)ze_0\eta/kT] - \exp(-\beta ze_0\eta/kT) \tag{12a}$$

or, for $ze_0\eta/kT \ll 1$,

$$V(\eta) = ze_0\eta/kT \tag{12b}$$

Here q_{mon} is the amount of electricity needed for the completion of one monatomic layer. The factor 2 in Eq. (12) accounts for the two equivalent fluxes from both sides of the step.

2.2.2. Direct Transfer

A fraction of the number of atoms incorporated into the step edge at a cathodic overpotential is supplied by direct transfer from the solution. The rate of this direct transfer reaction is determined by the frequencies of deposition and dissolution, Eqs. (1) and (2), applied to the step sites "st," i.e., sites adjacent to the step edge. We can define cathodic, anodic, and exchange current densities for these sites by analogy to the adsorption sites [see Eq. (7)]. Then, with $v_{\text{DT}} = i_{\text{DT}}\delta/q_{\text{mon}}$, the partial propagation rate v_{DT} due to direct transfer will be given by

$$v_{\text{DT}} = \frac{i_{0,\text{st}}\delta}{q_{\text{mon}}} V(\eta) \tag{13}$$

where $i_{0,\text{st}} = \omega_{\text{dep,st}}(E_{\text{rev}})ze_0/\delta a = \omega_{\text{diss,st}}(E_{\text{rev}})ze_0/\delta a$ is the exchange current density for the step site atoms and δ is the width of an atomic row added to the step edge and a is again the length per atom along the step.

If the exchange current densities $i_{0,\text{ad}}$ and $i_{0,\text{st}}$ are of the same order of magnitude, the ratio λ_s/δ predetermines a much higher contribution from surface diffusion.

2.2.3. The Exact Solution of the Surface Diffusion Problem

If two steps are closer than twice the mean displacement distance of adatoms, $x_0 < \lambda_s$, the regions of depleted adatom concentration overlap and the surface diffusion decreases in rate with respect to that obtained from Eq. (12).

The surface diffusion problem can be treated in greater detail by solving Fick's diffusion equations. The problem has been treated by a number of authors(7–12) who have come to almost identical conclusions. We shall follow a similar way of reasoning to that of Despić and Bockris,(8) but see also Ref. 10.

Consider an infinitesimal element, $dx\, dy$, of the surface at a distance x from the step element. The atom fluxes to and from this surface element are defined as follows:

$$\frac{dC_{\mathrm{ad}}(x,t)}{dt} = D_s \frac{d^2 C_{\mathrm{ad}}(x,t)}{dx^2} - \frac{i(x,t)}{zF} \tag{14}$$

$$i(x,t) = i_{0,\mathrm{ad}} \left\{ \frac{C_{\mathrm{ad}}(x,t)}{C^0_{\mathrm{ad}}} \exp\left[\frac{(1-\beta)ze_0\eta}{kT}\right] - \exp\left(-\frac{\beta ze_0\eta}{kT}\right) \right\} \tag{15}$$

$$i - C_{\mathrm{DL}} \frac{d\eta}{dt} = \frac{1}{x_0} \int_0^{x_0} i(x,t)\, dx \tag{16}$$

The $C_{\mathrm{DL}}(d\eta/dt)$ term accounts for the double-layer charging current. The right-hand part of Eq. (16) represents the mean Faradaic current to the crystal face.

The boundary conditions can be formulated in accordance with the specifics of the incorporation kinetics of the adatoms into the step edge, as follows:

(a) With a high incorporation rate constant, the adatom concentration in the close vicinity of the step edge changes insignificantly during growth and the boundary conditions are

$$C_{\mathrm{ad}}(x,0) = C_{\mathrm{ad}}(0,t) = C^0_{\mathrm{ad}}, \qquad [dC_{\mathrm{ad}}(x,t)/dx]_{x=x_0} = 0 \tag{17}$$

(b) With a low incorporation rate constant, the incorporation process needs a rise in the adatom concentration in the close vicinity of the step edge and the boundary conditions are in this case

$$\begin{gathered} C_{\mathrm{ad}}(x,0) = C^0_{\mathrm{ad}}, \qquad [dC_{\mathrm{ad}}(x,t)/dx]_{x=x_0} = 0, \qquad \text{and} \\ D_s[dC_{\mathrm{ad}}(x,t)/dx]_{x=0} = v_{\mathrm{inc}}[C_{\mathrm{ad}}(0,t) - C^0_{\mathrm{ad}}]/C^0_{\mathrm{ad}} \end{gathered} \tag{18}$$

where v_{inc}, mol $\mathrm{cm}^{-1}\,\mathrm{s}^{-1}$, is the incorporation rate constant.

This system of equations has been solved for the potentiostatic case.(7–10) The more informative galvanostatic case has not been solved yet. An equivalent electric circuit may be used for stimulation of galvanostatic transients at low overpotentials (Figure 2).(13) Many authors have solved this system of equations for different additional assumptions and approximations, e.g., as in Refs. 14 and 15. It is beyond the scope of this chapter to go into details of the problem and the reader is advised to consult the cited authors. A comprehensive review can be found in Vetter's monograph *Electrochemical Kinetics.*(10)

Three points may be worth emphasizing here:

(a) The adatom concentration distribution $C_{\mathrm{ad}}(x)$ in the steady state has been solved by a number of authors(7,8,10) and can be represented in the form

$$\frac{C_{\mathrm{ad}}(x)}{C^0_{\mathrm{ad}}} = \exp\left(-\frac{ze_0\eta}{kT}\right) + \left[1 - \exp\left(\frac{ze_0\eta}{kT}\right)\right] \frac{\mathrm{Chi}\,(x_0 - x)/\lambda_s}{\mathrm{Chi}\,(x_0/\lambda_s)} \tag{19}$$

where the substitution $\lambda_s = \lambda^0_s \exp[-(1-\beta)ze_0\eta/2kT]$ with $\lambda^0_s =$

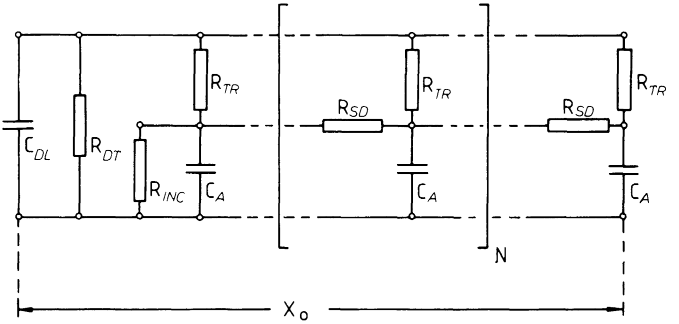

Figure 2. Equivalent electric circuit simulating the metal deposition process on a stepped surface (from E. Budevski and Z. Stoinov).(13) C_{DL}, Double-layer capacitance; C_A, adatom pseudocapacitance; R_{TR}, adatom transfer resistance; R_{SD}, adatom diffusion resistance; R_{INC}, adatom incorporation resistance; R_{DT}, direct transfer resistance; x_0, step half-distance.

$(zFD_sC^0_{\mathrm{ad}}/i_0)^{1/2}$ has the significance of a surface diffusion penetration depth and is equal to the mean displacement distance of adatoms defined by Eq. (10). Note that λ_s is an overpotential function. This relation is represented in Figures 3a and 3b for different η and λ^0_s/x_0 values. When $x > 4\lambda^0_s$, for sufficiently large x_0 values, $C_{\mathrm{ad}}(x)$ reaches its saturation value defined by Eq. (11), as seen, e.g., for the case $x_0/\lambda^0_s = 10$ and $\eta = 10$ mV in Figure 3b.

The local current densities, $i(x)$, are easily found by inserting Eq. (19) in Eq. (15) and are represented for different η and λ^0_s/x_0 values in Figures 3c and 3d.

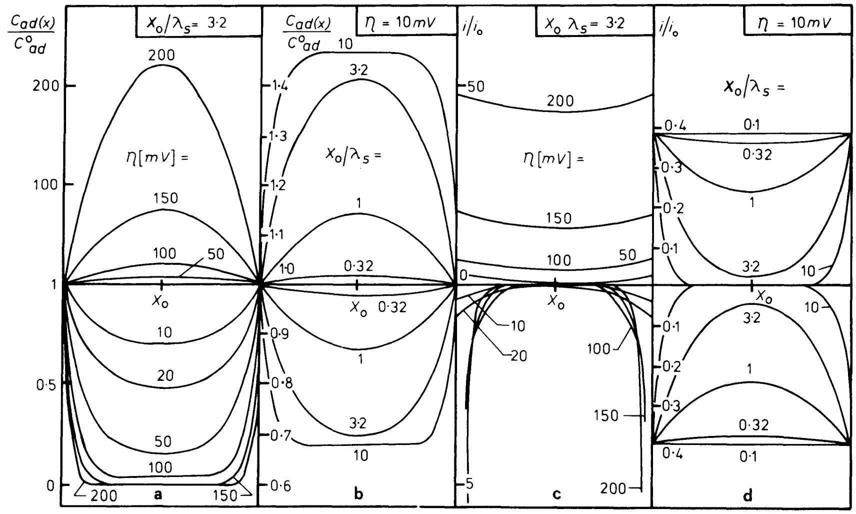

Figure 3. Adion concentration profiles, $C_{\mathrm{ad}}(x)/C^0_{\mathrm{ad}}$, and current density distribution, $i(x)/i_0$, between two growth steps at different x_0/λ_s and η values (Despić and Bockris).(8)

(b) The step propagation rate v, cm sec^{-1}, can be easily obtained by differentiation of Eq. (19) bearing also in mind Eq. (10):

$$v_{\mathrm{SD}} = \frac{2\lambda_s i_{0,\mathrm{ad}}}{q_{\mathrm{mon}}} V(\eta) \tanh\left(\frac{x_0}{\lambda_s}\right) \tag{20}$$

For $x_0 \gg \lambda_s$, this equation coincides with Eq. (12).

(c) The galvanostatic transient $\eta(t)_i$ can give information about the otherwise inaccessible adatom concentration. From the equivalent electric circuit simulating the deposition mechanism (Figure 2)[13] described by Eqs. (14)–(16) it can be assumed that after the double-layer charging $t > 4C_{\mathrm{DL}}\delta_D$, the initial slope i/C_{DL} should change to $i/(C_{\mathrm{DL}} + C_{\mathrm{A}})$, where $\delta_D = RT/zFi_0$ is the ion transfer resistance across the double layer and $C_{\mathrm{A}} = C^0_{\mathrm{ad}} z^2F^2/RT$ is the adatom pseudocapacitance. The further course of the transient before coming to saturation should follow a Warburg-impedance-like-$\sqrt{t}$ law due to the evolution of the surface diffusion process and, depending on λ_s/x_0, can hinder the evaluation of C_{A}. A large value of C_{A}, $C_{\mathrm{A}} > C_{\mathrm{DL}}$ (with $C_{\mathrm{DL}} \approx 20\ \mu\mathrm{F\ cm}^{-2}$ this requires C^0_{ad} 5×10^{-12} mol cm^{-2}) and a large value of x_0/λ_s are a prerequisite for a reliable determination of C_{A} and C^0_{ad}.

2.3. The Current Density on a Stepped Crystal Face

Consider a stepped singular face with a regular step spacing of $2x_0$. The step density L_s, cm^{-1}, or its equivalent, the total step length per unit area, cm cm^{-2}, is given by $L_s = 1/2x_0$. At a given overpotential all steps will propagate with a rate v determined by Eqs. (20) or (13), or the sum of both. The current density is given by

$$i = vL_s q_{\mathrm{mon}} \tag{21}$$

According to the mechanism prevailing we obtain the following:

(a) For the surface diffusion mechanism:

$$i = i_{0,\mathrm{ad}} V(\eta) \frac{\lambda_s}{x_0} \tanh\left(\frac{x_0}{\lambda_s}\right) \tag{22}$$

The first theoretical treatment of this mechanism was given by Lorenz,[7] who adapted the theory of Burton, Cabrera, and Frank[2] to the case of metal deposition. Later the problem was treated by Vermilyea,[12] Fleischmann and Thirsk,[11] Despić and Bockris,[8] Damjanović and Bockris,[9] and by Schnittler,[16] who brought the theory of surface diffusion to its present state.

Two limiting cases can be considered here:

(i) $\lambda_s \gg x_0$: Equation (22) yields a Butler–Volmer relation $i = i_0 V(\eta)$, i.e., the charge transfer is the rate-determining step and the current density is unaffected by the surface morphology.

(ii) $\lambda_s \ll x_0$: The tanh (x_0/λ_s) term in Eq. (22) is equal to unity and

$$i = 2i_{0,\mathrm{ad}} L_s \lambda_s V(\eta) \tag{23}$$

The surface diffusion process controls the reaction rate and the current density is proportional to the step density L_s.

(b) For the direct transfer mechanism, from Eqs. (21) and (13) we obtain

$$i = i_{0,st}\delta L_s V(\eta) \tag{24}$$

This equation is homologous to Eq. (23), and both are linear with respect to the step density L_s.

The direct transfer mechanism was suggested for the first time by Volmer(17) and was discussed later in the works of Lorenz,(7) Fleischmann and Thirsk,(11) Mott and Watts–Tobin,(18) and others. A comprehensive treatment of the problem may be found in Vetter.(10)

As seen from Eqs. (23) and (24) in both cases, i.e., for direct transfer or surface diffusion (with $\lambda_s < x_0$), the current density depends on the step density or in other words on the surface morphology. A high-indexed surface zone with a high density of steps or growth sites (kink positions), where $\lambda_s \gg x_0$, would follow the same growth law as a liquid metal, i.e., the Butler–Volmer relation. Special growth conditions are to be expected for perfect, defect-free singular faces. Vicinal faces characterized by low-index surface zones, separated by uniformly distributed monatomic steps, show an intermediate behavior. During growth, nonsingular surfaces would be faceted and transformed to vicinal faces. Owing to the growing out of the steps, vicinal faces are transformed to singular faces. Thus, in a later stage of growth, a perfect crystal will be bound by low-index singular faces. For a perfect defect-free crystal bound by singular faces, the only way for further growth is the formation of two-dimensional (2D) clusters of adatoms giving birth to a new lattice net which, with its peripheral step, would make atom incorporation into the crystal lattice possible. This mechanism of growth is known as the 2D nucleation mechanism of growth and will be discussed in the next section. Defect-free crystals are rarely found or produced, however. In the presence of defects and especially of screw dislocations, the step connected with this defect perpetuates during growth and produces a sufficient number of growth sites to make the 2D nucleation a not indispensable process. The mechanism of growth of real crystals will be treated in Section 4.

3. Metal Deposition on a Perfect Crystal Face

A perfect crystal bound by singular faces exhibits no sites for growth. A 2D nucleation process is required for the deposition of every new layer, as first noted by Gibbs(19) and developed later by Volmer and Weber,(20) Brandes,(21) and Kaischew.(22) This is because one atom deposited on the crystal face has a smaller bond energy to the crystal than a kink atom and it stays only temporarily on the surface as an adatom. A very important factor is the tendency of these surface atoms to cluster together thereby increasing their stability. Clusters of that kind are potential nuclei of a new lattice net.

3.1. Energy and Rate of Formation of Two-Dimensional Nuclei

3.1.1. Energy of Formation and Size of the Critical Nucleus

The Gibbs free energy of formation of a cluster consisting of N atoms is given (see also Section 5) by

$$\Delta G(N) = -Nze_0\eta_c + \Phi(N) \tag{25}$$

The first term accounts for the transfer of the N atoms across the double layer at the overpotential (cathodic) $\eta_c = E_{\text{rev}} - E$, the second term for the increase of the surface energy. The only change in the surface energy in the formation of a 2D cluster on a substrate of the like metal is the energy connected with the formation of the peripheral edge of the cluster. Then $\Phi(N) = \varepsilon P$, where P is the perimeter of the cluster and ε, J cm^{-1}, the specific periphery or edge energy. In the anisotropic case, where ε depends on orientation, the cluster has a polygonized form and $\Phi(N)$ is given by $\Phi(N) = \sum \varepsilon_i L_i$. From the Gibbs equilibrium form condition for the 2D case: $\Phi(N) =$ min at $S =$ const, the 2D Gibbs–Wulff rule: $\varepsilon_i/h_i =$ const, can be derived, where h_i are the distances of the sides of the polygon from a central (Wulff) point. From this rule a relation between N or S and L_i can be obtained.

As the periphery energy $\Phi(N) = \varepsilon P$ increases with $N^{1/2}$ while the first term is linear in N, the value of $\Delta G(N)$ [see Eq. (25)] after an initial rise passes through a maximum and becomes negative only for sufficiently large clusters. The maximum of $\Delta G(N)$ corresponds to the size of the critical nucleus; from there on the further growth of the cluster is connected with a decrease of the free energy and proceeds spontaneously. The differentiation of Eq. (25) with respect to N gives then for ΔG_c

$$\Delta G_c = bs\varepsilon^2/ze_0\eta_c \tag{26}$$

and for the size of the nucleus

$$N_c = bs\varepsilon^2/(ze_0\eta_c)^2 \tag{27}$$

Here b is the factor relating the surface area S of the nucleus to its perimeter $P = \sum L_i, b = P^2/4S$ ($b = \pi$ for a circular and $b = 4$ for a square form of the nucleus). s is the area occupied by one atom on the surface of the nucleus. When more than one type of sides with different specific edge energies confine the equilibrium form, ε has the meaning of an average value defined by $\sum \varepsilon_i L_i/L$.

From Eq. (27), using the Gibbs–Wulff rule: $h_i/\varepsilon_i =$ const, the size of the critical nucleus, described by the distances h_i from the Wulff point, is obtained: $h_i/\varepsilon_i = s/ze_0\eta_c$. When the equilibrium form is a regular polygon, the distance h is identical with the radius of the inscribed circle ρ, used very often as a measure for the size of the nucleus. Hence

$$\rho_c = s\varepsilon/ze_0\eta_c \tag{28}$$

which is the 2D equivalent of the Gibbs–Thomson equation.

3.1.2. The Rate of Formation of Two-Dimensional Nuclei

The rate of 2D nucleation, i.e., the rate of formation of clusters big enough to ensure spontaneous growth, is proportional to the population of critical nuclei and hence is given by an expression of the form

$$J = k_1 \exp(-\Delta G_c/kT) = k_1 \exp(-bs\varepsilon^2/ze_0kT\eta_c) \tag{29}$$

as first noted by Erdey–Gruz and Volmer.(23) Further development of the theory (Kaischew(22) and Hirth(24)) revealed that the preexponential term includes the so-called Zeldovich nonequilibrium factor $\Gamma = (\Delta G_c/3\pi kTN_c^2)^{1/2}$, taking into account the depletion of the population of nuclei due to their growth, as well as the probability ω_c for an adatom to join the critical nucleus, i.e., $k_1 = n_0\Gamma\omega_c$, where n_0 is the surface atomic density. Γ and ω_c are weakly dependent on overpotential and can very often be considered as constants. The J–η_c relationship according to Eq. (29) shows (Figure 4) a sharp rise of the nucleation rate at a critical value below which the rate is negligibly small. The existence of a supersaturation or overpotential threshold in the growth of a crystalline phase is a very characteristic feature of nucleation-induced processes.

3.1.3. The Experimental Investigation of the Kinetics of Two-Dimensional Nucleation

Based on this phenomenon, a double-pulse technique, originally developed for the study of the electrolytic phase formation by Scheludko and

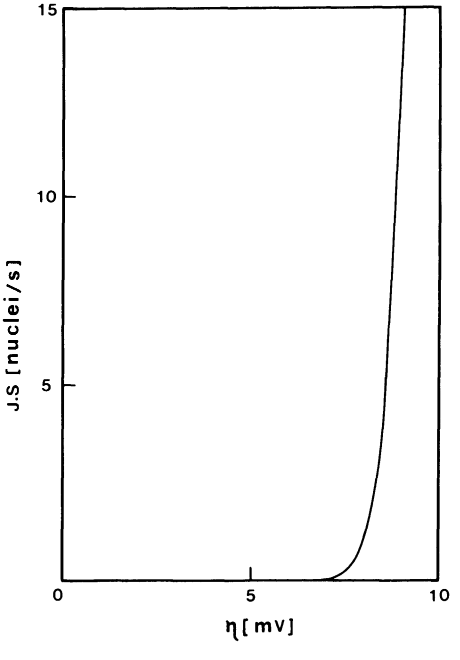

Figure 4. Overpotential dependence of the 2D nucleation rate JS, nuclei s^{-1} [Eq. (29)]. $k_1 = 10^{13}\,\mathrm{sec}^{-1}\,\mathrm{cm}^{-2}$, $\varepsilon = 2 \times 10^{-13}\,\mathrm{J\,cm}^{-1}$, $b = 4$, $T = 318\,\mathrm{K}$ with $ze_0/s = q_{\mathrm{mon}} = 2 \times 10^{-4}\,\mathrm{A\,sec\,cm}^{-2}$ for a Ag (100) face, $S = 2 \times 10^{-4}\,\mathrm{cm}^2$ from experimental data.(25)

Todorova$^{(28)}$ (see also Section 5.4) has been used by Budevski *et al.*$^{(25-27,29)}$ for the investigation of the 2D nucleation kinetics on screw dislocation-free faces. The only way to prepare a dislocation-free face is apparently by growth. For this purpose, an appropriately oriented single crystal is enclosed in a glass tube with a capillary ending and is used as a cathode in an electrolytic cell. The seed crystal is grown electrolytically into the capillary ending of the tube. Using an ac superimposed on the cathodic current, the front face can be grown as a perfect, dislocation-free face filling the whole cross section of the capillary usually of about 0.2-mm diameter. The preparation technique of dislocation-free faces of silver single crystals and their properties are described in Refs. 25–27. The nucleation overpotential threshold in 6 M $AgNO_3$ at 318 K has been found at about 5–8 mV, below which no current is observed. If, on a cell prepolarized at, e.g., 3–4 mV, an overpotential pulse exceeding the threshold value is applied, a current following this pulse shows that one or more nuclei have been formed. Under the applied low overpotential the nuclei grow out of the face and the initial state is restored. The nucleation pulse can be adjusted in amplitude η_c and duration τ in such a way that only in half of the pulse applications is a nucleus formed. Then the pulse duration can be considered as the time lapse needed for the formation of a single nucleus with 50% probability: $\tau = \tau_{0.5}$. Assuming a Poisson distribution of the probability Pr of nucleus formation: $\ln(1 - \mathrm{Pr}) = -JS$, S being the electrode surface, the nucleation rate J (nuclei $\sec^{-1}$ cm^{-2}) can be calculated from $J^{-1} = \tau_{0.5}S \ln 2$. Note that $\tau_{0.5}$ differs from the mean time $\tau_n = 1/JS$ of nucleation, as pointed out by Toshev *et al.*$^{(30)}$ The time lapse $\tau_{0.5}$ can be determined at different overpotentials. Figure 5 shows a $\ln J$ vs. $1/\eta_c$ plot of data obtained in this way. The relation between these two quantities is linear in this rep-

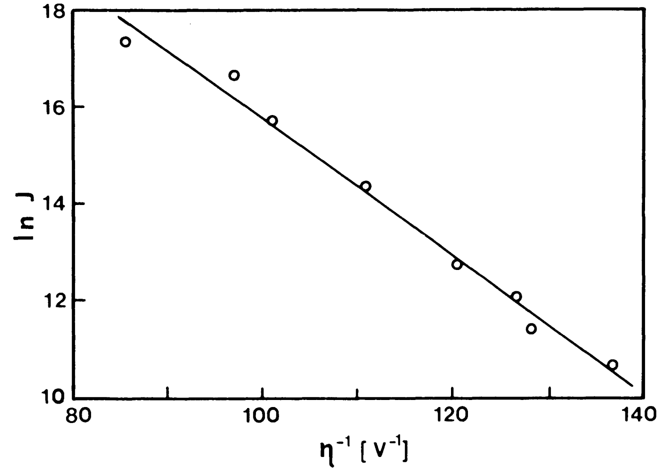

Figure 5. Logarithm of the 2D nucleation rate J, nuclei $\sec^{-1}$ cm^{-2}, as function of the reciprocal of the overpotential for (100) Ag in 6 M $AgNO_3$ at 318 K.$^{(25-27)}$

resentation, as required by Eq. (29). The contribution of the overpotential dependence of the Zeldovich factor Γ and the attachment frequency ω are obviously small enough to produce an appreciable effect on the general $\ln J - 1/\eta_c$ relation. From the slope, the specific edge energy $\varepsilon = 2 \times 10^{-13}$ J cm^{-1} can be calculated, whereby a square form ($b = 4$) of the critical nucleus has been assumed. From Eqs. (26) and (27), ΔG_c and N_c have been found to vary in the range of $10 \div 6.9 \times 10^{-20}$ J and 80–36 atoms, respectively. A value of interest is also the frequency factor $k_1 = n_0 \omega_c \Gamma$ in the rate equation (29) which can be calculated from the intercept of the $\ln J - 1/\eta_c$ curve.

The following values of the specific edge energy and the frequency factor k_1 are considered as most probable at the time being for the cubic and octahedral faces of silver in 6 M $AgNO_3$ at 318 K:

	(100)	(111)
ε (J cm^{-1})	$(1.9 \pm 0.2) \times 10^{-13}$	$(2.2 \pm 0.2) \times 10^{-13}$
k_1 (sec^{-1} cm^{-2})	10^{12}–10^{15}	10^{10}–10^{11}

The variation of ε and k_1 for both faces is within the limits of the experimental error so that no speculations can be made from the variation at this stage of experimental knowledge. An interesting fact is the variation of k_1 in a broad interval of several orders of magnitude showing that not all adsorption sites n_0 are equivalent for the nucleation process and that their number or activity changes from experiment to experiment.

3.2. Kinetics of Step Propagation and Mechanism of Metal Deposition

3.2.1. The Experimental Determination of the Rate of Step Propagation

In the experiments with dislocation-free faces described in the foregoing paragraph, after the nucleation pulse a current is observed indicating the formation of a nucleus (see, for example, Figure 9). Generally the current increases with time linearly in the beginning, goes through a maximum, and then falls to zero within a few seconds. The integral of the current–time curve gives an amount of electricity equivalent to the deposition of a monatomic layer. The shape of the i–t curves obviously follows the growth and decay of the peripheral edge of the spreading monolayer growing over and out of the face boundaries.(25–27) In the beginning, before the step has reached the face boundaries, the current should follow the linear law

$$i = q_{\text{mon}} 2 b v^2 t \tag{30}$$

where b is the same geometrical factor defined previously in Section 3.1.1. From the slope $(di/dt)_{t=0}$, the propagation velocity v of the step can be evaluated if the geometrical form of the spreading layer is known.

A more precise technique, which gives information not only on the propagation rate but also on orientation and form of the peripheral step confining the spreading monolayer, was developed by Bostanov *et al.*(31,32) by growing monatomic layers on dislocation-free faces with a rectangular elongated shape. For this purpose the crystal is grown in the usual way into a capillary of rectangular (100 × 400 μm) cross section to produce a dislocation-free face. As expected, it was found that the current–time curve following the formation of the nucleus shows a current plateau corresponding to the fact that, for a certain period of time, the step propagates with a constant length defined by the shorter side of the rectangular face.

Figure 6, curve b, shows a linear relation between the current plateau and the overpotential permitting the determination of the rate constant $v/\eta = x_v$, cm $\sec^{-1}$ V^{-1}, of step propagation. For this purpose, again, the form of the step and its orientation with respect to the rectangular boundaries of the face is needed. To solve the problem, two orientations of the rectangular cross section of the capillary with respect to that of the seed crystal have been used. In the case of the cubic face the orientations were chosen at an angle of 45° along the ⟨100⟩ and the ⟨110⟩ directions. The slopes of the current–overvoltage curves of Figure 6 would have been independent of orientation if the spreading monolayer had a circular form. Experiment showed, however,

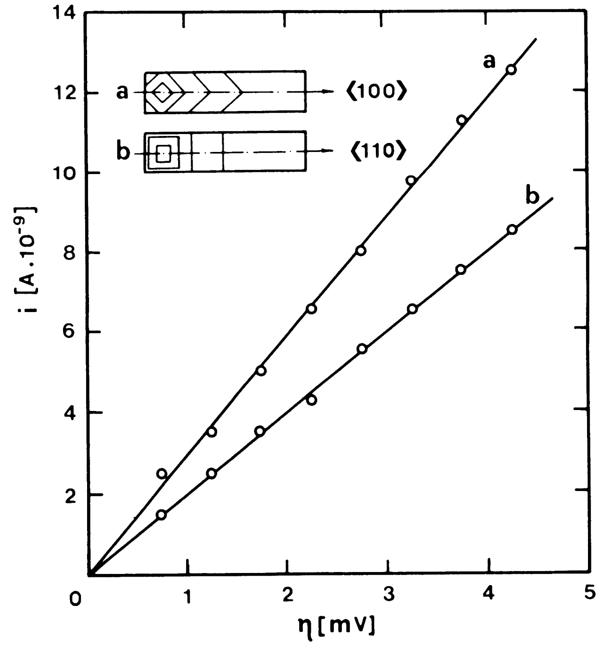

Figure 6. Current plateau values as function of the overpotential for two different orientations of the cross-section axis of a rectangular (0.2 × 0.4 mm) capillary with respect to the Ag single crystal. a, Along the ⟨100⟩, and b, along the ⟨110⟩ direction in the plane of the (100) front face.(31,32)

that the slopes for both orientations differ by a factor of $1.42 = \sqrt{2}$, the orientation $\langle 100 \rangle$ giving the higher value. It is evident that the growing monatomic layer has the form of a square with the sides oriented along the $\langle 110 \rangle$ direction.

Some preliminary investigations made by Bostanov(33) show that, in the case of the (111) face, a triangular symmetry of the process of propagation has been found indicating a triangular form of the spreading monolayer with the sides oriented parallel to the $\langle 110 \rangle$ direction. The technique, at this stage of development, does not reveal which three of all the six possible $\langle 110 \rangle$ directions in the (111) plane are preferred. We can only speculate that these are the same ones observed on the pyramids of growth in the presence of screw dislocations (see Section 4.2). Although the triangular symmetry observed in this case is consistent with the form of the pyramids of growth on an octahedral face, it is rather unexpected to find that three of the six very similarly structured close-packed steps are kinetically preferred for the process of deposition.

Knowing the forms and the orientations of the propagating steps, exact values of the propagation rate constants were found for monatomic steps on the (100) and (111) faces of silver crystals, viz.,

$$\kappa_v = (1.00 \pm 0.05)\ \text{cm sec}^{-1}\ \text{V}^{-1}$$

Under certain conditions, e.g., if a higher overvoltage pulse of a longer duration has been applied to the cell, an "activation" of the surface is observed.(32) On activated surfaces the value of κ_v is roughly twice as large, e.g., $\kappa_{v(100)} = 1.9\ \text{cm sec}^{-1}\ \text{V}^{-1}$.

3.2.2. Rate of Propagation of Polyatomic Steps and Mechanism of Metal Deposition

Under the cited conditions (higher pulses of longer durations), in some cases only one polyatomic step remains advancing on the face at the lower growth overvoltage. With the Nomarski differential contrast technique used in these experiments, some of these thicker steps can be observed directly. Figure 7 shows a 15-atom step moving along a (100) face in two consecutive positions in an interval of 2 sec. From the current and the propagation rate, which is easily determined from the photograph, the height of the step is obtained.

A rather unexpected fact is that the rate of propagation is independent of step height (up to heights of 5–10 nm where concentration polarization in the solution begins to interfere) giving a value of $\kappa_v = 1.9\ \text{cm sec}^{-1}\ \text{V}^{-1}$, very close to that found on "activated" surfaces with monatomic layers.

This fact could be taken as evidence for a direct transfer mechanism of ion incorporation which is independent of step distance down to atomic dimensions. We have to remember, however, that the steepness of the step

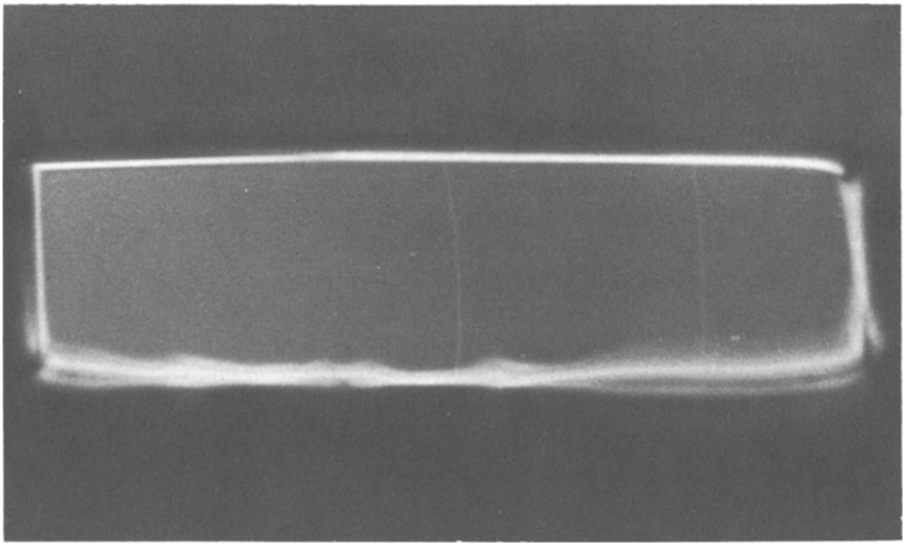

Figure 7. Two overlapping flashlight photographs of a 15-atomic-layer-thick step advancing on a dislocation-free Ag (100) face in a rectangular glass capillary (0.1 × 0.4 mm cross section) taken in an interval of 2 sec.(32)

front cannot be estimated from the interference picture obtained with the differential contrast technique, and if the individul monatomic steps forming the polyatomic step front are sufficiently distant, surface diffusion may not be excluded.

An estimation of the steepness of the front has been made by Bostanov *et al.*(32) using the decay curve of the current at the time when the step begins to disappear on the edge of the crystal face (Figure 8). Knowing the propagation velocity, the current gradient at the end of the current–time curve gives information on the mean step distance of the step train. A value of about 16 nm for the mean step distance was found for the case registered on Figure 7. It should be pointed out, however, that this value is the highest possible of this estimation, because a very steep but slightly curved (e.g., a radius of curvature of 25 cm for the 0.1-mm-long front) would produce the same gradient as that registered on Figure 8. Hence, we can assume that the mean step distance $2x_0$ is less than 16 nm. The independence of the step height on the propagation rate indicates, then, that $\lambda_s < 8$ nm.

To make an estimate of the surface diffusion contribution, the magnitude of the current density of adatoms on dislocation-free faces is needed. Exchange current densities were measured by Vitanov *et al.*(34,35) using the frequency dependence of the impedance on dislocation-free faces. A value of $i_{0,\mathrm{ad}} = 0.06\ \mathrm{A\ cm^{-2}}$ has been found in $6M$ $\mathrm{AgNO_3}$ at 318 K on (100) silver single-crystal faces. With this value and $\lambda_s < 8$ nm, the propagation rate constant $x_v = v_{\mathrm{SD}}/\eta$ can be calculated from Eq. (20), linearizing $V(\eta)$ and putting

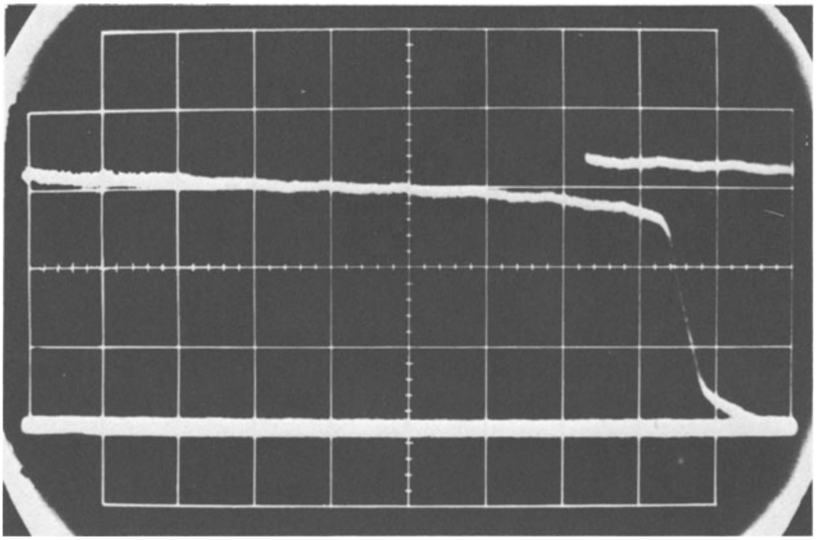

Figure 8. Oscillogram of the current decay at the moment of collision of a thick step on the face boundary edge. Time axis 20 msec div, current axis 10^{-7} A div.(32)

tanh $(x_0/\lambda_s = 1$: then χ_v 1.8×10^{-2} cm sec^{-1} V^{-1}, which is about 60 times lower than the experimental value 1.04 cm s^{-1} V^{-1}. We may conclude that surface diffusion plays a subordinate role in the electrolytic deposition of silver.(32,36) If direct transfer is predominant, from Eq. (13) with $\delta = 0.29$ nm and $\kappa_v = 1.04$ cm sec^{-1} V^{-1}, we obtain for $i_{0,\text{st}} = 200$ A cm^{-2}, an exchange current density for the step atoms of about four orders of magnitude higher than that for the adatoms (see also Section 4.2.3).

An intact, dislocation-free face as cathode represents an ideally polarizable electrode in the potential interval between the reversible potential and that of the nucleation overpotential threshold. In addition to impedance measurements, galvanostatic transients are useful for the determination of the double-layer capacitance C_{DL} and the adsorption pseudocapacitance C_A. For this purpose, the slopes $d\eta/dt$ at $t = 0$ and at $t \approx 4\tau_{\text{DL}}$ can be used, where $\tau_{\text{DL}} = C_{\text{DL}}\rho_D$ is the time constant for the double-layer charging, ρ_D being the resistance of the ion transfer reaction (see Section 2.2.3). The transient on a dislocation-free face should be linear after the inflection at $t \approx \tau_{\text{DL}}$ up to the nucleation overpotential of 5–8 mV. Owing to an appreciable penetration of the electrolyte between the walls of the glass capillary and the crystal, the transient is distorted to a $\sqrt{t}$ dependence in its very early stages. Because the second linear part of the transient is distorted by this effect, Vitanov *et al.*(35) have used $d\eta/dt$ at $t = 4\tau_{\text{DL}}$ to estimate the value of C_A. In agreement with impedance measurements,(37) a value of $C_{\text{DL}} = 30$ μF cm^{-2} for the cubic face of silver has been found from the initial slopes of the transients. The value of C_A found from the slope at $t = 4\tau_{\text{DL}}$ [where $i/(d\eta/dt)_{4\tau_{\text{DL}}} = C_A +$

C_{DL}] is $C_A = 10 \div 20$ μF cm^{-2}, indicating an adatom concentration of $C^0_{ad} = (2 \div 5) \times 10^{-12}$ mol cm^{-2}.(35) This very rough estimate gives an upper experimental limit of C^0_{ad} because the neglected penetration effect produces a false increase of C_A.

3.3. Deposition Kinetics on Perfect Crystal Faces

The kinetics of metal deposition on crystal faces free from screw dislocations is determined by the rate of nucleation J, nuclei cm^{-2} sec^{-1}, of new lattice nets and their rate of propagation v, cm sec^{-1}, over the face. Almost simultaneously Nielsen,(38) Chernov,(39) and Hillig(40) showed that, depending on the values of these two parameters, two different mechanisms can be distinguished, whereby the extension of the surface plays a significant role: (i) a layer by layer growth and (ii) a multinuclear multilayer growth.

3.3.1. The Layer-by-Layer Growth Mechanism

At low overpotentials, where the nucleation time $\tau_n = (JS)^{-1}$ is much larger than the time $\tau_p = S^{1/2}v^{-1}$ for propagation of one monatomic layer over the whole surface, each nucleus has sufficient time to spread over the surface before the next nucleus is formed. Under these conditions, each layer is formed by one nucleus only. The current following the development and the decay of the peripheral edge of each monolayer is not stable and fluctuates with nucleation and spreading of the layer over the face. The mean current density is given by the nucleation frequency $1/\tau_n = JS$ and is independent of rate of propagation v:

$$i = \frac{1}{\tau_n}\int_0^{\tau_n} i(t)\,dt = JSq_{\text{mon}} \tag{31}$$

With J given by Eq. (29), this equation goes back to Erdey-Grúz and Volmer.(23) Figure 9 shows the recorded fluctuations of the current in the deposition of silver on a (100) dislocation-free face at 8.5 mV. The time integral of the current in each fluctuation is equivalent to the deposition of one monatomic layer and the mean time interval between two acts of nucleation is inversely proportional to J.(41)

3.3.2. Multinuclear Monolayer Deposition

With growing overpotentials, the nucleation rate J increases much faster than the propagation rate [see Eqs. (13) or (20) and (29)] so that the mean nucleation time τ_n becomes much shorter than the propagation time τ_p, i.e., $(JS)^{-1} < S^{1/2}v^{-1}$. The deposition of each layer proceeds with formation of a large number of nuclei. The kinetics of deposition are determined in this polynuclear mechanism both by J and v.

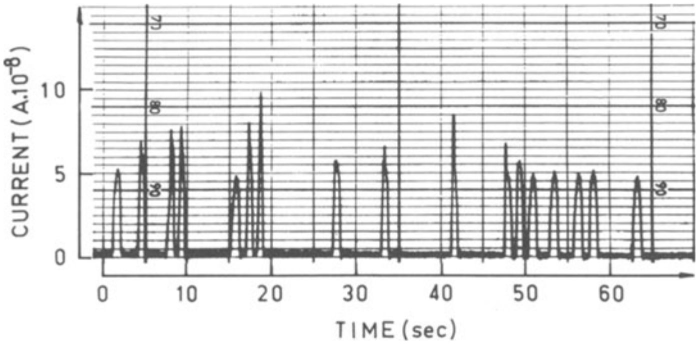

Figure 9. Fluctuations of the current on a dislocation-free Ag(100) face at 8.5 mV, indicating periodic nucleation and spreading of monatomic layers. The integrals under the *i–t* pulses are equal to $q_{\text{mon}} \approx 2 \times 10^{-4}$ As cm^{-2}. Different heights and forms of the pulses indicate that there are no preferential sites of nucleation on the face.

The kinetics of formation of one monatomic layer on an intact face are given[42,43] by

$$i = q_{\text{mon}} bJv^2t^2 \exp(-bJv^2t^3/3) \tag{32}$$

In this equation, the preexponential term gives the current flowing to the peripheries of the independently growing nuclei which are being progressively formed with time [see Eq. (30)]. The exponential term takes into account the overlap effect in terms of the Komogorov–Avrami formulation. In an early stage, before overlapping has occurred, the current follows the quadratic equation given by the preexponential term. Figure 10 shows a current vs.

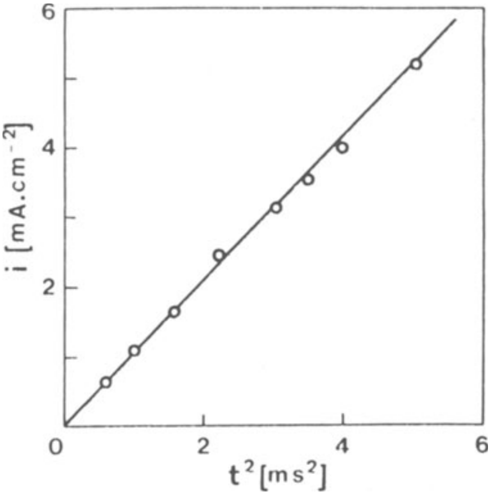

Figure 10. Current-time transient in an i vs. t^2 plot obtained on a dislocation-free Ag (100) face at 14 mV.[41]

time transient in a i vs. t^2 plot obtained on the (100) face of a silver single crystal.$^{(44)}$ From the slopes of a series of i vs. t^2 curves recorded at different overpotentials, the value of Jv^2 as function of η can be obtained. The propagation rate v and its dependence on η are known (see Section 3.2.1). A $\ln J$ vs. $1/\eta$ analysis can then be made, as described in Section 3.1.3. A value of $\varepsilon = 2$ to 2.8×10^{-13} J cm^{-1} was found,$^{(44)}$ in good agreement with that obtained from the time lag in formation of a single nucleus.

In some cases of 2D growth where active centers play a role, nucleus formation can proceed instantaneously in the beginning of the pulse. In this case, the current density is given according to Fleischmann and Thirsk$^{(43)}$ by

$$i = q_{\text{mon}} 2bN_0 v^2 t \exp(-bN_0 v^2 t^2) \tag{33}$$

The preexponential term gives the current flowing to the peripheries of the N_0 independently growing nuclei [see Eq. (30)]. The exponential term takes into account the overlap effect. On dislocation-free faces, the instantaneous nucleation can be simulated, thus extending the possibilities of investigation of the 2D nucleation.

For this purpose, a nucleation pulse ($\eta_{\text{nucl}} > 8$ mV and duration τ_{nucl}) is applied to the dislocation-free face prepolarized at a growth overpotential $\eta < 5$ mV. The nuclei created during the nucleation pulse are grown at the lower overpotential of growth and the current transient is recorded. Figure 11 shows a transient recorded in this way. In Figure 12 the same transient is represented as a $\ln(i/t)$ vs. t^2 plot giving a straight line as required by Eq. (33). From the slope, N_0 and $J = N_0/\tau_{\text{nucl}}$ are obtained. A $\ln J$ vs. $1/\eta$ analysis of J data obtained at different η_{nucl} values renders again ε ranging between 2 and 2.8×10^{-13} J cm^{-1}.$^{(44)}$

3.3.3. Multinuclear Multilayer Deposition

Equation (32) gives the kinetics of extension of a monatomic layer. As nucleation proceeds continuously, however, new nuclei are formed on top of the deposited first layer long before it has covered the whole area of the face. The same happens with the third, fourth, and so on layers as soon as their extensions become large enough to make the nucleation possible. The deposition process under these conditions is known as "multinuclear multilayer growth." Theoretically, up to seven layer levels of nucleation and propagation are expected to proceed simultaneously. This mechanism was extensively theoretically investigated by Borovinskii and Zindergosen,$^{(45)}$ Armstrong and Harrison,$^{(46)}$ and Rangarajan,$^{(47)}$ all treatments being based on the Kolmogorov–Avrami theory and by Bertocci$^{(48)}$ and Gilmer$^{(49)}$ using the Monte Carlo simulation technique.

The theoretical calculations have shown that after an initial rise, the current–time transient passes through several oscillations, and then after the deposition of several layers, steadies toward a final value, i_∞ (Figure 13). This

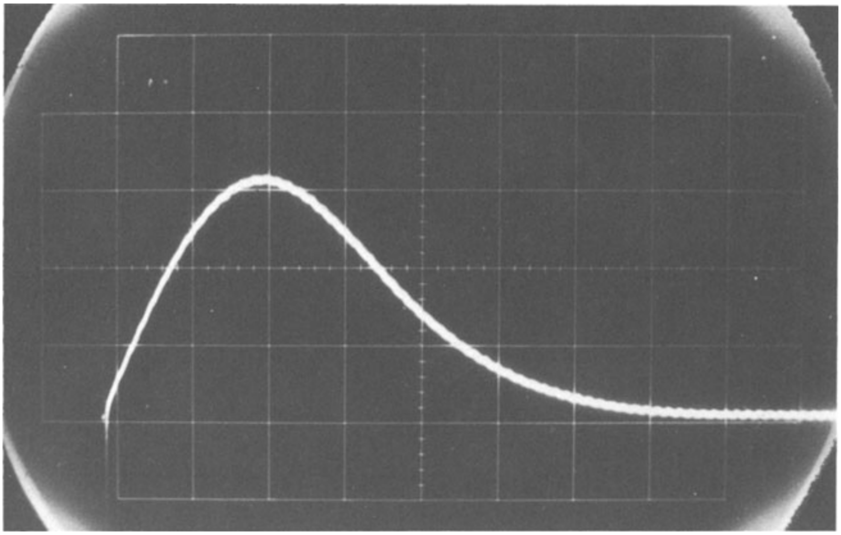

Figure 11. Current transient on a Ag (100) dislocation-free face at $\eta = 4\,\text{mV}$ following a nucleation pulse $\eta_{\text{nucl}} = 17\,\text{mV}$, $\tau_{\text{nucl}} = 120\,\mu\text{sec}$. Time scale 10 msec/div. Current scale 0.4 μA/div.(61)

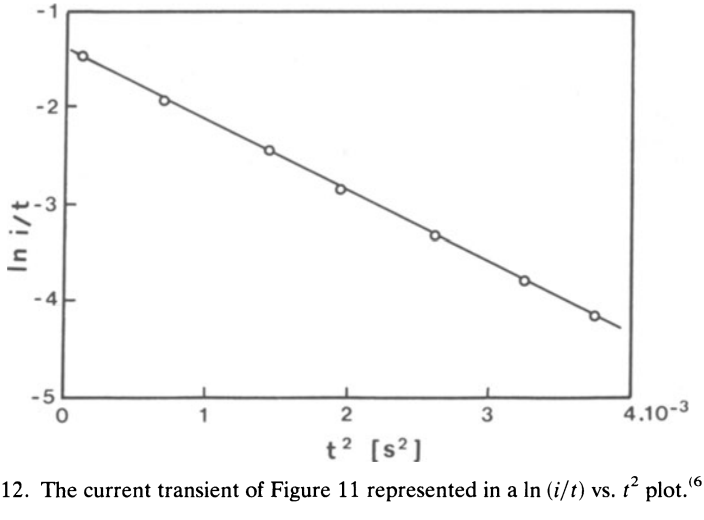

Figure 12. The current transient of Figure 11 represented in a ln (i/t) vs. t^2 plot.(61)

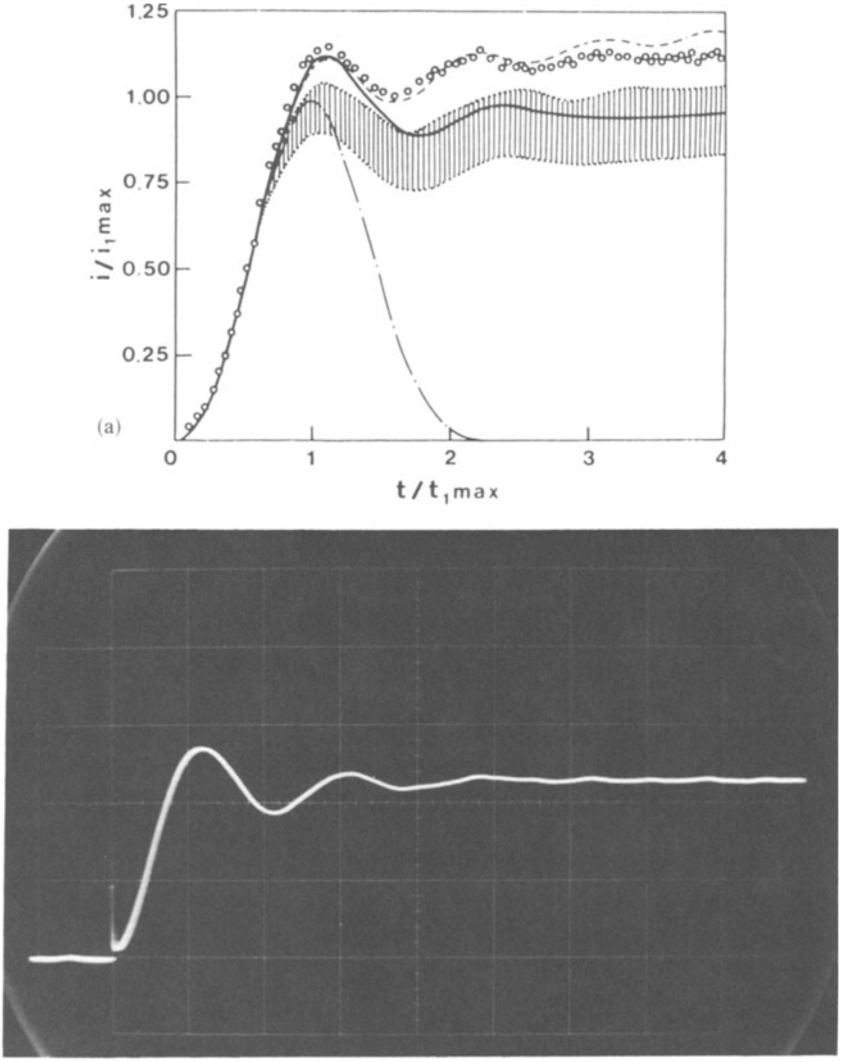

Figure 13. (a) Theoretical and experimental current–time transients for multinuclear multilayer growth. Drawn line, Ref. 46; dashed line, Ref. 45; circles Monte Carlo simulation, Ref. 49; dash–dot–dash line first monolayer formation. The hatched area represents the range of variation of the experimental i vs. t curves obtained at different overpotentials on dislocation-free Ag (100) faces.[41,50] All transients normalized to the i_{max} and t_{max} at the first layer formation. (b) Experimental current transient for multinuclear multilayer growth. $\eta = 14$ mV. Vertical sensitivity, 2 μA/div; time base, 5 msec/div.

steady state current density is given by

$$i_\infty = q_{\text{mon}}\beta(bJv^2)^{1/3} \tag{34}$$

where β is a constant varying around unity from theory to theory.

The transients of Figure 13 are normalized to the parameters of the maximum of the current of the first layer formation according to Eq. (32): $t_{1,\max} = (2/bJv^2)^{1/3}$ and $i_{1,\max} = q_{\text{mon}}(4bJv^2)^{1/3} \exp(-2/3)$. As seen from this figure, in the initial monolayer region all calculated transients follow the quadratic law given by the preeexponential term of Eq. (32). In the further course of the transients, the theoretical curves go slightly astray which seems to be connected with the different approximation used in the calculation of the $(n + 1)$st layer on top of the nth layer. The most reliable results seem to be obtained by the nucleation and disk growth Monte Carlo simulation (circles in Figure 13) calculated by Gilmer.(49)

As was already described, it has been found that the initial parts of the i vs. t transients follow the quadratic relation required by the preexponential term of Eq. (32). Values of Jv^2 obtained from the slopes of i vs. t^2 plots can be used for the calculation of $t_{1,\max}$ and $i_{1,\max}$ needed for the normalization of the experimental potentiostatic i vs. t transients and the comparison of these curves with the theoretical ones. Potentiostatic transients recorded at different overpotentials and normalized in the described way give a package of curves lying in the hatched region of Figure 13.(50)

An analysis of $\ln i_\infty$ as function of $\ln (bJv^2)$ obtained from the initial (i vs. t^2 region) parts of the transients showed a linear dependence with a slope of 1/3 as required by Eq. (34). The value of β has been found to be about 0.72. A $\ln i_\infty$ vs. $1/\eta$ plot gives the possibility for evaluation of the exponential term in J [see Eq. (29)], and an estimation of ε. The variation of v with η being linear can be neglected in the logarithmic representation of i_∞. Experimentally a value of $\varepsilon = 2.5 \times 10^{-13}$ J cm^{-1} was found, in good agreement with the values referred to above.(36,41)

3.3.4. Concluding Remarks and Outlook

Despite the reported agreement with the theory, the steady state parts of the transients as seen from Figure 13 lie in a range well below any of the theoretical curves. The most important fact, however, is that the first maximum of the experimental transients lies in a range around or below the maximum of the current–time curve for first layer formation as calculated from Jv^2 obtained from the initial part of the same transient. This is obviously impossible within the model of homogeneous nucleation. One possible explanation is to assume that nucleation proceeds on nucleation centers. There is much evidence that active sites play a role in this believed-to-be very simple case of metal deposition.

The logarithmic scale analysis used in the experiments referred to is sensitive to the energetics of the nucleation process. The good agreement between ε values obtained in so many different ways (see also Section 4) shows that the energetics is only slightly affected by eventual changes of the state of the surface. Larger deviations were observed in the kinetic factor k_1, showing a strong influence of the state of the surface, primarily due to active centers. This conclusion seems to be supported by the rather small influence of "fresh" and "aged" surfaces on the propagation rate, varying by not more than a factor of 2.

4. Metal Deposition on Faces Intersected by Screw Dislocations

4.1. The Theory of Spiral Growth

The two-dimensional mechanism of growth discussed hitherto is in fact very rarely encountered in real crystal growth. The main reason for this is that real crystals are never perfect and intact, while atomically smooth faces can be prepared only artificially by tedious growth techniques. F. C. Frank(57) first recognized in 1949 that the screw dislocations are one of the most important defects playing a role in crystal growth. Due to the helical structure of this type of defect a monatomic step originates from the point where the screw-dislocation line intersects the surfaces of the crystal face. This step being constrained to terminate at the dislocation emergence point, will wind up into a spiral if forced to advance over the surface in a supersaturated system. Because of the nature of its origin, the propagating spiral can never disappear on the surface and offers a sufficient number of growth sites so that growth can proceed at low overpotentials. A 2D nucleation can occur at high growth rates only but is not indispensable.

4.1.1. The Period of Rotation and Step Distance of a Spiral of Growth

The most important factors for the process of growth in the presence of screw dislocations is the Burgers vector of the screw dislocation and the rotation period T_r of the spiral of growth. In the steady state, when the form of the spiral remains unchanged with time, the current density is given by

$$i = q_{\text{mon}} \nu T_r^{-1} \tag{35}$$

where ν is the height of the spiral step in monatomic layer units and is related to the value and direction of the Burgers vector. The reciprocal of the rotation period gives the frequency of generation of new layers. When more than one spiral is operating on the surface, the current is given by the sum of the contributions of the individual spirals. In the steady state νT_r^{-1}, i.e., the normal growth rate in monolayer units, must be constant for all spirals, so that the contribution of each spiral is proportional to the area over which it operates. The average area of operation of each spiral, however, is inversely proportional to the number of dislocations, so that in the steady state the current density becomes independent of the number of screw dislocations intersecting the surface of the growing face.

The theory of spiral growth, leading to the evaluation of the form and rotation speed of the spirals of growth, was developed by Burton, Cabrera, and Frank.(2) The basic equation for the calculation of their form is the dependence of the propagation rate of a step on its radius of curvature in the isotropic case(2) or on its length in the anisotropic case;(52) $v(l) = v_\infty[1 - (lc/l)]$. This relation shows that a step cannot advance before reaching the length l_c of the side of the critical nucleus at the given supersaturation or overpotential, and only after it has reached that length can its propagation rate increase with l to the value v_∞ of an infinitely long step.

The analytical evaluation of the form and period of rotation of a spiral meets some difficulties. Different approximations have been made for the isotropic case. Burton, Cabrera, and Frank(2) found two approximations of the solution $r(\theta)$ describing the form of the stationary rotating spiral. The first approximation yields an Archimedian spiral with a radius of curvature at the center $\rho = \rho_c$. The step spacing is, in this case, uniform for the whole spiral: $d = 4/\pi\rho_c = 12.6\rho_c$. This result corresponds to a constant radial propagation rate, except for steps for which ρ is smaller than ρ_c. A second approximation is derived by the same authors by combining the solution for small r values, where the $v(\rho)$ relation is taken into account, with the former solution, valid for large r values. This solution yields 19.9 for the factor connecting d and ρ_c, which has been corrected later to 19.0 by Cabrera and Levine.(53)

The case of polygonized spirals has been discussed by Cabrera,(54) Kaischew *et al.*,(55) and by Chapon and Bonissent.(56) In all these treatments the step propagation rate is considered as constant, independent of the step length, except for steps shorter than the side length l_c of the 2D nucleus at the given overpotential. The calculation of the period of rotation T_r and the step spacing $d = T_r v_\infty$ of the polygonized spiral is simplified in this case. For a quadratic spiral the period T_r is four times the time lapse τ_c needed for a new step at the center to reach the curb length l_c. As the propagation rate has been assumed to be constant and the form of the spiral orthogonal, the time lapse $\tau_c = l_c/v_\infty$, hence $d = 4l_c$ or $d = 8\rho_c$. The spiral ledge spacings are constant, independent of their distance from the center of the spiral. For a k-cornered spiral, with $l_c = 2\rho_c \tan(\pi/k)$, the ledge spacings are given by $d = 4k\rho_c \sin^2(\pi/k)$.

The assumption $v = v_\infty$ for $l = l_c$ and $v = 0$ for $l < l_c$ is an oversimplification. It is obvious that the time lapse τ_c and hence the period of rotation should be in reality larger because the step adjacent to the new one propagates with a speed smaller than v_∞. The calculation is complicated because the propagation rates of all the adjacent steps are also dependent on l and hence the propagation rate of the spiral is given by a system of differential equations. A numerical calculation on this system of equations was given by Budevski *et al.*,(52) who found that irrespective of the form of the spiral, the period of rotation of a polygonized spiral is

$$T_r = 19\rho_c/v_\infty \tag{36}$$

and hence, from $d = T_r v_\infty$, with Eq. (28)

$$d = 19\rho_c = 19\varepsilon/q_{\text{mon}}\eta_c \tag{37}$$

4.1.2. The Interaction of Spirals of Growth

The situation becomes more complicated when two or more dislocations, with their centers located at distances comparable to the site length l_c of the critical nucleus, are operating simultaneously. If these distances are smaller than l_c and their vectors have the same sign, the group of dislocations acts as one with a correspondingly increased Burgers vector. The spiral of growth produced then has a double, triple, or (corresponding to the number of the dislocations forming the group) higher step height.(2)

When two dislocations have opposite signs they can form a pair connected by a step.(2,57,58) Both ends of this step terminate at the dislocation centers. If the distance between the two dislocation centers is smaller than l_c, this step is inactive for growth. Nucleation is, however, facilitated on such a step, so that it can serve as an active center with a reduced ΔG_c value. For greater distances, $L > l_c$, the dislocation pair produces loops of steps with a rate determined by v_∞ and the L/l_c ratio. Numerical calculations show(57,58) that with L approaching l_c the period of loop production decreases rapidly to zero or more precisely to the time lag for nucleation on a step edge with the respective length. For higher L/l_c ratios or, what is equivalent to it, higher overpotentials, it increases slightly above the value obtained for single dislocations to fall down to that curb value again for still higher overpotentials.

The growth pattern becomes even more complicated if more than two dislocations are interacting and especially if the component of the Burgers vector normal to the face is higher than the monatomic step height.

During growth, under conditions permitting a relaxation of the crystal lattice tension, the following processes are expected to occur: owing to forces of repulsion, screw-dislocation groups having the same sign can disintegrate into single dislocations with the lowest Burgers vector. Close opposite-sign screw-dislocation pairs attract, and thereby annihilate, each other. In an advanced stage of growth a relaxed face should show only well-separated single dislocations producing spirals of growth with a uniform step spacing or step density.

The step density L_s, important for the calculation of the current density according to Eqs. (22) or (24), is given by

$$L_s = d^{-1} = q_{\text{mon}}\eta_c/19\varepsilon \tag{38}$$

4.1.3. Morphology of Growth

The spirals of growth consisting of steps with a height of the order of the atomic radii are invisible with normal microscopic observation techniques.

A pyramidal pattern is observed instead with slopes of pyramids determined by the step height and the step distance:

$$\tan \alpha = \nu h_{\text{mon}}/d = \nu h_{\text{mon}} q_{mon} \eta_c / 19\varepsilon \qquad (39)$$

h_{mon} is the height of a monatomic layer on the respective face and ν the number of layers forming the spiral step, related to the Burgers vector of the dislocation. As seen from Eq. (39), the slope of a pyramid of growth is proportional to overvoltage.

In a number of cases of electrocrystallization, pyramidal growth patterns as well as spirals of growth have been observed.(27,55,59,60) In Figure 14 the relief of growth of a cubic silver single-crystal face is represented. Higher Burgers vectors and different rotation periods determine a complex relief of the growing crystal face, where regions of higher normal rates overgrow those of lower. Splitting of dislocations, smallest changes in their distances, and local changes of the overpotential can change abruptly the relief of the face. Simple conditions are found, as already mentioned, on a relaxed surface, where only a few dislocations are operating. Figure 15a shows the quadratic pyramids of growth observed on a cubic face. On an octahedral face, they are triangular as shown in Figure 15b. The pyramids of growth are obviously

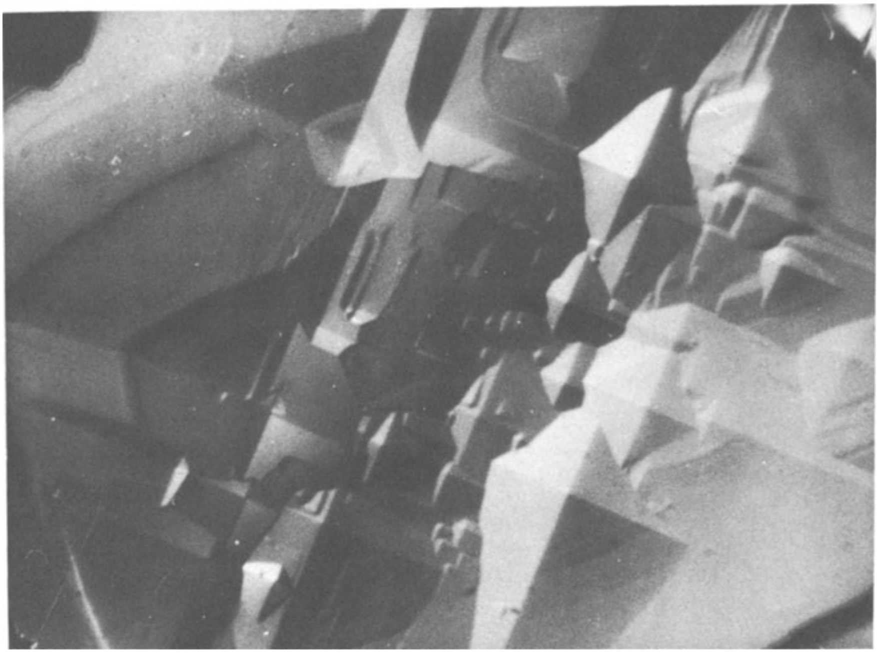

Figure 14. Morphology of growth of an Ag (100) face intersected by screw dislocations. Pyramids with different slopes can be recognized. Step bunching effects are observable at the left-hand side of the picture.

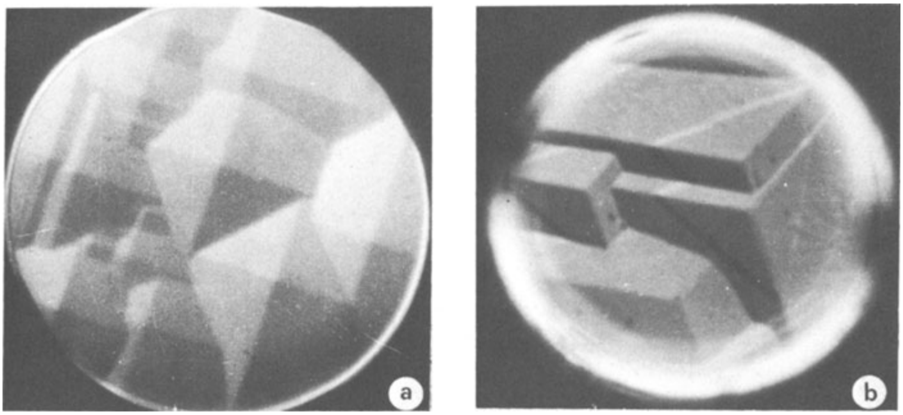

Figure 15. Pyramids of growth on an Ag (100) face (a) and on an Ag (111) face (b). A triangular stripe is visible on each of the triangular pyramids on the (111) face (b) propagating down to the base of the pyramids, produced by a short change of the overpotential during growth at constant overpotential. The photograph is made 1 sec after the pulse application.

the macroscopic representation of the spirals of growth. The following observations can be considered as evidence for this statement: (i) The slopes of the pyramids depend on overpotential. Changing the overpotential causes the slope also to be changed; see Figure 15b. (ii) The pyramids appear always on the same sites of the face. Upon anodic dissolution, an etch pit is produced at each of these sites.

4.2. Current Density and Morphology of Growth

4.2.1. The Steady State

On surfaces with a higher degree of perfection, as in the cases shown, e.g., in Figure 15, the growth patterns are relatively stable. The pyramids have equal and uniform slopes. The step density is also uniform and is defined by η. The current density as function of the overpotential is then easily obtained by insertion of Eq. (38) in Eqs. (22), (23), or (24). For small η_c values the exponential functions $V(\eta)$ and λ_s can be linearized giving a quadratic dependence of i on η_c, viz., $i = \text{const}\cdot\eta_c^2$.

From an experimental point of view, it is better to express the current density in terms of the propagation rate, v_∞, which under certain circumstances is directly experimentally accessible. From Eqs. (35) and (36) with Eq. (28), bearing in mind that $ze_0/s = q_{\text{mon}}$, one obtains

$$i = \frac{\nu q_{\text{mon}}^2}{19\varepsilon} v_\infty \eta_c \tag{40}$$

For theoretical considerations v_∞ can be taken from Eq. (20) for the surface

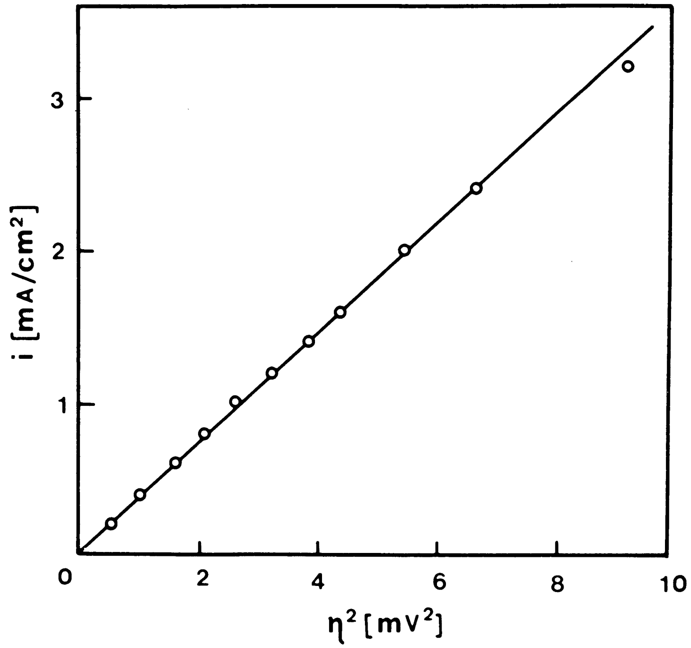

Figure 16. Steady state current–overvoltage dependence in an i vs. η^2 plot on an Ag (100) face in $6\,M$ $AgNO_3$ at 45°C. Screw-dislocation density $1 \div 5 \times 10^{-4}$ disl. cm^{-2}. Overvoltage is *IR* corrected.(29)

diffusion case or from Eq. (13) for the case of direct transfer; then identical equations are reached as described in the foregoing paragraph. The propagation rate v_∞ can be taken also from direct experimental measurements. It has been shown for instance that, in the case of silver, v_∞ is linearly dependent on overpotential: $v_\infty = \kappa_v \eta_c$, which is, *inter alia*, consistent with the theoretical equations (20) and (13) for the small η_c values used in the experiments. Hence

$$i = \frac{\nu q_{\text{mon}} 2\kappa_v}{19\varepsilon} \eta_c^2 \tag{41}$$

This current–overvoltage squared relation has been experimentally investigated in the case of silver deposition on (100) faces of Ag crystals by Vitanov *et al.*(35) From the experimental i–η_c^2 plot shown in Figure 16,(29) $\varepsilon = 2.4 \times 10^{13}\ \text{J cm}^{-1}$ has been found. The spiral steps have been assumed to be monatomic (i.e., $\nu = 1$) and κ_v has been taken from propagation rate measurements of single monatomic steps (Section 3.2.1) or from the spiral step propagation rate directly (Section 4.2.2).

4.2.2. The Transitional Period(58,61)

If the overpotential during growth is changed, the profile of the surface should also change because the step density L_s and hence the steepness of the pyramids are overpotential dependent. The change in the step density begins at the center of the spirals and spreads with a velocity equal to the propagation rate of the spiral steps at the given overpotential. In this way, a pyramid with a different slope is produced at every spiral center. The area covered by the new pyramid before it reaches the face boundary or the borders of its area of operation is

$$S(t) = br^2(t) = bv^2t^2 \tag{42}$$

Here $r(t) = vt$ is the radius of the circle inscribed into the geometrical form of the base of the new pyramid at time t after the overpotential change. The current distribution is not uniform over the face in the transitional period and can be divided in two parts:

$$i(t) = i(0)\left[1 - \frac{S(t)}{S_0}\right] + i(\infty)\frac{S(t)}{S_0}, \tag{43}$$

one flowing to the surface part of step density $L_s(\eta_1)$, corresponding to the initial overvoltage η_1, and the second flowing to the rest of the surface with a step density corresponding to the new overvoltage η_2. $i(0)$ and $i(\infty)$ are the current densities at the new overvoltage η_2 at $t = 0$ and at the steady state ($t = \infty$) when the whole surface is occupied by the new pyramid.

When a large number N of equally active ($\nu = 1$) screw dislocations distributed randomly over the surface are operating, a Kolmogorov–Avrami type of analysis can be made for the evaluation of the current transient:

$$S(t) = S_0\left[1 - \exp\left(-\frac{S_{\text{ex}}}{S_0}\right)\right] \tag{44}$$

with

$$S_{\text{ex}} = Nbv_2^2t^2 \tag{44a}$$

where S_{ex} is the expanded surface area which would be occupied by the new spirals after the time lapse t if there was no overlapping. Inserting Eq. (44) in (43)

$$i(t) = i(0)\exp\left(-\frac{Nbv_2^2t^2}{S_0}\right) + i(\infty)\left[1 - \exp\left(-\frac{Nbv_2^2t^2}{S_0}\right)\right] \tag{45}$$

For short times before an interaction of the growing pyramids has started,

$$i(t) = i(0) + [i(\infty) - i(0)]\frac{Nbv_2^2t^2}{S_0} \tag{46}$$

the current changes linearly with the square of t depending on the dislocation density N/S_0. In Figure 17 a transient obtained on a (111) face of an Ag crystal is represented. The initial part of the curve follows the predicted quadratic law as seen on the same figure. From the transient, $i(0)$ and $i(\infty)$ can be determined directly. With $N = 1$ the slope gives $\kappa_v = 0.78\ \text{cm sec}^{-1}\ \text{V}^{-1}$

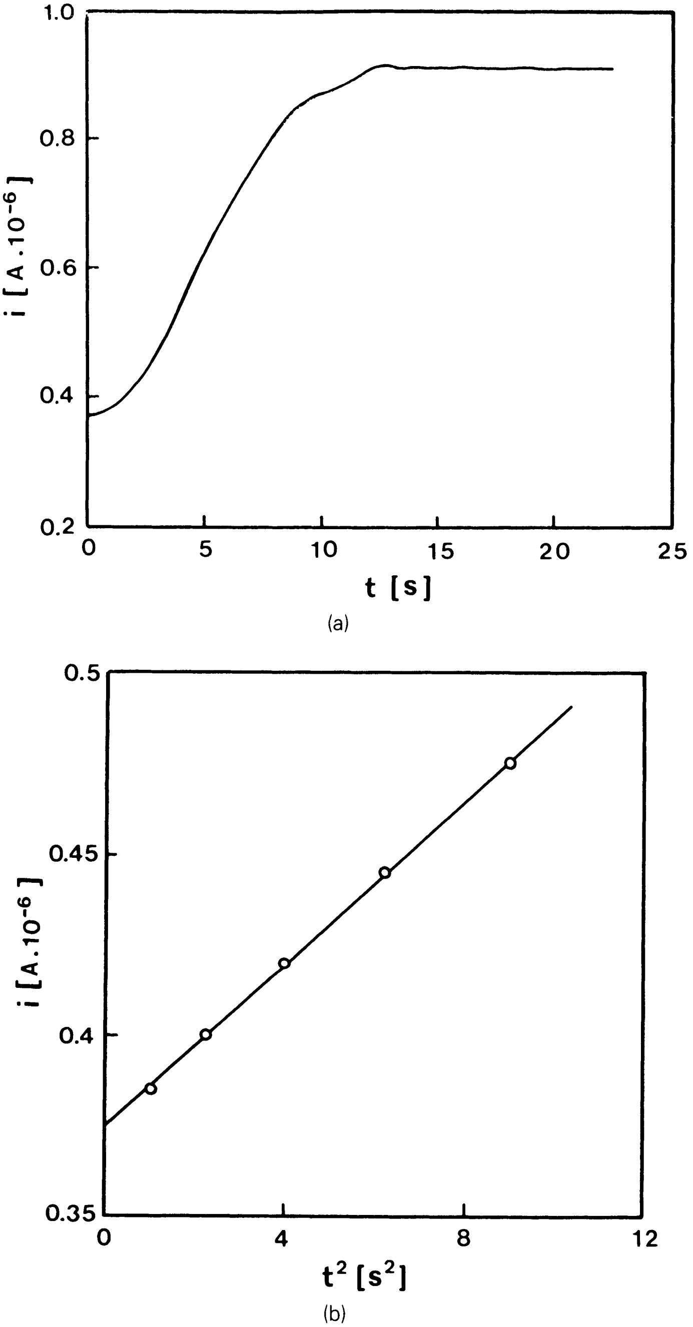

Figure 17. Current transient obtained on an Ag (111) face ($S = 2 \times 10^{-4}\ \mathrm{cm}^2$) intersected by one screw dislocation at 1.15 mV (*IR* correction) after a steady state growth at 0.25 mV (a). The initial part of the transient in an i vs. t^2 plot (b).(61)

so that, from $i(0)$ and $i(\infty)$, the value of $\varepsilon = 3 \div 5 \times 10^{-13}\,\mathrm{J\,cm^{-1}}$ can be found.(61) These figures are roughly in good agreement with values obtained by other methods.

The fact that the slope of the pyramids is changed on changing the overvoltage can be used for the determination of the propagation rate in a direct way.(29,62) If, for instance, during growth at constant potential the overvoltage is changed for a short period of time, a condensation of the spiral steps at the spiral center results. This condensed package of steps begins to propagate from the top of the pyramid downwards, as a stripe with a different shade. A stripe produced in this way is to be seen on the octahedral face represented in Figure 15b. A linear relation of the displacement velocity of these stripes with overpotential has been found(62) giving for the rate constant on the cubic face $\chi_v = 0.92\ \mathrm{cm\,sec^{-1}\,V^{-1}}$ as found also in the propagation rate measurements referred to above.

4.2.3. *The Exchange Current Density and the Surface Profile*(35)

The results of the experiments described can be taken as a very good quantitative verification of the theory of Burton, Cabrera, and Frank.

The verification of the theory of spiral growth makes it possible to grow crystal faces at a given overvoltage and after a regular surface profile is obtained to stop the growth and calculate the step density from Eq. (38). In addition to the technique of preparation of dislocation-free, atomically smooth faces, the technique described for preparation of electrode surfaces of known profile is of significant importance for the investigation of electrochemical phenomena on solid surfaces.

A very instructive example is the exchange-rate measurements on faces prepared by growth at different overpotentials.

It has been found by Vitanov *et al.*(35) that the exchange current density is strongly influenced by the surface profile and is proportional to step density as shown in Figure 18. The step density has been calculated from the overvol-

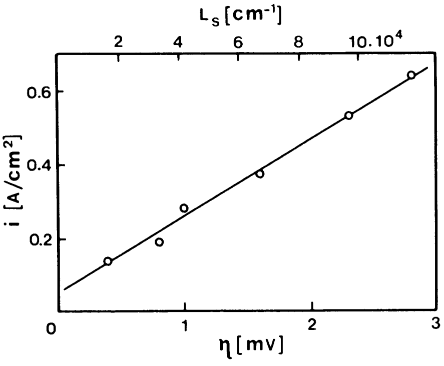

Figure 18. Dependence of the exchange current density on step density on an Ag (100) face intersected by screw dislocations ($\sim 5 \times 10^{-4}$ disl. cm^{-2}). Before each series of impedance measurements for the evaluation of the exchange current density, the face was grown at the indicated overpotential (*IR* corrected) until a steady state profile is obtained. Step densities L_S calculated from the overpotential of growth according to Eq. (38).(26,34,35)

tage at which the faces were grown and Eq. (38). As seen from Figure 18 the overall exchange current density depends linearly on step density L_s: $i_0 = i_{0,\mathrm{ad}} + i_{0,\mathrm{st}}^{(L)} L_s$, giving for the extrapolated (i.e., at $L_s = 0$) value an exchange current density equal to that obtained on dislocation-free faces, viz., $i_{0,\mathrm{ad}} = 0.06\ \mathrm{A\ cm^{-2}}$.(34)

From the slope of the dependence of i_0 on L_s the value of $i_{0,\mathrm{st}}^{(L)} = 5.2 \times 10^{-6}\ \mathrm{A\ cm^{-1}}$ has been found. This value can be used for the evaluation of the exchange current density of step atoms under the assumption that the observed "catalytic" effect of the step is extended to a distance not greater than one atomic diameter. With $d_{\mathrm{Ag}} = 0.29$ nm a value of $i_{0,\mathrm{st}} = 180\ \mathrm{A\ cm^{-2}}$ can be found, corresponding perfectly to the value obtained from the propagation rate measurements of Section 3.2.2.

5. Electrolytic Phase Formation

On a foreign metal substrate and in most of the cases on a substrate of the like metal, the first step of metal deposition is the formation of nuclei of the depositing metal. The kinetics of nucleation of the new metallic phase and its forms and rate of growth, in many cases play a dominant role in determining the overall deposition kinetics as well as the properties of the metal deposit.

5.1. Equilibrium Forms and Forms of Growth of Crystals

5.1.1. The Equilibrium Form

The equilibrium form of a crystal is defined as that possessing the minimal total surface free energy, $\Phi = \sum S_i \sigma_i$, for a given volume V. Here σ_i and S_i denote the specific surface energies and the surface areas of the respective crystallographic faces. This definition goes back to Gibbs and Curie.

If the crystal is in contact with the substrate with one of its faces, e.g., the face j, the contribution of that face to the surface free energy is given by the product of the area S_j^* of the contact interface and its specific free energy σ_j^* diminished by that of the substrate–solution interface σ_{sub} (note that with the creation of the contact interface an equivalent area of the substrate disappears). Hence $\Phi = S_j^* (\sigma_j^* - \sigma_{\mathrm{sub}}) + \sum S_i \sigma_i$, where the asterisk refers to quantities relating to the crystal–substrate interface.

The interaction of the crystal with the substrate can be described in a more perceivable way by the adhesion energy β, $\mathrm{J\ cm^{-2}}$, as introduced by Kaischew.(63–65) The adhesion energy is defined by $\beta = \sigma_j + \sigma_{\mathrm{sub}} - \sigma_j^*$, taking into account that with the separation of the crystal from the substrate, crystal–solution and the substrate–solution interfaces are created, while the equivalent crystal–substrate interface disappears.

Using the adhesion energy, β, the equilibrium condition for a crystal in contact with the substrate with its jth plane can be written as

$$\Phi = S_j^*(\sigma_j - \beta) + \sum S_i\sigma_i = \min \qquad \text{at } V = \text{const.} \tag{47}$$

5.1.2. The Gibbs–Wulff–Kaischew Theorem

The equilibrium form of a crystal can be described by the distances h_{hkl} of the respective faces from a central point (the Wulff point). Using the equilibrium condition (47), for geometrical reasons only it can be shown that these distances are related to the σ values by

$$\sigma_1/h_1 = \sigma_2/h_2 = \cdots = (\sigma_j - \beta)/h_j^* = \text{const} \tag{48}$$

which is a form of the Gibbs–Wulff theorem generalized by Kaischew(63–65) for the case of heterogeneous nucleation. Relation (48) allows the construction of the equilibrium form by drawing the faces (hkl) at distances h_i proportional to the respective σ_i values from a chosen point, the Wulff point. The contact interface j is to be drawn at a distance proportional to $(\sigma_j - \beta)$ as in Figure 19.

Depending on the adhesion energy β, the distance to the contact plane h_j^* can either be positive or negative. It is seen that the presence of the substrate does not generally affect the form of the crystal. It only becomes flatter in the direction of the substrate, leaving the distances of the faces in contact with the the solution unchanged.

The contact plane j lies normally parallel to one of the faces belonging to the equilibrium form so that the top face of the crystal lies very often parallel to the substrate surface. A thickness can be ascribed to the crystal in this case: $\delta = h_j + h_j^*$, where h_j is the distance of the top face j and h_j^* that of the crystal–substrate interface from the Wulff point. From Eq. (48), $h_j/\sigma_j =$

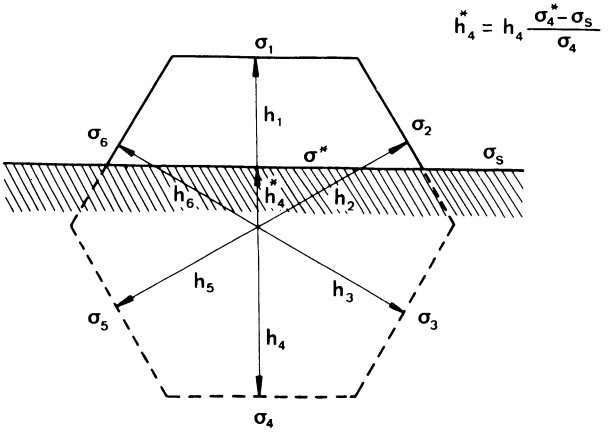

Figure 19. Illustration of the Gibbs–Wulff–Kaischew theorem. σ_1 to σ_6 are equal. The faces 1 to 6 are equidistant from the Wulff point. In the presence of the substrate, the distance h_4^* to the contact plane is reduced as indicated, becoming negative as $\sigma_s > \sigma_4^*$.

$h_j^*/(\sigma_j - \beta)$ or the thickness $\delta = h_j(2\sigma_j - \beta)/\sigma_j$. With increasing adhesion energy β, the thickness of the crystal decreases and becomes small compared to its other dimensions. Reaching the value of the thickness of one monatomic layer, δ becomes a constant and the crystal must be treated as two dimensional. The contact interface S_j^* of a 2D crystal is thus equal to the surface of its top face S_j so that in the sum $\sum S_i\sigma_i$ the term $S_j\sigma_j$ can be combined with the term $S_j^*(\sigma_j - \beta)$ giving $\Phi = S_j(2\sigma_j - \beta) + \sum S_i\sigma_i$. The first term vanishes with β tending to $2\sigma_j$, leaving for the surface energy of the 2D crystal the contribution of the side faces only from the second term. As with decreasing height, however, the specific surface energy of the side faces becomes a function of their height, it is better to introduce Φ in this case as the periphery energy $\sum \varepsilon_i L_i$, where L_i are the side lengths of the crystal. The specific periphery energies ε_i are related to the corresponding $\sigma_i(h)$ values by $\sigma_i(h)h = \varepsilon_i$.

In full analogy to the 3D case, the equilibrium form is defined here by $\Phi = \sum \varepsilon_i L_i = \min$ at $S = \text{const}$, which with a constant thickness is equivalent to $V = \text{const}$. In the same way, from geometrical considerations only, a Gibbs–Wulff equation $h_i/\varepsilon_i = \text{const}$ can be derived. When atom clusters are formed on a substrate of the like metal they are epitaxially oriented to the substrate. In such a case $\sigma_j^* = 0$ and $\sigma_{\text{sub}} = \sigma_j$ so that $\beta = \sigma_j + \sigma_{\text{sub}} - \sigma_j^* = 2\sigma_j$. Clusters formed on the like metal substrate are two dimensional.

The adhesion energy β, J cm^{-2}, is related to the adsorption energy, J mol^{-1}, but depends on the structure of the crystal face staying in contact with the substrate. If the adhesion energy β is larger than twice the specific surface energy of a closed packed face of the depositing metal, this shows that the atom–substrate interaction is higher than that between the atoms themselves. In this case, an appreciable adsorption and nucleation of compact monatomic layer can begin even at more positive potentials than the reversible potential of the depositing metal (underpotential deposition–see Part B).

The problem of the growth forms is much more complicated. Theoretically the growth form is confined by the slowest growing faces. Under idealized conditions these are the faces having a close-packed structure (singular faces) which are restricted to grow by the 2D nucleation mechanism. Crystal defects, particularly screw dislocations, can enhance the rate of growth of singular faces, while adsorption effects inhibit the growth of nonsingular faces. In electrolytic metal deposition, diffusion and electric field effects can influence additionally the forms of growth of crystals making at this stage of knowledge the prediction of the growth forms a difficult task.

5.2. The Nucleation Rate

The formation of nuclei of a new phase can be considered as a sequence of bimolecular reactions in which every cluster of one class transforms into the next higher or lower class by attachment or detachment of one atom:(66)

$$A_1 \overset{\pm A_1}{\rightleftarrows} A_2 \overset{\pm A_1}{\rightleftarrows} A_3 \cdots A_N \cdots \tag{49}$$

At equilibrium, all rates of the attachment and detachment reactions are equal:

$$\omega_a(N-1)Z^0(N-1) = \omega_d(N)Z^0(N) \tag{50}$$

where $\omega_a(N)$ and $\omega_d(N)$, sec^{-1}, are the frequencies of the attachment/detachment of one atom to/from a cluster of N atoms. $Z^0(N)$, cm^{-2}, are the corresponding cluster concentrations at equilibrium. $Z(N=0)$ corresponds to the number of adsorption sites Z_0 of the substrate per unit area and $\omega_a(N=0)$ to the impingement rate of atoms from the parent phase per adsorption site. If all $\omega_a(N)$ and $\omega_d(N)$ are known, the equilibrium cluster partition function $Z^0(N)$ can be calculated.

If an overpotential is applied, a net flux of clusters to higher classes is set. In the steady state the flux

$$J = \omega_a(N-1)Z(N-1) - \omega_d(N)Z(N), \qquad N = 1, 2, 3, \ldots, S \tag{51}$$

as well as the concentrations $Z(N)$, are constant with time. It can be shown that with increasing N the transformation rate to lower classes $\omega_d(N)Z(N)$ decreases so that, for a sufficiently large value of N, e.g., S, $\omega_d(S)Z(S)$ can be neglected in comparison to the flux rate J. The flux rate J is given then by the rate of transformation of clusters of the class $(S-1)$ to the higher class: $J = \omega_a(S-1)Z(S-1) \gg \omega_d(S)Z(S)$, and represents the rate of formation of new crystals of the new phase, i.e., equivalent to the nucleation rate.

According to Becker and Doring,(66) each one of these S equations except the first one are multiplied by the factor $\prod_{i=1}^{N} \omega_d(i)/\omega_a(i)$, where N varies from 1 to $S-1$, increasing by unity for every subsequent equation. By adding these equations, all right-hand terms cancel except the first one $\omega_a(0)Z_0$, while the last one $\omega_d(S)Z(S)$ can be neglected, so that(22,66,67)

$$J = \omega_a(0)Z_0 \bigg/ \left[1 + \sum_{N=1}^{S-1} \prod_{i=1}^{N} \omega_d(i)/\omega_a(i)\right] \tag{52}$$

This equation is quite general and does not depend on kind (two- or three-dimensional), state (liquid or crystalline), form and size of the clusters. If the clusters are crystalline, however, there are different ways of building them up to the size S, so that for each one of these parallel going reaction sequences a different value of J may be expected. Every one of them contributes to the overall nucleation rate independently.

Let us now scrutinize the products π in the denominator of Eq. (52) which can be rewritten in the form $[\omega_a(0)/\omega_a(N)] \prod_{i=1}^{N} \omega_d(i)/\omega_a(i-1)$. The detachment–attachment frequency ratio $\omega_{d,j}(N)/\omega_{a,j}(N-1)$ for a given site j of a crystalline cluster of N atoms can be obtained from Eqs. (1), (2), and (3)(68):

$$\frac{\omega_{d,j}(N)}{\omega_{a,j}(N-1)} = \frac{q_j p_k}{p_j q_k} \exp\left[-\frac{\phi_{j,s} - \phi_{k,s}}{kT}\right] \exp\left(-\frac{z e_0 \eta_c}{kT}\right) \tag{53}$$

where $\phi_{j,s} = -(\Delta G^*_{a,j} - \Delta G^*_{d,j})$ is the dissociation energy of an atom from the site j of the cluster (including its transfer as an ion from the solution at $E=0$, which is denoted by the index s). If the atom at the site j is in contact with the substrate, $\phi_{j,s}$ includes also the respective bond energy of this atom to the substrate. $\eta_c = E_{\text{rev}} - E$ is the (cathodic) overpotential. The product in the denominator of Eq. (52) is given then(68,69) by

$$\prod_{i=1}^{N} \frac{\omega_{d,j}(i)}{\omega_{a,j}(i-1)} = k_N \exp\left(\frac{N\phi_{k,s} - \sum^N \phi_{j,s}}{kT}\right) \exp\left(-\frac{Nze_0\eta_c}{kT}\right) \qquad (54)$$

where k_N includes the product of the N preexponential constants coming from Eq. (53), as well as an entropy term arising from the use of dissociation energies. The sum $\sum^N \phi_{j,s}$ gives the dissociation energy of the cluster, including its interaction with the substrate. The term $N\phi_{k,s} - \sum^N \phi_{j,s} = \phi(N)$ represents the difference in the energy of N atoms of the bulk crystal and that of the N atoms in the cluster. This difference can be considered as the surface free energy of the cluster because it arises from the unsaturated bonds of the surface atoms.(70) A comparison with Eq. (25) shows then that the exponent of Eq. (54) is equal to the free energy of formation of a cluster of size N:

$$\Delta G_N = -Nze_0\eta_c + \left(N\phi_{k,s} - \sum^N \phi_{j,s}\right) \qquad (55)$$

With increasing N, the sum $\sum^N \phi_{j,s}$ tends to $N\phi_{k,s}$ because more and more atoms are found in kink positions in the process of disintegration of the cluster. Therefore the ΔG_N value, being positive at small N values, rises initially, passes over a maximum and becomes negative only at larger N values. The cluster of size N_c at which ΔG_N reaches its maximum value ΔG_c is known as the "critical cluster" because its further growth is connected with a decrease of ΔG and proceeds spontaneously under the action of the overpotential η_c.

If the bond energies between the crystal atoms themselves and those between them and the substrate are known, the value of ΔG_N can be calculated as a function of N. In Figure 20, ΔG_N as calculated by Stoyanov(69) is shown as function of N at different $\Delta\mu (= ze_0\eta_c)$ values; ϕ_k and ϕ_j are calculated from the respective bond energies between first neighbors as well as ψ_1 for the cluster atoms and ψ_a for the cluster atom-substrate interaction (no solvation effects have been considered in this calculation). The procedure is complicated if a fixed crystal lattice arrangement of the atoms is imposed,(71) but this hardly has a physical meaning because, at room temperatures, small atomic aggregates have an increased mobility, so that only close-packed arrangements can be considered as in the calculation of Stoyanov referred to above.(69) It is of interest to note that with changing overpotentials, N_c being an integer changes, taking discrete values only. Hence, to each discrete value of N_c, a supersaturation interval of stability can be ascribed.

With increasing N, however, this atomistic method based mainly on lattice bond energies, becomes quite intricate and can be replaced by classical thermodynamic methods where macroscopic quantities can reasonably be applied.

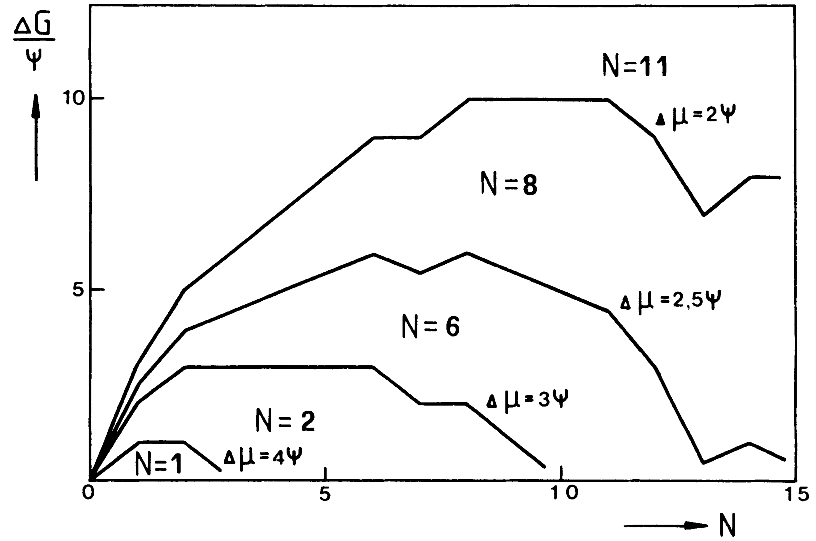

Figure 20. Gibbs free energy of formation of clusters as a function of size N at different supersaturations $\Delta\mu$. ϕ_k and ϕ_j are calculated from ψ_1 and $\psi_a = \psi_1$ and the number of first neighbors of the cluster configuration of lowest ΔG value (fivefold symmetry close-packed structure) according to Stoyanov.[69]

As shown already, the term $N\phi_{k,s} - \sum^N \phi_{j,s}$ gives the excess free energy σS of the small crystal attributed to the unsaturated bonds of its surface atoms. If a crystalline cluster in contact with a substrate is considered, the different crystallographic faces and the interface boundary have different σ values so that $\phi(N) = \sum \sigma_i S_i$ or $\phi(N) = S_j^*(\sigma_j - \beta) + \sum \sigma_i S_i$, as discussed already in Section 5.1.1, see Eq. (47). In this case ΔG_N is given by

$$\Delta G_N = -Nze_0\eta_0 + S_j^*(\sigma_j - \beta) + \sum \sigma_i S_i \tag{56}$$

The maximum value of ΔG_N can be obtained from the condition $d\Delta G_N/dN = 0$, but differentiation of Eq. (56) with respect to N is only possible if a relation between S_i, S_j^*, and N is found. Such a relation exists only if a specific geometrical form is considered. For any given geometrical form, the surface area S of the form is related to its volume by $S^3 = BV^2$, where B is a factor depending on the geometry, e.g., $B = 36\pi$ for a sphere and $B = 6^3$ for a cube. The maximum value of ΔG is found then at

$$N_c = 8Bv_m^2\sigma_g^3/27(ze_0\eta_c)^3 \tag{57}$$

with the value

$$\Delta G_c = \sigma_g S_c/3 = 4Bv_m^2\sigma_g^3/27(ze_0\eta_c)^2 \tag{58}$$

v_m is the volume occupied by one atom in the crystal lattice and $\sigma_g = [S_j^*(\sigma_j - \beta) + \sum \sigma_i S_i]/S$, having the meaning of an average specific surface energy, has been introduced for abbreviation (note that for a given geometrical form σ_g does not depend on the size of the crystal). Equations (57) and (58) are quite general and do not depend on the form of the nucleus for which they have been used. The only factors that have to be considered are the geometrical factor B and the mean specific surface energy σ_g, which vary from form to form changing the ΔG_c and N_c values accordingly.

The lowest value of ΔG_c which is of interest for the evaluation of the nucleation rate equation is that for which $\sum \sigma_i S_i$ has a minimum, i.e., the ΔG_c value of the Gibbs–Wulff–Kaischew equilibrium form. Recalling that for this form $\sigma_i/h_i = (\sigma_j - \beta)/h_j^* = \text{const}$ [Eq. (48)], the σ values in the surface energy term of Eq. (57) can be expressed by $\sigma_i = h_i\sigma_1/h_1$ and $\sigma_j - \beta = h_j^*\sigma_1/h_1$, respectively, for all faces but face 1. Then the term $\sigma_g S_c/3$ in Eq. (58) can be obtained in the form

$$\tfrac{1}{3}\sigma_g S_c = \frac{\sigma_1}{h_1}\frac{1}{3}\sum_{i,j} h_i S_i = \frac{\sigma_1}{h_1} V_c \tag{59}$$

where the sum $\sum_{i,j} h_i S_i$ includes all faces i of the cluster as well as the face j which is in contact with the substrate. The factor $(1/3)\sum h_i S_i$ is equal to the volume of the geometrical form of the crystal and, hence, in this case to that of the critical nucleus V_c. Inserting Eq. (59) in Eq. (57), bearing in mind that $V_c = v_m N_c$ and $S_c^3 = BV_c^2$, we obtain

$$\frac{\sigma_i}{h_i} = \frac{\sigma_j - \beta}{h_j^*} = \frac{ze_0\eta_c}{2v_m} \tag{60}$$

This is a general form of the well-known Gibbs–Thomson equation relating the size of the critical nucleus and its equilibrium form to the overpotential.

It is of significance for the electrochemist to note that, according to this relation, a small crystal has a more negative (cathodic) equilibrium potential than a large one. As an example, a cubic crystal of size $h = 10^{-4}$ cm (h is in this case equal to the half side length of the cube) with $v_m = 2 \times 10^{-23}$ cm^3 mol^{-1} and $\sigma = 500 \times 10^{-7}$ J cm^{-2} has a shift of the equilibrium potential of 0.1 mV to the negative side. It has to be emphasized, however, that the equilibrium between the supersaturated phase and the small crystal is metastable and the smallest change of its dimensions will make it either grow or dissolve under the acting overpotential.

Equation (60) in the general form presented here has been derived by Kaischew$^{(63-65)}$ and includes also the heterogeneous nucleation. According to Kaischew, the Gibbs free energy, ΔG_c^*, of nucleus formation in the heterogeneous case is related to ΔG_c for the nucleation in a homogeneous phase by

$$\Delta G_c^* = \Delta G_c V_c^*/V_c \tag{61}$$

where V_c and V_c^* are the volumes of the nucleus in the homogeneous phase and that in contact with the substrate. Equation (61) follows directly from

Eqs. (59) and (58). It is self-evident that Eq. (61) is valid only if clusters of the same geometrical form, e.g., the equilibrium form defined by Eq. (60), are compared.

The linear dimensions h_i of the critical cluster are determined according to Eq. (60) by the overpotential. The presence of the substrate affects only the value of h_j^*, i.e., the distance of the Wulff point from the contact interface.

The larger is the value of the adhesion energy β, the smaller is the thickness and hence the volume V_c^* of the critical cluster. If different orientations of the cluster with respect to the substrate are considered, this would mean that the orientation showing the highest crystal–substrate interaction, β, would be the one having the smallest volume and, according to Eq. (61), the lowest energy of formation. When the substrate is noncrystalline and does not exert orientational effects on the nucleus, the face with the most close-packed structure would correspond to this requirement; or, from the point of view of the energetics of the nucleation process, the most favorable orientation is that at which the nucleus is in contact with its most close-packed singular face with the substrate. As a matter of fact, no change or orientation of the nucleus can be expected going to higher overpotentials for energetical reasons only.

5.3. The Nucleation-Rate–Overpotential Relation

The interpretation of the nucleation rate equation in terms of its overpotential dependence is rather difficult to perceive as represented in the form of Eq. (52). It has been shown already that the terms $\prod_{i=1}^{N} \omega_d(i)/\omega_a(i)$ contain the energy of formation of the cluster of class N and that at a given overpotential ΔG_N has a maximum for the critically sized cluster, $N = N_c$. If all terms other than that for the critical cluster are neglected, Eq. (52) reduces to

$$J = k_1 \exp(-\Delta G_c/kT) \tag{62}$$

where k_1 includes constants which can be derived from Eq. (52): $k_1 = k_c \omega_{a,c} Z_0$. Equation (62) is known as the Volmer–Weber$^{(20)}$ equation derived as early as 1926 and gives, through ΔG_c, the overvoltage dependence of the nucleation rate. In the derivation made here, two significant approximations are made clear: (i) the contributions of all terms (other than that for the critical nucleus) to the nucleation rate are neglected and (ii) the existence of parallel going reaction sequences, to that selected by the equilibrium form condition, have been disregarded.

5.3.1. The Continuity Approach

At low overpotentials, where approximation (i) is rather poor, the size of the nucleus becomes large and the sum in the denominator in Eq. (52), being composed of a large number of terms, can be replaced by an integral.

The integration made first by Becker and Döring$^{(66)}$ for liquid droplets and by Kaischew$^{(22,72,73)}$ for cubic crystals leads to an expression of the form

$$J = \Gamma \omega_{a,c} Z_0 k^* \exp(-\Delta G_c/kT) \tag{63}$$

The comparison of this equation with Eq. (62) shows that the contribution of the omitted terms in the derivation of Eq. (62) can be accounted for by the introduction of the factor Γ known as the Zeldovich nonequilibrium factor. The factor is always less than unity, having an order of magnitude of 10^{-2} and accounts for the depletion of the cluster population due to the process of growth.$^{(74-76)}$ It seems that the Zeldovich factor depends on the geometrical form of the cluster (see Refs. 72 and 78) and for a liquid droplet has the value $\Gamma = (\Delta G_c/3\pi kTN_c^2)^{1/2}$.

The attachment frequency to the nucleus of the critical size, $\omega_{a,c}$, depends on the form of the nucleus and on the adopted mechanism of deposition (direct transfer, surface diffusion, etc.). Z_0 is the number of sites per unit area where nucleation can start. For a homogeneous surface, Z_0 is given by the number of adsorption sites for adatoms and is of the order of 10^{15} cm^{-2}. The factor k^* contains the vibrational frequencies of the cluster atom in the positions i with respect to the frequency of vibration of the kink atoms$^{(68)}$ and can be assumed to be of the order of unity. It has to be remembered, however, that the inclusion of an entropy term, particularly when dissociation energies are used for the calculation of ΔG_c, makes its value largely uncertain. It has been emphasized already that configurations other than equilibrium (Wulff–Kaischew) ones can contribute to the overall nucleation rate. Kaischew and Stoyanov have shown that, at low overpotentials, this contribution becomes appreciable.$^{(77)}$

The uncertainty in Z_0, $\omega_{a,c}$, k^* and the contribution ratio of nonequilibrium configurations, renders an attempt at a complete quantitative evaluation of the nucleation rate unsatisfactory. Nevertheless, significant progress toward a better understanding of the factors determining the preexponential term in Eq. (62) has been achieved. For more details, the reader should refer to the review articles by Hirth and Pound,$^{(78)}$ Neugebauer,$^{(79)}$ and by Toshev.$^{(76)}$

From an experimental point of view, however, it seems that little progress has been made since the evaluation of the Volmer–Weber equation in 1926. The experimentalist is bound to use Eq. (62), disregarding the small noninformative dependence of k_1 from η_c derived from the Zeldovich factor or the attachment frequency $\omega_{a,c}$.

Introducing ΔG_c from Eqs. (61) and (58) in Eq. (62), the overpotential dependence of the nucleation rate can be obtained in the form

$$\log J = \log k_1 - k_2/\eta_c^2 \tag{64}$$

where

$$k_2 = \frac{4Bv_m^2\sigma_g^3(V_c^*/V_c)}{27(ze_0)^2kT} \tag{65}$$

includes, through V_c^*/V_c, the cluster–substrate interaction parameter β. The J–η_c relation (64) shows a sharp rise of J above a critical value below which the rate of nucleation is negligibly small. The general course of the curve is very similar to that discussed already in Section 3.1 and presented in Figure 4.

5.3.2. The Small Cluster Model

With increasing overpotentials, the number of atoms, N_c, constituting the critical nucleus becomes reduced dramatically attaining values of the order of several atoms. Macroscopic quantities, such as volume, surface, surface energies, etc. lose their physical meaning in such cases and the use of atomic forces of interaction becomes more reasonable. The atomistic approach for the calculation of the dependence of nucleation rate on supersaturation was first used by Walton,(80,81) and then developed later to a general nucleation theory by Stoyanov *et al.*(68,82)

As shown by Stoyanov,(69,82) all terms in the denominator of Eq. (52) can reasonably be neglected with respect to the number of the critical nucleus where ΔG_N has its maximum, when small clusters are considered. An additional simplification can be made on the basis of the fact that only close-packed structures or atomic configurations can be considered because of the elevated mobility of the atoms of small atomic aggregates. Equation (52) then leads with Eqs. (54) and (55) to

$$J = Z_0 \omega_{a,c} k_c \exp\left[N_c z e_0 \eta_c / kT - \left(N_c \phi_{k,s} - \sum^{N} \phi_{j,s}\right)\Big/ kT\right] \tag{66}$$

where the index c denotes that the values ω_a, k, and N are referred to those of the critically sized nucleus. The attachment frequency of an atom to the critical cluster is also overpotential dependent. Being proportional to the cathodic component of the exchange current, $\omega_{a,c}$ is given by $\omega_{a,c} \sim \exp[(1-\beta) z e_0 \eta_c / kT]$. Taking the logarithm of J, Eq. (66) can then be rewritten as

$$\log J = A(N_c) + [N_c + (1-\beta)] z e_0 \eta_c / kT \tag{67}$$

where $A(N_c)$ includes all constants in the preexponential term of Eq. (66) as well as the N_c-dependent term $-(N_c \phi_{k,s} - \sum^N \phi_{j,s})$. In Eq. (67), N_c is over potential dependent but being an integer can take only discrete values. As seen from Figure 20, corresponding to any discrete value of N_c, an overpotential interval of stability can be found. Therefore, while the second term in Eq. (67) changes linearly with η_c with a slope depending on the discrete value of N_c, the first term, giving the intercept of the $\log J$ vs. η_c relation, takes only discrete values dpending on N_c. Consequently the log J vs. η_c relation at high overpotentials is composed of series of linear sections with slopes changing with the size N_c of the cluster as it changes from one overpotential interval to the other.

5.4. Comparison with Experimental Data

Several techniques have been developed for the investigation of the rate of nucleation. Earlier methods were based on galvanostatic techniques. The first to use this technique were Samartzev and Evstropiev.(83) Later it was developed and refined in experiments of Schottky(84) and Gutzow(85) but, because of the high sensitivity of the nucleation process on overpotential, the results are difficult to interpret. Potentiostatic techniques gave more comprehensible results. The simplest potentiostatic technique, used by Kaischew, Scheludko, and Bliznakov(86) and by Scheludko and Bliznakov,(67) is to apply an overpotential pulse to the electrode and to measure the time at which current is observed to flow. The technique allows an estimate to be made of the time lag τ_1 needed for the formation of the first nucleus. The identification of τ_1 with J^{-1} meets some difficulties connected with nonstationary processes discussed in detail by Toschew.(76)

The most straightforward test of the nucleation rate equation is to make a plot of the number of nuclei per unit area as function of time at different overpotentials. The double pulse technique developed by Scheludko and Todorova(28) has been successfully used in a wide range of experiments.(88–91) For this purpose, the electrode is conditioned at the equilibrium potential of the deposited metal and a short overpotential pulse is applied. The nuclei formed during this first nucleation pulse are grown with a second lower overpotential pulse. The amplitude of the second growth pulse is set at an overpotential lower than the critical value so that no further nucleation can proceed. The duration of this pulse is chosen so that the nuclei formed during the first nucleation pulse can grow to a size visible under the microscope. Figure 21 shows Hg droplets formed on a spherical Pt single-crystal electrode. The nuclei were formed with a cathodic pulse of 87 mV and a pulse duration of 1.5 msec and were grown at 20 mV for about 3 sec until they became visible. The density of nuclei is determined simply by counting the number of droplets for a given surface area of the electrode. The technique, being based on visual counting, allows determinations of the nucleation rate on different crystallographic zones of single-crystal electrodes to be made. In other words, it allows discrimination of differently active zones on the electrode surface.(90,91)

A modification of the double-pulse method is to record the current transient following the first pulse and from the slope of the i vs. $t^{1/2}$ plot to determine the number of growing nuclei. This technique has been successfully used by Gunawardena, Hills, and McKee(92) and Gunawardena, Hills, and Montenegro(93,94) for calculation of the number of nuclei formed following a galvanostatic or a potentiostatic pulse. From the experimental point of view, this modification is more easily performed especially where large numbers of nuclei have to be counted. It has to be pointed out, however, that this method, being connected with some additional assumptions and calculations, has always to be carefully checked by the visual technique described above.

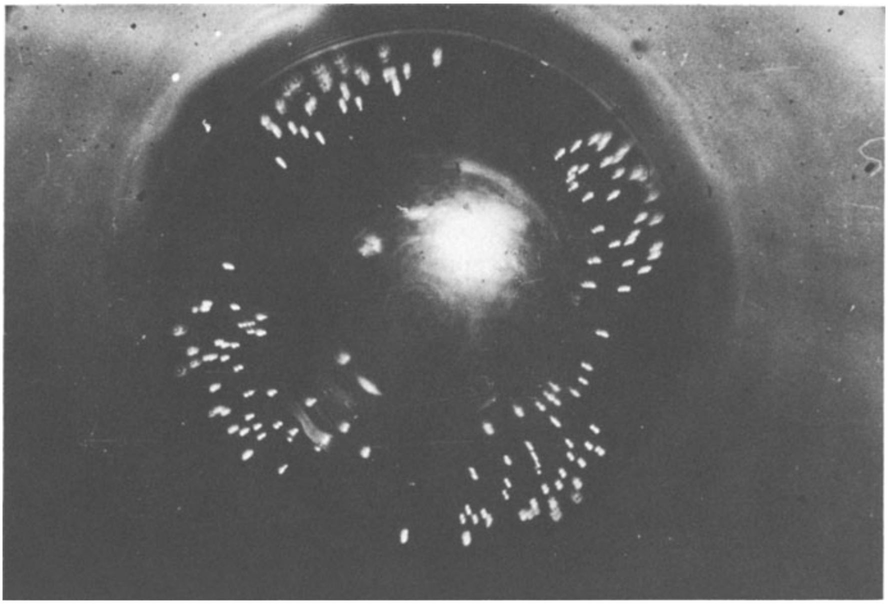

Figure 21. Hg droplets formed on a spherical Pt single-crystal electrode. Nuclei formed at $\eta_{\text{nucl}} = 87$ mV, $\tau_{\text{nucl}} = 1.5$ msec, $\eta_{\text{growth}} = 20$ mV, $\tau_{\text{growth}} = 3$ sec.(92)

Figure 22 shows experimental plots of the number of nuclei vs. time (i.e., vs. the nucleation pulse duration) at different overpotentials in the electrodeposition of mercury on platinum.(95) The steady state nucleation rate (dN/dt = const) is clearly attained only after an induction period of time. This induction period has been treated in terms of nonstationary effects connected with the readjustment of the surface to the new overpotential conditions. A detailed mathematical analysis based on the Zeldovich–Frenkel formulation of the nucleation kinetics has been given by Kashchiev(96) and Toshev.(76)

From the linear parts of the N/t curves of Figure 22 the steady state nucleation rate, J, for different overpotentials can be evaluated. Figure 23a represents a typical J vs. $1/\eta_c^2$ plot for the system of Figure 22. The analysis of the data according to Eq. (64) shows that, in the overpotential interval 84–106 mV studied, the value of ΔG_c varies between 8.4 and 5.3×10^{-20} J, while the number of atoms forming the critical nucleus varies between 13 and 6 [N_c is estimated from $N_c = 2\Delta G_c / ze_0\eta_c$, which follows directly from Eqs. (57) and (58)].

This low number of atoms (6–13) invalidates the use of Eqs. (64), (57), and (58), based on macroscopic quantities. The same experimental results are represented again in Figure 23b in a log J vs. η_c plot according to Eq. (67) of the small cluster model. The two slopes of the plot give ten and six

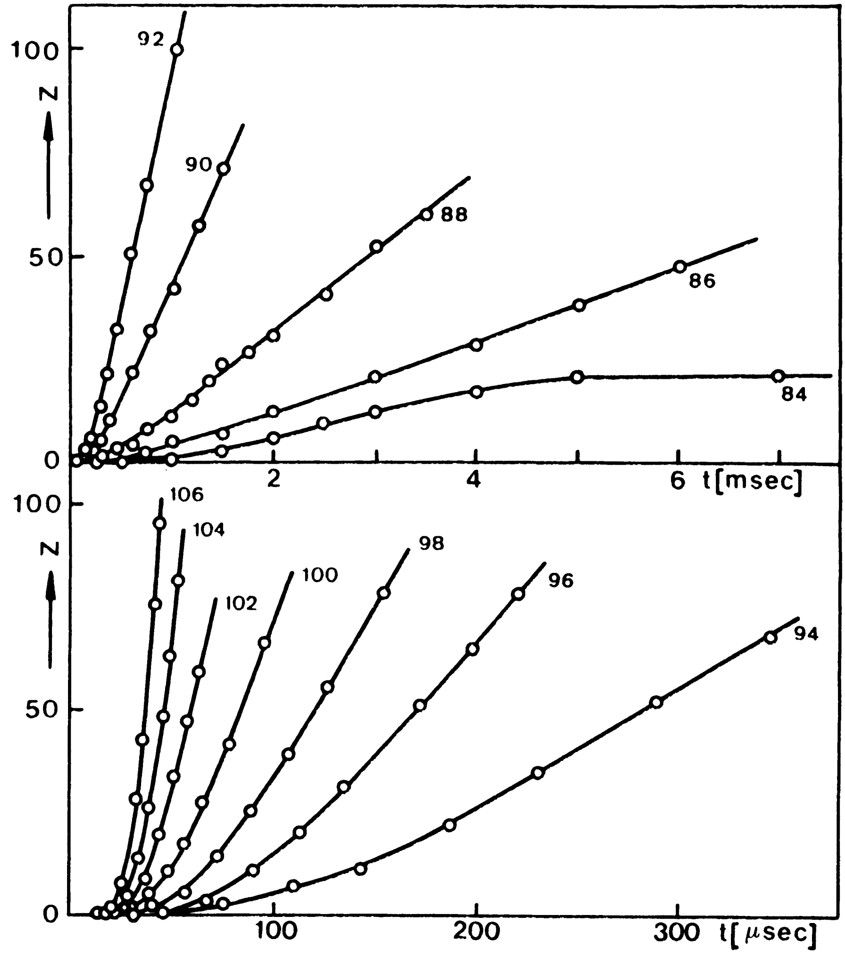

Figure 22. Experimental plots of the number of nuclei vs. time in the electrodeposition of mercury on Pt, after Toshev and Markov.(92) The figures denote the corresponding nucleation overvoltage.

atoms for the size of the critical nucleus in the intervals 84–96 and 96–106 mV, respectively.(69,97–99)

The apparent agreement with theory has, however, to be taken with caution. All experiments up to now have been made in a relatively small overpotential interval and no more than one cusp, i.e., two slopes, of the $\log J/\eta_c$ curve has been observed. The determination of the number of atoms in the critical nucleus is also quite uninformative as a criterion for the validity of the small cluster model equation. Furthermore it does not lead to any conclusions about the free energy of nucleation or forces of interaction between the cluster atoms themselves, and eventually between them and the substrate which would be the ultimate goal of a nucleation rate study.

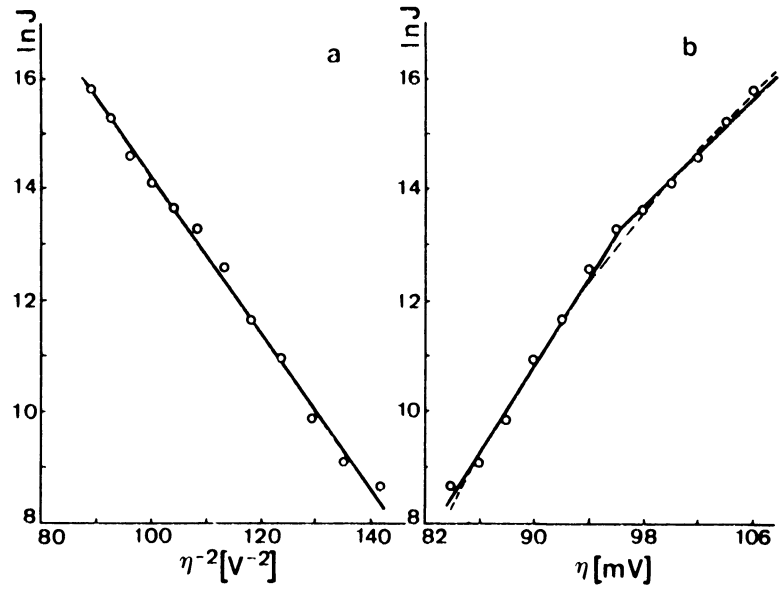

Figure 23. Experimental steady state nucleation rate J values calculated from the data of Figure 22; (a) in a ln J vs. $1/\eta^2$ plot and (b) in a ln J vs. η plot.(97)

Nevertheless, the comparison of a large number of experiments carried out by different authors, with theory, leads to the apparently important conclusion that the use of log J vs. $1/\eta_c^2$ plots gives reasonable results with respect to the number of atoms and eventually the free energy of formation of the critical nucleus. Table 1, based on data collected by Milchev and Stoyanov,(69,97) shows results treated according to both models. The number of atoms of the critical cluster in all cases is far too low to make a classical treatment acceptable but coincides well in both treatments. A comparison of the atomistic with the classical treatment is given in Figure 23b. The dashed line represents the straight line of the log J vs. $1/\eta_c^2$ plot of Figure 23a obtained by the least squares method, plotted in the coordinates of Figure 23b. The close course of both full and dashed lines observed in most of the cases suggests that both equations, the classical Eq. (64) and the atomistic Eq. (67), coincide in the high overpotential region, the atomistic model representing better the experimental results by the broken line as required by Eq. (67). Going to lower overpotentials, as the η_c intervals of constant cluster size N_c become narrower, the experimental results are expected to be represented better by the classical Eq. (64). How far the values of ΔG_c and the quantity $\sigma_g^3 V_c^* / V_c$ obtained from the classical plot at higher overpotentials can be trusted is still an open question. A detailed analysis of this problem has been made recently by Milchev and Vassileva.(99)

Table 1

Gibbs Free Energies of 3D Nucleation, ΔG_c, and Number of Atoms, N_c, Forming the Critical Nucleus in the Deposition of Different Metals on Pt as Calculated from the Classical and the Atomistic Model. η Indicates the Overpotential Interval Used in the Calculation.(97)

Experimental data	Ref.	Classical model			Atomistic model	
		η, V	ΔG_c, erg	N_c	η, V	N_c
Ag/Pt(100)	88	0.200–0.280	$(3.7\text{–}1.9) \times 10^{-13}$	2–1	0.200–0.240	1
					0.240–0.280	0
Ag/Pt(111)	88	0.200–0.250	$(4.8\text{–}3.1) \times 10^{-13}$	3–2	0.200–0.220	3
					0.220–0.250	1
Hg/Pt	88	0.090–0.102	$(10.1\text{–}7.9) \times 10^{-13}$	14–10	0.090–0.102	11
Hg/Pt	95	0.084–0.106	$(8.4\text{–}5.3) \times 10^{-13}$	13–6	0.084–0.096	10
					0.096–0.106	6
Ag/Pt	100	0.170–0.210	$(8.0\text{–}5.2) \times 10^{-13}$	6–3	0.170–0.193	5
					0.193–0.210	2
Cu/Pt	101	0.047–0.080	$(2.7\text{–}0.9) \times 10^{-13}$	7–1	0.047–0.051	14
					0.053–0.080	2

6. Conclusions and Outlook

The basic principles of electrocrystallization seem to be well established. Significant progress has been made in the last two decades in the understanding of the energetics of the nucleation and growth processes. The kinetics of growth have been well developed theoretically and have found a good experimental confirmation in isolated cases. Further development is needed in our concepts of the state and behavior of the crystal–solution interface as well as in the understanding of the activation and inhibition of the nucleation and growth processes.

Three-dimensional nucleation is still in a very early stage of development. Significant progress has, however, been evidently made by the introduction of the atomistic theory, but we are obviously still far from an adequate understanding of the processes of nucleation, cluster orientation, grain growth interaction, dendrite formation, and properties of bulk deposits.

Acknowledgments

The author is indebted for many helpful discussions to Drs. A. Milchev, W. Bostanov, G. Staykov, and Z. Stoinov as well as to Mrs. M. Kermekchieva and Mr. Yankulov for their technical help in the preparation of the manuscript.

References

1. F. C. Frank, in *Growth and Perfection of Crystals*, R. Doremus, R. Roberts, and D. Turnbull, eds., John Wiley and Sons, New York (1958), p. 3.
2. W. Burton, N. Cabrera, and F. Frank, *Philos. Trans.* A **243**, 299 (1958).
3. R. Kaischew, *Annu. Univ. Sofia Fac. Physiocomathem.* (*Chim.*) **42**, 109 (1945/1946).
4. A. A. Chernov, *Ann. Rev. Mater. Sci.* **3**, 397 (1973).
5. B. Conway and J. O'M. Bockris, *Proc. R. Soc.* **248**, 394 (1958); *Electrochim. Acta* **3**, 340 (1960).
6. J. O'M. Bockris and A. Damjanović, in *Modern Aspects of Electrochemistry*, J. O'M. Bockris and B. E. Conway, eds., Butterworths, London (1964), p. 224.
7. W. Lorenz, *Z. Naturforsch.* **9a**, 716 (1954).
8. A. Despić and J. O'M. Bockris, *J. Chem. Phys.* **32**, 389 (1960).
9. A. Damjanović and J. O'M. Bockris, *J. Electrochem. Soc.* **110**, 1035 (1963).
10. K. Vetter, *Electrochemical Kinetics*, Academic Press, New York (1967), p. 283.
11. M. Fleischmann and R. Thirsk, *Electrochim. Acta* **2**, 22 (1960).
12. D. A. Vermilyea, *J. Chem. Phys.* **25**, 1254 (1956).
13. E. Budevski and Z. Stoinov, *Izv. Inst. Phys. Chem. Bulg. Acad. Sci.* **4**, 35 (1964).
14. W. Mehl and J. O'M. Bockris, *J. Chem. Phys.* **27**, 817 (1957).
15. W. Mehl and J. O'M. Bockris, *Can. J. Chem.* **37**, 190 (1959).
16. Ch. Schnittler, Thesis, Techn. Hochschule Ilmenau, GDR (1969).
17. M. Volmer, in *Actualités Scientifiques et Industrielles*, Vol. **85**, Herrmann, Paris (1933), pp. 1–12.
18. N. Mott and R. Watts-Tobin, *Electrochim. Acta* **4**, 79 (1961).
19. J. W. Gibbs, in *Collected Works*, Vol. 1, Yale University Press, New Haven, Connecticut (1948).
20. M. Volmer and A. Weber, *Z. Phys. Chem.* **119**, 277 (1926).
21. H. Brandes, *Z. Phys. Chem.* **126**, 196 (1927).
22. R. Kaischew, *Acta Phys. Acad. Sci. Hung.* **8**, 75 (1957).
23. T. Erdey-Gruz and M. Volmer, *Z. Phys. Chem.* **157**, 165 (1931).
24. I. P. Hirth, *Acta Metall.* **7**, 755 (1959).
25. E. Budevski, V. Bostanov, T. Vitanov, Z. Stoynov, A. Kotzeva, and R. Kaischew, *Electrochim. Acta* **11**, 1697 (1966).
26. E. Budevski, V. Bostanov, T. Vitanov, Z. Stoynov, A. Kotzeva, and R. Kaischew, *Phys. Status Solidi* **13**, 577 (1966).
27. R. Kaischew and E. Budevski, *Contemp. Phys.* **8**, 489 (1967).
28. A. Scheludko and M. Todorova, *Bull. Acad. Sci. Bulg.* (*Phys.*) **3**, 61 (1952).
29. E. Budevski, in *Progress in Surface and Membrane Science*, Vol. 11, Academic Press, New York (1976), p. 71.
30. S. Toshev, A. Milchev, and S. Stoyanov, *J. Cryst. Growth* **13/14**, 123 (1972).
31. V. Bostanov, R. Roussinova, and E. Budevski, *Chem. Ing. Techn.* **45**, 179 (1973).
32. V. Bostanov, G. Staykov, and D. K. Roe, *J. Electrochem. Soc.* **122**, 1301 (1975).
33. V. Bostanov, private communication.
34. T. Vitanov, E. Sevastianov, V. Bostanov, and E. Budevski, *Elektrokhimiya*, **5**, 451 (1969).
35. T. Vitanov, A. Popov, and E. Budevski, *J. Electrochem. Soc.* **121**, 207 (1974).
36. V. Bostanov, *J. Cryst. Growth* **42**, 194 (1977).
37. T. Vitanov, E. S. Sevastianov, V. Bostanov, and E. Budevski, *Elektrokhimya* **5**, 451 (1969) (in Russian).
38. A. E. Nielsen, in *Kinetics of Precipitation*, Pergamon Press, New York (1964), p. 40.
39. A. A. Chernov and B. J. Lyubov, *Cryst. Growth USSR* **5**, 11 (1965).
40. W. B. Hillig, *Acta Metall.* **14**, 1868 (1966).
41. E. Budevski, V. Bostanov, and G. Staykov, *Ann. Rev. Mater. Sci.* **10**, 85 (1980).
42. A. Bewick, M. Fleischmann, and H. R. Thirsk, *Trans. Faraday Soc.* **58**, 2200 (1962).

43. M. Fleischmann and H. R. Thirsk, in *Advances in Electrochemistry and Electrochemical Engineering*, Vol. 3, P. Delahay, ed., John Wiley and Sons, New York (1963), p. 123.
44. G. Staikov, V. Bostanov, and E. Budevski, *Electrochim. Acta* **22**, 1245 (1977).
45. L. A. Borovinskii and A. N. Zindergosen, *Dokl. Acad. Nauk USSR* **183**, 1302 (1968).
46. R. D. Armstrong and J. A. Harrison, *J. Electrochem. Soc.* **116**, 328 (1969).
47. S. K. Rangarajan, *J. Electroanal. Chem.* **46**, 125 (1973).
48. U. Bertocci, *J. Electrochem. Soc.* **119**, 822 (1972).
49. G. Gilmer, *J. Cryst. Growth* **49**, 465 (1980).
50. W. Bostanov, W. Obretenov, G. Staikov, D. Roe, and E. Budevski, *J. Cryst. Growth.* **52**, 761 (1981).
51. F. C. Frank, *Discuss. Faraday Soc.* **5**, 48, 67 (1949).
52. E. Budevski, G. Staikov, and V. Bostanov, *J. Cryst. Growth* **29**, 316 (1975).
53. N. Cabrera and M. M. Levine, *Philos. Mag.* **1**, 450 (1956).
54. N. Cabrera, in *Structure and Properties of Solid Surfaces*, University of Chicago Press, Chicago (1953), p. 295.
55. R. Kaischev, E. Budevski, and J. Malinovski, *Z. Phys. Chem.* **204**, 348 (1955).
56. C. Chapon and A. Bonissent, *J. Cryst. Growth* **18**, 103 (1973).
57. V. Bostanov, E. Budevski, and G. Staikov, in *Faraday Symposium of the Chemical Society, London* No. 12, p. 83 (1977).
58. E. Budevski, G. Staikov, W. Bostanov, and G. Angelov, *Comm. Dept. Chem. Bulg. Acad. Sci.* **11**, 467 (1978).
59. H. Seiter, H. Fischer, and L. Albert, *Electrochim. Acta* **2**, 167 (1960).
60. E. Budevski, T. Vitanov, and W. Bostanov, *Phys. Status. Solidi* **8**, 369 (1965).
61. G. Staikov, W. Obretenov, W. Bostanov, E. Budevski, and H. Bort, *Electrochim. Acta* **25**, 1619 (1980).
62. W. Bostanov, R. Roussinova, and E. Budevski, *Comm. Dept. Chem. Bulg. Acad. Sci.* **2**, 885 (1969).
63. R. Kaischew, *Bull. Acad. Bulg. Sci.* (*Phys.*) **1**, 100 (1950).
64. R. Kaischew, *Bull. Acad. Bulg. Sci.* (*Phys.*) **2**, 191 (1951).
65. R. Kaischew, Arbeitstagung Festkörperphysik, Dresden (1952), p. 82.
66. R. Becker and W. Döring, *Ann. Phys.* (Leipzig) **24**, 719 (1935).
67. M. Volmer, in *Kinetik der Phasenbildung*, Theodor Steinkopf Verlag, Leipzig/Dresden (1939).
68. A. Milchev, S. Stoyanov, and R. Kaischew, *Thin Solid Films* **22**, 255, 267 (1974).
69. S. Stoyanov, in *Nucleation Theory for High and Low Supersaturations*, *Current Topics in Materials Science*, Vol. 3, E. Kaldis, ed., North-Holland, Amsterdam (1978), Chap. 4.
70. I. N. Stranski, *Annu. Univ. Sofia Fac. Phys.-Math. Livre 2* (*Chim.*) **30**, 367 (1936/1937).
71. B. Lewis, *Thin Solid Films*, **1**, 85 (1967).
72. R. Kaischew, *Z. Elektrochem.* **61**, 35 (1957).
73. R. Kaischew, in *Festkorperphysik und Physik der Leuchtstoffe*, Akademie Verlag, Berlin (1958), p. 133.
74. Ya. I. Frankel, in *Kinetic Theory of Liquids*, Dover, New York (1955).
75. Ya. B. Zeldovich, *J. Exp. Theoret. Phys.* (*USSR*) **12**, 525 (1942); *Acta Physicochim. URSS* **18**, 1 (1943).
76. S. Toshev, in *Homogeneous Nucleation in Crystal Growth*: *An Introduction*, M. Hartman, ed., North-Holland, Amsterdam (1973), p. 1.
77. R. Kaischew and S. Stoyanov, *Comm. Dept. Chem. Bulg. Acad. Sci.* **2**, 127 (1969).
78. J. P. Hirth and G. M. Pound, in *Condensation and Evaporation*, MacMillan, New York (1963).
79. C. A. Neugebauer, *Handbook of Thin Film Technology*, McGraw-Hill, New York (1970).
80. D. Walton, *J. Chem. Phys.* **37**, 2182 (1962); *Philos. Mag.* **7**, 1671 (1962).
81. D. Walton, T. Rhodin, and R. W. Rollins, *J. Chem. Phys.* **38**, 2698 (1963).
82. S. Stoyanov, *Thin Solid Films* **18**, 91 (1973).

83. A. G. Samartzev and K. S. Evstropiev, *Izv. Acad. Sci. USSR*, 603 (1934).
84. W. Schottky, *Z. Phys. Chem.* (*N.F.*) **31**, 40 (1962).
85. I. Gutzow, *Bull. Inst. Chim. Phys. Acad Bulg. Sci.* **4**, 69 (1964).
86. R. Kaischew, A. Scheludko, and G. Bliznakov, *Bull. Acad. Bulg. Sci.* (*Phys.*) **1**, 137 (1950).
87. A. Scheludko and G. Bliznakov, *Bull. Acad. Bulg. Sci.* (*Phys.*) **2**, 227 (1951).
88. R. Kaischew and B. Mutaftschiev, *Electrochim. Acta.* **10**, 643 (1965); *Z. Phys. Chem.* **204**, 334 (1955).
89. R. Kaischew, S. Toschew, and I. Markov, *Comm. Dept. Chem. Bulg. Acad. Sci.* **2**, 463 (1969).
90. R. Kaischew and B. Mutaftschiev, *Bull. Acad. Bulg. Sci.* **4**, 105 (1954); **5**, 77 (1955).
91. S. Toschew and B. Mutaftschiev, *Electrochim. Acta*, **9**, 1203 (1964).
92. G. A. Gunawardena, G. J. Hills, and J. Montenegro, *J. Electroanal. Chem.*, **138**, 241 (1982).
93. G. A. Gunawardena, G. J. Hills, and J. Montenegro, *Electrochim. Acta.*, **23**, 693 (1978).
94. G. A. Gunawardena, G. J. Hills, and J. Montenegro, *Discuss. Faraday Soc.*, **12**, 90 (Southampton) (1977).
95. S. Toshev and J. Markov, *Ber. Bunsenges. Phys. Chem.* **73**, 184 (1969).
96. D. Kashchiev, *Surf. Sci.* **14**, 209 (1969).
97. A. Milchev and S. Stoyanov, *J. Electroanal. Chem.* **72**, 33 (1976).
89. A. Milchev, E. Vassileva, and V. Kertov, *J. Electroanal. Chem.* **107**, 323 (1980).
99. A. Milchev and E. Vassileva, *J. Electroanal. Chem.* **107**, 337 (1980).
100. S. Toshev, A. Milchev, I. Markov, and K. Popova, *C. R. Acad. Bulg. Sci.* **22**, 1413 (1969).
101. R. Lackmann and H. J. Randig, *J. Cryst. Growth* **17**, 97 (1972).

7

Deposition and Dissolution of Metals and Alloys. Part B: Mechanisms, Kinetics, Texture, and Morphology

ALEKSANDAR R. DESPIĆ

1. Introduction

Electrochemical deposition and dissolution of metals obeys the following general stoichiometric equation†:

$$[\mathrm{M}(z)\mathrm{L}_p\mathrm{S}_\alpha]_{\mathrm{soln}} + [ze]_{\mathrm{metal}} \underset{\mathrm{dissol}}{\overset{\mathrm{depos}}{\rightleftarrows}} [\mathrm{M}]_{\mathrm{metal}} + [p\mathrm{L} + \alpha\mathrm{S}]_{\mathrm{soln}} \tag{1}$$

where M is metal atom, L atoms or atomic groups or molecules of a ligand, S solvent molecules, and z is the number of electrons, e, exchanged to form a z-valent metal ion $\mathrm{M}(z)$ from the metal M.

Electrochemical deposition of a metal from an ionic species present in bulk solution occurs in several steps as schematically represented in Figure 1.

Only for special conditions (very low pH, absence of complexation) is the species a simple solvated metal ion. In most cases, however, there is a

---

† Thermodynamic convention requires that the left-hand side of Eq. (1) (i.e., oxidized state) be considered as the initial state (reactants), and the right-hand side (i.e., the reduced state of M) as the final state (products). Hence, data on standard electrochemical potentials(1,2) refer to, and equations for electrochemical equilibria (the Nernst equations, cf. below) are written for, the overall process taken in the direction of *cathodic reduction.*

ALEKSANDAR R. DESPIĆ • Professor of Physical Chemistry, Faculty of Technology and Metallurgy, University of Belgrade, Belgrade, Yugoslavia.

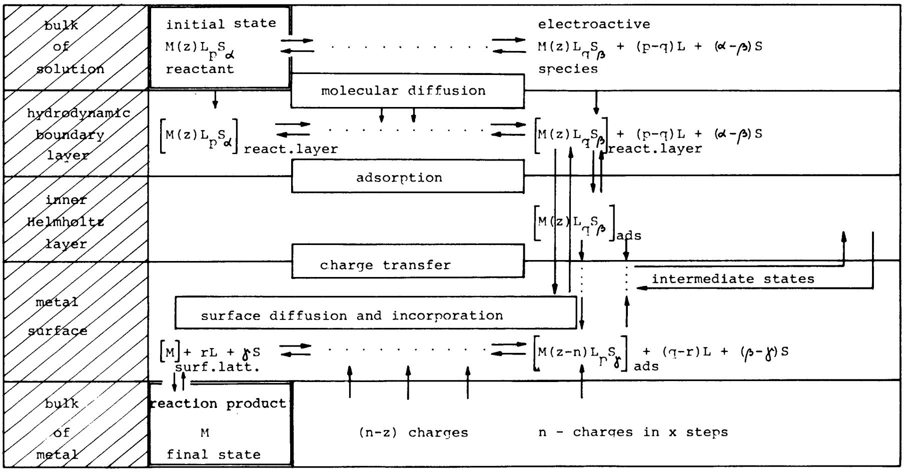
bulk of solution
initial state
M(z)L_pS_α
reactant
electroactive
M(z)L_qS_β + (p-q)L + (α-β)S
species
molecular diffusion
hydrodynamic boundary layer
[M(z)L_pS_α] react.layer
[M(z)L_qS_β] react.layer + (p-q)L + (α-β)S
adsorption
inner Helmholtz layer
[M(z)L_qS_β]ads
charge transfer
intermediate states
metal surface
surface diffusion and incorporation
[M] surf.latt. + rL + γS
[M(z-n)L_rS_γ]ads + (q-r)L + (β-γ)S
bulk of metal
reaction product
M
final state
(n-z) charges
n - charges in x steps

Figure 1. Schematic representation of the metal deposition and dissolution reaction: M, metal atom; L, ligand; S, solvent molecule; z, charge (valency) of the metal in solution; *p*, *q*, *r*, number of ligands per metal atom; α, β, γ, number of solvent molecules per metal atom.

complex grouping of ligands and solvent molecules around the central metal ion. Since this species may not be the one undergoing directly the charge transfer step, the first step in the metal deposition reaction may be its chemical transformation into the electroactive species. This step occurs during the transport (by diffusion) of the species to the electrode surface and takes place within the hydrodynamic boundary layer, or, in some cases, in the double layer. Before charge transfer, the electroactive species may be adsorbed at the outer or the inner Helmholtz layer on the electrode surface.

If multiple discharge ($z > 1$) is needed to obtain a neutral metal atom, the discharge itself may consist of several steps, possibly with some chemical transformation between them, and definitely followed by partial desolvation to form a species acceptable to the surface. This may not be a completely neutral and desolvated atom. Its state can depend on the strength of the attractive forces (adsorption) holding it at the surface in spite of, in some cases, considerable residual charge (electrosorption valency effect) and some corresponding residual solvation. Further changes in the properties of the species may occur along with the changes of its position and state on the surface, right up until its final incorporation into the crystal lattice.

The preceding chapter by Budevski has dealt with the phenomena of formation of the crystal lattice out of the products of charge transfer.

This present part considers the mechanism of the metal deposition and dissolution processes as a whole. It analyzes both the thermodynamic and the kinetic consequences of the postulated mechanisms, as well as the repercussions of the mechanisms on the properties of the deposits obtained. The electrode is also viewed as an electrical system, and the effects of the electrode processes on current–potential relationships, the impedance of the systems, etc. are discussed.

The effects of species not involved in the overall metal deposition reaction, but present at the electrode surface due to adsorption, and sometimes incorporated into the deposit, are also considered.

This chapter represents an attempt to give the reader an overview of the numerous phenomena encountered in electrochemical deposition and dissolution of metals. Particular metals are taken only as examples which serve as basis for, or which illustrate, the generalizations made. For a detailed review of the bulk of the work concerning each particular metal, which has been reported in the literature over the past decades, the reader is advised to consult recent monographs.†

2. Specific Features of the Thermodynamics of Metal and Alloy Phase Formation and Degradation

2.1. Equilibration of a Metal Surface with Electrolyte Containing Metal Ions—the Problem of the Reversible Potential

Equilibration results in establishment of an electrical potential difference across the metal–solution interface. This prevents any net transfer of reacting species involved in the electrode process described by Eq. (1), in spite of the fact that a chemical potential difference persists with respect to the exchangeable species. Hence, the particular feature of such an electrochemical equilibrium is that the electrode potential is a direct reflection of the chemical potential difference of the species involved or of the free energy change arising from the transformation of the reactants [left side of Eq. (1)] into the products [right side of Eq. (1)].

The equilibrium condition at an electrode interface is determined by equality of the Guggenheim "electrochemical potentials" for the charged species in the electrode (electrons) and the adjacent solution (cations and anions). This leads to an adjustment of the concentrations of the charged species across the interface, setting up an interfacial potential difference contribution, associated with the electronic and ionic charge separation. In addition to this coulombic contribution, there is a surface potential contribution in the single interface potential difference associated with asymmetry of the charge distribution at the metal surface and the moments of adsorbed and oriented dipoles of the solvent; the latter orientation is usually charge dependent.

The thermodynamic method is incapable of assessing the absolute value of that electrical potential difference at a single interface. Instead, it can derive its relative value with respect to a certain electrode reaction taken as a standard by using the free energy change (or Gibbs function) which results from a chemical equilibration between reactants and products of those two reactions.

---

† Particularly comprehensive ones are found in the series *Encyclopaedia of Electrochemistry of the Elements*, A. J. Bard, ed., Marcel Dekker, New York, 1980.

If, for example, the two reactions are:

$$Cu^{2+} + 2e \rightleftarrows Cu \tag{2}$$

and

$$2H_3O^+ + 2e \rightleftarrows H_2 + 2H_2O \tag{3}$$

the free energy change in the chemical reaction of reduction of cupric ions by hydrogen, viz.,

$$Cu^{2+} + H_2 + 2H_2O \rightleftarrows Cu + 2H_3O^+ \tag{4}$$

is related to the relative electrical potential difference (electrode potential) by

$$E = -\Delta G/zF \tag{5}$$

Reaction (4) is the cell reaction of the galvanic cell

$$\text{Pt, } H_2|H_3O^+|Cu^{2+}|Cu$$

which enables electrochemical reduction to take place, provided the hydrogen electrode is connected to the copper electrode by an external electronic conductor. Hence, the relative electrode potential is, in fact, the electromotive force of the couple in which the metal electrode is coupled with an electrode taken as a standard. If the hydrogen electrode is at a pressure of gaseous hydrogen $p^\ominus(H_2) = 101{,}325$ kPa and at a hydrogen ion activity in solution of $a^\ominus(H_3O^+) = 1$, the potential given by Eq. (5) is the relative potential, with respect to the standard hydrogen electrode, $E(Cu^{2+}|Cu)$ *vs.* SHE, and can be referred to as the electrode potential.

From the well-defined dependence of the free-energy change on the activity of each of the participating species of reaction (1) coupled with reaction (3), one can derive that

$$E = E^\ominus + \frac{RT}{zF}\ln\frac{a_{M(z)L_pS_\alpha}}{a_L^p a_S^\alpha} \tag{6}$$

where $a_{M(z)L_pS_\alpha}$, a_L, and a_S are relative activities of the metal-ion-containing species, of the ligand, and of the solvent, respectively, and $E^\ominus$ is the standard electrode potential for the electrode $M(z)L_pS_\alpha|M$[1,2] on the standard hydrogen scale.

Equation (6) is, of course, the Nernst equation for the metal electrode in the given solution, and it defines the reversible electrode potential as a starting point for performing cathodic deposition or anodic dissolution of the metal.

Truly reversible potentials of metals in solutions containing corresponding ions, reflecting the equilibrium described by the overall reaction (1), can be established only if the following conditions are fulfilled:

(a) All the processes in the transformation of the ion in solution into the metal in the lattice are considerably faster than the electrochemical reaction of the solvent or than any spurious redox process that may by chance be taking place, involving some foreign substance present in the solution (impurity of additive).

(b) All the intermediate species soluble in the electrolyte are present in bulk solution at equilibrium concentrations.

(c) The metal M is a pure and well-defined phase.

(d) The crystal grains constituting the surface are in their equilibrium form and state.

(e) The crystals are not too small.

If the first condition is not fulfilled, the driving force in a corrosion process will shift the established steady state electrode potential away from the reversible value. A typical example is that of metals the reversible potentials of which in an aqueous solution of their ions are more negative than that of the hydrogen electrode potential at the given pH of the solution. In such a case, hydrogen is being evolved from hydrogen ions or from water while the metal is dissolving anodically. The further away electrode potential adjusts itself in the positive direction from the true reversible potential of the metal, the lower is the rate constant for dissolution compared to that of hydrogen evolution.

The other three conditions are very often overlooked in experimental studies of metal deposition and dissolution, leading to ill-defined reference points from which overpotentials are measured in studies of electrode kinetics. For example, solutions are most often prepared by dissolving a salt containing cations corresponding to the metal with a single valency (e.g., cupric salts in copper deposition). Cations in intermediate oxidation states (e.g., cuprous ions) may have significantly large equilibrium concentrations, but these are often not reached within the limited time of the experiment, especially if the electrode is small and the amount of solution is large. Also, properties of metals are known to be affected by extremely small amounts of additives. For example, a whole selection of steels is obtained with relatively small additions of other metals, or minute percentages of carbon, sulfur, nitrogen, etc. The purity of the metal is, therefore, important in studies of electrode kinetics.

The problem of the equilibrium form of crystals has been discussed in the previous chapter. Attainment of such forms can be achieved only under special conditions and in most cases deviations from equilibrium forms constitute one reason for deviations of the electrode potentials from the expected reversible values.

All the above causes of deviation arise from a free-energy change different from that underlying the reversible potential, and hence the deviation of the established electrode potential from the reversible one can be expressed as:

$$\Delta E = -\Delta(\Delta G)/zF \tag{7}$$

If the crystal grains are decreasing in size, the reversible potential should shift to more negative values (Stockholm conversion) because of the increasing effect of surface free energy, known in vapor pressure or solubility measurements as the Kelvin effect. If the equivalent radius of a metal crystallite is r, the shift of the reversible electrode potential with respect to that of a large crystal grain ($r \to \infty$) will be

$$\Delta E = \frac{2\gamma V_m}{zFr} \tag{8}$$

where γ is the surface tension of the metal. Since the latter can have significant values (0.3–0.5 $\mathrm{N\,m^{-1}}$), the Kelvin effect becomes significant (>1 mV) as the grains become smaller than 27 nm.

2.2. Reversible Potentials of Alloys

Unless the standard potentials of the alloy components are very close to each other, an alloy can be electrochemically equilibrated only in solutions of ions corresponding to the less noble component (having a more negative value of the standard potential). In adverse cases, precipitation of the more noble component on account of dissolution of the less noble one (cementation) would occur until the surface is completely and tightly covered by the former.

If only ions of the less noble component are present, the reversible potential of the alloy electrode will be determined basically by the free-energy change of the less noble component in the alloy.

The possible cases reflect the variety of possibilities existing in solid phase formation by alloying.

2.2.1. Potential-Determining Component in Solid Solution

In an ideal case, the free energy of the less noble metal in the alloy, G, relative to that of a pure metal, $G^{\ominus}$, taken as the standard state, is given by the common thermodynamic relationship

$$\Delta G = G - G^{\ominus} = RT \ln x \tag{9}$$

where x is the mole fraction of the metal in the alloy. Hence, by substitution into Eq. (7), one obtains the change of the electrode potential of the alloy with respect to that of the pure metal:

$$\Delta E = -\frac{RT}{zF} \ln x \tag{10}$$

Since this implies the absence of any free energy of mixing, few alloys follow this relationship. Some dilute amalgams in aqueous solutions of corresponding ions at temperatures at which they are liquid do show linear relationships between E and $\log x$, e.g., sodium amalgams(3) up to mole fractions of 7×10^{-3}.

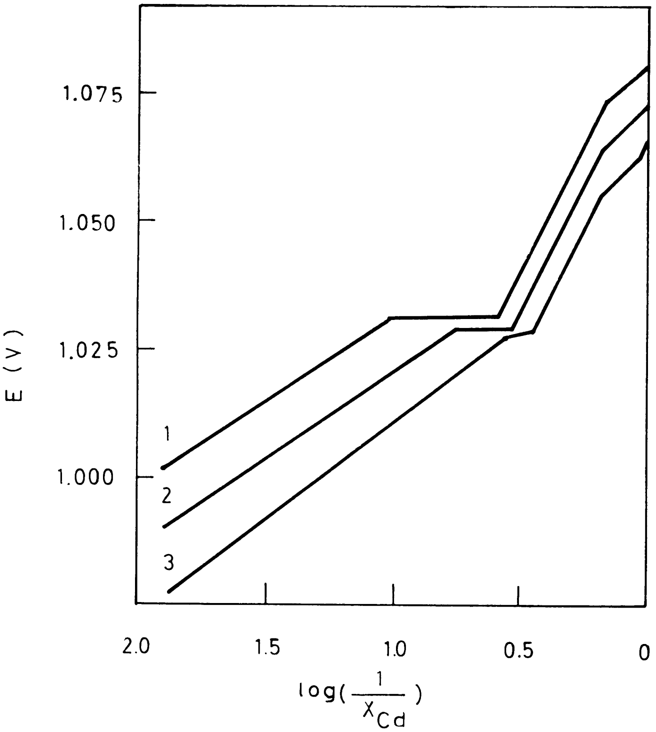

Figure 2. Potentials of cadmium amalgams as a function of composition: 1, 298°K; 2, 323 K; 3, 348 K.

The standard potentials to which they extrapolate, however, differ considerably from standard potentials of the corresponding metals, indicating significant free energies of amalgamation. Linearity observed is due merely to the constancy of that free energy over a range of amalgam concentrations.

In many cases, deviations from ideality arise, as, e.g., with the amalgam of cadmium,(4) as shown in Figure 2. Virtual independence of the potential on composition in the range of x around 0.4 makes this amalgam a good electrode for standard cells.(5)

2.2.2. Immiscible Components Forming Eutectics

If the components are strictly immiscible in the solid, the reversible potential of the alloy in the solution of ions corresponding to the less noble component should be the same as that of the pure, less noble metal, provided the conditions set forth earlier are fulfilled.

Since eutectics are usually formed of very small crystallites, the Kelvin effect [Eq. (8)] can be operative, and hence a shift of potential relative to that of the pure metal can be observed.

2.2.3. Formation of Intermetallic Compounds

The reversible potential of a metal alloyed with a component with which it forms an intermetallic compound should be more positive than that of the pure metal by effect of the free energy of formation of the compound, $\Delta G_f^\ominus$, which is always negative, i.e.,

$$\Delta E^\ominus = -\Delta G_f^\ominus / mzF \tag{11}$$

where m is the stoichiometric coefficient of the metal in the equation of formation. For example, zinc is known to form a compound when alloyed with silver, of the composition AgZn, with $\Delta G_f^\ominus = -10.46$ kJ mol^{-1}. Hence, the potential of the alloy in one and the same solution should be more positive than that of pure zinc by 0.054 V, i.e., the standard potential of the alloy should be $E^\ominus_{\mathrm{AgZn}} = 0.709$ V.

2.3. Underpotential Deposition of Metals on Foreign Substrates

The development of the ultrasensitive potential sweep technique, capable of detecting submonolayer amounts of substance on electrode surfaces and its application to metal deposition studies, resulted in detailed investigations of the phenomenon of deposition of metals on foreign substrates at potentials more positive than the thermodynamic reversible potential for the given conditions.(6) This phenomenon has been termed *underpotential deposition* (UPD).

This should be distinguished from findings(7) about the incorporation of alkali metals into the lattices of some other metals (e.g., lead, aluminum, zinc) occurring at potentials more than 1 V more positive than the normally expected deposition potentials of alkali metals, which represents a form of surface alloying (cf. amalgams).

Many examples of UPD are found (Ag, Tl, Pb, Cu, etc., on Au, Pb^{2+}, also on Ag, Pt, Bi), so that it appears to be a rather general phenomenon, preceding bulk deposition of metals negative to the reversible potential. A good example is found in the case of deposition of lead on gold,(8) where the voltammogram indicates strong adsorption coupled with discharge with a maximum at potentials some 0.416 V more positive than the potential of bulk deposition of lead and the presence of some two-dimensional phase transitions some 0.195 V more positive.

A striking example is seen in the potential sweep voltammogram shown in Figure 3 for the deposition of lead on the (111) plane of a silver single crystal. It indicates a sharp adsorption (desorption) of a full monolayer of lead atoms (charge transfer of 315 μC cm^{-2}) at a well-defined potential 137.5 ± 0.5 mV more positive than the reversible potential of lead (indicated by bulk deposition and dissolution at the left end of the voltammogram).

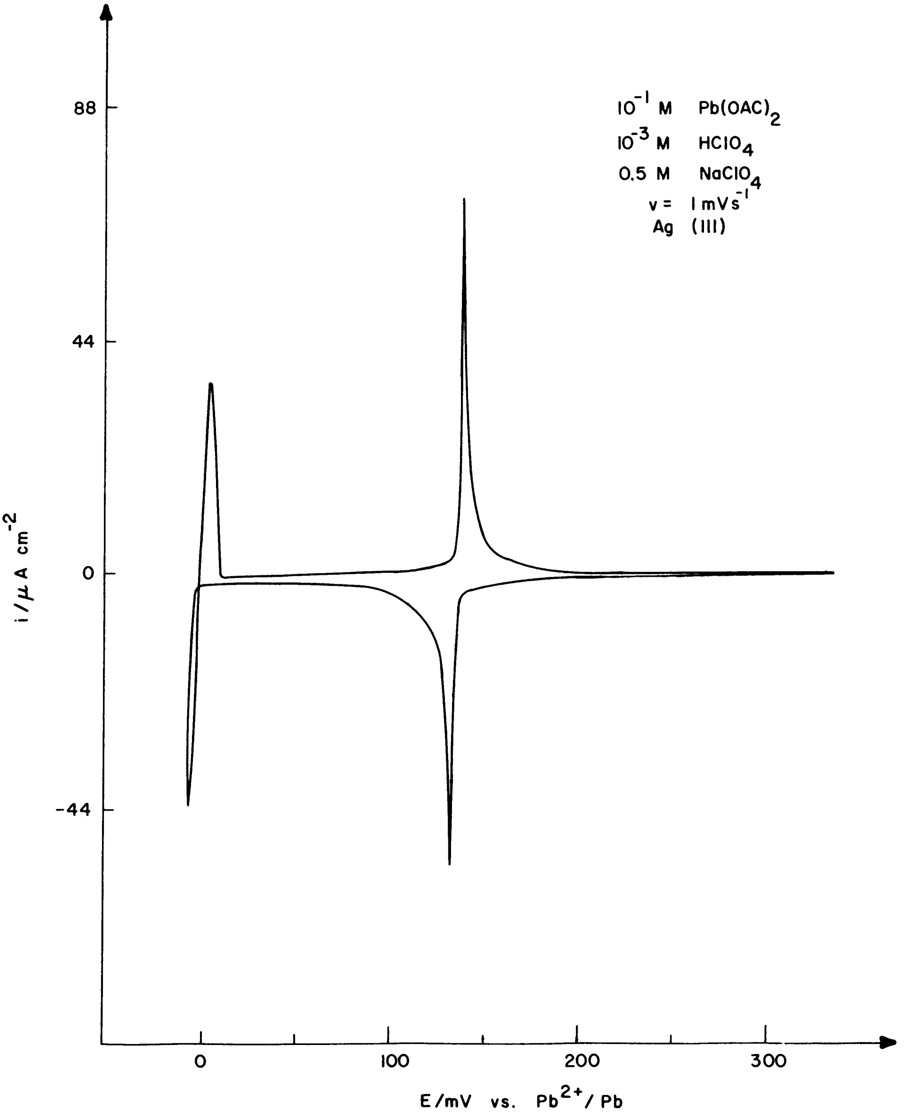

Figure 3. Experimentally recorded potential sweep voltammogram for the (111) plane of a silver single crystal in a solution noted in the figure.

The UPD is usually limited to a monolayer of metal (although there are certain indications that, in some cases, it can extend to 2 ~ 3 monolayers) and as soon as larger amounts are deposited, bulk metal phase is formed with a resulting shift of the potential to normal values. Sometimes a partial second layer is distinguished, e.g., on Pt.

The phenomenon can be explained in terms of the existence of stronger attraction forces between atoms of the depositing metal and the foreign atoms of the substrate than between like atoms of the bulk metal. If the reversible potential is considered to reflect the energy needed to take an adatom from the surface of the like metal and transfer it into the solution to form the product, the equilibrium established between adatoms and the foreign substrate at potentials 0.416 V more positive signifies an 80.3 kJ mol^{-1} larger energy of adsorption. Furthermore, if the free energy of sublimation, ΔG_s, of the metal reflects the bond energy between the metal atoms in the lattice, $W_{\text{M-M}}$, then neglecting all but the first neighbors,

$$W_{\text{M-M}} = \Delta G_s/n \tag{12}$$

where n is the coordination number, whereas the bond energy between an adatom and each of the m foreign atoms of the substrate should be

$$W_{\text{M-S}} = \frac{\Delta G_s}{n} + \frac{\Delta EzF}{m} \tag{13}$$

For lead with $n = 12$, the bond energy between atoms is obtained as 13.4 kJ mol^{-1}, while that between lead and gold atoms (with $m = 4$) has been estimated to be 33.4 kJ mol^{-1}.

This argument assumes that adatoms on the surface do not carry any charge and hence are neither complexed nor solvated. In the case of lead, this assumption seems to be fulfilled, since the so-called electrosorption valency equals 2, i.e., the ideal normal valency of the discharging plumbous ion. However, in most cases, this assumption is not quite fulfilled. The electrosorption valency differs usually from the full valency of the metal ion and, hence, some attraction from the solution side partly compensates the attractive force exerted by the substrate atoms. Thus, in such cases, the latter should actually be somewhat larger than could be calculated from Eq. (13).

2.4. Effect of Interactions of the Metal Ion in Solution on the Reversible Potential

The standard potentials of metals are usually given for the reaction of cathodic reduction from simple hydrated metal ions (see Section 1). It is of interest to analyze what changes in their values can be expected if (a) metal ions are deposited from some other solvent, and (b) metal ions form complexes with some components of the solution. Solvation itself is quite often a form of complexation, e.g., in the case of transition metal ions.

2.4.1. Reversible Potentials of Metals in Nonaqueous Solvents

Nonaqueous solvents, at the present time, play an increasingly important role in electrochemical deposition and dissolution of metals. Hence, the importance of knowing the standard potentials of metals relative to solutions of simple ions in such solvents.

There are experimental difficulties in establishing these values on the standard hydrogen scale of potentials pertaining to aqueous solutions. If the solvent is miscible with water, the difficulties can be overcome by measuring the potentials in solvent–water mixtures with respect to a reference electrode in pure aqueous solution, and extrapolating the measured values to pure solvent.

Some uncertainties still remain, however, because of ill-defined liquid junction potentials. Moreover, the method can be applied only in the case when the free energy of solvation is not much smaller than the free energy of hydration. Otherwise, the ion remains hydrated up to very low mole fractions of water in the solvent and the extrapolation becomes dubious.

Difficulties are even greater when the solvent is immiscible with water. Firstly, there appears an unknown value of the interfacial potential between the two solutions. Secondly, solvents are never ideally immiscible and, especially in the usual case of very large differences in free energies of solvation, trace amounts of water in the nonaqueous solvent may lead to erroneous results.

Hence, the usual procedure is to refer the potentials of metals to a reference electrode in the same solvent(9) and make theoretical calculations as to its relation to potentials in aqueous electrolytes. These require certain assumptions. If the free energies of solvation of the metal ion in water and the nonaqueous solvent are $\Delta G_{\mathrm{H_2O}}$ and $\Delta G_s^{\ominus}$, respectively, the difference in the standard potentials is

$$\Delta E^{\ominus} = \frac{\Delta G_s^{\ominus} - \Delta G_{\mathrm{H_2O}}^{\ominus}}{zF} \tag{14}$$

These quantities, however, are objectionable on account of the difficulty of estimating individual ionic properties.

It is usually assumed that the difference in the free energies of solvation of a cation in two solvents is equal to the difference in free energies of solvation of its salts with anions which are known to undergo little or no solvation. This is obviously only an approximation.

2.4.2. Reversible Potential of Metals in Solutions with Complexing Interactions

If a ligand L^{n-} is present in solution, with which the metal ion exhibits an affinity to form complexes, equilibria are established characterized by formal stability constants K_i(10) valid for a constant ionic strength of the solution.† Thus,

$$K_i = \frac{[\mathrm{M}(z)\mathrm{L}_i^{(z-in)+}]}{[\mathrm{M}(z)^{z+}][\mathrm{L}^{n-}]^i} \tag{15}$$

where square brackets denote concentrations of the species involved.

---

† True thermodynamic stability constants involve activities of all the species concerned. However, in that case, equations of type (15) cannot be simply combined with material balance equations to give Eq. (22).

Concentrations of different complex species are interrelated by equations of the type

$$\beta_j = \frac{[\mathrm{M}(z)\mathrm{L}_j^{(z-jn)+}]}{[\mathrm{M}(z)\mathrm{L}_{(j-1)}^{(j-1)n+}][\mathrm{L}^{n-}]} \tag{16}$$

There is a simple relationship between $K_i - s$ and $\beta_i - s$, i.e.,

$$K_i = \prod_1^i \beta_j \tag{17}$$

Hence, a number of species is present, each having a tendency to engage in the electrode reaction according to a corresponding stoichiometric equation of the type

$$[\mathrm{M}(z)\mathrm{L}_i^{(z-in)+}]_{\mathrm{soln}} + [ze]_{\mathrm{metal}} \rightleftarrows [\mathrm{M}]_{\mathrm{metal}} + [i\mathrm{L}^{n-}]_{\mathrm{soln}} \tag{18}$$

At equilibrium, the electrode potential can be calculated from any one of a series of Nernst equations

$$E_{r,i} = E_i^{\ominus} + \frac{RT}{zF} \ln \frac{[\mathrm{M}(z)\mathrm{L}_i^{(z-in)+}]}{[\mathrm{L}^{n-}]^i} \tag{19}$$

One can derive from Eqs. (19) and (15) that the standard potentials of different electrode reactions, $E_i^{\ominus}$, are related to the standard potential, $E^{\ominus}$, of the electrode reaction with the free metal ion as found in tables of electrochemical potentials(1,2) through

$$E_i^{\ominus} = E^{\ominus} - \frac{RT}{zF} \ln K_i \tag{20}$$

Usually, under a given set of conditions, a certain species is prevailing to the extent that concentrations of all the others can be neglected, and hence its concentration can be taken as equal to the total concentration of the metal in solution, $C^0_{\mathrm{M}(z)}$:

$$[\mathrm{M}(z)\mathrm{L}_i^{(z-n)+)}] = C^0_{\mathrm{M}(z)} \tag{21}$$

When this is not the case, the concentration of any one of the species can be calculated from the material balance equation combined with equations of type (15). So, for example, the concentration of the free metal ion is given by

$$\begin{aligned} C^0_{\mathrm{M}(z)} &= [\mathrm{M}^{z+}] + [\mathrm{ML}^{(z-n)+}] + [\mathrm{ML}_2^{(z-2n)+}] + [\mathrm{ML}_3^{(z-3n)+}] \\ &\quad \cdots + [\mathrm{ML}_i^{(z-in)+}] \cdots + [\mathrm{ML}_k^{(z-kn)+}] \\ &= [\mathrm{M}^{z+}] + K_1[\mathrm{M}^{z+}][\mathrm{L}^{n-}] + K_2[\mathrm{M}^{z+}][\mathrm{L}^{n-}]^2 + K_3[\mathrm{M}^{z+}][\mathrm{L}^{n-}]^3 \\ &\quad \cdots + K_i[\mathrm{M}^{z+}][\mathrm{L}^{n-}]^i + \cdots + K_k[\mathrm{M}^{2+}][\mathrm{L}^{n-}]^k \end{aligned} \tag{21a}$$

so that

$$\begin{aligned} [\mathrm{M}^{z+}] &= C^0_{\mathrm{M}(z)}\{1 + K_1[\mathrm{L}^{n-}] + K_2[\mathrm{L}^{n-}]^2 + K_3[\mathrm{L}^{n-}]^3 \\ &\quad \cdots + K_i[\mathrm{L}^{n-}]^i + \cdots + K_k[\mathrm{L}^{n-}]^k\}^{-1} \end{aligned} \tag{21b}$$

When the values of stability constants are close, so that the approximation implied in relationship (20) cannot be used, it is obvious that correct values of electrode potentials can be calculated only if Eq. (21a) is used in combination with the Nernst equation written in the usual manner with the activity of the free metal ions in solution. Since $[L^{n-}]$ represents the concentration of the free ligand in solution, a straightforward calculation of $[M^{z+}]$ can be made only if the ligand is present in a large excess over the metal salt, i.e., $C^0_{L(n)} \gg C^0_{M(z)}$. If not, the calculation must make use of the material balance equation with respect to the ligand, similar to Eq. (21).

A particularly important complexing interaction with metal ions is the formation of hydroxo complexes in aqueous solutions.

In an aqueous solution, OH^- ions are always present and their concentration is related to the pH value. Hence, the presence of hydroxo complexes is pH dependent and, depending on stability constants, there are pH regions in which free metal ions are practically nonexistent.

This type of complexing competes with complexing by other ligands present in solution. Hence, mixed ("basic") complexes can be expected, of the type $M(OH)_pL_q^{(z-p-q)+}$.

Amphoteric character of some metals leads further to acidic reaction of the hydroxo complexes in strongly alkaline solutions. This results in the formation of anions of the type $H_rMO_{(s+r)}^{(r+2s-z)-}$ (e.g., zincates, ferrites, nickelates, etc.).

Dimerization of some complexes has also been found and oligomerization should also be possible, in particular leading to precursors of precipitation of insoluble (usually neutral) complexes.

A typical example is that of the formation of species upon dissolution of zinc chloride to form an aqueous solution. Depending on pH and pCl^-, the following species are formed (in the order of increasing OH^- and Cl^- concentration):

$$\begin{tikzcd}
 & & \mathrm{Zn(OH)_2{\cdot}s} \arrow[d, leftrightarrow] & & \mathrm{Zn(OH)_3^-} \arrow[r, "+\mathrm{OH}^-", leftrightarrow] \arrow[dd, "-\mathrm{H_2O}", leftrightarrow] & \mathrm{Zn(OH)_4^{2-}} \arrow[dd, "-2\mathrm{H_2O}", leftrightarrow] \\
\mathrm{Zn^{2+}} \arrow[r, "+\mathrm{OH}^-", leftrightarrow] \arrow[ddd, "+\mathrm{Cl}^-"', leftrightarrow] & \mathrm{ZnOH^-} \arrow[r, "+\mathrm{OH}^-", leftrightarrow] \arrow[ddd, leftrightarrow] & \mathrm{Zn(OH)_2aq} \arrow[r, "+\mathrm{OH}^-", leftrightarrow] \arrow[ddd, leftrightarrow] & {} \arrow[ur, leftrightarrow] \arrow[dr, "-\mathrm{H}^+"', leftrightarrow] & & \\
 & & & & \mathrm{HZnO_2^-} \arrow[r, "+\mathrm{OH}^-\ -\mathrm{H}^+", leftrightarrow] & \mathrm{ZnO_2^{2-}} \\
 & & & & & \\
\mathrm{ZnCl^+} \arrow[d, "+\mathrm{Cl}^-"', leftrightarrow] & \mathrm{ZnOHCl} \arrow[d, leftrightarrow] & \mathrm{Zn(OH)_2Cl^-} \arrow[rr, leftrightarrow] \arrow[d, leftrightarrow] & & \mathrm{Zn(OH)_3Cl^{2-}} & \\
\mathrm{ZnCl_2} \arrow[d, "+\mathrm{Cl}^-"', leftrightarrow] & \mathrm{ZnOHCl_2^-} \arrow[d, leftrightarrow] & \mathrm{Zn(OH)_2Cl_2^{2-}} & & & \\
\mathrm{ZnCl_3^-} \arrow[d, "+\mathrm{Cl}^-"', leftrightarrow] & \mathrm{ZnOHCl_3^{2-}} & & & & \\
\mathrm{ZnCl_4^{2-}} & & & & &
\end{tikzcd} \qquad (22)$$

$$2Zn^{2+} + 3OH^- \rightleftarrows Zn_2(OH)_3^+$$

$$2Zn(OH)_3^- \rightleftarrows Zn_2(OH)_6^{2-}$$

The abundance of each species, $Zn(OH)_pCl_p^{(z-p-q)+}/C^0_{Zn(II)}$, could be calculated using Eqs. (21a) and (15), with stability constants of simple species

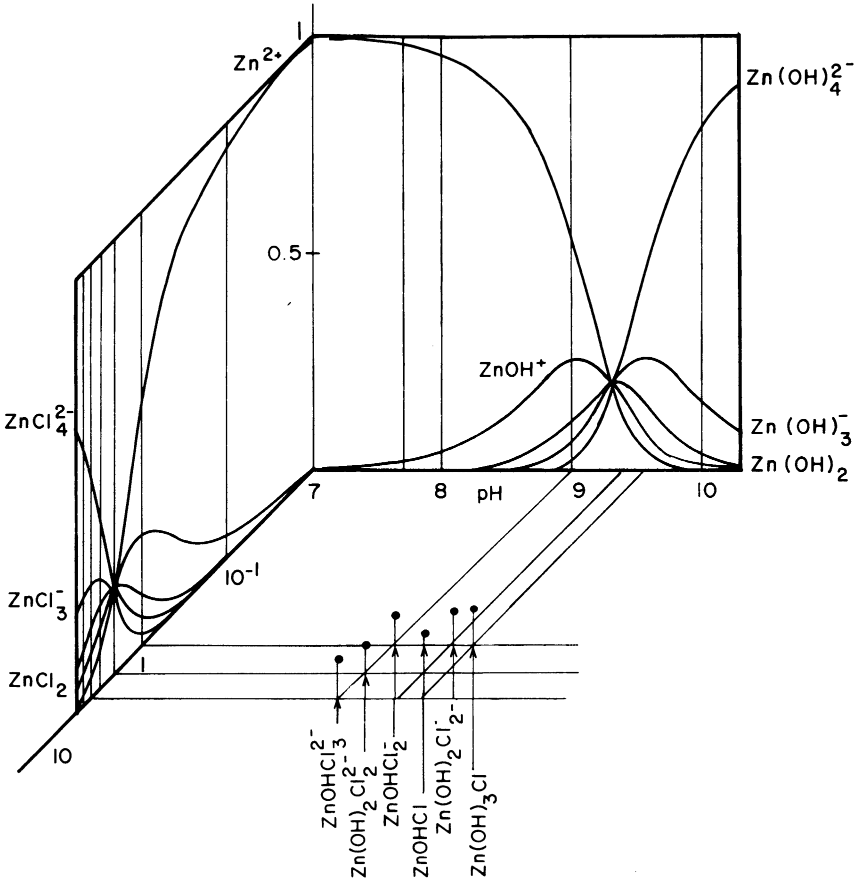

Figure 4a. Values of relative concentration of basic Zn chloride species in aqueous solution as a function of pH.

taken from the literature and those of mixed species derived on the basis of additivity of free energies upon attachment of ligands. Figure 4a shows the results. Maxima of abundance of each species are given as points in the pCl^-–pH plane, while the two sides demonstrate the distribution of simple chloro and hydroxo complexes under conditions in which the presence of mixed complexes can be neglected.† From the point of view of understanding phenomena in metal deposition and dissolution, it is an encouraging fact that, under any given conditions of pCl^- and pH, only a *few* species are present in significant amounts.

Figure 4b gives an example of the change of concentrations of different complex species with increasing concentration of ligand. When the values of

---

† The data needed to construct this figure were obtained from Professor Zlata Pavlović of the University of Banja Luka, whose help is duly acknowledged.

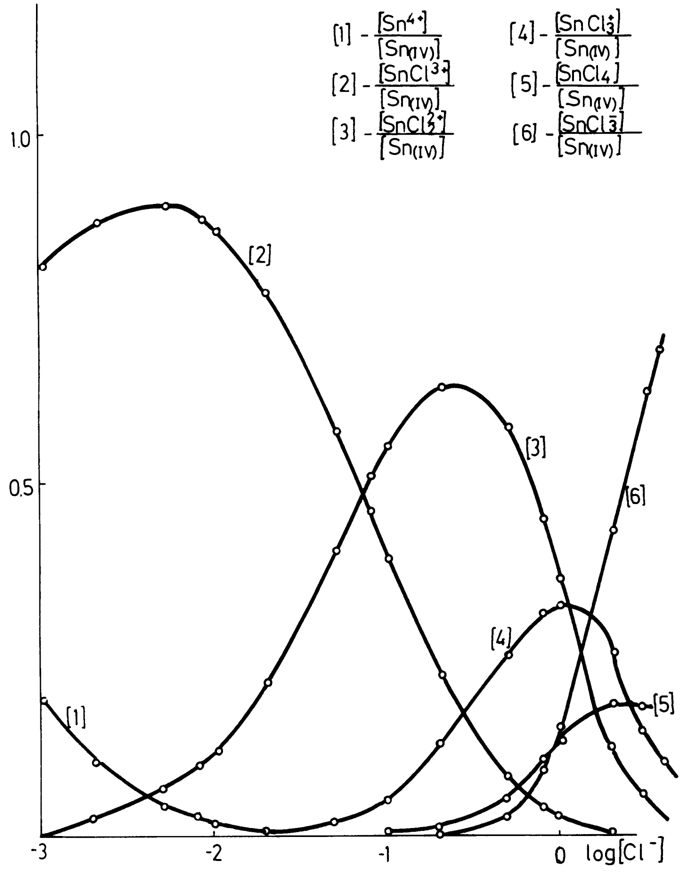

Figure 4b. Calculated values of relative concentrations of different Sn(IV) species as functions of Cl^- ion concentration.

stability constants in a sequence are close, as in this case, it is obvious that correct values of electrode potentials can be calculated only if the concentration of the relevant species is calculated using Eq. (21b).

2.5. Effect of pH on Electrode Potential

A particularly important complex interaction with metal ions is the formation of hydroxo complexes in aqueous solutions. In an aqueous solution, OH^- ions are always present and their concentration is related to the pH value. Hence, the presence of hydroxo complexes is pH dependent and, depending on stability constants, there are pH regions in which free metal ions are practically nonexistent (cf. Pourbaix diagrams).

A good representation of the effect of pH on electrode potential is due to Pourbaix. A Pourbaix diagram, such as the one shown in Figure 5, defines

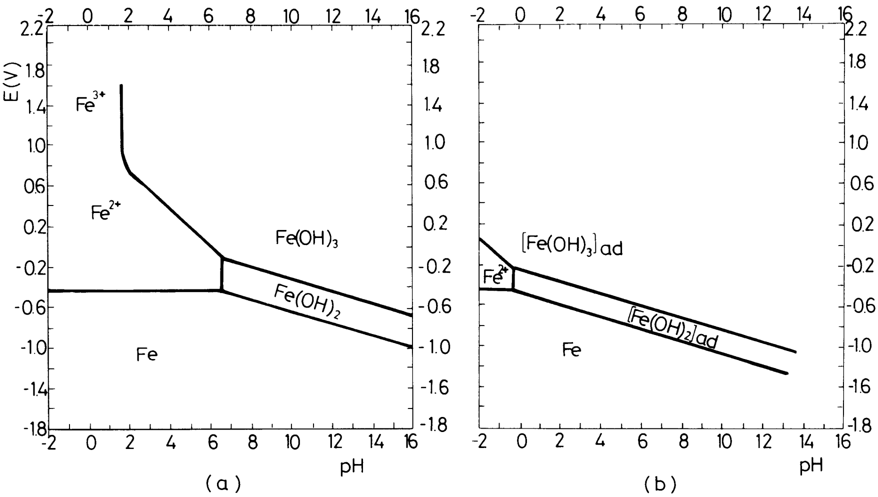

Figure 5. Potential–pH equilibrium diagrams for the system iron–water at 298 K [considering as solid substances only Fe, $Fe(OH)_2$, and $Fe(OH)_3$] for (a) the bulk-to-bulk equilibria (Pourbaix diagrams) and (b) the surface-to-bulk equilibria (Drazic–Pourbaix diagrams), for a concentration of all soluble species in solution of 1 M.

regions of stabilty of different species involving a given metal to the hydrogen- and oxygen-electrode potentials. Such diagrams(11) represent a useful tool in corrosion studies, since they define conditions under which hydrogen- or oxygen-type corrosion can take place.

One should note, however, that for electrode processes, including those determining corrosion, the relevant equilibria are those of species present at the electrode surface and, hence, their pH limits as well. Dražić has shown recently that those limits can be significantly shifted on the pH scale if energies of adsorption of those species are taken into account in the calculation of stability constants (fig. 56).(98)

3. Likely Mechanisms of Metal Ion Discharge and Their Kinetic Consequences

Let us consider first cathodic reduction processes. The general reaction path, depicted in Figure 1, shows the existence of three groups of events, each of which can control the reaction kinetics, if the respective rate constant is smaller than those of the other two.

These events are (a) transport of the reacting species from the bulk of solution to the position at which charge transfer takes place; (b) the electrode process itself, i.e., the act of reaction or a reaction sequence leading to the change of the valency state of the metal, as indicated by the stoichiometry of the electrochemical reaction; and (c) a sequence of events in the transformation of a surface species into an atom in the metal lattice. (The converse order of steps applied to anodic dissolution.)

This structure of the electrode process determines the electrical properties of the interface, i.e., the electrode impedance, the responses to electrical perturbations, and the current densities *vs.* potential relationship, which are normally measured in contemporary experimental electrochemistry.

The first group of events involves convective or molecular diffusion to the electrode, possibly with some chemical transformation of the dominantly present species into an electroactive form, and the adsorption step.

Transport by diffusion represents an integral part of any electrochemical process and has been extensively treated earlier (cf. Volume III). It has some specific effects, however, on metal deposition and the morphology of the deposit obtained which will be discussed at a later stage.

3.1. Mechanism and Kinetics of the Electrode Process

3.1.1. One-Electron Exchange Reactions

Relatively few metals form univalent ions, and these undergo relatively fast charge transfers (exchange current densities of the order of several A cm^{-2}). Hence, rates of charge transfer for such metals are difficult to determine experimentally, since other steps along the reaction path often have smaller rate constants, and are, thus, rate determining. Nevertheless, a number of methods have been developed for the study of fast electrode reactions and have been used for such systems.

They have revealed that, under appropriate conditions, where charge transfer is rate controlling (with liquid metals or with solid ones at short time intervals, before other types of control take over), in the vicinity of the reversible potential, the kinetics obey the Butler–Volmer relationship:

$$i = i_0\left\{\exp\left[\frac{(1-\beta)F}{RT}\eta\right] - \exp\left(-\frac{\beta F}{RT}\eta\right)\right\} = i_0[f_a(\eta) - f_c(\eta)] \tag{23}$$

where the anodic and cathodic transfer coefficients are determined solely by the symmetry factor, β, reflecting the symmetry of the activation energy barrier (slopes of potential energy surfaces at the region of intersection), and η is the overpotential (i.e., the difference between the actual electrode potential when $i > 0$ and the reversible potential E).

The exchange current density is given by

$$i_0 = F\bar{k}_s C_{\mathrm{M}^+}(1-\beta)C_{\mathrm{M}}^{\beta} \tag{24}$$

where $\bar{k}_s$ is the electrochemical rate constant defined by

$$\bar{k}_s = k_a \exp\left[\frac{(1-\beta)F}{RT}E\right] = k_c \exp\left(-\frac{\beta F}{RT}E\right) \tag{25}$$

The constants k_a and k_c are potential-independent heterogeneous rate constants for the anodic and cathodic directions of the reaction, respectively [all having dimensions of lt^{-1} (length per unit time) of the reaction].

Thus, thallium ion discharge on thallium amalgam was investigated, using the impedance method, by Randles,(12) and it was shown that log $\bar{k}_s$ changes linearly with the change of the reversible potential as indicated by Eq. (25). The plot rendered $\beta = 0.52$ (similar results were obtained from Faradaic rectification measurements by Barker *et al.*(13)).

Randles' analysis was based on the fact that, for transient responses to electrical perturbation, the electrical properties of electrodes at which the simple activation-controlled charge transfer is the rate-determining step (rds) can be represented by the equivalent circuit shown in Figure 6, where θ is a nonlinear and overpotential-dependent Faradaic resistance, which can be derived from Eq. (23). At very small values of η for which the exponential terms can be linearized ($\eta < 10$ mV), this is obtained as

$$\theta(\eta \rightarrow 0) = \frac{RT}{i_0 F} \tag{26}$$

The complex plane representation of the impedance of the above equivalent circuit is also shown in Figure 6. It is seen to give a semicircle which allows the determination of R, the ohmic resistance between the working

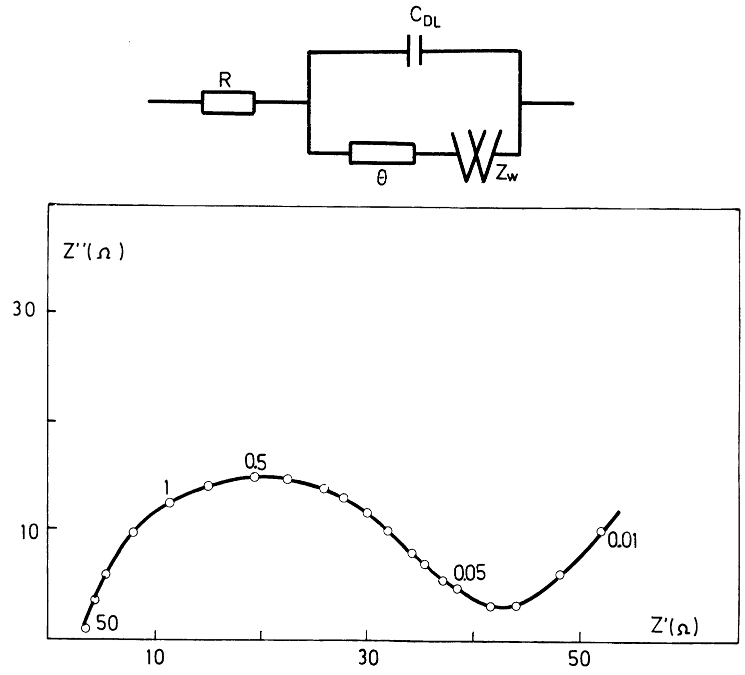

Figure 6. Randles equivalent circuit and complex plane diagram for activation control.

electrode and counterelectrode and θ from the diameter and the position on the abscissa and of C_{DL}, the double-layer capacitance from Z'', at the point of the maximum.

A detailed discussion of the capacities of this method to give accurate values of these electrode properties can be found elsewhere.(14)

Galvanostatic charging curves can also be used for that purpose, if Eq. (23) is extended to take into account the double-layer charging current, by the term $C_{\mathrm{DL}}(d\eta/dt)$, where C_{DL} is the double-layer capacitance. The solution of the differential equation was given by Roiter, Juza, and Poluyan(15) and rearranged by Despić and Bockris(16) to give

$$q = \log \frac{[\exp(-\eta_{\mathrm{A},\infty}/b') + \exp(\eta_{\mathrm{A},t}/b')][\exp(\eta_{\mathrm{A},\infty}/b') - 1]}{[\exp(\eta_{\mathrm{A},\infty}/b') - \exp(\eta_{\mathrm{A},t}/b')][\exp(-\eta_{\mathrm{A},\infty}/b') + 1]} = \frac{t}{2.3\tau_{\mathrm{DL}}} \tag{27}$$

where $b' = RT/F$, and the time constant τ_{DL},

$$\tau_{\mathrm{DL}} = \frac{\{b'[\exp(-\eta_{\mathrm{A},\infty}/b') + \exp(\eta_{\mathrm{A},\infty}/b')]^{-1}\}C_{\mathrm{DL}}}{i_0} \tag{28}$$

with $\eta_{\mathrm{A},t}$ and $\eta_{\mathrm{A},\infty}$ being the activation overpotential at time t and after the steady state is established, respectively. A linear plot of q vs. t can be obtained only if correct β values are introduced into the calculation of q. It was shown in the case of deposition of silver from silver perchlorate onto helium-treated and electrochemically activated silver that good linear plots are obtained if $\beta = 0.5$ is taken.

For the interpretation of the steady state data, the Butler–Volmer equation can be rearranged into the corrected Tafel plot,(16) i.e.,

$$y = \log \frac{i}{1 - \exp(-F\eta/RT)} = \log i_0 + \frac{(1-\beta)F\eta}{2.3\,RT} \tag{29}$$

which should be linear from the reversible potential upwards, giving log i_0 directly at $\eta \to 0$, if the process is truly activation controlled. Linear plots were, indeed, obtained in the case of silver, up to overpotentials of about 50 mV, in both the cathodic and the anodic direction, which were symmetrical with respect to the reversible potential, giving β values close to 0.5. The i_0 values were found to be 0.3–0.6 A cm^{-2} for 0.35 M silver perchlorate solution, decreasing in the expected manner with the decrease in silver ion concentration.

3.1.2. Charge Transfer Kinetics at High Relative Values of Overpotential

Since high values of i_0 indicate low activation energy barriers relative to the energy changes imposed by changing overpotentials, increase of over-

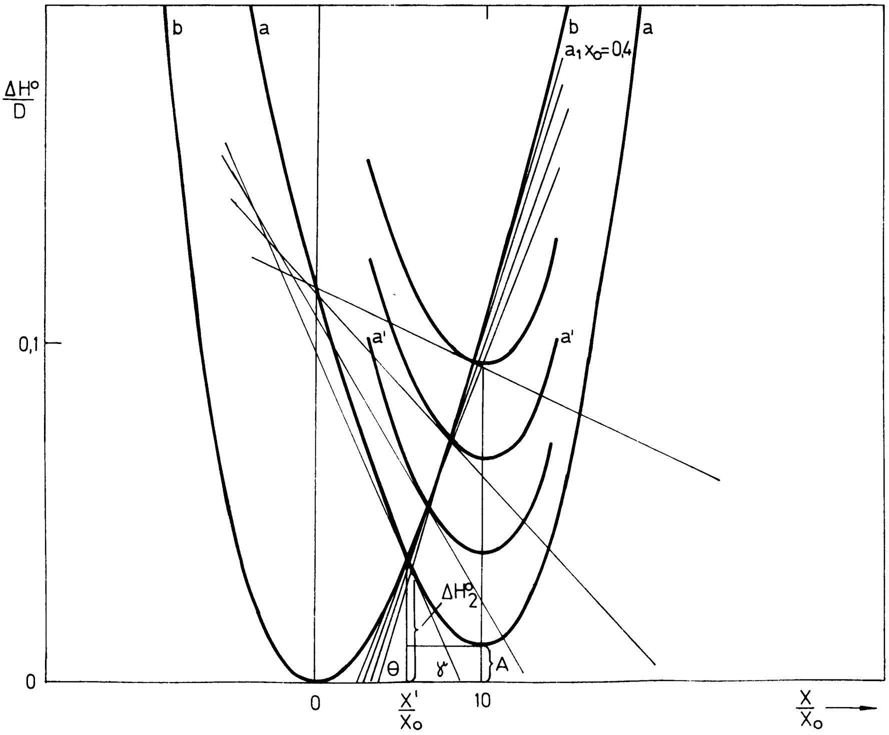

Figure 7. The potential-energy–distance relations (Morse functions with $ax_0 = 0.4$) at different values of electrode potential.

potential in the relatively low η-domain leads to a region of changing β as shown in Figure 7. There is a tendency to reach the "barrierless discharge" condition, where the current density stops being potential dependent, since in the Butler–Volmer equation $\beta \rightarrow 0$. Indeed, the experimentally observed dependence of current density on potential, as shown in Figure 8, is not exponential beyond $\eta = 0.050$ V, but shows a tendency toward an *activation-controlled limiting current.*(16)

3.1.3. Discharge of Simple Divalent Ions

The majority of metals of practical interest form divalent ions in solution. The kinetics of their deposition and dissolution have been extensively studied for the purpose of elucidating reaction mechanisms ever since the development of transient methods enabled measurements under conditions of pure activation control to be achieved. However, most divalent cations show a tendency toward complexing even with simple anions in solution. Moreover, strong interactions with OH^- ions lead to some hydroxo complex formation even at low pH values, which complicates the kinetic behavior.

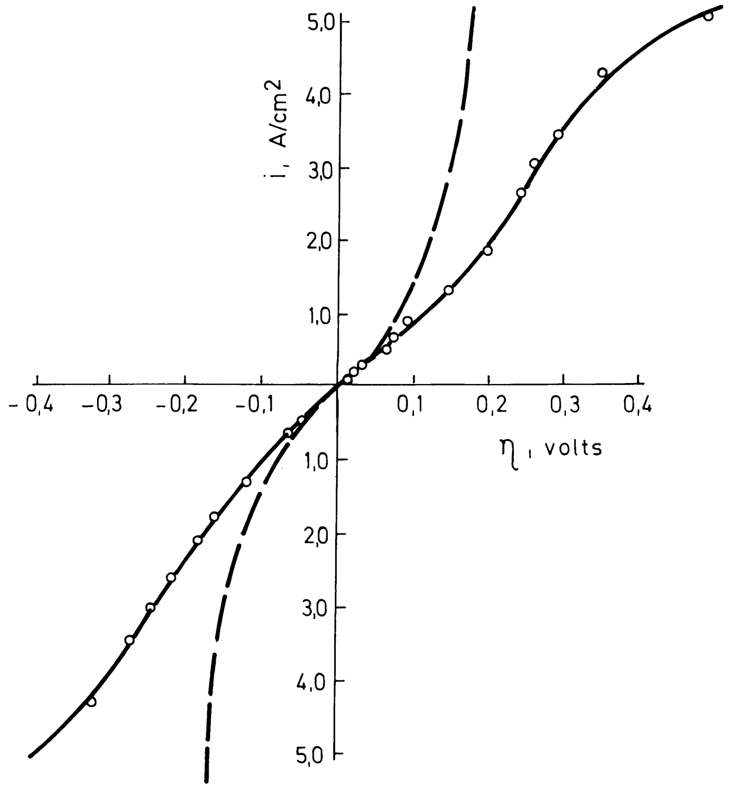

Figure 8. Typical i–η relation in the case of an activated silver electrode in 0.364 N $AgClO_4$ + 1 N $HClO_4$ solution. Dashed curve: Butler–Volmer curve with β = const.

The deposition of copper from acid copper salt solutions, and the converse dissolutions, have been extensively studied since the above interactions seem to be absent; then one can consider that only simple hydrated ions are involved in the electrode process. The work of a number of authors (Philbert, 1943; Randles and Somerton, 1952; Hilson, 1954; Kambara and Ishii, 1961; Mattson and Bockris, 1959; Bockris and Enyo, 1962; Bockris and Kita, 1962; Losev, 1972; and others) has contributed to the present understanding of the phenomena involved in that system.

The first question which arises in such a system concerns the distinction between two possible cases of charge transfer: that of a direct single-step two-electron exchange or a one-electron exchange in two steps, involving a species with an intermediate oxidation state between them. In the case of copper, the intermediate cuprous ion is known to have a relatively good stability in solution. Taking into account the standard potential of the cuprous/cupric redox couple of +0.17 V, one can calculate that, at the reversible potential of copper in cupric salt solutions, the equilibrium concentration of cuprous ions amounts to $[1.47 \times 10^{-3}(\sqrt{C_{\mathrm{Cu}^{2+}}})^{1/2}]$ of the concentration of cupric salt.

It was shown on theoretical grounds by Conway and Bockris$^{(17)}$ that the two-step transition should have a lower overall energy barrier than the single-step process with a two-electron exchange in one transition state. Hence, it could be expected that the prevailing mode of reaction will involve two single-electron transitions.

In such a case, a complex relationship is expected between the current density and the overpotential, as shown by Vetter in 1952,$^{(18)}$ i.e.,

$$i = 2i_{0,1}i_{0,2}\frac{\exp\left[(2-\beta_1-\beta_2)F\eta/RT\right]-\exp\left[-(\beta_1+\beta_2)F\eta/RT\right]}{i_{0,1}\exp\left[(1-\beta_1)F\eta/RT\right]+i_{0,2}\exp\left(-\beta_2 F\eta/RT\right)} \tag{30}$$

However, if the rate constant of one step in a reaction sequence is much smaller than those of all the others, so that that step controls the overall kinetics [the concept of the rate-determining step (rds)], while other steps are in the state of virtual equilibrium (i.e., the rates in each of them are practically equal in both directions), relation (30) simplifies into the usual Butler–Volmer type of equation

$$i = i_0 \exp\left(\frac{\alpha_a F}{RT}\eta\right) - \exp\left(-\frac{\alpha_c F}{RT}\eta\right) \tag{31}$$

with the transfer coefficients α_a and α_c reflecting the particular reaction path prevailing in the system. At higher overpotentials ($\eta \gg RT/F$) the equation becomes a simple Tafel relation, i.e., a linear η vs. $\log i$ plot is obtained.

It can also be shown that, when the concept of the rds is valid, if a single intermediate species is involved and adsorption effects are absent, the transfer coefficients are given by

$$\alpha_a = (1-\beta)z_d + z'/\mu_d \tag{32}$$

and

$$\alpha_c = -\beta z_d + z''/\mu_d \tag{33}$$

where z', z_d, and z'' are the numbers of electrons exchanged before, in, and after the rds, respectively, and μ_d is the stoichiometric number (i.e., the number of acts of the rds per act of the overall reaction).

Another important group of kinetic parameters which can be used as diagnostic criteria for determining the prevailing reaction mechanisms are the reaction orders. They are defined as

$$\begin{aligned} n_{a,\mathrm{ox}} &= \left(\frac{\log i_a}{\log C_{\mathrm{ox}}}\right)_E, & n_{a,\mathrm{red}} &= \left(\frac{\log i_a}{\log C_{\mathrm{red}}}\right)_E \\ n_{c,\mathrm{ox}} &= \left(\frac{\log i_c}{\log C_{\mathrm{ox}}}\right)_E, & n_{c,\mathrm{red}} &= \left(\frac{\log i_c}{\log C_{\mathrm{red}}}\right)_E \end{aligned} \tag{34}$$

where i_a and i_c are the anodic and cathodic current densities at a given constant electrode potential E, and C_{ox} and C_{red} are concentrations of the oxidized species (cupric ions) and reduced species (metallic copper, e.g., in amalgam), respectively.

For the case of a two-step reaction, three possible reaction paths can be envisaged, all involving the cuprous ion as intermediate:

$$\text{(a)}\quad Cu^{2+} + e \rightarrow Cu^{+} \qquad \text{(b)}\quad Cu^{+} + e \rightarrow Cu \tag{35}$$

$$\text{(a)}\quad Cu^{2+} + Cu \rightarrow 2Cu^{+} \qquad \text{(b)}\quad Cu^{+} + e \rightarrow Cu \tag{36}$$

$$\text{(a)}\quad Cu^{2+} + e \rightarrow Cu^{+} \qquad \text{(b)}\quad 2Cu^{+} \rightarrow Cu + Cu^{2+} \tag{37}$$

The step (37b) is a chemical step known to be operative in the bulk of solution as the so-called disproportionation reaction leading to the formation of powdery copper. The step (36a) is the reverse of (37b), constituting the chemical attack of cupric ions on copper when the solution is not equilibrated with respect to cuprous ions.

Table 1 lists the expected kinetic parameters for different possible reaction mechanisms of copper deposition and dissolution, including the single-step two-electron exchange, as well as the different cases of the single-electron exchange with cuprous ion as the intermediate.

Experimental investigations of the steady state dissolution and deposition have given Tafel plots, such as those shown in Figure 9. These indicate (a) that the concept of a single rds is valid and (b) that of all possible reaction paths, the transfer coefficients α_a and α_c, as calculated from the Tafel slopes, are consistent only with the reaction path (35). The same applies to the reaction orders that are obtained. Hence, it is the cupric–cuprous transition which has the lower rate of the two steps in the fastest of the possible reaction paths. This is to be expected, considering that cupric ion is the most heavily hydrated and protected from other interactions of all the species involved. The exchange current density for this step has been evaluated by this and a number of other methods. Table 2 lists the values obtained. They are seen to be several orders of magnitude smaller than those involving electron exchange with univalent ions.

The very fact that linear Tafel plots are obtained for the two-step mechanism of the electrode reaction of copper up to 0.28 V of overpotential indicates that the exchange current density of the faster step must be at least two orders of magnitude higher than that of the rds, and, considering the values of the latter (cf. Table 2), falls into the range obtained for the reaction rates of other univalent ions.

There are methods, however, by which this can be directly determined. Thus, under certain conditions, measurements of the Faradaic impedance could give values of i_0's for the faster step as well as the concentration of the intermediate. Such measurements, however, cannot indicate which of the two steps is the slower one.

Table 1
Kinetic Parameters for Possible Mechanisms of the Two-Electron Exchange Reaction[a]

Mechanism	RDS	$n_{a,ox}$	$N_{a,R}$	$N_{c,ox}$	$n_{c,R}$	α_a	α_c	μ_d
$Cu^{2+} + 2e \rightarrow Cu$	I	0	1	1	0	$2(1-\beta) \approx 1$	$-2\beta \approx -1$	1
(35)	I	0	1	1	0	$(2-\beta) \approx 1.5$	$-\beta \approx -0.5$	1
(35)	II	0	1	1	0	$(1-\beta) \approx 0.5$	$-(1+\beta) \approx -1.5$	1
(36)	I	0	1	1	1	1	0	1
(36)	II	0	1	1	1	$(1-\beta) \approx 0.5$	$-\beta \approx -0.5$	2
(37)	I	1	1	1	0	$(1-\beta) \approx 0.5$	$-\beta \approx -0.5$	2
(37)	II	1	1	1	0	0	-1	1

[a] $n_{a,ox}$ and $n_{a,R}$ are the reaction orders for the anodic reaction with respect to the oxidized form (divalent ion) and the reduced form (metal atoms), respectively; $n_{c,ox}$ and $n_{c,R}$ are the same quantities for the cathodic reaction.

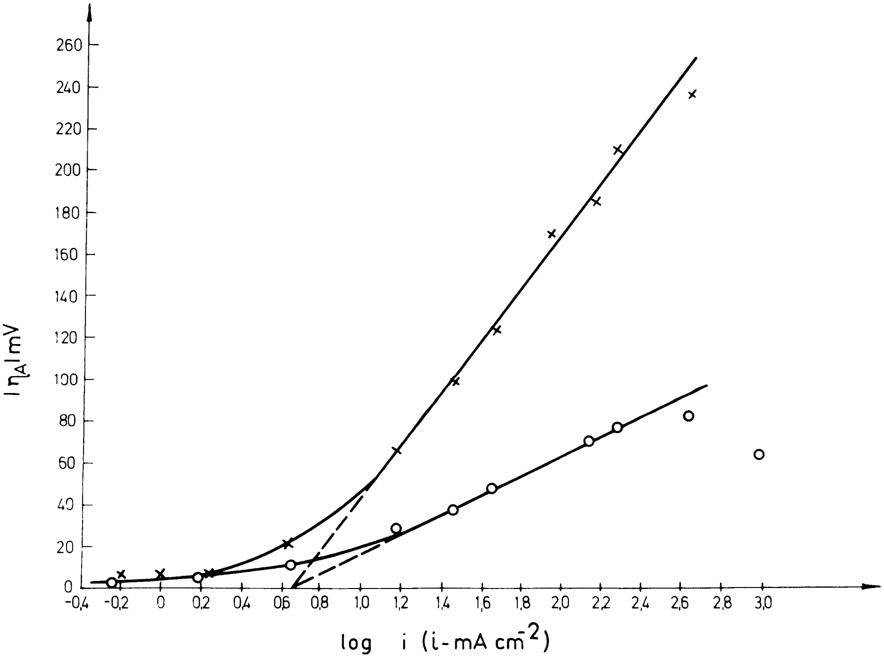

Figure 9. Tafel lines for electrode produced through electrodeposition ($C_{Cu^{2+}}$ = 0.15 equiv liter^{-1}); —O— anodic curve; —×— cathodic curve.

3.1.4. The Role of Hydroxo Complexes in Electrode Reactions with Divalent Ions

Results of kinetic investigations of metals forming divalent ions other than copper show a different behavior, especially at higher pH values, i.e., in slightly acidic or neutral solutions.

Table 2
Kinetic Parameters for the Reaction $Cu^{2+} + 2e \leftrightarrows Cu$

Type of Cu surface	Electrolyte	Temp. (°K)	Transfer coeff.		Exchange c.d. (mA cm^{-2})		Conc. of adions at surface (M cm^{-2})	Method
			α_a	α_c	From anodic	From cathodic		
Freshly electro-deposited copper	0.5 *M* $CuSO_4$ +0.5 *M* H_2SO_4	303	1.47	0.62	9.6	27.7	$5 \cdot 10^{-9}$	Galvanostatic; extrapol. from steady-state
Same	0.005 *M* $CuSO_4$ +0.5 *M* H_2SO_4	—	1.36	0.51	4.0	4.6	$5.8 \cdot 10^{-9}$	Same
Helium quenched after melting	0.46 *M* $CuSO_4$ +0.46 *M* H_2SO_4	303	1.51	0.42	5.2	8.0	—	Same
Helium quenched with oxide film	0.005 *M* $CuSO_4$	—	—	—	—	40.0	$0.17 \cdot 10^{-9}$	Same
Helium quenched, expos. to solution following anod. dissol.	0.005 *M* $CuSO_4$ +0.5 *M* H_2SO_4	—	1.25	0.48	16.0	30.0	$88 \cdot 10^{-2}$	Same
Polished copper	0.05 – 0.5 *M* $CuSO_4$ +0.5 *M* H_2SO_4	298	1.18	0.42	7.0	7.0	—	Galvanostatic double-pulse
Copper electroplated on platinum	0.01 – 0.02 *M* $CuSO_4$ +0.5 *M* H_2SO_4	298	—	0.32	—	3.38	—	Galvanodynamic
Same	0.125 *M* $CuCl_2$ +0.74 *M* HCl	—	—	0.51	—	2.4	—	Galvanostatic; extrapol. from steady-state
Same	0.1 *M* $Cu(ClO_4)_2$ +1 *M* $HClO_4$	303	1.31	0.51	6.7	1.1	—	Same
Same	0.1 *M* $Cu(Ac)_2$ +0.59 *M* HAc +0.5 *M* Na AC	303	1.26	0.5	0.8	2.4	—	Same
Same	0.1 *M* $Cu(SO_3NH_2)_2$ +1 *M* HSO_3NH_2	303	1.42	0.6	2.2	3.3	—	Same

Thus, for *cadmium* in neutral cadmium sulfate solutions, linear but symmetrical Tafel plots were obtained by Lorenz, with decadic Tafel slopes of 0.06 V, corresponding to the factor $2.3RT/F$, i.e., to transfer coefficients $\alpha_a = \alpha_c = 1$.

A similar behavior has been found much earlier for the reaction of *zinc* in zinc sulfate solution by Roiter *et al.*(15)

Iron, however, shows a more complex behavior. Good linear Tafel plots have been obtained by galvanostatic investigations(20) extending, in less acidic solutions (pH = 4.0), over two decades of current density, as shown in Figure 10. Decadic Tafel slopes of about 0.041 and 0.06 V for the anodic and cathodic direction, respectively, corresponding to the factors $2.3(2RT/3F)$ and $2.3(RT/F)$, or to transfer coefficients $\alpha_a = 1.5$ and $\alpha_c = 1$, were found. However, in some experiments, Tafel slopes corresponded to $2.3(2RT/F)$ for the cathodic direction, i.e., $\alpha_c = 0.5$, while in many anodic experiments, slopes of $2.3(RT/2F)$, i.e., $\alpha_a = 2$, were obtained.(21)

The first finding is contrary to the requirement that, in case one and the same mechanism governs both the cathodic and anodic processes, the sum $\alpha_c + \alpha_a = n$.

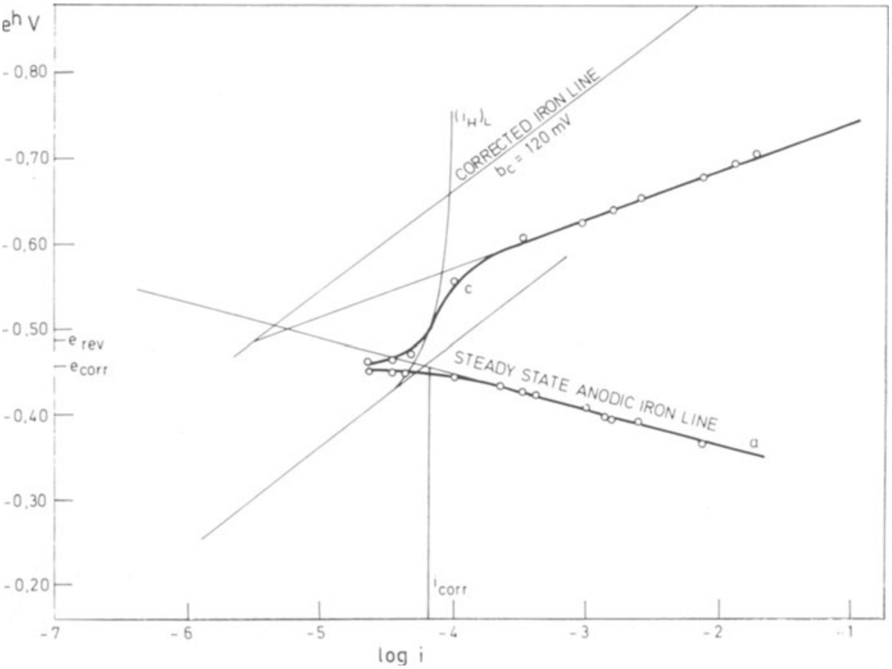

Figure 10. 0.5 *M* $FeSO_4$ + 0.5 *M* Na_2SO_4 (pH = 4.0), $b_{c,\text{expt}} = 60$ mV, $b_{c,\text{corrected}} = 120$ mV; $b_{\text{anodic}} = 42$ mV, $i_0 = 4.5 \times 10^{-6}$ A cm^{-2}; $e^h_{\text{corr}} = 7.1 \times 10^{-5}$ A cm^{-2}.

Moreover, the i_0 value was found to be pH dependent and a fairly good linear dependence gave $(\log i_0/\log C_{\mathrm{OH}^-})_{C_{\mathrm{Fe}^{2+}}} = 1$, suggesting that OH^- ions play a role in the reaction mechanism.

This fact is of particular importance for considering the problem of reaction mechanism. In slightly acidic or neutral solutions, complexing of heavy metal ions, like cadmium, zinc, and iron, with OH^- ions is quite considerable. Hence, species of the type $\mathrm{M(OH)}^+$ and $\mathrm{M(OH)_2}$ are present in sufficient concentrations to compete in charge transfer with the free metal ion. Their discharge should meet with a lower activation energy barrier, since they should be less heavily hydrated (cf. Ref. 17) because of smaller charge or no charge at all.

The symmetrical Tafel lines in the case of deposition of cadmium and zinc, giving $\alpha_a = \alpha_c = 1$, have been considered in the literature as an indication of a single-step, two-electron exchange mechanism. However, it should be borne in mind that Eqs. (27) and (28) offer two possibilities for obtaining such values of the transfer coefficients: (a) for $\beta = 0.5$ and $z_d = 2$, $z' = 0$ pertaining to the single-step mechanism and (b) for $z_d = 0$, $z' = 1$, and $z'' = 1$, with $\mu_d = 1$, which implies (at least) a three-step mechanism with two one-electron exchange steps and a chemical step in between rate determining. Two mechanisms could be envisaged involving the hydroxo complexes MOH^+ and $\mathrm{M(OH)_2}$, i.e., for metals exhibiting small stability of hydroxo complexes and/or at lower pH:

$$\begin{aligned} &\text{I} \quad \mathrm{M}^{2+} + \mathrm{OH}^- \rightleftarrows \mathrm{MOH}^+ \\ &\text{II} \quad \mathrm{MOH}^+ + \mathrm{e} \rightleftarrows \mathrm{MOH} \\ &\text{III} \quad \mathrm{MOH} + \mathrm{e} \rightleftarrows \mathrm{M} + \mathrm{OH}^- \end{aligned} \tag{38}$$

and, for metals with high affinity for OH^- ions and/or at higher pH:

$$\begin{aligned} &\text{I} \quad \mathrm{M}^{2+} + 2\mathrm{OH}^- \rightleftarrows \mathrm{M(OH)_2} \\ &\text{II} \quad \mathrm{M(OH)_2} + \mathrm{e} \rightleftarrows \mathrm{M(OH)_2}^- \\ &\text{III} \quad \mathrm{M(OH)_2}^- \rightleftarrows \mathrm{MOH} + \mathrm{OH}^- \\ &\text{IV} \quad \mathrm{MOH} + \mathrm{e} \rightleftarrows \mathrm{M} + \mathrm{OH}^- \end{aligned} \tag{39}$$

It is seen that mechanism (39) consists of four steps, including the above-mentioned sequence of three steps, with the possibility of the middle one being rate determining, and thus explains more adequately the observed behavior of cadmium or zinc than the single-step two-electron exchange mechanism.

This conclusion is supported by the fact that, in reduction of zinc-containing species in alkaline solutions, it has been found that electron transfer occurs predominantly with the $\mathrm{Zn(OH)_2}$ molecule (cf. below).

As for the electrochemical reaction of iron, a variety of results indicates that a number of mechanisms can be operative simultaneously in the system, and involve similar overall energy barriers sensitive to the conditions of the experiment. It is possible that the predominance of one reaction path is easily changed to the prevalence of another by changing the conditions. Indeed, a large number of possible reaction mechanisms has been suggested in the literature.(22)

In view of the above-mentioned discord with theory, cases for $\alpha_a = 1.5$ and $\alpha_c = 1$, which have been found experimentally, deserve special consideration. The disagreement could be resolved by assuming a reaction path similar to that applying to cadmium or zinc, but involving another phenomenon—that of *local change of pH at the electrode surface.*

Of the three metals considered, iron exhibits the lowest hydrogen overvoltage, especially if it contains some carbon and other impurities as with mild steel. Hence, as Figure 10 shows, the open-circuit potential of iron in ferrous sulfate or similar solutions is not the true equilibrium potential, but rather a hydrogen corrosion potential. Also, the Tafel line for iron deposition is reached only after the limiting current for hydrogen ion discharge has been surpassed. This indicates that conditions of considerably higher pH prevail at the electrode surface than in the bulk of solution and, since the iron deposition reaction is pH sensitive, the Tafel plot pertaining to the bulk pH value can be obtained only after experimental results are corrected for the local pH change. This is done in the following manner.

The discharge of H_3O^+ ions is assumed to occur under diffusion control. In such a case, for any potential of the iron electrode E_{Fe}, the concentration overpotential for hydrogen evolution is

$$\eta_c = E_{Fe} - E_{H\eta_c=0} = \frac{RT}{\alpha_H F}\ln\frac{(a_{H_3O^+})_s}{(a_{H_3O^+})_b} = \frac{RT}{\alpha_H F}\ln\frac{(a_{OH^-})_b}{(a_{OH^-})_s} \tag{40}$$

where the subscripts s and b denote the activities at the surface and in the bulk of solution, respectively. $E_{H,\eta_c=0}$ is the electrode potential at which hydrogen would evolve with the given hydrogen ion discharge current density, if there was no concentration polarization developed.

Knowing the reaction order with respect to OH^- to be 1, the kinetic equation for the cathodic reduction of the Fe(II) species can be written as

$$\overleftarrow{i}_{Fe} = i_{0,Fe}\frac{(a_{OH^-})_s}{(a_{OH^-})_b}\exp\left[-\frac{\alpha_{c,Fe}F}{RT}(E_{Fe} - E_{r,Fe})\right] \tag{41}$$

Taking the logarithmic form and differentiating, with i_0, $(a_{OH^-})_b$ and $E_{Fe,rev}$ as constant, one obtains

$$\frac{\partial(\ln \overleftarrow{i}_{Fe})}{\partial E_{Fe}} = \frac{-\alpha_{c,Fe}F}{RT}\frac{\partial \ln (a_{OH^-})_s}{\partial E_{Fe}} \tag{42}$$

Making use of Eq. (40), Eq. (42) can be transformed into

$$\frac{\partial(\ln \overleftarrow{i}_{\mathrm{Fe}})}{\partial E_{\mathrm{Fe}}} = \frac{-\alpha_{\mathrm{c,Fe}}F}{RT} - \frac{\partial}{\partial E_{\mathrm{Fe}}}(E_{\mathrm{Fe}} - E_{\mathrm{H},\eta_c=0})\frac{\alpha_{\mathrm{H}}F}{RT} \tag{43}$$

The left-hand side of Eq. (43) is the reciprocal of the experimentally observed Tafel slope, i.e., it is equal to $-F/RT$. Hence, the true value of the transfer coefficient for the deposition of iron is

$$\alpha_{\mathrm{c,Fe}} = 1 - \frac{\partial}{\partial E_{\mathrm{Fe}}}(E_{\mathrm{Fe}} - E_{\mathrm{H},\eta_c=0}) = 1 - \alpha_{\mathrm{H}} - \alpha_{\mathrm{H}}\frac{\partial E_{\mathrm{H},\eta_c=0}}{\partial E_{\mathrm{Fe}}} \tag{44}$$

The concentration overpotential is related to the difference between the actual hydrogen evolution current, i_{H}, and the diffusion-limiting current for the same process, i_{L}, as

$$\eta_c = (E_{\mathrm{Fe}} - E_{\mathrm{H},\eta_c=0}) = \frac{RT}{\alpha_{\mathrm{H}}F}\ln\frac{i_{\mathrm{L}} - i_{\mathrm{H}}}{i_{\mathrm{L}}} \tag{45}$$

Hence,

$$\frac{\partial E_{\mathrm{H},\eta_c=0}}{\partial E_{\mathrm{Fe}}} = \frac{1}{1 + i_{\mathrm{H}}/(i_{\mathrm{L}} - i_{\mathrm{H}})} \tag{46}$$

So that the Eq. (44) can be written as

$$\alpha_{\mathrm{c,Fe}} = 1 - \alpha_{\mathrm{H}} + \frac{\alpha_{\mathrm{H}}}{1 + i_{\mathrm{H}}/(i_{\mathrm{L}} - i_{\mathrm{H}})} \tag{47}$$

As $i_{\mathrm{H}} \rightarrow i_{\mathrm{L}}$, the last term in Eq. (47) vanishes and $\alpha_{\mathrm{c,Fe}} = 1 - \alpha_{\mathrm{H}}$. From the measurements of hydrogen evolution kinetics in the same system, the transfer coefficient α_{H} was found to be 0.51. Hence, $\alpha_{\mathrm{c.Fe}} = 0.49$ and the cathodic Tafel line would have a slope of $2RT/F$ (shown in Figure 10 in the form of the corrected Tafel plot), if the pH in the vicinity of the electrode were constant with changing current density. Considering this result, as well as the reaction order of 1 for $\mathrm{OH^-}$ ions, mechanism (38) is indicated for the deposition and dissolution of iron, with $\mathrm{FeOH^+}$ as the electroactive species and its discharge as the rds.

For the experimental situations in which Naperian Tafel slopes of $RT/2F$ are found, i.e., $\alpha_a = \alpha_c = 2$, a "catalytic" mechanism was suggested,(23) consisting of the following sequence of steps:

I $\mathrm{Fe^{2+} + H_2O \rightleftarrows FeOH^+ + H^+}$

II $\mathrm{FeOH^+ + Fe(OH)_{ads} + 2e \rightleftarrows Fe(FeOH) + OH^-}$

III $\mathrm{Fe(FeOH) \rightleftarrows Fe(OH)_{ads} + Fe}$

IV $\mathrm{FeOH_{ads} + H^+ + e \rightleftarrows Fe + H_2O}$

This involves simultaneous transfer of two electrons but on a complex species which need not be too heavily hydrated.

A similar effect of coevolution of hydrogen has been found in the deposition of nickel.$^{(120,121)}$

These findings suggest that whenever a kinetic investigation of metals whose potentials are more negative than the hydrogen electrode potential at the given pH is undertaken, the local change of pH has to be taken into account. Since this is sensitive to the hydrodynamic situation at the electrode, investigations should be made under well-controlled hydrodynamics (e.g., using the rotating disk technique). An instructive illustration of the changes of the composition of solution which can take place at the electrode surface compared to the bulk of solution is given by Harris.$^{(122)}$

3.1.5. Electrochemical Reaction of Zinc in Alkaline Solutions

Zinc is the only one of the heavy metals which forms species soluble in concentrated alkaline solutions. Presumably the dominant form is the species $[Zn(OH)_4]^{-2}\cdot 4H_2O$ or ZnO_2^-.

Early work of Gerischer,$^{(24)}$ using the impedance method, gave a reaction order with respect to OH^- of 2 for the cathodic reduction on to zinc amalgam, implying that the electroactive species is the neutral $Zn(OH)_2$ molecule. Further investigations, using the galvanostatic method,$^{(25)}$ gave linear Tafel plots extending over several orders of magnitude of current density, which were symmetrical around the equilibrium potential with slopes RT/F, i.e., $\alpha_a = \alpha_c = 1$.

As already discussed, this implies the dominance of the reaction mechanism (39), with the chemical transformation as the rds. However, going to higher cathodic overpotentials, the slopes changed to $2RT/F$, i.e., $\alpha_c = 0.5$, suggesting a change in the rds. It appears that, with increasing concentration of $Zn(OH)_2^-$, the rate of chemical decomposition becomes so high that the discharge of ZnOH starts limiting the rate. The shift of this transition to higher current densities with increasing concentration of zincate gives further support to such an interpretation.

Under certain conditions,$^{(26)}$ a complex behavior is indicated by both the current–potential relationship and the electrode impedance, represented in the complex plane as shown in Figure 11. This was interpreted by assuming a catalytic mechanism of deposition, similar to that suggested for iron.

3.2. *Pseudocapacitance Effects and the Concentration of Intermediate Species*

Reaction paths of the type found for the discharge of divalent species, involving univalent intermediates, must exhibit pseudocapacitance effects in transient or ac phenomena. This is due to the fact that a change in potential

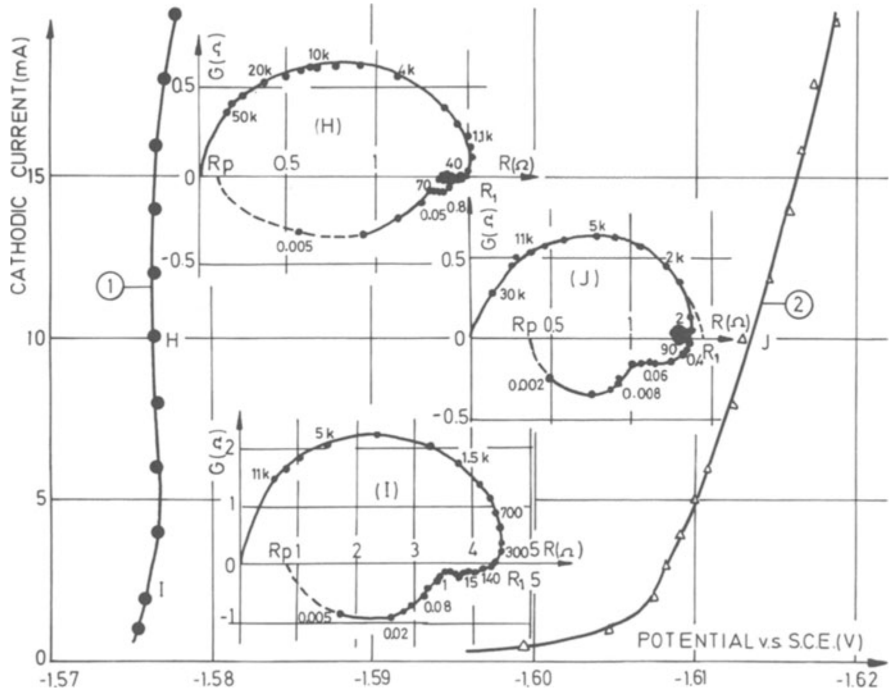

Figure 11. Influence of the concentration x of ZnO in 7 M KOH on the steady state current-potential curves relative to the electrocrystallization of zinc obtained with a rotating disk electrode (area, 0.28 cm^2) at 26 ± 0.5°C. Curve 1, x = 1.24 M, RPM = 3000; curve 2, x = 0.25 M, RPM = 5000. H (10 mA; −1.576 V vs. SCE); I (2 mA − 1.5755 V vs. SCE); J (10 mA − 1.613 V vs. SCE). Impedance diagrams (H), (I), and (J) obtained under the same conditions as for points I, J, and H (frequency in hertz).

must be accompanied by a corresponding change in the concentration of the intermediate, if equilibrium is to be maintained in steps other than the rds, and before a full steady state rate could be achieved. This can be done only by exchanging charge with the electrode.

Conversely, the appearance of pseudocapacitance can be taken as another proof of the correctness of the assumed mechanism and a way of finding out the concentration of the intermediate.

Two cases may arise. If the intermediate species is a surface species, i.e., strongly adsorbed and at a negligible concentration in solution, the change is limited practically to the surface concentration only, which can vary from surface coverage zero to unity. Hence, the maximum amount of the intermediate that can be formed or removed will be of the order of 10^{-9} mol cm^{-2}. However, when the intermediate has a finite stability in solution, as is the case with copper, the steady state can in theory be reached only after the concentration has been appropriately adjusted throughout the bulk of the solution. Hence, the amount of charge for charging the pseudocapacitance should be dependent on the amount of solution used in the experiment. In practice, the change in the concentration of the intermediate is limited to a "reaction layer," whose thickness depends on the rate of diffusion of the intermediate to and from the electrode surface. The slower the diffusion, the thinner should be the reaction layer, and the smaller the pseudocapacitance. The problem can be treated quantitatively for the first case, as well as for the second, assuming a fixed reaction layer, in the following way:

Suppose that, at any given potential, E, equilibrium between the univalent intermediate M^+ and one of the states, initial-M or final-M^{2+}, is established instantaneously by transfer of charge. The relationship between the equilibrium concentration of M^+ at that potential, C_{M^+}, and that at the reversible potential, $C_{M^+,0}$, is given by

$$E - E_{rev} = \frac{RT}{F} \ln \left(\frac{C_{M^+}}{C_{M^+,0}} \right) = \eta \tag{48}$$

where η is the overpotential required to drive the reaction as a whole at a given current density. The rate of change of C_{M^+} with time can be obtained by differentiation, i.e.,

$$\frac{dC_{M^+}}{dt} = \left[\frac{FC_{M^+,0}}{RT} \exp \left(\frac{F}{RT} \eta \right) \right] \frac{d\eta}{dt} \tag{49}$$

If C_{M^+} is the surface concentration (in mol cm^{-2}), the current density needed to produce this concentration change, i.e., the pseudocapacitance current density, is simply

$$i_{PC} = F\left(\frac{dC_{M^+}}{dt} \right) = \left[\frac{F^2 C_{M^+,0}}{RT} \exp \left(\frac{F\eta}{RT} \right) \right] \frac{d\eta}{dt} \tag{50}$$

At the very beginning of any perturbation (e.g., in a galvanostatic pulse) $\eta \to 0$, and hence

$$i_{PC} = \frac{F^2 C_{M^+,0}}{RT} \left(\frac{d\eta}{dt} \right)_{\eta \to 0} = C_{PC} \left(\frac{d\eta}{dt} \right)_{\eta \to 0} \tag{51}$$

where C_{PC} is the pseudocapacitance acting in parallel with the double-layer capacitance.

In the case of a soluble intermediate, assuming a reaction layer of thickness δ, the pseudocapacitance is

$$C_{PC} = \frac{F^2 C_{M^+,0} \delta}{RT} \tag{52}$$

If the concentration $C_{M^+,0}$ is known independently (e.g., from a known standard potential and the Nernst equation), the experimentally determined C_{PC} gives the reaction layer thickness. The pseudocapacitance determinations from galvanostatic transient analysis in the case of copper were first carried out by Bockris and Enyo(27); values of the order of 100 μF cm^{-2} were found.

With an equilibrium Cu^+ concentration of 3×10^{-7} mol cm^{-3}, this gives a reaction layer thickness of 8×10^{-5} cm.

Pseudocapacitances have also been found in the case of metals (zinc, nickel) whose univalent ions are not known normally to exist in solution. Hence, surface concentrations could be calculated, and it was found that, e.g., in the case of zinc,(25) they are of the order of 10^{-12} mol cm^{-2}.

Galvanostatic transients can be used also to observe trends in the change of the pseudocapacitance with potential which can have some diagnostic value. Thus, if, e.g., C_{PC} is found to decrease as the potential is changed in the cathodic direction, this means that the first of two electron exchange steps is the rds. Conversely, an increase in C_{PC} would arise if the fast step precedes the rds, since, in that case, an accumulation of M^+ occurs before the energy barrier. The method of analysis is based on the assumption that, at any potential along the galvanostatic transient, the rate of the activation-controlled rds is established instantaneously. This should be the case at potentials in the region where linear Tafel plots are obtained.

At any given potential along the transient, the capacitance current is obtained by subtracting the Faradaic current (indicated by the Tafel plot) from the total current, i.e.,

$$i_{PC} = i - i_F = i - i_0 \exp\left(-\frac{\beta F \eta}{RT}\right) \tag{53}$$

and the integral pseudocapacitance is obtained by graphical integration of the i_{PC}, time plot, i.e.,

$$C = \frac{\int_0^t i_{PC}\, dt}{\eta} \tag{54}$$

In the case of deposition of zinc from zincate solutions, it was found that it increases with increasing overpotential; not so sharply, however, as it would be expected if the concentration of one intermediate only was potential dependent. This is in accordance with the assumed mechanism which involves a chemical rds between two charge-transfer steps. In such a case, the pseudocapacitance is due to two effects—an accumulation of the $Zn(OH)_2^-$ intermediate before the rds and a decrease in concentration of the ZnOH species after it. Hence, there is a compensation effect in the change of C_{PC} with potential, and the values could even pass through a minimum.

3.3. Effect of Anions on the Kinetics of Metal Deposition and Dissolution

Anions can affect metal deposition and dissolution in several ways.

The most general effect is that due to the complexing of metal ions.

Anions of common strong acids, such as ClO_4^-, SO_4^{2-}, Cl^-, NO_3^-, etc. exhibit as a rule only weak complexing interactions, if any. Nevertheless, even weak complexation may be of importance in electrode kinetics if the complex ion undergoes electrode reaction more easily than the free metal ion, as is often the case, especially with chlorides. In such cases, the complex takes the role of an electroactive species, as already discussed for the hydroxo complexes. Thus, e.g., nickel can hardly be anodically dissolved at all if chloride ions are not present in the solution. In sulfate electrolytes, the oxidation product (some oxygen-containing species) forms a passive film and further dissolution is blocked soon after an anodic overpotential is imposed upon the electrode. The phenomenon of passivity is discussed elsewhere (cf. Volume 4). At this point, one should note that passivity is absent in the presence of chlorides.

Easily polarizable anions, like halides, can help charge transfer if adsorbed at the electrode surface. Some mechanism of transmission of charge, easier than when the surface is covered by water molecules only, results in catalysis of the activation-controlled electrochemical reaction of metals.

Other effects of yet unknown origin must also be significant in some cases, e.g., as in the deposition and dissolution of iron, since the i_0 values are found to decrease in the presence of different anions in the sequence

$$ClO_4^- > SO_4^{2-} > Cl^- > Ac^- > NO_3^-$$

3.4. Effect of Substrate on the Kinetics of Activation-Controlled Reactions of Metals

Differences found in the kinetics of one and the same reaction by different authors can often be ascribed to the effect of differences in the origin and method of preparation of the electrode. However, little is known about this subject and few experiments have been carried out with all the conditions the same except the nature of the substrate.

Careful experiments carried out on different preparations of copper electrodes (helium or hydrogen quenched, electrodeposited, anodically dissolved, or partly covered by oxide) under identical conditions of experimental determination of the kinetics,(28) have led to the same Tafel slopes (indicative of the same mechanism governing the process in all cases) and i_0 values changing within an order of magnitude (cf. Table 2). It appears that differences are due to different surface coverage of the electrode with adions, the electrodeposited copper and copper partly covered by oxide with higher surface coverage (about 0.8) giving a lower i_0 value, while at a smaller surface coverage (about 0.07), tenfold higher i_0 values were found for all the other preparations.

3.5. Kinetics of Codeposition of Metals and Effects on Alloy Phase Formation

Codeposition of two metals A and B at comparable rates occurs when

$$E_{r,\mathrm{A}} + \eta_{\mathrm{A},i_\mathrm{A}} \simeq E_{r,\mathrm{B}} + \eta_{\mathrm{B},i_\mathrm{B}} \tag{55}$$

where $\eta_{\mathrm{A},i_\mathrm{A}}$ and $\eta_{\mathrm{B},i_\mathrm{B}}$ are the cathodic overpotentials for the deposition of the two metals at comparable current densities, i_A and i_B, respectively.

This shows that there is a thermodynamic and a kinetic aspect of codeposition. The first has already been discussed (cf. Section 2.2). It is seen that, by modifying the kinetics, one can induce codeposition even if the reversible potentials of the deposition reactions are different. The metal with a more negative reversible potential requires a lower overpotential in order to be codeposited.

Codeposition at comparable rates is a precondition for alloy formation of any of the three types discussed earlier. The large field of electrochemical deposition of alloys, which is based upon the above considerations, has been intensively studied for practical purposes. Good reviews are available.(29,30)

3.5.1. Kinetics of Deposition of Binary Alloys in Systems with a Eutectic

In such systems, each metal is supposed to crystallize separately, although the discharge and adatom formation could, in principle, occur for both metals over the entire surface area of the electrode. However, it is observed experimentally, e.g., in the deposition of tin–zinc and tin–lead alloys from pyrophosphate solutions,(31) that the partial current for deposition of each metal at a given potential is lower than in the deposition onto the corresponding pure metal of the same electrode surface area. This is an indication that there is a preference for the deposition of metal adatoms onto the surface of crystallites of the same metal. If one assumes that this preference is absolute and that the kinetics of deposition of metal A are unaffected by the deposition of metal B (i.e., that the current-density–potential relationship for a microsurface of each crystal is the same as that for the macrodeposition of the metal concerned), then the apparent current density (per unit electrode surface area) for its deposition at a given overpotential will be given by

$$i'_\mathrm{A} = i_\mathrm{A}[S_\mathrm{A}/(S_\mathrm{A} + S_\mathrm{B})] \tag{56}$$

where S_A and S_B are the corresponding surface areas of microcrystallites of A and B, respectively.(30) Assuming the crystallites of both metals to be of similar size, the surface area covered by each metal will be proportional to the amount deposited. Thus,

$$\frac{S_\mathrm{A}}{S_\mathrm{A} + S_\mathrm{B}} = \frac{i_\mathrm{A}(\varepsilon_\mathrm{A}/\delta_\mathrm{A})}{i_\mathrm{A}(\varepsilon_\mathrm{A}/\delta_\mathrm{A}) + i_\mathrm{B}(\varepsilon_\mathrm{A}/\delta_\mathrm{B})} \tag{57}$$

where ε_A and ε_B are electrochemical equivalents, and δ_A and δ_B are the densities of metals A and B, respectively. Introducing (57) into (56), one obtains

$$i'_A = \frac{i_A^2}{i_A + (\varepsilon_B \delta_A / \varepsilon_A \delta_B) i_B} \tag{58}$$

The significance of this result becomes clear from the hypothetical case of codeposition of two metals shown in Figure 12. It is seen that although the deposition kinetics remains unchanged, there is a quasidecrease in the rate of the individual electrochemical reactions as compared with that for the process of pure metal deposition. The deposition of one of the components seems to reach limiting current conditions.

The assumption of exclusive deposition on to the surface of the like metal applies, of course, only as a limiting case. In practice, some codeposition at the molecular level is expected. Indeed, in some systems which show immiscibility in the solid phase under equilibrium conditions (e.g., Cu–Pb and Cu–Tl), there is evidence that, in an electrodeposited layer, each phase contains some concentration of the other component. Thus, reduction of the less noble component occurs at more positive potentials than those estimated on the basis of standard potentials of the pure metal. The potential shifts can be of the order of several tens of millivolts, and can be explained by the crystallites of the eutectic being supersaturated solid solutions of one component in the

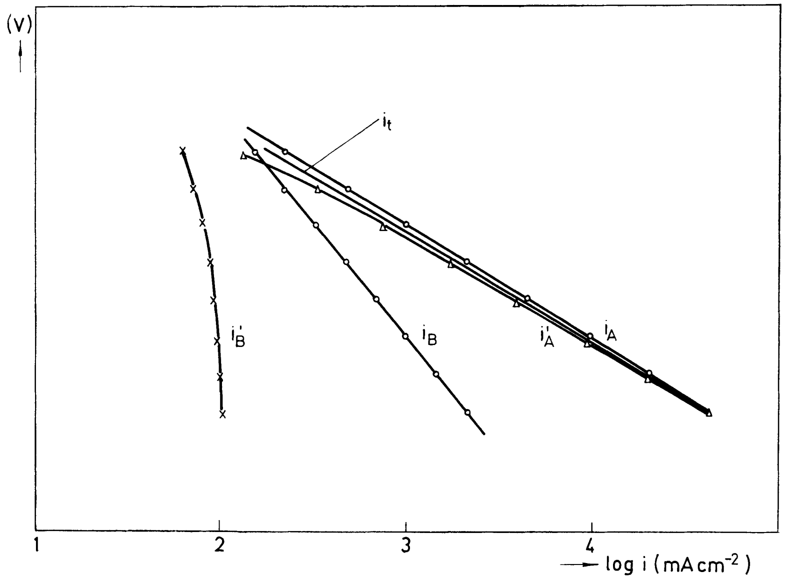

Figure 12. Comparison of hypothetical polarization curves for deposition of metals onto pure metal phases (i_A and i_B) with those that should be obtained for the deposition on a eutectic-type alloy, according to Eq. (58); i_t—the total current density line.

other, rather than pure metal phases. This possibility of achieving a special nonequilibrium state in the alloy obtained by electrochemical means may be of importance for some practical applications.

3.5.2. Codeposition into Solid Solutions

The changes in standard free energy for the depositing alloying metal compared with those for the corresponding pure metal due to the free energy of mixing, which were discussed earlier (cf. Section 2.2), can affect not only the reversible potential but also the kinetics of the deposition process by affecting the energy barrier, as shown schematically in Figure 13.

It can be shown that a simple vertical shift does not lead to a change in the height of the energy barrier and hence that, in such a case, the i_0 values or the chemical rate constant for the metal in the alloy should be the same as for pure metal. Similarly, no direct effect on deposition kinetics is expected from a change in the potential of zero charge (p.z.c.) from that of the pure metals to that of the alloy (cf. Frumkin(32)). However, Gorbunova and Polukarov(30) pointed out that a simple vertical shift of the potential energy curves may be an oversimplification. If potential energy is adequately represented by an equation of the Morse type, then any change in the parameter D (reflecting the change in the ground state energy) results not only in vertical

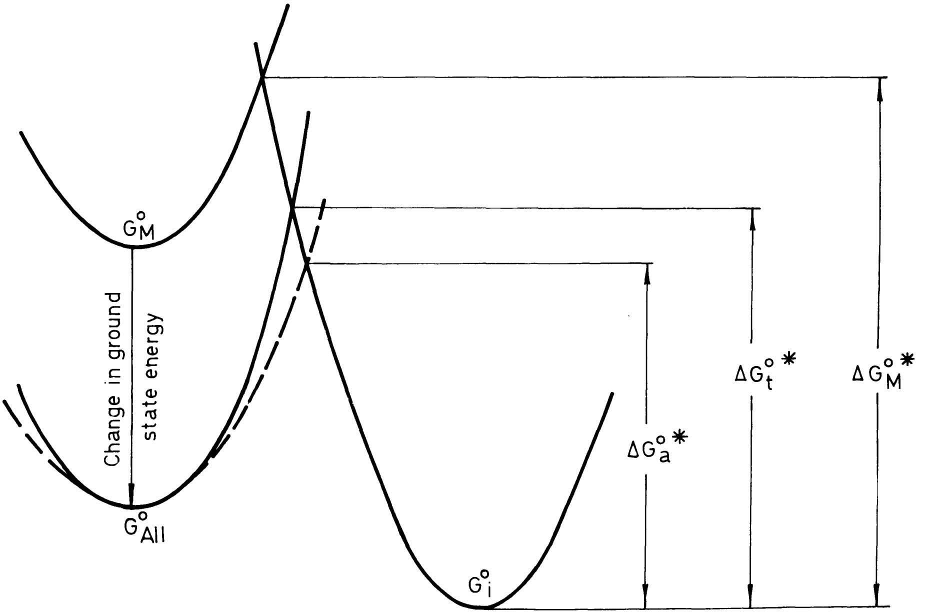

Figure 13. The approximate and the true values of the activation energy (ΔG^0_a and ΔG^0_t, respectively) obtained upon simple vertical shifting of the potential energy curve (dotted line) and upon taking into account the effect of the shape of the curve.

shifting but also in a change of slope. This contributes to the change in activation energy produced by shifting, as seen in Figure 13.

Hence, experimental observations made by a number of investigators showed that, at one and the same overpotential, the reduction rate for codeposition relative to the deposition of a pure metal decreases for the component with the more positive p.z.c. and increases for the one with the more negative p.z.c. This behavior can be explained by this model, as well as by some secondary effects of the change in the p.z.c.

4. Totally Irreversible Dissolution of Metals

The systems described so far have involved metals in solutions of their corresponding ions. In such systems, in principle, true (thermodynamic) electrochemical equilibria can be established, and departure of the potential from the equilibrium value results in a more or less reversible cathodic deposition of anodic dissolution. Both cathodic and anodic partial currents are present at any instant of time and undergo a continuous change with potential, leading to a situation when one becomes negligible compared to the other.

In practice, however, systems are often encountered in which the solution initially does not contain corresponding ions, and for that or some other reason, the cathodic partial current is negligible at any potential. In such cases, the system is not thermodynamically defined, and the concept of reversible potential cannot be used. Nevertheless, in many cases, well-defined steady states are established, giving stable potential values to the extent that some such systems are used as the most reproducible reference electrodes (e.g., Ag, AgCl, Cl^-; Hg, Hg_2Cl_2, Cl^-; Hg, Hg_2SO_4, SO_4^{2-}, etc.).

In others, well-defined steady states enable, e.g., the quantitative treatment of corrosion problems to be developed. Such situations are, therefore, important and will be given some attention here.

4.1. The "Floating" Electrode Potential

An electrode metal in the absence of its corresponding ions in solution, at open circuit, is likely to have a poorly defined potential. However, this is no longer so, as soon as some anodic dissolution current is applied, producing some corresponding ions in the vicinity of the electrode. In principle, a Butler–Volmer type of relationship analogous to Eq. (23), taking into account both the anodic and cathodic partial currents for a single electron exchange process, can be written$^{(33)}$ for any potential, E, measured with respect to an arbitrarily chosen reference state, as

$$i = i_{\mathrm{M}} - i_{\mathrm{M}^+} = k_a^0 C_{\mathrm{M}} f_a(E) - k_c^0 C_{\mathrm{M}^+} f_c(E) \tag{59}$$

where k_a^0 and k_c^0 are the anodic and cathodic heterogeneous rate constants at the reference potential (e.g., the standard potential of the M^+/M couple), and C_{M^+} is the concentration of M^+ ions in a reaction layer at the electrode surface.

On the other hand, when a steady state anodic dissolution is established, a diffusion flux of M^+ toward the bulk of solution competes with i_{M^+}. If the concentration of M^+ outside a diffusion layer of a defined thickness δ is maintained equal to zero, the material balance at the outer Helmholtz plane can be written as

$$\left(\frac{dC_{M^+}}{dt}\right)_{OHP} = \frac{k_a^0 C_M f_a(E)}{F} - \frac{k_c^0 C_{M^+} f_c(E)}{F} - \frac{D_{M^+} C_{M^+}}{\delta} = 0 \tag{60}$$

Hence,

$$C_{M^+} = \frac{k_a^0 C_M f_a(E)}{k_c^0 f_c(E) + (FD_{M^+}/\delta)} \tag{61}$$

and, substituting (61) into (59),

$$i = k_a^0 C_M f_a(E) \frac{FD_{M^+}/\delta}{k_c^0 f_c(E) + (FD_{M^+}/\delta)} \tag{62}$$

Equation (62) indicates that two regions of the E–i relationship are to be expected, both being Tafel-type functions.

At relatively negative potentials, where $k_c^0 f_c(E) \gg FD_{M^+}/\delta$ one obtains

$$E = \frac{RT}{F} \ln i - \frac{RT}{F} \ln \left(\frac{k_a^0}{k_c^0}\right) \left(\frac{FD_{M^+}}{\delta}\right) C_M \tag{63}$$

This is the region where diffusion is controlling the rate of the process and E is a reversible potential of the metal with respect to its ions, whatever the concentration established at the outer Helmholtz plane by the balance of fluxes.

As the potential becomes increasingly positive, after some transition region, an adverse condition is reached in which $k_c^0 f_c(E) \gg (FD_{M^+}/\delta)$ and hence rearranging (62) one obtains

$$E = \frac{RT}{(1-\beta)F} \ln i - \frac{RT}{(1-\beta)F} \ln k_a^0 C_M \tag{64}$$

which is the Tafel function for an activation-controlled anodic dissolution, with the same slope as that obtained in reversible systems, and with the intercept representing a kind of standard current density obtained at a potential equal to the reference potential.

Dissolution of divalent metals into a solution free of their corresponding ions, if they follow the two-step single-electron exchange mechanism, as, e.g., (35), gives a somewhat more complex relationship, since the existence of the univalent intermediate at the outer Helmholtz plane and its diffusion away from the electrode have to be taken into account. The total current is

$$i = \overleftarrow{i}_{\mathrm{M}} - \overrightarrow{i}_{\mathrm{M}^+} + \overleftarrow{i}_{\mathrm{M}^+} - \overrightarrow{i}_{\mathrm{M}^{2+}} = k^0_{a,1} C_{\mathrm{M}} f_a(E) - k^0_{c,1} C_{\mathrm{M}^+} f_c(E)$$
$$+ k^0_{a,2} C_{\mathrm{M}^+} f_a(E) - k^0_{c,2} C_{\mathrm{M}^{2+}} f_c(E) \qquad (65)$$

Moreover, the intermediate can either be a species which is relatively stable in solution, so as to exist at a finite concentration, as, e.g., in the case of Cu^+ ion, or it can be so strongly adsorbed at the surface that, although present there at kinetically significant concentration, its concentration in solution, even at $x = 0$, is negligible. This can be taken care of by assuming an adsorption equilibrium

$$C_{\mathrm{M}^+}/(C_{\mathrm{M}^+})_{x=0} = K \qquad (66)$$

Two material balance equations similar to Eq. (60) can now be set up. Solving them for C_{M^+} and $C_{\mathrm{M}^{2+}}$, and substituting into (65), one obtains

$$i = \frac{k^0_{a,1} C_{\mathrm{M}} f_a(E) \{P_1[k^0_{c,2} f_c(E) + P_2] + 2k^0_{a,2} f_a(E) P_2\}}{k^0_{c,1} k^0_{c,2} [f_c(E)]^2 + P_1 k^0_{c,2} f_c(E) + P_2[k^0_{c,1} f_c(E) + k^0_{a,2} f_a(E) + P_1]} \qquad (67)$$

where

$$P_1 = FD_{\mathrm{M}^+}/K\delta_{\mathrm{M}^+} \qquad (68)$$

and

$$P_2 = FD_{\mathrm{M}^{2+}}/\delta_{\mathrm{M}^{2+}} \qquad (69)$$

The diffusion layer thicknesses δ_{M^+} and $\delta_{\mathrm{M}^{2+}}$ are equal to each other and in some proportion to the hydrodynamic boundary layer, if the disproportionation reaction, as e.g., (36b), proceeds at a negligible rate. Otherwise, δ_{M^+} must be estimated by a complex treatment which is applied to cases when an electrochemical reaction is coupled with a chemical reaction. If the former condition is satisfied, a number of situations can arise, which can be distinguished by corresponding kinetic consequences. Hence, the study of *E–i* relationships for floating electrodes of divalent metals can have some diagnostic value. These situations are as follows:

(i) Both electron exchange steps are fast compared to diffusion of the univalent intermediate away from the electrode, but the second step is slower than the first one.

(ii) Same as (i) but the first of two electron exchange steps is slower than the second one.

(iii) The first step is faster, while the second one is slower than the diffusion of the univalent intermediate away from the electrode.

Table 3 lists the slopes of the Tafel relationships arising from Eq. (67) for the cited cases. It is seen that they can all be experimentally distinguished if a sufficiently wide range of potentials can be covered.

Experimentally, studies on "floating electrode" potentials have to be conducted with care, to avoid spurious potentials being established close to

Table 3

Tafel Slopes for Different Situations of Dissolution of Divalent Ions into Electrolytes Free of Corresponding Ions ("Floating" Electrode Conditions)

		Tafel slope		
Mechanism	Situation[a]	Low potentials	Highly positive potentials	
Single-step, two-electron exchange	—	RT/2F	RT/2(1 − β)F	RT/F
Two-step, one-electron exchange	(i)	RT/2F	RT/(2 − β)F	2RT/3F
	(ii)	RT/2F	RT/(1 − β)F	2RT/F
	(iii)	RT/F	RT/(1 − β)F	2RT/F

[a] See text for explanations of situations (i), (ii), and (iii).

O_2 imposition from the air being present or variations due to lack of pH stability, e.g., near 7.

4.2. Dissolution with the Formation of Insoluble Substances

4.2.1. Electrocrystallization of Substances Other than Metals

When anodic oxidation of a metal is followed by a chemical reaction with a component of the solution, insoluble substances are often formed. Considerable attention has been devoted to all the phases of such a process,(34) since this involves a number of electrochemical systems of great practical importance, as, e.g., the dissolution of lead to form $PbSO_4$, the formation of calomel in reference electrodes, etc. The formation of insoluble oxides can also be a cause of passivity.

Electrocrystallization of a nonmetallic phase can be a secondary effect, arising when saturation of the electrolyte by the product of the electrode reaction is reached. It can, however, also result from direct formation of the product by a solid state reaction.

A detailed study of each particular system is needed to distinguish between the two mechanisms. However, as far as the kinetics of the process is concerned, the dissolution–precipitation mechanism could be treated along the same lines of reasoning as used in the previous parts of this chapter, while a direct formation of insoluble product has a number of specific features which are treated elsewhere (Volume IV, Chapter 10, Volume VIII, Chapters 3 and 4) and are outside the scope of this review.

A good example of the dissolution–precipitation mechanism is found in the case of formation of calomel by anodic dissolution of mercury in chloride solutions. It has been realized(35) that the low-solubility product of calomel in aqueous solutions gives far too low a concentration of mercurous ions in equilibrium (10^{-18} M) to sustain the extremely high exchange current density of the calomel electrode (around 1 A cm^{-2}). Hence, it is assumed that an intermediate complex ion—the chloromercurous ion, Hg_2Cl^+, existing at much higher concentrations—serves as a transfer agent for mercury between the solid calomel and the electrode surface. Indeed, a simultaneous galvanostatic and ellipsometric investigation demonstrated(36) that steady state anodic dissolution is reached considerably before a change of the ellipsometer photomultiplier output indicated the appearance of a new phase at the mercury surface. Chronopotentiometric investigation allowed determination of the concentration of Hg_2Cl^+ ions from the $i(\tau_i)^{1/2}$ vs. i plot. It was found to be of the order of 10^{-4} M.

A generalization seems to be justified based on this and other similar experience with systems with insoluble reaction products not leading to passivation and those leading to fast or practically instantaneous passivation:

(a) If the overall reaction is controlled by the anodic oxidation of the metal and is without relatively soluble intermediates, the chances are that the insoluble substance will be formed in the double-layer region (direct precipitation), since ample supply of the reactant from the solution side is available;

(b) Conversely, if a relatively soluble intermediate participates in the mechanism underlying the overall reaction of formation of the precipitate and if anodic dissolution is a process with high i_0, and fast compared to the supply of reactants from the bulk of solution, the precipitate is likely to be formed sufficiently far away from the electrode as not to hinder continuous dissolution.

4.2.2. Electrochemical Dissolution of Metals through Oxide-Covered Surfaces

A number of metals (e.g., alkali metals, alkaline earths, magnesium, aluminum) have such a highly negative free energy of oxidation that, in contact with water, even in the absence of oxygen, they oxidize, noticeably evolving hydrogen. Some are unstable to the extent that the oxidation proceeds as long as there is any metal or water left. Others, however, may exhibit considerable stability if conditions are provided for the formation of a protective oxide layer.

In the case of aluminum, for example, the basic factor determining the qualities of that layer is the kind of anions present in the electrolyte.(37) There is a group of anions (e.g., borates), constituting the so-called barrier-forming electrolytes, in whose presence anodic polarization leads to the formation of a very compact film with good insulating and protective qualities. Maintaining a constant anodic current requires a voltage increase which is linear with time (i.e., with the quantity of electricity passed). This is an indication that anodization leads to a steady increase of the thickness of the oxide layer of constant resistivity. Hence, the structure of the layer does not change with increasing thickness, up to attainment of voltage across the layer in excess of a hundred volts, upon which an electrical breakdown arises.

The barrier-type oxide layer does not imbibe anions from the electrolyte.

In other electrolytes (e.g., sulphates), the surface oxide is found to consist of two layers: a compact one and a porous one. The compact layer is very thin (a fraction of a nanometer) and is impervious to the electrolyte, while the porous layer represents an oxide matrix through which the electrolyte is transported more or less freely.

It appears that it is the compact oxide film which prevents further oxidation. In that sense, these metals become similar to other metals which undergo passivity, e.g., transition metals. A number of phenomena connected with, and considerations of, the mechanism of passivity are given elsewhere (cf. Volume VIII, Chapters 3 and 4).

The highly reactive metals differ from those undergoing passivity, however, in two respects: (a) some electrochemical activity is preserved through the oxide as well, and (b) the anodic oxidation is totally irreversible, i.e., the oxide film cannot be reduced back to the metallic state from an aqueous solution under any conditions of potential, as their ions are heavily hydrated and are kinetically inert. Except for mercury, no substrate has been found so far at which decomposition of water would not precede any reduction of the cations of the highly electronegative metals. Even on mercury, some of them (e.g., Al) cannot be reduced to the metallic form.

The electrochemical activity of these metals is reflected in the fact that, in some electrolytes (e.g., aluminum in chloride-containing solutions), they establish relatively negative open-circuit potential values, although far from the theoretical equilibrium potential (−1.66 V). Also, if pseudo-ohmic overpotential is well accounted for, as seen in Figure 14, they exhibit relatively small change in polarization with increasing anodic dissolution current up to very large current densities of the order of $\mathrm{A\,cm^{-2}}$. In some cases, even negative resistance is found, i.e., anodic polarization decreases with increasing anodic current density, indicating change in the structure of the film toward lower resistivity.

An interesting phenomenon accompanies their anodic dissolution: with increasing anodic current density (and hence, with electrode potential shifting in the positive direction), an increase in hydrogen evolution rate is found instead of the expected decrease, which should take place if a simple hydrogen corrosion mechanism was operative and determined the open-circuit potential (cf. Volume VIII, Chapter 2). This phenomenon is termed traditionally *the negative difference effect.*(38) In most cases, the hydrogen evolution current increases linearly with increase in the anodic current density, so that the ratio between the two currents remains constant, and the negative difference effect can usually be expressed as a percentage figure.

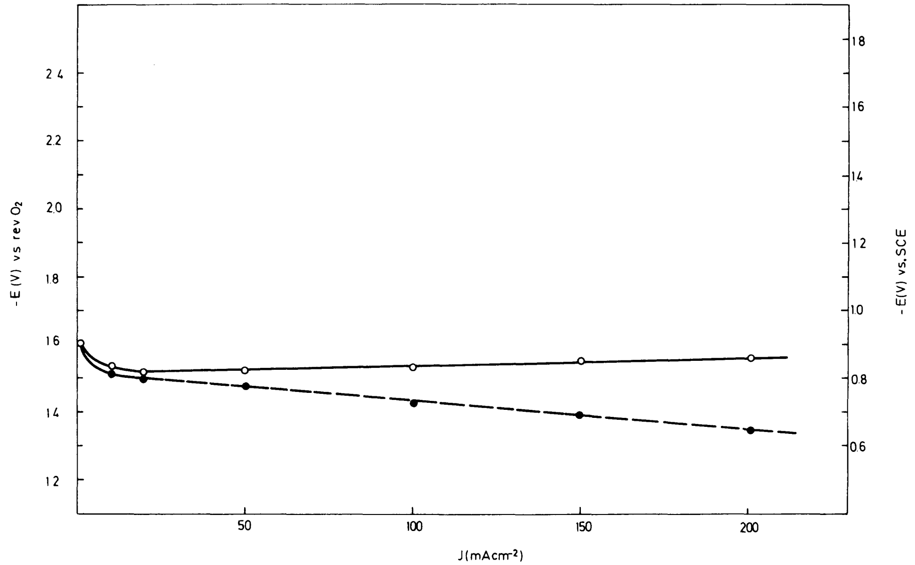

Figure 14. Polarization of aluminum in 2 *M* NaCl solution as a function of current density (dashed line, measured; full line, corrected for pseudo-ohmic overpotential).

Since hydrogen evolution is accompanied by a corresponding dissolution of the metal, the effect results in a reduced efficiency of obtaining electricity by anodic dissolution, independent of current density.

The shift of the open-circuit potential from the equilibrium potential of the metal under given conditions cannot also be accounted for by the simple hydrogen corrosion theory (the Wagner–Traud mechanism).

Hence, it is obvious that the voltage drop across the oxide layer accounts for most of the loss of potential when the metal is immersed in the solution and that equilibration with the solution implies creation of a space charge counteracting the electrochemical potential difference.

Several theories exist on the mechanism of dissolution of this type of metal, which explain the experimentally observed linearity of the Tafel plots.

It is possible that the dissolution rate is limited by the transport of species (metal ions and/or oxygen anions) through the nonporous oxide film (transport control). If so, the ionic mobility should increase exponentially with increase in the field strength across the film (anodic overpotential). This is not unlikely in solids submitted to ultrahigh fields of the order of 10^7 V cm^{-1}.

Another possibility is that the rds is the transition of the metal ion across the metal–oxide interface. Mott and Cabrerra have shown that an exponential relationship should apply in such a case between the ionic flux and the imposed potential difference at the interface.

Neither theories, however, explain the negative difference effect and this is considered independently as being due to three possible causes: (a) the splitting of small chunks of the metal away from the electrode during anodic dissolution for purely mechanical reasons (the "chunk effect"), (b) the rupture of the oxide layer, i.e., porosity of the film increasing with current density, and (c) the chemical reaction of uncommon valency state ions (e.g., M^+ ions) leaking through the film. In the case of the first mechanism, it is difficult to see why splitting off of chunks should be linearly dependent on current density as is found in most cases.

It is possible to treat the Mott–Cabrerra interfacial reaction as an activation-controlled electrochemical reaction between the metal and a solid electrolyte, since the latter would also follow an exponential dependence of the rate on potential (the Tafel relationship). If the mechanism of oxidation was

$$\begin{aligned} &\text{I} \quad M \rightleftarrows M^+ + e \\ &\text{II} \quad M^+ \rightarrow M^{3+} + 2e \end{aligned} \tag{70}$$

with the second step as the rds, this would fit well with the third concept of the negative difference effect. If step I is in equilibrium, the concentration of the intermediate M^+ at the metal–oxide interface should increase exponentially with change of potential (from the Nernst equation). Hence, there should be an exponential increase of the diffusion flux of M^+ through the film with a resulting increase of hydrogen evolution at the outer surface by chemical reaction with water. Since the overall anodic current is also increasing exponentially, the ratio of the two should stay constant as found experimentally.

4.3. Acceleration of Anodic Dissolution of Metals under Strain

The phenomenon of corrosive breaking of a metal under stress ("stress corrosion cracking"—cf. Volume VIII, Chapter 6) has been an indication that anodic dissolution of metals is for some reason sensitive either to any stress or to strain which is coupled with it.

Indeed, a number of authors have found that straining a metal produces some change in the freely established mixed potential of a metal in a corrosive medium(39) or in the anodic dissolution current under constant potential.(40–42)

The phenomenon is a transient one and dies out after the strain adjusts to stress, or else is continuous if the metal is strained continuously up to the breaking point of the sample. The effect is small when the metal is strained in the elastic region and increases rather sharply upon yielding to stress beyond the plastic deformation point. A typical recording of the stress–strain relationship and the accompanying anodic dissolution current is shown in Figure 15.(42) The maximum anodic dissolution current obtained at the breaking point is linearly dependent on the strain rate, the slope depending on the metal.

There seem to be two basically different reasons for the observed increase of electrochemical activity of metals, under stress(43):

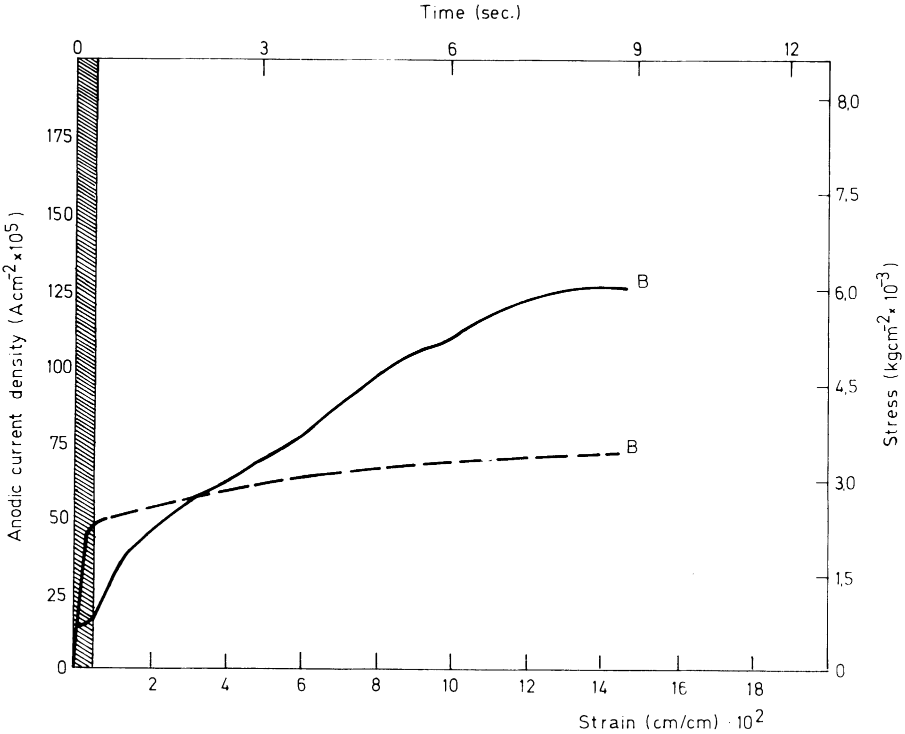

Figure 15. Simultaneous recording of stress (dashed line) and current (solid line) at an iron wire as a function of strain at a constant strain rate up to the breaking point B. Shaded area corresponds to the elastic region.

In the case of metals in media which promote passivity, it is the rupture of the protective film upon yielding which uncovers bare metal surface and hence causes fast anodic dissolution at the given potential before the film is repaired.

However, the phenomenon is observed also under conditions when no film is formed at the metal surface. There, the acceleration of anodic dissolution could be due to the appearance of loosely bound atoms at deformed grain boundaries, or, more likely, to uncovering high index planes as slip planes during plastic deformation, which exhibit higher rates of anodic dissolution than the surface which has been in contact with the solution before straining. A semiquantitative treatment based on this latter model could be made, assuming that, at the yield point, slip edges appear all along the metal surface and slip planes start emerging in succession to one another in discontinuous increments rather than simultaneously and continuously. As the overall surface area of the slip planes increases with straining, so does the anodic dissolution current. However, the new active planes dissolve preferentially and more stable, low index planes emerge as a result, ending the increased activity at those slip lines. A function following the experimentally recorded dependence (Figure 15) rather closely is obtained and the maximum current for this model depends linearly on strain rate.

The high-index plane theory is supported by the fact that metals which are known to develop high-index planes upon yielding (iron, molybdenum) exhibit considerably higher acceleration of anodic dissolution under stress, than those which develop planes of lower indices as slip planes (nickel, copper).

Both the protective-film-rupture theory and the high-index-plane theory may be valid for one and the same system, depending on conditions. This has been demonstrated by the behavior of an iron wire strained in an aerated nitrate solution.(41) When straining was done in the active region of potentials, the observed increase of anodic current was of the magnitude expected on the basis of the high-index-plane theory (within a power of 10). However, in the passive region, a 1500–2000-fold increase was observed which can be explained only in terms of the film-rupture mechanism.

5. Formation and Physical Properties of Metallic Deposits Obtained under Conditions of Slow Discharge and Incorporation

When discharge of ions and the formation of adatoms at the surface is the rate-determining step, compact deposits are always obtained, since the steady and random supply of adatoms all over the surface enables an even incorporation into the crystal lattice. However, the structure and properties of the deposit are influenced by numerous factors such as the substrate, the crystallographic properties of the depositing metals, the potential of deposition and/or the corresponding current density, the presence of impurities or additives in solution, temperature, etc.

Much of the work on electrochemical metal deposition has been preoccupied with attempts to establish correlations between these conditions and the structure of the deposits obtained. Classical work establishing the systematics of the phenomenology of the field and reviewing early work is due to H. Fischer.(45) Several problems are encountered in this connection. These are as follows:

(a) To what extent does the structure of the deposit follow the structure of the substrate underneath (epitaxy)?

(b) What determines the grain size in the deposit?

(c) What causes the appearance of texture in thick deposits?

(d) What determines the physical properties of the deposit and, in particular, the appearance of stress?

In general, a survey of the literature at the present time leads to the conclusion that the position reached concerning those problems is much less definitive than that concerning the other problems considered heretofore.

This is due to the great complexity of influences of the above factors in each particular case. Nevertheless, good qualitative and, in some cases, semiquantitative models exist, to help an understanding of most of the phenomena observed experimentally.

5.1. Effect of Substrate on the Growth of the Deposit

The substrate may affect the formation of a number of layers of depositing metal in two ways: (i) by exhibiting attractive forces which make the newly formed metal adhere to the surface, and (ii) by providing an ordered structure of its own crystal lattice as a support for newly created crystals.

The attractive forces can, in some cases, be stronger between the atoms in a foreign substrate and those of the depositing metal than between like atoms, as reflected in the appearance of underpotential deposition (cf. Section 2.3). Such a situation, as well as the substrate of the same metal which is being deposited, should favor two-dimensional layer growth, since thermodynamic affinity for the completion of the full layer adjacent to the substrate is, in such a case, larger than that of starting a new layer, and only kinetic reasons (piling-up of adatoms) may create a situation when several layers are being formed simultaneously on top of each other.

The depositing atoms would normally tend to replicate the crystal lattice of the substrate of the same or another metal, since attractive forces are strongest in the so-called half-lattice positions (kinks), steps or dislocations. Finally, in the center between any three atoms, they are stronger than on top of a single atom at the substrate surface (cf. Ref. 17).

This applies equally to deposition by extension of an already existing crystal lattice and to nucleation of new growth centers. However, in the case of a foreign substrate, if the attractive forces are smaller than between like atoms, three-dimensional nucleation will be favored instead of the two-dimensional one (cf. Volume IV, Chapter 7A).

The success of replicating the substrate and the extent to which its influence will be apparent with the thickening of the deposit depends, in the first instance, on the degree to which the dimensions of atoms of the two materials match. It has been shown(46) that a critical misfit, up to which a lattice of a natural spacing b and force constant γ can follow a substrate with lattice dimension a and with a potential field $\frac{1}{2}W$ (equal to the amplitude of the first harmonic of a Fourier series representing the substrate lattice), is given by

$$P = \frac{a-b}{b} = \frac{\pi}{2}m = \frac{\pi}{2}\left(\frac{\gamma a^2}{2W}\right)^{1/2} \tag{71}$$

The calculations using a Lennard-Jones potential give $m \sim 7$ and the critical misfit of about 9%. This represents the extent of misfit that the equilibrium lattice can stand. A larger misfit leads to formation of dislocations as sources of departure from replication. However, an activation barrier has to be overcome in forming a dislocation and hence, at sufficiently low temperatures, a metastable replication can be obtained up to a 14%–15% extent of misfit.

At smaller degrees of misfit, or at a substrate of the same metal, orientational influence of the substrate on the deposit obtained can be very strong. Nevertheless, with thickening of the deposit, epitaxy is lost in a continuous transition to a structure determined by other conditions of deposition. The departure is first reflected in the formation of a number of twins in the deposit. Eventually, the deposit turns polycrystalline, even if grown on a single crystal as a substrate. However, the orientational influence of a polycrystalline substrate with small crystallites (of the order of 100 nm) is lost at much earlier stages of deposition than that of a coarse grain substrate (with crystals of the order of 5000 nm). Apart from the misfit, the presence of any other factor causing dislocations makes this transition occur more readily.

5.2. Factors Affecting Grain Size in a Compact Deposit

Once the effect of the substrate is lost, the grain size is determined primarily by the number of grain-producing dislocations as well as by the number of nuclei formed during the deposition process. Except for coupled screw dislocations, the chances of two grains originating from two different sources merging into a single one are negligibly small for purely geometric reasons. Hence, the lines of coalescence form grain boundaries in the deposit.

Thus, the deposit will have a finer grain structure, the larger the density of grain precursors, and therefore all the factors promoting the formation of dislocations or nucleation would contribute to a reduction of the grain size. These are: high overpotential and/or current density, leading to a high degree of supersaturation of the surface by adatoms; foreign molecules (impurities or additives) adsorbed at the surface, which create disorder in the incorporation of adatoms into the lattice or inhibit surface diffusion of adatoms toward growing centers; or both. Inhibition of surface diffusion results in local supersaturation of the surface by adatoms, which increases the rate of nucleation (cf. Volume IV, Chapter 7A). The fact that electrodeposition can produce very coarse-grained metals indicates that, often, the rate of incorporation of adatoms into an already existing lattice is so fast that no significant supersaturation is attained, which is the necessary condition for formation of new nuclei.

5.3. The Appearance of Texture in Metal Deposits

As the deposit becomes free of the influence of the substrate structure upon thickening, instead of acquiring a randomly oriented grain structure, it often develops a preferred crystal orientation, which gives a definite texture to its cross section. Texture can be expressed in terms of degree of orientation of the grains constituting the deposit.(47) The orientation of each crystallite can be defined in terms of angles between its crystallographic axes and those of a reference coordinate system (e.g., based on the substrate). In the absence of texture, all three axes of all the crystallites under observation are randomly oriented. A one-degree orientation, sufficient for the appearance of texture, is obtained when one of the axes in most crystallites tends to be at a certain angle to the reference coordinates; 2° and 3° orientations are also possible. The 3° orientation (i.e., crystal lattices of several grains running parallel to each other) should be rare, since it provides conditions for dissolution of grain boundaries with merging into a single crystal.

In most deposits, one-dimensional texture can be observed using electron diffraction, X-ray diffraction, or electron micrography. Two types prevail(47): the "lateral growth" ("substrate-oriented" deposit(45)), in which the most densely populated crystal plane is parallel to the substrate surface, and the "outward growth" ("field-oriented" deposit(45)) in which most densely packed arrays of atoms extend perpendicularly to the surface. However, other orientations are also found.(48) Thus, cobalt, hexagonal nickel, and hexagonal silver tend to have the (1010) plane parallel to the surface.

Two factors seem to be dominant in determining texture: the base metal and the electrolyte (its composition, pH, temperature, and the presence of surface-active substances and colloidal additives). However, in the deposition of one and the same metal, different overpotentials can lead to different orientations.(48)

Several theories have been put forward for interpreting the appearance of texture. Early work(49) ascribed texture to the action of internal stress causing plastic deformation of the grains. This, however, does not seem to be substantiated by changes in other physical properties (e.g., hardness) which should be a normal consequence of such a situation.

A more likely reason could be a preferential orientation of nuclei, repeatedly formed at each new layer, thus providing continued growth of grains. It was suggested by Gorbunova *et al.*(50) that preferential orientation of two-dimensional nuclei is due to the minimum work of formation principle operating in the system. A semiquantitative theory has been developed(51) relating the work of formation to overpotential and showing that, at different overpotentials, different crystal planes could be formed with the minimal work, to lie flat on the substrate. If such a condition is maintained, repeated nucleation of the same orientation should produce oriented crystals.

Other factors could also promote oriented growth. In particular, different rates of deposition on to different crystal planes could be a cause of orientation in the deposit,(52) following the crystal growth principle that those planes grow fastest on which the rate of deposition is lowest. Differences in the rate of deposition have been found at different crystal planes, even in pure solutions. They can be exaggerated by preferential adsorption of foreign molecules (of impurities or additives). Hence, after some time of growth, crystals will develop well-defined, usually low-index planes aligned with each other along a certain crystallographic direction. Moreover, the rate of growth in a direction normal to the surface can be different from that parallel to the surface, because of the influence of the electric field.

Summing up the present state of the theory of texture, one must conclude that, although reasonable in providing an overview of possible causes, it is still weak when applied to real systems in making specific predictions.

5.4. Development of Stress in Metal Deposits

Internal stress appears to be a phenomenon inherent in all electrodeposited metals to the extent that only under special conditions and with utmost care can stress-free deposits be obtained.(53)

In considering the problem of stress, one should distinguish between *macrostress* ("stress of the first order") appearing over the entire electrodeposited layer, and *microstress* ("stress of the second order"), acting on metal atoms within each grain and extending only up to the grain boundary. The former can be measured by mechanical means based on experiments in which the bending properties of the deposit are recorded. The methods have been refined to such an extent that stress in deposits which are only 4 nm thick can be measured. Microstress manifests itself in distortion of the metal lattice within grains and hence can be measured by X-ray techniques. It causes changes in hardness compared with the bulk metal (cf. Volume VIII, Chapter 10).

Macrostress can be of two types: *tensile* and *compressive*. The first tends to compress the substrate, while the second tends to expand it. They are arbitrarily given a negative and a positive sign, respectively.

Finally, according to its origin, the stress can be *extrinsic* or *intrinsic*, depending on whether it is caused by the effect of the substrate upon the deposited layer or it appears in the layer independently of the substrate.

Stress reflects all the complexity of influences of various factors on formation of metal plates by electrodeposition and has, therefore, been the subject of extensive studies: they cover effects of substrate, plating solution composition, pH, deposit thickness, current density, or overpotential, deposition temperature. Detailed reviews are available.(54,55)

The phenomenon seems not to depend on the chemical nature or crystal structure of the metal. The most frequently encountered types of stress in different metals are listed in Table 4. It is seen that metals belonging to different groups of the periodic table as, e.g., Fe, Co, Ni (group VIII) and Cu (group I), or to different crystallographic systems (cubic-copper, hexagonal-cobalt, rhombic-gallium, etc.), all develop tensile stress under most conditions. On the other hand, e.g., lead (cubic), zinc and cadmium (hexagonal), develop compressive stress.

Table 4
Types of Stress Produced in Deposits of Different Metals

Metal	Group of periodic chart	Melting point (°C)	Sign of stress	Mode of changing the sign
Ag	I	961	±	– Changing current density, temperature, additives
Cu	I	1083	±	– Same as above
Cd	II	321	+	– Unknown
Zn	II	419.5	+	– Unknown
Ga	III	29.8	±	– Changing current density and concentration of gallium in solution
In	III	156	+	– Unknown
Sn	IV	231	+	– Application of ac together with introduction of additives
Pb	IV	327	+	– Unknown
Bi	V	271	+	– Unknown
Sb	V	630.5	±	– Changing current density, temperature, additives
Cr	VI	1875–1890	–	– Application of ac
Co	VIII	1492	–	1. same as for nickel 2. application of ac
Fe	VIII	1539	–	– Same as above
Pd	VIII	1552	–	– Unknown
Rh	VIII	1990	–	– Unknown

It has been pointed out(54) that the sign of stress appears to be in some relation to the melting point of the metal. Low-melting-point metals usually develop compressive stress, while tensile stress is associated with high-melting-point metals.

5.4.1. Extrinsic Stress

High internal stress was found, e.g., in thin layers of chromium plated at different face-centered-cubic metal substrates, and was insensitive to conditions of deposition, but varied markedly with the substrate lattice parameters. Indeed, a foreign substrate would normally be expected to play some role in the generation of stress at least in very thin deposits, because of the effects of misfit in lattice parameters. If the distance between positions of maximum attraction (between three atoms) in the substrate is larger than the equilibrium distance between atoms of the depositing metal in its crystal lattice, the new crystal lattice adhering to the substrate should be under tensile strain. Conversely, compressive stress should appear as a consequence of atoms in the deposited layer being forced against each other by the distances in the substrate lattice being smaller than the equilibrium distances in the lattice of the deposit.

However, both cases should result in microstress, while macrostress should depend basically on the mode of coalescence of two-dimensional grains into a continuous film. Such an effect could be replicated on layers piling up on top of each other. This is supported by experiments which have shown that, e.g., nickel plated on different substrates (copper-plated steel, beryllium–copper, and silver-plated steel) exhibits different internal stress which extends into layers 10^2–10^3 nm away from the substrate without any tendency to decrease.

5.4.2. *Intrinsic Stress*

Most of the stress, however, is intrinsic in origin. Intrinsic stress not only varies from metal to metal, but also strongly depends on plating conditions, as shown in Figure 16 for the plates of copper obtained from different electrolytes and under different conditions of electrolysis.(56) In one case only is there an asymptotic tendency to a constant stress, pointing to a possible extrinsic character. In other cases, tensile stress is proportional to thickness up to 25 nm (indicating one and the same stress in each new layer), while in

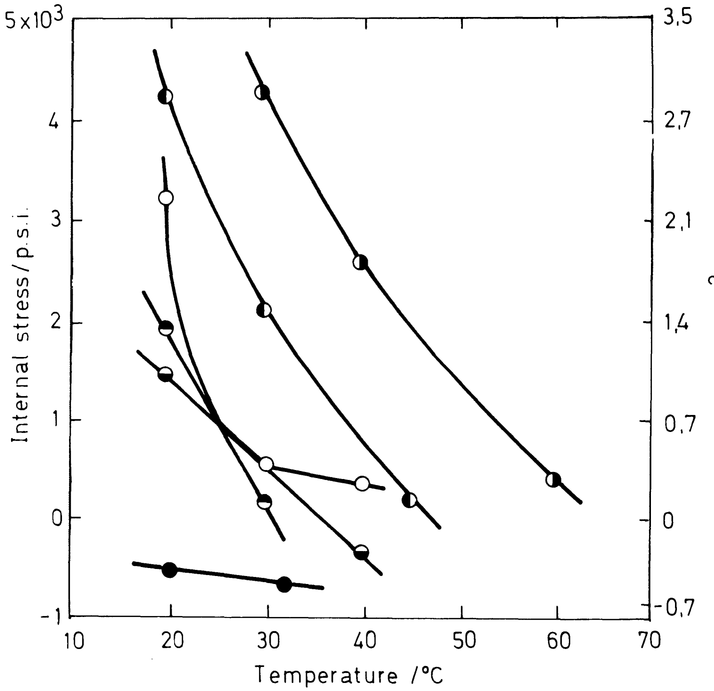

Figure 16. Relationship between bath temperature and internal stress in copper deposits from sulfate baths: ○, 0.35 *M* $CuSO_4$ + 0.4 *M* H_2SO_4, 20 mA cm^{-2}; ●, 0.75 *M* $CuSO_4$ + 0.40 *M* H_2SO_4, 5 mA cm^{-2}; ◒, same, 20 mA cm^{-2}; ◐, same, 40 mA cm^{-2}; ◓, 0.75 *M* $CuSO_4$ + 0.75 *M* H_2SO_4, 20 mA cm^{-2}; ◑, same, 80 mA cm^{-2}.

the case of a pyrophosphate bath, after overcoming some extrinsic tensile stress, the deposit develops compressive stress, again proportional to thickness.

Current density has a profound effect on stress. As shown for the case of copper plating from an acid sulfate bath,(56) increasing current density between, e.g., 0.5 and 4 A dm^{-2}, results in a steady change of stress from a low-compressive stress to a tensile stress which is higher, the lower the temperature, and at 293 K attains a value as high as 3 kg m^{-2}. On the other hand, tensile stress was shown to decrease rather sharply with increasing temperature of plating, e.g., in plating copper from acid sulfate electrolytes, while compressive stress obtained by plating from the same electrolyte but at lower current density exhibits some increase. Thus, in such a system, there are conditions of zero stress at a certain current density at each temperature.

Additives also have a complex effect on stress. Thus, when gelatine is added to the same electrolyte mentioned above, with increasing concentration, it causes first an increase of tensile stress in the copper deposit obtained. At a concentration an order of magnitude higher (0.1 g dm^{-3}) it leads to deposits with very high compressive stress.

Surprising may be the fact that addition of inorganic cations which do not deposit at the attained deposition potential may also cause significant increase in stress. Thus, it was observed that addition of zinc ions to chlorosulfate electrolyte for the deposition of nickel in increasing concentration results in a steady increase of stress in the deposit obtained, while cadmium ions at significantly lower concentrations produce an even stronger effect which passes through a maximum.

5.4.3. Interpretation of the Observed Phenomena

It is obvious that no single explanation can be put forward for interpreting such a complex phenomenon; many different models are offered in the literature for specific experimental results.(54,55) Nevertheless, some generalizations seem to be justified at the present time.

Thus, *tensile stress* seems to be related to the appearance and flow of dislocations. These can be due to the effect of misfit between the lattice of the depositing metal and that of the substrate, and hence account for the appearance of extrinsic stress. However, there are at least two intrinsic reasons for their appearance as well.

One is found in "accidents" in packing of atoms around a certain growth site. These can occur if atoms meet obstacles in the form of foreign atoms or molecules adsorbed at the surface, as are, e.g., molecules of gelatine or adatoms of zinc or cadmium deposited at underpotential. An increased dislocation density over the equilibrium one is then produced during deposition. A basic assumption of a semiquantitative theory of stress that was developed in this connection is that tensile stress is created when a dislocation moving through the crystal reaches its boundary and flows out (the energy it carries is then converted into stress energy).

The theory could account, at least qualitatively, for the increase of stress with increased concentration of additives and with increasing overpotential and/or current density.

Another cause is found in the merging of crystal nuclei into larger crystal grains. If one considers the problems of two-dimensional outgrowth from two nuclei on a flat plane meeting with each other, one can easily recognize that the chances of a seamless merging are very small. There is a high probability that a certain gap, smaller than the atomic dimensions, will remain. This, in itself, produces an attractive force between the two outgrowths which is different from the equilibrium force between atoms in the lattice, and hence, results in stress (the coalescence theory). Moreover, this gap becomes a source of a line dislocation, since an array of atoms landing on it is bound to be in a half-position between layers. Hence, the reasoning leading to the dislocation theory of stress also applies. This model seems particularly useful, since it links the appearance of stress not only to the dislocation theory, but also with the field of kinetics of nucleation (cf. Volume IV, Chapter 7A). It also gives a firmer foundation to a number of older theories.

The *compressive stress* is assumed to be due to occlusion of foreign material in the metal deposit. While adsorbed at the metal surface, the molecules are in the strong electric field (10^7–10^8 V cm^{-1}) of the Helmholtz part of the double layer. Most molecules undergo polarization and significant deformation under such conditions, their motion being hampered. As they become surrounded by metal atoms and buried in the metal, the field disappears and the molecule tends to assume its normal shape and modes of vibration. In this, it tends to compress the surrounding metal atoms, and this stress can extend over a considerable distance. "Softer" metals should be more sensitive to such an internal pressure, and this explains why compressive stress is found primarily in metals of lower melting point. Eventually, the sum of all such effects represents the observed compressive macrostress.

Statistical thermodynamics was applied to this problem to obtain some quantitative relationships. Orders of magnitude obtained on the basis of this theory were found to compare well with the experimentally found range of values (10^5–10^6 N cm^{-2}).

The effects causing tensile stress and compressive stress should be superimposed, and the observed stress should be the sum of the two. Since they have different relationships to conditions of deposition, it is reasonable that the net effect should change sign in changing some of these conditions. A criterion could be developed for the sign of the stress expected in a metal for a given overpotential.

A number, g, is found to be determined by a simple set of parameters such as: the latent heat of melting of the metal, ΔU_m (reflecting the cohesion energy), its density, d, and its atomic weight, A_{M}. Thus,

$$g = \left(\frac{\Delta U_m d}{A_{\mathrm{M}}} z\eta_c\right)^{1/2} \tag{72}$$

Although η_c is the crystallization overpotential, and therefore its range should be significantly lower than the range of total overpotential used in electrodeposition, as seen in Figure 17, a value of $g = 3.5$ seems to divide the metals according to the type of stress, in fair agreement with experimental findings summarized in Table 4.

Besides the above general causes of the appearance of stress, one can envisage the existence of some special ones in special situations. One such situation is connected with the codeposition of hydrogen during deposition of some metals. A mechanism of the appearance of stress has been developed, based on the consequences of the penetration of hydrogen, as H, into the metal as hydride. Hydrogen can also form gas pockets which are unstable. As hydrogen diffuses out after deposition is interrupted, the tensile stress should increase. Some experiments have shown that some residual increase in stress indeed occurs.

Hydrides can have different lattice parameters or belong to a different crystallographic system. Thus, in the case of chromium, the change of hexagonal lattice to body-centered cubic (twisting of lattice positions), which causes tensile stress, is found to be accompanied by hydrogen evolution.

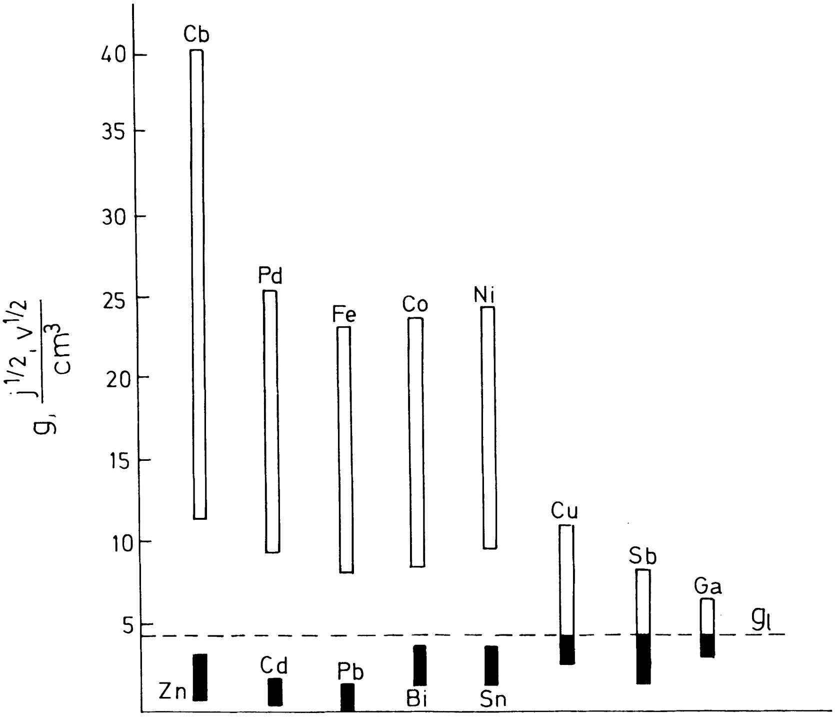

Figure 17. Expected values of the stress-sign criterion g according to Popereka, for different metals. White areas, tensile stress; black areas, compressive stress.

Compressive stress can be caused by hydrogen diffusing into lattice defects or cavities made around foreign atoms or molecules and forming gas under high pressure.

Secondary effects of the presence of hydrogen have also been suggested. Thus, e.g., hydrogen lowers the surface tension of metals, and hence, the flow of dislocations in the region of grain boundaries could be made easier.

6. Effect of Slow Transport of Species to the Electrode on Surface Morphology of Metal Deposits

Deposits obtained by electrochemical reduction can vary greatly in their outer appearance. They can be extremely smooth and bright, or be rough, granular, possibly dendritic, or even powdery.

Some kinds of surface morphology which can be obtained, e.g., in the deposition of zinc, are shown in Figure 18.

The phenomena underlying the appearance of different morphologies are (a) the amplification of surface roughness, (b) the appearance of dendrites, (c) the formation of powders, (d) the effect of periodically changing conditions of deposition, (e) electropolishing, (f) whisker growth and (g) leveling. A common feature of all of them is that transport of species from the bulk of solution to the electrode surface, during the process of metal deposition, plays a dominant role.(57) In four of them (d, e, f, and g), however, it is an interplay between transport and adsorption which determines the overall effect.

6.1. Amplification of Surface Roughness

Amplification of existing surface irregularities is a general phenomenon observed in metal deposition from pure metal salt solutions; it is the more pronounced the higher is the rate of deposition, and the lower is the concentration of metal ions in solution.

A typical example is shown in Figure 18. The amplification takes place obviously by virtue of the deposition being faster, and hence, the deposit thicker at elevations than at recesses.

Kritchmar(58) was the first to point out that this is to be expected in prolonged cathodic reduction for conditions close to those of complete diffusion control of the deposition process.

The reasons for the faster deposition at elevations are that a shorter diffusional path exists between the surface where the deposition takes place and the outer plane of the diffusion layer, than in the case of the recess, and also in the fact that, at tips of elevations, conditions of diffusion are approaching those of spherical diffusion which is always faster than the linear one, because of the wider diffusional field.(61)

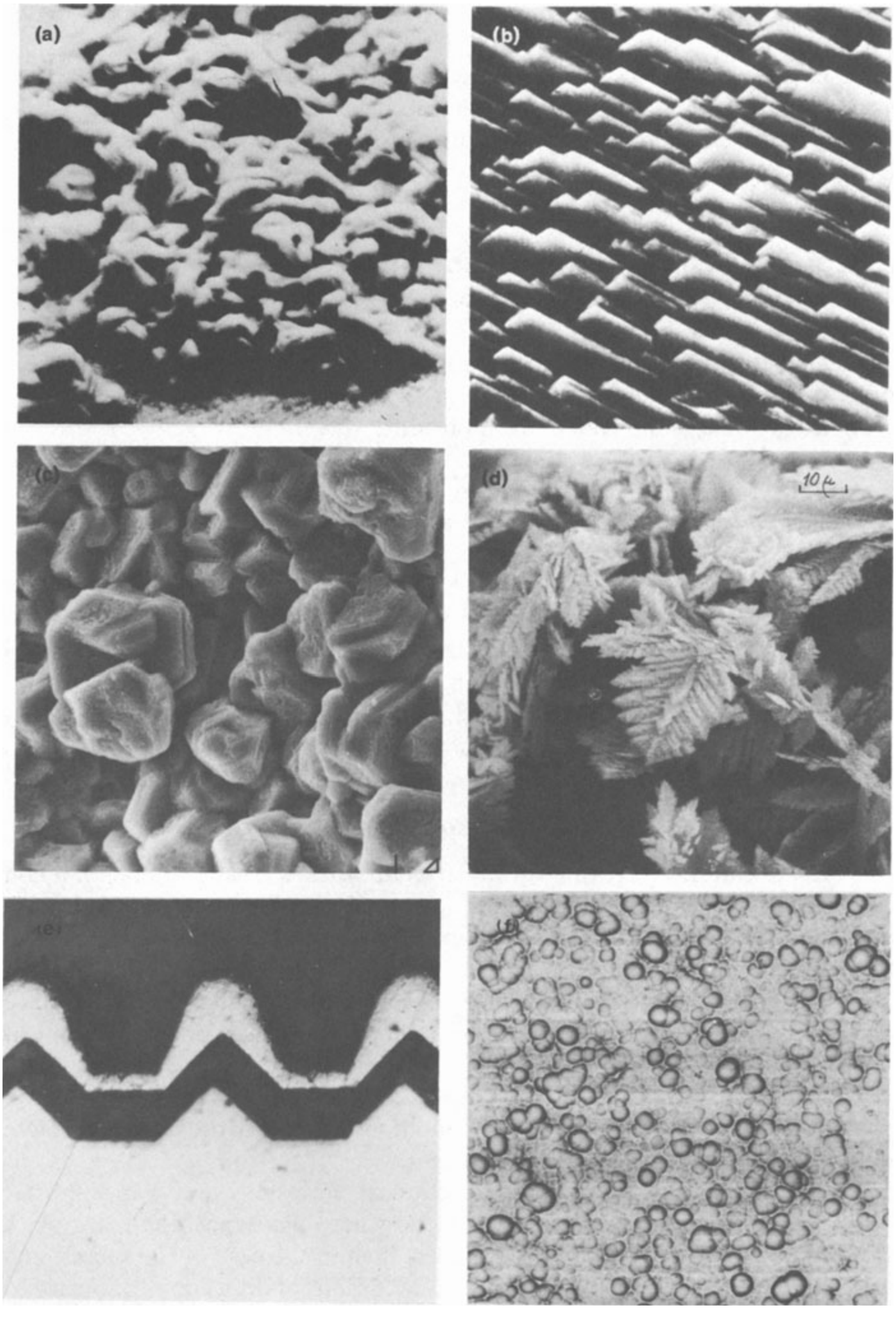

Figure 18. Surface morphology of zinc.

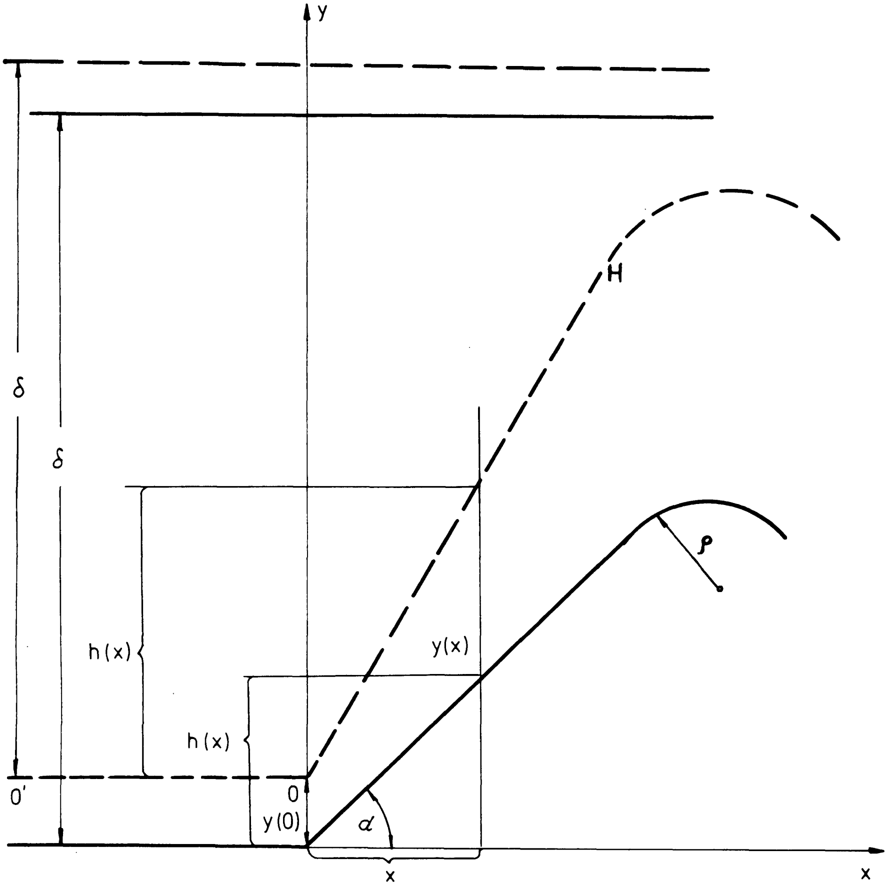

Figure 19. Model of metal deposition under diffusion control onto an elevation rising at an angle α from a surface plane.

An additional effect can be obtained at tips with very small radii of curvature, resulting from a Kelvin-type dependence of the rate of deposition on radius. The problem can be treated in a quantitative manner, assuming the model of the surface shown in Figure 19. One should assess first the limiting conditions, i.e., the highest attainable rates of transport at different parts of the surface.

At the flat part of the surface, the diffusion-limiting current density, in the case of steady state linear diffusion, is

$$i_{L(l)}(0) = zFDC^0/\delta \tag{73}$$

where D is the diffusion coefficient, C^0 the bulk concentration of depositing ions, and δ the Nernst diffusion layer thickness (its meaning indicated in Figure 19).

At the side of an irregularity any point at a distance x from the flat part of the surface is closer to the diffusion layer boundary by $y(x)$ than any point at the flat part of the surface. Hence, the diffusion-limiting current is correspondingly larger, i.e.,

$$i_{L(l)}(x) = \frac{zFDC^0}{\delta + y(0) - y(x)} = \frac{zFDC^0}{\delta - h(x)} \tag{74}$$

$h(x)$ being the height at x.

For a current density below the limiting one, a Butler–Volmer type of equation applies, taking into account the change in concentration of the depositing ions at the electrode surface for the cathodic direction, i.e.,

$$\begin{aligned} i(x) &= i_0\left[\exp\left(\frac{\alpha_a F}{RT}\eta\right) - \frac{C_i}{C_0}\exp\left(-\frac{\alpha_c F_\eta}{RT}\right)\right] \\ &= i_0\left[f_a(\eta) - \frac{C_i}{C_0}f_c(\eta)\right] \end{aligned} \tag{75}$$

The ratio of concentrations of the species M^{z+} to be reduced, at a current density i and in the absence of any current, is related to the ratio of the actual current density and the diffusion-limiting current density by

$$\frac{C_i}{C_0} = 1 - \frac{i}{i_L} \tag{76}$$

Introducing (76) into (75) and rearranging, one obtains

$$i(x) = i_{L(l)}(x)\frac{f_a(\eta) - f_c(\eta)}{i_{L(1)}(x) + i_0 f_c(\eta)} \tag{77}$$

The effective rate of growth of the deposit at the point x relative to the growth at the flat part of the surface is

$$\frac{dh(x)}{dt} = \frac{dy(x)}{dt} - \frac{dy(0)}{dt} = \frac{-M}{\rho zF}[i(x) - i(0)] \tag{78}$$

[the negative sign arising from the fact that the negative (cathodic) current produces positive change in height].

Hence, substituting (74) into (77) and then introducing the resulting relationship both for $i(x)$ and $i(0)$ into (78), and rearranging, one obtains,

$$\begin{aligned} \frac{dh(x)}{h(x)\,dt} &= \frac{MDC_0}{\rho}\,\frac{1 - [f_a(\eta)/f_c(\eta)]}{\{[zFDC_0/i_0 f_c(\eta)] + \delta\}\{[zFDC_0/i_0 f_c(\eta)] + \delta - h\}} \\ &= \frac{A}{B(B - h)} \end{aligned} \tag{79}$$

This can be termed the amplification factor, since it defines the relative rate of increase of the surface coarseness.

The height itself is seen to be an exponential function of time [integral of Eq. (79)], i.e.,

$$h(x) = h_0(x)\, e^{t/\tau_l} \tag{80}$$

with the time constant

$$\tau_l = \frac{\rho}{MD} \frac{[\delta + zFDC_0/i_0 f_c(\eta)]^2}{[1 - f_a(\eta)/f_c(\eta)]C_0} \tag{81}$$

If the surface roughness is defined as

$$\frac{\overline{OA}}{\overline{OB}} = \tan\alpha \tag{82}$$

it follows that the roughness factor is

$$f_r = \left[1 + \left(\frac{h_0}{x}\right)^2 \exp\left(\frac{2t}{\tau_l}\right)\right]^{1/2} \tag{83}$$

i.e., it is also an exponential function of time.

The increase of the height *at the tip of the surface irregularity* is even more intensive. Since the limiting rate of transport is governed there by the spherical diffusion law, i.e.,

$$i_{L(s)} = zFDC^*/r \tag{84}$$

where C^* is the concentration of the depositing species in the vicinity of the tip at a distance sufficiently great as to be considered outside the boundary of the spherical diffusion field. It can be deduced that this should be approximately

$$C^* = C_0(h/\delta) \tag{85}$$

Hence,

$$i_{L(s)} = i_{L(l)}(0)\frac{h}{r} \tag{86}$$

Taking into account that the rate of anodic dissolution at the tip can be somewhat larger than at a flat surface, owing to the Kelvin-type effect, Eq. (77), in this case, reads

$$i(x) = i_{L(s)} \frac{i_0[K(r)f_a(\eta) - f_c(\eta)]}{i_{L(s)} + i_0 K(r) f_c(\eta)} \tag{87}$$

with

$$K(r) = 2\gamma V_m/r \tag{88}$$

where γ is the surface tension, and the amplification factor is obtained as

$$\frac{dh(x)}{h(x)\,dt}=\frac{MDC_0 i_0}{\rho\delta r}\,\frac{K(r)f_a(\eta)-f_c(\eta)}{i_{L(1)}(0)(h/r)+i_0 f_c(\eta)}-\frac{r}{h}\times\frac{f_a(\eta)-f_c(\eta)}{i_{L(l)}(0)+i_0 f_c(\eta)} \tag{89}$$

In early stages of growth, this gives again an exponential dependence of the tip height on time. However, the time constant is now

$$\tau_s=\frac{\rho}{MDC_0[1-K(r)f_a(\eta)/f_c(\eta)]}\,\delta r=\tau_l\,\frac{r}{\delta} \tag{90}$$

Since $r \ll \delta$, the spherical diffusion time constant is smaller than that for linear diffusion, suggesting a faster growth on the tip than on the sides of an irregularity. This should result in a change of the shape of the elevation from a triangular to a paraboloidal one, as in fact is seen in Figure 18E.

At later stages of growth, a linear term in the integral of Eq. (89) prevails. However, as h approaches the value of δ, the model breaks down, and some considerations from the theory of dendritic growth must be applied (cf. below).

An important consequence of the amplification of surface roughness at a constant overpotential is the change of the apparent current density (per unit geometric surface area of the electrode) with time. This was first observed and explained in a qualitative manner by Ibl and Schadegg.$^{(59)}$

On the basis of the above model, a quantitative treatment gives for the local current density at a point (x, z)

$$i_{(x,z,t)}=i(0)+\frac{\rho zF}{M}\,\frac{dh(x)}{dt}=i(0)+\frac{\rho zFh_0(x)}{M\tau}\exp\frac{t}{\tau} \tag{91}$$

or, for the overall current density,

$$i=i(0)+\frac{\rho zF}{M}\left[\frac{S_s(h_0)_s}{\tau_l}\exp\frac{t}{\tau_l}+\frac{S_T(h_0)_T}{\tau_s}\exp\frac{t}{\tau_s}\right] \tag{92}$$

where S_s and S_T represent fractions of the surface pertaining to sides and tips of elevations, respectively.

It is seen that an increase of current density at a constant potential with time is a general phenomenon in metal deposition from pure salt solutions and that it is the more pronounced, the larger is the initial surface roughness (S_s, S_T, $(h_0)_s$, $(h_0)_T$).

The exponential character of the time dependence indicates that the latter can be divided into two periods: for some time after switching on the cathodic overpotential, no change should be observed either in surface roughness or in current. Then a sudden change should appear in both. The first period in phenomena of similar character is termed the *induction time*. In this case, and based on the above model, *the induction time of the amplification of surface roughness* could be derived as

$$t_i=\tau_s A \tag{93}$$

where τ_s is the time constant defined by Eq. (90) and A is a complex quantity reflecting initial surface roughness, diffusion layer thickness, and current density (or overpotential) of deposition.

6.2. The Appearance and Growth of Dendrites

This specific type of deposit (Figure 18, D) has been intensively studied in recent times. Types of morphology were worked out from a large amount of experimental material,(60) while a set of rules governing the kinetics of dendritic growth was established first by Barton and Bockris.(61) These are as follows: (a) A certain critical overvoltage must be exceeded in order to provoke dendritic growth; (b) growth exhibits a certain induction period before it becomes visible; (c) the critical current density for dendritic growth is directly related to the concentration of the depositing ions; (d) the incidence of dendrites increases with increasing overall current density; (e) once a dendrite is seen, it is found to grow at a constant velocity, dependent on overpotential; (f) the rates at which a number of dendrites grow at a given overpotential differ, but there appears to be an upper limit of velocity of propagation; (g) for a given applied overpotential, the dendrites that grow fastest are usually those that were initiated at higher overpotentials; (h) successive increments of overvoltage cause an increase in the velocity of propagation of a particular dendrite, up to a point at which the tip changes configuration, bursting into several smaller dendritic outgrowths or branches; after that the velocity of advancement becomes much less than that of the original dendrite; and (i) upon decreasing the overvoltage, the growth ceases, with the dendrite tip turning from a paraboloidal into a prismatic form.

The basic cause for the appearance of dendrites is the same as that for the amplification of surface roughness, i.e., the formation of a diffusional field of depositing ions, favoring protrusions developing in the direction of increasing concentration. There are, however, three basic differences which make for the specific appearance of dendritic deposits:

(i) There appears to be a critical overpotential needed for the dimension of a dendrite precursor in the direction of the field to start becoming significantly larger than those in the other two directions (change in shape of a screw dislocation with overpotential).

(ii) The development of a definite structure reflects the effect of the crystalline nature of a dendritic protrusion.

(iii) The period of intensive growth of the dendrite is that when it has penetrated through the linear diffusion boundary layer into the bulk solution richer in depositing ions. Hence, the model used in describing the amplification of the surface roughness can be applied only to account for initiation and the induction time of dendritic growth.

For the intensive growth at a constant velocity of propagation (cf. fig. 20), Barton and Bockris(61) compared the rate of deposition onto a moving para-

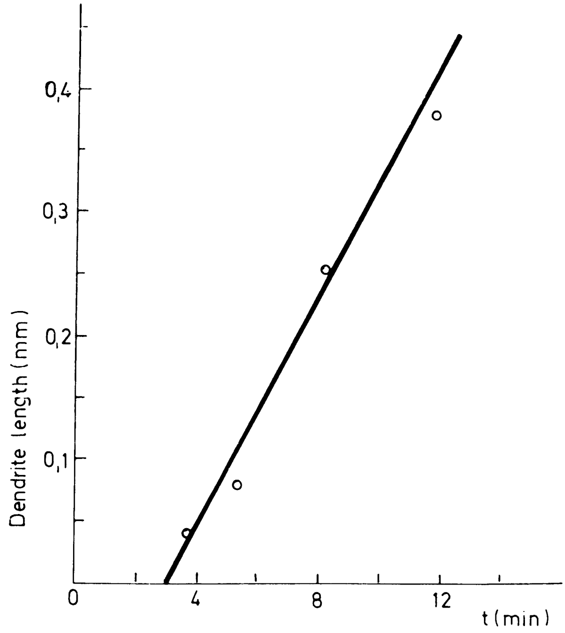

Figure 20. The time dependence of the length of a silver dendrite grown from a molten salt solution of silver ions.

boloidal dendrite tip in its own hemispherical diffusional field with the rate of growth at the flat surface governed by linear diffusion. An exact solution for diffusion toward the former was found in some earlier work.[(62)] In such a case the limiting current density is

$$i_{L(P)} = \frac{zFDC_0}{\rho/2} \frac{\exp(-V_m \Delta C/2)}{E_i(-V_m \Delta C/2)} = \frac{zFDC_0}{\rho/2} \nabla f \tag{94}$$

where ρ is the characteristic tip radius, $\Delta C = (C_0 - C_i)$, E_i is the exponential integral, and ∇f is the Hamilton factor.

This result can be employed with an equation similar to (87) to obtain current densities at dendrite tips over the whole range of overpotentials and tip radii.

At low overpotentials ($\eta \ll RT/F$) and relatively large tip radii, the equation reduced to the original one of Barton and Bockris, viz.,

$$-\eta = \frac{i}{i_0}\frac{RT}{F} + \frac{i(\rho/2)RT}{\nabla_f DC_0 F^2} + \frac{2V_m}{F(\rho/2)} \tag{95}$$

showing contributions due to activation and to diffusion control, and of the Kelvin effect to the overpotential at a dendrite growing at a current density i. (Note that, as a dendrite grows at constant current, the current density decreases owing to increasing crystallite area.)

The use of the full equation indicated the existence of an optimal tip radius at each overpotential for maximum growth rate of the dendrite.[(57)]

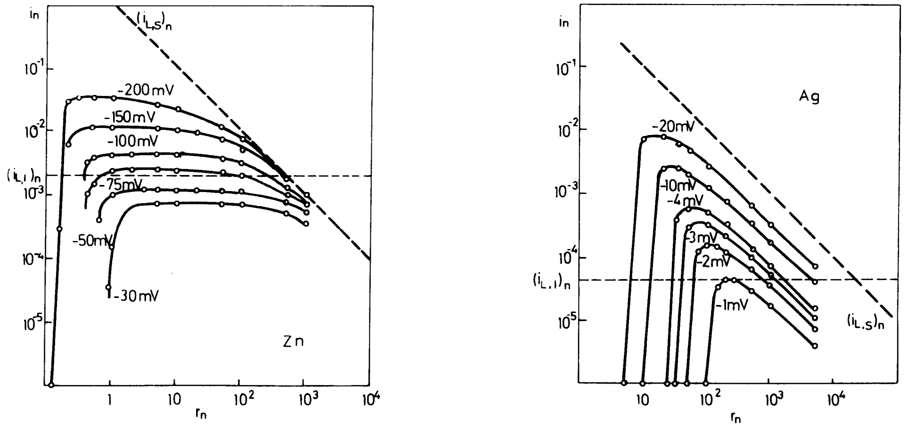

Figure 21. Dependence of the current density at the dendrite tip on the tip radius at different constant overpotentials for the deposition of divalent (Zn) and univalent (Ag) metals: $(i_{L,1})_n$ is the value of the limiting current density of linear diffusion; $(i_{L,s})_n$ is that of the spherical diffusion.

Also criteria for a critical value of current density and of overpotential at which dendritic growth could be detected within a reasonable time were established as

$$i_c = i_0[f_c(\eta) - f_a(\eta)] \gg i_{L(l)} \tag{96}$$

and

$$\eta_c \geq (RT/F)i_{L(l)}/i_0 \qquad \text{for } \eta \ll RT/F \tag{97}$$

$$\eta_c \geq (RT/F)\ln(i_{L(l)}/i_0) \qquad \text{for } \eta \gg RT/F \tag{98}$$

The critical current density depends solely on conditions of diffusion to the flat surface, while the overpotential depends also on the i_0 for the deposition process.

It can be shown that the mechanism of ion reduction, and even more so the i_0 value, has an influence on the range of tip radii in which dendrite propagation should be favored. Thus, as shown in Figure 21, the very fast and simple single-electron exchange with silver leads to sharp peaks of growth rate in a narrow range of tip radii, while the reduction of zinc as a two-step, relatively slow process, exhibits broad plateaus over a wide range of tip radii. This is in accordance with the observation that dendrites of silver propagate rapidly at low overpotentials but arise so infrequently that single incidents can be caught, while zinc dendrites propagate more slowly but are abundant at any overpotential above the critical one because of abundance of precursors in the broad range of radii.

6.3. The Formation of Metal Powders

Powdery metal deposits differ from visibly dendritic ones mainly by a very high degree of dispersion (crystallites being often in the range of 10 μm) which makes the electrode turn black as soon as powder deposition starts, as well as by the fact that they are so loosely adherent to the substrate that they fall off at the slightest provocation.

They were obtained first with silver in the earliest experiments in electrochemistry (Pristley, 1803), and a large number of metals have been obtained in that form by electrodeposition processes since that time. Examples include Cu, Ni, Co, Fe, Pb, Sn, Mn, Zn, Cd, Pd, W, Pt. Detailed surveys of the field are available.(63,64)

Features common to all electrochemical metal powder deposition are the following:

(i) There exists a certain critical value of the current density, i_p, above which powdery deposits are obtained. With some metals (Zn, Cd) and for specific reasons, powders are obtained also in the low-current-density region, lower than that needed for obtaining a compact deposit.

(ii) When the condition of critical current density is overcome, an induction period is found before powder is formed, during which a compact deposit is obtained. This time, t_p, needed for the appearance of powder, can be recorded visually as the electrode is seen to turn suddenly from lustrous to black.

(iii) Powder formation is enhanced by decreasing the concentration of depositing ions, increasing that of the supporting electrolyte, increasing solution viscosity, decreasing the deposition temperature, and slowing down the motion of electrolyte. All these factors lead to a decrease of the particle size.

(iv) It was shown for a large number of electrolytes and depositing metals that the product between the current density and square root of t_p depends linearly on concentration. This is a characteristic of diffusion-controlled processes obeying the Sand equation:

$$i\tau^{1/2} = [zF/2(1 - n_c)]\pi^{1/2}D^{1/2}C_0 \tag{99}$$

where τ is the chronopotentiometric transition time and n_c the transference number of the discharging ion.

In fact, when the current density is corrected for the transference number and t_p is normalized by the value of D, a single linear dependence on concentration is obtained for different depositing metals as seen in Figure 22.

Hence, there is little doubt that the reasons behind powder formation are the same as those for the amplification of surface roughness or the formation of dendritic deposits, i.e., propagation of metal particles depositing under transport control, up the concentration gradient toward solutions ever richer in depositing species.

However, while amplification of surface roughness starts taking place as soon as there appears any significant change in concentration at the electrode surface with respect to the bulk of solution and while dendrites start developing significantly below the diffusion-limiting current, powders are formed only under limiting current conditions or, in the case of constant current density, close to the transition time leading to some other electrode process.

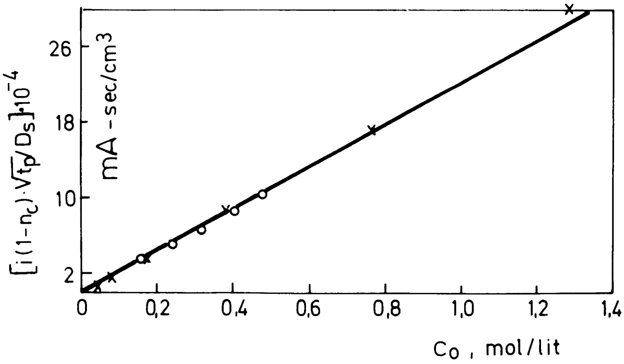

Figure 22. Dependence of $i(1 - n_c)(t_p/D_s)^{1/2}$ on bulk concentration of $CdSO_4$ (×) and $CuSO_4$ (O).

This fact led to explanations of small size and poor adherence of powder particles. The former is likely to be due to a high nucleation rate as a result of the high polarization needed for achieving limiting current conditions, causing distribution of depositing material onto a very large number of small particles. The latter is suggested(65) to be due to increasing distance from the electrode surface at which the reduction of ions takes place by quantum mechanical electron tunneling, resulting in a kind of homogeneous phase nucleation and growth of metal crystals.

6.4. Effect of Periodically Changing Conditions of Deposition

It is a rather old experience in electroplating practice that periodic changes of current lead to improvement in the quality of the deposit. Such changes are of three types: periodic current reversal, sinusoidal ac superimposed on direct cathodic current, and pulsating current. A detailed review of the subject is available.(57) The effect is well demonstrated in Figure 23, showing the yield of dendrites during cathodic deposition of zinc as a function of the ratio of the superimposed ac density to the basic direct current density.(66)

Understanding the reasons behind the above-cited effects can be achieved by a quantitative consideration of the deposition of a metal with a very high exchange current density, under conditions of potential pulsation between a value providing a high cathodic current density and a value bringing the current to zero (reversible potential). The calculations showed that under such conditions, the change in concentration with distance away from the electrode indicates the existence of two different diffusion layers superimposed on each other.

After a steady state is established, there exists a stable concentration profile from a point close to the electrode surface (where the concentration is half of that in the bulk) toward the bulk of solution, which determines a diffusion layer similar to that obtained with direct current deposition at the

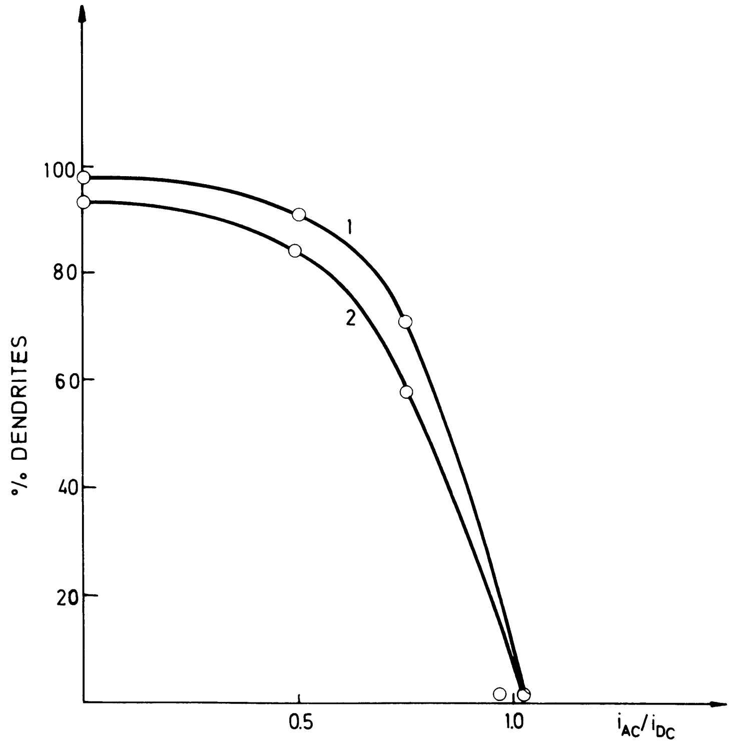

Figure 23. Yield of dendritic deposit as a function of the ratio i_{ac}/i_{dc} in the deposition of zinc from alkaline zincate solution.

same average current density. This profile is insensitive to the amplitude or frequency of pulsation.

At the electrode surface, however, there is another, periodically changing concentration profile due to the fact that the pulsating potential causes the concentration at the surface to oscillate between the bulk value (at the reversible potential—"off" period) and a value close to zero (limiting current). This concentration profile defines another diffusion layer, whose thickness again becomes stabilized, when a steady state is achieved, to a value

$$\delta_N = \frac{C_0}{(\partial c/\partial x)_{x=0}} = \frac{D^{1/2}\tau^{1/2}T^{1/2}}{(2n+1)^{-1/2} - (2n)^{-1/2} + (2n-1)^{-1/2} - \cdots + 1}$$
$$= \frac{D^{1/2}\tau^{1/2}T^{1/2}}{a} \qquad (100)$$

where T is the pulse duration, n is the number of pulses, and $a = 0.606$ represents the asymptotic value of the denominator.

Since T is inversely proportional to the frequency of pulsation, it is seen that this diffusion layer is thinner the higher is the frequency. At some frequency, it becomes comparable to or smaller than the dimensions of surface irregularities. When deposition is carried out under such conditions, the diffusion layer follows closely the surface profile, providing a constant diffusion flux at all points. Hence, the basic conditions for the amplification of surface roughness do not exist, (i.e., the diffusion boundary layer displaced from the surface profile and flat), so that the surface profile is reproduced during growth without any amplification.

With some differences in the quantitative aspects, the effects of the diversity of periodically changing conditions of deposition seem all to have basically the same origin.

6.5. The Phenomenon of Electropolishing

In some electrolytes (e.g., phosphoric acid) an effect opposite to amplification of surface roughness is found upon anodic dissolution, i.e., the surface becomes increasingly smooth, until a mirrorlike finish is achieved. This phenomenon has been widely used for practical purposes of electropolishing, since the work of Jacquet in 1936.(67)

It was found(68) that electropolishing occurs in systems which, under anodic dissolution, exhibit a limiting current characteristic of diffusion control, i.e., currents are dependent on flow rate of the electrolyte past the anode, as shown in Figure 24. Over a certain range of potentials at the limiting current plateau, at which maximum brilliance is obtained, oscillations of potential occur at a virtually constant current density, with an amplitude of over 0.40 V, and without appreciable damping.(69) Also, a significant photoelectrochemical effect is found.(70)

This indicates the existence of a photosensitive semiconducting film and its possible role in obtaining the electropolishing effect.

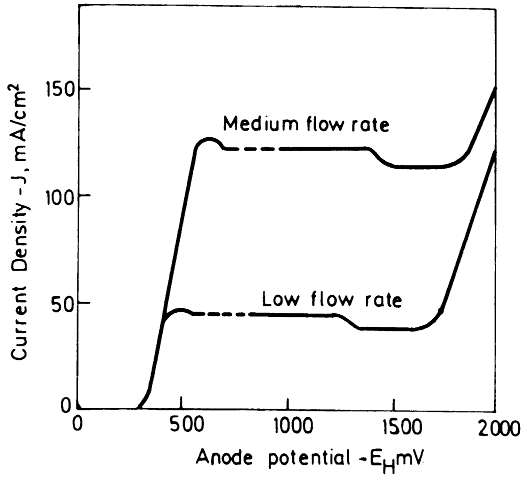

Figure 24. Schematic polarization curves of the copper–phosphoric acid electropolishing system.

Nevertheless, there seems to be sufficient evidence that electropolishing is an essentially transport-controlled process. Thus, the transition time, τ, is observed under galvanostatic conditions, with the Sand product, $i\tau^{1/2}$, being constant for a given electrolyte and reciprocal with the square root of its viscosity. Yet the Faradaic efficiency is found to be virtually 100%, and hence there can be no doubt that there is no other process leading to electropolishing except anodic dissolution of the metal.

Experiments with a phonograph record negative(71) revealed that a decrease in the depth of the prismatic microgroove is a function of quantity of electricity passed, and that this effect is at a maximum in a unstirred bath, decreasing with stirring. Similar experiments with a sinusoidal profile(72) demonstrated a very regular exponential decrease of the amplitude with time; the slope of the plots in semilog coordinates, as shown in Figure 25, depends on the concentration of phosphoric acid.

A number of reasons have been put forward for the smoothing effect of the anodic dissolution current. Thus, Jacquet(67) ascribed it to the primary current distribution, i.e., higher concentrations of current lines arrive at the more elevated parts of the surface than on the bottoms of recesses. However, although it should exist in principle, this effect cannot be significant under normal conditions of conductivity of the metal and the electrolyte. Moreover, if this model was valid, no dependence on stirring should be observed.

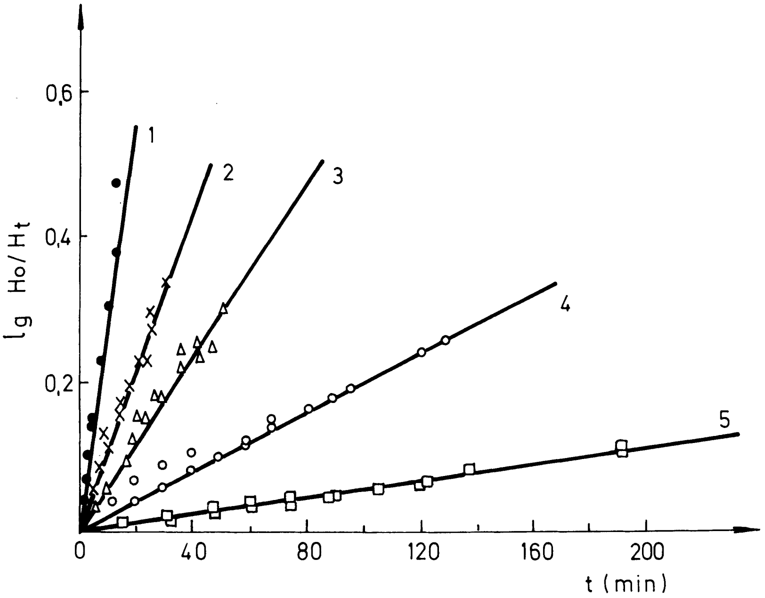

Figure 25. Dependence of log of depth of recess of the profile on bronze on time for different wavelengths a in 10 M H_3PO_4. Concentrations of H_3PO_4 (mol liter^{-1}); 2(1), 5(2), 7.5(3), 10(4), and 15(5).

The Kelvin-type effect has also been forwarded as a reason, since the surface free energy of metal atoms should be larger at peaks of elevations than at flat portions of the surface.(73) This should be true also of any defects or imperfections caused, e.g., by mechanical treatment of the surface.(74)

Passive films may be formed more easily at recesses than at peaks, thus producing a beneficial variation in current density of dissolution over the surface.(75,76) In special cases, preferential adsorption of some species (e.g., ClO_4^- at aluminum) at peaks may lead to destruction of the passive film at those points, with resulting faster dissolution.(77)

Nevertheless, the basic reason should still be found in transport phenomena similar to those leading to amplification of the surface profile in the opposite process of cathodic deposition: the diffusion flux of products of anodic dissolution away from the surface is larger at elevated points than at recesses, since the effective diffusion layer thickness is smaller at the former than at the latter,(78,79) and there is also an increased diffusion flux in the convex diffusion field at the peaks, leading to conditions close to those of spherical diffusion. However, diffusion away from the electrode in anodic processes is known not to lead to any limiting current, unless the solubility limit of the reaction product is reached or a very steep viscosity increase follows increase in concentration. Hence, a more likely cause could be found in the limitations of diffusion toward the electrode of an agent complexing the reaction product.(71,80)

A quantitative treatment,(80) essentially similar to that of amplification of surface roughness, results in an exponential decrease in the amplitude of the surface profile, viz.,

$$h = h_0 e^{-t/\tau} \tag{101}$$

with

$$\tau = a\delta/2\pi DVC^0 \tag{102}$$

For electropolishing a copper surface with sinusoidal grooves of 70 nm in wavelength in phosphoric acid baths, the time constant was found to be in the range between 3.6×10^3 and 2.2×10^4 for phosphoric acid concentrations ranging from 5 to 13 mol dm^{-3}, respectively.

7. Effect of Adsorption of Foreign Substances on Surface Morphology of Metal Deposits

Adsorption of species other than the depositing ions, and in particular of organic molecules or inorganic and organic colloids, can have significant effects on the surface morphology of deposits.

Thus, granular growth of the type shown in Figure 18c is likely to be due to adsorption of colloidal particles of zinc hydroxide, stopping the growth after a certain size of the crystallite is reached and preventing coalescence.

When soluble organic macromolecules are added (e.g., polyvinylpyridine copolymerized with methyl methacrylate) spheroidal forms of metal crystallites tend to be produced, as shown in Figure 18f.

In homogeneous phase crystallization, adsorption is known to affect morphology by selective adherence of foreign molecules on some crystal planes. Those planes are known to develop most, at which adsorption is strongest. Development of spheroids is an indication of such strong adsorption on all possible crystal planes, so that no set of planes is favored. Hence, although the crystal structure is preserved inside the metal phase (the particles can even be monocrystalline), it is lost in the globular outer appearance.

Interesting effects are obtained when adsorption is in competition with transport control of the deposition process. Two phenomena can then appear, as will be described below.

7.1. The Growth of Whiskers

Whiskers are long, threadlike metal crystals which differ from dendrites in that (i) they have significantly larger ratios between the longitudinal and the lateral dimensions, (ii) they exhibit no tendency to form side growths or branch, (iii) they exhibit an increased electrical resistivity (e.g., with silver, 2–3 times compared to the pure metal) and increased tensile strength (an order of magnitude larger than in pure metal crystals), and (iv) they are often single crystals.

A typical case is the growth of silver whiskers by cathodic reduction from concentrated silver nitrate solutions (0.3 M) containing certain organic additives such as oleic acid, gelatine, albumin, or n-heptyl, n-octyl, and n-nonyl alcohols, or, from silver nitrate solutions "aged" for several weeks.(81) Copper whiskers can be grown from solutions containing a variety of additives or hydroxylamine ions in the presence of chlorides.

It appears that the following set of phenomena is generally met in the growth of whiskers:

(i) A critical current density exists for formation of each whisker and is related to its lateral dimensions: the thinner the whisker, the higher is the critical current density needed for its growth.

(ii) Whiskers grow in a single direction but dissolve anodically at a uniform rate on all sides, with much lower overpotential than that needed for growth. Hence, anodic dissolution produces thinning of whiskers.

(iii) Initiation requires a higher overpotential than that for the subsequent growth.

(iv) If the growth is interrupted for a longer period, it may be continued at the tip upon repeating the overpotential step, but usually assuming a new direction; or else it may not continue to grow at all, but a new one could appear elsewhere.

(v) The interruption time needed for cessation of growth is related to the concentration of the additive.

The phenomenon of whisker growth presents a good example of competition between agglomeration of additive molecules by adsorption and that of metal atoms produced by discharge. According to the model of Price, Vermilyea, and Webb,(85) adsorption is overwhelming at all crystal planes except one. At this particular one, deposition of metal atoms is favored and the adsorbing molecules of the additive are buried inside the metal phase.

An equation was derived based on such a model. It defines the critical current density as

$$i_c = \left(4 \times 10^{-14} \frac{hM^2\gamma^2 D_i b^2}{\alpha a\rho^2 zF} \frac{C_i}{r}\right)^{1/3} = A\left(\frac{C_i}{r}\right)^{1/3} \tag{103}$$

where h and a are heights of the molecule of the additive at the surface, and the surface step, respectively, α is the area covered by each metal atom. γ is the work of building a crystal edge of unit length, b is the proportionality constant between overpotential ($\eta < 10$ mV) and current density, D_i and C_i are the diffusion coefficient and the concentration of the additive, respectively, and r is the whisker radius.

The theory seems to be in good agreement with experiment, with the order-of-magnitude calculation of A being based on independently assessed parameters.

The minimum time of interruption could also be calculated, assuming this to be equal to the time needed to block the surface completely by adsorption of the additive. This is, then,

$$t = mr/ND_iC_i \tag{104}$$

where m is the number of molecules needed to block 1 cm^2 of the surface (10^{13} cm^{-2}). The fit of experimentally observed values is seen in Figure 26.

7.2. Leveling in Metal Deposition

An effect opposite of amplification of surface roughness, yet under similar conditions of plating, has been known to occur when specific substances are added to the electrolyte: surface irregularities are increasingly buried within the deposit in prolonged cathodic deposition and smooth surfaces result. Early work of Meyer,(86) Schmellenmeier,(87) and Gardam(88) showed that this effect of leveling is due to more rapid metal deposition at recesses than at elevated points of the surface.

This phenomenon involves irregularities not larger than 100 nm in amplitude, and the quality of an electrolyte required to produce such an effect was measured by the so-called "microthrowing power."

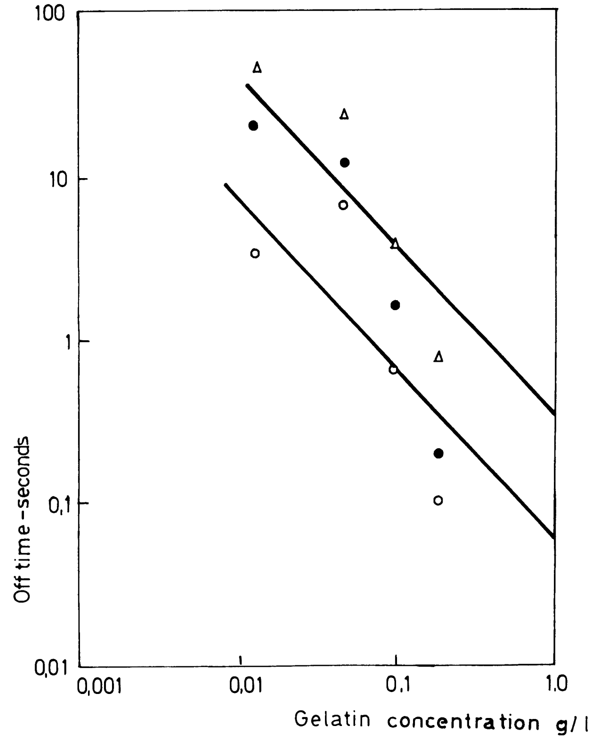

Figure 26. Effect of impurity concentration on the time required for contamination of the tip of a whisker during the period of zero current flow.

Detailed reviews exist on this phenomenon, which is of great importance for the practice of plating.(89–92)

It has been demonstrated(93) that, very much as in electropolishing, the amplitude of a sinusoidal surface profile decreases exponentially with time of deposition, the time constant increasing with increasing wavelength of the profile and decreasing proportionally to deposit. When this condition is achieved, the supply of the additive is faster at the elevations than at recesses.

Hence, its surface concentration, which is determined by the balance between the rate of supply and the rate of burial, is larger at elevations with a resulting stronger inhibition of the deposition process.

A quantitative interpretation can be made using this model and a result similar to the ones described earlier, for other transport-controlled processes, is obtained. The observed exponential decay of surface roughness is obtained with the time constant

$$\tau = \frac{\mathrm{a}}{A[B(C^0_{\mathrm{ad}}/\delta) - i]} \coth\left(\frac{2\pi\delta}{\mathrm{a}}\right) \tag{105}$$

i.e., it is seen to depend on the difference between a term reflecting the

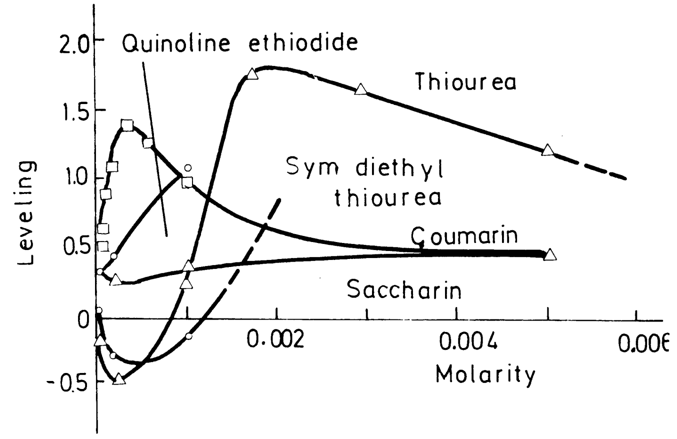

Figure 27. Experimental graphs of leveling versus addition-agent concentration.

diffusion flux of the additive (being proportional to the additive concentration, C^0_{ad}, and the diffusion layer thickness, δ) and the current density of metal deposition, as well as on the ratio between the "wavelength" of the surface profile, a, and δ.

The surface concentration of the additive can also be evaluated$^{(92)}$ as

$$C^s_{ad} = \frac{C^0_{ad}}{(K_d/K_a) + \{(1/K_a) + [1/(D/\delta_N)]\}\{(M/zF\rho h) + [K^0_r/(i_0)^\alpha]i^{(\alpha-1)}\}i} \tag{106}$$

where K_a and K_d are rate constants of the adsorption–desorption process, K^0_r is the rate constant of the potential-dependent reduction of the additive at the electrode, and α is the ratio of transfer coefficients for the additive reduction and the metal deposition processes. When the additive is strongly adsorbed, Eq. (106) reduces to

$$C^s_{ad} = \frac{DC^0_{ad}/\delta}{\{(M/zF\rho h) + [K^0_r/(i^0)^\alpha]i^{(\alpha-1)}\}i} \tag{107}$$

i.e., it is determined essentially by the limiting rate of diffusion of the additive and the rate of its disappearance in the two ways. The theory has been compared with experiment and a good agreement is claimed.

8. Conclusion

Based on the above considerations, it seems justified to say, in conclusion, that basic phenomena in electrochemical deposition and dissolution of metals have been well-defined and rather well understood, in some cases even in a semiquantitative manner, so that correlations between electrochemical parameters and kinetic and morphological features can be established.

There are still many details, however, which could be of considerable significance in practice, which require further study before a satisfactory level of predictability of behavior of these complex electrochemical systems is reached.

Acknowledgments

The author is indebted to Dr. Milica Beck for useful remarks and to Mr. Vladimir Jović for his assistance in the technical preparation of the manuscript.

References

1. W. M. Latimer, *The Oxidation States of the Elements and Their Potentials in Aqueous Solutions*, 2nd ed., Prentice-Hall, Englewood Cliffs, New Jersey (1952).
2. G. Milazzo and S. Caroli, *Tables of Standard Electrode Potentials*, John Wiley & Sons, New York (1978).
3. L. J. Antropov and V. P. Tchviruk, *Elektrokhimiya* **3**, 1351 (1967).
4. L. F. Kozin, *Amalgamnaya Metallurgiya*, Kiev (1970), p. 14.
5. J. O'M. Bockris and A. K. N. Reddy, *Modern Electrochemistry*, Vol. 2, Plenum Press, New York (1970).
6. Cf., e.g., W. J. Lorenz, H. D. Hermann, N. Wuthrich, and F. Hilbert, *J. Electrochem. Soc.* **121**, 1167 (1974).
7. B. N. Kabanov, J. G. Kiseleva, and J. J. Astakhov, *Elektrokhimiya* **8**, 955 (1972).
8. H. Gerischer, D. M. Kolb, and J. K. Sass, *Advances in Physics* **27**, No. 3 (1978), p. 437.
9. G. J. Hills, in *Reference Electrodes*, D. J. G. Ives and G. J. Janz, eds., Academic Press, New York (1961), Chap. 10, p. 433.
10. *Stability Constants of Metal-Ion Complexes*, IUPAC Chemical Data Series, No. 22, Compl. by D. D. Perrin, Pergamon Press, Oxford (1979).
11. M. Pourbaix, *Atlas of Electrochemical Equilibria in Aqueous Solutions*, Pergamon Press, Oxford (1966).
12. J. E. B. Randles, in *Trans. Symp. Electrode Processes, Philadelphia, 1959*, John Wiley & Sons, New York (1961), p. 209.
13. G. C. Barker, R. L. Fairdoth, and A. W. Gardner, *Nature* **181**, 247 (1958).
14. A. R. Despić, V. D. Jović, and M. V. Djorović, *Isr. J. Chem.* **18**, 65 (1979).
15. V. A. Roiter, V. A. Juza, and E. S. Poluyan, *Acta Physicochim. USSR* **10**, 389 (1939); **10**, 845 (1939).
16. A. R. Despić and J. O'M. Bockris, *J. Chem. Phys.* **32**, 389 (1960).
17. B. E. Conway and J. O'M. Bockris, *Proc. R. Soc. London Ser. A* **248**, 394 (1958).
18. K. J. Vetter, *Z. Naturforsch.* **7a**, 328 (1952); cf. also K. Vetter, *Elektrochemische Kinetik*, Springer Verlag, Berlin (1961).
19. W. Lorenz, *Z. Naturforsch.* **9a**, 716 (1954); *Z. Elektrochem.* **58**, 912 (1954).
20. J. O'M. Bockris, D. M. Drazic, and A. R. Despić, *Electrochim. Acta* **4**, 325 (1961).
21. T. P. Hoar and T. Hurlen, in *Proceedings of the 8th CITCE Meeting, Madrid, 1956*, Butterworths, London (1958).

22. J. O'M. Bockris and A. R. Despić, in *Physical Chemistry*, Vol. 9B, Eyring, Henderson, Jost, eds., Academic Press, New York (1970), Chap. 7, p. 639.
23. K. E. Heussler, *Z. Elektrochem.* **62**, 582 (1958).
24. H. Gerischer, *Z. Elektrochem.* **57**, 605 (1953); *Z. Phys. Chem.* (*Leipzig*) **A202**, 302 (1953).
25. A. R. Despić, Dj. Jovanovic, and T. Rakic, *Electrochim. Acta* **21**, 63 (1976).
26. I. Epelboin, M. Ksouri, and R. Wiart, *J. Electrochem. Soc.* **122**, 1206 (1975).
27. J. O'M. Bockris and M. Enyo, *Trans. Faraday Soc.* **58**, 1187 (1962).
28. J. O'M. Bockris and H. Kita, *J. Electrochem. Soc.* **109**, 928 (1962).
29. A. Brenner, *Electrodeposition of Alloys. Principles and Practices*, Academic Press, New York (1963).
30. K. M. Gorbunova and Yu. M. Polukarov, *Adv. Electrochem. Electrochem. Eng.* **5**, 249 (1967).
31. T. L. Rama-Char and J. Vaid, *Plating* **48**, 871 (1961); *Met. Finish.* **59**, 44 (1961); *Metalloberfl.* **16**, 70 (1962).
32. A. N. Frumkin, *Elektrokhimiya* **1**, 394 (1965); **1**, 1288 (1963).
33. G. E. Kimball, *J. Chem. Phys.* **8**, 199 (1940).
34. M. Fleischmann and H. R. Thirsk, *Adv. Electrochem. Electrochem. Eng.* **3**, 123 (1963).
35. G. J. Hills and D. J. G. Ives, *J. Chem. Soc.* 311 (1951).
36. J. O'M. Bockris, M. A. V. Devanathan, and A. K. N. Reddy, *Proc. R. Soc. London Ser. A* **279**, 327 (1964).
37. J. W. Diggle, T. C. Downie, and C. W. Goulding, *Chem. Rev.* **69**, 365 (1969).
38. W. O. Kroenig and V. N. Uspenskaja, *Korros. Metallschutz.* **11**, 10 (1935).
39. R. G. Raicheff, A. Damjanovic, and J. O'M. Bockris, *J. Chem. Phys.* **47**, 2198 (1967).
40. M. A. V. Devanathan and M. J. Fernando, *Electrochim. Acta* **15**, 1623 (1970).
41. H. Gerischer and H. Rickert, *Z. Metallk.* **46**, 681 (1955).
42. T. P. Hoar and J. M. West, *Nature* **181**, 835 (1958).
43. Cf. A. R. Despić, in *MTP International Rev. of Sci. Physical Chem.*, Ser. 1, Vol. 5, Electrochem., Butterworths, London (1973), Chap. 3.
44. R. G. Raicheff and A. R. Despić, *C. R. Acad. Bulg. Sci.* **23**, 535 (1970).
45. H. Fischer, *Elektrolytische Abscheidung und Elektrokrystallisation von Metallen*, Springer Verlag, Berlin (1954).
46. F. C. Frank and J. H. Van der Merve, *Proc. R. Soc. London Ser. A* **198**, 205 (1949); **198**, 216 (1949); **200**, 125 (1949).
47. G. J. Finch, H. Wilman, and L. Yang, *Discuss. Faraday Soc.* **1**, 144 (1947).
48. N. A. Pangarov and St. Rashkow, *Bull. Inst. Phys. Chem.* **1**, 79 (1960); *C. R. Acad. Bulg. Sci.* **13**, 555 (1960).
49. R. M. Bozorth, *Phys. Rev.* **26**, 390 (1925).
50. K. M. Gorbunova, O. S. Popova, A. A. Sutyagina, and Y. M. Polukarov, *Crystal growth*, Rept. Congr. Crystal Growth, Moscow, Izd. Akad. Nauk SSSR, Moscow, p. 58.
51. N. A. Pangarov, *Electrochim. Acta* **9**, 721 (1964).
52. A. K. N. Reddy, *J. Electroanal. Chem.* **6**, 141 (1963).
53. R. Weil, *Plating* **57**, 881 (1970).
54. M. Ya. Popereka, *Internal Stress in Electrolytically Deposited Metals*, Indian Nat. Sci. Center, New Delhi (1970).
55. R. Weil, *Plating* **57**, 1231 (1970); **58**, 50 (1971); **58**, 137 (1971).
56. V. A. Lamb and D. R. Valentine, *Plating* **52**, 1289 (1965).
57. Cf. A. R. Despić and K. I. Popov, in *Modern Aspects of Electrochemistry*, Vol. 7, B. E. Conway and J. O'M. Bockris, eds., Plenum Press, New York (1972), Chap. 4, p. 199.
58. S. J. Kritchmar, *Elektrokhimiya* **1**, 609 (1965).
59. N. Ibl and K. Schadeg, *J. Electrochem. Soc.* **114**, 54 (1967).
60. G. Wranglen, *Electrochim. Acta* **2**, 130 (1960).
61. J. L. Barton and J. O'M. Bockris, *Proc. R. Soc. London Ser. A* **268**, 485 (1962).
62. G. P. Ivantsov, *Dokl. Akad. Nauk SSSR* **58**, 567 (1947).

63. N. Ibl, *Advances in Electrochemistry and Electrochemical Engineering*, Vol. 2, Interscience, New York (1962).
64. A. Calusaru, *Depunerea Electrolitica a purberilor metalica*, Editura Stiutifica si enciclopedica, Bucharest (1976); A. Calusaru, *Electrodeposition of Metal Powders*, Elsevier, Amsterdam (1979).
65. J. Atanasiu and A. Calusaru, *Studii si cercetari de metalurgie* **2**, 337 (1957); *CA* **52**, 1347oh (1958).
66. V. V. Romanov, *Zh. Priklad. Khim.* **34**, 2692 (1961).
67. P. A. Jacquet, *Bull. Soc. Chim. France* **3**, 705 (1936); *Trans. Electrochem. Soc.* **69**, 629 (1936).
68. T. P. Hoar and G. P. Rothwell, *Electrochim. Acta* **9**, 135 (1964).
69. B. Pointu, *Electrochim. Acta* **14**, 1207 (1969).
70. T. V. Grechukhina and A. Sh. Valeyev, *Elektrokhimiya* **3**, 1080 (1967).
71. J. Edwards, *J. Electrochem. Soc.* **100**, 189C (1953); **100**, 223C (1953).
72. S. J. Krichmar, *Zh. Priklad. Khim.* **37**, 2244 (1964).
73. U. R. Evans, *Trans. Electrochem. Soc.* **69**, 652 (1936).
74. G. S. Vozdvizhenskii, *Dokl. Akad. Nauk SSSR* **59**, 1587 (1948).
75. T. P. Hoar and J. A. S. Mowat, *Nature* **165**, 64 (1950).
76. K. Huber, *Chimia* **4**, 54 (1950); see also *Z. Elektrochem.* **55**, 165 (1951).
77. E. Darmois and M. J. Epelboin, *Bull. Soc. France Electriciens.* **4**, 344 (1954).
78. W. C. Elmore, *J. Appl. Phys.* **10**, 724 (1939); **11**, 797 (1940).
79. S. J. Krichmar, *Dokl. Akad. Nauk SSSR* **100**, 481 (1955).
80. C. Wagner, *J. Electrochem. Soc.* **101**, 225 (1954).
81. K. M. Gorbunova and A. J. Zhukova, *Zh. Fiz. Khim.* **23**, 605 (1949).
82. K. M. Gorbunova, *Dankov. Zh. Fiz. Khim.* **23**, 616 (1949).
83. P. A. Van der Meulen and H. V. Lindstrom, *Trans. Electrochem. Soc.* **103**, 390 (1956).
84. T. C. J. Ovenston, C. A. Parker, and A. E. Robinson, *Trans. Electrochem. Soc.* **104**, 607 (1957).
85. P. B. Price, D. A. Vermilyea, and M. B. Webb, *Acta Metal.* **6**, 524 (1958).
86. W. R. Meyer, *Proc. Am. Electroplaters Soc.* **23**, 116 (1935); **23**, 135 (1935); **24**, 135 (1936).
87. H. Schmellenmeier, *Korrosion u. Metallsch.* **21**, 9 (1945).
88. G. E. Gardam, *J. Electrodep. Techn. Soc.* **22**, 155 (1947).
89. E. B. Leffler and H. Leidheizer, *Plating* **44**, 388 (1957).
90. A. T. Vagramyan and Z. A. Solovyova, *Methody Issledovaniya Electroosazhdeniya Metallov*, Moscow (1960).
91. O. Kardos and D. G. Foulke, in *Advances in Electrochemistry and Electrochemical Engineering*, Vol. 2, Interscience, New York (1962).
92. O. Kardos, *Proc.* "*Surface 66*", Forster Verl., Zurich (1967), p. 62.
93. S. J. Krichmar and A. Ya. Pronskaya, *Zh. Fiz. Khim.* **39**, 741 (1965).
94. S. A. Watson and J. Edwards, *Trans. Inst. Met. Finish.* **34**, 167 (1957).
95. R. C. V. Piatti, A. J. Arvia, and J. J. Podesta, *Electrochim. Acta* **14**, 541 (1969).
96. K. E. Heussler and L. Gaiser, *Electrochim. Acta* **13**, 59 (1968).
97. L. B. Harris, *J. Electrochem. Soc.* **120**, 1036 (1973).
98. D. M. Dražić, L. Ž. Vorkapić, *Bull. Soc. Chim. Beograd* **46**, 595 (1981).

8

Processes at Semiconductor Electrodes

R. MEMMING

1. Introduction

Until about 1960 the metal–electrolyte interface was probably the most extensively investigated surface. Semiconductor electrodes also have a considerable history, dating back at least as far as Bequerel's work on silver halides.(1) Almost all the early studies with semiconducting electrodes were performed with materials of uncontrolled and generally unknown properties.

The modern work on semiconductor electrodes dates back to the growth of well-defined single crystals of germanium. It is interesting to note that the first semiconductor amplifier ever built was, in fact, the field device of Brattain and Gibney(2) in which the modulating field was applied across an electrolyte contact. The first systematic investigations of the semiconductor–electrolyte interface were conducted by Brattain and Garrett.(3) Since then much research has been done with many semiconducting electrodes and most of the basic processes are now well understood.

From electrochemical investigations with semiconductor electrodes, not only information about properties of the electrode material has been obtained, but also information about basic mechanisms of electron transfer processes between the solid electrode and molecules in the electrolyte. In the latter case, semiconductor and organic electrodes have certain advantages over metal electrodes: (i) In a semiconductor or organic crystal, well-defined energy

---

R. MEMMING • Philips GmbH Forschungslaboratorium Hamburg, D-2000 Hamburg 54, Postfach 540840, Federal Republic of Germany.

bands or states exist which are involved in the electron transfer process; (ii) the carrier density is much smaller than in a metal and can be varied over many orders of magnitude; (iii) the occupation of energy levels by electrons and holes can be increased by optical excitation.

Following the early stage of germanium and silicon electrochemistry, a considerable number of compound semiconductors have been studied during the last 15 years. Especially investigations with materials of large band gaps ($E_g \geq 1.4$ eV) have contributed to a better understanding of the energy parameters and kinetics of electrochemical reactions. In recent years, the interest in semiconductor electrodes has ever increased because of its possible application in solar energy conversion systems.

In the present chapter, the basic processes at semiconductor electrodes are described, mainly in terms of energy diagrams. The main emphasis is laid on electron transfer reactions stimulated by light excitation, the light being absorbed either by the electrode or by molecules in the electrolyte. For comparison some results are also discussed, which are obtained with electrodes consisting of organic molecular crystals.

2. Potential and Charge Distribution at Solid–Electrolyte Interfaces

At the interface of a solid and electrolyte a double layer is formed by adsorption of ions or molecules, by oriented dipoles, or by the formation of surface bonds between the solid and species in the solution. The thickness of such a Helmholtz double layer is of the order of a few nanometers. Between the two phases a potential difference U_H occurs. The charges on the solid surface are electrons and in the electrolyte they are ions. In very dilute solutions (low ion concentration), the countercharges in the electrolyte are not only located at the outer side of the Helmholtz double layer but are distributed over a certain distance in the electrolyte (space charge Gouy layer in the electrolyte). In the following, only those cases are considered in which the ion concentration is sufficiently large, so that any space charge in the electrolyte can be neglected.

A space charge region in the solid exists if the electron density is very small, as in the case of semiconductors and insulators. In metals the electron density is very high so that at a metal–electrolyte interface only the potential drop across the Helmholtz layer, U_H, exists, as shown in Figure 1a. In the case of a semiconductor electrode, however, a potential drop U_{SC} also occurs across the space charge layer due to the low electron density as shown in Figure 2a. The existence of such a space charge layer is not limited to semiconductor–electrolyte interfaces but occurs also at other interfaces between semiconductors and metals and between semiconductors of different doping (*pn* junctions), as was realized by Brattain and Garrett(3) already in 1955.

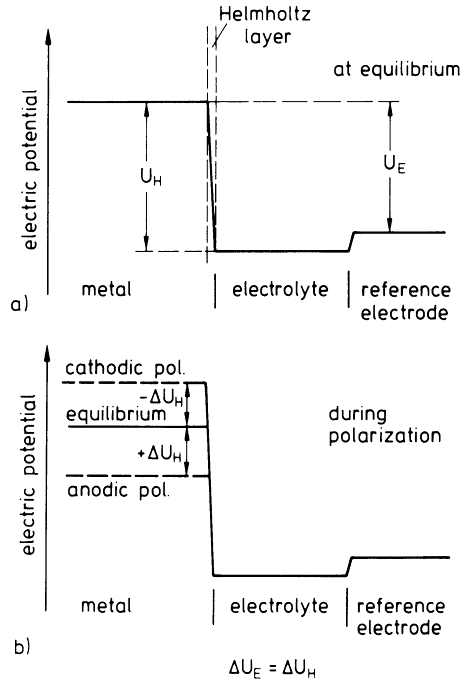
Helmholtz layer
at equilibrium
electric potential
U_H
U_E
metal
electrolyte
reference electrode
a)
cathodic pol.
$-\Delta U_H$
equilibrium
$+\Delta U_H$
anodic pol.
during polarization
electric potential
metal
electrolyte
reference electrode
b)
$\Delta U_E = \Delta U_H$

Figure 1. Potential distribution at metal–electrolyte interface (a) at equilibrium and (b) at polarization.

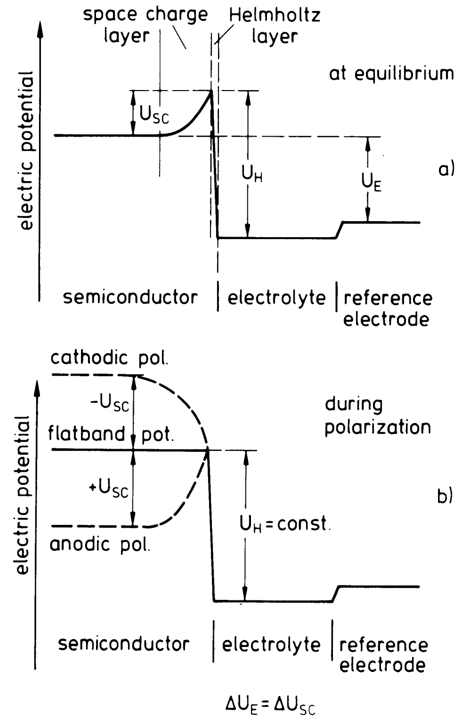
space charge layer
Helmholtz layer
at equilibrium
electric potential
U_{SC}
U_H
U_E
a)
semiconductor
electrolyte
reference electrode
cathodic pol.
$-U_{SC}$
flatband pot.
$+U_{SC}$
anodic pol.
during polarization
electric potential
$U_H = \text{const.}$
b)
semiconductor
electrolyte
reference electrode
$\Delta U_E = \Delta U_{SC}$

Figure 2. Potential distribution at semiconductor–electrolyte interface (a) at equilibrium and (b) at polarization.

The potential and charge distribution within the space charge region below the semiconductor surface is quantitatively described by the Poisson equation:

$$\frac{d^2U}{dx^2} = -\frac{e}{\varepsilon\varepsilon_0}[N_D - N_A - n(x) + p(x)] \tag{1}$$

in which x is the distance from the surface and N_D and N_A are the donor and acceptor densities, respectively, which are given by the doping of the semiconducting material. The electron and hole densities, $n(x)$ and $p(x)$, vary with the distance x. Assuming a Boltzmann distribution, they are given by:

$$n(x) = n_0 \exp\left(-\frac{eU_{\mathrm{SC}}}{kT}\right) \xrightarrow{x=0} n_s = n_0 \exp\left(-\frac{eU_{\mathrm{SC}}}{kT}\right) \tag{2a}$$

$$p(x) = p_0 \exp\left(\frac{eU_{\mathrm{SC}}}{kT}\right) \xrightarrow{x=0} p_s = p_0 \exp\left(\frac{eU_{\mathrm{SC}}}{kT}\right) \tag{2b}$$

in which n_0 and p_0 are the bulk electron and hole densities, respectively. The equilibrium condition is then given by

$$n_s p_s = n_0 p_0 = \text{const} = n_i^2 \tag{3}$$

in which n_i is the intrinsic carrier density. Integrating Eq. (1) one obtains the field strengths at the surface as given by

$$E_s = \left(\frac{dU_{\mathrm{SC}}}{dx}\right)_{x=0} = \frac{kT/e}{L_{\mathrm{D}}}\left\{\frac{p_0}{n_i}\left[\exp\left(\frac{eU_{\mathrm{SC}}}{kT} - 1\right)\right] + \frac{n_0}{n_i}\left[\exp\left(-\frac{eU_{\mathrm{SC}}}{kT}\right) - 1\right]\right.$$

$$\left. - \frac{e}{kT}\frac{(N_A - N_D)}{n_i}U_{\mathrm{SC}}\right\}^{1/2} \tag{4}$$

in which L_{D} is the so-called Debye length given by

$$L_{\mathrm{D}} = \left(\frac{\varepsilon\varepsilon_0 kT}{2n_i e^2}\right)^{1/2} \tag{5}$$

and which is valid for an intrinsic semiconductor.

The space charge Q_{SC} which produces the electrical field E_s is given by

$$Q_{\mathrm{SC}} = \varepsilon\varepsilon_0 E_s \tag{6}$$

and can easily be determined by using Eq. (4).

The potential, U_E, of a metal or a semiconductor electrode is always measured *vs.* a reference electrode [normal hydrogen electrode (NHE) or calomel electrode] as indicated in Figures 1 and 2. When an external potential is applied at a cell containing a metal electrode, only the potential drop across the Hemholtz layer is varied, i.e.,

$$\Delta U_E = \Delta U_{\mathrm{H}} \qquad \text{(metal electrode)} \tag{7}$$

as is schematically shown in Figure 1b. In the case of semiconductor electrodes, the situation is different. Here it has to be tested experimentally whether an externally applied potential leads to a variation of U_H or U_{SC}, or both. This is usually investigated by capacity measurements. The interface of a semiconductor can be considered as two capacities in series, one of the Helmholtz double layer, C_H, and the other of the space charge layer, C_{SC}. The latter capacity is defined as

$$C_{SC} = \frac{dQ_{SC}}{dU_{SC}} \tag{8}$$

and can be calculated quantitatively by inserting Eqs. (3) and (6) into (8). Since the corresponding equation is rather complex,(4) we shall restrict ourselves to two limiting cases which can be applied in most investigations. They correspond to

$$C_{SC} = \frac{\varepsilon\varepsilon_0}{L_D} \cosh\left(\frac{eU_{SC}}{kT}\right) \tag{9}$$

for intrinsic semiconductors and

$$1/C^2_{SC} = \left(\frac{2L_{D,\text{eff}}}{\varepsilon\varepsilon_0}\right)^2 \left(\frac{eU_{SC}}{kT} - 1\right) \tag{10}$$

for doped semiconductors, in which $L_{D,\text{eff}}$ is the effective Debye length given by

$$L_{D,\text{eff}} = \left(\frac{\varepsilon\varepsilon_0 kT}{2n_0e^2}\right)^{1/2} \tag{11}$$

[compare also with Eq. (5)].

The thickness of the space charge layer can be derived using the relation $d = \varepsilon\varepsilon_0/C$ for a normal capacitor, and then one obtains from (10)

$$d_{SC} = 2L_{D,\text{eff}}\left[\frac{eU_{SC}}{kT} - 1\right]^{1/2} \tag{12}$$

The thickness increases with increasing potential drop, U_{SC}, across the space charge region and $d_{SC} = L_{D,\text{eff}}$ for $U_{SC} \approx kT/e$. Taking a semiconductor with a typical doping of, e.g., $n_0 = 10^{17}\ \text{cm}^{-3}$, one obtains $L_{D,\text{eff}} = 10^{-6}$ cm ($\varepsilon \approx 10$).

The capacity–potential relation, given by Eq. (10), is the so-called "Mott–Schottky" equation which is strictly valid only in the exhaustion region, i.e., for space charges in which the majority carrier density at the surface is smaller than the corresponding bulk concentration ($n_s < n_0$ for n-type and $p_s < p_0$ for p-type electrodes).

Quantitative measurements of the space charge capacity (C_H can be neglected, since $C_H \gg C_{SC}$ in a series relationship) and a consecutive comparison with theoretical C_{SC} values, performed at first with intrinsic germanium,(5–7) has shown that an externally applied potential appears only across the space charge layer, whereas, in contradiction to the case of metal electrodes, the potential across the Helmholtz layer remains unchanged, i.e.,

$$\Delta U_E = \Delta U_{SC} \qquad \text{(at semiconductors)} \tag{13}$$

The same result has been found with most other semiconductor electrodes. One example is shown for GaP (Figure 3) for which the capacity is shown in a Mott–Schottky plot vs. electrode potential.(8) According to Eq. (10),

$$\frac{1}{C_{SC}{}^2} \rightarrow 0 \qquad \text{for } U_{SC} = \frac{kT}{e} \sim \hat{0} \tag{14}$$

i.e., the extrapolation of the curves in Figure 3 to $1/C_{SC}{}^2 \rightarrow 0$ leads to an electrode potential for which no potential drop occurs across the space charge layer ($U_{SC} = 0$). This potential is usually called the "flatband potential" (see also Figure 2b):

$$\frac{1}{C_{SC}{}^2} \rightarrow 0 \rightarrow U_{SC} \approx 0 \rightarrow U_E = U_{fb} \tag{15}$$

At this potential, the potential distribution is given by

$$U_{fb} = U_H + U_0 \tag{16}$$

in which U_0 is a constant which contains all other potentials such as the reference electrode at ohmic contacts.

According to Figure 3, different flatband potentials are obtained for *n*- and *p*-type GaP. At first sight, this result is surprising because it could lead to the assumption that *n*- and *p*-type electrodes of the same material exhibit different potentials, U_H, across the Helmholtz layer. This conclusion, however, is not correct because there is also a potential drop across the ohmic contact

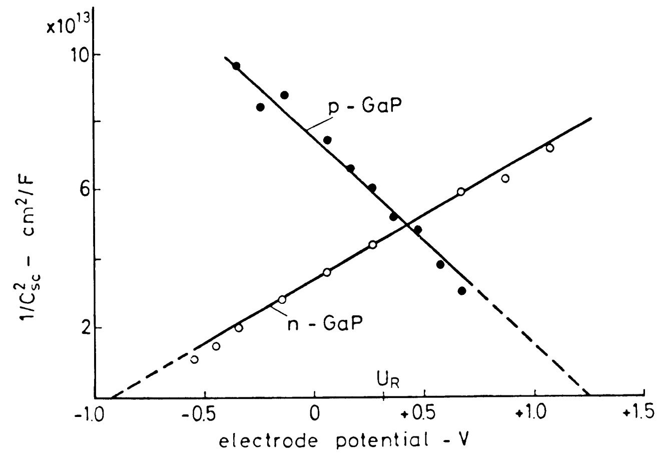

Figure 3. Mott–Schottky plot of space charge capacity vs. electrode potential at *n*- and *p*-type GaP in 0.1 *N* H_2SO_4.(8)

at the back side of the electrode. This potential is constant, although different for n- and p-type electrodes of the same material. Accordingly, U_H is equal in Eq. (16), but U_0 is different for both types of electrodes.(9)

The Helmholtz potential, U_H, which depends, of course, on the composition of the electrolyte, can be determined quantitatively by flatband potential measurements using Eq. (16). A strong pH dependence has been found for most semiconductors. Especially in the case of oxide semiconductors, the pH dependence has been measured quantitatively. Such experiments have yielded a shift of 0.059 V/pH as shown by various authors.(10–13) These results indicate that the adsorption or bonding of hydroxyl groups determines the behavior of the Helmholtz layer. A pH dependence has also been observed for some III–V compounds(14) and II–IV compounds.(15) In these cases, however, hydroxyl groups are not necessarily the potential-determining species. For instance, Ginley and Butler identified such species to be HS^- and H^+ at CdS electrodes.(15)

In the very early stage of semiconductor electrochemistry germanium electrodes were extensively studied. Here also a strong pH dependence was measured yielding again 0.059 V/pH.(6,9,16,17) In this case, however, two types of Helmholtz layers could be identified. One, a Ge–OH surface, was detected after anodic prepolarization,(6,16,18,19) and another, a Ge–H surface, after cathodic polarization.(16) In both cases the 0.059 V/pH dependence was observed which was interpreted in terms of dissociation of the surface groups. In strong hydrofluoric acid, according to Mehl and Lohmann,(20) the dissociation of surface hydroxyl groups seems to be suppressed.

In the case of silicon, the pH dependence could not be investigated because of oxide formation in aqueous solutions. Reasonable capacity and flatband potentials could only be obtained in hydrofluoric acid solutions.(21)

Finally, it should be mentioned that various peculiarities in the capacity measurements have been observed. In many cases a certain frequency dependence of the slope of the Mott–Schottky plots [Eq. (10)] and of the series was found. Gomes and co-workers have analyzed these effects in detail.(22–24) The physical origin is still unknown. Fortunately, however, the flatband potential showed mostly no frequency dispersion.

3. Energy Levels in Solids and Electrolytes

In the previous chapter we have reported results from which the potential distribution at the semiconductor–electrolyte interfaces was derived without referring to energy bands in the solid or to energy levels in the electrolyte. In this chapter the electrode potential and flatband potential will be correlated to energy levels.

Some problems arise because different reference points are used in solid state physics and in electrochemistry. In the first case, an absolute scale with vacuum as a reference is applied, whereas, in the second case, a standard reference electrode (normal hydrogen electrode) is used. This problem can be solved as follows.

3.1. Absolute and Conventional Electrode Potentials

The electrons at the Fermi level of the metal in a normal hydrogen electrode (NHE) have an exactly defined energy, E_{ref}, relative to the energy of the free electron in vacuum. Taking a redox system as an example, then the absolute energy scale of a redox system is only shifted against the conventional scale by the free energy, E_{red}, i.e.,

$$E = E_{\mathrm{ref}} - eU_0 \tag{17a}$$

in which U_0 is the standard redox potential. The negative sign of U_0 in this equation is due to convention of signs in the conventional and in the absolute electron scale. E_{ref} has a negative sign. The determination of the absolute value of E_{ref} has been the subject of various investigations during the last decade. In semiconductor electrochemistry, a value of $E_{\mathrm{ref}} = -4.5$ eV for the NHE, as derived by Lohmann,(25) is mostly used. Recently Trasatti(26) recalculated E_{ref} and obtained -4.31 eV. The calculations are based on a reaction cycle (see, e.g., Ref. 27) which contains energy terms such as sublimation energy, ionization energy, and the single-ion hydration energy. The latter is rather difficult to determine because it contains a term describing the potential difference, $\chi_{\mathrm{H_2O}}$, between the solution surface and its interior. Trasatti estimated this potential, whereas Lohmann neglected it, which explains the difference of the two E_{ref}'s. Both authors used experimental values obtained by Randles.(28)

Recently, Gomer and co-workers have taken up this problem again.(29) They determined absolute potentials experimentally by using the vibrating condenser method and obtained $E_{\mathrm{ref}} = -4.73$ eV for the NHE. This value is considerably larger than Trasatti's value. According to Gomer the difference from the other value is due to an incorrect value for the work function of Hg in air, the reference electrode used by Randles. In addition, the same author showed(29) that $\chi_{\mathrm{H_2O}} \leq 0.05$ eV and decreases considerably at electrolyte concentrations above 9.1 *M*.

Because of these discrepancies, we also use Lohmann's value of $E_{\mathrm{ref}} = -4.50$ for NHE, so that the electron energy of any redox system is given by

$$E_{\mathrm{abs}} = -4.5\ \mathrm{eV} - eU_0 \tag{17b}$$

as schematically shown in Figure 4.

3.2. Energy Levels in Solids

The energy levels in a semiconductor are characterized by the conduction E_C and the valence band E_V values, and by the Fermi level E_F. In the bulk

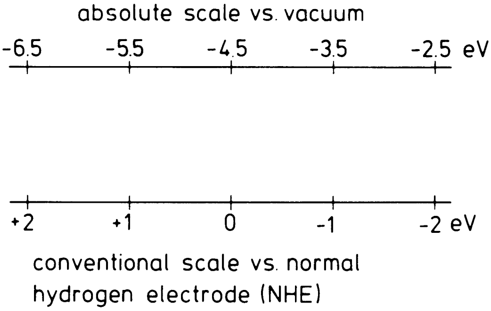
absolute scale vs. vacuum
-6.5
-5.5
-4.5
-3.5
-2.5 eV
+2
+1
0
-1
-2 eV
conventional scale vs. normal hydrogen electrode (NHE)

Figure 4. Absolute and conventional electrode potential scale.

of a semiconductor, the Fermi level is equivalent to the chemical potential μ_e of the electrons as given by

$$\mu_e = E_F = E_C + kT \ln \frac{n}{N_C} \tag{18}$$

and an equivalent expression is valid for the chemical potential of holes as given by

$$\mu_h = E_V - kT \ln \frac{p}{N_V} \tag{19}$$

Here N_C and N_V are the effective densities of energy states at the bottom of the conduction band and at the top of the valence band, respectively. Since, at equilibrium, $\mu_e = \mu_h$, one can derive from Eqs. (18) and (19)

$$n \cdot p = N_C N_V \exp\left(-\frac{E_C - E_V}{kT}\right) = n_i^2 = \text{const} \tag{20}$$

In the absolute energy scale, the position of the conduction band with respect to the vacuum level is given by the electron affinity E_A (Figure 5). The position of the Fermi level depends on the free carrier density, n, and consequently on the doping. The electron affinity, E_A, is usually given in the

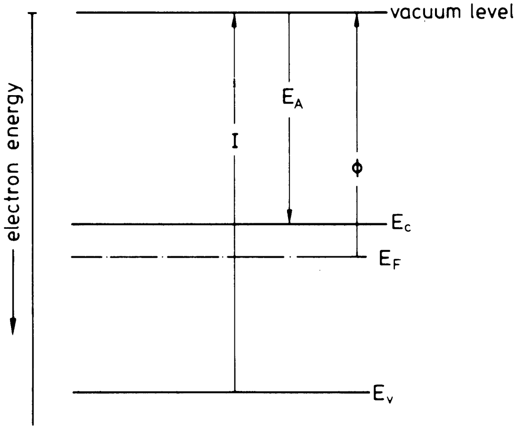
vacuum level
electron energy
E_A
I
Φ
E_c
E_F
E_v

Figure 5. Position of conduction and valence band and Fermi level in a semiconductor with the vacuum as a reference. E_A, electron affinity; I, ionization energy.

absolute scale; it can also be expressed in the conventional scale according to Eq. (17a). Accordingly the position of energy bands can be predicted from E_A values provided that no specific adsorption of ions occurs at the electrode surface. If the electron affinity, E_A, is not known, it can also be calculated from electronegativities.(30) The bulk electronegativity,† χ, of a compound has been postulated to be the geometric mean of the electronegativities of the constituent atoms.(31) In a semiconductor, the bulk electronegativity corresponds to an energy halfway between the conduction and valence band levels. Thus the electron affinity of the compound is given by

$$E_A = \chi - 1/2E_g \tag{21}$$

where E_g is the band gap energy. Examples of the application of this equation will be given in Section 3.4.

3.3. Energy Levels in Electrolytes

Taking a redox system as an example, the chemical potential of the electrons is given by

$$\mu_{e,\text{redox}} = \mu^{\circ}_{\text{redox}} + kT \ln \frac{C_{\text{ox}}}{C_{\text{red}}} \tag{22}$$

where C_{ox} and C_{red} are the concentrations ($\simeq$ activities) of the oxidized and reduced species of the redox system, respectively. Usually the corresponding redox potentials are given on the conventional scale. Using the absolute scale with the vacuum level as a reference point, then the chemical potential of the electrons is equivalent to the Fermi level $E_{\text{F,redox}}$ of the redox system,(32) i.e.,

$$E_{\text{F,redox}} = \mu_{e,\text{redox}} \tag{23}$$

in the absolute scale.

Information about further energy levels in a redox system can be derived from the theory of electron transfer to electrodes which has been worked out by several authors.(32–36) In all these theories it is assumed that the Frank–Condon principle is valid, i.e., it is assumed that the vibration of molecules and their surrounding solvation shell is slow compared to the actual electron transfer between redox system and electrode. Following Gerischer's treatment, then this assumption leads to the consequence that the energy levels involved in the electron transfer differ from the thermodynamic value $E_{\text{F,redox}}$. This can be illustrated by considering a reaction cycle as shown in Figure 6. The total energy of a redox system in its reduced state is given at equilibrium by $\text{Red}_{(\text{solv,red})}$, the ions being surrounded by a certain solvation shell (solv,red). Starting now from this state, a certain electron energy E°_{red} is required for an electron transfer to the vacuum level. During this process, forming the oxidized

---

† The symbol, χ, is employed here for electronegativity; it is not to be confused with χ for the surface dipole potential at single interface, mentioned earlier.

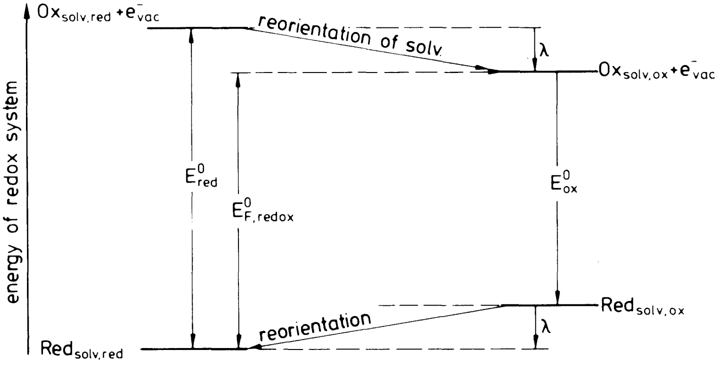

Figure 6. Energies of a redox system in its oxidized and reduced states. The energy difference E°_{red}, E°_{ox}, and $E_{\text{F,redox}}$ are electron energies.

species of the redox system $\text{Ox}_{(\text{solv,red})}$, the solvation shell, however, remains unchanged (Frank–Condon principle). Afterwards the solvent dipoles of the original solvation shell (solv,red) are reoriented and the oxidized molecule $\text{Ox}_{(\text{solv,red})}$ relaxes to its equilibrium state $\text{Ox}_{(\text{solv,ox})}$. The energy involved in the relaxation process is the so-called reorientation energy λ. The reverse process, electron transfer from the vacuum to the oxidized species, proceeds in a similar way (E°_{ox}) followed again by a slow relaxation to its original state. One can also see from Figure 6 that the electronic energy E°_{red} is larger and E°_{ox} is smaller than the thermodynamic value $E_{\text{F,redox}}$. Plotting now only the electron energies (energy differences in Figure 6) in a pure electron energy diagram, using vacuum as a reference level (absolute scale), one obtains Figure 7a. This energy diagram is very similar to the corresponding picture derived for solids (see Figure 5).

The electron energy states of a redox system are not very discrete energy levels because one cannot attribute only a single Frank–Condon energy state to a molecule in solution. The energy states are distributed over a certain energy range due to fluctuations in the solvation shell surrounding the molecule. This is demonstrated by the distribution of energy states around the energies E°_{ox} and E°_{red} (Figure 7b). In this figure, D_{red} is the density of occupied states (in relative units) represented by the reduced component of the redox system and D_{ox} the density of empty states represented by the oxidized component.$^{(32,36)}$ The distribution curves, D_{ox} and D_{red}, are described by a Gaussian type of function which can be derived quantitatively assuming a harmonic oscillation for the solvation shell. One obtains

$$D_{\text{red}} = D^{\circ}_{\text{red}} \exp\left[-\frac{(E - E^{\circ}_{\text{red}})^2}{4kT\lambda}\right] = D^{\circ}_{\text{red}} \exp\left[-\frac{(E - E_{\text{F,redox}} - \lambda)^2}{4kT\lambda}\right] \quad (24a)$$

$$D_{\text{ox}} = D^{\circ}_{\text{ox}} \exp\left[-\frac{(E - E^{\circ}_{\text{ox}})^2}{4kT\lambda}\right] = D_{\text{ox}} \exp\left[-\frac{(E - E_{\text{F,redox}} + \lambda)^2}{4kT\lambda}\right] \quad (24b)$$

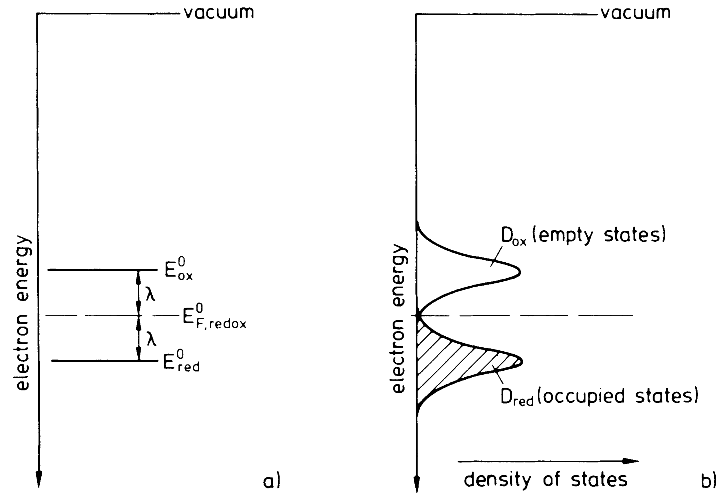

Figure 7. Electron energies of a redox system (differences in Figure 6). E°_{red}, occupied states; E°_{ox}, empty states (a); the corresponding distribution D functions are given in (b).

D°_{red} and D°_{ox} are normalizing factors making $\int (D) E \, dE = 1$ from which follows that

$$D^\circ_{ox} = D^\circ_{red} = (4kT\lambda)^{-1/2} \tag{25}$$

The half-width of the distribution curve is given by

$$\Delta E_{1/2} = 0.53\lambda^{1/2}\,\mathrm{eV} \tag{26}$$

Accordingly, not only the energy distance of the maxima of the distribution curves from $E_{F,redox}$ but also the half-width depends on the reorientation energy, λ. Typical values of λ are in the range from a few tenths of an eV up to 2 eV(9) (see Section 4.5). It is assumed here that the reorientation energy λ after electron transfer is equal for the oxidation and reduction processes.

It should be emphasized that, in principle, the same energy diagram can also be derived from other theories on electron transfer processes. Since all these authors(33-35) used a harmonic oscillator picture, one obtains the same distribution curves.(9) The question arises, however, whether this kind of approach can be used for electron transfer processes with real redox systems. This problem will be discussed in the chapter on electrode kinetics. Certainly this model is applicable only for weak interaction between an electrode and the species of the redox system.

3.4. Energy Levels at Semiconductor–Electrolyte Interfaces

Combining now a semiconductor with a redox system, equilibrium is achieved if the electrochemical potential is constant throughout the whole half-cell, i.e., the Fermi levels of the semiconductor and the redox system must be equal on both sides of the interface:

$$E_F = E_{F,\text{redox}} \tag{27}$$

To achieve equilibrium electrons cross the interface until a corresponding potential difference occurs. The latter depends on the difference of the chemical potential of the two phases, i.e., on the difference of the two Fermi levels before contact is made. Neglecting any specific adsorption on H^+ and OH^- ions or the formation of a dipole layer on the surface, the potential difference is given by

$$\underset{E_A+(E_C-E_F)_{\text{bulk}}}{\mu_{\text{sem}}} - \underset{E_{F,\text{redox}}}{\mu_{\text{redox}}} = eU_{SC} \tag{28}$$

It can be calculated provided that E_A and $(E_C - E_F)$, the latter being dependent on the doping, are known. Examples are given in Figures 8a and 8b for two redox systems and differently doped semiconductors (left and right sides).

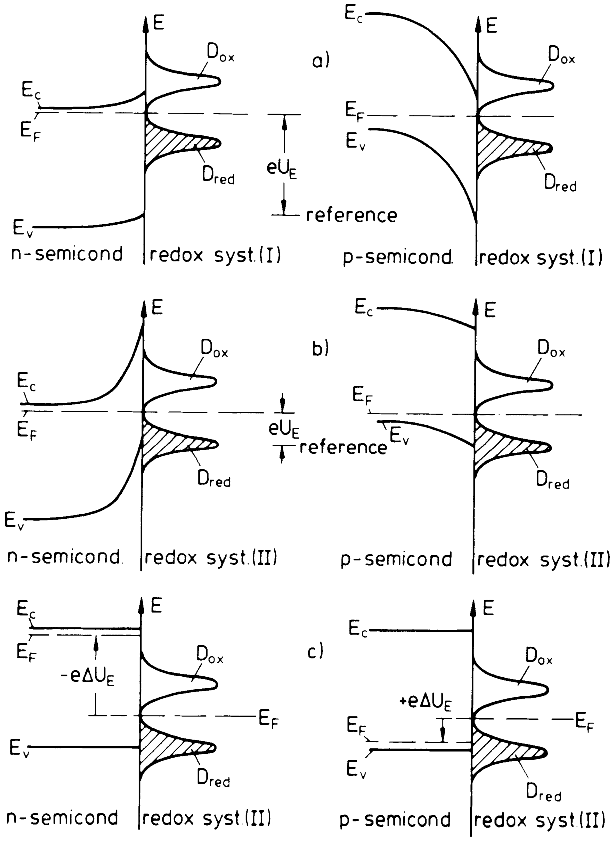
a)
E
E_c
E_F
E_v
D_{ox}
D_{red}
eU_E
reference
n-semicond
redox syst.(I)
p-semicond.
redox syst.(I)
b)
reference
E_v
n-semicond.
redox syst.(II)
p-semicond
redox syst.(II)
c)
$-e\Delta U_E$
$+e\Delta U_E$
n-semicond
redox syst.(II)
p-semicond
redox syst.(II)

Figure 8. Relative position of energy levels at the interface semiconductor–redox system; (a) and (b) two different redox systems, (c) the same as (b) at flatband potential.

It can be clearly seen from this figure that the potential difference developed for achieving equilibrium occurs within the semiconductor below its surface. The magnitude of band bending and its sign depends on the standard potential (conventional scale) or Fermi level (absolute scale) of the redox system (compare Figures 8a and 8b). It also depends on the electron affinity and the doping of the semiconductor (compare left and right sides of Figure 8).

As mentioned above, the potential difference occurs across the space charge layer of the semiconductor. This is only true provided that the ion concentration in the electrolyte is sufficiently large (Gouy layer neglected).

In principle, the energy diagram in Figure 8 is also valid for "real" interfaces at which H^+ or OH^- ions are adsorbed or bonded to the semiconductor which leads to the formation of the Helmholtz double layer. In this case, however, the position of the conduction band with respect to the vacuum level is not anymore entirely determined by the electron affinity E_A and the potential difference cannot be simply calculated from Eq. (28). The distance between the conduction band and vacuum level is now given by $E_A + eU_H$, in which the last term represents the potential drop across the Helmholtz layer, as also indicated in Figure 8.

This result makes it impossible to predict theoretically the position of energy bands without further experiments, since U_H is unknown. Fortunately, however, the position of energy levels can be obtained experimentally by determining the "flatband" potential using capacity measurements. As already discussed in Section 2, an externally applied potential only arises across the space charge region [$\Delta U_E = \Delta U_{SC}$, see Eq. (14)]. Since eU_H is constant during polarization, the position of energy levels on both sides of the interface remain also unchanged.

From capacity measurements one obtains the potential change, ΔU_E, required for making the energy bands flat up to the surface (flatband potential) as shown in Figure 8c. Since the energy distance between the conduction band and the Fermi level in the bulk of the semiconductor can be determined from the carrier density [Eqs. (18) and (19)], the position of E_C^S and E_V^S can be easily calculated. One obtains values either given in the conventional or in the absolute scales.

A selection of semiconductors is given in Figure 9.(37) Other examples are given in the literature.(32,38) It must be emphasized that the external voltage required for making the energy bands flat is different for *n*- and *p*-type doping, where the position of energy bands at the surface are equal because the same Helmholtz layer is expected for *n*- and *p*-type doping. This has been proved experimentally in many cases(11,14,19) (see also Figure 3).

In the constant search for semiconducting electrode materials suitable for solar cells (Section 5.2.4) there is still a great demand to predict in advance the position of energy bands or the flatband potential. In connection with this problem, a very interesting method for predicting flatband potentials has

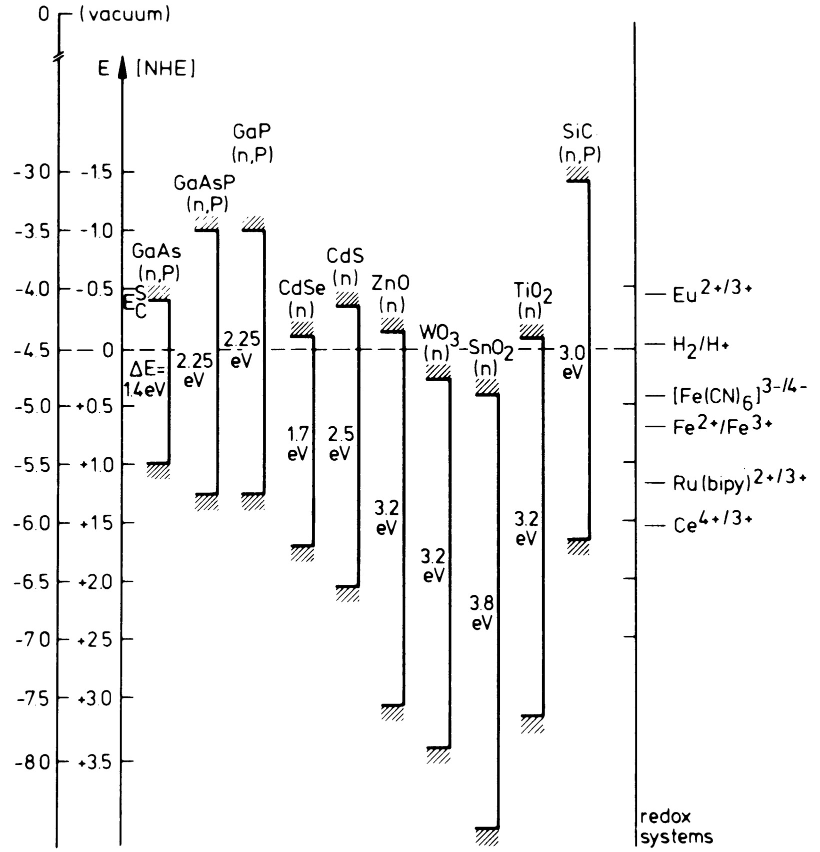
0 (vacuum)
E [NHE]
-3.0 -1.5
-3.5 -1.0
-4.0 -0.5
-4.5 0
-5.0 +0.5
-5.5 +1.0
-6.0 +1.5
-6.5 +2.0
-7.0 +2.5
-7.5 +3.0
-8.0 +3.5
GaAs (n,P)
ΔE= 1.4eV
GaAsP (n,P)
2.25 eV
GaP (n,P)
2.25 eV
CdSe (n)
1.7 eV
CdS (n)
2.5 eV
ZnO (n)
3.2 eV
WO3 (n)
3.2 eV
SnO2 (n)
3.8 eV
TiO2 (n)
3.2 eV
SiC (n,P)
3.0 eV
Eu2+/3+
H2/H+
[Fe(CN)6]3-/4-
Fe2+/Fe3+
Ru(bipy)2+/3+
Ce4+/3+
redox systems

Figure 9. Position of energy bands at the surface of various semiconductor electrodes at pH 1.(37)

recently been published by Butler and Ginley.(30) They solved the problem as follows:

According to Figure 8c one can derive the relation

$$E_A + eU_H = E_{\text{ref}} + eU_{\text{fb}} - (E_C - E_F) \quad (29)$$

If the flatband potentials are measured vs. NHE then they are also known in the absolute scale [$E_{\text{ref}} = -4.50$ eV according to Eq. (17a)]. Butler and Ginley considered a Helmholtz layer to be due to specific adsorption of OH^- and H^+ ions. There exists some unique point for each semiconductor where the number of positively and negatively charged potential-determining ions at the interface are equal. At this point, which is called the point of zero zeta potential (pzzp),(39) the potential drop across the Helmholtz layer U_H due to adsorbed ions is zero ($eU_H = 0$). The U_{fb} can be easily calculated from Eq. (29). A corresponding plot of E_A vs. U_{fb} is given by the solid line in Figure 10. The authors tested this method by measuring the pzzp of various

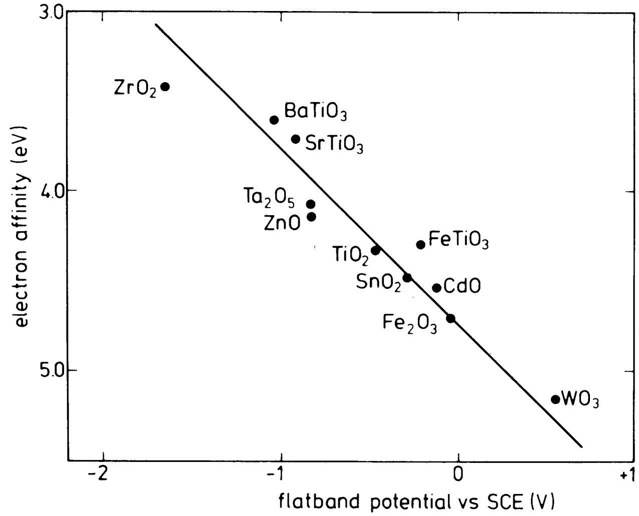

Figure 10. Electron affinity calculated using atomic electronegativities vs. measured flatband potentials for labeled semiconductors corrected to their respective pzzp's. The solid line is expected from Eq. (29).(30)

oxide semiconductors. The pzzp is actually the pH value at which the zeta potential is zero, provided that OH^- and H^+ determine the charge balance in the Helmholtz layer. They also determined the flatband potential at the same pH values, as given by the closed circles in Figure 10.

According to this figure, the experimental values agree well with the theory. Butler and Ginley neglected any fraction of the Helmholtz layer due to the formation of a surface dipole layer which is not determined by zeta potential measurements. In any case they claim that the flatband potential can be predicted from electronegativities with an accuracy of about 0.3 V. The authors also applied the same method successfully to CdS.(15)

4. Electrode Kinetics

4.1. Rate of Electron Transfer (Theory)†

Since the early work by Gurney(40) in 1931 a number of theories on electron transfer processes have been published by Hush,(41) Marcus,(33) Levich,(34) Dogonadze,(35,42) and by Gerischer.(26,32) These theories have not only been applied to semiconductor, but also to metal–electrodes. Following Gerischer's model, electron transfer can only occur between two electronic energy states of equal energies, one being occupied, the other vacant. An electron transfer from a molecule (electron donor) in the electrolyte to the electrode is represented by an anodic current i_A given by

---

† See also Chapter 1 by Dogonadze and Koznetsov and Chapter 2 by Khan and Bockris in this volume.

$$i^+ = F \cdot Z \cdot c \int_{-\infty}^{\infty} \kappa(E) \cdot N_{\text{un}}(E) D_{\text{red}}(E)\, dE \tag{30}$$

in which $Z \cdot c$ means the number of molecules which reach the electrode surface, $\kappa(E)$ is the transition coefficient which strongly depends on the distance of the reacting molecules from the surface, $N_{\text{un}}(E)$ is the density of empty (unoccupied) states in the electrode, and $E_{\text{red}}(E)$ is the density of occupied energy states in the electrolyte, as defined by Eq. (24a). It is now necessary to distinguish between an electron transfer into the conduction band ($E \geq E_C$) or into the valence band ($E \leq E_V$).

In the first case (conduction band process), the density of unoccupied energy states ($N_{\text{un}} = N_C$) in the conduction band can be taken to be constant because only a few of them are occupied, even in n-type material, so that the corresponding current is given by

$$i_c^+ \frac{F \cdot Z \cdot c}{(\pi k T \lambda)^{1/2}} \int_{E_c}^{+\infty} \kappa(E) N_c \exp\left[-\frac{(E - E_{\text{F,redox}} - \lambda)^2}{4kT\lambda}\right] dE \tag{31a}$$

The situation is different in the case of a valence band process because most of the energy states are occupied by electrons. Here an electron transfer into the valence band is only possible if holes are present at the surface, i.e., the density of empty states, N_{un}, is equal to the density of holes at the surface, p_s. The corresponding current is given by

$$i_v^+ = \frac{F \cdot Z \cdot c}{(\pi k T \lambda)^{1/2}} \int_{-\infty}^{E_V} \kappa(E) p_s \exp\left[-\frac{(E - E_{\text{F,redox}} - \lambda)^2}{4kT\lambda}\right] dE \tag{31b}$$

The integral can only be analytically solved by making some approximations as follows: since the distribution functions vary exponentially with E^2 and since, in most cases, the overlap between energy states on both sides of the interface is mostly limited to a rather small energy range (see, e.g., Figure 8), the electron transfer is assumed to occur mainly within 1 kT of the edge of the conduction or valence band (v.b.). Using this approximation, the integrals in Eq. (31) can be replaced by inserting $\Delta E = 1$ kT and $E = E_c$ (conduction band process) or $E = E_V$ (v.b. process). Assuming further $\kappa(E)$ to be constant, one obtains for the anodic current:

$$i_c^+ \sim F \cdot Z \cdot c \left(\frac{kT}{\pi\lambda}\right)^{1/2} \kappa N_c \exp\left[-\frac{(E_c - E_{\text{F,redox}} - \lambda)^2}{4kT\lambda}\right] \tag{32a}$$

$$i_v^+ \sim F \cdot Z \cdot c \left(\frac{kT}{\pi\lambda}\right)^{1/2} \kappa p_s \exp\left[-\frac{(E_c - E_{\text{F,redox}} - \lambda)^2}{4kT\lambda}\right] \tag{32b}$$

In a similar procedure, also the cathodic currents, representing the electron transfer from the electrode to the electrolyte, can be derived. The current is given by

$$i^- = F \cdot Z \cdot c \int_{-\infty}^{\pi\infty} \kappa(E) N_{\mathrm{occ}}(E) D_{\mathrm{ox}}(E)\, dE \tag{33}$$

In this case, the density of occupied states N_{occ} in the conduction band is given by the density of electrons at the surface n_s, whereas the corresponding density of occupied states in the valence band is given by its density of states (N_v) itself. Using the same approximation, one obtains for the conduction band process using also Eq. (24b)

$$i_c^- = F \cdot Z \cdot c \left(\frac{kT}{\pi\lambda}\right)^{1/2} \kappa n_s \exp\left[-\frac{(E_c - E_{\mathrm{F,redox}} + \lambda)^2}{4kT\lambda}\right] \tag{34a}$$

and for the valence band process,

$$i_v^- - F \cdot Z \cdot c \left(\frac{kT}{\pi\lambda}\right)^{1/2} \kappa N_v \exp\left[-\frac{(E_v - E_{\mathrm{F,redox}} + \lambda)^2}{4kT\lambda}\right] \tag{34b}$$

According to Eqs. (32) and (34), there are four possible partial currents. Two of them (i_c^+ and i_c^-) are illustrated by using the energy diagram shown in Figure 11 which is similar to that in Figure 8. In this example, energy levels

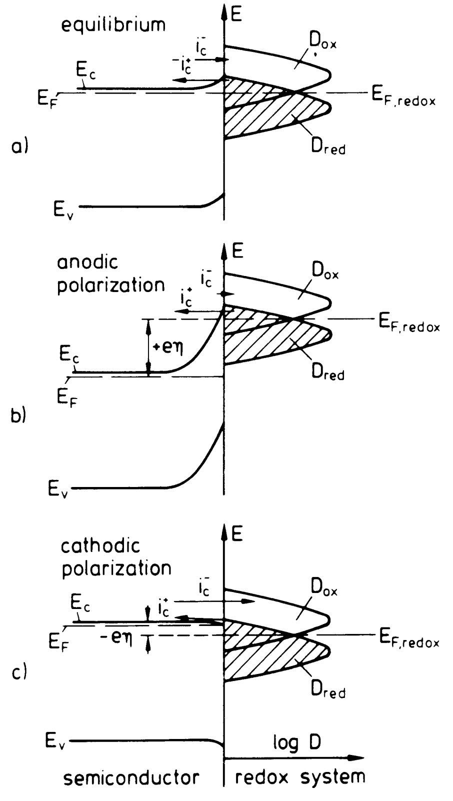
a)
equilibrium
E
i_c^-
$-i_c^+$
E_c
E_F
D_{ox}
$E_{F,redox}$
D_{red}
E_v
b)
anodic polarization
E
i_c^-
i_c^+
$+e\eta$
E_c
E_F
D_{ox}
$E_{F,redox}$
D_{red}
E_v
c)
cathodic polarization
E
i_c^-
i_c^+
E_c
E_F
$-e\eta$
D_{ox}
$E_{F,redox}$
D_{red}
E_v
log D
semiconductor
redox system

Figure 11. Electron transfer (arrows) via the conduction band of a semiconductor (a) at equilibrium, (b) at anodic, and (c) at cathodic polarization.

of a redox system occur at the same energy as that for the conduction band (Figure 11a). From this figure and also from Eqs. (32) and (34), the potential dependence of currents can easily be derived as follows:

At equilibrium the Fermi level is constant throughout the system [$E_F = E_{F,\text{redox}}$; see Eq. (27)]. Polarizing the electrode, the Fermi levels on both sides differ by the externally applied potential ΔU_E. Since any potential variation occurs only across the space of the semiconductor [$\Delta U_E = \Delta U_{SC}$; see Eq. (13) of Section 2] we have

$$E_F + E_{F,\text{redox}} + e\Delta U_{SC} \tag{35}$$

Since the potential across the Helmholtz layer is constant, also the relative position of energy states on both sides of the interface, and consequently the energy difference between the energy bands at the surface and the Fermi level in the redox system, remain unchanged. Accordingly, the exponential terms in the current equations (32) and (35) are independent of any applied voltage. The only potential-dependent quantities in these equations are the carrier densities n_s and p_s. They depend exponentially on U_{SC} as given by Eqs. (2a) and (2b). Since n_s and p_s occur only in two current equations (32b) and (34a), i_c^- and i_v^+ depend on U_{SC} and therefore on the applied potential, whereas the other two partial currents i_c^+ and i_v^- are always potentially independent, i.e.,

$$i_c^+ = i_c^\circ \qquad \text{and} \qquad i_v^- = i_v^\circ$$

in which

$$i_c^\circ = F \cdot c\kappa \left(\frac{kT}{\pi\lambda}\right)^{1/2} N_c \exp\left[-\frac{(E_c - E_{F,\text{redox}} - \lambda)^2}{4kT\lambda}\right] \tag{36a}$$

and

$$i_v^\circ = F \cdot c\kappa \left(\frac{kT}{\pi\lambda}\right)^{1/2} N_c \exp\left[-\frac{(E_c - E_{F,\text{redox}} + \lambda)^2}{4kT\lambda}\right] \tag{36b}$$

At equilibrium, the anodic and cathodic currents across each energy band must be equal, i.e.,

$$i_c^+ = i_c^- = i_c^\circ \qquad \text{and} \qquad i_v^+ = i_v^- = i_v^\circ \tag{37}$$

In order to fulfill this equilibrium condition, the surface carrier concentrations n_s, p_s in Eqs. (34a) and (32b) must attain corresponding values. Denoting the equilibrium concentrations by n_{s0} and p_{s0}, they are related to the band bending, eU_{SC} [see Eq. (2)] by

$$n_{s0} = n_0 \exp\left(-\frac{eU_{SC}^\circ}{kT}\right) \qquad \text{and} \qquad p_{s0} = p_0 \exp\left(\frac{eU_{SC}^\circ}{kT}\right) \tag{38}$$

in which eU_{SC}° is the band bending at equilibrium, as shown in the upper part of Figure 11. Polarizing now an electrode, we only vary the band bending and the surface carrier densities as given by

$$n_s = n_{s0} \exp\left(-\frac{e\eta}{kT}\right) \quad \text{and} \quad p_s = p_{s0} \exp\left(\frac{e\eta}{kT}\right) \tag{39}$$

in which η is the overpotential. The anodic current can now be written in the usual way by using Eqs. (32) to (39):

$$\begin{gathered} i_c^+ = i_c^\circ, \qquad i_v^+ = i_v^\circ \exp\left(\frac{e\eta}{kT}\right) \\ i_c^- = i_c^\circ \exp\left(-\frac{e\eta}{kT}\right) \quad \text{and} \quad i_v^- = i_v^\circ \end{gathered} \tag{40}$$

Various possibilities are given in Figure 11. The lengths of arrows indicate the currents. The absolute values of currents depend mainly on the density of energy states on both sides of the interface at the energy level across which the charge transfer occurs.

Finally it should be mentioned that, in principle, the same current–potential behavior can be obtained from Marcus's(33) or Levich's(34) theory. Although not mentioned in these theories, one can actually derive from them the same distribution functions of energy states, since the exponential terms in Eqs. (32) and (34) are equal in all theories. This result is entirely due to the assumption of a harmonic oscillation model of the motion in the ion's solvation shell. The main advantage of Gerisher's model is the description of electron transfer reactions in terms of an energy picture (Figure 11), which is especially useful for the processes occurring at semiconductor or insulator electrodes. The same description, of course, can also be applied for metal electrodes,† which will not be discussed here (see, e.g., Ref. 91).

4.2. Electrode Reactions in Electrolytes without Redox Systems

During polarization, various electrode processes can occur such as electrochemical dissolution, O_2 evolution and oxide formation during anodic polarization, and surface reduction and H_2 formation during cathodic polarization. It must be emphasized that the theory derived above is not quantitatively applicable here because, in most processes, a strong interaction between semiconductor and electrolyte is involved, whereas the electron transfer theory is only valid for weak interactions, i.e., it is applicable only for redox processes. The other processes, electrochemical dissolution, etc., will be treated briefly before discussing pure electron transfer reactions (redox processes) because they present the basic behavior of semiconducting electrodes.

---

† See Chapter 1 Dogonadze and Koznetsov in this volume.

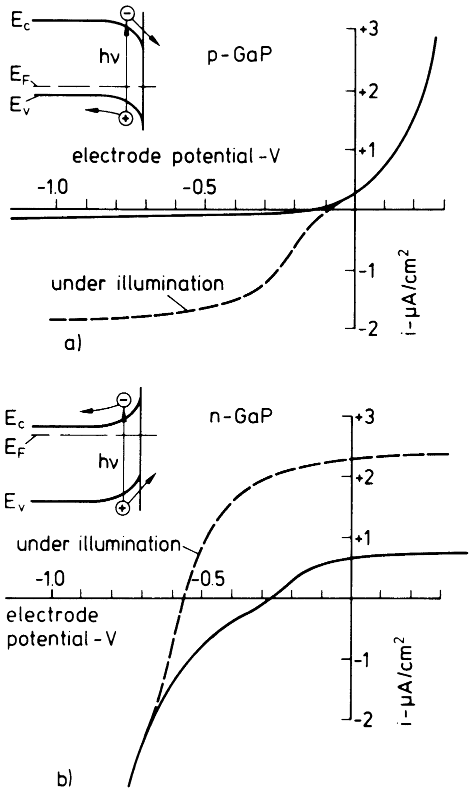

Figure 12. Current–potential dependence at *n*- and *p*-type GaP in 0.1 *N* H_2SO_4.(14)

A typical current–potential behavior of a semiconductor electrode is shown in Figure 12 for *n*- and *p*-GaP.(14) Here the cathodic process corresponds to H_2 evolution whereas, in the anodic range, the electrode is dissolved. The current–potential curves yield immediately information on which energy band of the semiconductor is involved in the reaction process. For instance, the increase of the cathodic current with potential, observed only with *n*-type GaP, must be interpreted by a conduction band process, i.e., by electron transfer from the conduction band to water leading to the formation of hydrogen. The current increase is entirely determined by the increase of the electron density n_s at the surface upon cathodic polarization, as already discussed in the previous section. In the case of a *p*-type electrode, the density of electrons in the bulk is extremely low so that almost no electrons are available in the conduction band to be transferred across the interface. Accordingly, the current is low. It is not determined by the band bending but entirely by the diffusion of the electrons (minority carriers) from the bulk toward the surface. The diffusion-limited current is given by(43,44)

$$i_{\text{diff}}^{-} = \frac{eD_n \cdot n_p}{L_n} \tag{41}$$

in which D_n, L_n are the diffusion constant and diffusion length of electrons, respectively, and n_p is the electron density in a p-doped semiconductor. This typical behavior of a semiconductor electrode can be proved by illuminating the electrode by light absorbed by the semiconductor. Then electrons are excited into the conduction band which leads to the well-known corresponding current increase as shown in Figure 12.

Similar conclusions can be made for anodic processes. Since here a current increase is only observed with p-type electrodes, it can be concluded that the dissolution process is a valence band process. The density of holes at the surface determines the reaction rate.

These basic properties of semiconductor electrodes were observed at first by Brattain and Garrett(3) with germanium electrodes. It was further shown for germanium that the small cathodic current at p-type and small anodic current at n-type germanium are quantitatively determined by the diffusion of minority carriers.(3,45–47)

4.2.1. Anodic Dissolution Processes

In the early state of research on semiconductor electrochemistry, the anodic dissolution was the subject of many investigations. Especially the dissolution mechanisms of germanium(45,48,49) and silicon(46,50–53) were studied in detail. It has been shown for all semiconductors at which anodic dissolution occurs that this process arises mainly via the valence band. Various dissolution reactions have been investigated quantitatively; examples are given in Table 1. In all cases, besides germanium, the anodic reaction is entirely a valence band process, i.e., holes (p) are required. This is reasonable because surface bonds between atoms have to be broken. It is interesting to note that germanium is an exception in so far as here only two holes are required, whereas the two other charges are electrons being transferred into the conduction band.(48) (If both electron and hole transfer are involved, one can distinguish between them by using the so-called "thin slice method,"(3,77) which will not be described here.) This phenomenon can be interpreted as follows (see also Figure 13).(38,59,78)

If one or two holes are consumed at the surface for breaking one bond, then the remaining bond of such a surface group is already weakened and the electron energy state at or near this surface group occurs no longer in the valence band but is located somewhere above this band (surface state). Since the energy gap of Ge is relatively small ($E_G = 0.8$ eV), an electron can now be transferred from this surface group into the conduction band by thermal activation. A detailed analysis of the anodic dissolution of Ge has been given by Gerischer and Beck.(48) This model is also applicable for all other semiconductors. However, other materials have a larger band gap and the energy distance between surface state and conduction band is too large for electron transfer into the conduction band.

Table 1
Decomposition Products of Various Semiconductor Electrodes during Anodic and Cathodic Polarization(59)

Electrode material	E_g, eV	Anodic decomposition products[a]	Cathodic decomposition products[a]
Ge(*n*, *p*)	0.8	Ge^{4+} (48)	H_2 (48)
Si(*n*, *p*)	1.1	Si^{2+}, Si^{4+} (in HF) (50–53)	H_2 (50,51)
GaAs(*n*, *p*)	1.4	Ga^{3+}, A^{3+} (53,54)	AsH_3, H_2 (56)
CdSe(*n*, *P*)	1.75	Cd^{2+}, Se° (57)	Cd, (H_2Se) (57)
GaP(*n*, *p*)	2.35	Ga^{3+}, $p°$ or p^{3+} (14)	H_2 ($PH_3 < 0.1\%$) (14)
CdS(*n*)	2.4	Cd^2, $S°$ (57)	Cd, H_2S (57)
WO_3(*n*)	2.5	O_2 (60,62,63)	H_xWO_3, H_2 (61,62)
SiC(*n*, *p*)	3.0	Si^{4+}, C (in HF) (37)	H_2 (37)
ZnO(*n*)	3.2	Zn^{2+}, O_2 (64)	Zn, H_2O (64)
TiO_2(*n*)	3.2	(Ti^{4+}), O_2 (65–69)	Ti, H_2 (66–69)
K_3TaO_4(*n*)	3.5	O_2 (70)	H_2 (70)
SnO_2(*n*)	3.8	O_2 (11)	H_2, Sn (in HCL) (11)
Fe_2O_3	2.2	O_2 (71–73)	
$SrTiO_2$	3.2	O_2 (74)	H_2
MoS_2	2.5	$Mo(SO_4)O_2$ (75,76)	

[a] Reference numbers are in parentheses.

A detailed model has also been given for the anodic dissolution of silicon(50) in hydrofluoric acid. In this case it is interesting to note that the number of charges required for the elementary process depends on the HF concentration, a result which will not be discussed here.

In connection with the dissolution process of compound semiconductors, the question has been raised whether different crystal faces (e.g., Ga or P faces in GaP) show a different dissolution behavior. This has never been found, probably because the dissolution occurs mainly at dislocations or steps.(14,59)

There are other examples such as sulfide compounds where dissolution has also been observed. In these cases, however, the corresponding anodic

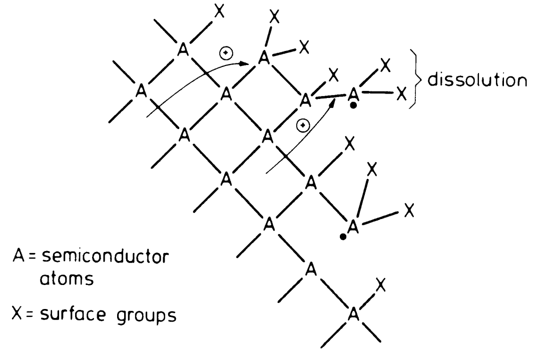

Figure 13. Schematic presentation of anodic dissolution process of a semiconductor electrode.(38)

current decreases always to a rather low value after a certain polarization time, owing to the formation of sulfur on the surface which blocks any further charge transfer.(9) Another example is silicon in electrolytes free from HF.(50,51)

4.2.2. Oxygen Evolution

Various other semiconductors are known at which no anodic dissolution occurs. These stable materials, mainly oxides, show O_2 evolution during anodic polarization. Most of them exhibit large band gaps; examples are given in Table 1.

The question arises which factors really determine the stability of semiconductors, a problem of great importance for application of semiconductor electrodes in solar energy conversion devices. An indication whether O_2 evolution or dissolution should be expected can be derived from thermodynamic considerations. In corresponding calculations, dissolution potentials are determined from the energies of the compounds and are given in Table 2. According to these results, for instance, the decomposition potentials of TiO_2 and SnO_2 occur at potentials more positive than that for H_2O/O_2 equilibrium. Accordingly, these compounds are expected to be stable. On the other hand, the valence band of these compounds is far below (i.e., at a more positive potential) (see Figure 9) the Fermi energies (standard potentials) of the H_2O oxidation and for the crystal decomposition. Therefore, both reactions are, in principle, possible with high liberation of free energy provided that holes are present in the valence band. The stability of TiO_2, SnO_2, and others is therefore not a thermodynamic but a kinetic problem.(83)

It has recently been reported also that certain chalcogenides such as, e.g., MoS_2 or $MoSe_2$, are relatively stable, which has been interpreted in terms of the layer structures involved and by the existence of an upper valence band consisting mainly of *d* electrons.(75,76,83)

Table 2
Calculated Dissolution Potentials(38,79–82)

Semiconductor	Anodic reaction	$\frac{\Delta G}{nF}$ *vs.* NHE
GaAs (1.4 eV)	$GaAs + 5H_2O + 6p^+ \rightleftarrows Ga(OH)_3 + HAsO_2 + 6H^+$	−0.38 V
GaP (2.35 eV)	$GaP + 6H_2O + 6p^+ \rightleftarrows Ga(OH)_3 + H_3PO_3 + 6H^+$	−0.71 V
CdS (2.5 eV)	$CdS + 2HCl + 2p^+ \rightleftarrows Cd^{2+} + 2Cl^- + 2H^+ + S$	−0.09 V
TiO_2 (3.0 V)	$TiO_2 + 4HCl + 4p^+ \rightleftarrows TiCl_4 + O_2 + 4H^+$	+1.4 V
ZnO (3.25 eV)	$2ZnO + 4H_2O + 4p^+ \rightleftarrows 2Zn(OH)_2 + O_2 + 4H^+$	+0.81 V
SnO_2 (3.8 eV)	$SnO_2 + 4HCl + 4p^+ \rightleftarrows SnCl_4 + O_2 + 4H^+$	+1.05 V

4.2.3. Cathodic Processes

As mentioned earlier, most cathodic processes are due to hydrogen evolution. In other cases a decomposition of the electrode was also observed. Typical examples are rather polar compounds such as CdS, CdSe, and ZnO (see Table 1). In these cases, cathodic polarization leads to production of a metal surface according to the reaction

$$\mathrm{ZnO} + 2\mathrm{e}^- + \mathrm{H}^+ \rightarrow \mathrm{Zn} + \mathrm{H_2O}$$

A series of compounds and their decomposition products is given in Table 1.

An interesting case is the nature of cathodic processes at Ge electrodes. Although H_2 evolution was observed, this process is preceded by reduction of the surface, as given by the reaction(84,85)

$$\rangle\!\!-\mathrm{Ge{-}OH} + \mathrm{H}^+ + \mathrm{e}^- \rightarrow \mathrm{Ge}\cdot + \mathrm{H_2O} \tag{42a}$$

$$\rangle\!\!-\mathrm{Ge}\cdot + \mathrm{H}^+ \rightarrow \mathrm{Ge{-}H} + \mathrm{p}^+ \tag{42b}$$

Cyclic voltametric measurements shown in Figure 14 indicate that only one surface layer is reduced. It is interesting to note that the reduction and reoxidation depends on the crystal faces.(86) Capacity measurements proved that a new Helmholtz layer is formed after cathodic polarization(84) (see also Chapter 2). It could be further shown that the electronic level of the surface radical Ge· is a surface state which is located between the conduction and valence bands, and which appears only as an intermediate state during the surface reduction process.(87) Since the same surface state was detected again in the potential range in which H_2 is finally formed, it has been postulated that the radical occurs as an intermediate state also in the mechanism of H_2 evolution as given by(86)

$$\rangle\!\!-\mathrm{Ge{-}H} + \mathrm{H}^+ + \mathrm{e}^- \rightarrow \mathrm{Ge}\cdot + \mathrm{H_2} \tag{43}$$

followed by reaction (42b).

4.2.4. Influence of Crystal Perfection and Doping on Surface Reactions

As already discussed above and shown in Figure 12, anodic currents at *n*-type electrodes are limited to a low value if the electrode process occurs via the valence band. Low cathodic currents are observed with *p*-type electrodes if a conduction process exists. These currents should be determined by the diffusion of minority carriers (electrons in *p* types and holes in *n*

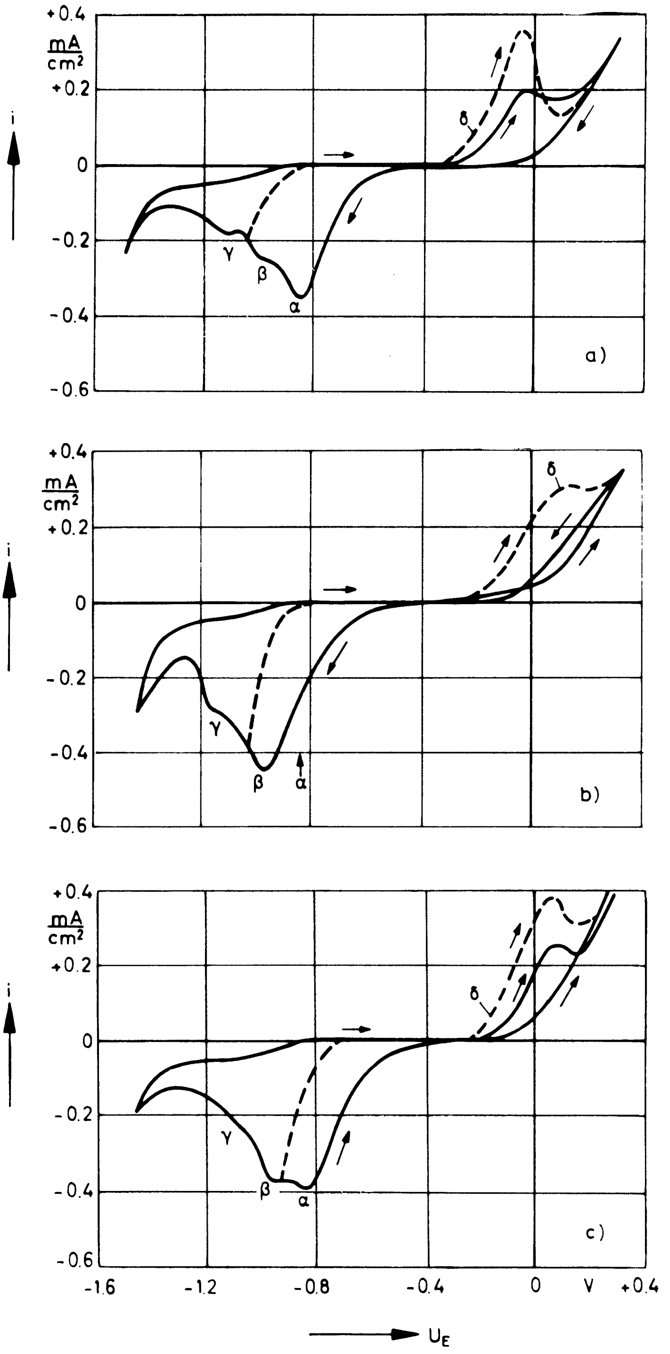

Figure 14. Current–potential dependence for differently oriented germanium crystals in 0.1 *N* H_2SO_4.[86] a) (111); b) (100); c) 110 faces.

types). Frequently, especially in the case of *p*-type electrodes, the current limitation is not very satisfying, i.e., a rather undefined current increase was observed. The situation has considerably improved since expitaxial layers of extremely low dislocation densities and excellent surface smoothness are available. This experience indicates that local high fields at dislocations and kinks lead to thermal activation of minority carriers.

The situation is much less severe for *n*-type electrodes in the anodic range. Here kinks disappear obviously during the anodic dissolution, so that mostly small diffusion-limited currents are observed. On the other hand, a sharp current increase has frequently been observed at higher anodic polarizations. Two examples are given in Figure 15 from which it can be deduced that the doping of the crystals is of importance. The interpretation for the sharp current increase is, however, completely different for these two examples. In the case of highly doped SnO_2 ($N_D \sim 10^{19}$ cm^{-3}), the dark current rises sharply around +1.2 V vs. SCE, i.e., slightly above the H_2O/O_2 potential;

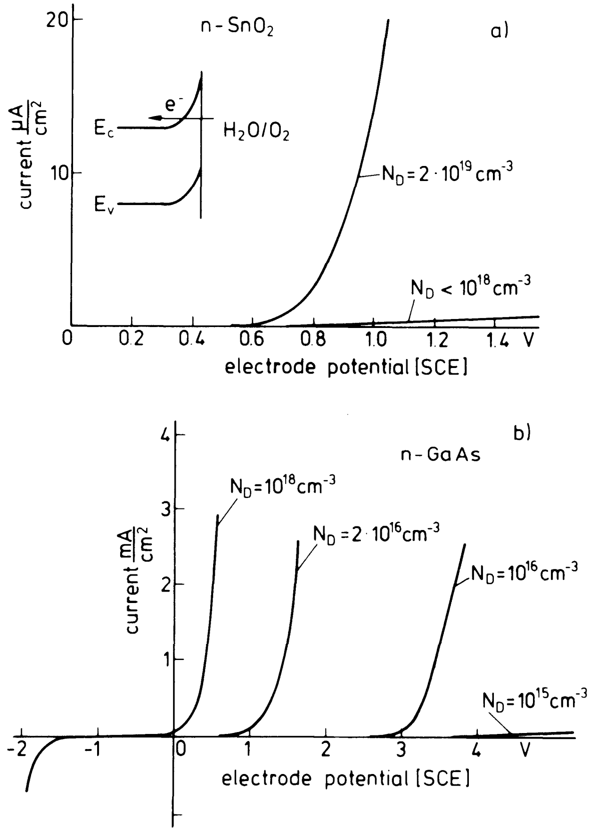

Figure 15. Current–potential dependence for differently doped semiconductor electrodes (a) *n*-SnO_2 at pH 9 (11) (b) *n*-GaAs at pH 14.(93)

although the conduction band occurs at +0.2 V (see insert of Figure 15a). Here the current must be interpreted in terms of electron tunneling through the space charge layer into the conduction band.(89,90) Such a tunneling mechanism seems to be quite reasonable since the thickness of the space charge layer is only about 0.3 nm as calculated from Eq. (13). Similar tunneling processes have also been reported for heavily doped ZnO.(91,92)

There are other examples given in the literature for which a similar sharp current rise was reported, although tunneling had to be ruled out because the thickness of the space charge layer is too large. An example is epitaxially grown *n*-GaAs (Figure 15b). According to the Debye length [Eqs. (12) and (13)], tunneling is not possible for a level of doping below $N_D = 10^{18}\,\text{cm}^{-3}$. In the case of *n*-GaAs, the current–potential behavior was explained quantitatively by an avalanche breakdown, occurring primarily at dislocations.(93)

4.3. Redox Processes

The theory of electron transfer processes given in Section 4.1 should be applicable for simple redox processes at semiconductors so long as the chemical interaction between redox ions and the electrode is weak. At an early stage of semiconductor electrochemistry, Gerischer and Beck(48) already experimentally showed that charge transfer to a redox system at Ge electrodes occurs via one of the energy bands, although there was much interference by anodic dissolution. More quantitative information was obtained later with semiconductor electrodes having much larger band gaps as with CdS, GaP, ZnO, and SnO_2. In these cases, anodic dissolution and H_2 evolution occurs at higher potentials, so that the potential range in which redox reactions can be measured is much larger.

Qualitatively, the same results were obtained as with germanium. However, at different semiconductor electrodes, the same redox process can occur via different energy bands. Two typical examples as found with GaP(14) and SnO_2(11) are given in Figures 16 and 17, respectively. In the case of cathodic processes at GaP electrodes, *p*-type material was used to avoid H_2 evolution. According to Figure 16, the limiting cathodic currents vary with the redox system. The largest current was obtained with Ce^{3+}/Ce^{4+} ($U^{\circ}_{\text{redox}} = +\,1.6$ V vs. NHE). Since its redox energy (Fermi level) occurs near the valence band (compare with Figure 9), the electron transfer should occur via the valence band, as observed experimentally. The current is already diffusion limited. In the three other cases, redox systems having smaller redox potentials are presented. Here the observed currents are not diffusion limited. They are more or less equal to the exchange current $i_v^- = i_v^{\circ}$ [compare with Eq. (40)].

Similar results were obtained with SnO_2 electrodes (*n* type) as shown in Figure 17. Since the energy bands of SnO_2 occur at rather low energies (see Figure 9), it should mainly be expected that an electron transfer via the conduction band would occur as proved experimentally. Here electrons are

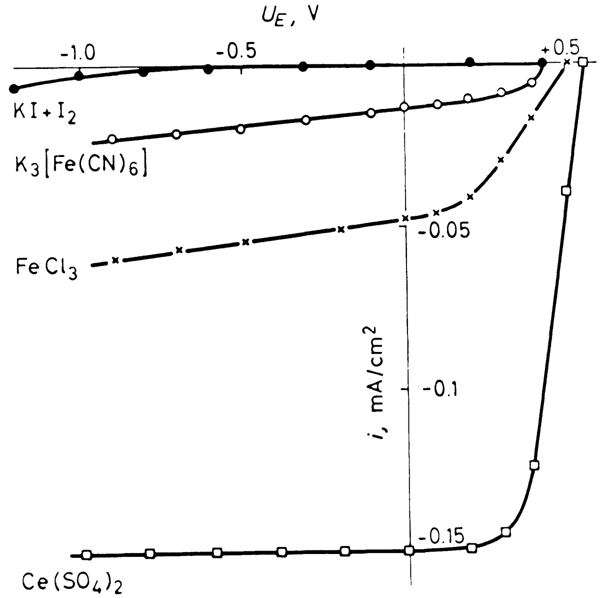

Figure 16. Cathodic currents at p-GaP with various redox systems in 0.1 N H_2SO_4.(14)

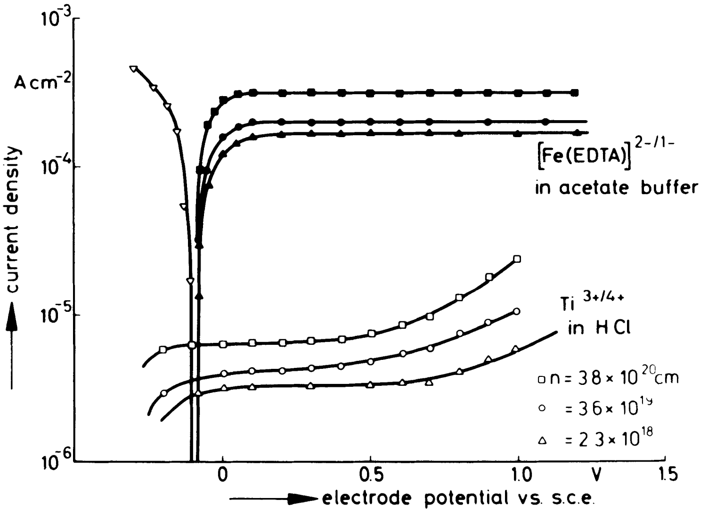

Figure 17. Anodic currents at n-SnO_2 with various redox systems in 2 M HCl.

injected from occupied states of the redox system into the conduction band, and the anodic currents are given by $i_c^+ = i_c^\circ$ as indicated by Eq. (40) (see also Figure 11a).

A large number of other semiconductors and redox systems have been investigated. A selection is given in Table 3 including references.

Table 3
Redox Reactions at Semiconductors

	Redox potential band gap, eV	Ce^{4+}/Ce^{3+} [a] 1.6 V	$IrCl^{2-}/IrCl^{3+}$ [a] 1.02	$[Fe^{3+}/Fe^{2+}]$ [a] 0.77	$[Fe(CN)_6]^{3-/4-}$ [a] 0.36	$[Fe(EDITA)]^{1-/2-}$ 0.15	V^{2+}/V^{3+} [a] −0.26	Ti^{3+}/Ti^{2+} −0.37	Eu^{4+}/Eu^{3+} [a]
Ge	0.88	v.b.[b] (48)	v.b.[c]	v.b. (50)	v.b. (50)	?	c.b. (50)	c.b.[c]	c.b.[c]
Si	1.1	v.b. (50)	v.b.[c]	v.b.[e]	v.b.[e]	?	?	?	?
GaAs	1.4	v.b. (56)	v.b.[c]	v.b. (56)	v.b. (56)	?	?	?	c.b.[d] (79)
GaP	2.25	v.b. (14)	v.b.[c]	v.b. (74)	v.b. (14)	v.b.[e]	?	?	c.b. (79)
CdS	2.5	v.b. (94)	v.b.[c]	v.b. (79)	c.b. (94)	c.b.[c]	c.b.[c]	c.b.[c]	c.b. (94)
SiC	3.0	v.b. (37)	?	v.b. (37)	v.b. (37)	c.b.[c]	c.b.[c]	c.b.[c]	c.b.[c]
ZnO	3.25	c.b.[c]	c.b.[c]	c.b.[c]	c.b. (95)	c.b.[c]	c.b.[c]	c.b.[c]	c.b.[c]
SnO	3.8	c.b. (11)	c.b. (11)	c.b. (11)	c.b. (11)	c.b.[e]	c.b.[e]	c.b.[e]	c.b.[e]

[a] Reference numbers are in parentheses.
[b] v.b., valence band mechanism.
[c] Estimated by comparison with similar redox systems.
[d] c.b., conduction band mechanism.
[e] Unpublished results.

The question also arises whether quantitative information can be obtained from the experimentally determined exchange currents (i_c° or i_v°). This problem will be treated in Section 4.5.

4.4. Electron Transfer Processes at Organic Insulator Electrodes

For comparison, some basic properties of organic electrode materials should also be briefly discussed. In organic molecular crystals, the orbital overlap between neighboring molecules is so small that the energy bands are extremely small, in the order of a few kTs.(96) Accordingly, the electron energy levels are similar to those of the crystal-forming molecules. These have large energy gaps and exhibit insulating properties, i.e., the Fermi level in the bulk is far above the occupied states and far below the unoccupied states (at least by 0.5 eV).(97)

Combining now a molecular crystal with an electrolyte, the Fermi levels must be equal again on both sides of the interface. According to Mehl,(97) the potential drop across the Helmholtz layer, U_H, at such an interface can be neglected since usually strong specific adsorption of ions does not occur. Lohmann(98) calculated U_H and obtained values for anthracene of the order of 0.1–0.3 V. Neglecting the Helmholtz layer, the relative position of energy levels can simply be calculated by the procedure given in Section 3.4. As an example, the energy levels of the interface anthracene/Ce$^{3+/4+}$ are given in Figure 18a.

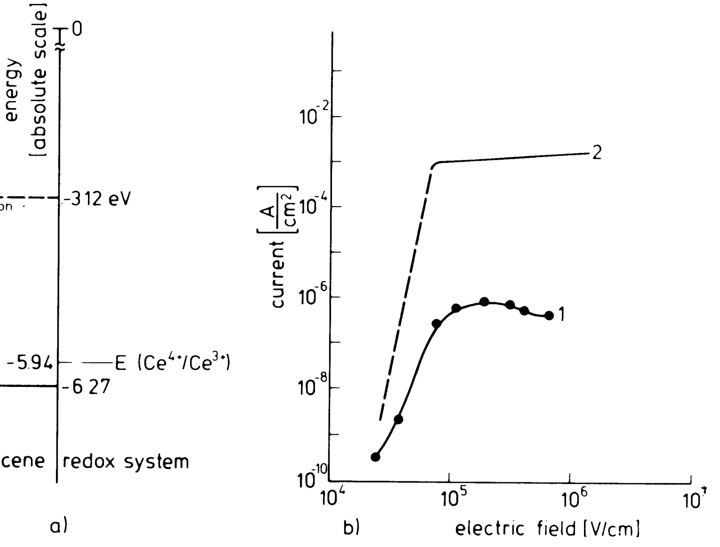

Figure 18. (a) Relative position of energy levels at the interface anthracene electrode–redox system (Ce^{4+}/Ce^{3+}). (b) Dependence of cathodic current on applied field.(105)

As far as electron transfer at the interface is concerned the same conclusions can be drawn from Figure 18a as was done before for ordinary semiconductors. Moreover, the same electron transfer relations, as given by Eqs. (34) and (35), should be applicable. Difficulties arise, however, because the electrodes are insulators. Accordingly, when a charge carrier is injected into an insulator, then the current potential behavior can be entirely determined by the bulk properties of the crystal. In this case the injected carriers produce a space charge which forms a counterforce. Such space-charge-limited currents rise steeply with increasing external voltage.(99) Accordingly, the external voltage has to be raised to a very high level before the current becomes controlled by the electrolytic contact. The thickness of the crystal has to be kept $\leq 50\ \mu m$ in order to allow measurements of the real exchange current at field strengths up to $10^6\ V\ cm^{-1}$.

The first experiments with anthracene electrodes were performed by Kallmann and Pope.(100,101) More detailed investigations were performed by Mehl and co-workers (see Ref. 97 and literature cited there). These authors analyzed quantitatively various charge transfer processes. They observed, for instance, a cathodic limiting current for anthracene using $Ce^{4+/3+}$ as a redox system (curve 1 in Figure 18b). This current is controlled by the interface properties and was interpreted by injection of positive carriers into the valence band of anthracene as expected from the energy picture in Figure 18a. The sharp increase of current at lower field strengths is determined by the bulk properties (space-charge-limited current). The same research group also showed that electron injection into a higher energy level of anthracene is possible using Li/Li^+ in ethylenediamine as a sufficiently negative redox system.(103)

Unfortunately, these crystals are not completely inert. Injected charge carriers at the surface, especially holes, undergo slow side reactions which lead to a change of the chemical nature of the crystal surface.(104) This effect has a remarkable influence on the interface-controlled limiting current, as shown by Willig *et al.*(105) These authors developed a kind of pulse technique in which the contact between organic crystal and electrolyte was made immediately before measurement. The currents were then determined within about 3 msec. This technique ensured a low density of injected carriers. A typical result is given by curve 2 in Figure 18b.

4.5. Evaluations of Exchange Currents and Determination of Reorientation Energies

At first sight, it should be possible to determine the reorientation energy, λ, from Eqs. (36a) and (36b) if the exchange current i_c° or i_v° is measured. Difficulties arise, however, since assumptions have to be made concerning the collision frequency Z and the transition factor κ. Z has been calculated by Marcus,(33) who suggests a value of $10^4\ cm\ sec^{-1}$. It is impossible, however, to estimate a reasonable value of κ. It should be unity for a pure adiabatic process.(33) If, however, the reaction is nonadiabatic, then $\kappa \ll 1$, which depends on the interaction between initial and final state in the transition state. Accordingly, κ varies with the electrode material and the reacting molecules in the electrolyte.(33,106) Consequently, it is impossible to determine λ directly from i_c° or i_v°.

It should be mentioned that the same problem arises for metal electrodes. The corresponding exchange current is given here by (see, e.g., Ref. 19)

$$i_{\text{met}}^\circ = F \cdot Z \cdot c\rho(E_F)\kappa\left(\frac{kT}{\pi\lambda}\right)^{1/2} \exp\left(-\frac{\lambda}{4kT}\right) \tag{44}$$

[$\rho(E_F)$ in the density of states at the Fermi level].

Several years ago, two other methods for determining λ were reported in the literature which are independent of knowledge of κ. The first method is based on the fact that, at heavily doped semiconductors, electron transfer can also occur via tunneling through the space charge layer, as schematically shown in Figure 19 for anodic processes at SnO_2.(9,89,107) In this example, the occupied levels D_{red} of the redox system overlap only slightly with the conduction band, i.e., the usual exchange current i_c° is small. Provided that the thickness of the space charge layer is sufficiently small, then electrons can also tunnel at lower energies from the occupied states D_{red} into the conduction band. The corresponding tunnel current, i_T, can be larger than the usual exchange current, i_c°, because more occupied states are available at lower energies. The tunneling probability, $T(E)$, depends on the thickness of the space charge layer. Since the latter depends on the potential across the space charge layer according to Eq. (12), also $T(E)$ varies with the applied potential (see Figure 10). In addition, the tunneling probability can also be influenced by the doping of the crystal because the layer thickness depends, via the Debye length [Eq. (12)], on the donor density. The exchange current is now given [cf. Eq. (36a)] by

$$i_c^\circ = \frac{F \cdot Z \cdot c}{(\pi kT\lambda)^{1/2}}\kappa N_c \int_{E_c}^{\infty} T(E, N_D) \exp\left[-\frac{(E_c - E_{\text{F,redox}} - \lambda)^2}{4kT\lambda}\right] dE \tag{45}$$

Corresponding current–potential curves measured with differently doped SnO_2 electrodes could be quantitatively evaluated by using the above equation.(89) The whole set of curves could be interpreted by assuming one single λ value. Values obtained for various redox systems are given in Table 4.

The other method is based on investigations at organic electrodes.(108) In this case, λ values were obtained by comparing cathodic exchange currents obtained with different organic electrode materials. Taking one redox system (e.g., Ce^{4+}/Ce^{3+}) then the energy difference $E_v - E_{\text{F,redox}}$ changes from one crystal to the other (see Figure 18a) and can be calculated as discussed in Section 3.4, provided that the potential across the Helmholtz layer can be neglected. The latter has been proved as follows:

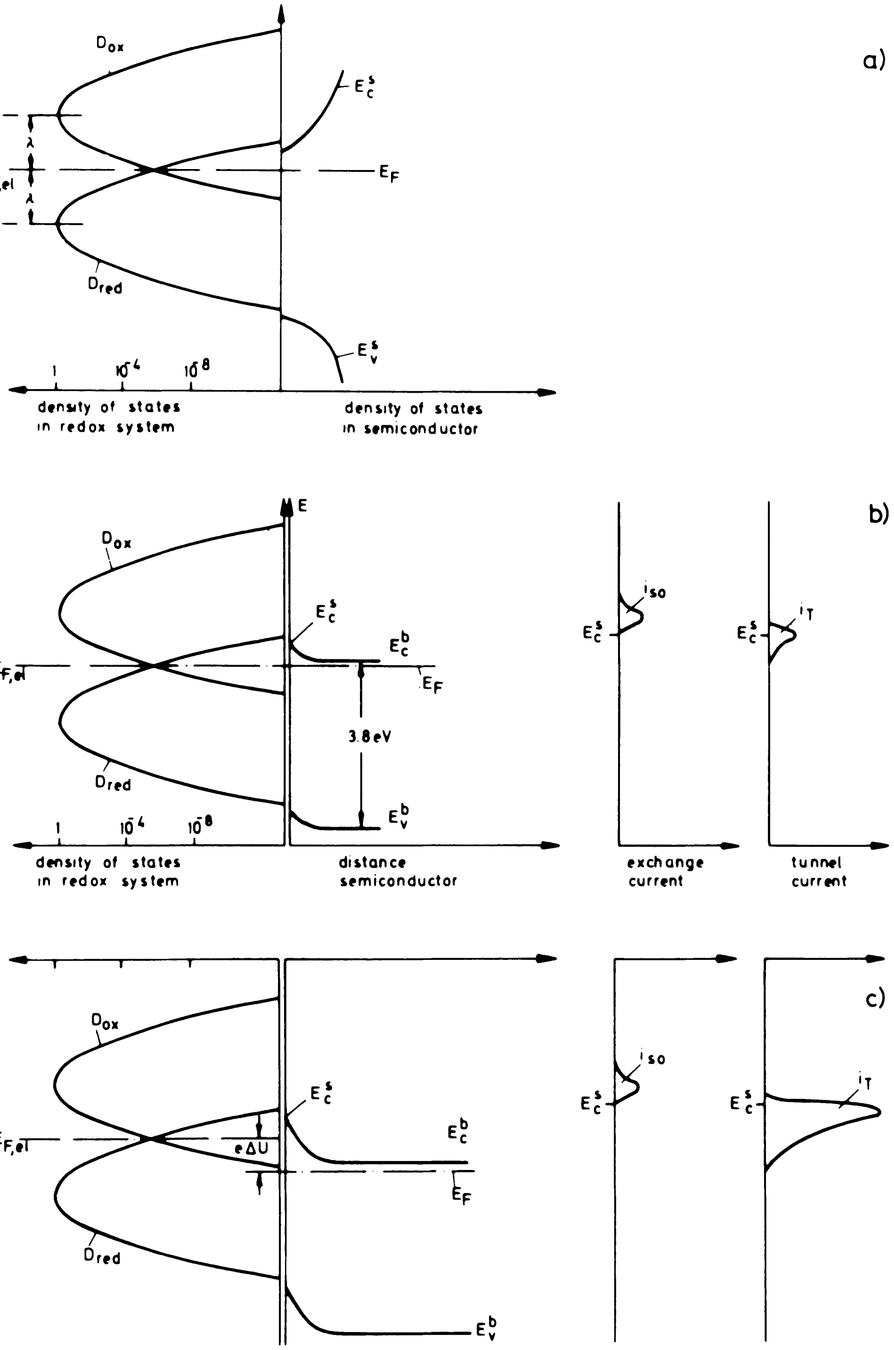
a)
D_{ox}
E_c^s
λ
$E_{F,el}$
λ
E_F
D_{red}
E_v^s
1
10^{-4}
10^{-8}
density of states in redox system
density of states in semiconductor
b)
E
D_{ox}
E_c^s
E_c^b
$E_{F,el}$
E_F
3.8 eV
D_{red}
E_v^b
1
10^{-4}
10^{-8}
density of states in redox system
distance semiconductor
E_c^s
i_{so}
exchange current
E_c^s
i_T
tunnel current
c)
D_{ox}
E_c^s
E_c^b
$E_{F,el}$
eΔU
E_F
D_{red}
E_v^b
E_c^s
i_{so}
E_c^s
i_T

Figure 19. Schematic diagram for electron transfer via tunneling through the space charge of a heavily doped semiconductor.

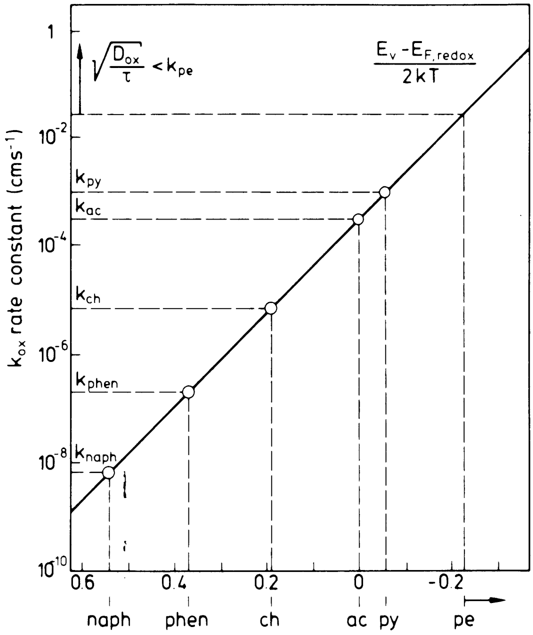

Figure 20. Rate constants vs. relative positions of the valence of various organic crystals with respect to anthracene. (naphthalene, naph; phenanthrene, phen; crysene, ch; pyrene, py; anthracene, ac). Redox system: Ce^{4+}/Ce^{3+} in 1 N H_2SO_4.(109)

The cathodic exchange current given by Eq. (36b) can be approximated to

$$i_v^\circ = Fc\kappa\left(\frac{kT}{\pi\lambda}\right)^{1/2} N_v \exp\left[-\frac{\lambda + 2(E_v - E_{\mathrm{F,redox}})}{4kT}\right]$$

provided that

$$\frac{E_v - E_{\mathrm{F,redox}}}{\lambda} \ll 1$$

Rearranging the above equation, one obtains

$$\ln k_{\mathrm{ox}} = \ln\left(\frac{i_v^\circ}{F_c}\right) = \ln\left[\kappa\left(\frac{kT}{\pi\lambda}\right)^{1/2} N_v\right] - kT^{-1}\left[\frac{\lambda}{4} + \frac{(E_v - E_{\mathrm{F,redox}})}{2}\right] \quad (46)$$

This relation was confirmed by using various electrode materials with $Ce^{4+/3+}$ as a redox system (Figure 20).(109) It can be concluded that the transition factor and the density of states is equal for all organic crystals given in Figure 20. Accordingly, the measurement of i_v° for the two different electrodes is sufficient for determining λ. The experimental values are very similar to those given in Table 4.(108)†

According to Table 4, the reorientation energies differ considerably from one redox system to another. The unusually high λ value obtained for

---

† According to more recent experiments by Willig, the λ value for $[Fe(CN)_6]^{4-/3-}$ is about 1 eV (private communication).

Table 4
Comparison of λ Values (eV)

Redox system	From SnO_2 electrodes[a]	From Pt electrodes[b]	Theoretical values $\lambda_0 + \lambda_i = \lambda$
Fe^{2+}/Fe^{3+} (0.5 M H_2SO_4)	1.2 ± 0.2 (89)	1.49	1.14 + 0.46 = 1.60
Ce^{3+}/Ce^{4+} (0.5 M H_2SO_4)	1.7 ± 0.2 (89)	2.06	1.07 + 0.1 = 1.17
$[Fe(CN)_6]^{4-/3-}$ acetate buffer	0.4 ± 0.2 (89)	1.2	0.86 + 0.38 = 1.24
Quinone 0.5 M H_2SO_4	0.5 ± 0.2 (131)		

[a] Reference numbers are in parentheses.
[b] From Ref. 106.

Ce^{3+}/Ce^{4+} is interpreted in terms of different ligand configurations in Ce^{3+} and Ce^{4+} ions.(109)

Further details on the analysis of exchange currents, and experimental and theoretical λ values, are given in other review papers.(9,106)

5. Photoeffects

5.1. Photopotentials and Photocurrents

In Section 4.2 we have described electrode reactions which were partly limited by the deficiency of electrons or holes in the corresponding energy bands. A typical example was the current–potential behavior in Figure 12. The anodic current at the *n*-type electrode was limited by the diffusion of holes and the cathodic current at the *p*-type electrode by the diffusion of electrons toward the surface. It was further mentioned that these currents could be enhanced by light absorbed by the electrode.

In the present chapter, the nature of the photopotential and the efficiency of photocurrents will be treated in more detail.

As described in Section 2, a certain potential drop, U_{SC}, arises across the space charge layer of the semiconductor and corresponds to a certain band bending. Taking a weakly doped *n*-type semiconductor as an example, the energy bands may be bent upward or downward, as schematically shown in Figure 21. Illuminating such an electrode by light, electrons are excited from the valence band into the conduction band, i.e., electron–holes are created as indicated in Figure 21. Since an electric field exists across the space charge region the electron–hole pairs are separated. In the case of a negative space charge (Figure 21a), the electrons are drawn toward the surface and the holes toward the interior of the crystal. In the other case (positive space charge; Figure 21b), electrons and holes move in the opposite directions. In both cases, the potentials across the space charge, and consequently the resulting band bending, are reduced as indicated by the dashed curves in

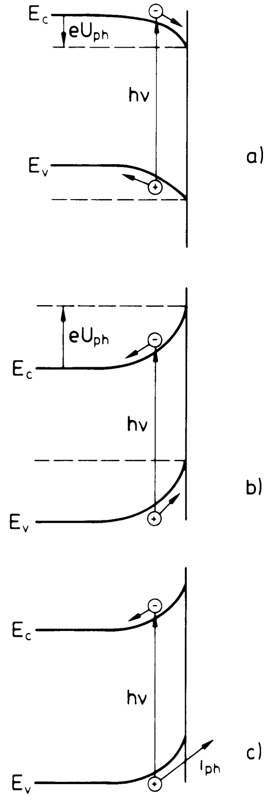

Figure 21. Production of electron–hole pairs by light excitation, of photovoltage under open-circuit conditions (a) and (b) and the production of a photocurrent under short-circuit conditions.

Figure 21. The photopotential, U_{ph}, developed across the space charge region can be detected as a change of the electrode potential under galvanostatic conditions. It is quite clear that the photopotential depends on the light intensity and on the original band bending in the dark U_{SC}°. The maximum photopotential is obtained when the energy bands become flat. A quantitative relation between U_{ph} and the increase of carrier densities, Δn and Δp, which are proportional to the light intensity, can be derived from the field equation (4) in Section 2 as follows:

Rewriting Eq. (4) in an abbreviated form, one obtains in the dark

$$E_s^{\circ} = \frac{kT/e}{L_{\text{D}}} f_{\text{SO}}(U_{\text{SC}}^{\circ}, n_0, p_0) \tag{47}$$

and during illumination

$$E_s = \frac{kT/e}{L_{\text{D}}} f_s(U_{\text{SC}}, n_0 + \Delta n, p_0 + \Delta p) \tag{48}$$

Δn and Δp are the concentration changes at the edge between the bulk and space charge regions. To conserve electroneutrality, $\Delta n = \Delta p$. Since the total charge of the semiconductor is not changed upon illumination, the surface field remains, in accordance with Eq. (6), also unchanged, i.e.,

$$E_s = E_s^\circ$$

By equating expressions (47) and (48), one obtains

$$U_{\text{ph}} = U_{\text{SC}} - U_{\text{SC}}^\circ = f(U_{\text{SC}}^\circ, n_0 + \Delta n, p_0 + \Delta n) \tag{49}$$

which is a rather complex expression as derived by Johnson$^{(110)}$ (see also Ref. 19), which will not be given here. Experimental values of the photovoltage, as obtained with silicon, are given in Figure 22,$^{(111)}$ which corresponds, qualitatively, with the theoretical values. The sign of the photovoltage changes at $U_{\text{SC}}^\circ = 0$, i.e., at the flatband potential. Similar results were also obtained with germanium.$^{(112)}$

Large photovoltages of the order of the band gap can be obtained for heavily doped semiconductors (N_D or $N_A \geq 10^{17}$ cm^{-3}) for a large degree of band bending. The above equation can be approximated by

$$\begin{aligned} U_{\text{ph}} &= -\frac{kT}{e}\ln\frac{\Delta p}{p_{0(n)}} \quad \text{for } n \text{ type} \\ U_{\text{ph}} &= +\frac{kT}{e}\ln\frac{\Delta n}{n_{0(p)}} \quad \text{for } p \text{ type} \end{aligned} \tag{50}$$

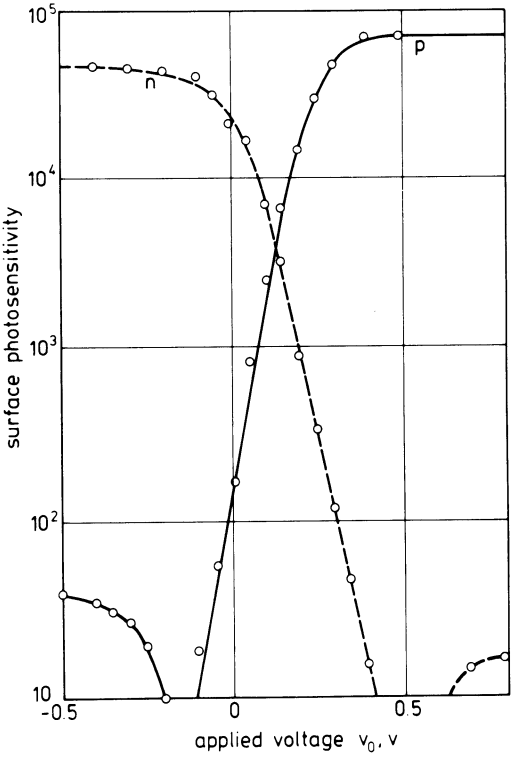

Figure 22. Photopotential vs. applied potential at n- and p-type silicon electrode in 0.1 N H_2SO_4.$^{(111)}$

They are valid for exhaustion or inversion layers as long as $|U_{\text{ph}}| < |U^{\circ}_{\text{SC}} - 0.1\text{ V}|$. Above this value, U_{ph} saturates. According to Eq. (50), large photovoltages are already obtained at rather low intensities because the carrier density created by light excitation can easily exceed the minority carrier density $p_{0(n)}$ in n-type or $n_{0(p)}$ in p-type material.

According to these results, it is in principle possible to determine the flatband potential (Section 2) by measuring the electrode potential of an illuminated electrode under open circuit conditions. This method, as will be shown later, can lead, however, to rather inaccurate results.

Under potentiostatic conditions, no photopotential can be developed since the potentials across the space charge region and the Helmholtz layer are kept constant. In this situation, the electron–hole pairs created by light excitation are still separated by the field within the space charge region. Now the charge carriers drawn toward the electrode surface are forced to cross the interface which leads to a corresponding photocurrent, as schematically shown in Figure 21c. According to this model a photocurrent is expected as long as a field exists across the space charge layer, i.e., the photocurrent should start to rise around the flatband potential. This result leads to the interesting consequence that light-induced reactions occur in a potential range where they are not expected from a thermodynamic point of view. This has been proved experimentally for many semiconductor electrodes. It has also been shown that the photocurrent, i_{ph}, is proportional to the intensity I_0 of light since

$$i_{\text{ph}} \sim \Delta n \sim I_0 \tag{51}$$

In addition, the photocurrent also depends on the wavelength or energy of the exciting light. The photocurrent sets in at about a light energy equivalent to the band gap energy. An example is given in Figure 23.(79) i_{ph} rises until it reaches a constant value at higher energies. The limiting value is obtained if all excited minority carriers reach the surface where they are used in the reaction process.

It must be emphasized that the carriers produced by light excitation are not only drawn toward the surface by diffusion. It depends on the penetration depth of light whether the field effect or the diffusion dominates. A quantitative treatment of the problem has recently been given by Butler,(113) who used formulas applied to pure solid–solid interfaces given by Gärtner.(114) Following arguments given by Butler for photons incident upon the interface, the generation of electron–hole pairs is given by

$$G(x) = I_0 \alpha \exp(-\alpha x) \tag{52}$$

where I_0 is the photon flux, α the optical absorption coefficient, and x is the distance into the semiconductor. It is assumed that all carriers created in the space charge region contribute to the current. The latter is then given by

$$i_{\text{ph,field}} = e \int_0^{d_{\text{SC}}} g(d)\, dx = -eI_0[\exp(-\alpha d_{\text{SC}}) - 1] \tag{53}$$

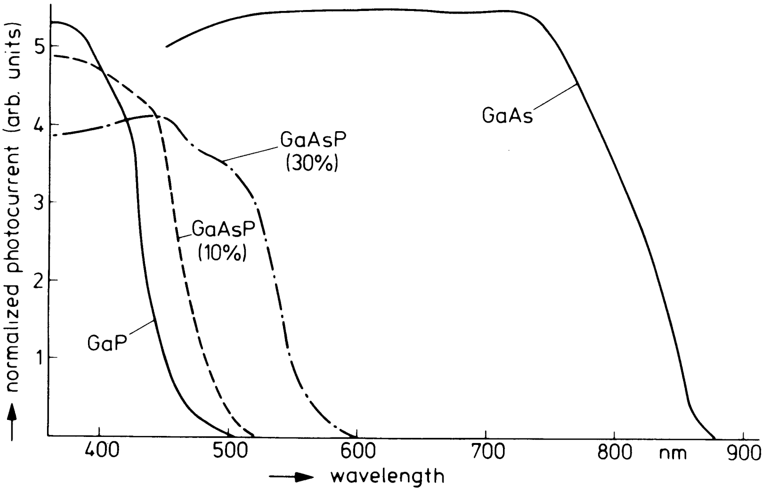

Figure 23. Excitation spectra of photocurrents at various semiconductor electrodes in 0.1 *N* H_2SO_4.(79)

where d_{SC} is the thickness of the space charge region as given by Eq. (12) in Section 2.

The contribution of diffusion to the current is obtained by solving the diffusion equation for minority carriers created by light. Using the boundary conditions given by Gärtner,(114) that $\Delta n = 0$ for $x \to \infty$ and for $x = d_{SC}$, one obtains

$$i_{\text{ph,diff}} = eI_0 \frac{\alpha L}{1 + \alpha L} \exp(-\alpha d_{SC}) \tag{54}$$

in which L is the diffusion length of the minority carriers. The boundary conditions imply that diffusion occurs only outside the space charge region and that any electron–hole reaching the space charge layer is immediately separated. Combining the two contributions to the total photocurrent one obtains

$$i_{\text{ph}} = i_{\text{ph,field}} + i_{\text{ph,diff}} = eI_0\left[1 - \frac{\exp(-\alpha d_{SC})}{1 + \alpha L}\right] \tag{55a}$$

Inserting d_{SC} from Eq. (13) leads to

$$i_{\text{ph}} = eI_0\left\{1 - \frac{\exp[-2\alpha L_{\text{D,eff}}(eU_{SC}/kT - 1)^{1/2}]}{1 + \alpha L}\right\} \tag{55b}$$

in which the effective Debye length $L_{\text{D,eff}}$ is given by Eq. (11). Two extreme cases are of interest here:

(i) The absorption (α) or the thickness of the space charge is very large so that $\alpha d_{SC} \gg 1$. Then we have $i_{\text{ph}} = eI_0$ [see Eq. (55a)], i.e., all created carriers contribute to the photocurrent. An example is given in Figure 24a.

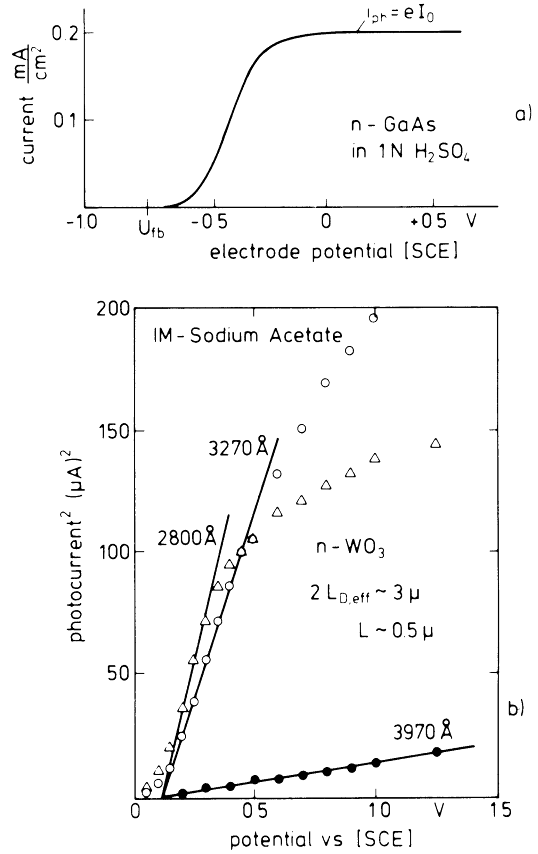

Figure 24. Photocurrent vs. electrode potential (a) n-GaAs$^{(127)}$ (b) n-WO_3 (photocurrent plotted as i_{ph}^2; see text).

(ii) We assume $\alpha L \ll 1$. We can further expand the exponential term in (55a) or (55b) for

$$\alpha L_{D,eff}\left(\frac{eU_{SC}}{kT} - 1\right)^{1/2} \ll 1$$

Then we obtain from (55)

$$i_{ph} \sim eI_0\alpha(L + d_{SC}) = eI_0\alpha\left[L + eL_{D,eff}\left(\frac{eU_{SC}}{kT} - 1\right)^{1/2}\right] \tag{56}$$

In this case the photocurrent can also be potential independent if $L \gg d_{SC}$. Theoretically a photocurrent should even occur at the flatband potential ($d_{SC} = 0$). In practice, however, such a situation would not occur because on inverse polarization (accumulation) we have a reverse sign of field and the minority carriers would be drawn toward the bulk. In other cases, L can be neglected ($L \ll d_{SC}$). Then one obtains a rather simple relation after rearranging Eq. (56), viz.,

$$i_{\mathrm{ph}}^2 \sim (2eI_0\alpha L_{\mathrm{D,eff}})^2\left(\frac{eU_{\mathrm{SC}}}{kT} - 1\right)$$

$$\sim (2eI_0\alpha L_{\mathrm{D,eff}})^2 \frac{e}{kT}(U_E - U_{\mathrm{fb}}) \qquad (57)$$

in which U_E is the electrode potential.

The potential dependence of the photocurrent was qualitatively found by Morrison.(115) Quantitatively the above relation has been tested for various wavelengths (i.e., different α values) by using *n*-type WO_3,(113) as shown in Figure 24b. Butler has also suggested using this procedure for determining the flatband potential by extrapolating the linear plot of i_{ph}^2 vs. U_E to $i_{\mathrm{ph}} \rightarrow 0$. The flatband potential obtained from Figure 24b agrees quite well with the value derived from capacity measurements.(60)

There are other examples in the literature where the photocurrent does not rise near the flatband potential and then considerable band bending is required before any photocurrent can be detected. This inhibition is due to surface recombination, which will be treated in Section 5.2.3.

5.2. Applications in Electrode Kinetics

5.2.1. Competition between Redox Processes and Other Reactions

As discussed previously, anodic currents at *n*-type electrodes can be increased by light excitation if holes are required for the corresponding electrode process. In many cases such a process is the anodic dissolution of the semiconductor material. The question arises now, what kind of process occurs under illumination, if a redox system is added to the electrolyte?

This question cannot be answered by measuring only the photocurrent because the latter depends only on the light intensity. More specific information can be obtained by chemical analysis or by application of a special rotating ring–disk electrode system. The latter consists of a semiconductor disk and a Pt ring as the collector electrode. Taking redox processes at *n*-type CdS electrodes as an example, one can discriminate between alternative courses of reactions at the semiconductor disk electrode as follows:

Without any redox system, illumination leads to an anodic corrosion process represented by

$$\mathrm{CdS} + p^+ \rightarrow \mathrm{Cd}^{2+} + \mathrm{S} \qquad (58)$$

(compare with Table 1 in Section 4.2.1) in which the holes (p^+) are created by light absorption in the CdS electrode. If a redox system, such as $[\mathrm{Fe(CN)_6}]^{4-}$, is added to the electrolyte, the holes may also be consumed in the oxidation of this compound by the reaction

$$[\mathrm{Fe(CN)_6}]^{4-} + p^+ \rightarrow [\mathrm{Fe(CN)_6}]^{3-} \qquad (59)$$

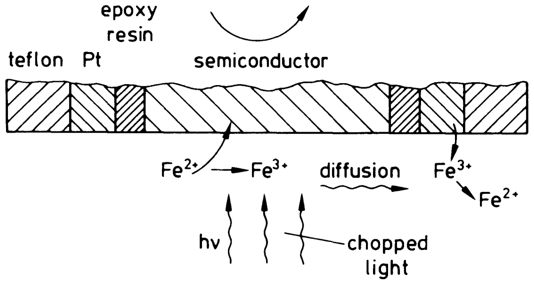

Figure 25. Ring–disk electrode.(118)

Illuminating the semiconductor in the rotating arrangement (Figure 25) then the $[Fe(CN)_6]^{3-}$ ions produced at the CdS electrode can be reduced at the Pt-ring if its potential is well negative with respect to the standard potential of the redox system.

This method was applied to this kind of problem at first by Honda *et al.*(116,117) for the oxidation of I^- and CdS. Some other authors(89,118–120) used the same technique for the quantitative analysis of various other redox reactions and semiconductors. Results obtained with CdS and $[Fe(CN)_6]^{4-}$ are presented in Figure 26. According to this figure, both the photocurrent i_D and the ring current i_R start to rise at the same potential. A quantitative analysis has shown(119) that, in this range, the photocurrent is entirely due to the oxidation of $[Fe(CN)_6]^{4-}$. At higher potentials, at which i_D still increases and the ring current decreases, the anodic dissolution reaction (58) proceeds obviously at the expense of the generation of $[Fe(CN)_6]^{3-}$. This result can be interpreted as follows: The disk current due to the oxidation of $[Fe(CN)_6]^{4-}$ is controlled by the diffusion of these ions toward the electrode ($i_{\text{diff}} = 102\ \mu A$

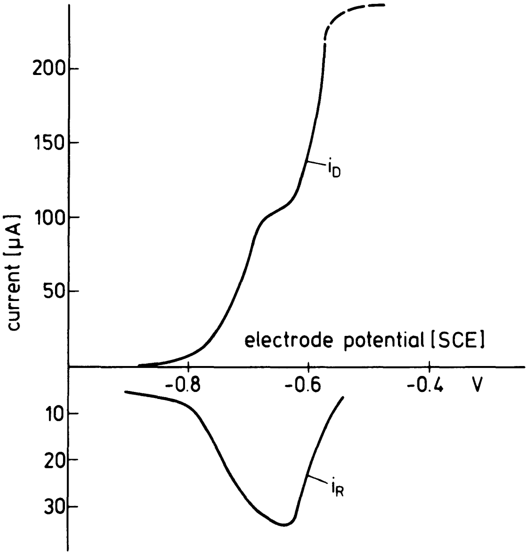

Figure 26. Disk current i_D (photocurrent) and ring current i_R vs. electrode potential(119) disk: CdS electrode, redox system $[Fe(CN)_6]^{4-}$.

in this case). Since the photocurrent determined only by the light intensity is much higher, the surface reaction (58) must occur. Since, however, the ring current does not remain constant but decreases, it must be concluded that the oxidation of CdS [reaction (58)] leads to changes of the electrode surface which inhibits the redox process. This is confirmed by measurements at low light intensities ($i_{\mathrm{ph}} \ll i_{\mathrm{diff}}$) which yielded a constant ring current.(118)

Various other combinations of semiconductors and redox systems have been studied(79,116,121) with the aim to understand the factors which determine the competition between dissolution and redox process. According to the energy model (Figure 9) derived in Section 3.3 one should expect that the redox reaction is predominant if its energy levels overlap well with the valence band. In the case of CdS, this condition is very well fulfilled for the redox systems Fe^{2+}/Fe^{3+} or Ce^{3+}/Ce^{4+} but not really for $[Fe(CN)_6]^{4-/3-}$. Measurements with the ring–disk electrode have shown, however, that the oxidation of Fe^{2+} and Ce^{3+} does not compete with the dissolution reaction whereas the oxidation of $[Fe(CN)_6]^{4-}$ turned out to be no problem if $i_D \ll i_{\mathrm{diff}}$ (see above).(118)

This result seems to be in contradiction to the energy model. Similar observations have also been made with other semiconductors such as GaAs and GaP.(79) The problem can only be solved on the basis of the energy model by assuming an electron transfer from the occupied states of the $[Fe(CN)_6]^{4-/4-}$ system into surface states of CdS from which electrons recombine with a hole in the valence band as shown schematically in Figure 27a. Such a surface state can be the electronic level of a partly separated surface group (indicated by A) which is formed as an intermediate state in the dissolution process. The final separation can be prevented if an electron is transferred from a suitable redox system to such a surface group. In this process the bond is restored (Figure 27b) and the surface state disappears.(38)

5.2.2. Recombination and Reactions via Surface States

Most effects discussed in earlier sections could be interpreted without assuming the presence of surface states. This may be surprising because the periodicity of crystal lattice of the semiconductor is interrupted at the surface. In many cases, certainly surface states are present but they are not recognized. They can be detected by surface recombination measurements using the so-called thin slice method,(3,77) schematically shown in Figure 28a. This method consists of using a semiconductor electrode, e.g., *n*-type material, with a *pn* junction on the reverse side. If electron–hole pairs are created near the surface by light of small penetration depth, these pairs can diffuse through the crystal to the *pn* junction where they can be detected by measuring a short-circuit current. The electron–hole pair may also, however, recombine via surface states as indicated in Figure 28b. The corresponding surface recombination velocity S was derived by Stevenson and Keyes,(122) who

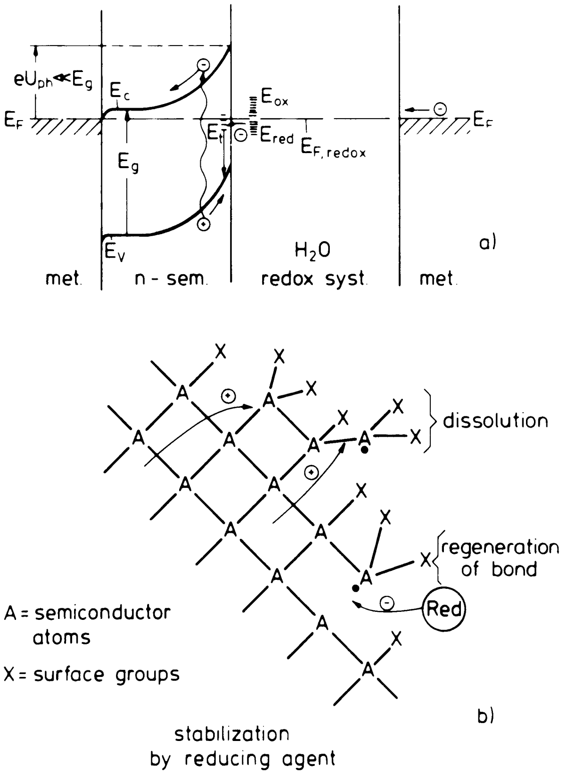
eU_ph ≪ E_g
E_F
E_c
E_g
E_t
E_V
E_ox
E_red
E_F, redox
E_F
H2O
met.
n - sem.
redox syst.
met.
a)
A
X
dissolution
regeneration of bond
Red
A = semiconductor atoms
X = surface groups
stabilization by reducing agent
b)

Figure 27. Surface states and stabilization of electrode surface of *n*-type semiconductor by a redox system.[38]

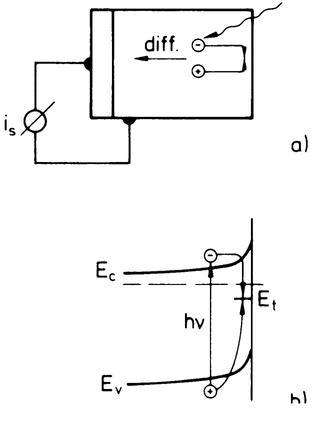
hν
diff.
i_s
a)
E_c
E_t
hν
E_v
b)

Figure 28. (a) "Thin-slice" method (schematic) for measuring surface recombination; (b) recombination of electron–hole pairs via surface states obtained

$$S = \frac{N_t C_n C_p (n_0 + p_0)}{C_n\{n_0 \exp(-eU_{SC}/kT) + N_c \exp[(E_t - E_c)/kT]\} + C_p\{p_0 \exp(eU_{SC}/kT) + N_v \exp[(E_v - E_t)/kT]\}} \tag{60}$$

in which C_n and C_p are capture probabilities for electrons and holes, and N_t and E_t are the density and energy of surface states, respectively. This equation is only valid in this form for $\Delta n \ll n_0$ and p_0.(123) The recombination velocity S depends on the band bending, eU_{SC}; it tends toward zero for strong upward and downward band bending, i.e., a maximum is expected at some U_{SC} value. The short-circuit current i_s, measured on the back side of the thin slice arrangement, is related to the surface recombination by(123,124)

$$i_s \sim I_0\left(\frac{1}{S} + \frac{D}{L}\right) \tag{61}$$

in which L is the diffusion length of the created electron–hole pairs in the bulk of the semiconductor, D the diffusion constant, and I_0 the incident light intensity.

This method has been successfully applied to Ge and Si electrodes. Brattain and Boddy(5) found, for example, that a Ge–OH surface was nearly free from surface states ($N_t \leq 10^8\ \text{cm}^{-2}$), whereas, upon adsorption of Cu^{2+}, Ag^{2+}, and Au^{3+} ions on such a surface, about 10^{10}–$10^{11}\ \text{cm}^{-2}$ surface states were found.(125,126) Later it was found that during the reduction of a Ge–OH surface [see reaction (42)] to Ge–H, surface states appeared as intermediates which could be correlated to Ge· radicals.(88) After completion of the Ge–H surface, again no surface states were detectable. Also in the case of silicon surface states were measured,(111,123) but their chemical nature could not be explained.

Since created electron–holes can recombine via surface states, the question arises whether this process effects also the quantum yield of photocurrents discussed earlier. Such an effect has been indeed observed. An example is *p*-GaAs, as shown in Figure 29. Here the cathodic current (solid line) does not set in at the flatband potential as normally expected, but only at a much more negative potential. In this case obviously the recombination (steps 1 and 2 in Figure 29b) is much faster than the electron transfer to H^+ ions. Since the recombination is potential dependent [see Eq. (60)] the electron transfer is only efficient at higher potentials. It is interesting to note that the photocurrent occurs already near U_{fb} if a redox system is added, the energy levels of which exist at the level of the surface states.(127) In this case, the electron transfer (step 4) competes efficiently with the second recombination step 2. Similar results were obtained with *p*-GaP.(127) In the case of an *n*-type electrode, recombination seems to be a less severe problem.(128,129)

The recombination via surface states can also be observed without any light excitation. In the case of *n*-GaP, for instance, it has been found that luminescence occurs if holes are injected by an electrochemical process.(69,130)

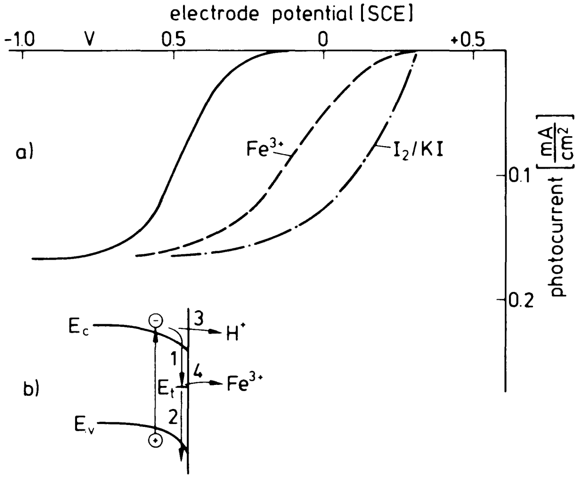

Figure 29. (a) Cathodic photocurrent vs. electrode potential at *p*-GaAs at pH 1; (b) electron transfer via surface states.(127)

5.2.3. Two-Step Redox Processes

Two-step redox processes are understood as reactions in which two electrons are exchanged at the electrode. Typical examples involve H_2O_2, $S_2O_8^{2-}$, quinones, HCOOH, and various other organic substances. Taking H_2O_2 as an example, its reduction can be studied by using photoexcitation techniques as follows:

As already discussed in Section 4.3, the reduction of a redox system having a large positive standard potential is expected to occur via the valence bands of many semiconductors. Experiments have shown, for instance, that the reduction of Ce^{4+} ions ($U_{redox} = +1.4$ V) at GaP electrodes is already a valence band process. Since H_2O_2 has a standard potential ($U_{redox} = +1.77$ V) even larger than that of Ce^{4+}/Ce^{3+}, one also expects a valence band process, i.e., a corresponding cathodic current should be measured at a *p*-type GaP electrode. Experiments have shown, however, that no current (in the dark) is detectable. On the other hand, a photocurrent was measured which was twice as large as that measured without H_2O_2 (Figure 30a), although the photocurrent is only determined by the light intensity. This "current doubling" was interpreted through the assumption that half of the electrons required for the reduction of H_2O_2 are created by light excitation.(8) Accordingly, it was postulated that, in the first step, an electron is transferred from the conduction band to the redox system and the second one from the valence band, as schematically shown in Figure 30b. The corresponding reaction scheme is given by(8)

$$H_2O_2 + e^- \rightarrow \dot{O}H + OH^- \tag{62a}$$

$$\dot{O}H \rightarrow OH^- + p^+ \tag{62b}$$

This reaction scheme, especially reaction (62b), was proved as follows:

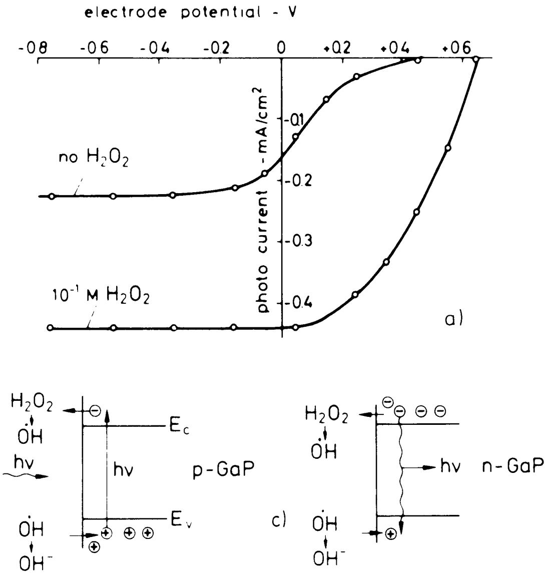

Figure 30. "Current-doubling" processes. (a) Cathodic photocurrent at *p*-GaP with 10^{-1} *N* H_2O_2 at pH 1 (8); (b) two-step electron transfer at *p*-type GaP upon light excitation; (c) the same as (b) for *n*-type in the dark leading to light emission.

Using *n*-type instead of *p*-type GaP electrodes, the whole process occurred already without light excitation because sufficient electrons were available. In the second step, holes (here minority carriers) were injected into the valence band which recombined with electrons of the conduction band. Such a recombination in GaP is a radiative transition, which would be detected by measuring the emitted light intensity(8,9,13) (see Figure 30c).

Since the reduction of H_2O_2 consists of two consecutive steps, it seems reasonable to describe its redox properties by *two* standard potentials given by

$$E_1 = eU_1 = eU_1^\circ + \frac{RT}{F}\ln\frac{C_{H_2O_2}}{C^\circ_{OH}C_{OH^-}} \tag{63a}$$

$$E_2 = eU_2 = eU_2^\circ + \frac{RT}{F}\ln\frac{C_{OH}}{C_{OH}C_{OH^-}} \tag{63b}$$

in which U_1° and U_2° are the standard potentials of each step, whereas the standard potential U_0 of the whole system is an average value given by

$$E_0 = eU^\circ = \frac{eU_1^\circ + eU_2^\circ}{2} \tag{64}$$

At equilibrium, the concentration of OH radicals is very low, i.e.,

$$E = E_1 = E_2 = E_{F,\text{redox}} \tag{65}$$

As far as the energetics of the charge transfer is concerned, the standard potential of each step is of importance. According to the experimental results, the energy eU_1° must be located near the conduction band and eU_2° far below the upper edge of the valence band, as indicated in Figure 30b.

Very similar results were obtained for reduction of $S_2O_8{}^{2-}$ (8) and of various quinones.(131) It is impossible to discriminate between the two reaction steps at metal electrodes because $U_2^\circ > U_1^\circ$.

An analogous description can be given for the oxidation of various organic compounds. For instance, Morrison and co-workers,(132,133) who were actually the first to observe the "current doubling," used *n*-ZnO electrodes for the oxidation of formic acid. They found a doubling of the anodic photocurrent after addition of HCOOH to the electrolyte which they interpreted in terms of the reaction

$$\mathrm{HCOO^- + \mathit{p}^+ \rightarrow HCOO^{\bullet}} \qquad \text{(valence band process)} \qquad \text{(66a)}$$

$$\mathrm{HCOO^{\bullet} \rightarrow CO_2 + H^+ + e^-} \qquad \text{(conduction band process)} \qquad \text{(66b)}$$

In this case, holes had to be created by light excitation and were consumed in the first reaction step. The radical formed as an intermediate product has a much more negative redox potential and is further reduced by electron transfer into the conduction band. Similar observations have been made for the oxidation of alcohols at CdS electrodes.(78)

Further information about the energetics of two-step redox process is given in Ref. 9.

5.2.4. Applications to Solar Energy Conversion Systems

The photoeffects discussed in the previous sections have been used in investigations of solar energy conversion either into electrical or chemical energy. It was possible to produce stable cells suitable for production of electrical energy by using a redox system as an electrolyte. It would be beyond the scope of this chapter to discuss this problem in detail and reference should be made to appropriate review articles: Refs. 34, 38, 83, and 135–137. It should be mentioned that in connection with this problem, semiconductors in organic electrolytes have also been studied (see, e.g., Refs. 138 and 139 and literature cited therein). As far as the production of a chemical fuel (H_2) is concerned, the photolysis of water has also been realized. In this case, however, only large band gap semiconductors (band gap energy $E_g > 3$ eV) could be applied because only these were found to be sufficiently stable against corrosion. The energetics of these processes have recently been reviewed by Nozik(140) (see also Refs. 38, 83, and 141). Some first attempts have been made to use semiconductors as a photocatalyst for organic reactions.(142–145)

5.3. Photostimulated Reactions at Organic Electrodes

Photocurrents have also been measured with organic crystals such as, e.g., anthracene. The creation of charge carriers upon light excitation is here, however, completely different. In a molecular crystal, light absorption leads to an excitation of individual molecules, i.e., we have to consider a certain density of excited states ("excitons"). These excitons are not split into charge carriers directly in the bulk of the crystal. They diffuse over a certain distance, depending on their lifetime. If such an exciton reaches the surface between crystal and electrolyte it may react with an electron-donating or -accepting molecule in the electrolyte which finally leads to the generation of charge carriers in the crystal. The photocurrent is therefore expected to be controlled by the diffusion of excitons toward the surface. This effect was discovered at first by Steketee and de Jonge,(146) who determined quantitatively the diffusion length of excitons ($L \sim 40$–80 nm) from measurements of the photocurrent and absorption spectra.

Further results and theoretical treatments are given in other review articles.(97,147)

6. Reactions of Excited Molecules at Electrodes

In the previous section discussion has centered on electrode reactions stimulated by light absorption in the semiconductor electrode. In the present section, electron transfer processes between electrodes and excited molecules will be treated. In order to avoid any light absorption by the electrode itself, only large band gap semiconductors can be used.

The first investigations in this field were made with organic crystals (anthracene) as electrodes and electrolytes containing rhodamine B as an excitable species.(148,149) In this case photocurrents were measured upon excitation of the dye only. Since the lifetime of an excited molecule is very short, only excitation of *adsorbed* molecules leads to electron transfer. Several years later, similar experiments were also started with typical semiconductor electrodes, at first with ZnO and solutions of rhodamine B (see Ref. 150).

Before discussing the experimental results, we have to derive an energy scheme, which is actually an extension of the usual model (Section 3) to excited molecules.

6.1. Energy Levels of Excited Molecules

In Section 3.2 we have characterized a redox system by its Fermi level $E_{\mathrm{F,redox}}$ (redox potential), in terms of occupied and empty energy levels (E°_{red} and E°_{ox}) and their distribution, and by the reorientation energy λ (Figure 7). Now it is well known that an excited molecule is more easily reduced or oxidized because the excitation energy ΔE^* is stored in the molecule. Possible reactions are

$$\mathrm{M}^* \rightleftarrows \mathrm{M}^+ + e^- \tag{67a}$$

and

$$M^* + e^- \rightleftarrows M^- \tag{67b}$$

The stored energy ΔE^* is given by the 0–0 transition (between the lowest vibrational levels in the ground and excited states) in the electron spectra, i.e., $\Delta E^* = \Delta E_{0\text{-}0}$. The excited state may be either a singlet or triplet state (see below). It is now possible to estimate the redox potentials of excited molecules by adding or subtracting $\Delta E_{0\text{-}0}$ from the redox potential for the molecules in the ground state. One obtains

$$^*E_{\mathrm{F,redox}}(M^*/M^+) = E_{\mathrm{F,redox}}(M/M^+) - \Delta E_{0\text{-}0}(M/M^*) \tag{68a}$$

or

$$^*E_{\mathrm{F,redox}}(M^*/M^-) = E_{\mathrm{F,redox}}(M/M^-) + \Delta E_{0\text{-}0}(M/M^*) \tag{68b}$$

(The sign is valid using the conventional scale.) Provided that the standard potentials in the ground state are known, the $^*E_{\mathrm{F,redox}}$ can easily be determined. In most organic systems the redox potentials in the ground state $E_\mathrm{F}(M/M^+)$ and $E_\mathrm{F}(M/M^-)$ differ considerably because different molecular orbitals are involved. Therefore also the corresponding values for the excited molecules will occur at different values, as schematically shown in Figure 31.

The situation can be very well illustrated taking $M = \mathrm{Ru(II)(bipy)_3}^{2+}$ as an example. This compound is very stable and the ruthenium can exist in various oxidation states (+3 to −2)$^{(151)}$ and most standard potentials in the ground state are known, i.e., $E_\mathrm{F}(\mathrm{Ru}^{2+}/\mathrm{Ru}^{3+}) = 1.26$ eV, $E_\mathrm{F}(\mathrm{Ru}^{1+}/\mathrm{Ru}^{2+}) = -1.28$ eV, and $^*\Delta E_{0\text{-}0}(\mathrm{Ru}^{2+}) = 2.12$ eV.$^{(152)}$ The calculated $^*E_\mathrm{F}$'s are given in Figure 32. They were experimentally confirmed by investigations of electron transfer reactions of excited $^*\mathrm{Ru(bipy)_3}^{2+}$ with other redox systems which acted as electron donors or acceptors.$^{(152-154)}$

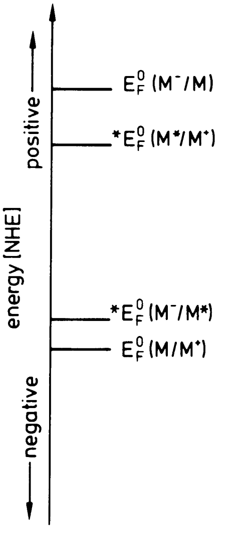

Figure 31. Fermi levels (standard potentials) of a redox system in its ground and excited states in the absolute and conventional scale.

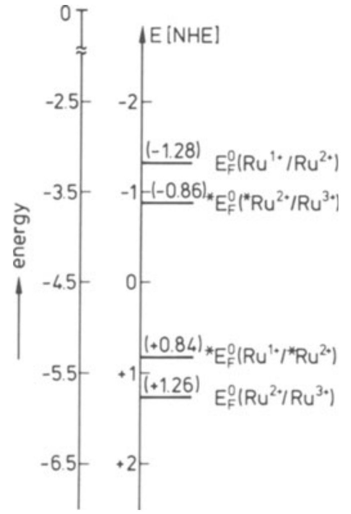
0
-2.5
-3.5
-4.5
-5.5
-6.5
energy
E [NHE]
-2
-1
0
+1
+2
(-1.28) E$_F^0$(Ru^{1+}/Ru^{2+})
(-0.86) *E$_F^0$(*Ru^{2+}/Ru^{3+})
(+0.84) *E$_F^0$(Ru^{1+}/*Ru^{2+})
(+1.26) E$_F^0$(Ru^{2+}/Ru^{3+})

Figure 32. Fermi levels (standard potentials) of $Ru(bipy)_3{}^{2+}/Ru(bipy)_3{}^{3+}$ and $Ru(bipy)_3{}^{2+}/Ru(bipy)_3{}^{1+}$ in the ground and excited state.

As already mentioned (Section 3.2), a redox system is also characterized by occupied and empty states which are distributed over a certain energy range. These states are also important here because they are involved in the actual electron transfer process. Introducing the corresponding states in Figure 31, one obtains Figure 33 in which the two reactions (67a) and (67b) are treated separately.

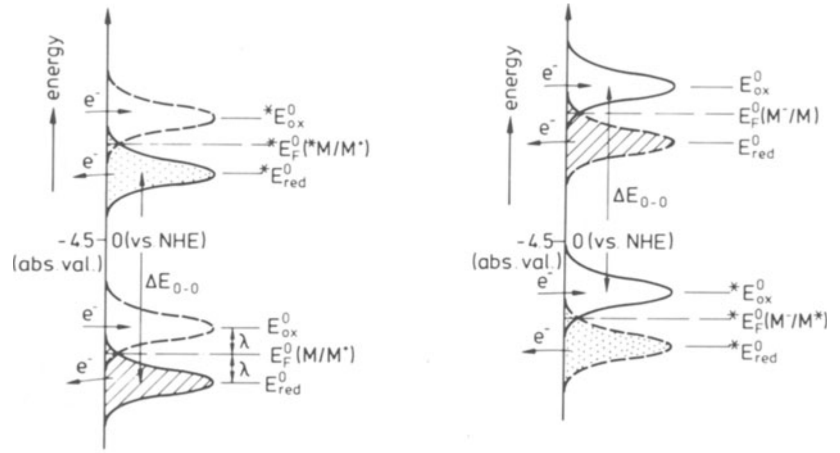
energy
e⁻
e⁻
*E$^0_{ox}$
*E^0_F(*M/M$^+$)
*E$^0_{red}$
-4.5
(abs val.)
0 (vs NHE)
ΔE$_{0-0}$
e⁻
e⁻
λ
λ
E$^0_{ox}$
E^0_F(M/M$^+$)
E$^0_{red}$
energy
e⁻
e⁻
E$^0_{ox}$
E^0_F(M$^-$/M)
E$^0_{red}$
ΔE$_{0-0}$
-4.5
(abs. val.)
0 (vs. NHE)
e⁻
e⁻
*E$^0_{ox}$
E^0_F(M$^-$/M)
*E$^0_{red}$

a) $M^* \rightleftharpoons M^+ + e^-$

b) $M^* + e^- \rightleftharpoons M^-$

Figure 33. Energy states and their distributions and the optical excitation energy ΔE_{0-0} for different electron transfer reactions.

6.2. Electron Transfer Process

As far as the electron transfer between an excited molecule and an electrode is concerned, the same rules have to be applied as already derived for ordinary redox systems. It depends on the relative position of energy states on both sides of the interface whether a charge transfer occurs via the conduction or the valence band. Taking as examples the combinations $SnO_2/Ru(bipy)_3^{2+}$ and $SiC/Ru(bipy)_3^{2+}$, one can derive quantitatively the position of energy states by using data from Figures 9 and 32. The results are shown in Figures 34a and 34b. Here only those energy terms of the molecules are shown which are involved in the process. According to this energy scheme, excitation of $Ru(bipy)_3^{2+}$ should lead to an electron transfer from the excited state into the conduction band of SnO_2 (Figure 34a), whereas an electron transfer into the conduction band of SiC is not possible. On the other hand, the reverse process, electron transfer from SiC to the excited Ru-complex, is expected (Figure 34b) by hole injection into the valence band. The energy scheme has been proved by photocurrent measurements,(155,156) as shown in Figure 35. The spectra resemble practically the absorption spectrum of the Ru-complex.

The photocurrent sets in around the flatband potential (Figure 36) and reaches a saturation value about 0.4 V positive from the flatband potential. The photocurrents increase linearly with light intensity.

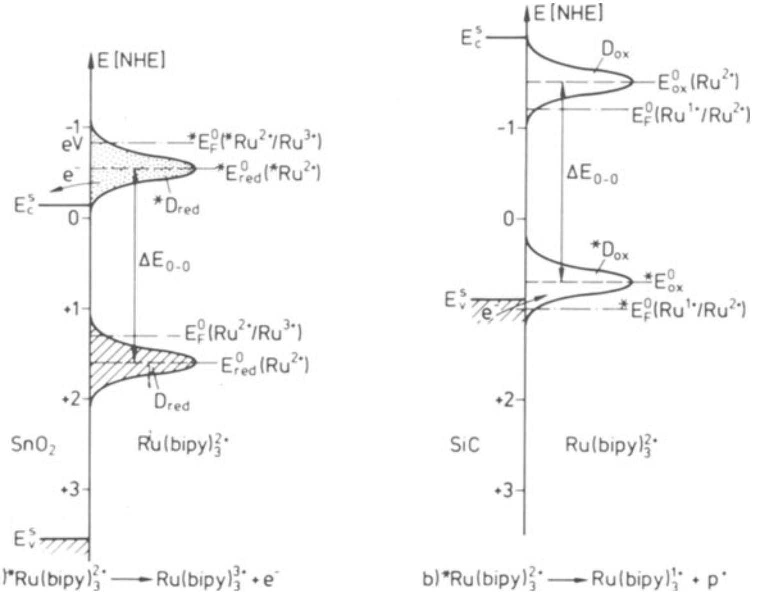
E [NHE]
-1 eV
e⁻
E_c^s
0
$*E_F^0(*Ru^{2+}/Ru^{3+})$
$*E_{red}^0(*Ru^{2+})$
$*D_{red}$
ΔE_{0-0}
+1
$E_F^0(Ru^{2+}/Ru^{3+})$
$E_{red}^0(Ru^{2+})$
D_{red}
+2
SnO_2
$Ru(bipy)_3^{2+}$
+3
E_v^s
a) $*Ru(bipy)_3^{2+} \rightarrow Ru(bipy)_3^{3+} + e^-$
E [NHE]
E_c^s
D_{ox}
$E_{ox}^0(Ru^{2+})$
$E_F^0(Ru^{1+}/Ru^{2+})$
-1
ΔE_{0-0}
0
$*D_{ox}$
$*E_{ox}^0$
E_v^s
e
$*E_F^0(Ru^{1+}/Ru^{2+})$
+2
SiC
$Ru(bipy)_3^{2+}$
+3
b) $*Ru(bipy)_3^{2+} \rightarrow Ru(bipy)_3^{1+} + p^+$

Figure 34. Energy levels and transfer processes with excited $Ru(bipy)_3^{2+}$ at semiconductor electrodes (a) SnO_2 and (b) SiC.

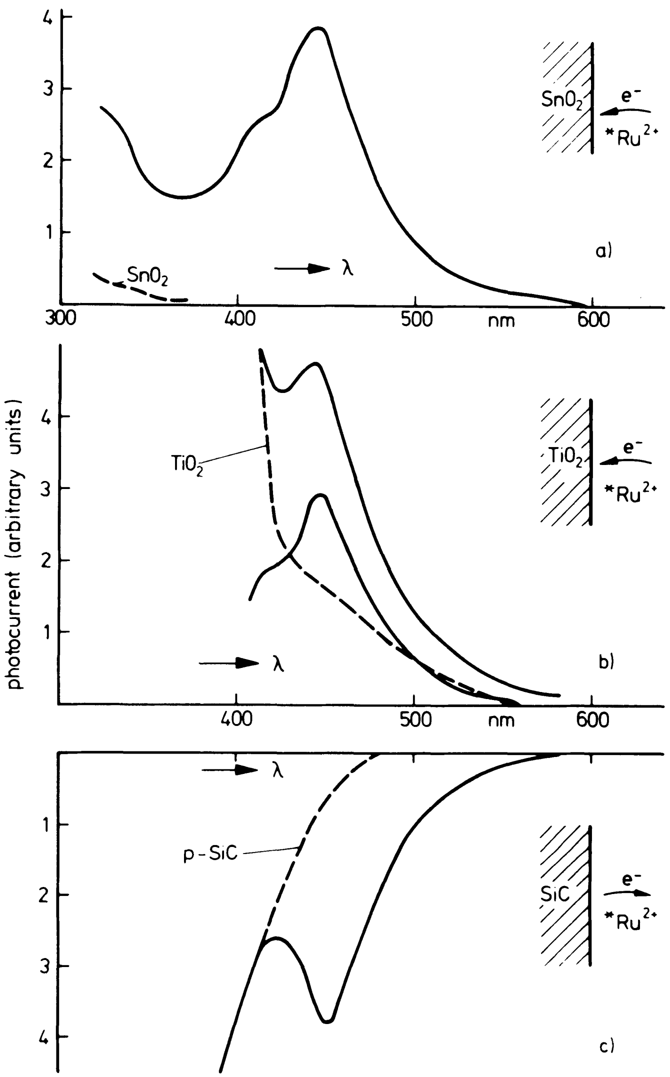

Figure 35. Photocurrent spectra upon excitation of $Ru(bipy)_3^{2+}$ at various semiconductor electrodes in 0.1 *N* H_2SO_4.(156)

As mentioned before, $Ru(bipy)_3^{2+}$ was selected as an example because of its excellent reversible redox properties and defined potentials. Most investigations have been performed, however, with xanthene and cyanine dyes. Electron injection from the excited dyes has been observed with ZnO_2,(150,158,164) SnO_2,(157,165,168) TiO_2,(156,169,170) and CdS electrodes.(171-174) Hole injection was detected with GaP,(156,175) and SiC electrodes.(155,156) In all cases similar results were obtained and discussed for $Ru(bipy)_3^{2+}$. In the

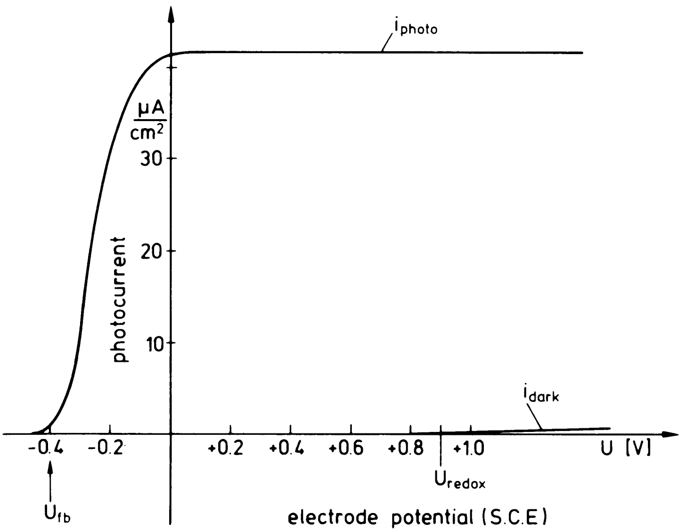

Figure 36. Photocurrent–potential dependence at SnO_2 electrode during excitation of $Ru(bipy)_3^{2+}$ ($\lambda_{excit} = 488$ nm).(157)

case of typical dyes, the photocurrent spectra are slightly shifted toward longer wavelengths compared to the corresponding absorption spectra (measured in solution). This must be attributed to an interaction of the adsorbed species with the electrode.(176) Since only adsorbed molecules are involved, the photocurrents were found to be very small. The quantum yields, however, can be high; values vary from a few percent up to 90%.

In principle, electron transfer can occur via an adsorbed molecule excited into its singlet or triplet state. In the case of $Ru(bipy)_3^{2+}$, it has been proved by quenching experiments that only the triplet state (charge transfer triplet; see, e.g., Ref. 152) is involved.(155) In the presence of Fe^{3+} ions in the electrolyte, which act as electron acceptors,(152) the anodic photocurrent was quenched at the same rate as that found in pure photochemical investigations.(155) Gerischer and co-workers(177) also used quenching agents in the case of xanthene dyes. Their results also provide some evidence that the triplet state participates in the reactions.

It should be mentioned that similar processes have also been observed with organic electrodes (see, e.g., Refs. 147–149). Here, especially, energy transfer processes and magnetic effects are of interest.

6.3. Relaxation Phenomena, Quenching, Supersensitization

The electron transfer processes described above lead either to a photooxidation or -reduction of the excited molecules. Since only adsorbed molecules participate in the electron transfer reaction, it would be expected that all adsorbed molecules are oxidized or reduced after a certain illumination.

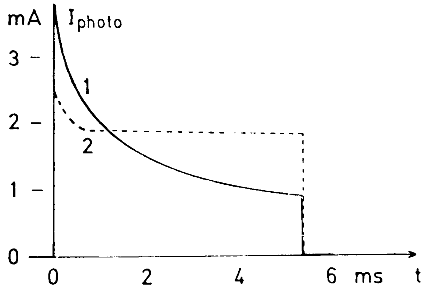

Figure 37. Photocurrent during light pulse (λ = 514 nm) at ZnO electrode with rhodamine B in the absence (1) and in the presence of hydroquinone (2).(157)

Consequently the photocurrent is generally found to decrease after a certain time (Figure 37), which shows that also the product remains on the electrode, i.e., the exchange with molecules in the solution is very ineffective. The decrease can be avoided by addition of a redox system which regenerates the oxidized or reduced molecule directly in its adsorbed state.(159) An example is given by curve 2 in Figure 37. The whole process is then given by

$$M^*_{ads} \rightarrow M^+_{ads} + e^- \quad \text{(electron injection into conduction band)} \qquad (69a)$$

$$M^+_{ads} + X \rightarrow M_{ads} + X^- \quad \text{(regeneration)} \qquad (69b)$$

in which X is a suitable redox system, or by

$$M^*_{ads} \rightarrow M^-_{ads} + p^+ \quad \text{(hole injection into valence band)} \qquad (70a)$$

$$M^-_{ads} + X \rightarrow M_{ads} + X^+ \quad \text{(regeneration)} \qquad (70b)$$

These processes are also illustrated in a corresponding energy scheme (Figure 38). Such regeneration has turned out to be necessary in all cases. $Ru(bipy)_3{}^{2+}$ seems to be an exception insofar as H_2O acts as a regeneration agent.(157,167)

The regeneration is not really a supersensitization process. The latter term is only applicable if the original electron transfer between an excited molecule and an electrode is enhanced by addition of a redox system. In principle, such a process is possible if the excited molecule reacts at first with the redox system before an electron is transferred across the interface. Then we have

$$M^*_{ads} + S \rightarrow M^-_{ads} + S \quad \text{(supersensitization)} \qquad (71a)$$

$$M^-_{ads} \rightarrow M_{ads} + e^- \quad \text{(electron injection)}$$

or

$$M^*_{ads} + S \rightarrow M^+_{ads} + S^- \quad \text{(supersensitization)} \qquad (71b)$$

$$M^+_{ads} \rightarrow M_{ads} \quad \text{(hole injection)}$$

There are several examples in the literature where an enhancement of the photocurrent was observed. Since most of these experiments were made

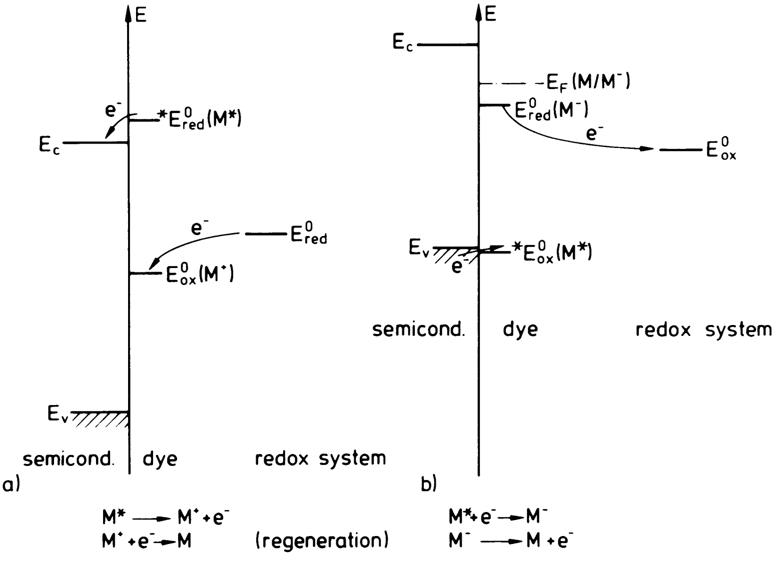

Figure 38. Schematic diagram for regeneration of adsorbed dye molecule.

under stationary conditions, it is not clear whether real supersensitization or regeneration occurred. At present, no unambiguous example has been found.

6.4. Competitive Photochemical Reactions in the Electrolyte

Frequently the direct electron transfer process between excited molecules and electrodes is obscured by photochemical reactions in the solution followed by a pure electrochemical reaction of the products. Since excitation of dissolved molecules cannot be avoided, these molecules can also react with a regeneration agent leading to formation of dye radicals. These radicals can exhibit a considerable lifetime so that they reach the electrode by diffusion where they are oxidized or reduced. In this case, one also measures a "photocurrent," which can be considerably larger than the normal photocurrent.(178) Even the presence of oxygen in the electrolyte may lead to photocurrents based on photochemical processes in the bulk of the solution. An example, $\mathrm{Ru(bipy)_3}^{2+}$ at $\mathrm{SnO_2}$, is illustrated in Figure 39. In $\mathrm{O_2}$ free solutions an anodic photocurrent occurs which follows the light intensity (curve a). This current is due to the normal electron injection from excited molecules adsorbed on the electrode. In the presence of oxygen, however, the anodic photocurrent relaxes during illumination, and returns slowly to zero after the light has been turned off (curve b). This effect was proved to be due to the following reaction(157):

$$(^3\mathrm{CT})\mathrm{Ru(II)(bipy)_3}^{2+} \xrightarrow{\mathrm{O_2}} \mathrm{Ru(III)(bipy)_3}^{3+} \qquad (72)$$

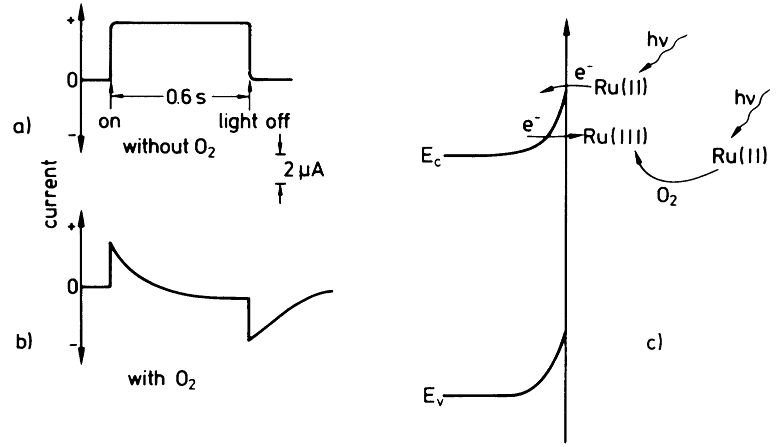

Figure 39. Photocurrent during light pulse (488 nm) at heavily doped SnO_2 with $Ru(bipy)_3^{2+}$ at heavily doped SnO_2 with $Ru(bipy)_3^{2+}$ in the absence (a) and in the presence of O_2 (b). Schematic reaction process in (c).[157]

The Ru(III) complex diffused toward the electrode where it was reduced according to the reaction

$$Ru(III)(bipy)_3^{3+} + e^- \xrightarrow{SnO_2} Ru(III)(bipy)_3^{2+} \qquad (73)$$

The latter process was responsible for the cathodic current. It must be emphasized that such cathodic currents were only observed with heavily doped SnO_2 electrodes. Therefore it was concluded that reaction (73) occurred via tunneling of electrons through the thin space charge layer from the conduction band to Ru(III) molecules produced photochemically.[157]

Similar relaxation phenomena were also observed with ZnO electrodes and rhodamine B. Gerischer and co-workers[179] interpreted this result by electron transfer from the adsorbed dye (anodic current), followed by a back reaction via tunneling. Any photochemical process or oxygen effect, however, was not mentioned.

6.5. Production of Excited Molecules by Electron Transfer

In the previous sections, we have discussed electron transfer reactions between optically excited molecules and semiconductor electrodes. The question arises whether the opposite effect, the production of an excited state by electron transfer, is also possible. In principle it can be realized if we select a semiconductor, the conduction band (c.b.) of which is located above the energy level of the excited species $[E_F(M^*/M^+)]$. The reaction process is then given by

$$M^+ + e^-(c.b.) \rightarrow M^* \qquad (74)$$

followed by

$$M^* \rightarrow M + h\nu \tag{75}$$

This condition can be met, for instance, by using n-SiC and an aqueous solution of $\mathrm{Ru(II)(bipy)_3}^{3+}$. In this case, luminescence was observed during cathodic polarization. This result proved the formation of an excited $\mathrm{Ru(II)(bipy)_3}^{2+}$ by electron transfer.(180)

Bard and co-workers(181,182) have analyzed the whole problem in more detail and emphasized that it is frequently difficult to attribute the electrogenerated luminescence unambiguously to the process discussed above. In several cases, instead of reaction (74), electron transfer occurred to the neutral molecule according to

$$M + e^- \rightarrow M^- \tag{76}$$

followed by

$$M^- + M^+ \rightarrow M + M^* \tag{77}$$

Here a radical anion (M^-) is formed which reacts with the cation (M^+) in the solution ("radical ion annihilation"). This process leads also to the production of excited molecules which are detected by luminescence measurements. The process can also be observed with metal electrodes.(183)

In many cases, reaction (76) cannot be avoided at semiconductor electrodes because the energies $^*E_F(M^*/M^+)$ and $E_F(M^-/M)$ are rather close.(184) Luttmer and Bard(182) found only one system, rubrene, with which reaction (74) could be verified, although in a somewhat modified form. The results, as obtained with rubrene (R) at ZnO, are shown in Figure 40. According to

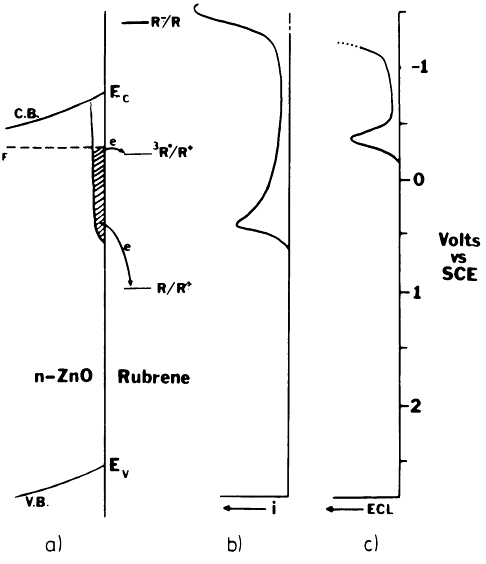

Figure 40. (a) Schematic energy diagram for the production of a rubrene triplet $^3R^*$ by electron transfer from a ZnO electrode(182); (b) current i vs. energy E; (c) electrochemiluminescence (ECL) vs. energy E.

the energy scheme (Figure 40a), the energies $E(R/R^-)$ and $^*E(R^*/R^+)$ are far above the conduction band, so that an electron transfer from the conduction band to these levels is not possible. The authors observed, however, the rubrene fluorescence around an electrode potential of −0.30 V. Since, at this potential, the Fermi level passes the $R^+/^3R$ potential, they concluded that primarily a rubrene triplet (^3R) was formed. It was assumed that the electrons were not directly transferred from the conduction band to the $^3R/R^+$ term but via surface states (E_{ss}). We have then

$$R^+ + e^-(\text{s.s.}) \rightarrow {}^3R \tag{78}$$

followed by a triplet–triplet annihilation process given by

$$^3R + {}^3R \rightarrow {}^*R + R \tag{79}$$

In the latter process, rubrene is formed in its excited singlet state (R^*) which was detected by fluorescence measurements.

It is interesting to note that the onset of current occurred already around +0.5 V (Figure 40b) which is interpreted in terms of electron transfer from surface states into the R/R^+ term (see Figure 40a). In this process no excited species is involved.

7. Conclusions

In this chapter, the essential properties of semiconductor electrodes and their interfaces with solutions have been described. Various reactions were discussed in terms of energy diagrams. Most processes are qualitatively well understood. In many cases, reactions were also quantitatively described. However, some problems, especially the role of surface states within the forbidden gap, have to be further analyzed.

Hamburg, August 1979

References

1. E. Bequerel, *C. R. Acad. Sci.* **9**, 561 (1939).
2. W. H. Brattain and T. B. Gibney, U.S. Patent 2,524,034 (1948).
3. W. H. Brattain and C. G. B. Garrett, *Bell Syst. Tech. J.* **34**, 129 (1955).
4. K. Bohnenkamp and H. J. Engell, *Z. Elektrochem.* **61**, 1184 (1957).
5. W. H. Brattain and P. J. Boddy, *J. Electrochem. Soc.* **109**, 574 (1962).
6. M. Hoffmann-Perez and H. Gerischer, *Z. Elektrochem.* **65**, 771 (1961).
7. R. Memming, *Philips Res. Rep.* **19**, 323 (1964).
8. R. Memming, *J. Electrochem. Soc.* **116**, 785 (1969).
9. R. Memming, in *Electroanalytical Chemistry*, Vol. 11, A. J. Bard, ed., Marcel Dekker, New York (1970), p. 1.
10. F. Lohmann, *Ber. Bunsenges. Phys. Chem.* **70**, 428 (1966).
11. F. Möllers and R. Memming, *Ber. Bunsenges. Phys. Chem.* **76**, 469 (1972).
12. J. M. Bolts and M. S. Wrighton, *J. Phys. Chem.* **70**, 428 (1966).
13. Yu. V. Pleskov, *Croat. Chem. Acta* **44**, 179 (1972); *Prog. Surf. Membr. Sci.* **7**, 57 (1973).

14. R. Memming and G. Schwandt, *Electrochim. Acta* **13**, 1299 (1968).
15. D. S. Ginley and M. A. Butler, *J. Electrochem. Soc.* **125**, 1968 (1978).
16. H. Gerischer, M. Hoffmann-Perez, and W. Mindt, *Ber. Bunsenges.* **69**, 130 (1965).
17. H. U. Harten and R. Memming, *Phys. Lett.* **3**, 95 (1962).
18. Yu. V. Pleskov, *Eletrokimiya* **1**, 4 (1965).
19. V. A. Myamlin and Yu. V. Pleskov, *Semiconductor Electrochemistry*, Plenum Press, New York (1967).
20. W. Mehl and F. Lohmann, *Ber. Bunsenges.* **71**, 1055 (1967).
21. R. Memming and G. Schwandt, *Surf. Sci.* **5**, 97 (1966).
22. E. C. Dutoit, R. L. Meirhaeghe, W. P. Gomes, and F. Cardon, *Ber. Bunsenges. Phys. Chem.* **79**, 1209 (1975).
23. W. H. Laflére, R. L. Meirhaeghe, F. Cardon, and W. P. Gomes, *Surf. Sci.* **59**, 401 (1976).
24. M. J. Madou, F. Cardon, and W. P. Gomes, *J. Electrochem. Soc.* **124**, 1623 (1977).
25. F. Lohmann, *Z. Naturforsch.* **22a**, 843 (1967).
26. S. Trasatti, in *Advances in Electrochemistry and Electrochemical Engineering*, Vol. 10, H. Gerischer and C. W. Tobias, eds., John Wiley, New York (1977), p. 213.
27. B. Case, in *Reactions of Molecules at Electrodes*, N. S. Hush, ed., Wiley Interscience, New York (1971), p. 46.
28. J. E. B. Randles, *Discuss. Faraday Soc.* **24**, 194 (1957).
29. R. Gomer, *J. Chem. Phys.* **66**, 4413 (1977).
30. M. A. Butler and D. S. Ginley, *J. Electrochem. Soc.* **125**, 228 (1978).
31. A. H. Nethercot, *Phys. Rev. Lett.* **33**, 1088 (1974).
32. H. Gerischer, *Z. Phys. Chem. N.F.* **26**, 223, 325 (1960); **27**, 48 (1961).
33. R. A. Marcus, *Ann. Rev. Phys. Chem.* **15**, 155 (1964).
34. V. G. Levich, in *Advances in Electrochemistry and Electrochemical Engineering*, Vol. 4, P. Delahay and C. W. Tobias, eds., Wiley Interscience, New York (1966), p. 249.
35. R. R. Dogonadze, in *Reactions of Molecules at Electrodes*, N. S. Hush, ed., Wiley Interscience, New York (1971), p. 135.
36. H. Gerischer, in *Physical Chemistry*, Vol. IX A, Eyring, Henderson, and Jost, eds., Academic Press, New York (1970), p. 463.
37. M. Gleria and R. Memming, *J. Electroanal. Chem. Interfac. Electrochem.* **65**, 163 (1975).
38. R. Memming, *Electrochim. Acta* **25**, 77 (1980).
39. G. A. Parks and P. L. deBruyn, *J. Phys. Chem.* **66**, 967 (1962).
40. R. W. Gurney, *Proc. R. Soc. London Ser. A* **134**, 137 (1931).
41. N. S. Hush, *J. Chem. Phys.* **28**, 962 (1958); *Trans. Faraday Soc.* **57**, 557 (1961).
42. A. M. Kuznetsov and R. R. Dogonadze, *Izv. Akad. Nauk* **10**, 1787 (1964).
43. W. Shockley, *Electrons and Holes in Semiconductors*, D. Van Nostrand Co., Princeton, New Jersey (1950).
44. J. F. Dewald, in *Semiconductors*, N. B. Hannay, ed., Reinhold Publishing, New York (1959), p. 727.
45. E. A. Efinov and I. G. Jerusalimchik, *Zh. Fiz. Khim.* **32**, 413 (1958); **32**, 1103 (1958).
46. J. B. Flynn, *J. Electrochem. Soc.* **105**, 715 (1958).
47. H. Gerischer, in *Advances in Electrochemistry and Electrochemical Engineering*, Vol. 1, P. Oclahay and C. W. Tobias, eds., Interscience Publishers, New York (1961), p. 139.
48. F. Beck and H. Gerischer, *Z. Elektrochem.* **63**, 500 (1959); **63**, 943 (1959).
49. D. R. Turner, *J. Electrochem. Soc.* **103**, 252 (1956).
50. R. Memming and G. Schwandt, *Surf. Sci.* **4**, 109 (1966).
51. A. Uhlir, *Bell Syst. Tech. J.* **35**, 333 (1956).
52. D. R. Turner, *Electrolytic Etching of Semiconductors*, Symposium of the Electrochemical Society, Columbus, Ohio, 1959.
54. H. Gerischer, *Ber. Bunsenges. Phys. Chem.* **69**, 578 (1965).
55. H. Gerischer and J. Wallem-Mattes, *Z. Phys. Chem.* **64**, 187 (1969).
56. H. Gerischer and J. Mattes, *Z. Phys. Chem.* **49**, 112 (1966).

57. R. Williams, *J. Chem. Phys.* **32**, 1505 (1960).
58. M. H. Madou, F. Cardon, and W. P. Gomes, *Ber. Bunsenges.* **81**, 819 (1977); **81**, 1186 (1977).
59. R. Memming, in NBS Publ. 455, Electrocatalysis of Non-Metallic Surfaces, Gaithersburg, Md. (1976), p. 267.
60. W. Gissler and R. Memming, *J. Electrochem. Soc.* **124**, 1710 (1977).
61. B. S. Hobbs and A. C. C. Tseung, *J. Electrochem. Soc.* **120**, 766 (1973).
62. B. Reichmann and A. J. Bard, *J. Electrochem. Soc.* **126**, 2133 (1979).
63. M. A. Butler, R. D. Nashby, and R. K. Quin, *Solid State Commun.* **19**, 1011 (1976).
64. U. D. Justice and R. M. Hard, *J. Electrochem. Soc.* **118**, 1417 (1971).
65. P. J. Boddy, *J. Electrochem. Soc.* **115**, 199 (1968).
66. F. Möller, H. Tolle, and R. Memming, *J. Electrochem. Soc.* **121**, 1160 (1974).
67. W. Gissler, P. L. Lensi, and S. Pizzini, *J. Appl. Electrochem.* **6**, 9 (1976).
68. S. N. Frank and A. J. Bard, *J. Am. Chem. Soc.* **98**, 2774 (1976).
69. R. N. Noufi, P. A. Kohl, S. N. Frank, and A. J. Bard, *J. Electrochem. Soc.* **125**, 246 (1978).
70. M. S. Wrighton, A. B. Ellis, P. T. Woldczanski, D. L. Morse, and D. S. Ginley, *J. Am. Chem. Soc.* **98**, 2774 (1976).
71. W. Gissler and J. G. Curran, *J. Electrochem. Soc.* **126**, 56 (1979).
72. K. L. Hardee and A. J. Bard, *J. Electrochem. Soc.* **123**, 1924 (1976); **124**, 215 (1977).
73. J. H. Kennedy and K. W. Freese, *J. Electrochem. Soc.* **125**, 709 (1978); **125**, 723 (1978).
74. M. S. Wrighton, D. L. Morse, A. B. Ellis, D. S. Ginley, and H. B. Abrahamson, *J. Am. Chem. Soc.* **98**, 44 (1976).
75. H. Tributsch and J. C. Bennett, *J. Electroanal. Chem. Interfac. Electrochem.* **81**, 97 (1977).
76. H. Tributsch, *Z. Naturforsch.* **32a**, 972 (1977).
77. Yu. V. Pleskov, *Dokl. Akad. Nauk SSSR* **126**, 111 (1959).
78. H. Gerischer, *Surf. Sci.* **18**, 17 (1969).
79. R. Memming, *J. Electrochem. Soc.* **125**, 117 (1978).
80. R. Memming, in *Proceedings of Conference on Semiconductor Liquid Junction Solar Cells 77-3*, A. Heller, ed., Electrochemical Society, Princeton, New Jersey (1977), p. 38.
81. A. J. Bard and M. W. Wrighton, *J. Electrochem. Soc.* **124**, 1706 (1977).
82. A. J. Bard and M. S. Wrighton, in *Proceedings of Conference on Semiconductor Liquid Junction Solar Cells 77-3*, A. Heller, ed., Electrochemical Society, Princeton, New Jersey (1977), p. 195.
83. H. Gerischer, in *Topics in Applied Physics 31*, B. O. Seraphin, ed., Springer Verlag, Berlin (1979), p. 115.
84. H. Gerischer and W. Mindt, *Surf. Sci.* **4**, 440 (1966).
85. H. Gerischer, A. Mauerer, and W. Mindt, *Surf. Sci.* **4**, 431 (1966).
86. R. Memming and G. Neumann, *J. Electroanal. Chem. Interfac. Electrochem.* **21**, 295 (1969).
87. R. Memming and G. Neumann, *Phys. Lett.* **A24**, 19 (1967).
88. R. Memming and G. Neumann, *Surf. Sci.* **10**, 1 (1968).
89. R. Memming and F. Möllers, *Ber. Bunsenges. Phys. Chem.* **76**, 475 (1972).
90. J. A. Laitinen, C. A. Vincent, and T. M. Bednarski, *J. Electrochem. Soc.* **115**, 1924 (1970).
91. B. Pttinger, H. R. Schöppel, T. Yokoyama, and H. Gerischer, *Ber. Bunsenges. Phys. Chem.* **78**, 450 (1974).
92. B. Pettinger, H. R. Schöppel, and H. Gerischer, *Ber. Bunsenges. Phys. Chem.* **78**, 450 (1974).
93. J. C. Tranchart, L. Hollen, and R. Memming, *J. Electrochem. Soc.* **125**, 1185 (1978).
94. W. Mehl and F. Lohmann, *Electrochim. Acta* **13**, 1495 (1968).
95. R. A. L. van den Berghe, F. Cardon, and W. P. Gomes, *Surf. Sci.* **39**, 368 (1973).
96. R. W. Munn and W. Siebrand, *J. Chem. Phys.* **52**, 6391 (1970).
97. W. Mehl, in *Reaction of Molecules at Electrodes*, N. S. Hush, ed., Wiley Interscience, New York (1971), p. 305.
98. F. Lohmann, *Surf. Sci.* **14**, 431 (1969).
99. P. Mark and W. Helfrich, *J. Appl. Phys.* **33**, 205 (1962).

100. H. Kallmann and M. Pope, *J. Chem. Phys.* **32**, 300 (1960).
101. H. Kallmann and M. Pope, *Nature* **186**, 31 (1960).
102. W. Mehl, *Ber. Bunsenges. Phys. Chem.* **69**, 583 (1965).
103. W. Mehl and W. Bücher, *Z. Phys. Chem. N. F.* **47**, 76 (1965).
104. F. Lohmann and W. Mehl, *Electrochim. Acta* **13**, 1469 (1968).
105. F. Willig, G. Scherer, and W. Rothämel, *Z. Naturforsch.* **29a**, 131 (1974).
106. J. M. Hale, in *Reactions of Molecules at Electrodes*, N. S. Hush, ed., Wiley Interscience, New York (1971), p. 229.
107. R. Memming, in *Proceedings of the Symposium on Electrocatalysis*, M. Breiter, ed., Electrochemical Society, Princeton, New Jersey (1974), p. 178.
108. F. Willig, G. Scherer, and W. Rothämel, *Ber. Bunsenges. Phys. Chem.* **77**, 921 (1973).
109. F. Willig and G. Scherer, *Chem. Phys. Lett.* **53**, 128 (1978).
110. E. O. Johnson, *Phys. Rev.* **111**, 153 (1958).
111. H. U. Harten, *J. Phys. Chem. Solids* **14**, 220 (1960).
112. P. J. Boddy and W. H. Brattain, *Ann. N.Y. Acad. Sci.* **101**, 683 (1963).
113. M. A. Butler, *J. Appl. Phys.* **48**, 1914 (1977).
114. W. Gärtner, *Phys. Rev.* **116**, 84 (1953).
115. S. R. Morrison and T. Freund, NBS Publ. 455, Electrocatalysis of Nonmetallic Surfaces, Gaithersburg, Md. (1976), p. 139.
116. A. Fujishima, E. Sugiyzma, and K. Honda, *Bull. Chem. Soc. Jpn.* **44**, 304 (1971).
117. T. Inoue, T. Watanabe, A. Fijishima, H. Honda, and K. Kohayakawa, *J. Electrochem. Soc.* **124**, 719 (1977).
118. R. Memming, *Ber. Bunsenges. Phys. Chem.* **81**, 732 (1977).
119. B. Miller, S. Memezes, and A. Heller, in *Proceedings of Conference on Semiconductor Liquid Junction Solar Cells 77-3*, A. Heller, ed., Electrochemical Society, Princeton, New Jersey (1977), p. 196.
120. B. Miller, S. Menezes, and A. Heller, *J. Electrochem. Soc.* **126**, 1483 (1979).
121. T. Inoue, T. Watanabe, A. Fijishima, and K. Honda, in *Proceedings of Conference on Semiconductor Liquid Junction Solar Cells 77-3*, A. Heller, ed., Electrochemical Society, Princeton, New Jersey (1977), p. 210.
122. D. T. Stevenson and R. J. Keyes, *Physica* **20**, 1041 (1954).
123. R. Memming, *Surf. Sci.* **1**, 88 (1964).
124. H. U. Harten and W. Schultz, *Z. Phys.* **141**, 319 (1955).
125. P. J. Boddy and W. H. Brattain, *J. Electrochem. Soc.* **109**, 812 (1962).
126. R. Memming, *Surf. Sci.* **2**, 436 (1964).
127. R. Memming and J. Kelly, *Proc. of III Int. Conf. on Photochem. Energy Conversion and Storage*, Acad. Press, New York (1981), p. 243.
128. R. H. Wilson, *J. Appl. Phys.* **48**, 4292 (1977).
129. R. H. Wilson, in *Proceedings of Conference on Semiconductor Liquid Junction Solar Cells 77-3*, A. Heller, ed., Electrochemical Society, Princeton, New Jersey (1977), p. 67.
130. K. H. Beckmann and R. Memming, *J. Electrochem. Soc.* **116**, 368 (1969).
131. R. Memming and F. Möllers, *Ber. Bunsenges. Phys. Chem.* **76**, 609 (1972).
132. S. R. Morrison and T. Freund, *Electrochim. Acta* **13**, 1343 (1968).
133. S. R. Morrison and T. Freund, *J. Chem. Phys.* **47**, 1543 (1967).
134. A. Heller, *Electrochim. Acta*, in press.
135. H. Gerischer, in *Solar Power and Fuels*, J. R. Bolton, ed., Academic Press, New York (1977), p. 77.
136. H. Gerischer, in *Solar Power and Fuels*, J. R. Bolton, ed., Academic Press, New York (1977), p. 77.
137. H. Tsubomura, in *Progress in Batteries and Solar Cells*, Vol. 1, A. Kozawa *et al.*, eds., IEC Press, Cleveland, Ohio (1978), p. 204.
138. P. A. Kohl and A. J. Bard, *J. Electrochem. Soc.* **126**, 603 (1979).
139. K. Nakatani, S. Matsudaira, and H. Tsubomura, *J. Electrochem. Soc.* **125**, 406 (1978).

140. A. J. Nozik, *Rev. Phys. Chem.* **29**, 189 (1978).
141. L. A. Harris and R. H. Wilson, *Ann. Rev. Mater. Sci.* **8**, 99 (1978).
142. A. J. Bard, *J. Photochem.* **10**, 59 (1979).
143. C. R. Dickson and A. J. Nozik, *J. Am. Chem. Soc.* **100**, 8007 (1978).
144. M. Halmann, *Nature* **275**, 115 (1978).
145. T. Inoue, A. Fujishima, S. Konishi, and K. Honda, *Nature* **227**, 637 (1979).
146. J. W. Steketee and J. de Jonge, *Proc. K. Ned. Akad. Wet.* **B66**, 76 (1963).
147. H. Gerischer and F. Willig, in *Topics in Current Chemistry*, Vol. 61, Springer Verlag, Berlin (1976), p. 31.
148. *B. J. Mulder and J. de Jonge, Proc. K. Ned. Akad. Wet.* **B66**, 303 (1963).
149. B. J. Mulder, *Philips Res. Rep.* **22**, 553 (1967).
150. H. Gerischer, M. E. Michel-Beyerle, F. Rebentrost, and H. Tributsch, *Electrochim. Acta* **13**, 1509 (1968).
151. N. E. Tokel-Takvoryan, R. E. Hemmingway, and A. J. Bard, *J. Am. Chem. Soc.* **95**, 6582 (1973).
152. V. Balzani, F. Bolletta, M. T. Gandolfi, and M. Maestri, in *Topics in Current Chemistry*, Vol. 75, Springer Verlag, Berlin (1978), p. 1.
153. N. Sutin and C. Creutz, *Adv. Chem. Ser.* **168**, *Inorg. Organomet. Photochem.* (1978), p. 1.
154. C. R. Bock, T. J. Meyer, and D. G. Whitten, *J. Am. Chem. Soc.* **97**, 2911 (1975).
155. M. Gleria and R. Memming, *Z. Phys. Chem. N.F.* **98**, 303 (1975).
156. R. Memming, in *Topics in Surface Chemistry*, E. Kay and P. S. Bagus, eds., Plenum Press, New York (1978), p. 1.
157. R. Memming, F. Schröppel, and U. Bringmann, *J. Electroanal. Chem. Interfac. Electrochem.* **100**, 307 (1979).
158. H. Gerischer and H. Tributsch, *Ber. Bunsenges. Phys. Chem.* **72**, 437 (1968).
159. H. Tributsch and H. Gerischer, *Ber. Bunsenges. Phys. Chem.* **73**, 251 (1969).
160. H. Gerischer, *Photochem. Photobiol.* **16**, 243 (1972).
161. H. Tsubomura, M. Matsumura, Y. Nomura, and T. Amamiya, *Nature* **261**, 402 (1976).
162. H. Tributsch, *Photochem. Photobiol.* **14**, 95 (1971).
163. K. Hauffe, H. J. Danzamann, H. Pusch, J. Range, and H. Volz, *J. Electrochem. Soc.* **117**, 933 (1970).
164. K. Hauffe and J. Range, *Z. Naturforsch.* **23b**, 736 (1968).
165. R. Memming, *Photochem. Photobiol.* 325 (1972).
166. R. Memming, *Faraday Discuss.* **58**, 261 (1974).
167. R. Memming and F. Schröppel, *Chem. Phys. Lett.* **62**, 207 (1979).
168. W. Arden and P. Fromherz, *Ber. Bunsenges.* **82**, 868 (1978).
169. W. D. K. Clark and N. Sutin, *J. Am. Chem. Soc.* **99**, 4676 (1977).
170. M. T. Spitler and M. Calvin, *J. Chem. Phys.* **66**, 4294 (1977).
171. H. Tributsch and H. Gerischer, *Ber. Bunsenges. Phys. Chem.* **73**, 850 (1969).
172. A. Fujishima, T. Watanabe, O. Tatsuoki, and K. Honda, *Chem. Lett.* **1**, 13 (1975).
173. T. Watanabe, T. Takizawa, and K. Honda, *J. Phys. Chem.* **81**, 1845 (1977).
174. T. Takizawa, T. Watanabe, and K. Honda, *J. Phys. Chem.* **82**, 1391 (1978).
175. R. Memming and H. Tributsch, *J. Phys. Chem.* **75**, 562 (1971).
176. H. Gerischer, *Discuss. Faraday Soc.* **58**, 219 (1974).
177. M. Spitler, M. Lübke, and H. Gerischer, *Chem. Phys. Lett.* **56**, 577 (1978).
178. R. Memming and G. Kürsten, *Ber. Bunsenges. Phys. Chem.* **76**, 4 (1972).
179. B. Pettinger, H. R. Schöppel, and H. Gerischer, *Ber. Bunsenges.* **77**, 960 (1973).
180. M. Gleria and R. Memming, *Z. Phys. Chem. N.F.* **101**, 171 (1976).
181. L. S. R. Yeh and A. J. Bard, *Chem. Phys. Lett.* **44**, 339 (1976).
182. J. D. Luttmer and A. J. Bard, *J. Electrochem. Soc.* **125**, 1423 (1978).
183. L. F. Faulkner and A. J. Bard, in *Electroanalytical Chemistry*, Vol. 10, A. J. Bard, ed., Marcel Dekker, New York (1978), p. 1, and literature cited therein.
184. E. W. Grabner, *Electrochim. Acta* **20**, 7 (1975).

9

Electrochemistry in Molten Salts

D. INMAN and D. G. LOVERING

1. Introduction

1.1. General

According to recent developments in the field, the term *molten salts* can advantageously be widened in scope to encompass many molten media which may not be wholly ionic or derived from simple salts. Thus, many systems studied within this broad classification may change their ionicity and hence conductivity according to temperature, pressure, or composition, e.g., silicates, group IIB chlorides, and chloroaluminates, respectively. Nevertheless, the majority of melts that have been studied are substantially dissociated in the liquid state, and *all* processes conducted in these are *ipso facto* electrochemical. Many of the processes considered here, therefore, involve charge transfer systems, particularly between solids (mainly metals) and melts, viz., electrode processes.(1)

Molten salts are still rather unfamiliar amongst chemists, so that it is appropriate first to present some general considerations concerning their properties and constitution.(2) Melts derived from inorganic materials may often remain as stable liquids up to very high temperatures (~1800 K), giving them a much larger liquidus range than is normally encountered with other liquids, other than metals. The lowest melting systems are liquid below 373 K, but the inclusion of simple organic molecules, often rather polar ones such

---

D. INMAN • Department of Metallurgy & Materials Science, Imperial College, London SW7 2BP, United Kingdom. **D. G. LOVERING** • Chemistry Branch, R.M.C.S., Shrivenham, Swindon, SN6 8LA, United Kingdom.

as those present in pyridine salts and amides, can bring eutectic melting temperatures down below room temperature.

In some respects, as for example in the aqueous or hydrate melts, water itself may be considered a proper component of the molten mixture.(3) Other terms used for this general group of liquids are ionic liquids, fused salts, and molten or liquid electrolytes. Particularly common are the mixed salts of the alkali metals and alkaline earth metals which find application in the metallurgical industries owing to their excellent thermal and electrochemical stabilities, and good heat capacities.(4)

Molten salts form the largest proportion of *nonaqueous* solvents, a term frequently reserved for organic solvents.(5) Each anion type leads to a range of melts, e.g., nitrates, within which the physical and electrochemical properties are determined, in a second-order way, by the conjugate cation or cation mixture.(6) Thus, molten eutectic LiCl–KCl, for example, needs to be distinguished on points of detail from molten NaCl–KCl, although both systems exhibit the essential features of chloride melts.(7)

With increasing difficulty, one may discern a number of general types of molten salts, according to the following classification:

(a) *Simple ionic salt melts*, e.g., NaCl. These are, to a good approximation, completely ionic, with spherically symmetrical anions and cations, capable of being described in classical statistical mechanical terms and responding well to molecular dynamic modelling of properties.(8)

(b) *Oxyanionic melts*, e.g., $NaNO_3$. These have relatively low melting points, may be prone to thermal decomposition, still remaining essentially ionic, but, while responding reasonably well to modelling, require greater attention to polarization forces and other factors associated with the deformable anion.(9)

(c) *Polymeric or network melts*, e.g., $Na_2O{\cdot}2B_2O_3$. These are stable, viscous, glass-forming systems, in which the extent of polymerization and fragmentation determining their properties depends on the acid–base level, e.g., $Na_2O:B_2O_3$ ratio, and temperature.(10)

(d) *Molecular melts*, e.g., $HgCl_2$. These are largely covalent liquids which exhibit limited self-dissociation. They have short, stable liquid ranges and show pressure-dependent properties.(11) Many organic melts, e.g., $N_{2226}B_{2226}$ and liquid crystals must be included in this group, as well as, perhaps, water.

(e) *Aqueous melts*, e.g., $Zn(NO_3)_2{\cdot}6H_2O$. These melt at very low temperatures, to form viscous, ionic liquids that need to be handled under controlled water vapor pressures, to prevent composition changes.(12)

There are an increasing number of intermediate types, such as $AlCl_3$–MCl mixtures, whose Lewis acidity (and ionicity) is composition dependent.(13) Notwithstanding, more attention will focus on essentially fully ionized melts [types (a) and (b)], which are classically regarded as molten salts and have, therefore, been most studied.

Close to their melting temperatures, the time-averaged structures of the simplest molten salts resemble the well-defined arrays of their parent crystals.(8,14) However, while the strongest short-range ion forces persist, the long-range ordering is lost. From an electrochemical viewpoint, the most important consequence of melting is the reorganization of the constituent atoms into simple and complex ions, with the creation of space. Considerable controversy has surrounded the concept of complex ions in wholly ionic media, as well as the form of the space created (holes? defects? mobile interstices?).(1,15,16)

Some properties associated with simple molten salts include (i) good thermal stability, (ii) good electrochemical stability, (iii) high heat capacity, (iv) good heat transfer properties, (v) rapid chemical and electrochemical reaction rates, (vi) high electrolytic conductivity, and (vii) good solvent properties.

Many of these properties are advantageous to their commercial exploitation and also important in considering electrode processes therein.

1.2. Complex Ions(1,15,16)

It is particularly difficult to define a complex ion in a matrix which consists solely of anions and cations; each of these necessarily constitutes the nearest neighbor to the other, in order to preserve both local and overall charge neutrality, regardless of extra-Coulombic interactions. Thus, well-defined instantaneous arrangements of anions about a static, reference cation do not necessarily indicate the formation of a discrete complex in the aqueous solution sense, even though that cation may usefully be regarded as being solvated by those anions. Moreover, it is important to distinguish between dilute solutions of one salt in a binary mixture, where no competition exists between anions for cation-adjacent sites, and dilute solutions in reciprocal melts where such competition does occur. In the latter case, specific interactions can be quantified in terms of the familiar stability constant calculations, whereas in the former case, recourse to measured lifetimes, translational mutual displacements, and distances of approach need to be made in order to identify discrete kinetic entities. A limited number of techniques are available to make the distinction between such species and time-averaged assemblages. Thus, observation times of measurements need to exceed the general quasilattice relaxation time of $\sim 10^{-11}$ sec.(17) Most recently, molecular dynamic calculations definitely indicate the formation of complex ions in single and binary molten halides, particularly of akaline earth ions with bromides and iodides.(16) The presence of such species clearly influences the electrochemical behavior of these melts.

1.3. Acidity and Basicity

The proton is generally a less important species in melts, although it features prominently in molten bisulfates and hydroxides, as well as in dilute solutions of water and, for example, HCl, in anhydrous molten salts. Generally, the Lux–Flood (L–F) concept of acidity(18) has been adopted in place of the Lowry–Brønsted scheme, although the Lewis and the Pearson formalizations are sufficiently universal to remain valid in melts. A L–F acid is defined as an oxide ion acceptor leading to the formation of the conjugate base:

$$\text{L–F acid} + O^{2-} \rightleftharpoons \text{base}$$

This system is especially applicable to the oxyanionic melts, including polymeric or network ones, in which bulk anions can participate in the equilibria and determine, *inter alia*, electrode potentials (see later sections), viz.,

$$CO_3{}^{2-} \rightleftharpoons CO_2 + O^{2-}$$

Likewise, solutions of oxide ions and related species, perhaps produced by hydrolysis, for example, in nonparticipating melts, can be represented by a pO^{2-} scale,† defined as $-\log a_{O^{2-}} \simeq -\log c_{O^{2-}}$, which finds application in corrosion studies in molten salts; this is analogous to pH in aqueous solutions.(19)

The Lewis acidity scheme, on the other hand, has been particularly useful for treating melts based on $AlCl_3$,(13) viz.,

$$AlCl_3 + Cl^- \rightleftharpoons AlCl_4{}^- \qquad (1)$$

According to this notation, the chloride ion would act as a Lewis base.

1.4. emf Series and Reference Electrodes

emf series have now been determined for a number of molten salt solvents, but the most comprehensive compilations are for halide melts in which the largest number of ions and oxidation states can be identified.(2,4,20) The more restricted emf series reported for other melts,(21) such as nitrates and sulfates, reflects their limited ranges of electrochemical stability, arising mainly from the cathodic (but also anodic) electroactivity of the oxyanion itself, e.g.,

$$NO_3{}^- + 2e^- \rightarrow NO_2{}^- + \text{“}O^{2-}\text{”} \qquad (2)$$

In halide melts, unlike the oxyanion systems, the gas/gas ion electrode corresponding to the melt anion, e.g., Cl_2/Cl^- for chloride melts, naturally suggests itself as the best primary reference point for these series.(22)

Among the secondary reference half cells which have been employed in work on many melt types, the Ag/Ag^I system has proved most popular, although the Pt/Pt^{2+} is also useful in higher-melting media.(1) Even in halide melts, however, these series may be slightly restricted because the metals are disposed to dissolve in their own salt melts, e.g., Na in NaCl.(23) This causes a lowering of their thermodynamic activity, resulting in deposition at more noble potentials than that predicted on the basis of the defined standard state of unit activity.

† Care is needed in these media to ascertain that O^{2-} is the sole oxide ion present.(9b)

A related phenomenon is the common occurrence of secondary deposition in molten salts. Thus, a metal may be deposited as a result of a chemical reaction between a metallic ion in the melt and another preferentially-deposited, reactive metal corresponding to the solvent cation(s). (Notably, there is still discussion as to whether sodium or aluminum is the primarily deposited metal during operation of the Hall–Héroult cell.(24)) Such occurrences can be rationalized in theoretical terms if the primary deposition of the solute metal is precluded by an observed limiting current exceeding that predicted, or if its deposition potential is displaced in a cathodic direction by activation overpotential. Some authors have preferred an explanation which involves *underpotential* deposition (*vide infra*).

2. Electroanalytical Aspects

2.1. General Methodology

For a complete understanding of any electrochemical process, it is necessary to acquire information, not only concerning the mechanism of the primary charge transfer step in which a bulk species becomes discharged at the melt–electrode interface, but also about the form of that bulk species and its rate of transport up to the reaction plane. A knowledge of the final, equilibrium state of the product is also necessary, e.g., whether or not it becomes incorporated into the original electrode substrate.

Electroanalytical techniques, essentially similar to those employed in aqueous solutions, can be adapted for use in melts to provide data on solution equilibria by way of stability constant determinations, ion transport through diffusion coefficient measurements, as well as mechanistic analysis and product identification from mathematical data treatment.(25) Indeed, techniques such as linear sweep voltammetry and chronopotentiometry may often be applied rapidly to assess or confirm general characteristics or overall stoichiometry of electrode processes in melts, prior to more detailed kinetic or mechanistic investigations requiring more elaborate instrumentation and equipment, e.g., as demanded by impedance studies. Thus, answers to such preliminary questions as

- does the solution species give rise to any well-defined product following charge transfer?
- does the electrode process involve the predeposition of alkali metal or alkaline earth metal?
- is there a slow step in the overall charge transfer process?
- are there adsorption or chemical processes coupled with the main charge transfer step?
- does the charge transfer occur in single or separately identifiable successive stages?

may often be found at an early time.

Advantageously, electroanalytical techniques may also be employed for *in situ* analysis(26) and control of industrial processes, e.g., as currently practiced for "anode effect" control in aluminum electrowinning.(27)

Most of the commonly used electroanalytical techniques such as polarography, chronopotentiometry, linear sweep, cyclic and potential step voltammetry, chronoamperometry, and the rotating disk method have now been applied in molten salt work. Nevertheless, for many years, chronopotentiometry found the widest appeal for different melt systems, because of its inherent simplicity of application in otherwise experimentally difficult situations.(28) As a consequence, difficulties were transferred to data handling and interpretation of results, since theoretical limitations associated with rate control rather than process selection, and with assignment of a precise transition time from an often poorly defined signal response, proved particularly intractable in some cases. More recently, improvements in cell design, equipment, instrumentation, and data handling have permitted other techniques, especially linear sweep voltammetry, to be successfully applied to molten salts.(29) For detailed studies of electrode processes, it is advisable, and now possible, to follow up a preliminary voltammetric experiment which establishes general features, with additional techniques such as potentiostatic or galvanostatic pulse methods designed to retrieve the more esoteric information.(30) This approach may then be coupled to structural studies. A natural corollary follows, that caution is needed in the application of the newer semiquantitative techniques so that the (rapid) generation of unsubstantiated data, which may cloud the central issues, is avoided.

With modern instrumentation, the coupling of several techniques in series can advantageously be performed. In their study of thin oxide on platinum in molten LiCl–KCl, Inman and Weaver(31) formed their films at constant potential, but examined them by galvanostatic stripping. Similarly, Kisza and Twardoch(32) were able to generate unstable species by anodic dissolution and analyze them by chronopotentiometry. With the advent of microprocessor control, such manipulations are likely to increase in molten salt experimentation, as has occurred in work on aqueous solution systems. Computer control and data collection is even more desirable in molten media, since it is necessary to maximize information retrieval when the hardware *is* performing according to plan!

Notwithstanding, the experimental simplicity of chronopotentiometry may still make it a first-choice electroanalytical technique for higher-temperature molten systems. Furthermore, in the current-reversal mode, it is one of only a few diagnostic techniques for assessing the classical reversibility of an electrode process. A recent review(33) has surveyed many of its applications in this context, and so, bearing in mind the authors' own interests, it seems appropriate to use examples of chronopotentiometric studies to illustrate some of the present aspects of current interest.

2.2. Ion Transport

While standard polarographic techniques at mercury electrodes and ionophoretic methods on glass plates or papers provide straightforward means of determining ionic interdiffusion coefficients in the lowest melting salts such as nitrates, as mentioned above, chronopotentiometry may offer a more attractive approach for higher melting and more reactive melts. However, because of the difficulties of assigning a precise transition time and the generally poor reproducibility of results among works of different authors which seems to characterize high-temperature studies, controversy has been generated by apparent systematic discrepancies in reported diffusion coefficients. Nevertheless, the internally self-consistent results of individual workers for a range of ions can provide a useful basis for testing models of ion transport.(34) For example, Figures 1 and 2 show some chronopotentiometrically determined diffusion coefficients for a range of ions at platinum microcathodes in molten Li_2SO_4–20 mol % K_2SO_4 at 873 K, together with some other data for ions in molten LiCl–KCl eutectic at 723 K, taken from the literature, plotted against Z^2/r and $\sum I/r$, respectively. The former plot is based on an electrostatic Born model for solvation, and assumes that the rate-determining step for diffusion is the escape of the cation from its anion solvation sheath. Although there is some correlation in this plot, bunching of

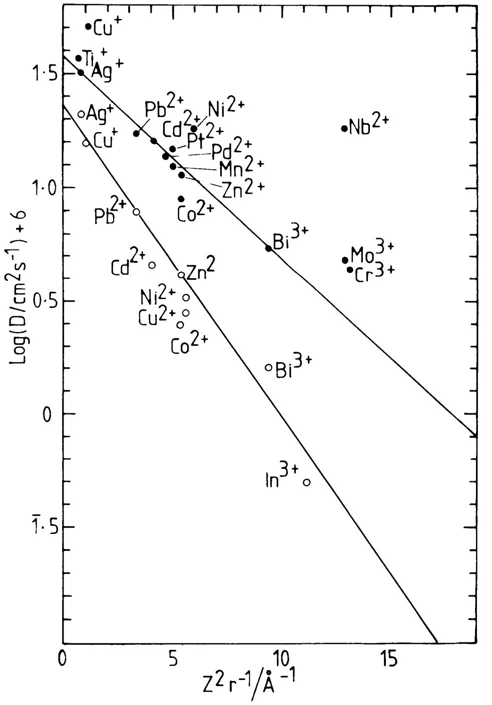

Figure 1. Plot of log D vs. Z^2/r for ions in Li_2SO_4–20 wt % K_2SO_4 at 873 K, this work (○), and in LiCl–41 mol % KCl at 723 K (●). (Reproduced from Ref. 34 by kind permission Elsevier Sequoia S.A.)

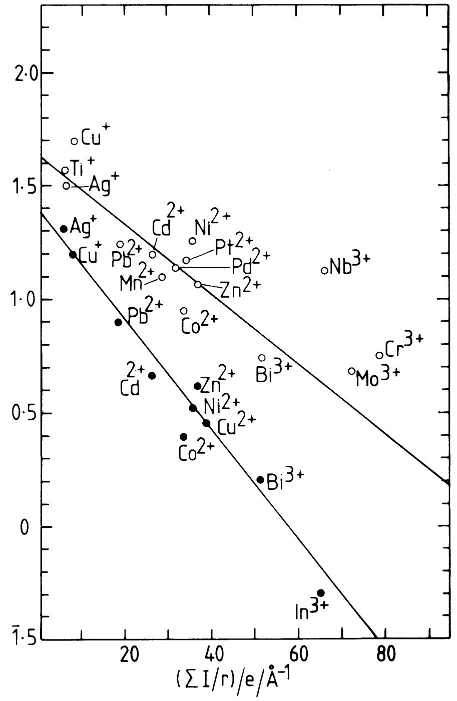

Figure 2. Plot of log D vs. $\sum I/r$ for data shown in Figure 1. (Reproduced from Ref. 34 by kind permission Elsevier Sequoia S.A.)

data occurs with the transition metal ions, which have similar radii, and other anomalies are evident; realistically, the Born equation is inappropriate to ionic melts. Some smoothing of the data can be observed in the $\sum I/r$ plot. This semiempirically accounts for the redistribution of charge around the metal ion required to stabilize it in a highly negative field, through a correlation with the ionization potential—a measure of the cations' ability to accept charge from the anions. Further refinements are clearly indicated, especially to take account of the strong charge dependence of ionic motion in melts noted by several workers.(35)

Persistent reports(36–38) indicate that the Stokes–Einstein equation may be valid in molten salts and that a suitable choice for the "hydrodynamic" friction constant "a" will be ~4.6π, approximating to nearly complete slippage. The only explanation for this that has been offered so far is that the near-square potential energy wells in which ions reside in melts fortuitously resemble the Van der Waals interaction wells operating in the dielectric continuum envisaged in the original formulation in all respects except their strength.

2.3. Ionic Adsorption

A number of electrochemical studies in molten salts have invoked ionic adsorption to explain the observed results. Although extrapolation from aqueous solution data would suggest that such effects should cease at $\lesssim 373$ K, in the absence of water there is no *a priori* reason why ions should not interact strongly and specifically with excess charge at the interface. Christie and Osteryoung(39) reported polarographic maxima at the dropping mercury electrode (dme) in molten $LiNO_3$–KNO_3 at 453 K for Cd^{II} and Pb^{II} ions in the presence of Br^- ions. Laitinen and Gaur(40) reported phase angles in excess of 45° in a Faradaic impedance study of Cd^{II}, Pb^{II}, Ni^{II}, and Zn^{II} ions at platinum electrodes in molten LiCl–KCl at 723 K. These observations, together with other evidence derived from polarographic, chronopotentiometric, and interfacial capacitance studies, may best be interpreted in terms of ionic specific adsorption.

The first calculation of surface excess charge was performed by Narayan, Lovering, and Inman(41) arising from a chronopotentiometric study, supported by polarographic evidence, of the $Cd^{II} + Br^-$ and $Pb^{II} + Br^-$ systems in nitrate melts, at platinum and mercury electrodes, respectively. Particular care was taken in the chronopotentiometric measurements to ensure that the electrodes were free from reducible oxide films, that the quantity of metal deposited was minimized in order to avoid changes in surface area, that these deposits were rapidly stripped from the electrode in a reverse current pulse, and that transition times were sufficiently long to limit charging contributions but short enough to avoid convective transport complications.

Perhaps the clearest support(42) for the occurrence of ionic adsorption in molten salts comes from an extension of the study of the $Cd^{II} + Br^-$ system at a slow-dropping mercury electrode ($t \sim 15$ sec) in molten $NaNO_3$–KNO_3 at 523 K. The electronic circuitry employed allowed short transition times (1–85 msec) to be recorded at predetermined drop times, such that reproducible and approximately constant electrode surface areas were presented for each current pulse. Thus, the chronopotentiometric transitions were extremely sharp, owing to the smooth electrode surface, the absence of oxide films, and the mercury-soluble product. Precise adherence to the Sand equation for solutions of Cd^{II} ions alone confirmed that the interfacial charging term was negligible. Positive intercepts on the ordinates of $\tau^{1/2}$ vs. I^{-1}, in the presence of Br^- ions, provided diagnostic evidence for the occurrence of adsorption. A precise model of adsorption could not be distinguished, although the parallel depletion of adsorbed and diffusing species was favored. Surface excess terms and diffusion coefficients were determined and are shown in Table 1. Likewise, broadly similar phenomena were shown to persist down to 323 K in molten $Ca(NO_3)_2 \cdot 4H_2O$ for the $Cd^{II} + Br^-$ system.(43) Polarographic maxima, enhanced but split chronopotentiometric transition times, as well as double-peaked linear sweep voltammograms (l.s.v.) were observed at hanging and dropping mercury electrodes. However, in this case, by varying the sweep rate in l.s.v. experiments, it was evident that the adsorbed film was being reduced at higher energies than the diffusing species. Not only were surface excess terms able to be evaluated (Table 2), but some consideration

Table 1
Surface Excesses and Diffusion Coefficients Determined from Chronopotentiograms[a]

$C_{\mathrm{KBr}} \times 10^3$, m	$\Gamma \times 10^{10}$, mol cm^{-2}	$D \times 10^6$, cm^2 sec^{-1}
28.29	0.899 ± 0.183	4.6 ± 0.1
44.49	0.941 ± 0.394	4.2 ± 0.2
64.88	1.315 ± 0.149	3.9 ± 0.1
91.16	1.440 ± 0.224	3.4 ± 0.1

[a] $[\mathrm{Cd^{II}}] = 0.698 \times 10^{-3}$ m in $NaNO_3$-KNO_3 at 523 K with added KBr, according to the SAR adsorption model. Slow dme, $t = 15$ sec.

Table 2
Surface Excesses Determined from Linear Sweep Voltammograms[a]

$C_{\mathrm{KBr}} \times 10^3$, m	Total charge consumed q, μC	∴ Excess charge q^*, μC	∴ $\Gamma \times 10^{10}$, mol cm^{-2}
—	0.287	—	—
2.00	0.665	0.378	0.93
4.72	3.959	3.673	8.99
9.16	4.015	3.728	9.12
18.27	3.987	3.700	9.05
44.54	0.850	0.563	1.38
163.00	0.556	0.269	0.66

[a] $[\mathrm{Cd^{II}}] = 0.376 \times 10^{-3}$ m in $Ca(NO_3)_2 \cdot 4H_2O$ at 323 K with added KBr. hmde area = 0.0212 cm^2, sweep rate = 5 V sec^{-1}, start potential = −0.4 V vs. Ag/Ag$^{\mathrm{I}}$ (0.03 m), sweep range = 0.5 V. Charge manually integrated.

was given to a more detailed model in which the $CdBr_3^-$ entity appeared principally responsible for the adsorption behavior. More recently,(44) chronocoulometric studies for similar systems have been interpreted in terms of the formation of insoluble mixed white metal halide phases on the mercury electrodes used. Notwithstanding semantic arguments(45) concerning the difference between a monolayer of adsorbed ions and a monolayer of a distinct phase which *includes* the surface of the electrode itself, the chronocoulometric technique may introduce undesirable experimental artifacts associated with the choice of initial and step potentials.

2.4. Coupled Chemical Reactions

The formation of complex ions in molten salts is considered elsewhere. However, in certain cases, where the complex ions themselves are electroinactive, they can dissociate to form electroactive species. The "kinetic effects" which are then manifested may be detected and quantified by electroanalytical techniques following aqueous solution procedures, viz., in a redox reaction:

$$Z \rightleftarrows O + ne \rightarrow R \tag{3}$$

At high temperatures, it is difficult to identify unambiguously phenomena such as these because artifactual processes, especially convective stirring, can manifest themselves in similar ways. Nevertheless a clear example is provided by the system $MoCl_3$–58.5 mol % LiCl–41.5 mol % KCl at 838 K.(46) This will be discussed in detail in Section 4.

2.5. Solution Stability

It is sometimes very difficult to obtain stable, homogeneous solutions of inorganic compounds in molten salt.(47) This is particularly so for the compounds of the transition metals which characteristically exhibit a range of oxidation states for each element. Tantalum, which can exist in the oxidation states V, IV, II, I, −I, may form cluster compounds in the lower states; these are capable of disproportionating, whereas the higher oxidation state compounds are rather volatile at the operating temperatures of many molten salts. Some further details of these phenomena are also given in Section 4.

The important point to be made here is that electroanalytical techniques are particularly useful for monitoring the occurrence of these chemical phenomena. Furthermore, disproportionation can occur as an integral part of an electrode reaction and gives rise to "catalytic effects" when a lower oxidation state ion is formed as an intermediate during an electroreduction process. Again, electroanalytical techniques can be particularly useful for investigating such effects.

3. The Metal–Molten Salt Interface

3.1. General Aspects

At first sight, perhaps, the metal–molten salt interface might not be expected to resemble the metal–aqueous solution interface too closely, having regard to the complex role of water in the latter case, and the hydration of ions. Nevertheless, in practice, their experimentally determined interfacial properties do appear strikingly similar. Thus, minimum double-layer capacitances are of the same order of magnitude, and even zero charge potentials occur in the same general region of solvent electroactivity. Furthermore, the development of second-order effects, such as the "hump" in aqueous solution capacitance plots, appears to develop only very slowly when a melt is titrated with water.(48) Moreover, the phenomenon of electrocapillarity, expressing the relationship between interfacial capacitance–electrode potential behavior also holds good for metals in contact with molten salts.(49)

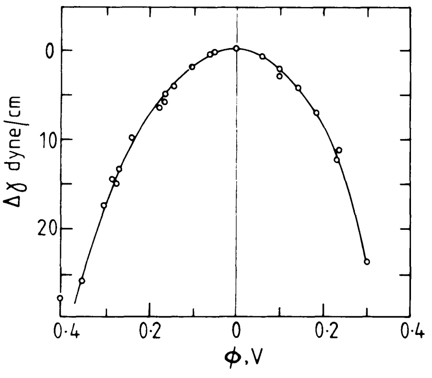

Figure 3. Electrocapillary data for Pb in molten KCl at 1093 K. Experimental data shown as points, solid curve corresponds to double-integrated capacitance curve, and ϕ is the rational potential for the Pb electrode. (Reproduced from Ref. 1 by kind permisssion John Wiley and Sons, Inc.)

One advantage of investigating interfacial properties in melts arises from the wider range of *liquid*, i.e., clean and reproducible, metal surfaces that may be employed, subject to the limitations of metal–melt interactions and reactions mentioned earlier. Thus, zero charge potentials for many liquid metals, especially in alkali halide melts, have been tabulated from results of extensive measurements of electrocapillary curves and interfacial capacitances, notably by several Russian schools.(49,50) That these two approaches are self-consistent is evident from Figure 3, which compares the doubly integrated capacitance data for molten Pb in contact with molten LiCl–KCl with the experimentally observed electrocapillary curves.(49) Agreement between zero charge potentials determined in the two different ways is generally good.

Unfortunately, owing to experimental difficulties, interfacial measurements in molten salts often need to be made at solid metal substrates, and these give rather less reliable results.(53) For example, the agreement between the reported values of the minimum capacitance for both solid and liquid metals tends to be quite poor. This may be ascribed to melt impurities, especially water and, at the higher temperatures, spurious parallel components arising from materials' instabilities. However, progress has been achieved in a number of experimentally difficult situations, notably in the alumina–cryolite melt system(51) which is so important in aluminum production.

3.2. The Electrical Multilayer Close to $E_q = 0$

Early investigations,(52) particularly by the Russian schools, indicated that the interfacial tension and capacitance for liquid metals in contact with melts were symmetrical, parabolic functions of electrode potential with common principal axes through their points of zero charge. While the characteristics of these electrical multilayers appear to be largely independent of the nature of the metal phase, the observed capacitances do depend, both in magnitude and in potential response, on the composition of the molten salt phase; the cationic composition seems to exert the greater influence.

Some general features of the interfacial capacitance/potential plots can be summarized as follows:

(a) Approximately parabolic profiles are observed with minima at $E_q = 0$, i.e., the zero-charge potential.

(b) A general independence of $E_q = 0$ is found on the anion composition (with the exception of F^-), but variation of $C_{\min}$ in the series $Cl^- < Br^- < I^-$.

(c) A dependence of $E_q = 0$ on the cation composition, e.g., for the melts LiCl, KCl, CsCl, is found.

(d) Positive temperature coefficients for $C_{\min}$ and markedly different capacitance curve shapes in the low (~673 K) and high (~1073 K) temperature regions (but see below) are observed.

These comments apply to the molten alkali metal halides. In molten nitrates,(53–55) the capacitance–potential curves are also parabolic, with a minimum at $E_q = 0$; however, the cathodic branch cannot be properly discerned owing to the onset of the reduction of the nitrate ion. Furthermore, the minimum multilayer capacity appears invariant within the rather more restricted temperature range accessible in these media.

The foregoing observations have proved a durable guide to interfacial properties over a number of years. However, in the light of more recent studies, including those of electrode processes in melts, it may be necessary to revise certain detailed aspects, particularly concerning the higher-temperature behavior of the two branches of the capacitance–potential curves.

Esin suggested(56) in 1956 that the excess charge on the melt side of a liquid metal–molten salt interface may be distributed across several ionic layers; hence, it seems more appropriate to consider the electrified interface as a "multilayer" *for molten salt systems* rather than as the double layer associated with aqueous systems. The first theoretical description of this layer was given by Dogonadze and Chizmadzhev.(57) Using binary distribution functions previously employed for interpreting X-ray diffraction measurements of *bulk* melt structures, they obtained a description of the melt structure at the interface. They concluded that the charge distribution was characterized by a sharply attenuated oscillation, in agreement with Esin.

Unfortunately, rather too many approximations were made in their formulation:

$$C_{\min} = \kappa^2 \cdot \lambda \cdot d/8\pi^4$$

where d is the distance to the first maximum in the distribution function, λ^{-1} is the correlation radius, characterizing the dimension of short-range order in the melt and being $>d$, and κ^{-1} is the Debye length for $C_{\min}$, the minimum interfacial capacitance. Moreover, the values of some parameters chosen to calculate $C_{\min}$, notably a correlation radius for liquid cesium *metal*, provided a less than favorable comparison with experimental data.

A damped oscillating charge distribution of the interfacial structure was also obtained by Sotnikov and Esin,(58) assuming a Boltzmann distribution of ion vacancies in the interface; cf. the case of dilute solutions of ions in water. Additionally, they introduced a polarizability factor to account for the deformation of ion charge under the influence of the electric field within the multilayer. Their revised formula for the interfacial capacitance gave

$$\frac{1}{C}=\frac{1}{C_k}-\frac{4\pi\delta}{1-4\pi\delta\beta|\varepsilon|} \tag{4}$$

where

$$C_k=\frac{D}{4\pi r}$$

represents the capacitance of a parallel plate capacitor with a separation equal to the radius, r, of the cation, D being the dielectric constant of the medium,

$$\delta^2 = kT/[8\pi q^2 C_0(z-2)]$$

and (5)

$$\beta = 8\pi\alpha q C_0(z-1)/kT$$

where q is the charge on the vacancy, C_0 the concentration of vacancies of appropriate sign in the bulk melt, z is the number of ions in the rigid coordination sphere surrounding the ion, and α is its polarizability. For the potassium, rubidium, and cesium halides, agreement between experiment and theory was good. For sodium halides, agreement was fair at the melting point, but for the lithium halides it was poor. However, the anion and cation vacancies have very different sizes and properties in the latter case, while the theoretical treatment necessarily assumes them to be identical.

Bukun and Ukshe(59) calculated the integral capacitance from an infinite series, for a multilayer interface by treating the net-charged ionic layers as the plates of a parallel multiplate capacitor. In practice, it was only necessary to consider three layers to approximate the series. They were able to define a set of parameters, derived from the experimentally determined temperature coefficient of capacitance, which enabled them to obtain reasonable verification of their theory as indicated by the agreement between calculated and observed capacitances.

3.3. The Electrical Multilayer Remote from $E_q = 0$

The remarkable changes which occur in the shapes of the capacitance–potential curves as the temperature is raised and the accompanying rapid increase of capacitance with potential cannot be adequately accounted for by the foregoing theories. Therefore, Graves and Inman(60) repeated the measurements of Ukshe and Bukun,(59) made at 723 K, using the single galvanostatic pulse (rise time <10 nsec) technique rather than the ac impedance method.

In this way, clear-cut separation can be obtained between capacitative charging and Faradaic processes, although spurious pseudocapacitances are still indistinguishable (*vide infra*). While these capacitance data obtained *at potentials close to* $E_q = 0$ were in substantial agreement with those of Ukshe and Bukun, at potentials removed from $E_q = 0$ (on the positive side for experimental convenience) the value of the multilayer capacitance increased quite rapidly with potential, as had been observed at the higher temperatures. It was proposed that the liquid lead electrode was manifesting nearly ideally reversible behavior at these potentials, because the exchange current density for the $Pb \rightleftarrows Pb^{2+} + 2e$ electrode reaction is very high (see Section 4). Although Bek and Lifshits(61) obtained similar results using an impedance method designed to account for a charge transfer component by deliberate addition of Pb^{2+} ions to the melt, natural corrosion of the lead electrode complicates the data treatment. Charge transfer processes are instrumentally eliminated in the galvanostatic pulse technique.

Graves and Inman(60) surmised that the capacitance–potential curves comprised two regions: quasi-ideally reversible behavior, on the one hand, and quasi-ideally polarizable behavior on the other. In the former case, the predicted log ΔC–potential relationship is experimentally observed, where ΔC represents the enhanced interfacial capacitance for the quasi-ideally reversible region.

An attractive proposition is that the change in shape of the capacitance–potential curves with increasing temperature arises from a decrease in the *range* of potentials over which quasi-ideally polarizable behavior prevails. Thus, the sharply rising extremities of these curves become compressed at higher temperatures. Graves and Inman were able subsequently to quantify this hypothesis.(62)

Interestingly, Ukshe and Bukun(59) indicated a negligible range of ideally polarizable behavior at 1073 K from their results. However, Graves and Inman(62) predicted a small but finite residual range which was confirmed by Bek and Lifshits(61) after applying their charge transfer corrections. Notably, the minimum capacitance of 25 $\mu F\ cm^{-2}$ reported by the last-named authors for the Pb/NaCl–KCl system at 1073 K is similar to the value obtained at lower temperatures and in conflict with the value of 40 $\mu F\ cm^{-2}$ reported by Ukshe and Bukun,(59) whose capacitance curves do not exhibit a horizontal region.

Another factor influencing the apparent temperature dependence of the minimum capacitance is that the data analyses may not have adequately allowed for a dc polarized charge transfer component. Heus, Tidwell, and Egan(63) certainly could not detect any temperature dependence using an extensively purified molten salt (i.e., low in Pb^{2+} ions), although their minimum value was rather high at 30 $\mu F\ cm^{-3}$. Fellner and Matiasovsky(64) reported virtually temperature and frequency independence of the minimum capacitances for the systems $Hg/LiNO_3$–$NaNO_3$–KNO_3 between 413 and 473 K, and Pb/LiCl–KCl between 673 and 773 K, from 1–20 kHz. The small increases in capacitance of the latter system from ~23 μF cm^{-2} to ~26 and 29.5 μF cm^{-2} at 873 and 973 K, respectively, showed a frequency dependence up to 12 kHz which was ascribed to a parallel pseudo-capacitance. This conflicts with the interpretation of Ukshe and Bukun,(59) who claimed that the agreement between their interfacial tension–potential curves and those obtained by double integration of the capacitance data was diagnostic proof that "true" capacitance was being measured.

Inman, Bowling, Lovering, and White(65) attempted to resolve this issue by pointing out that, if the interface is behaving in a quasi-ideally reversible manner, then adsorption capacitances will appear as "true" capacitances *and* the interfacial tension curves will correspond with the doubly integrated capacitance curves because the discharge of adsorbed ions proceeds at a rate which is infinitely faster than the measuring frequency.

In conclusion, it appears that few metal–molten salt systems behave in the ideally polarizable sense generally associated with the mercury/aqueous solution interface at 298 K. Possible exceptions include some noble liquid metal/melt systems such as mercury/molten nitrates and lead/molten halides at low temperatures (<773 K), but only when the molten electrolyte is extensively purified. Otherwise, systems need to be analyzed as complex impedances, using ac or pulse techniques, to determine whether the minimum interfacial capacitance is affected by extensive factors, leading to parallel pseudocapacitances and Faradaic components.(1,64) The range of potentials and measuring frequencies for which the interface approaches ideally polarizable behavior also needs to be established. It now seems clear that the multilayer ionic model of charge distribution at the metal/melt interface is more pertinent to molten media than the familiar "double layer" associated with aqueous solutions. However, the quantitative theories derived for the former model will have to be revised if it is confirmed that the interfacial capacitance is, indeed, independent of temperature in the ideally polarizable region.

Some assistance in resolving these issues may eventually come from molecular dynamical simulations of charged interfaces.(66) These calculations are still in their infancy, and at the moment, scarcely give even reasonable agreement with experiment. Nevertheless, the technique is a powerful one and offers considerable promise.

4. Kinetics and Mechanisms of Electrode Reactions

4.1. Problems and Methods of Approach

Many electrode reactions in molten salts, especially metal–metal ion systems, are purely diffusion controlled. However, it is now recognized that the whole range of electrode process mechanisms may be encountered in appropriate circumstances. In ionic molten salts, migration of solute ions will, of course, be absent and mass transfer will generally proceed, under laboratory conditions, according to linear diffusion. At very high temperatures and in industrial processes, convective transport may become important. In certain cases, convective mixing may arise from Joule heating at high current densities, and this can be deliberately encouraged in order to sustain the cell temperature.(67) Nevertheless, useful *in situ* electroanalytical monitoring of such systems may be performed, using pulse and transient techniques of very short duration.(68) Notwithstanding, caution is sometimes required in the analysis of apparently straightforward laboratory experiments, since the effects of convection and spherical diffusion (particularly to liquid metal drops) are not always readily distinguishable from kinetic complications arising from chemical reactions coupled to charge transfer processes (see previous section) at long observation times. On the other hand, an experimental time scale >10 msec is essential, as in aqueous solutions, if non-Faradaic multilayer charging is to be distinguished from the discharge of adsorbed species. Slow, i.e., classically irreversible, processes are becoming increasingly apparent in molten salt systems and often respond to traditional analytical treatment (*vide infra*). Processes involving ionic adsorption were considered earlier; some more complex phenomena such as the "anode" effect, in aluminum extraction, for example, are beyond the scope of this chapter and are dealt with elsewhere.

4.2. Electrode Reactions Involving Homogeneous Redox Reactions

A number of unique difficulties pertain to oxidation states of metal ions encountered in molten salt solutions. For example, for first-row transition metals, the highest oxidation state prevailing is often +3, as in the case of Fe^{3+} and Cr^{3+}. Frequently, for chlorides in particular, the +3 state compounds are volatile at suitable operating temperatures and, hence, their solutions are thermally unstable.(69) Other problems encountered include rapidly disproportionating states, the formation of oxyhalides, and precipitation of complexes by reaction with the melt.(70) While redox reactions *per se* involve very fast charge transfer steps, these may occur at the extremes of the range of electrochemical stability, thus leading to concomitant solvent melt decomposition. Nevertheless, suitable processes such as Fe^{2+}/Fe^{3+} on vitreous carbon in chloride melts can be employed to determine the effective electrochemical areas of electrodes where diffusion coefficients are accurately known.(71)

4.3. Electrode Reactions at Liquid Metal Electrodes

Mercury, lead, bismuth, and silver have been the most frequently studied liquid metal electrodes; the dme has been employed to study metal–metal ion reactions, mainly in nitrate(72) and chloroaluminate melts(73) (but also

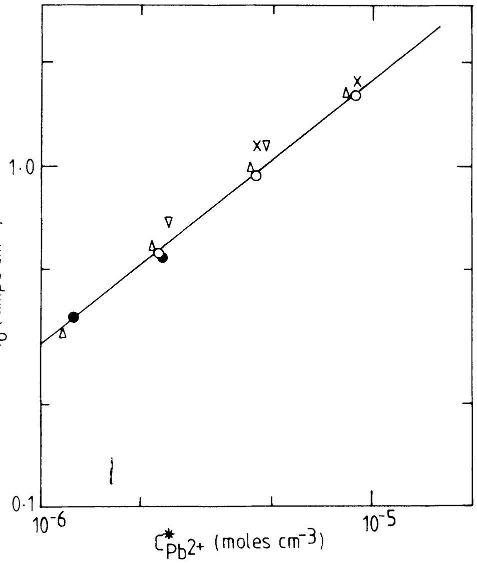

Figure 4. Logarithmic plot of exchange current density vs. concentration for the Pb/Pb^{2+} couple in eutectic LiCl–KCl at 723 K. (Reproduced from Ref. 60 by kind permission The Institution of Mining and Metallurgy.)

some organic systems), while the remainder have been used in halide,(74) especially chloride melts, as pools or hanging drops.(45) Most investigations have been of metal–ion reduction reactions. Randles and White(53) were the first to determine the rate constants for a quasireversible Ni^{II}/Ni (Hg) reaction in a molten medium, a eutectic nitrate mixture, by using an impedance method at a hanging drop mercury electrode (hdme). The Pb^{II}/Pb (liq) reaction has received considerable attention, particularly in chloride melts (see previous section).(60,76) Where a single oxidation state is stable for the ion in the melt, and that ion is deposited onto a liquid electrode of its parent metal, the electrode process can be very fast. Some typical exchange current densities for the above reaction in molten LiCl–KCl are plotted in logarithmic co-ordinates in Figure 4.(60) Even at quite low Pb^{2+} concentrations, $\sim 5.10^{-3}$ M, the exchange current density can approach as high a value as 1 A cm^{-2}.

Given the interfacial capacitance studies of this system may be interpreted in terms of quasi-ideally reversible reactions at potentials remote from $E_{q=0}$ (Section 3), then such a high exchange current density reaction might be ascribed to the rapid discharge of an absorbed layer. In this case, interaction between ions in the bulk phase and the electrode should be facilitated by anion or complex-ion bridging;(77) if one species is prone to form extended arrays, e.g., $PbCl_2$, then an electronically conducting adsorbed layer could act to accelerate electron transfer between complex species such as $PbCl_4{}^{2-}$ diffusing from the bulk and the electrode. The absence of water in these media must surely aid rapid electron and/or ion transfer also, even if notions of simple ion transport followed by rapid electron transfer to unsolvated ions are too naive. Nevertheless, the velocities of multiple-bridged reactions of this type can readily be appreciated.

4.4. Electrode Reactions at Solid Metal Electrodes

These may be divided into those processes which exhibit solution chemical reaction complications and those that do not. At first sight, an electrode process apparently in the latter category is the $Ag^+ + e^- \rightleftarrows Ag^0(M)$ reaction for which the exchange current density is usually large.(78) However, a number of unusual features attend the behavior of silver in molten salts. Firstly, in nitrate melts, the activity coefficient of $AgNO_3$ can vary from ~0.5–3.3 according to the temperature and cationic composition.(79) Furthermore, electrochemically determined diffusion coefficients for Ag^+ in several melt systems sometimes appear to be anomalous,(80,35) even though suggestions of binuclear complexes seem to be without foundation.(81) Moreover, this metal also seems to be particularly prone to post-charge-transfer complications, such as in nucleation and growth.(82). The overpotential attending the nucleation of metals on foreign substrates readily manifests itself as an initial potential overshoot in constant current experiments(83) and can best be studied by examining current–time profiles at selected constant potentials.(82) At constant current, potential decay occurs during the subsequent crystal growth step, but before depletion of reactant at the electrode surface leads to the final inflection characterizing the diffusion-controlled transition time.

However, *underpotential* deposition of a metal on a foreign substrate may also be encountered in molten salts. For example, when metals are deposited at high temperatures from molten salt baths, they may be in the form of either a liquid or a solid. If this liquid metal wets the electrode substrate and the two materials are miscible, then an alloy may be formed. Alternatively, regardless of the state of the deposited metal, rapid interdiffusion of metal atoms into the electrode can lead to solid solutions or the formation of intermetallic compounds. These effects are deliberately exploited in metal treatment processes, including metalliding (see following section). In these cases, the thermodynamic activity of the deposited metal can be less than unity and, consequently, the deposition potential may be more positive than that predicted by the Nernst equation in which the metal appears in its standard state. Sometimes these phenomena can lead to the semilogarithmic plots of the current or time functions vs. potential, exhibiting slopes more appropriate to a soluble product rather than that expected for a solid deposit.(84) Such effects are obviously unique to systems operated at elevated temperatures; on the other hand, it is especially interesting to examine nucleation and growth processes in melts, even though they pertain equally to aqueous solutions at 298 K.

For charge transfer processes which are coupled with chemical steps, it might be expected that the overall mechanism would be too rapid at high temperatures to exhibit measurable overpotentials and that reversible electrode reactions would result. This has not always proved to be the case. Apparent "irreversibility" in cathodic reactions can often arise from slow coupled chemical processes rather than from slow charge transfer. Interest in this area has been promoted by a desire to obtain smooth, thick, adherent electrodeposits by molten salt electrolysis (see following section). One important feature of this work is that our knowledge of the inorganic chemistry of many elements in molten salts has benefited from recent electrochemical studies, not least because electrons are clean, controllable reducing agents.

Recent interest has focused especially on the role of the coupled chemical steps mentioned above in determining the overall kinetics and mechanisms of electrode reactions. Although this leads to an increase in the amount of chemical information that can be obtained, it may also lead to various complications and ambiguities. Schematically, a complex ion which is normally electroinactive itself dissociates to form an electroactive species O, viz.,

$$Z \rightleftarrows O \tag{6}$$

and then

$$O + ne \rightarrow R \tag{7}$$

the concentration of which can be detected and monitored by an electroanalytical technique.

As explained earlier, it may be difficult to identify unambiguously phenomena such as these, because of the intervention of artefactual processes, especially convective mass transfer. In both the chemical and convective mass transfer cases, the transport rate corresponding to the linear diffusion case is enhanced. A clear example of a chemical complication is provided by the system $MoCl_3$ in molten NaCl–80 mol % KCl at 1033 K.(85) A single chronopotentiometric wave is observed for $MoCl_3$ concentrations $<2.10^{-2}\,M$. Although the transition times themselves obeyed Sand's equation, the shifts of $e_{\tau/4}$ with applied current density and the slopes of the Karaoglanoff plots suggest an irreversibility having chemical rather than electrochemical origin. Thus, if the rate-determining step (rds) is indeed one of the type $Z \leftrightarrows O$, the dissociation rate $Z \rightarrow 0$ must be rather high. Thus, using Vetter's treatment for a homogeneous rate-controlling prior chemical step, and identifying the reaction overpotential η_τ with $e_{\tau/4}$ to a first approximation, the following overall reaction pathway was postulated:

$$Mo^{6+} \xrightarrow{\text{slow}} 2Mo^{3+} \qquad \text{(rds)} \tag{8}$$

$$Mo^{3+} + 3e \rightarrow Mo^0 \qquad \text{(fast)} \tag{9}$$

At high Mo^{III} concentrations, two chronopotentiometric reduction waves are observed; the more cathodic one, which is absent at low concentrations, is shorter than the first. The parameters of this second wave were not consistent with it being due to the reduction of another oxidation state of molybdenum. A higher oxidation state would have produced a new wave at more anodic potentials, while a lower oxidation state would have produced a wave having a longer transition time than the initial one and be apparent at all concentrations. However, this second wave is certainly due to molybdenum, since

Table 3
Stability of Solutions of Refractory Metal Chlorides in Molten Alkali Metal Chlorides

Solution instability	Refractory metal W	 Mo	 Cr	 Ti	 Ta
Volatility of solute (generally exhibited by high oxidation states)	√	√ ($MoCl_3$)	× ($CrCl_2$)	× ($TiCl_2$)	√ ($TaCl_5$) ($TaCl_4$)
Disproportionation of solute (generally exhibited by low oxidation states)	√	×	×	√	√
Formation of cluster compounds	√	√ (Soluble)	?	√	√

Factors which control the stability of these solutions:

1. Solvent anion composition
2. Solvent cation composition
3. Concentration of solute
4. Temperature
5. Complexation reactions

addition of more $MoCl_3$ causes the transition time of the second wave to increase. Thus, this second wave probably corresponds to the direct reduction of a multi(probably di-)nuclear complex to metallic molybdenum. This study provides additional quantitative support for the earlier observations of Mellors and Senderoff, who employed the eutectic melt LiCl–KCl as solvent.

The attainment of stable solutions of some refractory metal compounds in molten solvents can present major problems. Thus, solutes can be lost through vaporization; the volatility of $TiCl_4$, for example, has undoubtedly hindered the commercial exploitation of electrolytic routes for extracting titanium, since the tetrachloride is the feedstock of choice. The formation of insoluble cluster compounds and the disproportionation of dissolved species also present added complications;(86) Table 3 shows some of the systems in which these effects occur and the factors which control the stability of the solutions.

4.5. The Electroactivity of Nonmetallic Anions

4.5.1. Cathodic Reactions

Although negatively charged, anions are susceptible to electroreduction so long as they contain an element whose oxidation state can be lowered within the range of melt electrochemical stability. For example, nitrate ions contain N^{V} which can be reduced to N^{III}, forming nitrite ions well within the stability range of most melts, including chlorides. This occurs in nitrates themselves, of course, as a limiting reaction (but see below).(87) Such electrochemical behavior might be rationalized in terms of the Lux–Flood acid–base formalization; for many years the reduction of nitrate ions was written(88)

$$NO_3^- \rightleftarrows NO_2{}^+_{\text{Lux–Flood acid}} + O^{2-} \rightarrow NO_2^+ + 2e^- \rightarrow NO_2^- \qquad (10)$$

However, recent thermodynamic and kinetic data indicates that neither O^{2-} nor NO_2^+ have any significance, even as transient species, at least in nitrate melts.(89)

The reductions of several anions, both within their own melts and dissolved in other molten solutions, have received considerable attention. One complication which can occur is the formation of an insoluble oxide film on the electrode surface; this leads to partial passivation, limiting the current rise in voltammetry until the potential at which the succeeding process, often alkali metal deposition, is reached.(90) Such a phenomenon takes place in all alkali metal nitrate melts except pure KNO_3, which has no insoluble oxide species.

Apart from nitrate ions, the direct reduction of carbonate,(91) phosphate,(92) and silicate(93) anions have all been reported. Some controversy surrounds the electroreduction of sulfate ions; water may be implicated in this process. Inman and Wrench(94) could only induce cathodic electroactivity of sulfate ions dissolved in a chloride melt by release of SO_3, the conjugate acid, with a stronger Lux–Flood acid, metaphosphate, PO_3^-. While the alkali metal and alkaline earth sulfates, carbonates, and nitrates are clearly ionic, borate, phosphate, and silicate melts are highly polymerized. In such systems, the mobile cations move freely about the anion lattice network, which comprises a temperature- and compositional-dependent equilibrium between ion fragments of variable chain length. Inman and Franks observed kinetically limited electroreduction processes in a phosphate melt, as might be expected if only the smallest fragments of the dynamic polymer equilibrium are electroactive.(95)

The study of the cathodic generation of alkali metals in molten salts, particularly halides, is always attended by the complication of a back reaction in which the metal dissolves to form an electronically conducting solution.

4.5.2. Anodic Reactions

The limiting anodic reaction in melts may either involve the straightforward evolution of a gaseous product, or the oxidation of an oxyanion. For halide melts, the parent halogen is usually produced, and such reactions might intuitively be expected to compare with, for example, the evolution of oxygen in aqueous solution.

The simplicity of the oxygen evolution reaction in molten chlorides, viz.,

$$O^{2-} \rightarrow 1/2O_2 + 2e^- \qquad (11)$$

as compared to the complicated mechanisms established in aqueous solutions, e.g.,

$$OH^- \rightarrow H^+ + 1/2O_2 + 2e^- \tag{12}$$

$$H_2O \rightarrow 2H^+ + 1/2O_2 + 2e^- \tag{13}$$

is deceptive. The former reaction turns out to be quite irreversible, with an exchange current density comparable with that for hydrogen evolution in aqueous solution.(96) Evidently, complications may arise owing to the formation of other oxide species such as $O_2{}^{2-}$ and $O_2{}^-$, both in the bulk phase and as surface oxides on the electrodes.(97) Post-charge-transfer chemical reactions, such as $M + 1/2O_2 \rightarrow MO$, or direct participation of the metal substrate in the electrode reaction, $M + O^{2-} \rightarrow MO + 2e^-$, or, yet again, dissolution–precipitation reactions of the type $M \rightarrow M^{2+} + 2e^-$ followed by $M^{2+} + O^{2-} \rightarrow MO\downarrow$ might well be responsible for the observed behavior, thus disposing of any notion of simplicity surrounding molten salt oxide electrochemistry. Furthermore, as described in the final section, the molten salt container itself may well become involved in the stabilization, or otherwise, of oxide species.

Thus, it appears imperative to complement equilibrium measurements, such as cell emf determinations, by transient electrochemical investigations (as well as nonelectrochemical or spectroelectrochemical techniques, where possible), in order to definitively establish the nature of the process being examined.

As a final example, the anodic response of sulfur electrodes in molten salts can be considerably more complicated even than that of oxygen electrodes, not least because both sulfur atoms and ions have a tendency toward catenation. Hence, it is always necessary to consider families of polynuclear species like $S_x{}^-$ and $S_x{}^{2-}$, rather than their dimeric persulfide, $S_2{}^{2-}$ and supersulfide, $S_2{}^-$, derivatives. Frequently, it becomes impossible to resolve the electrochemical behavior of these species and spectroscopic methods are required in support of data interpretations.

In addition, of course, complications arise because elemental sulfur is completely nonconducting; however, one interesting possibility is that the deposition of liquid sulfur may be compared with the evolution of gaseous sulfur.

It is not possible to review all the work concerning sulfur electrode reactions in molten salts but only to highlight the main features.(98) Much of this work has been motivated by interests in high-temperature batteries and in the electrolytic recovery of metals from their sulfides. Solvents such as LiCl–KCl and KCNS have been employed, but many studies have concerned pure molten polysulfide melts (cf. the Na–S battery).

Much controversy has surrounded the work carried out in LiCl–KCl at temperatures around 673–723 K. Up-to-date reviews and discussions of this field are available elsewhere.

Nevertheless, certain conclusions may be drawn from even a brief perusal of this work. These include the necessity of positively identifying electrochemical waves by methods such as the standard addition technique. Moreover, there is a clear need to control the sulfur partial pressure over melts. Lastly, more attention must be given to the role of solvent and solute cation composition, since many of the apparent disagreements in the literature have arisen because authors have employed different alkali and alkaline earth sulfides.

5. Applications

5.1. General

Molten salts are widely used in industrial processes and the number of new applications is still increasing. Many of these are electrochemically based, especially in the fields of materials recovery and power generation. Progress in these areas is well documented. Thus, attention will be focused here on selected areas of metals deposition, power devices, and materials aspects in this section, in order to illustrate the principles underlying the diverse applications. Further developments are proceeding rather rapidly; hence, it is neither possible nor desirable to discuss any one aspect in detail.

5.2. Metals Recovery and Processing

Metals electrowinning, electrorefining, and electroplating represent major fields of molten salt electrochemical endeavor. Few metals may be deposited in pure form at 100% current efficiency from aqueous solutions, owing partly to the intervention of the hydrogen evolution reaction (which, if it occurred without substantial overpotential, would preclude the electrodeposition of most metals). However, other factors such as oxide film formation, hydride formation, oxide deposition from stable oxycations, chemical reduction, or oxidation reactions, especially for high and low oxidation states, with the solvent water, all impede the primary electrodeposition of pure metal from aqueous media. Therefore, molten salts offer attractive nonaqueous environments for metals processing which possess distinct advantages over the only other possibility—use of organic solvents.

These benefits, evident from the introductory remarks, include wide limits of electrochemical stability, high ionic conductivity, good solvent properties for inorganic feedstocks, especially oxide ores, and relatively small cathodic deposition overvoltages. Two disadvantages occurring from these properties include the solubility of many refractory container materials and the frequent mass-transfer-controlled rate to the electrodeposition reaction. The former problem may be overcome in most cases, reverting to metallic vessels if necessary; the latter problem will be discussed below.

5.2.1. Liquid Metals

Most success in the recovery of metals has been achieved for those which are themselves molten within the liquidus range of the molten electrolyte employed. The reason for this lies in the consequent ease of separation of the metal generated from its parent melt; this represents a further advantage of the molten salt electrolytic route. Although all the group IA and IIA metals may be extracted, either directly or indirectly, by means of molten salt electrolysis, the most important and well-known example in this category which well illustrates the principles of electrometallurgical extraction and electrorefining is aluminum; only this metal will, therefore, be considered here.

Some coverage of the Bayer–Hall–Heroult extraction process(99) can be found in most chemistry textbooks; less attention is given to the Hoopes three-layer process(100) for the further electrorefining of aluminum. The Hall–Heroult extraction process could not be supplanted in the short term, because it represents considerable capital investment; however, its energy-intensive nature, requiring remote location, close to hydroelectric power, will ensure continued research and development on alternative processes. A typical modern cell will operate at ~1233 K, ~130,000 A, and ~4.6 V, to produce 340 tonnes of aluminum per year, for a 600-kW power input.(101) This voltage is more than that predicted by elementary thermodynamics, about 0.6 V being dissipated as anodic overvoltage. Thus, specific aims of present research and development efforts in Hall–Heroult technology seek to reduce this overvoltage. The savings in cost, consequent upon voltage reductions, have been estimated at $100,000's per millivolt per annum.

Significant cost savings can be achieved in other ways, too. Automated process control may be used to monitor the alumina content of cells, upon which the onset of the anode effect (see earlier) is critically dependent. The operating temperature may be reduced by the incorporation of other fluoride salts such as LiF, MgF_2, and CaF_2. Furthermore, the replacement of the consumable carbon anodes presently in use by dimensionally stable, permanent anodes of refractory interstitial compounds, such as TiB_2, and conducting ceramics may indirectly contribute to economies. While the application of such materials inevitably results in an increase of cell voltage and greater dissipation of heat, it may lead to increases in current efficiency if deployed in a redesigned sloping configuration, for example, which would permit the continuous drainage of molten aluminum from a smooth, solid cathode; in this way, metal turbulence and backreactions could be minimized.

In spite of these continual improvements to the established technology, the search for alternative production routes for primary aluminum provides a worthwhile goal.(102) The ALCOA scheme(103) for the electrolysis of aluminum chloride seems particularly attractive at the present time, and full-scale trials are being assessed. According to this process, molten NaCl–LiCl–$AlCl_3$ is electrolyzed at 973 K and ~3.3 V. Other chloride salts, together with the $AlCl_3$, have been investigated, and both mono- and bipolar cells have been reported in the patent literature. Apparently the performance of the electrolytic cell is entirely satisfactory. However, the process involves the recycling of the chlorine evolved at the anodes for conversion of the bauxite ore. This is an expensive and apparently difficult stage upon which the ultimate commercial success, or otherwise, of the overall process may depend. Ironically, other proposed conversion routes also initially pass through a chlorination stage to produce $AlCl_3$ and, thus, for this and other reasons, fail to compete.

Several principles are exemplified in the Hoopes aluminum electrorefining process.(100) Accordingly, crude aluminum is comelted to form a dense, lower-layer anode beneath a molten chloride electrolyte. A pure aluminum cathode floats above the melt. Since copper is more noble than aluminum, during electrolysis, the crude aluminum is preferentially dissolved into the molten chloride phase prior to electrodeposition as pure metal in the upper metal layer.

5.2.2. Solid Metals

Apart from the most electropositive metals, most other metals extracted through molten salt routes are recovered as solids; these include many important refractory and other transition metals, the lanthanides, and some actinides. Particularly interesting problems arise in the electrowinning of the refractory metals. Attempts to deposit these metals in a coherent, massive form of theoretical density usually meet with a number of difficulties.(104) Deposits may be dendritic, for example, if electrodeposition proceeds under mass transfer control, or they may be powdery and nonadherent if secondary reactions, such as alkali metal deposition, followed by backreaction with the solute, occurs. Moreover, powdery deposits may also arise if low oxidation states, formed as intermediates during the reduction process, disproportionate in the metal–melt interphase. Charge-transfer-controlled electrodeposition or coupled chemical steps appear to be a prerequisite for obtaining dense, coherent, and adherent deposits.(105,106) Such deposits have been obtained for most the group IVA, VA, and VIA metals in the Union Carbide electroforming process which utilizes an all-fluoride molten electrolyte. Of these nine refractory metals, only chromium may be electrowon from aqueous solution, albeit at low current efficiency.

Unfortunately, the Union Carbide process does not provide satisfactory deposits of titanium, technologically the most important member of this group. This fact, together with other evidence, suggests that the unified mechanism proposed for the process may not be entirely adequate. The original explanation offered for the success of this process focused on the formation of fluorocomplexes in the bulk solution.(107) The essential role of potassium ions was also stressed in this context. However, it now appears that no single explanation is valid for all the metal electroforming reactions, and that surface effects, not previously considered, also need to be taken into account.(108) Furthermore, it follows from the foregoing arguments, that the overall electrode reaction must, in every case, include at least one stage which is not controlled by mass transfer.

An interesting example of the operation of the process is provided by the case of niobium.(109) This metal can be electroformed from molten eutectic LiF–NaF—KF (FLiNaK), mp 727 K, using the bath operated at temperatures between 973 and 1098 K. Niobium pentafluoride is employed as solute at ~10% wt and with current densities between 5 and 125 mA cm^{-2}. The resulting electroform has good mechanical properties; the throwing power of the bath is exceptional, as might be expected. The presence of potassium ions in the melt certainly seems to be necessary in this case. Also anionic impurities such as oxide and chloride ions can lead to unsatisfactory hard and brittle deposits, although the niobium bath can tolerate chloride concentrations up to ~10%; if 100% current efficiency is to be achieved, then at least 90% of the dissolved niobium must be present as Nb^{4+} prior to the electrolysis stage. Otherwise, the niobium metal produced can backreact with the +5 oxidation state:

$$\text{Nb} + 4\text{Nb}^{5+} \rightarrow 5\text{Nb}^{4+} \tag{14}$$

Thus, preliminary reduction of the feedstock NbF_5 is necessary. Oxygen must be rigorously excluded from the electrolysis cell.

Much research and development has been carried out on possible electrowinning routes for these metals; however, except for tantalum,(110) which is used in relatively large quantities for making capacitors, no other process has been operated on a commercial scale. This contrasts sharply with the extraction of liquid metals via molten salt routes, mentioned above. The reasons for this are complex but include innate conservatism and historical factors, as well as more obvious considerations such as capital investment and the high cost of preparing suitable feedstocks. One inherent factor stands out, however, and that is the form of the deposit: if this is dendritic and/or powdery, as frequently happens, then postelectrolytic separation of the metal from entrained melt can be costly, time consuming, and lead to contamination of the product, especially with oxides. Nevertheless, some quantities of mischmetal as well as certain actinides are recovered in this way, in spite of their pyrophoric nature.(111)

A potentially valuable development arising from these earlier investigations is the process of "metalliding".(112) According to this invention, virtually any element in the periodic table can be deposited and simultaneously diffused into the surface of a substrate metal. Fluoride melts are normally employed at temperatures close to the melting point of the metal to be treated. This is essentially a surface finishing process, which may be used to upgrade the performance of relatively cheap bulk materials. In the original article, the boriding and chromiding of steel and the berylliding of copper were shown to markedly improve their hardness and tensile strength, respectively.

5.3. Batteries

Molten salt electrolytes are a natural choice for advanced battery systems.(113–116) Their high conductivity minimizes internal resistance, their electrochemical stability permits the choice of extremely electropositive and electronegative electrode materials, and their elevated operating temperatures ensure high discharge rates since i_0's are quite large. As a result, molten salt batteries are advocated for load-leveling, traction, and thermal reserve applications; some versions of the latter are already in military service.(117,118) Although self-discharge can be serious at these operating temperatures, most of the problems encountered in manufacturing viable units have been concerned with corrosion of the cell components, particularly seals.

The most attractive candidates for electrodes are thus a combination of an alkali metal (possibly an alkaline earth metal) anode with a halogen or chalcogenide cathode. These might well be immersed in a eutectic alkali metal halide melt electrolyte.

The $Li/LiCl/Cl_2$ cell operating just below 973 K has been well studied,(119,120) providing outputs up to 40 W cm^{-2} and an open circuit voltage (o.c.v.) of 3.45. For fast discharge in a primary mode, a specific power of ~1000 kg^{-1} and specific energy of 400 W hr kg^{-1} have been projected. However, severe material problems cloud the future of such units; while the operating temperature may be reduced by employing a eutectic melt, such as LiCl–KCl, or even $NaCl–KCl–AlCl_3$, so also are the exchange current densities significantly diminished.

Considerable effort has been expended recently on the development of a sodium–sulfur cell,(121,122) particularly for traction applications. These units incorporate a solid electrolyte of so-called β-alumina (actually $Na_2O \cdot 11Al_2O_3$), in which the transport number of sodium ions is close to unity. Operating at ~360°C (633 K) power densities of ~0.04 W cm^{-2} with an *initial* o.c.v. of 2.08, have been achieved. A specific power of ~100 W kg^{-1} and a specific energy of 160 W hr kg^{-1} have been reported. The electrochemical reaction at the sulfur–β-alumina interface leads to the formation of complex molten polysulfides, notably Na_2S_5 and Na_2S_3, some of which form immiscible phases; two distinct discharge plateaus are associated with these compounds, and eventually Na_2S_2 may precipitate out. Although field trials of these cells have been promising and include a successful demonstration of an electric van, problems concerned with the mass production of β-alumina, its conductivity and satisfactory seals, still remain.

Emphasis has switched to lithium–sulfur cells at the present time, both for traction(123) and for load-leveling application.(124) Most attention is focussed on $Li\text{-}Al/LiCl\text{-}KCl/FeS_2$ or FeS units, since iron sulfides are good electronic conductors. An FeS-based cell, operating between 673 and 873 K, is favored. Specific energies ~130 W hr kg^{-1} are projected for 10-kW modules, based on the demonstrated performance of single units; an o.c.v. ~1.7 is obtained. Other lithium alloys, including those with silicon, alternative sulfide electrodes such as NiS_2, and electrolyte composition variants are being examined.(125) These batteries are most likely to meet performance goals in the short-to-medium term.

The main thermal reserve battery deployed at present is the Ca/LiCl-KCl/$CaCrO_4$/Fe cell which is pyrotechnically activated to $\sim$873 K. However, problems of side reactions of the calcium electrode and the $CaCrO_4$ limit their operational time to $\ll$1 hr and/or their output current density to $<$15 mA cm^{-2}. Research, particularly by the USAF, is directed to developing replacement units based on the lower melting ($<$473 K) chloroaluminate systems, with an Li–Al anode and various transition metal chloride cathodes, e.g., $FeCl_3$, $CuCl_2$, or $MoCl_5$.(126) With suitable reconfiguration, these designs may also be suitable in primary and secondary roles. Notably, the inclusion of an organic component in the chloroaluminate electrolyte permits a room temperature molten salt to be realized.(127)

5.4. Fuel Cells

Only molten carbonate electrolytes figure in molten salt fuel cell designs.(128) Other melts are not compatible with the use of hydrocarbon fuels, or, indeed, hydrogen and air feeds which have not been scrubbed free from carbon dioxide. Viable molten carbonate devices are based on eutectic mixtures of alkali-metal salts and are operated in the range 923–973 K. The overall electrode reactions are novel:

$$\text{cathode:} \quad O_2 + 2CO_2 + 4e^- \rightarrow 2CO_3^{2-} \tag{15}$$

$$\text{anode:} \quad \text{“}H_2\text{”} + CO_3^{2-} \rightarrow H_2O + CO_2 + 2e^- \tag{16}$$

in that oxide ions are transferred from the oxidizer electrode as the Lux–Flood conjugate base, carbonate:

$$CO_2 + O^{2-} \rightarrow CO_3^{2-} \tag{17}$$

in a mechanism which apparently consumes and regenerates electrolyte anions continuously. The detailed electrode processes are more complicated, but open circuit voltages range from $\sim$1.05–1.1, according to operating conditions and fuel. Importantly, the use of mixed low-grade hydrocarbon gaseous fuels is envisaged,(129) ideally derived, perhaps, from a molten carbonate coal gasification reactor.(130) Sulfur tolerance of the electrodes is a limiting parameter, although recent work has shown that a severely poisoned system can be returned to normal operating performance simply by flushing with “clean” fuel for a period.(131)

Considerable commitment to fuel cell technology has been made in the United States; experience has been gained of well over 13,000-hr operation of stable cells, with 40,000-hr cells underway. A 635-MW coal-fired power plant consisting of 96 cells of 4.7 MW (dc) each is envisaged.(132) Although noble metal electrocatalysts can be avoided in molten salt fuel cells, considerable quantities of nickel are required. Precautions necessary to prevent long-term blocking of the sintered nickel electrodes include the incorporation of silver particles, since no solid solution forms between these two metals.(133) Advantageously, the molten electrolyte is immobilized within a ceramic matrix, the principal candidates being the lithium aluminates.(134) Temperature, composition, and environmental factors can lead to complex phase changes in these materials. Corrosion of metallic cell components remains a problem, especially in the anode wet-seal area, which can lead to gas leaks.(135) In spite of the many predictable difficulties, the prospects for advancement of molten carbonate fuel cells seem to be favorable. Overall efficiencies of ~50% are projected for the fuel-to-power process, if waste heat is recovered, for example, by a steam-bottoming cycle.

5.5. Corrosion

Metals and ceramics come into contact with molten salts, either by design or by accident, in many high-temperature industrial processes, as in oil-fired boilers used for generating electricity, for example. The mechanisms of corrosion at elevated temperatures have received far less attention than those pertaining to aqueous solutions. The important differences between corrosion by molten salts and by aqueous media therefore need to be considered, together with the special features which distinguish the former phenomena.(136,137)

5.5.1. Special Features

Except in aqueous melts, molten bisulfates, and melts exposed to hydrogen atmospheres, the hydrogen ion is of little importance in molten systems, which can generally be regarded as aprotic solvents. Rather, it is the oxide ions which are of central importance in corrosion schemes. This is particularly so in oxyanionic melts, wherein acidity and basicity are best defined according to the Lux–Flood formalization (see earlier). Thus, for example, when a deposit of molten sulfates accumulates on boiler tubes, it arises through the corrosion equilibrium(138,139):

$$\begin{array}{ccccc} SO_3(g) & + & O^{2-} & \rightleftarrows & SO_4^{2-} \\ \text{fuel effluent} & & \text{boiler} & & \text{molten deposit} \\ \text{L–F acid} & & \text{tube} & & \text{L–F conjugate base} \end{array} \qquad (18)$$

in which the function pO^{2-} ($\equiv pH$ in aqueous environments), approximated by $-\log C_{O^{2-}}$, defines the oxide ion activity. The higher the value of the pO^{2-} function of a melt, the more it will corrode a metal in contact with it and vice versa. Although this general rule holds in the case of ceramics, the melt's corrosive effects will also depend on the relative acidity or basicity of the ceramic itself. Furthermore, the concentration of oxide ions influences the corrosive effects of nonoxyanionic melts which have been subject to hydrolysis, by contact with atmospheric moisture. For example,

$$2LiCl + H_2O \rightarrow \uparrow HCl + Li_2O \tag{19}$$

Since molten salts are very reactive, due especially to the appearance of temperature in the exponential part of rate equations, it is unlikely that corrosion will be kinetically inhibited if thermodynamically predicted, as is often encountered in aqueous solutions. Moreover, when assessing corrosion possibilities, the whole system including container materials needs to be considered, since the latter are rarely inert in contact with melts.

Because molten salts are such good solvents for inorganic compounds, opportunities for passivation by surface blocking due to precipitation of insoluble oxides or other salts generally do not arise. Thus, sometimes, predicted regions of passivity for a metal may not be observed in practice.

5.5.2. Cathodic Sinks

In aqueous solutions, the corrosion process may be represented as

$$M^0 \rightarrow M^{n+} + ne^- \tag{20}$$

if solvation is neglected. The conjugate cathodic reaction which provides the electron sink for corrosion to proceed is usually

$$H^+ + e^- \rightarrow 1/2H_2 \tag{21}$$

Clearly, in molten salts, where hydrogen ions are absent, alternative electron sinks operate. These include the following:

(a) *Ions of metals more noble than the corroding metal.* These can occur as impurities in the system, and it should be noted that salts employed in their pure, molten state, i.e., in the absence of an inert solvent, are generally not intended for such application.

(b) *Alkali and alkaline earth metal ions.* This is perhaps unexpected, at least on the basis of the thermodynamics of the pure compounds: cf.

$$Ag + NaCl \rightarrow Na + AgCl \tag{22}$$

(i.e., the corrosion of silver in molten NaCl).

In this case, the reaction proceeds to the right-hand side, because sodium can dissolve in molten sodium chloride and also distill out of the system. The practical consequence of these processes is that the Nernst electrode potential for the alkali or alkaline earth metal–metal ion couple will be shifted in the positive direction as a result of the metal activity being less than unity, its normally defined standard state. Hence, the overlap of the current–electrode potential profiles for the conjugate pair of processes contributing to the overall corrosion reaction becomes more probable, and corrosion occurs.

(c) *Reduction of the anion itself in many oxyanionic melts.* This will occur when the principal element in the oxyanion has a stable, lower oxidation state to which it can be reduced within the range of electrochemical stability of the melt, as in the case of $N^V \rightarrow N^{III}$ in nitrates, cited in the previous section. When this type of reaction occurs, viz.,

$$NO_3^- + 2e^- \rightarrow NO_2^- + O^{2-} \tag{23}$$

oxide ions, in some form, are liberated. While the overlap of current–potential profiles is still a condition under which corrosion occurs, it is evident that such corrosion may be reduced or prevented by increasing the concentration of dissolved oxides in the melts. This is, perhaps, better visualized in terms of a lowering of the concentration of the acid component in the acid–base couple:

$$\begin{array}{c} CO_3^{2-} \rightarrow CO_2 + O^{2-} \\ \qquad\downarrow \\ \qquad CO + O^{2-} \end{array} \tag{24}$$

(d) *Oxygen itself as the cathodic sink.* This may occur via

$$1/2O_2 + 2e^- \rightarrow O^{2-} \tag{25}$$

However, since gases generally have limited solubility in molten salts, corrosion will be restricted to a narrow region in the three-phase boundary.

5.5.3. Corrosion Diagrams

For some years, a plot(140) of E vs. pO^{2-} has served as a molten salt equivalent of the E vs. pH Pourbaix diagrams used to delineate stability characteristics of metals in aqueous solutions. While both these diagrams have drawbacks to their routine application, the frequent absence of kinetic limitations at high temperatures make E vs. pO^{2-} diagrams more realistic in this sense than their Pourbaix counterparts. A typical example is given in Figure 5 of the E vs. pO^{2-} diagram for nickel(137); many metal–molten salt systems have now been treated in this way.(141,142) Some of the difficulties which may be experienced in their application include (i) an inadequate knowledge of many molten salt electrode reactions, particularly those involving oxyanions, making the choice of thermodynamic data from which to construct the diagrams somewhat restricted; (ii) a frequent loss of products from the system by vaporization, etc., rendering predictions based on closed systems at equilibrium invalid; (iii) gross departures from ideality, even for dilute solutions, through complex formation, for example, making diagrams based on pure-component thermodynamic data unrealistic; (iv) a lack of passivity due to oxide solubility in molten salts; and (v) the stable existence of the other oxides, notably O_2^{2-} and O_2^-, in molten salt solutions, leading to errors in the diagrams which relate solely to the O^{2-} species.

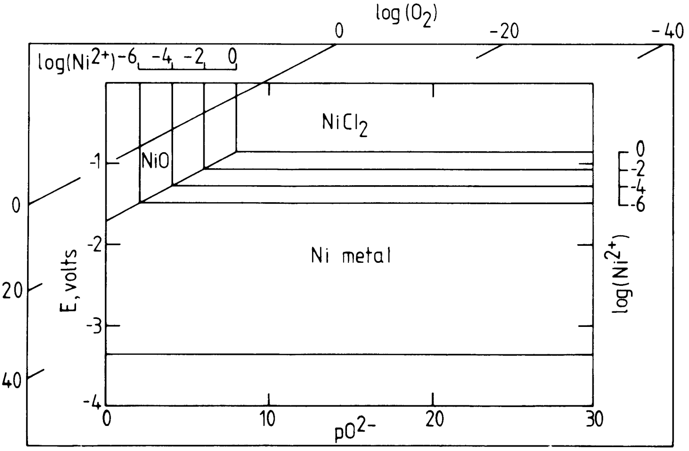

Figure 5. E vs. pO^{2-} diagram for Ni in molten LiCl at 1073 K. (Reproduced from Ref. 137 by kind permission The Metals Society.)

5.6. Anodizing

Although anodizing in aqueous solutions constitutes an important and long-established industrial metal finishing process, the application of molten salts in this field represents a recent innovation. Impetus for the current efforts in these directions comes from the aerospace and electronics industries. Improved dielectric properties, enhanced corrosion resistance and better adhesive bonding have been claimed to result from anodizing in these *apparently* nonaqueous media. Unfortunately, however, many of the studies carried out have been conducted under poorly characterized conditions. This is especially true with respect to melt dryness, which emerges as a crucial parameter in determining the morphology of the grown oxide film.

A majority of studies have been concerned with anodizing aluminum and its alloys,(143–148) although tantalum,(149,150) titanium,(151,152) zirconium,(153) and other transition and coinage metals have been of interest. The Italian school under Conte has been particularly active in these investigations which have mainly centered on nitrate melts, over the temperature interval 343–723 K. A bisulfate mixture is used in a Japanese commercial process.(154) Table 4 shows some of the melt systems that have been studied.

Thick white and thin transparent oxide films can be grown anodically on aluminum and its alloys in nitrate melts at the lower temperatures. Claims that the films contain α-, γ-, η-, and hydrated alumina have variously been made, but the techniques used to characterize these (e.g., eddy current, weight loss, double replication) have not always been entirely suitable. Films may be formed both at constant voltage or under constant current conditions. The latter seems less desirable, since morphological changes may occur as the voltage rises; the application of reverse cathodic current pulses(147) is positively

Table 4
Melts and Conditions Used in Molten Salt Anodizing

Melt	Melting point, °C	Range studied, °C	Metals anodized	References
$NaHSO_4$-$KHSO_4$	~125	130-180	Al	154, 160
NH_4HSO_4		184-207	Al	154, 160
$NaHSO_4$		178-207	Al	154, 160
$Ca(NO_3)_2 \cdot 4H_2O$	42.7	50-100	Al, Zr	145, 153
$NaNO_3$-KNO_3	220	250-300	Al, Ti, Zr	145, 157, 152, 153
$LiNO_3$-KNO_3	133.5	140-260	Al, alloys	144, 161, 148, 155, 156, 159
$LiNO_3$-NH_4NO_3	~98	110-140	Al	156, 159
$NaNO_3$-NH_4NO_3	121	140	Al	156, 159
$LiNO_3$-KNO_2	108	110-120	Al, alloys	147
$NaNO_2$-KNO_2		227-352	Al	162
$NaNO_3$-$Ca(NO_3)_2$		300-370	Ti	151
KNO_3	337	400-450	Al, Ti	145, 146
$NaNO_3$-$NaNO_2$-KNO_3	142	150-200	Zr	153
$LiNO_3$-$NaNO_3$-KNO_3	125	217-340	Al, Ta	158, 149, 150
$NaNO_2$	271	315	Ti	218,
$NaNO_3$-$NaNO_2$	146	315	Ti	219
NH_4NO_3-$CO(NH_2)_2$	43.5	45-80	Al, Ti	161
$NaNO_3$	310	330-390	Ti	220
$RbNO_3$	316	350-390	Ti	220

dangerous, since alkali metal deposition and nitrate reduction can occur explosively.

The criteria of dryness of the molten salt, coupled with anodizing voltage, has been shown to influence significantly the morphology of oxide films grown on pure aluminum, according to a recent fundamental investigation.(155)

Surprisingly, previous workers had employed elaborate purification and drying operations in preparing their melts, only to expose them to the atmosphere during anodizing! Under totally anhydrous conditions, thin, transparent, amorphous oxide films are formed at all voltages. When water is present, however, thick, white, poorly compacted crystalline films containing α-Al_2O_3 and $Al_2O_3 \cdot H_2O$ are formed between ~10–50 V, while thin, flawed films grow at higher and lower voltages. Only in $LiNO_3$–NH_4NO_3 melts at 383 K (not 413 K) are thick, white, flaw-free, coherent oxide layers formed, at >50 V, in the presence of water.(156) The presence of water in the molten salt may also affect the structure of oxide films grown anodically onto titanium.

There appear to be some inconsistencies in the assignment of the growth mechanism of the oxide film in melts for aluminum(157,158) and tantalum(149,150) owing to an apparent *negative* temperature coefficient of the Tafel slopes. Also, the apparently improved stress corrosion cracking (s.c.c.) resistance for melt-anodized aluminum alloy specimens may not be due to the nature of the oxide film, as claimed,(147,148) but to recrystallization in the surface layers of the alloy itself.(156,159) While molten-salt-anodized films seem to be quite unique, a considerable amount of further work is required if they are to become a widespread commercial reality.

6. Experimental Procedures

6.1. Materials, Electrodes, and Operating Conditions

Unfortunately, considerable molten salt expertise lies hidden in generations of higher-degree theses, and it will be the specific aim of a forthcoming series of texts to expose this knowledge in a coherent form.(163) Nevertheless, well-defined areas of essential expertise can readily be identified for molten salt electrochemical studies. These include preliminary preparation, purification, and properties of the melt itself, aspects of melt handling, including materials choice, cell design, and selection of electrodes. While some of the operating procedures and parameters will obviously be determined by the specific type of melt, especially relating to the temperature range and materials used, some common features of molten salt investigations are evident. Water, for example, is the most ubiquitous contaminant in most melt systems;(164) it gives rise to particular problems in hygroscopic melts containing lithium and magnesium salts, for example. The removal of it, and its hydrolytic products, represents the most crucial and necessary stage in purification procedures.(165) In low concentrations, this may largely be achieved by long-term drying over P_2O_5, followed by pumping, but at higher concentrations and high temperatures more elaborate techniques may be required. Preelectrolysis between inert electrodes is another commonly employed pretreatment; however, while heavy metals can be removed by this means, caution is needed to avoid undesirable side reactions of other impurities, especially anionic ones.(166) Zone refining might be the purification method of choice, were it not for problems of scale, time, and expense.

In general, materials selection will be determined mainly by the operating temperature and the aggressiveness of the melt. Of course, at the highest temperatures, most ceramic materials become conducting and, thus, susceptible to corrosion: noble metals or vitreous carbon in inert atmospheres may then be required. Above about 1273 K, experimental limitations are quite considerable. Creep, materials porosity, and intercalation, solvent and solute volatility, solute disproportionation and reaction can all add to the experimental difficulties encountered with molten salts. The use of well-dried and deoxygenated inert atmospheres is a general requirement, not only to limit oxidation but to prevent the generation of the several soluble and electroactive oxide species stable in melt systems.(167) For the lowest melting salts and mixtures, a wide range of heating equipment is available, including liquid (silicone oil, paraffin oil, and nitrate–nitrite melts) thermostats, air or organic vapor ovens, metal block furnaces, and resistance-heated furnaces. At higher temperatures (>773 K) only the latter are practicable. Outer containment envelopes can be made from borosilicate glass, silica, or a refractory according to temperature, while simple flange or cone-and-socket cell heads need to be changed to water-cooled metal designs above ~523 K. Thus, the electrical layout of cells for fast-pulse and high-frequency measurements encounters severe design limitations, which generally increase with increasing temperature.(163,168,192)

The dropping mercury electrode has been successfully applied up to ~500 K and the hdme to 523 K.(169) Conceivably, mercury film electrodes might extend that range by a little, but the vapor pressure of mercury presents serious stability, as well as toxicological, problems at higher temperatures. Dropping bismuth(170) and silver electrodes [up to 1273 K (171)] have achieved success in the hands of a few skilled operators, while liquid lead hanging drops have been extensively used in interphasial studies in molten halides (see Section 3). However, as explained earlier, studies at solid, mainly noble, electrodes such as platinum, gold, but also tungsten and molybdenum, have often been preferred in molten salt studies, in spite of the inherent difficulties associated with their use. Most recently, vitreous carbon electrodes have been employed in nonoxidizing melts.(172) The choice of counterelectrode poses no special problems; both liquid metal pools and large masses of inert metals (Pt, Au, and vitreous C) have been employed. The choice and design of reference electrodes, however, is rather more restricted. Reference potentials are often a good deal less stable and reproducible than those encountered in aqueous solutions,(163) and this has variously been ascribed to metal recrystallization,(173) membrane exchange reactions,(174) and envelope instability(175) among other phenomena aggravated by elevated operating temperatures. Most universally used has been the Ag/Ag^I half-cell made up in the same melt as that in the main cell compartment;(176) Osteryoung(177) has even recommended this unit for chloroaluminate melts rather than the more popular aluminum wire.(178) Nevertheless, the Pt/Pt^{2+} couple has provided a suitable secondary standard in halide melts,(179) whereas the Ni/Ni^{II} has been adopted for fluoride systems,(180) and the Cu/Cu^I for hydroxide systems.(181) Generally, the membrane material has been soda or borosilicate glass, asbestos fibers, or sintered glass disks in lower melting nitrates and halides. While an asbestos plug in an insulating ceramic, such as boron nitride, remains viable at high temperatures, free-diffusion capillary junctions have also been used. Provided the ion in the reference compartment is relatively large and at low concentration, and the interdiffusion between half-cells sufficiently impeded, then liquid junction potentials can be very small. In fluoride melts, a lanthanum trifluoride membrane is used.(180)

The problem of introducing solutes into melts may not always be inconsiderable. A number of entry-port systems have been described,(182) but the most elegant solution to the problem for fundamental studies may be anodic dissolution. Otherwise, the availability or ease of preparation of adequately anhydrous material can present serious difficulties.(183)

Once the principles of operating in a molten salt environment have been grasped, suitable extrapolations or interpolations of materials requirements and cell and equipment designs can be made between different systems. In bringing a molten salt process into commercial operation, unique materials problems requiring special solutions often limit its progress, but practically never prevent it. Thus, if a desired result may not be achieved for theoretical reasons in any alternative electrolyte, because of electrochemical instability, for example, then initial development costs and difficulties become inconsequential. Such has been the case with thermal batteries,(184) sodium–sulfur batteries,(185) molten fluoride nuclear reactors,(186) and molten carbonate fuel cells.(187) In view of the above contention and partly because they have provided most of the accumulated molten salt expertise, only nitrate and some halide melt systems will be given detailed consideration in this chapter (see below).

6.2. Nitrates

Apart from the applications mentioned previously, these media, which constitute one of the most studied groups of molten salts, are now being used in the heat-treatment, heat-storage, and pyrolysis areas. The use of the eutectic mixtures $LiNO_3$–59 mol % KNO_3, mp 406.5 K, and $NaNO_3$–50 mol % KNO_3, mp 490 K, enables the operating temperature to be minimized, thermal dissociation to be limited, and materials constraints to be eased. Supplies of good-quality anhydrous $LiNO_3$ are limited to only a few suppliers and, although the purification and drying of alternative hydrated material represents a major undertaking, some workers have attempted this. Firstly, the chloride and sulfate levels need to be reduced to micromolar quantities by repeated recrystallization as $LiNO_3 \cdot 1/2H_2O$ from hot solution; the efficiency is low. Limited preelectrolysis may be applied with caution, and peroxides can be discharged with dry silica powder (to what?). Further purification is then limited to the standard procedures of prolonged drying in the solid state, gradual fusion under vacuum, followed by filtration. Purging the melt with oxygen or nitrogen dioxide (claimed to oxidize nitrite)(188,189) is probably best avoided, since this procedure can lead to new impurities(190):

$$O_2 + H_2O + 4e^- \rightleftarrows 4OH^-, \qquad E_{1/2} = -0.49\text{V vs. Ag/Ag}^{\text{I}}\ (0.07\ m) \tag{26}$$

$$O_2 + O_2^{2-} \rightleftarrows 2O_2^-, \qquad k^{503\,\text{K}} = 2.0 \times 10^6 \tag{27}$$

$$2NO_2 + H_2O \rightleftarrows NO_3^- + NO_2^- + 2H^+ \tag{28}$$

Nitrite is particularly difficult to remove and is best avoided by using pure starting materials as well as limiting its production by working at low temperatures for short times, over restricted potential ranges (*vide infra*).

The assessment of melt purity can be carried out spectroscopically, or better, voltammetrically.(191) Notably, the appearance of the cathodic "water wave" in wet nitrate melts has given rise to considerable controversy and confusion. It does *not* represent the direct reduction of water, but is due to its coreduction with another species. According to Lovering *et al.*,(192) the other species is not nitrate,(193) but nitrite ions, which take part in an autocatalytic process:

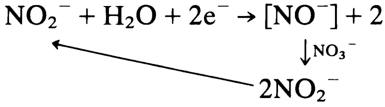

$$\begin{tikzcd} NO_2^- + H_2O + 2e^- \arrow[r] & {[NO^-] + 2OH^-} \arrow[d, "NO_3^-"] \\ & 2NO_2^- \arrow[ul] \end{tikzcd} \qquad (29)$$

Since nitrite ions are produced *cathodically* during the reduction of nitrate ions and by thermal dissociative mechanisms, the greatest of caution is required in both the electrochemical *and* thermal treatments of these melts—matters which hitherto have received insufficient attention by a majority of workers.

A further area of controversy surrounded the operation of oxygen electrodes in nitrate melts, for many years. Claims that the mechanism proceeds by one-(194) and two-electron(195) steps were recorded. Kerridge(196) resolved the issue by pointing out that apparent two-electron slopes were only obtained by workers utilizing glass vessels, and that they were monitoring the potential of the oxygen–silicate reduction:

$$x SiO_2 + 1/2 O_2 + 2e^- \rightleftarrows (SiO_2)_x \cdot O^{2-} \qquad (30)$$

On the other hand, a one-electron process can be observed when the melt is contained in a noble metal or Teflon cell:

$$O_2 + e^- \rightleftarrows O_2^-, \qquad E_{1/2} = -0.64\,V \text{ vs. } Ag/Ag^I\,(0.07\,m) \qquad (31)$$

In the presence of water, a four-electron process prevails, as given above. In view of all these complications, the superficial attraction of working with low-melting nitrates loses some of its appeal. Moreover, work previously reported in these media may need careful reassessment.

6.3. Halides

Molten chlorides have also been widely studied, especially the low-melting eutectic LiCl–41.5 mol % KCl, mp 628 K, and the very low-melting chloroaluminates. The latter, which can be handled in standard apparatus under an inert atmosphere, are purified by first subliming the $AlCl_3$ component. The melt may then be treated either with pure aluminum powder or by preelectrolysis at ~1.5 mA cm^{-2}, followed by filtration; the resulting melt should be colorless.(197) Water contamination does not seem to present problems, because instantaneous precipitation of solid alumina occurs. Much interest stems from the ability to vary their ionicity, and hence Lewis acidity, according to the position of the equilibria(198):

$$2AlCl_3 + 2Cl^- \rightleftharpoons 2AlCl_4^- \rightleftharpoons Al_2Cl_7^- + Cl^- \tag{32}$$

The formation of oxychlorides can affect the electrochemical, as well as solution behavior(199):

$$AlCl_4^- + O^{2-} \rightleftharpoons AlO^+Cl_x^- + (4-x)Cl^- \tag{33}$$

For the preparation of the LiCl–KCl eutectic, reasonable purity anhydrous LiCl is readily available, although in the United States, the fully purified eutectic can be obtained. Otherwise, treatment with dry HCl followed by dry Cl_2 prior to preelectrolysis at 2.7 V, and, finally, filtration, is recommended.(200) Similar procedures, with suitable modifications to the gas purges and electrolysis voltages, may be adopted for $MgCl_2$–KCl, NaCl–KCl, $CaCl_2$–KCl, $ZnCl_2$–KCl, and for the bromides and iodides. Advantageously, vitreous carbon crucibles can be used for halide melts; they are reusable and can form the counterelectrode. Purity of these systems may again be assessed voltammetrically. Surprisingly,(201) water is reversibly soluble at low partial pressures, but hydrolysis occurs at $\gtrsim 18$ mm:

$$H_2O + 2Cl^- \rightarrow 2HCl + O^{2-} \tag{34}$$

The eutectic mixture LiF–11.5 mol % NaF–42 mol % KF, mp 727 K, has received considerable attention. Although the constituents are available in very pure grades, further purification, especially to remove water and oxides, is desirable.(202) The main hydrolytic reaction product, HF, is particularly undesirable(203):

$$H_2O + F^- \rightarrow OH^- + HF \tag{35}$$

$$H_2O + 2F^- \rightarrow O^{2-} + 2HF \tag{36}$$

Purification may be effected either with an H_2/HF gas purge, or by comelting under vacuum with NH_4HF_2.(204) Preelectrolysis at ~3 V is recommended.(205) Fluoride melts are excellent scavenging fluxes for oxides, so the rigorous exclusion of oxygen and water from experimental cells is called for. Given this precaution, they may then be safely handled in pure or cast iron, nickel, nickel- or molybdenum-based alloy, or vitreous carbon containers, preferably with an outer vessel as a safety measure. Care is needed to limit cathodic potential excursions if alkali metal reduction is to be avoided, since these may alloy or react with other cell components. Although slowly penetrated by the melt,(206) boron nitride has been employed as an electrode-insulating sheath. The handling and pretreatment of the eutectic melts LiF–34 mol % BeF_2, mp 727 K, and LiF–29.4 mol % BeF_2–5 mol % ZrF_4, mp 707 K, which have been used in the Oak Ridge Molten Salt Reactor Experiment, follow similar lines as for other fluorides.(207)

Cryolite melts (Na_3AlF_6, mp 1273 K), which are of considerable importance in aluminum refining studies, need to be purified from refractory oxides (silica, alumina, etc.) and iron, among others. Preelectrolysis at 1.6 V using a molten silver cathode in a graphite or molybdenum crucible is recommended.(208,209)

6.4. Other Salts

Among the remaining melt systems, those of special technological or academic interest at the present time are shown in Table 5. To this list must be added melt types of lesser immediate importance, but certainly possessing interesting possibilities, such as carbides, alkanoates, sulfides, thiocyanates, and aqueous (or hydrate) melts. The latter are quite different from the others and generally melt at very low temperatures,(210) e.g., $CaCl_2{\cdot}6H_2O$, mp 302.88 K. These systems present special problems and need to be handled under precisely controlled water vapor pressures in order to maintain constant composition. They hold promise as heat collection and storage media, and as catalysts.

Rather less detailed information concerning the purification of these additional melts exists. Routinely, salts are recrystallized from aqueous solutions and dried over P_2O_5 for prolonged periods. When one component is normally recovered as a hydrate, e.g., $Li_2SO_4{\cdot}H_2O$, the fate of that water of crystallization in succeeding processing is frequently ignored. Otherwise, the procedures outlined above may variously be adopted, e.g., gas purges, preelectrolysis, and filtration.

In some cases, great care is needed to avoid undesirable side reactions, including thermal dissociation. For example, in sulfate melts, for which alumina(211) crucibles may be used, the SO_3 partial pressure needs to be controlled in order to fix the position of the equilibrium(212):

$$SO_4^{2-} \rightleftarrows SO_3 + O^{2-} \tag{37}$$

which itself can give rise to pyrosulfate species:

$$SO_4^{2-} + SO_3 \rightleftarrows S_2O_7^{2-} \tag{38}$$

and, unless the supernatant atmosphere is perfectly dry, then

$$SO_4^{2-} + SO_3 + H_2O \rightleftarrows 2HSO_4^- \tag{39}$$

tends to occur.

In hydroxide melts, which are generally contained in Teflon ware, the greatest of care is needed to avoid thermal dissociation,(213) according to

$$2OH^- \rightleftarrows H_2O + O^{2-} \tag{40}$$

since the water generated is reversibly reduced(213,214):

$$2H_2O + 2e^- \rightleftarrows H_2 + 2OH^-, \qquad E_{1/2} = -0.815\text{V vs. Cu/Cu}^{\text{I}}\ (1\ m) \tag{41}$$

although the addition of oxide can be utilized to aid the removal of impurity water levels. Gas streams clearly need to be rigorously freed from CO_2 if carbonate buildup is to be prevented.

Acetate melts, contrary to early reports, have now been shown to be very stable, even up to 773 K. However, this stability can only be achieved when the salts are extensively dried and when the supernatant atmosphere is devoid of oxygen.(215,216)

The composition of polymeric melts such as the silicates needs to be very closely controlled; quite minor variations in, for example, the sodium content can modify their physical properties, such as viscosity, which, in turn, can affect the transport rate of dissolved ions.

Molten thiocyanates tend to form colloidal sulfur (blue coloration) if overheated, and this can have deleterious effects on the performance of any electrode! The avoidance of hydrolytic reactions in molten sulfides, cyanides, and carbides would seem to be mandatory, even from an elementary school chemistry standpoint(217)!

Many mixed-anion melt systems are emerging, as well as those containing organic components, which can reduce the melting temperature considerably. If one key feature of molten salt techniques and technology is selected for a concluding reiteration, it must be that each melt type needs to be *separately* considered as an individual and unique system, since the common features between different types of systems are often only discernible as fine detail by the experienced eye.

Finally, in spite of the extra energy requirements for operating at elevated temperatures, it seems probable that the attractions of fast, clean processes will ensure a continued expansion in molten salt electrochemistry.

Table 5
Types of Molten Salt Mixtures and Their Applications

Anion type	Popular eutectic mix, mol % compositions	Melting point, °C	Applications/interest
Carbonates	Li_2CO_3–Na_2CO_3–K_2CO_3 43.5 : 31.5 : 25	397	Fuel cell, coal gasification
Sulfates	Li_2SO_4–Na_2SO_4–K_2SO_4 78 : 13.5 : 8.5	512	Corrosion studies
Hydroxides	NaOH–KOH 49.4 : 50.6	170	Fuel conversion
Oxides	PbO–B_2O_3 66 : 34	497	Glasses
Silicates Phosphates Borates	Various compositions	Generally >700°C	Glasses, fluxes, lubricants

References

1. A. D. Graves, G. J. Hills, and D. Inman, in *Advances in Electrochemistry and Electrochemical Engineering*, Vol. 4, P. Delahay and C. W. Tobias, eds., Wiley Interscience, New York (1966).
2. G. J. Janz, *Molten Salt Handbook*, Academic Press, New York (1967).
3. J. Braunstein, *Inorg. Chim. Acta. Rev.* **2**, 19 (1968).
4. *Encyclopaedia of Electrochemistry*, Ç. A. Hampel, ed., Reinhold, New York (1964), and *Characterization of Solutes in Non-Aqueous Solvents*, G. Mamantov, ed., Plenum Press, New York (1978).
5. *The Chemistry of Non-Aqueous Solvents*, Vol. I, J. J. Lagowski, ed., Academic Press, New York (1966); *Non-Aqueous Solvent Systems*, T. C. Waddington, ed., Academic Press, New York (1965); *Inorganic Chemistry in Non-Aqueous Solvents*, A. K. Holliday and A. G. Massey, eds., Commonwealth and International Library, Pergamon, New York (1965).
6. J. Lumsden, *Thermodynamics of Molten Salt Mixtures*, Academic Press, New York (1966).
7. *Phase Diagrams for Ceramists*, E. M. Levin, C. R. Robbins, and H. F. McMurdy, eds., American Ceramics Society, Columbus, Ohio (1964), (1965), (1975).
8. L. V. Woodcock and K. Singer, *Trans. Farad. Soc.* **67**, 12 (1971); F. H. Stillinger, Jr., in *Molten Salt Chemistry*, M. Blander, ed., Wiley Interscience, New York (1964).
9. See, for example, (a) C. A. Angell and C. T. Moynihan, (b) J. Jordan, W. B. McCarthy, and P. G. Zambonin, in *Molten Salts: Characterization and Analysis*, G. Mamantov, ed., Marcel Dekker, New York (1969).
10. H. Bloom and J. O'M. Bockris, in *Fused Salts*, B. Sundheim, ed., McGraw-Hill, New York (1964); F. D. Richardson, *Physical Chemistry of Melts in Metallurgy*, Vols. 1 and 2, Academic Press, New York (1974).
11. L. Grantham and S. J. Yosim, *J. Phys. Chem.* **67**, 2506 (1963); *J. Chem. Phys.* **45**, 1192 (1966); B. Cleaver and S. I. Smedley, *Trans. Faraday Soc.* **67**, 1115 (1971); B. Cleaver, in *Advances in Molten Salt Chemistry*, Vol. 4, G. Mamantov and J. Braunstein, eds., Plenum Press, New York (1980).
12. D. G. Lovering, thesis, City University (1969).
13. G. Charlot and B. Tremillon, *Chemical Reactions in Solvents and Melts*, transl. P. J. J. Harvey, Pergamon Press, Braunschweig (1969); G. Mamantov and R. A. Osteryoung, in *Characterization of Solutes in Non-Aqueous Solvents*, G. Mamantov, ed., Plenum Press, New York (1978).
14. H. A. Levy and M. D. Danford, in *Molten Salt Chemistry*, M. Blander, ed., Wiley Interscience, New York (1964); F. G. Edwards, R. A. Howe, J. E. Enderby, and D. I. Page, *J. Phys. C* **8**, 3483 (1975).
15. M. A. Bredig, in *Molten Salts: Characterization and Analysis*, G. Mamantov, ed., Marcel Dekker, New York (1969), but see also discussion by D. Inman, A. D. Graves, and R. S. Sethi, in *Specialist Periodical Reports—Electrochemistry*, Vol. I, The Chemical Society, London (1970), p. 187; Y.-T. Hsu, R. B. Escue, and T. H. Tidwell, Jr., *J. Electroanal. Chem.* **15**, 245 (1967).
16. J. Michielsen, P. Woerlee, F. v. d. Graff, and J. A. A. Ketelaar, *J. Chem. Soc. Faraday Trans. 2,* **71**, 1730 (1975).
17. J. K. Wilmshurst, *J. Chem. Phys.* **39**, 1779 (1963).
18. H. Lux, *Z. Elektrochem.* **45**, 303 (1939) *et seq.*; H. Flood and T. Førland, *Acta Chem. Scand.* **1**, 592 (1947).
19. R. Littlewood, *J. Electrochem. Soc.* **109**, 525 (1962); D. Inman and N. S. Wrench, *Brit. Corr. J.* **1**, 246 (1966).
20. J. A. Plambeck, in *Encyclopaedia of Electrochemistry of the Elements*, Vol. X, A. J. Bard, ed., Marcel Dekker, New York (1976).

21. K. E. Johnson and P. Fullman, Abstract 358, in Extended Abstracts, Vol. 78-2, Fall Meeting, The Electrochemical Society, Princeton, New Jersey (1978), p. 966.
22. A. F. Alabyshev, M. F. Lantratov, and A. G. Morachevskii, *Reference Electrodes for Fused Salts*, transl. A. Pieperl, Sigma Press, Washington D.C. (1965).
23. J. D. Corbett, in *Fused Salts*, B. R. Sundheim, ed., McGraw-Hill, New York (1964); M. A. Bredig, in *Molten Salt Chemistry*, M. Blander, ed., Wiley Interscience, New York (1964).
24. G. A. Wolstenholme, in *Molten Salt Technology*, D. G. Lovering, ed., Plenum, N.Y., (1982); also see Ref. 27 and K. Grojotheim, C. Krohn, and H. Øye, in *Trends in Electrochemistry*, J. O'M. Bockris, D. A. J. Rand, and B. J. Welch, eds., Plenum Press, New York (1977).
25. K. W. Fung and G. Mamantov, in *Advances in Molten Salt Chemistry*, Vol. 2, J. Braunstein, G. Mamantov, and G. P. Smith, eds., Plenum Press, New York (1972).
26. D. Inman, *New Scientist* **25**, 220 (1965).
27. N. E. Richards, in *Electrochemistry—The Past Thirty and the Next Thirty Years*, H. Bloom and F. Gutmann, eds., Plenum Press, New York (1977).
28. M. Paunovic, *J. Electroanal. Chem.* **14**, 447 (1967); R. K. Jain, H. C. Gaur, and B. J. Welch, *J. Electroanal. Chem.* **79**, 211 (1977).
29. See, for example, W. K. Behl and H. C. Gaur, *J. Electroanal. Chem.* **32**, 293 (1971).
30. G. J. Hills, D. J. Schiffrin, and J. Thompson, *J. Electrochem. Soc.* **120**, 157 (1973).
32. A. Kisza and U. Twardoch, *Bull. Acad. Polon. Sci.* **20**, 1063 (1972).
33. P. H. Davies, E. J. Frazer, M. Skyllas, and B. J. Welch, in *Trends in Electrochemistry*, J. O'M. Bockris, D. A. J. Rand, and B. J. Welch., eds., Plenum Press, New York (1977).
34. D. Inman, Dj. Jovanovic, and S. H. White, *J. Electroanal. Chem.* **43**, 37 (1973).
35. D. G. Lovering, *Collect. Czech. Chem. Commun.* **38**, 1719 (1973).
36. J. O'M. Bockris, S. R. Richards, and L. Nanis, *J. Phys. Chem.* **69**, 1627 (1965).
37. S. Forcheri and V. Wagner, *Z. Naturforsch.* **22a**, 1171 (1967).
38. D. G. Lovering and R. M. Oblath, *J. Electrochem. Soc.*, **127**, 1997 (1980).
39. J. H. Christie and R. A. Osteryoung, *J. Am. Chem. Soc.* **82**, 1841 (1960).
40. H. A. Laitinen and H. C. Gaur, *J. Electrochem. Soc.* **104**, 730 (1957).
41. R. Narayan, D. G. Lovering, and D. Inman, *Chem. Commun.* **386** (1966).
42. D. Inman, R. S. Sethi, and R. Spencer, *J. Electroanal. Chem.* **29**, 137 (1971).
43. D. G. Lovering, *Trans. Faraday Soc.* **67**, 2659 (1971).
44. E. Temmerman and R. A. Osteryoung, *J. Electroanal. Chem.* **64**, 1 (1975).
45. D. Inman and D. G. Lovering, *J. Electrochem. Soc.* **121**, 778 (1974).
46. D. Inman and R. Spencer, in *Advances in Extractive Metallurgy and Refining*, I.M.M., London (1974).
47. G. F. Warren, S. H. White, and D. Inman, in *International Symposium on Molten Salts*, J. P. Pemsler, J. Braunstein, K. Nobe, D. R. Morris, and N. E. Richards, eds., The Electrochemical Society, Princeton, New Jersey (1976).
48. V. Sh. Palanker, A. M. Skundin, and V. S. Bagotskii, *Sov. Electrochem.* **2**, 592 (1966).
49. E. A. Ukshe, N. G. Bukun, D. I. Leikis, and A. N. Frumkin, *Electrochim. Acta* **9**, 431 (1964).
50. N. G. Bukun and E. A. Ukshe, *Russ. J. Phys. Chem.* **37**, 750 (1963); S. Karpachev and A. Stromberg, *Zh. Fiz. Khim.* **18**, 47 (1944); V. A. Kuznetsov, T. D. Dyakova, and V. D. Mal'tseva, *Russ. J. Phys. Chem.* **33**, 48 (1959).
51. E. W. Dewing and P. Desclaux, in *Molten Salt Electrolysis in Metal Production*, I.M.M., London (1977).
52. S. Karpachev and W. Patzug, *Zh. Fiz. Khim.* **13**, 1831 (1939).
53. J. E. B. Randles and W. White, *Z. Elektrochem.* **59**, 666 (1955).
54. G. J. Hills and P. D. Power, *Trans. Faraday Soc.* **64**, 1629 (1968).
55. P. Fellner and K. Matiasovsky, *Chem. Zvesti* **26**, 36 (1972).
56. O. A. Esin, *Zh. Fiz. Khim.* **30**, 3 (1956).
57. R. R. Dogonzdze and Yu. A. Chizmadev, *Proc. Acad. Sci. SSSR Phys. Chem. Sect. (Engl.)* **157**, 778 (1964).

58. A. I. Sotnikov and O. A. Esin, in *Physical Chemistry and Electrochemistry of Molten Salts and Slags*, Proceedings 3rd All-Soviet Conference, May 1966, Khimiya, Leningrad (1968).
59. N. G. Bukun and E. A. Ukshe, Ibid.
60. A. D. Graves and D. Inman, in *E.m.f. Measurements in High Temperature Systems*, C. B. Alcock, ed., I.M.M., London (1968).
61. R. Yu. Bek and A. S. Lifshits, *Siber. Chem. J.* **6**, 713 (1967).
62. A. D. Graves and D. Inman, *J. Electroanal. Chem.* **25**, 357 (1970).
63. R. H. Heus, T. Tidwell, and J. J. Egan, in *Molten Salts: Characterization and Analysis*, G. Mamantov, ed., Marcel Dekker, New York (1969).
64. P. Fellner and K. Matiasovsky, *Electrochim. Acta.* **17**, 233 (1972).
65. D. Inman, J. E. Bowling, D. G. Lovering, and S. H. White, in *Specialist Periodical Reports—Electrochemistry*, Vol. 4, Chemical Society, London (1974).
66. D. M. Heyes, M. Barber, and J. H. R. Clarke, Abstract No. 365, in Second International Symposium on Molten Salts, Extended Abstracts 78-2, from 154th Meeting, Electrochemical Society, Pittsburgh, October 15–20 (1978), p. 980.
67. E. H. Amstein and W. D. Davis, *Molten Salt Electrolysis in Metal Production*, I.M.M., London (1977), p. 62.
68. D. Inman, *Chem. Eng.* (*London*) **51** (1967).
69. D. Inman, J. C. L. Legey, and R. Spencer, *J. Electroanal. Chem.* **61**, 289 (1975).
70. D. Inman and S. H. White, *J. Appl. Electrochem.* **8**, 375 (1978).
71. F. Lantelme, J. P. Hanselin, and M. Chemla, *J. Electroanal. Chem.* **97**, 49 (1979).
72. H. C. Gaur and R. S. Sethi, *J. Electroanal. Chem.* **7**, 474 (1974).
73. R. M. de Froment *et al.*, in *Polarography 1964*, G. J. Hills, ed., Macmillan, London (1966).
74. For example, see J. J. Egan and R. Heus, *J. Electrochem. Soc.* **107**, 824 (1960).
75. D. Inman and J. O'M. Bockris, *J. Electroanal. Chem.* **3**, 126 (1962).
76. E. A. Ukshe and N. G. Bukun, *Russ. J. Phys. Chem.* **35**, 1330 (1961).
77. B. A. Parkinson and F. C. Anson, *Anal. Chem.* **50**, 1886 (1978), but see also H. B. Harvey, R. L. McNeey, P. Surana, C. M. Ellion, and R. W. Murray, *Anal. Chem.* **46**, 1258 (1974).
78. D. Inman, J. O'M. Bockris, and E. Blomgren, *J. Electroanal. Chem.* **2**, 506 (1961).
79. L. G. Boxall and K. E. Johnson, *Trans. Faraday Soc.* **67**, 1433 (1971).
80. S. Sterberg and C. Herdlicka, *Rev. Roum. Chim.* **17**, 343 (1972).
81. D. Inman, S. H. White, I. Wilmot, and B. Jones, *J. Electroanal. Chem.* **33**, 225 (1971).
82. G. J. Hills, D. J. Schiffrin, and J. Thompson, *Electrochim. Acta* **19**, 657 (1974).
83. J. C. L. Legey, thesis, London (1973).
84. H. C. Gaur, H. L. Jindal, and R. S. Sethi, *Electrochim. Acta.* **15**, 845 (1970); H. C. Gaur and H. C. Jindal, *J. Electraoanal. Chem.* **23**, 289 (1969).
85. D. Inman, R. S. Sethi, and R. Spencer, *J. Electroanal. Chem.* **29**, 137 (1971).
86. P. G. Dudley, D. Inman, and S. H. White, in Extended Abstracts, 78-2, The Electrochemical Society, Princeton, New Jersey (1978).
87. G. J. Mills and K. E. Johnson, in *Advances in Polarography*, Vol. 3, I. Longmuir, ed., Pergamon Press, Oxford (1960).
88. F. R. Duke and M. L. Iverson, *Anal. Chem.* **31**, 1233 (1959).
89. For a lucid discussion, see J. Jordan, *J. Electroanal. Chem.* **29**, 127 (1971), but also see A. F. J. Goeting and J. A. A. Ketalaar, *Electrochim. Acta* **19**, 267 (1974) and J. D. Burke and D. H. Kerridge, *J. Electrochim. Acta* **19**, 251 (1974).
90. G. J. Hills and K. E. Johnson, *J. Electrochem. Soc.* **108**, 1013 (1961).
91. Yu. K. Delimarskii, V. I. Sherpoval, and V. A. Vasilenko, *Sov. Electrochem.* **7**, 1255 (1971).
92. E. Franks and D. Inman, *J. Electroanal. Chem.* **26**, 13 (1970).
93. E. Franks and A. Mukherjee, *J. Electroanal. Chem.* **49**, 456 (1974).
94. D. M. Wrench and D. Inman, *Electrochim. Acta* **12**, 1601 (1967).
95. E. Franks and D. Inman, *J. Appl. Electrochem.* **1**, 73 (1971).
96. D. Inman, in *Electroactive Force Measurements in High-Temperature Systems*, C. B. Alcock, ed., I.M.M., London (1968).

97. P. G. Zambonin, *J. Electroanal. Chem.* **24**, Appl. 25 (1970); D. Inman and M. J. Weaver, *J. Electroanal. Chem.* **51**, 45 (1974).
98. See, for example, R. P. Tischer and F. A. Ludwig, in *Advances in Electrochemistry and Electrochemical Engineering*, Vol. 10, C. W. Tobias and H. Gerischer, eds., Interscience, New York (1964).
99. See, for example, C. R. Dillard and D. E. Goldberg, *Chemistry: Reactions, Structure and Properties*, 2nd ed., Macmillan, New York (1979).
100. *The Encyclopaedia of Electrochemistry*, C. A. Hampel, ed., Reinhold, New York (1964), p. 31.
101. F. R. A. Smith, *Met. Mater.* (March 1974), p. 182.
102. G. A. Wolstenholme, *Chem. Ind.* **9**, 383 (1975); J. G. Peacey and W. G. Davenport, *J. Met.* (July, 25, 1974).
103. See Ref. 102.
104. D. Inman and S. H. White, *J. Appl. Electrochem.* **8**, 375 (1978).
105. S. Senderoff, G. W. Mellors, and W. J. Reinhart, *J. Electrochem. Soc.* **112**, 266 (1965).
106. S. Senderoff, G. W. Mellors, and W. J. Reinhart, *J. Electrochem. Soc.* **112**, 840 (1965).
107. G. W. Mellors, *Proceedings of the 1st Australian Conference on Electrochemistry*, A. Friend and F. Gutmann, eds., Pergamon Press, Oxford (1964).
108. A. D. Graves and D. Inman, *Electroplat. Met. Finish.* **19**, 314 (1966).
109. S. Senderoff and G. W. Mellors, *J. Electrochem. Soc.* **113**, 66 (1966).
110. See Ref. 100, p. 1100.
111. T. A. Henrie and E. Morrice, *J. Met.* **18**, 1207 (1966); **21**, 34 (1969).
112. N. C. Cook, *Sci. Am.* (August, 38, 1969).
113. D. A. J. Swinkels, in *Advances in Molten Salt Chemistry*, Vol. 1, J. Braunstein, G. Mamantov, and G. P. Smith, eds., Plenum Press, New York (1971).
114. E. J. Cairns and R. K. Steunenberg, in *Progress in High Temperature Physics and Chemistry*, Vol. 5, C. A. Rouse, ed., Pergamon Press, Oxford (1973).
115. K. V. Kordesch, in *Modern Aspects of Electrochemistry*, Vol. 10, J. O'M. Bockris and B. E. Conway, eds., Plenum Press, New York (1975).
116. R. Roberts, in *Electrotechnology*, Vol. 2, R. P. Ouellette, F. Ellerbusch, and P. N. Cheremisinoff, eds., Ann Arbor Science, Ann Arbor, Michigan (1978).
117. D. H. Thow, in *Power Sources 3*, D. H. Collins, ed., Oriel Press, Newcastle (1971).
118. G. Bowser *et al.*; U.S. Patent 3,891,460.
119. D. A. J. Swinkels and R. N. Seefurth, *J. Electrochem. Soc.* **115**, 994 (1968).
120. E. H. Hietbrink, J. J. Petraits, and G. M. Craig, in *Advances in Energy Conversion Engineering*, A.S.M.E., New York (1967).
121. M. W. Breiter, in *Trends in Electrochemistry*, J. O'M. Bockris, D. A. J. Rand, and B. J. Welch, eds., Plenum Press, New York (1977).
122. J. L. Sudworth, A. R. Tilley, and J. M. Bird, in Extended Abstracts 77-2 (1977); J. L. Sudworth and M. D. Hames, in Extended Abstracts, 78-2 (1978), The Electrochemical Society, Princeton, New Jersey (1977).
123. R. Hudson and K. Gentry, in Extended Abstracts 78-2, The Electrochemical Society, Princeton, New Jersey (1978).
124. P. A. Nelson *et al.*, Development of Lithium/Metal Sulphide Batteries at Argonne National Laboratory: Summary Report 1977, ANL-78-20 (1978).
125. See, for example, S. K. Preto, S. von Winbush, and M. F. Roche, Extended Abstracts, 78-2, The Electrochemical Society, Princeton, New Jersey (1978).
126. J. C. Nardi, J. K. Erbacher, C. L. Hussey, and L. A. King, *J. Power Sources* **3**, 81 (1978).
127. R. A. Osteryoung, R. J. Gale, J. Robinson, R. Bugle, and B. Gilbert, Extended Abstracts 78-2, The Electrochemical Society, Princeton, New Jersey (1978).
128. For early background material, see F. Jones, in *An Introduction to Fuel Cells*, K. R. Williams, ed., Elsevier, Amsterdam (1966) and D. P. Gregory, *Fuel Cells*, Mills and Boon, London (1972). For recent technical detail see 1st–5th National Fuel Cell Seminar Proceedings

(1976–1980), *Extended Abstracts* of Electrochemical Society Meetings, especially Vol. **80-2**, Hollywood (1980) which includes a Symposium on Molten Carbonate Fuel Cell Technology.

129. K. F. Blurton, L. G. Marianowski, and E. H. Camara, in *Power Sources 11*, J. Thompson, ed., Academic Press, N.Y. (1979).
130. S. J. Yosim, K. M. Barclay, K. J. Miller, and C. A. Trilling, *Extended Abstracts*, **78-2**, The Electrochemical Society, Princeton, N.J. (1978).
131. J. M. King, W. E. Houghtby, and R. A. Sederqvist, in National Fuel Cell Seminar, Boston, MA (1977).
132. J. M. King, E.C.A.S. Phase II, Final Report on NAS 3-19586 Contract to NASA, United Technologies Corp., Conn. (1976).
133. A. C. C. Tseung, *J. Appl. Electrochem.* **1**, 279 (1971); **2**, 137 (1972).
134. K. Kinoshita, J. W. Sim, and J. P. Ackerman, in National Fuel Cell Seminar, Boston, MA (1977).
135. L. G. Marianowski, K. F. Blurton, E. H. Camara, and H. C. Maru, *ibid.*
136. Corrosion, Vol. I, 2nd Ed., L. L. Shrier, ed., Newnes-Butterworth, London (1976), Section 2-10.
137. D. Inman and N. S. Wrench, *Brit. Corr. J.* **1**, 246 (1966).
138. B. W. Burrows and G. J. Hills, *J. Inst. Fuel* **39**, 168 (1966).
139. A. J. B. Cutler *et al.*, A.S.M.E. Publicn. 67-WA/CD-4 (1967).
140. R. Littlewood, *J. Electrochem. Soc.* **109**, 525 (1962).
141. R. Littlewood, *Trans. A.I.M.E.* **233**, 772 (1965).
142. M. D. Ingram and G. J. Janz, *Electrochim. Acta* **10**, 783 (1965).
143. L. Campanella, *Brit. Corr. J.* **2**, 219 (1967).
144. L. Campanella and A. Conte, *J. Electrochem. Soc.* **116**, 144 (1969).
145. L. Campanella, *Plating* **56**, 813 (1969); **57**, 807 (1970); **59**, 575 (1972).
146. L. Campanella, *Trans. Inst. Met. Finish.* **51**, 97 (1973).
147. F. H. Cocks, D. R. Cogley, G. H. Hurley, and C. R. Mitchell, *Corrosion* **32**, 135 (1976).
148. R. E. Herfert, Tech. Rept. AFML-TR-76-142, U.S.A.F. (1976).
149. R. K. Nigam and R. S. Chaudhary, *Ind. J. Chem.* **8**, 343 (1970).
150. R. K. Nigam and R. S. Chaudhary, *Electrochim. Acta.* **17**, 1765 (1972).
151. A. Yamashita and H. Hagiwara, *J. Electrochem. Soc.* **112**, 279 (1965).
152. E. L. Krongauz, V. D. Kashcheev, and V. B. Busse-Machukas, *Sov. Electrochem.* **8**, 1219 (1972).
153. A. Conte, A. Borello, and A. Cabrini, *J. Appl. Electrochem.* **6**, 293 (1976).
154. S. Tajima, M. Soda, and T. Mori, *Electrochim. Acta* **1**, 205 (1959).
155. A. K. Turner and D. G. Lovering, *Trans. Inst. Met. Finish.*, in press (1980).
156. A. K. Turner and D. G. Lovering, Final Report to M.O.D. (P.E.) on contract AT/2160/027 MAT (1978).
157. V. Saifullin and F. F. Faizullin, *Sb. Aspir. Rab. Kazan. Gos. Univ. Estecto. Nauki Khim.* **25** (1973).
158. R. K. Nigam and I. K. Arora, *Electrochim. Acta* **17**, 2133 (1972).
159. A. K. Turner, thesis, London (1978).
160. S. Tajima, Y. Tanabe, M. Shimura, and T. Mori, *Electrochim. Acta* **6**, 127 (1962).
161. G. L. Holleck, F. H. Cocks, D. R. Cogley, and I. W. Frutkoff, Tech. Rept. AFML-TR-72-191, USAF (1978).
162. S. Ikonopisov, *Electrodep. Surf. Treat.* **2**, 303 (1973–1974).
163. *Molten Salt Techniques*, D. G. Lovering and R. J. Gale, ed., Plenum Press, New York, 1983 et seq.
164. D. G. Lovering and R. M. Oblath, in *Ionic Liquids*, D. Inman and D. G. Lovering, eds., Plenum Press, New York (1981).
165. S. H. White, in *Ionic Liquids*, D. Inman and D. G. Lovering, eds., Plenum Press, New York (1981).
166. P. G. Zambonin and J. Jordan, *J. Am. Chem. Soc.* **91**, 2225 (1969).

167. P. G. Zambonin, *J. Electroanal. Chem.* **32**, App. 1 (1971).
168. A. D. Graves and D. Inman, in *Electromotive Force Measurements in High-Temperature Systems*, C. B. Alcock, ed., I.M.M., London (1968).
169. Yu. K. Delimarskii and B. F. Markov, *Electrochemistry of Fused Salts*, Sigma Press, New York (1961).
170. J. J. Egan and R. Heus, *J. Electrochem. Soc.* **107**, 824 (1960).
171. H. Hoff, *Electrochim. Acta* **16**, 1059 (1971).
172. W. H. Bell, *J. Electrochem. Soc.* **118**, 889 (1971).
173. H, Hoff, *Electrochim. Acta* **16**, 1357 (1971).
174. Yu. K. Delimarskii and A. A. Kolotii, *Zavod. Lab.* **22**, 75 (1956).
175. R. W. Laity, in *Reference Electrodes: Theory and Practice*, D. J. G. Ives and G. J. Janz, eds., Academic Press, New York (1961).
176. D. Inman, *J. Sci. Instrum.* **39**, 391 (1962).
177. H. L. Jones, L. G. Boxall, and R. A. Osteryoung, *J. Electroanal. Chem.* **38**, 476 (1972).
178. B. S. Del Ducca, *J. Electrochem. Soc.* **118**, 405 (1971).
179. J. O'M. Bockris, G. J. Hills, D. Inman, and L. Young, *J. Sci. Instrum.* **33**, 438 (1956).
180. H. R. Bronstein and D. L. Manning, *J. Electrochem. Soc.* **119**, 125 (1972).
181. G. Schiavon, S. Zecchin, and G. G. Bombi, *J. Electroanal. Chem.* **38**, 473 (1972).
182. G. J. Hills, D. Inman, and L. Young, in *Proceedings of 8th Meeting of the C.I.T.C.E.*, Butterworth Scientific Publications, London (1958), p. 90.
183. D. Inman, D. G. Lovering, and R. Narayan, *Trans. Faraday Soc.* **63**, 3017 (1967).
184. M. D. Baird, A. J. Clark, C. R. Feltham, and L. J. Pearce, in *Power Sources 11*, J. Thompson, ed., Academic Press, London and New York (1978).
185. R. Roberts, in *Electrotechnology*, Vol. 2, *Applications in Manufacturing*, R. P. Ouellette, F. Ellerbusch, and P. N. Cheremisinoff, eds., Arbor Science Publishers, Ann Arbor, Michigan (1978).
186. W. R. Grimes and S. Cantor, in *The Chemistry of Fusion Technology*, R. M. Gruen, ed., Plenum Press, New York (1972).
187. See, for example, 1st–5th National Fuel Cell Seminars, Palo Alto, California, 1976; Boston 1977; San Francisco 1978; Bethesda, Maryland 1979; San Diego 1980.
188. G. J. Hills and P. D. Power, *J. Pol. Soc.* **13**, 71 (1967).
189. E. Desimoni, F. Palmisano, and P. G. Zambonin, *J. Electroanal. Chem.* **84**, 323 (1977).
190. See, for example, P. G. Zambonin, *Anal. Chem.* **43**, 1571 (1971) and other papers by this author.
191. M. Peleg, *J. Phys. Chem.* **71**, 4553 (1967).
192. D. G. Lovering, R. M. Oblath, and A. K. Turner, *J. Chem. Soc., Chem. Commun.*, 673 (1976).
193. A. Espinola and J. Jordan, in *Characterization of Solutes in Nonaqueous Solvents*, G. Mamantov, ed., Plenum Press, New York (1978).
194. P. G. Zambonin, *J. Electroanal. Chem.* **33**, 243 (1971).
195. R. N. Kust and F. R. Duke, *J. Am. Chem. Soc.* **85**, 3338 (1963); M. Fredericks and R. B. Temple, *J. Electroanal. Chem.* **38**, App. 5 (1972).
196. J. D. Burke and D. H. Kerridge, *Electrochim. Acta* **19**, 151 (1974).
197. K. W. Fung, G. Mamantov, and J. P. Young, *Inorg. Nucl. Chem. Lett.* **8**, 219 (1972).
198. L. G. Boxall, H. L. Jones, and R. A. Osteryoung, *J. Electrochem. Soc.* **120**, 223 (1973).
199. H. Schaefer, C. Joeser, and L. Bayer, *Z. Anorg. Allg. Chem.* **263**, 87 (1950).
200. D. Inman, G. J. Hills, L. Young, and J. O'M. Bockris, *Ann. N.Y. Acad. Sci.* **29**, 803 (1960); H. A. Laitinen, W. S. Ferguson, and R. A. Osteryoung, *J. Electrochem. Soc.* **104**, 516 (1957).
201. W. J. Burkhard and J. D. Corbett, *J. Am. Chem. Soc.* **79**, 6361 (1957).
202. D. L. Manning, *J. Electrochem. Soc.* **7**, 302 (1964).
203. S. Pizzini and R. Morlotti, *Electrochim. Acta* **10**, 1033 (1965).
204. H. Kojima, S. G. Whiteway, and C. R. Masson, *Can. J. Chem.* **46**, 2905 (1968).

205. D. W. Townsend, in *International Symposium on Molten Salts*, J. P. Pemsler, J. Braunstein, K. Nobe, D. R. Morris, and N. E. Richards, eds., The Electrochemical Society, Princeton, New Jersey (1976).
206. J. Thonstad, *J. Electrochem. Soc.* **9**, 346 (1968).
207. F. R. Clayton, G. Mamantov, and D. L. Manning, *J. Electrochem. Soc.* **120**, 111C (1973).
208. S. Vire and D. Inman, unpublished work.
209. J. Thonstad, F. Nordmo, and J. F. Rodreth, *Electrochim. Acta* **19**, 751 (1974).
210. D. G. Lovering, *Collect. Czech. Chem. Commun.* **37**, 3697 (1972).
211. D. G. Hill, B. Porter, and A. S. Gillespie, *J. Electrochem. Soc.* **105**, 408 (1958).
212. B. W. Burrows and G. J. Hills, *Electrochim. Acta* **15**, 445 (1970).
213. J. Goret and B. Tremillon, *Bull. Soc. Chim. France*, 67 (1966).
214. J. Goret and B. Tremillon, *Electrochim. Acta* **12**, 1065 (1967).
215. G. G. Bombi, M. Fiorani, and C. Macca, *J. Chem. Soc., Chem. Commun.*, 455 (1966).
216. F. J. Hazlewood, E. Rhodes, and A. R. Ubbelohde, *Trans. Faraday Soc.* **62**, 3101 (1966).
217. E. Rhodes and A. R. Ubbelohde, *Trans. Faraday Soc.* **55**, 1705 (1959).
218. K. Hirata, H. Yoneyama, and H. Tamura, *Electrochim. Acta* **17**, 793 (1972).
219. K. Hirata, H. Yoneyama, and H. Tamura, *Electrochim. Acta* **17**, 804 (1972).
220. V. P. Yurinskii, N. V. Vorob'eva, A. G. Morachevskii, and E. Yu. Riskina, *Zh. Priklad. Khim.* **52**(2), 221 (1979).

10

Organic Electrode Processes: Kinetics, Mechanisms, and Prospects for Commercial Development

E. J. RUDD and B. E. CONWAY

1. Historical Aspects

Organic electrochemistry has its origins in the last century when quite a number of now well-known electrochemical oxidations and reductions had been achieved at electrodes and Kolbe's unique oxidative dimerization of aliphatic carboxylates had been described.(1–7) Developments in the dye industry in the early 1900s stimulated many studies on electro-organic procedures, e.g., reduction of nitro compounds to amines. In 1926, Brockman(7) gave an excellent account in his book of the many types of electrochemical routes for functionalizing organic compounds and for modifying existing functionalities by oxidation or reduction.

Unfortunately, mechanisms of elementary steps, e.g., electron transfer, in electrode processes were not at all well understood during the period of early development of electro-organic chemistry, and the significance of the fundamental relation between overpotential ("polarization") and current density was not appreciated until the work of Volmer, Gurney, Bowden,

---

E. J. RUDD • Eltech Systems Corporation, Technical Center, Fairport, Ohio.
B. E. CONWAY • Chemistry Department, University of Ottawa, Ottawa, Ontario, Canada.

Rideal, and Butler in the early 1930s.(8,9) Similarly, the role of adsorption in electrode interface processes,(10) which is of great importance in many, if not all, electrode reactions involving organics, was hardly appreciated until Frumkin's pioneering work, which formed a cornerstone of the research of the Russian school of electrochemistry.

To those who have been involved with electrochemical technology, it has often seemed somewhat illogical that there are so few established industrial processes based on organic electrochemistry. Indeed, the number of processes "on stream" at any time could probably be counted on the fingers of one hand. Yet, electrochemical processes are firmly established in the manufacture of some inorganic chemicals and extraction and purification of metals.(11,12) For example, the production of chlorine and sodium hydroxide alone accounts for approximately 2% of the total consumption of electricity in the United States and, together with that for Al, much more. This apparent lack of acceptance of organic electrode processes as viable means for (certain types) of syntheses (see later) is perhaps all the more surprising when it is noted that electrolytic reactions are simply very direct oxidation and reduction processes which do not produce in the solution other conjugate reduced or oxidized species, respectively, such as would occur with homogeneous redox reagents.

The development of organic electrochemistry can be conveniently illustrated by the scheme shown as Figure 1. Early in the nineteenth century, the oxidation of acetic acid by Faraday(13) demonstrated the ability of an electric current to decompose organic substances, and by the end of that century, Gatterman, Kolbe, Haber, and others(7,14) had extended the field of electro-organic chemistry substantially. However, after this initial activity, the scientific community paid only minimum attention to organic electrode processes for some time until the resurgence of interest in the field took place in the 1960s.

Limitations to the acceptance of organic electrochemistry, particularly as a synthetic technique, may have been connected with the fact that electrode reactions are normally "two-dimensional," i.e., they are restricted to a *surface* and therefore require mass transport (see elsewhere in this chapter) and also because many reactions yield a complex mixture of products(15) when the electrolyses are carried out using a constant current. However, as early as 1898, Haber(14) had pointed out the importance of control of the electrode *potential* for the overall process, in his work where nitrosobenzene, phenylhydroxylamine and aniline were isolated *selectively* from the reduction of nitrobenzene. However, design of suitable controlled-potential equipment proved to be a practical barrier, even in laboratory studies, until 1942, when the potentiostat—an instrument capable of automatically controlling the electrode potential—was introduced.(16) Without question, this instrument has facilitated electro-organic syntheses, mechanistic studies, and specific electro-oxidation and electroreduction processes. More modern and electronically

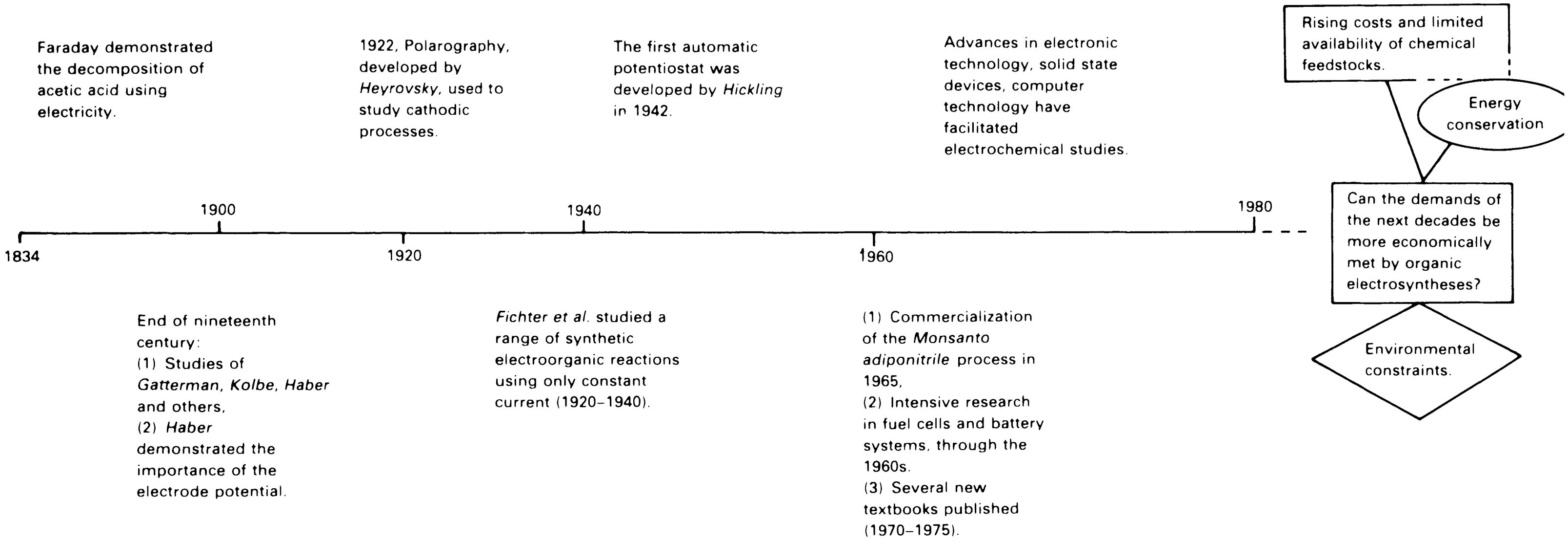
Faraday demonstrated the decomposition of acetic acid using electricity.
1922, Polarography, developed by *Heyrovsky*, used to study cathodic processes.
The first automatic potentiostat was developed by *Hickling* in 1942.
Advances in electronic technology, solid state devices, computer technology have facilitated electrochemical studies.
Rising costs and limited availability of chemical feedstocks.
Energy conservation
1834
1900
1920
1940
1960
1980
Can the demands of the next decades be more economically met by organic electrosyntheses?
End of nineteenth century: (1) Studies of *Gatterman, Kolbe, Haber* and others, (2) *Haber* demonstrated the importance of the electrode potential.
Fichter et al. studied a range of synthetic electroorganic reactions using only constant current (1920–1940).
(1) Commercialization of the *Monsanto adiponitrile* process in 1965, (2) Intensive research in fuel cells and battery systems, through the 1960s. (3) Several new textbooks published (1970–1975).
Environmental constraints.

Figure 1. Illustrating developments in electro-organic chemistry.

better designed potentiostats became available from Germany (Wenking) in 1961, and later from other suppliers.†

It is also important to note that the development in 1922 of the dropping mercury electrode and the polarographic method did allow a sustained interest in electroreduction (cathodic) reactions of organic molecules,(17) but not from the synthetic direction. Classical polarography may be regarded as a slow, potentiodynamic method, i.e., the electrode potential is varied in a controlled manner and an average current is determined as a function of potential. In more recent applications of the polarographic technique, rotating solid bead or wire electrodes have been used, particularly in studies of anodic (oxidation) processes. Efforts have been made to understand the mechanisms of the electrode reactions involving organic molecules, and in this area the Czechoslovak school has been a major contributor.(18) It must be remembered, however, that in polarography the concentrations of the reactants are deliberately maintained at low levels (10^{-3}–10^{-5} M) to ensure that the reaction is *diffusion controlled* (see Section 7.3). Consequently, little or no information is afforded concerning the products or yields of the reaction.

The relative neglect of organic electrochemistry is also reflected in the absence of consistent reference to electro-oxidation and electroreduction processes in the textbooks and in experimental university courses. Ironically, it may be that, in some cases, superior synthetic routes were ignored. It is evident that the lack of effective communication between organic chemists, organic electrochemists, and physical electrochemists is another contributing factor. In the last decade, however, new textbooks and monographs have been published in which electrode kinetics, physical electrochemical techniques, the theory and practice of cell design and operation electrodes and electrolytes, as well as extensive reviews of anodic and cathodic reactions of organic molecules, have been presented.(1,19–27) Forums for the discussion of new work have become available considerably enhancing the communication between the physical and synthetic electro-organic chemists.

Advances in electronics technology and the development of solid state devices have allowed in recent years design of a variety of potentiostats, providing high current capability, e.g., in instruments developed by Allen and by the Newcastle school, for syntheses and rapid response for the application of potential-step or pulse techniques in mechanistic and preparative studies.

The use of nonaqueous electrolytes in more recent work has considerably extended the range of electrode potentials available for oxidation and reduction of a variety of organic molecules. Also, the advent of superior materials for cell construction, electrodes, separators, and ion exchange membranes, e.g., Nafion®, and the application of computer technology to control of electrochemical systems and process engineering, are further factors that have contributed to the renewed interest in organic electrode processes in the last two decades.

† See p. 667.

2. Introduction and Nature of Organic Electrode Processes

Much of organic electrochemistry from the "electrochemical" point of view is concerned with the consequences of using the electron as a "reagent" in a heterogeneous reaction at a metal or metal oxide surface—electron addition in cathodic processes or electron withdrawal in anodic processes. These two fundamental types of steps in electrode processes involving reactions of organics are normally coupled, or involve consecutively, proton addition or removal, respectively, in protic media, depending on pH, or in aprotic media, various follow-up steps involving reactions such as dissociation, rearrangement, disproportionation, dimerization, or reaction with the solvent or ions of the electrolyte present. Dimerization is also observed in a number of reactions in protic media, following electron and proton transfer.

In some cases, the chemistry of reactions prior to the electron transfer step is important, e.g., enolization rearrangements, protonation, and conformational changes in the electrode double-layer field.

In aqueous and related media, most of the chemistry of organic electrode reactions is concerned with species resulting from the eventual uptake of one electron and one proton or, more usually, two electrons and two protons (in cathodic reactions) and the reverse processes in some anodic reactions. However, in the latter reactions, the formation of radical intermediates as a result of de-electronation may lead to other chemical changes, e.g., in the total oxidation of hydrocarbons to carbon dioxide in aqueous media and in other ways in the Kolbe,(5) Hofer-Moest and Crum Brown-Walker reactions,(4,5) and some other carbonium ion type rearrangements.

The uptake (or loss) of electrons and protons usually occurs in successive steps, possibly coupled with chemical rearrangements (see below), and the order in which these steps proceed is a matter of great importance; it can sometimes be elucidated by means of polarography or related techniques, such as cyclic voltammetry.

In aprotic nonaqueous media, the organic electrochemistry of anodic and cathodic reactions is concerned predominantly with radical-ion chemistry: in many cases involving aromatic substances, the radicals are of sufficient stability for them to be characterized spectroscopically by conventional absorption spectrophotometry and by esr spectroscopy. Linear relations are found(28) between the cathodic and anodic half-wave potentials and the ionization potentials or electron affinities determined in the gas phase. The oxidation and reduction potentials can also be related to the theoretically calculated(28,29) energies of the highest occupied (anodic process) or lowest vacant (cathodic process) molecular orbitals.

An important and different class of electroorganic reaction is that which may be called "electrocatalytic" in type. In such cases, the organic molecule undergoes an initial dissociative chemisorption step (or steps) at the electrode surface$^{(30,31)}$ (usually that of a transition metal), which is followed by successive coupled electrochemical steps of hydrogenation (cathodic) or oxidation of dissociated H (anodic) and/or oxidation of the adsorbed carbon structure fragments with the "elements of oxygen" electrochemically discharged from H_2O or OH^-, depending on pH. This class of reactions has attracted much interest in fuel cell technology,$^{(32-37)}$ e.g., with molecules such as CH_3OH, EtOH, HCOOH, hydrocarbons from CH_4 to C_8H_{18}, and some olefins such as C_2H_4 and C_3H_6. Mechanistically, with the smaller molecules, the basic elementary steps in these reactions are relatively well understood. Oxidation of H_2, e.g., at Pt, is an elementary prototypical reaction of this kind.$^{(38)}$

In most of these types of electrocatalytic organic electrode reactions, the electron transfer event is involved in production or maintenance of a surface layer of chemisorbed H (cathodic processes) or oxygen species (OH, O, anodic processes), which then participates in electrochemical hydrogenation or oxidation, respectively, of the organic compound often through heterogeneous reactions at the electrode surface between chemisorbed H or OH/O species and the temporarily adsorbed organic reactant. The electrochemical reaction in such cases is hence indirect.

Other types of indirect electrochemical reaction arise when a bulk phase is generated on or at the electrode surface and is maintained by passage of current. Usually, this type of reaction$^{(39,40)}$ involves the formation of higher oxides of some anode metal, e.g., PbO_2 at Pb, Ni·O·OH, or "NiO_2" at Ni or corresponding compounds at Co, and "AgO" at Ag. Again, such reactions are heterogeneous and the electrochemistry is really secondary. Another type of bulk phase electrochemical reaction is that arising when some reactive, solution–soluble reactant species is generated, e.g., Cl_2 or Ag^{3+} at anodes or reactive low-valent cations in cathodic processes, e.g., Cr^{2+}, V^{2+}, and perhaps Zn^+ or Mg^+ in less well understood cases. Cathodic production of solvated electrons also falls into this class.

It is useful to distinguish two types of mechanistic problems in organic electrochemistry: (a) the basic steps, and their sequence,$^{(31)}$ in the processes at the electrode involving electron transfer, electrocatalysis and adsorption, recombination disproportionation or rearrangement assisted by the electrode surface and possibly by the metal–solution field,$^{(31)}$ and (b) follow-up reactions which are essentially steps familiar as regular organic reaction processes and take place following the elementary act of electron transfer or withdrawal. Such steps are usually relatively independent of the electrode surface, especially if the latter is rather nonchemisorptive (e.g., Hg, Pb as cathodes). A third, but different, point is that unlike most other types of electrode reactions, organic electrode processes can involve, with appropriate reactants, important steric effects related to adsorption at the surface or accessibility of functional groups (see Section 9), and possible electrode field-dependent orientation of the principal dipole in the molecule. For example, in studies of the adsorption of polar molecules such as pyridine or the quinolines at the

Hg/solution interface, strong orientation effects are experimentally demonstrable.

In this chapter, emphasis will be placed on same basic *electrochemical* mechanistic aspects of studies in electro-organic chemistry rather than the myriad of specific, essentially organic reaction mechanisms that involve eventual product formation from the initial, electrochemically generated intermediate. We shall, however, refer in a later section of this chapter to a selection of reactions that are mechanistically better understood and may lead, or have led, to commercially viable processes (Section 13). In other chapters in this series of volumes(41) will be found accounts of electroorganic reactions which are presented more specifically from the point of view of the organic chemistry involved, e.g., in follow-up reactions after electron transfer.

3. Classification of Organic Electrode Reactions

The many known organic electrode reactions(1,7,15,22,24) may be conveniently classified in several ways. For example, based on the type of reaction, it is possible to describe processes in terms of (a) electron transfer reactions (often a primary step), (b) conversion reactions, (c) addition reactions, (d) substitution reactions, (e) elimination reactions, (f) coupling reactions, (g) cleavage reactions, and (h) electrocatalytic reactions. All of these types of reactions have been observed in both anodic and cathodic processes. However, it is important to be aware that, as in organic syntheses, electro-organic reactions may involve more than one of the above reactions, resulting in the formation of several products. It is necessary to establish the optimum reaction conditions for isolation of a particular product.

An alternative and electrochemically more significant method for classification of electroorganic reactions is based upon the type of mechanism of the electrode process. This may be described in terms of the *number* and *sequence* of electrochemical steps (involving the transfer of electrons) and chemical steps. A useful example of both types of classification is the electro-oxidation of an aliphatic amide, e.g., *NN*-dimethylformamide:

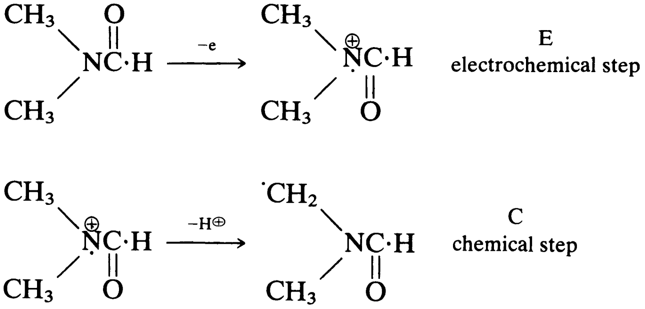

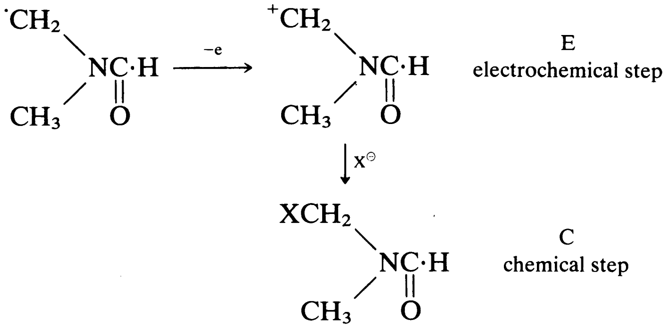

(I)

Thus, the formation of the substituted amide (I) may be classified as a *substitution* reaction or, in terms of the electrode process, as an ECEC reaction.

Based on the material given in several textbooks and reviews published in recent years,(19–26,30) one may simply summarize the many electroorganic processes in a more general way, as in Table 1. In the discussion which follows later in Section 13, the examples can be readily classified in the above terms

Table 1
Summary of Organic Electrode Processes

Electroreduction cathodic processes	Electro-oxidation anodic processes	Other electrochemical processes
Reduction of alkenes and alkynes	Oxidation of aliphatic hydrocarbons	Indirect oxidation and reduction
Reduction of aromatic hydrocarbons	Oxidation of aromatic hydrocarbons	
Reduction of carbonyl compounds	Substitution reaction of aromatic compounds	Anodic halogenation
Reduction of nitro compounds	1. Hydroxylation	
Reduction of nitriles, imines oximes	2. Alkoxylation	Electroinitiated polymerization
Reduction of carbon–halogen bonds	3. Acyloxylation	
Reduction of organosulfur compounds	4. Acetamidation	Electrosynthesis of organometallic compounds
	5. Cyanation	
	Kolbe and Hofer–Moest reactions	Electrocoating
	Oxidation of amines	
	Oxidation of amides	
	Oxidation of alcohols and phenols	
	Oxidation of ethers	
	Oxidation of oximes, nitroalkanes, hydrazines	

by the reader, so that, beyond this point, no consistent effort to do so will be made by the authors.

A general electrochemical classification of reaction type is as follows:

(a) electron transfer controlled
 / anodic → radical cations → follow-up products
 \ cathodic → radical anions → follow-up products

(b) electrocatalytic
 / anodic—general oxidations, sometimes to CO_2
 \ cathodic—hydrogenations

(c) reactions with electrochemically produced bulk species—thick oxide layers, solution–soluble ions, reactive gases evolved at anodes, solvated electrons

A more specific classification can be made in terms of the types of radical ion produced in the initial electron transfer (1e) step (i.e., in reactions not of the electrocatalytic type), viz., radical anions or radical cations, and their subsequent reactions to form stable products, which may include processes such as a further 1e transfer step, a dimerization after proton transfer, a rearrangement or cleavage, etc.

Examples of this type of classification for anodic and cathodic processes are given in the two schemes shown below as Figures 2 and 3. In some cases, the existence of the radical ions involved and their nature has been proved by means of electron spin resonance spectroscopy.

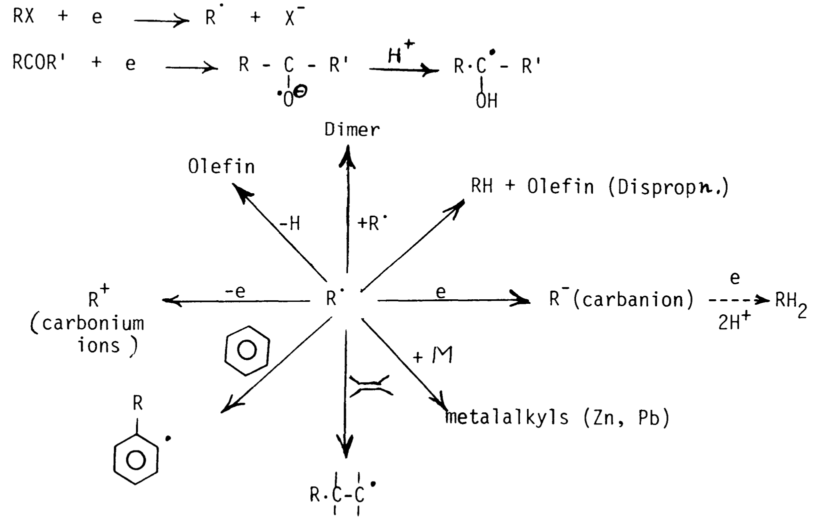

Figure 2. Follow-up processes occurring after electrochemical cathodic production of a carbanion. Aromatics in nonaqueous aprotic solvents give $R^{+\bullet}$ and $R^{-\bullet}$ species which are relatively stable; $R^{-\bullet} > R^{+\bullet}$.

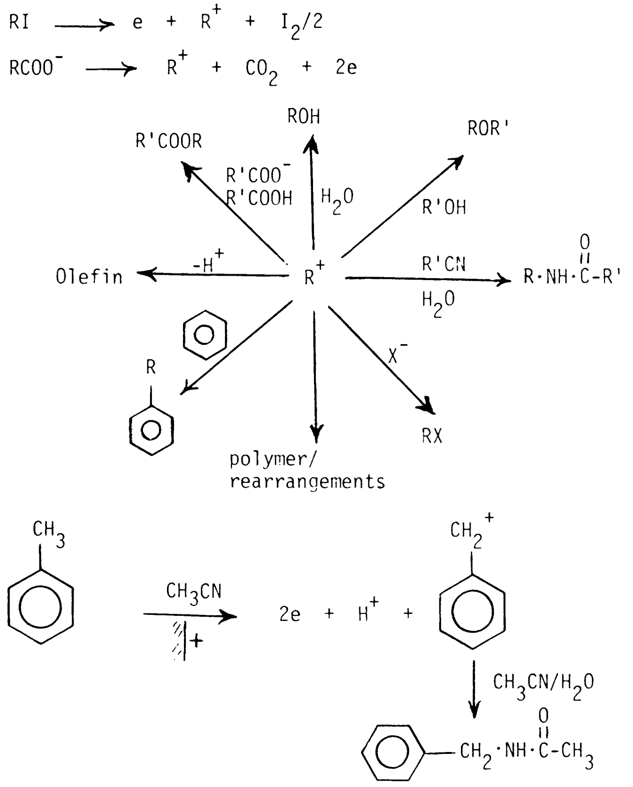
RI → e + R+ + I2/2
RCOO- → R+ + CO2 + 2e
ROH
R'COOR
R'COO-
R'COOH
H2O
ROR'
R'OH
Olefin
-H+
R+
R'CN
H2O
R·NH·C(=O)-R'
R
X-
RX
polymer/
rearrangements
CH3
CH3CN
2e + H+ +
CH2+
CH3CN/H2O
CH2·NH·C(=O)-CH3

Figure 3. Follow-up processes occurring after electrochemical anodic production of a carbonium ion.

4. Kinetic Equations for Electrochemical Reactions

We shall first present for reference purposes some basic aspects of electrode kinetics, as they may apply to electro-organic reactions, outlining the dependence of electrode reaction rates on potential, electrode material, adsorption behavior, etc., and the role of consecutive reaction steps.

4.1. Factors in the Kinetics of Organic Electrode Reactions

Electrode reactions are heterogeneous processes, so that their rates will be influenced (a) by the concentration of the reactant at the surface which is related to the bulk concentration by an adsorption isotherm, (b) by the presence of any intermediates and/or products which are adsorbed on the surface, and (c) by the nature of the electrode material and solvent, also, (d) depending on concentration and/or solution agitation or flow rate, by diffusional or convective mass transport of reagents and/or products to or from the electrode surface (see Section 7). Additionally, because the reactions are electrochemical, their rates will be determined also by (e) the potential difference across the metal/solution interphase (see below) and the sign of surface charge on the electrode surface. The former factor, which is of primary importance in all electrochemical reactions, results in (i) a potential dependence of adsorption of solvent, ions, and reactant, and orientation at the surface, as well as (ii) a potential dependence of the activation energy, and hence, rate, of the heterogeneous electron transfer reaction and subsequent steps.

In addition to the factors (a), (b), (c), and (e), which determine the actual rate of the electrochemical reaction *at* the interface, there is usually the important question of diffusion of the reactant *to* the interface, factor (d). If the electrochemical rate constant for the reaction at the interface tends to be large, then the overall rate of the process can become limited by the rate of diffusion [(d) above] to the electrode surface from the bulk. In such cases, the surface concentration is no longer related to the bulk concentration by an adsorption isotherm as indicated in (e) above and tends to zero as the diffusion-limited current is approached. Diffusion limitation will always become significant, even for slower electrode surface processes, if the concentration of reactant in the bulk of the solution is sufficiently small. This situation is taken advantage of in the technique of polarography to be discussed later in this chapter. It is to be noted that since the rates of electrochemical reactions can readily be modified by changing the electrode potential, conditions can always be reached where diffusion limitation eventually becomes important, i.e., at low concentrations, high enough potentials, or at elevated temperatures.

4.2. Electrode Potential, E, and the Rate Equations for Electron Transfer Reactions

A single metal–solution potential difference cannot, in principle, be measured so that E must be expressed with respect to the potential of some reference electrode, preferably in the same solution. In certain cases, it is possible to employ a reference electrode at which the *same* electrode process is occurring (but reversibly) as that being studied [for example, in studies of the hydrogen evolution reaction at a cathode, the reference electrode is simply a hydrogen electrode (H_2/platinized platinum) on open circuit with no current passing]. For this case, the quantity $E - E_{\text{ref}}$, which can be measured directly, is called the polarization† or "overpotential" (η).(31)

---

† Kortum (*Treatise on Electrochemistry*, Elsevier, New York, 1965, p. 441) distinguishes between the true overpotential defined as $E - E_{\text{ref}}$ and the "polarization" defined as $E - E_{\text{rest}}$ when no true reversible potential is set up, but a rest potential E_{rest} is attained at zero net current. Overpotential and polarization are, however, usually synonymous and even if E_{ref} for the electrode reaction concerned cannot actually be measured, it may in many cases be calculated on some other practical reference potential scale, as has been done in the case of the Kolbe reaction.(5)

In the study of many organic electrode processes, however, the electrode reaction is often too slow for a practical reversible electrode, employing the same reaction, to be used as the reference for the scale of potentials investigated. (Quinone–hydroquinone and some nitroso-compound reference electrodes are the few exceptions.) In these cases, the reference potential against which the potential of the current carrying electrode is measured is provided by an electrode such as the calomel electrode, silver–silver chloride electrode, mercury–mercuric oxide, or silver–silver ion electrode,† etc. Use of such electrodes usually introduces a liquid junction into the measuring circuit since the salt solutions (e.g., potassium or sodium chloride in the case of the Ag/AgCl or Hg/Hg_2Cl_2 electrodes) required for operation of the reference electrode may not be suitable solutions in which to conduct the actual electro-organic kinetic study or preparation.

In most cases, the metal–solution potential difference E can be expressed in a rigorous manner in terms of the potential profile in the double layer at the electrode interface. In the absence of so-called specifically adsorbed (i.e., chemisorbed) ions such as I^-, CNS^-, E is made up of a sharp potential drop, $\psi_m - \psi_1$, from the metal surface to the first layer of hydrated ions of the electrolyte (that region usually called the outer Helmholtz plane, OHP) and a less rapidly varying potential difference, $\psi_1 - \psi_3$, in the so-called diffuse part of the double layer.(31) With certain organic ions, and in the presence of specifically adsorbed anions, the potential profile involves an initial drop of potential, $\psi_m - \psi_2$, across the so-called inner Helmholtz plane, IHP, where the specifically adsorbed anions reside.(31,42) The diffuse layer potential difference, $\psi_1 - \psi_s$, varies with electrolyte concentration (decreasing with increasing ionic strength) and may have significant effects on the kinetics of an electrode process which can usually be calculated or experimentally evaluated. The distribution of potential is important in determining reaction rates and organic molecule adsorption.

The effect of electrode potential on the rate of an electrode reaction arises in two principal ways. Firstly, the surface concentration of the reactant must be related to its bulk concentration by an electrochemical distribution function, which includes the potential-dependent, electrochemical free energy of adsorption, $\Delta\bar{G}^\circ_{ads}$. Secondly, and more significantly, the potential difference modifies the electrochemical standard free energy of activation, $\Delta\bar{G}^{\circ\ddagger}$. This energy term will include (a) any chemical effects associated with the "activation" of the reactant particle, e.g., configurational changes, solvation, bond deformation, and (b) changes of the electrical energy experienced by the particle in its progress along the reaction coordinate. $\Delta\bar{G}^{\circ\ddagger}$ is, therefore, analogous to the chemical free energy of activation, $\Delta G^{\circ\ddagger}$, and will be dependent on the electrochemical nature of the reactant and the catalytic and adsorptive properties of the surface.

---

† A useful review on special reference electrodes for aprotic organic solvents has been given by J. N. Butler, *Adv. Electrochem. Electrochem. Eng.* **7**, 77 (1970), P. Delahay and C. W. Tobias, eds., Interscience, New York.

In general, $\Delta\bar{G}^{\circ\ddagger}$ can be written as

$$\Delta\bar{G}^{\circ\ddagger} = \Delta G^{\circ\ddagger} + \beta FE \tag{1}$$

where β is a symmetry factor† similar to the Brønsted coefficient and expresses that fraction of the potential E across the interface which appears as a change in the chemical free energy of activation. For a simple electron transfer process, $\beta = 0.5$, but extreme values of β are possible with $\beta = 0$ for a so-called "activationless" reaction(44) and $\beta = 1$ for a "barrierless" discharge.(44) In some cases, β may vary with the potential, depending on the height and shape of the potential energy barrier corresponding to the activation energy. The E can change the activation energy in electrode processes in well-known ways.[31]

In terms of modern theories of electron transfer, the reactant molecule near the electrode (i.e., within 0.1 ~ 0.3 nm of it) acquires thermal energy randomly according to the Boltzmann distribution and its solvation and/or conformation becomes modified about "halfway" ($\beta = 0.5$) toward that characteristic of the *product* of the electron transfer step (which is usually an intermediate in the overall reaction). Suitably activated reactant molecules can then accept (or donate, in an anodic reaction) an electron in a so-called adiabatic electron transfer process and the resulting species then suffers further exchange of energy to form the product of the electron transfer step, usually a radical or a radical ion, which can then undergo further reactions or suffer a second electron transfer. The term *adiabatic* used for this kind of process simply refers to the situation that conformational and/or solvation shell rearrangements usually take place on a much longer time scale (10^{-11}–10^{-13} sec) than that for electron redistribution (*ca.* 10^{-16} sec). The effects are analogous to those described by the Franck–Condon principle in photochemical excitation of molecules. All electron transfer reactions at electrodes in solution are radiationless; photoemission that is sometimes observed is a chemiluminescence (e.g., in oxidation/reduction of rubrene) due to follow-up reactions.

Thus, electron transfer to or from the electrode always takes place to or from electronic energy levels in the metal at or near the so-called Fermi level, defined as the energy state having a probability of occupancy by electrons of 0.5 at finite temperatures. The electron transfer is always between states in the organic molecule which have the same energy as those in the electrode, i.e., there is no radiation emitted or adsorbed in the transfer ("radiationless transition"). Electrochemical reactions which emit light do so for quite different reasons, associated with radical ion reactions.

---

† Various interpretations of the parameter β have been discussed by Conway(31) and the use of α and β in rate equations for electrode processes has been reviewed by Bauer.(42) There is a close correlation between the β factor and Brønsted's α factor in acid–base proton transfer processes.

In many cases, the activation of the reactant and the electron transfer to the resulting transition state occur in the double layer near the electrode surface. It is for this reason that the adsorption and orientation of the organic molecule or its reactive functional group in the electrode–solution interphase is of great importance in connection with the primary act of electron transfer and any subsequent reactions the resulting intermediate may undergo. The understandable preoccupation of organic chemists employing electro-organic processes with reaction products, yields, etc., has tended to result in neglect of factors such as adsorption which are involved in the "chemical physics" of the basic electrochemical act of charge transfer to or from organic molecules. In many cases, for example, adsorption and orientation of molecules such as ketones, heterocyclic bases, and alcohols has been demonstrated experimentally at various electrode materials, particularly Hg, and quantitative information on these aspects of the interaction of reactant molecules with the electrode metal surface are available (see Section 6.5).

We now examine the mathematical representation of electrochemical reaction rates in terms of current, rate constant, and electrode potential. The velocity $\bar{v}$ of a chemical reaction may be written as

$$\bar{v} = \frac{kT}{h} C_{\mathrm{R}} \exp\left(-\frac{\Delta G^{\circ\ddagger}}{RT}\right) \tag{2}$$

where C_{R} is the bulk concentration of reactant R (and, if more than one reactant is involved, then the concentration term is $C_{\mathrm{R}} \cdot C_{\mathrm{R}_1}$, etc.), k is Boltzmann's constant, and h is Planck's constant.

For an electrochemical process $\mathrm{R} + \mathrm{e} \rightarrow \mathrm{P}$, the current density (i) specifies the rate in mol liter^{-1} (or mol cm^{-3}) per second *per unit area* of electrode surface and i directly measures the rate of the process concerned provided that its coulombic efficiency is 100%. For a reaction involving the passage of z faradays per mole, i.e., z electrons per molecule,

$$i = zF\bar{v} \tag{3}$$

and the rate expression in terms of the current density is hence of the form

$$i = zF(C_{\mathrm{R}})_s \frac{kT}{h} \exp\left(-\frac{\Delta G^{\circ\ddagger}}{RT}\right) \exp\left(-\frac{\beta FE}{RT}\right) \tag{4}$$

$(C_{\mathrm{R}})_s$ is the surface concentration of the reactant. The term $(kT/h)\exp(-\Delta G^{\circ\ddagger}/RT)$ is the chemical rate constant at the particular condition $E = 0$, although on a practical reference scale the potential at which this situation is realized cannot be experimentally known. It is convenient to regard the current density i as determined by an electrochemical rate constant

$\bar{k}$, where $\bar{k}$ is defined, from Eq. (4), as

$$\bar{k} = \frac{kT}{h} \exp\left(-\frac{\Delta G^{\circ\ddagger}}{RT}\right) \exp\left(-\frac{\beta FE}{RT}\right) \tag{5}$$

from which it can be seen that in an electrochemical reaction the rate constant is potential dependent.

The potential difference E can be written as

$$E = E_r + \eta \tag{6}$$

where E_r is the reversible electrode potential for the particular processes and η is the overpotential. At the potential E_r, the system is at equilibrium ($\eta = 0$) and the rates of the forward and reverse reactions are hence equal. Hence, i_c (cathodic current density) = i_a (anodic current density), and the net current density is zero. The velocity of the forward or reverse reaction is then expressed as the exchange current density i_0, where

$$i_a = i_c = i_0 = zF(C_\mathrm{R})_s \frac{kT}{h} \exp\left(-\frac{\Delta G^{\circ\ddagger}}{RT}\right) \exp\left(-\frac{\beta FE_r}{RT}\right) \tag{7}$$

The general rate expression at *any* potential E can then be conveniently written in terms of η and E_r as

$$i = zF(C_\mathrm{R})_s \bar{k}' \exp\left(-\frac{\Delta G^{\circ}}{RT}\right) \exp\left(-\frac{\beta FE_r}{RT}\right) \exp\left(\frac{\beta F\eta}{RT}\right) \tag{8}$$

and therefore

$$i = i_0 \exp\left(\frac{\beta F\eta}{RT}\right) \tag{9}$$

The logarithmic form of Eq. (9) is

$$\eta = \frac{RT}{\beta F} \ln i - \frac{RT}{\beta F} \ln i_0 \tag{10}$$

which is equivalent to the familiar relation due to Tafel, $\eta = a + b \ln i$, where the first term a is a constant, characteristic of the kinetics of the reaction at $E = E_r$. The slope of the relation between η and $\ln i$ is usually written as $b = RT/\alpha F$, the so-called Tafel slope, where α is referred to as the transfer coefficient. The term *symmetry coefficient* is usually reserved for β to distinguish it from the transfer coefficient since β refers to the energy barrier for electron transfer. $\alpha \equiv \beta$ in the simple case of an electron-transfer-controlled reaction. In favorable cases, the Tafel slope can be a diagnostic aid in elucidation of the mechanism of an electrode reaction, but for most organic reactions, full chemical characterization is usually a prerequisite for further electrochemical investigations.

As E approaches E_r, the reverse reaction becomes increasingly important, and it is then necessary to write the *net* current density as the difference between the cathodic and anodic current densities, so that

$$i = i_c - i_a \tag{11}$$

Also, if α is the transfer coefficient for the forward process, then $(1 - \alpha)$ is the value of the transfer coefficient for the reverse reaction, since, at equilibrium $i_c = i_a$ and the equilibrium condition corresponding to Nernst's relation must be independent of any kinetic parameters such as α. Then since

$$i_c = i_0 \exp\left(-\frac{\alpha FE}{RT}\right) \tag{12}$$

$$i_a = i_0 \exp\left[\frac{(1-\alpha)FE}{RT}\right] \tag{13}$$

when $\alpha = 0.5$, the current expression takes the convenient form

$$i = i_0 \exp\left(-\frac{FE}{2RT}\right) - \exp\left(\frac{FE}{2RT}\right)$$

or

$$i = 2i_0 \sinh\left(-\frac{FE}{2RT}\right) \tag{14}$$

which represents the whole of the current–potential curve at low or high overpotentials. An alternative means of treating results when the back-reaction is significant is to plot $\ln i$ *vs.* $\eta + \ln[1 - \exp(-\eta F/RT)]$.

4.3. Treatments for More Complex Electrochemical Reactions

In more complex organic reactions involving several charge transfer or chemical steps in the reaction sequence, it is often possible for one step to have a smaller rate constant than another. If this situation applies to the second or subsequent steps in a sequence, then the steps prior to the rate-controlling step can usually be regarded as almost at equilibrium, and the surface concentrations of intermediates, θ, can then be expressed as a function of potential, so that there are *two* parts of the rate equation where potential-dependent terms are involved.

The following example may be considered in order to illustrate the principles involved. Acetophenone reduction in acid medium follows the pathway

$$\phi\mathrm{CO{\cdot}CH_3} + \mathrm{H^+} \underset{k_{-a}}{\overset{k_a}{\rightleftharpoons}} \phi\mathrm{{\cdot}COH^+{\cdot}CH_3} \tag{a}$$

$$\phi\mathrm{{\cdot}COH^+{\cdot}CH_3} + \mathrm{e} \underset{k_{-b}}{\overset{k_b}{\rightleftharpoons}} \phi\mathrm{{\cdot}\dot{C}OH{\cdot}CH_3} \tag{b}$$

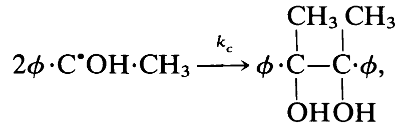

$$2\phi\cdot C^{\bullet}OH\cdot CH_3 \xrightarrow{k_c} \phi\cdot\underset{OH}{\overset{CH_3}{C}}-\underset{OH}{\overset{CH_3}{C}}\cdot\phi, \quad \text{the pinacol} \qquad \text{(c)}$$

In neutral or basic medium, an alternative pathway exists, leading to formation of the alchohol

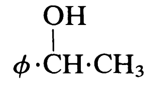

$$\phi\cdot\overset{OH}{C}H\cdot CH_3$$

through a step following (b), viz.,

$$\phi\cdot CH^{\bullet}OH\cdot CH_3 + e \rightarrow \phi C^{-}OH\cdot CH_3 \qquad \text{(d)}$$

$$\phi\cdot C^{-}OH\cdot CH_3 + H_2O \rightleftharpoons \phi\cdot CHOH\cdot CH_3 + OH^{-} \qquad \text{(e)}$$

Except at high or medium pH, step (a) is a rapid protonation equilibrium. If, however, step (c) were rate controlling, i.e., if the rate constants were such that $k_c \ll k_b$, k_{-b} or k_a, then step (b), as well as step (a), would be almost at equilibrium (this occurs, e.g., in some polarographically reversible systems; see Section 8.2). Under these conditions, the surface coverage† θ_K of the ketyl radical $\phi\cdot\dot{C}OH\cdot CH_2$ ("K") at the electrode surface could be represented approximately by

$$\theta_K = K_b C C_{\mathrm{H}^+} \exp[-EF/RT] \qquad (15)$$

where K_b is a quasi-equilibrium constant for step (b) when (c) is rate controlling, C is the concentration of acetophenone reactant in step (a), and C_{H^-} is the proton concentration in solution (neglecting here any effects due to the double layer). The velocity of the rate-determining step (c) will involve the square of θ_K, i.e., the net current density will be given by

$$i_c = 2Fk_c(\theta_K)^2 \qquad (16)$$

since k_c is the rate constant of the chemical step (c) and for each mole of pinacol formed, *two* faradays of charge (2 electrons per molecule) must be passed. Then, substituting for θ_K from Eq. (15), the overall rate of the reaction is given by

$$i_c = 2Fk_{cb}^2 C^2 C_{\mathrm{H}^+}^2 \exp(-2EF/RT) \qquad (17)$$

from which a logarithmic current–potential relation results with a slope

$$\frac{dE}{d\ln i_c} = -\frac{RT}{2F} \qquad (18)$$

(E is usually taken negative for cathodic potentials). Had the electron transfer step (b) been rate determining, the slope of the logarithmic current–potential relation would have been simply

---

† Here it is assumed that the recombination of ketyl radicals occurs as a surface reaction. In some work, homogeneous recombination in solution near the electrode has been assumed and leads to a different final result.[45]

$$\frac{dE}{d\ln i_b} = -\frac{RT}{\beta F} = -\frac{-2RT}{F} \tag{19}$$

with β taken as 0.5 (see above). Hence, a distinction between the mechanisms of reduction proceeding with step (b) or with step (c) rate determining can, in principle, be made by measurement of Tafel slopes of the steady state current–potential relations.

In practice, there are often complications in this kind of approach, e.g., the relation (15) is more complex for intermediate surface coverages, and displacement of adsorbed solvent molecules in step (b) requires a more sophisticated treatment than that given above. It is of interest to note that if the pathway were (a), (b), (d), (e) giving the alcohol, and the *second* electron transfer step was rate determining [step (d)], the slope $dE/d\ln i_\alpha$ would be $-RT/(1+\beta)F$, since another electron transfer step follows the prior one (b) at equilibrium.

The numerical values of these slopes, if the current is plotted on a *decadic* logarithm scale, are $2.3RT/\beta F(\beta = 0.5) = 118$ mV, $2.3RT/(1+\beta)F = 39$ mV, and $2.3RT/2F = 29.5$ at 298 K.

We have seen that the Tafel slope is usually written for the general case as, $b = RT/\alpha F$, so that α in the above case will be as follows:

rate-controlling step:	(b)	(d)	(c)
slope $dE/d\ln i$:	$RT/\beta F$	$RT/(1+\beta)F$	$RT/2F$
value of α:	$1/2(\equiv\beta)$	$3/2$	2

Only for single electron transfer steps is $\alpha = \beta$, i.e., $b = RT/\beta F$.

Other types of situations can arise in reductions where a halide ion is displaced, e.g.,

$$RX + e \rightarrow R^{\bullet} + X^{-}$$

$$R^{\bullet} + e \rightarrow R^{-}$$

$$R^{-} + H^{+} \rightarrow RH$$

or, by H abstraction between $R^{\bullet}$ radicals or by recombination, the following steps giving different products can arise:

$$2R^{\bullet} \rightarrow R_2, \qquad 2R^{\bullet} \rightarrow R' + RH$$

where R′ is an olefin.

For processes in which an adsorbed intermediate [see Eq. (15) and below] is formed as a result of electron transfer, the rate equation for a discharge must take into account the fraction of unit surface occupied in the steady state. Since discharge can only occur at a vacant surface site, in the simplest case the current is then

$$i = \bar{k}'(1-\theta_j)C_R \exp(-\beta EF/RT) \tag{20}$$

where θ is that fraction of the surface area covered by the adsorbed intermediate. If the organic reagent, R, is also adsorbed in the initial state of the reaction, as will be commonly the case, the free space available on the surface will be, fractionally, $1 - \theta_j = \theta_R$. However, in many cases, the intermediate j will arise directly by electron transfer from R, so that the space requirement for j will usually be quite similar to that for R, so that the current density i in Eq. (20) will contain the term θ_R directly rather than $1 - \theta_j$.

Usually when adsorbed species are involved in an electrochemical reaction, there is an extra exponential effect on the rate constant as well as a surface blocking effect, i.e., Eq. (20) takes the related form

$$i = \bar{k}' \exp(-\beta r \theta_j) \cdot (1 - \theta_j) C_R \exp\left(-\frac{\beta FE}{RT}\right) \tag{21}$$

where r is a factor expressing the change of energy of chemisorption of the intermediate with coverage.(46) The latter quantity enters into the kinetics, since the $\Delta G^{\circ\ddagger}$ in the $\bar{k}'$ term is determined in part by the energy of chemisorption of the intermediate produced as a result of electron transfer, and the chemisorption energy depends on coverage. One of the best and simplest examples of this effect arises with the hydrogen evolution reaction, where the first step is

$$H_3O^+ + M \rightarrow MH_{ads} + H_2O$$

at a site on a metal M. In this case, the adsorbed H intermediate can be electrochemically and optically detected by means of reflectivity changes. In the case of organic electrode reactions, examples are less well characterized, but in the Kolbe reaction at noble metals, the first step is

$$CH_3COO^- + M \rightarrow CH_3COO^\bullet/M + e$$

where the acetoxyl radical intermediate is believed(5) to be chemisorbed and to undergo subsequent decarboxylation leading to evolution of CO_2 and C_2H_6 after $CH_3^\bullet$ radical recombination. Alkyl radicals are also involved in ketone reduction at Pt and Ni.

The energy of activation for the carboxylate discharge step will tend to be lower the stronger is the intermediate acetoxyl radical chemisorbed to the surface, but the energy of the chemisorption process itself will usually tend to become smaller with increasing coverage by the radical due to heterogeneity and interaction effects at the surface, which determine the magnitude of r in Eq. (18b). These effects are particularly important in the more "electrocatalytic" types of organic electrochemical reactions(30) that can be carried out at the noble catalytic and adsorptive metals, e.g., Pt, Rh, Ir, Ni.

Examples of the latter types of process are where simple molecules, such as HCOOH, CH_3OH, C_3H_8, become dissociatively chemisorbed at Pt and the molecular fragments then become oxidized in coupled, succeeding electrochemical reactions steps; thus, for CH_3OH, steps such as

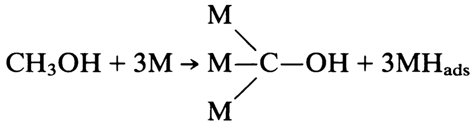

$$CH_3OH + 3M \rightarrow (M)_3C{-}OH + 3MH_{ads}$$

$$3MH_{ads} \rightarrow 3H^+ + 3e$$

and

$$(3M)C{-}OH + H_2O \rightarrow CO_2 + 3H^+ + 3e$$

occur in a complex reaction sequence of coupled electrochemical steps on the surface. Chemisorption of intermediates arising from the methanol can, in this case, again be experimentally demonstrated. In these types of reaction, charge transfer steps often *follow* heterogeneous (dissociation) steps, while in other types of reactions discussed above, the chemical steps follow the production of radicals or radical ions by the electron transfer process (see the classification of reaction types, e, c, etc.; see Section 3). Consequently, the rates of such electrocatalytic processes depend, not only on potential, but on the rate of the dissociative chemisorption step, and hence, on the coverage, at a particular potential, of the electroactive intermediates. In some cases, limiting (i.e., potential–independent) currents can arise corresponding to the rate of the *chemical* step at the electrode surface producing the adsorbed intermediates, which are subsequently desorbed in one or more following electron transfer steps. Such reactions are usually very complex and Tafel slope analysis is, in most cases, inadequate for a full elucidation of the mechanism and role of intermediates. For example, self-inhibition and passivation processes often set in as the potential is changed, e.g., with oxidation of methanol and formic acid at noble metals, owing to build-up of coverage by adsorbed intermediates on the electrode and by surface oxidation of the metal at more anodic potentials (>0.8 V E_H at Pt, Rh).

The self-inhibition effects which often arise in electroorganic experiments due to coverage of the electrode by (a) adsorbed intermediates, (b) reaction products, and/or (c) by side-reaction products such as adsorbed polymers, are usually a source of difficulty both in kinetic and preparative experiments, particularly in controlled potential experiments where the current tends to fall with time during the run. If this effect is a basic one arising from inhibition of the reaction by its own intermediates, little can be done to improve the situation except by relatively radical changes of experimental conditions such as elevation of the temperature or change of the electrode material (this, however, may also result in change of the reaction pathway). Increasing the potential in such cases often results in a *decrease* of current or even a change of reaction pathway. If the effect is due to (b) or (c), some alleviation of difficulties may be achieved by change of solvent or by continuously scraping the electrode (e.g., a cylindrical one) to maintain a clean and active surface.

For example, addition of pyridine facilitates Kolbe preparations by diminishing surface blocking by polymeric byproducts which arise in some aromatic systems.

4.4. Dependence of Rates of Organic Electrode Reactions on the Electrode Material

An important characteristic of most electrode reactions, particularly those involving organic substances, is the dependence of their rates (at a given measured potential) on the electrode material. However, it is possible to show that if the reaction involves *only* electron transfer or electron transfer followed by further steps *in solution*, as often assumed in polarography, then the kinetics experimentally investigated at constant potential must be independent of the metal. Since this is not a well understood effect in the electro-organic field, we present an examination of its origin; the conclusions are of great importance for organic electrode reactions that may involve adsorbed species, and for the choice of electrode materials.

Consider a reduction reaction:

$$\mathrm{O} + ne \rightarrow \mathrm{R}$$

in which adsorbed species are *not* involved, proceeding at two metals M_1 and M_2 for which the electronic work functions (energies for extraction of an electron from the metal) are Φ_1 and Φ_2, respectively. Let $\Phi_2 > \Phi_1$ and consider for simplicity $n = 1$. Then the energy of activation for the above reaction at metal M_2 is *greater* than that at M_1 by the quantity $\beta(\Phi_2 - \Phi_1)$ at a given metal–solution potential difference (p.d.) at the interface of M_1 or M_2 (the latter p.d. is not, however, a measurable experimental quantity), since electrons are more difficult to remove from M_2 than from M_1 ($\Phi_2 > \Phi_1$ was assumed). The rate equations at M_1 and M_2 are:

$$i_1 = nFk_1C_0 \exp\left[-\frac{\Delta G_1^\circ}{RT}\right] \exp\left[-\frac{\beta EF}{RT}\right] \tag{22}$$

or, referred to the metal solution p.d. $E_{r,1}$ at M_1 when the above reaction is at equilibrium:

$$i_1 = nF\frac{kT}{h}C_0 \exp\left[-\frac{\Delta G_1^{\circ\ddagger}}{RT}\right] \exp\left[-\frac{\beta E_{r,1}F}{RT}\right] \cdot \exp\left[-\frac{\beta\eta F}{RT}\right] \tag{23}$$

where η is again the overpotential [see Eqs. (6) and (8)]. For metal 2,

$$i_2 = nF\frac{kT}{h}C_0 \exp\left[-\frac{\Delta G_2^{\circ\ddagger}}{RT}\right] \cdot \exp\left[-\frac{\beta E_{r,2}F}{RT}\right] \cdot \exp\left[-\frac{\beta\eta F}{RT}\right] \tag{24}$$

Now $\Delta G_2^{\circ\ddagger}$ differs from $\Delta G_1^{\circ\ddagger}$ by $\beta(\Phi_2 - \Phi_1)$ as shown above but the single metal–solution p.d.'s set up by the reaction proceeding reversibly at M_1 and M_2 also differ by $\Phi_2 - \Phi_1$; on the international convention of signs and directions of polarity, the reaction $O + e \rightarrow R$ proceeding at M_2 will tend to establish a more *negative* potential† of the metal phase than when it proceeds at M_1 if $\Phi_2 > \Phi_1$ since metal M_2 has greater electron affinity than M_1. Hence, if the kinetics are studied at a given *measured* potential using M_1 and M_2 also as reference electrodes with $O + e \rightleftarrows R$ as the reference electrode reversible reaction (this can, for example, be done with studies on the H_2 evolution reaction, e.g., at Pt or Rh), then this is equivalent to examining the current densities i_1 and i_2 at constant overpotential η. $E_{r,2}$ will be more negative than $E_{r,1}$, but this rate-increasing effect will just be counterbalanced by the difference in $\Delta G^{o\ddagger}$ equal to $\beta(\Phi_2 - \Phi_1)$. Hence, $i_2 = i_1$ at a given measured overpotential so that the *rates are independent of the metal.*

A common experimental situation is where a given reference electrode is used in conjunction with various metals examined in the kinetic study of an organic electrode reaction. It may be then asked whether the rates would be different using this constant reference electrode metal (e.g., M_1 or Hg in a calomel electrode) for evaluation of the potential dependence of currents i_1 and i_2 in the kinetic experiments carried out at M_1 and M_2 working electrodes. The systems are now

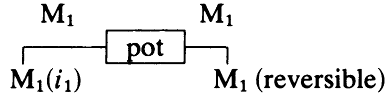

and

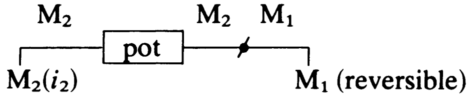

and we are again considering constant overall potential difference in the cell as *measured* on the potentiometer (no other potential differences at interfaces in these circuits are susceptible to experimental measurement). Again the free energy of activation of the reaction at M_1 will tend to be different from that at M_2. Although the reversible potential at the reference electrode will remain the same for the two cases, since the metal of the reference electrode is kept the same, a contact potential between M_1 and M_2 has now been introduced in the external circuit (marked $\underline{M_2 \nmid M_1}$). At such a contact there is a tendency for electron flow from one metal to the other until the electrochemical potentials are equal. An electric p.d. is thus set up equal to the work function difference $\Phi_2 - \Phi_1$, with the metal having the higher work function taking the negative sign. Hence, the tendency for the reaction $O + e \rightarrow R$ to occur at different rates at M_1 and M_2 electrodes at a given measured potential is exactly compensated by the change of the contact p.d. which is included in the measured p.d. when the same reference electrode is used in the two experiments with different working electrodes M_1 and M_2. Thus, again, at constant experimentally measured potential difference in a cell, the rates of a pure electron transfer process should be independent of the metal.

---

† This arises because a larger work function Φ, corresponding to a greater electron affinity of the metal (M_2 in this case), will tend to drive the equilibrium $O + e \rightleftarrows R$ more to the left-hand side at M_2 than M_1 and thus "accumulate" electrons in the metal phase, establishing the metal M_2 at a more negative potential with respect to the solution than in the case of M_1.

The fact that, experimentally, the rates of many reactions, at constant potential, *do* depend on the electrode metal must therefore indicate involvement of adsorption of (a) the reactant, (b) the product or (c) intermediates formed in the electron transfer or subsequent step; adsorption of all three types of species is often involved and will, of course, give rise to a metal-dependent factor in the kinetics, e.g., due to local concentration of reactant at the electrode surface, through changes of the energy of activation of various steps or through blocking and interaction effects among the species adsorbed at the electrode interface. Simple inorganic redox reactions, e.g., Fe^{2+}/Fe^{3+}, $[Fe(CN)_6]^{4-}/[Fe(CN)_6]^{3-}$, are some of the few reactions the kinetics of which are (almost) independent of the metal substrate, indicating absence of adsorption and interaction effects. The kinetics of organic reactions commonly depend on the metal, so that adsorption effects are usually of great importance. With suitable high-area electrode materials or by means of sensitive methods such as *in situ* reflectivity, adsorption of many organic substances may be directly measured. Generally speaking, more attention to the role of adsorption in electro-organic reaction studies than has hitherto been given, is desirable, although this factor has been well recognized by workers of the Russian school for many years.(10)

A brief account of treatments of adsorption at electrodes, particularly as they involve organic molecules, will be given in the next section.

5. Reaction Yields in Relation to Coulombic Efficiency and Conditions of Electrolysis

5.1. Current Efficiencies and Coulombic Yields

In all organic electrochemical reactions, analysis and characterization of the product or products are prerequisites for determination of the mechanism. This should normally include characterization of by-products since in favorable cases the type of by-products formed may give an indication of the reaction mechanism and/or the nature of any intermediates involved. In electrochemical processes, not only is the chemical yield of product(s) significant but the coulombic yield, i.e., the Faradaic efficiency with respect to the number of electrons per mole of product formed, is of interest, especially in commercial operations.

The yield of various products may also depend on electrode potential, so that *potentiostatic* preparative conditions are often desirable. Two cases may be exemplified here: the reduction of nitrobenzene which, depending on the potential, may lead to the formation of nitrosobenzene, phenylhydroxylamine, and eventually aniline(14); also in the case of anodic oxidation of carboxylic acids RCOOH, and Kolbe product R_2 ($+2CO_2$) is commonly formed at Pt or Ir at high potentials(5) (>2.2 V E_H), while other products derived from oxidation of the R function are generated at lower potentials (0.8–1.5 V E_H), particularly if the electrode is a catalytically active one, such as platinized platinum.

In cases where more than one product may be formed, particuarly when the relative yield is potential dependent, potentiostatic electrolysis is particularly desirable. If a controlled constant current electrolysis is carried out in such a case, the potential will generally increase with time as the reactant is consumed, so that eventually the diffusion-limited current is reached, which itself eventually becomes smaller and smaller and the remaining fraction of the current is then passed by decomposition of the solvent or supporting electrolyte, usually with evolution of hydrogen (cathodic processes) or oxygen (anodically) in the case of an aqueous medium.

In noncatalytic types of reaction, the potentials at which one reaction product or another arise (in cases where parallel or successive two- or multipathway reactions are involved), may sometimes be evaluated conveniently by means of polarography (see Section 8).

In any parallel reactions, the relative yields of products will depend on the relative values of the component currents passing at a given potential.(47) Since for different processes, the parameters characterizing the current/potential relations at a given metal are usually different, the relative yields of products in parallel reactions will be potential dependent if the Tafel slopes for the two or more electrochemical reactions are different. Adsorption effects, e.g., the effect of products of one reaction on the course of the parallel reaction, may alter the Tafel slopes as the current is varied so that complex effects arise.

For a dual parallel pathway 1 and 2, the total current I may be written

$$I = I_1 + I_2 \tag{25}$$

$$= I_{0,1} \exp[\alpha_1 \eta_1 F/RT] + I_{0,2} \exp[\alpha_2 \eta_2 F/RT] \tag{26}$$

where α_1, α_2 are the transfer coefficients determining the Tafel slope b ($=RT/\alpha F$), η_1 and η_2 are the overpotentials for each reaction at a given electrode potential V ($\eta_1 = V - V_{1,r}$; $\eta_2 = V - V_{2,r}$, where $V_{1,r}$ and $V_{2,r}$ are the respective reversible potentials for the alternative processes) and I_0 terms are the respective exchange currents. Obviously various cases can arise depending on (a) the relative values of I_0, (b) the relative values of α, and (c) the involvement of coverage effects. The latter may be specified by introducing into the terms for I_1 and I_2 coverage terms of the form

$$I_1 = I'_{0,1}(1 - \theta_{1,v}) \exp[\alpha \eta_1 F/RT] \tag{27}$$

$$I_2 = I'_{0,2}(1 - \theta_{2,v}) \exp[\alpha \eta_2 F/RT] \tag{28}$$

i.e., I_1 and I_2 may depend on the free surface $1 - \theta_{1,v}$ or $1 - \theta_{2,v}$, which can change with potential due to potential-dependent adsorption of the product and/or intermediates of the parallel processes. Various cases can arise.

In the absence of adsorption effects, with $I_{0,1} > I_{0,2}$ and $\alpha_1 > \alpha_2$, the relative yield of products measured by I_1/I_2 from the pathways 1 and 2 will always increase with increasing η (Figure 4a).

If $I_{0,2} > I_{0,1}$ (Figure 4b) but α_1 is still $> \alpha_2$, the relative yield $I_1/I_2 < 1$ at low η becomes unity at a characteristic value of η and eventually $I_1/I_2 > 1$ (as in Figure 4b). Related cases arise obviously if $I_{0,2} < I_{0,1}$ and $\alpha_2 > \alpha_1$.

In cases where diffusion limitation of the main reaction (say, 1) can arise but process 2 is decomposition of the supporting solution, conditions are usually chosen such that $I < I_{1,\text{lim}}$ but $I > I_2$ over the experimental range of potentials. For total currents $\geq I_{1,\text{lim}}$, obviously an increasing fraction of the

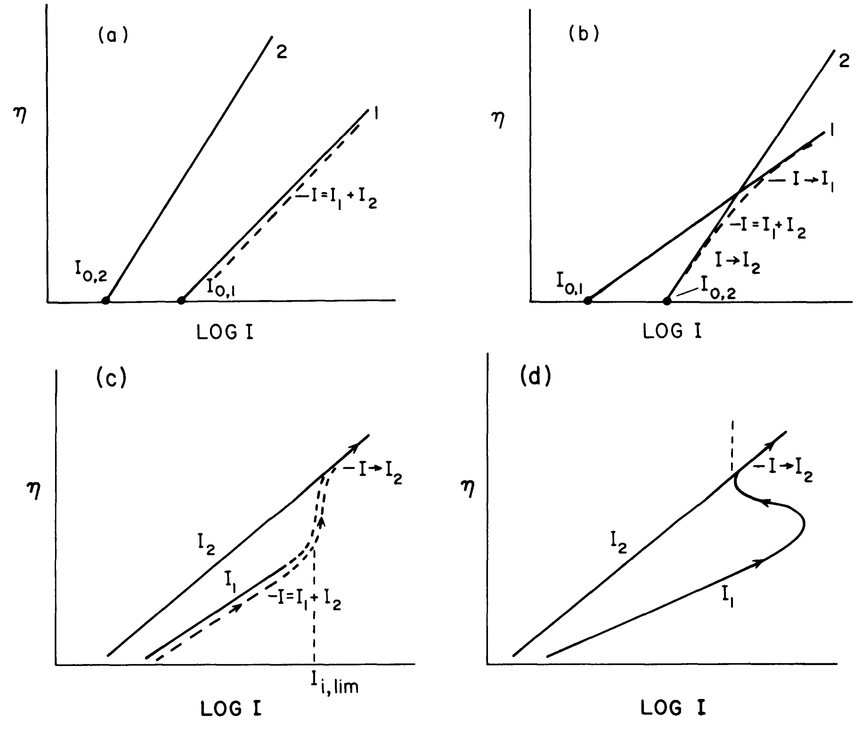

Figure 4. Current–potential relations for parallel processes determining coulombic yields at various overpotentials, η. (a) Separated $\log I$–η lines giving increasing yield of 1 with increasing η. I is total current, I_1, I_2 partial currents for processes 1 and 2. $I_{0,1}$ and $I_{0,2}$ are the respective exchange currents (note: the reversible potentials for the two processes may not, in the general case, be identical). (b) Crossing $\log I$–η lines for two processes. Predominant yield of 2 will be replaced by predominant yield of 1 at higher η. Relative yields will be strongly potential dependent. (c) $\text{Log}\, I$–η relations for two processes, one of which (1) exhibits a diffusion limited current. Main yield will then pass from 1 to 2 with increasing η. (d) $\text{Log}\, I$–η relations for two processes, one of which (1) suffers an inhibition at a critical current or potential. Predominant production of 1 ($I_1 > I_2$) then passes over to predominant production of 2 at high η.

current is passed by the side reaction of background electrolyte or solvent decomposition as potential is increased. This case is illustrated in Figure 4c. The course of the current–potential curve is then that indicated by the line with arrows in this figure. The lower dashed line is the total current I which is obviously $>I_1$ or I_2 at all potentials. In preparative and mechanistic work, it is, of course, desirable to maintain the potential in the region where $I_1(=I) \gg I_2$. When $I > I_{1,\text{lim}}$, the side reaction increasingly participates with increasing potential. Potentiostatic relative yields are found from the intersections of constant potential lines with the I–V relations.

If the individual Tafel relations are known for the two or more pathways in the reaction, a general equation can be derived for the respective current efficiencies for the production of each of the products as a function of the electrode potential. However, interaction effects between the two processes, e.g., because of competitive adsorption among the reactant, intermediate, and product species, must usually be taken into account, making an *a priori* evaluation of current efficiencies difficult in all but the simplest cases.

A number of reactions (usually, but not exclusively anodic ones) show self-passivation effects so that linear relations of Figures 4a or 4b are no longer an adequate basis for representation of the relative yields. This type of case is illustrated in Figure 4d.

5.2. Significance of Controlled Potential Electrolysis

In many descriptions of electrochemical preparations of organic substances, only the overall current and voltage applied across the cell have been specified. It must be emphasized that this information is generally inadequate for a proper electrochemical specification of the experimental conditions and a characterization of the reaction mechanism. Under constant *current* conditions, as consumption of the reactant occurs, the potential normally becomes increased (greater polarization) until eventually some new electrode process becomes predominant (see Section 5.1). This may either be decomposition of the solvent or supporting electrolyte or, in some cases, a further reaction with the substrate involved in the electroorganic preparation. In the latter case, it is clear that the preparation will yield more than one principal product. A classical case, first investigated by Haber,(14) is the electroreduction of nitrobenzene referred to above and also the Kolbe reaction.(5)

It is evident that controlled potential electrolysis is, in principle, the preferred technique. In large-scale preparations, potentiostatic electrolysis with wholly electronic equipment may be economically unfeasible, but electromechanical systems may be constructed more easily.

From the electrode-kinetic point of view (Section 4), operation of electrochemical reactions at constant potential enables the rates to be treated exactly like rates of other heterogeneous processes with, e.g., corresponding evaluation of reaction orders leading to mechanism elucidation (see Section 6.3). This approach can be applied at various selected, controlled potentials.

For preparative purposes it is usually not necessary to control the potential more closely than 20–100 mV, depending on the type of reaction and the possibility of parallel reaction pathways (Section 5.1).

Various potentiostats are available commercially, the best known being constructed by the following companies:

U.K.	Chemical Electronics, Ltd., Durham, England.
W. Germany and USA	"Wenking" Potentiostats supplied by Gerhard Bank, Göttingen.
France and USA	"Tacussel" Potentiostats, Tacussel Co., Paris.
USA	Continental Oil Company, "Anotrol" preparative potentiostat.
USA	"P.A.R." Princeton Applied Research Corp., Princeton, New Jersey (with "logarithmic" current response plug-ins or digital coulometer plug-ins and built-in *IR* compensation arrangement).
USA	Stonehart Associates Corp., New Haven, Connecticut, with built-in *IR* compensation.

Higher-power potentiostats have been described by Allen(50) and a lower-power potentiostat of sophisticated design has been described by Brown(51) for transient processes. A high-power system has also recently been designed and constructed by this author.

A quasipotentiostatic method, employed in following the oxidation of formic acid, was first used by Muller.(48) A true potentiostatic device was not, however, at that time available; potentiostasis was effectively achieved by using a low-impedance circuit with a relatively unpolarizable counterelectrode (cathode) so that changes of cell voltage were approximately equal to changes of the p.d. at the working metal electrode/solution interface.

The first true potentiostatic arrangement was that developed by Hickling(49) but the value of "potentiostatic" experiments, particularly in studies of relaxation and reversibility in electrode kinetics by application of ramp and step functions of potential with respect to time, were not fully appreciated until the post-1950 period. From the 1960s onward, many applications were made to organic electrode processes of procedures based on the use of potentiostats(52) operating in a dynamical mode, programmed by a function generator, especially in a repetitive way in the method known as cyclic voltammetry. The latter technique has proved particularly valuable in investigations of the reversibility or otherwise of many electro-organic reactions and its relation to the role and rates of follow-up reactions succeeding electron transfer steps.

5.3. Coulometry

The fundamental principle of coulometry originates in Faraday's laws, which relate the quantity of a substance transformed in an electrolysis to the quantity Q coulombs of electricity that has been passed, viz.,

$$W = \frac{MQ}{9.648z} \times 10^{-4} \text{ grams} \tag{29}$$

where W (g) is the weight of substance oxidized or reduced, M is the atomic or molecular weight of the electroactive species and z has its usual significance. Coulometry is therefore a useful technique in electroorganic chemistry ($W \propto Q$) provided (i) that only one process is occurring at the electrode, i.e., the current efficiency of the reaction is virtually 100%, and (ii) that the reaction is carried out to virtual completion.

High efficiency in an electrode process will be mainly dependent upon the absence of side reactions occurring simultaneously with the desired reaction at the electrode surface. Various side reactions can often be distinguished(53) and may involve the solvent, or the electrode itself, or the product(s) of the electrolysis or possibly the supporting electrolyte. Many polarographic reactions involving organic substances have been carried out in water or in a mixture of water and an organic solvent but protic solvents such as water, methanol, ethanol, acetic acid, etc., are decomposed cathodically to evolve hydrogen; hence the potential at which the current attributable to decomposition of the solvent becomes significant (say, $\geq 10\%$ of the total current), provides a practical limitation to the range of potentials available for the efficient preparative or polarographic reductions of the other electroactive species. Fortunately, H_2 evolution is a reaction which at Hg is relatively slow, i.e., a high overpotential is required for significant solvent decomposition. This overpotential may be conveniently increased by addition of tetraalkylammonium salts, thus suppressing H_2 evolution and improving coulombic yields in reduction experiments. This is important in electrochemical organic preparations and for electric power economy.

Mercury electrodes, however, cannot be used in many, if any, anodic (oxidation) processes since the metal itself is readily oxidized. Anodic polarographic or preparative studies are therefore conducted at platinum, gold, or graphite electrodes, where the side reactions involving the oxidation of the electrode do not become important at low anodic potentials.

Experimentally, coulometry may be carried out by controlling either the potential of the working electrode or the electrolysis current itself. In a coulometric experiment under conditions of controlled potential, the current decreases continually since the concentration of the electroactive substances decreases as the electrolysis proceeds (Section 5.1). The condition $I = 0$, $(C_{\text{ox}})_b = 0$, is never actually reached and normally a coulometric experiment is considered as complete when the current has become very small when compared with the initial current.(53)

The current availability of digital coulometers from instrument suppliers such as Wenking or P.A.R. makes coulometric monitoring of organic electrode reactions much more convenient than has hitherto been the case. Also computer data acquisition of coulometric information can readily be arranged.

The principles and applications of coulometry under conditions of controlled potential or controlled current have been discussed by Delahay(54) and by Charlot *et al.*(53)

5.4. Preparative Methods

An obvious consequence of coulometric studies of electro-organic reactions is that the product(s) of the electrode reaction are also obtained. Many years ago Haber(14) pointed out that the degree of completion of an electrochemical process is determined by the potential of the electrode at which this process occurs. The importance of control of the potential (Section 5.2) is a factor which unfortunately has been ignored in many electro-organic syntheses. This situation becomes all the more anomalous when it is realized that a number of chemical reductions are, in fact, electrochemical in nature, and proceed effectively under conditions of controlled potential, e.g., the Clemmensen reduction (Zn/Hg) and reductions with Na/Hg or Mg/Hg. Here a mixed potential is established which corresponds to both the corrosion of the amalgam and the reduction of the organic compound (itself adsorbed at the surface of the amalgam) occurring at equal rates at a common, almost constant potential.

It would therefore seem logical to directly control the potential of the working electrode, and it is likely that well-known electrolytic preparations in organic chemistry could be improved with respect to product purity by a more systematic application of controlled-potential electrolysis. However, potentiostatic reductions can be slow, and this is one reason for the preferred use of a large current, even if controlled, in many electro-organic syntheses.

Controlled-potential electrolysis yields a product which may be identified *in situ*, e.g., spectrometrically, or after isolation from the solution. In the former case, both stable and unstable products may be studied, whereas isolation is usually limited to stable compounds. The methods used for identification of the product will also depend upon the stability of that product. Electron spin resonance, ultraviolet spectrophotometry, and cyclic voltammetry have proved useful techniques for the identification of unstable (radical) species. The presence of water in the electrolyzed solution usually prevents the use of *in situ* infrared (but not Raman) spectrophotometric analysis, and the use of such powerful techniques as nuclear magnetic resonance and mass spectrometry is also excluded unless the product can be isolated in a reasonably pure state.

Electrolysis may be carried out continuously, i.e., the selected potential is applied to the working electrode for the duration of the reaction, or an intermittent procedure may be used in which the potential is periodically changed or interrupted so that electrolysis ceases. The use of a dropping mercury electrode is not desirable in preparative methods since the low currents which can be passed provide only very low rates of formation of product. It is therefore preferable to use a hanging drop mercury electrode or preferably a mercury pool electrode having a large surface area.

The use of preparative methods in studies of organic electrochemical reactions has been reviewed(55) and examples of the identification of both unstable and stable intermediates and products have been presented. This review includes some interesting observations upon the fact, referred to above, that different products may be obtained from a given reaction if it is carried out at a mercury pool rather that a dropping mercury electrode.

6. Role of Adsorption in Electro-Organic Reactions

As was mentioned earlier, surprisingly little attention has been paid to the role of adsorption of organic substances in electro-organic chemistry, although clear indications of its significance have existed for some years, especially in the Russian literature (Frumkin, Bagotzky, Vassil'ev, Damaskin, and other). Here we shall outline some of the treatments that have been given for adsorption of neutral molecules at electrodes, and the role of adsorption in the kinetics of organic electrode processes.

6.1. Factors in Adsorption and the Formulation of Isotherms

An electrode in solution presents an interface for electron transfer and other coupled reactions. The electron transfer event is hence almost certainly heterogeneous for most organic oxidations and reductions and in the case of oxidation of hydrocarbons, formic acid, formaldehyde, and methanol, for example, direct electrochemical evidence exists for chemisorption of C-containing intermediates. Much thermodynamic evidence from capacity, surface tension and radiotracer experiments (see below) exists which enables the adsorption of organic substances at electrode/solution interfaces involving Hg, amalgams, and Pt to be characterized. In most cases, the adsorption is significant in the sense that in the concentration range 10^{-3}–10^{-1} m, fractional coverages θ of the electrode surface by the organic reactant can vary from ~10% to almost 100%. For large aromatic or heterocyclic molecules such as anthracene or acridine, significant adsorption arises already at 10^{-6}–10^{-5} m concentrations. Adsorption is hence usually an important factor in electroorganic chemistry and has often been neglected in considering reaction mechanisms and possible pathways, e.g., in polarography. The extent of adsorption corresponding to the standard free energy of adsorption and solution concentration is often related to the solubility of the reactant in the solvent concerned: smaller solubilities, of course, tend to promote stronger adsorption.

The main interactions leading to adsorption at electrode interfaces are the following:

(i) Hydrophobic or lyophobic interactions which lead to expulsion of the reactant from the solution, especially when it is aqueous, at the electrode interface even though little or no specific interaction with the metal itself is involved;

(ii) Field–dipole interactions of the electrode double layer with functional groups on the organic reactant in relation to corresponding interactions with solvent molecules in an equal volume of the interphase; also image potential effects with polar groups;

(iii) Specific or chemisorption of certain electron and atomic groups with the electrode metal surface, e.g., >S or ⩾SH or ⩾N at Hg, π-orbital groupings at electron-deficient (anode) surfaces;

(iv) Dissociative chemisorption at *d*-band metals such as Ni, Pt, Pd, etc., where formation of adsorbed alkyl or alkylene radicals arises with coadsorption of dissociated H atoms;

(v) Chemisorption of organic radicals arising from coupled electron transfer and solvent protonation events. Such adsorption processes are significant at many metals but may specifically determine the organic chemistry of the electrochemical reaction when organometallic intermediates can be formed, e.g., in certain reductions at Zn, Cd, Hg, Pb, etc.

When ionic intermediates (radical ions) are formed as a result of the primary electron transfer event, the strength (standard free energy) of adsorption may usually be expected to be substantially smaller than that of the initial neutral reactant. The intermediate may hence tend to be desorbed from the surface both on account of (a) its stronger solvation due to electrostatic charge–solvent interactions, and (b) repulsion between the electrode charge and the ion in the double layer since, necessarily, the sign of charge on an ionic intermediate will usually† tend to be the same as that of the electrode metal at which it is produced.

The first calculations of field-dependent adsorption of organic substances at electrode interfaces were made by Frumkin(56) and Butler.(57) In Frumkin's approach, the change of energy associated with the charged capacitance of the double layer when organic adsorbate replaced solvent was estimated from electrostatic theory. This energy change was then employed in a distribution function determining the relative concentration of the organic substance in the interphase and in solution. In the theory of Butler,(57) a more explicit calculation of the electrostatic distribution effect was made by calculation of the difference of electric polarization energy of equal volume elements of the solvent and the adsorbate in the double-layer field. At higher double-layer fields, the less polar molecules tend to be electrostatically squeezed out from the interphase, which then tends to be more populated by the more polar component. In aqueous solutions of most organic substances, the water molecule tends to be the preferentially adsorbed species at large positive and negative electrode surface charges owing to its relatively high dipole moment and its small size. Thus, adsorption of a substance the size of pyridine requires, for example, the desorption of about four water molecules. The adsorption of amyl alcohol at Hg electrodes from water serves as a good example of a case where relatively sudden adsorption/desorption processes occur at a critical double-layer field or electrode surface charge. At Hg, amyl alcohol is only adsorbed over a limited range of potentials near the p.z.c., dependent on the solution concentration.

---

† This is not always the case, however, since under certain circumstances, anionic intermediates could, e.g., be formed in a cathodic reaction at potentials *anodic* to the potential of zero charge where the metal bears a net *positive* surface charge. Such cases are rare but may arise at Pb which has a potential of zero charge which is unusually high on the negative side, viz., $\sim -0.8\ \mathrm{V}\ E_{\mathrm{H}}$.

The electrode field will also tend to cause *orientation* of (a) solvent dipoles and (b) the reactant molecule if it is polar, or has a polar functional group within it. Also, in molecules where conformational fluctuations are possible, conformations having higher dipole moments will be preferred in the double-layer field at the electrode interface. Examples are molecules such as dioxane and morpholine.

Factor (b), the orientation of a functional group, may be important in the kinetics of reduction of such polar reactants as alkyl halides or ketones; in the latter case, the orientation of the functional group will be the significant factor as discussed by Elving and Pullman.(58)

At finite temperatures, a distribution of orientations will be involved and the mean orientation will be determined by a function involving the ratio of the energy of the dipole group in the electrode field, $\mu\mathscr{E}$, to the thermal energy kT. For an angle of orientation θ to the electrode surface, the energy W_θ of interaction with the field will be $-\mu\mathscr{E}\cos\theta$ and the distribution function for orientation will be(31)

$$\frac{dN}{N} = \frac{\exp(\mu\mathscr{E}\cos\theta/kT)\cdot d\cos\theta}{\int_{-1}^{1}\exp(\mu\mathscr{E}\cos\theta/kT)\,d\cos\theta} \tag{30}$$

$$\frac{1}{N}\frac{dN}{d\cos\theta} = \frac{\exp\mu\mathscr{E}\cos\theta/kT}{(2kT/\mu\mathscr{E})\sinh(\mu\mathscr{E}/kT)} \tag{31}$$

which gives an increasingly sharp maximum the higher the electrode field or the lower the temperature. In the absence of lateral interaction of hydrogen-bonding effects giving rise to orientation correlation (cf. the theory of dielectric constant for polar and associated liquids), substantial orientation would already arise at electrode potentials of ±0.2 V from the potential of zero field. (The potential of zero net field is not necessarily the same as the potential of zero net charge (the electrocapillary maximum at Hg and liquid metals) owing to the presence of oriented dipoles and the intrinsic surface potential at the electronic surface of the metal electrode.)

A more elaborate theory of orientation effects was developed by Watts-Tobin and Mott(59) and applied by Bockris, Devanathan, and Muller(60) and Bockris and Habib(61) to the calculation of isotherms for adsorption of organic substances. Solvent molecules were regarded as being present in the double layer in two orientations, "up" or "down" (cf. theories of ferromagnetism) at respective surface coverages of $N\uparrow$ or $N\downarrow$. The sum $N\uparrow + N\downarrow$ is equal to the total coverage of the electrode by solvent molecules.

Adsorption of an organic substance results in displacement of the oriented solvent dipoles with an energy change determined by (i) the number of $\uparrow$ dipoles displaced; (ii) the number of $\downarrow$ dipoles displaced; (iii) the polarization energy of the adsorbed organic residue in the field (induced dipole, permanent dipole and electronic polarization energy in the field, due to the charged electrode); (iv) any quadrupole interaction with field gradients at the interface (the latter effect may contribute to differences of energy of an organic dipole at corresponding positive and negative net surface charges on either side of the p.z.c.).

The equilibrium between water adsorbed in the "up" and the "down" positions,† and that in solution is considered. By means of Langmuir's kinetic representation of adsorption, the equilibrium condition is written

$$k_w C_w (1 - \theta\uparrow - \theta\downarrow) = k\uparrow\theta\uparrow \tag{32}$$

for the adsorption of "up" molecules and

$$k_w C_w (1 - \theta\uparrow - \theta\downarrow) = k\downarrow\theta\downarrow \tag{33}$$

for the "down" molecules, where k's are the indicated rate constants for adsorption and desorption processes. C_w is the concentration of water.

Then,

$$\theta\uparrow/\theta\downarrow = e^{2x} \tag{34}$$

where kTx is the total energy of adsorption of dipoles in the electrode field including lateral interactions. Alternatively,

$$\frac{\theta\uparrow - \theta\downarrow}{\theta\uparrow - \theta\downarrow} - \tanh x = \frac{N\uparrow - N\downarrow}{N\uparrow - N\downarrow} = \frac{N\uparrow - N\downarrow}{N_T} \tag{35}$$

where N_T is the total number of solvent dipoles corresponding to full coverage in the absence of an adsorbed organic substance. N_T may change with field and temperature due to electrostriction in the double-layer field and structure-breaking effects similar to those which arise in bulk water.

The energy of the system of dipoles in the electrode field X is written

$$E\uparrow = \mu X + UC\frac{N\downarrow}{N_T} - UC\frac{N\uparrow}{N_T} \tag{36}$$

---

† A more recent treatment by Fawcett(62) considers three states of solvent dipole orientation, "up," "down," and "flat," i.e., parallel with the electrode surface. Another treatment by Parsons, communicated at a recent conference,(63) envisages a hexagonal array of dipoles oriented parallel to the electrode surface at the potential of zero charge with some orientation at finite + or − charges.

for the up water molecules, and

$$E{\downarrow} = -\left(\mu X + UC\frac{N{\downarrow}}{N_T} - UC\frac{N{\uparrow}}{N_T}\right) = -kTx \tag{37}$$

for the down, where μ is the dipole moment, C the surface coordination number in the interphase, and U the lateral interaction energy between nearest-neighbor dipoles. The distribution function for orientations of solvent dipoles is then

$$\frac{N{\uparrow} - N{\downarrow}}{N_T} = \tanh\left[-\frac{UC}{kT}\frac{(N{\uparrow} - N{\downarrow})}{N_T} + \frac{\mu X}{kT}\right] \tag{38}$$

This relation enables the surface dipole potential χ_d to be evaluated together with other functions for adsorption of organic substances which displace the field-oriented solvent dipoles.

In the absence of lateral interaction effects among the solvent dipoles, the standard electrochemical free energy, $\Delta\bar{G}^\circ_x$, of water molecules at the electrode where the field is X at the center of the water dipole is

$$\Delta\bar{G}^\circ_x = \Delta G^\circ + \frac{N{\uparrow}}{N_T}\mu X - \frac{N{\downarrow}}{N_T}\mu X \tag{39}$$

Now consider the adsorption of an organic molecule which *displaces*† n water molecules; the standard electrochemical free energy of adsorption $\Delta\bar{G}^\circ_{X,\text{ads}}$ is given by

$$\begin{aligned}\Delta\bar{G}^\circ_{X,\text{ads}} &= G^\circ_{\text{org in soln}} + nG^\circ_{\text{H}_2\text{O in soln}} - (G^\circ_{\text{org on electrode}} \\ &\quad + nG^\circ_{\text{H}_2\text{O on electrode}}) \\ &= \Delta G^\circ_{\text{ads}} - n\mu X(N{\uparrow} - N{\downarrow})/N_T \end{aligned} \tag{40}$$

The isotherm corresponding to this free energy of adsorption was written

$$\frac{\theta_{\text{org}}}{1-\theta_{\text{org}}} = \frac{C_{\text{org}}}{C_w}\exp\left(\frac{-\Delta G^\circ_{\text{ads}}}{RT}\right), \qquad \exp\left(\frac{-n\mu X}{kT}\cdot\tanh\frac{\mu X}{kT}\right) \tag{41}$$

using the relation given above for $(N{\uparrow} - N{\downarrow})/N_T$ as $f(\mu X/kT)$.

This relation gives a fair account of the adsorption of 0.1 N n-butanol at a mercury electrode but an improved comparison results if lateral solvent dipole interactions are taken into account. Then

$$\Delta\bar{G}^\circ_{X,\text{ads}} = \Delta G^\circ_{\text{ads}} + \left[\tanh\left(\frac{\mu X}{kT} - \frac{N{\uparrow} - N{\downarrow}}{N_T}\frac{UC}{kT}\right)\right]\left(\frac{\mu X}{kT} - \frac{RUC}{kT}\right) \tag{42}$$

where R is defined as $R = (N{\uparrow} - N{\downarrow})/N_T$, i.e.,

$$\Delta\bar{G}^\circ_{X,\text{ads}} = R\left(\frac{\mu X}{kT} - \frac{RUC}{kT}\right) \tag{43}$$

---

† The concept of displacement of previously oriented, adsorbed water (or solvent) by an adsorbing organic substance is of basic importance and is closely related to the hydrophobicity of the organic substances, and/or the nature of the solvent.

This gives an adsorption isotherm of the form

$$\frac{\theta_{\text{org}}}{1-\theta_{\text{org}}} = \frac{C_{\text{org}}}{C_w} \exp\left(-\frac{\Delta G^{\circ}_{\text{ads}}}{RT}\right), \qquad \exp nF\left(\frac{\mu X}{RT} - \frac{RUC}{RT}\right) \tag{44}$$

The field X is taken as that due to a surface charge density q_{M}, i.e., $X = 4\pi q_{\text{M}}/\varepsilon$, where ε is the effective dielectric constant of the interphase. This theory provides a good basis for quantitative interpretation of organic molecule adsorption but when the organic molecule is n times as large as the adsorbed solvent, the form of the isotherm will be

$$\frac{\theta_{\text{org}}}{n(1-\theta_{\text{org}})^n} = \frac{C_{\text{org}}}{C_w} \exp\left(-\frac{\Delta \bar{G}^{\circ}_{\text{X,ads}}}{\text{RT}}\right) \tag{45}$$

rather than the simpler Langmuir form in $\theta_{\text{org}}/(1-\theta_{\text{org}})$.

Also, in further developments of this kind of treatment, specific structure-forming and structure-breaking effects of the organic adsorbate must be considered in relation to the orientation of solvent molecules, e.g., as indicated(64) by entropies and heats of adsorption of pyridine at Hg electrodes. Analysis of various types of isotherms which represent organic molecule adsorption has been made by Kovac and Bockris(65) and by Wroblowa and Mueller(66) in relation to the theory presented above.

Free energies of adsorption or more particularly the standard free energies $\Delta G^{\circ}_{\text{ads}}$ may be evaluated if θ_1 is known as $f(C_i)$ at constant potential. If data are available over a range of potentials, then $\Delta G^{\circ}_{\text{ads}}$ may also be evaluated as a function of potential of q_{M}. For many organic substances less polar than water (per unit volume), $\Delta G^{\circ}_{\text{ads}}$ varies as q^2_{M} around the p.z.c. where q_{M} may take positive or negative values. Adsorption is often a maximum at or near the p.z.c., depending on coadsorption of anions and asymmetry of solvent molecule adsorption with respect to $\pm q_{\text{M}}$; the latter effect can arise from (a) the noncentral location of the electric dipole in the solvent molecule, (b) solvent structure effects in the interphase, and (c) field-gradient/quadrupole interactions in the double layer if the field is not locally uniform.

When $\Delta G^{\circ}_{\text{ads}}$ is evaluated and found to be a function of C or correspondingly θ_i, interaction effects (and/or heterogeneity effects if the metal electrode is a solid) are indicated. $\Delta G^{\circ}_{\text{ads}}$ can then be extrapolated with respect to θ_i to obtain the free energy of adsorption at zero coverage, i.e., for infinite dilution in the two-dimensional interphase. In the Russian literature, coverage-dependent adsorption and kinetic behavior has usually been treated in terms of the Temkin isotherm, although evidence for the required heterogeneity of the surface has not often been given.

6.2. Methods for Investigation of Adsorption of Organic Substances

Experimental determinations of adsorption at electrodes can be made by a number of methods; the following are the most important:

(1) At liquid metals, by surface tension measurements, using the Gibbs adsorption equation in a form appropriate for a charged interface. For surface tension values, γ, the thermodynamic treatment for an ideally polarizable electrode leads to the following derivatives:

$$\text{(a)}\quad \left(\frac{\partial \gamma}{\partial E}\right)_{\mu,T} = q_{\mathrm{M}} \tag{46}$$

where E is the electrode potential measured with respect to a reference electrode of constant potential and μ is the chemical potential of adsorbate in solution. q_{M} is the surface charge density on the metal and is, thus, thermodynamically determinable;

$$\text{(b)}\quad \left(\frac{\partial \gamma}{\partial \mu}\right)_{E,T,\mu_i,\mu_k} = -\Gamma_{i,E} \tag{47}$$

where $\Gamma_{i,E}$ is the surface excess of the adsorbate component i in a solution where chemical potentials of other components are constant. For dilute adsorbate solutions, Γ_i is approximately equal to the surface concentration. $\Gamma_{i,E}$ can be evaluated as $f(E)$ so that the adsorption as a function of the electrical variables E or q_{M} may be evaluated.

The second derivative of γ with respect to E may also be obtained, giving the interfacial double-layer capacitance(42,67) but its determination by this method is inaccurate owing to the double differentiation which is required. The capacity is usually measured directly by an ac impedance technique (see below).

(2) By double integration of capacity values directly determined by an ac impedance method. Here the capacity C must be evaluated as $f(E, \mu_i)$ and the integration performed using integration constants derived from an electrocapillary experiment (coordinates of the p.z.c.) and from the theory of the diffuse double layer. For liquid metals, the capacity method gives results of considerable precision.(42) At solid metals it is less reliable owing to frequency variation of the capacity(67,68) and the problem of evaluation of integration constants.

(3) By direct measurements, usually at solid metals, of the uptake of radioactively labeled molecules at the metal itself or from solution by difference.(69)

(4) By electrochemical determination of extents of blocking of electrochemisorption of H at noble metals.(70)

(5) By spectrophotometric determination of uptake of suitable organic substances (conjugated aromatics and heterocyclics) at large-area electrodes from small volumes of solution.(71)

(6) Indirectly, and less quantitatively, by studies of effects of adsorption of an organic substance on the kinetics of another reaction, e.g., cathodic hydrogen evolution.

6.3. Reaction Order and Adsorption in Kinetics of Electro-Organic Processes

In examination of mechanisms of organic electrochemical reactions, it is useful to apply procedures which are employed for ordinary chemical reactions in addition to the methods which arise because the reaction is electrochemical.

Thus, the reaction order in the "reactant" itself is useful to evaluate. If the reactant is likely to be adsorbed significantly, then the reaction order must be interpreted, as in other types of heterogeneous reactions, with due attention to the type of adsorption isotherm and the extent of coverage. Since the kinetics of electrode reactions depend in a primary way on the potential (see Section 4), the reaction order must be specified and evaluated with respect to a constant electrode potential. Usually a supporting (electrochemically inactive) electrolyte is used so that effects of ion distribution and potential in the double layer remain approximately constant as other quantities are varied in the experimental analysis, viz., pH, reactant concentration.

When adsorption is significant in an electro-organic reaction, interpretations of reaction order in terms of mechanisms must be made with care. Consider a case where the current density at a given constant potential E is

$$i_E = k_E \theta_i^n \tag{48}$$

where θ_i is the coverage of reactant i and the surface reaction molecularity is n which is given by $d(\ln i_E)/d(\ln \theta_i) = n$. The reaction order R is, however, determined experimentally with respect to bulk concentration c, i.e.,

$$R = d(\ln i_E)/d(\ln c) \tag{49}$$

By writing

$$R = [d(\ln i_E)/d(\ln \theta_i) \cdot d(\ln \theta_i)/d(\ln c)] \tag{50}$$

it is readily seen that n may be evaluated from

$$n = R/[d(\ln \theta)_i/d(\ln c)] \tag{51}$$

The quotient $d(\ln \theta)_i/d(\ln c)$ is the derivative of the adsorption isotherm $\theta_i = f(c)$ at constant potential and may be obtained from experimental evaluation of the isotherm. Usually it is convenient(72) to express $d(\ln \theta)_i/d(\ln c)$ as $d\theta_i/dc \cdot c/\theta_i$, since the latter derivative is usually easier to obtain, particularly in cases of isotherms having linear and transcendental terms.

It is useful to exemplify the calculation with respect to a process obeying the Langmuir isotherm:

$$\frac{\theta_i}{1-\theta_i} = Kc \qquad \text{or} \qquad \theta_i = \frac{Kc}{1+Kc}, \tag{52}$$

then

$$\frac{d\theta_i}{dc} = \frac{(1+Kc)K - K^2c}{(1+Kc)^2} = \frac{1}{(1+Kc)^2} \tag{53}$$

c/θ_i is $(1+Kc)/K$, so that

$$\frac{d(\ln\theta_i)}{d(\ln c)}=\frac{K}{(1+Kc)^2}\cdot\frac{1+Kc}{Kc}=\frac{1}{1+Kc}\tag{54}$$

Therefore

$$n=R(1+Kc)$$

or

$$\frac{R}{n}=\frac{1}{1+Kc}=(1-\theta_i)\tag{55}$$

i.e., $R=n$ only for low coverage where $\theta_i \ll 1$. Hence, n can be evaluated from measurements of R if the adsorption isotherm has been determined.

In more complex cases, e.g., isotherms with interaction terms, R/n can usually be evaluated by the method exemplified above. The results for several isotherms that have been investigated for adsorption of organic substances at electrodes are summarized in Table 2.

Cases are frequently encountered(72) where the rate constant is also a function of coverage θ_i, e.g., in a rate equation of the form

$$v=i/zF=k\exp(\alpha' nr\theta)\cdot\theta^n\exp(\alpha EF/RT)\tag{56}$$

then the molecularity n of the surface reaction is

$$n=(\partial\ln i/\partial\ln\theta)_E/(1+\alpha' r\theta)\tag{57}$$

or, in terms of the experimental order R, using Eq. (51):

$$n=R\Big/\frac{(\partial\ln\theta)}{(\partial\ln c)_E}\cdot(1+{}'\alpha r\theta)=\frac{R_s}{(1+\alpha' r\theta)}\tag{58}$$

where R_s has been written as an apparent order of the surface reaction defined by

$$R_s=R(\partial\ln\theta/\partial\ln c)_E\tag{59}$$

R_s and n are only identical when the rate constant is independent of θ or when $\theta \to 0$, as in the first case examined above.

While $(\partial\ln\theta/\partial\ln c)_E$ is usually <1 as $\theta > 0$, it is of interest to note that R can be $>n$ when attractive interactions (or equivalent solvent structure changes in the interphase) arise (i.e., for positive r in the equations of Table 2). For the case of the Hg-solution interphase, the virial or the Frumkin isotherms are of special interest, as these represent the effects of interactions in the adlayer. Some calculated values(72) for $(\partial\ln\theta/\partial\ln c)_E$ for the virial isotherm are shown in Table 3.

6.4. Adsorption and Solvation: Solvent Effects in Organic Adsorption

Change of solvent from the aqueous medium can appreciably modify the kinetics of many organic electrochemical reactions and in certain cases the

Table 2
Forms of a Number of Adsorption Isotherms and the Corresponding Reaction Order Factors $(\partial \ln \theta/\partial \ln c)_E$ Which Relate R to n

Type of isotherm	Form of isotherm[a]	$(\partial \ln \theta/\partial \ln c)_E$
"Henry's law"	$K(C_R)_b = RT\theta\Gamma_m$	1
Volmer	$K(C_R)_b = RT\frac{\theta\Gamma_m}{1-b\theta}\exp\left(\frac{b\theta\Gamma_m}{1-b\theta}\right)$	$1+\frac{b\theta}{1-b\theta\Gamma_m}+\frac{b\theta\Gamma_m}{1-b\theta\Gamma_m}$
Langmuir	$K(C_R)_b = \frac{\Gamma}{\Gamma_m-\Gamma} = \frac{\theta}{1-\theta}$	$1-\theta$
Flory–Huggins	$K(C_R)_b = \frac{\theta}{x(1-\theta)^x}$	$\frac{1-\theta}{1+(x-1)\theta}$
Virial	$K(C_R)_b = RT\theta\Gamma_m \exp(-r\theta\Gamma_m)$	$\frac{1}{1-r\theta\Gamma_m}$
Frumkin	$K(C_R)_b = \frac{\theta}{1-\theta}\exp(-r\theta\Gamma_m)$	$\frac{1-\theta}{1-r\theta\Gamma_m+r\theta^2\Gamma_m\cdot}$
Temkin	$K(C_R)_b = \exp(-r\theta\Gamma_m)$	$\frac{1}{r\Gamma_m\theta}$

[a] Γ, surface concentration of adsorbate $\doteqdot$ surface excess; Γ_m, surface concentration corresponding to a monolayer at the surface; K, $\exp(-G^\circ_{ads}/RT)$; b, molecular area of adsorbate species; θ, degree of coverage of the electrode surface by adsorbate, given by Γ/Γ_m; x, ratio of relative sizes of adsorbate and solvent molecules in the Flory–Huggins type of isotherm; r, interaction parameter characterizing two-dimensional attraction or repulsion in the adsorbed layer in the virial or Frumkin isotherm or is a heterogeneity parameter in Temkin's isotherm. Units of r depend on how coverage is expressed, i.e. as $\Gamma(=\theta\Gamma_m)$ or in terms of θ.

Table 3
Coverage Dependence of the Reaction Order Factor $(\partial \ln \theta/\partial \ln c)_E$ Derived from the Virial Isotherm

Virial equation[a]: $K(C_R)_b = RT\theta\Gamma_m \exp(-r\theta\Gamma_m)$; $(\partial \ln \theta/\partial \ln c)_E = 1/(1-r\theta\Gamma_m)$

$(\partial \ln \theta/\partial \ln c)_E$

	Attraction			Zero interaction		Repulsion	
$\theta\Gamma_m$	$r=5$	$r=1$	$r=0.5$	$r=0.1$	$r=0$	$r=-0.1$	$r=-1$
0.1	2	1.11	1.05	1.01	1	0.99	0.91
0.2	[∞]	1.25	1.1	1.02	1	0.98	0.83
0.4	−1	1.67	1.25	1.04	1	0.96	0.71
0.6	−0.5	2.5	1.43	1.06	1	0.94	0.63
0.8	−0.33	5	1.67	1.08	1	0.93	0.55

[a] Here the parameter r (introduced for conformity with other isotherms in Table 2) is equal to -2β, where β is the second virial coefficient for the adlayer of organic substance.

reaction products.(5) This is presumably due to the changing adsorption conditions and/or changing strength of solvation of intermediates or transition states. Change of solvent may thus modify the partial molar free energy of the initial reactant, the transition state, or the product, or modify all three of these quantities. Many substances containing hydrophobic nonpolar residues, e.g., alkyl or aryl groups, normally suffer a tendency to be expelled from the water phase at its interface with air or with the electrode metal. Change to a less polar solvent diminishes this effect and usually decreases the numerical value of the free energy of adsorption. This is the situation with alcohol–water mixtures and series of alcohols with progressively longer alkyl functions. Radical modification of the solvent from a protic to an aprotic one may, of course, completely change the mechanism and products of a reaction, since protonation of ionic intermediates is no longer possible and the reaction is characterized by the chemistry of radical ions.

The equilibrium adsorption process is determined formally by the condition

$$\mu_{i,s} = \mu_{i,b} \tag{60}$$

for an organic substance i in the interphase s and in the bulk b. In terms of surface and bulk mole fractions $x_{i,s}$ and $x_{i,b}$,

$$\mu_{i,s}^{\circ} + RT \ln x_{i,s} = \mu_{b}^{\circ} + RT \ln x_{i,b} \tag{61}$$

where $\mu_{i,s}^{\circ} - \mu_{i,b}^{\circ}$ is the standard free energy of adsorption.

In the case of appreciable specific adsorption, i.e., if the adsorption is due largely to metal–i interactions rather than lyophobic interactions with the solvent, changes of solvent will mainly modify $\mu_{i,b}^{\circ}$. Better solvents for i will lower the energy $\mu_{i,b}^{\circ}$ and diminish the magnitude of the standard free energy of adsorption. In cases where the adsorption arises mainly from lyophobic interactions, better solvation of i in the bulk will usually have a similar effect, since at the interface it is coordinated only by about half the number of solvent molecules that coordinate i in the bulk phase. Since for a given pure solute (chemical potential μ_{i}°) in saturation equilibrium with its saturated solution:

$$\mu_{i}^{\circ} = \mu_{i,b}^{\circ\prime} + RT \ln a_{i,\text{sat}}^{\prime} = \mu_{i,b}^{\circ\prime\prime} + RT \ln a_{i,\text{sat}}^{\prime\prime}, \text{ etc.} \tag{62}$$

where ′ and ″ represent solutions in different solvents, it is evident that the differences of standard chemical potentials of i in various solvents varies as the difference of the logarithms of the solubilities, i.e., as the logarithm of the *ratio* of solubilities.

Consider now the adsorption of i from two solvents designated ′ and ″ but from solutions of the *same* mole fraction $x_{i,b}$ (or activity). Then

$$\mu_{i,s}^{\circ\prime} + RT \ln x_{i,s}^{\prime} = \mu_{b}^{\circ\prime} + RT \ln x_{i,b} \tag{63}$$

and

$$\mu_{i,s}^{\circ\prime\prime} + RT \ln x_{i,s}^{\prime\prime} = \mu_{b}^{\circ\prime\prime} + RT \ln x_{i,b} \tag{64}$$

Then finally

$$\mu_{i,s}^{\circ\prime} - \mu_{i,s}^{\circ\prime\prime} + RT \ln \frac{x'_{i,s}}{x''_{i,s}} = \mu_b^{\circ\prime} - \mu_b^{\circ\prime\prime} = -RT \ln a'_{i,\text{sat}}/a''_{i,\text{sat}} \tag{65}$$

so that the ratio of mole fractions in the interphase is related to the ratio of the saturation solubilities and the difference of standard chemical potentials in the interphase. In the case where the interaction of i with the metal is much stronger (chemisorption case) than changes of interaction in the interphase due to the solvents, then differences of adsorption $x^{i}_{i,s}/x''_{i,s}$ will be determined mainly by the solubility difference.

6.5. Adsorption and the Electrode Metal

The electrode metal can determine the role of adsorption in an electroorganic reaction in several ways: (a) through specific interactions with the reactant, a product, or an intermediate, e.g., metal alkyls can be formed at Hg or Zn electrodes: S and N functions may be chemisorbed at Hg; π-orbitals in olefinic or aromatic substances may interact with positively charged metal electrode interfaces; (b) through electrostatic effects, referred to above, depending on the potential of zero charge of the metal. The p.z.c. is usually related to the electronic work function of the metal. This type of effect was recognized in many of Frumkin's papers and has been specially treated by Antropov. The value of the p.z.c. in relation to the thermodynamic reversible potential for a reaction is of particular importance, for it may determine the orientation of the reactant molecule, its surface coverage, and the competitive adsorption between the reactant, the product(s), and the solvent in the region of potentials where the electro-organic reduction is thermodynamically feasible; and (c) through coadsorption of solvent and supporting electrolyte ions, e.g., halide anions, R_4N^+ cations such as are commonly employed as salts in supporting electrolyte solutions. The energy and potential dependence of solvent adsorption is important since it determines the net free energy of adsorption or organic substances on account of the solvent displacement required for adsorption of the organic reactant. The specificity of solvent adsorption and orientation at the potential of zero charge as a function of the electrode metal has been demonstrated in recent work by Trasatti.(73)

7. Organic Reactions under Diffusion Control at Electrodes

7.1. Introduction

With most organic substances, particularly those of limited solubility in electrochemically useful solvents (e.g., water, alcohols, acetone–water mixtures, acetonitrile, propylene carbonate, formamide, dimethyl formamide, hexamethylphosphoramide, dimethylsulfoxide, sulfolane) the reaction current will eventually become limited by the rate of *diffusion* of the reactant to the electrode surface. The limiting diffusion current density, i_{lim}, for a plane electrode is obtained from an equation derived from Fick's so-called first law:

$$i_{\text{lim}} = -zFD\frac{dC_R}{dx} = zFD\frac{C_R}{\delta} \tag{66}$$

where C_R is the concentration in mol cm^{-2}, D is the diffusion constant (usually 10^{-5}–10^{-6} cm sec^{-1}), and δ is a diffusion boundary layer thickness corresponding to the thickness of the layer across which the concentration gradient is set up in the "x" direction, normal to the electrode surface.

7.2. Diffusion-Limited Electrode Processes at Solid Metals

While diffusion-controlled conditions are deliberately introduced when organic electrochemical reactions are to be studied by means of polarography (see Section 8) at the Hg electrode, the situation often arises in practice that diffusion control becomes operative at solid electrodes, e.g., for fast reactions or toward the end of a preparative organic electrolysis.

At solid electrodes, conditions of *planar* diffusion normally operate in distinction to the situation at growing spherical drops in polarography (see below), where *spherical* diffusion conditions obtain with the mass transport occurring along radial directions toward (or away from) the center of the drop. Planar diffusion occurs, however, at most solid electrode interfaces unless the surface exhibits roughness or crystallinity giving rise to local asperities and depressions of dimensions† comparable with those of the diffusion layer (viz., 0.05–0.01 cm); then the diffusion conditions are more complex.

An important method for examining electrode processes at solid electrodes under reproducibly controlled mass transport conditions employs the so-called rotating disk and ring–disk electrodes.(74)

In the former case, an electrode ~0.5 cm in diameter is set into a plastic cylinder (Teflon or epoxy) mounted concentrically with a metal shaft which can be rotated at known, precisely controlled rotation rates up to ~20,000 rpm. Rotation speeds up to 5000 or 10,000 rpm can easily be attained with commercially available motors. Motor speed is regulated by means of electronic circuits; rotation velocities can be determined by means of a commutator operating in conjunction with an oscilloscope or with an auxiliary ac armature generating an ac frequency which can be counted. Speeds may also be monitored optically by means of a stroboscopic device.

---

† In organic preparations at solid metals, a macroscopically rough electrode is preferable in order to attain the maximum diffusion-controlled limiting current consistent with the size of the electrolytic cell employed in the experiment. Larger currents and shorter electrolysis times can then be employed in the preparation provided cooling arrangements are introduced.

The rotating disk electrode provides, in effect, a hydrodynamically controllable, forced convection arrangement which brings material from the bulk of the solution to the electrode reaction interface at the disk. The unconsumed reactant is sucked into the central region of the electrode and the products and unconsumed reactant are spun out across the surface of the rotating electrode. Diffusion-controlled electrochemical reaction occurs across a diffusion layer (as at a static electrode or at a dropping Hg electrode) but the steady state thickness of this boundary layer is effectively variable with rotation rate, being inversely proportional to the *square root* of the angular rotation frequency (ω). Reactions that, under given static conditions, proceed at a certain diffusion-controlled rate, then give currents that increase with $\omega^{1/2}$. In some cases, the diffusion-controlled rate may be sufficiently increased that activation control of the process eventually sets in at a high enough rotation frequency. The current density then increases, but not linearly with $\omega^{1/2}$, and eventually (in an idealized case) becomes almost independent of ω when activation control is reached.

Under diffusion-controlled conditions, the limiting current at a rotating disk electrode is given by Levich's equation, for a z electron process, as

$$i_d = z\,0.62\,FC_0D^{2/3}\nu^{-1/6}\omega^{1/2} \tag{67}$$

Extensions to the Levich equation, involving small corrections, were made by Riddiford and Gregory, who obtained

$$i_d = \frac{0.62\,zFD^{2/3}\nu^{-1/6}C_0\omega^{1/2}}{1 + 0.34\,(D/\nu)^{0.36}} \tag{68}$$

where F is the Faraday, C_0 is the bulk concentration in g equiv cm^{-2}, D the diffusion constant, ν the kinematic viscosity of the solution in cm^2 sec^{-1}, and ω the angular frequency in radians sec^{-1} ($\omega = 2\pi f$, where f is in rotations sec^{-1}).

In some circumstances, the Levich equation provides a useful way of determining diffusion coefficients of electroactive organic molecules, e.g., for use in polarographic calculations. From the Levich equation for the disk current, D may be readily calculated from the slopes of the current-$\omega^{1/2}$ relations.

A very important development of the rotating disk technique was envisaged by Frumkin and described by Frumkin and Nekrassov. It consists of a disk electrode surrounded by a ring separated from the disk by a narrow annular region of insulation. An electrode process is carried out at the disk and any electroactive diffusible intermediates, or products, are transferred across the annular region, in the flowing solution, and can be reoxidized or rereduced at the ring which is provided with a separate potential-controlling circuit. Also, further reduction or oxidation stages can be achieved by using appropriate potentials at the ring.

In cases where intermediates are formed in an electro-organic reaction, this method provides an important way of indicating their existence. If the intermediates have limited lifetime, e.g., because of reaction with each other or with the solvent, the *kinetics* of processes leading to their removal may be determined by measuring ring currents (for a given disk current at a different potential) as a function of rotation velocity. Electrochemical collection at the ring will be favored by higher rotation rates for a species with a given lifetime, τ. In fact, τ must be comparable with the transit time in transport of the intermediate from the disk to the ring. Ketyl radical intermediates in aromatic ketone reduction have been indicated by this method. In other systems, more stable intermediates such as HO_2^- or H_2O_2 have been indicated in studies on the reduction of O_2.

An important parameter in ring–disk experiments is the *collection efficiency*, i.e., the fraction of, e.g., a reduced species (produced at the disk) which can be reoxidized under forced transport conditions at the ring. Expressions for the collection efficiency have been derived by Levich and by Bruckenstein, and may be numerically evaluated for various radii of the disk and ring.

A further recent development consists in employing a *split* ring surrounding the disk. Intermediates produced at the latter may be either reduced *or* oxidized at the two insulated sections of the ring. Three independent electrochemical current/potential controlling systems are then required.

These methods deserve further application in the study of organic electrochemical reactions where unstable intermediates are produced; the intermediates must, however, be capable of undergoing further, or reverse, electron transfer at the ring electrode, i.e., they must remain electroactive during their transit from the disk to the ring.

7.3. Polarographic Conditions: Diffusion at Mercury Drops

By operating at relatively low concentrations, most reactions can be made to become largely diffusion controlled and use is made of this situtation in the technique of polarography, first developed in 1922 by Heyrovsky.(17) At that time, the term denoted an electrolytic method based on the measurement of the dependence of a current averaged over the size of growing drops, upon a controlled but progressively varying potential at a dropping mercury electrode.† Thus, classical polarography may, in fact, be regarded as a slow potentiodynamic method for a series of mercury drops where the average current is determined. The general subject of polarography nowadays commonly includes the interpretation as well as the measurement of such current–potential relationships and is the most well-known and experimentally important example of techniques based upon the evaluation of diffusion-controlled currents at a nonstationary surface.

---

† In more recent applications of polarography, rotating solid bead or wire electrodes of platinum have been employed, particularly for anodic processes which could not be studied at Hg due to dissolution or anodic attack of the metal.

Since its introduction, the technique has been associated with important applications in many branches of chemistry; a principal example is in analytical chemistry, including that of organic substances. The method provides a simple technique for the detection and estimation of electroreducible ions and compounds present in solution at very small concentrations. The sensitivity of conventional polarography allows the measurement of concentrations of various ions to approximately 10^{-5} mol liter^{-1}. Several procedures have been developed to extend the analytical range, notably the compensation method(73) and the square wave polarographic technique introduced by Barker and Jenkins.(74)

In a later section (Section 8), some of the fundamental aspects of polarography will be briefly considered with particular reference to the question of reversibility of various electro-organic reactions studied by means of polarography. Finally, an attempt will be made to discuss those techniques complementary to the basic polarographic method, but essential for any deductions regarding the nature of intermediates and products in an organic electrode reaction, and therefore regarding its overall reaction mechanism.

Numerous reference books are available on the principles, technique, and results of polarography,(58,75–78) and the mechanisms of organic electrode processes studied by means of this technique have been discussed in several reviews.(79–83)

Before proceeding with that topic, however, we shall first discuss some practical problems involving mass transfer and diffusion in preparative electro-organic operations and in the field or electrolytic cell design for such processes.

7.4. The Mass Transport Problems in Preparative Electro-Organic Chemistry and Cell Design

Electrode processes, being necessarily heterogeneous, suffer the general difficulty that reagents must be transferred from the bulk solution to the reactive electrode surface and products in the opposite direction. Under quiescent conditions, therefore, the maximum currents attainable in a preparative experiment would be those dictated by the diffusion-limited current determined by the bulk concentration of reagent(s), the diffusion constant(s), of the reagent(s) and the viscosity of the solution. Higher rates could be obtained at rotated disk or cylinder electrodes in proportion to the square root of the angular rotation frequency.(74)

In organic reactions at electrodes, more so than with most inorganic ones, problems of slow desorption of products or side reactions that produce polymeric materials on the electrode surface, limit the currents that can be passed and often cause undesirable decreases of these currents with time of electrolysis. Various conditions may be adopted in order to mitigate these problems, e.g., change to a solvent in which products are more soluble or less adsorbed, or to a solvent (or other conditions) in which polymerization side reactions are minimized. Thus, for example, attempts to perform the Kolbe reaction with α-phenylacetic acid in aqueous media are impaired by build-up of side reaction products on the electrode and insolubility of dibenzyl. However, yields of desired products are much improved when pyridine is present in substantial quantity. It has probably both a chemical (as a base) and a physical effect on the course of the reaction.

The general mass transport problem in preparative electrochemistry, which is especially important in organic systems, can be circumvented by several routes of a more practical kind than the use of a rotating disk electrode. The following three approaches have been employed in various systems:

(a) Use of a fluidized bed of electrode reagent pellets which are mobilized by circulation of the electrolyte through the bed. This method can be used with a variety of electrode metals, and even mercury can be employed in the form of an amalgamated surface of copper beads. Various evaluations of fluidized bed systems have been made in recent years(84) but overall efficiencies are not good and utilization of the available bed electrode surface is incomplete, depending on the density of the bed, the conductivity of the electrolyte, the solution flow rate, and the overall current distribution. The method does have advantages over other geometries, however, with regard to optimizing electrode–surface to solution–volume ratios and to scale-up to potentially large installations. This system was developed by Fleischmann and Goodridge.(84)

(b) The second type of system employs rotating vanes constructed of gauze electrodes, i.e., the electrode surface is moved *through* the reagent solution permitting good contact with the reagent and satisfactory opportunity for products to be swept away from the vicinity of the electrode. This type of system has been employed in some industrial applications, e.g., for reduction of nitro compounds. A variant of this method is the use of a vibrating electrode.

(c) The third system employs a fixed bed electrode (a porous matrix) *through* which the reagent plus electrolyte solution is pumped at a rate allowing an optimum residence time of the reagent within the matrix of the bed. This type of system has been studied by the Soviet workers(85) and by Wroblowa.(86)

Since the problem of mass transport of reagents and products is a major one in any large, or even smaller, scale preparative development in organic electrochemistry, this is now more of a problem in electrochemical engineering than in mechanistic electrochemistry.

The mass transport problem can be mitigated in another, quite different, way by having the electrode produce a *solution-soluble* reagent that can react *homogeneously* with an appropriate organic substance. Examples are the cathodic production of low-valent inorganic ions, such as Cr^{2+}, V^{2+} in aqueous solutions, or solvated electrons in nonaqueous media, that are strong reducing agents, of the anodic production of high-valency-state cations such as Ag^{3+}, or molecules such as F_2, Cl_2, Br_2 that are oxidizing agents. The electrode processes are then secondary to the organic reduction or oxidation reactions that take place in the solution some way from the electrode surface depending on conditions of solution agitation.

The electrochemical production of solvated electrons directly from cathodes(87) at high potentials in nonaqueous, prefereably aprotic, solutions is of special interest as the reactions which are possible are similar to those which can be achieved with the Birch reagent (Na in liquid NH_3) and interesting selective reductions, e.g., of naphthalene, can be carried out.(88) Unfortunately, methods based on electrochemical generation of solvated electrons have not found industrial applications. An interesting feature of the generation of solvated electrons in cathodic processes in aprotic media, or even in water, is the photoeffect(89) which lowers the threshold potential for cathodic solvated electron production.

Depending on the type of reaction desired, and the reversibility or otherwise of the overall electrode processes, separators may or may not be required between the anode and the cathode regions of the cell. However, for most preparative processes, an anode/cathode separator is desirable to minimize cross-flow of products between the +, − pair of electrodes and the consequent mutual depolarization effects with possible, or probable, contamination of the main electroorganic product desired. This is a practical factor determining product coulombic efficiency and yields. The usual engineering problems with separator properties, their design, and mounting, arise in scale-up for preparative applications.

Methods such as fluidization(84) of the electrode material, use of rotating vanes, or flow-through bed electrodes,(85,86) which improve the mass transport situation, usually involve problems in designing a counterelectrode arrangement with a satisfactory geometry having a sufficiently low *IR* dop in the cell. The flow-through bed electrode presents the least difficulty in this regard as it can be set up in a "thin-layer," parallel plate configuration with flow down and through a porous bed in the form of a rectangular electrode as in a battery or fuel cell configuration.

8. Polarographic Methods and Related Techniques for the Study of Electro-Organic Reactions

8.1. Introduction

Conventional or slow scan polarography has received wide use in the study of organic electrode processes, although it must be recognized, as Brown and Harrison(90) have remarked in their review, that this technique "... used alone ... is in general inadequate for the unambiguous elucidation of complex reaction schemes." This applies particularly when a reaction is irreversible (see below), as is often the case with organic electrode processes.

Apart from analytical applications, polarography is useful in electroorganic reaction studies as a means for establishing ranges of potential over which one or more reduction (or oxidation) steps occur and thus as a basis for choice of conditions for a potentiostatic preparation. Of course, information obtained at the Hg surface normally used in (cathodic) polarography cannot always be transferred to behavior at other metals where different reaction pathways may arise due to adsorption effects and catalysis.

Athough reductions of organic compounds were among the earliest electrochemical reactions to be studied using a dropping mercury electrode,(91–93) organic polarography has developed relatively slowly even as an analytical method. This may have been partly due to the relatively complex nature of organic electrode processes and to the difficulty of directly relating polarographic results to other electrochemical data available at that time. However, in the last two decades, particular efforts have been made to understand the pathways and mechanisms of organic electrode processes by means of polarography and the contributions† of the Czechoslovak school, especially Zuman, have been the principal ones in this area. For example, attention has been focused on the chemical reactions occurring in the electrical double layer which precede, are parallel to, or succeed the actual electron transfer step. This interest has resulted in the development of both theoretical equations and experimental techniques (a) to characterize and correlate chemical and electrochemical steps involved in the overall reaction, (b) to define the importance of adsorption at the electrode surface, and (c) to determine the role of the proton and the effects of changes of solvent composition upon the electrode reaction (see below).

8.2. Fundamental Aspects of Polarography

8.2.1. Electrochemical Equilibrium and Kinetic Factors

For a simple redox process,

$$\mathrm{Ox} + ze \underset{k_b}{\overset{k_f}{\rightleftharpoons}} \mathrm{R} \tag{69}$$

where z is the number of electrons involved in the overall reaction and k_f and k_b are heterogeneous, potential-dependent rate constants for the forward (cathodic) and reverse (anodic) electrochemical reactions, the reversible electrode potential $E = E_r$ can be written according to the well-known Nernst equation§ as

$$E_r = E_r^\circ - \frac{RT}{zF}\ln\left[\frac{(C_{\mathrm{R}})_s}{(C_{\mathrm{Ox}})_s}\right] \tag{70}$$

---

† In particular the work of J. Heyrovsky, Koryta, Brdicka and Mairanovskii in the USSR.

§ The International Stockholm Convention is used here with E° values for elements baser than H_2 taking a negative sign. The E° (or E) values refer to the direction of the process written above.

Here E_r° is the standard reversible potential for the electrode process, F is the Faraday, and R and T have their usual significance. For simplicity, the concentrations $(C_\mathrm{R})_s$ and $(C_\mathrm{Ox})_s$ in the electrode surface region are used in place of surface activities.

At any potential E, the net current density is

$$i = i_0[\exp - \beta zF(E - E_r)/RT - \exp(1 - \beta)zF(E - E_r)/RT] \qquad (71)$$

where i_0 is the exchange current density for $E = E_r$, the reversible potential [see Section 4, Eqs. (7) and (8)] and β has been referred to in Section 4. i_0 can be written

$$i_0 = \bar{k}_{f,0} zF(C_\mathrm{Ox})_s \qquad (72)$$

where $\bar{k}_{f,0}$ is standard electrochemical rate constant at the reversible potential $E = E_r$. $\bar{k}_{f,0}$ can be represented by

$$\begin{aligned} \bar{k}_{f0} &= k_f \exp(-\beta zFE_r/RT) \\ &= \frac{kT}{h} \exp\left(-\frac{\Delta G^{\circ\ddagger}}{RT}\right) \cdot \exp\left(-\frac{\beta zFE_r}{RT}\right) \end{aligned} \qquad (73)$$

where k_f is the *chemical* forward rate constant related to the chemical free energy of activation, $\Delta G^{\circ\ddagger}$. $\bar{k}_{f,0} = k_f$ only for the condition of zero absolute metal–solution pc, an experimentally indeterminable condition.

For other potentials more negative than E_r, a net cathodic current passes corresponding to the current of the polarographic wave and E_r, of course, depends on the activities of oxidized and reduced forms in a reversible process. The net current density is given by Eq. (71) with i_0 given by Eq. (72) and $\bar{k}_{f,0}$ by (73).

The net current is the algebraic sum of the cathodic and anodic currents (see Section 4), corresponding to the reduction and oxidation reactions. However, in polarography the solution usually contains only one electroactive species and the contribution from the reverse reaction can usually be neglected in the case of many organic reactions which behave irreversibly. It can be seen that as the applied potential is increased the cathodic current increases exponentially until it becomes diffusion limited, and this is shown in the current–potential curve, or polarogram (Figure 5).

8.2.2. Reversible and Irreversible Polarographic Waves

In a typical polarographic study, the concentration of the electroactive species may vary from 10^{-6} to perhaps 10^{-3} mol liter^{-1} and if the rate of electron transfer is "fast," then with increasing potential the rate of reaction (and therefore the current) becomes eventually limited by the rate of diffusion of the reducible species to the surface of the electrode. It should be noted that the current may also be limited by adsorption, or by the rate of a chemical

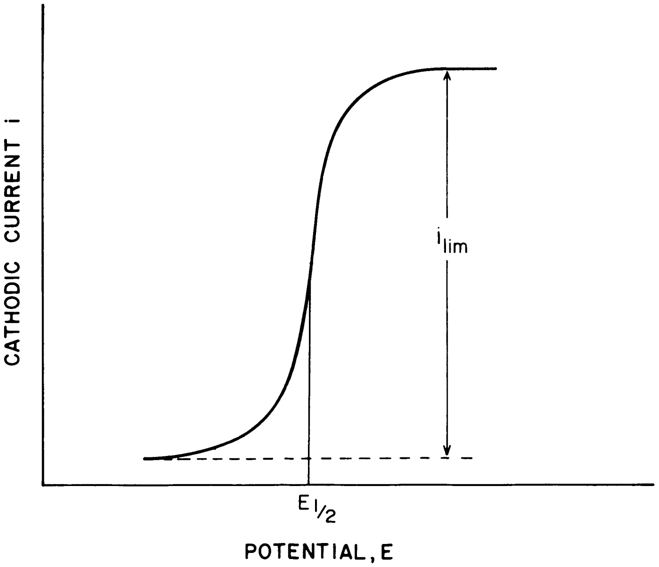

Figure 5. Typical polarogram (schematic) showing diffusion-limited current i_{lim} and half-wave potential $E_{1/2}$.

or a catalytic reaction which is occurring at the electrode surface, and it is essential to determine the nature of a limiting current before further interpretation of polarographic current–potential curves is made (see Section 8.2.3 for further discussion of polarographic limiting currents).

In a polarographic wave for a reversible process, the ratio of activities of R and Ox species at the electrode surface progressively increases from zero at the foot of the wave, through unity at the half-wave potential to infinity as the limiting current is approached. The potentials throughout the wave are determined by the Nernst equation in $(RT/F)\log a_R/a_{Ox}$ and the current densities by Eq. (71) with both forward and backward component terms comparable. With increasing potential, the rate of the reaction and therefore the current increases and eventually becomes limited by the maximum rate of diffusion determined by the bulk solution concentration, the solution viscosity, and the diffusion constant.

In an irreversible process, the potential is no longer given by a Nernst relation throughout the wave and only the forward current–potential term in Eq. (71) applies, especially at elevated potentials. Many electro-organic processes behave in the latter manner.

An equation which describes the diffusion-limited current at an expanding spherical electrode was first derived by Ilkovic.(94) The limiting current, averaged over the lifetime of the drop, is given by

$$I_{lim} = 607zm^{2/3}t^{1/6}D_{Ox}^{1/2}C_{Ox} \tag{74}$$

where the current is measured in microamperes, m is the rate of flow of mercury (mg $\sec^{-1}$), t is the drop time (sec), D_{Ox} is the diffusion coefficient of the reducible species ($\mathrm{cm}^2 \sec^{-1}$), and C_{Ox} is the bulk concentration of the reducible species (m mol liter^{-1}). Although the Ilkovic equation for diffusion-controlled processes is not regarded as entirely satisfactory,(95,96) it can be shown that relations based on this simple equation are valid if the polarographic currents are obtained in the usual way.

The limiting current is independent of potential and is directly proportional to the bulk concentration of the reducible substance (hence, the importance of polarography in analytical chemistry). The half-wave potential ($E_{1/2}$) is that potential for which the condition

$$I = \frac{I_{\mathrm{lim}}}{2} \tag{75}$$

is realized, and it is this parameter which is characteristic of a particular redox system. The half-wave potential for a reversible polarographic process can be expressed as follows:

$$E_{1/2} = E_r^\circ - \frac{RT}{zF} \ln \left(\frac{D_{\mathrm{Ox}}}{D_{\mathrm{R}}}\right)^{1/2} - \frac{RT}{zF} \ln \left(\frac{f_{\mathrm{R}}}{f_{\mathrm{Ox}}}\right) \tag{76}$$

where f_{R} and f_{Ox} are the activity coefficients of the oxidizable and reducible species, respectively. Since $D_{\mathrm{Ox}} \simeq D_{\mathrm{R}}$ at a given ionic strength, it follows that, for a reversible process,†

$$E_{1/2} = E_r^\circ \tag{77}$$

and

$$E_{1/2} = -\frac{\Delta G^\circ}{zF} \tag{78}$$

where ΔG° is the standard free energy change for the redox reaction. Studies of reversible systems therefore allow conclusions to be drawn regarding the states of the oxidized and reduced forms (e.g., involvement of protons, dimerization, etc.), and the effects of structural changes upon ΔG°.

However, only a few organic compounds behave in a polarographically reversible manner; although many may involve a reversible electron transfer step, this is often followed by irreversible chemical reactions. Irreversible processes are those for which the current is limited mainly by the kinetics of the process at the electrode surface and not by diffusion. The nature of such current–potential curves can be described by reference to Figure 6. If electrochemical equilibrium obtains at the electrode surface, then a reversible wave is obtained (curve a). The irreversible wave (curve b) is more "drawn out," i.e., for a given current, say, I_1 or I_2, a higher cathodic potential is required.

† This equivalence of $E_{1/2}$ and E_r° is only true if there is no specific interaction of the reduction product with Hg. For example, $E_{1/2}$ for metals that may be deposited in the Hg phase are much lower than the respective true E_r° values in the electrochemical series.

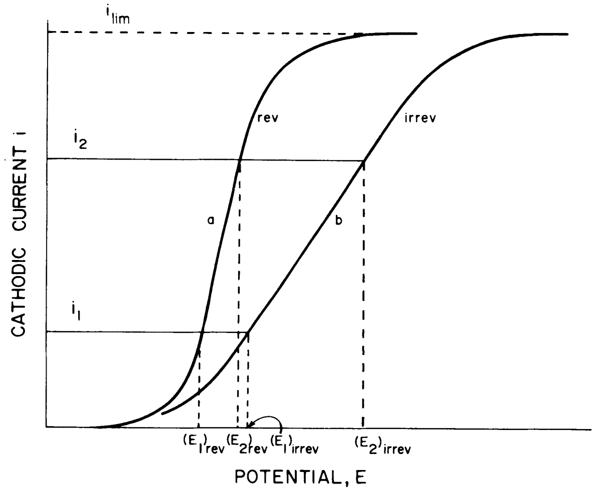

Figure 6. Comparison of reversible (a) and irreversible (b) polarographic waves showing corresponding current I and potentials E at two points on the waves.

In other words, a larger driving force (overpotential) is required to provide a particular current since the electrode process is now activation controlled. However, at very cathodic potentials, the rate of the electrode process becomes relatively "fast" so that the rate of reaction becomes eventually limited by the rate of diffusion of the reducible species to the surface of the electrode, as in a reversible reaction.

The theory of such polarographic currents is based on the work of a number of authors (e.g., see references 54 and 75–77), and an approximate form of the exact solution is given below:

$$\frac{I}{I_{\text{lim}}} = \frac{0.886\,\lambda}{1 + 0.866\,\lambda} \tag{79}$$

where $\lambda = k_b D_{\text{Ox}}^{-1/2} t^{1/2}$. The half-wave potential for irreversible processes depends on the drop time, t,(54,97,98) and although the change in $E_{1/2}$ with changes in t is small, it is nevertheless significant. There is also a dependence upon D_{Ox}, k_b° (the rate constant for the cathodic process when $E = 0$) and the parameter αz_a, where z_a is the number of electrons involved in the activation step.(54) This should be kept in mind in organic polarography where it is customary to seek relations between $E_{1/2}$ and some characteristic property of a series of compounds, e.g., the energy of the highest occupied molecular orbital (HOMO).

A simplified relation between $(E_{1/2})_{\text{irrev}}$ and $\Delta G^\ddagger$, the free energy of activation, has been given by Zuman(83):

$$E_{1/2} = E_r^\circ - \frac{\Delta G^\ddagger}{\alpha z} \log 0.886 \left(\frac{t}{D_{\text{Ox}}}\right)^{1/2} \tag{80}$$

and from this it is concluded that the half-wave potential may reflect the structure and energy distribution of the transition state of the electrode process. Thus, conclusions regarding the mechanism of electrode reactions have been made from analyses of irreversible polarograms, (cf. the determination of rate constants in homogeneous chemical reactions). However, Delahay(54) has pointed out that variations in the half-wave potential can reflect changes in *both* k_b° and αz_a, and it is only for compounds which are very similar in structure that the quantity αz_a will not vary appreciably. Furthermore, in order that conclusions regarding the mechanism of the electrode reaction can be drawn from polarographic waves of irreversible processes, it is essential that only a single rate-determining step be involved. In fact, when an electro-organic reaction is highly irreversible, polarography is probably not the best method for its study, e.g., with regard to elucidation of the kinetics and mechanism of the reaction, since the diffusion control limitations which the polarographic method necessarily imposes on the experimental study of the reaction restrict the information that can be obtained on the kinetics. Reaction order and polarization information is then required but this is better obtained by means of steady state(99,100) or special transient experiments.(101–106) In many cases, insufficient attention has been paid to the *lack* of reversibility of organic electrode reactions studied polarographically. In fact, only relatively few types of reaction approach practical reversibility, e.g., reduction of quinones, some nitroso compounds, chloramines, and some radical-ion-producing reactions in nonaqueous aprotic solvents.

8.2.3. Polarographic Currents

It has already been pointed out that the character of a polarographic limiting current must be established before any interpretation of a polarogram is made. Although several reviews and textbooks(75–83,107) are available in which discussions of polarographic limiting currents have been presented, a brief summary will be given here for reference purposes in this treatise.

8.2.3.1. Charging Currents. A small current ($\sim 10^{-7}$ A) is usually observed in the absence of an electroactive substance and is due to the charging of the electrical double layer at the mercury/solution interface as each new mercury drop forms. In this respect, the dropping mercury electrode behaves as a varying capacitance. The magnitude of this capacitative current in the presence of oxidizable and/or reducible substances may indicate the onset of adsorption or desorption processes which can occur as the applied potential is increased.

8.2.3.2. Diffusion Current. The rate of the electrode reaction increases with increasing potential, and there is a decrease in the concentration of the reducible species in the reaction layer, i.e., in that "layer" of solution adjacent to the electrode surface within which electron transfer to or from the electroactive substance can occur. As $(C_{\mathrm{Ox}})_s \rightarrow 0$, the rate of the reaction becomes limited by the diffusion of the reducible species to the electrode surface, and limitingly $(C_{\mathrm{Ox}})_s$ is effectively zero, so that the electroactive substance is reduced as fast as it diffuses to the electrode. It can be shown(31,54) from a consideration of the diffusion process in terms of Fick's first law that the maximum limiting value for a diffusion current is

$$I_{\lim} = \frac{zFD_{\mathrm{Ox}}A(C_{\mathrm{Ox}})_b}{\delta} \tag{81}$$

where $(C_{\mathrm{Ox}})_b$ is the bulk concentration of the reducible species and δ is the so-called diffusion layer thickness. The proportionality between the limiting current and the bulk concentration, which has formed the basis for development of polarography as an analytical technique, is indicated by this equation.

8.2.3.3. Migration Current. Such currents arise from the movement of charged particles in an applied electric field. In polarography, a supporting electrolyte is used, the concentration of which is large relative to that of the electroactive species. In this way, the contribution to the total current from migration of the reducible ionic species is negligible. Furthermore, neutral molecules are usually involved in organic electrode processes and migration of these species in the applied field is not significant.

8.2.3.4. Kinetic Currents. The discovery of kinetically controlled polarographic waves by Brdicka and Wiesner(108,109) is now considered an important stage in the development of polarography. In these waves the current (and particuarly the limiting current) may be controlled by diffusion of the electroreducible species from the bulk solution *and* by the rate of a chemical reaction occurring before or after electron transfer, or parallel to the electrochemical stage. The most frequently encountered type of kinetic current arises from an antecedent chemical reaction and reactions of this kind have been treated by Mairanovskii(107) together with examples of the other two cases.

The significance of kinetic currents may be indicated by considering the reaction scheme below, which represents an electrode process with a preceding first-order chemical reaction (c, e, type):

$$C \underset{k_2}{\overset{k_1}{\rightleftharpoons}} \mathrm{Ox} \xrightarrow[e]{k_3} \mathrm{R} \tag{82}$$

where $\mathrm{Ox} \rightarrow \mathrm{R}$ is the electron transfer step. The electroactive species is present in solution in two forms, C and Ox, which are different in their depolarizing properties, i.e., Ox is reduced more readily or at lower cathodic potentials than is C. If the rate of the chemical reaction is sufficiently high, then the overall rate of the reaction (and hence the current) will be almost entirely limited by the rate of diffusion of the two species to the electrode surface. However, when the rate of the chemical reaction is slow compared with that of the electron transfer step, the species Ox is reduced as rapidly as it reaches the electrode surface, so that the current is limited partly by diffusion and partly by the rate of formation of the reducible species.

The kinetics of c,e-type processes are also conveniently studied by means of fast-sweep cyclic voltammetry where the current measured depends on sweep-rate due to the time required for the electroactive species Ox to be produced from the initial reactant, C. Information on k_3 in relation to the magnitude of k_1 and k_2 can be obtained from suitably designed experiments.

The limiting current of a kinetically controlled polarographic wave often shows a strong dependence on temperature (unlike I_{lim} for a reversible wave) and is independent of the height (h) of the head of mercury (cf. for reversible waves $I_{\text{lim}} \propto \sqrt{h}$).

8.2.3.5. Catalytic Currents.(107) Many nitrogen and sulfur-containing organic compounds, e.g., alkaloids, pyridine, and quinoline derivatives, lower the overvoltage of the hydrogen evolution reaction at a mercury electrode.(110–112) Thus, in the presence of these compounds, hydrogen discharge waves are observed at potentials less cathodic than the usual hydrogen wave in the same solution. Furthermore, the N- or S-containing compound does not act as a depolarizer but remains unchanged during the electrode process, thus behaving as a catalyst which facilitates the hydrogen evolution reaction. This type of polarographic wave is therefore called a catalytic hydrogen wave and is a special example of a kinetic wave. In fact, catalytic waves show many properties of kinetic waves but, in contrast, a limiting catalytic current can significantly exceed the limiting current corresponding to the given catalyst concentration.

The mechanism of catalytic hydrogen wave formation in the presence of organic bases was discussed by Conway, Bockris and Lovrecek.(112) Essentially the reaction requires the formation of an adsorbed onium compound, i.e., the addition of a proton to the heterocyclic compound which is adsorbed at the electrode surface. Electron transfer to the onium compound occurs at potentials less negative than those required to discharge H_3O^+ or other protonated solvent molecules and the product, which has characteristics of a radical, decomposes to liberate hydrogen and regenerate the heterocyclic base(80):

$$\text{R}\cdot\text{N}_{\text{soln}} \rightleftarrows \text{R—N}_{\text{ads}}$$

$$\text{R—N}_{\text{ads}} + \text{H}_3\text{O}^+ \rightleftarrows \text{R—NH}^+_{\text{ads}} + \text{H}_2\text{O}$$

$$\text{R—NH}^+_{\text{ads}} + e^- \rightarrow \text{R—NH}^\bullet_{\text{ads}} \rightarrow \text{R—N}_{\text{ads}} + 1/2\text{H}_2$$

Catalytic currents of this kind appear to be of little value in the polarography of heterocyclic compounds and are difficult to utilize in quantitative analytical applications. Other examples of catalytic currents have been discussed by Delahay(54) and by Kolthoff and Lingane.(75)

8.2.3.6. Adsorption Currents. In general, adsorption currents appear in a polarographic current–potential curve in one of the two following ways: (i) as one of two kinds of polarographic maxima from which information can be obtained regarding the adsorption of surface active molecules at a dropping mercury electrode, or (ii) due to adsorption of the electroactive species or the product of the electrode process.

Polarographic current–potential curves often exhibit pronounced maxima† which are reproducible and can usually be eliminated by the addition of surface-active agents. These maxima are caused by the tangential movement of the mercury surface, due either to nonuniform polarization (maximum of the first kind) or due to the fast outflow of mercury from the capillary (maximum of the second kind). The adsorption of surface active compounds dampens this movement and therefore reduces the polarographic maxima. The ability of surface-active compounds to suppress maxima arises only in the potential region where their adsorption occurs, a fact which permits the determination of this potential range. Furthermore, at low surface coverages ($\theta \ll 0.5$) where θ represents the fraction of the electrode surface covered by adsorbed organic species) the rate of decrease of this tangential movement depends upon the rate of transfer of the surface-active molecules to the electrode surface. The theory of polarographic maxima and their suppression has been developed by Frumkin and his co-workers, notably Kryukova.(113)

The polarographic waves of many organic compounds show a prewave at potentials less cathodic than the main wave. The height of this prewave is proportional to the bulk concentration of the organic compound only at low concentrations and a limiting height is reached as C_{bulk} increases. This wave is usually attributed to the presence of an absorbed layer and the limiting wave height corresponds to the condition of full surface coverage ($\theta = 1$). In the case of the prewave, it has been suggested that the product of the electrode reaction is adsorbed(99,114) and the adsorption energy facilitates the electron transfer of forward electrochemical process. If the electroreducible compound is adsorbed, then an adsorption postwave is observed on the polarogram, i.e., a wave at potentials *more* cathodic than the main wave.

The effects of adsorption upon electrochemical reactions at a dropping mercury electrode have been discussed in some detail by Mairanovskii.(107)

8.3. Criteria of Polarographic Reversibility

In potentiometric studies of redox reactions, the dependence of the potential of an inert electrode upon the concentrations of the electroactive substances in the solution is measured but a distinction between reversible and irreversible reactions is not provided. The establishment of equilibrium at the electrode surface may be only a matter of time and provided that this time period does not exceed several minutes the redox process can be regarded as reversible. On the other hand, polarographic data reflect the kinetics of electrode processes and conditions for reversibility must be defined more rigorously. Here a system must be sufficiently mobile to rapidly (almost instantly) establish the equilibrium at the electrode surface as the applied potential is changed,† but, as has been stated earlier, few organic systems are polarographically reversible.

---

† A maximum may be defined as an abnormal increase in current above the usual limiting current and is most frequently observed at the beginning of the polarographic wave.(78)

An electrochemical reaction occurring without any significant overpotential (η) is said to be "reversible" and conversely an electrode process occurring with a substantial overpotential is said to be "irreversible." The latter term is, however, relative since all reactions when driven at a net rate require application of a potential E in excess of the reversible potential E_r [Eq. (71)]. In diffusion-controlled processes, as in polarography, the degree of reversibility of an electrode reaction can, however, be usefully(54) regarded as determined by the overpotential required to drive the electron transfer at a velocity equal to or comparable with the rate of diffusion at or near the I_{lim}. The distinction between reversible and irreversible electrode processes is thus somewhat artificial, since a sufficiently large increase in current will, in any reaction, establish an overpotential and hence so-called irreversibility. Quantitatively, it may be concluded(54) that when $k_b > 2 \times 10^{-2}$ cm sec^{-1} the rate of the electrochemical step is so high that the overall rate of reaction will be diffusion limited and the process may be regarded as virtually reversible. Hence, the current and the electrode potential are then determined, through Nernst's equation, very largely by the surface concentration of the electroactive species. As the value of k_b decreases, the shape of the polarographic wave changes, and it becomes more "drawn out" (as in Figure 6). Delahay(54) calculated that the effect of the reverse reaction can be neglected for any value of k_b less than 3×10^{-5} cm sec^{-1} and the wave is then totally irreversible.

Normally, if $I_{\text{lim}} \ll i_0 A$ (where i_0 is the exchange current density, see Section 4), the wave will be reversible unless the reaction has an unusually high Tafel slope. The magnitude of the exchange current density (i_0) may therefore be regarded as an equivalent criterion of the reversibility of an electrochemical reaction, although it involves the additional factor of reactant concentration. A high value of i_0 is usually taken to indicate a reversible process, as in the hydrogen evolution reaction at platinized platinum ($i_0 \simeq 10^{-3}$ A cm^{-2}). Conversely, the very low i_0 value (10^{-13} A cm^{-2}) which arises for the same reaction at a mercury electrode reflects the irreversibility of the process under these conditions.

At currents appreciably displaced from the exchange current, the rate of the reverse reaction of the process is negligible and the current is then essentially an exponential function of the potential. Consequently, the logarithm of the current varies linearly with the potential (Tafel behavior).

† Under typical polarographic experimental conditions, the rate of change of the applied potential is between 30 and 60 mV/sec and therefore a process with a half-time of about 10^{-5} sec will be regarded as instantaneous.

Extrapolation of the linear (Tafel) region of the relation between log (current) and the potential to the condition $\eta = 0$ gives the exchange current density i_0. This presupposes that the potential corresponding to this condition ($\eta = 0$) is known, i.e., that the reversible potential for the electrode reaction is known or can be determined, e.g., from appropriate thermodynamic data. For many organic electrode processes, however, the required thermodynamic data are not available so that E_r cannot be calculated.

Under these circumstances, the Tafel slope may be used to indicate another aspect of the degree of reversibility of the electrode reaction. Since a reversible reaction should occur essentially without significant overpotential, then not only should i_0 be preferably large but the slope of the log $[i]$–E curve should be low; hence, large values (~118 mV) of the Tafel slope therefore reflect irreversiblity of the electrode process in another way.

The magnitude of the exchange current and Tafel slope are useful indications of irreversibility in electrode processes but it is appropriate to consider three conditions that must be fulfilled before a redox system may be regarded as *polarographically* reversible:

(a) The shape of the polarographic curve must correspond to the equation derived for the particular type of electrode process which is involved.

(b) The half-wave potentials of the oxidized and reduced forms of the redox couple must be identical and practically the same as E_r° obtained (where possible) from potentiometric measurements;

(c) The change of the instantaneous current with time for each drop (so-called *i–t* curves) must correspond to the theoretically predicted shape for the electrode process concerned. This agreement should not be confined to the potential region in which the current is limited by diffusion but also should apply to that region of potential in which the current is rising rapidly.

For a diffusion-controlled reversible system, which does not involve semiquinone formation or dimerization of either the oxidized or the reduced forms, the correct shape of the polarographic current–potential curve is described by an equation derived by Heyrovsky and Ilkovic(115) [cf. Eq. (70)]:

$$E = E^\circ + \frac{RT}{zF}\ln\left(\frac{I_{\text{lim}} - I}{I - I_{\text{lim}}}\right)\left(\frac{D_R}{D_{\text{Ox}}}\right)^{1/2} \tag{83}$$

where I_{lim} is the mean diffusion-limited cathodic current, I_d is the mean diffusion-limited anodic current, and i is the mean current at the potential E. Usually, in (cathodic) polarographic experiments, only the oxidized form is present in solution, so that the equation may be simplified as follows:

$$E = E_{1/2} + \frac{RT}{zF}\ln\left(\frac{I_{\text{lim}} - I}{I}\right) \tag{84}$$

Hence, for a reversible system, the well-known linear relation is obtained between the potential E and $\log (I_{\text{lim}} - I/I)$. Other equations have been derived for those reversible systems that involve semiquinone formation, dimerization, or the formation of complex compounds with mercury. Logarithmic analysis of the polarographic wave is often the only proof of reversibility which is considered but recently several authors, in particular Zuman(83) and Delahay,(54) have pointed out that it is inadequate to assume that an electrode process is reversible on this evidence alone. For a reversible reaction, plots of E vs. $\ln (I_{\text{lim}} - I/I)$ give the electron number z from the slope of the plot, RT/zF. A clearer indication of irreversibility is the evaluation of slopes of log i–E curves for higher concentrations (for $i < I_{\text{lim}}$). Irreversible processes will give Tafel behavior.(99)

Comparison of the half-wave potentials of the oxidizable and reducible forms of the redox reactants with the potentiometrically determined value of the standard redox potential is the simplest method for proof of reversibility and agreement between these two sets of data provides strong support for reversibility of the process being studied. However, in many polarographic reactions, it is found that one form of the conjugate redox pair is not sufficiently stable to be prepared or to permit determination of E°_r potentiometrically. In some of these cases, auxiliary methods can be used, particularly where the reactive species is relatively stable when formed at the surface of the mercury electrode. Such methods include the commutator method, an anodic stripping technique which has recently been reviewed by Barendrecht,(116) and oscillopolarographic and cyclic voltammetric techniques.

In 1948 Kalousek(117) introduced the commutator method to establish the reversibility of certain inorganic and organic redox processes. In this method, the electrode potential is alternately switched from a potential at which the reduction product is formed to that potential at which it is reoxidized (cf. cyclic voltammetry). The mean current is recorded against the increasing potential and, for a polarographically reversible process, the observed cathodic (reduction) current is equal but opposite to the anodic (oxidation) current.

A third method for indicating reversibility of an electrode process is based upon the changes of the instantaneous current with time for successive mercury drops.(55) At all potentials along a reversible wave, $\log I$ (the instantaneous current) is linearly dependent upon $\log t$ (when $t > 0.5$ sec). The data for irreversible processes do not exhibit this linearity.

8.4. What Information May Be Obtained from Classical Polarography?

Classical polarography makes possible a rapid evaluation of an electrode process over a wide range of potentials, and at any potential the behavior is not influenced by the prehistory of the electrolysis as occurs in other methods. However, there is little possibility in polarography of ascertaining the chemical nature of intermediates, except intuitively, or of the final products of the electrode reaction, although some conclusions can be drawn from the dependence of the half-wave potential upon drop time and concentration of the reactant if the wave is irreversible. If, however, the overall reaction is polarographically reversible nothing is known of the product of the electron transfer process (except the number of electrons consumed as determined from the wave height of curve analysis). On the other hand, it has already been shown that there is a correlation between $E_{1/2}$ and $\Delta G°$ for a reversible process and between $E_{1/2}$ and $\Delta G^{\ddagger}$ for a completely irreversible process. Therefore, some insight into the thermodynamics or kinetics of the electrode reaction may be gained particularly from studies of homologous series of compounds and from substituent effects in the behavior of a certain parent molecule.

In most cases, electrode processes studied in organic polarography do not involve simply an electron transfer, but also preceding and/or subsequent chemical reactions, and adsorption–desorption phenomena. A single method cannot therefore be expected to elucidate the electrode process fully and information must be obtained from several approaches(99) in order to identify the steps involved in the reaction.(55) From polarographic waves themselves, conclusions regarding the nature of the electroactive species can be drawn from the relative contributions from diffusion and kinetically controlled currents and from the dependence of the half-wave potential upon pH (see below) or the solvent. It is also possible to establish participation of preceding, parallel, or consecutive chemical reactions. However, more information is required, particularly with regard to intermediates and products of the reaction, and this may be obtained from (i) preparative methods and (ii) from other electrochemical techniques.†

8.5. Other Electrochemical Techniques Related to Polarography

8.5.1. Oscillographic Polarography

The development of the fast potential sweep method, which was introduced by Matheson and Nichols(118) and later improved by Randles(119) and Sevcik,(120) is a logical step in the evolution of polarography. Current–potential curves are determined with a stationary electrode, the potential of which varies either linearly or sinusoidally with time. The dropping mercury electrode can be used in this method provided that its area does not vary appreciably during the recording of the complete *i–E* curve. Because of the short duration of the transient, a cathode ray oscilloscope is usually employed as the recorder and the method is generally referred to as oscillographic polarography. The hanging mercury drop electrode provides a useful form of stationary but renewable mercury electrode, and has proven particularly successful in the characterization of intermediates and products by non-steady-state methods such as the potential sweep method.

---

† Such electrochemical techniques have been the subjects of several reviews, e.g., see *Progress in Polarography*, Vols. I and II, P. Zuman and I. M. Kolfhoff, Eds., Interscience, New York, 1962.

Distinction should be made between the so-called single-sweep technique$^{(119)}$ and the multisweep method.$^{(120)}$ In the former method, a single current–potential curve is recorded and the system is brought back to its original condition before a second sweep is made. On the other hand, in the multisweep method, several consecutive *i–E* curves are recorded and the concentration gradient of the electroactive species changes from one sweep to another, particularly from the first to the subsequent ones.

A current–potential curve obtained by the application of a triangular impulse of potential is shown in Figure 7, this curve being recorded at a dropping mercury electrode,$^{(121)}$ and is typical of the current–potential relationship for a markedly irreversible electrode process. In the first case, for a single sweep, from stationary initial conditions, there is zero concentration gradient. Application of the potential ramp causes consumption of reactant and a nonsteady concentration gradient is established. The combination of reactant consumption and exponential increase of rate with increasing potential in the sweep leads to a current–potential curve exhibiting a

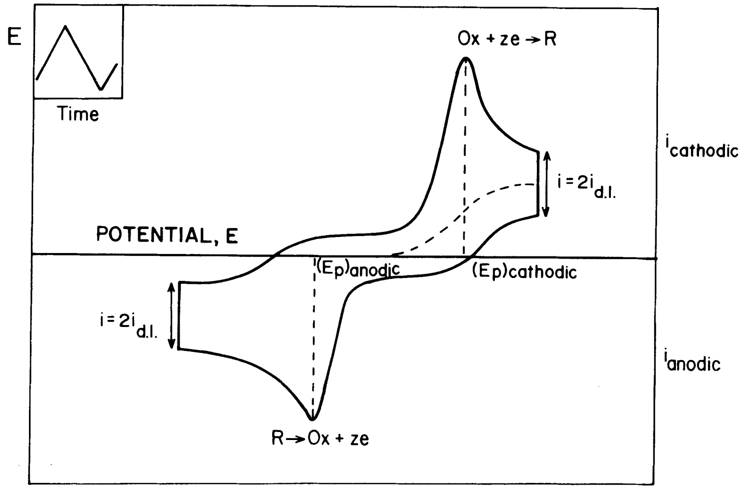

Figure 7. Typical cyclic–voltammetry curve for anodic and cathodic directions of polarization in the case of a diffusion-controlled reversible redox process. i_{dl} is the double-layer charging current density and E_p's the anodic and cathodic peak potentials. Inset shows potential *E*—time program applied to the electrode through a "potentiostat" used in a potentiodynamic configuration. The diagram is schematic.

maximum, I_p; the current then decreases toward a diffusion-limited value as in conventional polarography. The relation between fast sweep behavior and slow polarographic behavior (dotted line) is also illustrated in Figure 7.

If the direction of the applied potential is reversed, i.e., the applied potential then becomes more anodic (or less cathodic) with time, the current suddenly decreases. This rapid change (Figure 7) of current is equal to twice the double-layer charging current for the electrode.$^{(54)}$ The current continues to decrease until the potential becomes sufficiently anodic that oxidation of the product of the reduction reaction can then occur. Again a maximum current $[(I_p)_{\text{anodic}}]$ is obtained and the current then decreases with the continuing change of potential until the direction of the applied potential is again reversed.

In cyclic voltammetry, the forms of the curves will be different from that for the first sweep since the concentration gradients will not be the same at various times during the first and subsequent sweeps. Each cycle gives a cathodic and an anodic branch and the comparison of these cycles can serve as an indication of the reversibility of the electrode process. The following relation between the half-wave potential $E_{1/2}$, obtained from conventional polarography, and the peak potential E_p has been derived by Delahay$^{(54)}$ for a reversible electrode process assuming linear diffusion to the electrode:

$$E_p = E_{1/2} - 1.1RT/zF \tag{85}$$

where R, T, z, and F have their usual significance. The difference in potential between the anodic and cathodic peaks is

$$\Delta E_p = \frac{0.056}{z}\,\text{V} \tag{86}$$

at 25°C. Hence for a one-electron process, a value of ΔE_p, $[(E_p)_{\text{anodic}} - (E_p)_{\text{cathodic}}]$, greater than say 70 mV indicates that the process is irreversible. A note of caution must be introduced here, in that if the product of the electrode process undergoes chemical reactions subsequent to the electron transfer then large differences may be observed between the peak potentials, although the electron transfer step itself may be reversible.$^{(122)}$ For ireversible systems, the displacement between the peaks may be larger or the reverse peak may not be observed at all.

The peak current I_p for the reversible reaction cases is given by

$$I_p = 2.72 \times 10^5\, z^{3/2} A D_{\text{Ox}}^{1/2} (C_{\text{Ox}})_b v^{1/2} \tag{87}$$

for the single-sweep case, where $(C_{\text{Ox}})_b$ is the bulk concentration of the electroreducible species and v is the frequency of the potential sweep (in cycles per second).

The current–potential curves for a totally irreversible process have also been derived by Delahay$^{(121)}$ and the expression for the peak current is then

$$I_p = 3.01 \times 10^5\, z(\alpha z_a)^{1/2} A (D_{\text{Ox}})^{1/2} (C_{\text{Ox}})_b v^{1/2} \tag{88}$$

in which the dependence of I_p upon bulk concentration of the electroactive species and upon the rate of change of potential is again evident. However, the peak current now depends on the product $z(\alpha z_a)^{1/2}$ and since $\alpha < 1$ and $z_a < z$, peak currents for an irreversible process will be smaller than those expected for a reversible electrode reaction. The expression for the peak potential has also been given$^{(122)}$ and E_p is dependent logarithmically upon the rate of charge of the potential but again independent of the bulk concentration of the electroactive substance:

$$E_p = E_i - \frac{RT}{\alpha z_a F}\left(0.77 - \ln k_i + \ln (D_{\text{Ox}})^{1/2} + 0.5 \ln \frac{\alpha z_a F v}{RT}\right) \tag{89}$$

where E_i is the initial potential, i.e., at which the sweep begins, and k_i is the rate constant for the electrode process at that potential. From the equations for the peak potentials for reversible and irreversible electrode processes a further distinction is evident. The peak potential for an irreversible process will become more *cathodic* with increasing sweep rate although the shift is rather small, whereas E_p for a reversible process is independent of the sweep rate.

The discussion hitherto has been concerned only with reversible and totally irreversible electrode processes. However, recent developments in the theory of cyclic voltammetry$^{(101-103)}$ have led to methods for quantitative resolution of electrochemical and preceding or succeeding chemical steps in electrode processes. Nicholson and Shain$^{(102)}$ made a detailed study of the current–potential (time) behavior in stationary electrode polarography for single-scan and cyclic methods ("cyclic voltammetry") applied to reversible, irreversible, and "kinetic" systems.

It will be convenient to list the cases which were treated mathematically; the current functions were evaluated numerically and enable the current-potential scans to be obtained for various cases. They are of great value for comparing the observed experimental behavior in a given system with predictions for various reaction mechanisms: (a) reversible charge transfer (cf. Randles$^{(119)}$ and Sevcik$^{(120)}$), (b) irreversible charge transfer (cf. Delahay$^{(121)}$), (c) chemical reaction preceding a reversible charge transfer, (d) chemical reaction preceding an irreversible charge transfer, (e) charge transfer followed by a reversible chemical reaction, (f) charge transfer followed by an irreversible chemical reaction, (g) catalytic reaction with reversible charge transfer (e.g., $\text{O} + ze \rightarrow \text{R}$; $\text{R} + \text{Z} \rightarrow \text{O}$), and (h) catalytic reaction with irreversible charge transfer.

In particular, the variations of peak current and peak potentials with scan rate are of interest. Normally, the behavior in single-scan and cyclic voltammetry will be different since the initial conditions for diffusion in a single scan experiment are necessarily different from those in a cyclic experiment where the time of relaxation of the concentration gradients in relation to the scan repetition time is an important factor.

Non-steady-state methods such as cyclic or single-sweep voltammetry are able to give both kinetic and (implicit) mechanistic information on organic electrode reactions in the following ways.

Firstly, if the current vs. potential curve generated in a potential sweep experiment is of the irreversible type, and corresponds only to the electron transfer step, then rate constant information can be extracted from the behavior by standard procedures. Secondly, and of more interest, if a chemical step is coupled before or after it, then the magnitude of currents observed will depend on the ratio of the rate constants for the electrochemical and chemical steps, and the relation between the rate constant of the rate-controlling step and the time scale of the experimental measurement, i.e., the potential sweep rate.

The general shape of current vs. potential curves in cyclic voltammetry arises because at the foot of the curve (or corresponding wave) the current tends to increase in the normal way exponentially with potential, while, as potential and time increase in the course of the sweep, the diffusion layer becomes depleted from the electroactive material giving rise to the current in the Faradaic process at the electrode, so the current eventually decreases again, giving rise to the well-known maximum. If a chemical step is coupled to the electrochemical one, either prior to or succeeding, it determines the concentration of the electroactive species in the diffusion layer and the time course of this concentration (related to the sweep rate). Hence, characteristic dependencies of the current vs. potential profiles arise, depending on the type of reaction mechanism, the rate constants of the two (or more) steps, and the sweep rate. Complementary information of a related kind can be obtained in ring–disk rotated electrode experiments by measuring ratios of ring and disk currents (collection ratios) as a function of rotation frequency. Such experiments can also interestingly be conducted in a potential sweep mode and a special system developed by Albery also enables *in situ* photoelectrochemical experiments with organic molecules to be conducted at rotated disk–ring electrodes.

Two-dimensional surface processes also give rise to a current vs. potential curve in cyclic voltammetry having a maximum but the curves are distinguished from those for diffusion-controlled processes by a dependence of the currents on the first power of the sweep rate, while the latter processes give currents related to square root of sweep rate. Coupled chemical steps give similar behavior with respect to changing sweep rate and type of mechanism as do the diffusion-controlled processes except that the curves exhibit maxima determined by depletion of the two-dimensional adlayer rather than the three-dimensional diffusion layer. The characteristic "$t^{1/2}$" behavior found in diffusion-controlled or -influenced processes is therefore not observed. Section 8.5.2 which follows discusses briefly the case of "surface" reactions.

It will be useful next to consider some examples of the behavior of coupled reactions.

The case of dimerization following electron transfer, e.g., in ketone reduction and reduction of some RMe_3N^+ salts, is a special case of a chemical reaction following charge transfer (e and f above). This type of situation has been dealt with specially in papers by Koutecky and Hanus,(45) Saveant and Vianello,(104,105) and by Olmstead, Hamilton, and Nicholson.(106)

A useful analysis of single-scan voltammetric curves was given by Saveant and Vianello(104) and developed for cases where a chemical reaction of any order precedes, follows, or runs in parallel with an electron transfer step. Limiting cases of pure kinetic or complete diffusion control were considered. In a further paper,(105) these authors extended their treatment to the special cases of "monomerization" (isomerization) or dimerization as the coupled chemical step, i.e., for processes such as

$$\mathrm{Ox} + ze \rightarrow \mathrm{R} \qquad 2\mathrm{R} \rightarrow \mathrm{I}$$

or

$$\mathrm{Ox} + ze \rightarrow \mathrm{R} \text{ coupled with } \mathrm{I} \rightarrow 2\mathrm{Ox}$$

where Ox and R are oxidized and reduced forms of the charge transfer reactant. The "monomerization" process corresponds to formation of the electroactive species by a chemical dissociation step. The dimerization process is a common one(123) and arises, e.g., in the well-known case of pinacol formation in ketone reduction. In the case of dimerization, the removal of R from the system by the radical coupling reaction, which is often irreversible, disturbs any equilibrium or quasiequilibrium in the charge transfer process and modifies the polarographic or kinetic behavior.

In the case of "monomerization," the form of the current–potential curve and the values of peak current and potential as a function of sweep rate provide a useful means of characterizing this mechanism. In the case of the dimerization type of reaction, however, the *i–E* curves are not appreciably affected by the chemical reaction. Also, unless the dimerization is relatively slow, the detection of an intermediate in the anodic direction corresponding to a reversed scan is difficult. With acetophenone reduction, for example, reoxidation of the ketyl radical intermediate formed in the cathodic direction of sweep in acid solutions ($CH_3{\cdot}COH^+{\cdot}\phi + e \rightarrow CH_3{\cdot}\dot{C}OH{\cdot}\phi$) is not observed.

Some characteristics of the voltammetric curves as deduced by Saveant and Vianello(105) are given in Table 4. The conclusions of these authors are to be compared with those of Nicholson and Shain(102) (cf. Ref. 106).

Cyclic voltammetry may also be conveniently used in conjunction with the rotating disk technique so that the mass transfer conditions can be independently controlled. This approach is useful for reactions where adsorption effects arise and/or pure kinetic control becomes important.

8.5.2. Cyclic Voltammetry Applied to Surface Processes

Here we shall briefly refer to the use of cyclic voltammetry techniques to surface processes at electrodes, i.e., where chemisorbed species are involved. More detailed reviews of this area have been given elsewhere.

Table 4
Diagnostic Criteria in Linear Sweep Voltammetry(105)

Character of kinetics	Reaction scheme	Shape of polarization curve	Current (peak or plateau) proportionality to		Potential (peak, half-peak or half-plateau) variations with v and $C°$			
			ν_v^{ν}	$(C°)^{\nu}c$	$(\Delta E_v/z)\log \nu$		$(\Delta E_c/z)\log C°$	
			ν_v	ν_c	Direction of variation	$\lvert\Delta E_v\rvert$ mV	Direction of variation	$\lvert\Delta E_c\rvert$, mA
Pure kinetic current	$I \rightleftarrows Ox$	Wave	0	1	Anodic	30	Cathodic	0
	$I \rightleftarrows 2Ox$	Wave	0	3/4	Anodic	30	Cathodic	15
	$R \rightleftarrows Ox$	Wave	0	1	—	0	—	0
	$R \rightleftarrows I$	Peak	1/2	1	Cathodic	30	Anodic	30
	$2R \rightleftarrows I$	Peak	1/2	1	Cathodic	20	Anodic	20
Diffusion current corresponding to a fast establishment of equilibrium	$I \rightleftarrows Ox$	Peak	1/2	1	—	0	—	0
	$I \rightleftarrows 2Ox$	Peak	1/2	1	—	0	Cathodic	30
	$R \rightleftarrows I$	Peak	1/2	1	—	0	—	0
	$2R \rightleftarrows I$	Peak	1/2	1	—	0	Anodic	30
Diffusion current corresponding to a slow establishment of equilibrium	$I \rightleftarrows Ox$	Peak	1/2	1	—	0	—	0
	$I \rightleftarrows 2Ox$	Peak	1/2	1/2	—	0	—	0
	$R \rightleftarrows Ox$	Peak	1/2	1	—	0	—	0
	$R \rightleftarrows I$	Peak	1/2	1	—	0	—	0
	$2R \rightleftarrows I$	Peak	1/2	1	—	0	—	0

In cases where electroactive intermediates arise in an adsorbed state on the electrode, e.g., in reactions such as

$$e + Pt + H_3O^+ \rightarrow PtH_{ads} + H_2O$$

or

$$Pt + H_2O \rightarrow \text{“PtOH”} + H^+ + e$$

current peaks arise, but i_p is found to be proportional the *first* power of the sweep rate v. This arises because in the formation or removal of reversibly electrodeposited ad-species a pseudocapacitance C_ϕ arises, associated with the potential dependence of the coverage θ ($C_\theta = k\, d\theta/dE$) and the charging or discharging current brought about by a linearly varying potential is then given by

$$i_\theta = C_\phi\, dE/dt \tag{88}$$

i.e., the current in the charging process is always proportional to sweep rate except when irreversibility sets in, e.g., as it must eventually at sufficiently high sweep rates. The linearity of i_θ with v provides an important diagnostic indication of the role of electroactive adsorbed species in a reaction. Unlike the curve of Figure 7 for a reversible, diffusion-controlled reaction, the anodic and cathodic curves for a simple $1e$ surface reaction are mirror images.

Many electrocatalytic processes involve a complex combination of surface charging processes (H or OH or O deposition and removal) and net Faradaic reactions, in which the surface species are themselves involved and cause effects associated with inhibition of the main reaction sequence or of coreactions. The Faradaic reactions may also be partly diffusion controlled, which leads to the most complex behavior. In cases where surface oxide films arise which are substantially thicker than a monolayer, e.g., as at Ni or Ag electrodes, the time-dependent current in a sweep experiment reverts to a square root dependence on sweep rate and this effect arises either because of a dissolution–precipitation mechanism of oxide layer growth or because of solid state diffusion effects.

It should be mentioned that few, if any, examples are known of carbon-containing species chemisorbed at electrodes that are directly electroactive like H or OH/O species. Only in the case of adsorbed quinones or polymer-bound redox functions at chemically modified electrodes is direct surface electroactivity known. Some organic sulfide/disulfide pairs such as cystine/cysteine are also electroactive when adsorbed.

The time-dependent currents which arise in sweep experiments in anodic oxidations which proceed in the presence of, or through reaction with, surface oxides (e.g., methanol oxidation, oxidation of hydrocarbons at Pt) were considered by Conway, Kozlowska, Klinger, MacDougall, and Tilak,(124) who obtained numerical solutions for the kinetics in selected cases.

The currents arising in the sweep under such conditions are determined by (a) diffusion and adsorption of the reactant, (b) coreaction between a surface oxide and the oxidizable organic substance, (c) inhibition of the adsorption of the reactant by electrochemisorbed oxygen species at noble metal electrodes at potentials more anodic than $\sim +0.8\text{ V}$ *vs.* E_{H}, (d) inhibition of the reaction itself by effects on its activation energy due to the presence of coadsorbed surface oxide. All these processes are dependent on sweep rate in a complex manner and make the quantitative analysis of cyclic voltammetric curves a matter of difficulty. The use of single-sweep techniques coupled with an electrochemical pretreatment program of the type used by Gilman(125) offers the most satisfactory approach to the study of processes accompanied by electrochemisorption and oxidation of the electrode surface.

Other applications of cyclic methods have been discussed, e.g., by Badoz-Lambling(53) and by Heyrovsky.(126)

Recent technical developments include the use of on-line minicomputers for data acquisition and processing of cyclic voltammetry data and, in some applications, for the control of the experiments themselves. The work of Perone(127) should be mentioned especially here as well as that of Mark.(128)

8.5.3. Alternating Current Polarography

In this method, a superimposed ac signal is applied to the potential sweep and a *derivative* response is generated, i.e., at the midpoint of the regular polarographic (dc) wave, a peak in the ac response curve is generated like the peak current in a fast sweep voltammetry curve. The method has some advantages in sensitivity, especially in distinguishing processes having close half-wave potentials.

The development of ac polarography and its application to the study of processes occurring at a dropping mercury electrode (or a hanging drop mercury electrode) was a direct result of the fundamental studies of several workers(129–131) in the middle and late 1940s. Increasing interest has been shown in this technique through the last two decades and it may now be regarded as a highly important addition to recent methods available for electrochemical studies.(54,132–135)

Basically, the ac polarographic experiment involves measurement of the impedance of an electrolytic cell under polarographic conditions, using an alternating potential of small amplitude ($<10\text{ mV}$) which is superimposed upon the potential of the working (indicator) electrode. This impedance may be related to the kinetics and mechanism of the electrode reaction as well as to the concentration of the electroactive species.

Although the Faradaic process is frequently the primary subject of ac polarographic experiments, the simultaneous study of the capacity of the double layer which the method allows has provided valuable information upon the influence of adsorption of organic substances upon this capacity and therefore its role in electroorganic reactions.(136–138)

8.5.4. Current-Potential Curves at Stationary Mercury Pool Electrodes

Although the renewability of the electrode surface is often considered to be a necessary prerequisite for useful analytical applications of polarography, current–potential curves can be obtained with a stationary pool electrode(99,139,140); with stirring, measurements can be made at concentrations as low as 5×10^{-7} mol liter^{-1}. The curves were shown to be similar to those obtained by a single-sweep method at a dropping mercury electrode (dme), i.e., they exhibited characteristic maxima, the heights of which varied linearly with the concentration of the reactant. It is found that at scan rates comparable with those used in conventional polarography ($\simeq 400$ mV min^{-1}) and at comparable current densities to those encountered in a polarographic wave, the curves recorded at a stirred mercury pool electrode are quite reproducible (cf. Ref. 99).

Comparison of polarographic curves at the dme with the current–potential curves obtained at a stirred mercury pool is important with regard to the identification of products of electrolysis.(141) In most cases, the number, the shape, and the half-wave potentials of the waves are identical, e.g., as in the behavior of *p*-diacetylbenzene referred to by Zuman.(55) However, cases have been reported in which differences are observed and in some there is no resemblance at all between the results obtained at a dropping mercury electrode and at a stationary mercury pool. This may arise because extents of adsorption of the reactant are different, since studies at the dme are usually conducted with solutions of low concentration, 10^{-5}–10^{-3} *M*, while preparative experiments at a pool electrode are conducted at much higher concentrations.

8.6. Polarographic Studies of pH Effects and Reaction Mechanisms

In protic media, electron transfer must be followed, or be coupled with, *proton transfer* in organic reduction processes, except in the case of high pH when an anion may be formed. For the production of a stable product which is not a free radical, two electrons must be transferred and up to two protons will also be involved depending again on the pH. The course of electro-organic reductions depends on the stage at which the first proton is taken up, i.e., before or after the first electron transfer. Rates of protonation can also determine the kinetics. A considerable variety of different cases can be recognized, depending on the order of electron and proton transfer, and may be distinguished by appropriate steady state kinetic experiments or by means of polarography where the dependence of (a) half-wave potential $E_{1/2}$ and (b) wave height of diffusion limited current on pH can be investigated and related to the kinetic pathway of the reaction. A thorough discussion of these matters has been presented by Zuman(142) in a monograph and in various papers and the brief account given below is based on his classification of the types of case encountered.

Most work in aqueous media has been carried out on reductions owing to the limited range of potentials which can be explored anodically at the mercury surface. Oxidations involving simply electron transfer steps have, however, been extensively investigated by polarographic and other techniques in *aprotic* media at inert (Pt) anodes but in aqueous media, anodic reactions at Pt are mainly determined by heterogeneous processes involving the oxidized Pt surface.(124,125) The products of such reactions are often complex and the mechanism of the reactions usually involves dissociative adsorption at the electrode surface. Here the discussion of pH effects will be restricted mainly to reactions proceeding reductively at "noncatalytic" electrode surfaces, principally Hg.

pH effects may be studied in two principal ways: (a) by means of evaluation of reaction orders in $[H^+]$ at various controlled potentials in steady state electrolysis, or (b) by polarography. In the latter procedure, the two quantities that may depend on pH are the half-wave potential $E_{1/2}$ and the diffusion-limited current density i_{lim}. $E_{1/2}$ may vary if the type of species undergoing reduction depends on pH and i_{lim} will depend on its concentration plus that of any other type of species reducible at, or near, the same $E_{1/2}$ value. Various cases may arise depending on the complexity of the reaction and the type of protonation equilibria that are involved, and also the kinetics of protonation. In the following section are summarized the various principal possibilities arising polarographically.

(i) In the simplest case of a single reduction wave which exhibits an $E_{1/2}$ and i_{lim} independent of pH, the substance in the bulk of the solution is usually the only electroactive species and diffuses as such to the electrode surface. No proton transfer event precedes the electron transfer step. Any transformation which the substance in the bulk may undergo in its approach to the electrode must also be pH independent. In these cases, electron transfer steps must precede proton transfer steps.

(ii) In the case where the $E_{1/2}$ is dependent on pH but the i_{lim} is not, a fast acid–base equilibrium involving the electroactive species must be involved, e.g.,

$$\text{HA} \rightleftarrows \text{A}^- + \text{H}^+$$

where either HA or A^- is the species reduced at the electrode. $E_{1/2}$ varies since the concentration of the reducible species at the electrode depends on pH. Similar effects may arise in an anodic process.

A further case in the above category arises when the protonation rate depends on pH and becomes slow under certain pH conditions. If both the acidic and basic forms of the organic substance in solution can be reduced, a common wave may arise in the pH range where slow protonation occurs. Since the total amount of the substance available for reduction is the same, independent of pH (α the fraction in the form HA and $1-\alpha$ in the form

A^-) $i_{\lim}$ will remain constant. In all these cases, protonation *precedes* electron transfer (H^+, e, H^+, e or H^+, e, e, H^+).

For a system in which an equilibrium protonation precedes electron transfer to the acidic form HA, the variation of $E_{1/2}$ with pH near the pK for the protonation equilibrium (constant K) is given by

$$E_{1/2} = C + \frac{RT}{\alpha zF} \ln \frac{[\mathrm{H}^+]}{K + [\mathrm{H}^+]^m} \tag{89}$$

where m is usually 1 for a monobasic acid and C is a constant. In this case, $E_{1/2}$ undergoes an inflection near pH = pK as pH is increased.

(iii) The third type of case arises in polarograms where both $E_{1/2}$ and $i_{\lim}$ are dependent on pH. The latter complication obviously indicates that the amount of electroactive species diffusing to the surface depends on pH, an effect that may arise for thermodynamic or kinetic reasons. Usually the kinetic effect arises in a pH dependent acid/base reaction where only *one* of the species HA or A^- is electroactive; $i_{\lim}$ decreases as soon as a pH-limited rate of formation of the electroactive species determines the rate of reduction. Alternatively, the electroactive form may be generated from an inactive form in an acid- or base-catalyzed reaction or it may arise in a tautomeric equilibrium. Another possibility is that both forms of the conjugate acid/base pair are reducible but differ with respect to the total number of electrons (z_{HA}, z_{A^-}) that can be transferred. This will cause $i_{\lim}$ to vary with pH, as well as $E_{1/2}$, since the type of species reduced changes with pH. Usually the values of $i_{\lim}$ at low and high pH will bear a simple relation to one another, viz., $z_{\mathrm{A}^-}/z_{\mathrm{HA}} = 2$.

In the case of a protonation-limited rate, the ratio of currents due to Ha reduction and that of $i_{\lim}$ at low pH is given(143) by

$$\frac{i_{\mathrm{HA}}}{i_{\lim}} = \frac{0.886(k_r t_l [\mathrm{H}^+]/K)^{1/2}}{1 + 0.886(k_r t_l [\mathrm{H}^+]/K)^{1/2}} \tag{90}$$

where K is the dissociation constant for

$$\mathrm{HA} \rightleftarrows \mathrm{A}^- + \mathrm{H}^+$$

and k_r is the recombination rate constant for A^- with H^+.

Reduction of the tropylium ion investigated by Zuman *et al.*(144) provides an example of the above type of behavior. In the case of a chemical step dependent on pH, e.g., hydration or acid-catalyzed rearrangement, the relation analogous to (90) above is

$$\frac{i}{i_{\lim}} = \frac{0.886(K_c k_c t_l)^{1/2}}{1 + 0.886(K_c k_c t_l)^{1/2}} \tag{91}$$

where K_c is the equilibrium constant for the chemical step, k_c its forward rate constant, i.e., in the direction of production of the electroactive species, and $i_{\lim}$ is the wave height in the pH-independent limit, or in the absence of an observed value for this, a calculated value based on the diffusion constant.

The commonest examples of this behavior arise with aldehydes,$^{(142)}$ viz.,

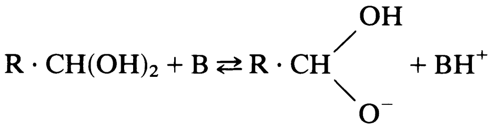

$$\mathrm{R \cdot CH(OH)_2 + B \rightleftarrows R \cdot CH\begin{matrix} \diagup \mathrm{OH} \\ \diagdown \mathrm{O^-} \end{matrix} + BH^+}$$

hydrated form

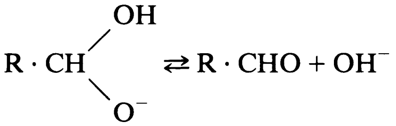

$$\mathrm{R \cdot CH\begin{matrix} \diagup \mathrm{OH} \\ \diagdown \mathrm{O^-} \end{matrix} \rightleftarrows R \cdot CHO + OH^-}$$

$$\mathrm{RCHO + 2e + 2H^+ \rightarrow RCH_2OH}$$

(iv) Various more complex cases arise where the polarograms exhibit two waves. The wave heights may (a) remain constant, (b) vary with pH due to protonation steps prior to the first electron transfer step, or (c) change with pH due to other chemical steps arising between the two stages of electron transfer.

In the case where the *ratio* of wave heights remains constant with pH, either (α) or $E_{1/2}$ of the more positive wave is dependent on pH, while that of the second is independent or (β) the $E_{1/2}$ of the more negative wave is shifting while that of the more positive one remains constant. For the first of these two cases, (α), the resolved polarogram in acid media coalesces to one wave at higher pH, while the reverse effect arises in the second case (β). Zuman has considered the following scheme for these two cases. The initial step is fast (equilibrium) protonation prior to the first electron transfer but no further protonation is envisaged until the second electron has been transferred:

$$\mathrm{A^- + H^+ \rightleftarrows HA}$$

$$\mathrm{HA + e \rightarrow HA^-}$$

$$\mathrm{HA^- + e \rightarrow HA^{2-} \rightarrow product}$$

Reductions of certain carbonyl compounds in acid media proceed by this mechanism but not in the case of pinacol formation where dimerization of a ketyl radical follows electron transfer.

Case β can be accounted for in terms of a reaction mechanism such as

$$\mathrm{A + e \rightarrow A^-}$$

$$\mathrm{A^- + H^+ \rightleftarrows HA}$$

$$\mathrm{HA + e \rightarrow HA^-}$$

Many examples arise where the ratio of wave heights is not constant and varies with pH due to acid/base protonation reactions occurring before the first electron transfer step. A scheme which accounts(142) for the case of the *sum* of the wave heights remaining constant is

$$\mathrm{HA} \rightleftharpoons \mathrm{A}^- + \mathrm{H}^+$$

$$\mathrm{HA} + z_{\mathrm{HA}}\mathrm{e} \rightarrow \mathrm{P}_1 \qquad E_{1/2}(1)$$

$$\mathrm{A}^- + z_{\mathrm{A}^-}\mathrm{e} \rightarrow \mathrm{P}_2 \qquad E_{1/2}(2)$$

where $E_{1/2}(1)$ and $E_{1/2}(2)$ are the half-wave potentials for reduction of the two types of species. At low pH, a single wave arises for HA reduction, while at high pH A^- is predominant and gives again a single wave. At intermediate pH, two waves with half-wave potentials $E_{1/2}(1)$ and $E_{1/2}(2)$ are resolved corresponding to the distinguishable reductions of A^- and HA.

It must also be noted that the *shapes* of the waves may be different if the reduction of one species is less reversible than that of the other or if differential adsorption effects are significant. For example, the ionized form of a conjugate acid/base pair is usually less adsorbed than the neutral (acid) form. Adsorbability also usually changes inversely as solubility and will depend on protonation.

The reaction scheme in which a pH-dependent intermediate process arises between the two stages of electron transfer may be represented as follows:

$$\mathrm{A} + z_{\mathrm{A}}\mathrm{e} \rightarrow \mathrm{P}_1 \qquad E_{1/2}(1)$$

$$\mathrm{P}_1 \rightleftharpoons \mathrm{P}_2;\, f(\mathrm{pH})$$

$$\mathrm{P}_2 + z_{\mathrm{B}}\mathrm{e} \rightarrow \mathrm{P}_3 \qquad E_{1/2}(2)$$

Two waves arise with the indicated half-wave potentials. The wave height for the process $\mathrm{P}_2 + z_{\mathrm{B}}\mathrm{e} \rightarrow \mathrm{P}_3$ occurring at the more negative potential will obviously depend on the rate at which electroactive P_2 is generated from P_1, which is itself assumed to be electroinactive. Examples where this type of behavior arises are the reductions of α-substituted ketones, aromatic bicarbonyl compounds such as p-diacetylbenzene, terephthaldialdehyde and α,β-unsaturated ketones. Restricting ourselves to one type of example discussed by Zuman,(142) the following is the scheme for reduction of an α-substituted ketone $\mathrm{R\cdot CO\cdot CH_2X}$, where $\mathrm{X = NR_2}$,(147–147) $\mathrm{N^+R_3}$.(147) SR,(148) $\mathrm{S^+R}$,(149), OR,(148) $\mathrm{P^+R_3}$,(146) or a halogen residue(150):

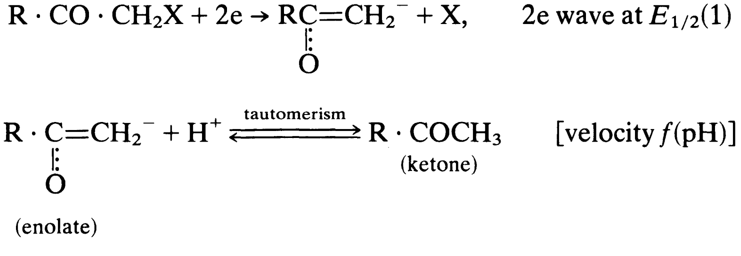

$$\mathrm{R\cdot CO\cdot CH_2X + 2e \rightarrow R\underset{\substack{\vdots \\ O}}{C}{=}CH_2^- + X}, \qquad \text{2e wave at } E_{1/2}(1)$$

$$\mathrm{R\cdot \underset{\substack{\vdots \\ O}}{C}{=}CH_2^- + H^+ \xrightleftharpoons{\text{tautomerism}} R\cdot COCH_3} \qquad [\text{velocity } f(\mathrm{pH})]$$

(ketone)

(enolate)

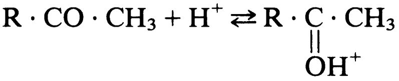

$$R\cdot CO\cdot CH_3 + H^+ \rightleftharpoons R\cdot \underset{\underset{OH^+}{\|}}{C}\cdot CH_3$$

[equilibrium or rate f(pH)]

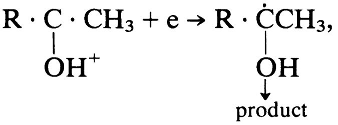

$$R\cdot \underset{\underset{OH^+}{|}}{C}\cdot CH_3 + e \rightarrow R\cdot \underset{\underset{\text{product}}{\underset{\downarrow}{\underset{OH}{|}}}}{\dot{C}}CH_3,$$

1e wave at $E_{1/2}(2)$

The tautomerism is acid/base catalyzed and its rate controls the height of the more negative wave. The second reduction in the case R = phenyl can be identified with acetophenone but at a concentration determined by the rate of enolization to produce the keto form which is electroactive in the protonated condition.

9. Steric Aspects of Electro-Organic Reaction Mechanisms

9.1. Adsorption of Intermediates and Stereochemical Effects

Considerable interest arises in electrochemical·reactions in which a chemisorbed radical may be formed from an initially optically active center. In certain cases, chirality of the radical produced may be preserved if chemisorption occurs and leads to stereochemically different products from those which may arise in the corresponding homogeneous reaction. Examples which have been considered are products arising from reduction of certain ketones and in decarboxylation. For example, the stereochemistry at the C* center in a radical RR′R″C· derived from an acid RR′R″C · COOH may be preserved if the radical is chemisorbed. Also, the radio of *dl* to *meso* diastereoisomers in the case of dimeric products may differ according to whether the products are formed heterogeneously or homogeneously. Steric effects can also influence the reduction of *cis* and *trans* reactants or the formation of *cis* and *trans* products in appropriate cases.

Various cases of the above effects have been considered by Brewster,(151,152) including the question of reduction of cycloalkyl ketones to equatorial or axial alcohols depending on the orientation at the electrode surface and the pH. In neutral medium, the equatorial alcohol is produced according to the scheme

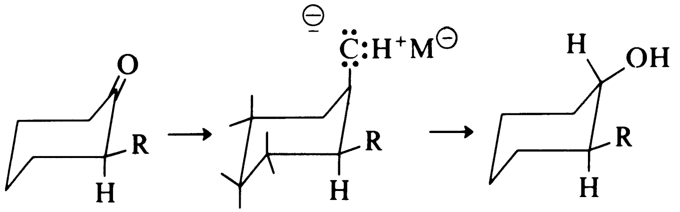

involving participation of the electrode as adsorbent for the OH group. In acid medium, where the protonated form of the ketone is reduced,(48) it is proposed that the reduction proceeds according to the scheme

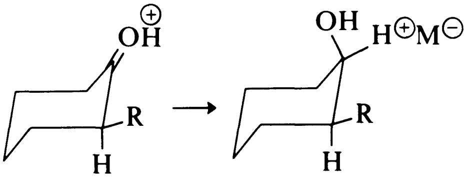

These effects are observed in a more pronounced fashion in reduction of steroid ketones where the structure is rigid.

In many cases of organic reductions, direct participation of metal–organic intermediates is indicated, e.g., in the Clemmensen reduction of ketones at Pb and Hg where hydrocarbons are formed as well as pinacols or alcohols.

With ketones in acid media, Brewster(152) suggests the following path with interaction with the electrode surface:

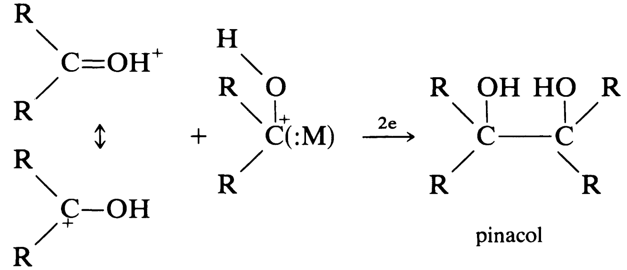

Clemmensen reductions of saturated, unsaturated, and α-substituted ketones were discussed.

A concerted effect of the negative electrode surface was also recognized by Elving(58) and Elving and Leone(153) in their studies in ketone reduction. A progressive polarization of the $>$C=O bond by the field of the cathode was proposed with uptake of a proton to give an adsorbed ketyl radical K which could either become further reduced (neutral or alkaline solution) or dimerize to form the pinacol as in other reaction schemes.

The question whether significant adsorption of an intermediate is involved, and hence, whether dimerization is heterogeneous or homogeneous, has received some attention(154) in relation to the stereochemistry of the pinacol product in ketone reduction; either a *d–l* racemic mixture or the *meso* form, or both, can be produced. Under acidic conditions, in 80% aq. EtOH, it has been argued that because the *dl* : *meso* ratio is dependent only slightly on the electrode material (Cu, Sn, or Hg), recombination of K radicals is homogeneous. This evidence does not necessarily indicate absence of adsorption of radicals but, alternatively, comparable adsorption of the three electrodes. In alkaline solutions, where the intermediates are radical anions, adsorption will be less favored and the *d* : *l* : *meso* ratios are in fact then quite different from those found in acid solutions. Arguments for heterogeneous recombinations have, however, been proposed by Brewster(152) and the observation by Puglisi *et al.*,(155) that the *dl* : *meso* ratio in hydrobenzoin produced in the electrolytic reduction of benzaldehyde at Hg is substantially modified by specific adsorption of I^- indicates recombination among adsorbed radicals.

In the observations of Stocker and Jenevein,(154) the diastereomeric ratios in the formation of acetophenone pinacol were substantially different in acidic and basic media being 0.9–1.4 *dl*/*meso* and 2.5–3.2 *dl*/*meso*, respectively, a fact which led these authors to conclude that the combining intermediates are not the same in acidic and basic media.

Dimerization resulting from bimolecular reaction among free radicals resulting from electronation of the protonated forms of the ketone (acetophenone) can occur according to the following stereochemical representations of the formation of pinacols:

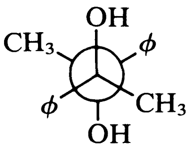

A (yields *meso*)

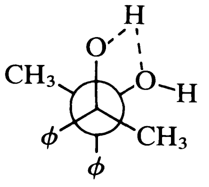

B (yields *dl*)

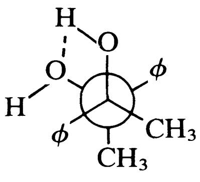

C (yields *dl*)

A is included on steric grounds and B and C show the H bonding which can arise.(154)

In acidic media, almost the *same* amount of the two diastereoisomers are formed, a fact which leads to the conclusion that H bonding (B, C) plays an important role in the pinacol C–C bond formation.

In more basic media radical anions are produced by electron transfer to the neutral ketone and the anions become protonated in the course of the reaction. It is proposed that this mixture of radicals and radical anions can react in three ways; i.e., combination of like species or cross-coupling as may be visualized(154) by replacing one of the hydroxyl groups in A and the donor O in B and C with an oxygen *anion*, yielding the corresponding conformers at the time of coupling in basic solution. The relatively enhanced (see above)

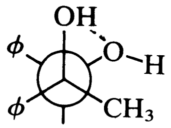

D

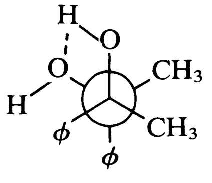

D′

production of the *dl* form would then follow from the increased preference of radical–radical anion conformation derived from B or C relative to A. A final possibility involving H bonding and leading to the *meso* form can be formulated (D, D′). Either formulation involves both nonbonded interactions between CH_3 and CH_3, and between ϕ and ϕ.

9.2. Alkyl Halide Reduction and Stereochemical Effects

A type of reaction of considerable mechanistic interest in the kinetics of electrochemical and solvolytic reactions is the reduction of alkyl halides RX where a nucleophilic substitution type of reaction occurs with the "electrode" acting as the nucleophile. The anion X^- and the hydrocarbon RH are the main products. In some cases, organometallic intermediates are produced, e.g., in the reduction of alkyl iodides or bromides at Pb. Here the process which leads to lead tetraalkyls is of considerable commercial significance.

Stereochemical studies have been carried out by Annino *et al.*(156) on reduction of 1-bromo-2,2-diphenylcyclopropane carboxylic acid where the role of adsorption at the electrode surface and inversion of configuration was investigated. The following summary of their conclusions illustrates the value of stereochemical considerations but, at the same time, exemplifies some of the problems that arise depending on reaction conditions. A general mechanism for electroreduction of carbon–halogen (X) bonds was considered by Elving and Pullman(58) involving the steps

$$RX + e \rightarrow [R^\cdot] + X^-$$

$$[R^\cdot] \rightarrow R^\cdot$$

$$2R^\cdot \rightarrow R_2$$

and

$$[R^\cdot] + e \rightarrow [R^-]$$

$$R^- + SH \rightarrow RH \qquad (SH = \text{solvent proton source})$$

where $[R^\cdot]$ and $[R^-]$ are adsorbed species associated with the electrode surface. It is evident that this mechanism involves both carbanions and radicals with corresponding products (dimers RR or disproportionation or H abstraction types of products, e.g., an olefin R′ and the paraffin RH). An example is the reduction of benzyl halides.(157) The scheme of Elving and Pullman(58) involves a nucleophilic attack by electrons from the metal surface on the C atom of the CX bond polarized in the double-layer field as in their mechanism for ketone reduction. On the other hand, various proposals have been made that in bridgehead halides,(158) and perhaps generally, initial attack occurs on the X atom. By examination of reduction of X at an asymmetric center, Annino *et al.*(156) sought to provide a basis for distinction between the above two pathways. Cyclopropyl bromides were employed as these can exist in optically active forms and the cyclopropyl carbanions invert at a very low rate. Thus, it would be possible to observe stereospecificity in the reaction even if the electrode adsorption complex becomes desorbed to free carbanions before reaction with a source of protons. On the other hand, if a free radical intermediate were formed, rapid racemization would be expected since cyclopropyl radicals suffer relatively rapid inversion. If a carbonium intermediate were formed, rearranged products would obviously be expected. Reductions of 1-bromo, 2-diphenylcyclopropane carboxylic acid and its derivatives were carried out at Hg and Zn electrodes. The reactions were

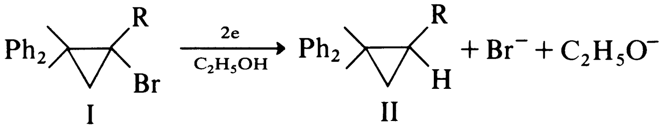

with R = (a) COOH, (b) $COOCH_3$, or (c) CH_3. The products II were obtained in high yield with 2e per mole passed in the electrolysis. Dimeric or rearranged products were absent, indicating negligible participation of free radical or carbonium ion intermediates.

Although preliminary experiments of Annino *et al.*(156) with optically active I yielded inverted II which suggested that an SN_2-type mechanism was operative followed by either an SE_2 reaction at the electrode complex III or protonation of the inverted carbanion IV (see below) after diffusion into the bulk of the solution, the complete set of data (reproduced in Table 5) indicate a more complex situation. The more important indications in this table are the predominant *retentions* of configuration observed in the cases of Ic and Ia reductions in basic solution. For an SN_2-type addition of electrons shown below (the electrode surface acting as the nucleophile providing a delocalized source of 3), a double inversion is required if overall retention is exhibited; i.e., a second inversion after electron transfer of the intermediate carbanion is necessary, followed by protonation from the side not shielded by the electrode before diffusion occurs into the bulk of the solution. Such a sequence of reactions is, however, more likely with Ia and Ib than with Ic and Ia anion (in the basic medium) since the COOH and COOMe groups are expected to diminish the barrier to inversion. Also the carbanions from the Ia anion and from Ic are more likely to retain their inverted configuration until protonated in solution. These results were regarded as important evidence against the SN_2-type mechanism, and results obtained in the reductions with Zn supported this viewpoint (Table 6).

A schematic course of the reaction is shown in Scheme 1, and as the authors point out, is not intended to represent the exact details of the electroreduction mechanisms.

The observed stereochemistry (Table 5) may be explained(156) by means of two main proposals: (i) that the initial attack by the electrode occurs on the *same* side of the molecule as the Br atom to give an adsorbed complex with the same configuration as the reactant; (ii) the overall stereochemistry is then determined by a stereoselective reaction of the free or electrode-

Table 5

Electrolytic Reduction of 1-Bromo-2,2-diphenylcyclopropanecarboxylic Acid (Ia), Methyl 1-Bromo-2,2-diphenylcyclopropanecarboxalate (Ib), and 1-Bromo-1-methyl-2,2-diphenylcyclopropane (Ic)[(156)]

			Electrolyte				
Compound	% Inversion	% Retention	Salt (0.1 *M*)	Acetic acid, *M*	OH^-, *M*	E_c, V[a]	% Yield
Ia	26		TBABr	0.04–0.17	0	−1.2 to −1.4	90–96
Ia	35		TEABr	0.17	0	−1.1 to −1.2	86
Ia	30		LiCL	0.17	0	−1.2 to −1.5	86–90
Ia		31		0	0.02–0.05	−1.7	91
Ia		38	TBABr	0	0.02	−1.7	85
Ib	43			0.17–0.34	0	−1.1 to −1.5	85–90
Ib	35		TEABr	0.17	0	−1.2	73
Ib	30		LiCL	0.17–0.34	0	−1.3 to −1.4	86
Ib	56		TBABr	0	0.02	−1.6	87
Ib	46		TEABr	0	0	−1.3 to −1.6	86–95
Ib	34		LiCL	0	0	−1.3 to −1.5	95
Ic		21	TEABr	0	0	−2.2	73–80

[a] E_c, effective potential at which material was electrolyzed, reported vs. aqueous sce.

shielded carbanion with solvent or a proton. In Scheme 1, IIIa or IIIb result from transfer of the first electron; the addition of the second electron yields the absorbed carbanion species IV. Following steps may occur along two

Table 6
Zinc Metal Reduction of Compounds 1a, b, c(156)

Compound		% Inversion	% Retention	% Yield
Ia	Glacial acetic acid, room temp., 48 hr,	21		61
	10% KOH–ethanol, room temp., 18 hr		26	82
Ib	Glacial acetic acid, room temp., 48 hr	15		68
	Neutral ethanol and zinc, 48 hr	11		95
Ic	10% KOH-ethanol, room temp., 30 hr		21	80

Scheme 1

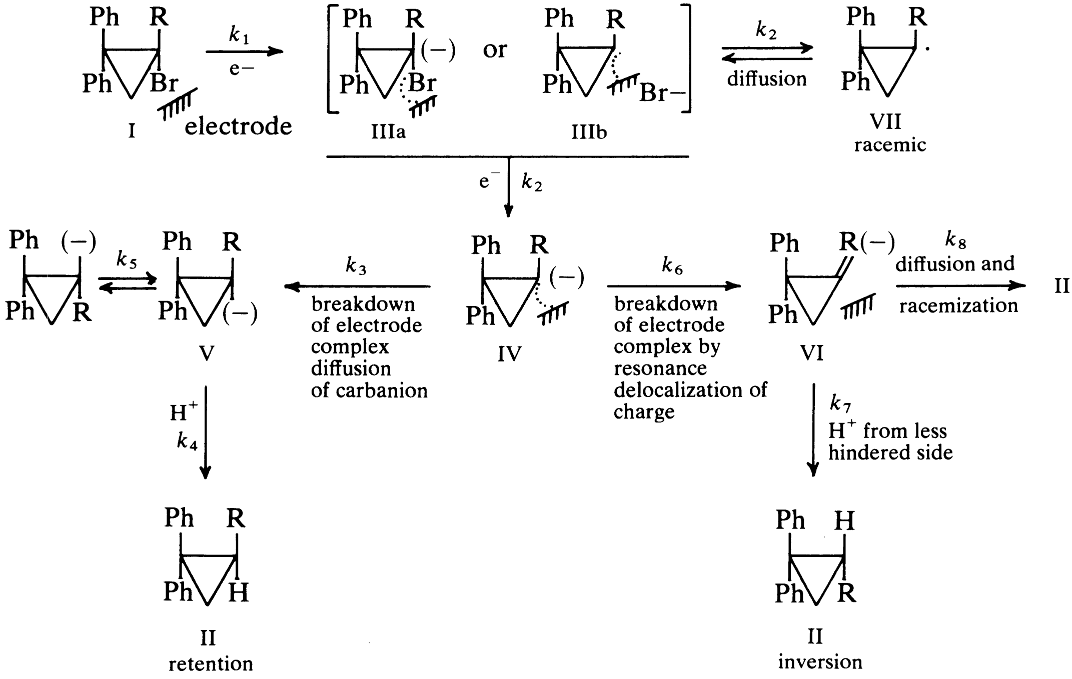
Ph R
Ph Br
I
electrode
k1
e−
Ph R (−)
Ph :Br
IIIa
or
Ph R
Ph Br−
IIIb
k2
diffusion
Ph R
Ph
VII
racemic
e−
k2
Ph (−)
Ph R
k5
Ph R
Ph (−)
V
k3
breakdown of electrode complex diffusion of carbanion
Ph R (−)
Ph
IV
k6
breakdown of electrode complex by resonance delocalization of charge
Ph R(−)
Ph
VI
k8
diffusion and racemization
II
H+
k4
Ph R
Ph H
II
retention
k7
H+ from less hindered side
Ph H
Ph R
II
inversion

alternative pathways: if R = Me or COO$^-$, desorption yields the carbanion V, which is then protonated giving a product, the optical purity of which depends on the stability of V with respect to inversion. Since usually $k_5 < k_4$, retention of configuration is significant. When, however, R = COOH or COOMe, either a planar carbanion VI is produced or inversion is rapid relative to protonation. For complete desorption of the carbanion, a racemic product can result since solvent attack from either side may occur with comparable rates. Racemization may also occur by desorption IIIb to give the planar radical VII. Inverted product will be formed if VI is protonated before desorption. The observed situation is somewhere between these extremes and illustrates the difficulty of establishing reaction pathways uniquely by means of investigations based on stereoselectivity.

Grabowski$^{(159)}$ examined the stereospecificity of a number of electrode reductions of organic substances and considered the question of reduction of alkyl halides in terms of the following three reaction pathways related to those discussed above:

$$RX \xrightarrow[\text{field}]{\text{electrode}} [R^+ \cdots X^-] \xrightarrow{2e} R^- + X^- \xrightarrow{H^+} RH$$

$$RX \xrightarrow{e} R^{\cdot} + X^- \xrightarrow{e} R^- \xrightarrow{H^+} RH$$

$$RX \xrightarrow{2e} R^- + X^- \xrightarrow{H^+} RH$$

S_{N_1}- and S_{N_2}-type processes may be regarded$^{(160)}$ as indistinguishable in electrode processes and may be jointly called "ionic mechanisms" in contrast to the free radical pathway S_R discussed by Elving and Pullman.$^{(58)}$ S_R or S_{N_1} should lead to racemization, while S_{N_2} will lead to inversion (cf. the conclusions and experiments of Annino *et al.*,$^{(156)}$ with cyclopropylbromide derivatives). Grabowski$^{(159)}$ studied the reduction of 2-phenyl-2-chloropropionic acid. The possible mechanism for reduction is

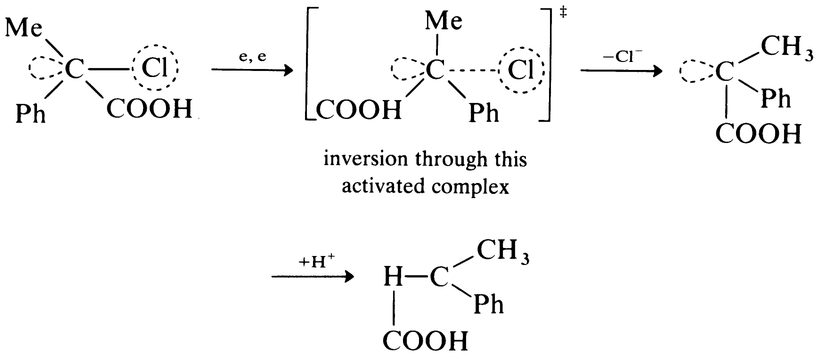

Electron addition is regarded as occurring between the electrode surface (Fermi level) and the lowest vacant (antibonding) orbital. This is the σ^* antibonding orbital corresponding to the weakest σ bond in the molecule, i.e., at the C–Cl linkage.(161) The results which demonstrate inversion do not, however, clarify the controversial question regarding the orientation of RX at the electrode surface in relation to the act of electron transfer.(162) By analogy with the activation process of solvation "shell" reorganization in the theory of adiabatic electrochemical electron transfer processes,(163) it may be supposed that the acquisition of a favorable orientation of the C–Cl bond (or of the reacting functional group, in general, in cathodic reductions, e.g., of $-NO_2$ in nitro compounds, of C=O in ketone and aldehyde reductions) in the double layer assisted by the electrode field (as referred to by Elving and Pullman(58)) is an intimate part of the process of activation in reaching the transition state at which adiabatic transfer of the electron is accomplished. In independent studies of adsorption of polar molecules at the mercury/solution interface by means of surface tension and capacitance measurements, orientation of the molecules is indicated by the observation of significant Esin and Markov effects(164) which may arise not only at the potential of zero charge but also at other more negative potentials. It seems unlikely that orientation of polar groups in the double-layer field at electrodes is not a significant factor in the kinetics and mechanism of reductions. However, the role of structural and polar interactions with the adsorbed water or alcohol at the electrode interface (in aqueous or alcoholic media) is an equally important matter to which relatively little attention has been given (but cf. Ref. 165).

It is of interest in relation to the distinction between "electron transfer" and "electrolytic hydrogenation" mechanisms that catalytic reduction on Pd of the halides studied by Grabowski does not give inversion, while with Zn or the Hg electrode, inverted products predominate to the extent of 80%–90% in the product yields. In the electronic reduction, the transfer to RCl is the step with the smallest rate constant and it is in this step that inversion probably occurs. Subsequent protonation of the carbanion occurs with retention of configuration as discussed with regard to the cases treated by Annino *et al.*,(156) so that the intermediate carbanion having sp^3 hybridization (contrast the corresponding radical) is almost certainly formed in the inverted configuration.(166) The analogy between Zn reduction and the controlled electrolytic reduction of alkyl halides or derivatives was also noted by Annino *et al.*(156) It is a behavior to be expected on account of the electrolytic nature of corrosion processes which are effectively involved in metallic reductions in aqueous acid or alkaline media.

Grabowski(159) also studied steric effects in the reduction of benzoin (the diketone "dibenzoyl"). This reduces to stilbenediol but steric effects allow *cis* and *trans* forms of the benzoin to exist. Electrode double-layer field effects then determine the ratio of *cis* and *trans* stilbenediol in the two-electron product and this ratio varies from about 0.4 to 2 with increasing cathodic potential at Hg in the range −0.7 to −1.1 V exhibiting a maximum at a potential of ~0.85 V. This is an interesting example of electrode interfacial effects on the course of an electroorganic reaction. The reaction is shown below:

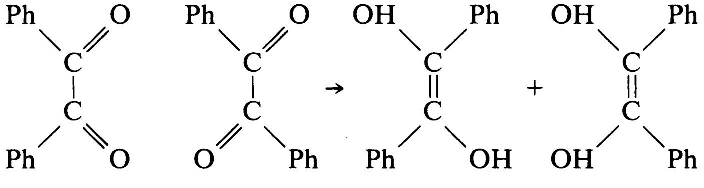

cis-
benzil

trans-
benzil

trans-
stilbenediol

cis-
stilbenediol

The two stilbenediol products were identified by means of cyclic voltammetry which exhibited two peaks on the reoxidation sweep. The fact that two products are formed is clearly the result of the existence of two conformations of the reactant at equilibrium; however, the *trans* conformer predominates (as may be expected on steric and energetic grounds) at equilibrium so that the corresponding *trans*-stilbenediol exhibits a larger reoxidation peak in the cyclic voltammetry than that for the *cis* form.

Another reduction reaction involving *cis* and *trans* isomers is that studied by Elving and Teitelbaum,(167) who examined the reduction of fumaric and maleic acids at mercury electrodes by polarographic techniques and proposed the following mechanism for the formation of the product succinic acid:

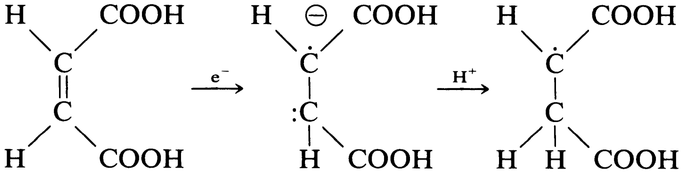

The pH dependence of the reduction seems to indicate that a proton is added *before* the second reduction step, which then proceeds as follows:

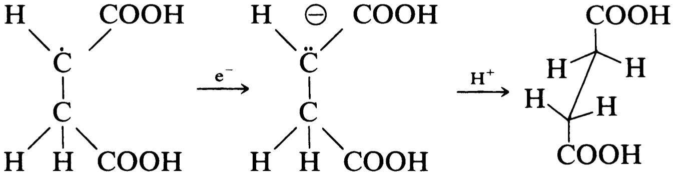

succinic acid
(most stable conformer)

The radical intermediate would be expected to be able to rotate freely about the central bond and therefore is the same for both maleic and fumaric acid reductions.

A comparison of polarographic results for reduction of maleic and fumaric acids indicates that the fumaric acid waves occur at more negative potentials. The greater thermodynamic stability of fumaric acid (the *trans* isomer), is consistent with this behavior.

Now if one of the protons of maleic (or fumaric) acid is replaced by a methyl group to form citraconic acid and this dibasic acid is electrochemically reduced, the product is expected to be methyl succinic acid. This acid now contains an asymmetric center, so that it may be possible to form an optically active product under conditions of electrolytic reduction; citraconic acid would be expected to yield the racemic mixture:

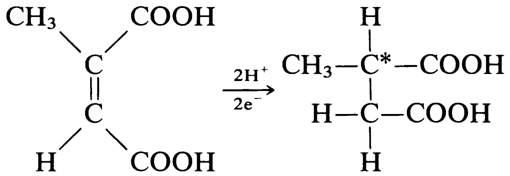

citraconic acid

methyl succinic acid

However, if the electrochemical reduction is perturbed by the presence of an optically active but electrochemically unreactive organic base, e.g., α-phenylethylamine, it is possible to obtain preferential formation of one enantiomer over the other. The basis of this principle lies in the results of work by Gourley, Grimshaw, and Millar,(168) who obtained an optically active 3,4-dihydro-4-methyl coumarin product upon electrochemical reduction of 4-methyl coumarin in the presence of optically active organic bases, such as codeine, brucine, and yohimbine.

It is known that the presence of an organic base lowers the overpotential for hydrogen evolution at mercury; therefore it appears reasonable that the presence of an amine should alter the course of the reduction of the coumarin. The mechanism for the hydrogen evolution reaction required the formation of a quaternary radical:

$$R_3N^+H + e^- \rightarrow R_3\dot{N}H \rightarrow R_3N + 1/2H_2$$

If the organic base is adsorbed on the electrode to a sufficient extent together with the 4-methyl coumarin, an optically active product is obtained as well as the dimer. The dimerization indicates that the reaction proceeds through a radical mechanism:

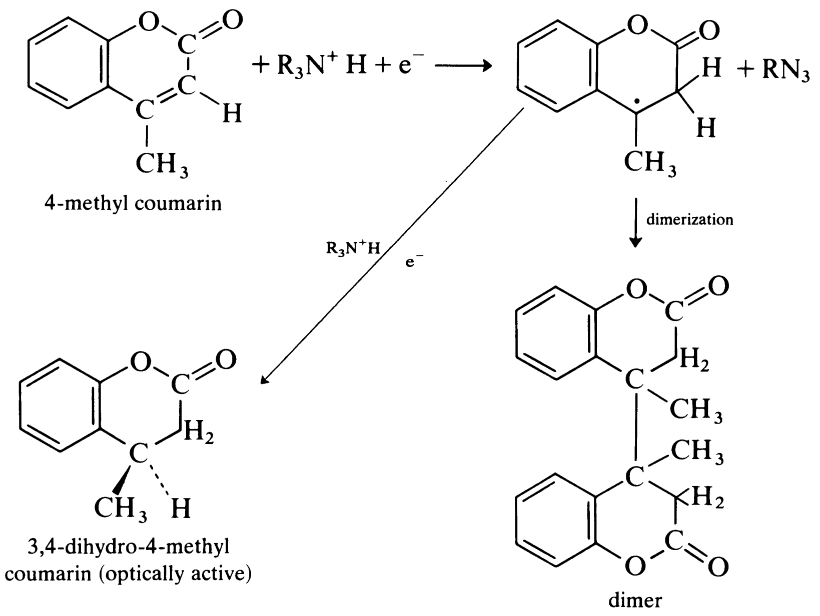

10. Isotope Effects in Mechanistic Studies

The only isotope effects which are usually of significance in electroorganic mechanism considerations are those involving H and D in (a) primary kinetic isotope effects, (b) secondary solvent isotope effects where reactions are compared in pure H_2O and D_2O or pure *h*- and *d*-alcohols, and (c) in prior protonation equilibria, e.g., with ketone reduction. Primary kinetic isotope effects having a magnitude of $\geq \sim 2.5$ may be expected in reactions that involve a rearrangement with proton participation, e.g., keto–enol tautomerism prior to an electron transfer step. Most other H/D isotope effects arise from protonation equilibria prior to the rate-controlling electron transfer step (e.g., in ketone reduction: $RR'CO + H^+ \rightleftarrows RR'COH^+$) and the isotope effect is then usually small, in the range 0.8–1.5. Secondary solvent isotope effects may arise when the free energies of solvation of reactants, intermediates or transition states differ in the pure *h* and pure *d* solvents. Such effects are usually significant but small.

Examination of the magnitude of an H/D isotope effect in appropriate cases usually enables a distinction to be made between an "equilibrium" or a rate-determining protonation step. It may also be useful in distinguishing between the electrochemical hydrogenation pathway and the electron transfer/fast protonation pathways in cathodic reduction at metals of intermediate hydrogen overvoltage and moderate affinity for H (Cu, Ag, W; contrast Ni, Pt, Rh). Correspondingly, oxidations, e.g., of hydrocarbons and derivatives such as aldehydes, alcohols which may proceed in part by dehydrogenation mechanisms, will give kinetic isotope effects for the *h*- and *d*-labeled compounds which will differ from the effects associated with oxygen participation from the water solvent coupled with proton transfer to the solvent, e.g., in the pathways I and II illustrated schematically below:

$$\mathrm{RH + M + e \rightarrow RM + HM} \qquad \mathrm{I}$$

$$\left.\begin{array}{c}\mathrm{RM + H_2O \rightarrow MROH + H^+ + e}\\ \mathrm{HM \rightarrow M + H^+ + e}\end{array}\right\} \qquad \mathrm{II}$$

Cases of this kind have been investigated in studies of anodic hydrocarbon oxidation.(169,170) While *a priori* calculations of the values of electrochemical kinetic isotope effects, particularly with complex organic molecules, cannot be regarded as quantitatively reliable owing to the difficulty of evaluation of the relevant reactant and transition state partition functions for particles in solution, nevertheless sufficient experimental data exist which, coupled with theoretical evidence of trends of values of the isotope effect for different types of reaction pathway, enable useful distinctions in mechanism to be made on the basis of H/D kinetic isotope experiments on electrochemical reactions.

11. Electrocatalytic Types of Reaction with Small Organic Molecules

In this class of reaction,(100) an initial dissociative chemisorption step occurs in which the molecule is split, usually into adsorbed H and adsorbed carbonaceous fragments, which are subsequently electrochemically oxidized either directly, as with H ($\mathrm{MH \rightarrow M + H^+ + e}$), or indirectly, as with the carbonaceous residues, by heterogeneous reaction with anodically electrodeposited monolayer surface oxide species, e.g., at Pt.

Much of the electrocatalytic work on small organic molecule oxidations was stimulated by fuel cell research(125) in the 1960s. While many interesting results were found, it is regrettable that in 1980 no fuel cell directly operating on a small organic molecule as fuel, e.g., CH_3OH, at ambient temperatures has found commercial or technological success.

The simplest model reaction for the electrocatalytic type of electroorganic reaction is really that of H_2 at catalytic noble metals, especially Pt.(38) In this case, molecular H_2 becomes dissociatively chemisorbed in the potential range 0.05–0.75 V and the adsorbed H is oxidized directly to H^+ or H_2O, with electrode transfer.

At metals such as Pt, where underpotential deposition of H occurs in the potential range 0–0.35 V E_H, the H_2 dissociation process appears to take place independently of the H deposition/ionization apart from the surface sites occupied by the electrodeposited H. Beyond ~0.35 V, however, the surface is almost free from deposited H. Beyond ~0.75 V surface oxidation of Pt begins and inhibition of H_2 oxidation sets in and is complete by ~0.95–

1.0 V E_H. This is due to passivation of active sites required for H_2 dissociation by a relatively small OH coverage. A complete oxide film at Pt will, however, react with H_2 in an autocatalytic way, depending on opening up holes in the oxide which exposes metal sites where the dissociation of H_2 can occur. The oxide film is then stripped in a mixed cathodic/anodic (oxidation of H) process.(171–173)

Most other simple organic substances react in an analogous way by chemisorptive dehydrogenation giving an adsorbed carbonaceous residue, e.g., in the cases of oxidation of formic acid, methanol, ethanol, olefins, and paraffins. Oxidation of hydrocarbons will be treated in Section 13.1.

The carbonaceous residues require(100,125) the "elements of oxygen" to complete their oxidation to CO_2 and this is usually achieved by a "bifunctional" type of heterogeneous reaction with electrochemically maintained surface oxide species. There is no evidence of O species being taken up directly from water by formation of adsorbed carbonium ions and their reaction with H_2O or OH^-.

A model reaction for this type of heterogeneous oxidation is the oxidation of CO studied by Gilman,(174) who proposed a nearest-neighbor reaction between chemisorbed CO (at Pt or Au) and electrogenerated OH or O species.

The extensively studied reaction of methanol oxidation exemplifies both types of processes, dissociative dehydrogenation and heterogeneous oxidation. According to Bagotzky and Vassilyev,(175) the initial chemisorptive oxidation steps are

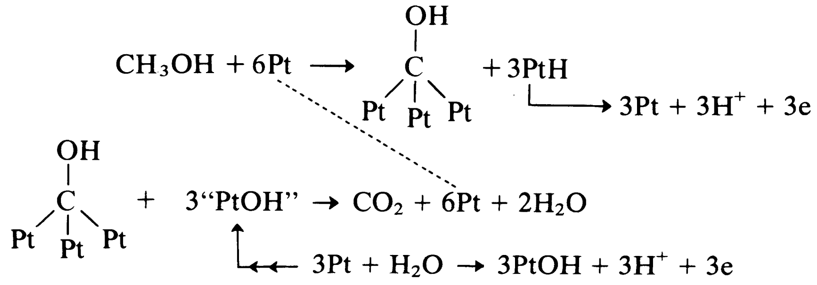

$$\mathrm{CH_3OH + 6Pt \longrightarrow \overset{OH}{\underset{Pt\;Pt\;Pt}{C}} + 3PtH}$$

$$\mathrm{3PtH \longrightarrow 3Pt + 3H^+ + 3e}$$

$$\mathrm{\overset{OH}{\underset{Pt\;Pt\;Pt}{C}} + 3\text{“PtOH”} \longrightarrow CO_2 + 6Pt + 2H_2O}$$

$$\mathrm{3Pt + H_2O \longrightarrow 3PtOH + 3H^+ + 3e}$$

The reaction may be more complex than this, or side reactions are significant, since in electro-oxidation of CH_3OH, depending on potential, pH, and electrode metal, some HCOOH and HCHO are known to be formed. These species are probably the cause of deactivation of methanol anodes which occurs at, e.g., Pt, and makes a direct methanol fuel cell at present impractical despite attempts at developing mixed-electrode materials, such as Sn-doped Ru or Ru-treated Pt.

Much work has also been done on formic acid oxidation at various noble metals.(100) The reaction should be apparently very simple, e.g., at Pt:

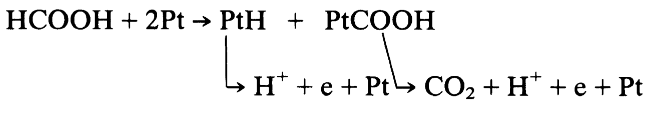

$$\mathrm{HCOOH + 2Pt \rightarrow PtH + PtCOOH}$$

$$\mathrm{PtH \rightarrow H^+ + e + Pt}$$

$$\mathrm{PtCOOH \rightarrow CO_2 + H^+ + e + Pt}$$

However, a self-inhibiting species "P" is generated from chemisorbed COOH and H, which covers most of the surface at low anodic potentials preventing appreciable rates of direct oxidation. Oxidation is then only possible at potentials where "P" is oxidatively desorbed by the heterogeneous "surface-oxide" oxidation type of pathway.(174) The action of the inhibitor "P" is much diminished at Pd and Pt/Au alloys(176) in comparison with Pt and is also attenuated by other competitively adsorbing species such as Hg, SH^-, Pb, CH_3CN. Formation of "P" is a "site-demanding" surface process which is easily interfered with by changes of the available catalytic/adsorptive sites at Pt.

Electrochemical hydrogenations of unsaturated organic molecules at transition metals proceed by an initial associative chemisorption with uptake of electrodeposited, presumably chemisorbed H. Unfortunately, only at Pt, Rh, and Ir can surface coverages of electrodeposited (upd) H be unambiguously evaluated, e.g., by cyclic voltammetry. Unsaturated organics chemisorb with diminution of coverage by upd H, some of which presumably reacts with the organic chemisorbate. Less work has been done on electrocatalytic hydrogenations than on oxidation of organic molecules. Some hydrogenations have been effected by electrochemical transfer of H through Pd or Pd/Ag membrane cathodes.

More detailed reviews on the electrocatalytic-type reactions have been given elsewhere(100) from the point of view more of "electrocatalysis" than "electro-organic chemistry." From the preparative point of view, electrolytic hydrogenations have been used more than electrocatalytic oxidations, but it must be admitted that most preparations that can be carried out by electrolytic hydrogenation can equally well be achieved by high-pressure catalytic hydrogenation with H_2. The electrolytic method at cathodic H_2 overpotentials provides, however, a way of effectively working at high H activity without employing high-pressure H_2.

The techniques for studying the electrocatalytic types of reaction involve programmed linear sweep voltammetry, galvanostatic charging curves, and potential-step i vs. t transients.(100,177) A full description of these methods and their applications is outside the scope of this chapter.

12. Anodic Reactions with Thick-Film Oxides on Electrodes

12.1. Reactions at Bulk-Type Base Metal Oxide Films

Apart from Pt, PbO_2 or anodically oxidized Pb and Ni electrodes were used the most in both early(7) and more modern work(178,179) to effect a variety of anodic oxidations. PbO_2 has also been used chemically as an oxidant for many years and effects oxidation of olefins and 1,2-glycol cleavages(181) in a way similar to lead tetraacetate of $KMnO_4$. An older review of PbO_2 oxidations in organic chemistry was given by Sa.(182) Oxidations of H_2 (183) and CH_4 (184) in the gas phase can be effected with PbO_2 but at elevated temperatures (175–200°C with H_2; 50°C with H_2 and Ag_2O). Various oxides are reduced by CH_4, PbO_2 giving Pb_3O_4 at 440°C or Pb at 750°C.(186,187) The preparation of PbO_2 electrodes by an electrolytic procedure was described by Kitahara and Ohsuga.(185)

A number of functional group oxidations can be carried out at PbO_2 anodes, e.g., $PhCh_3CN$ to PhCHO,(186,187) toluene-sulfonamide to benzoylsulfonamide.(188,189) However, at Pt, the first and third compounds are the main products, while the second is formed only in traces. These results indicate that the reaction products depend on the type of electrode and for a given reaction, the influence of electrode material on the kinetics of formation of several products is evidently appreciable.

Elbs and Brunner(190) also showed that a variety of alcohols are oxidized to corresponding acids at Pt and PbO_2 electrodes, while *iso*-propyl alcohol is oxidized to acetone (70%) plus some CH_3COOH, CO_2, and HCOOH. "Oxygen carrier" additives such as $Ce(SO_4)_2$ were used in the solution and presumably act as redox mediators.

PbO_2 electrodes have also been used as substrates for the Kolbe and related anodic oxidations.(187,191) Generally the electrochemical behavior of these reactions is different at PbO_2 from that at Pt.

p-Toluic acid is easily converted to terephthalic acid(192) while the CH_3 group on DNT and TNT is smoothly oxidized(7) to COOH at PbO_2 anodes, paralleling the chemical reaction of Sacks and Kempf.(193) Similarly, *p*-nitrotoluene is converted to *p*-nitrobenzoic acid.(194) The power of PbO_2 as an oxidizing agent is indicated by the observation(195,196) that under certain conditions, a suspension of toluene is oxidized *completely* to CO_2 by PbO_2. However, Pt and PbO_2 give different products. PbO_2 also oxidized CH_3OH almost completely to CO_2 while, at Pt, intermediate products (HCHO) can be isolated in good yield.(190)

The ability of PbO_2 anodes to effect complete oxidation of a variety of organic substances, all the way to CO_2 and H_2O (or H^+), was the basis of an air purification device, developed by Cyanamid Co., in which polluted air was passed over a high-area PbO_2 matrix, wet with H_2SO_4 and polarized anodically against a counterelectrode.

The question whether PbO_2 anodes act simply in a heterogeneously chemical fashion but are regenerated electrochemically is to some extent answered by the early observation of Michler and Pattinson(197) that a PbO_2 anode gives good yields of tetramethylbenzidine and tetramethyldiaminodiphenylmethane plus traces of trimethyl, phenyl-*p*-phenylenediamine from dimethylaniline but the chemical reaction with PbO_2 gives only poor yields. Hence, there is a specific effect of PbO_2 as an *electrode* interface.

A large variety of organic oxidations can be carried out at oxidized Ni electrodes(198) or heterogeneously at "nickel peroxide" in alkaline solution.(39,40,199) The electrochemistry of the states of oxidation of Ni in nickel oxide films has been extensively studied in work on nickel oxide cathodes for Ni/Cd batteries.(200–204) The oxides normally are the bulk materials or thick (40 ~ 100 layers)(204–206) oxide films. The valence state of Ni varies from II in the discharged state, through III (Ni · O · OH), to IV at low temperatures and elevated potentials.

The oxidations of a range of phenylethanols, benzyl alcohols, and allyl alcohols was investigated by Amjad, Pletcher, and Smith(40) in *t*-butanol/H_2O mixtures in NaOH or Et_4NOH solutions. The alcohols give well-defined, kinetically controlled oxidation waves at the potential of the Ni(II)/(Ni(III) valence change. The phenyl alcohols and allyl alcohols give only carboxylic acids in good yields. The benzyl alcohols give acid and aldehyde, the total being in good yield, dependent on the OH^- ion concentration. The latter can determine the extent of any Ni(IV) formation at high OH^- concentrations. Simple normal alcohols are also oxidized to the corresponding *n*-carboxylic acid in 90% yield by anodized Ni electrodes.(39)

It was proposed that the rate-controlling step in processes of this kind was the abstraction of the H at the α-carbon of the alcohol by the anodic nickel oxide film which is chemically closely related to the so-called(207) nickel peroxide reagent (not really a "peroxide"). The reaction mechanism suggested can be represented as follows:

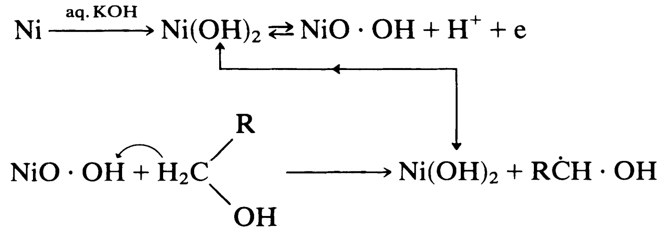

$$\mathrm{Ni} \xrightarrow{\text{aq.KOH}} \mathrm{Ni(OH)_2} \rightleftarrows \mathrm{NiO\cdot OH} + \mathrm{H^+} + \mathrm{e}$$

$$\mathrm{NiO\cdot OH} + \mathrm{H_2C}(\mathrm{R})(\mathrm{OH}) \longrightarrow \mathrm{Ni(OH)_2} + \mathrm{R\dot{C}H\cdot OH}$$

$$\mathrm{R\dot{C}H\cdot OH} \rightarrow \text{product via other steps}$$

The further steps presumably involve another oxidation stage in order to reach R · COOH products, but detailed mechanisms were not formulated. It is to be noted that a free radical type of mechanism was suggested, as was also discussed in the general review of reactions with "nickel peroxide" given by George and Balachandran.(207) Free radicals in aromatic oxidations at nickel peroxide were indicated from esr experiments.

The general reactivity of oxidized Ni anodes in various *t*-butanol/H_2O mixtures was followed by cyclic voltammetry.(40) The coulombic and organic product yields of aldehyde and acid were determined for various primary alcohol derivatives. Substituent effect on the anodic oxidation rates of a series of benzyl alcohols were evaluated. Attempts were made to relate the oxidation rates to the Hammett σ parameter for substituent properties.

Table 7
Current Yields of Oxidation Products of ROH and RNH_2 Molecules on Anodes Coated with Oxides(39)

Reactant	Product(s)	Current yield % Ni (0.55 V)	Ag (0.75 V)	Cu (0.70 V)
n-Propylamine	Proprionitrile	84	83	85
	Propionaldehyde	11	2	2
n-Butylamine	Butyronitrile	85	85	—
	Butyraldehyde	6	2	—
Iso-propylamine	Acetone	80	70	85
Diethylamine	Acetonitrile	46	27	30
	Acetaldehyde	3	3	5
	Acetic acid	36	29	40
Ethanol	Acetic acid	98	—	96
1-Propanol	Propionic acid	95	—	—
2-Propanol	Acetone	80	—	9

At oxidized Ni anodes, the general product pattern is(179,180) (Table 7)

Primary alcohols → carboxylic acids

Secondary alcohols → ketones

Aliphatic amines → nitriles

With hydrazine,(208) similar oxidation of the reactant molecule (to N_2) occurs readily at the nickel oxide electrode surface. The rate constant for oxidative reaction(208) increases progressively in the series $N_2H_4 > CH_3NH_2 > C_2H_5NH_2 > NH_2C_2H_4NH_2 > (C_2H_5)_2NH$. In the case of N_2H_4, however, two types of mechanisms arise, depending on electrode potential: at low potentials, reaction is said to occur by direct electron transfer to the electrode metal (bare Ni sites) or more likely by dissociative chemisorption followed by electron transfer events with adsorbed H, while at more positive potentials, the reaction involves(208) the Ni (III) oxide with electrochemical regeneration after reductive reaction with the N_2H_4.

Anodic oxidations of amines and alcohols can also be effected by reaction with the oxide films formed anodically at Ag, Cu, and Co electrodes (Table 7), as well as at Ni.(39) An H abstraction mechanism to the oxide film was proposed (cf. Ref. 40) rather than electron transfer to the anode surface. The latter would lead to organic ion reactions with proton transfer rather than free radical reactions which appear to be the indicated type of process in these anodic oxidations.

Rate constants for a series of oxidations of amines and alcohols at anodically oxidized Ni, Ag, Cu, and Co electrodes were measured. The oxidations proceed by reaction with the oxide layer coupled with its electrochemical regeneration by an anodic reoxidation step. Reaction with solution-free transition metal ions derived from the oxide films was considered unlikely although oxidations with Ag^{3+} are known. The H abstraction mechanism at the α-C atoms was confirmed by the demonstration of an appreciable primary H/D isotope effect in the rate-controlling step, producing the $R \cdot \dot{C}H \cdot OH$ radical. Such radical steps were discussed by Pickering(209) for the chemical reaction between reactive transition metal oxides and organic substances, and the H abstraction route was indicated by esr studies.

Generally,(40) the products of oxidation at each of these electrodes are identical with those from heterogeneous reactions with the corresponding bulk materials. Hence, in these cases, the electrochemical system serves only to provide a way of continuously generating the higher valence state of the oxide which is the reactive oxidant. The behavior of these electrodes may differ somewhat from that of PbO_2 where, on account of the high positive potentials attainable at oxidized Pb electrodes, electrochemical reactions different from those which can be effected in a heterogeneous chemical manner can arise with some reagents.

12.2. Reactions of Organic Substances at High Anodic Potentials on Thick Noble Metal Oxide Films

Several electrochemically important reactions occur *on* the surface of oxidized noble metal electrodes without reaction *with* the surface oxide. The oxide film then behaves as a new type of electrocatalyst surface on which the reaction proceeds, in distinction to the underlying metal. The oxide films are normally only one to three oxygen layers in thickness. The following inorganic reactions are of this class: (a) O_2 evolution, (b) Cl_2, (c) Br_2 (to a small extent, since adsorbed Br^- blocks surface oxidation) and N_2 evolution (from N_3^-) while, in the case of organic reactions, (a) the Kolbe and Crum-Brown/Walker syntheses, as well as (b) the Hofer-Moest reaction, are of this type.(5)

Recently, interesting claims have been made that organic substances can react with, and be adsorbed at, "thick" (about two to three monolayers) oxide films on noble metals.

Both at Pt and Rh electrodes Tyurin *et al.*(210,211) have given evidence that a special so-called "phase-oxide" type of surface oxide is formed above ~2.0 V after the normal, more easily reducible oxide is formed up to a limiting "monolayer" level of oxidation corresponding to the stoichiometry "PtO_2." A similar phase oxide film can be formed on Rh. These kinds of oxides presumably correspond to those referred to by Shibata(171,172) and to the oxidized surface of Pt on which the Kolbe reaction proceeds at potentials >2.2 V *vs.* E_H.

The term *phase oxide* used by Tyurin for the oxides formed at high anodic potentials on Pt and Rh refers to a state of the oxidized metal surfaces rather different from that which has also been referred to as phase oxide by other authors. The latter usage normally refers to the rearranged state of the monolayer surface oxide which is already established at or below 1.1 V *vs.* E_H.

In an extensive series of papers, Tyurin and Fioshin, with various coauthors,(210–221) have studied the supposed (see below) adsorption of a variety of organic compounds on the oxide films formed at Pt and Rh at high anodic potentials. Compounds such as acetonitrile, thiourea, thiazole, acetic, propionic and butyric acids, benzene, cyclohexane, and 3,4-diphenyl-2-(4-dimethylamino)-benzylidenehydrazono-1,2-dihydro-1,3-thiazole (on Rh (218)) were studied.

The adsorption was measured by two methods(219): (a) from the change of the capacitance of the electrode and (b) from the decrease of the oxidation charge of the electrode surface as measured by the charge associated with reduction peaks in a cathodic sweep taken from high (1.8 ~ 2.2 V) potentials. The surface oxide state that is influenced by adsorption of organic molecules is that which is reduced at the most cathodic potentials, ~0.2 V, over the potential range that is normally associated with H underpotential deposition.

Adsorption isotherms are logarithmic in adsorbate concentration, e.g., on Rh,(218) exhibiting two almost linear regions. Adsorption depends on molecular size and functionality: e.g., RCN is adsorbed more strongly than $R \cdot CO^-$.(221) Adsorption is believed to be associated with a change of state of the oxide surface (oxide "coverage" is diminished) and has a maximum around 1.9 ~ 2.0 V with various organic substances, e.g., as at Rh.(217,218)

In most of this work, little is said about the fate of the adsorbed organic molecules: it is difficult to regard them as remaining adsorbed in a chemically unchanged state at such high anodic potentials. Some oxidation of various functions on the molecules would be expected, and this may be the reason for the observed diminution of extent of surface oxidation of the anodes in the presence of such molecules. More work is required in this interesting potential range to characterize what oxidations of organic molecules might be possible.

The adsorption of various organic molecules, including carboxylic acids, claimed in this work, helps to answer the question whether adsorbed species are involved in the Kolbe reaction. The work of Tyurin *et al.* in the various papers quoted above would appear to support such a view. The adsorption of the organic species also promotes inhibition of O_2 evolution,(220) a phenomenon often noted (e.g., Ref. 5) in kinetic and yield studies on the Kolbe reaction.

13. Discussion of Some Reactions and Their Mechanisms That Have Possibilities for Commercial Development

In earlier sections of this chapter, we have discussed mainly electrochemical methods of approach for the study of kinetics and mechanisms of organic electrode reactions. A fuller understanding of the pathways involved in electro-organic reactions can only be gained by considering some of the organic-mechanistic aspects of the reactions in a way complementary to the elementary electrode processes and to any chemisorption steps. In this section, we shall examine some of these mechanistic matters with reference to a selection of organic electrode processes that have some possibilities for commercial exploitation or have already been developed in that direction.

13.1. Oxidation of Aliphatic Hydrocarbons

It is well known today that perhaps the most dramatic application of the fuel cell—an electrochemical device that may be based in the future upon the oxidation of aliphatic hydrocarbons—was in the Gemini Space Mission. In this application, the cell was based upon the use of a "solid polymer electrolyte"—a cation-exchange membrane in its acid form—but with hydrogen and oxygen as the fuels rather than an aliphatic hydrocarbon. Considerable research and development preceded and supported these successful missions and the units demonstrated that indeed the H_2/O_2 fuel cell was capable of extended performance at relatively high current densities—a capability of fundamental importance in commercial applications.

Other applications for fuel cells have been identified and development continues today,(32a,b) an important one being to provide an alternative and economically competitive source of electrical energy to meet the projected demand through the next decade. United Technologies has expended considerable effort toward this goal, believing that success can only be achieved if commercially available hydrocarbons and air are the reactants in the fuel cell.

The extensive research into the fundamental electrochemistry of the anodic oxidation of low-molecular-weight hydrocarbons in aqueous electrolytes is summarized as part of Table 8. Parallel programs to develop effective catalysts, to design optimum electrode and membrane or separator structures, and to engineer the electrochemical power generation unit have been undertaken through the 1960s and 1970s. The first generation power plant—a 4.5-MW unit based on phosphoric acid technology—is currently being installed in New York City for operation in 1985.(32b)

13.1.1. Electro-Oxidation of Hydrocarbons in Aqueous Electrolytes

The fundamental studies of the electro-oxidation of low molecular weight, saturated hydrocarbons in aqueous electrolytes such as sulfuric and phosphoric acid, showed that adsorption of the organic molecule upon the surface of the *catalytic electrode* is a critical step.(125,222–230) Partial oxidation occurs rapidly, and it has been postulated(228) that the adsorbate then contains two types of intermediate, one a so-called O type and the second a CH type. Thus, the overall reaction is represented as

$$\underset{\text{in solution}}{C_xH_{2x+2}} \rightarrow \underset{\text{adsorbed}}{C_xH_{2x+2}} \qquad \text{(a diffusion-controlled process)}$$

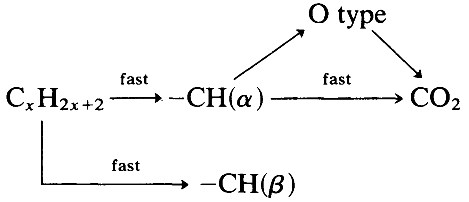

unreactive to further oxidation:
also cannot be electrochemically reduced

The electrocatalytic oxidation of alkenes has similarly been the subject of extensive study, as part of the development of fuel cell technology. The overall reaction is thought to be similar to gas phase oxidation processes, involving both adsorption of the olefin and oxidative adsorption of water molecules, the latter forming intermediate species which react with the olefin$^{(222,224,229,230)}$:

$$\underset{\text{in solution}}{C_2H_4} \rightleftarrows \underset{\text{adsorbed}}{C_2H_4}$$

$$H_2O \rightleftarrows \underset{\text{adsorbed}}{OH^{\cdot}} + H^{\oplus} + e^{\ominus}$$

$$C_2H_4 + OH^{\cdot} \rightarrow C_2H_4OH^{\cdot} \rightarrow CO_2 + \text{other products}$$

13.1.2. Electro-Oxidation of Hydrocarbons in Nonaqueous Electrolytes

The reaction pathways involved in the anodic oxidation of a hydrocarbon molecule are shown below:

$$\begin{tikzcd}
RH \arrow[r, "-e"] & \underset{\text{cation radical}}{RH^{\oplus\cdot}} \arrow[r, "-e"] \arrow[d, "-H^{+}"] & \underset{\text{dication}}{RH^{\oplus\oplus}} \\
 & \underset{\text{radical}}{R^{\cdot}} \arrow[r, "-e"] & \underset{\text{monocation}}{R^{\oplus}}
\end{tikzcd}$$

If it is realized that the cation radical, dication, and monocation are all subject to attack by nucleophilic species and that the cation radical and radical may undergo product formation by pathways available to radicals, then it becomes evident that anodic oxidation can lead to a variety of products. The overall reaction mode can be addition, dimerization, or substitution and the products obtained will depend upon (i) the relative stabilities of the intermediate species, (ii) the nucleophiles present, (iii) availability of proton acceptors, and (iv) the electrode potential applied.

Table 8
Oxidation of Aliphatic Hydrocarbons

Alkanes, cycloalkanes	Aqueous electrolytes E.g., H_2SO_4, H_3PO_4, KOH, usually at elevated temperatures	Platinum, Raney platinum, silver, palladium nickel	Typically 0.3–0.9 V vs. NHE but involves complex electrode processes, i.e., adsorptive dissociation of the organic substrate	The use of low molecular weight hydrocarbons such as methane, ethane, and propane was considered to be an economic alternative to the anodic oxidation of hydrogen in the fuel cell. Extensive research and development was undertaken in this area in the 1960s.	Refs. 33–37
	Nonaqueous electrolytes Ambient temperatures			The products of these reactions are typically α,β-unsaturated ketones, acetamido-alkanes and polymeric alkanes. It is considered that reaction proceeds through the direct or indirect formation of a carbocation, which subsequently reacts with the solvent or supporting electrolyte.	Refs. 231–234
	Acetonitrile/lithium perchlorate	Platinum	1.5–2.0 V vs. SCE		
	Nitromethane/tetraalkyl ammonium Tetrafluoroborate ($TEA_{\bullet}{}^{\oplus}BF_4{}^{\ominus}$)		2.6–2.8 V vs. ferrocene/ferrocinium		
	Propylene Carbonate/ $TEA^{\oplus}BF_4{}^{\ominus}$		2.6–2.8 V vs. ferrocene/ferrocinium		
	Acetonitrile/$TEA^{\oplus}BF_4{}^{\ominus}$		>3 V vs. $Ag/Ag^{\oplus}$ (0.01 N)		
	Fluorosulphonic acid/ acetic acid		1.6–1.8 V vs. Pd/H_2		

	Aqueous electrolytes H_2SO_4 Na_2SO_4 (pH 0.3–12) 35 weight % KOH at elevated temperatures, 80–200°C	Platinum Platinized platinum Gold Carbon-supported platinum Platinum/gold alloys	Typically 0.2–0.1 V vs. NHE. The anodic oxidation processes have been extensively studied and involve adsorptive dissociation of the organic substrate at the catalytic electrode surface.	Again the electro-oxidation of alkenes, particularly the low-molecular-weight alkenes such as ethylene and propylene, have been evaluated as an alternative fuel for application in fuel cells. A major limitation appears to be the incomplete oxidation and subsequent poisoning of the catalysts. Aldehydes have been identified as an intermediate product.	Refs. 36, 37, 222–227
Alkenes, cycloalkenes	Nonaqueous electrolytes Ambient temperatures Acetonitrile/tetraethyl ammonium Tetrafluoroborate ($TEA^{\oplus}BF_4^{\ominus}$) Acetonitrile/$LiClO_4$ Nitromethane/$TEA^{\oplus}BF_4^{\ominus}$ Methylene chloride/$TEA^{\oplus}BF_4^{\ominus}$ Propylene carbonate/$TEA^{\oplus}BF_4^{\ominus}$	Platinum	2.5–3 V vs. $Ag/Ag^{\oplus}$ (0.01 *N*) for isolated double bonds. 1.8–2 V vs. $Ag/Ag^{\oplus}$ (0.01 *N*) for conjugated dienes	The products of these reactions include heterocycles and polymers.	Refs. 237–242

The stability of aliphatic hydrocarbons is reflected in the high anodic potentials required to effect oxidation at normal temperatures so that the electrochemical studies have necessarily involved non-aqueous electrolytes.(231–242) In solvents such as acetonitrile, nitromethane, methylene chloride, or propylene carbonate, oxidation of hydrocarbons containing allylic or tertiary CH bonds has been demonstrated.(231) These reactions have led to the formation of acetamidoalkanes, $\alpha\beta$-unsaturated ketones and isomerized alkane polymers.

Similar reaction products have been observed in the electro-oxidation of alkenes in nonaqueous electrolytes.(236–242) Several mechanisms have been postulated to describe the overall reactions(238,239,242):

(a) Direct electron transfer to form a cation radical and subsequent reaction with a nucleophile, the product then either dimerizing or being further oxidized:

$$\begin{tikzcd}
\mathrm{RCH{=}CHR'} \arrow[r, "-e"] & \mathrm{R\overset{\oplus}{C}H{-}\dot{C}HR'} \arrow[d] \\
\mathrm{RCH(Y)\cdot CH(Y)R'} & \mathrm{RCH(Y){-}\dot{C}HR'} \rightarrow \arrow[l, "-e", "Y^-"']
\end{tikzcd}$$

(b) Successive one-electron steps leading to the formation of an allylic carbenium ion, which subsequently reacts with the nucleophile Y^-:

$$\begin{tikzcd}
\mathrm{RCH = CHR'} \arrow[r] & \mathrm{RCH = CH\overset{+}{C}HR'' + H^+ + 2e} \arrow[d] \\
 & \mathrm{RCH = CH\cdot CH(Y)R''}
\end{tikzcd}$$

(c) Electro-oxidation of the solvent or the supporting electrolyte to yield radicals which react with the olefin by addition or hydrogen abstraction.

These alternate mechanisms are exemplified by the oxidation of propylene in acetic acid.(238) With lithium perchlorate as the supporting electrolyte, direct electron transfer from the alkene occurs to form an allylic carbenium ion, e.g., mechanism (b) above. However, in the presence of lithium nitrate, oxidation of the nitrate ion has been shown to occur preferentially and the resulting nitrate radical, $NO_3^{\cdot}$, reacts with the alkene, i.e., mechanism (c).

A summary of oxidation reactions of aliphatic hydrocarbons is given in Table 8.

13.2. Anodic Substitution Reactions with Aromatic Hydrocarbons

As with the electro-oxidation of aliphatic hydrocarbons, several pathways may be involved in anodic reactions of aromatic molecules: (a) direct electron transfer from the aromatic substrate to form cationic species, (b) reaction of the aromatic hydrocarbon with an electrogenerated oxidant, e.g., radicals from oxidation of the supporting electrolyte, hydroxy radicals, transition metal cations such as Cr^{6+}, Co^{3+}, or Ce^{4+}, (c) dissociative chemisorption, an oxidation pathway observed in aqueous electrolytes with catalytic electrodes (fuel cell technology).

Furthermore, and again as with alkanes and alkenes, the mechanism of the oxidation and the products of the reaction will depend upon factors such as the electrolyte, the electrode material, the electrode potential, the stability of the various intermediates, and the nucleophilicity of the anion species.

It appears that many of the anodic reactions of aromatic hydrocarbons—and particularly those in nonaqueous electrolytes—proceed by way of the formation of a cation radical:

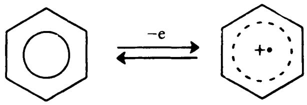

Indeed the polarographic half-wave potential is a direct measure of the ease with which the electron transfer is effected, provided that it is the potential of the reversible, one-electron process that is measured. Available data for the half-wave potentials for the oxidation of series of aromatic hydrocarbons is extensive(240,243–247) and series of the early $E_{1/2}$ values were shown to correlate linearly with the energies of the highest filled molecular orbitals(248) and ionization potentials.(249,250) Later studies indicated that only in specific cases did the published data actually apply to the reversible one-electron process represented above.(251–253)

Several synthetically useful substitution reactions can be carried out through anodic oxidation of an aromatic hydrocarbon:

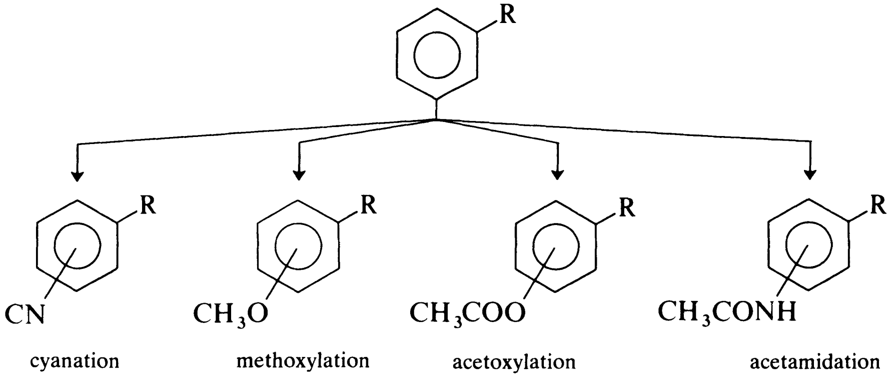

The importance of the nature of the solvent and supporting electrolyte is clearly illustrated by these several reactions. The final products of these substitution reactions will largely depend upon the distribution of positive charge in the intermediate cation radical,(254,255) since this will determine the ring site at which nucleophilic attack occurs. However, other factors such as steric requirements and ion solvation should also be considered.(256)

The oxidation of an aromatic hydrocarbon in the presence of acetate ions leads to the formation of aryl acetates. Detailed studies of the electrode reaction using polarographic and cyclic voltammetric techniques have established that direct oxidation of the aromatic molecule is the initial reaction.(244) Certainly the facile decarboxylation of acetoxy radicals appears to preclude their involvement in this reaction.(257) It has also been shown that the electro-oxidation strongly resembles an electrophilic substitution reaction, particularly with respect to the distribution of *ortho*-, *meta*-, and *para*-substituted products.(258)

In solution of perchlorates and tosylates in acetic acid, the primary products of electro-oxidation of aromatic hydrocarbons are shown to be benzylic acetates, i.e., substitution occurs preferentially in the side chain. A large, primary isotope effect, $k_H/k_D = 2.6$, provided strong evidence that in this type of substitution reaction the rate-determining step involved the loss of a proton.(258) Further refinement of the mechanism correlated isomeric product ratios to the distribution of positive charge density in the intermediate cation radical.(259)

The electro-oxidation of an aromatic hydrocarbon containing a benzylic hydrogen, using solutions of perchlorates, tetrafluoroborates, or hexafluorophosphates in acetonitrile as the electrolyte, results in the formation of an acetamido derivative. This is essentially the electrochemical analog of the Ritter reaction. Again direct oxidation of the aromatic molecule has been regarded as the initial step in the overall reaction,(260) e.g., in the reaction with toluene (II) (Scheme 2). Increasing amounts of the nucleophile, water,

Scheme 2

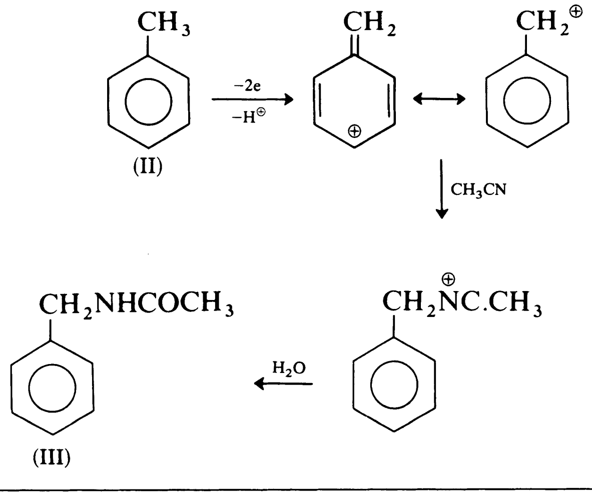

in the electrolyte allows a competitive reaction to occur, forming benzyl alcohols (and subsequently benzaldehydes by further oxidation). Study of the competing reactions showed that *less* reactive cations were selective to acetonitrile, the weaker nucleophile.(261)

However, this simple mechanism shown in Scheme 2 does not adequately account for all aspects of all acetamidation reactions with aromatic hydrocarbons. For example, it has been shown(262) that in the acetamidation of toluene the distribution of five products—the acetamido derivative (III), a dimeric hydrocarbon (IV), benzyl alcohol (V), benzaldehyde (VI), and benzoic acid (VII)—is dependent upon the electrode potential, the concentration of water in the electrolyte, and the supporting electrolyte itself:

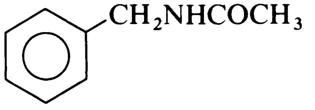

(III)

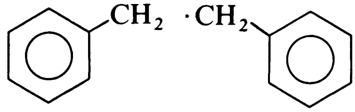

(IV)

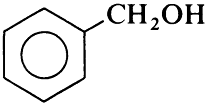

(V)

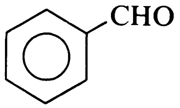

(VI)

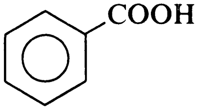

(VII)

The experimental data indicated that indirect oxidation must occur under some conditions, i.e., the anion of the supporting electrolyte is more readily oxidized than the hydrocarbon. Furthermore, the presence of bibenzyl (IV) in the products strongly suggests that an intermediate benzyl radical is formed, so that it is likely that dual reaction pathways must be considered (Scheme 3).

Extensive discussions of these substitution reactions may be found elsewhere (see Refs. 19, 22, 23, and 24, for example) providing the information to support the mechanistic conclusions and indicating the areas of controversy. A comprehensive literature survey through 1971 was presented in tabular form by (N.L.) Weinberg(263) to include experimental conditions such as electrolyte, electrode material, temperature, and current density as well as the reaction products. The oxidations of alkylaromatics(264) and polynuclear aromatics(265) are also reviewed in separate chapters in the recently published encyclopedia.

13.3. Electroreduction Processes

In general the electroreduction of organic molecules can be conveniently divided into three classes: (a) Involvement in the reaction of a direct electron transfer to the organic molecule, producing initially a radical anion; (b) electrochemical hydrogenation; (c) generation of a reducing agent *in situ* by the electrode reaction. Electrochemical hydrogenation typically involves electrodes (cathodes) which exhibit low hydrogen overpotential, i.e., the so-called

Scheme 3

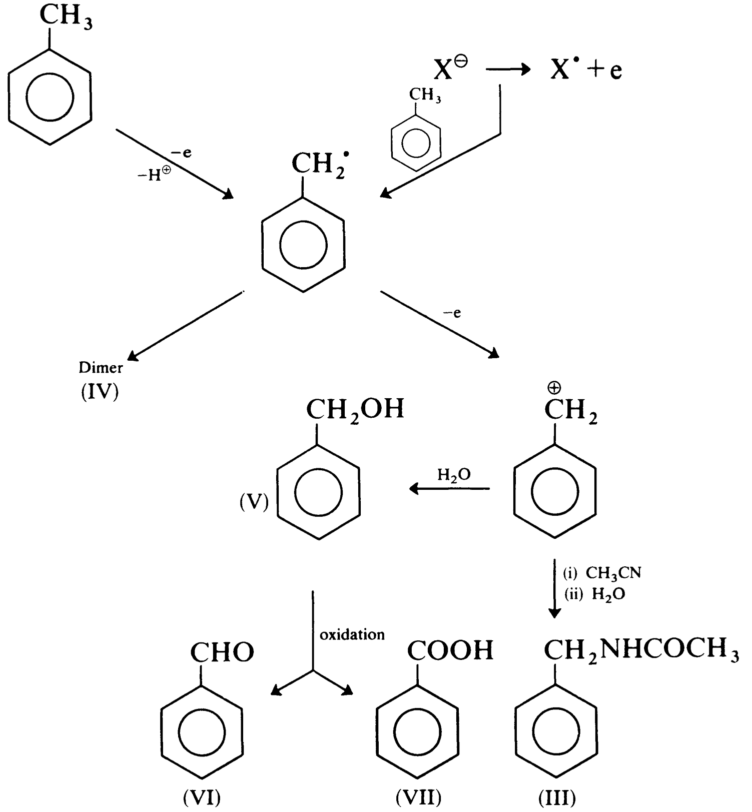
CH_3
$X^{\ominus} \longrightarrow X^{\bullet} + e$
CH_3
$-e$
$-H^{\oplus}$
$CH_2^{\bullet}$
Dimer
(IV)
$-e$
CH_2OH
$\overset{\oplus}{C}H_2$
(V)
H_2O
(i) CH_3CN
(ii) H_2O
oxidation
CHO
COOH
$CH_2NHCOCH_3$
(VI)
(VII)
(III)

catalytic electrodes such as platinum and palladium, and an electrolytic medium of high proton availability (low pH). The key intermediate in these electrode processes is believed to be an adsorbed hydrogen atom, formed either by dissociation of hydrogen molecules or by discharge of a proton:

$$\left.\begin{matrix} H_2 \rightleftharpoons \\ 2H^{\oplus} + 2e \rightleftharpoons \end{matrix}\right. \underset{\text{(adsorbed)}}{2H^{\cdot}} \xrightarrow{R} RH_2$$

The extent to which the electrode surface is covered by chemisorbed hydrogen atoms has been classically demonstrated by cyclic voltammetry and chronopotentiometry, particularly with respect to elucidation of the mechanism of the hydrogen evolution reaction and in the electrochemistry of fuel cells. The involvement of such intermediates is also consistent with the known mechanisms of catalytic hydrogenation, both from the vapor phase and the liquid phase. These results also indicate coadsorption of R species.

Recent reviews and textbooks$^{(19-22,24,25,266)}$ focus primarily upon electroreductions that involve electron transfer directly to the organic molecule. Chemical, spectroscopic, and electrochemical evidence has established that, in these reduction processes, the formation of free radicals, adsorbed radicals, radical anions, carbanions, and dianions is involved. Reaction pathways may be distinguished according to whether they follow a simple electron–proton uptake sequence or vice versa:

$$\text{(a)}\quad R \xrightarrow{+e} \underset{\substack{\text{radical}\\ \text{anion}}}{R^{\cdot -}} \xrightarrow{+H^{\oplus}} \underset{\text{radical}}{RH^{\cdot}}$$

$$\text{(b)}\quad R \xrightarrow{+H^{\oplus}} \underset{\text{cation}}{RH^{\oplus}} \xrightarrow{+e} RH^{\cdot}$$

In other cases a chemical process such as dimerization, hydrogen abstraction, or disproportionation may either precede the initial electron transfer or follow the electron–proton uptake step. The particular reaction pathway and the intermediates formed will depend upon such factors as (i) the substrate itself, (ii) the electrode potential, (iii) the electrode material, (iv) the supporting electrolyte and solvent, and (v) the pH of the environment. The importance of the overall reaction conditions can be effectively illustrated by the electroreduction of carbonyl compounds and nitro compounds.

13.3.1. Electroreduction of Carbonyl Compounds

The molecular properties and the chemistry of aldehydes and ketones are reflected in the electrochemistry observed, e.g., the involvement of keto–enol tautomeric equilibria, addition reactions, protonation in acidic media, and the effects of α substituents. Extensive studies of the products of these electrolytic reactions have been undertaken$^{(267-270)}$ yet, although some initial interest has been shown, none of the syntheses are of commercial significance today.

The electroreduction of the carbonyl group in aqueous or partially aqueous electrolytes primarily yields the corresponding alcohol and alkane, metal alkyl compounds, and a 1,2-diol:

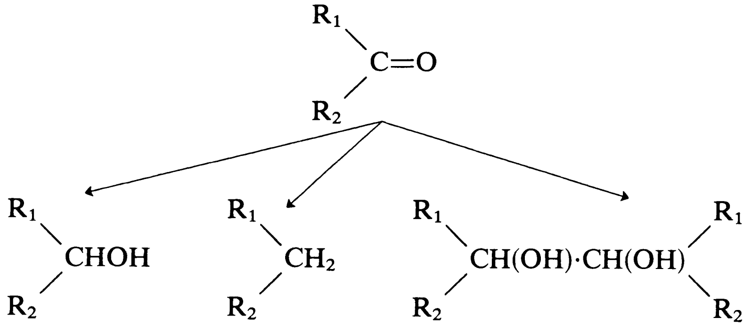

Formation of the alkane is believed to require a strongly acidic electrolyte and the highest yields have been obtained using lead, zinc, and zinc-amalgam cathodes.(271),† In contrast, low yields of the 1,2-diol (VIII) have been isolated from the electroreduction of acetone in an alkaline electrolyte.(272) The possibility of synthesizing this diol electrochemically attracted attention(273) in the chemical industry since it offered a practical route to dimethylbutadiene (IV):

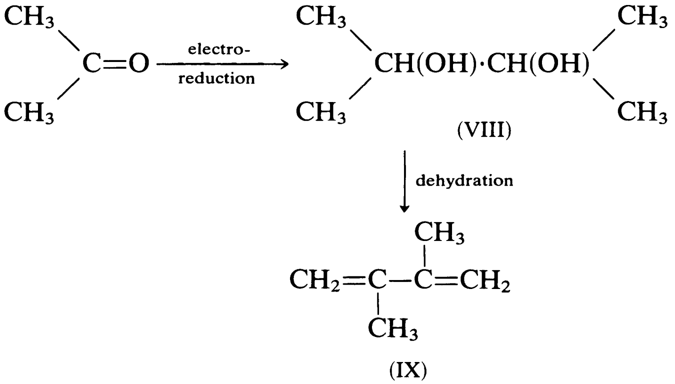

(VIII)

(IX)

Considerable attention has been focused upon the electroreduction of the aromatic carbonyl compounds, the ease of reduction making them ideal candidates for studies of the effects of molecular structure, electrode potential, electrode material, pH, and the nature of the electrolyte upon the overall electrode process. For example, a detailed experimental study of the electroreduction of a series of aromatic aldehydes and ketones, perhaps the most complete to date, has recently been published by Nadjo and Saveant.(274) From this data, the authors have constructed diagrams showing the distribution of the thermodynamically favored species as a function of pH and electrode potential.

Overall electrochemical reduction processes may be represented in terms of several electron transfers, proton transfers, and chemical reactions, as is shown below by the electroreduction of acetophenone(99) [(X), Scheme 4].

Although there is always an element of risk in attempting to fit the electrochemical behavior of the numerous aromatic carbonyl compounds to a common framework, a general summary may be presented:

(a) *In acidic solutions* a single-electron transfer occurs to the protonated form of the carbonyl compound, with subsequent dimerization of the neutral radical to form a pinacol (XI).

---

† The reduction of carbonyl compounds (and other organic molecules) using sodium in ethanol or zinc amalgam in strongly acidic solution (the Clemmensen reduction) may be considered as an electrochemical process occurring at a controlled potential, that potential being the mixed potential related to the organic reduction and metal corrosion processes, as mentioned in relation to potentiostatic electrolyses.

Scheme 4

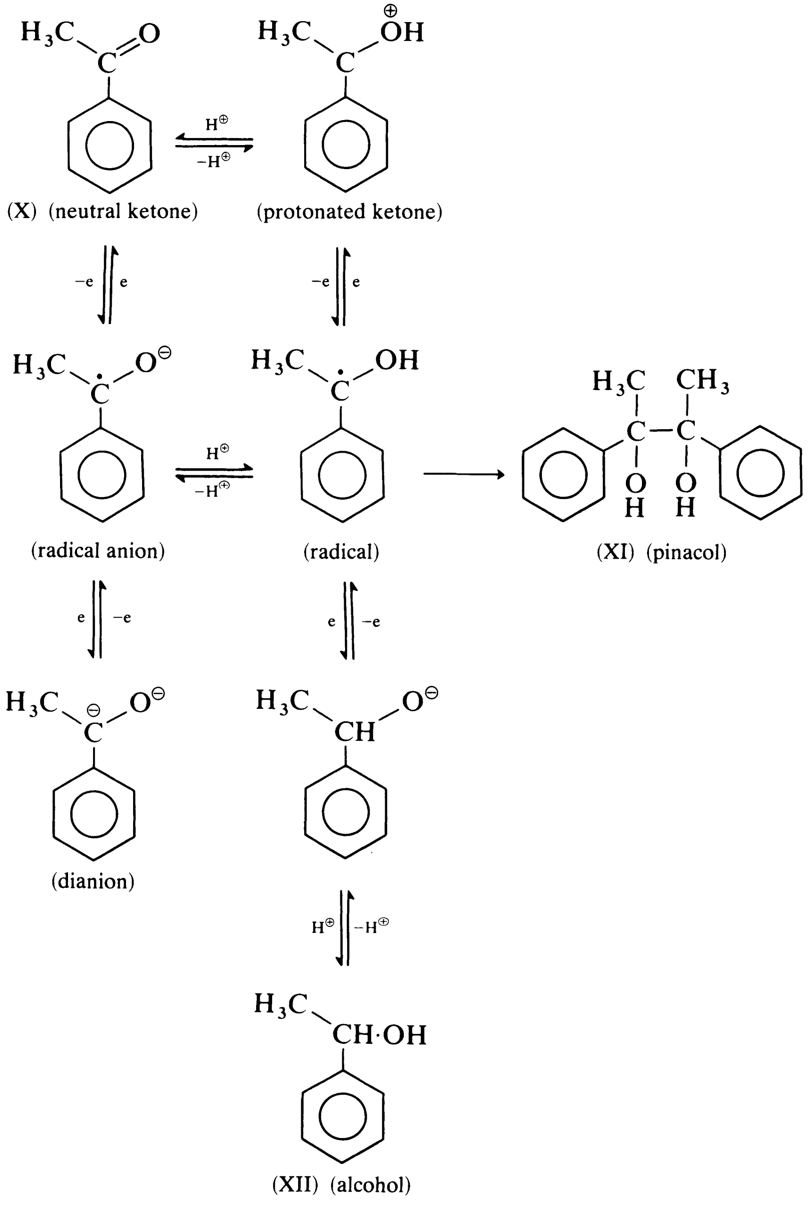
(X) (neutral ketone)
(protonated ketone)
(radical anion)
(radical)
(XI) (pinacol)
(dianion)
(XII) (alcohol)

(b) *In neutral solutions* the reaction pathway is dependent upon the relative ease of reduction of the various intermediates and therefore sensitive to molecular structure.

(c) *In alkaline solutions* the reaction becomes very sensitive to the structure of the aromatic molecule. For example, fluorenone is reduced in a stepwise manner to the carbinol (XII), whereas benzaldehyde has been shown to form a radical anion which undergoes dimerization.

Certainly polarographic and cyclic voltammetric techniques(274) have been used effectively to elucidate the mechanisms of the electroreduction of both aromatic and aliphatic carbonyl compounds (and indeed a wide variety of electrode processes) but in synthetic studies the very different conditions, particularly with respect to the concentrations of reactants and products, can influence both the reaction kinetics and reaction pathway.

The electroreduction of acetophenone in acidic electrolytes has been the subject of detailed studies of both the electrode kinetics and the reaction products.(275–278) One important question that has arisen from this work concerns the dimerization reaction, i.e., does this process occur heterogeneously *at* the surface of the electrode or homogeneously in the boundary layer *near* the electrode. In aqueous-alcoholic solutions, the rate-determining step becomes distinctly irreversible at both high and low concentrations of alcohol, this being attributed to adsorption effects.(276,277) Here, adsorption may involve the reactant molecules, intermediate species, and product molecules as well as the solvent molecules—all of which are, of course, competitive processes. However, more recently, similar kinetic data were observed at several cathode materials,(278) suggesting that perhaps adsorption is not significant and that the dimerization process occurs homogeneously. Again, it may equally well be argued that comparable (but significant) adsorption occurs at the various electrodes.(279)

13.3.2. Electroreduction of Nitrocompounds

The reduction of aliphatic and aromatic nitrocompounds, considering in particular the polarographic and voltammetric data, has been recently reviewed by Kemula and Krygowski.(280)

(a) *Aliphatic nitrocompounds.* Polarographic reduction of aliphatic nitrocompounds shows two irreversible processes,(281,282) the first corresponding to the formation of an alkyl hydroxylamine and the second to an amine:

$$\mathrm{R{\cdot}CH_2NO_2 \xrightarrow[4H^+]{4e} RCH_2NHOH \xrightarrow[2H^+]{2e} RCH_2NH}$$

The polarographic half-wave potentials for both processes are strongly dependent upon the pH of the electrolyte, becoming more cathodic as the solutions become basic. Detailed studies(283,284) using both the conventional dropping mercury electrode and a rotating platinum electrode formed the basis for a general reaction mechanism for the electroreduction of primary and secondary nitroalkanes (Scheme 5).

Scheme 5

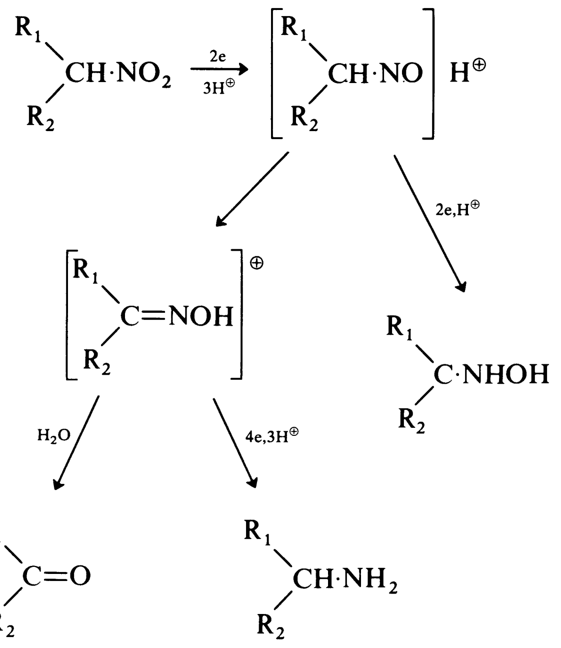
R_1
CH·NO$_2$
R_2
2e
3H$^\oplus$
CH·NO
H$^\oplus$
2e,H$^\oplus$
C=NOH
$\oplus$
C·NHOH
H$_2$O
4e,3H$^\oplus$
C=O
CH·NH$_2$

Tertiary nitroalkanes are primarily reduced to the alkylhydroxylamine. Under anhydrous conditions, the first intermediate of the electroreduction is an anion radical, which undergoes cleavage to the corresponding free radical.(285,286)

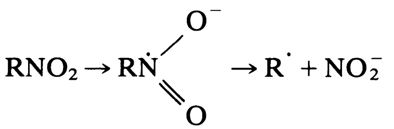

$$RNO_2 \rightarrow R\dot{N}\begin{array}{l}\diagup O^-\\ \\ \diagdown\!\!\diagdown O\end{array} \rightarrow R^{\cdot} + NO_2^-$$

This free radical may, of course, dimerize or abstract hydrogen or disproportionate:

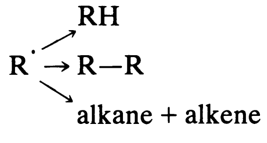

$$R^{\cdot}\begin{array}{l}\nearrow RH\\ \rightarrow R{-}R\\ \searrow \text{alkane + alkene}\end{array}$$

(b) *Aromatic nitrocompounds.* A general mechanism for the electroreduction of aromatic nitrocompounds was proposed by Haber(14) as long ago as

Scheme 6

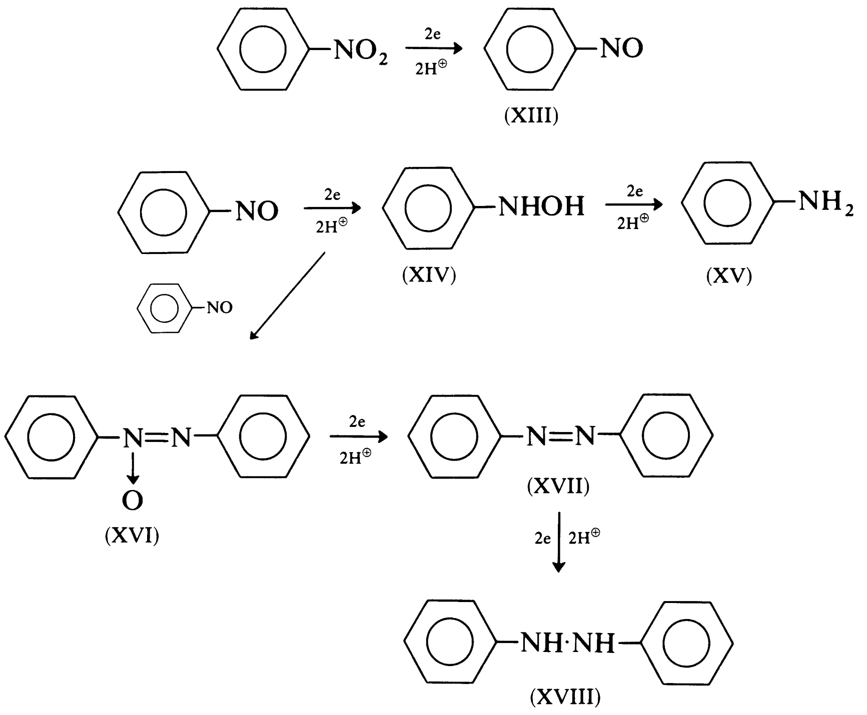
NO₂
2e
2H⊕
NO
(XIII)
NO
NHOH
(XIV)
NH₂
(XV)
N=N
O
(XVI)
(XVII)
NH·NH
(XVIII)

1898. As mentioned earlier, it was these electrochemical syntheses that clearly demonstrated the importance of control of the potential to electrode processes. Reduction sequences are shown in Scheme 6.

A variety of compounds can be obtained from this single electroreduction reaction. For example, the formation of the hydroxylamine (XIV) occurs at a platinum cathode (low hydrogen overpotential) in dilute aqueous acid. It is interesting to note that in aqueous sulfuric acid the hydroxylamine rearranges to yield *p*-aminophenol (XIX).(287)

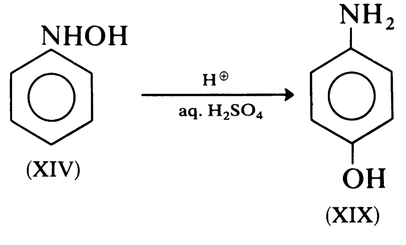
NHOH
H⊕
aq. H₂SO₄
NH₂
OH
(XIV)
(XIX)

However, in aqueous hydrochloric acid, the chloride ion is a stronger nucleophile than water, so that a mixture of *ortho*- (XX) and *para*-chloroaniline

(XXI) is also obtained.(288,289) Thus

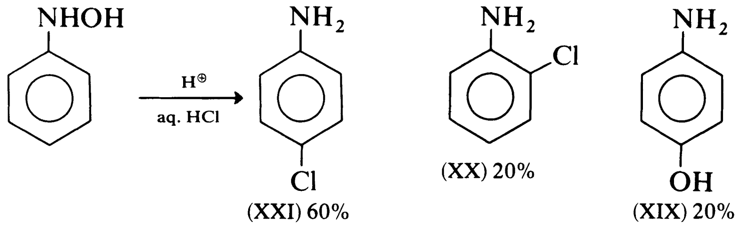

(XXI) 60%

(XX) 20%

(XIX) 20%

The use of electrodes with a high hydrogen overpotential such as mercury and lead favor formation of aniline (XV) in strongly acidic solutions, but in a basic electrolyte the coupling products (XVII) and (XVIII) are formed preferentially.

The role of adsorption in the electroreduction of aromatic nitrocompounds has been studied by several electrochemical techniques. Kastening *et al.*(290,291) calculated adsorption coefficients for *p*-chloronitrobenzene in various aqueous methanolic solutions of sodium hydroxide and in the presence of several concentrations of an inhibitor. From these studies, it was concluded that electron transfer occurred to an adsorbed species but that subsequent reactions of the anion radical may take place in the boundary layer:

$$\begin{array}{ccccc} RNO_2 & \xrightarrow{\text{diffusion}} & RNO_2 & \underset{-e}{\overset{e}{\rightleftharpoons}} & RNO_2^{\cdot\ominus} \\ \text{(bulk solution)} & & \text{(adsorbed)} & & \text{(adsorbed)} \end{array}$$

13.4. Coupling Reactions

The dimerization reaction, illustrated by the formation of the pinacol in the electroreduction of acetophenone, is an obvious example of a *coupling* reaction. Such reactions may occur between radicals or radical ions generated in either an anodic or a cathodic process. For example, an electrochemical process in which radicals are generated anodically is the classical Kolbe reaction, the electrolysis of carboxylates:

$$\begin{tikzcd} 2RCOO^{\ominus} \arrow[r] & 2R^{\cdot} + 2CO_2 \arrow[d, "\text{dimerization}"] \\ & R{-}R \end{tikzcd}$$

13.4.1. The Kolbe Reaction

This reaction has also been studied extensively and has broad synthetic applications. A simple route to the synthesis of many dicarboxylic acids is an extension of the Kolbe electrosynthesis, being the electrolysis of the half esters of dicarboxylic acids(292):

$$CH_3CH_2OOC{-}(CH_2)_nCOO^{\ominus} \rightarrow CH_3CH_2OOC{-}(CH_2)_{2n}COOCH_2CH_3$$

By way of a further extension of this oxidation process, it was shown that, under specific conditions, the dimerization reaction could be suppressed, allowing formation of alcohols and esters—the so-called Hofer–Moest reaction(293):

$$\mathrm{RCOO}^{\ominus} \rightarrow \mathrm{R{\cdot}OH} + \mathrm{RCOOR}$$

Some aspects of the mechanism of the Kolbe reaction are still very much a matter for debate as in some respects is the mechanism of electroreduction of aldehydes and ketones; key questions appear to be the nature of the intermediates and if they are adsorbed or not. It has been well established(294) that in aqueous electrolytes the Kolbe reaction does not occur below a certain critical anodic potential (~1.9 V vs. normal hydrogen electrode). The results of a thorough study of this electrosynthesis in both aqueous and anhydrous systems(295) were interpreted in terms of adsorbed carboxyl radicals. With increasing anodic potential, these intermediate species gradually cover the electrode surface until discharged to a second adsorbed radical at anode potentials above the critical potential.(5,99) Subsequent dimerization and desorption occurs to yield the product hydrocarbon:

$$\mathrm{RCOO}^{\ominus} + \mathrm{M} \rightleftarrows \underset{\text{(adsorbed)}}{\mathrm{RCOO}^{\cdot}/\mathrm{M}} + \mathrm{e}$$

$$\mathrm{RCOO}^{\cdot}/\mathrm{M} \rightarrow \underset{\text{(adsorbed)}}{\mathrm{R}^{\cdot}/\mathrm{M}} + \mathrm{CO_2}$$

$$\mathrm{R}^{\cdot}/\mathrm{M} + \mathrm{R}^{\cdot}/\mathrm{M} \rightarrow \mathrm{R{-}R}$$

A significantly different viewpoint has been expressed(296) wherein it is suggested that the formation of an oxide layer at the platinum anode is necessary for the formation of the hydrocarbon. The presence of a layer of platinum oxide at high anodic potentials appears to be supported by data obtained from a study of the platinum electrode surface using ESCA.(297)† On the other hand, polaromicrotribometry(298,299)—the measurement of the coefficient of friction of a metal surface—showed that in the electro-oxidation of acetate ions an organic film is formed in that region just below the critical potential.

An alternative approach to the elucidation of a reaction mechanism is by way of analysis of the products obtained under a variety of conditions.(300) It is also possible to compare and contrast these data with the data obtained from homogeneous reactions. Several electrolyses using the salts of selectively deuterated carboxylic acids, e.g., $\mathrm{CD_3COOH}$,(301) $\mathrm{CD_3CH_2COOH}$, and $\mathrm{CH_3CD_2COOH}$,(302) yielded products consistent with the formation of intermediate free radicals in that (a) the intermediates react with a –CH bond of a second anion and not with a water molecule:

---

† It should be remembered that ESCA is an ultrahigh vacuum technique for surface analysis and the surface studied is necessarily neither immersed in an electrolyte nor polarized.

$$CD_3COO^{\ominus} \rightarrow CD_3COO^{\cdot} \rightarrow CD_3^{\cdot} \xrightarrow{CD_3COO^{\ominus}} CD_4 + {}^{\cdot}CD_2COO^{\ominus}$$

and (b) disproportionation is a primary reaction pathway:

$$\begin{tikzcd}
CD_3CH_2COO^{\ominus} \arrow[r] & CD_3CH_2COO^{\cdot} \arrow[r] & CD_3CH_2^{\cdot} \arrow[d] \\
 & & CH_2=CD_2 + CD_3CH_2D \\
 & & CH_2=CD_2 + CH_3CHD_2 \\
CH_3CD_2COO^{\ominus} \arrow[r] & CH_3CD_2COO^{\cdot} \arrow[r] & CH_3CD_2^{\cdot} \arrow[u]
\end{tikzcd}$$

Further evidence of the involvement of radical species is afforded by the polymerizations observed during the electrolyses of carboxylates in the presence of olefins such as styrene, vinyl acetate, and vinyl chloride.(302)

It can be seen that the involvement of free radicals in the Kolbe electrosynthesis is actually not the question. Rather, it is whether these radicals are free to react *homogeneously* in solution(303)—although formed by a concerted electron transfer/decarboxylation process at the electrode surface—or are *adsorbed*.(5) In an excellent review of the anodic reactions of carboxylates, Utley(304) has presented a reaction scheme (shown in part below) which is adequate for most purposes. In a concluding section of this review, the question of free radical intermediates vis à vis adsorbed radicals is discussed in considerable detail. However, it would seem that the only conclusion one can draw is that the mechanism of this electro-organic process is still by no means settled. However, the following steps are likely to be involved:

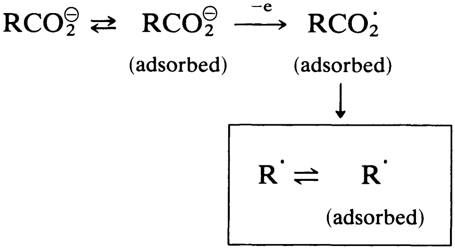

$$\begin{tikzcd}
RCO_2^{\ominus} \arrow[r, shift left] & \underset{\text{(adsorbed)}}{RCO_2^{\ominus}} \arrow[l, shift left] \arrow[r, "-e"] & \underset{\text{(adsorbed)}}{RCO_2^{\cdot}} \arrow[d] \\
 & & \boxed{R^{\cdot} \rightleftharpoons \underset{\text{(adsorbed)}}{R^{\cdot}}}
\end{tikzcd}$$

(a) disproportionation of $R^{\cdot} \rightarrow$ alkane + alkene
(b) dimerization of $R^{\cdot} \rightarrow$ higher alkane
(c) hydrogen abstraction by $R^{\cdot} \rightarrow$ alkane
(d) further oxidation of $R^{\cdot} \rightarrow R^{+}$, carbonium ion

The other anodic reactions of carboxylates, e.g., the Hofer–Moest reaction, are believed to involve carbonium ion intermediates.

13.4.2. Other Anodic Coupling Reactions

A variety of substituted radicals may be generated by the electro-oxidation of salts of 1,3-dicarbonyl compounds, aliphatic nitrocompounds, phenols, oximes, alkynes, and organometallic compounds. In all of these reactions, an anionic (or partially anionic) species is formed from which the intermediate radical is generated, e.g., in the anodic oxidation of diethylmalonate (XXII)(305):

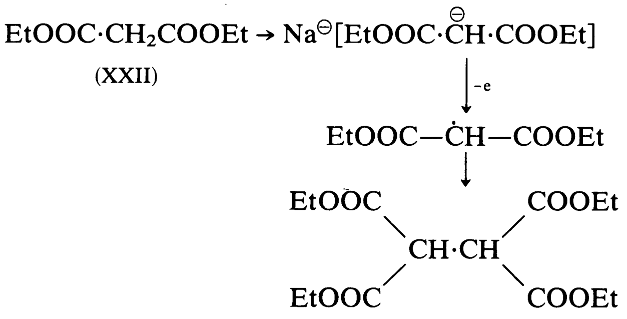

(XXII)

Other examples are summarized in Table 9.

Grignard reagents or lithium alkyls exhibit low oxidation potentials and provide an excellent source of both alkyl and aryl radicals. It appears that subsequent oxidation of intermediate species, as is observed in some Kolbe electrosyntheses, is often avoided in the anodic reactions of these organometallic compounds, but practical difficulties have tended to limit progress in this area. It is anticipated that improved design of electrochemical cells will alleviate these problems.(314)

Table 9
Coupling Reactions via Anodic Oxidation

Reactant	Product	References
Diethyl malonate	Tetraethyl ethane-1,1,2,2-tetracarboxylate	305
Ethyl acetoacetate	Diethyl diacetyl-succinate	305
Ethyl cyanoacetate	Diethyl α,α'-dicyanosuccinate	306
1-Nitropropane	3,4-Dinitrohexane and 3-nitro-3-hexene	307
2-Nitropropane	2,3-Dinitro-2,3-dimethylbutane	308, 309
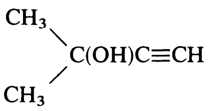	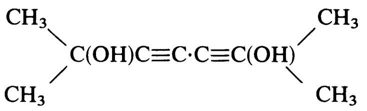	310
Sodium phenyl mercaptide	Diphenyl disulfide	311
Potassium thioacetate	Diacetyl disulfide	311
Phenyl magnesium bromide or diphenyl zinc	Biphenyl	312
Nitrocyclohexane	1-Azido-1-nitrocyclohexane	313

Coupling of different anions is achieved by the simultaneous electrolysis of both species. It has been postulated that intermediate radical ions are formed and subsequently further oxidized.(308,313) For example, in the coelectrolysis of sodium azide and a nitroaliphatic compound:

$$Na^{\ominus}N_3^- \rightarrow N_3^{\bullet}$$

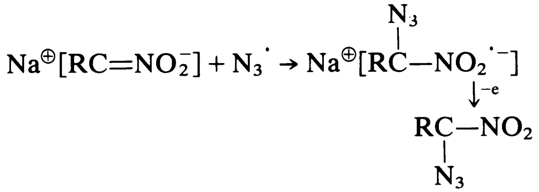

$$Na^{\oplus}[RC{=}NO_2^-] + N_3^{\bullet} \rightarrow Na^{\oplus}[R\overset{N_3}{\overset{|}{C}}{-}NO_2^{\bullet -}] \xrightarrow{-e} R\underset{N_3}{\underset{|}{C}}{-}NO_2$$

13.4.3. Cathodic Coupling

Again the dimerization or coupling reactions will involve free radicals or radical ions, but the intermediates are generated cathodically. Suitable substrates are electrophiles such as activated olefins and carbonyl compounds. In this section, it is intended to focus only upon the electroreduction of activated olefins, partly because the electrode reactions of aldehydes and ketones has been discussed earlier. However, it is the electrohydrodimerization of an activated olefin that has become a successful, commercial electroorganic process, i.e., the electroreduction of acrylonitrile developed by Monsanto:

$$CH_2{=}CHCN \xrightarrow[2H^{\oplus}]{2e} CN{-}(CH_2)_4{-}CN$$

More generally, the electrode reaction can be written as

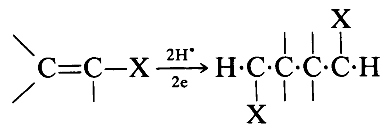

$$\rangle C{=}\underset{|}{C}{-}X \xrightarrow[2e]{2H^{\bullet}} H{\cdot}\underset{|}{C}{\cdot}\underset{\underset{X}{|}}{\overset{|}{C}}{\cdot}\underset{|}{\overset{|}{C}}{\cdot}\overset{\overset{X}{|}}{C}{\cdot}H$$

where X = CN, C = O, COOR, or CONH$_2$.

Cathodic coupling of α,β-unsaturated carbonyl compounds may yield three types of dimers, namely "head-to-head," "tail-to-tail," and "head-to-tail" (Scheme 7).

A comparison of the electrochemical and chemical reduction—the latter using potassium or lithium amalgams—of a series of α,β-unsaturated esters has shown that in all cases the electrochemical syntheses were superior (see Table 10).(315) The products of several of these reactions also showed that the stereochemical requirements of the electrode process led to exclusive tail-to-tail dimerization.(316)

The yields and stereochemistry of the products obtained from the electrochemical reduction and chemical reduction (using sodium amalgam,

Scheme 7

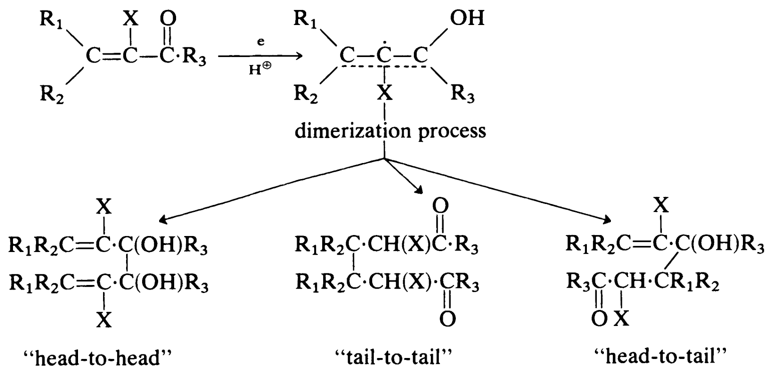
e
H⊕
dimerization process
"head-to-head"
"tail-to-tail"
"head-to-tail"

magnesium, or zinc) or 2-cyclohexenone (XXIII) showed that (a) both head-to-tail (XXIV) and tail-to-tail (XXV) dimerization occurs and (b) the yields from chemical reduction were sensitive to the solvent.[(316)]

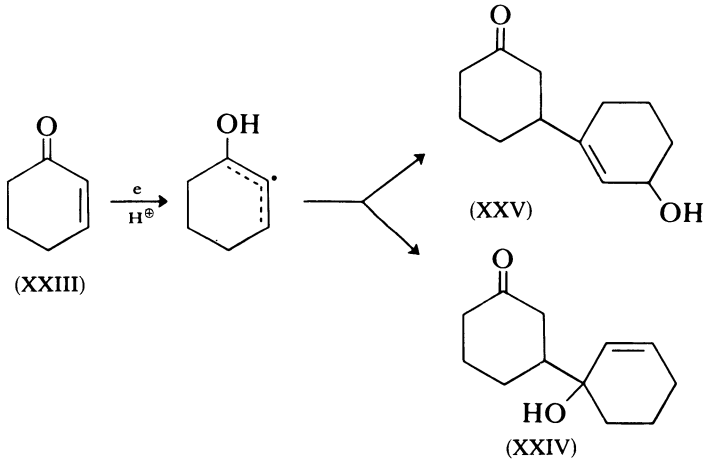
e
H⊕
(XXIII)
(XXV)
(XXIV)

Table 10
Electrohydrodimerization of α,β-Unsaturated Esters

Ester	Yield from electroreduction	Yield from chemical reduction
Ethyl acrylate	85%	52%
Diethyl maleate	65%	31%
Acrylamide	40%	Zero

Intramolecular cyclization has been observed in several electrohydrodimerization reactions,(317) another indication of the versatility of this type of electrode process. High yields of cyclopropanes, cyclopentanes, and cyclohexanes have been obtained from α,β-unsaturated esters.(317,318)

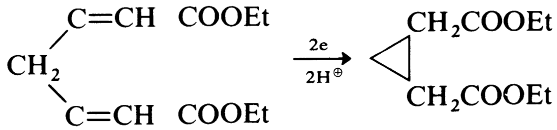
C=CH COOEt
CH2
C=CH COOEt
2e
2H⊕
CH2COOEt
CH2COOEt

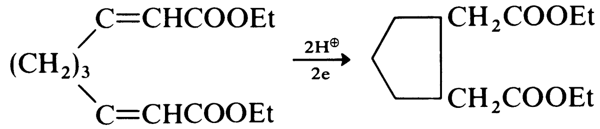
C=CHCOOEt
(CH2)3
C=CHCOOEt
2H⊕
2e
CH2COOEt
CH2COOEt

Bicyclic esters and therefore bicyclic dicarboxylic acids may also be synthesized(317,318):

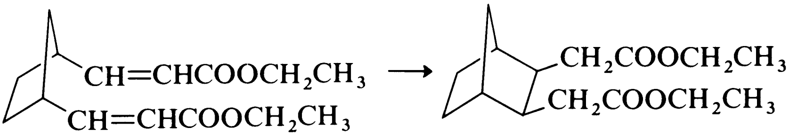
CH=CHCOOCH2CH3
CH=CHCOOCH2CH3
CH2COOCH2CH3
CH2COOCH2CH3

The overall mechanism of the intramolecular cyclization has been discussed by Anderson and Baizer(319) and a *concerted* process is favored (Scheme 8) (cf. the mechanism proposed by Eberson for the Kolbe reaction).

Scheme 8

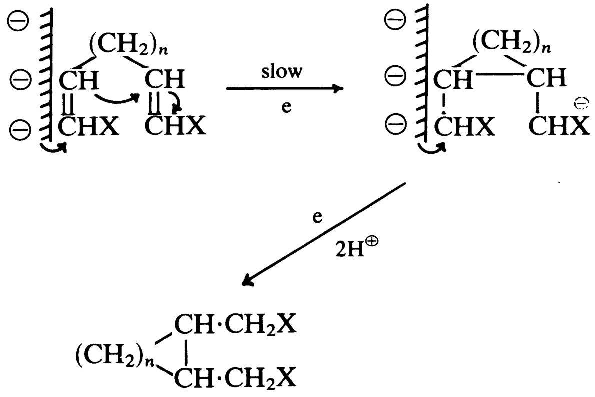
(CH2)n
CH
CH
CHX
CHX
slow
e
(CH2)n
CH
CH
CHX
CHX
e
2H⊕
CH·CH2X
(CH2)n
CH·CH2X

13.5. Electroinitiated Polymerizations

It is obvious that an electric current may be used to generate reactive intermediates—radicals, radical anions, radical cations, cations, and anions—so that it is logical that such intermediates may be used in some polymerization reactions. Thus, the overall polymerization process may be *initiated* either by direct electron transfer to or from the monomer itself or by the generation of an active species in the electrolyte.

Electroinitiated polymerization of organic molecules was recognized perhaps three decades ago, and since that time the cathodic and anodic polymerization of activated olefins, cyclic ethers, carboxylic acids, esters, anhydrides, amines, phenols, and heterocyclic compounds have been described.(320,321) However, polymerizations not achieved by "more conventional" techniques have yet to be demonstrated, and presently this technique has not been chosen for a large-scale polymerization process. This is perhaps surprising, since one advantage of electroinitiated polymerization processes is that relatively mild conditions of temperature and pressure are required, thus tending to minimize branching and cross-linking reactions. It has been pointed out(321) that, in order to be applicable industrially, it is essential that the electrochemistry be used only to generate the active intermediates. In other words, a multimillion pound bulk polymerization process in an electrochemical cell may never be feasible!

One area that does appear to be of industrial interest is electrocoating,(322) i.e., the formation of adherent, impermeable coatings on various metal shapes. Here the control of the process gained by the "throwing power" of the cell and electrodes assures deposition over the *total* surface.

The diversity of electropolymerization reactions is also of interest, i.e., the ability to generate other anionic or cationic polymerizations from the same monomer simply by reversing the polarity of the electrodes in the system. Furthermore, it has been shown that grafting(323) and cross-linking(324) have been demonstrated by electrochemical techniques. Funt *et al.*(325,326) established that control of the molecular weight and distribution of molecular weight could be achieved from the total charge (faradays) passed in the reaction process.

An interesting extension of electroinitiated polymerization techniques is the formation of block copolymers. For example, it has been found that after polymerization of styrene and tetrahydrofuran in a *divided* cell, further reaction of the two homopolymers provided an A–B–A block copolymer (Scheme 9) (where A is tetrahydrofuran and B is styrene).

It is important to realize that in both homopolymerization processes a "living polyion" is formed and the subsequent reaction is a combination of these ions. Here a "living ion" is one whose molecular weight can be reversibly changed by the conditions of the reaction, e.g., concentration of the monomer,

Scheme 9

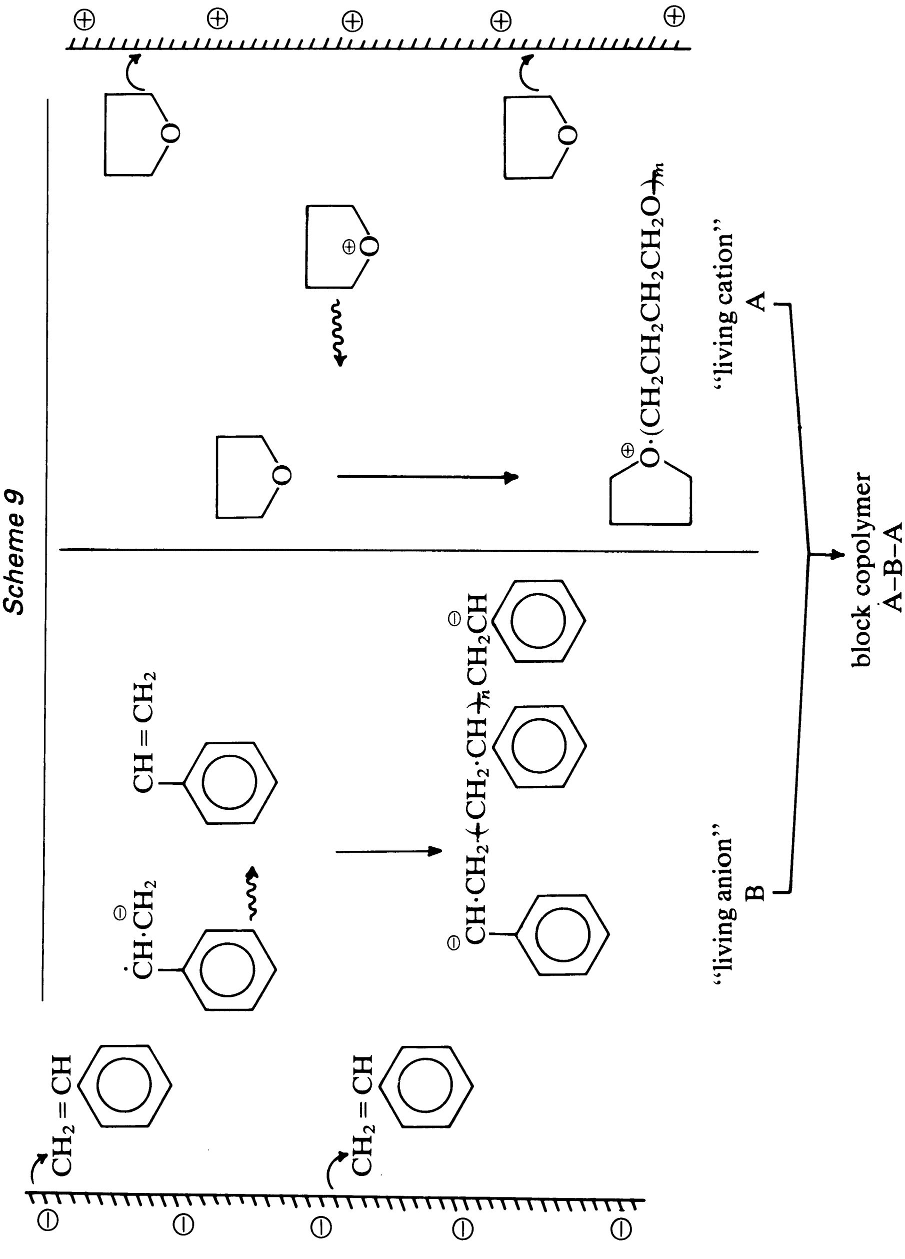
⊕ ⊕ ⊕ ⊕ ⊕
⊖ ⊖ ⊖ ⊖ ⊖
CH₂ = CH
ĊH·CH₂ ⊖
CH = CH₂
⊖ CH·CH₂–(CH₂·CH)ₙ CH₂CH ⊖
O
⊕O
⊕O·(CH₂CH₂CH₂CH₂O)ₙ
"living anion"
B
"living cation"
A
block copolymer
A–B–A

temperature, etc.:

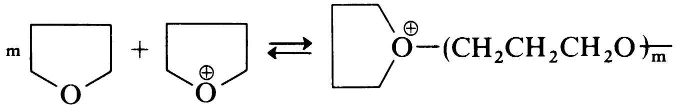

This living polyion is susceptible to quenching by nucleophilic species even in trace quantities, e.g., anionic (or cationic) species, water, hydrophilic solvents.

An obvious disadvantage to electroinitiated polymerization is that the method is restricted to polar media, in that the electrolyte or solution of the monomer must be able to conduct a small current at least. Furthermore, the presence of solvent molecules may be detrimental to the overall polymerization. In several instances, however, the monomer is sufficiently polar in nature to ionize a suitable supporting electrolyte, e.g., solutions of perchlorates or tetrafluoroborates in tetrahydrofuran.

Electroinitiated polymerization has been reviewed in two recent monographs(320,321) describing the experimental procedures, mechanistic features, potential advantages, and obvious limitations of this type of process.

14. Economic and Commercial Aspects of Organic Electrode Processes

The preceding sections have highlighted but a fraction of the many organic electrode reactions that have been reported in the literature, as may be readily appreciated from the available monographs and review articles.(19–27) In this light, one again must ask the question, why are there so few established industrial processes based on organic electrochemistry? Perhaps the engineering skills necessary for the successful scale-up of electrochemical syntheses have developed too slowly to be effective. Preference of a competitive "chemical" route—even if only marginally competitive—may also be a factor.(327–330) (Indeed it often seems that the emergence of a potentially economic electrochemical synthesis stimulates considerable activity toward identifying an even better chemical route!) But perhaps more important is the commitment of labor and resources required to commercialize any process that has been defined in the laboratory.

The single most successful industrial process based upon organic electrochemistry is the electrohydrodimerization of acrylonitrile to yield adiponitrile, introduced commercially in 1965 by Monsanto. The discovery, development, and commercialization of this process have been described in detail in recent articles(331,332) that provide excellent insight into the commitment that is required to bring a process to commercial success.

The motivation for Monsanto to pursue this technology may be understood by an awareness of the synthesis of Nylon "66," shown schematically below. Adipic acid (XXVI) is a key intermediate in the process, being a precursor to hexamethylenediamine (XXVII) and itself polymerized with the diamine to form Nylon.

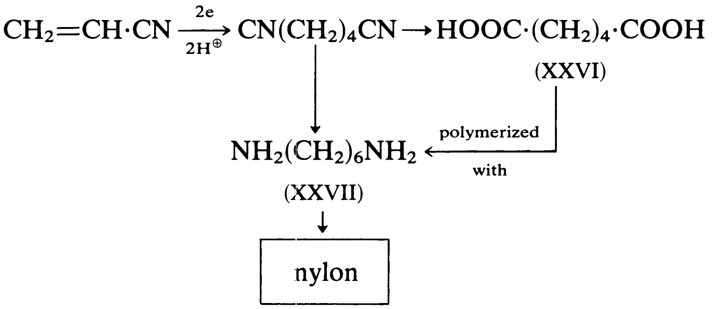

$$\begin{tikzcd}
CH_2{=}CH{\cdot}CN \arrow[r, "2e", "2H^{\oplus}"'] & CN(CH_2)_4CN \arrow[r] \arrow[d] & HOOC{\cdot}(CH_2)_4{\cdot}COOH\ (XXVI) \arrow[dl, "polymerized", "with"'] \\
 & NH_2(CH_2)_6NH_2\ (XXVII) \arrow[d] & \\
 & \boxed{\text{nylon}} &
\end{tikzcd}$$

Thus, the electrochemical route for synthesis of adiponitrile effectively halved the demand for adipic acid.

The development of a laboratory scale synthesis of adiponitrile—perceived to be viable *only* by the electrochemical route—is delightfully recounted by Baizer in his recent paper.(136) It is interesting to note that a key factor was the introduction of the tetraalkylammonium salts as the supporting electrolyte in the aqueous-organic system, allowing essentially quantitative yields to be achieved. Scale-up was undertaken and completed in approximately 18 months(332) and involved an organization of 20 chemists and engineers (none of whom were experienced in electrochemistry). The successful completion of this stage allowed plant construction to begin in sufficient time to provide the required capacity of adiponitrile in 1965. Today it is estimated that 220,000 tons of adiponitrile are produced annually by the electrohydrodimerization process.

Several factors must be considered before a commitment of resources can be made to the commercialization of any synthetic process. The type of process that has been identified from the laboratory and pilot studies must show distinct advantages over existing and emerging technology, and the risk associated with achieving the desired production levels must be reasonable. The management of any organization will probably also consider the "fit within corporate strategy and business" and evaluate where the particular process can utilize the company's technological and/or marketing strengths. A major consideration is the availability of capital and resources, which, for all but the largest chemical companies, may be the most critical decision, i.e., which projects to fund and which to delay.

Recent publications(333,334) concerning the industrial applicability of organic electrosyntheses have included tabular summaries of electro-organic processes that have been developed beyond the laboratory stage (though not necessarily to commercial production). A similar summary is included here, using those reactions and types of reaction that have been discussed (Table 11).

An economic study(334) has reviewed the commercial status of electro-organic processes and attempted to estimate where significant *energy savings* might be achieved by introduction of an electrode process to replace a

Table 11

Type of reaction	Starting compound	Product	Status	Company and country	References
Crum Brown–Walker	Half ester of adipic acid	Diester of sebacic acid	Formerly pilot plant	BASF (FRG)	335
Crum Brown–Walker	Monomethyl azelaic acid	Hexadecane dioic ester	Commercial	Soda Aromatic Co. (Japan)	
Anodic substitution	2-Methyl naphthalene	2-Methyl-α-naphthol acetate	Formerly pilot plant	BASF (FRG)	336
Anodic substitution	Naphthalene	1-Naphthyl acetate	Pilot plant	BASF (FRG)	
Anodic substitution	Furan	Dimethoxydihydrofuran	Commercial	BASF (FRG)	337
Indirect oxidation	Toluene	Benzaldehyde	Pilot plant		338
Indirect oxidation	Benzene	Hydroquinone	Pilot plant	Stavely (UK) Carus (US)	339
Indirect oxidation	Anthracene	Anthraquinone	Commercial	Holliday (UK)	340, 341, 342
Organometallic	Methyl chloride (THF/Diglyme, RMgCl)	Tetraalkyl lead	Commercial (may now have been terminated)	Nalco (US)	343, 344
Electrohydrodimerization	Acrylonitrile	Adiponitrile	Commercial	Monsanto (US & UK) Asahi (Japan)	345
Reductive coupling	Acetone	Pinacol	Formerly pilot plant	Diamond Shamrock (US) BASF (FRG)	346, 347
Reductive coupling	*p*-Hydroxypropiophenone	Pinacol	Pilot plant	Sorapec (France)	
Reductive rearrangement	Nitrobenzene	*p*-Aminophenol	Commercial	Japan Holliday (UK) CJB (UK) India	348
Reduction	Nitrobenzene	Aniline	Pilot plant	India	349
Reduction	Salicyclic acid	Salicaldehyde	Commercial	USSR, India	350
Reduction	Tetrahydrocarbazole	Hexahydrocarbazole	Commercial	BASF (FRG)	347, 351, 352
Reduction	Pyridine	Piperidine	Commercial	Robinson Bro. (UK)	353

Table 12
Energy Requirements in kcal/lb for Electrochemical and Chemical Syntheses of Selected Compounds

	Electrochemical	Chemical
Adiponitrile	950,000	1,450,000
Aniline from nitrobenzene	796,000	306,000
Sorbitol	208,000	21,000
Terephthalic acid	382,000	1,540
Phenol	783,000	270,000
Dichloroethane	391,000	135,000
Hydroquinone	1,160,000	678,000
Melamine	664,000	340,000

conventional chemical process. Two hundred and twenty chemicals were identified, the production of which exceeded 10,000 tons per year in the United States according to 1975 data. From the extensive literature of electro-organic chemistry, it was found that 95 of these chemicals had been synthesized electrochemically. It was then possible to select a small number of these and obtain detailed calculations of the energy consumption for the two types of synthesis—chemical vs. electrochemical.

The results of these calculations are shown in Table 12. It can be seen immediately that the only distinct advantage in terms of *energy savings* is obtained with the production of adiponitrile. However, this is only one aspect, and it is also necessary to consider the factors discussed above, the relative yields obtained and the costs of the raw materials and process equipment required. Then a selection of a particular process should be made. Nonetheless, Table 12 serves to show the "handicap" that electro-organic processes must overcome.

15. Conclusions Regarding Industrial Applications

The chemical industry is today faced with several challenges: (i) the continual increase in the cost of raw materials, (ii) environmental constraints, which grow ever more stringent, and (iii) the need for energy conservation.

Thus, processes are being examined and reexamined, improvements and modifications considered, and alternate processes studied in an effort to define technology that might alleviate or eliminate these problems. Organic electrode processes are presently being carefully assessed in this light.(334)

Baizer(333) suggests that if certain conditions prevail, the future for organic electrochemistry may be strong:

(a) Advances in the technical aspects of this field must continue, e.g., cell designs of higher space-time yields, superior membranes and electrodes, more predictability in scale-up.

(b) A stronger rapport between the laboratory chemist and process chemist must develop at early stages.

(c) Emphasis must be placed on the *unique* aspects of electrochemical syntheses.

(d) The specialty chemical and drug industries must become more aware of the selectivity and specificity of organic electrode processes.

Finally, and perhaps most importantly, an assessment of the capital and resources requirement must be made at the early stages of the project and the *commitment maintained* steadfastly throughout the life of that project.

References

1. N. Weinberg and H. Weinberg, *Chem. Rev.* **68**, 449 (1968).
2. S. Swann, Jr., in *Techniques of Organic Chemistry*, Vol. II, 2nd Ed., A. Weissberger, ed., Interscience, New York (1956).
3. M. J. Allen, *Organic Electrode Processes*, Reinhold, New York (1958).
4. S. Glasstone and A. Hickling, *Chem. Rev.* **25**, 407 (1939).
5. A. K. Vijh and B. E. Conway, *Chem. Rev.* **67**, 623 (1967).
6. B. C. L. Weedon, *Quart. Rev. Chem. Soc. London* **6**, 300 (1952).
7. C. J. Brockman, *Electroorganic Chemistry*, John Wiley and Sons, New York (1926); *Bibliography of Electroorganic Syntheses (1801–1975)*, R. Alkire and S. Swann, Electrochemical Society, Pennington, New Jersey (1980).
8. T. Erdey-Gruz and M. Volmer, *Z. Phys. Chem.* **A150**, 203 (1930).
9. J. A. V. Butler, *Electrocapallarity*, Methuen, London (1940).
10. B. B. Damaskin, O. A. Petrii, and V. V. Batrakov, *Adsorption of Organic Compounds on Electrodes*, Plenum Press, New York (1971).
11. A. Schmidt, *Angewandte Elektrochemie*, Verlag Chemie, New York (1976).
12. A. Kuhn, *Industrial Electrochemical Processes*, Elsevier, Amsterdam (1971).
13. M. Faraday, *Ann. Phys. Chem.* **33**(2), 438 (1834).
14. F. Haber, *Z. Elektrochem.* **22**, 506 (1898); see also F. Haber and C. Schmidt, *Z. Phys. Chem.* **32**, 271 (1900).
15. F. Fichter, *Organische Electrochemie*, Steinkopff, Dresden (1942).
16. A. Hickling, *Trans. Faraday Soc.* **38**, 27 (1942).
17. J. Heyrovsky, *Chem. Listy* **16**, 256 (1922).
18. In particular, the work of Heyrovsky, Koutecky, Koryta, Brdicka, and Zuman.
19. L. Eberson and H. Schafer, *Fortsch. Chem. Forsch.*, No. 21, 1, Springer-Verlag, Berlin (1971).
20. A. J. Fry, *Synthetic Organic Electrochemistry*, Harper and Row, New York (1972).
21. F. Beck, *Elektroorganische Chemie*, Verlag Chemie, Weinheim, BRD (1974).
22. N. Weinberg, ed., *Technique of Electroorganic Synthesis*, Parts I and II, Wiley Interscience, New York (1974/1975).
23. S. Ross, M. Finkelstein, and E. J. Rudd, *Anodic Oxidation*, Academic Press, New York (1975).
24. M. M. Baizer, ed., *Organic Electrochemistry*, Marcel Dekker, New York (1973).
25. M. R. Rifi and R. H. Covitz, *Introduction to Organic Electrochemistry*, Marcel Dekker, New York (1974).
26. A. J. Bard and H. Lund, eds., *Encyclopedia of Electrochemistry of the Elements*, Vol. XI, XII, XIII, and XIV, Marcel Dekker, New York (1978).

27. D. T. Sawyer and J. L. Roberts, Jr., *Experimental Electrochemistry for Chemists*, Wiley Interscience, New York (1974).
28. A. Streitweiser, *Molecular Orbital Theory for Organic Chemists*, John Wiley and Sons, New York (1961).
29. G. J. Hoytink, *Rec. Tav. Chim.* **77**, 555 (1958); see also P. J. Elving and M. Pullman, *Adv. Chem. Phys.*, I. Prigogine, ed., **3**, 1 (1961).
30. For discussion of chemical factors in electrochemical processes, see B. E. Conway, in *Progress in Kinetics*, Vol. 4, G. Porter, ed., Pergamon Press, London (1967), Chap. 10, p. 399.
31. B. E. Conway, *Theory and Principles of Electrode Processes*, Ronald Press, New York (1965).
32. (a) Fuel Cells, A survey of B. J. Crowe, NASA SP-5115, Washington, D.C. (1973); (b) E. A. Gillis, *Chem. Eng. Prog.* **76**, 88 (1980).
33. B. J. Piersma and E. Gileadi, in *Modern Aspects of Electrochemistry*, Vol. 4, J. O'M. Bockris and B. E. Conway, eds., Plenum Press, New York (1966).
34. J. O'M. Bockris, E. Gileadi, and G. E. Stoner, *J. Phys. Chem.* **73**, 427 (1969).
35. H. Binder, A. Kohling, H. Krupp, K. Richter, and G. Sandstede, *J. Electrochem. Soc.* **112**, 355 (1965).
36. H. A. Liebhafsky, Fuel cells and fuel batteries—an engineering view, *IEEE Spectrum* **3**(12), 48 (1966).
37. F. T. Bacon, The development and practical application of fuel cells, in *Trends in Electrochemistry*, J. O'M. Bockris, D. A. J. Rand, and B. J. Welch, eds., Plenum Press, New York (1977).
38. M. W. Brieter, *Electrochim. Acta* **7**, 601 (1962); see also S. Schuldiner, M. Rosen, and D. R. Flinn, *J. Electrochem. Soc.* **117**, 1251 (1970).
39. M. Fleischmann, K. Korinek, and D. Pletcher, *J. Chem. Soc. Perkin Trans. II*, 1396 (1972).
40. M. Amjad, D. Pletcher, and C. Smith, *J. Electrochem. Soc.* **124**, 203 (1977).
41. See Vol. of this treatise.
42. D. C. Grahame, *Chem. Rev.* **41**, 441 (1947).
43. H. H. Bauer, *J. Electroanal. Chem.* **12**, 524 (1966).
44. L. I. Krishtalik, *Elektrokhimiya* **2**, 1123 (1966); *J. Electroanal. Chem.* **21**, 421 (1969); see also *Advances In Electrochemistry and Electrochemical Engineering*, Vol. 7, P. Delahay and C. W. Tobias, eds., Interscience, New York (1970), p. 283.
45. J. Koutecky and V. Hanus, *Collect. Czech. Chem. Commun.* **20**, 124 (1955).
46. The kinetic behavior corresponding to this equation is often referred to as "Temkin kinetics" in relation to the Temkin isotherm [M. I. Temkin, *Zh. Fiz. Khim.* **15**, 296 (1941); see also A. N. Frumkin, *Z. Phys. Chem.* **116**, 466 (1925)], but the latter refers to heterogeneity rather than interaction effects with regard to the origin of the $\exp(-\beta r\theta j)$ term.
47. E. Gileadi and S. Srinivasan, *J. Electroanal. Chem.* **7**, 452 (1964).
48. E. Muller, *Z. Elektrochem.* **29**, 264 (1923); **33**, 561 (1927); **34**, 256 (1928).
49. A. Hickling, *Trans. Faraday Soc.* **38**, 27 (1942).
50. M. J. Allen, *Organic Electrode Reactions*, Reinhold, New York (1958), p. 21.
51. O. R. Brown, *Electrochim. Acta* **13**, 317 (1968).
52. F. G. Will and C. A. Knorr, *Z. Elektrochem.* **64**, 258; 270 (1960).
53. J. Badoz-Lamling, G. Charlot, and M. Tremillon, in *Electrochemical Reactions*, Elsevier, Amsterdam (1963).
54. P. Delahay, *New Instrumental Methods in Electrochemistry*, Interscience, New York (1954).
55. P. Zuman, *J. Polarographic Soc.* **13**, 53 (1967).
56. A. N. Frumkin, *Z. Phys.* **35**, 792 (1926).
57. J. A. V. Butler, *Proc. Roy. Soc. London Ser. A* **122**, 399 (1929).
58. P. J. Elving and M. Pullman, *Adv. Chem. Phys.*, I. Prigogine, ed., **3**, 1 (1961).
59. N. F. Mott and R. J. Watts-Tobin, *Electrochim. Acta* **4**, 79 (1960); see also *Philos. Mag.* **7**(8), 483 (1962).

60. J. O'M. Bockris, M. A. V. Devanathan, and K. Muller, *Proc. Roy. Soc. London Ser. A* **274**, 55 (1963).
61. M. A. Habib and J. O'M. Bockris, in *Comprehensive Treatise of Electrochemistry*, Vol. 1, J. O'M. Bockris, B. E. Conway, and E. Yeager, eds., Plenum Press, New York (1980); see also B. E. Conway, *Ionic Hydration in Chemistry and Biophysics*, Elsevier, Amsterdam (1981).
62. R. W. Fawcett, S. Levine, R. M. De Nobriga, and A. C. McDonald, *J. Electroanal. Chem.* **111**, 163 (1980).
63. Micro-Symposium on the Double Layer, International Conference Solute–Solute–Solvent Interactions, Florence, Italy, May (1980), *J. Electroanal. Chem.* **123**, 81 (1981).
64. B. E. Conway and L. G. M. Gordon, *J. Phys. Chem.* **73**, 3609 (1969).
65. H. Wroblowa, Z. Kovac, and J. O'M. Brockris, *Trans. Faraday Soc.* **61**, 1523 (1965).
66. H. Wroblowa and K. Muller, *J. Phys. Chem.* **73**, 3528 (1969).
67. D. C. Grahame, *J. Am. Chem. Soc.* **76**, 4819 (1954); **79**, 2093 (1957).
68. R. S. Hansen and B. H. Clampitt, *J. Phys. Chem.* **58**, 908 (1954); R. S. Hansen, R. E. Minturn, and D. A. Hickson, *J. Phys. Chem.* **60**, 1185 (1956).
69. N. A. Balashova, *Dokl. Akad. Nauk SSSR* **103**, 639 (1959); *Zh. Fiz. Khim.* **32**, 2266 (1958); *Z. Phys. Chem.* (*Leipzig*) **207**, 340 (1957).
70. S. Gilman, *Trans. Faraday Soc.* **61**, 2546; 2561 (1965); **62**, 466; 481 (1966).
71. B. E. Conway, R. G. Barradas, and T. Zawidski, *J. Phys. Chem.* **62**, 676 (1958).
72. E. J. Rudd and B. E. Conway, *Trans. Farday Soc.* **67**, 440 (1971).
73. S. Trasatti, *J. Electroanal. Chem.* **33**, 351 (1971); see also *J. Chem. Soc. Faraday Trans. 1*, **70**, 1752 (1974).
74. A. N. Frumkin, I. Nekrassov, B. Levich, and Y. Ivanov, *J. Electroanal. Chem. I* **84**, (1959/1960).
74. (a) D. Ilkovic and G. Semerano, *Collect. Czech. Chem. Commun.* **4**, 176 (1932); (b) G. C. Barker and I. L. Jenkins, *Analyst* **77**, 685 (1952).
75. I. M. Kolthoff and J. J. Lingane, *Polarography*, Interscience, New York (1952).
76. P. Zuman, Organic Polarographic Analysis, Macmillan, New York (1964).
77. L. Meites, *Polarographic Techniques*, 2nd Ed., Interscience, New York (1965).
78. O. H. Muller, in *Physical Methods of Organic Chemistry*, Vol. I, Part IV, A. Weissberger, ed., 3rd Ed., Interscience, New York (1960).
79. J. E. Page, *Quart. Rev.* **6**, 262 (1952).
80. P. J. Elving, *Record Chem. Prog.* (*Kresge Hooker Sci. Lib.*) **14**, 99 (1953).
81. P. Zuman and S. Wawzonek, in *Progress in Polarography*, Vol. I, P. Zuman and I. M. Kolthoff, eds., Interscience, New York (1962).
82. C. L. Perrin, in *Progress in Physical Organic Chemistry*, Vol. III, S. G. Cohen, A. Streitweiser, Jr., and R. W. Taft, eds., Interscience, New York (1965).
83. P. Zuman, in *Progress in Physical Organic Chemistry*, Vol. V, S. G. Cohen, A. Streitseiser, Jr., and R. W. Taft, eds., Interscience, New York (1967).
84. J. R. Backhurst, J. M. Coulson, R. E. Plimley, M. Fleischmann, and F. Goodridge, *J. Electrochem. Soc.* **116**, 1600 (1969); see also M. Fleischmann, J. W. Oldfield, and L. Pennakoon, *J. Appl. Electrochem.* **1**, 103 (1971); M. Fleischmann and J. W. Oldfield, *J. Electroanal. Chem.* **29**, 211 (1971); and G. Kreysa, S. Pioteck, and E. Heitz, *J. Appl. Electrochem.* **5**, 305 (1975).
85. I. G. Gurevich and V. S. Bagotzky, *Electrochim. Acta* **3**, 1151 (1964).
86. H. Wroblowa, *J. Electroanal. Chem.* **42**, 321, 329 (1973); **49**, 355 (1969); **69**, 299 (1976); see also R. E. Sioda, *J. Electroanal. Chem.* **34**, 411 (1972).
87. D. C. Walker, *Can. J. Chem.* **44**, 2226 (1966); **45**, 807 (1967); see also B. E. Conway and D. J. MacKinnon, *J. Phys. Chem.* **74**, 3663 (1970).
88. H. W. Sternberg, R. E. Markby, I. Wender, and D. M. Mohilner, *J. Am. Chem. Soc.* **89**, 187 (1967); see also T. Asahara, M. Seno, and K. Kaneko, *Bull. Chem. Soc. Jpn.* **41**, 2985 (1968).

89. M. Heyrovsky, *Proc. Roy. Soc. London Ser. A* **301**, 411 (1967).
90. O. R. Brown and J. A. Harrison, *J. Electroanal. Chem.* **21**, 387 (1969).
91. M. Shikata, *Trans. Faraday Soc.* **21**, 42, 53 (1925).
92. M. Shikata, *J. Agr. Chem. Soc. (Jpn)* **1**, 533 (1925).
93. J. B. Conant and M. F. Pratt, *J. Am. Chem. Soc.* **48**, 2468 (1926).
94. D. Ilkovic, *Collect. Czech. Chem. Commun.* **6**, 498 (1934).
95. S. G. Mairanovskii and M. B. Neiman, *Izv. Akad. Nauk. SSSR Otd. Khim. Nauk.*, No. 3, 420 (1955).
96. J. J. Lingane and B. A. Loveridge, *J. Am. Chem. Soc.* **66**, 1425 (1944); **68**, 395 (1946); **72**, 438 (1950).
97. P. Delahay, *J. Am. Chem. Soc.* **75**, 1430 (1953).
98. P. Kivalo, K. B. Oldham, and H. A. Laitinen, *J. Am. Chem. Soc.* **75**, 4148 (1953).
99. B. E. Conway, E. J. Rudd, and L. G. M. Gordon, *Discuss. Faraday Soc.* **45**, 87 (1968).
100. B. E. Conway, *Progress in Reaction Kinetics*, Vol. 4, G. Porter, ed., Pergamon Press, London (1967), p. 399.
101. R. S. Nicholson, *Anal. Chem.* **37**, 1351 (1965); **38**, 1406 (1966).
102. R. S. Nicholson and I. Shain, *Anal. Chem.* **36**, 706, 1212 (1964); **37**, 178, 190(1965).
103. M. L. Olmstead and R. S. Nicholson, *Anal. Chem.* **38**, 150 (1966).
104. J. M. Saveant and E. Vianello, *Electrochim. Acta* **12**, 629 (1967).
105. J. M. Saveant and E. Vianello, *Electrochim. Acta* **12**, 1545 (1967).
106. M. L. Olmstead, R. G. Hamilton, and R. S. Nicholson, *Anal. Chem.* **41**, 260 (1969).
107. S. G. Mairanovskii, *Catalytic and Kinetic Waves in Polarography*, (English trans.), Plenum Press, New York (1968).
108. R. Brdicka and K. Wiesner, *Naturwiss.* **31**, 247 (1943).
109. K. Wiesner, *Z. Elektrochem.* **49**, 164 (1943).
110. J. Kuta and I. Drabek, *Collect. Czech. Chem. Commun.* **20**, 902 (1955).
111. M. Stackelberg and H. Fassbender, *Z. Elektrochem.* **62**, 834 (1958); see also M. Stackelberg and H. W. Nurnberg, *Rev. Polarog. (Kyoto)* **6**, 27 (1958).
112. B. E. Conway, J. O'M. Bockris, and B. Lovrecek, *Proc. CITCE Meeting 1954*, Butterworths, London (1955), p. 207.
113. T. A. Kryukova, C. I. Sinyakova, and T. V. Aref'eva, *The Polarographic Method*, Goskhimizdat, Moscow (1959).
114. M. Stackelberg, in *Houben–Weyl: Methoden der organischen Chemie*, Vol. 3, 4th Ed., E. Mueller, ed., G. Theime, Stuttgart (1955).
115. J. Heyrovsky and D. Ilkovic, *Collect. Czech. Chem. Commun.* **7**, 198 (1935).
116. E. Barendrecht, in *Electroanalytical Chemistry*, Vol. 2, A. J. Bard, ed., Marcel Dekker, New York (1967).
117. M. Kalousek, *Collect. Czech. Chem. Commun.* **13**, 105 (1948).
118. L. A. Matheson and N. Nichols, *Trans. Am. Electrochem. Soc.* **73**, 193 (1938).
119. J. E. B. Randles, *Trans. Faraday Soc.* **44**, 322 (1948).
120. A. Sevcik, *Collect. Czech. Chem. Commun.* **13**, 349 (1948).
121. P. Delahay, *J. Am. Chem. Soc.* **75**, 1190 (1953).
122. L. I. Smith, I. M. Kolthoff, S. Wawzonek, and P. M. Ruoff, *J. Am. Chem. Soc.* **63**, 1018 (1941).
123. A. P. Tomilov and M. Y. Fioshin, *Chem. Rev. USSR* **32**, 30 (1963).
124. B. E. Conway, H. A. Kozlowska, B. MacDougall, and B. V. Tilak, in *Proc. 3rd Int. Cong. on Fuel Cells*, SERAI, Brussels (1969), p. 163.
125. S. Gilman, *J. Phys. Chem.* **66**, 2657 (1962); **67**, 78 (1963); **67**, 2898 (1963); **68**, 2098 (1964).
126. M. Heyrovsky and K. Micka, in *Electroanalytical Chemistry*, Vol. 2, A. J. Bard, ed., Marcel Dekker, New York (1967).
127. S. P. Perone and D. O. Jones, *Digital Computers in Scientific Instrumentation: Applications to Chemistry*, McGraw-Hill, New York (1973).

128. *Electrochemistry: Calculations, Simulation and Instrumentation*, J. S. Mattson, H. B. Mark, and H. C. MacDonald, eds., Marcel Dekker, New York (1972).
129. D. C. Grahame, *J. Am. Chem. Soc.* **63**, 1207 (1944).
130. B. Breyer and F. Gutmann, *Trans. Faraday Soc.* **42**, 645, 650 (1947); **43**, 785 (1947); see also *Discuss. Faraday Soc.* **1**, 19 (1947).
131. J. E. B. Randles, *Discuss. Faraday Soc.* **1**, 11, 47 (1947).
132. W. H. Reinmuth, *Anal. Chem.* **36**, 200R (1964).
133. D. N. Hume, *Anal. Chem.* **36**, 211R (1964).
134. B. Breyer and H. H. Bauer, in *Alternating Current Polarography and Tensammetry in Chemical Analysis*, Vol. 13, P. J. Elving and I. M. Kolthoff, eds., Wiley, New York (1963).
135. D. E. Smith, in *Electroanalytical Chemistry*, Vol. I, A. J. Bard, ed., Marcel Dekker, New York (1966).
136. B. Breyer and S. Hacobian, *Austr. J. Chem.* **9**, 7 (1956).
137. A. N. Frumkin and B. Damaskin, *J. Electroanal. Chem.* **3**, 36 (1962).
138. B. Breyer and S. Hacobian, *J. Electroanal. Chem.* **3**, 45 (1962).
139. C. A. Steuli and W. D. Cooke, *Anal. Chem.* **25**, 1691 (1953).
140. C. A. Streuli and W. D. Cooke, *J. Phys. Chem.* **57**, 824 (1967).
141. P. J. Elving, *Pure Appl. Chem.* **15**, 297 (1967).
142. P. Zuman, *The Elucidation of Organic Electrode Processes*, Academic Press, New York (1969).
143. J. Koutecky, *Collect. Czech. Chem. Commun.* **18**, 587 (1953).
144. P. Zuman, J. Chodkowski, and F. Santavy, *Collect Czech. Chem. Commun.* **26**, 380 (1961).
145. F. Micheel and E. Heiskel, *Chem. Ber.* **94**, 143 (1961).
146. J. M. Saveant, *C.R. Acad. Sci. Paris.* **257**, 448 (1963); **258**, 585 (1964).
147. P. Zuman and V. Horak, *Collect. Czech. Chem. Commun.* **26**, 176 (1961).
148. H. Lund, *Acta Chem. Scand.* **14**, 1927 (1960).
149. P. Zuman and S. Tang, *Collect. Czech. Chem. Commun.* **28**, 829 (1961).
150. V. Delaroff, M. Billa, and M. Legrand, *Bull. Soc. Chim. France*, 1912 (1961).
151. J. H. Brewster, *J. Am. Chem. Soc.* **76**, 6361 (1954).
152. J. H. Brewster, *J. Am. Chem. Soc.* **76**, 6364 (1954).
153. P. J. Elving and J. T. Leone, *J. Am. Chem. Soc.* **80**, 1021 (1958).
154. J. H. Stocker and R. M. Jenevein, *J. Org. Chem.* **33**, 294, 2145 (1968).
155. V. J. Puglisi, G. L. Clapper, and D. H. Evans, *Anal. Chem.* **41**, 279 (1969).
156. R. Annino, R. E. Erickson, J. Michalovic, and B. McKay, *J. Am. Chem. Soc.* **88**, 4424 (1966).
157. S. Wawzonek, R. C. Doty, and J. H. Wagenknecht, *J. Electrochem. Soc.* **111**, 74 (1964); see also G. Klopman, *Helv. Chim. Acta* **44**, 1908 (1961).
158. J. W. Seare, P. Chang, and J. L. Groth, *J. Am. Chem. Soc.* **86**, 3154 (1964).
159. S. Grabowski, *Discuss. Faraday Soc.* **46**, 145 (1968).
160. W. A. Bonner, J. A. Zderic, and G. A. Casaletto, *J. Am. Chem. Soc.* **74**, 5086 (1952).
161. K. Fukui, *Bull. Chem. Soc. Jpn.* **35**, 38 (1962); **36**, 217 (1963).
162. L. G. Feokistov, *Uspekhi Elektrokhimii Org. Soyedinening*, A. N. Frumkin and Y. V. Vasil'ev, eds., Izdat Nauka, Moscow (1966), p. 135.
163. R. A. Marcus, *Ann. Rev. Phys. Chem.* **15**, 155 (1964).
164. R. G. Barradas, P. G. Hamilton, and B. E. Conway, *J. Phys. Chem.* **69**, 3411 (1965).
165. B. E. Conway and L. G. M. Gordon, *J. Phys. Chem.* **73**, 3523, 3609 (1969).
166. P. J. Cram, *Fundamentals of Carbanion Chemistry*, Academic Press, New York (1965).
167. P. J. Elving and C. Teitelbaum, *J. Am. Chem. Soc.* **71**, 3916 (1949).
168. R. Gourley, J. Grimshaw, and P. Millar, *Chem. Commun.*, 1278 (1967).
169. H. Wroblowa, B. Piersma, and J. O'M. Bockris, *J. Electroanal. Chem.* **6**, 401 (1963).
170. A. T. Kuhn, H. Wroblowa, and J. O'M. Bockris, *Trans. Faraday Soc.* **63**, 1458 (1967).
171. S. Shibata and M. P. Sumino, *Electrochim. Acta* **20**, 739 (1975).
172. S. Shibata, *J. Electroanal. Chem.* **89**, 37 (1978).
173. M. W. Breiter, *J. Electrochem. Soc.* **109**, 425 (1962).

174. S. Gilman, *J. Phys. Chem.* **67**, 1898 (1963); **68**, 70 (1964).
175. V. S. Bagotzky and Y. B. Vassilyev, *Electrochim. Acta* **11**, 1439 (1966).
176. B. E. Conway, H. Angerstein-Kozlowska, and G. Czartoryska, *Z. Phys. Chem. N.F.* **112**, 195 (1978).
177. B. E. Conway and H. Angerstein-Kozlowska, *Acc. Chem. Res.* **14**, 49 (1981).
178. A. Rius, J. Llopis, and M. C. Servet, *An. Real. Soc. Espan. Fiz. Quim.* **49**, 447 (1953); **52B**, 601 (1956).
179. S. Terabe and R. Konaka, *J. Chem. Soc. Perkin Trans.* **2**, 2163 (1972).
180. M. Fleischmann, K. Korinek, and D. Pletcher, *J. Electroanal. Chem.* **31**, 39 (1971).
181. Y. Matushima, *J. Chem. Soc. Jpn.* **69**, 159 (1948).
182. A. Sa, *Rev. Centrol Estud. Farm. Biquim.* **27**, 19, 48 (1937).
183. J. M. Dunoyer, *C.R. Acad. Sci. Paris* **214**, 556 (1942).
184. J. Racine, *C.R. Acad. Sci. Paris* **220**, 823 (1945).
185. S. Kitahara and T. Ohsuga, *J. Electrochem. Assoc. Jpn.* **10**, 409 (1942); *J. Electrochem. Soc. Jpn.* **10**, 409 (1940).
186. J. Mitzuguchi and S. Matsumoto, *J. Pharm. Soc. Jpn.* **71**, 737 (1951).
187. T. Sekine and K. Sugino, *J. Electrochem. Soc.* **115**, 242 (1968).
188. German Pat. No. 865,740 (1953); *C.A.* **53**, 292 (1959).
189. British Pat. No. 766, 578 (1957); *C.A.* **51**, 10278 (1957).
190. H. Elbs and S. Brunner, *Z. Elektrochem.* **6**, 604 (1900).
191. K. Chida and T. Sekine, *Denki Kagaku* (*Japan*) **38**, 130 (1970).
192. J. Labhard and K. Zschoche, *Z. Elektrochem.* **8**, 93 (1902).
193. D. Sacho and O. Kempf, *Ber. Bunsenges. Phys. Chem.* **35**, 2704 (1902).
194. H. Elbs, *Z. Elektrochem.* **2**, 552 (1896).
195. C. Merzbacher and M. Smith, *J. Am. Chem. Soc.* **22**, 223 (1900).
196. H. D. Law and F. M. Perkin, *Chem. News* **91**, 54 (1905); **92**, 69 (1905).
197. K. Michler and J. Pattison, *Ber. Bunsenges. Phys. Chem.* **14**, 2163 (1891).
198. F. Fichter and K. Brizard, *Helv. Chim. Acta* **4**, 928 (1921).
199. G. Vertes, G. Horanyi, and F. Nagy, *Acta Chim. Acad. Sci. Hungary* **67**, 145 (1971).
200. G. Vertes and G. Horanyi, *Acta Chim. Acad. Sci. Hungary* **68**, 217 (1971).
201. G. Horanyi, G. Vertes, and F. Nagy, *Acta Chim. Acad. Sci. Hungary* **67**, 357 (1971).
202. I. A. Avrutskaya, M. Y. Fioshin, and T. E. Mulina, *Elektrokhimiya* **9**, 897 (1973).
203. M. Fleischmann, K. Korinek, and D. Pletcher, *J. Electroanal. Chem.* **33**, 478 (1971).
204. M. Fleischmann, K. Korinek, and D. Pletcher, *J. Chem. Soc., Perkin Trans. II*, 1396 (1972).
205. B. E. Conway and P. L. Bourgault, *Can. J. Chem.* **38**, 1557 (1960); **40**, 1690 (1962).
206. B. E. Conway and P. L. Bourgault, *Trans. Faraday Soc.* **58**, 693 (1962).
207. M. V. George and K. S. Balachandran, *Chem. Rev.* **35**, 491 (1975).
208. M. Fleischmann, K. Korinek, and D. Pletcher, *J. Electroanal. Chem.* **34**, 499 (1972).
209. W. F. Pickering, *Rev. Pure Appl. Chem.* **16**, 185 (1966).
210. B. E. Conway and M. A. Sattar, *Electrochim. Acta* **14**, 695 (1969).
211. R. Konaka, S. Terabe, and K. Kuruma, *J. Org. Chem.* **34**, 1334 (1969).
212. S. Terabe, K. Kuruma, and R. Konaka, *Chem. Lett.* **115** (1972).
213. A. Crum-Brown and A. Walker, *Ann.* **261**, 107 (1891).
214. H. Hofer and M. Moest, *Ann.* **323**, 285 (1902).
210. Y. M. Tyurin and G. F. Volodin, *Elektrokhimiya* **6**, 1186 (1970).
211. Y. M. Tyurin, G. F. Volodin, L. A. Smirnova, and Y. B. Battalova, *Elektrokhimiya* **9**, 532 (1973).
212. L. A. Mirkind and M. Y. Fioshin, *Dokl. Akad. Nauk. SSSR* **154**, 1163 (1964).
213. L. M. Mirkind, M. Y. Fioshin, and D. Constantinescu, *Elektrokhimiya* **2**, 1085 (1966).
214. Y. M. Tyurin, G. F. Volodin, Y. V. Battalova, and L. A. Smirnova, V, 8b, XI Mendeleevsk S'ezd po Obshch, i Prikl Khimii. Ref. Dokl. i Soobshch 1975 (3) 282; *C.A.* **84**, 171, 429 (1976).

215. V. E. Kazarinov, A. G. Dubinin, L. A. Mirkind, and Y. A. Fioshin, in *The Double Layer Adsorption on Solid Electrodes*, Vol. 3, Tartu, (1972), p. 123.
216. V. L. Naumov, L. A. Smirnova, G. N. Afonshin, and Y. M. Tyurin, *Elektrokhimiya* **7**, 1872 (1971).
217. V. I. Naumov and Y. M. Tyurin, *Elektrokhimiya* **8**, 1228 (1972).
218. V. I. Naumov and Y. M. Tyruin, *Elektrokhimiya* **9**, 427 (1973).
219. L. A. Mirind and Y. M. Tyurin, *Coll. Electrosynthesis and Organic Reaction Mechanisms*, Nauka, Moscow (1973), p. 181.
220. Y. M. Tyurin, G. F. Volodin, and V. S. Paducheva, *Elektrokhimiya* **7**, 1309 (1971).
221. Y. M. Tyurin, V. I. Naumov, V. N. Flerov, and Y. V. Battalova, *Elektrokhimiya* **10**, 1119 (1974).
222. J. O'M. Bockris, H. Wroblowa, E. Gileadi, and B. J. Piersma, *Trans. Farday Soc.* **61**, 2531 (1965).
223. J. W. Johnson, S. C. Lai, and W. J. James, *Electrochim. Acta* **16**, 1763 (1971).
224. H. Wroblowa, B. J. Piersma, and J. O'M. Bockris, *J. Electroanal. Chem.* **6**, 401 (1963).
225. T. N. Hartley and D. Price, *J. Electrochem. Soc.* **117**, 448 (1970).
226. R. Thacker and D. D. Bump, *Electrochem. Technol.* **3**, 9 (1965).
227. C. Cwiklinski and J. Perichon, *Electrochim. Acta* **19**, 297 (1974).
228. S. Brummer, J. Ford, and M. Turner, *J. Phys. Chem.* **69**, 3424 (1965); **71**, 2825, 3494, 3902 (1967).
229. H. Dahms and J. O'M. Bockris, *J. Electrochem. Soc.* **111**, 728 (1964).
230. A. T. Kuhn, H. Wroblowa, and J. O'M. Bockris, *Trans. Faraday Soc.* **63**, 1458 (1967).
231. M. Fleischmann and D. Pletcher, *Tetrahedron Lett.* **60**, 6255 (1968).
232. D. B. Clark, M Fleischmann, and D. Pletcher, *J. Chem. Soc. Perkin Trans. 2*, 1578 (1973).
233. J. Bertram, M. Fleischmann, and D. Pletcher, *Tetrahedron Lett.* **4**, 349 (1971).
234. J. Bertram, J. P. Coleman, M. Fleischmann, and D. Pletcher, *J. Chem. Soc. Perkin Trans. 2*, 374 (1973).
235. C. Pitti, F. Bibilliart, A. Thiebault, and M. Herlem, *Anal. Lett.* **8**, 241 (1975).
236. T. Shono and A. Ikeda, *J. Am. Chem. Soc.* **94**, 7892 (1972).
237. M. Fleischmann and D. Pletcher, *Chem.-Ing.-Techn.* **44**, 187 (1972).
238. L. Formaro, G. Fioro, and M. Colombi, *J. Electroanal. Chem.* **44**, 255 (1973).
239. M. Katz, O. E. Saygin, and H. Wendt, *Electrochim. Acta* **19**, 193 (1974).
240. W. C. Neikam, G. R. Dimeler, and M. M. Desmond, *J. Electrochem. Soc.* **111**, 1190 (1964).
241. D. B. Clark, M. Fleischmann, and D. Pletcher, *J. Electroanal. Chem.* **42**, 133 (1973).
242. H. Schafer and E. Steckhan, *Chem.-Ing.-Techn.* **44**, 186 (1972); *Angew. Chem. Int. Ed.* **8**, 518 (1969).
243. H. Lund, Acta Chem. Scand. **11**, 1323 (1957).
244. L. Eberson and K. Nyberg, *J. Am. Chem. Soc.* **88**, 1686 (1966).
245. M. E. Peover and B. S. White, *J. Electroanal. Chem.* **13**, 93 (1967).
246. K. K. Barnes and C. K. Mann, *J. Org. Chem.* **32**, 1322 (1967).
247. C. K. Mann and K. K. Barnes, *Electrochemical Reactions in Non-Aqueous Systems*, Marcel Dekker, New York (1970), Chap. 3.
248. G. J. Hoijtink, *Rec. Trav. Chim. Pays-Bax* **77**, 555 (1958).
249. J. W. Loveland and G. R. Dimeler, *Anal. Chem.* **33**, 1196 (1961).
250. E. S. Pysh and N. C. Yang, *J. Am. Chem. Soc.* **85**, 2124 (1963).
251. J. Phelps, K. S. V. Santhaman, and A. J. Bard, *J. Am. Chem. Soc.* **89**, 1752 (1967).
252. R. E. Sioda and W. S. Koski, *J. Am. Chem. Soc.* **87**, 5573 (1965).
253. L. S. Marcoux, J. M. Fritsch, and R. N. Adams, *J. Am. Chem. Soc.* **89**, 5766 (1967).
254. S. Andreades and E. W. Zahnow, *J. Am. Chem. Soc.* **91**, 4121 (1969).
255. A. Zweig, W. H. Hodgson, and W. H. Jura, *J. Am. Chem. Soc.* **86**, 4124 (1964).
256. G. Klopman, *J. Am. Chem. Soc.* **90**, 223 (1968).
257. L. Herk, M. Feld, and M. Szwarc, *J. Am. Chem. Soc.* **83**, 2998 (1961).
258. L. Eberson, *J. Am. Chem. Soc.* **89**, 4669 (1967).

259. C. Magnusson, B. Olofsson, and K. Nyberg, *Chemi. Scripta* **1**, 57 (1971).
260. L. Eberson and K. Nyberg, *Tetrahedron Lett.* 2389 (1966).
261. L. Eberson and B. Olofsson, *Acta Chem. Scand.* **23**, 2355 (1969).
262. V. D. Parker and B. E. Burgert, *Tetrahedron Lett.* 2411 (1968).
263. N. L. Weinberg, in *Technique of Electroorganic Synthesis*, N. L. Weinberg, ed., Part I, Wiley Interscience, New York (1974), Chap. IV.
264. K. Nyberg, in *Encyclopedia of Electrochemistry of the Elements*, Vol. XI, A. J. Bard and H. Lund, eds., Marcel Dekker, New York (1978).
265. J. Perichon, in "Encyclopedia of Electrochemistry of the Elements", Vol. XI, A. J. Bard and H. Lund, eds, Marcel Dekker, New York (1978).
266. O. R. Brown and J. A. Harrison, *J. Electroanal. Chem.* **21**, 387 (1969).
267. F. D. Popp and H. P. Schultz, *Chem. Rev.* **62**, 19 (1962).
268. A. J. Fry, *Fortsch. Chem. Forsch.* **34**, 1 (1972).
269. L. Eberson and L. Horner, in *Organic Electrochemistry*, M. M. Baizer, ed., Marcel Dekker, New York (1973).
270. M. M. Baizer and J. P. Petrovich, in *Progress in Physical Organic Chemistry*, Vol. 7, A. Streitweiser, ed., Wiley, New York (1970).
271. T. Sekine, A. Yamura, and K. Sugino, *J. Electrochem. Soc.* **112**, 439 (1965).
272. V. A. Smirnov, L. I. Antropov, M. G. Smirnova, and L. A. Dimchuk, *Zh. Fiz. Khim.* **42**, 1713 (1968).
273. J. H. Stocker and R. M. Jenevein, *J. Org. Chem.* **33**, 294, 2415 (1968); **34**, 2807 (1969).
274. L. Nadjo and J. M. Saveant, *J. Electroanal. Chem.* **33**, 419 (1971).
275. E. Laviron, *Collect. Czech. Chem. Commun.* **30**, 4219 (1965).
276. B. E. Conway, E. J. Rudd, and L. G. M. Gordon, *Discuss. Faraday Soc.* **45**, 87 (1968).
277. E. J. Rudd and B. E. Conway, *Trans. Faraday Soc.* **67**, 440 (1971).
278. M. P. J. Brennan and O. R. Brown, *J. Chem. Soc., Faraday Trans. 1*, **69**, 132 (1973).
279. B. E. Conway and E. J. Rudd, *Techniques of Electroorganic Chemistry*, N. Weinberg, ed., Part I, Wiley Interscience, New York (1974), Chap. III.
280. W. Kemula and T. M. Krygowski, *Encyclopedia of Electrochemistry of the Elements*, Vol. XIII, A. J. Bard and H. Lund, eds., Marcel Dekker, New York (1979), Chap. 2.
281. F. Petru, *Collect. Czech. Chem. Commun.* **12**, 620 (1947).
282. M. Suzuki and P. J. Elving, *Collect. Czech. Chem. Commun.* **25**, 3502 (1960).
283. S. Wawzonek and Tsung-Yuan Su, *J. Electrochem. Soc.* **100**, 745 (1973).
284. H. Lund, *Organic Electrochemistry*, M. M. Baizer, ed., Marcel Dekker, New York (1973), Chap. VII.
285. H. Sayo, Y. Tsukitani, and M. Masui, *Tetrahedron* **24**, 1717 (1968).
286. H. Sayo and M. Masui, *Tetrahedron* **24**, 5075 (1968).
287. M. W. Leeds and G. B. Smith, *J. Electrochem. Soc.* **98**, 129 (1951).
288. W. Lob, *Ber. Bunsenges. Phys. Chem.* **29**, 1896 (1896).
289. K. Elbs and F. Silberman, *Z. Elektrochem.* **7**, 590 (1902).
290. L. Holleck, B. Kastening, and R. D. Williams, *Z. Elektrochem.* **66**, 396 (1962).
291. B. Kastening, H. Gastmann, and L. Holleck, *Electrochim. Acta* **9**, 741 (1964).
292. A. C. Brown and J. Walker, *Justus Liebigs Ann. Chem.* **261**, 107 (1891).
293. H. Hofer and M. Moest, *Justus Liebigs Ann. Chem.* **323**, 285 (1902).
294. T. Dickinson and W. F. K. Wynne-Jones, *Trans. Faraday Soc.* **58**, 382 (1962).
295. B. E. Conway and M. Dzieciuch, *Can. J. Chem.* **41**, 38 (1963); *see also Proc. Chem. Soc. London*, 121 (1962).
296. M. Fleischmann, J. R. Mansfield, and W. F. K. Wynne-Jones, *J. Electroanal. Chem.* **10**, 511, 522 (1965).
297. K. S. Kim, N. Winograd, and R. E. Davis, *J. Am. Chem. Soc.* **93**, 6296 (1971).
298. J. M. Cesbron, R. Courtel, J. E. DuBois, M. Herlem, and P. C. Lacaze, *C.R. Acad. Sci. Paris (C)* **266**, 1667 (1968).

299. J. E. DuBois, P. Comille, and F. Bruno, *C.R. Acad. Sci. Paris* (*C*) **271**, 791 (1970).
300. L. Eberson, *Chemistry of the Carboxylic Acids and Esters*, S. Patai, ed., Wiley Interscience, London (1969), Chap. 2.
301. W. B. Smith and H. Gilde, *J. Am. Chem. Soc.* **82**, 659 (1960).
302. W. B. Smith and D. T. Manning, *J. Polym. Sci.* **59**, 545 (1962).
303. L. Eberson, *Electrochim. Acta* **12**, 1473 (1967).
304. J. P. Utley, in *Technique of Electroorganic Chemistry*, N. Weinberg, ed., Part I, Wiley Interscience, New York (1974), Chap. IV.
305. T. Okubo and S. Tsutsumi, *Bull. Soc. Chem. Jpn.* **37**, 1794 (1964).
306. T. Okubo and S. Tsutsumi, *Nippon Kagaku Zasshi* **87**, 449 (1966).
307. C. T. Bahner, U.S. Patent No. 2,485,803 (1949).
308. C. T. Bahner, *Ind. Eng. Chem.* **44**, 317 (1952).
309. C. Walling and E. S. Huyser, in *Organic Reactions*, Vol. 13, A. C. Cope, ed., John Wiley and Sons, New York (1963), p. 91.
310. A. J. Lebedeva, *Dokl. Akad. Nauk SSSR* **42**, 71 (1944).
311. N. Bunge, *Chem. Ber.* **3**, 295, 911 (1870).
312. J. L. Morgat and R. Palland, *C.R. Acad. Sci. Paris* (*C*) **260**, 5579 (1965).
313. C. M. Wright, R. F. Heck, and W. Yokoyama, Extended Abstracts, Meeting of Electrochemical Society, May 1969.
314. F. Beck and H. Guthke, *Chem. Ing-Tech.* **41**, 943 (1969).
315. M. M. Baizer and J. D. Anderson, *J. Electrochem. Soc.* **111**, 223 (1964).
316. E. Touboul, F. Weisbuch, and J. Weimann, *C.R. Ser. C* **268**, 1170 (1969).
317. J. D. Anderson, M. M. Baizer, and J. P. Petrovich, *J. Org. Chem.* **31**, 3890 (1966).
318. J. D. Anderson and M. M. Baizer, *Tetrahedron Lett.* 511 (1966).
319. J. D. Anderson and M. M. Baizer, *J. Org. Chem.* **31**, 3897 (1966).
320. B. L. Funt and J. Tanner, in *Technique of Electroorganic Chemistry*, N. Weinberg, ed., Wiley Interscience, New York (1975), Part II, Chap. XI.
321. M. Rifi and F. H. Covitz, *Introduction to Organic Electrochemistry*, Marcel Dekker, New York (1974), Chap. 6.
322. M. Rifi and F. H. Covitz, *Introduction to Organic Electrochemistry*, Marcel Dekker, New York (1974), Chap. 7.
323. J. A. Epstein and A. Bar-nun, *J. Polym. Sci. Part B* **2**, 27 (1964).
324. W. R. Grace and Co., *Brit. Pat. No.* 1,156,309 (1968).
325. B. L. Funt, S. N. Bhadani, and D. Richardson, *J. Polym. Sci.* (*A-1*) **4**, 2871 (1966).
326. B. L. Funt and D. R. Richardson, *J. Polym. Sci. Polym. Chem. Ed.* **8**, 1055 (1970).
327. N. L. Weinberg, in *Techniques of Electroorganic Synthesis*, N. L. Weinberg, ed., Wiley Interscience, New York (1974), Part I, Chap. 1.
328. F. Goodridge, *Chem. Process Eng.* **49**, 93 (1968).
329. R. B. MacMullin, *Electrochem. Tech.* **2**, 106 (1964).
330. F. Beck, *Chem.-Ing.-Tech.* **42**, 153 (1970).
331. M. M. Baizer, Armstrong Lecture, 1979, Part I, Chem. and Ind., London, 435 (1979).
332. D. E. Danly, Armstrong Lecture, 1979, Part II, Chem. and Ind., London, 439 (1979).
333. M. M. Baizer, *J. Appl. Electrochem.* **10**, 285 (1980).
334. Electrochemical Technology Corp., Final Report on a Survey of Organic Electrolytic Processes, ANL-OETM-79-5. Prepared for the office of Electrochemical Project Management, Argonne National Laboratories, under Contract No. 31-109-38-4209 (1979).
335. W. Himmele, N. Kutepow, and W. Schwab, Ger. Pat. No. 1,162,347 (1964); see also F. Beck, H. Nohe, and J. Haufe, Ger. Pat. No. 2,014,985 (1971), and N. T. Kobzeva, *Sov. Electrochem.* **11**, 667 (1975).
336. W. J. Koehl, Jr., U.S. Pat. No. 3,252,876 (1966).
337. N. Clauson-Kaas, F. Limborg, and K. Glens, *Acta Chem. Scand.* **6**, 531 (1952); see also U.S. Pat. No. 2,714,576 (1955).

338. B. B. Dey and R. K. Maller, *J. Sci. Ind. Res.* (*India*) **12B**, 255 (1953).
339. J. P. Millington, *Chem. Ind.* (*London*) 780 (1975); U.K. Electricity Council, Brit. Pat. No. 1,377,681 (1974).
340. C. J. Thatcher, Can. Pat. No. 222,264 (1922).
341. S. Krishan, V. A. Vyas, M. S. V. Pathy, and H. V. K. Udupa, *J. Electrochem. Soc. India* **14**, 32 (1964).
342. N. Niki, T. Sekine, and K. Sugino, *J. Electrochem. Soc. Japan* **37**, 74 (1969).
343. L. Bott, *Hydrocarbon Proc.* **44**, 115 (1965).
344. D. G. Braithwaite, U.S. Pat. Nos. 3,256,161 (1966), 3,391,066 and 3,391,067 (1968).
345. M. M. Baizer, *J. Electrochem. Soc.* **111**, 215 (1964); U.S. Pat. Nos. 3,193,480 and 3,193,481 (1965), 3,440,154 (1969).
346. N. Shuster, K. J. O'Leary, and A. D. Babinsky, Extended Abstracts, 76–1, 694, Electrochemical Society Meeting, Washington, D.C., May 1976.
347. H. Nohe and F. Beck, *Ger. Pat. No.* 2,343,054 (1975).
348. H. C. Rance and J. M. Coulson, *Electrochim. Acta* **14**, 283 (1969).
349. T. D. B. Lakrishnan *et al.*, *Chem.-Ing.-Tech.* **41**, 776 (1969).
350. U.S. Army Technical Translation, FSTC-HT-23-258-68; Industrial Electrosynthesis of Organic Compounds, M. Y. Fioshin and A. P. Tomilov (1966); see also T. D. Balakrishnan *et al.*, *Chem. Ind.* (*London*), 1(22) (1970).
351. W. H. Perkin and S. G. Plant, *J. Chem. Soc.* (*London*) **125**, 1503 (1924).
352. M. Lukes, *Chem. Listy* **27**, 392 (1933).
353. Robinson Bros. and D. W. Parkes, *Brit. Pat. No.* 395,741 (1933).

Index

Ackerman and Moor, spectroscopic contributions, 51
Activation controlled limiting current, formulated by Despić and Bockris, 470
Activation energies
  and their detection, 120
  ideal, 110
  real, 110
  true and apparent, 101
  of various electrode reactions, 94, 157
Activationless processes, 116
Activity coefficient, in electrode reactions, 108
Adatoms, 400
  and mean displacement, 403
Additives, in the hydrogen evolution reaction, 281
Adiabaticity, 76
Adiabatic reactions, theory of, 24
Adiabatic transfers, 3
Adion concentration, in surface diffusion, 406
Adion distribution between surface planes, 407
Adions, introduced by Conway and Bockris, 403
Adsorbed films and oxides, studied by ellipsommetry, 336
Adsorbed oxygen molecules, and reduction schemes, of Wroblowa, 357
Adsorbed species, on platinum, 328
Adsorption coefficient, on platinum, studied by McIntyre and Kolb, 338
Adsorption energy, and electrode kinetics, 101
Adsorption equilibrium, and electrode reactions, 130
Adsorption isotherm, for atomic hydrogen, 244
Adsorption and rate-determining step, formulated, 195
Adsorption theory
  and kinetic approach to oxygen adsorption, 323
  for oxygen reactions, of Biegler and Woods, 323
Adsorption of water molecules, and hydrogen overpotential, 152
Advancing front, in metal deposition, 416
Affinity, and rate determining steps, 266
Affinity distribution
  and absence of rate determining step, 264
  as function of total overpotential, 276
Agar, and temperature dependence of electrode reactions, 111
Alloys
  mechanism of deposition, 451
  their reversible potentials, analyzed by Damjanovic, 456
Angerstein–Kozlowska, and adsorbed oxygen species, 317
Anion effects, on hydrogen reaction rate, 249
Anions, reduction of, 155
  and work of Krylov, 163
Anodic layers of platinum, originally investigated by Bockris, 323
Antropov, potential of zero-charge effects in organic reactions, 166
Appleby, Fleisch, and Savy, rotating disk electrode techniques on macrocycles, 384
Appleby
  and adsorption theory of oxide layers on platinum, 318

Appleby (*cont.*)
  and complicated dependences between kinetic parameters and specific properties of electrodes, 343
  and linear sweep voltammograms, 317
  and oxygen reduction reaction, 343
  and structural effects, 291
Applicability, of Bornian theory, examined, 44
Applied potential, and free energy of reaction, 186
Armstrong and Harrison, mechanism of multilayer deposition, 420
Arrhenius plots, work of Schultze and Vetter, 348
Arvia and Folgner, and history of electrochemistry, 326
Arvia and Giordano, monograph on electrocatalysis, 32
Atom incorporation, and metal deposition, 400
Audubert, and zero activation energy, 116
Auger spectroscopy
  and films in electrode kinetics, 217
  and investigation of platinum surfaces, 340
Avrami formulation, 419

Bagotski
  and charge remaining on adsorbed species on repulsion, 323
  and currents as a function of crystal structure, 291
  and the disk-ring plots, as function of reaction rate, 357
  and a general formulation of oxygen reduction, 354
  and oxygen reduction reactions with parallel steps, 356
Balandin, volcano relationship, 98
Barker, and faradaic rectification, 468
Barrett and Parsons, studies of platinum films, 338
Barrier, for photo emission and metal-electrode surface, 65
Barrier height, estimated by Sen and Bockris, 57
Barrierless conditions, 126
Barrierless discharge, originated by Despić and Bockris, 470
Barrierless processes, 116, 122
  and activation of energy, 119
Bates, his criticism of Landau–Zener, 78
Beck, and investigation of hydrogenation, 288
Becker and Döring, and nucleation, 436
Bell-shaped diagrams, invalid for distribution of electron states in solution, 75
Bewick and Tuxford, ac modulation reflectance for platinum films, 339
Biegler and Woods, adsorption theory for oxygen reactions, 323
Blocking material, and electrocatalysis, 203
Bockris group, its work on iridium, 351
Bockris and coworkers, and open circuit potentials involving oxygen, 306
Bockris and Damjanovic, and diagnostic criteria from the disk-ring data, 354
Bockris and Enyo, rate determining step in copper deposition, 471
Bockris and Huq
  first establishment of the reversible oxygen potential, 307
  intensive purification of solution, 307
Bockris and Khan
  agreement of George and Griffith theory with experiment, 43
  and transition probability, 47
Bockris, Khan, and Matthews, experimental free energy of activation and continuum theory, 43
Bockris and Kita, mechanism of copper deposition, 471
Bockris and Koch
  hydrogen evolution on iron, 226
  stoichiometric number, 226
Bockris and Matthews
  use of Eckart barrier, 54
  and quantum character of proton, 52
Bockris and Mauser, their formulation of the kinetics of hydrogen evolution, 191
Bockris and Potter
  and the potential of zero charge in electrocatalysis, 184
  role of the substrate in electrode reactions, 174
Bockris and Sen
  and fluctuation theory, 42
  and water bond, 213
Bockris and Subramanyan, pressure of hydrogen in metal, 283
Bockris and Uosaki, theory of photoelectrochemical kinetics,
  quantum mechanical, 62
Bockris
  and adiabaticity, 213
  basic theory of electrode kinetics, 1
  and coupled reactions, 264

Bockris (*cont.*)
  and the disk-ring criterion for hydrogen peroxide formation, 354
  and first work on tungsten bronzes, 376
  impurity effects on oxygen evolution, 308
  and initial investigations of anodic layers of platinum, 323
  and kinetic data on oxygen evolution, 342
  relationship between rate and work function, 181
  and surface conductivity, 339
  and volcano plots, 224
Bohr condition, compared with that of Gurney, 49
Bold and Breither, expansion of the surface layer, 335
Boltzmannian or Gaussian?, 74
Bond energies, and crystal growth, 437
Bonding, at electrodes, and electrode kinetic formulations, 101
Bonhoeffer, his pointing out of a parallelism between hydrogen overpotential and catalytic reaction rates, 241
Born contribution, small, in electrode kinetics, 43
Bornian theories
  and Tafel plots, comprehensive comparison, 45
  tested, 44
Born–Oppenheimer, 25
Bostanow
  and peripheral steps in metal deposition, 414
  and the 111 face, 415
  and steepness of the advancing front, in metal deposition, 416
Bowden and Rideal, their well-known 1928 paper, 173
Bowden, and oxygen evolution on platinum, 348
Brandes, and nucleation processes, 409
Breitner, and pre-exponential plots, 225
Brodskii and Gurevich, quantum theory of photon emission, 61
Bronsted–Polanyi relation, 93
Buckley and Burke
  charge capacity of surface oxides, 334
  their work for oxygen evolution on iridium, 350
Budewski
  and the calculation of spirals, 425
  and crystal lattice formation, 453
  two dimensional nucleation, 412
Burton, Caberra, and Frank
  and metal deposition, 408
  and the spiral growth mechanism, 425
Butler model, for charge transfer, 207
Butler's theory, 51
Butler–Volmer relation, 467

Cabrerra–Mott mechanisms on platinum, 325
Cabrerra–Mott model, proposed by Damjanovic, 325
Cahan, and surface conductivity measurements showing adsorption, 339
Carbon, 363
  and oxygen reduction, 363
Carbon materials, and oxygen reduction thereon, 377
Catalysis and electrocatalysis, 177
Catalysts, nonmetallic, 376
Catalytic activity
  examined by Collman, Anson, and others, 388
  and metal cobaltites, 376
Central metal ion, 380
Chain processes, and electrocatalysis, 180
Charge, along reaction coordinates, in electrocatalysis, 181
Charge transfer kinetics, at high overpotentials, 469
Chlorine evolution, in work of Novak, Tilak, and Conway, 234
Chlorine reactions
  kinetics of, 124
  and rate determining step, 125
Christov
  and linearity of Tafel lines, 46
  and part played by harmonic oscillator, 46
  thermal theory of electrode kinetics, 1
Clamroth and Knorr, and decay of hydrogen overpotential, 271
Classical rates, for electron transfer, 53
Clusius and Hinshelwood, intermediates in catalytic reactions, 179
Cobalt Porphyrins, coming "face-to-face", 233
Colman, Anson, and others, face-to-face situation in porphyrins, 388
Compensation effect, 225
  in oxygen electrode reactions, 230
Complex processes, rate solved, 190
Complex reactions, and Bockris and Mauser, 191
Complexes in solutions, as function of concentration, for zinc, 464

Complexing interactions, and reversible potentials, 462
Complexity, as a theme in electrode kinetics, 196
Continuity approach, metal deposition, 441
Continuum, in vibrational levels in solutions, 51
Continuum solvent coordinate, considered by Ovchinnikov and Benderskii, 60
Continuum theory
  inconsistencies, 46
  tested by calculation, 43
Conway and Bockris
  and adions, 403
  and electrocatalysis, 174
  and the equilibrium step in hydrogen evolution, 221
  and the first fitting of volcano plots in electrochemistry, 205
  first relations of electrode kinetics to calculated heats of adsorption, 223
  heats of adsorption versus overpotential, 223
  and hydration energy for surface atoms, 403
  relation to heat of adsorption in electrode kinetics, 106
  and two kinds of reactions in volcano plots, 224
Conway and Curry, electrode kinetics as a function of pressure, and inner shell, 43
Conway and Gottesfeld, study of anodic layers by reflectance measurements, 39
Conway and Novak, and the chlorine evolution reaction, 234
Conway
  and computer simulation of linear sweep voltammograms, 317
  and irreversibility of formation of anodic layers on platinum, 315
  and kinetic equations used in two-step oxygen adsorption reactions, 318
  and solvated electrons, 105
  and sweep voltammetry for oxygen deposition on platinum, 316
  and voltage sweeps of oxygen reactions, 317
Copper deposition, 471
Correlations
  in electrocatalysis, 204
  between George and Griffith theory and stretching constants, 43
Coverage, effects on electrode kinetics, 100
  in electrode reactions, and volcano plots, 216
  its effects upon electrocatalysis, 201
  low, in hydrogen evolution reactions, 257
Criteria, of rate determining step, 193
Crystalline surfaces, and metal deposition, 400
Crystals
  their form of growth, 433
  and size in crystal growth, 439
Current density, to stepped crystal faces, 408
Current-overpotential relationship, and nucleation, 412
Current-overpotential relationships in metal deposition on perfect crystal faces, 414
Current-potential profiles, for platinum single crystals, 249
Current-time transients, in multi-layer deposition, 421, 422

d-character, and hydrogen evolution, 290
Davydov, on poloron theory, 2
Damjanovic and Bockris, and treatment of set crystal planes, 408
Damjanovic, Genshaw and Bockris, their criterion for oxygen reduction using disk ring, 354
Damjanovic and Brusic, rate determining step in oxygen reduction reaction, 231
Damjanovic and Jovanovic
  and mechanism of oxygen evolution reaction on platinum, 347
  parameters in oxygen evolution reaction, 344
  reaction orders less than one, 346
  their unconventional explanation, 348
Damjanovic
  discrepancy of results with those of Bockris and Huq, 346
  and the disk ring criterion for oxygen reduction, 354
  and disk-ring plots as function of rotation rate, 357
  his evaluation of the electrochemical oxide part on iridium, 351
  and field-enhanced oxide growth, 326
  irreversibility of oxide formation, 325
  and kinetic equations for evidencing Cabrerra–Mott mechanisms, 325
  and the mechanism of oxygen evolution, 345
  and the model of oxygen buildup, 324
  oxide formation is uniform, 330
  and oxygen evolution reaction, 330
  and oxygen reduction, 369
  his parameters for oxygen evolution, 344
  and phase oxides, 324
  his review on oxygen evolution reaction, 342

Damjanovic (*cont.*)
  and the slow desorption of hydrogen peroxide, 358
Decoupling in, 18
Delahay and Ruetschi, relations to heat of adsorption in electrode kinetics, 106
Delahay
  corrected Tafel slopes, 156
  his monograph, 140
  Tafel plots for gallium ion reduction, 163
Density matrix, for calculations at electrodes, 14
Deposition, multi-layer, 420
Deposition of metal, 451
Desorption of hydrogen, step of, 31
Despić and Bockris
  their formulation of activation controlled limiting current, 470
  their treatment of surface diffusion, 405
  and treatment of certain crystal planes, 408

Di-electric constant optical, experiments to test Bornian theories, 43
Diffusion of atoms into metals, hypothesis tested by Bagotskii, 310
Direct transfer mechanisms, 415
Discharge, of metal ions, kinetic consequences, 466
Discharge step, model for in proton transfer, 58
Disk mutation-desorption step, in oxygen reduction, 380
Disk ring
  analysis of oxygen reduction, 354
  criteria of reaction mechanisms, evaluated by Damjanovic and Bockris, 354
Disk-ring method, proposed by Frumkin and Nekrasov, 353
Disk-ring plots as function of reaction rate, and oxygen reduction, 357
Disk-ring studies of oxygen reduction, 359
Dislocation-free cathodes, their use as ideally polarizable electrodes, 417
Dissolution of metals, 399
  of rhodium, as established by Wood, 334
Distribution, of electron states in solution, 74
Distribution function, in electrode kinetics, 30
Dogonadze and Kuznetsov, on the Frank–Condon approximation, 6
  proton transfer processes in liquids, 4
Dogonadze and Levich, and frequency factor on electrode reactions, 210
Dogonadze–Levich theory, and separation factor, 212
Dogonadze, Chizmadzhev, and Kuznetsov, nonadiabatic electron transfer at semiconductors, 4
Dogonadze, Kutznetsov, and Levich, proton transfer theory, 45
Dogonadze, Kuznetsov, and Levich, proton transfer processes and liquids, 4
Dogonadze
  and activation processes, 209
  transition probability for nonadiabatic transfers, 3
Double layer effects in electrode kinetics, general reactions, 141
Double layer structure, and electrode kinetics, 140
  general reactions, 141
Double layer and drop in potentials involving semiconductors, 68
Double layer, effect on electrode kinetics, 27
Double-barrier model, of MacDonald and Conway, 346
Dubrovina and Nekrasov, and formation of a negative oxygen complex, 306

EXAFS, 340
Eckart barrier, use by Bockris and Matthews, 54
Efrima and Bixon, fast reactions at electrodes, 99
Electrocatalysis, 7
  and catalysis, 177
  and chemical potentials, 183
  and Conway and Bockris, 174
  in correlations, 204
  and electrode materials, 289
  its etymology, 173
  first mention of, 174
  first theoretically treated by Horiuti and Polanyi, 199
  formulated in terms of appropriate potentials, 182
  for oxygen, and Appleby, 343
  and potential energy diagrams, 197
  practical, 234
  and quantum mechanics, 205
  and Temkin isotherm, 202
Electrocatalytic reactions, general consideration, 217
Electrochemical kinetics, and work function, 101
Electrochemical nucleation, and Fleischmann and Thirsk, 330

Electrochemical processes compared with spectroscopic, 46
Electrochemistry of oxygen, 301
Electrocrystallization, 399
Electrode kinetics
  a basic formulation, 250
  calculated without approximations, 192
  and double layer structure, 140
  effects of coverage, 100
  as effected by the double layer, work of Frumkin, 27
  elementary equations, 89
  formulated at high coverage for hydrogen evolution reaction, 258
  formulated with respect to coverage, 200
  more complex formulation, 131
  multi-step reactions, 132
Electrode materials, and electrocatalysis, 289
Electrode processes, steps in, 87
Electrode reaction rates, and temperature dependence, 110
Electrode reactions
  dual, 264
  linked, 264
Electrolyte effects, on oxygen reduction, 383
Electron states in solution
  bell shaped curves, 75
  distribution of, 74
Electronic properties, and hydrogen evolution, 291
Electronic work functions, and metal solution interfaces, 105
Electrons
  coming from Fermi level, 208
  and phonon interaction, 35
Electrons, and reduction of organic compounds, 285
Electron transfer, as a rate determining step, in oxygen reduction, 384
Electron transfer processes, and time dependent perturbation theory, 49
Ellipsometric data
  interpreted by Angerstein-Kozlowska, 338
  and the model of oxygen buildup, 324
Ellipsommetry
  original studies by Reddy in Bockris' group, 336
  reflectance studies by Kim, Paik, and Bockris, 338
Elovich equation, 312
Embrittlement effects, Bockris and Subramanyan, 283
Energy profiles, in complex processes, 201
Entropy, and electrode reactions, 111
Enyo
  and palladium electrodes, 272
  and use of term "coupled", 264
Equations in electrode kinetics, the first, by Erdey-Gruz and Volmer, 411
Equilibrium potential, reaction rates at, 90
Erdey-Gruz and Volmer, first equations in electrode kinetics, 411
Errors, in Landau-Zener theories, 78
Exchange current density, 90
  definition of, 129
  and surface profile, 432

Faradaic rectification, and Barker, 468
Fermi level
  and electrode reactions, 117
  in solution, invalid concept?, 71
  as source of electrons, 208
Fermi's golden rule
  applied to electrodes, 56
  and transitions at semiconductor-solution interfaces, 66
Field-enhanced oxide transitions, work of Damjanovic, 326
Films, properties of, on platinum, 337
Fleischmann and Thirsk
  electrochemical nucleation, 330
  and treatment of set crystal planes, 408
Fluctuation theory, calculation of, Bockris and Sen, 42
Folgner and Arvia, and aging effects in electrode reactions, 326
Formulation, of electrode kinetics, complex, 256
Fourier transform, of inertial polarization, 10
Frank-Condon barrier, and solvent polarization, 21
Frank-Condon factor, in transition, 58
Frank-Condon transitions, in electrocatalysis, 212
Free energy of adsorption in electrocatalysis, and Parsons, 204
Free energy change, in electrochemical reactions, 454
Frequency dependence of the impedance, and the exchange current density measurements, 416
Frequency factor, and metal deposition, 413
Frumkin
  and Bronsted's theory, 94
  and the electronic work functions in electrode kinetics, 101

Frumkin (*cont.*)
  free energies and electrode processes, 94
  his isotherm, 312
  his monograph, 140
  and potential distribution at interface, its influence in hydrogen, ion discharge, 241
Frumkin and Aladjalova, and palladium electrodes, 271
Frumkin and Florianovich, an interpretation of anion reduction phenomenon, 155
Frumkin and Nekrasov, and the disk ring method, 353
Frumkin and Nikolaeva-Fedorovich, and kinetics of persulfate reduction, 103
Fuel cells, and electrocatalysis, 176

Gadzuk
  initial state of electrons at electrodes, 50
  solution to problems in time dependent perturbation theory, 50
Galvani potential difference
  in electrode kinetic formulations, 185
  in electrode kinetics, 103
  and rate of electrode reaction, 181
Gamow
  formula applied to electrode kinetics, 3
  and tunneling, 3
Garten and Weiss, and the surface quinone groups in oxygen reduction, 379
Gaussian distribution
  failure in reproduction of Tafel line, 76
  of states in energy gap, 66
Gaussian or Boltzmannian?, 74
  distribution of states in solution, 75
  and electrocatalysis, 174
  and first discussion of adsorption on semiconductors, 213
  and nonadiabatic transfers, 3
  and promulgation of invalid concepts, 75
  theory of Fermi energy in solutions, doubtful?, 72
  and volcano plots, 205
Gibbs' adsorption equations, applied by Frumkin to electrode kinetics, 158
Gibbs free energy
  as function of size and nucleation, 438
  for 3-D nucleation, 446
Gibbs-Wulff-Kaischew theorem, 434
Gierst
  and co-adsorption of ions, 146
  and Cornelissen, the anodic oxidation of europium, 164
Gierst (*cont.*)
  graphical method of correcting Tafel slopes, 156
  and ion pairs on electrode reactions, 161
  and Psi effects, 162
Gilroy
  and nucleation mechanisms in oxygen reactions, 330
  his oxide concept, 324
  and reduction of oxide layers, 330
Gnanamuthu and Petrocetli, and Tafel slopes larger than 2RT/F, 187
Gold, mechanism for oxygen reduction thereon, 365
Gold rate constants, for oxygen reduction on palladium, 361
Grahame and the rational potential scale, 184
Grahame and Soderberg, their study of the outer Helmholtz plane, 190
Graphite, and oxygen reduction, 361
Ground state protons, and electrode reactions, 46
Grubb, and electrocatalysis, 174
Gunawardena, Hills, and Montenegro, calculation of nucleii in galvanostatic pulse, 443
Gurney
  founding paper in quantum theory of electrochemical kinetics, 1
  and radiationless transfer theory, 206
  transition probability, 48
Gurney condition, 48
Gurney model, for charge transfer, 207

Hale, limiting currents in activationless processes, 8
Hamiltonian
  of oscillators in homogeneous systems, 11
  for redox reactions, 79
Harmonic oscillator, Christov's calculations, 46
Heat of adsorption
  as function of coverage, on electrodes, 246
  and reduction of activation energy, 198
Heat of adsorption in electrode kinetics
  work of Conway and Bockris, 106
  work of Delahay and Ruetschi, 106
Helmholtz double layer, transfer across of species in electrode reactions, 188
Helmholtz plane, and location of discharging particles, 29
Heterogeneity, and Temkin effects, 217
Heterogeneous nucleation, theory of Kaischew, 439
Heyrovsky step, 88, 269

Hickling and Hill, and oxygen overvoltage, 343
Hillig, and layer growth, 418
Hirth and Pound, their review of nucleation, 441
Hoar, and calculation of reversible potential for oxygen, 307
Hoare
  and oxygen diffusion in the bulk of metals, 310
  and reversible oxygen potential, 307
  and thermodynamics of oxygen electrodes, 303
Horiuti and Polanyi
  basic theory of phenomenological electrochemical kinetics, 1
  and first treatment of electrocatalysis, 199
Horiuti, and stoichiometric number, 137
Horkans, oxide films on platinum, 338
Hush, adiabatic changes with solvent polarization, 3
Hydrodynamics, of disk ring method, 353
Hydrogen
  adsorption on metal electrodes, 242
  and reduction of organic compounds, 285
  step for desorption, 31
Hydrogen adsorption isotherm, 245
Hydrogenation
  and the effect of hydrogen, 288
  and electrode potentials, 287
  of organic substances, 285
Hydrogen dissolution, anodic limiting currents, 279
Hydrogen electrode reactions, formulated, 218
Hydrogen evolution
  from alkaline solutions, 153
  its complexity, 196
  and d-character, 290
  and Psi effects, 142
  and Tafel lines, 290
Hydrogen evolution reaction, model of, 57
Hydrogen overpotential
  and barrierless processes, 121
  on lead electrodes, 152
  on mercury, 144, 153
  in nonaqueous solutions, 107
  on platinum and nickel, 263
  on silver cathodes, 122
Hydrogen peroxide
  analyzed by the disk-ring, 354
  appearing in oxygen reduction reactions, 354
  indicated by oxygen reduction, 354
Hydrogen pressure, and hydrogen overpotential, 282
Hydrogen waves, 242
  and experiments on single crystal planes, 247
Hydroxonium ions, a continuum in vibrational levels, 51

Impedance diagram, for activation control, 468
Impedance method, of Randall, 468
Inconsistencies, in continuum theory, 46
Initial state, shifted in electrode reactions, 113
Inner potential, of solution, left out in Fermi level in solution calculation, 74
Inner shell, predominant in electrode reactions, 43

Intermediates, in oxygen evolution reaction, 341
Ion pair formation, near electrodes, 161
Ion pairs, and electrode reactions, 161
Iridium, and oxygen evolution, 350
Iron, among more weakly absorbing metals?, 226
Irreversible oxide formation, Damjanovic's work, 325
Isotope effects, 38
Isotopic labelling experiments, and oxygen reduction, 354
Isotopic work, on oxygen evolution reaction, 332
Iwakura, and oxygen evolution on platinum, 349

Jofa and Kabanov, specific adsorption of anions, 146

Kabanov, incorporation of alkaline metal in cathode, 154
Kaischew
  and the continuity approach, 441
  frequencies of deposition and dissolution step roughness, 402
  and growth of crystals, 433
  and heterogeneous nucleation, 439
  and nucleation processes, 409
  and poliganized spirals, 425
Kaischew and Toshnev, analysis of nucleii formation, 444
Kaischew and Zelevich, nonequilibrium factor, 411
Kelvin effect, with small crystal, 457
Kestner, electron transfer between complexes, 7

Khan
  and application of Fermi's golden rule, 213
  his book with Bockris, 53
  and invalidity of Fermi level in solution, 75
  and the testing of Bornian theories, 44
Khanova, and adsorbed oxygen, 331
Khartkatz and Ulstrup, polarization characteristics in hydrogen evolution, 7
Kim, Paik, and Bockris, reflectance studies connected to ellipsommetry, 338
Kinetic analysis, of oxygen evolution reaction, 345
Kinetic equations, basic, and electrode kinetics, 248
Kinetic parameters for oxygen adsorption and desorption reactions, 320
Kinetics
  of electrode reactions, general, 127
  of hydrogen evolution, results gathered, 290
  of hydrogen evolution reaction, 268
  of metal deposition, on perfect crystal faces, 418
  of two-dimensional nucleation, experimental investigation, 411
Kink positions on surface, 401
Kirchoff's equations, in electrode kinetics, 135
Kita, and selection of heat of adsorption values, 223
Kobosev and Monblanowa, Elektrokatalyse, 174
Kolotyrkin, and the potential of zero charge, 151
Kossel and Stranski, first work on "half crystal" positions, 400
Kotz and Yeager, and electrochemically formed films on silver, 339
Krasilchikow, his mechanism for oxygen evolution, 351
Krishtalik
  activation processes, 3
  and an anomalous formation of volcano plots, 226
  barrierless transitions, 8
Krylov, and anion reductions, 163
Kryukova, minimum in the persulfate anion reduction, 155
Kubo and Toyozawa
  basic theory of radiationless transfers, 2
  density matrix method, 8
Kuhn, and screening of electrocatalysts, 217

Labelling experiments, for oxygen evolution reactions, 342
Landau and Zener, and nonadiabatic reactions, 77
Landau–Zener expression, used by Dogonadze and Levich, 211
Landau–Zener theory
  its errors, 78
  formulation, 77
Langmuir adsorption, isotherm, 246
Langmuir isotherm
  applied to electrode reactions, 98, 245
  and electrocatalysis, 187
Latimer, and free energy data, 304
Lax, radiationless transfers for polyatomic molecules, 2
Layer growth, and Chernov, 418
Ligand structure, 380
Legendre polynomial, and orientation of hydrogen molecule, 32
Leites, and pH effects on oxygen reduction, 370
Levich
  continuum theory, 42
  and equilibrium between ions in bulk and surface, 162
  polaron mechanism, 41, 42
  rate constant in homogeneous proton transfer, 6
Levich and Dogonadze, nonadiabatic transfers, 3
Lewis, and experiments on palladium electrodes, 272
Libby
  continuum theory, 2
  solvent polarization, 2
Limiting current observed under activation conditions, 471
Liquids, decoupling in, 18
Lorenz, and metal deposition, 408
Losev, and work on metal deposition, 471

MacDonald and Conway, and oxygen evolution on palladium-gold alloys, 345
Macrocycles, 380
Marcos and Yeager
  oxygen reduction work on pyrolytic graphite, 363, 364
  and stoichiometric numbers, 365
Marcus
  and BEBO model, 213
  and inner sphere reactions, 213
  outersphere electron transfer reaction, 2
  simplified model, 3
Matthews and Bockris, and relation of transfer coefficient to stoichiometric number, 257

Mattson and Bockris, work on metal deposition, 471
Maxwellian distribution, and Tafel lines, 76
Mayoka and Enyo
  and effect of surfactants on hydrogen overpotential, 281
  and experiments on palladium electrodes, 272
  pressure phenomena on palladium electrode, 284
Mechanism of oxygen evolution reaction, 344
Mechanism for oxygen reduction, on pyrolytic graphite, 364
Mechanistic aspects of oxygen evolution reaction, 341
Meeting, of rotating loops, 426
Meier, and Mössbauer spectra on carbon supports, 385
Metal cobaltites, 376
Metal deposition, 399
  on perfect crystal phase, 409
Metal electrodes, adsorption of hydrogen, 242
Metal oxides, and oxygen evolution, 351
Miles, the oxygen evolution reaction on nickel, 351
Model, for electron transfer at interface, 59
Molecular reduction, of oxygen, 360
Monolayer deposition, 418
Moore, translater frequencies in water, 41
Morphology, 451
  of growth, 426
Morse-type potential, in proton transfer, 22
Mössbauer spectroscopy, first applied to electrodes by O'Grady and Bockris, 340
Mueller and Nekrasov, and use of the rotating disk method, 353
Multi-layer deposition, 420
  multi-nuclear, 420
Multi-step reactions, 134

Neél temperature, 351
Nernst relationship, in electrode kinetics, 99
Newton, his contribution to transmission coefficient theory, 78
Nielsen, and layer growth, 418
Nikolic, Adzic, and Yeager, models of adsorbed iron and cobalt phthalocyanines, 387
Noble metals, and oxide formation, 333
Nonadiabaticity, 76, 77
Nonadiabatic reactions, 3, 20
Nonadiabatic transitions, and general formula, 4
Nonaqueous solutions, and hydrogen overpotential, 107
Novak, Tilak, and Conway, and the chlorine evolution reaction, 234
Nucleation, and Gibbs free energy, 438
Nucleation, and time elapse, 412
Nucleation overpotential, 412
Nucleation rate, 435
  as a function of current density, 445
Nucleation-rate-overpotential relation, 440
Nucleii, as a function of time, in crystal growth, 444
Nucleii formation, in galvanostatic pulse, 443

O'Grady, and oxygen evolution, on oxides, 352
  studies of oxygen evolution, 335
Open circuit potentials, 306
  and oxygen electrode reactions, 306
Operator, of interactions near electrodes, 13
Orbitals, for oxygen interaction, 373
Organic compounds and reduction of, 165
Organic molecules, large, and electrode reactions, 167
Organic oxidations, and electrocatalysis, 233
Orientation of water molecules, and hydrogen overpotential, 152
Outer shell, and electrode reactions, 46
Ovchinnikov and Benderskii, quantum mechanical model of hydrogen evolution, 57
Overall kinetics, and hydrogen evolution reaction, 267
Overpotential components, on palladium electrode, 275
Overpotential, at the steady state, 273
Overpotential
  and clusters, 436
  its decay, 274
  and different orientations, of crystal faces, 414
  and nucleation, 412
  at steady state, 273
Oxidation of HO– on gold, 367
Oxide catalysts, 375
Oxide-covered interfaces, and tunneling, 68
Oxide films, and adsorbed oxygen, study by ellipsommetry, 336
Oxide films on platinum, work of Yeager, 338
Oxide formation
  and temperature dependence illustrated by Damjanovic, 326
  uniformity established by Damjanovic, 330
Oxide thickness, and reaction rate, 348

Oxides
  and oxygen evolution, 348
  and thickness on platinum, 333
Oxygen adsorbed on metal sites, reaction pathways, and oxygen reduction, 373
Oxygen adsorption
  distinguished from oxygen phase formation, 312
  on noble metals, 321
Oxygen buildup of platinum, and ellipsometric data, 324
Oxygen deposition on platinum and sweep voltammetry, 316
Oxygen diffusion into metals, and the work of Hoare, 310
Oxygen electrochemistry, 301
Oxygen electrode reactions, 228
Oxygen electrode reduction on platinum, 368
Oxygen electrode
  thermodynamics of, 302
  and Vetter and Schultze, 328
Oxygen evolution mechanisms, on nickel, 351
Oxygen evolution reaction, 341
  and Damjanovic, 345
  intermediates in, 341
  a kinetic analysis, 345
  and Tafel slopes, 343
  treated by Damjanovic, 330
Oxygen evolution, Rosenthal and Veselovskii, and studies with O, 341
Oxygen evolution on palladium–gold alloys, 345
Oxygen evolution on platinum, studies of high anodic potentials, 338
Oxygen gas reduction, 355
Oxygen reactions, and voltage sweeps, 317
Oxygen reduction, 363
  on basal plane of graphite, 379
  and Damjanovic, 369
  and electrolyte effects, 383
  on metal monolayers, 385
  on nonmetallic material, 374
  in parallel reactions, 356
  on pyrolytic graphite, 364
  in stoichiometric numbers, 364
  and Tafel plots on pyrolytic graphite, 386
  and Tafel slopes, 362
  as treated by Wroblowa, 357
Oxygen reduction mechanisms, alternatives, 371
Oxygen reduction reaction
  formulation of Temkin adsorption isotherm, 312
  suggestion of Damjanovic and Brusic, 231
Oxygen reduction studies, and Tafel plot, 372
Oxygen species, thermodynamic data, 303
Oxygen, reduction to hydrogen peroxide, 368
Oxygen, and anodic films on platinum, 312

pH, and electrode potential, 466
pH dependence, of peak potentials in voltammograms, 322
pH effects, on hydrogen overpotential, 153
Palladium hydrogen electrode, and transient experiment, 270
Palm and Tenno, potential of zero charge in respect to electrode reactions, 151
Parallel reactions
  in electrode kinetics, 139
  in oxygen reduction, 356
Parallel and series reactions, for oxygen evolution, 353
Parsons and Visscher, and optical studies of oxygen evolution on platinum, 338
Parsons' group, its studies of platinum oxides, 340
Parsons
  and double layer structure effects on electrode kinetics, 146
  and electrocatalysis, 174
  free energy of adsorption in electrocatalysis, 204
  and pre-exponential plots, 225
  relationship between changes in overpotential and Psi potential, 147
  and use of term "coupled", 264
  and volcano plots, 205, 224, 233
Pathways, and complex electrode kinetics, 196
Pekar, radiationless theory for polar crystals, 2
Perfect crystal faces, in metal deposition, 418
Perfect crystal phase, and metal deposition thereon, 409
Perfluoro sulphonic acid, 350
Peroxide theory, to explain resting potentials at oxygen electrodes, 308
Phase oxides, and work of Damjanovic, 324
Phase oxide theory, and investigation of platinum electrodes, 323
Phenomenological theory, of electrode kinetics, 93
Phonon, and electron interactions, 35
Photo-current, and non-Tafel behavior, 63
Photoelectrochemical kinetics
  aspects of, 61
  formulated by Bockris and Uosaki, 62
  quantum theory of, 62
Phthalocyanines, 380

Platinum
  anodic films with oxygen, 312
  anodic layers, their irreversibility, 315
  and oxide layers, 318
  and oxygen electroreduction, 362
  and oxygen evolution, 349
  and oxygen formation, depicted, 317
  studies of oxygen adsorption, 314
Platinum dissolution, and effect on electrode reactions, 311
Platinum electrodes, and surface modifications, involving higher catalytic activity, 291
Platinum films
  refractive index for, 337
  study by electromodulation, 339
Platinum oxides, including individual species of PtOH, studied by Parsons' group, 340
Platinum single crystals, and Will, 247
Platinum surfaces, investigated by Auger Spectroscopy, 340
Platzmann and Frank, radiationless theory of transitions, 2
Pleskov, photo-emission experiments, 104
Pleskov and Rotenberg, limiting activation currents for hydrogen discharge, 123
Polarization, its meaning in electrode kinetics, 92
Polarization curves
  for oxygen reduction, 376
    on palladium, 370
  for oxygen evolution on oxides, 352
Polaron theory, Levich, 42
Potential
  of electrode, its effect on the rate of reaction, 181
  as a function of composition, for cadmium amalgams, 457
Potential drop, in double layer, space charge region, and potential drop, 68
Potential energy barrier, at electrodes, 7
Potential energy curves
  and effect of potential, 97
  and electrode processes, 95
  harmonic, 96
Potential energy diagrams, and electrocatalysis, 197
Potential energy surfaces, 9
  in proton transfer, 23
Potential sweeps, for silver single crystals, 459
Potential sweep technique, with hydrogen waves, 242
Potential of zero charge
  its effect on organic reactions, 166
  and electrocatalysis, 184
  and rational potential scale, 184
Pourbaix, his diagrams, 466
Pre-exponential factors in electrode reactions, 114
  and barrierless transitions, 114
  and electrode kinetics, 28
Pre-exponential plots, and Parsons, 225
Pre-exponentials, related in oxygen evolution reaction, 343
Pressure
  effect on electrode reactions, 115
  and hydrogen overpotential, 282
Probability, of transition, 16
Proton transfer
  and splitting energy, 57
  Gurney's model, 51
  kinetic parameters for, 37
  model for, 11
  weak coupling case, 25
  a model for, 21
  and model of electrode processes, 83
Proton transfer reactions, 20
Psi potential in Helmholtz plane and elsewhere, 161
Pyramids, and metal deposition, 429, 432
Pyrolytic graphite and oxygen reduction, 363

Quantum character, of proton transfer, 52
Quantum mechanical aspects, of electrocatalysis, 205
Quantum mechanical calculations of electron transfer probability, 4
Quantum mechanical rates for electron transfer, 53

Radiationless transfer theory, 206
Raman spectroscopy, of silver oxide layers, 339
Randall's, his impedance method, 468
Rangarajan, and multi-layer deposition, 420
Rate determining steps
  and chlorine reactions, 125
  and electrocatalysis, 180
  as formulated by Bockris and Mauser, 194
  sometimes absent, 261, 264
  and volcano plots, 222
Rate of formation of two-dimensional nucleii, 411
Rate of step propagation, rate of, 404
Rates, virtual, 219
Reaction orders
  definition, 260

  and Tafel lines, 262
  and Vetter, 259
Reaction routes, and mechanism, 251
Recombination kinetics, 91
Reddy, Genshaw, and Bockris, studies of anodic films on platinum using ellipsommetry, 336
Reddy, original studies in potential-controlled ellipsommetry, 339
Reddy, *et al.*, two types of layers on platinum, 337
Reddy, his book with Bockris, 399
Redox catalysts, and concepts of Beck, 231
Redox potentials, on vacuum scale, 71
Redox reactions, and volcano relations, 232
Reduction
  of anions, 155
  organic materials, near electrodes, 167
Reduction of oxygen, for electron mechanisms, 356
Reduction of oxygen on high pressure, and stress-neel pyrolytic graphite, 377
Reflectance, modulated, on the electrode, 339
Refractive index for platinum films, 337
Relaxation, and the double layer, and electrode kinetics, 190
Reorganization energy, 5
  calculated, 44
Resonance time, of adatoms, 404
Rest potential on platinum, in presence of oxygen, and surface oxides, 309
Reversible potential for oxygen, and characteristics observed, 308
Reversible potentials
  alloys, 456
  of metals in solutions with complex interactions, 461
  in nonaqueous solutions, 460
Rhodium, analyzed by Damjanovic, 351
Ross
  and activities in rhodium-platinum alloys, 291
  and weak peaks, 317
Rotating disk-ring data, and oxygen reduction, 354
Rotation and spiral growth, 424
Roughness, of surface, 400
Rudolph and Zimmermann, quasi continuum vibrational levels in H_2O, 51
Ruetschi and Delahay, correlation of oxygen overvoltage to energies of MOH bond, 343
Ruthenium oxide
  mechanism of oxygen evolution on, 353
  studied by Trasatti, 335

Salami and Weaver, electrode kinetics in nonaqueous media, 43
Salt effects, on hydrogen overpotential, 145
  theory of, 148
Salzano, studies on hydrogen, 222
Sawyer, and the one electron transfer of reduction of oxygen, 366
Scans, cyclic, 219
Schmickler
  calculation of transition probability, 18
  harmonic approximations, 70
  transition probability, 18
  and treatment of set crystal planes, 408
  tunneling, 68
Schmickler and Vielstich, Frank–Condon approximation, 6
Schmidt, the quantum mechanical probability of crossing for bridge-assisted reactions, 8
Schrödinger's equation, and electrode reactions, 55
Schuldiner, and diffusion of atoms into metals, 310
Schultze and Vetter, modelistic approaches to oxygen evolution on oxides, 348
Screening action, of ammonium ion, in electrode kinetics, 146
Selectivity, in electrode reaction rates, 175
Semiconductors, and rate of reaction on, 215

Semiconducting properties, of graphite, and oxygen reduction, 378
Semiconductor-solution interface, photo current at, 64
Sen and Bockris, calculation of fluctuating barrier height, 57
Sen and Bockris, validity of WKB method, 54
Separation factor, as a function of potential, 150
Silver single crystals, and potential sweeps, 459
Single atom incorporation paths, 401
Single crystal planes, and experiments on hydrogen waves, 247
Single crystals, and two dimensional nucleation, 412
Small cluster model, 442
Solvated electrons, and Conway's treatment, 105
Solvent polarization, 3

Spectroscopic processes
  compared with electrochemical, 46
  and probability of transition, 47
Spillover theory, and volcano plots, 233
Spiral growth, 425
Spiral growth mechanism, and Burton, Caberra, and Frank, 425
Spirals
  and the calculations of Budevski, 425
  interacting, 426
Splitting energy, and proton transfer, 57
Spreading layers, the formation of monoatomic layers, Komogorov–Avrami, formulation, 419
Spreading monolayers, propagation, of polyatomic steps, 415
Stackelberg and Weber, reduction on palladium electrodes, 286
Standard electrode potentials, for oxygen reactions, 303
Standard pre-energy in rate determining steps, 184
Steady state hypothesis, in electrode kinetics, 178
Steady state polarization, 273
Stepped crystal faces, and current density, 408
Step propagation, 413
  and metal deposition, 413
Stoichiometric number, 133, 252, 254
  as determined by Morcos and Yeager, in oxygen reduction, 364
  general formulation, 136
  introduced by Horiuti and Ikusima, 136
  methods of determination, 255
  and oxygen reduction studies, 371
  and rate determining steps, 267
  related to transfer coefficient, 257
Stoichiometry, and electrode reactions, formulated, 189
Stonehart and Kolhlmayr, and hydrogen evolution on rotating disk electrode, 281
Stoner, and surface conductivity measurements of adsorption, 339
Summary, of basic aspects of electrode process theory, 83
Surface active agents, and hydrogen overpotential, 149
Surface atoms, and partial hydration energy, of Conway and Bockris, 403
Surface concentration, in electrode reactions, 167
Surface coverage, with hydrogen, 280
Surface diffusion
  in metal deposition, 406
  treatment of Despić and Bockris, 405
  treatment of Mehl and Bockris, 404
Surface oxides, studied by Buckley and Burke, 334
Surface profiles, and current densities, 432
Surfaces of electrodes in solution, methods of examination, 340
Symmetry factor, 49

Tafel
  his law, 94
  his step, 88
Tafel curves, corrected and uncorrected, 157
Tafel equation, proof of, 128
Tafel line, with respect to components of overpotential on palladium, 277
Tafel lines
  as function of overpotential on palladium electrodes, 278
  and Gaussian distribution, 76
  and hydrogen evolution, 290
  and Maxwellian distribution, 76
  on nickel, 263
  and reaction orders, 262
Tafel plots
  from Butler–Volmer equation, 469
  compared with predictions of Bornian theory, 45
  connected to volcano plots, 223
  for oxide solution interfaces, 71
  for oxygen reduction, 386
  and the potential energy surface, 213
Tafel region
  and hydrogen discharge, 123
  and stoichiometric number, 138
Tafel slopes, 254
  greater than 2RT/F, and Parsons' explanation, 187
  on pyrolitic graphite, 363
  and oxygen evolution reaction, 343
  low, 121
  and stoichiometric number, 253
  their magnitudes, 255
Tafel–Volmer route, 267
Takehara, and experimental techniques at palladium electrodes, 286
Tarasevich
  and Tafel slopes, for oxygen reduction, 362
  and pH dependence of potential in oxygen reduction, 362

Tarasevich (*cont.*)
  and the shift of isotopic distribution in oxygen reduction, 355
  and kinetic treatment of oxygen adsorption, 318
  and oxygen layers on platinum, 318
  and oxygen reduction, 363
  and tephlon bonded electrodes in establishing reversible potential for oxygen, 307
  and tephlon-bonded high area platinum, 372
Tedoradze, high coverage effects in electrode kinetics, 168
Tempkin
  and affect of heat adsorption on electrode reaction rates, 97
  and entropy in electrode reactions, 112
  and oxygen evolution reaction, 345
  and "real" activation energies, 110
  and temperature dependence of electrode reactions, 110
Temkin adsorption
  as applied to oxygen evolution reaction, 344
  isotherm, and oxygen reactions, 323
Temkin conditions, and oxygen electrode reactions, 228
Temkin effects, and induced heterogeneity, 217
Temkin isotherm, 276
  and electrocatalysis, 202
  and hydrogen evolution reaction, 268
  negative, 246
Temkin region, and volcano plots, 225
Temkin's treatment, of true and apparent activation energies, 101
Temperature dependence of electrode reaction rates, 110
Tests, of Bornian theories, 44
Texture, 451
Theory of oxygen evolution reaction, by Damjanovic and Jovanovic, 348
Thermodynamic data, for oxygen species, 303
Thermodynamics
  applied to metal deposition, 453, 455
  of oxygen electrode, 302
Time dependent perturbation theory, 49
  applied to electrode reactions, 47
  calculation of transition probability, 80
Tracer experiments
  for hydrogen evolution reaction, 262
  and rate determining steps, 261
Transfer, to stepped crystal planes, 408
Transfer coefficient
  related to stoichiometric numbers, 257
Transfer coefficient (*cont.*)
  true and false, 143
  values, 189
Transients, in metal deposition, 423
Transition configuration, near electrodes, 17
Transition metal complexes, 380
Transition morphology, of growth, 428
Transition period, and growth morphology, 429
Transition probability
  and accoustical modes, 15
  affected by tunneling, 52
  calculated by Bockris and Khan, 47
  of electrons, at electrode-solution interfaces, 80
  equal by time dependent perturbation theory and tunneling theory, 55
  general expression for, 11
  and quantum number of electrons at electrodes, 12
Translater frequencies, Moore's work, 41
Transmission coefficient for homogeneous redox reactions, 78
Trasatti, orientation of water molecules, 151
Trasatti and Buzzanca, properties of ruthenium oxide, 335
Tseung and Bevan, investigation of perovskites, 311
Tunneling, at oxide covered interfaces, 68
Tunneling probability, for proton transfer, 54
Two-dimensional nucleation, 410
Two-dimensional nucleii, rate of formation, 411

Underpotential deposition, 243
  of metals, 458
Uosaki, and photoelectrochemical kinetics, 62

Vacuum scale potentials, 72
Vandenbrink, Barendercht, and Visscher, obtaining *five* rate constants, 357
Vermilyea, and treatment of set crystal planes, 408
Veselovskii, and oxide formation of anodic situations, 332
Vetter
  and comprehensive treatment of metal deposition mechanisms, 409
  and formulation of reaction orders, 259
  and limiting values of overpotential in Heyrovsky–Volmer reaction, 272

Vetter and Schultze
  and exponential decrease of reaction as a function of oxide thickness, 348
  and models for oxygen electrodes, 328
  and oxide concepts for platinum, 324
  and reduction of oxides, 330
Vischer and Devanathan, and phase oxide theory, 323
Vitanov and exchange current densities
  using frequency dependence of the impedance, 416
  for surface profile explanations, 432
Volcano plots
  and activation energy data, 229
  Balanden–Parsons–Gerischer model, 231
  and Brönsted slope, 220
  and the Conway–Bockris formulation, 224
  early calculations of Bockris, 224
  effected by overpotential, 222
  first fitted with experimental data by Conway and Bockris, 205
  for oxygen electrode reactions, 229
  for oxygen reaction, 344
  and Parsons, 224
  and the results of Bockris and Koch, 226
  and theoretical discussion of Parsons, 205
  theory of, 216
Volcano relationships
  interpreted for oxygen electrode
Volmer
  and direct transfer mechanism in metal deposition, 409
  electrode processes, 87
Volmer–Heyrovsky mechanism, 252
Volmer reaction, 243
  and redox reactions, 232
  and steady state formulations, 273
Volmer–Tafel, 265
  mechanism, 252
Volmer and Weber, and nucleation processes, 409
Volodin, and adsorbed oxygen, 331
Voltammogram
  and computer simulations, 317
  for oxygen, 315
  for platinum, 319

WKB approximation, used in Gurney's theory, 51
WKB method, validity examined by Sen and Bockris, 54
Wagner, and reduction on palladium electrodes, 286
Walker, his invalid attempts on solvated electrons, 105
Watanabe and Devanathan, and reversible oxygen potential, 307
Water discharge, on mercury, 153
Water electrolysis, at high current density, 349
Wave length dependence for platinum films, work of Horkans, 338
Weak coupling and proton transfer, 26
Weaver, Tyma, and Mettlesky, ratio of redox reaction rates in water-duterium oxide, 43
Will, and platinum single crystals, 247
Wood, and anodic charge on rodium, 334
Work function
  correlations to hydrogen overpotential, 106
  and dark electrode reactions, 105
  and related values in electrode kinetics, 101
Wright, Khan, and Bockris, on nonadiabaticity, 213
  transition probability calculation, 82
Wroblowa, Rao, Damjanovic, and Bockris, pressure relationship for reversible oxygen evolution, 308
Wroblowa, and Bockris, first presentation of factors in electrocatalysis, 174
Wroblowa's treatment, of oxygen reduction, 357

Yanagihara, and electrocatalytic activity on cobalt electrodes, 291
Yeager
  and oxide films on platinum, 338
  oxygen reduction on other carbons, 363
  and the peroxide dismutation-desorption step, in oxygen reduction, 379
Yeager and Kozawa, and open circuit electrode potentials involving oxygen, 304
Yofa and Frumkin, hydrogen overpotential in concentrated solutions, 109

Zagal, and catalytic properties, of certain graphite surfaces, 382
Zagal and Yeager
  and mechanisms for chemical limiting currents, 386
  and oxygen reduction on monolayers, 385
Zeta potential, and reaction orders, 260
Zinc chloride species, in solution, 465
Zurilla, and mechanism for oxygen reduction on gold, 365